

รายงานวิจัยฉบับสมบูรณ์

โครงการ

องค์ความรู้ใหม่ทางเคมีวิเคราะห์เพื่อนวัตกรรม

ทางการตรวจวัด

โดย ศาสตราจารย์ ดร. อรรธรณ ชัยลภากุล

และคณะ

สิงหาคม 2560



รายงานวิจัยฉบับสมบูรณ์

โครงการ

องค์ความรู้ใหม่ทางเคมีวิเคราะห์เพื่อนวัตกรรม

ทางการตรวจวัด

โดย ศาสตราจารย์ ดร. อรรธรณ ชัยลภากุล

และคณะ

สิงหาคม 2560

รายงานวิจัยฉบับสมบูรณ์

โครงการ

องค์ความรู้ใหม่ทางเคมีวิเคราะห์เพื่อนวัตกรรมทางการตรวจวัด

ผู้วิจัย

ศาสตราจารย์ ดร. อรรพรรณ ชัยลภากุล	จุฬาลงกรณ์มหาวิทยาลัย
รองศาสตราจารย์ ดร. นาทยา งามโรจนวณิชย์	จุฬาลงกรณ์มหาวิทยาลัย
รองศาสตราจารย์ ดร. ณรงค์ ประไพรัชสิทธิ์	จุฬาลงกรณ์มหาวิทยาลัย
รองศาสตราจารย์ ดร. วิณา เสียงเพราะ	มหาวิทยาลัยศรีนครินทรวิโรฒ
ผู้ช่วยศาสตราจารย์ ดร. สุชาดา จูณวัฒน์กุล	จุฬาลงกรณ์มหาวิทยาลัย
ผู้ช่วยศาสตราจารย์ ดร. วนิดา หลายวัฒนไพศาล	จุฬาลงกรณ์มหาวิทยาลัย
ผู้ช่วยศาสตราจารย์ ดร. เกียรติศักดิ์ ส่งศรีโรจน์	มหาวิทยาลัยศรีนครินทรวิโรฒ
ผู้ช่วยศาสตราจารย์ ดร. วิจิตรา เตือนฉาย	มหาวิทยาลัยเทคโนโลยีพระจอมเกล้าธนบุรี
ดร. นาฏนิตดา รอดทองคำ	จุฬาลงกรณ์มหาวิทยาลัย
ดร. มนพิชา ศรีสอาด	จุฬาลงกรณ์มหาวิทยาลัย
ดร. อมรา อภิลักษณ์	มหาวิทยาลัยมหิดล

สนับสนุนโดยสำนักงานกองทุนสนับสนุนการวิจัย

และจุฬาลงกรณ์มหาวิทยาลัย

(ความเห็นในรายงานนี้เป็นของผู้วิจัย สกว. และจุฬาลงกรณ์มหาวิทยาลัย)

ไม่จำเป็นต้องเห็นด้วยเสมอไป)

เลขหมู่

เลขทะเบียน 017495

วัน, เดือน, ปี 22 พ.ย. 60

Project title: องค์ความรู้ใหม่ทางเคมีวิเคราะห์เพื่อนวัตกรรมทางการตรวจวัด
Novelty in Analytical Chemistry for Innovation of Detection

Project duration: 3 years

Total budget: 7,500,000.00 Baht

Principal investigator: Professor Dr. Orawon Chailapakul
Department of Chemistry, Faculty of Science, Chulalongkorn
University

Abstract

Analytical chemistry is the one of the most importance not only to all branches of chemistry but also to all the biological sciences, to engineering, and, more recently, medicine, public health, food, environment and the supply of energy in all forms. Therefore, the developments of novel detection methods play an important role to obtain both qualitative analysis and quantification of the chemical or biomolecule components of natural and artificial materials. This work has been separated into 3 groups for finishing the novelty in detection methods. First, novel nanomaterials-based or nanocomposite chemical sensors based on nanomaterial/conducting polymer will be prepared and used to modify the electrode surface for sensitive electrochemical and/or optical detection of chemicals and biomolecules. The bioreceptor functionalization will be applied if it is necessary. Under the optimal conditions, the proposed system will be used for sensitive detection of target analytes (e.g. heavy metals, pesticides, food contaminants and biomolecules). This approach is an alternative tool for environmental monitoring, food inspection as well as clinical diagnosis. Second, the paper-based device is proposed. They have the potential to be good alternatives for point-of-care testing because they are portable, easy to use, require only a small volume of sample and provide rapid analysis. To create the detection method for lab-on-paper, colorimetric and electrochemical detection are proposed. These provide the benefits of simplicity, speed, low cost, and portability for applying to various applications. Last, a simple microfluidic or sequential injection system for chemical or biomedical analysis will be developed. Exploiting a microfluidic or sequential injection system, short analysis times can be achieved with high analytical performances. In addition, only small amount of samples and reagents are required, which is beneficial for samples which are expensive or limited, especially biological samples. Moreover, microfluidic or sequential injection analysis holds great

promise for high-throughput analysis and screening, which offers an alternative platform for analysis and would be an ideal tool for a portable analysis system for clinical diagnosis.

Keywords: nanomaterial-based chemical sensors, metal nanoparticles, graphene, conducting polymer, pesticides, heavy metals, paper-based device, microfluidics, sequential injection

บทคัดย่อ

เคมีวิเคราะห์เป็นศาสตร์หนึ่งของเคมีที่มีความสำคัญมากไม่ใช่เฉพาะต่อทุกสาขาของเคมีแต่ยังเป็นศาสตร์ที่มีความสำคัญยิ่งต่อสาขาอื่น ๆ เช่น ชีววิทยา วิศวกรรมศาสตร์ การแพทย์ การอาหาร สิ่งแวดล้อม และพลังงานทดแทน ดังนั้นการพัฒนาเพื่อให้ได้มาซึ่งวิธีการตรวจวัดแบบใหม่จึงมีความสำคัญยิ่งทั้งต่อการวิเคราะห์เชิงคุณภาพและการวิเคราะห์เชิงปริมาณเพื่อตรวจสอบองค์ประกอบทางเคมีและทางชีวภาพสารธรรมชาติและสารสังเคราะห์ โครงการวิจัยนี้ถูกแบ่งออกเป็น 3 กลุ่มย่อยเพื่อสร้างสรรค์นวัตกรรมทางการตรวจวัด กลุ่มย่อยที่หนึ่ง เป็นการพัฒนาวัสดุนาโนหรือวัสดุนาโนคอมโพสิทระหว่างวัสดุนาโนและพอลิเมอร์นำไฟฟ้าแบบใหม่เพื่อใช้เป็นขั้วไฟฟ้าหรือเพื่อการดัดแปรผิวหน้าขั้วไฟฟ้าเพื่อการตรวจวัดทางเคมีไฟฟ้าและ/หรือเพื่อการตรวจวัดเชิงสีเพื่อตรวจวัดสารเคมีที่มีความสำคัญ เช่น โลหะหนัก ยาฆ่าแมลง สารปนเปื้อนในอาหาร และสารชีวภาพ เป็นต้น ซึ่งวิธีที่พัฒนาขึ้นมานี้จะสามารถใช้เป็นวิธีทางเลือกใหม่ของการตรวจวัดทางสิ่งแวดล้อม อาหาร และทางคลินิกได้ กลุ่มย่อยที่สอง คือการพัฒนาอุปกรณ์ฐานกระดาษร่วมกับกการตรวจวัดทางเคมีไฟฟ้าและ/หรือการตรวจวัดเชิงสี เพื่อสร้างเป็นอุปกรณ์การตรวจวัดนอกห้องปฏิบัติการ เนื่องจากกระดาษเป็นวัสดุที่หาง่ายและกำจัดได้ง่าย มีราคาถูก สามารถออกแบบอุปกรณ์ได้หลากหลายให้สอดคล้องกับการประยุกต์ใช้ อีกทั้งยังใช้สารตัวอย่างและรีเอเจนต์ในปริมาณที่น้อย พบว่าได้สะดวก กลุ่มสุดท้าย คือการพัฒนาของไหล เช่น ไมโครฟลูอิดิกและระบบซีเควินเซียลอินเจคชัน เพื่อการตรวจวัดสารเคมีหรือสารชีวภาพที่สำคัญ เพื่อได้มาซึ่งวิธีที่ง่าย รวดเร็ว มีประสิทธิภาพ และใช้สารตัวอย่าง รีเอเจนต์ ในปริมาณน้อย ทำให้ได้วิธีการที่ประหยัดและเหมาะสมต่อการประยุกต์กับตัวอย่างทางชีวภาพ นอกจากนี้ระบบไมโครฟลูอิดิกและระบบซีเควินเซียลอินเจคชันสามารถสร้างเป็นระบบการตรวจวัดแบบอัตโนมัติทำให้สามารถจัดการกับงานที่มีจำนวนสารตัวอย่างมาก ๆ ได้ มีความเหมาะสมกับทั้งงานคัดกรองและการตรวจปริมาณ จึงนับเป็นระบบการตรวจวัดในอุดมคติแบบพกพาที่อาจสามารถประยุกต์เพื่อการวิเคราะห์ทางคลินิกสืบต่อไปได้

คำสำคัญ: ระบบรับรู้เคมีฐานวัสดุนาโน โลหะขนาดนาโนเมตร แกรฟีน พอลิเมอร์นำไฟฟ้า ยาฆ่าแมลง โลหะหนัก อุปกรณ์ฐานกระดาษ ไมโครฟลูอิดิก ซีเควินเซียลอินเจคชัน

Chapter I

Executive Summary

1. Inspiration of this project

Analytical chemistry is the study of the separation, identification, and quantification of the chemical or biomolecule components of natural and artificial materials. Qualitative analysis provides an indication of the identity of the chemical species in the sample, and quantitative analysis determines the amount of certain components in the substance. The separation of components is often performed prior to analysis. In addition, analytical chemistry is also focused on improvements in experimental design and the creation of new measurement tools and/or method to provide higher potential of detection. Analytical chemistry is of the most fundamental importance not only to all branches of chemistry but also to all the biological sciences, to engineering, and, more recently, medicine, public health, food, the environment and the supply of energy in all forms. Such a beautiful importance as mentioned, finding novelty or developing fundamental concept in analytical area for various applications are really important and challenging, especially to obtain the sensitive, simpler, smaller, faster, and cheaper tool or method. In addition, sensitive detection of chemicals and biomolecules is crucial for various fields of application, such as food inspection, environmental monitoring as well as medical diagnosis. Recently, there has been increasingly interest in development of sensitive system for the detection of food contaminants (e.g. sulfonamide, paraben, toxic heavy metal) and clinical biomarkers (e.g. cancer markers, proteins, DNA/RNA) because the abnormal level of these compounds

seriously affects the living system and human health. Early detection of contaminants and diseases is greatly desired since the early stage is commonly treated with the highest probability of success.

Various traditional methods have been used for the determination of food, environment contaminants and clinical biomarkers, such as colorimetric and fluorescence based methods. However, these methods are still limited for accurate quantitation of trace level analytes in complex samples, leading to false negative results. Even though, some of basic methods (*e.g.* ELISA) have been created to sensitively determine the disease markers, it still has some disadvantages including high operating cost, long development lead time and complicated labeling processes. These issues lead to an upsurge of interests in development of novel systems for sensitive detection of chemicals and biomolecules. The discovery and advances development in nanotechnology leading more easily available the novel chemical and physical properties of nanomaterials. A wide variety of nanoscale materials of different sizes, shapes and compositions are currently available. The important interest in nanomaterials is driven by their many desirable properties. In particular, the ability to reduce the size and structure and hence the properties of nanomaterials offers excellent prospects for designing novel sensing systems and enhancing the performance of analytical assay. Many kinds of nanomaterials, including metal, metal-oxide, semiconductor, composite-metal nanoparticles and even graphene, have been used for constructing electrochemical sensors.

Recently, paper-based microfluidic devices, representing the next generation of paper strip test devices. A paper-based microfluidic device combines many advantages of

paper strip tests with the utility of microfluidics. They have the potential to be good alternatives for point-of-care testing over traditional paper strip tests because they are capable of simultaneous multiplex analyte detection. In addition, they are portable, easy to use, require only a small volume of sample and provide rapid analysis.

Microfluidic systems have been utilized for analysis in a variety of applications, including chemical, biological, medical, environmental and pharmaceutical fields. Taking advantages from micron-scale systems, microfluidic devices offer a number of advantages, including small amount of samples and reagents required, fast analysis time, high analytical performances, portability and possibility for high-throughput analysis. Nowadays, microfluidics for medical analysis has attracted considerable attraction because of its high potential to be developed as point-of-care (POC) medical diagnostic systems. One of the most challenging tasks for developing microfluidic systems for POC analysis is that a system should be rapid, simple to use (less equipment and training), cost-effective, reliable and easily interpretable. Herein, a simple microfluidic system is developed for medical applications and further applied to be a microfluidic-based POC system and would be eventually attained to be a home-care device.

From research problem and its significances, in our team, we separate work into 3 groups. First, the development of new nanomaterial-based chemical sensors for electroanalysis will be proposed. Second, creation the novel analytical method as an alternative choice for detection of various compounds using lab-on-paper will be established. Final, a simple microfluidic system for chemical or biomedical analysis will be developed.

The finding and developing using analytical concepts will provide new assays or new prototype for innovative detection of various important analytes in food, environment, clinical and medical samples.

2. Objectives of this project

To achieve the research goals, the following objectives are set.

- 1) To develop new nanomaterial-based chemical sensors by modification surface with nanomaterial, nanocomposite, and polymer for analysis of chemical or biochemical components in food or environment or disease markers
- 2) To develop paper-based analytical tools coupled with colorimetric or chemical or electrochemical detection for food, environment and medical analysis
- 3) To develop a simple, cost-effective and reliable microfluidic method for medical applications and flow-based system for food or environmental applications
- 4) To apply the novel tools or novel methods for detection the target analytes in real samples

3. Scope of Research

To achieve the research objectives, the following scope was set.

- The nanomaterial-based chemical sensors such as gold nanoparticles and graphene were developed and used for studying the electrochemical properties of various chemical and biological compounds . Particular attention was given towards studying the electrochemical properties of these analytes using various techniques of electrochemistry. Comparison results were obtained by carbon-based electrodes. The effect of pH, concentration and scan rate were studied in detail. The developed sensor was employed

as a detector in the HPLC system for separation and detection of herbicides. Chromatographic and electrochemical condition for the separation and detection of herbicides were studied as well as the analytical figures. In addition, silver nanoparticles were used as colorimetric reagent for detection of heavy metals and pesticides.

- The paper-based analytical sensors were coupled with colorimetric, electrochemical and dual detection for quantitative analysis of target analytes. The effects of detection potential, linear dynamic range, accuracy, precision were also studied and compared to those obtained from the standard methods.

- The microfluidic system and sequential injection analysis with electrochemical detection were developed for the separation and detection of important chemical and biological compounds. The electrophoresis conditions or flow-based condition as well as the detection methods were investigated.

- The microfluidic system and sequential injection analysis with electrochemical detection were designed for rapid screening and identification of target analytes. Also, pH effect, separation voltage, sampling time, and sample loading were investigated.

- The developed methods were applied for the determination of target analytes in real samples. Analytical recoveries were determined as well as the precision.

There are five chapters in this report. Chapter I is the executive summary. Chapter II is the detail for development of nanomaterial-based chemical sensors. This chapter also covers the output obtained from this project. Chapter III gives details of the

development of paper-based analytical devices coupled with colorimetric and electrochemical detection. Chapter IV reports on the use of microfluidic and sequential injection systems for the automatic detection of heavy metals and biological compounds. Lastly, Chapter V is the conclusion and future perspectives.

Chapter II

The development of nanomaterial-based chemical sensors

In this chapter, the motivations and creations for new electrochemical sensors and/or optical sensors were introduced. In this chapter, various materials such as gold nanoparticles, silver nanoparticles, and graphene-based were applied as sensor to detect the target analytes in many applications. There are 13 publications obtained from the development under this objective. The list of publications are shown below.

1. K. Charoenkitamorn, O. Chailapakul, W. Siangproh, Development of gold nanoparticles modified screen-printed carbon electrode for the analysis of thiram, disulfiram and their derivative in food using ultra-high performance liquid chromatography, *Talanta*, 132 (2015) 416-423.
2. Y. Boonyasit, A. Heiskanen, O. Chailapakul, W. Laiwattanapaisal, Selective label-free electrochemical impedance measurement of glycated haemoglobin on 3-aminophenylboronic acid-modified eggshell membranes, *Analytical and Bioanalytical Chemistry*, 407 (2015) 5287-5297.
3. C. Bardpho, P. Rattanarat, W. Siangproh, O. Chailapakul, Ultra-high performance liquid chromatographic determination of antioxidants in teas using inkjet-printed graphene-polyaniline electrode, *Talanta*, 148 (2016) 673-679.
4. S. Kajornkavinkul, E. Punrat, W. Siangproh, N. Rodthongkum, N. Praphairaksit, O. Chailapakul, Graphene/polyvinylpyrrolidone/polyaniline nanocomposite-modified electrode for simultaneous determination of parabens by high performance liquid chromatography, *Talanta*, 148 (2016) 655-660.

5. S. Jampasa, W. Siangproh, K. Duangmal, O. Chailapakul, Electrochemically reduced graphene oxide-modified screen-printed carbon electrodes for a simple and highly sensitive electrochemical detection of synthetic colorants in beverages, *Talanta*, 160 (2016) 113-124.
6. R. Tirawattanakoson, P. Rattanarat, N. Ngamrojanavanich, N. Rodthongkum, O. Chailapakul, Free radical scavenger screening of total antioxidant capacity in herb and beverage using graphene/PEDOT: PSS-modified electrochemical sensor, *Journal of Electroanalytical Chemistry*, 767 (2016) 68-75.
7. S. Chaiyo, E. Mehmeti, K. Zagar, W. Siangproh, O. Chailapakul, K. Kalcher, Electrochemical sensors for the simultaneous determination of zinc, cadmium and lead using a Nafion/ionic liquid/graphene composite modified screen-printed carbon electrode, *Analytica Chimica Acta*, 918 (2016) 26-34.
8. N. Akkarachanchainon, P. Rattanawaleedirojn, O. Chailapakul, N. Rodthongkum, Hydrophilic graphene surface prepared by electrochemically reduced micellar graphene oxide as a platform for electrochemical sensor, *Talanta*, 165 (2017) 692-701.
9. A. Jirasirichotea, E. Punratb, A. Suea-Ngama, O. Chailapakula, S. Chuanuwatanakula, Voltammetric detection of carbofuran determination using screen-printed carbon electrodes modified with gold nanoparticles and graphene oxide, *Talanta*, 175 (2017) 331-337. (IF 2015 =4.035)
10. J. Yukird, T. Wongtangprasert, R. Rangkupan, O. Chailapakul, T. Pisitkun, N. Rodthongkum, Label-free immunosensor based on graphene/polyaniline nanocomposite for neutrophil gelatinase-associated lipocalin detection, *Biosensors and Bioelectronics*, 87 (2017) 249-255. (IF 2015 =7.476)

11. N. Ratnarathorn, O. Chailapakul, W. Dungchai, Highly sensitive colorimetric detection of lead using maleic acid functionalized gold nanoparticles, *Talanta*, 132 (2015) 613-618.
12. W. Siangproh, O. Chailapakul, K. Songsrirote, Simple and fast colorimetric detection of inorganic arsenic selectively adsorbed onto ferrihydrite-coated silica gel using silver nanoplates, *Talanta*, 153 (2016) 197-202.
13. W. Siangproh, T. Somboonsuk, O. Chailapakul, K. Songsrirote, Novel colorimetric assay for paraquat detection on-silica bead using negatively charged silver nanoparticles, *Talanta*, 174 (2017) 448-453.

In addition, we have 1 publication reviewed on the application of nanoparticles used as the probes for biological applications as shown below.

14. A. Yakoh, C. Pinyorosphatum, W. Siangproh, O. Chailapakul, Biomedical Probes Based on Inorganic Nanoparticles for Electrochemical and Optical Spectroscopy Applications, *Sensors*, 15 (2015) 21427-21477.

The detail of each work is presented in the following part.



Development of gold nanoparticles modified screen-printed carbon electrode for the analysis of thiram, disulfiram and their derivative in food using ultra-high performance liquid chromatography



Kanokwan Charoenkitamorn^a, Orawon Chailapakul^{a,c,*}, Weena Siangproh^{b,**}

^a *Electrochemistry and Optical Spectroscopy Research Unit, Department of Chemistry, Faculty of Science, Chulalongkorn University, 254 Phayathai Road, Patumwan, Bangkok 10330, Thailand*

^b *Department of Chemistry, Faculty of Science, Srinakharinwirot University, Sukhumvit 23, Wattana, Bangkok 10110, Thailand*

^c *National Center of Excellent of Petroleum, Petrochemicals and Advanced Materials, Chulalongkorn University, Patumwan, Bangkok 10330, Thailand*

ARTICLE INFO

Article history:

Received 16 July 2014

Received in revised form

10 September 2014

Accepted 11 September 2014

Available online 30 September 2014

Keywords:

Dithiocarbamates

Fungicides

Screen-printed carbon electrode

Gold nanoparticles

Simultaneous determination

Ultra-high performance liquid chromatography

ABSTRACT

For the first time, gold nanoparticles (AuNPs) modified screen-printed carbon electrode (SPCE) was developed as working electrode in ultra-high performance liquid chromatography (UHPLC) coupled with electrochemical detection (UHPLC-ED) for simultaneous determination of thiram, disulfiram, and *N,N*-diethyl-*N,N'*-dimethylthiuram disulfide, their derivative compound. The separation was performed in reversed-phase mode using C18 column, mobile phase consisting of 55:45 (v/v) ratio of 0.05 M phosphate buffer solution (pH 5) and acetonitrile at a flow rate of 1.5 mL min⁻¹. For the detection part, the amperometric detection was chosen with a detection potential of 1.2 V vs. Ag/AgCl. Under the optimal conditions, the good linear relationship was obtained in the range of 0.07–15, 0.07–12, and 0.5–15 μg mL⁻¹ (correlation coefficient more than 0.9900) for thiram, *N,N*-diethyl-*N,N'*-dimethylthiuram disulfide, and disulfiram, respectively. The limits of detection (LODs) of thiram, *N,N*-diethyl-*N,N'*-dimethylthiuram disulfide, and disulfiram were 0.022, 0.023, and 0.165 μg mL⁻¹, respectively. Moreover, this method was successfully applied for the detection of these compounds in real samples (apple, grape and lettuce) with the recoveries ranging from 94.3% to 108.8%. To validate this developed method, a highly quantitative agreement was clearly observed compared to standard UHPLC–UV system. Therefore, the proposed electrode can be effectively used as an alternative electrode in UHPLC-ED for rapid, selective, highly sensitive, and simultaneous determination of thiram, disulfiram, and *N,N*-diethyl-*N,N'*-dimethylthiuram disulfide.

© 2014 Elsevier B.V. All rights reserved.

1. Introduction

Nowadays, the designing of electrochemical sensor has been developed in the field of electrochemistry to improve the analytical efficiency in the terms of sensitivity, selectivity, reliability, ease of fabrication and use, and low cost. Screen printing is the technology used for fabrication of biosensors and chemical sensors instead of using large-scale electrode. Their various advantages such as miniaturization, versatility, and low cost of production are really attractive [1]. In addition, many laboratories use the screen-printing for in-house production of sensors. Screen-printed carbon electrode (SPCE) is an alternative material used instead of using the traditional electrodes based on economic substrate. Recently, SPCE have been successfully used as the electrochemical sensor for various researches due to the

simplicity to produce and still give the rapid responses [2]. Moreover, the main advantage of SPCE is able to use only once and then is discarded. This advantage can be used to solve the problems of surface fouling compared with those of conventional electrodes. However, the limitation of SPCE is small surface area of working electrode leading to the lack of sensitivity [3]. Therefore, electrode modification is necessary to solve this problem.

For electrode modification, metal-nanoparticles modified SPCE is focused to improve the electrochemical efficiency. Metal-nanoparticles are attractive catalyst in the electrochemical applications. Transition metals, especially precious metals, show very high catalytic abilities for catalyzing the redox process of some interested molecules, making the use of electroanalytical techniques for applications are extended [4]. Particularly, gold nanoparticles (AuNPs) have received significant attention in recent years. AuNPs are widely used in many fields due to their unique optical and physical properties, such as surface plasmon oscillations for labeling, imaging, and sensing [5]. For the electrochemical fields, AuNPs have been widely used for modification of electrode because of their benefits including catalysis, mass

* Corresponding author. Tel.: +662 218 7615.

** Corresponding author. Tel.: +662 249 5000x18208.

E-mail addresses: corawon@chula.ac.th (O. Chailapakul), weenasi@hotmail.com (W. Siangproh).

transport, and high effective surface area [1]. AuNPs have the ability to improve the detection signal, electron transfer, which make the limit of detection in electrochemical sensor is reduced. Moreover, the most importance is AuNPs showed strong specific interaction with the sulfur-containing compounds [6]. Therefore, AuNPs became an interesting nanomaterial used as modifier onto working electrode for electrochemical detection of sulfur-containing compounds.

Thiram (tetramethyl thiuram) and disulfiram (tetraethyl thiuram) are organosulfur compounds in the group of dithiocarbamates (DTCs) fungicides. DTCs have been used in agriculture as fungicides in foliage vegetable and fruit [7]. Besides these agricultural applications, DTCs are also used in industry such as vulcanization accelerator and antioxidant in rubber. The use of DTCs results in their release into the environment causing the contamination in food and water which leads to hazardous effect in the living organisms through diverse pathways [8]. Environmental problem resulting from uncontrollable use of fungicides in agriculture is one of the most important evidence. Therefore, it is necessary to continuously develop simple, selective, and sensitive methods for analysis of fungicides [9].

Various methods have been developed for analysis of DTCs. Spectrometry [10–12] and head space gas chromatography [13] have been used as the methods for the determination of DTCs after their decomposition to carbon disulfide (CS_2). From these methods, most of DTCs can degrade to CS_2 . Therefore, they are unable to distinguish among different DTCs. Moreover, gas chromatography [14,15], capillary electrophoresis [16–20], and high performance liquid chromatography (HPLC) were used for simultaneous determination of DTCs coupled with UV detection. Especially, HPLC is the simple technique used for easy separation of the disulfide substance. However, the drawback of the UV detection is low sensitivity. Therefore, HPLC coupled with electrochemical detection became an important choice for the determination of disulfides [21]. The main advantage of electrochemical detection compared to those of spectrometry is that the derivatization step is not needed, which makes the analysis time and cost reduced. In addition, the use of electrochemical detection after the separation by HPLC can provide more sensitive detection than UV [22].

Recently, ultra-high performance liquid chromatography coupled with electrochemical detection (UHPLC-ED) is a high potential alternative method for various analysis. UHPLC concerns to the development of short column packed with small particles for working at high pressures (> 400 bar). The use of UHPLC can enhance chromatographic performances in terms of efficiency, resolution, and analysis time [23]. In the detection part, AuNPs modified electrode was used as amperometric detection. Amperometry is an attractive potential technique because of its fast response, high sensitivity, relatively low cost of equipment, no need for complicated operation, and simplicity for direct sulfur assay [24].

With such benefits from the mentioned background, the objective of this work is to develop AuNPs modified SPCE in UHPLC-ED system for simultaneous determination of DTCs with high sensitivity, specificity, and rapid analysis. Thiram (tetramethyl thiuram) and disulfiram (tetraethyl thiuram) are chosen as representative compounds of DTCs because they are importantly applied to control a variety of pest [25]. Typically, when thiram and disulfiram are mixed together, the intermediate of *N,N*-diethyl-*N',N'*-dimethylthiuram disulfide (DEDMTDS) appears as the derivative of thiram and disulfiram. This compound is one of DTCs that affects human health and has the same effect of thiram and disulfiram. The presence of *N,N*-diethyl-*N',N'*-dimethylthiuram disulfide can also use to monitor thiram and disulfiram in samples. Therefore, the detection of *N,N*-diethyl-*N',N'*-dimethylthiuram disulfide is important. This derivative compound is also determined along with the measurement of thiram and disulfiram.

To the best of our knowledge, there is no publication report about the use of AuNPs modified SPCE as working electrode for ED

after the UHPLC separation to simultaneously determine thiram, DEDMTDS, and disulfiram. Moreover, this developed UHPLC-ED using AuNPs modified SPCE was applied for the first time to analyze thiram, DEDMTDS, and disulfiram in fruits and vegetables collected from local markets.

2. Materials and methods

2.1. Chemicals and reagents

All chemicals used in this work were of analytical grade, and all solutions were prepared using Milli-Q water from Millipore ($R \geq 18.2 \text{ M } \Omega \text{ cm}^{-1}$). Acetonitrile (HPLC-grade), chloroform, and sulfuric acid were obtained from Merck (Darmstadt, Germany). Potassium dihydrogen phosphate (KH_2PO_4) was acquired from BDH laboratory supplies (VWR International Ltd., England). Disodium hydrogen phosphate (Na_2HPO_4) and sodium hydroxide (NaOH) were purchased from Merck (Darmstadt, Germany). Standard thiram (tetramethyl thiuram) was obtained from Chem Service (West Chester, PA, USA). Standard disulfiram (tetraethyl thiuram) and gold (III) chloride solution were obtained from Sigma-Aldrich (St. Louis, MO, USA).

All of stock standard solutions ($1000 \mu\text{g mL}^{-1}$) were prepared by dissolving 10 mg of each analyte in acetonitrile. The solutions were then placed in an amber bottle and stored at 4°C . To prepare working standard solution, the standard solution was mixed and diluted in suitable proportions of acetonitrile:Milli-Q water (50:50; v/v), and kept for 5 min before measurement. All solutions and solvents were filtered by $0.22 \mu\text{m}$ nylon membranes prior to use in UHPLC separation.

2.2. Fabrication and modification of screen-printed carbon electrode

The working electrode was fabricated using screen printing and modified by electrodeposition techniques. The Ag/AgCl electrode and Pt wire was used as reference and auxiliary electrodes, respectively. To fabricate the in-house screen-printed carbon electrode (Fig. S1), the Ag/AgCl ink was first printed on the PVC substrate for using as a conductive pad. Then, the carbon ink was printed to create a working electrode. The each step of printing electrode was allowed to dry in an oven at 55°C for 1 h. The screen-printed carbon electrode was ready to modify in the next step.

For the electrodes modification, the 10 mM of gold (III) solution was used to modify onto electrode surface by electrodeposition technique. The three-electrode system was placed into cell containing 2 mL of solution of 10 mM of gold (III) solution in 0.5 M H_2SO_4 followed by deposition of gold onto the SPCE at a deposition potential of -0.6 V (vs. Ag/AgCl) for 50 s while the solution was stirred (by means of a mechanical stirrer bar). The gold nanoparticles (AuNPs) were obtained onto the electrode surface. After the modification, the AuNPs modified SPCE was carefully rinsed with distilled water and dried under N_2 gas prior to use.

2.3. Cyclic voltammetry

The electrochemical reaction and optimal parameters for electrodeposition step were studied by cyclic voltammetry (CV) using a CH instrument potentiostat 1232 A (CH Instrument, Inc., USA). The working electrodes used in this work were bare SPCE and AuNPs modified SPCE. The reference and auxiliary electrode were silver/silver chloride electrode and Pt wire, respectively. All experiments were done at room temperature.

2.4. UHPLC experiment and apparatus

The UHPLC system was performed in reversed-phase mode using an LC-20ADXR solvent deliver unit (Shimadzu Corporation,

Japan), an autosampler (SIL-20 A) with 0.1–100 mL loop and a Kinetex™ core-shell C18 column (50 mm x 4.6 mm i.d.; particle size, 2.6 μm , Phenomenex). The UHPLC-electrochemical measurement was carried out in 45:55 (v/v) ratio acetonitrile: 0.05 M phosphate buffer solution (pH 5), which was adjusted to pH 5 with 0.1 M sodium hydroxide solution, as mobile phase with an applied potential of 1.2 V vs. Ag/AgCl, an injection volume of 50 μL , and a flow rate of 1.5 mL min^{-1} . All chromatographic separations were performed at room temperature.

2.5. Electrochemical measurement

The thin-layer flow cell consisted of a working AuNPs modified SPCE, a reference Ag/AgCl electrode (Bioanalytical system Inc., USA), and a stainless steel tube counter electrode. The geometric area of the AuNPs modified SPCE in the flow cell was estimated to be 0.40 cm^2 with 1 mm thick silicon rubber gasket as a spacer. An electrochemical measurement for amperometric control and signal processing was performed using CH instrument potentiostat 1232 A.

2.6. Sample preparation

The three real samples including apple, grape and lettuce were obtained from local markets in Thailand. For analysis, 50 g of cut sample was weighted accurately and transferred to a blender. Then 50 μL of 500 $\mu\text{g mL}^{-1}$ of standard mixture solution and chloroform were added. The mixture was homogenized with blender and transferred into centrifuge tubes. After centrifugation at 4000 rpm for 10 min, all of the organic phases were filtered through a Buchner funnel with Whatman filter paper No. 4 and transferred to 250 mL vessel of the rotary vacuum evaporator for evaporation to dryness at room temperature. The residues were dissolved in 4.5 mL of acetonitrile using ultrasonic stirring, filtered through the 0.2 μm pore size of nylon membrane, and collected in 5 mL of volumetric flask. After that, acetonitrile filtered through the 0.2 μm pore size of nylon membrane was added to adjust volume to 5 mL of solution. Finally, 50 μL of the solution was injected into the UHPLC system. The determination of DTCs in samples was analyzed within the linear dynamic range that obtained by adding different volume of 500 $\mu\text{g mL}^{-1}$ of standard mixture solution into the blank sample and prepared following the above treatment.

2.7. Method validation

Standard solutions and samples were analyzed, and the currents were integrated. A calibration curve of standard solutions was performed under optimal conditions and treated with linear least square regression analysis using the Excel software package. The limit of detection (LOD) and limit of quantification (LOQ) were determined from the $3 S_{\text{bl}}/S$ and $10 S_{\text{bl}}/S$, respectively, where S_{bl} is standard deviation of blank ($n=10$), and S is sensitivity of method, obtained from the slope of the linearity. For the precision of intra-day and inter-day, three concentrations of DTCs (1, 6, and 12 $\mu\text{g mL}^{-1}$) were observed for three times within a day and three different days. To validate the developed method, UHPLC-ED was compared to the standard method of UHPLC coupled with ultraviolet detection (UHPLC-UV) using the paired t -test.

3. Results and discussion

3.1. Surface morphology of AuNPs modified SPCE

Gold (III) solution was used to generate the AuNPs on the electrode surface by electrodeposition. The surface morphology of bare SPCE and AuNPs modified SPCE was investigated using

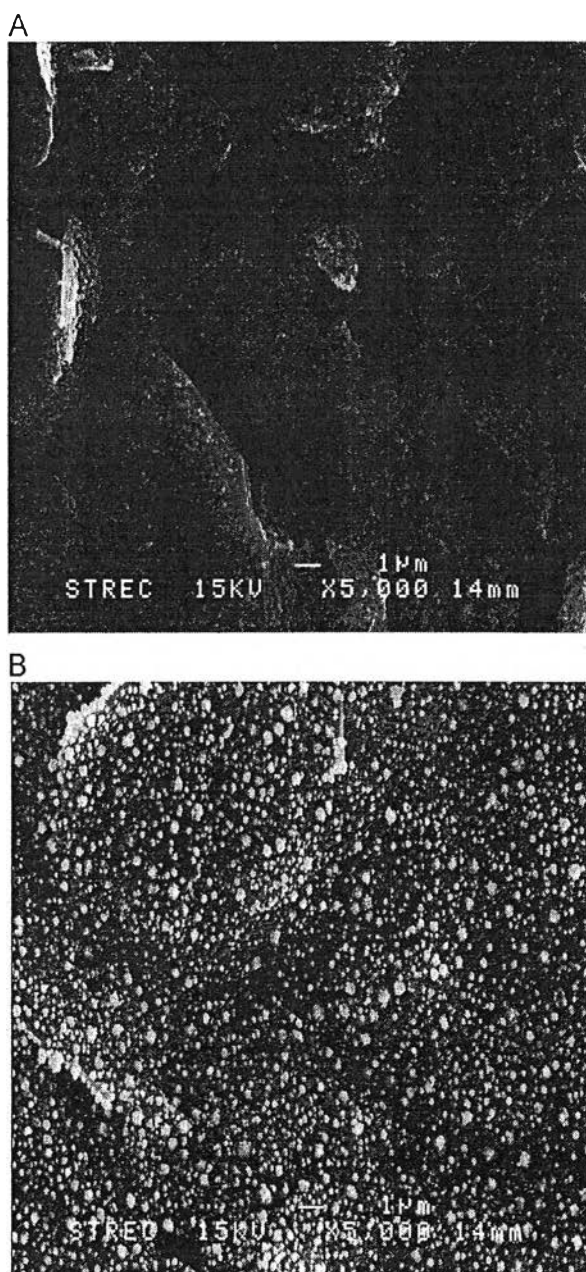


Fig. 1. SEM images of (A) bare SPCE and (B) AuNPs modified SPCE prepared by electrodeposition of 10 mM gold (III) solution at applied potential of -0.6 V for 50 s.

scanning electron microscope (SEM) as shown in Fig. 1A and B, respectively. After the modification, the well dispersed gold particles in nanoscale was observed (Fig. 1B). The distribution of AuNPs on the electrode surface led to increase the surface area and improve the electrochemical sensitivity of the modified electrode.

3.2. Optimization of the electrode modification

For the electrode modification using electrodeposition technique, the deposition potential and deposition time were optimized because these factors can effect to the analytical results. First, thiram was selected as the representative compounds because it is the best electrochemically active species at bare carbon electrode. Therefore, it is easy to observe the signal obtained from modified and unmodified electrode. To obtain the optimal condition of AuNPs modified SPCE, the dependence of deposition potential and

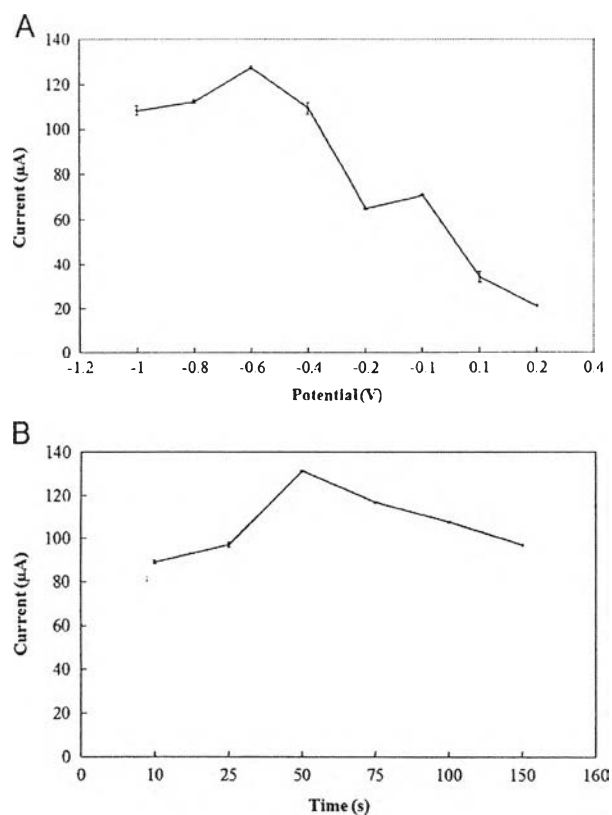


Fig. 2. Effect of the (A) deposition potential and (B) deposition time of thiram at AuNPs modified SPCE. Data are shown as the mean \pm SD derived from three replicates.

deposition time were studied using cyclic voltammetry, and the relationship between the studied parameter and current response of thiram was plotted. The deposition potential was studied in the range of -1.0 to 0.2 V. The current signal of thiram was initially increased as the function of deposition potential from -1.0 to -0.6 V and then decreased (Fig. 2A). For the deposition time, the current signal of thiram increased from 10 s to 50 s and then decreased (Fig. 2B). Therefore, the deposition potential of -0.6 V and the deposition time of 50 s were chosen as optimal parameters for modification of AuNPs onto the electrode surface.

3.3. Electrochemical response of thiram at AuNPs modified SPCE

As mentioned above, thiram is the best electrochemically active species. Thus, it was used as the representative of DTCs to study the electrochemical response. The cyclic voltammogram (CV) of $10 \mu\text{g mL}^{-1}$ of thiram obtained from bare SPCE and AuNPs modified SPCE at the potential range of 0.0 to 1.4 V was shown in Fig. 3. From CV results, the anodic current of thiram was investigated, and the current at AuNPs modified SPCE was significantly higher than the current obtained from bare SPCE due to the distribution of AuNPs on the electrode surface. We believe that the AuNPs on the electrode surface can enhance electron transfer and also improve the electrochemical determination of DTCs. For the comparison of oxidation current density between AuNPs modified SPCE and bare SPCE (Fig. 3B), the higher current density about nine times was observed at AuNPs modified SPCE. This result indicated that the AuNPs modified SPCE can be assuring electrode for the detection of thiram, disulfiram, and DEDMTDS. Therefore, this modified electrode can be an alternative electrode

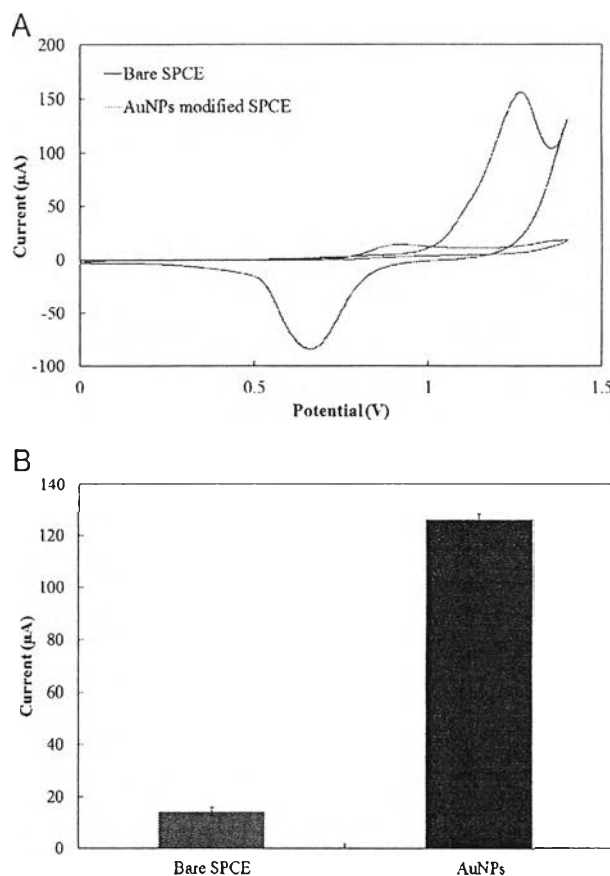


Fig. 3. (A) Cyclic voltammogram of thiram at the AuNPs modified SPCE (red line) compared to bare SPCE (blue line) and (B) comparison of oxidation current density between AuNPs modified SPCE (red rod) and bare SPCE (blue rod) vs. Ag/AgCl at the concentration of $10 \mu\text{g mL}^{-1}$ in 55:45 of 0.05 M phosphate solution pH 5: acetonitrile, scan rate 100 mV s^{-1} .

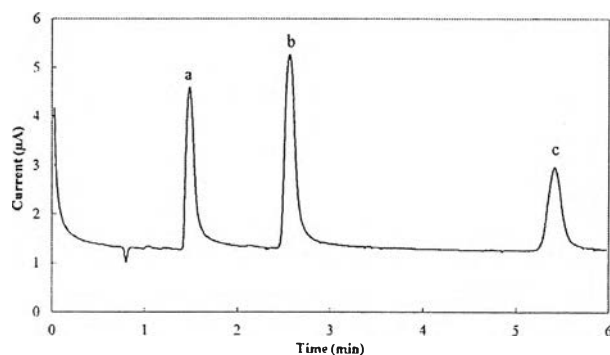


Fig. 4. Representative UHPLC-ED chromatogram of $12 \mu\text{g mL}^{-1}$ of thiram (a), DEDMTDS (b), and disulfiram (c) in a mobile phase (0.05 M phosphate solution (pH 5): acetonitrile), the detection potential of 1.2 V vs. Ag/AgCl using AuNPs modified SPCE, the injection volume of $50 \mu\text{L}$, and the flow rate of 1.5 mL min^{-1} . Chromatograms are representative of at least three independent repetitions.

for using as working electrode with the advantages of low-cost material, simple fabrication and high sensitivity in case of detection DTCs.

3.4. UHPLC separation

In this work, C18 column was used to separate thiram, DEDMTDS, and disulfiram by isocratic elution. The effect of percentage of acetonitrile used in the mobile phase on the

retention characteristics was first evaluated. When the percentage of acetonitrile ≤ 40 was used, the separation time was higher than 20 min and peak broadening of disulfiram was observed. On the other hand, at higher content of acetonitrile in mobile phase, the current signal of thiram, DEDMTDS, and disulfiram were decreased due to the low of diffusion coefficient with changing ionic strength of the medium. Therefore, the acetonitrile of 45% was selected as

compromise to achieve the completely separated them within 6 min with good sensitivity. In addition, 0.05 M phosphate buffer solution (pH 5) was chosen as the electrolyte solution because the high concentration of salt in buffer solution was not suitable for the UHPLC system. The chromatogram for the separation of standard mixture solution was shown in Fig. 4. The retention time of thiram, DEDMTDS, and disulfiram was 1.5, 2.6, and 5.4 min, respectively, and the retention time stability was found in the range of 0.1% to 1.5%. The peak widths were 11.6 s for thiram, 14.2 s for DEDMTDS, and 18.8 s for disulfiram. Therefore, this proposed system offers the rapid time for separating DTCs.

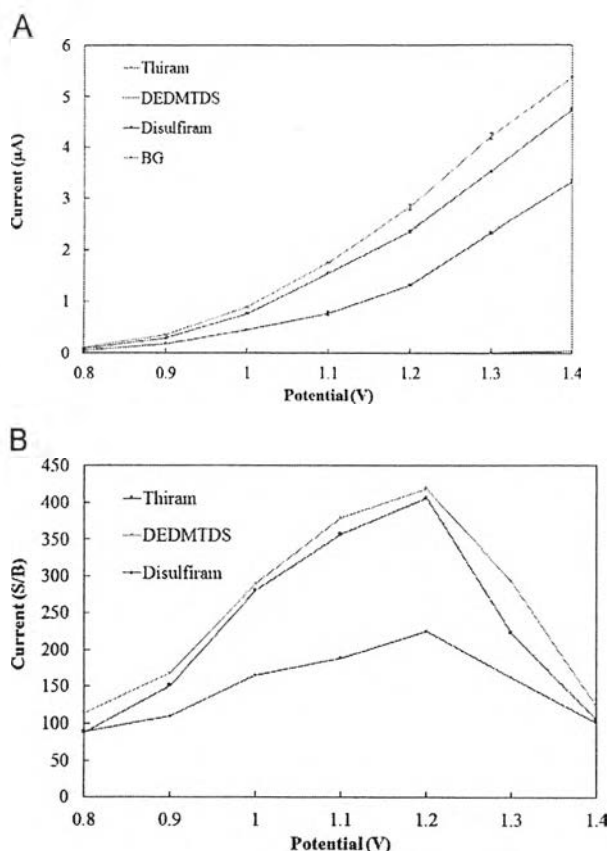


Fig. 5. Hydrodynamic voltammetric results at the AuNPs modified SPCE for a $10 \mu\text{g mL}^{-1}$ each mixture ($50 \mu\text{L}$ total) of thiram and disulfiram. (A) thiram (blue line), DEDMTDS (green line), disulfiram (red line), and background (purple line); (B) hydrodynamic voltammogram of signal-to-background ratios. The other conditions are the same as in Fig. 4. Data are shown as the mean ± 1 SD derived from three independent repetitions.

3.5. Hydrodynamic voltammetry

Hydrodynamic voltammetry was used to optimize the detection potential. The potential was studied in the range of 0.8 to 1.4 V. The peak current after each injection at different potential was recorded corresponding to the background current. These data were plotted as a function of applied potential to obtain the hydrodynamic curves as shown in Fig. 5. The detection potentials significantly affected the oxidation current of the thiram, DEDMTDS, and disulfiram as well as the background current (Fig. 5A). Therefore, the net current after background subtraction was studied, and signal-to-background (S/B) ratios were plotted corresponding to the detection potential. It was found that the current increased when the potential increased up to 1.2 V for all compounds (Fig. 5B). Therefore, the detection potential of 1.2 V was selected as optimal detection potential for amperometric detection of thiram, DEDMTDS, and disulfiram after their separation with UHPLC.

3.6. Method validation

3.6.1. Analytical performance

The analytical performance of this proposed system was studied. The calibration curve between the concentration and current response of analytes was plotted as shown in Fig. 6. Under the optimal conditions, the linearity was observed in the range of 0.07 to $15 \mu\text{g mL}^{-1}$ for thiram, 0.07 to $12 \mu\text{g mL}^{-1}$ for DEDMTDS, and 0.5 to $15 \mu\text{g mL}^{-1}$ for disulfiram. The limit of detection (LOD) and limit of quantification (LOQ) were calculated from $3 S_{bl}/S$ and $10 S_{bl}/S$, where S_{bl} is the standard deviation of blank measurements ($n=10$), and S is the sensitivity of the method or the slope of linearity. Good linearity value with $r^2 > 0.99$ was obtained. LODs and LOQs were summarized in Table 1. In addition, when the performance of AuNPs

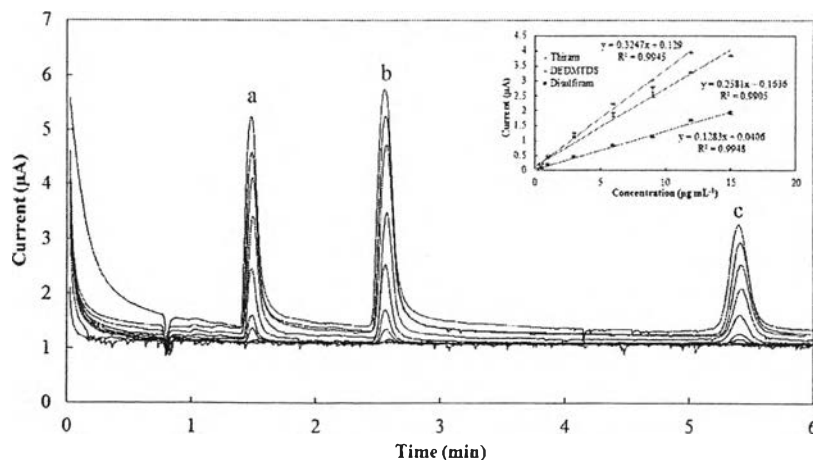


Fig. 6. The amperometric voltammogram for different concentrations of thiram (a), DEDMTDS (b), and disulfiram (c) (0.07 to $15 \mu\text{g mL}^{-1}$) using AuNPs modified SPCE and the corresponding calibration plots (inset). Measurements were performed under the optimal conditions.

Table 1
Linearity, limit of detection (LOD) and limit of quantitation (LOQ) of the UHPLC-ED method (n=3).

Analyte	Linear range ($\mu\text{g mL}^{-1}$)	Slope (peak height) ($\mu\text{A}/\mu\text{g mL}^{-1}$)	Intercept (μA)	r^2	LOD ($\mu\text{g mL}^{-1}$)	LOQ ($\mu\text{g mL}^{-1}$)
Thiram	0.07–15	0.2585	0.1636	0.9905	0.022	0.074
DEDMTDS	0.07–12	0.3247	0.129	0.9945	0.023	0.076
Disulfiram	0.5–15	0.1283	0.0406	0.9948	0.165	0.551

Table 2
Recent report using different types of electrodes for electrochemical determination of DTCs.

Modified electrode	Detection method	Linearity range ($\mu\text{g mL}^{-1}$)	LOD ($\mu\text{g mL}^{-1}$)	Analyte	Real sample	Reference
Cylindrical carbon fiber microelectrode	Square-wave voltammetry	0.24–144	0.10	Thiram	Grape	[7]
Graphite-poly (tetrafluoroethylene)	Amperometry	2–100	0.14–1.0	Thiram and disulfiram	Apple	[26]
Hanging mercury drop electrode	Differential pulse voltammetry	0.01–0.6	0.01	Ziram	rice	[27]
Hanging mercury drop electrode	Square-wave voltammetry	0.01–0.19	0.0072	Ziram	Potato, cabbage and tomato	[28]
AuNPs modified SPCE	Amperometry	0.07–15	0.022–0.165	Thiram, DEDMTDS and disulfiram	Grape, apple and lettuce	This work

Table 3
The intra- and inter-precisions and recoveries of the UHPLC-ED method (n=3).

Samples	Spiked level ($\mu\text{g mL}^{-1}$)	Analyte	Intra-day		Inter-day	
			Recovery (%)	RSD (%)	Recovery (%)	RSD (%)
Apple	1	Thiram	97.1	1.1	99.0	3.7
		DEDMTDS	101.5	0.2	100.6	1.0
		Disulfiram	104.1	3.3	100.6	4.9
	3	Thiram	102.7	0.1	100.7	5.7
		DEDMTDS	102.7	0.3	102.0	1.4
		Disulfiram	108.5	0.3	103.3	4.4
	6	Thiram	109.0	0.9	104.0	4.4
		DEDMTDS	109.2	1.3	104.8	4.0
		Disulfiram	97.4	0.6	98.1	2.4
	9	Thiram	109.3	0.6	107.0	1.8
		DEDMTDS	109.2	0.3	107.7	1.7
		Disulfiram	103.6	0.6	104.2	4.9
12	Thiram	101.5	0.2	101.9	0.7	
	DEDMTDS	106.5	0.4	102.5	3.4	
	Disulfiram	102.6	0.2	101.4	2.5	
Grape	1	Thiram	100.1	0.2	102.3	3.3
		DEDMTDS	101.5	2.3	99.7	1.9
		Disulfiram	108.8	0.7	104.2	7.7
	3	Thiram	103.9	0.6	100.7	2.8
		DEDMTDS	105.2	0.2	102.2	2.5
		Disulfiram	107.9	0.3	104.7	2.7
	6	Thiram	103.5	1.0	103.3	2.9
		DEDMTDS	98.9	1.5	102.6	4.9
		Disulfiram	98.4	0.2	100.6	3.4
	9	Thiram	107.4	0.5	107.2	0.1
		DEDMTDS	100.4	1.0	102.6	4.7
		Disulfiram	97.5	0.4	98.0	2.6
12	Thiram	106.1	0.4	103.3	2.4	
	DEDMTDS	102.1	0.7	101.9	0.8	
	Disulfiram	100.5	0.3	100.9	5.0	
Lettuce	1	Thiram	98.8	0.8	101.9	3.4
		DEDMTDS	102.6	1.4	101.6	1.4
		Disulfiram	102.4	1.7	100.8	4.3
	3	Thiram	105.1	0.9	99.7	4.8
		DEDMTDS	102.4	1.0	103.4	3.6
		Disulfiram	104.1	1.9	99.0	4.9
	6	Thiram	98.9	0.2	96.7	4.4
		DEDMTDS	98.7	0.5	101.7	4.7
		Disulfiram	106.0	0.5	101.3	4.1
	9	Thiram	108.0	1.8	105.8	2.5
		DEDMTDS	100.5	3.7	101.8	3.8
		Disulfiram	103.1	0.8	102.6	4.2
12	Thiram	102.6	1.3	101.6	2.5	
	DEDMTDS	100.5	2.9	101.1	0.8	
	Disulfiram	100.1	0.6	102.5	2.3	

Table 4
Determination of DTCs level in different samples ($n=3$) by traditional UHPLC-UV method and the developed UHPLC-ED method reported here.

Samples	Spiked level ($\mu\text{g mL}^{-1}$)	Analyte	Amount found ($\mu\text{g mL}^{-1}$) ($\bar{x} \pm \text{SD}$)		% recovery		
			UHPLC-ED	UHPLC-UV	UHPLC-ED	UHPLC-UV	
Apple	1	Thiram	0.99 \pm 0.04	1.02 \pm 0.03	99.0	102.2	
		DEDMTDS	1.01 \pm 0.01	1.01 \pm 0.02	100.6	101.1	
		Disulfiram	0.98 \pm 0.05	1.01 \pm 0.05	97.5	100.6	
	6	Thiram	6.24 \pm 0.27	5.79 \pm 0.26	104.0	96.5	
		DEDMTDS	6.15 \pm 0.10	6.12 \pm 0.19	102.5	101.9	
		Disulfiram	5.89 \pm 0.14	5.72 \pm 0.13	98.1	95.4	
	12	Thiram	12.23 \pm 0.50	11.90 \pm 0.36	101.9	99.2	
		DEDMTDS	12.30 \pm 0.49	11.78 \pm 0.62	102.5	98.1	
		Disulfiram	12.42 \pm 0.25	12.26 \pm 0.23	103.5	102.1	
	Grape	1	Thiram	1.02 \pm 0.03	1.02 \pm 0.02	102.3	102.2
			DEDMTDS	1.01 \pm 0.02	1.00 \pm 0.01	100.8	99.7
			Disulfiram	1.04 \pm 0.08	0.99 \pm 0.01	104.2	98.7
6		Thiram	6.20 \pm 0.18	5.92 \pm 0.19	103.3	98.7	
		DEDMTDS	6.15 \pm 0.30	6.01 \pm 0.22	102.6	100.1	
		Disulfiram	6.04 \pm 0.21	6.04 \pm 0.12	100.6	100.7	
12		Thiram	12.17 \pm 0.34	12.09 \pm 0.41	101.4	100.8	
		DEDMTDS	12.23 \pm 0.60	12.00 \pm 0.60	101.9	100.0	
		Disulfiram	12.40 \pm 0.41	12.30 \pm 0.20	103.3	102.5	
Lettuce		1	Thiram	1.02 \pm 0.03	0.98 \pm 0.03	101.9	98.1
			DEDMTDS	1.02 \pm 0.01	1.02 \pm 0.04	102.2	101.6
			Disulfiram	1.01 \pm 0.04	0.97 \pm 0.09	100.8	97.1
	6	Thiram	5.80 \pm 0.26	5.75 \pm 0.25	96.7	95.8	
		DEDMTDS	6.10 \pm 0.28	5.99 \pm 0.22	101.7	99.8	
		Disulfiram	6.08 \pm 0.25	5.99 \pm 0.13	101.3	99.8	
	12	Thiram	12.20 \pm 0.41	11.98 \pm 0.27	101.6	99.9	
		DEDMTDS	12.13 \pm 0.47	11.94 \pm 0.62	101.1	99.5	
		Disulfiram	12.30 \pm 0.20	12.11 \pm 0.35	102.5	100.9	
	Paired two-tail test	t values (at 1 $\mu\text{g mL}^{-1}$)	Thiram	0.104			
			DEDMTDS	0.898			
			Disulfiram	0.792			
t values (at 6 $\mu\text{g mL}^{-1}$)		Thiram	2.293				
		DEDMTDS	3.029				
		Disulfiram	1.747				
t values (at 12 $\mu\text{g mL}^{-1}$)		Thiram	2.808				
		DEDMTDS	2.989				
		Disulfiram	-0.243				
t critical			4.303				

modified SPCE was compared to the other previous electrodes for the detection of DTCs as shown in Table 2. It was found that the LODs obtained from the proposed electrode were lower than using cylindrical carbon fiber [7] and graphite-poly (tetrafluoroethylene) composite electrode [26]. However, few researches used the mercury electrode to provide lower LOD than this method but the mercury is toxic [27,28]. Therefore, the proposed electrode offers less toxicity, uncomplicated, and low cost. Additionally, the proposed electrode shows good electrocatalytic properties for DTCs detection to obtain a high electrochemical sensitivity.

3.6.2. Application to real samples

To assess the applicability of the proposed method, target compounds in samples from local supermarkets were investigated. The proposed method was applied for the detection of three different samples, including apple, grape, and lettuce. The standard addition method was chosen to investigate the reliability of this proposed system. The precision of the analytical process was evaluated by the repeatability of the process. The spiked concentrations in the dynamic linearity between 1 to 15 $\mu\text{g mL}^{-1}$ were studied to calculate the RSD percentage. The summary of intra- and inter-day precision, and recovery that obtained from the proposed method was shown in Table 3. The RSDs and recoveries of intra-day were found in the range of 0.1–3.7% and 94.3–108.8%, respectively, while the inter-day RSDs and recoveries were found in the range of 0.1–5.7% and 95.8–107.7%, respectively. Therefore,

this method is an alternative and suitable for rapid separation and simultaneous determination of DTCs.

To validate the proposed method, UHPLC-UV was used as a standard method to compare the acceptable and reliable. The results obtained from UHPLC-ED and UHPLC-UV were compared by a paired t -test at the 95% confidence for three samples that spiked with three standard concentrations (1, 6, and 12 $\mu\text{g mL}^{-1}$ to represent the low, medium, and high level, respectively). The critical t -value was significantly higher than calculated t -values between two assays. From the results shown in Table 4, the calculated t -values of three concentrations were found in the range of -0.243 to 3.029 and lower than critical t -values (4.303). It can be concluded that there is no significant difference between UHPLC-ED and conventional UHPLC-UV method. Therefore, the results obtained from UHPLC coupled with amperometric detection using AuNPs modified SPCE is acceptable and reliable for applying to simultaneous determination of DTCs in food.

4. Conclusions

AuNPs modified SPCE was firstly developed for the determination of thiram, disulfiram, and DEDMTDS after their separation with UHPLC system. Under the optimal conditions, the separation was complete within 6 min, and the high current response signal was obtained at AuNPs modified SPCE. The main advantages for the use of AuNPs modified SPCE are in term of high sensitivity, low-cost and simple fabrication-based material. Reproducible signal from %RSD for intra- and inter-day were below 5%. These

results indicated that the high reproducibility was obtained using this system for long time. Moreover, the proposed UHPLC-ED system is an acceptable and reliable method compared to standard UHPLC-UV system using paired *t*-test. Ultimately, the UHPLC coupled with AuNPs modified SPCE amperometry is successfully applied for real samples. This proposed electrode could be a novel or an alternative electrode in UHPLC-ED system for the simultaneous determination of DTCs in fruits and vegetables with low cost material, simple fabrication, and high sensitivity.

Acknowledgments

KC gratefully acknowledges the partially financial supports from Thailand Research Fund (TRF) through the Royal Golden Jubilee Ph.D. program (Grant Number PHD/0049/2553). OC and WS greatly thank the Thailand Research Fund through Research Team Promotion Grant (RTA5780005), the Thai Government Stimulus Package 2 (TKK2555), under the Project for Establishment of Comprehensive Center for Innovative Food, Health Products and Agriculture, Chulalongkorn University. We also thank the financial support from the 90th Anniversary of Chulalongkorn University Fund (Ratchadphiseksomphot Endowment Fund).

Appendix A. Supporting information

Supplementary data associated with this article can be found in the online version at <http://dx.doi.org/10.1016/j.talanta.2014.09.020>.

References

- [1] M. Albareda-Sirvent, A. Merkoci, S. Alegret, *Sensor Actuat. B-Chem.* 69 (2000) 153–163.
- [2] J. Li, H. Xie, L. Chen, *Sensor Actuat. B-Chem.* 153 (2011) 239–245.
- [3] K.C. Honeychurch, J.P. Hart, *TrAC, Trends Anal. Chem.* 22 (2003) 456–469.
- [4] D. Hernandez-Santos, M.B. Gonzalez-García, A.C. García, *Electroanalysis* 14 (2002) 1225–1235.
- [5] M. Das, K. Shim, S. An, D. Yi, *Toxicol. Environ. Health Sci* 3 (2011) 193–205.
- [6] L. Agüí, C. Peña-Farfal, P. Yáñez-Sedeño, J.M. Pingarrón, *Talanta* 74 (2007) 412–420.
- [7] M.A. Hernández-Olmos, L. Agüí, P. Yáñez-Sedeño, J.M. Pingarrón, *Electrochim. Acta* 46 (2000) 289–296.
- [8] S. Rastegarzadeh, S. Abdali, *Talanta* 104 (2013) 22–26.
- [9] L.G. Shaidarova, G.K. Budnikov, S.A. Zaripova, *J. Anal. Chem.* 56 (2001) 748–753.
- [10] E.D. Caldas, M.H. Conceicao, M.C.C. Miranda, L. de Souza, J.F. Lima, *J. Agr. Food Chem.* 49 (2001) 4521–4525.
- [11] S. Heise, H. Weber, L. Alder, *Fresen. J. Anal. Chem.* 366 (2000) 851–856.
- [12] W. Schwack, S. Nyanzi, *Z. Lebensm. Unters. Forsch* 198 (1994) 8–10.
- [13] O.H.J. Szolar, *Anal. Chim. Acta* 582 (2007) 191–200.
- [14] N. Ahmad, L. Guo, P. Mandarakas, S. Appleby, *J. AOAC Int.* 78 (1995) 1238–1243.
- [15] R.C. Perz, H. van Lishaut, W. Schwack, *J. Agric. Food Chem.* 48 (2000) 792–796.
- [16] A. Kumar Malik, W. Faubel, *Talanta* 52 (2000) 341–346.
- [17] A.W.M. Lee, W.F. Chan, F.S.Y. Yuen, C.H. Lo, R.C.K. Chan, Y. Liang, *Anal. Chim. Acta* 339 (1997) 123–129.
- [18] A.K. Malik, W. Faubel, *Crit. Rev. Anal. Chem.* 31 (2001) 223–279.
- [19] A.K. Malik, B.S. Seidel, W. Faubel, *J. Chromatogr. A* 857 (1999) 365–368.
- [20] M. Rossi, D. Rotilio, *HRC-J. High Res. Chrom* 20 (1997) 265–269.
- [21] W.A. Kleinman, J.P. Richie Jr, *J. Chromatogr. B* 672 (1995) 73–80.
- [22] M.D. da Silva, J.R. Procopio, L. Hernandez, *J. Liq. Chromatogr. R. T.* 22 (1999) 463–475.
- [23] D.T.T. Nguyen, D. Guillarme, S. Rudaz, J.L. Veuthey, *J. Sep. Sci.* 29 (2006) 1836–1848.
- [24] P.Y. Chen, C.H. Luo, M.C. Chen, F.J. Tsai, N.F. Chang, Y. Shih, *Int. J. Mol. Sci.* 12 (2011) 3810–3820.
- [25] C. Fernández, A.J. Reviejo, J.M. Pingarrón, *Anal. Chim. Acta* 305 (1995) 192–199.
- [26] C. Fernández, A.J. Reviejo, L.M. Polo, J.M. Pingarrón, *Talanta* 43 (1996) 1341–1348.
- [27] L. Mathew, M.L.P. Reddy, T.P. Rao, C.S.P. Iyer, A.D. Damodaran, *Talanta* 43 (1996) 73–76.
- [28] P. Qiu, Y.N. Ni, *Chin. Chem. Lett.* 19 (2008) 1337–1340.

Selective label-free electrochemical impedance measurement of glycated haemoglobin on 3-aminophenylboronic acid-modified eggshell membranes

Yuwadee Boonyasit¹ · Arto Heiskanen² · Orawan Chailapakul^{3,4} · Wanida Laiwattanapaisal⁵

Received: 27 January 2015 / Revised: 31 March 2015 / Accepted: 7 April 2015 / Published online: 10 May 2015
© Springer-Verlag Berlin Heidelberg 2015

Abstract We propose a novel alternative approach to long-term glycaemic monitoring using eggshell membranes (ESMs) as a new immobilising platform for the selective label-free electrochemical sensing of glycated haemoglobin (HbA1c), a vital clinical index of the glycaemic status in diabetic individuals. Due to the unique features of a novel 3-aminophenylboronic acid-modified ESM, selective binding was obtained via cis–diol interactions. This newly developed device provides clinical applicability as an affinity membrane-based biosensor for the identification of HbA1c over a clinically relevant range (2.3–14 %) with a detection limit of 0.19 %. The proposed membrane-based biosensor also exhibited good reproducibility. When analysing normal and abnormal HbA1c levels, the within-run coefficients of variation were 1.68 and 1.83 %, respectively. The run-to-run

coefficients of variation were 1.97 and 2.02 %, respectively. These results demonstrated that this method achieved the precise and selective measurement of HbA1c. Compared with a commercial HbA1c kit, the results demonstrated excellent agreement between the techniques ($n=15$), demonstrating the clinical applicability of this sensor for monitoring glycaemic control. Thus, this low-cost sensing platform using the proposed membrane-based biosensor is ideal for point-of-care diagnostics.

Keywords Glycated haemoglobin (HbA1c) · Diabetes mellitus · 3-aminophenyl boronic acid · Eggshell membrane · Membrane-based biosensor · Selective label-free electrochemical detection

Electronic supplementary material The online version of this article (doi:10.1007/s00216-015-8680-8) contains supplementary material, which is available to authorized users.

✉ Wanida Laiwattanapaisal
Wanida.L@chula.ac.th

¹ Graduate Program in Clinical Biochemistry and Molecular Medicine, Faculty of Allied Health Sciences, Chulalongkorn University, Bangkok 10330, Thailand

² Department of Micro- and Nanotechnology, Technical University of Denmark, 2800 Kgs. Lyngby, Denmark

³ Electrochemistry and Optical Spectroscopy Research Unit (EOSRU), Department of Chemistry, Faculty of Science, Chulalongkorn University, Bangkok 10330, Thailand

⁴ Center of Excellence on Petrochemical and Materials Technology (PETROMAT), Chulalongkorn University, Bangkok 10330, Thailand

⁵ Department of Clinical Chemistry, Faculty of Allied Health Sciences, Chulalongkorn University, Bangkok 10330, Thailand

Introduction

The alarming increases in mortality and health care expenditures resulting from diabetes have brought about considerable efforts to make disease-related measurements outside clinical settings, especially at a patient's bedside. High blood glucose contributes significantly towards many chronic complications, e.g., atherosclerosis, kidney failure, retinopathy, and cognitive degeneration [1, 2]. The frequent monitoring of glycaemic levels is of great importance for preventing the serious complications associated with diabetes and also for delaying the clinical progression of the disease. Traditionally, glycated haemoglobin (HbA1c) has been used as a predominant biomarker for the long-term assessment of glycaemic control in clinical practice. HbA1c is irreversibly formed by a slow, non-enzymatic glycation process at one or both of the N-terminal valine residues of the β -chains of haemoglobin over a long period of time, which corresponds to the average lifespan of erythrocytes in the preceding 2–3 months. The American

Diabetes Association (ADA) strongly recommends maintaining tight control over the level of HbA1c, with recommended values lower than 7 % and using HbA1c level as a diagnostic criterion for diabetes [3]. A quantitative measurement of HbA1c should be performed at least twice a year in patients with good glycaemic control and at least once every 3 months in individuals with poor glycaemic control [3].

Currently, the quantitative analysis of HbA1c is performed with a variety of analytical techniques, including electrophoresis [4], ion-exchange chromatography [5], boronate affinity chromatography [6], mass spectrometry [7–9], immunoassays [10–13], electrochemical detection [14–19], piezoelectric sensors [20–22], chemiluminescence [23], surface plasmon resonance [24] and surface-enhanced resonance Raman spectroscopy [25]. Among these available techniques, the major drawbacks are that such methods are rather complicated, take a long time for the analysis [10] and require the use of labelled antibodies [16], expensive equipment [20, 22] and/or sample preparation prior to the analysis [26]. Additionally, the effects of haemoglobin variants and chemically modified derivatives could also complicate these methods of HbA1c measurement [4]. Although boronate affinity chromatography and mass spectrometry appear to be unaffected by interference from haemoglobin derivatives, the high-priced cost of analysis and the need for sophisticated instruments making these methods unsuitable for routine clinical usage [7].

Due to the unique features of boronic acid binding, this compound is of interest in developing an alternative detection method to distinguish between non-glycated haemoglobin (HbAo) and HbA1c. Boronate groups are able to form stable complexes with the diol groups from glycated proteins under alkaline conditions [27]. Consequently, a boronate derivative is a critical component of an affinity biosensor for the analysis of glycosylated biomolecules. More recently, to amplify the electrochemical signal, Song et al. proposed the competition assay between HbA1c and glucose oxidase on the boronate-modified electrode surface for HbA1c determination in whole blood samples [17]. The proposed biosensor provided a linear response covering the clinical reference range found in diabetic patients (4.5–15 %). However, in contrast to the voltammetric and amperometric methods, impedimetric measurements gain the full benefits of understanding the chemical reaction mechanisms, including electron transfer, absorption, conductance, and mass transport of the redox probe [28]. Therefore, for this purpose, the use of electrochemical impedance spectroscopy for investigating chemical characteristics is highly desirable. A technique for selective HbA1c biosensing by impedance spectroscopy has been previously reported to enable the determination of HbA1c concentrations with high sensitivity [29–31]. This previously reported technique depended primarily on a self-assembled monolayer (SAM) of thiophene-3-boronic acid (T3BA) on gold electrodes. However, the dynamic detection range has yet to match the

physiological range of HbA1c in real blood samples (3–13 mg mL⁻¹) [21]. Thus, improvements of the sensing interface are needed to achieve an acceptable linear range for the clinical assessment of HbA1c.

Porous fibres consisting of proteins, e.g., eggshell membranes (ESMs), have attracted much attention because of the wide potential applications of these fibres as low-cost platforms for immobilisation. Previous studies on other selective microporous membranes [32, 33] suggested the potential problems of delicate operation and high cost as important barriers for the development of membrane-based biosensors. ESM, a naturally occurring biological polymer, has a distinct property of an interconnected porous structure, making ESM a useful biomaterial to use as a template for surface modification. ESM is generally available, affordable, abundant, biocompatible and environmentally friendly. Moreover, the amines and amides on its surface present positively charged functional groups can be functionally modified [34]. Because of these properties, ESM has currently been used in several biomedical applications as a membrane for guided bone regeneration [35], a biological dressing to promote the infection-free healing of wounds [36] and a platform for protein immobilisation [37, 38].

To date, no data is currently available on label-free biosensing with boronate affinity applications. Therefore, the primary aim of this work was to investigate the possibility of using ESM as a new immobilising platform for surface modification with boronate derivatives. Such a platform can be applied to the generation of an affinity-based biosensor to identify HbA1c. In this study, a novel ESM-based analytical device for the quantitative measurement of HbA1c in patient blood samples was constructed and evaluated. The selective 3-aminophenylboronic acid (APBA)-modified ESM was constructed as a specific binding component of a device for the label-free electrochemical impedance spectroscopy measurement. The APBA plays a key role in the selective binding of HbA1c via cis-diol interactions with a boronate-recognition group. To our knowledge, this newly proposed device is the first ESM-based biosensors for determining HbA1c in blood samples. Using ESM as a new immobilising platform, our study demonstrated that ESM can be used in the development of a reliable and inexpensive device for assaying HbA1c.

Materials and methods

Reagents and chemicals

For assaying HbA1c levels, a Lyphochek® HbA1c Linearity Set and Lyphochek® Diabetes Controls were purchased from BioRad Laboratories (Hercules, CA, USA). Analytical grade chemicals were used throughout this study. APBA, 4-ethylmorpholine, sodium chloride, potassium chloride,

potassium hexacyanoferrate II, potassium hexacyanoferrate III, a glutaraldehyde solution (25 %, w/w), ethanolamine, sodium acetate trihydrate, potassium cyanide, sodium phosphate monobasic, sodium phosphate dibasic, potassium ferricyanide, sodium bicarbonate and haemoglobin-Ao were obtained from Sigma (St. Louis, MO, USA). Hydrochloric acid, Brij® 35 (polyoxyethylene (23) lauryl ether detergent) and acetic acid were acquired from Merck (Dannstadt, Germany). The materials used to determine the haematocrit (Hct) values, including microhaematocrit tubes, a microcapillary reader, and a microhaematocrit centrifuge, were manufactured by Vitrex Medical A/S (Herlev, Denmark), International Equipment Company (Needham Heights, MA, USA) and Hawksley and Sons Ltd. (Sussex, England), respectively. A cyanmethaemoglobin standard solution was available from a local service provider. The commercial platinum screen-printed electrode was supplied by DropSens (Asturias, Spain). To determine the HbA1c levels in the whole blood samples, commercial in2it™ (II) A1c test kits from BioRad Laboratories (Hercules, CA, USA) were employed to validate the method based on well-established boronate affinity chromatography.

ESM preparation

Chicken eggs were purchased from the local supermarket and stored at 4 °C before use. The ESM is a double-layered membrane inside the eggshell composed of highly cross-linked proteins. According to the method described by Yeni et al. [39], to obtain the whole ESMs, eggs were soaked in absolute acetic acid at 4 °C for 18 h and the membrane was subsequently peeled off of the broken eggshell. Afterwards, the membranes were cleansed with a copious amount of deionised water before cutting into circles with a diameter of approximately 13 mm. The circular ESMs were stored in a 10-mM 4-ethylmorpholine buffer containing 0.25 M KCl and 0.1 M NaCl until further use.

To characterise the microstructure of the ESM with and without the immobilised HbA1c, a scanning electron microscope (JSM-5410LV, JEOL, Tokyo, Japan) and transmission electron microscope (TEM-2100, JEOL, Tokyo, Japan) were used to study the surface and internal structure of the ESMs. For scanning electron microscopy (SEM), the dried circular membranes were placed on a specimen stub and coated with a thin layer of gold before analysis. To prepare the ESMs for transmission electron microscopy (TEM), the membranes were initially fixed with a 2.5 % (w/w) glutaraldehyde solution and 1 % (w/w) osmium tetroxide before being dehydrated with a series of washes with ethanol at concentrations ranging from 35 to 95 %. The membranes were further immersed in propylene oxide, embedded in an epoxy resin solution, dried, and then cut to 90-nm thickness using an ultramicrotome before being placed on a copper grid. Finally, to increase the contrast

level of the image, the membranes were stained with uranyl acetate and lead citrate before the TEM investigation.

Surface modification with APBA

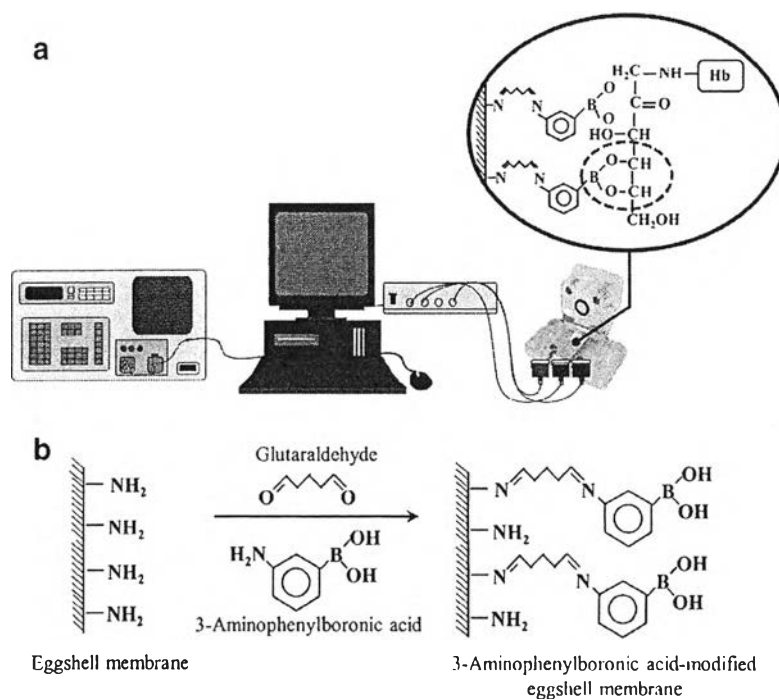
Unless otherwise stated, for fabrication of the APBA-modified ESM, a drop of glutaraldehyde solution was placed on the surface of the membrane, which was then thoroughly washed with 10 mM 4-ethylmorpholine buffer before the addition of 2.5 mg mL⁻¹ of APBA. The excess aldehyde groups were subsequently removed by rinsing with 10 mM ethanolamine followed by an additional wash. Finally, various concentrations of HbA1c were used to investigate whether HbA1c could bind to the selective sensing surface via cis-diol interactions. Each consecutive step was carried out on the same piece of platinum screen-printed electrode with the use of the electroactive redox probe. The electrochemical impedance spectroscopy measurement was conducted in a step-wise manner. The APBA-modified ESMs could be used repeatedly after washing with a regeneration buffer, 10 mM sodium acetate at pH 5, which reversed the HbA1c binding reaction. A sodium acetate buffer could be used to remove HbA1c from the APBA-modified membranes because the binding of boronate groups with diol groups has been shown to be quite unstable under acidic conditions [40].

Glutaraldehyde was used as a coupling agent and served as a homo-bifunctional crosslinker between the amine moiety of APBA and the amine groups on the surface of the ESM, as depicted in Fig. 1b. The aldehyde group is expected to attach to the amine group of APBA. Afterwards, any remaining aldehyde groups were then blocked with the ethanolamine buffer. In such a case, the specific binding between the boronic acid groups and HbA1c occurs via cis-diol interactions.

Sample preparation

Healthy participants and diabetic patients, as defined by the American Diabetes Association criteria [41], volunteered to take part in our study. Written informed consent was obtained from all the individuals before the study began. The project regarding the development of membrane-based biosensors was approved by the Ethics Review Committee for Research Involving Human Research Subjects, Health Sciences Group, Chulalongkorn University (ECCU) under approval number COA No. 057/2557. Whole blood samples were collected in vacuum blood collection tubes using tripotassium ethylenediaminetetraacetic acid (K₃EDTA) as an anticoagulant. The Hct and total haemoglobin (Hb) were quantified using the microcapillary and cyanmethaemoglobin methods (Drabkin's reagent), respectively. After measuring the Hct and total Hb, centrifugation was used to separate the plasma from cells, and then the plasma was discarded to eliminate glucose and other glycosylated proteins existing in the plasma.

Fig. 1 Schematic diagram of the proposed ESM-based biosensor illustrating (a) a configuration of the label-free electrochemical impedance system setup and (b) a reaction scheme for immobilising APBA on the surface of ESMs



The red blood cells remaining were carefully washed three times with physiological saline (a 0.9 % sodium chloride solution) to remove the plasma completely. To prepare the red blood cell lysates, a haemolysing buffer solution (26 mM NaH_2PO_4 , 7.4 mM Na_2HPO_4 and 13.5 mM KCN), as prepared according to a previous study [14], was used to lyse the red blood cells prior to the electrochemical impedance measurement.

Label-free electrochemical impedance spectroscopy system setup

The label-free electrochemical impedance spectroscopy measurement was carried out with a potentiostat/galvanostat instrument (Autolab PGSTAT30, Eco Chemie, The Netherlands) equipped with the Frequency Response Analyser system software. In this study, the impedance detection system was connected to a commercial platinum screen-printed electrode (DropSens, Asturias, Spain) for the selective electrochemical sensing of HbA1c. This new configuration is illustrated in Fig. 1a. A circle-sized APBA-modified ESM (13 mm) was well positioned on the platinum screen-printed electrode surface and covered all of the three electrodes, consisting of the counter (CE), working (WE) and reference electrodes (RE). The membrane was carefully placed over the electrode to prevent the formation of air bubbles between both layers. The whole assembly, i.e., an integrated electrode with a thin layer of ESM, an O-ring and a custom-ordered holder, was clamped together through a magnetic force. The electronic connections were accomplished by a customised designed

electronic connector. The impedance measurement was conducted over a frequency range of 10 Hz to 100 kHz with an applied current potential of 10 mV. The redox ions, i.e., a 5-mM $(\text{Fe}(\text{CN})_6)^{3-/4-}$ solution containing 0.25 M KCl and 0.1 M NaCl dissolved in 10 mM 4-ethylmorpholine buffer, were prepared and used as an electroactive probe throughout the experiment. The impedance data were fitted to an equivalent-circuit model using the NOVA 1.9 software.

Results and discussion

Surface characterisation of the ESM

The ESM, a thin film adhering inside the eggshell, is composed of three thin membranes, namely, the outer ESM, inner ESM and limiting membrane, from outside to inside [42]. In our study, the entire ESM was used as a sheet membrane, and the membrane surface that contacts the shell was called the outer surface, whereas the opposite surface was called the inner surface. Figure 2 displays scanning electron micrographs (a-d) and transmission electron micrographs (e, f) of ESMs with and without the immobilised red blood cell lysates. The surface structure was found to be different side of an ESM, as shown in Fig. 2a. The total thickness of the ESM was approximately 60–70 μm , which is in agreement with the work of Takiguchi et al. [43]. A network-like structure was observed on the ESM surface (Fig. 2b), indicating that the ESM consisted of highly cross-linked protein fibres and cavities. The fibres of the inner layer were smaller and smoother

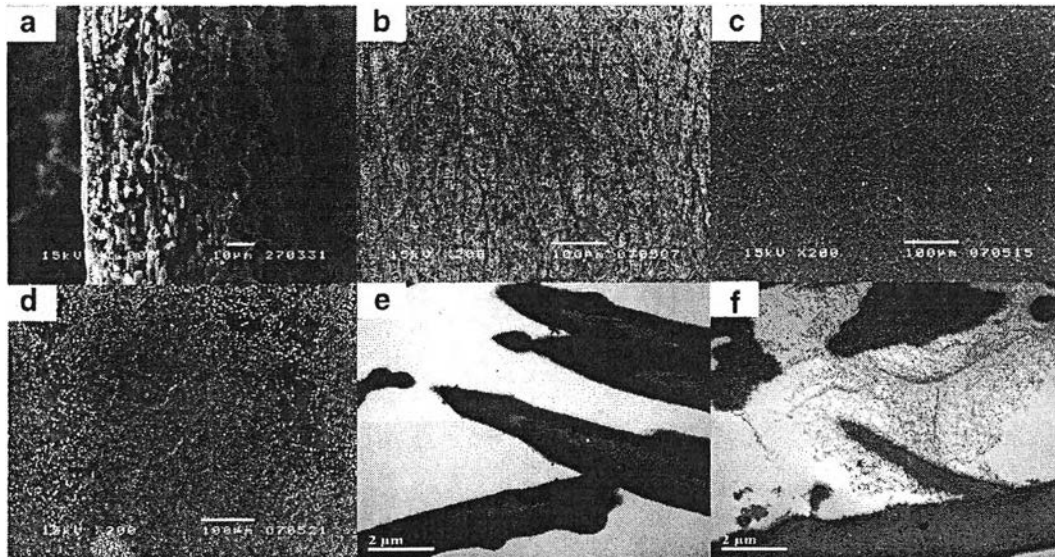


Fig. 2 SEM images of the ESM: (a) cross-section, (b) outer surface, (c) inner surface and (d) after exposure to HbA1c; and TEM images of ESM: (e) membrane fibres consisting of a collagen-rich core surrounded by a mantle layer and extra-fibre spaces and (f) after exposure to HbA1c

than those of the outer layer (Fig. 2c). After the immobilisation of APBA, the red blood cell lysates were able to adhere to the surface of the ESM, as depicted in Fig. 2d. Our analysis indicated that the red blood cell lysates were successfully immobilised on the surface of the ESM. Figure 2e presents the TEM micrograph showing that the membrane fibres are 1–4 μm in diameter and separated by extra-fibre spaces. Each fibre consists of a collagen-rich core that is surrounded by a glycoprotein-rich mantle [44]. The internal cavity of the ESM was occupied by HbA1c after exposure to the red blood cell lysates (Fig. 2f). These results implied that some components of the red blood cell lysates attached to the surface of the ESM, while other components entered into the interlacing network of ESM fibres.

HbA1c optimisation of the assay

Effect of pH

The effect of pH has been widely perceived to be the most crucial factor for affinity binding between HbA1c and the boronate groups. In general, under alkaline conditions, boronic acid is transformed to its tetrahedral anionic form, which subsequently reacts with the diol group of a glycosylated protein to form a cyclic ester. A pH above the pK_a value of APBA is typically considered optimal for this reaction; however, it has been suggested that determining the optimum pH for binding is not this simple [45]. Therefore, in this study, the effect of pH on binding was investigated with a 10-mM 4-ethylmorpholine buffer solution containing 0.25 M KCl and 0.1 M NaCl to maintain the pH at 8, 8.5, 9 or 9.5. As shown in Fig. 3, the normalised ratio of stimulated resistance plotted against the

HbA1c concentration was greatly impacted by pH. The results revealed that the sensitivity of the HbA1c assay increased with increasing pH. Although the binding of HbA1c to the boronate complexes at pH 9.5 provided the highest sensitivity, this pH was disregarded due to the narrow linearity also obtained at this pH. Furthermore, under extremely alkaline conditions, the tertiary and quaternary structures of glycosylated proteins would be subject to denaturation. Thus, a pH of 8.5 was instead selected for all subsequent experiments because this pH provided a wider linear range that extended to 14 % HbA1c. At pH values close to the pK_a of APBA, the boronate group is expected to exist in an anionic form, which is able to bind specifically with a diol to form the boronate ester. Similarly, Příbýl et al. also suggested that a pH above 8 can generally be accepted as an optimum condition [22].

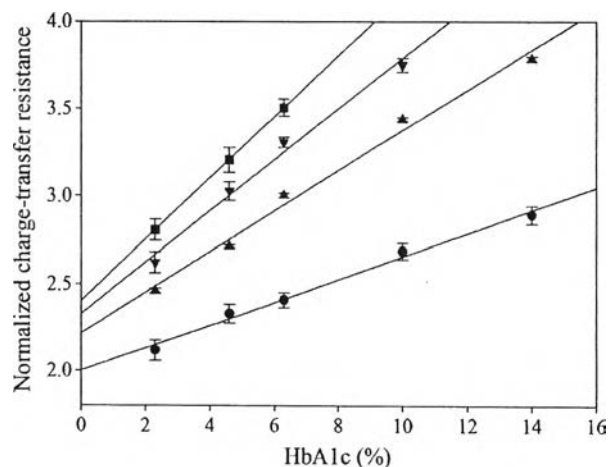


Fig. 3 The effect of pH on HbA1c binding: circles pH 8, triangles pH 8.5, inverted triangles pH 9 and squares pH 9.5

Effects of glutaraldehyde and APBA concentrations

In our system, the glutaraldehyde solution was used as a cross-linking agent to achieve covalent bonding between the amino groups of the ESMs and amine functional groups of APBA. Two levels of an HbA1c standard solution were employed to investigate the effect of glutaraldehyde concentration on the impedance signal response of the APBA-modified ESMs at a concentration of 0.25 mg mL^{-1} APBA. After 5 min of glutaraldehyde immobilisation, when normal and high levels of HbA1c were assayed, the impedance response of the membrane-based biosensor increased with increasing concentrations of glutaraldehyde, as depicted in Fig. S1A in the Electronic supplementary material. Hence, a 25 % (w/w) glutaraldehyde solution was the optimum condition and was selected for all subsequent experiments. In comparison, when using ESM as an enzyme immobilisation platform, higher glutaraldehyde concentrations lead to a decrease in the sensitivity of the biosensor due to the denaturation of the enzyme. In general, a 2.5 % (w/w) glutaraldehyde solution has been chosen as the optimal cross-linking agent for enzyme immobilisation; however, the immobilisation normally occurs over a prolonged period ranging from 30 min to 8 h, permitting long-term contact of the enzymes with glutaraldehyde [46–48]. In contrast, the method of choice in this study involved an immobilisation strategy that utilised a higher concentration of glutaraldehyde and a short contact time. This approach is not without precedent because several instances of using high concentrations of glutaraldehyde have been reported in the literature [49–51].

The concentration of APBA was also a relevant factor that directly affected the binding of HbA1c to the ESM-based biosensor. The signal response increased with an increasing concentration of APBA, as depicted in Fig. S1B in the Electronic supplementary material). However, when the concentration of APBA was higher than 0.25 mg mL^{-1} , the response reached a maximum value, indicating that the amount of APBA had achieved equilibrium. Thus, 0.25 mg mL^{-1} of APBA was used for all subsequent experiments.

Effect of incubation time

Alteration of the times for the APBA and HbA1c immobilisations on the ESMs could affect the amount of immobilised boronic acid functional groups and HbA1c molecules, respectively, on the surface of the ESMs, which are in direct proportion to the sensitivity of the membrane-based biosensors. Thus, the effect on HbA1c detection of APBA immobilisation times from 10 to 40 min was also investigated (Fig. S2A in the Electronic supplementary material). When assaying two levels of HbA1c with 0.25 mg mL^{-1} of APBA, the impedance signal increased gradually as the immobilisation time increased from 10 to 20 min and the signal reached a

steady state after 20 min of incubation. Therefore, the optimum immobilisation time for APBA was determined to be 20 min. Figure S2B in the Electronic supplementary material illustrates the effect of HbA1c immobilisation time on the impedance signal obtained from the APBA-modified ESM. In this case, when assaying two levels of HbA1c, the signal response increased with an increasing incubation time and approached the maximum value after 15 min. Thus, considering a compromise between the signal response and analysis time, a 15-min incubation time was used throughout our studies.

Analytical characteristics

EIS characterisation of the sensing interface

One of the distinctive features of ESM is that its structure is composed of an intricate lattice meshwork of large and small fibres interlocking with each other, and the ESM surface is expected to contain the reactive functional groups, i.e., amines and amides, that are expected to react with APBA via a glutaraldehyde coupling agent. In our study, the inner surface of the ESM was subjected to step-wise boronate modifications with a platinum screen-printed electrode underneath. Label-free electrochemical impedance measurements were subsequently performed following each step of the surface modification. Figure 4 has Nyquist plots for the kinetic redox process, using $(\text{Fe}(\text{CN})_6)^{3-/4-}$ as an electroactive probe, on a bare platinum screen-printed electrode and on the ESM, glutaraldehyde-activated ESM and APBA-modified ESM. Compared with the impedance data obtained from a bare electrode, a twofold increase in the charge-transfer resistance (R_{ct}) was observed when the membrane was placed on the

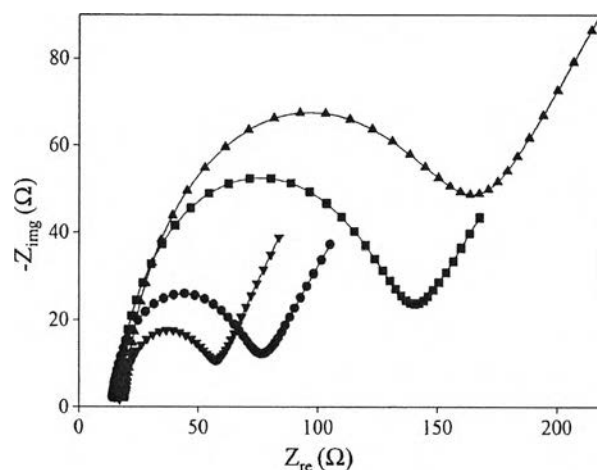


Fig. 4 Nyquist plots for the stepwise analysis of the *circles* bare electrode, *squares* ESM, *triangles* glutaraldehyde-treated ESM and *inverted triangles* APBA-modified ESM surface in the presence of a 5 mM $(\text{Fe}(\text{CN})_6)^{3-/4-}$ redox probe in 10 mM 4-ethylmorpholine buffer (pH 8.5)

electrode. This evidence implies that the fibrous ESM immobilised on the surface of platinum electrode was blocking redox species movement. When the glutaraldehyde solution was applied, the curve broadened significantly, indicating a dramatic increase in resistance. Surprisingly, when the glutaraldehyde-activated ESM was further modified with APBA, the R_{ct} significantly decreased, indicating neutralisation of the negative charges of the redox probes. The observed decrease in the R_{ct} may result from the almost neutral net charge of APBA in a buffer with a pH close to the pK_a of APBA. In addition, APBA may directly bind to the surface of the ESM because the network of protein fibres in this type of membrane is composed of a collagen-rich core and a glycoprotein-rich mantle [52]. To investigate whether the impedance changes were due to the resistance of the membrane, a control experiment was also performed using the screen-printed electrode without ESM prepared in the same manner as the electrode in the proposed system. Nyquist plots for the stepwise modification of screen-printed electrodes are shown in Fig. S3 (Electronic supplementary material). The impedance response obtained from the glutaraldehyde-treated electrode was significantly decreased compared with that obtained from the bare electrode. Additionally, the glutaraldehyde-treated electrode was not responsive to the 0.25 mg mL^{-1} APBA. The impedance signals of the APBA-modified electrode were not in direct proportion to the various concentrations of HbA1c, implying that the changes in impedance of the proposed membrane-based system were due to the resistance of the membrane.

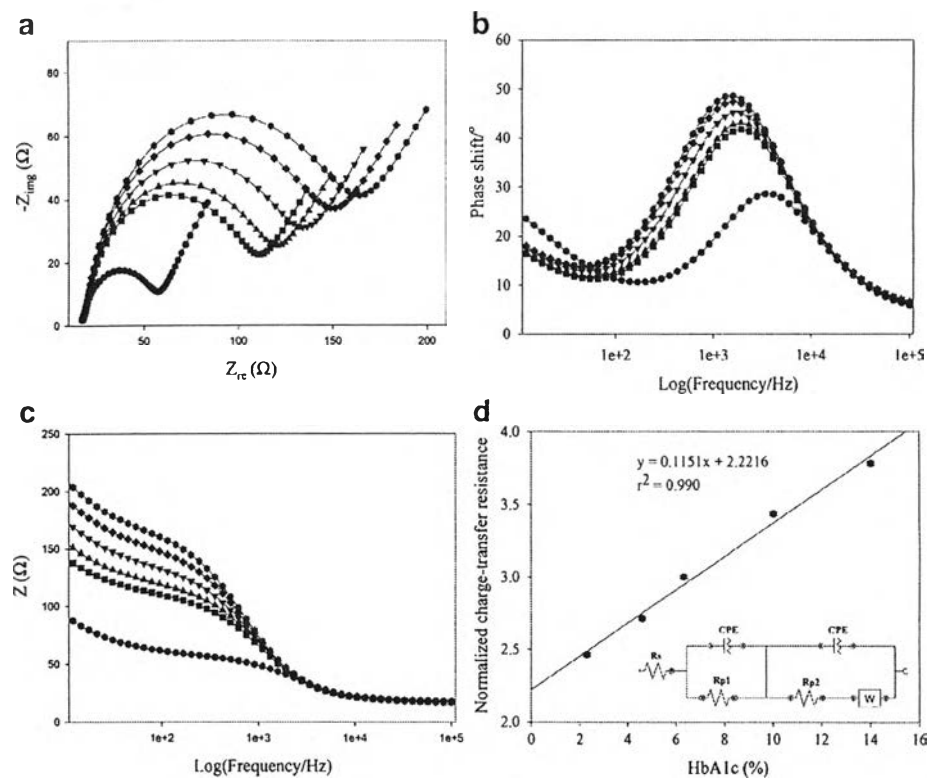
Calibration curve for the detection of HbA1c

The differential change in impedance with increasing HbA1c concentrations is clearly indicated in the Nyquist plot, as depicted in Fig. 5a. After exposure to the HbA1c, the R_{ct} was significantly increased due to the ability of HbA1c to interact with APBA on the modified ESM and thus hinder the movement of redox species to the platinum electrode surface below the ESM. A control experiment was also carried out using an ESM without immobilised APBA, which was prepared in a manner similar to the proposed system. The impedance signal response towards HbA1c over the concentration range of 2.3 to 14 % remained unchanged compared with the baseline signal of the ESM (Fig. S4 in the Electronic supplementary material). This result confirmed that the impedance signal arose from the specific binding between the APBA-modified ESM and HbA1c via cis-diol interactions. Additionally, as shown in Fig. 5b, a significant phase shift was observed after attachment of the HbA1c and a less obvious change occurred with increasing concentrations of HbA1c. Dramatic changes in impedance were noticed at the lower frequency ranges (Fig. 5c), thereby demonstrating the sensitive response of the APBA-modified ESM towards HbA1c.

The impedance data are satisfactorily described by the behaviour of a system with the equivalent circuit shown in Fig. 5d (inset), which comprises a series of two constant-phase elements (CPEs) in parallel with two resistances (R_p) and the Warburg impedance element (W), along with the solution resistance (R_s). The good fitting results are shown in Fig. S5 (Electronic supplementary material). In this model, R_s corresponds primarily to the resistance of the electrolyte solution, whereas R_{p1} and R_{p2} are the R_{ct} values that correspond to the membrane resistance and charge-transfer kinetics at the platinum screen-printed electrode, respectively. A CPE is used to describe the non-Faradic process at the membrane solution and electrode-solution layers. The CPE is defined as $Z_{CPE} = (A\omega)^{-\alpha}$, where A is a proportionality factor, ω is the angular factor and α is an exponential term with a value between 0 and 1. When the value of α is equal to 1, the CPE acts as a resistor [28]. Based on the results of fitting the electrochemical impedance data to this equivalent circuit, an increase in the membrane resistance R_{p1} response is observed in the presence of increasing HbA1c concentrations. These results implied that the immobilised HbA1c could fully occupy the porous network of the ESM; therefore, the electroactive probe was not accessible to the surface of the platinum electrode, resulting in an increase in the R_{ct} . The rate constant for the Faradic reaction of $(\text{Fe}(\text{CN})_6)^{3-/4-}$, an electroactive probe, has been described using the electrochemical basis of the R_{ct} , as indicated in the following equation [53]: $R_{ct} = RT / (n^2 F^2 A k_{app}^0 C)$ where R is the gas constant, T is the temperature, n is the number of electrons transferred, F is the Faraday constant, A is the electrode surface area, k_{app}^0 is the rate constant of the redox process and C is the concentration of the redox species. In our proposed system, the A and the k_{app}^0 can be altered by the stepwise modification process.

The normalised ratio of the resistances derived from the fitted resistance values was plotted versus the various concentrations of HbA1c, as illustrated in Fig. 5d. The results revealed that the normalised response was linear up to 14 % of HbA1c, with a regression equation of $y = 0.1151x + 2.2216$ ($r^2 = 0.990$). The detection limit, defined by a signal-to-noise ratio of 3, was found to be 0.19 %, a slightly higher sensitivity than that described by Kim et al. [14]. These findings suggest that the proposed system provides sufficient sensitivity to measure the concentration of HbA1c within the required clinically relevant range of HbA1c, where 4–6 % is considered normal and covers the clinical reference range of diabetes (6.5–15 %) [3]. Compared with other electrochemical impedance measurements of HbA1c, the proposed membrane-based biosensor provides a wider linear range for assaying HbA1c [29–31]. ESM has a distinctive property. The higher the porous fibres, the higher the immobilisation surface areas, is available for boronate-binding sites. Hence, the high surface density of the available boronate groups increases the sensitivity and linearity of the proposed biosensor. With the

Fig. 5 Impedance data obtained from (a) Nyquist plot, (b) Bode-phase plot of the APBA-modified ESM before and after it was exposed to various concentrations of HbA1c: circles APBA-modified ESM, squares 2.3 %, triangles 4.6 %, inverted triangles 6.3 %, diamonds 10 % and hexagons 14 % HbA1c; (c) Bode-modulus plot and (d) variation of the normalised charge-transfer resistance (R_{ct}) with respect to the concentration of HbA1c (%). *Inset right*, an equivalent circuit for analysing the impedance data; R_s solution resistance, R_{p1} membrane resistance, R_{p2} charge-transfer kinetics, CPE constant-phase element, W Warburg impedance



proposed ESM biosensor, samples can be directly tested without requiring additional sample dilution steps and avoiding pipetting errors. In addition, this label-free affinity platform provides us with a better understanding of interfacial sensing mechanisms and a great tool for glycaemic monitoring in diabetic patients, especially those in developing countries. A favourable comparison of the analytical characteristics for HbA1c determination using boronate-based electrochemical methods is provided in greater detail in Table S1 (Electronic supplementary material). Importantly, according to the standard interpretation norms of HbA1c in clinical practice, the HbA1c concentration should be expressed as the percentage of total haemoglobin (i.e., mmol mol^{-1} or %). Thus, in our studies, the HbA1c haemolysate standards (% HbA1c), which are currently used for commercial instruments, were selected as being representative of real clinical samples. As demonstrated here, the proposed membrane-based system leads to a substantial improvement in the dynamic detection range of HbA1c (up to 14 %) and also exhibits excellent sensitivity. Such capabilities make this method useful for real sample analysis and for assessing the glycaemic levels for clinical diagnosis.

Reproducibility

The reliability of the proposed membrane-based biosensor was determined with a precision assay that included two levels of HbA1c, i.e., normal (4.6 %) and diabetic (10 %) HbA1c

concentrations, performed on the same day and on three consecutive days. The results revealed that the within-run reproducibility (each concentration; $n=10$) was indicated by CVs of 1.68 and 1.83 % when assaying normal and abnormal levels of HbA1c, respectively. Furthermore, the run-to-run reproducibility studies at normal and abnormal levels resulted in CVs of 1.97 and 2.02 %, respectively, assessed on three consecutive days (each concentration; $n=30$). The regeneration experiment is also demonstrated in Fig. S6 (Electronic supplementary material). Due to the reversible binding between HbA1c and boronate-recognition groups, the proposed membrane-based biosensor could be used as a reusable sensing platform. After repeated usage of the proposed membrane-based biosensor, similar signal responses were observed up to 10 cycles without losing APBA activity. Recently, Sacks et al. recommended that an intra-laboratory CV should be less than 2 % (National Glycohemoglobin Standardisation Programme (NGSP) units) because a difference of 0.5 % HbA1c between successive patient samples represented a significant change in glycaemic control [54]. Therefore, these findings clearly demonstrate that our proposed system provides an accurate assessment of HbA1c with great precision and also meets the performance goal for HbA1c measurement. Additionally, the storage stability of the screen-printed electrode covered with the boronate-modified ESM was also investigated by soaking the system in ultrapure water. Unfortunately, our results showed that the activity of APBA sensing interface was

greatly diminished after storing the electrode for a few days. The decrease in signal response could be due to detachment of the boronate group from the ESM. Thus, future studies on the storage stability of the boronate-modified ESM will be needed to be investigated.

Selectivity study

For clinical purposes, a whole blood specimen is the most complex matrix because there are many interfering molecules present, including endogenous (unconjugated bilirubin, glucose, glycosylated proteins or high hypertriglyceridaemia) and exogenous substances (commonly prescribed drugs and supplements). Considering the underlying principles of the boronate affinity measurement method, this analytical concept is based on a unique structural characteristic of HbA1c. The boronate-recognition group is able to covalently bind to the diol group of any glycosylated protein or sugar. Accordingly, the method described here may not be specific only to HbA1c but may also bind to glucose, glycosylated albumin, and other glycosylated proteins interfering in whole blood samples. However, in our study, these endogenous interfering substances present in plasma were negligible because these substances were completely removed from the red blood cells by centrifugation and washing with physiological saline. As stated earlier, the red blood cell lysates were prepared before being subjected to the impedance analysis. Therefore, to evaluate the selectivity of the proposed membrane-based biosensor for the determination of HbA1c in authentic blood samples, the use of HbAo was one possible way to investigate whether the non-glycosylated protein could interfere with the specificity of the proposed assay. The experiment was carried out utilising the boronate-modified ESM prepared in a manner similar to that for HbA1c determination, as described in the ‘Materials and methods’, but HbAo was used instead. Compared with the signal response of boronate-modified membranes, the impedance data in the response towards HbAo remained unchanged over the concentration range of 10 to 20 g dL⁻¹ (data not shown). These results imply that our proposed membrane-based system is able to very precisely determine the HbA1c content in authentic blood samples, indicating the clinical applicability of the present method to monitor glycaemic levels in diabetic individuals.

Most importantly, for the correct interpretation of HbA1c measurements in clinical practice, the analytical interference of genetic variants, i.e., HbS, HbC, HbD, HbF and HbE and chemical derivatives of haemoglobin, i.e., carbamyl-Hb and pre-HbA1c, is of particular note when guaranteeing the reliability of the results. However, to our knowledge, compared with the other available methods for HbA1c determination, the boronate affinity binding method is generally considered to be less affected by the presence of haemoglobin variants and modified derivatives [55, 56]. Recent data obtained from a comparison between the International Federation of Clinical Chemistry and Laboratory Medicine (IFCC) reference method

and boronate affinity method showed that boronate affinity method was not affected by the presence of most common haemoglobin variants [56]. However, the characteristics of the patient population should be carefully considered during the selection of HbA1c assay method, including the prevalence of haemoglobin variants. Additional physiological factors, such as severe iron-deficiency anaemia, haemolytic anaemia or any conditions that directly affect the erythrocyte lifespan, should be considered as potential restrictions for interpreting HbA1c assay results.

Assay comparison

Fifteen red blood cell lysate samples obtained from non-diabetic and diabetic volunteers were analysed for HbA1c levels using the proposed membrane-based system in parallel with the current commercially available method. All of the

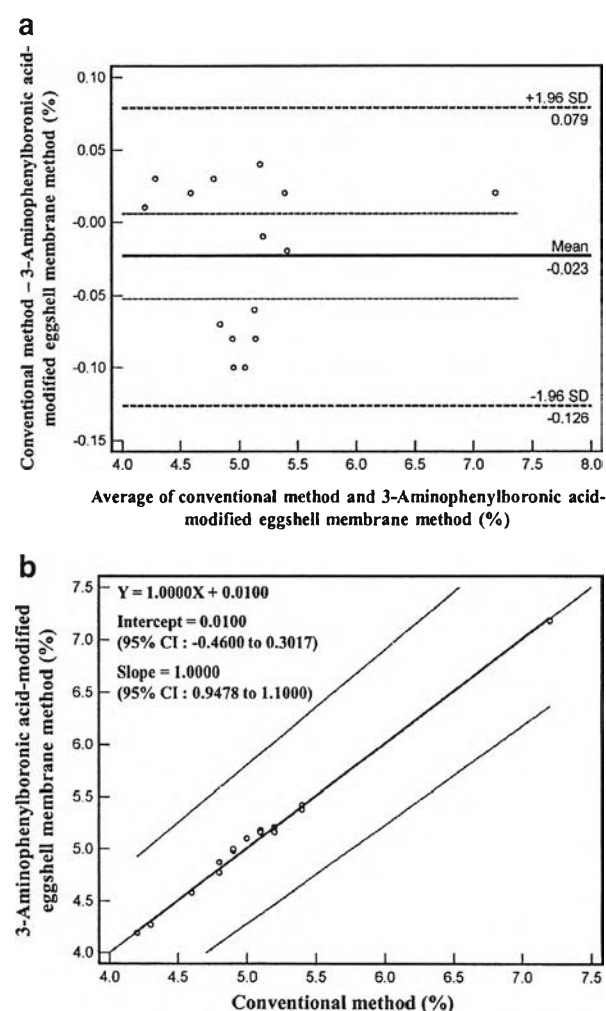


Fig. 6 Comparison of the proposed ESM-based analytical system and the current commercially available method for HbA1c measurement using (a) a Bland–Altman bias plot and (b) Passing–Bablok regression analysis

samples were analysed for haemoglobin and haematocrit values, which were determined to be within the ranges of 11–18 g dL⁻¹ and 30–47 %, respectively. The agreement and correlation between the two approaches were assessed using the Bland–Altman bias plot and a Passing–Bablok regression analysis, respectively. The results revealed a reliable relationship between the proposed membrane-based system and the commercially available method within an agreement interval of ± 1.96 SD. As demonstrated in Fig. 6a, these results suggest that the two methods could be used interchangeably. The results derived from our system were highly correlated with those obtained using the commercially available kit, with a Passing–Bablok regression equation of $y = 1.0000x + 0.0100$, as shown in Fig. 6b. Based on a 95 % confidence interval, the values of the y-intercept (0.0100) and the slope (1.0000) were trustworthy and covered a range of -0.4600 to 0.3017 and 0.9478 to 1.1000 , respectively. In other words, these data demonstrate a good agreement between these two methods, and the proposed ESM-based method provides an alternative approach to monitoring HbA_{1c} levels in authentic blood samples. In this case, the glycaemic status of each individual can be determined.

Conclusions

The proposed ESM-based biosensor was remarkably selective in determining HbA_{1c} levels because this method was successfully applied to the analysis of authentic samples via a label-free electrochemical impedance measurement, in which the results demonstrated good agreement with the commercially available affinity method. The results showed in a step-wise process that the boronate-modified ESM was highly responsive to a wide range of HbA_{1c} levels, indicating that this method is suitable for the clinical monitoring of glycaemic control. A novel APBA-modified ESM also provides a cost-effective biosensor for the diagnosis of diabetes, which is highly desirable in under-developed countries. Without the use of other detection labels, such as antibodies, dyes, or fluorescent materials, the proposed system has the merit of great simplicity. With the utilisation of an affinity membrane-based biosensor, this method has the potential for continuously monitoring glycaemic levels in diabetic patients and can be applicable to determining the presence of other glycosylated proteins, e.g., glycosylated albumin, found in plasma.

Acknowledgements This research was financially supported by the Ratchadaphiseksomphot Endowment Fund of Chulalongkorn University (RES 560530212-HR) and the Thailand Research Fund (RTA5780005). Y.B. acknowledges the Thailand Research Fund through the Royal Golden Jubilee Ph.D. Programme (under grant No. PHD/0164/2553) and the Graduate School, Chulalongkorn University for the tuition fee scholarship.

References

- Brownlee M (2001) Biochemistry and molecular cell biology of diabetic complications. *Nature* 414:813–820
- Baynes JW, Thorpe SR (1999) Role of oxidative stress in diabetic complications: a new perspective on an old paradigm. *Diabetes* 48:1–9
- American Diabetes Association (2013) Standards of medical care in diabetes—2013. *Diabetes Care* 36:S11
- Weykamp CW, Penders TJ, Siebelder CW, Muskiet FA, Slik WVD (1993) Interference of carbamylated and acetylated hemoglobins in assays of glycohemoglobin by HPLC, electrophoresis, affinity chromatography, and enzyme immunoassay. *Clin Chem* 39:138–142
- Eckerbom S, Bergqvist Y, Jeppsson JO (1994) Improved method for analysis of glycosylated haemoglobin by ion exchange chromatography. *Ann Clin Biochem* 31:355–360
- Frantzen F, Grimsrud K, Heggli DE, Sundrehagen E (1995) Protein-boronic acid conjugates and their binding to low-molecular-mass cis-diols and glycosylated hemoglobin. *J Chromatogr B* 670:37–45
- Roberts NB, Amara AB, Morris M, Green BN (2001) Long-term evaluation of electrospray ionization mass spectrometric analysis of glycosylated hemoglobin. *Clin Chem* 47:316–321
- Castillo ED, Montes-Bayón M, Añón E, Sanz-Medel A (2011) Quantitative targeted biomarker assay for glycosylated haemoglobin by multidimensional LC using mass spectrometric detection. *J Proteomics* 74:35–43
- Jeppsson JO, Kobold U, Barr J, Finke A, Hoelzel W, Hoshino T, Miedema K, Mosca A, Mauri P, Paroni R (2002) Approved IFCC reference method for the measurement of HbA_{1c} in human blood. *Clin Chem Lab Med* 40:78–89
- Chen HH, Wu CH, Tsai ML, Huang YJ, Chen SH (2012) Detection of total and A1c-glycosylated hemoglobin in human whole blood using sandwich immunoassays on polydimethylsiloxane-based antibody microarrays. *Anal Chem* 84:8635–8641
- Stöllner D, Stöcklein W, Scheller F, Warsinke A (2002) Membrane-immobilized haptoglobin as affinity matrix for a hemoglobin-A1c immunosensor. *Anal Chim Acta* 470:111–119
- Liu G, Khor SM, Iyengar SG, Gooding JJ (2012) Development of an electrochemical immunosensor for the detection of HbA_{1c} in serum. *Analyst* 137:829–832
- Wangoo N, Kaushal J, Bhasin KK, Mehta SK, Suri CR (2010) Zeta potential based colorimetric immunoassay for the direct detection of diabetic marker HbA_{1c} using gold nanoprobe. *Chem Commun* 46:5755–5757
- Kim DM, Shim YB (2013) Disposable amperometric glycosylated hemoglobin sensor for the finger prick blood test. *Anal Chem* 85:6536–6543
- Liu S, Wollenberger U, Katterle M, Scheller FW (2006) Ferroceneboronic acid-based amperometric biosensor for glycosylated hemoglobin. *Sens Actuators B Chem* 113:623–629
- Tanaka T, Tsukube S, Izawa K, Okochi M, Lim TK, Watanabe S, Harada M, Matsunaga T (2007) Electrochemical detection of HbA_{1c}, a marker for diabetes, using a flow immunoassay system. *Biosens Bioelectron* 22:2051–2056
- Song SY, Han YD, Park YM, Jeong CY, Yang YJ, Kim MS, Ku Y, Yoon HC (2012) Biocatalytic detection of glycosylated hemoglobin (HbA_{1c}) based on the competitive binding of target and signaling glycoproteins to a boronate-modified surface. *Biosens Bioelectron* 35:355–362
- Song SY, Yoon HC (2009) Boronic acid-modified thin film interface for specific binding of glycosylated hemoglobin (HbA_{1c}) and electrochemical biosensing. *Sens Actuators B Chem* 140:233–239
- Zhou Y, Dong H, Liu L, Hao Y, Chang Z, Xu M (2015) Fabrication of electrochemical interface based on boronic acid-modified pyrroloquinoline quinone/reduced graphene oxide composites for

- voltammetric determination of glycosylated haemoglobin. *Biosens Bioelectron* 64:442–448
20. Haláček J, Wollenberger U, Stöcklein W, Scheller FW (2007) Development of a biosensor for glycosylated hemoglobin. *Electrochim Acta* 53:1127–1133
 21. Příbyl J, Skládal P (2005) Quartz crystal biosensor for detection of sugars and glycosylated hemoglobin. *Anal Chim Acta* 530:75–84
 22. Příbyl J, Skládal P (2006) Development of a combined setup for simultaneous detection of total and glycosylated haemoglobin content in blood samples. *Biosens Bioelectron* 21:1952–1959
 23. Adamczyk M, Chen YY, Johnson DD, Mattingly PG, Moore JA, Pan Y, Reddy RE (2006) Chemiluminescent acridinium-9-carboxamide boronic acid probes: application to a homogeneous glycosylated hemoglobin assay. *Bioorg Med Chem Lett* 16:1324–1328
 24. Liu JT, Chen LY, Shih MC, Chang Y, Chen WY (2008) The investigation of recognition interaction between phenylboronate monolayer and glycosylated hemoglobin using surface plasmon resonance. *Anal Biochem* 375:90–96
 25. Kiran MS, Itoh T, Yoshida KI, Kawashima N, Biju V, Ishikawa M (2010) Selective detection of HbA_{1c} using surface enhanced resonance Raman spectroscopy. *Anal Chem* 82:1342–1348
 26. Fang L, Li W, Zhou Y, Liu CC (2009) A single-use, disposable iridium-modified electrochemical biosensor for fructosyl valine for the glycosylated hemoglobin detection. *Sens Actuators B Chem* 137:235–238
 27. Stolowitz ML, Ahlem C, Hughes KA, Kaiser RJ, Kesicki EA, Li G, Lund KP, Torkelson SM, Wiley JP (2001) Phenylboronic acid-salicylhydroxamic acid bioconjugates. 1. A novel boronic acid complex for protein immobilization. *Bioconjugate Chem* 12:229–239
 28. Raistrick ID, Franceschetti DR, Macdonald JR (2005) In: Barsoukov E, Macdonald JR (eds) *Impedance spectroscopy: theory, experiment, and applications*. Wiley, New Jersey
 29. Park JY, Chang BY, Nam H, Park SM (2008) Selective electrochemical sensing of glycosylated hemoglobin (HbA_{1c}) on thiophene-3-boronic acid self-assembled monolayer covered gold electrodes. *Anal Chem* 80:8035–8044
 30. Hsieh KM, Lan KC, Hu WL, Chen MK, Jang LS, Wang MH (2013) Glycosylated hemoglobin (HbA_{1c}) affinity biosensors with ring-shaped interdigital electrodes on impedance measurement. *Biosens Bioelectron* 49:450–456
 31. Chuang YC, Lan KC, Hsieh KM, Jang LS, Chen MK (2012) Detection of glycosylated hemoglobin (HbA_{1c}) based on impedance measurement with parallel electrodes integrated into a microfluidic device. *Sens Actuators B Chem* 171:1222–1230
 32. Tanvir S, Pantigny J, Boulnois P, Pulvin S (2009) Covalent immobilization of recombinant human cytochrome CYP2E1 and glucose-6-phosphate dehydrogenase in alumina membrane for drug screening applications. *J Membr Sci* 329:85–90
 33. Deng J, Toh CS (2013) Impedimetric DNA biosensor based on a nanoporous alumina membrane for the detection of the specific oligonucleotide sequence of dengue virus. *Sensors* 13:7774–7785
 34. Tsai WT, Yang JM, Lai CW, Cheng YH, Lin CC, Yeh CW (2006) Characterization and adsorption properties of eggshells and eggshell membrane. *Bioresour Technol* 97:488–493
 35. Durmuş E, Celik I, Ozturk A, Ozkan Y, Aydin MF (2003) Evaluation of the potential beneficial effects of ostrich eggshell combined with eggshell membranes in healing of cranial defects in rabbits. *J Int Med Res* 31:223–230
 36. Yang JY, Chuang SS, Yang WG, Tsay PK (2003) Egg membrane as a new biological dressing in split-thickness skin graft donor sites: a preliminary clinical evaluation. *Chang Gung Med J* 26:153–159
 37. Xiao D, Choi MMF (2002) Aspartame optical biosensor with bienzyme-immobilized eggshell membrane and oxygen-sensitive optode membrane. *Anal Chem* 74:863–870
 38. Tang J, Liu Z, Kang J, Zhang Y (2010) Determination of salbutamol using R-phycoerythrin immobilized on eggshell membrane surface as a fluorescence probe. *Anal Bioanal Chem* 397:3015–3022
 39. Yeni F, Odaci D, Timur S (2008) Use of eggshell membrane as an immobilization platform in microbial sensing. *Anal Lett* 41:2743–2758
 40. Liu S, Wollenberger U, Haláček J, Leupold E, Stöcklein W, Warsinke A, Scheller FW (2005) Affinity interactions between phenylboronic acid-carrying self-assembled monolayers and flavin adenine dinucleotide or horseradish peroxidase. *Chem Eur J* 11:4239–4246
 41. Executive summary: standards of medical care in diabetes—2013 (2013) *Diabetes Care* 36:S4–S10
 42. Tan CK, Chen TW, Chan HL, Ng LS (1992) A scanning and transmission electron microscopic study of the membranes of chicken egg. *Histol Histopathol* 7:339–345
 43. Takiguchi M, Igarashi K, Azuma M, Ooshima H (2006) Flowerlike agglomerates of calcium carbonate crystals formed on an eggshell membrane. *Cryst Growth Des* 6:2754–2757
 44. Li N, Niu LN, Qi YP, Yiu CKY, Ryou H, Arola DD, Chen JH, Pashley DH, Tay FR (2011) Subtleties of biomineralisation revealed by manipulation of the eggshell membrane. *Biomaterials* 32:8743–8752
 45. Yan J, Springsteen G, Deeter S, Wang B (2004) The relationship among pK_a, pH, and binding constants in the interactions between boronic acids and diols—it is not as simple as it appears. *Tetrahedron* 60:11205–11209
 46. Li B, Lan D, Zhang Z (2008) Chemiluminescence flow-through biosensor for glucose with eggshell membrane as enzyme immobilization platform. *Anal Biochem* 374:64–70
 47. Zhang G, Liu D, Shuang S, Choi MMF (2006) A homocysteine biosensor with eggshell membrane as an enzyme immobilization platform. *Sens Actuators B Chem* 114:936–942
 48. Wu B, Zhang G, Shuang S, Choi MMF (2004) Biosensors for determination of glucose with glucose oxidase immobilized on an eggshell membrane. *Talanta* 64:546–553
 49. Choi MMF, Yiu TP (2004) Immobilization of beef liver catalase on eggshell membrane for fabrication of hydrogen peroxide biosensor. *Enzyme Microb Technol* 34:41–47
 50. Tembe S, Kubal BS, Karve M, D'Souza SF (2008) Glutaraldehyde activated eggshell membrane for immobilization of tyrosinase from *Amorphophallus compamulatus*: application in construction of electrochemical biosensor for dopamine. *Anal Chim Acta* 612:212–217
 51. Choi MMF, Pang WSH, Xiao D, Wu X (2001) An optical glucose biosensor with eggshell membrane as an enzyme immobilisation platform. *Analyst* 126:1558–1563
 52. Nys Y, Gautron J, Garcia-Ruiz JM, Hincke MT (2004) Avian eggshell mineralization: biochemical and functional characterization of matrix proteins. *CR Palevol* 3:549–562
 53. Bard AJ, Faulkner LR (2001) *Electrochemical methods: fundamentals and applications*. Wiley, New Jersey
 54. Sacks DB, Arnold M, Bakris GL, Bruns DE, Horvath AR, Kirkman MS, Lemmark A, Metzger BE, Nathan DM (2011) Guidelines and recommendations for laboratory analysis in the diagnosis and management of diabetes mellitus. *Diabetes Care* 34:e61–e99
 55. Bry L, Chen PC, Sacks DB (2001) Effects of hemoglobin variants and chemically modified derivatives on assays for glycohemoglobin. *Clin Chem* 47:153–163
 56. Jaisson S, Leroy N, Desroches C, Tonye-Libyh M, Guillard E, Gillery P (2013) Interference of the most frequent haemoglobin variants on quantification of HbA_{1c}: comparison between the LC-MS (IFCC reference method) and three routinely used methods. *Diabetes Metab* 39:363–369



Ultra-high performance liquid chromatographic determination of antioxidants in teas using inkjet-printed graphene–polyaniline electrode[☆]



Chayanee Bardpho^{a,b}, Poomrat Rattanarat^a, Weena Siangproh^c, Orawon Chailapakul^{a,b,*}

^a Electrochemistry and Optical Spectroscopy Research Unit (EOSRU), Department of Chemistry, Faculty of Science, Chulalongkorn University, Patumwan, Bangkok 10330, Thailand

^b Center of Excellence on Petrochemical and Materials Technology, Chulalongkorn University, Patumwan, Bangkok 10330, Thailand

^c Department of Chemistry, Faculty of Science, Srinakharinwirot University, Sukhumvit, Bangkok 10110, Thailand

ARTICLE INFO

Article history:

Received 27 February 2015

Received in revised form

30 April 2015

Accepted 7 May 2015

Available online 18 May 2015

Keywords:

UHPLC

Electrochemical detection

Inkjet-printing

Graphene

Polyaniline

Polyphenolic

Antioxidants

ABSTRACT

A development of ultra-high performance liquid chromatographic coupled with a novel inkjet-printed conductive ink-modified electrode for a fast and simultaneous determination of polyphenolic antioxidants was achieved. Two printing techniques were selected for fabrication and modification including (i) an in-house screen-printing method and (ii) an inkjet-printing method, respectively. A conductive ink containing graphene and polyaniline nanocomposite (G–PANI) was precisely casted onto the surface of screen-printed carbon electrode (SPCE) using a dimatix inkjet material printer. Compared to a bare SPCE, the G–PANI-modified screen-printed carbon electrode (G–PANI/SPCE) exhibited higher electrochemical sensitivity with increase (2–4 times) of peak current of each antioxidant. Moreover, four antioxidants were successfully separated and determined within 3 min using a reverse phase ultra-high performance liquid chromatography (UHPLC) with a mobile phase containing phosphate buffer and acetonitrile (90:10 v/v). Under an optimal detection potential at +1.2 V vs. Ag/AgCl, linear calibrations and limits of detection ($S/N=3$) for antioxidants were found to be 0.01–10 $\mu\text{g mL}^{-1}$ and 1.38–1.94 ng mL^{-1} , respectively. Finally, this proposed method has been successfully used for the determination of antioxidants in tea samples, the results obtained from our presented method were within a highly good agreement those obtained from a standard UHPLC–UV method.

© 2015 Elsevier B.V. All rights reserved.

1. Introduction

Tea is one of the most widely consumed beverages in the world. A commercial dried tea has been normally collected from tea leaves which a scientific name is *Camellia sinensis* from an Aceae family of the Theales order [1,2]. Tea consumption has linked with decreased risks including cancer, cardiovascular abnormalities, arthritis, and pathogenic infections [3]. A tea infusion provides numerous essential compounds for a human health such as polyphenolic antioxidants, caffeine, amino acids, vitamins, carbohydrates, and trace elements [4]. The conventional tea beverage contains a variety of major polyphenols

consisting of epicatechin (EC), epicatechin-3-gallate (ECG), epigallocatechin (EGC), epigallocatechin-3-gallate (EGCG), catechin (C), gallic acid (GA), and caffeic acid (CFA). To monitor a quality control of tea, a determination of these polyphenol contents in the tea as well as in the beverages is very important in the various research fields including nutritional and epidemiological studies. Therefore, it is necessary to develop an appropriate approach to determine the phenolic compounds simultaneously in tea samples to evaluate their qualities and health promoting properties.

Various conventional analytical methods for separation and simultaneous determination of polyphenolic antioxidants have been reported [5–7]. One of the remarkable technique to measure these antioxidants is high performance liquid chromatography (HPLC). However, the HPLC method provided the limitation in term of time-consuming which all separation and determination processes were longer than 30 min approximately [8,9]. To decrease the separation time for simultaneous measurement of polyphenolic antioxidants, ultra-high performance liquid chromatography (UHPLC) has become an interesting technique to produce high-throughput analysis

[☆] Selected papers presented at The 19th International Conference on Flow Injection Analysis and Related Techniques and Related Techniques, Fukuoka, Japan, November 30–December 5, 2014.

* Corresponding author at: Electrochemistry and Optical Spectroscopy Research Unit (EOSRU), Department of Chemistry, Faculty of Science, Chulalongkorn University, Patumwan, Bangkok 10330, Thailand.
Tel.: +66 2 218 7614; fax: +66 2 254 1309.

E-mail address: corawon@chula.ac.th (O. Chailapakul).

because of its fast analysis and high resolution [10,11]. For detection mode, an electrochemical detection offers high potential of interest. They can be used as a detector in the UHPLC system for the determination of varietal electroactive antioxidants [12–14]. Various electrode materials have been also applied to detect these electroactive polyphenolic compounds such as metal electrode (platinum electrode [15]), glassy carbon electrode (GCE) [16,17], carbon-paste electrode (CPE) [18] and screen-printed carbon electrode (SPCE) [19]. Among these electrode materials, SPCEs have been paid much interest due to its significantly low cost, disposability, and easy to couple with a thin-layer flow cell for the electrochemical detector in the flow-based system.

To enhance the electrochemical sensitivity of working electrode, the electrode modification has been a remarkable issue for current ongoing research. Several modification techniques have been applied such as simple drop-casting [20], electropolymerization [21,22], spin-coating [23,24], electrospraying [25] and electrospinning [26]. An inkjet printing has been demonstrated to be an attractive method for the electrode modification providing low cost, high production speed, selectivity, and compatibility with a wide range of materials and substrates. This technique is able to precisely deposit very small droplets of modifier in a picoliter level (2–12 pL) to prepare ultra-thin film onto the surface of substrate with a high production speed and a high pattern resolution [27–33]. For another strategy to improve the electrode surface area in the electrochemical system, an electrode modification using a noticeable nanomaterial has played an important role to enhance the electrochemical sensitivity of the sensors. Various kinds of nanomaterials have been used as an electrode modifier such as metallic nanoparticles (i.e. gold, silver, and platinum) [34], carbon-based nanoparticles (i.e. fullerene, single-wall carbon nanotube and multi-wall carbon nanotube) [35].

Currently, graphene (G) is a distinguished nanomaterial modifier which is highly useful for electroanalysis due to its very large two-dimensional electrical conductivity, and excellent electron transfer rate. However, the drawback of using G to modify electrode is agglomeration; therefore, to prevent this limitation of G, polyaniline (PANI) has been also used as an electrode modifier to improve the G distribution on the electrode surface. PANI is a versatile conducting polymer owing to its high electrical conductivity, thermal and chemical stability, simplicity to synthesize, and wide range of potential applications [36,37].

Such the benefits of G and PANI, in this work, we interested in the use of the inkjet printing technology to print the conductive G–PANI ink onto the SPCE. They would be an alternative way to enhance the electrochemical sensing and catalytic capabilities of the electrochemical detection in the UHPLC system.

Therefore, the aim of this work is to develop an outstanding inkjet-printed G–PANI-modified SPCE (G–PANI/SPCE) to use as a new electrochemical sensor for chromatographic determination of antioxidants in tea samples. The inkjet printing technology was applied to produce thin-film of G–PANI among on the surface of SPCE with high reproducibility. The physical and electrochemical properties of G–PANI/SPCE were then characterized. The optimal G–PANI/SPCE was coupled with the UHPLC system for amperometric and simultaneous determination of four antioxidants in teas.

2. Experimental

2.1. Reagents

HPLC-grade acetonitrile and methanol were obtained from Merck (Darmstadt, Germany). Graphene (G) was ordered from A.C. S (Medford, USA). Gallic acid (GA), (–)-epigallocatechin (EGC), (+)-catechin (C), caffeic acid (CFA), ortho-phosphoric acid 85%,

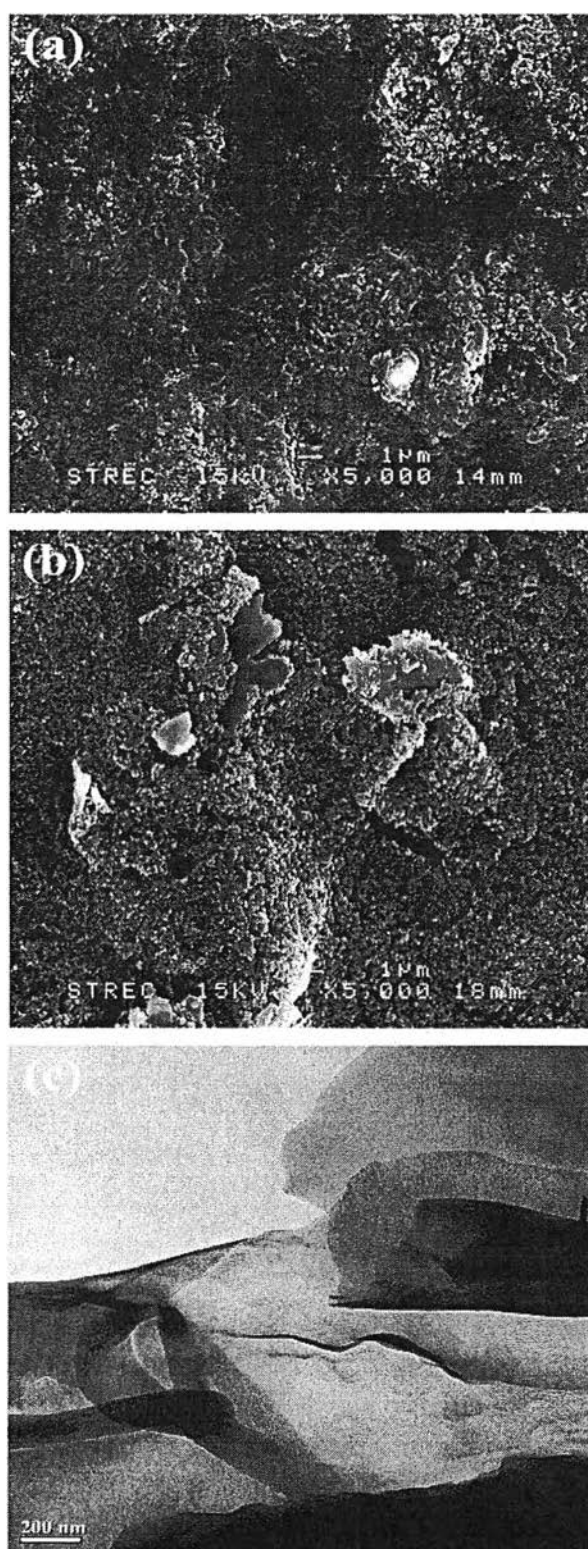


Fig. 1. SEM images of (a) bare SPCE and (b) inkjet-printed G–PANI/SPCE prepared by inkjet printing and (c) TEM image of G–PANI.

potassium dihydrogen phosphate (KH_2PO_4), polyaniline, camphor-10-sulfonic acid ($\text{C}_{10}\text{H}_{16}\text{O}_4\text{S}$) and N-methyl-2-pyrrolidone (NMP) were purchased from Sigma-Aldrich (St. Louis, USA). Milli-Q water from Millipore ($R \geq 18.2 \text{ M } \Omega \text{ cm}^{-1}$) was used to prepare buffers and stock standard solutions. Stock standard solutions of GA, EGC,

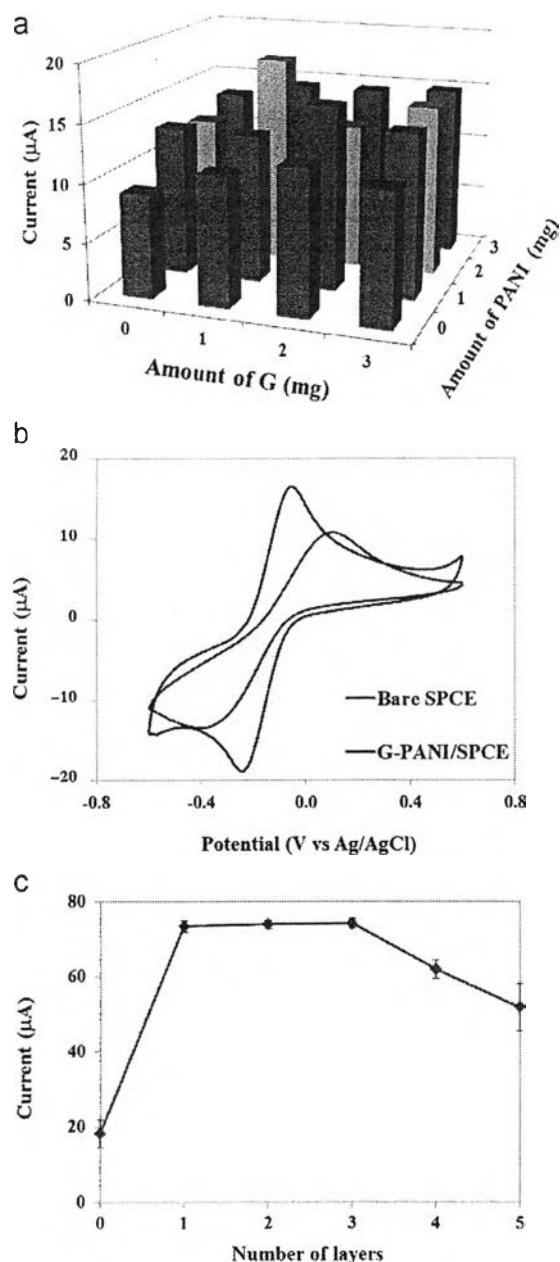


Fig. 2. (a) Comparison of oxidation current of the ratios between graphene and polyaniline. (b) cyclic voltammogram of 1 mM ferri(III)cyanide in 0.1 M KCl with scan rate 100 mV s^{-1} when compared G-PANI/SPCE with bare SPCE and (c) effect of number of inkjet-printed layer on anodic peak current of 1 mM gallic acid. (For interpretation of the references to color in this figure, the reader is referred to the web version of this article.)

C and CFA were prepared by dissolving each compound at a concentration of 1.0 mg mL^{-1} in phosphate buffer (pH 3). Stock solutions were stored at -4°C and resulted to be stable for a month. All solutions and solvents were filtered by $0.22 \mu\text{m}$ nylon membranes before to use in the UHPLC system.

2.2. Electrode fabrication and modification

A disposable screen-printed carbon electrode (SPCE) was fabricated using an in-house screen-printing method. Firstly, a carbon ink was screen-printed onto a polyethylene terephthalate (PET) substrate to form a working electrode pattern. A silver/silver

chloride (Ag/AgCl) was then printed as a conductive pad. The printed electrodes were baked in an oven at 65°C for 30 min to remove solvent and organic residues.

For the electrode modification procedure, an electrode modifier was initially prepared by a physical mixing between graphene (G) and polyaniline (PANI) solutions. Graphene powder (10 mg) was dispersed in 10 mL N-methyl-2-pyrrolidone (NMP). PANI solution was prepared by dissolving 20 mg of PANI (emeraldine base) and 25.8 mg of camphor-10-sulfonic acid ($\text{C}_{10}\text{H}_{16}\text{O}_4\text{S}$) in 10 mL of NMP. After that, the well-mixing PANI solution was stirred for 5 h. The solutions of G and PANI were mixed together and stirred for 1 h to produce conductive ink. After that, the mixture was centrifuged at 5000 rpm for 30 min and filtered at $0.43 \mu\text{m}$. The remaining conductive ink is ready to use for the inkjet-printing. The conductive G-PANI ink was loaded into a cartridge and printed onto the working electrode area of SPCE by using a piezoelectric Dimatix™ Materials Printer (DMP-2800, FUJIFILM Dimatix, Inc., Santa Clara, USA). The optimal inkjet printing conditions including drop spacing of $25 \mu\text{m}$ and a firing frequency of 17 V was chosen for applying a small droplet size of 10 pL on the SPCE surface. The inkjet-printed G-PANI/SPCE was heated in an oven at 120°C for 5 min to evaporate an organic solvent in the conductive ink.

2.3. Electrochemical measurement

Cyclic voltammetric experiments were performed on eDAQ (eDAQ Pty Ltd., Australia) with a standard three-electrode system. In this work, the working electrodes (WE) consisted of bare SPCE and G-PANI/SPCE. The platinum wire and Ag/AgCl electrodes were used as the auxiliary (AE) and reference electrodes (RE), respectively. Cyclic voltammetric responses of the standard solution such as 1 mM potassium ferri(III)cyanide ($\text{K}_3[\text{Fe}(\text{CN})_6]$) in 0.1 M KCl, $170.12 \mu\text{g mL}^{-1}$ gallic acid, $50.00 \mu\text{g mL}^{-1}$ epigallocatechin, $10.00 \mu\text{g mL}^{-1}$ catechin, and $180.16 \mu\text{g mL}^{-1}$ caffeic acid in 0.1 M phosphate buffer (pH 3):acetonitrile (90:10) were investigated at the scan rate of 100 mV s^{-1} .

2.4. UHPLC separation and electrochemical detection (UHPLC-ECD)

The UHPLC analysis was achieved using a UFLCXR (Shimadzu Corporation, Japan), comprising of a 20 ADXR solvent deliver unit, an auto sampler (SIL-20A) with 0.1–100 μL loop, an Kinetex™ core-shell C18 column (50 mm \times 4.6 mm i.d.; particle size, 2.6 μm , Phenomenex), a thin-layer flow cell (GL Science Inc.), and an amperometric detector. The thin-layer flow cell composed of a working G-PANI/SPCE, an auxiliary stainless steel electrode, and a reference Ag/AgCl electrode (Bioanalytical system Inc., USA). A 1 mm thick silicon rubber gasket was used as a vacancy in the flow cell for limiting the surface area of G-PANI/SPCE. The separation of four antioxidants was carried out with an isocratic elution consisting of 0.1 M phosphate buffer (pH 3): ACN (90:10 v/v) with an injection volume of 50 μL , flow rate of 0.8 mL min^{-1} , and an applied potential of +1.2 V vs. Ag/AgCl. For hydrodynamic voltammetry, the applied potential in the amperometric detection was examined in a range of 0.8–1.4 V vs. Ag/AgCl. The hydrodynamic voltammogram was plotted between peak current and applied potential. Limits of detection (LOD) and quantification (LOQ) were calculated from the $3\text{SD}_b/S$ and $10\text{SD}_b/S$, respectively, where SD_b is the standard deviation of blank ($n=10$), and S is the slope of the linearity. For the precision of intra-day and inter-day, five concentrations of antioxidants (1, 3, 5, 7, and 9 $\mu\text{g mL}^{-1}$) were examined for 3 times within a day and three different days. To validate this proposed method, UHPLC-ECD was compared to UHPLC coupled with ultra-violet detection (UHPLC-UV) using the same chromatographic conditions. Furthermore, the recovery was

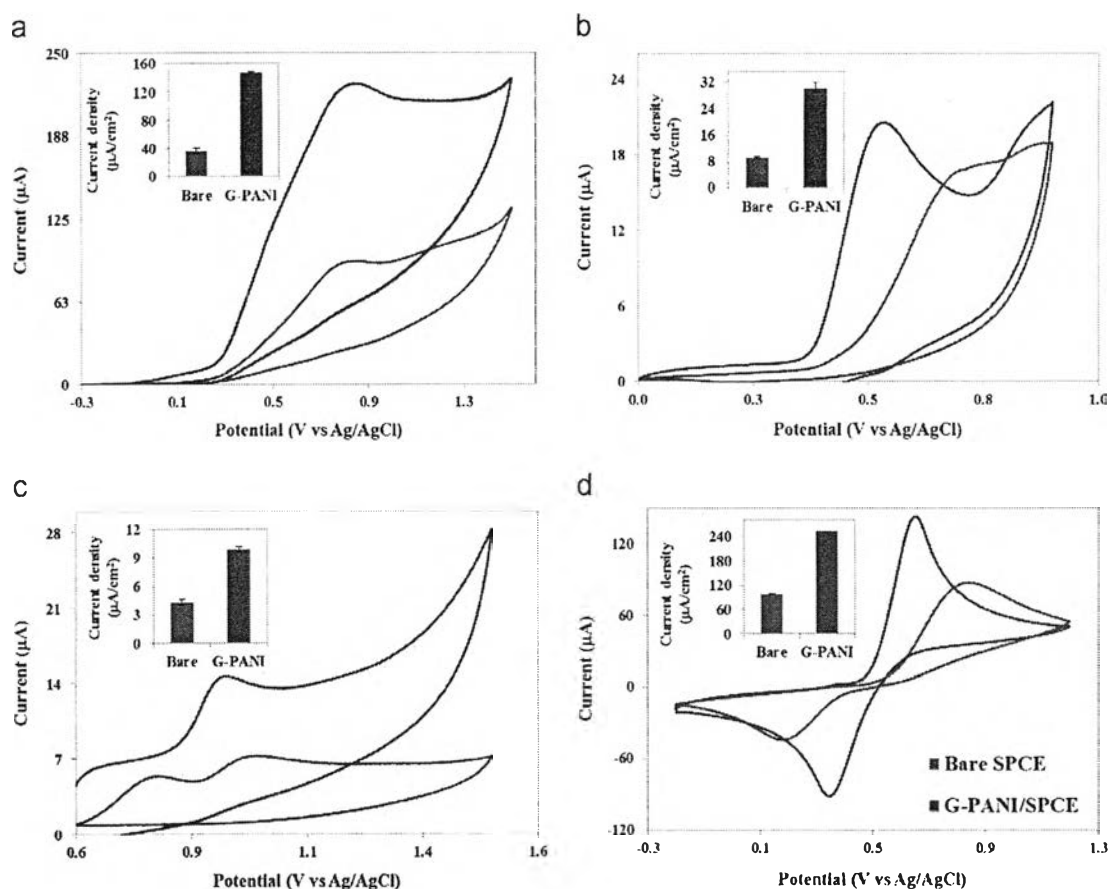


Fig. 3. Cyclic voltammogram of (a) 170.12 μg mL⁻¹ GA, (b) 50.00 μg mL⁻¹ ECG, (c) 10.00 μg mL⁻¹ C and (d) 180.16 μg mL⁻¹ CFA measured on the G-PANI/SPCE compared to the bare SPCE in the 0.1 M phosphate solution pH 3: acetonitrile (90:10) at a scan rate of 100 mV s⁻¹. (Inset) The comparison of oxidation current density between bare SPCE and G-PANI/SPCE vs. Ag/AgCl.

determined by spiking known antioxidant concentrations. The results obtained between the proposed UHPLC–ECD and the standard UHPLC–UV methods were compared.

2.5. Preparation of tea extracts

Dried tea leaves of 0.1 g were weighted and crushed with a mortar and pestle. The tea infusion was prepared by an extraction of tea leaves with 10 mL freshly hot water at 80 °C, and stirred with a magnetic stirrer bar for 10 min. Tea extracts were filtered through paper filters, then through 0.22 μm syringe filter and diluted with MilliQ grade water. Tea infusions were daily prepared and resulted to be stable over the experiment duration.

3. Results and discussion

3.1. Surface morphology of G-PANI/SPCE

The solution of G-PANI with a ratio of 1:2 was inkjet-printed onto the SPCE surface in order to form a thin layer of G-PANI nanomodifier on the surface. The morphology of G-PANI nanocomposite onto the SPCE surface was examined by a scanning electron microscope (SEM), and its image has been shown in Fig. 1. As shown in the SEM and TEM images, a well uniform dispersion of G-PANI nanocomposites was clearly observed on the SPCE surface with unprecedented number of G, leading to increase surface area of SPCE and thus improve electrochemical sensitivity of the modified SPCE.

3.2. Electrochemical characterization of G-PANI/SPCE

Influence of G:PANI ratio on a cyclic voltammetric response was initially investigated using 1 mM ferri(III)cyanide in 0.1 M KCl. The G:PANI modifier concentration in the different proportions was varied as shown in Fig. 2a. It was found that the anodic peak currents were related to the amount of G-PANI on the electrode surface. The G:PANI ratio of 1:2 provided the highest anodic peak current response, compared to other ratios. For higher ratio than 1:2, anodic peak currents decreased while the capacitive current (background current) increased. Thus, this ratio could be the optimal condition for electrode preparation. We believed that the decrease of redox peak current at higher ratio between G and PANI is due to the G agglomeration within the G-PANI modifier layer. Cyclic voltammetric behaviors of 1 mM ferri(III)cyanide were also measured using bare SPCE and G-PANI/SPCE. The comparison was shown Fig. 2b. Using G-PANI/SPCE, the well-defined anodic and cathodic peaks with an increase of peak current and a decrease of potential difference ($\Delta E = E_{p,a} - E_{p,c}$) were obtained. The ΔE_p of ferri/ferrocyanide measured on G-PANI/SPCE was found to be 0.19 V vs. Ag/AgCl (red solid line) while ΔE_p obtained from bare SPCE was found to be 0.42 V vs. Ag/AgCl (blue solid line). These results indicated that the proposed inkjet-printed G-PANI nanocomposites can increase the electron transfer kinetics for measurement.

Moreover, the electrochemical response of G-PANI/SPCE could be affected by the number of inkjet-printed G-PANI layers. The number of printed layer in the range of 0–5 layers was optimized as shown in Fig. 2c. The result shows that, when the number of

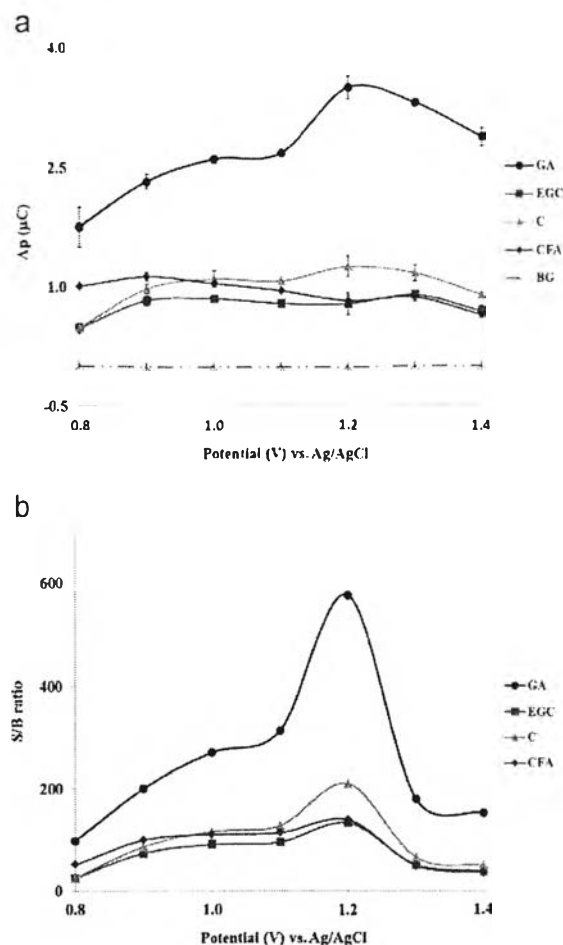


Fig. 4. (a) Hydrodynamic voltammetric results at the G-PANI/SPCE for a $1 \mu\text{g mL}^{-1}$ each mixture of antioxidants. (b) Hydrodynamic voltammogram of signal-to-background ratios. Conditions: the flow rate of 0.8 mL min^{-1} and injection volume of $50 \mu\text{L}$. Data are shown as the mean ± 1 SD derived from three independent repetitions.

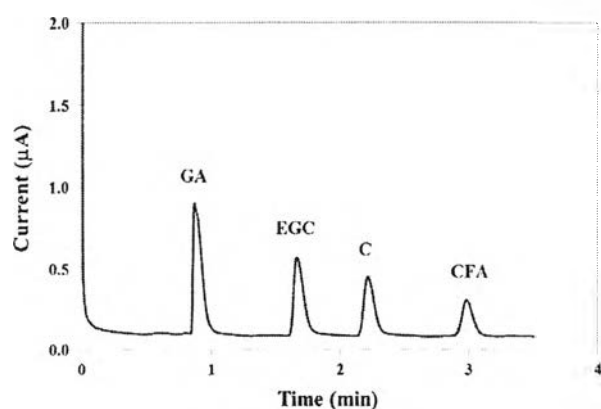


Fig. 5. UHPLC-ECD chromatogram of $1 \mu\text{g mL}^{-1}$ GA, EGC, C, and CFA in a mobile phase (0.1 M phosphate solution pH 3; acetonitrile (90:10)). Conditions: the optimal flow rate of 0.8 mL min^{-1} , applied potential of $+1.2 \text{ V vs. Ag/AgCl}$, and injection volume of $50 \mu\text{L}$.

layers increased from 0 to 2 layers, the current dramatically increased. Then over 3 printing layers, the current significantly decreased. We believed that the decrease of anodic current is due to the aggregation of excess G among on the SPCE surface. Therefore, the optimal number of printed layers was 2 layers.

Table 1

Linearity, limit of detection (LOD) and limit of quantitative (LOQ) of four antioxidants.

Analyte	Linear range ($\mu\text{g mL}^{-1}$)	Calibration equations	R^2	LOD (ng mL^{-1})	LOQ (ng mL^{-1})
GA	0.1–10	$y = 3.7314x - 0.1214$	0.9950	1.38	4.59
EGC	0.01–10	$y = 3.0202x - 0.2870$	0.9962	1.80	5.97
C	0.01–10	$y = 2.2018x - 0.2082$	0.9946	1.94	6.46
CFA	0.01–10	$y = 1.5108x - 0.1982$	0.9942	1.93	6.43

3.3. Electrochemical detection of antioxidants using G-PANI/SPCE

Using the optimized G-PANI/SPCE, cyclic voltammeteries of GA, EGC, C, and CFA were performed at scan rate of 100 mV s^{-1} as shown in Fig. 3. The well-defined irreversible peaks of GA, EGC, and C were observed while an obviously reversible peak of CFA was obtained. As expected, the cyclic voltammetric results showed that the proposed G-PANI/SPCE exhibited the higher current response and well-defined cyclic voltammograms when compared to those of bare SPCE. Compared between bare SPCE and G-PANI/SPCE, the peak potentials of EGC and CFA significantly shifted with the potential difference of 200 mV while the anodic peak potential of C slightly shifted with the potential difference of 50 mV approximately. From all results obtained, it is clearly seen that using G-PANI/SPCE can enhance the peak current around 2–4 times and the shift of peak potential can also increase. This indicated that the nanocomposite of G-PANI/SPCE provide the electrocatalysis toward the electrooxidation of all analytes. As results shown, it can be seen that the proposed electrode could be a promising and alternative choice of working electrode for sensitive detection of antioxidants due to inexpensive electrode material, simple fabrication, and high-throughput modification process of G-PANI/SPCE. Next, the inkjet-printed G-PANI/SPCE will be coupled with UHPLC separation system for simultaneous determination of four polyphenolic antioxidants.

3.4. Optimization of the detection potential

To optimize the detection potential of each polyphenolic antioxidant for the electrochemical detection in UHPLC system, hydrodynamic voltammetry was employed within a detection potential range of 0.8–1.4 V vs. Ag/AgCl as shown in Fig. 4. Hydrodynamic voltammetric curves, which displayed the peak area (A_p) of antioxidant and background, were significantly affected by each detection potentials. It is evident that the A_p of four antioxidants initially increased as the detection potential increased until the detection potential of $+1.2 \text{ V vs. Ag/AgCl}$. Thus, the detection potential of $+1.2 \text{ V}$ was chosen as optimal detection potential for amperometric detection of all four polyphenolic antioxidants, following their UHPLC separation.

3.5. UHPLC separation coupled with electrochemical detection (UHPLC-ECD)

In order to provide additional selective determination of antioxidant in tea, UHPLC systems coupled with G-PANI/SPCE was used for the separation and simultaneous detection of polyphenolic antioxidant. In this work, the reversed phase C18 column was selected for the separation of four antioxidants using the UHPLC-ECD system. The 0.1 M phosphate buffer solution pH 3 was selected because it offers the preferable separation and peak shapes. Moreover, the influence of acetonitrile percentage used in the mobile phase on the retention characteristics of polyphenolic antioxidants was investigated (data not shown). For 5% acetonitrile, the total elution time was higher than 10 min. Above 10%

Table 2
Comparison of recent report using different types of electrodes for electrochemical determination of antioxidants.

Modified electrode	Detection method	Analyte	LOD (ng mL ⁻¹)	Real sample	Refs.
Ru(bpy) ₃ ³⁺ modified Boron-doped diamond	Chronoam-perometry	C	35.12	–	[38]
Nickel(II) complex and 3-mercapto-propionic acid on a gold electrode	Square wave voltammetry	C	239.76	Green tea	[39]
Glassy carbon electrode	Amperometry	GA	2.21	Green tea, black tea	[40]
		C	6.74		
Pencil-graphite electrode	Differential pulse voltammetry	CFA	15.91	Tea	[41]
		EGC	0.37	Green tea, human plasma	[42]
Glassy carbon electrode	Amperometry	C	0.35	Green tea, white tea, oolong tea, black tea	This work
		GA	1.38		
		EGC	1.80		
		C	1.94		
Inkjet-printed G-PANI/SPCE	Amperometry	CFA	1.93		

Table 3
Content of polyphenol in tea samples.

Samples	Analyte	Amount found (mg g ⁻¹) (x ± SD)	
		UHPLC-ECD	UHPLC-UV
Black tea	GA	1.8442 ± 0.10	1.3073 ± 0.01
	EGC	0.0986 ± 0.02	0.1120 ± 0.01
	C	0.3215 ± 0.09	0.6047 ± 0.01
	CFA	0.4325 ± 0.04	0.4871 ± 0.01
White tea	GA	1.4032 ± 0.15	0.7030 ± 0.03
	C	2.5617 ± 0.02	2.0877 ± 0.37
	CFA	0.3851 ± 0.08	0.1703 ± 0.17
Oolong tea	GA	0.5750 ± 0.05	0.6690 ± 0.06
	C	0.6865 ± 0.06	0.5140 ± 0.57
	CFA	0.6828 ± 0.20	0.2661 ± 0.01
Green tea	GA	0.1516 ± 0.11	0.2325 ± 0.03
	C	0.4813 ± 0.15	0.5472 ± 0.04
	CFA	0.1522 ± 0.06	0.1966 ± 0.02
Paired two-tail test	t V alues	1.7318	
	t Critical	2.1788	

(v/v) acetonitrile, a shorter elution time was obtained, but low resolution and sensitivity were observed. Thus, a 0.1 M phosphate buffer pH 3 and acetonitrile in the ratio of 90:10 v/v was selected as the optimal mobile phase, resulting the proper resolution of sharp peaks with the high current response.

Using the optimized parameters, four antioxidants were completely separated within 3 min, and the high current responses were observed for all antioxidants as shown in the UHPLC chromatogram in Fig. 5. The retention time of GA, EGC, C and CFA was 0.8, 1.6, 2.2 and 2.9 min, respectively. It can be seen that this proposed UHPLC-ECD system provides not only rapid measurement but also high sensitivity for simultaneous determination of antioxidants.

3.6. Analytical performance

Linear regression analysis for the four polyphenolic antioxidants including GA, EGC, C, and CFA was performed. The A_p and concentration of polyphenolic antioxidants was subjected to linear regression analysis. The analytical performance of our UHPLC-ECD system (linear range, calibration equation, correlation coefficients (R^2), limit of detection (LOD), and limit of quantification (LOQ)) are summarized and reported in Table 1. Under the optimal conditions, the linear calibration of GA was found to be 0.1–10 $\mu\text{g mL}^{-1}$ while the linear calibrations of EGC, C, and CFA were 0.01–10 $\mu\text{g mL}^{-1}$. The linearity of the plots ($n=3$) is better than 0.994. Furthermore, the performance of the G-PANI/SPCE was compared to the other previous electrodes used for the determination of electroactive antioxidants as shown in Table 2. Our proposed UHPLC-ECD method provided a good linearity and

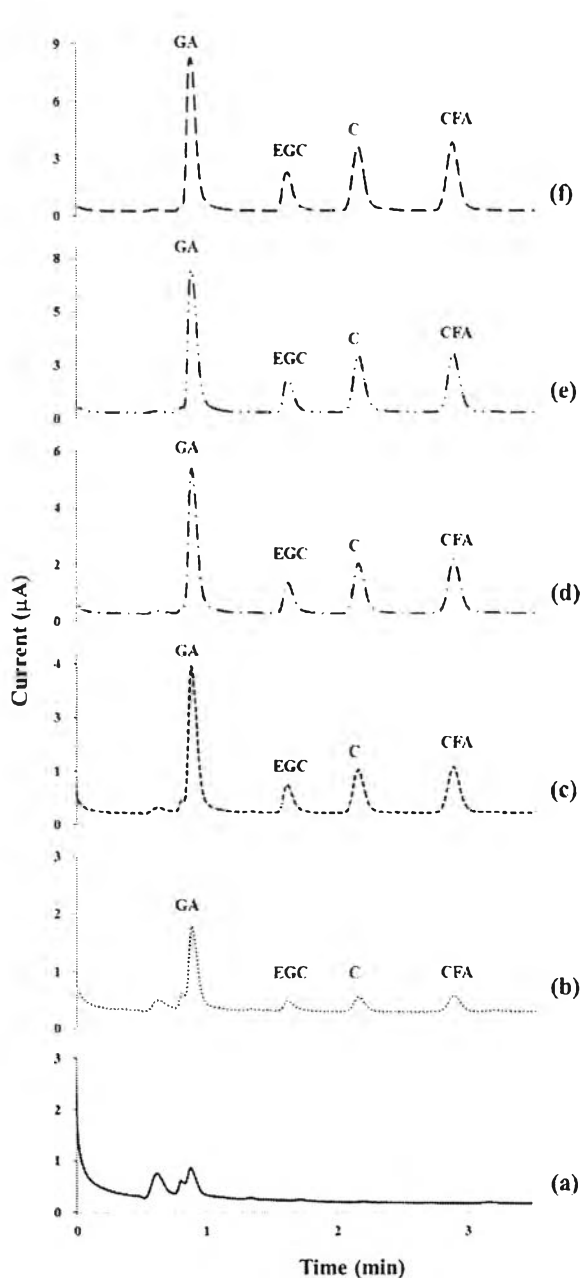


Fig. 6. UHPLC-ECD chromatograms of blank black tea sample (a) and black tea sample with spiked polyphenols concentration in the range of (b) 1, (c) 3, (d) 5, (e) 7 and (f) 9 $\mu\text{g mL}^{-1}$ measured on the G-PANI/SPCE under the optimal conditions.

comparable LODs. The LODs obtained from our proposed method are better than those obtained from previous reports [38–42]. It means that this proposed method can be further useful, sensitive, and rapid for the simultaneous determination of polyphenolic antioxidant in the tea samples.

3.7. Application in real samples

The antioxidants of interest in green tea, white tea, oolong tea and black tea were determined using the proposed method. Quantification of antioxidants was achieved by the standard addition method to investigate the reliability of this proposed system (Table 3). UHPLC–ECD chromatogram (Fig. 6) shows the peak current of four antioxidants in blank and in black tea sample that spiked each analyte at five concentrations (1, 3, 5, 7, and 9 $\mu\text{g mL}^{-1}$). To assess the precision of the method, the repeatability and reproducibility of the process was determined by calculating the relative standard deviation (RSD, $n=3$), and the accuracy was reported as the recovery percentage. Table S1 shows the intra-day and inter-day precision and recovery for the detection of antioxidants in all tea samples which obtained from the proposed method. These results indicated recovery percentages of GA, EGC, C, and CFA were in a range of 83.9–110.0% with RSDs < 5. Hence, this proposed method is an alternative for rapid separation and simultaneous determination of antioxidants in teas.

The proposed method was also validated by the standard method of UHPLC coupled with ultra-violet detection (UHPLC–UV). A paired *t*-test at 95% confidential interval was achieved on the results obtained by spiked three concentrations of standard GA, EGC, C and CFA (1, 5 and 9 $\mu\text{g mL}^{-1}$) in tea samples. The experimental *t*-values (*t* calculated) obtained by this novel method is 1.7318 and lower than critical *t*-values (2.1788). It can be concluded that there is no significant difference between UHPLC–ECD system and conventional UHPLC–UV method. Therefore, our proposed method is very useful and can be used as a new alternative assay for the determination of antioxidant compounds with highly sensitive and rapid analysis.

4. Conclusions

G–PANI conductive ink was modified on SPCE by inkjet printing for providing a superb electrochemical performance of electrode, leading to improve the sensitivity of the antioxidants detection in the UHPLC system. Four antioxidants were successfully separated and quantified within 3 min with good recovery and low LOD. The sensitivity, accuracy, and precision of our developed method were acceptable to measure the antioxidants. Therefore, this proposed method could be a new or an alternative and rapid method for the determination of antioxidants in tea samples.

Acknowledgments

The authors are grateful for the financial support from the Center of Excellence on Petrochemical and Materials Technology and the Thailand Research Fund through Research Team Promotion Grant (RTA5780005). We would also like to thank Nanoelectronics and MEMS Laboratory, National Electronics and Computer Technology Center (NECTEC) for preliminary use of inkjet printing equipment.

Appendix A. Supplementary material

Supplementary data associated with this article can be found in the online version at <http://dx.doi.org/10.1016/j.talanta.2015.05.020>.

References

- [1] Q. Chen, Z. Guo, J. Zhao, *J. Pharm. Biomed. Anal.* 48 (2008) 1321–1325.
- [2] M. Naldi, J. Fiori, R. Gotti, A. Périat, J.-L. Veuthey, D. Guilleme, V. Andrisano, *J. Pharm. Biomed. Anal.* 88 (2014) 307–314.
- [3] T. Yi, L. Zhu, W.-L. Peng, X.-C. He, H.-L. Chen, J. Li, T. Yu, Z.-T. Liang, Z.-Z. Zhao, H.-B. Chen, *IWT – Food Sci. Technol.* 62 (2015) 194–201.
- [4] M. Jeszka-Skowron, M. Krawczyk, A. Zgola-Gizeszkowiak, *J. Food Compos. Anal.* 40 (2015) 70–77.
- [5] P.A. Kilmartin, C.F. Hsu, *Food Chem.* 82 (2003) 501–512.
- [6] H.H.F. Koolen, F.M.A. da Silva, F.C. Gozzo, A.Q.L. de Souza, A.D.L. de Souza, *Food Res. Int.* 51 (2013) 467–473.
- [7] M.S. El-Shahawi, A. Hamza, S.O. Bahaffi, A.A. Al-Sibaai, T.N. Abduljabbar, *Food Chem.* 134 (2012) 2268–2275.
- [8] O. Kenny, T.J. Smyth, C.M. Hewage, N.P. Brunton, *Food Chem.* 141 (2013) 4295–4302.
- [9] J. Cheng, K. Weijun, L. Yun, W. Jiabo, W. Haitao, L. Qingmiao, X. Xiaoho, *J. Pharm. Biomed. Anal.* 53 (2010) 43–49.
- [10] Y. Foo Wong, A. Makahleh, B. Saad, M.N.M. Ibrahim, A. Abdul Rahim, N. Brosse, *Talanta* 130 (2014) 299–306.
- [11] P.V. Hung, D.W. Hatcher, W. Barker, *Food Chem.* 126 (2011) 1896–1901.
- [12] K. Narumi, J.-I. Sonoda, K. Shiotani, M. Shigeru, M. Shibata, A. Kawachi, E. Tomishige, K. Sato, T. Motoya, *J. Chromatogr. B* 945–946 (2014) 147–153.
- [13] S. Magiera, I. Baranowska, A. Lautenszleger, *J. Pharm. Biomed. Anal.* 102 (2015) 468–475.
- [14] N. Thammasoontaree, P. Rattananat, N. Ruecha, W. Siangproh, N. Rodthongkum, O. Chailapakul, *Talanta* 123 (2014) 115–121.
- [15] C. Bianchini, A. Curulli, M. Pasquali, D. Zane, *Food Chem.* 156 (2014) 81–86.
- [16] D. Vega, I. Aguil, A. González-Cortés, P. Yáñez-Sedeño, J.M. Pingarrón, *Talanta* 71 (2007) 1031–1038.
- [17] J. Piljac-Zegarac, L. Valek, T. Stipčević, S. Martinez, *Food Chem.* 121 (2010) 820–825.
- [18] P. Mailley, E.A. Cummings, S. Mailley, S. Cosnier, B.R. Eggins, E. McAdams, *Bioelectrochemistry* 63 (2004) 291–296.
- [19] F. Matemadombo, C. Apetrei, T. Nyokong, M.L. Rodríguez-Méndez, J.A. de Saja, *Sens. Actuators B: Chem.* 166–167 (2012) 457–466.
- [20] C.W. Foster, J. Pillay, J.P. Metters, C.E. Banks, *Sensors* 14 (2014) 21905–21922.
- [21] P. Najafisayar, M.E. Bahrololoom, *Electrochim. Acta* 114 (2013) 462–473.
- [22] D.K. Ariyanayagamkumarappa, I. Zhitomirsky, *Synth. Met.* 162 (2012) 868–872.
- [23] J.C. Arrebola, Á. Caballero, L. Hernán, M. Melero, J. Morales, E.R. Castellón, *J. Power Sources* 162 (2006) 606–613.
- [24] M.B. Sahana, C. Sudakar, C. Thapa, G. Lawes, V.M. Naik, R.J. Baird, G.W. Auner, R. Naik, K.R. Padmanabhan, *Mater. Sci. Eng. B* 143 (2007) 42–50.
- [25] N. Ruecha, R. Rangkupan, N. Rodthongkum, O. Chailapakul, *Biosens. Bioelectron.* 52 (2014) 13–19.
- [26] N. Promphet, P. Rattananat, R. Rangkupan, O. Chailapakul, N. Rodthongkum, *Sens. Actuators B: Chem. Part A* 207 (2015) 526–534.
- [27] C. Karuwan, C. Sriprachubwong, A. Wisitsoraat, D. Phokharatkul, P. Sritongkham, A. Tuantranont, *Sens. Actuators B: Chem.* 161 (2012) 549–555.
- [28] T.C. Gomes, C.J.L. Constantino, E.M. Lopes, A.E. Job, N. Alves, *Thin Solid Films* 520 (2012) 7200–7204.
- [29] W. Kit-Anan, A. Olarnwanich, C. Sriprachubwong, C. Karuwan, A. Tuantranont, A. Wisitsoraat, W. Srituravanich, A. Pimpin, *J. Electroanal. Chem.* 685 (2012) 72–78.
- [30] A. Määttä, U. Vanamo, P. Ihalainen, P. Pulkkinen, H. Tenhu, J. Bobacka, J. Peltonen, *Sens. Actuators B: Chem.* 177 (2013) 153–162.
- [31] A. Morrin, O. Ngamna, E. O'Malley, N. Kent, S.F. Moulton, G.G. Wallace, M. R. Smyth, A.J. Killard, *Electrochim. Acta* 53 (2008) 5092–5099.
- [32] M. Schneider, A. Türke, W.-J. Fischer, P.A. Kilmartin, *Food Chem.* 159 (2014) 428–432.
- [33] T. Öhlund, J. Ortegren, S. Forsberg, H.-E. Nilsson, *Appl. Surf. Sci.* 259 (2012) 731–739.
- [34] K. Charoenkitamorn, O. Chailapakul, W. Siangproh, *Talanta* 132 (2015) 416–423.
- [35] A. Lesch, F. Cortés-Salazar, M. Prudent, J. Delobel, S. Rastgar, N. Lion, J.-D. Tissot, P. Tacchini, H.H. Girault, *J. Electroanal. Chem.* 717–718 (2014) 61–68.
- [36] Z. Stempien, T. Rybicki, E. Rybicki, M. Kozanecki, M.I. Szykowska, *Synth. Met.* 202 (2015) 49–62.
- [37] Y. Xu, I. Hennig, D. Freyberg, A. James Strudwick, M. Georg Schwab, T. Weitz, K. Chih-Pei Cha, *J. Power Sources* 248 (2014) 483–488.
- [38] J. Wu, H. Wang, L. Fu, Z. Chen, J. Jiang, G. Shen, R. Yu, *Talanta* 65 (2005) 511–517.
- [39] S.K. Moccellini, S.C. Fernandes, T.P. de Camargo, A. Neves, I.C. Vieira, *Talanta* 78 (2009) 1063–1068.
- [40] I. Novak, M. Šeruga, Š. Komorsky-Lovrić, *Food Chem.* 122 (2010) 1283–1289.
- [41] I.G. David, A.-M.C. Bizgan, D.E. Popa, M. Buleandra, Z. Moldovan, I.A. Badea, T.A. Tekiner, H. Basaga, A.A. Ciucu, *Food Chem.* 173 (2015) 1059–1065.
- [42] A. Kotani, K. Takahashi, H. Hakamata, S. Kojima, F. Kusu, *Anal. Sci.* 23 (2007) 157–163.



Graphene/polyvinylpyrrolidone/polyaniline nanocomposite-modified electrode for simultaneous determination of parabens by high performance liquid chromatography

Suphunnee Kajornkavinkul^a, Eakkasit Punrat^a, Weena Siangproh^b,
Nadnudda Rodthongkum^c, Narong Praphairaksit^a, Orawon Chailapakul^{a,*}

^a Electrochemistry and Optical Spectroscopy Research Unit, Department of Chemistry, Faculty of Science, Chulalongkorn University, Phayathai Road, Patumwan, Bangkok 10330, Thailand

^b Department of Chemistry, Faculty of Science, Srinakharinwirot University, Sukumvit 23 Road, Wattana, Bangkok 10110, Thailand

^c Metallurgy and Materials Science Research Institute, Chulalongkorn University, Phayathai Road, Patumwan, Bangkok 10330, Thailand

ARTICLE INFO

Article history:

Received 26 February 2015

Received in revised form

14 May 2015

Accepted 18 May 2015

Available online 21 May 2015

Keywords:

Parabens

Graphene/polyvinylpyrrolidone/polyaniline nanocomposite

Electrospraying

Simultaneous determination

High performance liquid chromatography

ABSTRACT

A nanocomposite of graphene (G), polyvinylpyrrolidone (PVP) and polyaniline (PANI) modified onto screen-printed carbon electrode (SPCE) using an electrospraying technique was developed for simultaneous determination of five parabens in beverages and cosmetic products by high performance liquid chromatography. PVP and PANI were used as the dispersing agents of graphene, and also for the enhancement of electrochemical conductivity of the electrode. The electrochemical behavior of each paraben was investigated using the G/PVP/PANI nanocomposite-modified SPCE, compared to the unmodified SPCE. Using HPLC along with amperometric detection at a controlled potential of +1.2 V vs Ag/AgCl, the chromatogram of five parabens obtained from the modified SPCE exhibits well defined peaks and higher current response than those of its unmodified counterpart. Under the optimal conditions, the calibration curves of five parabens similarly provide a linear range between 0.1 and 30 $\mu\text{g mL}^{-1}$ with the detection limits of 0.01 $\mu\text{g mL}^{-1}$ for methyl paraben (MP), ethyl paraben (EP) and propyl paraben (PP), 0.02 and 0.03 $\mu\text{g mL}^{-1}$ for isobutyl paraben (IBP) and butyl paraben (BP), respectively. Furthermore, this proposed method was applied for the simultaneous determination of five parabens in real samples including a soft drink and a cosmetic product with satisfactory results, yielding the recovery in the range of 90.4–105.0%.

© 2015 Elsevier B.V. All rights reserved.

1. Introduction

Parabens (alkyl esters of p-hydroxybenzoic acid) have been widely used for a long time as antimicrobial preservatives in beverages, foods, pharmaceutical products and especially cosmetic products because of their biodegradability, stability, efficiency in wider pH range, non-volatility and other properties such as low cost and no color [1,2]. When the length of alkyl chain increases, the antimicrobial activities of the parabens increase while its water solubility decreases. Moreover, two or more parabens can often be used together to achieve synergistic effects [3,4]. However, high dose of these compounds are dangerous for customers because they can cause allergic contact dermatitis [5,6]. In addition, they can produce inhibitory effects on mitochondrial respiratory capacity, and eliminate the human reproductive

potential [7–9], as well as promote breast cancer [10,11]. Therefore, the use of parabens has been limited by the European Economic Community (EEC), i.e. the maximum concentration allowed in cosmetics is 0.4% (w/w) for single paraben and up to 0.8% (w/w) for their mixtures, and the maximum thresholds of paraben concentration in foodstuffs and pharmaceutical products are 0.1% (w/w) and 1% (w/w), respectively [12,13].

Various analytical methods have been utilized for the determination of parabens, for instance, UV-spectroscopy coupled with high performance liquid chromatography (HPLC) [14–16], flame ionization detection in gas chromatography (GC) [17], and mass spectrometry (MS) [11,18]. Electrochemical detection (ECD) is an alternative and very attractive detection method for the determination of parabens because of its low cost, simplicity, fast analysis, portability and high sensitivity. A variety of working electrodes have been established for the detection of parabens, including molecularly imprinted polymers (MIPs) film on glassy carbon electrode [19], boron doped-diamond (BDD) electrode [20] and multi-wall carbon nanotubes (MWNTs) coupled with nafion

* Corresponding author.

E-mail address: corawon@chula.ac.th (O. Chailapakul).

modified glassy carbon electrode [21]. In this work, screen-printed carbon electrode (SPCE) was chosen as the working electrode due to its inexpensiveness and ease of preparation and modification. However, a bare SPCE may be limited by its inadequate sensitivity. To improve the sensitivity, nanomaterials such as carbon nanotubes (CNTs), carbon nanofibers (CNFs) and carbon nanodots (CNDs) have been employed to modify the working electrodes and increase its surface area [22–24].

Graphene (G) is a monolayer, crystalline allotrope of carbon which is densely packed in a regular sp^2 -bonded atom into a two dimensional honeycomb lattices. Graphene has been widely studied in different fields due to its excellent physical and chemical properties. Recently, graphene has been adopted as a popular nanomaterial in electrochemistry because it exhibits many desirable electrochemical properties such as large surface area, high electrical conductivity and rapid electron transfer [25–27]. Despite these numerous advantages, the uncontrolled agglomeration of graphene due to attractive Van der Waals forces can occur and result in inhomogeneity. Therefore, polyaniline (PANI) and polyvinyl pyrrolidone (PVP) were additionally used to increase the dispersion of graphene. PANI is an outstanding conducting polymer that is widely used for electrode modification in electrochemical biosensors because of its excellent electrochemical properties, ease of synthesis and functionalization, high environmental stability, and low toxicity [28,29]. Meanwhile, it has been reported that PVP can stabilize graphene at high concentration by dispersing it in any organic solvent [30].

Recently, there has been reported that G/PVP/PANI nanocomposite-modified, paper-based biosensor was successfully developed for the determination of cholesterol in a complex biological fluid [31]. In addition, G/PANI nanocomposite-modified SPCE was also effectively coupled with ultra-performance liquid chromatography (UPLC) system for determination of eight sulfonamides (SAs) in shrimp. The sensitivity of eight SAs was higher than the unmodified electrode including BDD electrode [32].

In this research, therefore, G/PVP/PANI nanocomposite-modified SPCE was fabricated and used as the working electrode of electrochemical detection coupled with HPLC. Electro spraying technique was chosen as the fabrication means because of its simplicity, homogeneity of droplets and cost efficiency. The coupled devices were utilized for simultaneous determination of five parabens with satisfactory results. This proposed method is simple and inexpensive hence it can be an alternative approach for sensitive determination of parabens in soft drinks and cosmetic products.

2. Experimental

2.1. Chemicals and materials

All solutions were prepared by dilution with ultra-purified deionized ($R \geq 18.2 \text{ M}\Omega \text{ cm}^{-1}$), Milli-Q water (Merck Millipore, Germany). Stock standard solutions of five parabens ($1000 \mu\text{g mL}^{-1}$), namely methyl paraben (MP), ethyl paraben (EP), propyl paraben (PP), butyl paraben (BP) (Sigma-Aldrich, USA) and isobutyl paraben (IBP) (Tokyo Chemical Industry, Japan), were prepared in Milli-Q water: acetonitrile (1:1, v/v). The standard working solutions were diluted from these stock solutions to the desired concentrations.

In HPLC, all solutions were filtered through $0.22 \mu\text{m}$ Nylon membrane filter paper (Vertical Chromatography Co., Ltd, Thailand). The mobile phase was a mixture of buffer solution and acetonitrile (60:40, %v/v). The buffer solution was 0.05 M phosphate buffer prepared from potassium dihydrogen phosphate (KH_2PO_4 ; Carlo Erba Reagenti-SDS, France) and di-sodium

hydrogen phosphate (Na_2HPO_4 ; Merck, Germany), and then precisely adjusted to the desired pH with ortho-phosphoric acid (85%) and sodium hydroxide (NaOH) (Merck, Germany).

2.2. Instruments

Cyclic voltammetry was carried out by a potentiostat (CHI 1232A, CHI Instrument, USA) with three-electrode system; a G/PVP/PANI nanocomposite-modified screen-printed carbon electrode as working electrode, silver/silver chloride (Ag/AgCl) as reference electrode, and platinum wire as counter electrode. Electrochemical measurement was performed in a home-made cell at room temperature.

An HPLC system (Shimadzu LC-20AD XR UFLC Shimadzu, Japan) with a chromatographic column of Luna $5 \mu\text{m}$ C18 column ($150 \text{ mm} \times 4.6 \text{ mm}$ i.d.) from Phenomenex (CA, USA) was used. A thin-layer flow cell (GL Sciences, Inc., USA) was assembled to the HPLC as a detection unit which was comprised of three electrodes; a G/PVP/PANI-modified SPCE working electrode, a Ag/AgCl reference electrode (Bioanalytical System, Inc., USA) and a stainless steel tube counter electrode.

2.3. Fabrication of G/PVP/PANI nanocomposite-modified SPCE

SPCEs used in this research were produced in our laboratory by a screen-printing technique. First, Ag/AgCl ink (Gwent group, United Kingdom) was printed onto a PVC substrate as an electrical connector and then dried in an oven at $55 \text{ }^\circ\text{C}$ for 1 h. After that, carbon ink (Gwent group, United Kingdom) was printed as an active area of working electrode and dried in an oven under the same condition.

For the modification of SPCE, a G/PVP/PANI nanocomposite solution was sprayed onto the SPCE by the electro spraying technique. The conditions used including flow rate, the distance between the needle and the ground collector, and applying voltage were 1.0 mL min^{-1} , 5 cm, and 9 kV, respectively [31]. Twenty milligrams of graphene nanopowder (SkySpring Nanomaterials, Inc., USA) and 20 mg of PVP (Sigma-Aldrich, USA) were dispersed in 10 mL of dimethylformamide (DMF) and sonicated for 6 h at room temperature. Next, PANI was doped with camphor-10-sulfonic acid (CSA) to make it conductive and subsequently dissolved in chloroform [28]. The G/PVP/PANI nanocomposite solution was then prepared by mixing of a dispersed graphene solution and a doped PANI solution with a ratio of 1:1 v/v.

2.4. Electrochemical measurement

The electrochemical characteristic of G/PVP/PANI nanocomposite-modified SPCE was investigated by cyclic voltammetry (CV) of ferri/ferrocyanideredox couple. CV was also used for the study of electrochemical behavior of each concerned paraben in 0.05 M phosphate buffer solution (pH 6) on the G/PVP/PANI modified SPCE. The potential range of CV was scanned from -0.6 V to $+1.0 \text{ V}$ for ferri/ferrocyanide and $+0.4 \text{ V}$ to $+1.3 \text{ V}$ for parabens with a scan rate of 100 mV s^{-1} .

A mixture of five parabens was separated by HPLC using 0.05 M phosphate buffer (pH 6):acetonitrile (60:40, %v/v) as mobile phase, flow rate of 1.5 mL min^{-1} , and injection volume of $50 \mu\text{L}$. The resulting chromatograms were obtained with amperometry with an applied constant potential of $+1.2 \text{ V}$ vs Ag/AgCl at room temperature ($\sim 25 \text{ }^\circ\text{C}$).

2.5. Analysis of real samples

The developed method was applied for the determination of five parabens in a soft drink sample and a cosmetic product

(makeup remover). One milliliter of sample was extracted with 2.5 mL of methanol. The solution was sonicated in an ultrasonic bath for 15 min. Prior to the sample injection, the extracted samples were filtered through 0.22 μm Nylon membrane filters (Vertical Chromatography Co., Ltd, Thailand), spiked (if no parabens were present) and analyzed by the proposed technique.

3. Results and discussion

3.1. Characterization of G/PVP/PANI nanocomposite-modified SPCE

Firstly, the morphology of the G/PVP/PANI nanocomposite on the electrode surface was investigated by scanning electron microscopy (SEM) Fig. 1(A) shows the SEM image presenting a uniform distribution of the homogeneous nanocomposites on the SPCE surface. Furthermore, the transmission electron microscopy (TEM) image, shown in Fig. 1(B), indicated that the dispersed graphene did not agglomerate.

In this work, the electrochemical characterization of G/PVP/PANI nanocomposite-modified SPCEs was initially investigated using ferri/ferrocyanide redox couple. The resulting cyclic voltammograms are shown in Fig. 2(A). It was observed that the cyclic

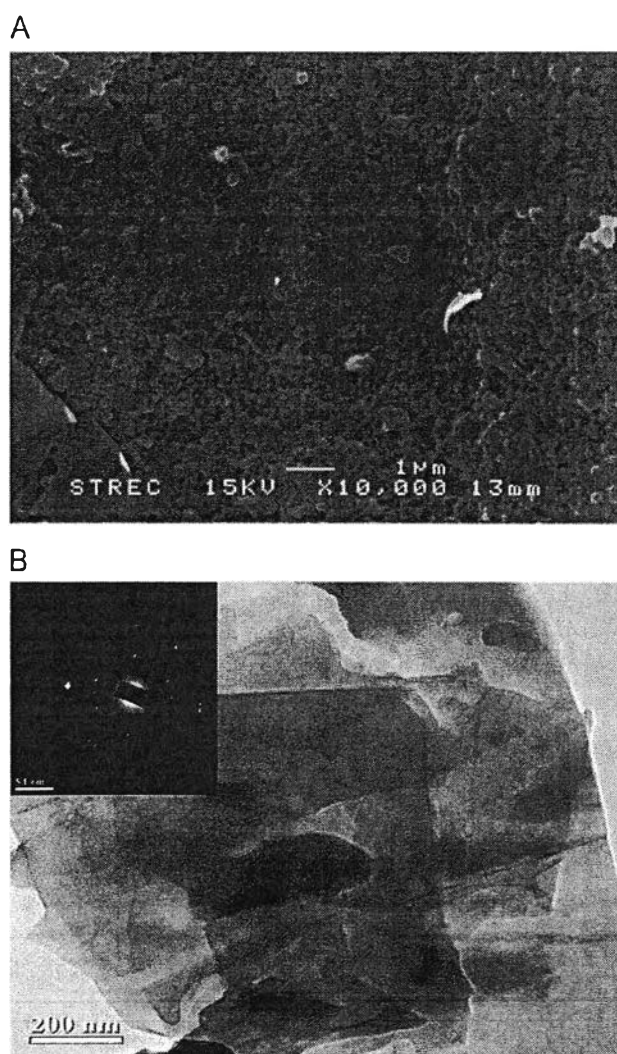


Fig. 1. SEM image (A) and TEM image (B) with the electron diffraction pattern of graphene (inset picture) of the G/PVP/PANI nanocomposite-modified SPCE.

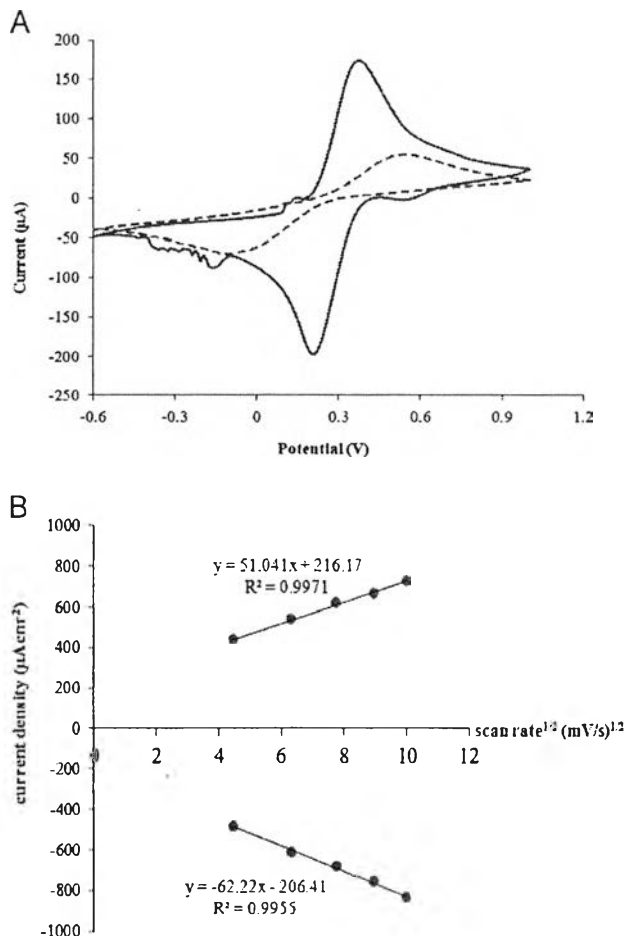


Fig. 2. (A) Cyclic voltammograms of 1 mM ferri/ferrocyanide redox couple in 0.5 M KCl on the G/PVP/PANI nanocomposite-modified SPCE (solid line) and the unmodified SPCE (dashed line).

(B) The relationship between square root of the potential scan rate and cathodic and anodic peak current density for electrochemical characterization of the G/PVP/PANI nanocomposite-modified SPCE.

voltammogram exhibited a well-defined peak shape illustrating the kinetic of electron transfer process on the G/PVP/PANI nanocomposite-modified SPCE. In addition, the oxidation peak at +0.15 V and the reduction peak at around -0.6 to -0.2 V and +0.5 V derived from the modified electrode using G/PVP/PANI nanocomposite were usually found in the cyclic voltammogram. However, there is no overlapping from these peaks with the target analytes. The response current of ferri/ferrocyanide obtained from G/PVP/PANI nanocomposite-modified SPCE was remarkably higher than those of the unmodified SPCE. It indicates that the proposed modified electrode could be very useful for electroanalysis applications. In addition, to investigate the mass transfer process of the modified electrode, the potential scan rates of CV in the ferri/ferrocyanide solution were varied in the range of 20 to 100 mV s^{-1} , and the currents were measured. The relationship between the anodic and cathodic peak currents, and the square root of scan rate were linear as shown in Fig. 2(B). It was verified that the mass transfer process of G/PVP/PANI nanocomposite-modified SPCE was controlled by the diffusion process.

3.2. Electrochemical behavior of parabens

The electrochemical behaviors of five parabens in each single standard solution were investigated in 0.05 M phosphate buffer (pH 6) on the G/PVP/PANI nanocomposite-modified SPCE

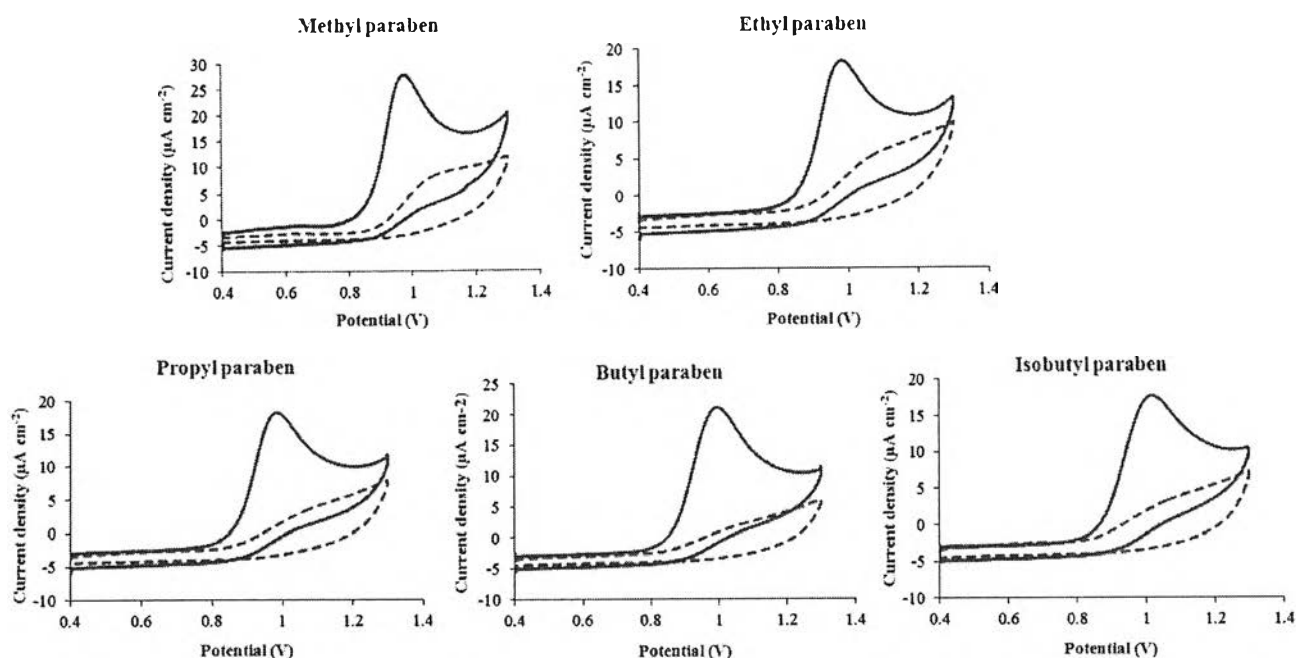


Fig. 3. Typical cyclic voltammograms of each single standard solution ($10 \mu\text{g mL}^{-1}$) of the five parabens in phosphate buffer solution (pH 6) on G/PVP/PANI nanocomposite-modified SPCE (solid line) and the unmodified SPCE (dashed line); potential scan rate of 100 mV s^{-1} .

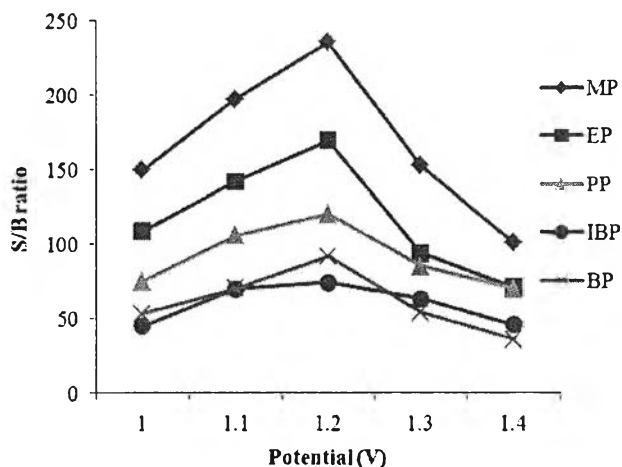


Fig. 4. Hydrodynamic voltammogram signal-to-background ratios at G/PVP/PANI nanocomposite-modified SPCE of $10 \mu\text{g mL}^{-1}$ parabens in 0.05 M phosphate buffer solution (pH 6):acetonitrile (60:40, %v/v).

compared with the unmodified SPCE by CV technique. The cyclic voltammograms in Fig. 3 show that all five parabens presented the anodic peaks with the irreversible reaction, and the peak currents of each paraben obtained by the modified SPCE were approximately between 3–8 times higher than those using the unmodified

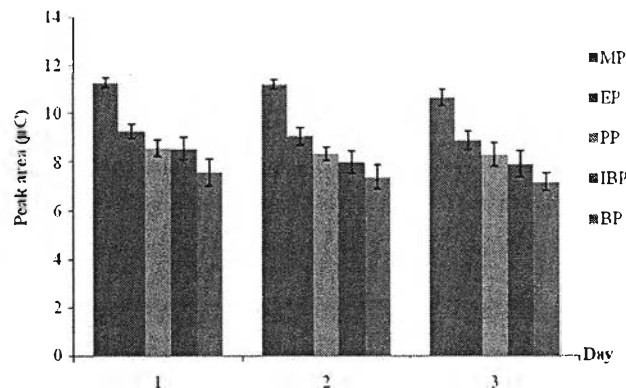


Fig. 5. The inter-day study of $10 \mu\text{g mL}^{-1}$ of five parabens in 0.05 M phosphate buffer solution (pH 6):acetonitrile (60:40, %v/v) on G/PVP/PANI nanocomposite-modified SPCE.

electrode. Furthermore, the five parabens were oxidized at a similar anodic peak potential of about +1.0 V vs Ag/AgCl.

3.3. Ratio of mobile phase

Prior to the investigation of the mobile phase ratio, pH value of phosphate buffer solution were examined in the range of 4–8. The phosphate buffer solution pH 6 was found to be the most

Table 1

Summary of analytical performances of the proposed method (HPLC-ECD) using G/PVP/PANI nanocomposite-modified SPCE for the simultaneous determination of five parabens ($n=3$).

Analyte	Linear range				LOD ($\mu\text{g mL}^{-1}$)	LOQ ($\mu\text{g mL}^{-1}$)
	Linearity ($\mu\text{g mL}^{-1}$)	Slope ($\mu\text{C mL } \mu\text{g}^{-1}$)	Y-intercept (μC)	R^2		
Methyl paraben	0.1–30	0.1665 ± 0.0112	0.0732 ± 0.0249	0.9923–0.9960	0.01	0.04
Ethyl paraben	0.1–30	0.1138 ± 0.0110	0.0341 ± 0.0195	0.9934–0.9984	0.01	0.04
Propyl paraben	0.1–30	0.0725 ± 0.0084	0.0254 ± 0.0115	0.9958–0.9997	0.01	0.04
Isobutyl paraben	0.1–30	0.0357 ± 0.0086	0.0256 ± 0.0116	0.9954–0.9996	0.02	0.06
Butyl paraben	0.1–30	0.0333 ± 0.0078	0.0221 ± 0.0085	0.9948–0.9994	0.03	0.10

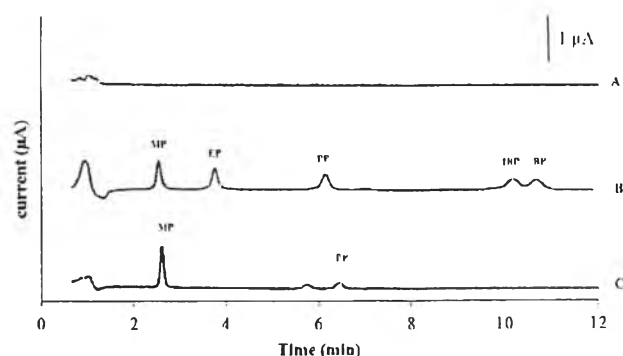


Fig. 6. Chromatograms of five parabens in real samples, a soft drink sample (A), a soft drink sample spiked with $5 \mu\text{g mL}^{-1}$ parabens (B) and a cosmetic product sample (C), in the mobile phase of 0.05 M phosphate buffer solution (pH 6):acetonitrile (60:40, %v/v).

beneficial for paraben detection. Using HPLC with C18 packed column in an isocratic system for the simultaneous determination of five parabens, the ratio of mobile phase between 0.05 M phosphate buffer solution (pH 6) and acetonitrile was examined by varying percentages of acetonitrile in the range of 35–55% (v/v). It was found that the separation time was longer than 15 min when the percentage of acetonitrile was lower than 40%. Faster separation was achieved by increasing the percentage of acetonitrile; however, the peaks of the isomeric compounds of BP and IBP were not resolved when the percentage of acetonitrile was above 45% (S1). Therefore, the ratio between 0.05 M phosphate buffer (pH 6) and acetonitrile of 60:40 (%v/v) was chosen as optimal for the mobile phase for further experiments.

3.4. Hydrodynamic voltammetry

Hydrodynamic voltammetry was utilized for the optimization of applied potential to determine five parabens. The applied potentials were examined from +1.0 to +1.4 V vs Ag/AgCl. The ratios of oxidation peak currents and background currents (S/B) of five parabens continually increased when higher potentials were applied; however, the S/B significantly decreased when the potentials above +1.2 V were applied partly due to the increasing background currents (shown in Fig. 4). The potential of +1.2 V vs Ag/AgCl was clearly the optimal applied potential and hence was adopted for the simultaneous determination of five parabens with amperometric detection.

Table 2

Summarized results of the simultaneous determination of five parabens in real samples by the proposed method (HPLC-ECD) using the G/PVP/PANI nanocomposite-modified SPCE, compared with the traditional standard method (HPLC-UV).

Sample	Analyte	Spiked ($\mu\text{g mL}^{-1}$)	Found ($\mu\text{g mL}^{-1}$)		Recovery (%)		t-Value of the two method ($t_{\text{critical (95\% CI)}} = 2.3060$)
			HPLC-ECD	HPLC-UV	HPLC-ECD	HPLC-UV	
Soft drink	MP	–	ND	ND	–	–	–
	EP	–	ND	ND	–	–	–
	PP	–	ND	ND	–	–	–
	IBP	–	ND	ND	–	–	–
	BP	–	ND	ND	–	–	–
Soft drink	MP	5	4.52 ± 0.31	4.78 ± 0.28	90.4	95.6	1.39
	EP	5	5.10 ± 0.39	4.82 ± 0.28	102.0	96.4	1.30
	PP	5	5.13 ± 0.32	4.87 ± 0.27	102.6	97.4	1.39
	IBP	5	5.25 ± 0.32	4.91 ± 0.24	105.0	98.2	1.90
	BP	5	4.92 ± 0.42	4.90 ± 0.25	98.4	98.0	0.09
	MP	–	498.67 ± 16.62	504.00 ± 5.25	–	–	0.68
Cosmetic	EP	–	–	–	–	–	–
	PP	–	134.60 ± 16.62	134.75 ± 11.81	–	–	0.02
	IBP	–	–	–	–	–	–
	BP	–	–	–	–	–	–

3.5. Analytical performance

Under the optimal conditions, the calibration curves obtained for various concentrations of five parabens, were established. Key analytical from these measurements were summarized in Table 1. The calibration curves of five parabens were linear in similarly equal range of 0.1 and $30 \mu\text{g mL}^{-1}$ with the coefficients of determination (R^2) of higher than 0.99 ($n=3$). The limit of detection (LOD) and the limit of quantitation (LOQ) were calculated from $3S_b/S$ and $10S_b/S$, respectively, where S_b is the standard deviation of repeated blank measurements ($n=10$) and S is the slope of the calibration curve. LOD and LOQ of five parabens were found to be in the range of $0.01\text{--}0.03 \mu\text{g mL}^{-1}$ and $0.04\text{--}0.10 \mu\text{g mL}^{-1}$, respectively.

The intra-day precision of 30 measurements was evaluated to ascertain the stability of this proposed method. It was found that the obtained peak currents did not significantly change in repeated measurements with the relative standard deviation (RSD) in the range of 3.42–7.20% for all five parabens. In addition, the inter-day precision was also investigated for 3 days with the same electrode. It was found that the modified electrode can be used more than 3 days because the sensitivity did not significantly change as shown in Fig. 5.

3.6. Analysis of real samples

Eventually, the proposed method using the G/PVP/PANI nanocomposite-modified SPCE coupled with HPLC was applied to simultaneously detect five parabens in real samples. A soft drink and a cosmetic product were selected as a model of sample because they were reported to have a chance to contaminate with parabens.

The chromatogram in Fig. 6(A) of the soft drink sample apparently showed no sign of any paraben. Therefore, the soft drink sample was spiked with standard parabens at a concentration of $5 \mu\text{g mL}^{-1}$ to investigate the accuracy of this proposed method from the recovery by the standard addition method and the typical chromatogram of the spiked sample is shown in Fig. 6(B). The peaks of MP, BP, PP, IBP and BP were obtained at the retention times of 2.5, 3.7, 6.0, 10.0 and 10.5 min, respectively. The recovery was in the range of 90.4–105.0% for five parabens which is well within the acceptance range of the Association of Official Analytical Chemists (AOAC) recommended values (80–115% recovery for $10 \mu\text{g mL}^{-1}$ of analyte concentration).

For the cosmetic product, the chromatogram in Fig. 6(C) reveals

peaks of MP and PP at the retention times of 2.6 and 6.4 min, respectively. The remaining peak at retention time of 5.7 min is an unknown electrochemically active specie in the cosmetic sample. To investigate accuracy, the results of this proposed method (HPLC-ECD) using the G/PVP/PANI nanocomposite-modified SPCE were then compared to those obtained from a standard traditional method, HPLC-UV. The student's *t*-test was used to evaluate the two different methods. The calculated *t*-values obtained were smaller than the *t*-critical value, indicating that there is no significant difference between the proposed method and the HPLC-UV method at a confidence interval (CI) of 95%. The summary of real samples analyses is shown in Table 2.

4. Conclusion

A novel G/PVP/PANI nanocomposite-modified SPCE for the simultaneous determination of five parabens using HPLC was successfully developed. The SPCE is inexpensive and easy to modify. The G/PVP/PANI nanocomposite solution was sprayed onto the SPCE resulting in the increase in sensitivity of the electrode. The homogeneous and well distributed G/PVP/PANI on SPCE was demonstrated. The determination of five parabens by the modified electrode exhibited higher sensitivity than that of the conventional electrode. The modified electrode was not only easy to prepare but also readily coupled with HPLC for simultaneous determination of five parabens. The separation was completed in 12 min. In addition, the proposed method has been successfully applied to analyze beverages and cosmetic products with good agreement to the HPLC-UV method.

Acknowledgments

The authors are grateful for the financial support from the Thailand Research Fund (RTA5780005), The Thai Government Stimulus Package 2 (TKK2555), under the Project for Establishment of Comprehensive Center for Innovative Food, Health Products and Agriculture, Chulalongkorn University and the National Research University Project of CHE and Ratchadaphiseksomphot Endowment Fund of Chulalongkorn University (RES560530040-AM), and the 90th Anniversary of Chulalongkorn University Fund. E. Punrat also thanks Ratchadaphiseksomphot Endowment Fund, Chulalongkorn University for Postdoctoral Fellowship.

Appendix A. Supplementary material

Supplementary data associated with this article can be found in the online version at <http://dx.doi.org/10.1016/j.talanta.2015.05.044>.

References

- [1] R. Hájková, P. Solich, M. Pospíšilová, J. Šícha, *Anal. Chim. Acta* 467 (2002) 91–96.
- [2] S. Ho Kang, H. Kim, *J. Pharm. Biomed.* 15 (1997) 1359–1364.
- [3] P.E. Mahuzier, K.D. Altria, B.J. Clark, *J. Chromatogr. A* 924 (2001) 465–470.
- [4] K.-I. Kuo, Y.-Z. Hsieh, *J. Chromatogr. A* 768 (1997) 334–341.
- [5] M.G. Soni, I.G. Carabin, G.A. Burdock, *Food. Chem. Toxicol.* 43 (2005) 985–1015.
- [6] P. Furrer, J.M. Mayer, R. Gurny, *Eur. J. Pharm. Biopharm.* 53 (2002) 263–280.
- [7] R.S. Tavares, F.C. Martins, P.J. Oliveira, J. Ramalho-Santos, F.P. Peixoto, *Reprod. Toxicol.* 27 (2009) 1–7.
- [8] F. Martins, A. Margarida, M.M. Oliveira, P.J. Oliveira, F.P. Peixoto, *Biochim. Biophys. Acta* 1777 (2008) S60–S61.
- [9] J.G. Chen, K.C. Ahn, N.A. Gee, S.J. Gee, B.D. Hammock, B.L. Lasley, *Toxicol. Appl. Pharmacol.* 221 (2007) 278–284.
- [10] G. Shanmugam, B.R. Ramaswamy, V. Radhakrishnan, H. Tao, *Microchem. J.* 96 (2010) 391–396.
- [11] X.Y. Ye, A.M. Bishop, L.L. Needham, A.M. Calafat, *Anal. Chim. Acta* 622 (2008) 150–156.
- [12] D. Casoni, I.A. Tuhutiu, C. Sarbu, J. Liq. Chromatogr. Relat. Technol. 34 (2011) 805–816.
- [13] M.G. Soni, G.A. Burdock, S.L. Taylor, N.A. Greenberg, *Food. Chem. Toxicol.* 39 (2001) 513–532.
- [14] B. Saad, M.F. Bari, M.I. Saleh, K. Ahmad, M.K.M. Talib, *J. Chromatogr. A* 1073 (2005) 393–397.
- [15] P.D. Tzanavaras, T.D. Karakosta, P.G. Rigas, D.G. Themelis, A. Zotou, *Cent. Eur. J. Chem.* 10 (2012) 1459–1463.
- [16] W.H. Gao, C. Legido-Quigley, *J. Chromatogr. A* 1218 (2011) 4307–4311.
- [17] J. Lopez-Darias, V. Pino, Y.J. Meng, J.L. Anderson, A.M. Alfonso, *J. Chromatogr. A* 1217 (2010) 7189–7197.
- [18] B. Albero, R.A. Perez, C. Sanchez-Brunete, J.L. Tadeo, *J. Hazard. Mater.* 239 (2012) 48–55.
- [19] Y. Wang, Y.H. Cao, C. Fang, Q.Q. Gong, *Anal. Chim. Acta* 673 (2010) 145–150.
- [20] I. Martins, F.C. Carreira, L.S. Canaes, F.A.D. Campos, L.M.D. Cruz, S. Rath, *Talanta* 85 (2011) 1–7.
- [21] P.L. Luo, J. Liu, Y.M. Li, Y.R. Miao, B.X. Ye, *Anal. Lett.* 45 (2012) 2445–2454.
- [22] L. Wang, X.Y. Wang, G.S. Shi, C. Peng, Y.H. Ding, *Anal. Chem.* 84 (2012) 10560–10567.
- [23] N. Rodthongkum, N. Ruecha, R. Rangkupan, R.W. Vachet, O. Chailapakul, *Anal. Chim. Acta* 804 (2013) 84–91.
- [24] H. Dai, G.F. Xu, L.S. Gong, C.P. Yang, Y.Y. Lin, Y.J. Tong, J.H. Chen, G.N. Chen, *Electrochim. Acta* 80 (2012) 362–367.
- [25] K.S. Novoselov, A.K. Geim, S.V. Morozov, D. Jiang, Y. Zhang, S.V. Dubonos, I. V. Grigorieva, A.A. Firsov, *Science* 306 (2004) 666–669.
- [26] K.P. Loh, Q.L. Bao, P.K. Ang, J.X. Yang, *J. Mater. Chem.* 20 (2010) 2277–2289.
- [27] D. Li, R.B. Kaner, *Science* 320 (2008) 1170–1171.
- [28] Y.J. Shin, J. Kameoka, *J. Ind. Eng. Chem.* 18 (2012) 193–197.
- [29] C. Dhand, M. Das, M. Datta, B.D. Malhotra, *Biosens. Bioelectron.* 26 (2011) 2811–2821.
- [30] A.S. Wajid, S. Das, F. Irin, H.S.T. Ahmed, J.L. Shelburne, D. Parviz, R.J. Fullerton, A.F. Jankowski, K.C. Hedden, M.J. Green, *Carbon* 50 (2012) 526–534.
- [31] N. Ruecha, R. Rangkupan, N. Rodthongkum, O. Chailapakul, *Biosens. Bioelectron.* 52 (2014) 13–19.
- [32] N. Thammasoontaree, P. Rattanasat, N. Ruecha, W. Siangproh, N. Rodthongkum, O. Chailapakul, *Talanta* 123 (2014) 115–121.



Electrochemically reduced graphene oxide-modified screen-printed carbon electrodes for a simple and highly sensitive electrochemical detection of synthetic colorants in beverages



Sakda Jampasa^a, Weena Siangproh^b, Kiattisak Duangmal^c, Orawon Chailapakul^{d,e,*}

^a Program in Petrochemistry, Faculty of Science, Chulalongkorn University, Pathumwan, Bangkok 10330, Thailand

^b Department of Chemistry, Faculty of Science, Srinakharinwirot University, Bangkok 10110, Thailand

^c Department of Food Technology, Faculty of Science, Chulalongkorn University, Pathumwan, Bangkok 10330, Thailand

^d Electrochemistry and Optical Spectroscopy Research Unit, Department of Chemistry, Faculty of Science, Chulalongkorn University, Pathumwan, Bangkok 10330, Thailand

^e Nanotec-CU Center of Excellent on Food and Agriculture, Chulalongkorn University, Phayathai Road, Patumwan, Bangkok 10330, Thailand

ARTICLE INFO

Article history:

Received 20 April 2016

Received in revised form

1 July 2016

Accepted 3 July 2016

Available online 5 July 2016

Keywords:

Electrochemically reduced graphene oxide (ERGO)

Tartrazine (TZ)

Sunset yellow (SY)

Screen-printed carbon electrode (SPCE)

Electrochemical detection

ABSTRACT

A simple and highly sensitive electrochemical sensor based on an electrochemically reduced graphene oxide-modified screen-printed carbon electrode (ERGO-SPCE) for the simultaneous determination of sunset yellow (SY) and tartrazine (TZ) was proposed. An ERGO film was coated onto the electrode surface using a cyclic voltammetric method and then characterized by scanning electron microscopy (SEM). In 0.1 M phosphate buffer at a pH of 6, the two oxidation peaks of SY and TZ appeared separately at 0.41 and 0.70 V, respectively. Surprisingly, the electrochemical response remarkably increased approximately 90- and 20-fold for SY and TZ, respectively, using the modified electrode in comparison to the unmodified electrode. The calibration curves exhibited linear ranges from 0.01 to 20.0 μ M for SY and from 0.02 to 20.0 μ M for TZ. The limits of detection were found to be 0.50 and 4.50 nM (at $S/N=3$) for SY and TZ, respectively. Furthermore, this detection platform provided very high selectivity for the measurement of both colorants. This electrochemical sensor was successfully applied to determine the amount of SY and TZ in commercial beverages. Comparison of the results obtained from this proposed method to those obtained by an in-house standard technique proved that this developed method has good agreement in terms of accuracy for practical applications. This sensor offers an inexpensive, rapid and sensitive determination. The proposed system is therefore suitable for routine analysis and should be an alternative method for the analysis of food colorants.

© 2016 Elsevier B.V. All rights reserved.

1. Introduction

With the beginning of a new era in the food industry, more food additives have been introduced to aid in food preservation and processing. The use of food additives has also been proven to extend the shelf-life and/or enhance the food quality and texture [1]. However, these food additives can only be incorporated in certain food products, and they must fall within a specified dosage as well as have a justified purpose. A food additive overdose is considered as food adulteration, as these foods possess toxicity or lack any technical-functional purpose. Therefore, the use of food additives in the food industry requires ethical consideration [2].

Food colorants, either synthetic or in a natural form, are

normally used as food additives to enhance consumer acceptance. Sunset yellow (SY, E110) and tartrazine (TZ, E102), classified as azo dyes, are common synthetic colorants that are extensively employed in the food industry due to their low production cost, charming color uniformity and excellent water solubility as well as their high stability to light, oxygen and pH [3–5]. However, they can cause detrimental effects to health when they are excessively consumed. In recent studies, extensive consumption of SY and TZ was found to significantly decrease the thymus weight and alter the monocyte counts as well as induce allergic responses including contact urticaria, angioneurotic edema, asthma, contact anaphylaxis and immunosuppression in humans [6,7]. Because they are harmful to human health, the use of colorants as food additives is strictly controlled by laws and regulations. The maximum acceptable content by the international and national legislation is 100 μ g/mL when they are employed individually or in

* Corresponding author.

E-mail address: corawon@chiula.ac.th (O. Chailapakul).

combination [8]. The European University Association and some European countries such as Finland and Norway have already excluded these colorants and consider them to be carcinogenic agents [9]. According to Thai Food Act B. E. 2547, notification 281, colorants are not permitted to be incorporated into many food categories such as pickled/osmosed fruit, fresh-cut fruit, processed meat, smoked meat and dried meat. Yet, some manufacturers illegally incorporate these substances into their products. The presence of colorants in food samples indicates that some food producers lack responsibility and ethics, and it also indicates that these colorants are still widely used in foods beyond the use permitted by rules and regulations [10].

Various techniques have been developed and applied over the last few decades for the examination of SY and TZ. Currently, the most widely used techniques for the determination of colorants are spectrophotometry [11], high performance liquid chromatography (HPLC) [12], column chromatography [13], and capillary electrophoresis [14]. Nevertheless, the first two aforementioned techniques have some disadvantages. In particular, these two techniques exhibit low sensitivity and specificity, require expertise, are time-consuming, and require instrumentation that is complicated as well as expensive. Therefore, a detection method that offers a short analysis time, a simple and low cost process, high sensitivity and high selectivity is still in demand and important for food safety and human health.

Different electrochemical methods for the simultaneous determination of SY and TZ in commercial beverages have been reported. The high sensitivity, small sample volume requirement, low cost, simplicity, short analysis time and portability are the key requirements of a detection method. Various types of electrodes have been employed to successfully fabricate a sensor that allowed simultaneous measurement of SY and TZ. Examples of such electrodes include a pretreated boron-doped diamond electrode, a graphene phosphotungstic-modified glassy carbon electrode (GN-PTA/GCE), a graphene TiO₂-modified GCE (GN-TiO₂/GCE), a gold nanoparticle-modified carbon paste electrode (Au NPs/CPE), a multi-walled carbon nanotubes-modified GCE (MWCNT/GCE) and a platinum wire-coated electrode [15–20]. Unfortunately, these electrodes are non-disposable and rather expensive to use for the routine analysis of food colorants. Therefore, a critical step towards routine analysis is the development of a disposable sensor that simultaneously detects SY and TZ without compromising the electrochemical sensitivity and selectivity.

Graphene, a single sheet of carbon atoms settled in a honeycomb lattice, has recently received research interest due to its potential in improving the conductivity of the modified sensor. It has been applied in many applications, especially in the electrochemical field. Graphene-modified electrochemical sensors have been reported in the detection of phytohormones, biomolecules, pharmaceuticals, food additives and environmental pollutants [21–25]. However, it was found that graphene tends to form irreversible agglomerates through strong π - π stacking and Van der Waals interactions, which restricts its application and storage [26].

Chemically synthesized graphene has been considered to be a new substitute for graphene because of its similar characteristics and ease of synthesis. Synthetic graphene is usually obtained from reduced graphite oxide prepared via Hummers's method, followed by reducing the ultrasonically exfoliated graphene oxide (GO) with hydrazine [27]. An alternative method reported for the preparation of graphene involves reacting sodium metal and ethanol, followed by thermal exfoliation and reduction of the GO intermediate [28]. Although a simpler method for graphene synthesis has been reported, preparation of a graphene solution for further electrode modification is troublesome. Recently, the GO intermediate has received intense research interest due to its convenience in storage and fast dissolution in water without any

dispersing agents. However, among these reduction methods, both chemical and physical reduction of an intermediate still possess some disadvantages because of the toxicity of reducing agents, expense and several steps in the reduction process.

Recently, an environmentally friendly electrochemical reduction of GO with controllable size and thickness has been reported. This technique is an attractive alternative method for the reduction of GO to obtain a graphene sheet due to its simple instrumental setup. Moreover, it also offers easy preparation, cost-effectiveness and non-toxicity. The electrochemical reduction of GO film (ERGO) obtained by employing this technique can enhance the large specific surface area and electrochemical conductance of the electrochemical sensor, thus improving the analytical performance [29].

An electrochemical sensor for the simultaneous determination of SY and TZ using an electrochemically reduced graphene oxide-modified screen-printed carbon electrode (ERGO-SPCE) has not yet been reported. Therefore, the main objective of this work is to propose a simple and highly sensitive electrochemical sensor based on an ERGO-SPCE to use as a novel method for the determination of SY and TZ. A green and facile routine electrochemical reduction method was employed to produce an ERGO film onto the electrode surface in one step. This disposable SPCE employed was inexpensively and easily prepared. Analytical parameters, such as the sensitivity, selectivity and reproducibility, were also investigated. This developed electrochemical sensor was also applied to quantify the amounts of SY and TZ in practical samples to validate the performance of the developed sensor.

2. Experimental

2.1. Chemicals and apparatus

Graphite powder (mesh size < 100 μm) was purchased from Sigma Aldrich (CA, USA). Carbon ink and silver/silver chloride were purchased from Acheson (CA, USA). The screen-printed block was made by Chaiyaboon Co. Ltd. (Bangkok, Thailand). Analytical grade diethylene glycol monobutyl ether and ethylene glycol monobutyl ether acetate, as binder solution in the ink preparation step, and other analytical grade reagents were purchased from Merck (CA, USA). Food grade, sunset yellow (batch: 21,023) and tartrazine (batch: 20,633) standard samples were obtained from BRENNTAG Co. Ltd. (Bangkok, Thailand). Graphene oxide (GO) was purchased from XF Nano, Inc. (Nanjing, China).

All electrochemical measurements were performed on a PGSTAT 30 potentiostat (Metrohm Siam Co. Ltd.) and controlled with the general purpose electrochemical system (GPES) software (Utrecht, Netherlands). A disposable screen-printed carbon electrode (SPCE) was fabricated using an in-house screen-printing method. All measurements were conducted using a differential pulse voltammetric method at room temperature (25 °C). The surface morphologies of the unmodified and modified electrode were verified using scanning electron microscopy (SEM). The presence of the ERGO film on the electrode surface was monitored employing infrared spectroscopy (IR).

For the analysis employing compendium of method, used in parallel with the proposed approach to confirm the accuracy and acceptability of method, the system consisted of a pump (Model CM 3200), UV-vis detector (absorbance at 235 nM, model SM 3200), C18 column (250 mm \times 4.6 mm i.d.; particle size, 5 μm , Phenomenex). The separation was carried out with an isocratic elution consisting of 5 mM tetra-n-butyl ammonium hydroxide (TBAH), pH 4.5:ACN (52:48v/v) with an injection volume of 20 μL , flow rate of 1.2 mL min^{-1} .

2.2. Preparation of the screen-printed carbon electrode (SPCE)

A disposable SPCE was used in this present work because of its cost-effectiveness and ease of preparation. The design and preparation of the three-electrode system were previously described [30]. A pattern of electrode, designed using Adobe Illustrator program (Fig. S1. Supporting information (SI)). The SPCE was fabricated using an in-house screen-printing method. The ink composition included graphite powder and carbon ink at a ratio of 0.2:1 (w/w). Silver/silver chloride ink was first printed onto a polyvinyl chloride (PVC) substrate to be used as both the pseudo-reference electrode (RE) and the conductive pads. Next, the carbon ink was printed onto the same PVC substrate as the second layer to form both the working electrode (WE, 3 mm i.d.) and counter electrode (CE). The finished electrode was then heated at 55 °C for 1 h to remove the solvent and dry the electrode.

2.3. Electrochemical reduction of graphene oxide (ERGO)

A protocol of ERGO preparation was previously described [29]. GO sheet (1 mg) was first dissolved in 1 mL deionized water with applying sonication for 1 h to achieve homogeneous solution. The GO solution was subsequently diluted with 0.1 M phosphate buffer (0.1 M Na_2HPO_4 and 0.1 M KH_2PO_4) of pH 6 to give a final concentration of GO in working solution of 70% (v/v). The working solution (40 μL) was then dropped onto the electrode surface, and followed by the electrochemical reduction of GO using a cyclic voltammetric technique. The reduction potential was scanned from 0.1 to -1.5 V with a scan rate of 100 mV/s for 16 cycles. The modified electrode was then rinsed twice with deionized water.

The schematic illustration of an ERGO is shown in Fig. 1.

2.4. Preparation of standard solutions and electrochemical measurements

Food grade synthetic colorants, SY and TZ, were selected as the analytes in this work. A stock standard solution (5 mM) was freshly prepared for each determination in phosphate buffer of pH 6. For the study of pH effect, a solution pH was adjusted using NaOH (1 M) and conc. H_3PO_4 . The designated concentrations of analytes were diluted from stock solutions. For electrochemical measurement, the analytes solution (40 μL) was dropped onto a freshly prepared electrode and subsequently accumulated at open-circuit for 3 min (otherwise stated see Section 3.2), and followed by electrochemical measurement. Limits of detection (LOD) and quantification (LOQ) were calculated from the $S/N=3$ and $10SD_b/S$, respectively, where SD_b is the standard deviation of blank ($n=10$), and S is the slope of the linearity.

Evaluation of the selectivity, largely reflects the analytical performance, was also examined using the same protocol as mentioned above using 50-fold excess of interfering substances. The selectivity was determined by comparing the signals obtained from the ERGO-SPCE with and without the presence of interferences such as glucose, ascorbic acid, sodium and iron, which are commonly added in drinks.

In all cases, the differential pulse voltammetry (DPV) was performed with 60 mV amplitude, 50 mV/s scan rate and 10 mV step potential. These employed experimental parameters were the optimized parameters. For the optimization of each parameter, the amplitude interval was investigated from 10 to 80 mV (Fig. S2(A),

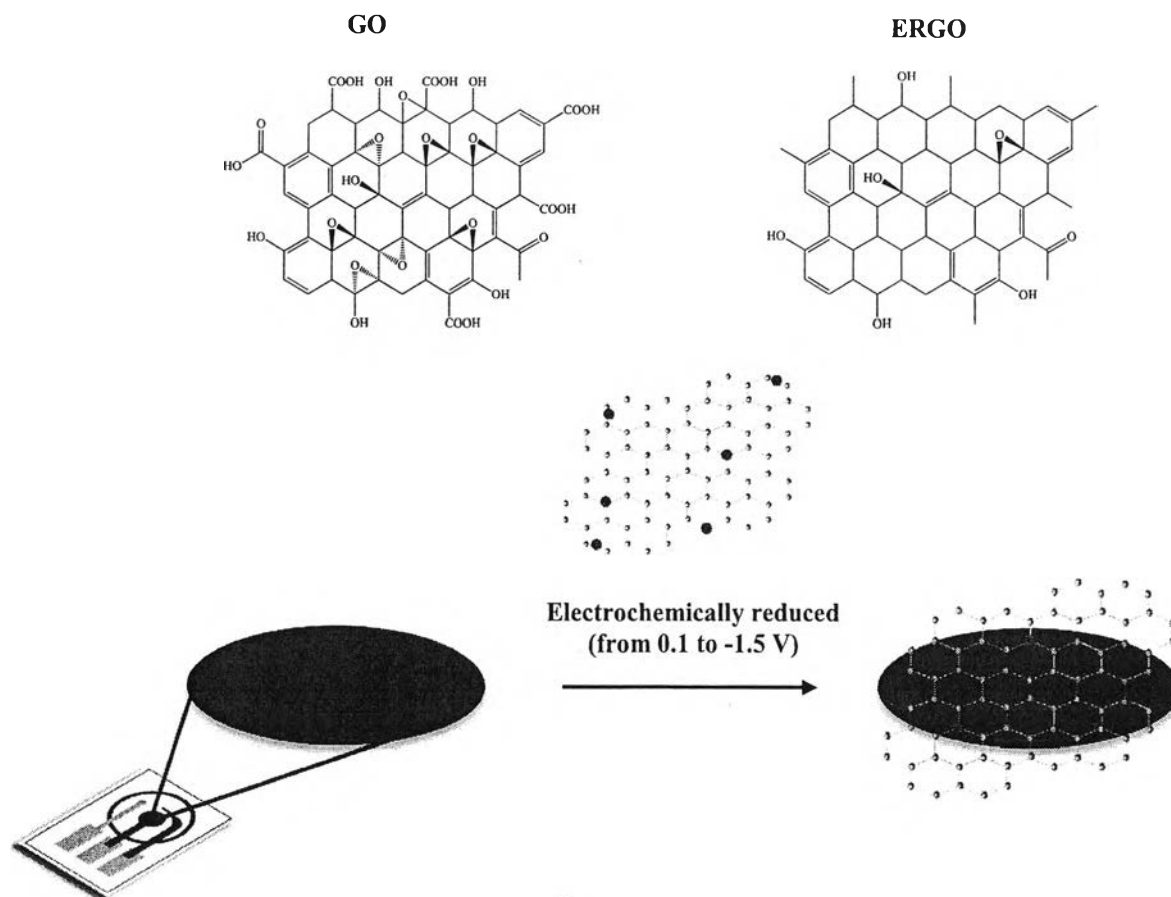


Fig. 1. Schematic illustration of ERGO-modified SPCE. Condition: CV was scanned from 0.1 to -1.5 V for sixteen cycles, scan rate of 100 mV/s.

SI), and the step potential was from 2 to 20 mV (Fig. S2(B), SI).

2.5. Sample preparation

The seven beverages employed in this work consisted of two soft drinks, two juice concentrate drinks, two energy drinks and one thirst quencher sample, which were purchased from a local supermarket and used directly without further pretreatment. When measuring SY and TZ using a ERGO-SPCE, a designated sample concentration was diluted employing 0.1 M phosphate buffer of pH 6, and then analyzed according to the analytical procedure.

In addition, compendium of methods for food analysis was also used to determine the amount of SY and TZ in these samples in parallel with the results obtained from the proposed approach to confirm the accuracy and acceptability of method. Compendium of method is applicable to the determination of food containing SY and TZ by high performance liquid chromatography method (HPLC). The preparation of sample was performed as previously described [31]. Briefly, liquid sample of 10 g was weighed accurately (or appropriate amount) and 50 mL of distilled water was subsequently added into the samples with constant stirring. After that, 10 mL of each sample was pipetted into each 50 mL beaker, followed by the addition of 30 mL of distilled water and acidified using glacial acetic acid. Finally, polyamide powder of 0.2–5.0 g is added into the adjusted samples, stirred with a stirring rod and left for 10 min or until all colors from the solution are adsorbed onto polyamide. Next, polyamide was subsequently added into the column and followed by a washing step using 5 mL acetone until no color is adsorbed onto polyamide and then combined all eluted fraction. These fractions were evaporated until nearly dry and small amount of distilled water was subsequently added into the samples to dissolve residue as final step. The results obtained from the ERGO-SPCE and compendiums of method were compared.

Furthermore, the recovery was determined by spiking known SY and TZ concentrations into the samples and then analyzed according to the same procedure.

3. Results and discussion

3.1. Characterization of the ERGO-SPCE

3.1.1. Scanning electron microscopy (SEM)

The surface morphologies of bare and ERGO-modified SPCEs were verified using SEM to confirm the presence of ERGO sheets on the electrode surface. As shown in Fig. 2B and C, after the electrochemical reduction of GO, the surface became more rough and non-exquisite compared to the bare electrode (Fig. 2A). SEM images of the electrode surface obviously showed that the surface

was dominantly covered by the irregularly crumbled and sheet-like structure of ERGO. Furthermore, it seemingly appears that the density and thickness of the ERGO sheet was gradually increased with increasing the number of scan cycle, as shown in Fig. 2A and B (eight cycles) and C (sixteen cycles), respectively. This led to an increase in the effective surface on the electrode and improvement in the conductivity of the modified sensor, which helps determine the detection sensitivity [29]. The obtained results indicated that GO was electrochemically reduced onto the electrode surface during the operation.

3.1.2. Electrochemical impedance spectroscopy (EIS)

To confirm the improvement of the conductivity of the modified sensor, an experiment using the EIS technique for measuring the charge transfer resistance (R_{ct}) of active species on electrode surface was carried out. The obtained results displayed that a semicircle with a large diameter was observed on the unmodified electrode (SPCE), and the semicircle became much smaller on the modified electrode (ERGO-SPCE) (Fig. S3, SI). In a Nyquist plot, the semicircle diameter represents the R_{ct} of the active species, which is $\text{Fe}(\text{CN})_6^{3-/4-}$, on the electrode surface. Herein, the R_{ct} values of $\text{Fe}(\text{CN})_6^{3-/4-}$ on the SPCE, GO-SPCE and ERGO-SPCE were found to be 20.29 k Ω , 8.09 k Ω and 0.43 k Ω , respectively. The greatly depressed R_{ct} values revealed that conductivity of the developed sensor was improved after the formation of the ERGO-SPCE, consequently resulting in higher signals and sensitivity [32].

From the relationship between R_{ct} and the heterogeneous electron-transfer rate constant (K_{et}) according to Eq. (1), the K_{et} value could be successfully obtained.

$$K_{et} = \frac{RT}{n^2 F^2 R_{ct} A C_{\text{redox}}} \quad (1)$$

In Eq. (1), A is the geometrical area of the electrode surface, and C_{redox} corresponds to the concentration of the redox couple. According to Eq. (1), the K_{et} values were calculated to be $3.74 \times 10^{-5} \text{ cm s}^{-1}$, $9.39 \times 10^{-5} \text{ cm s}^{-1}$ and $176.9 \times 10^{-5} \text{ cm s}^{-1}$ for the SPCE, GO-SPCE and ERGO-SPCE, respectively. The ERGO-SPCE exhibited a noticeable increase in the K_{et} value in comparison to the SPCE. Based on this evidence, it can be concluded that the electron transfer process on the ERGO-SPCE is easier and faster than that on the SPCE [33].

Furthermore, to illustrate that the ERGO could improve the surface area of the SPCE, the electroactive surface areas (A) of ordinary SPCE and ERGO-modified electrodes were determined employing CV in a 5.0 mM $\text{Fe}(\text{CN})_6^{4-/3-}$ solution containing 0.1 M KCl at various scan rates (v) according to the Randles-Sevcik equation, as follows: $i_p = 2.69 \times 10^5 \text{ A D}^{1/2} n^{3/2} v^{1/2} C$, where D is the diffusion coefficient of $\text{Fe}(\text{CN})_6^{4-/3-}$, C is the concentration of $\text{Fe}(\text{CN})_6^{4-/3-}$, and n is the number of involved electrons. As shown in Fig. 3, both the peak currents (i_p) of ERGO-modified (Fig. 3A)

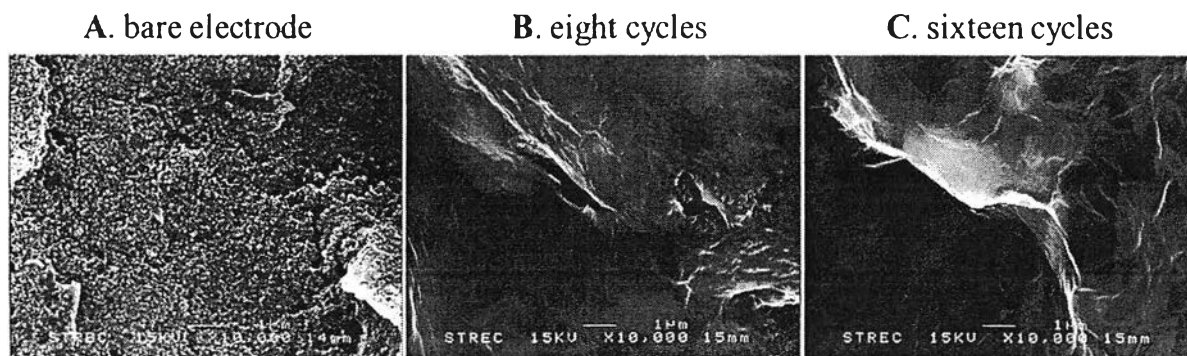


Fig. 2. SEM images of the bare (A) and ERGO-modified SPCE at eight (B) and sixteen (C) scan cycles.

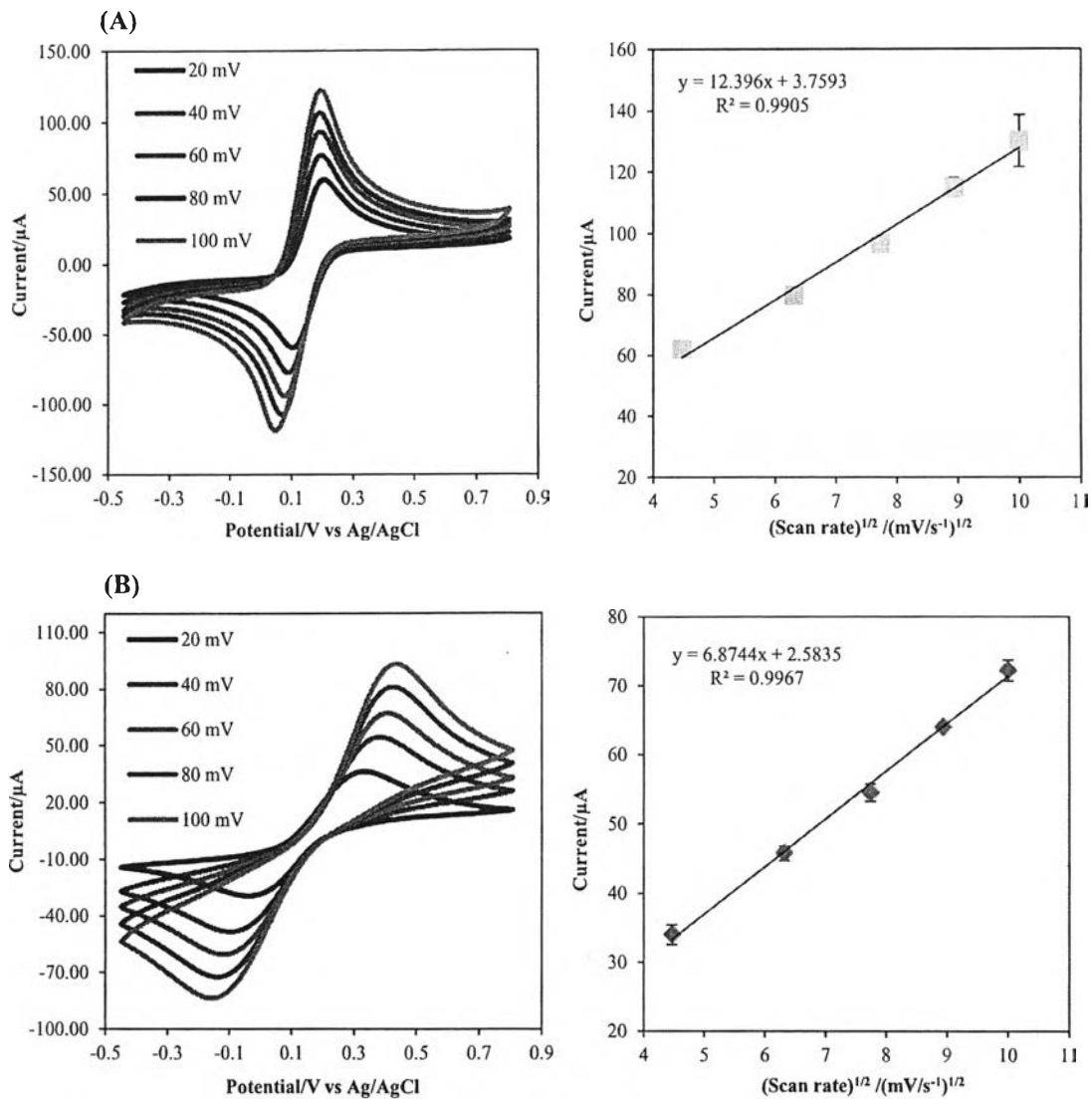


Fig. 3. CVs of the modified (A) and unmodified SPCE (B) in 5.0 mM $\text{Fe}(\text{CN})_6^{4-/3-}$ at different scan rates from 20 to 100 mV/s.

and unmodified electrodes (Fig. 3B) were proportional to the square root of the scan rate. With the constant parameters of D ($7.6 \times 10^{-6} \text{ cm}^2 \text{ s}^{-1}$), C (5 mM) and n (1 electron), an approximate value of A according to the Randles-Sevcik equation could be successfully achieved. The electroactive surface areas were calculated to be 0.335 cm^2 and 0.186 cm^2 for the modified and unmodified electrodes, respectively, where the electroactive surface area of the electrode increased 1.86-fold. This result provided effective evidence for the superior conductivity of ERGO as expected [34].

3.1.3. Infrared spectroscopy (IR)

According to sensor preparation, to prove that GO was electrochemically reduced by voltammetric cycling, an IR technique was carried out. The IR spectrum of the GO-SPCE showed all of the characteristic bands for GO including the following: C=O stretching at 1574 cm^{-1} , C–O stretching at 1051 cm^{-1} , and finally the OH stretching at 3350 cm^{-1} . The IR of the ERGO-SPCE preserved all of the characteristic bands of GO, except that the peak due to C=O stretching at 1574 cm^{-1} completely disappeared. This result indicates that the C=O functional group in GO was reduced during the voltammetric cycling (Fig. S4, S1). Moreover, the IR of ERGO-SPCE also exhibited the appearance of the new

peak at 2949 cm^{-1} , which is due to the CH_2 vibrations. This suggests that GO was converted to ERGO by voltammetric cycling [35].

3.2. Electrochemical behaviors of food colorants on the developed sensor

The electrochemical behaviors of SY and TZ on the SPCE, GO-SPCE and ERGO-SPCE were first investigated by a cyclic voltammetric (CV) technique to differentiate the oxidation peak potential of each colorant. As shown in Fig. 4A, the SPCE and GO-SPCE showed almost no anodic peaks of SY and TZ. This was due to that GO is electrochemically insulating by nature [26]. In contrast, the comparison exhibited that the peak currents of SY and TZ were significantly improved and well-defined peaks were observed on the ERGO-SPCE. Using a DPV technique, the results displayed that the peak separation between SY and TZ was increased at the ERGO-SPCE. The potential difference of the modified electrode was higher than that of the bare electrode by approximately 0.3 mV. The oxidation peaks appeared separately at approximately 0.41 and 0.70 V for SY and TZ, respectively, on the modified electrode (Fig. 4B). Surprisingly, the oxidation current was remarkably increased by approximately 90- and 20-fold for SY and TZ, respectively, in comparison to the unmodified electrode. These results

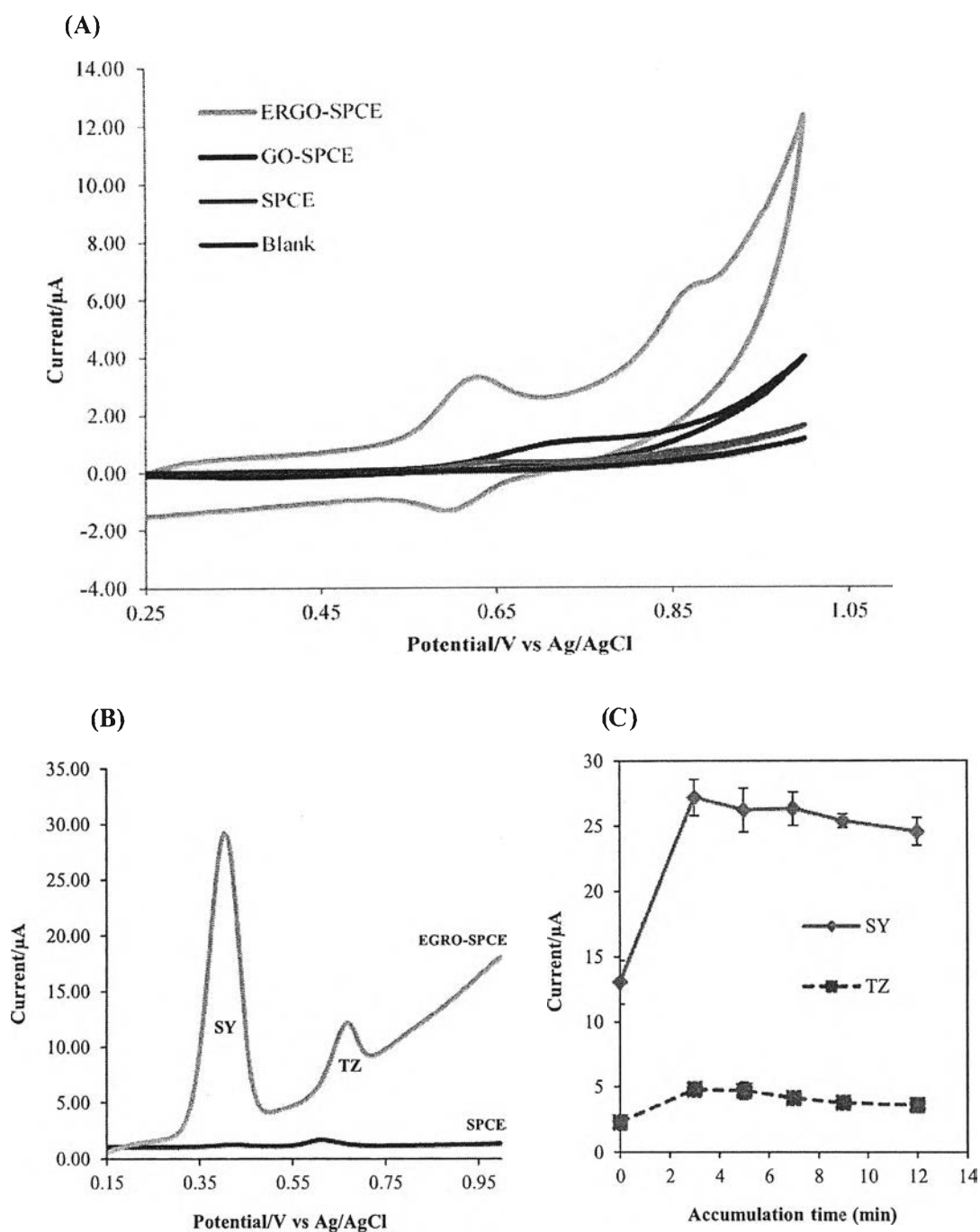


Fig. 4. CV (A) and DPV voltammograms (B) of the modified and unmodified SPCE, (C) accumulation time effect on the oxidation current of SY and TZ (10 μM) in 0.1 M phosphate buffer solution of pH 6.0.

suggested that the ERGO-modified electrode could improve the sensitivity of detection, which is consistent with the previously reported results [36].

To enhance the sensitivity of detection, the effect of accumulation time with and without applying potential on the current response of these colorants was examined. With applying potential, (at +0.4 V with various times from 0 to 120 s), the current signal was almost unchanged or negligible for the oxidation current of both SY and TZ (data not show). More interestingly, as shown in Fig. 4C, the current signals of both colorants with different accumulation times at the open-circuit were enhanced and reached maximums at 3 min. The current signal then reached a

plateau after further increasing the accumulation time, and an accumulation time of 3 min was therefore selected. As a result, it can be concluded that the accumulation time affects the increase of the current signal. In other words, it can be assumed that the accumulation potential has no effect on the current responses of SY and TZ, which is consistent with the previous report [37].

3.3. Influence of the GO concentrations on the current responses of SY and TZ

As the electrochemical reduction of GO can control the thickness and size of the produced ERGO film by varying either the

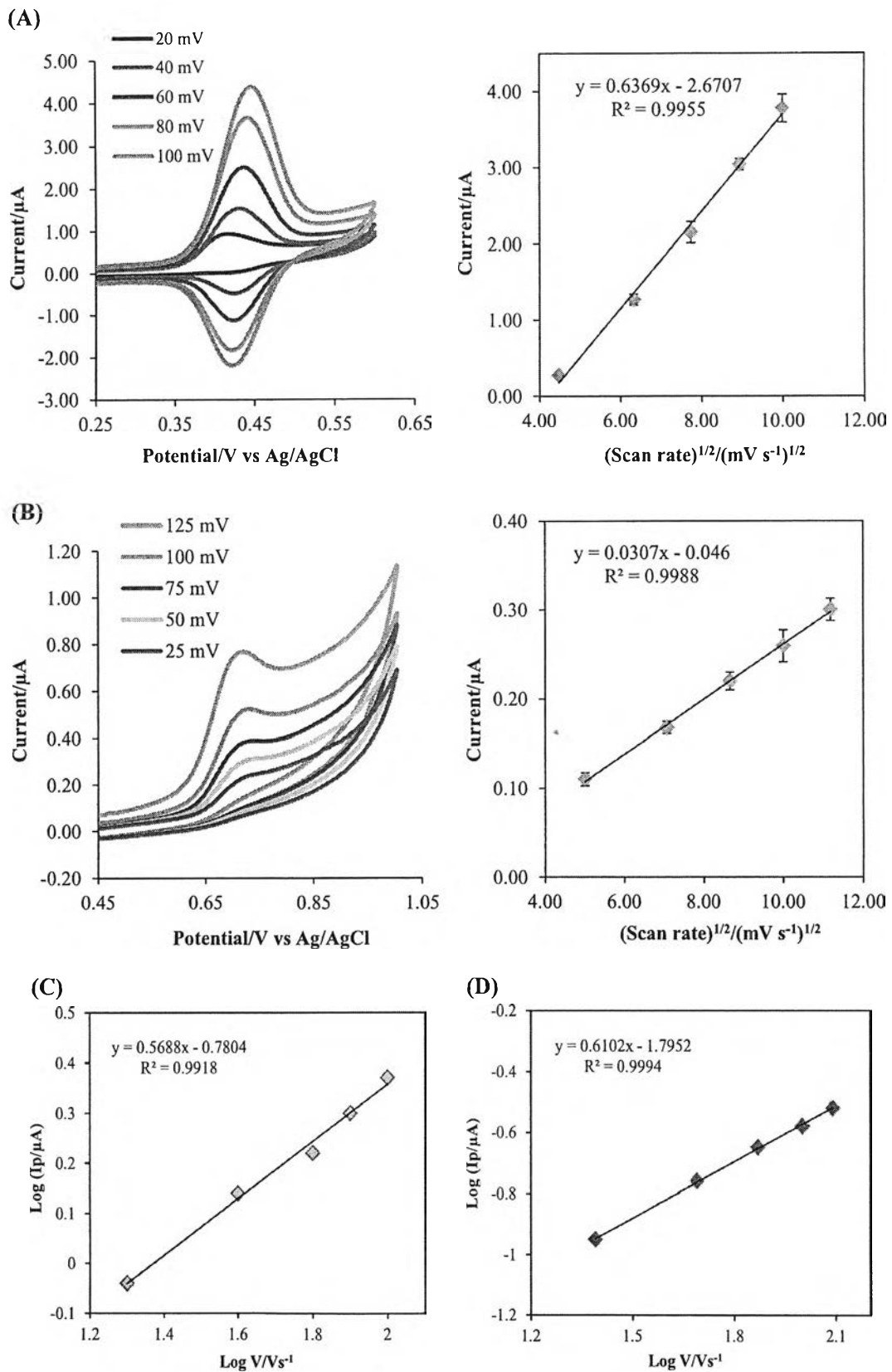


Fig. 5. CV curves of 10 μM SY (A) and TZ (B) in phosphate buffer solution of pH 6 under different scan rates and linear relation between logarithm of peak current and logarithm of scan rate for SY (C) and TZ (D).

electrochemical parameters or GO concentration [29], to achieve proper conditions for detection, the effects of the GO concentration and number of reduction cycles on the current responses of SY and TZ were examined. For the optimization of the GO loading, a

gradual increase in the concentrations of GO in the working solution from 0 to 0.7 mg/mL results in remarkable increases in the oxidation peak currents of both colorants (Fig. S5(A), S1). During this period, the surface concentration of GO greatly increases,

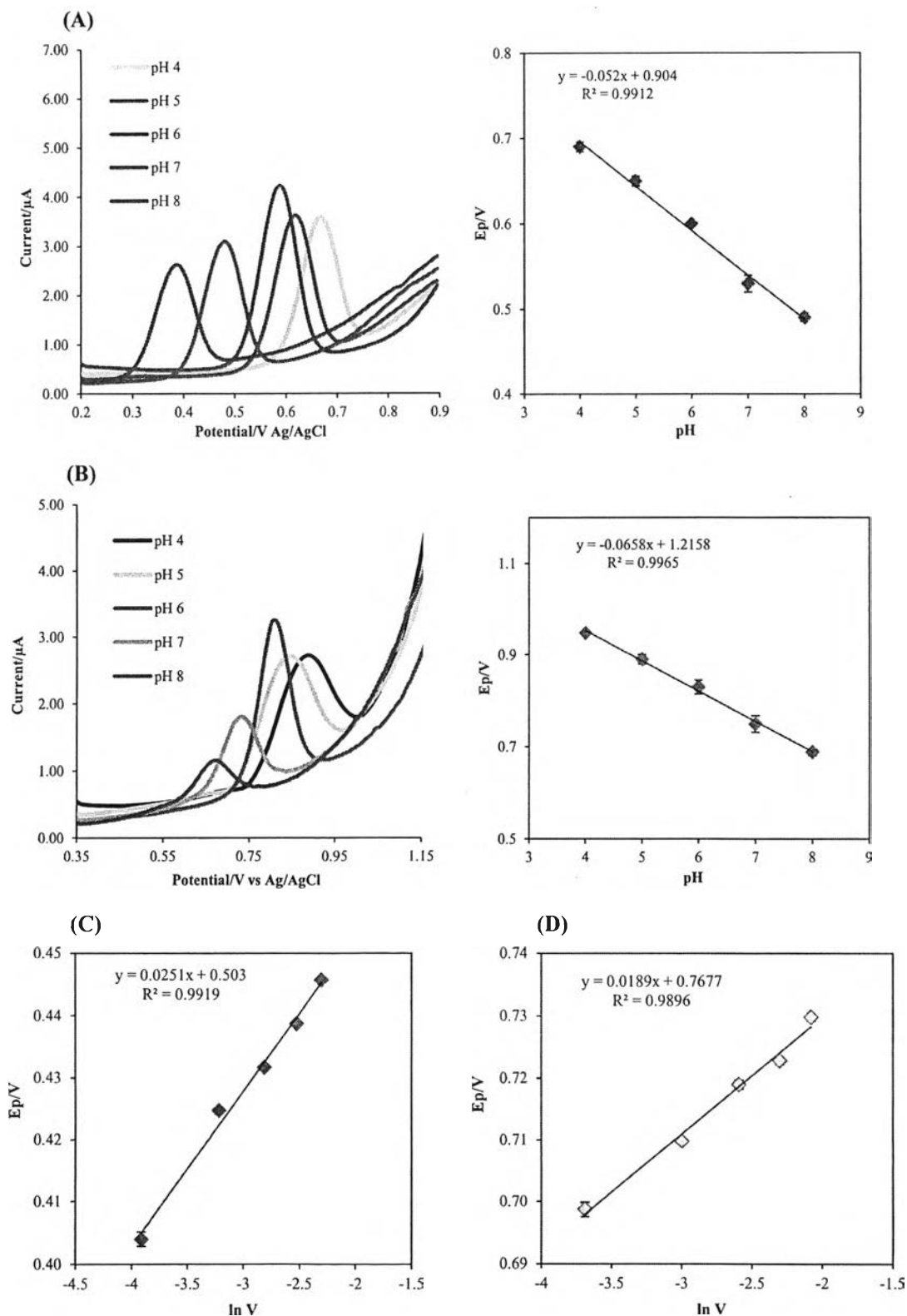


Fig. 6. DPV voltammograms represent the influence of pH values on the Ep of 7 μM SY (A) and 10 μM TZ (B) and dependence of Ep on the natural logarithms of scan rate of SY (C) and TZ (D) at ERGO-SPCE under the optimized condition.

showing a higher accumulation efficiency and current responses to SY and TZ. The maximum currents of both colorants were obtained at 0.7 mg/mL of GO, and the oxidation peak currents gradually decrease as the GO concentration was further raised from 0.7 to 1.1 mg/mL. As for the decreases in the analytical signals of both analytes, a possible explanation could be that multiple layers of graphene (more than 10 layers) are generated on the electrode surface when a high concentration of GO is employed, which makes it characteristically similar to graphite material. The GO concentration of 0.7 mg/mL was therefore selected to modify the sensors.

Additionally, to achieve the optimal conditions, the effect of the number of scan cycles was examined. The obtained results exhibited that the current responses of both colorants gradually increase with increasing the number of scan cycles (Fig. S5(B), S1) and reach a maximum current at sixteen scan cycles. After more cycles, the decreased signal might be caused by the same reason aforementioned, which is that multiple layers of the ERGO film are generated on the electrode surface affecting the electron transfer between the analytes and the electrode surface.

3.4. Effect of the scan rate

In this section, to fit a diffusion-controlled redox process, the influence of the scan rate on the peak currents of SY and TZ was examined by cyclic voltammetry. From this study, the results revealed that the peak potentials (E_p) of both colorants shifted positively with faster scan rates. As shown in Fig. 5A and B, linear relationships between the square root of the scan rate and current response were obtained from 20 to 100 mV s^{-1} and 25–125 mV s^{-1} for SY and TZ, respectively, which are typical of diffusion controlled currents, and the equations can be expressed as follows: $i_p(\text{SY}) = 0.6369 v^{1/2} - 2.6707$, $R^2 = 0.9955$; $i_p(\text{TZ}) = 0.0307 v^{1/2} - 0.0460$, $R^2 = 0.9988$.

In addition, to confirm a diffusion-controlled redox process, plots of the $\log i_p$ versus the $\log v$ were established in Fig. 5 corresponding to the following equation: $\log i_p(\text{SY}) = 0.5688 \log v - 0.7804$, $R^2 = 0.9918$; $\log i_p(\text{TZ}) = 0.6102 \log v - 1.7952$, $R^2 = 0.9994$. The slopes of 0.56 (Fig. 5C) and 0.61 (Fig. 5D) for SY and TZ, respectively, were close to the theoretically expected value of 0.5 for a purely diffusion controlled current [38]. This result further confirms that the electro-oxidation of SY and TZ was a diffusion controlled process.

3.5. Study of the electrochemical mechanism at the ERGO-SPCE

To determine the number of electrons and protons in the reaction of each analyte at the ERGO-SPCE, the influence of pH on the E_p of SY and TZ was examined using a DPV technique. A plot of E_p vs pH values was first constructed to obtain the ratio between protons and electrons in the reaction. As exhibited in Fig. 6, the anodic potentials of SY (Fig. 6A) and TZ (Fig. 6B) were found to be dependent on pH values and shifted to more negative values when the pH of the medium was increased. This suggested that a proton participates in the oxidation of both SY and TZ. The equations of pH dependency can be expressed as follows: $E_{pa}(\text{SY}) = -0.0520 \text{ pH} + 0.904$, $R^2 = 0.9912$ and $E_{pa}(\text{TZ}) = -0.0658 \text{ pH} + 1.215$, $R^2 = 0.9965$. Slopes of -0.052 mV and -0.065 mV for SY and TZ, respectively, were obtained and are near the theoretical value of -0.059 mV per unit. This result confirms that an equal number of electrons and protons are involved in the reaction [16]. The highest peak current was obtained at a pH of 6. This pH was then employed in this study. It is noted that the oxidation signals of both SY and TZ gradually increased with increasing pH values from 4 to 6 and then slightly decreased with further pH increases. Thus, pH values higher than 6 were unsuitable for electrochemical

determination of these colorants. The decreases of oxidation signals at pH higher than 6 could be attributed to the oxidation of phenolic hydroxyl group with one proton transferred in the electrochemical reaction [40]. The pK_a values of these synthetic colorants are 9.4 and 10.4 for TZ and SY, respectively. As the obtained results, it can be concluded that pH value is the most important parameter for electrochemical detection of these colorants.

To propose a possible mechanism, the electrochemical behaviors of SY and TZ on the ERGO-SPCE were studied using a CV technique at the different scan rates. The oxidation currents of SY (Fig. 5A, section 3.4) and TZ (Fig. 5B, section 3.4) increased linearly with the square root of the scan rate, which is typical of diffusion controlled currents. The oxidation peaks of both SY and TZ shifted positively with ascending scan rates. Additionally, the oxidation peak of SY exhibited a reversible process, while TZ displayed an irreversible electrode process. This relationship is in accordance with Eq. (2).

$$E_p = E^\circ + \frac{RT}{\alpha n F} \left[0.780 + \ln \left(D_r^{\frac{1}{2}} \div k^\circ \right) + \ln \left(\frac{\alpha n F v}{RT} \right)^{1/2} \right] \\ = K + \frac{RT}{2\alpha n F} \ln v \quad (2)$$

In Eq. (2), α is the transfer coefficient, k° is the standard heterogeneous rate constant of the reaction, n is the number of electrons transferred, v is the scan rate, and E° is the formal redox potential. Other symbols have their usual meanings. Based on this result, to obtain the number of electrons participating in the reaction, plots of E_p vs $\ln v$ for SY (Fig. 6C) and TZ (Fig. 6D) were constructed.

According to Eq. (2), the plots of E_p vs $\ln v$ have good correlation, and the values of αn can be calculated to be 0.51 and 0.67 for SY and TZ, respectively, from the slope of each (0.0251 and 0.0189). Commonly, α is assumed to be 0.5. Consequently, the involvement of one electron was concluded for the reactions of both SY and TZ.

According to the relationship of E_p and pH, we know that an equal number of electrons and protons participated in the oxidation reaction of both SY and TZ. Based on this result, it can be concluded that the oxidation mechanisms of SY and TZ involve one electron and one proton being transferred, which is consistent with the previously reported results [16,39]. The proposed mechanisms are illustrated in Fig. 7A and B for SY and TZ, respectively.

3.6. Calibration curve

After the formation of the ERGO-SPCE and obtaining the optimized conditions, calibration plots of the current signals obtained from the DPV analysis and various tested colorant concentrations were constructed. Fig. 8A and B illustrate the DPV responses of SY and TZ under different concentrations, respectively. To observe the synergistic interference of them, the concentrations were fixed at 0.2 μM and 5 μM for SY and TZ, respectively. As shown in Fig. 8A, it was found that the oxidation signal of 5 μM TZ was almost unchanged as the concentration of SY increased from 0.01 to 20 μM . A similar experiment was also carried out for TZ, as shown in Fig. 8B. When the concentration of TZ was increased from 0.02 to 20 μM , the oxidation current of 0.2 μM SY appeared to be stable. Therefore, the oxidation signals of SY and TZ on ERGO-SPCE were independent, and their synergistic interference was negligible. The calibration curve of SY exhibited a linear range from 0.01 to 20.0 μM with a R^2 value of 0.9958. For TZ determination, it was found that the oxidation peak current plotted against various tested concentrations of TZ exhibited linear correlation in the range from 0.02 to 20.0 μM with a R^2 value of 0.9949. The LODs were experimentally obtained and found to be 0.50 nM for SY and 4.50 nM for TZ. The LOQs were calculated to be 0.029 and 0.190 μM

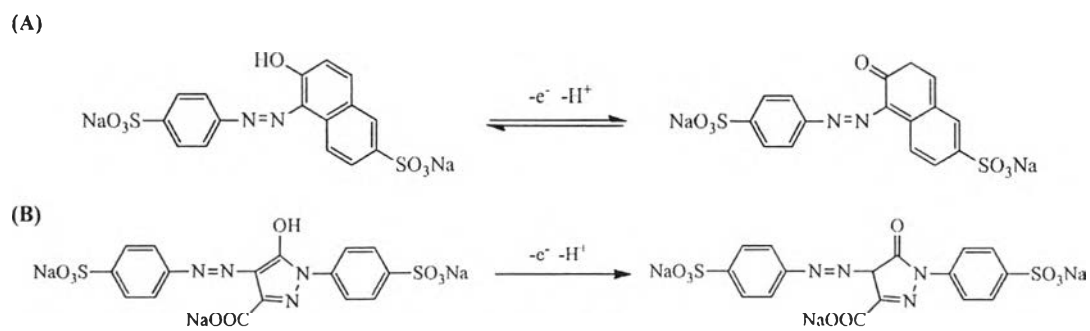


Fig. 7. The mechanisms for electrochemical process of SY (A) and TZ (B).

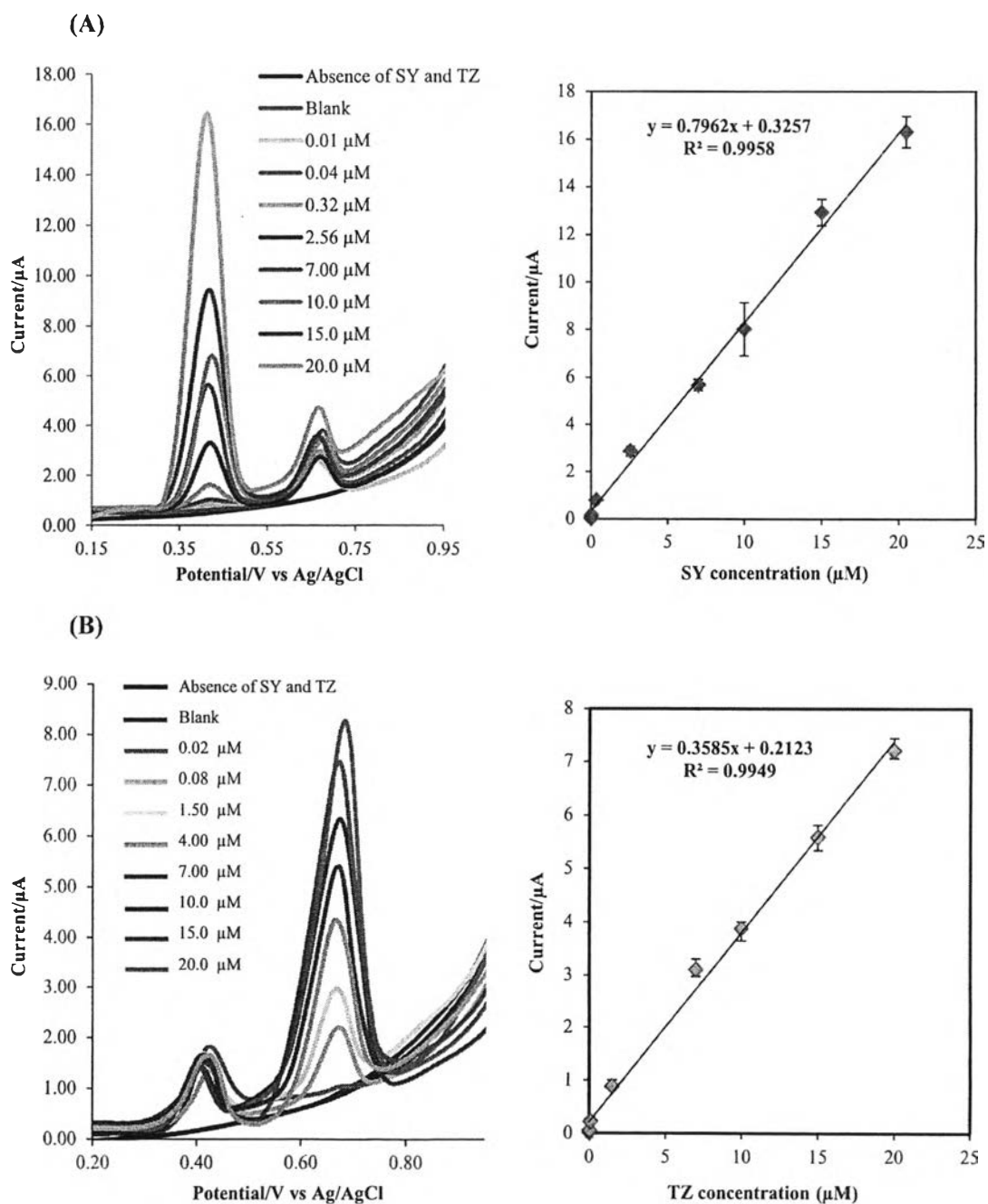


Fig. 8. Representative DPV of ERGO-SPCE with various SY (A) and TZ (B) concentrations, under the optimized parameters.

Table 1

Comparison of the analytical performance between the developed and previously reported electrochemical sensor for the simultaneous determination of both colorants.

Working electrode	pH	Linear range (μM)		Limit of detection (μM)		Reference
		SY	TZ	SY	TZ	
β -CD-PDDA-GR ^a /GC-RDE ^b	5	0.05–20	0.05–20	0.0120	0.0140	[9]
Pretreated-BDD ^c	H ₂ SO ₄ (0.1 M)	0.02–4.76	0.0999–5.660	0.0131	0.0627	[15]
GN-PTA ^d /GCE ^e	4.4	0.0332–0.464	0.112–2.810	0.0011	0.0561	[16]
GN-TO ₂ /CPE ^f	H ₂ SO ₄ (0.1 M)	0.02–2.050	0.02–1.180	0.0060	0.0080	[17]
Au NPs/CPE	4	0.1–2.0	0.05–1.6	0.0300	0.0020	[18]
MWCNT ^g /GCE	8	0.0553–11.053	0.374–74.86	0.0200	0.1880	[19]
ERGO/SPCE	6	0.01–20	0.02–20	0.0005	0.0045	This work

^a β -cyclodextrin-coated poly (diallyldimethylammonium chloride)-functionalized graphene.

^b Glassy carbon-rotating disk electrode.

^c Boron-doped diamond electrode.

^d Graphene layer-wrapped phosphotungstic acid hybrid.

^e Glassy carbon electrode.

^f Carbon paste electrode.

^g Multi-walled carbon nanotubes.

(at S/N=10) for SY and TZ, respectively. The percent relative standard deviations (%RSD) for each set of SY and TZ determinations (n=3) including the slope, intercept, LOD and LOQ were found to be in the range from 2.07 to 11.51. These %RSD values indicated that excellent reproducibility was achieved. The %RSD was calculated according to Eq. (3), where SD is the standard deviation of the current signal.

$$\%RSD = (SD/\text{mean}) \times 10 \quad (3)$$

Compared with the previously reported electrochemical methods for the simultaneous determination of SY and TZ, this new sensing platform exhibited a wider dynamic range and higher sensitivity. Additionally, the detection limits were as low as 0.50 and 4.50 nM for SY and TZ, respectively, as confirmed in Table 1.

3.7. Selectivity and reproducibility of the detection

The selectivity of a method is a crucial factor for a practical measurement due to various interfering substances present in the system, such as glucose, ascorbic acid, sodium and iron. The results displayed that when interfering substances are present, the peak current changed insignificantly, indicating that the developed ERGO-SPCE sensor had good selectivity for the determinations of SY and TZ (see Fig. S6(A) and (B), SI).

To evaluate the reproducibility of the proposed method, seven sensors were prepared by the same process. The electrochemical sensor was tested at concentrations of 2, 5 and 10 μM for each colorant. For SY determination, %RSDs of 7.8%, 4.5% and 1.6% were obtained, respectively. An excellent reproducibility was also obtained for TZ detection, and the %RSDs of reproducibility were found to be 7.11%, 6.82% and 2.15%, respectively. The obtained results suggested that the proposed method remarkably minimized the sensor-to-sensor deviation, and excellent fabrication reproducibility was achieved.

Table 2

Comparison of the obtained results between the proposed method and HPLC for detection of SY and TZ in seven beverages. Accumulation time was 3 min at open circuit.

Sample no.	Analyte	By developed sensor (mg/L)	Compendium of method (HPLC) (mg/L)	Relative error (%)
1	SY	4.10 \pm 0.04	3.95 \pm 0.02	3.79
	TZ	19.04 \pm 0.91	18.55 \pm 0.07	2.64
2	SY	5.70 \pm 0.05	5.56 \pm 0.24	2.51
	TZ	5.04 \pm 0.09	4.83 \pm 0.01	4.34
3	SY	4.54 \pm 0.53	4.75 \pm 0.03	-4.42
	TZ	16.56 \pm 0.16	15.80 \pm 0.01	4.81
4	SY	28.95 \pm 0.75	30.43 \pm 0.01	-4.86
	TZ	31.49 \pm 1.21	32.45 \pm 0.03	-2.95
5	SY	43.33 \pm 1.70	43.14 \pm 0.03	0.44
	TZ	-	-	-
6	SY	10.17 \pm 0.41	9.93 \pm 0.05	2.41
	TZ	-	-	-
7	SY	-	-	-
	TZ	1.49 \pm 0.07	1.55 \pm 0.02	-3.87

Note: values reported are mean of three replicates (n=3).

3.8. Application of a ERGO-SPCE for the determination of SY and TZ in practical samples

To demonstrate its suitability and potential application for practical sample analysis, the proposed method was applied to determine SY and TZ in seven selected beverages, which were purchased from a local supermarket. The seven beverages employed in this work consisted of two soft drinks, two juice concentrate drinks, two energy drinks and one thirst quencher sample. In one type of soft drink, in 0.1 M phosphate buffer at a pH of 6 after 3 min of accumulation time, two oxidation peaks appeared at approximately 0.4 V and 0.7 V with the ERGO-SPCE, which imply that both SY and TZ were present. After standard solutions of both colorants were added, it was found that the oxidation peak currents increased (Fig. S7, SI). Otherwise, the contents of SY and TZ in the sample can be achieved according to the oxidation peak current ratio.

The contents of both colorants were also validated employing the compendium of methods to confirm the accuracy of this method. The comparison of the results between the proposed system and compendium method agreed as displayed in Table 2. Each reported value is a mean of three replicates (n=3), and the relative standard deviation ($RSD \leq 5$) using this method was acceptable, indicating good repeatability. A paired *t*-test at a 95% confidence interval was achieved on the results obtained from real samples analysis. The experimental *t*-value (*t* calculated) obtained by this novel method is in the range from 1.2318 to 2.0334 and is lower than the critical *t*-value (2.920). It can be concluded that there is no significant difference between proposed method and the compendium of methods. Therefore, our proposed strategy is reliable and can be used as a new alternative assay for the determination of SY and TZ with highly sensitive and rapid analysis.

In addition, the accuracy of the proposed method was evaluated by performing a recovery test after introducing known amounts of SY and TZ into the samples and then analyzing them according to the same procedure. The amounts of SY and TZ were determined using the standard addition method. The %recovery values are in the range from 80.74 to 117.59, suggesting that the determination of SY and TZ using an ERGO-SPCE is precise and feasible (Table S1, SI).

4. Conclusions

A novel electrochemical sensor for the simultaneous determination of SY and TZ based on an ERGO-modified disposable SPCE was successfully developed and applied to detect the SY and TZ contents in some commercial beverages. The ERGO-modified SPCE can greatly enhance the electrochemical signals of both colorants, suggesting remarkable surface enhancement effects. The calibration curves of SY and TZ exhibited linear correlation from 0.01 to 20.0 μM , and 0.02–20.0 μM , respectively, and the corresponding LODs were as low as 0.50 and 4.50 nM, respectively. Furthermore, the peak current was changed insignificantly in the presence of interfering substances, suggesting that the selectivity of the developed sensor was excellent. For practical analysis, the obtained results from this proposed method agreed well with those obtained from the compendium of methods, in-house standard technique. The advantages of this sensor include the ease of preparation, reduced time consumption and non-toxicity. The electrode is easily and inexpensively prepared, and it requires only a small sample volume (40 μL). The instrument set-up is also simple. Therefore, the present technique should be suitable as a novel method for the rapid determination of these food colorants. Additionally, this sensing platform may provide a promising alternative choice for practical application in biological and environmental analysis.

Acknowledgments

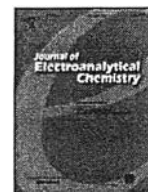
The authors thank financial supports from Science Achievement Scholarship of Thailand (SAST), Electrochemistry and Optical Spectroscopy Research Unit (EOSRU), and Program in Petrochemistry, Chulalongkorn University. In addition, we thank The National Nanotechnology Center (NANOTEC), NSTDA, Ministry of Science and Technology, Thailand through its program of Center of Excellence Network, the Thailand Research Fund through Research Team Promotion Grant (RTA5780005), the National Research University Project of CHE and Ratchadaphiseksomphot Endowment Fund (Project codes AM10091-56 and AM1006A-56) for support.

Appendix A. Supporting information

Supplementary data associated with this article can be found in the online version at <http://dx.doi.org/10.1016/j.talanta.2016.07.011>.

References

- [1] R.C. Lindsay, Food additives, in: S. Damodaran, K.L. Parkinn, O.R. Fennema (Eds.), *Fennema's Food Chemistry*, 4th ed., CRC Press, Boca Raton, 2008, pp. 689–749.
- [2] K. Duangmal, P. Hemptarasuwan, P. Somsong, Current situation on food additives in Thailand use and awareness, in: S. Hongladarom (Ed.), *Proceedings of the APSAFE2013 Food Security and Food Safety For The Twenty-first Century*, New York, Springer, 2015, pp. 45–60.
- [3] Y.Y. Zhang, T. Gan, C.D. Wan, K.B. Wu, *Anal. Chim. Acta* 764 (2013) 53–58.
- [4] Y. Zhang, X.J. Zhang, X.H. Lu, J.Q. Yang, K.B. Wu, *Food Chem.* 122 (3) (2010) 909–913.
- [5] P. Wang, X.Z. Hu, Q. Cheng, X.Y. Zhao, X.F. Fu, K.B. Wu, *J. Agric. Food Chem.* 58 (23) (2010) 12112–12116.
- [6] L. Koutsogeorgopoulou, C. Maravelias, G. Methenitou, A. Koutselini, *Vet. Hum. Toxicol.* 40 (1998) 1–4.
- [7] A. Yadav, A. Kumar, P.D. Dwivedi, A. Tripathi, M. Das, *Toxicol. Lett.* 208 (2012) 239–245.
- [8] S.M. Ghoreishi, M. Behpour, M. Golestaneh, *Food Chem.* 132 (2012) 637–641.
- [9] X. Ye, Y. Du, D. Lu, C. Wang, *Anal. Chim. Acta* 779 (2013) 22–34.
- [10] Food Act, Notification of the Ministry of Public Health No. 281 B.E. 2547, RE: Food Additive. Thailand. Bangkok: Cabinet and Royal Gazette Publishing, 2004. (<http://www.foodadditives.org/pdf/cochran%20present.pdf>). (Retrieved November 17, 2013).
- [11] L.H. Oakley, D.M. Fabian, H.E. Mayhew, S.A. Svoboda, K.L. Wustholz, *Anal. Chem.* 84 (18) (2012) 8006–8012.
- [12] M. Ma, X. Luo, B. Chen, S. Su, S. Yao, *J. Chromatogr. A* 1103 (2006) 170–176.
- [13] S.P. Alves, D.M. Brum, E.C.B. de Andrade, A.D.P. Netto, *Food Chem.* 107 (1) (2008) 489–496.
- [14] A.V. Jager, F.G. Tonin, M.F.M. Tavares, *J. Sep. Sci.* 28 (2005) 957–965.
- [15] R.A. Medeiros, B.C. Lourencao, R.C. Rocha, O. Fatibello, *Talanta* 97 (2012) 291–297.
- [16] T. Gan, J. Sun, S. Cao, F. Gao, Y. Zhang, Y. Yang, *Electrochim. Acta* 74 (2012) 151–157.
- [17] T. Gan, J. Sun, W. Meng, L. Song, Y. Zhang, *Food Chem.* 141 (2013) 3731–3737.
- [18] S.M. Ghoreishi, M. Behpour, M. Golestaneh, *Food Chem.* 132 (2012) 637–641.
- [19] W. Zhang, T. Liu, X. Zheng, W. Huang, C. Wan, *Colloids Surf. B* 74 (2009) 28–31.
- [20] S. Rouhani, *Anal. Lett.* 42 (2009) 141–153.
- [21] T. Gan, C.G. Hu, Z.L. Chen, S.S. Hu, *Talanta* 85 (1) (2011) 310–316.
- [22] K.J. Huang, Y.X. Miao, L. Wang, T. Gan, M. Yu, L.L. Wang, *Process Biochem.* 47 (7) (2012) 1171–1177.
- [23] Q. Wei, Y.F. Zhao, B. Du, D. Wu, H. Li, M.H. Yang, *Food Chem.* 134 (3) (2012) 1601–1606.
- [24] C. Wu, D. Sun, Q. Li, K.B. Wu, *Sens. Actuators B* 168 (2012) 178–184.
- [25] T. Gan, J. Y. Sun, K.J. Huang, L. Song, Y.M. Li, *Sens. Actuators B* 177 (2012) 412–418.
- [26] S. Stankovich, D.A. Dikin, R.D. Piner, K.A. Kohlhaas, A. Kleinhammes, Y. Jia, Y. Wu, S.T. Nguyen, R.S. Ruoff, *Carbon* 45 (2007) 1558–1565.
- [27] W.S. Hummers, R.E. Offeman, *J. Am. Chem. Soc.* 80 (6) (1958) 1339.
- [28] M. Choucair, P. Thordarson, J.A. Stride, *Nat. Nanotechnol.* 4 (2009) 30–33.
- [29] X.Y. Peng, X.X. Liu, D. Diamond, K.T. Lau, *Carbon* 49 (2011) 3488–3496.
- [30] S. Jampasa, W. Wonsawat, N. Rodthongkum, W. Siangproh, P. Yanatatsaneejit, T. Vilaivan, O. Chailapakul, *Biosens. Bioelectron.* 54 (2014) 428–434.
- [31] J.F. Lawrence, F.E. Lancaster, H.B.S. Conacher, *J. Chromatogr. A* 210 (1981) 168–173.
- [32] L. Ji, Q. Cheng, K. Wu, X. Yang, *Sens. Actuators B* 231 (2016) 12–17.
- [33] E. Arslan, S. Çakır, *J. Electroanal. Chem.* 646 (2010) 114–123.
- [34] L. Bai, R. Yuan, Y. Chai, Y. Yuan, Y. Wang, S. Xie, *Chem. Commun.* 48 (2012) 10972–10974.
- [35] W.J. Basirun, M. Sookhikian, S. Baradaran, M.R. Mahmoudian, M. Ebadi, *Nanoscale Res. Lett.* 8 (2013) 387–397.
- [36] C. Liu, K. Wang, S. Luo, Y. Tang, L. Chen, *Small* 7 (2011) 1203.
- [37] M. Wang, J. Zhao, *Sens. Actuators B* 216 (2015) 578–585.
- [38] S.N. Azizi, S. Ghasemi, F. Amiripour, *Sens. Actuators B* 227 (2016) 1–10.
- [39] X. Qiu, L. Lu, J. Leng, Y. Yu, W. Wang, M. Jiang, L. Bai, *Food Chem.* 190 (2016) 889–895.
- [40] X. Song, Z. Shi, X. Tan, S. Zhang, G. Liu, K. Wu, *Sens. Actuators B* 197 (2014) 104–108.



Free radical scavenger screening of total antioxidant capacity in herb and beverage using graphene/PEDOT: PSS-modified electrochemical sensor



Ruksuda Tirawattanakoson^a, Poomrat Rattanarat^b, Nattaya Ngamrojanavanich^b,
Nadnudda Rodthongkum^{c,*}, Orawon Chailapakul^{b,d,**}

^a Program in Biotechnology, Faculty of Science, Chulalongkorn University, Pathumwan, Bangkok 10330, Thailand

^b Electrochemistry and Optical Spectroscopy Research Unit (EOSRU), Department of Chemistry, Faculty of Science, Chulalongkorn University, Pathumwan, Bangkok 10330, Thailand

^c Metallurgy and Materials Science Research Institute, Chulalongkorn University, Pathumwan, Bangkok 10330, Thailand

^d Nanotec-CU Center of Excellence on Food and Agriculture, Bangkok 10330, Thailand

ARTICLE INFO

Article history:

Received 1 July 2015

Received in revised form 26 October 2015

Accepted 24 November 2015

Available online 29 January 2016

Keywords:

Graphene

PEDOT:PSS

Electrospraying

Total antioxidant capacity

DPPH

ABSTRACT

This work describes the development of a novel nanocomposite- graphene/poly (3,4-ethylenedioxythiophene): poly (styrenesulfonate) modified screen-printed carbon electrode (G/PEDOT:PSS/SPCE) for the evaluation of total antioxidant capacity (TAC) based on 2,2-diphenyl-1-picrylhydrazyl (DPPH) assay. Droplet-like nanostructures of G/PEDOT: PSS were fabricated on the SPCE surface via electrospraying. The electrochemical behaviors of both unmodified SPCE and G/PEDOT: PSS modified SPCE were investigated by cyclic voltammetry (CV) using a standard ferri/ferrocyanide $[\text{Fe}(\text{CN})_6]^{3/4-}$. Interestingly, electrosprayed G/PEDOT: PSS can enhance the current response due to simple increase of the SPCE surface area. Compared to an unmodified SPCE, the peak potential difference (ΔE_p) between anodic and cathodic peak potential of G/PEDOT: PSS modified SPCE substantially decreased, indicating the faster electron transfer kinetics. Moreover, our system can be used for quantitation of TAC by chronoamperometric detection of residual non-reacted DPPH level at the interference free cathodic region. With addition of standard Trolox antioxidant, the cathodic DPPH current decreased. The calibration curve of Trolox antioxidant was found in a range of 5–30 μM with a limit of detection ($S/N = 3$) of 0.59 μM and a limit of quantification ($S/N = 10$) of 1.97 μM . Finally, this novel electrochemical sensor was successfully applied for TAC evaluation in Thai herb and herbal beverage. The results showed a good agreement with the conventional UV-visible spectrophotometric results.

© 2015 Published by Elsevier B.V.

1. Introduction

An antioxidant is defined as a molecule diminishing the risk of harmful abnormalities arising from an oxidative stress including Alzheimer's disease, cancer, asthma, atherosclerosis, inflammation, rheumatoid arthritis, and cardiovascular disorder [1]. The antioxidants neutralize adverse free radicals by either donating a hydrogen atom or a single electron transfer mechanism [2]. Natural antioxidants found in fruits, vegetables and herbs such as vitamin C, vitamin E, phenolic compounds and flavonoids have high potential to scavenge the free radicals. The consumed plants and foods containing an appropriate amount of antioxidant play an important role as a source of antioxidants [3]. Nowadays, the antioxidants become the major contents in various

industrial products, such as health-care goods, foods and cosmetics. Thus, researchers have been continuously developed the methods to evaluate antioxidant capacity in natural products and foods, which might be beneficial for quality control of herbs and herbal beverages.

Various conventional analytical approaches have been used for the determination of total antioxidant capacity (TAC) including spectrophotometry [4], chemiluminescence spectroscopy [5], fluorescence spectroscopy [6], and chromatographic related techniques [7]. Spectrophotometry measures the color change of oxidant, which is either an increase or decrease of absorbance at a specific wavelength. The absorbance change is correlated to the concentration of antioxidant. Common spectrophotometric assays have been reported for the determination of TAC in various natural products and biological fluids such as 2,2'-azino-bis (3-ethylbenzothiazoline-6-sulphonic acid) (ABTS) [8] 2,2-diphenyl-1-picrylhydrazyl (DPPH) [9,10], and ferric reducing ability plasma (FRAP) [11] assays. One of the most interesting assays for evaluation of TAC is spectrophotometric DPPH assay [12,13]. DPPH is a stable free radical which has an unpaired valence electron at one atom of nitrogen bridge [14]. Antioxidant can donate an H-atom to DPPH structure, leading to the color change of DPPH solution from violet to pale yellow.

* Corresponding author.

** Correspondence to: O. Chailapakul, Electrochemistry and Optical Spectroscopy Research Unit (EOSRU), Department of Chemistry, Faculty of Science, Chulalongkorn University, Pathumwan, Bangkok 10330, Thailand.

E-mail addresses: nadnudda.r@chula.ac.th (N. Rodthongkum), corawon@chula.ac.th (O. Chailapakul).

However, independence of sample turbidity and matrix color is required for spectroscopic measurement [12,13].

Nowadays, an electrochemical technique has attracted much interest because it offers a great promise with excellent features such as high sensitivity, minimal power demand, inherent miniaturization of electrode and controlled instrumentation [15]. Moreover, electrochemical sensing of an electroactive DPPH radical is undisturbed by turbidity and color of testing solution. Several studies focus on the electrochemical measurement of TAC using DPPH assay. For instance, Amatongchai et al. developed a simple chronoamperometric flow injection coupled with DPPH assay for TAC evaluation using carbon nanotube modified glassy carbon electrode (CNT/GC) [16]. Schulte et al. introduced an accurate computer-controlled chronoamperometric DPPH assay using an automated electrochemical microtiter plate for quantification of antioxidants in food samples [17]. Nonetheless, the previously reported electrochemical systems are designed to be small size, resulting in decrease of electrochemical sensitivity.

To improve the sensitivity of electrochemical system, electrode modification using nanomaterials has become an attractive approach for ongoing researches. Especially, graphene (G), which is a single planar sheet of sp^2 -bonded carbon atom densely packed honeycomb two-dimensional lattice [18], has become an outstanding nanomaterial for improving the electrode performance due to its large surface area (theoretical value $2630\text{ m}^2\text{ g}^{-1}$), high electrical conductivity, strong mechanical strength, and good biocompatibility [19]. Nevertheless, the pure form of G has a high tendency to agglomerate and restack to form graphite through p - p stacking and van der Waals interaction. To solve this problem, G and conducting polymer have been used to form composite materials in order to reduce the agglomeration of G [20–22]. Conducting polymer has become a material of interest for electrode surface modification because of its unique conduction ability and high environmental stability. Various conducting polymers, such as polyaniline (PANI) [23], polypyrrole (PPy) [24] and poly(3,4-ethylenedioxythiophene): poly(styrenesulfonate) (PEDOT:PSS) [22] have been incorporated with G layer to improve the electrochemical performances of electrode [25]. PEDOT:PSS is one of an interesting conducting polymers for electrode modification owing to its high conductivity, low redox potential and thermal stability [26]. Karuwan et al. developed the inkjet-printed G/PEDOT:PSS modified screen-printed carbon electrode (SPCE) for electrochemical determination of salbutamol in pharmaceutical products [26]. Moreover, electrochemical biosensor based on G/PEDOT:PSS and glucose oxidase modified electrode was developed for highly sensitive detection of glucose [27]. Several electrode modification techniques such as drop-casting [28], electrodeposition [29], inkjet-printing [26], electrospinning [30,31], and electro spraying [32–34] have been used. In this work, electro spraying was selected as an electrode modification procedure to generate uniform three-dimension droplet-like composite on electrode surface by applying high voltage electric field. This technique significantly increases the specific surface area of electrode and provides fast electron transfer process, which is highly appropriate for the development of a highly sensitive electrochemical sensor [32–34].

This research aims to develop a chronoamperometric sensor using an electro sprayed G/PEDOT: PSS modified SPCE coupled with DPPH assay for free radical scavenger screening of TAC and then applies the developed system for evaluation of TAC content in Thai herb and beverage. When adding the testing solution, the decrease of the DPPH signal from the baseline was obtained and related to the antioxidant amount in the sample solution. For chronoamperometric sensing, the cathodic detection region was used to monitor DPPH consumption with no observed interference from easily oxidizable species such as polyphenolic antioxidants [35]. For food sample analyses, this system was successfully validated and compared to standard spectrophotometric assay with the satisfactory results. This novel approach might be an alternative tool for TAC screening in food products.

2. Experiment

2.1. Reagent and material

Graphene (G) nanopowder was purchased from SkySpring Nanomaterials, Inc. (Houston, TX, USA). Poly(3,4-ethylenedioxythiophene): poly(styrenesulfonate) (PEDOT:PSS), 2,2-diphenyl-1-picrylhydrazil (DPPH), potassium ferricyanide ($K_3[Fe(CN_6)]$), Trolox (6-hydroxy-2,5,7,8-tetramethylchroman-2-carboxylic acid), and potassium ferrocyanide ($K_4[Fe(CN_6)]$) were obtained from Sigma-Aldrich (St. Louis, Mo, USA). Dimethylformamide (DMF), absolute ethanol (C_2H_5OH), and potassium dihydrogen phosphate (KH_2PO_4) were purchased from Carlo Erba Reagenti-SDS (Val de Reuil, France). Disodium hydrogen phosphate (Na_2HPO_4), potassium chloride (KCl), sodium chloride (NaCl), and ascorbic acid (AA) were received from Merck (Darmstadt, Germany). Carbon and silver/silver chloride inks were purchased from Gwent group (Torfean, United Kingdom). All analytical grade reagents and milliQ water ($R \geq 18.2\text{ M}\Omega\text{ cm}$) were used for all experiments. Phosphate buffer saline (0.1 M, pH 7.0) and absolute ethanol were used as the supporting electrolyte for all electrochemical measurements. An ethanolic phosphate buffer solution (EPBS) was prepared by mixing between 60% ethanol and PBS solution and used as a supporting electrolyte. The stock solution of 2,2-diphenyl-1-picrylhydrazil (DPPH) and 2 mM standard Trolox was freshly prepared in 0.1 M EPBS at a pH of 7.0. After that, DPPH in ethanol was sonicated using ultrasonicator to provide completely dissolved DPPH solution.

Thai herb (Indian gooseberry) and herbal drinks (Thai blueberry, mulberry, bamboo grass and gotu kola) were purchased from local supermarket in Thailand. Botanical names of these herbs are *Phyllanthus emblica* L. (Indian gooseberry), *Antidesma ghaesembilla* Gaertn. (Thai blueberry), *Antidesma ghaesembilla* Gaertn. (mulberry), *Tiliacora triandra* (Colebr.) Diels (bamboo grass) and *Centella asiatica* (L.) Urban (gotu kola).

2.2. Screen-printed carbon electrode (SPCE) fabrication

For the electrode fabrication, the screen-printed carbon electrodes (SPCEs) were prepared in-house on polyvinyl chloride (PVC) substrate as described in previous studies [30,36]. Firstly, silver/silver chloride ink was printed on PVC surface to form a reference electrode (RE) and conducting pad. Then, carbon ink was printed onto PVC substrate as a working electrode (WE) and counter electrode (CE), respectively. In each screen-printing step, SPCEs were dried in an oven at $55\text{ }^\circ\text{C}$ for 1 h to evaporate the solvent. The projective surface area of working electrode is 50 mm^2 .

2.3. Preparation of G/PEDOT: PSS modified SPCE using electro spraying fabrication

G/PEDOT: PSS composite solution was prepared by physical mixing method. Firstly, 4 mg of G nanopowders was dispersed in 1 mL of DMF and sonicated for 24 h at room temperature. Then, 10 mg of PEDOT: PSS was dissolved in 1 mL of DMF and sonicated for 24 h at room temperature. After that, G and PEDOT:PSS solution was mixed together with magnetic stirrer.

An electro spraying system consists of a high-voltage power supply (Gamma High Voltage Research, Ormond Beach, FL, USA), syringe pump (Kent Scientific Corp., Torrington, CT, USA), ground collector (5 cm from the needle tip), plastic syringe, and stainless-steel needle. The composite solution was filled in the plastic syringe and inserted into the syringe pump with a constant flow rate of 1.0 mL h^{-1} . A high-voltage power supply was connected between stainless-steel needle and ground collector. The counter (CE) and reference electrodes (RE) were covered with aluminum foil to prevent spray from the electro spraying process. The optimal electro spraying conditions including 7.5 kV of applied voltage, and 6 min of spraying time were used for

all experiments. A well-mixed G/PEDOT:PSS nanocomposite solution was electrosprayed onto the working electrode (WE) and then attached to a ground collector. Finally, the SPCE modified by G/PEDOT:PSS nanodroplet was obtained and used as a novel WE for further step.

The morphology of G/PEDOT:PSS nanodroplet and the dispersion of G were investigated by using a JSM-6400 field emission scanning electron microscope (Japan Electron Optics Laboratory Co., Ltd., Japan) and a JEM-2100 transmission electron microscope (Japan Electron Optics Laboratory Co., Ltd., Japan).

2.4. Electrochemical measurement

Electrochemical measurement was performed using a potentiostat with e-corder 410 (eDAQ, Australia). Three electrode system consists of Ag/AgCl electrode as reference electrode, and carbon electrode as both working electrode and counter electrode. Cyclic voltammetry (CV) was performed for electrochemical characterization of various SPCEs including bare SPCE, PEDOT:PSS/SPCE, and G/PEDOT:PSS/SPCE. First, the electrochemical behaviors of these electrodes were investigated by CV using a standard solution of $[\text{Fe}(\text{CN})_6]^{3-/4-}$ in 0.1 M KCl with a scanning potential range between -0.2 to 1.2 V vs. Ag/AgCl and a scan rate of 250 mV/s.

For electrode optimization, 2.5 mM DPPH in 0.1 M EPBS solution at pH of 7.0 was used. SWV measurements were performed over a scanning potential range from 0 to $+0.6$ V with a pulse amplitude of 25 mV, frequency of 15 Hz, and step height of 1 mV. For the determination of TAC, DPPH scavenging upon addition of antioxidant was monitored by chronoamperometric measurement. The testing solution was mixed with 6 mM DPPH at the ratio of 1:1 (v/v). Commercial vortex mixer (LMS Co., LTD., Tokyo, Japan) was used to mix the solution for 30 s. Then, only 40 μL of mixture was dropped onto the SPCE and measured the electrochemical response by chronoamperometric detection. The chronoamperometric experiment was performed at the detection

potential of 0.2 V vs. Ag/AgCl. An amperometric response was recorded at 40 s, which was a 95% steady-state current. The linear calibration between the difference of cathodic DPPH current (between the adding and no adding standard Trolox solution) and Trolox concentration in a range of 5–30 μM was constructed and treated with linear least square regression analysis.

2.5. Preparation of plant extract

For antioxidant extraction, fresh indian gooseberry pulps were grinded and dried. 10 g of dried powder was extracted using 100 mL ethanol for 24 h and then filtered through 0.45 μm filter paper. Ethanol was removed from filtered using a rotary evaporator at 40 °C. The crude plant extract was freeze-dried and then stored at 4 °C until analysis as described in the previous report [17,37]. In case of herbal drink samples, these liquid samples were diluted 1000 times and then directly tested with our proposed method without any sample preparation step.

For the method validation, UV-vis spectrophotometry was used to determine TAC and compared with the results obtained from our proposed system [3]. 0.2 mM DPPH solution, real samples and a standard Trolox were dissolved in ethanol-water. The solution of DPPH and diluted real samples was mixed for 10 s, and absorbance of DPPH activity was measured at 523 nm using ultraviolet-vis spectrophotometer with ethanol as blank. [38].

3. Results and discussion

3.1. Optimization of electrode modification

Firstly, the parameters influencing on the electrochemical sensitivity of G/PEDOT:PSS/SPCE were investigated and optimized. The amount of PEDOT:PSS loading and G loading in the range of 0–12 mg/mL and 0–10 mg/mL, respectively was studied. Then, the optimized electrodes

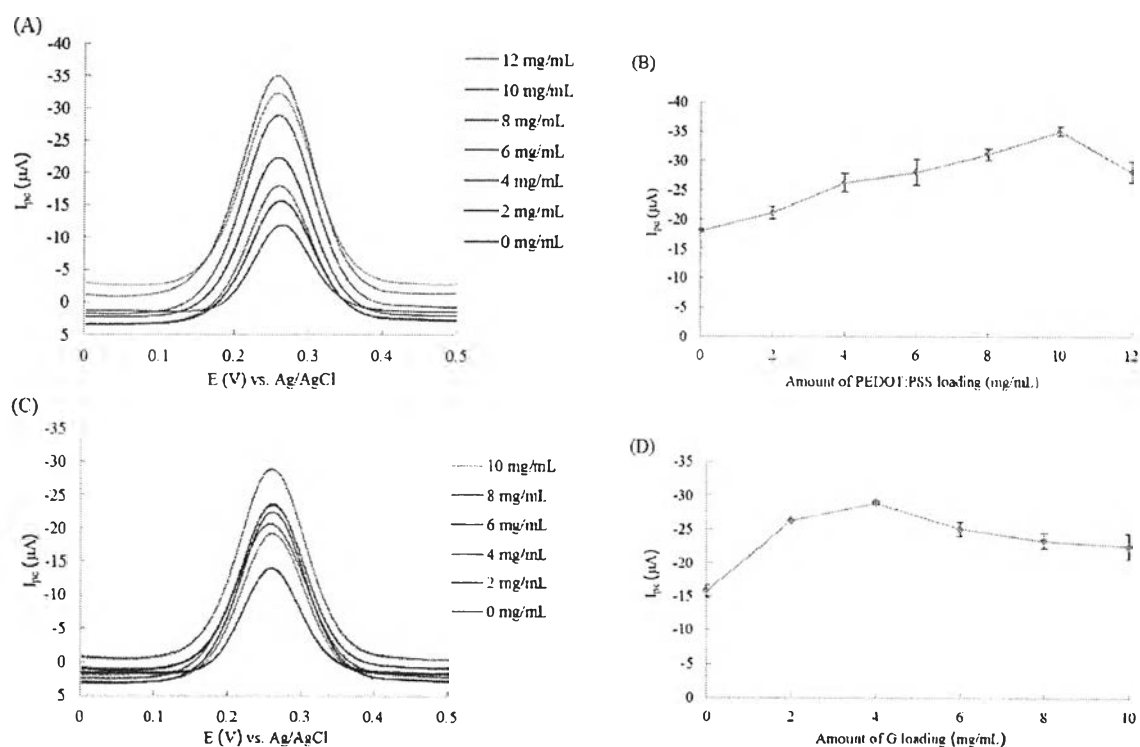


Fig. 1. Influence of the amount of PEDOT:PSS loading (A and B) and amount of G loading (C and D) using square-wave voltammetric detection of 2.5 mM DPPH. G concentration employed during the optimization of the amount of PEDOT:PSS is 4 mg/mL while PEDOT:PSS concentration employed during the optimization of the amount of G is 10 mg/mL. SWV conditions: scanning potential range of 0 to $+0.6$ V with a pulse amplitude of 25 mV, a square wave frequency of 15 Hz, and a step height of 1 mV.

were tested towards the electrochemical detection of DPPH by using SWV. Initially, the effect of PEDOT: PSS loading (mg/mL) on the electrochemical sensitivity in the detection of DPPH was explored as shown in Fig. 1A and B. When the amount of PEDOT: PSS loading (mg/mL) increases from 2 to 10 mg/mL, the cathodic peak current slightly increases, and the current is highest when the amount of PEDOT: PSS loading is 10 mg/mL. At 12 mg/mL of PEDOT: PSS loading, the cathodic peak current starts decreasing, which is probably the limited solubility of the polymers. Therefore, 10 mg/mL of PEDOT: PSS loading was selected as an optimum condition for the subsequent experiments.

Next, the optimal amount of G loading was investigated as shown in Fig. 1C and D, respectively. These results verify that incorporation of G into PEDOT: PSS tends to improve the electrochemical conductivity of modified electrode. However, the cathodic peak currents decrease when the amount of G loading is above 4 mg/mL. The decrease of cathodic current response is probably caused by the agglomeration of G within the nanocomposites [25]. Thus, 4 mg/mL of G loading was chosen as an optimal G loading for further experiments.

3.2. Physical characterization of G/PEDOT: PSS/SPCE

The surface morphology of G/PEDOT:PSS/SPCE was characterized by scanning electron microscopy (SEM). As shown in Fig. 2A, a SEM image displays the uniform 3D droplet-like structure of G/PEDOT:PSS on the electrode surface. Furthermore, a TEM image (Fig. 2B) shows the ultra-thin sheets of G verifying that G is well dispersed within the nanocomposites without severe agglomeration and the electron diffraction pattern of G is demonstrated in Fig. 2C.

3.3. Electrochemical characterization of G/PEDOT: PSS/SPCE

Fig. 3A shows the well-defined cyclic voltammograms of standard ferri/ferrocyanide $[\text{Fe}(\text{CN})_6]^{3/4-}$ measured on the unmodified SPCE and G/PEDOT:PSS/SPCE. The results reveal that the current response measured on G/PEDOT: PSS/SPCE is approximately 3-fold higher than the current response measured on unmodified SPCE. Moreover, a significant decrease of potential difference (ΔE_p) between anodic and cathodic peak potential of G/PEDOT:PSS/SPCE ($\Delta E_p = 0.1$ V) compared to unmodified SPCE ($\Delta E_p = 1.0$ V) indicating that G/PEDOT:PSS nanocomposite can also improve the electron transfer kinetics of this electrochemical system.

Fig. 3B shows the cyclic voltammograms of DPPH solution measured on the unmodified SPCE compared to G/PEDOT:PSS/SPCE. Two reversible redox couples were observed (1st couple $E_{pc} = 0.22$ V, $E_{pa} = 0.31$ V and the 2nd couple $E_{pc} = 0.66$ V, $E_{pa} = 0.74$ V vs. Ag/AgCl). Unmodified and modified SPCEs provide the similar ΔE_p obtained from the cyclic voltammogram indicating that both are high conducting material. The current response measured on G/PEDOT: PSS/SPCE is approximately 2-fold higher than the current response measured on unmodified SPCE. Furthermore, the electrochemical performance of DPPH is well matched with the previous reports [39,40]. These results suggest that G/PEDOT: PSS/SPCE can be an alternative electrochemical sensor for the detection of free radical DPPH.

To investigate the mass transfer process of DPPH on the G/PEDOT: PSS/SPCE, the effect of scan rate on the current response was studied. As shown in cyclic voltammogram (Fig. 4A), two reversible redox couples are observed, which can be explained by the Randle-Sevcik equation [41]. As shown in Fig. 4B, both anodic and cathodic

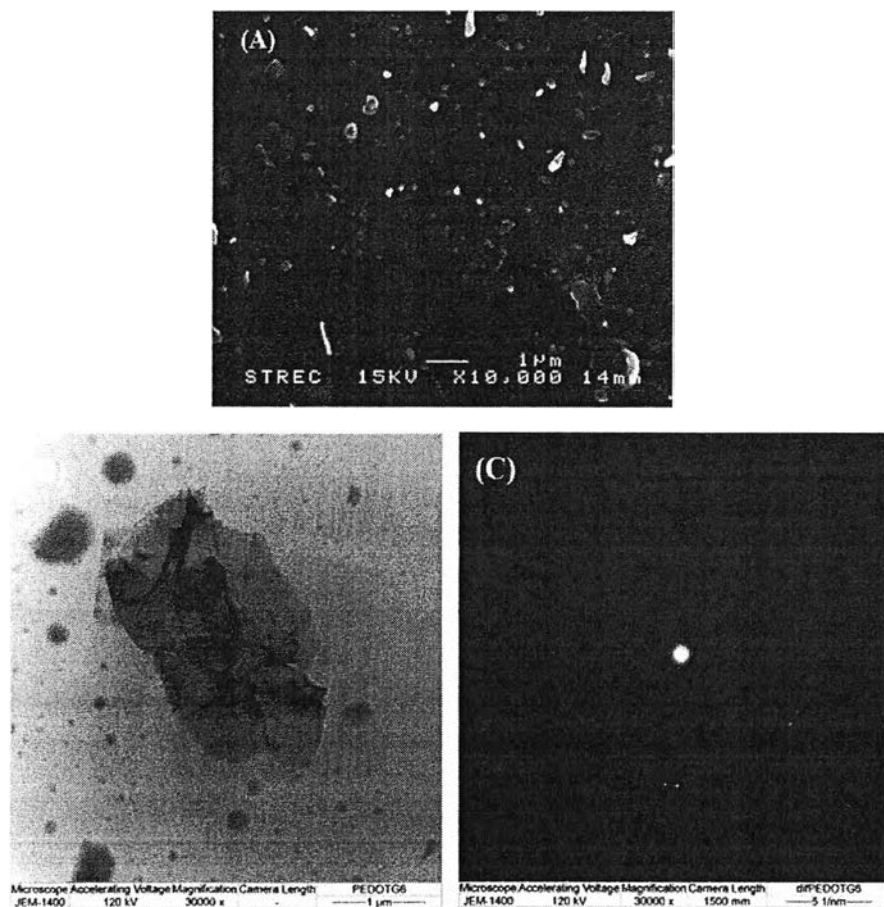


Fig. 2. (A) SEM image of G/PEDOT: PSS/SPCE, (B) TEM image of G dispersed in nanocomposites and (C) electron diffraction pattern of G in nanocomposites.

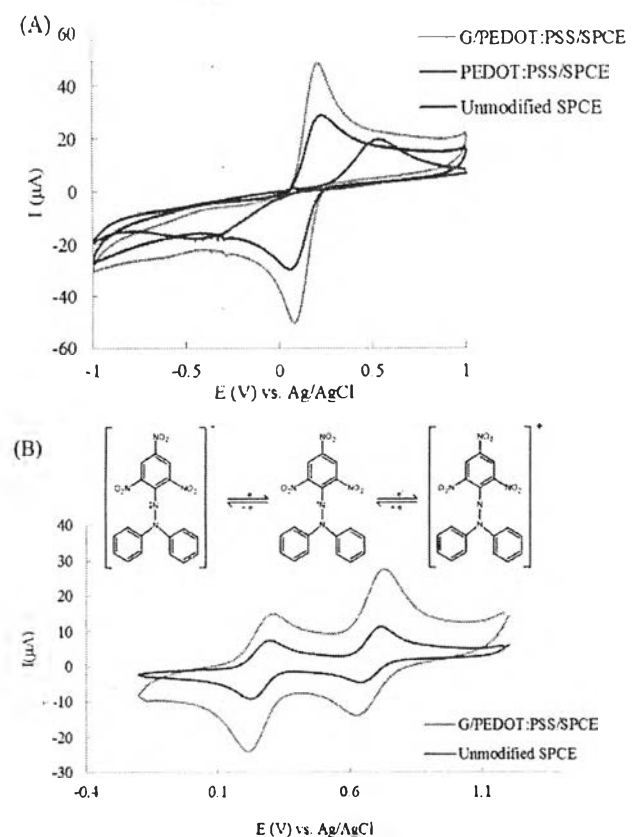


Fig. 3. (A) Cyclic voltammograms of 1.0 mM [Fe(CN)6]3-/4- in 0.1 M KCl with a scan rate of 250 mV/s measured on unmodified SPCE (blue line), PEDOT:PSS modified electrode (red line) and G/PEDOT:PSS modified electrode (green line). (B) cyclic voltammograms of 2.5 mM DPPH in 0.1 M EPBS solution (pH 7.0) measured on unmodified SPCE (blue line) and on G/PEDOT:PSS/SPCE (green line). (inset) redox reaction of DPPH.

current responses are linearly proportional to the square root of scan rate ($v^{1/2}$) in the range of 100–400 mV/s. Thus, the redox process on G/PEDOT:PSS/SPCE is controlled by diffusion process which is no adsorption and a coupled reaction to electrochemical processes [38].

3.4. Electrochemical investigation of DPPH in the presence of Trolox

Fig. 5A shows a representative cyclic voltammogram of DPPH in the presence and absence of Trolox. With adding 5 mM of Trolox in the DPPH solution, the peaks corresponding to the redox reactions of DPPH disappeared. We believed that the decrease of current in the presence of Trolox antioxidant is due to consumption of electroactive DPPH, corresponding to hydrogen atom transfer (HAT) mechanism as shown in Eqs. (1) and (2).



Where DPPH• is 2,2-diphenyl-1-picrylhydrazine radical, AH is protonated antioxidant and A• is deprotonated antioxidant. As the DPPH-H occurred, concentration of DPPH- and DPPH• which is available for electrochemical detection also decreased. However, only anodic current (I_{pa2}) in the Fig. 5A dramatically increased. We believed that this is caused by the direct electro-oxidation of Trolox. Thus, electrochemical detection of non-reacted DPPH- and DPPH• at cathodic region

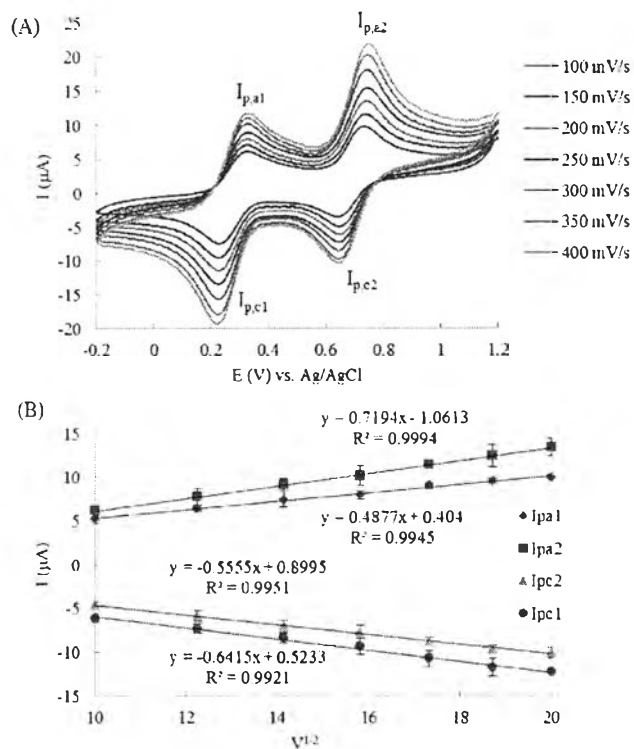


Fig. 4. (A) Cyclic voltammogram of 2.5 mM DPPH in 0.1 M EPBS solution (pH 7.0) measured on G/PEDOT:PSS/SPCE at scan rate of 100, 150, 200, 250, 300, 350 and 400 mV/s and (B) relationship between anodic and cathodic peak currents (μA) versus (scan rate) $^{1/2}$.

was selected for the further experiments to avoid interfering response obtained from a directly electrochemical oxidation of antioxidant.

3.5. Selection of detection potential

According to previous literatures [2,42], the common antioxidants which are able to detect by using electrochemical method are ascorbic acid, gallic acid, catechin and caffeic acid. Thus, the detection of these antioxidants was investigated by cyclic voltammetry focusing on the detection at cathodic region as shown in the Fig. S1. We found that the antioxidants which provided the cathodic peak response are only catechin and caffeic acid (Fig. S2). The cathodic peak potentials of catechin and caffeic acid were found to be -0.03 V and -0.025 V vs. Ag/AgCl, respectively. Moreover, the difference in the cathodic peak potential between DPPH and catechin was found to be 250 mV while potential difference between DPPH and caffeic acid was 245 mV vs. Ag/AgCl. Consequently, the chronoamperometric detection potential higher than 0 V vs. Ag/AgCl might be useful to provide a selectively electrochemical detection of DPPH without any interfering response from direct reduction of the electroactive antioxidants.

Next, chronoamperometry was performed for indirect electrochemical determination of TAC by DPPH assay. The sensitivity and selectivity of the system can be readily tuned by the selection of appropriate detection potential. To investigate the optimal detection potential for chronoamperometric detection of DPPH, the relationship between detection potential in a range of -0.1 to 0.4 V vs. Ag/AgCl and current response of DPPH (blue line) versus 0.1 M EPBS (green line) was constructed as shown in Fig. 5B [43]. When the applied potential is changed from -0.1 to 0.2 V, the cathodic current response drastically decreases. The cathodic current response reached a plateau when the applied potential is lower than 0.2 V (Fig. 5B). The S/B ratios are calculated, and the resulting curve between S/B ratio and detection potential is shown in Fig. 5C. The maximum S/B ratio is found to be 0.2 V vs. Ag/AgCl,

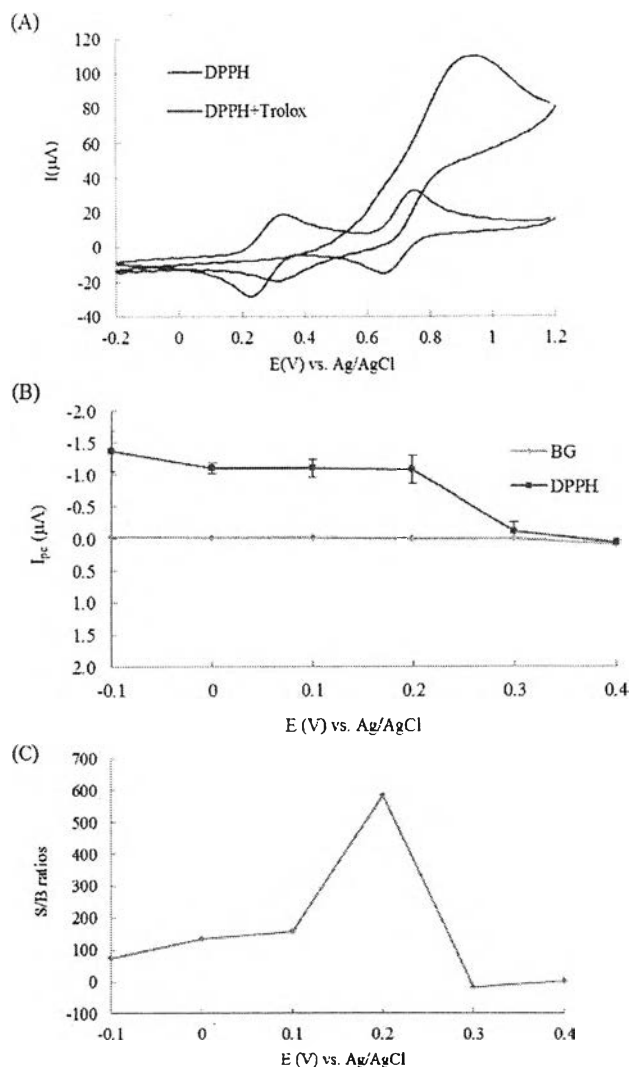


Fig. 5. (A) Cyclic voltammogram of 2.5 mM DPPH in the absence (blue solid line) and presence (red solid line) of Trolox (5 mM). (B) relationship between current and detection potential of 6.0 mM DPPH (blue line) and background (green line) at 40 s sampling time measured on G/PEDOT:PSS/SPCE and (C) signal-to-background (S/B) ratio obtained from the data in the Fig 5A.

therefore, this potential is chosen for cathodic chronoamperometric detection of DPPH solution.

3.6. 3.5 Analytical performance of this system

G/PEDOT:PSS/SPCE was used for the measurement of different standard Trolox concentrations in a range of 0–30 μM as shown in Fig. 6A, and the steady-state chronoamperometric current responses at a current of 40 s were recorded. Then, linear calibration curve was obtained (Fig. 6B) by plotting the current responses versus standard Trolox concentrations. The limits of detection (LOD, $S/N = 3$) and limits of quantification (LOQ, $S/N = 10$) were found to be 0.59 μM and 1.97 μM , respectively. Moreover, the reproducibility (7 different electrodes) and repeatability (7 different measurements) of G/PEDOT:PSS/SPCE were investigated by chronoamperometric detection of 20 μM Trolox in EPBS (pH 7.0). The relative standard deviations (RSDs) of reproducibility and repeatability were found to be 2.13% and 2.78%, respectively, indicating that our proposed system provides a good reproducibility and repeatability.

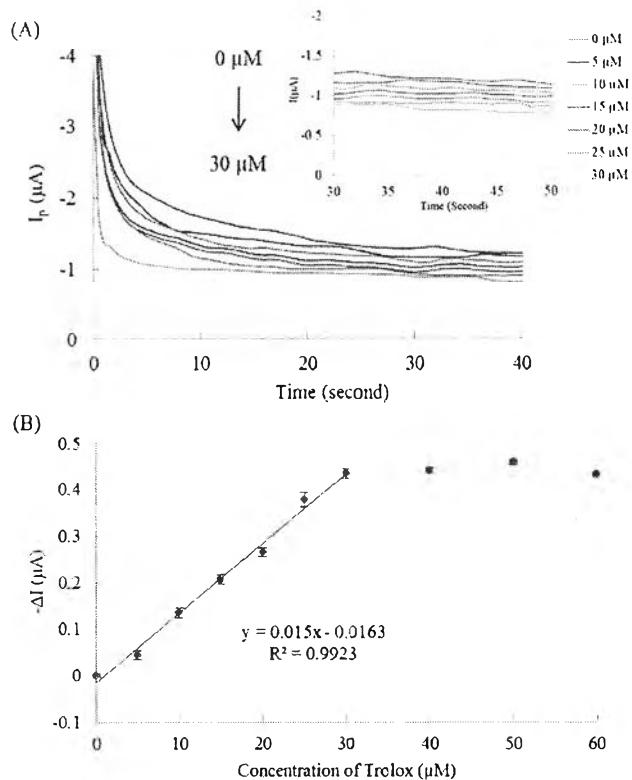


Fig. 6. (A) Chronoamperogram and (B) calibration curve of Trolox detection in a concentration range of 5 to 30 μM in the EPBS solution at pH 7.0 measured on G/PEDOT:PSS/SPCE.

3.7. 3.6 Evaluation of TAC in herb samples and herbal beverages

G/PEDOT:PSS/SPCE was applied to evaluate the TAC of five samples. Prior to analysis, dried herb sample was prepared using ethanolic extraction to separate antioxidants from a dried plant matrix while TAC of herbal beverages was directly determined without sample preparation step. In case of dried plant, TAC value was expressed as mg Trolox equivalent per gram of dry plant ($\text{mg of Trolox g}^{-1}$ of sample). As shown in Table 1, the TAC values obtained from our method are compared to those obtained from conventional Uv–vis spectrophotometry using a paired T-test analysis at the 95% confidence. The results obtained from our system were not significantly different between these methods. Therefore, it can be concluded that G/PEDOT:PSS/SPCE can be successfully applied for the determination of TAC in both herb and herbal beverages.

4. Conclusions

A novel electrospayed G/PEDOT:PSS modified electrochemical sensor was developed for TAC evaluation in various herbal samples.

Table 1

TAC values of five samples obtained from our developed system versus a conventional ultraviolet–visible spectrophotometry (spectrometric, [3]).

Scientific name of sample	Type of sample	Found TAC value	
		Our proposed method	Spectrophotometric method
<i>P. emblica</i> L.	Dried plant	$513.29 \pm 3.39 \text{ mg/g}^*$	$508.30 \pm 4.03 \text{ mg/g}^*$
<i>A. ghaesembilla</i> Gaertn.	Beverage	$5.25 \pm 0.15 \text{ g/L}$	$5.00 \pm 0.15 \text{ g/L}$
<i>Morus alba</i> Linn.	Beverage	$3.69 \pm 0.14 \text{ g/L}$	$3.56 \pm 0.13 \text{ g/L}$
<i>T. triandra</i> (Colebr.) Diels	Beverage	$3.89 \pm 0.12 \text{ g/L}$	$3.75 \pm 0.14 \text{ g/L}$
<i>C. asiatica</i> (L.) Urban.	Beverage	$4.65 \pm 0.15 \text{ g/L}$	$4.49 \pm 0.09 \text{ g/L}$

* mg of Trolox/g of sample.

G/PEDOT: PSS nanostructures can increase the electrochemical activity and current response for TAC monitoring via the detection of DPPH. Moreover, this sensing system shows a substantial improved sensitivity, reproducibility, repeatability and requires only small volume of sample (40 μL). Finally, G/PEDOT: PSS/SPCE was successfully applied for the determination of antioxidant content in Thai herbs and herbal beverages. The obtained results showed a good agreement with the results from conventional UV–visible spectrophotometry. This system might be an alternative tool for TAC evaluation in plants, which is applicable to all sample types without any interference effect from sample color and sample turbidity.

Novelty statement

This work presents a novel graphene/poly (3,4-ethylenedioxythiophene):poly (styrene sulfonate) nanocomposite-modified screen-printed carbon electrode (G/PEDOT:PSS/SPCE) for evaluation of TAC content using chronoamperometric detection of DPPH. The modified electrodes exhibit excellent electrochemical sensitivity for TAC determination. Interestingly, the matrix color of sample does not interfere our proposed method in the electrochemical measurement of TAC. In addition, the G/PEDOT:PSS/SPCE can be applied for the determination of TAC in herb and herbal beverages with good reproducibility and repeatability. Finally, this presented method is a satisfactory agreement with the conventional UV–Visible spectroscopic method.

Acknowledgments

Authors gratefully acknowledge the financial support from the Thailand Research Fund through Research Team Promotion Grant (RTA5780005) and the National Nanotechnology Center (NANOTEC), NSTDA, Ministry of Science and Technology, Thailand. P. R. Would like to thank the financial support from the Graduate School of Chulalongkorn University for a Postdoctoral Fellowship (Ratchadaphiseksomphot Endowment Fund).

Appendix A. Supplementary data

Supplementary data to this article can be found online at <http://dx.doi.org/10.1016/j.jelechem.2015.11.037>.

References

- [1] M. Laguerre, J. Lecomte, P. Villeneuve, Evaluation of the ability of antioxidants to counteract lipid oxidation: existing methods, new trends and challenges, *Prog. Lipid Res.* 46 (2007) 244–262.
- [2] S. Milardović, D. Iveković, B.S. Grabarić, A novel amperometric method for antioxidant activity determination using DPPH free radical, *Bioelectrochemistry* 68 (2006) 175–180.
- [3] A.M. Pisoschi, M.C. Cheregi, A.F. Danet, Total antioxidant capacity of some commercial fruit juices: electrochemical and spectrophotometric approaches, *Molecules* 14 (2009) 480–493.
- [4] D. Ozyurt, B. Demirata, R. Apak, Determination of total antioxidant capacity by a new spectrophotometric method based on Ce(IV) reducing capacity measurement, *Talanta* 71 (2007) 1155–1165.
- [5] S. Girotti, F. Fini, L. Bolelli, L. Savini, E. Sartini, G. Arfelli, Chemiluminescent determination of total antioxidant capacity during winemaking, *Luminescence* 21 (2006) 233–238.
- [6] A. Ghiselli, M. Serafini, G. Maiani, E. Azzini, A. Ferro-Luzzi, A fluorescence-based method for measuring total plasma antioxidant capability, *Free Radic. Biol. Med.* 18 (1995) 29–36.
- [7] K. Sözgen Başkan, E. Tütem, N. Özer, R. Apak, Spectrophotometric and chromatographic assessment of contributions of carotenoids and chlorophylls to the total antioxidant capacities of plant foods, *J. Agric. Food Chem.* 61 (2013) 11371–11381.
- [8] O. Erel, A novel automated direct measurement method for total antioxidant capacity using a new generation, more stable ABTS radical cation, *Clin. Biochem.* 37 (2004) 277–285.
- [9] P. Molyneux, The use of the stable free radical diphenylpicrylhydrazyl (DPPH) for estimating antioxidant activity, *Songklanakarin J. Sci. Technol.* 26 (2004) 211–219.
- [10] M.S. Blois, Antioxidant determinations by the use of a stable free radical, *Nature* 181 (1958) 1199–1200.
- [11] C. Guo, J. Yang, J. Wei, Y. Li, J. Xu, Y. Jiang, Antioxidant activities of peel, pulp and seed fractions of common fruits as determined by FRAP assay, *Nutr. Res.* 23 (2003) 1719–1726.
- [12] F. Abderrahim, S.M. Arribas, M.C. Gonzalez, L. Condezu-Hoyos, Rapid high-throughput assay to assess scavenging capacity index using DPPH, *Food Chem.* 141 (2013) 788–794.
- [13] A.C. Moț, R. Silaghi-Dumitrescu, C. Sârbu, Rapid and effective evaluation of the antioxidant capacity of propolis extracts using DPPH bleaching kinetic profiles, FT-IR and UV–vis spectroscopic data, *J. Food Compos. Anal.* 24 (2011) 516–522.
- [14] O.P. Sharma, T.K. Bhat, DPPH antioxidant assay revisited, *Food Chem.* 113 (2009) 1202–1205.
- [15] J. Wang, Portable electrochemical systems, *TrAC Trends Anal. Chem.* 21 (2002) 226–232.
- [16] M. Amatongchai, S. Laosing, O. Chailapakul, D. Nacapricha, Simple flow injection for screening of total antioxidant capacity by amperometric detection of DPPH radical on carbon nanotube modified-glassy carbon electrode, *Talanta* 97 (2012) 267–272.
- [17] S. Intarakham, A. Schulte, Automated electrochemical free radical scavenger screening in dietary samples, *Anal. Chem.* 84 (2012) 6767–6774.
- [18] K.S. Novoselov, A.K. Geim, S. Morozov, D. Jiang, Y. Zhang, S. Dubonos, I. Grigorieva, A. Firsov, Electric field effect in atomically thin carbon films, *Science* 306 (2004) 666–669.
- [19] B.-T. Zhang, X. Zheng, H.-F. Li, J.-M. Lin, Application of carbon-based nanomaterials in sample preparation: a review, *Anal. Chim. Acta* 784 (2013) 1–17.
- [20] Y. Fan, J.-H. Liu, C.-P. Yang, M. Yu, P. Liu, Graphene–polyaniline composite film modified electrode for voltammetric determination of 4-aminophenol, *Sensors Actuators B Chem.* 157 (2011) 669–674.
- [21] P. Ekabutr, O. Chailapakul, P. Supaphol, Modification of disposable screen-printed carbon electrode surfaces with conductive electrospun nanofibers for biosensor applications, *J. Appl. Polym. Sci.* 130 (2013) 3885–3893.
- [22] C. Sriprachuabwong, C. Karuwan, A. Wisitsoratt, D. Phokharatkul, T. Lomas, P. Sritongkham, A. Tuantranont, Inkjet-printed graphene-PEDOT: PSS modified screen printed carbon electrode for biochemical sensing, *J. Mater. Chem.* 22 (2012) 5478–5485.
- [23] S. Liu, X. Xing, J. Yu, W. Lian, J. Li, M. Cui, J. Huang, A novel label-free electrochemical aptasensor based on graphene–polyaniline composite film for dopamine determination, *Biosens. Bioelectron.* 36 (2012) 186–191.
- [24] A. Ramanavičius, A. Ramanavičienė, A. Malinauskas, Electrochemical sensors based on conducting polymer–polypyrrrole, *Electrochim. Acta* 51 (2006) 6025–6037.
- [25] N. Rodthongkum, N. Ruecha, N. Promphet, R. Rangkupan, R.W. Vachet, O. Chailapakul, Graphene-Loaded Nanofiber-Modified Electrode: A Novel and Sensitive Electrochemical Detection System, *Image*, DOI 2015.
- [26] C. Karuwan, C. Sriprachuabwong, A. Wisitsoratt, D. Phokharatkul, P. Sritongkham, A. Tuantranont, Inkjet-printed graphene–poly(3,4-ethylenedioxythiophene):poly(styrene-sulfonate) modified on screen printed carbon electrode for electrochemical sensing of salbutamol, *Sensors Actuators B Chem.* 161 (2012) 549–555.
- [27] A. Wisitsoratt, S. Pakongpan, C. Sriprachuabwong, D. Phokharatkul, P. Sritongkham, T. Lomas, A. Tuantranont, Graphene-PEDOT: PSS on screen printed carbon electrode for enzymatic biosensing, *J. Electroanal. Chem.* 704 (2013) 208–213.
- [28] X.-M. Feng, R.-M. Li, Y.-W. Ma, R.-F. Chen, N.-E. Shi, Q.-L. Fan, W. Huang, One-step electrochemical synthesis of graphene/polyaniline composite film and its applications, *Adv. Funct. Mater.* 21 (2011) 2989–2996.
- [29] Y. Tang, N. Wu, S. Luo, C. Liu, K. Wang, L. Chen, One-step electrodeposition to layer-by-layer graphene–conducting-polymer hybrid films, *Macromol. Rapid Commun.* 33 (2012) 1780–1786.
- [30] N. Promphet, P. Rattanasat, R. Rangkupan, O. Chailapakul, N. Rodthongkum, An electrochemical sensor based on graphene/polyaniline/polystyrene nanoporous fibers modified electrode for simultaneous determination of lead and cadmium, *Sensors Actuators B Chem.* 207 (Part A) (2015) 526–534.
- [31] N. Rodthongkum, N. Ruecha, R. Rangkupan, R.W. Vachet, O. Chailapakul, Graphene-loaded nanofiber-modified electrodes for the ultrasensitive determination of dopamine, *Anal. Chim. Acta* 804 (2013) 84–91.
- [32] N. Ruecha, R. Rangkupan, N. Rodthongkum, O. Chailapakul, Novel paper-based cholesterol biosensor using graphene/polyvinylpyrrolidone/polyaniline nanocomposite, *Biosens. Bioelectron.* 52 (2014) 13–19.
- [33] N. Ruecha, N. Rodthongkum, D.M. Cate, J. Volckens, O. Chailapakul, C.S. Henry, Sensitive electrochemical sensor using a graphene–polyaniline nanocomposite for simultaneous detection of Zn(II), Cd(II), and Pb(II), *Anal. Chim. Acta* 874 (2015) 40–48.
- [34] N. Thammasonaree, P. Rattanasat, N. Ruecha, W. Siangproh, N. Rodthongkum, O. Chailapakul, Ultra-performance liquid chromatography coupled with graphene/polyaniline nanocomposite modified electrode for the determination of sulfonamide residues, *Talanta* 123 (2014) 115–121.
- [35] M. Amatongchai, S. Laosing, O. Chailapakul, D. Nacapricha, Simple flow injection for screening of total antioxidant capacity by amperometric detection of DPPH radical on carbon nanotube modified-glassy carbon electrode, *Talanta* 97 (2012) 267–272.
- [36] P. Noyrod, O. Chailapakul, W. Wonsawat, S. Chuanwatanakul, The simultaneous determination of isoprotruron and carbendazim pesticides by single drop analysis using a graphene-based electrochemical sensor, *J. Electroanal. Chem.* 719 (2014) 54–59.
- [37] X. Liu, M. Zhao, J. Wang, B. Yang, Y. Jiang, Antioxidant activity of methanolic extract of emblica fruit (*Phyllanthus emblica* L.) from six regions in China, *J. Food Compos. Anal.* 21 (2008) 219–228.
- [38] S. Ahmed, S. Tabassum, F. Shakeel, A.Y. Khan, A facile electrochemical analysis to determine antioxidant activity of flavonoids against DPPH radical, *J. Electrochem. Soc.* 159 (2012) F103–F109.

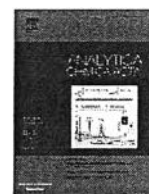
- [39] A.W. Taylor, S. Puttick, P. Licence, Probing solvation in ionic liquids via the electrochemistry of the DPPH radical, *J. Am. Chem. Soc.* 134 (2012) 15636–15639.
- [40] I. Vasilescu, S.A. Eremia, C. Albu, A. Radoi, S.-C. Litescu, G.-L. Radu, Determination of the antiradical properties of olive oils using an electrochemical method based on DPPH radical, *Food Chem.* 166 (2015) 324–329.
- [41] M. Olmstead, R. Nicholson, Experimental evaluation of cyclic stationary electrode polarography for reversible electron transfer, *Anal. Chem.* 38 (1966) 150–151.
- [42] C. Bardpho, P. Rattanasat, W. Siangproh, O. Chailapakul, Ultra-high performance liquid chromatographic determination of antioxidants in teas using inkjet-printed graphene-polyaniline electrode, *Talanta* 148 (2016) 673–679.
- [43] S. Nantaphol, O. Chailapakul, W. Siangproh, Sensitive and selective electrochemical sensor using silver nanoparticles modified glassy carbon electrode for determination of cholesterol in bovine serum, *Sensors Actuators B Chem.* 207 (Part A) (2015) 193–198.



ELSEVIER

Contents lists available at ScienceDirect

Analytica Chimica Acta

journal homepage: www.elsevier.com/locate/aca

Electrochemical sensors for the simultaneous determination of zinc, cadmium and lead using a Nafion/ionic liquid/graphene composite modified screen-printed carbon electrode



Sudkate Chaiyo^a, Eda Mehmeti^b, Kristina Žagar^c, Weena Siangproh^{d,***},
Orawon Chailapakul^{a, e, **}, Kurt Kalcher^{b, *}

^a Electrochemistry and Optical Spectroscopy Research Unit (EOSRU), Department of Chemistry, Faculty of Science, Chulalongkorn University, 254 Phayathai Road, Patumwan, Bangkok, Thailand

^b Institute of Chemistry, Department of Analytical Chemistry, Karl-Franzens University, Universitätsplatz 1, Graz A-8010, Austria

^c Department for Nanostructured Materials, Jozef Stefan Institute, Ljubljana, Slovenia

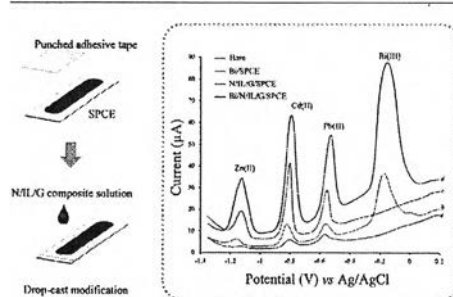
^d Department of Chemistry, Faculty of Science, Srinakharinwirot University, Sukhumvit 23, Wattana, Bangkok, Thailand

^e Center of Excellence on Petrochemical and Materials Technology, Chulalongkorn University, Patumwan, Bangkok, Thailand

HIGHLIGHTS

- Nafion/ionic liquid/graphene composite modified electrode was fabricated.
- Simultaneous determination of Zn, Cd and Pb in real samples was studied.
- Zn, Cd and Pb could be sensitively measured as low as 90, 60 and 80 pg mL^{-1} .

GRAPHICAL ABSTRACT



ARTICLE INFO

Article history:

Received 21 December 2015

Received in revised form

29 February 2016

Accepted 10 March 2016

Available online 19 March 2016

Keywords:

Nafion/ionic liquid/graphene composite

Screen-printed carbon electrode

Bismuth film

Zinc

Cadmium

Lead

ABSTRACT

A simple, low cost, and highly sensitive electrochemical sensor, based on a Nafion/ionic liquid/graphene composite modified screen-printed carbon electrode (N/IL/G/SPCE) was developed to determine zinc (Zn(II)), cadmium (Cd(II)), and lead (Pb(II)) simultaneously. This disposable electrode shows excellent conductivity and fast electron transfer kinetics. By in situ plating with a bismuth film (BiF), the developed electrode exhibited well-defined and separate peaks for Zn(II), Cd(II), and Pb(II) by square wave anodic stripping voltammetry (SWASV). Analytical characteristics of the BiF/N/IL/G/SPCE were explored with calibration curves which were found to be linear for Zn(II), Cd(II), and Pb(II) concentrations over the range from 0.1 to 100.0 ng L^{-1} . With an accumulation period of 120 s detection limits of 0.09 ng mL^{-1} , 0.06 ng L^{-1} and 0.08 ng L^{-1} were obtained for Zn(II), Cd(II) and Pb(II), respectively using the BiF/N/IL/G/SPCE sensor, calculated as 3σ value of the blank. In addition, the developed electrode displayed a good repeatability and reproducibility. The interference from other common ions associated with Zn(II), Cd(II) and Pb(II) detection could be effectively avoided. Finally, the proposed analytical procedure was applied to detect the trace metal ions in drinking water samples with satisfactory results which demonstrates the

* Corresponding author.

** Corresponding author, Electrochemistry and Optical Spectroscopy Research Unit (EOSRU), Department of Chemistry, Faculty of Science, Chulalongkorn University, 254 Phayathai Road, Patumwan, Bangkok, Thailand.

*** Corresponding author.

E-mail addresses: weena@swu.ac.th, weenasi@hotmail.com (W. Siangproh), corawon@chula.ac.th (O. Chailapakul), kurt.kalcher@uni-graz.at (K. Kalcher).

<http://dx.doi.org/10.1016/j.aca.2016.03.026>

0003-2670/© 2016 Elsevier B.V. All rights reserved.

suitability of the BiF/N/IL/G/SPCE to detect heavy metals in water samples and the results agreed well with those obtained by inductively coupled plasma mass spectrometry.

© 2016 Elsevier B.V. All rights reserved.

1. Introduction

Trace and toxic elements, such as zinc (Zn(II)), cadmium (Cd(II)) and lead (Pb(II)) in various matrices, like environmental, food and biological samples have been of great interest due to several hazardous effects that these elements could provide to humans [1,2,48]. Therefore, the determination of heavy metals in environmental, food and biological samples has drawn significant attention due to the toxic and nutritional effects of these elements [3,4]. Several analytical techniques such as atomic absorption spectrometry (AAS) [5], inductively coupled plasma atomic emission spectrometry (ICP-AES) [6] and inductively coupled plasma mass spectrometry (ICP-MS) [7] are available for the determination of trace heavy metals with sufficient sensitivity for most of applications. Usually, these methods are more expensive and time-consuming as compared to electrochemical methods.

Electrochemical methods, especially electrochemical stripping analysis, have been widely recognized as a powerful tool for determination of heavy metals due to its low cost, easy operation, good specificity, excellent stability, high sensitivity and low limit of detection [8,9]. Mercury-based electrodes, such as mercury film electrodes (MFE) [10,11] and hanging mercury drop electrodes (HMDE) [12], have traditionally been used in stripping techniques because of their advantages, like high sensitivity, reproducibility, purity of the surface, high hydrogen overpotential, and possibility of amalgam formation [10–12]. However, the toxicity of mercury restricts the use of these electrodes in today's ecologically oriented analysis [13]. Numerous attempts have consequently been made to replace mercury electrodes by alternative electrode materials with good analytical performance and environment friendly characteristics. The bismuth-film electrode (BiFE) was introduced around the year 2000 as an alternative to mercury electrodes due to its stripping behaviors similar to those of mercury electrodes and the environmentally friendly nature of bismuth [14]. The ability of bismuth to form intermetallic alloys with heavy metals, as well as its insensitivity towards dissolved oxygen are just some of remarkable electrochemical features of bismuth-based electrodes that stay behind their widespread use [14–16]. The bismuth film can be constructed by electrodeposition on substrates including glassy carbon electrodes (GCE) [17], carbon paste electrodes (CPE) [18], boron doped diamond electrode (BDDE) [19] and screen-printed carbon electrodes (SPCE) [20,21]. SPCE was chosen as the electrode material in this research because screen printed technology is a rapid and cost-reducing way to fabricate robust and solid electrodes. It offers several advantages, among which the versatility of the design, reproducibility in the sensor preparation and low cost production are notable, which permits the sensors to be disposed after a single use [22,23].

Graphene (G) has attracted attention among researchers for its properties like extremely high thermal conductivity, good mechanical strength, high mobility of charge carriers, large specific surface area and outstanding electrical properties [24,25]. Ionic liquid (IL) is a promising material adopted in the field of electrochemistry. Due to the high ionic conductivity and wide electrochemical window, it has been widely used as electrochemical solvents and electrode modifiers for the fabrication of sensors [26,27]. Recently, a synergistic effect of G and IL composite

modified SPCE can enable a sensitive determination of heavy metals [28,29]. To enhance the detection sensitivity towards heavy metals, Nafion (N), a perfluorinated sulphonated cation exchanger with properties of excellent antifouling capacity, chemical inertness, and high permeability to cations, has been extensively employed as an electrode modifier for organic molecules [30,31]. The integration of G, IL and N could elicit synergistic effects in the electrochemical applications. Thus, G, IL and N composite could be used as a kind of robust and advanced electrode material for the determination of heavy metals.

In the present work, a graphene, ionic liquid (1-butyl-2,3-dimethylimidazolium tetrafluoroborate) (IL) and Nafion composite and bismuth film-modified screen-printed carbon electrode, was developed. Tetrafluoroborates usually show good combined properties of high electric conductivity and electrochemical stability; for this reason we have chosen 1-butyl-2,3-dimethylimidazolium tetrafluoroborate as a proper candidate for our studies whose moderate lipophilic properties should cope well with graphene [49]. After in situ deposition of the bismuth film, the sensor was applied to determine traces of Zn(II), Cd(II) and Pb(II) by square wave anodic stripping voltammetry (SWASV). Finally, this highly sensitive, simple and low-cost sensor was applied to the determination of Zn(II), Cd(II) and Pb(II) in drinking water samples.

2. Experimental

2.1. Apparatus

Voltammetric experiments were performed using an Autolab electrochemical system with a potentiostat PGSTAT 128 (EcoChemie, Utrecht, Netherlands) controlled by the NOVA 10.1 software. The three-electrode system consisted of a Nafion/ionic liquid/graphene/screen-printed carbon electrode (N/IL/G/SPCE) as the working electrode, an Ag/AgCl/sat.KCl electrode as the reference and a platinum wire as the auxiliary electrode.

2.2. Reagents

Industrial-quality graphene was obtained from ACS Material, LLC (Medford, USA). The ionic liquid 1-butyl-2,3-dimethylimidazolium tetrafluoroborate, Nafion (5% in lower alcohols), N,N-dimethylformamide (DMF) and sodium acetate (CH₃COONa) were purchased from Sigma–Aldrich (Buchs, Switzerland). Stock solutions of Zn(II), Cd(II), Pb(II), phosphate (PO₄³⁻), chloride (Cl⁻), sulfate (SO₄²⁻), fluoride (F⁻), calcium (Ca(II)), potassium (K(I)), magnesium (Mg(II)), iron (Fe(III)), arsenic (As(III)), mercury (Hg(II)), copper (Cu(II)), cobalt (Co(II)), and nickel (Ni(II)) in concentrations 1000 mg L⁻¹ were purchased from Carl Roth GmbH + Co. KG (Austria). The stock solutions of bismuth (Bi(III)) and manganese (Mn(II)) (1000 mg L⁻¹) were obtained from CPI International (USA). Acetic acid was purchased from Merck (Darmstadt, Germany). All reagents were of analytical grade, and were used without further purification. All solutions were prepared using ultra-purified water (> 18 MΩ cm) refined by a cartridge purification system (Millipore, UK).

2.3. Preparation of the N/IL/G casting solution and fabrication of the modified electrode

To prepare the N/IL/G composite, 1.0 mg of the graphene was dispersed in 1.0 mL of DMF by ultrasonic agitation for about 2 h. Next, 0.5% (m:v) of the ionic liquid and 0.1% (v:v) of the Nafion solution were added to the graphene dispersion and sonicated for further 30 min. The N/G composite and the IL/G composite were prepared under the same experimental conditions but without adding the IL and N, respectively.

SPCEs were prepared by printing carbon ink (Acheson, USA) onto a ceramic substrate (Coors Ceramic, Chattanooga, TN, USA). The printed electrode was allowed to dry in an oven at 55 °C for 1 h. After that, 5 mm diameter-punched adhesive tape was attached to the working electrode for limiting the surface area of the sensor (area = 0.196 cm²) (Fig. 1). For the electrode modification by drop-casting, 1.0 μL of the N/IL/G composite solution was dropped onto the working electrode and allowed to dry completely at room temperature for approximately 10 min.

2.4. Electrochemical measurements

Cyclic voltammetry (CV) and square wave anodic stripping voltammetry (SWASV) were carried out in a 10 mL electrochemical cell. For the determination of Zn(II), Cd(II) and Pb(II) square wave voltammograms were recorded in 0.1 M acetate buffer solutions pH 4.5 in the presence of 200.0 ng mL⁻¹ Bi(III). Standard solutions of Zn(II), Cd(II) and Pb(II) were added to the cell and the mixed solution was stirred at a potential of -1.4 V for 120 s. Following the preconcentration step, the stirring was stopped. After 5 s of quiescence time, square wave stripping voltammetric measurement was performed by a potential scan from -1.4 V to +0.2 V with a frequency 25 Hz, a pulse amplitude 20 mV and a potential step of 5 mV. To obtain reproducible results the electrode was regenerated by polarizing the electrode at +0.3 V for 60 s prior to the next cycle.

2.5. Sample preparation

Drinking water samples were bought from a local supermarket (Graz, Austria). These samples were filtered through a 0.45 μm filter. Generally, 2.0 mL of drinking water sample was mixed with 8.0 mL of 0.1 M acetate buffer (pH 4.5) and then analyzed by the optimized square wave anodic stripping voltammetry (SWASV) method.

3. Results and discussion

3.1. SEM characterization of the prepared electrodes

The scanning electron microscopy (SEM) of SPCE, G/SPCE and N/IL/G/SPCE are shown in Fig. 2. The surface of the SPCE was predominated by isolated and irregularly shaped graphite flakes and separated layers were seen (Fig. 2A). Therefore, the charges could not be transferred along the vertical direction of planes because of

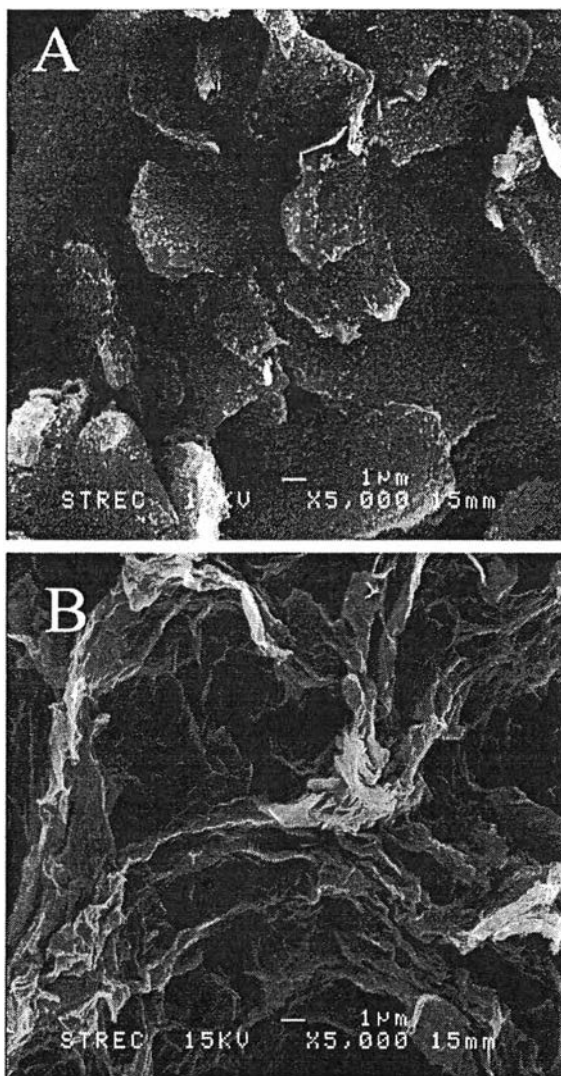


Fig. 2. SEM images of surface morphologies of SPCE (A) and N/IL/G/SPCE.

the block of non-conductive binder. The SEM image of N/IL/G/SPCE showed more uniform surface (Fig. 2B). As a liquid with good conductivity and high viscosity, IL and N are capable of better dispersing the G in the paste than the conditional paraffin, thus, could better bridge the G sheets together. Thus, the conductive performance of the N/IL/G/SPCE was notably improved due to a mixed carbon-ionic contribution.

3.2. Electrochemical characterization of the prepared electrodes

Cyclic voltammetry can provide interface information of the

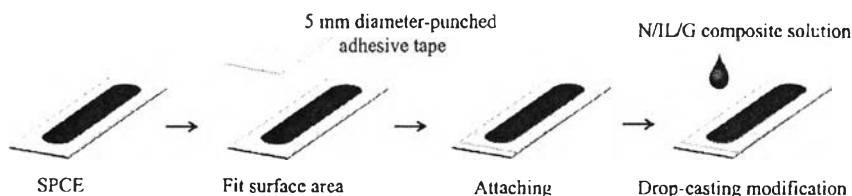


Fig. 1. Schematic drawing of the electrochemical sensor fabrication and drop-casting modification.

electrode surface in dependence of the modification process. The cyclic voltammetric behavior of 1.0 mM $K_3[Fe(CN)_6]$ containing 0.1 M KCl at different electrodes was studied at a potential scan rate of 100 V s^{-1} (Fig. 3A). On the bare SPCE (curve a), a pair of weak redox peaks with the peak-to-peak separation (ΔE_p) of 0.31 V was observed, indicating the lethargic electron transfer rate at the interface. On the G/SPCE (curve b), a pair of well-defined peaks appeared with a peak potential separation ΔE_p of 0.28 V. On the N/G/SPCE (curve c), a higher peak current than that on both SPCE and G/SPCE was observed, but ΔE_p extended to 0.39 V which is due to the presence of a membrane which deteriorates the diffusion process. The presence of the ionic liquid in IL/G/SPCE (curve d) causes well-defined and enhanced redox peaks with a small ΔE_p of 0.22 V, which could be ascribed to the high ionic conductivity and maybe an electrocatalytic activity of the IL. After N was added to the IL/G/SPCE, the anodic and cathodic peaks current even improved showing a ΔE_p of 0.20 V, indicating that the ionic liquid slightly overcompensates and synergically improves the otherwise negative influence of the Nafion membrane in the N/IL/G/SPCE (curve e).

The relative peak separations, $\chi^0 = (E_{pa} - E_{pc})/0.058$, and anodic to cathodic peak current density ratios (I_{pa}/I_{pc}) are given in Table 1. The theoretical χ^0 -values for this redox reaction is 1. The closer the

χ^0 -values are to the theoretical value, the faster the electron transfer kinetics on the electrode [32,33]. The N/IL/G/SPCE electrodes showed a value of 3.45, which is closer to the theoretical value and much smaller than 5.34 for the bare SPCE.

The effective surface area of the N/IL/G/SPCE was evaluated using $K_3[Fe(CN)_6]$ as a probe based on the Randles–Sevcik equation. The experiment was performed with a 1.0 mM $K_3[Fe(CN)_6]$ solution at various scan rates (Fig. 3B). For a reversible process, the following equation can be utilized [34]:

$$I_{pc} = 2.69 \times 10^5 \times (D_0) \times A \times \nu^{1/2} \times n^{3/2} \times C_0$$

where I_{pc} is the reduction peak current, D_0 is the diffusion coefficient of $K_3[Fe(CN)_6]$ ($\text{cm}^2 \text{ s}^{-1}$), A is the apparent electrode area (cm^2), ν is the scan rate (V s^{-1}), n is the electron transfer number and C_0 is the concentration for $K_3[Fe(CN)_6]$ (mol cm^{-3}), in consequence, the calculated effective surface area of the modified electrode is estimated as 0.648 cm^2 . This surface is about 2.9 times that of the bare SPCE assuming that the diffusion coefficient is unaltered by the ionic liquid and the membrane.

Fig. 3B shows the cyclic voltammogram of the N/IL/G modified SPCE at different scan rates (20–200 mV s^{-1}). The oxidation and reduction peak current increases with the increasing scan rates. Further, the oxidation and reduction peak current exhibits a linear dependence on the square root of the scan rate (Fig. 3B inset) in the range of 20–200 mV s^{-1} . The result suggests that the kinetics of the overall process is mainly controlled by diffusion.

3.3. Electrochemical detection of Zn(II), Cd(II), and Pb(II)

Fig. 4 shows the square wave anodic stripping voltammograms (SWASVs) of 50 ng L^{-1} Zn(II), Cd(II) and Pb(II) at the bare SPCE, bare bismuth film-modified SPCE (BiF/SPCE), N/IL/G/SPCE and bismuth film-modified N/IL/G/SPCE (BiF/N/IL/G/SPCE) in 0.1 M acetate buffer solution pH 4.5. As shown, relatively small stripping current responses are observed on the bare SPCE (curve a) due to the difficulty to deposit target metals onto the bare SPCE surface. The BiF/SPCE (curve b) yielded peak currents higher than those obtained with the bare SPCE, which is due to the bismuth providing an increased surface and facilitating a better deposition due to the formation of “fused” alloys with lead and cadmium. If graphene, Nafion or the ionic liquid were individually spread on the electrode surface only slight increases of the signal could be observed (not shown). An obvious increase in stripping currents could be detected upon casting Nafion, graphene and the ionic liquid to the bare electrode surface (N/IL/G/SPCE, curve c); the improvement can be attributed to the high ionic conductivity and ion exchange properties of the polymer and IL as well as to the surface area increase and electric conductivity of graphene. If this electrode was combined with in situ bismuth film formation, the highest stripping peaks were observed (BiF/N/IL/G/SPCE, curve d). The stripping voltammograms clearly demonstrate that the bismuth film in combination with the N/IL/G composite possesses very attractive electrochemical characteristics with highest sensitivity, compared with other electrodes studied in this work.

Table 1
Influence of the modifiers on the characteristics of the electrode.

Electrode	ΔE_p (V)	χ^0	I_{pa}/I_{pc}
SPCE	0.31	5.34	1.12
G/SPCE	0.28	4.83	1.17
N/G/SPCE	0.39	6.72	1.28
IL/G/SPCE	0.22	3.79	1.15
N/IL/G/SPCE	0.20	3.45	1.08

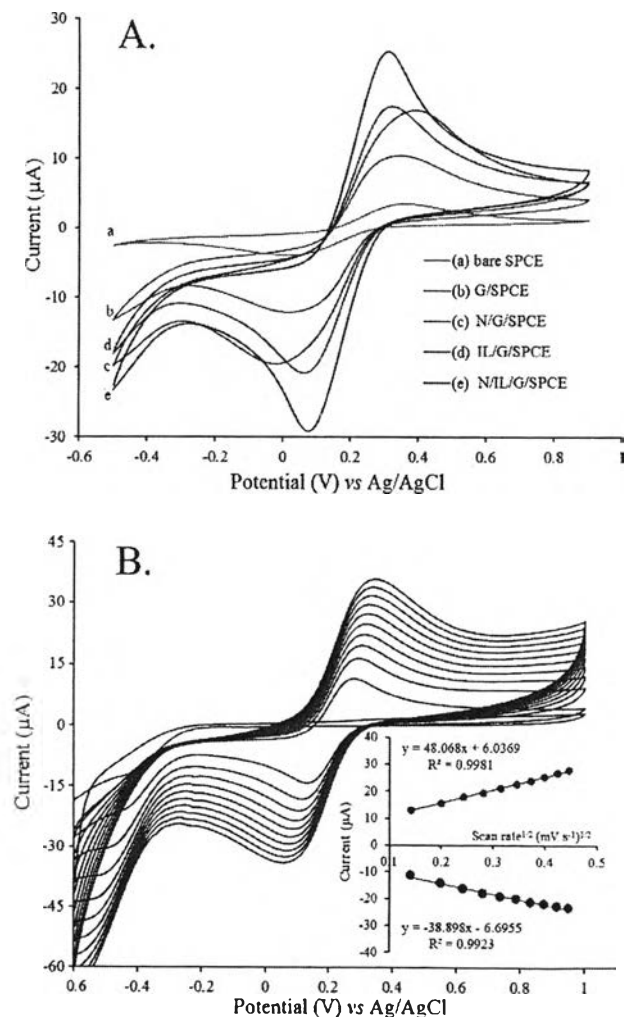


Fig. 3. Cyclic voltammograms for 2 mM $K_3[Fe(CN)_6]$ in 0.1 M KCl (A) obtained with a (a) bare SPCE, (b) G/SPCE, (c) IL/G/SPCE, (d) N/G/SPCE and (e) N/IL/G/SPCE with a scan rate of 100 mV s^{-1} ; (B) at scan rates of 20–200 mV s^{-1} on a N/IL/G/SPCE. Inset: dependence of the peak current on the square root of the scan rate.

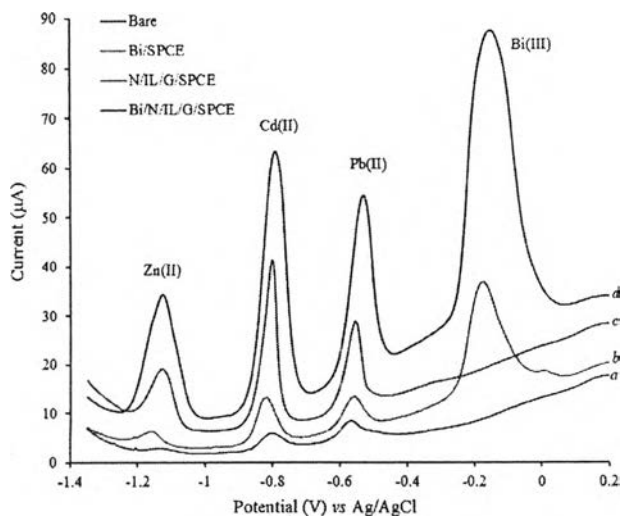


Fig. 4. SWASVs of 50 ng mL⁻¹ Zn(II), Cd(II) and Pb(II) in 0.1 M acetate buffer solution (pH 4.5) on the (a) bare SPCE, (b) Bi(III) film-modified SPCE, (c) N/IL/G/SPCE and (d) Bi(III) film-modified N/IL/G/SPCE. Deposition time: 120 s. Deposition potential: -1.4 V. Concentration of Bi(III): 200 ng mL⁻¹.

3.4. Optimization of experimental parameters

3.4.1. Effect of concentration of G, IL and NA

Different concentrations of G, IL and NA that benefited the electrochemical performance of Zn(II), Cd(II) and Pb(II) were dropped on the surface of SPCE, leading to various electrocatalytic actions. Fig. 5 shows the stripping currents variations of 50.0 ng mL⁻¹ Zn(II), Cd(II) and Pb(II) with 1 µL of casting solution at different concentrations. The stripping currents of Zn(II), Cd(II) and Pb(II) first gradually increased with rising the concentration of G, IL and NA in the casting-solution from 0.1 to 1.0 mg mL⁻¹, 0.05–0.5% (m:m) and 0.01–0.1% (m:v), respectively, and decreased thereafter. The film formed by N/IL/G composite, if too thick, probably weakens the plane structure of the N/IL/G composite and reduces the electrical conductivity. Taking all these into consideration, 1.0 mg mL⁻¹ of G, 0.5% of IL and 0.1% of NA composites were used to modify the surface of SPCE. Concerning the cast volume 1 µL per 0.2 cm² seemed optimal.

3.4.2. Effect of pH, deposition potential, deposition time and concentration of Bi(III)

SWASV was used to study the effect of pH of the supporting electrolyte, deposition potential, deposition time and concentration of Bi(III) on the stripping peak current of 50.0 ng mL⁻¹ Zn(II), Cd(II) and Pb(II) (Fig. 6). Different pH of 0.1 M acetate buffer were tested in the range of 2.5–6.5. It was found that a pH of 4.5 produced the highest stripping currents (Fig. 6A). Thus, for further studies, 0.1 M acetate buffer at pH 4.5 was chosen as the supporting electrolyte. A pH of 4.5 seems to be an optimum for the deposition of bismuth and is in accordance with other literature data [29,50].

The effect of deposition potential on the stripping peak current of Zn(II), Cd(II) and Pb(II) was evaluated over the potential range from -1.0 to -1.6 V (Fig. 6B). As can be seen, the current increased by applying the potential from -1.0 to -1.4 V (vs. Ag/AgCl), and then dramatically decreased due to hydrogen formation. Therefore, a deposition potential of -1.4 V was chosen to record the voltammograms. The deposition time is another important parameter in stripping procedures that has a pronounced effect on both sensitivity and the dynamic range. The results showed that Zn(II), Cd(II) and Pb(II) were accumulated on the modified electrode surface

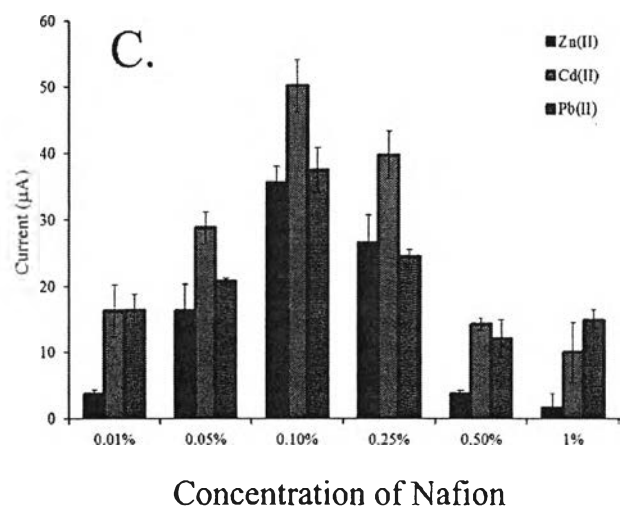
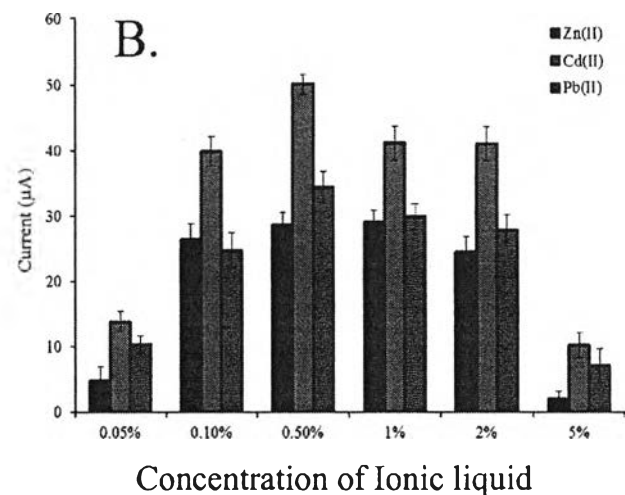
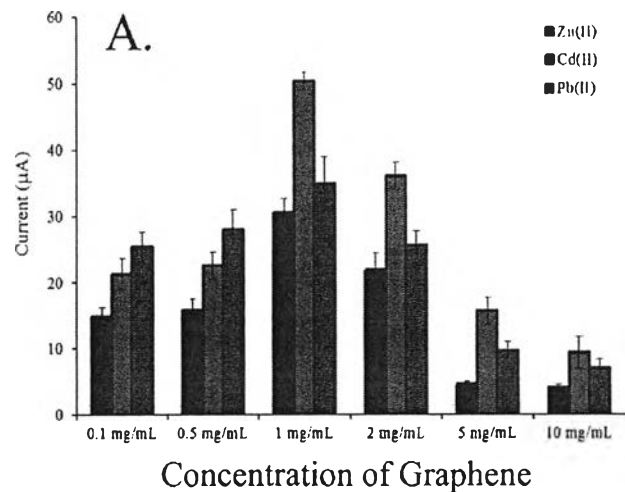


Fig. 5. Effects of (A) concentration of graphene, (B) concentration of ionic liquid and (C) concentration of Nafion on the stripping peaks current of 50 ng mL⁻¹ Zn(II), Cd(II) and Pb(II) in 0.1 M acetate buffer solution (pH 4.5). Error bar: n = 3.

within 120 s and further time did not improve the peak current (Fig. 6C). In order to achieve high sensitivity within relatively short analysis time, a deposition time of 120 s was chosen.

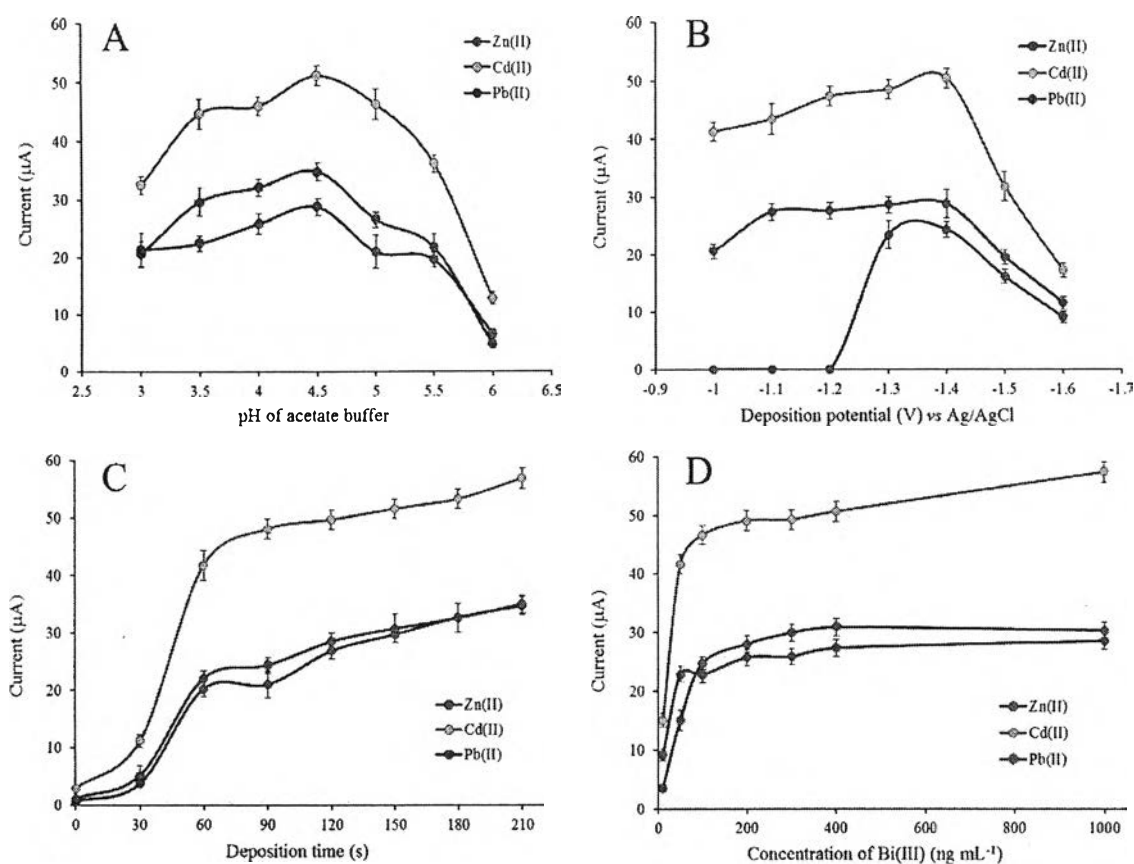


Fig. 6. Effects of (A) pH, (B) deposition potential, (C) deposition time and (D) concentration of Bi(III) on the stripping peaks current of 50 ng mL⁻¹ Zn(II), Cd(II) and Pb(II). Error bar: n = 3.

The stripping peaks are affected by the thickness of the bismuth film, which can be controlled by varying the concentration of Bi(III) in the plating solution. The effect of the concentration of the Bi(III) was examined in the range from 10 to 1000 ng mL⁻¹ (Fig. 6D). The results show that even at very low concentrations of bismuth, the response of the modified electrode towards Zn(II), Cd(II) and Pb(II) was very sensitive. As the Bi(III) concentration increased, the stripping peaks became more prominent, and the stripping peak currents of Zn(II), Cd(II) and Pb(II) increased only slightly when increasing the concentration above 200 ng mL⁻¹ Bi(III). Therefore, the Bi(III) concentration of 200 ng mL⁻¹ was chosen for the simultaneous determinations of Zn(II), Cd(II) and Pb(II).

3.5. Analytical performance of BiF/N/IL/G/SPCE

The analytical performance of the BiF/N/IL/G/SPCE for the determination of Zn(II), Cd(II), and Pb(II) was evaluated with SWASV under the optimized experimental conditions, and the results are shown in Fig. 7. It can be seen that an increase in target metals concentration is accompanied by an increase in stripping peak current. The sensor exhibits excellent linear concentration ranges of 0.1–100 ng mL⁻¹ for Zn(II), Cd(II) and Pb(II). Beyond these concentrations the graphs level off. The limits of detection based on 3σ value of the blank are 0.09 ng L⁻¹, 0.06 ng L⁻¹ and 0.08 ng L⁻¹ for Zn(II), Cd(II) and Pb(II), respectively. The obtained detection limits are very low and more sensitive than for the previously reported methods. Table 2 summarizes the linear range and the detection limits of Zn(II), Cd(II) and Pb(II) by various modified electrodes. The detection limit and linear range of the proposed electrode are

comparable with and even better than those obtained by other modified electrodes.

The repeatability estimated in terms of the relative standard deviation (RSD %) for ten repetitive measurements of 5.0, 30.0 and 60.0 ng mL⁻¹ of Zn(II), Cd(II) and Pb(II) was less than 8.0%. The reproducibility with different BiF/N/IL/G/SPCE (n = 10 sensors) was always lower than 12%. These results indicate that this sensor can be successfully applied to the simultaneous determination of heavy metal ions with excellent sensitivity and repeatability.

3.6. Interference study

The effect of some possible interferences was investigated by adding them to a solution containing 50.0 ng mL⁻¹ of Zn(II), Cd(II) and Pb(II) in 0.1 M acetate buffer pH 4.5. The tolerance limit is estimated to be less than 5% of the error. The experimental results reveal that 1000-fold mass ratios of PO₄³⁻, Cl⁻, SO₄²⁻, F⁻, Ca²⁺, K⁺, Mg²⁺ and Mn²⁺; 500-fold mass ratios of Fe³⁺, As³⁺ and Hg²⁺ 200-fold mass ratio of Zn²⁺, Cd²⁺ and Pb²⁺ and 10-fold mass ratios of Cu²⁺, Co²⁺ and Ni²⁺ did not interfere with the analysis of Zn(II), Cd(II) and Pb(II) (Table 3). Hence the determination of Zn(II), Cd(II) and Pb(II) was not considerably affected by common interfering species, which shows that the method is more selective toward the three target metals.

3.7. Sample analysis

The BiF/N/IL/G/SPCE sensor was applied on treated drinking water samples using the standard addition method. Recovery

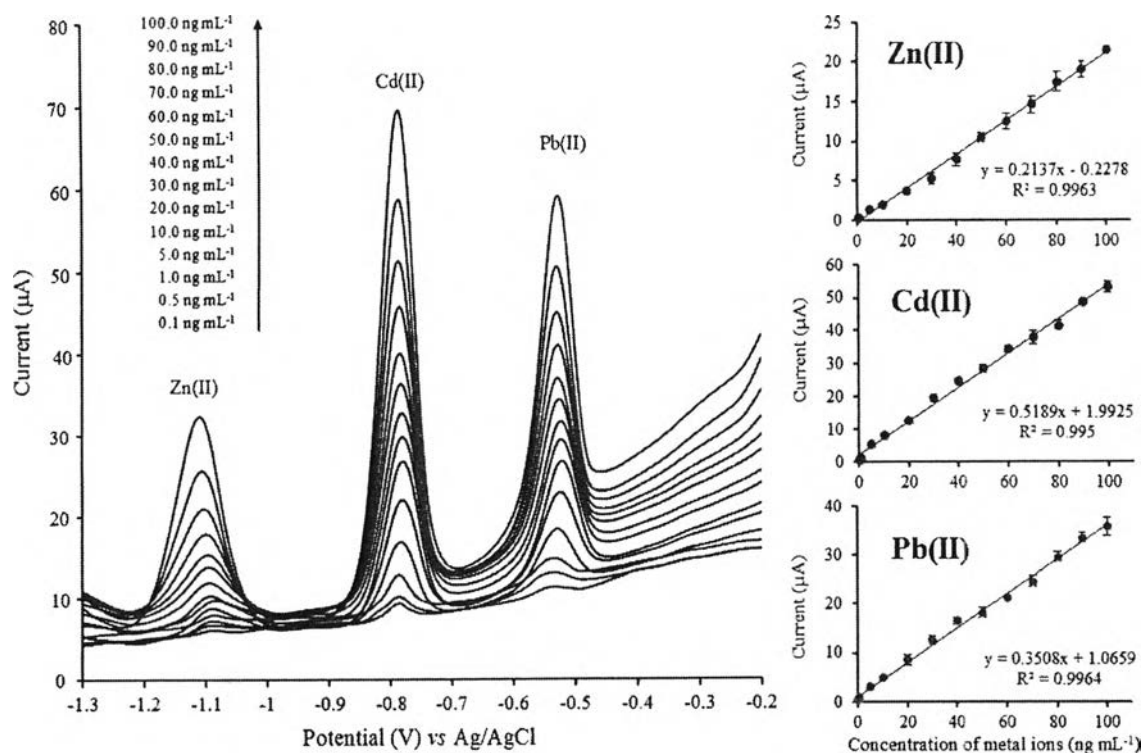


Fig. 7. SWASVs of Zn(II), Cd(II) and Pb(II); concentrations of Zn(II), Cd(II) and Pb(II) 0.1, 0.5, 1.0, 5.0, 10.0, 20.0, 40.0, 60.0, 80.0 and 100.0 ng mL⁻¹. Other conditions are the same as in Fig. 3. The insets show the calibration curves.

Table 2

Comparison of this method for the determination of Zn(II), Cd(II) and Pb(II) with other stripping techniques at modified electrodes.

Electrodes	Method	Linear range (ng mL ⁻¹)			Detection limit (ng nL ⁻¹)			References
		Zn(II)	Cd(II)	Pb(II)	Zn(II)	Cd(II)	Pb(II)	
Mercury film/SPCE	SWASV	N.M.	1–1000	1–1000	N.M.	1.0	0.3	[35]
Bismuth film/SPCE	SWASV	N.M.	0–70	0–70	N.M.	0.69	0.89	[36]
Bismuth film/carbon nanotubes/SPCE	SWASV	12–100	2–100	2–100	11	0.8	0.2	[21]
Bismuth film/carbon nanotubes/N/SPCE	DPASV	0.5–100	0.5–80	0.5–100	0.3	0.1	0.07	[37]
Bismuth film/G/IL/SPCE	SWASV	N.M.	1–80	1–80	N.M.	0.08	0.1	[28]
IL/G/CPE	SWASV	N.M.	N.M.	2.6–41.4	N.M.	N.M.	0.09	[29]
Bismuth film/N/G/polyaniline nanocomposite/SPCE	SWASV	1–300	1–300	1–300	1	0.1	0.1	[38]
Hydroxyapatite/IL/CPE	SWASV	N.M.	0.1–11.2	0.2–20.8	N.M.	0.06	0.04	[39]
IL mediated hollow fiber/CPE	SWASV	N.M.	2–13000	0.6–6500	N.M.	0.61	0.19	[40]
Mercury Film/N/IL/Electrode	AdSV	N.M.	0.1–16.0	1.0–16.0	N.M.	0.13	0.12	[41]
IL/Mesoporous Silica/CPE	DPASV	N.M.	67.5–3372.3	82.9–18648	N.M.	9.0	8.3	[42]
Bismuth film/G/polyaniline/polystyrene nanoporous fibers/SPCE	SWASV	N.M.	10–500	10–500	N.M.	4.43	3.30	[43]
Bismuth film/N/IL/G/SPCE	SWASV	0.1–100	0.1–100	0.1–100	0.09	0.06	0.08	This work

SPCE: screen-printed carbon electrode; NA: Nafion; G: graphene; IL: ionic liquid; CPE: carbon paste electrode; DPASV: differential pulse anodic stripping voltammetry; AdSV: adsorptive stripping voltammetry; N.M.: not measured.

Table 3

Tolerance ratio of interfering ions in the electrochemical determination of 50 ng mL⁻¹ of Zn(II), Cd(II) and Pb(II) on BiF/N/IL/G/SPCE.

Common ions	5% tolerance ratio ($W_{ions}/W_{target\ metals}$)		
	Zn(II)	Cd(II)	Pb(II)
PO ₄ ³⁻ , Cl ⁻ , SO ₄ ²⁻ , F ⁻ , Ca ²⁺ , K ⁺ , Mg ²⁺ , Mn ²⁺	>1000	>1000	>1000
Fe ³⁺ , As ³⁺ , Hg ²⁺	500	500	500
Cu ²⁺ , Co ²⁺ , Ni ²⁺	25	25	25
Pb ²⁺	200	200	–
Cd ²⁺	200	–	200
Zn ²⁺	–	200	200

studies were carried out by spiking Zn(II), Cd(II) and Pb(II) to the drinking water samples (with analyte concentrations below the detection limit) at three concentration levels of 5.0, 30.0 and 60.0 ng mL⁻¹. The obtained recoveries of Zn(II), Cd(II) and Pb(II) were in the range of 90.3–112.5% (Table 4). The recoveries were satisfactory reasonable, which indicated the capability of the method for determination of Zn(II), Cd(II) and Pb(II) in such samples. Commercially available drinking waters were analyzed, the results obtained by BiF/N/IL/G/SPCE were compared with those from inductively coupled plasma-mass spectrometry (ICP-MS) (Table 5). The applicability of the method to natural water matrices was additionally confirmed with the analysis of a reference material (NIST standard reference material 1640 a, "Trace Elements in

Table 4
Recovery for the determination of Zn(II), Cd(II) and Pb(II) in drinking water samples (n = 3).

Samples	Added (ng mL ⁻¹)	% Recovery			% RSD		
		Zn(II)	Cd(II)	Pb(II)	Zn(II)	Cd(II)	Pb(II)
Drinking water 1	5.0	94.7 ± 3.5	90.3 ± 2.9	110.4 ± 1.7	3.7	3.2	1.6
	30.0	101.6 ± 5.8	103.0 ± 4.2	96.8 ± 3.6	5.7	4.1	3.7
	60.0	99.6 ± 3.0	99.3 ± 2.3	100.7 ± 2.3	3.0	2.3	2.3
Drinking water 2	5.0	96.2 ± 4.3	93.0 ± 2.3	105.4 ± 5.7	4.5	2.4	4.6
	30.0	101.2 ± 0.9	102.2 ± 5.3	101.4 ± 1.2	0.9	5.2	1.2
	60.0	99.8 ± 4.1	99.5 ± 3.2	102.1 ± 5.1	4.1	3.2	5.0
Drinking water 3	5.0	105.3 ± 9.8	91.9 ± 5.6	112.5 ± 1.9	9.3	6.1	1.7
	30.0	98.4 ± 2.0	107.2 ± 4.8	93.4 ± 2.0	2.0	4.4	2.1
	60.0	100.4 ± 7.1	98.4 ± 6.6	101.5 ± 7.6	7.1	6.7	7.5

Table 5
The comparison of the proposed method and standard method for the determination of Zn(II), Cd(II) and Pb(II) in drinking water samples (n = 3).

Samples	Found (ng mL ⁻¹)					
	Proposed method			ICP-MS		
	Zn(II)	Cd(II)	Pb(II)	Zn(II)	Cd(II)	Pb(II)
Drinking water 1	7.6 ± 0.4	3.0 ± 0.5	8.7 ± 0.4	8.0 ± 0.8	3.2 ± 0.4	9.2 ± 0.4
Drinking water 2	24.9 ± 0.9	2.5 ± 0.6	8.6 ± 0.3	25.3 ± 1.2	2.1 ± 0.3	8.8 ± 0.4
Drinking water 3	13.5 ± 0.4	<1.0	6.3 ± 0.3	13.8 ± 1.5	<2.0	6.6 ± 0.2
Drinking water 4	9.6 ± 0.5	<1.0	<1.0	9.9 ± 1.4	<2.0	<2.0
NIST SRM 1640a	56.0 ± 1.3	4.1 ± 0.5	12.5 ± 0.6	55.64 ± 0.35 ^a	3.992 ± 0.074 ^a	12.101 ± 0.050 ^a

^a Certified value.

Natural Water"). The significance of the developed method was also tested. The results thus obtained clearly reveal that the concentrations of Zn(II), Cd(II) and Pb(II) in the drinking samples obtained by the proposed stripping voltammetry are in satisfactory agreement with those determined by ICP-MS and the proposed stripping sensor has promising feasibility for trace-level determination of Zn(II), Cd(II) and Pb(II) in even more complex samples.

4. Conclusions

In this study, a Nafion/ionic liquid/graphene composite and bismuth film-modified screen-printed carbon electrode (BiF/N/IL/G/SPCE) was developed and used for the simultaneous determination of Zn(II), Cd(II) and Pb(II) by square wave anodic stripping voltammetry (SWASV). To the best of our knowledge, such a multiple composite - bismuth film electrode was used for the first time as a working electrode. The modified electrode exhibited greatly improved stripping performance for the determination of Zn(II), Cd(II) and Pb(II). This was attributed to the increased surface area, improved conductivity and mass transfer on the electrode surface due to the incorporation of Nafion, ionic liquid and graphene. Under optimized conditions, the relevant calibration curves were linear in the range of 0.1–100 ng mL⁻¹ for three metal ions, with a detection limit of 0.09 ng L⁻¹, 0.06 ng L⁻¹ and 0.08 ng L⁻¹ for Zn(II), Cd(II) and Pb(II), respectively, with 120 s deposition time. Good repeatability and reproducibility of the voltammetric responses was achieved. Compared to approaches with carbon nanotubes [21] the new type of sensor shows significantly lower detection limits, improved baseline and signal characteristics particularly for zinc, but also for the other analytes, and may be used simply in batch stripping analysis without sequential injection at very low concentration levels which will favor its application to matrices with low contents of the analytes, such as rain water. The reason for this drastic improvement can be found in many characteristics of graphene which are superior to CNTs, such as electric conductivity and surface area [44–47].

Furthermore, the utility of the proposed method was

successfully tested by the determination of heavy metals in drinking water samples and the results were in satisfactory agreement with ICP-MS determination. This sensor can be used as an excellent alternative to more expensive spectrometric methods for the determination of heavy metals in real samples.

Acknowledgments

This work was financially supported by Thailand Research Fund (TRF) through the Royal Golden Jubilee Ph.D. program (Grant number PHD/0127/2556), and the Thailand Research Fund (TRF) through Research Team Promotion Grant (RTA5780005). Financial support by Asea UniNet is kindly acknowledged.

References

- [1] J. Ferguson, *The Heavy Elements. Chemistry Environmental Impact and Health Effects*, Pergamon Press, 1990.
- [2] R. Hassanzadeh, A. Abbasnejad, M.A. Hamzeh, Assessment of groundwater pollution in Kerman urban areas, *J. Environ. Stud.* 36 (2011) 101–110.
- [3] R.A. Mandour, Y.A. Azab, Toxic levels of some heavy metals in drinking groundwater in Dakahlyia Governorate, Egypt in the year 2010, *Int. J. Occup. Environ. Med.* 2 (2011) 112–117.
- [4] R.A. Goyer, T.W. Clarkson, Toxic effects of metals, in: C.D. Klaassen (Ed.), *Casarett and Doull's Toxicology*, sixth ed., McGraw-Hill, New York, 2001, pp. 811–867.
- [5] E.L. Silva, P.S. Roldan, Simultaneous flow injection preconcentration of lead and cadmium using cloud point extraction and determination by atomic absorption spectrometry, *J. Hazard. Mat.* 161 (2009) 142–147.
- [6] K.S. Rao, T. Balaji, T.P. Rao, Y. Babu, G.R.K. Naidu, Determination of iron, cobalt, nickel, manganese, zinc, copper, cadmium and lead in human hair by inductively coupled plasma-atomic emission spectrometry, *Spectrochim. Acta Part B At. Spectrosc.* 57 (2002) 1333–1338.
- [7] A.A. Ammann, Speciation of heavy metals in environmental water by ion chromatography coupled to ICP-MS, *Anal. Bioanal. Chem.* 372 (2002) 448–452.
- [8] E. Nagles, V. Arancibia, C. Rojas, R. Segura, Nafion-mercury coated film electrode for the adsorptive stripping voltammetric determination of lead and cadmium in the presence of pyrogallol red, *Talanta* 99 (2012) 119–124.
- [9] R. Güell, G. Aragay, C. Fontàs, E. Anticó, A. Merkoçi, Sensitive and stable monitoring of lead and cadmium in seawater using screen-printed electrode and electrochemical stripping analysis, *Anal. Chim. Acta* 627 (2008) 219–224.
- [10] M.F. de Oliveira, A.A. Saczk, L.L. Okumura, A.P. Fernandes, M. de Moraes, N.R. Stradiotto, Simultaneous determination of zinc, copper, lead, and

- cadmium in fuel ethanol by anodic stripping voltammetry using a glassy carbon-mercury-film electrode, *Anal. Bioanal. Chem.* 380 (2004) 135–140.
- [11] C.L. da Silva, J.C. Masini, Determination of Cu, Pb, Cd, and Zn in river sediment extracts by sequential injection anodic stripping voltammetry with mercury film electrode, *Fresenius J. Anal. Chem.* 367 (2000) 284–290.
 - [12] T. Rojahn, Determination of copper, lead, cadmium and zinc in estuarine water by anodic-stripping alternating-current voltammetry on the hanging mercury drop electrode, *Anal. Chim. Acta.* 62 (1972) 438–441.
 - [13] J. Wang, Real-time electrochemical monitoring: toward green analytical chemistry, *Acc. Chem. Res.* 35 (2002) 811–816.
 - [14] J. Wang, J. Lu, S.B. Hocevar, P.A.M. Farias, B. Ogorevc, Bismuth-coated carbon electrodes for anodic stripping voltammetry, *Anal. Chem.* 72 (2000) 3218–3222.
 - [15] A. Economou, Bismuth-film electrodes: recent developments and potentialities for electroanalysis, *Trends Anal. Chem.* 24 (2005) 334–340.
 - [16] C. Kokkinos, A. Economou, Stripping analysis at bismuth-based electrodes, *Anal. Chem.* 4 (2008) 183–190.
 - [17] G. Kefala, A. Economou, A. Voulgaropoulos, M. Sofoniou, A study of bismuth-film electrodes for the detection of trace metals by anodic stripping voltammetry and their application to the determination of Pb and Zn in tapwater and human hair, *Talanta* 61 (2003) 603–610.
 - [18] W. Wonsawat, S. Chuanuwatanakul, W. Dungchai, E. Punrat, S. Motomizu, O. Chailapakul, Graphene-carbon paste electrode for cadmium and lead ion monitoring in a flow-based system, *Talanta* 100 (2012) 282–289.
 - [19] K.E. Toghill, C.G. Wildgoose, A. Moshar, C. Mulcahy, R.G. Compton, The fabrication and characterization of a bismuth nanoparticle modified boron doped diamond electrode and its application to the simultaneous determination of cadmium(II) and lead(II), *Electroanalysis* 20 (2008) 1731–1737.
 - [20] S. Chuanuwatanakul, W. Dungchai, O. Chailapakul, S. Motomizu, Determination of trace heavy metals by sequential injection-anodic stripping voltammetry using bismuth film screen-printed printed carbon electrode, *Anal. Sci.* 24 (2008) 589–594.
 - [21] U. Injang, P. Noyrod, W. Siangproh, W. Dungchai, S. Motomizu, O. Chailapakul, Determination of trace heavy metals in herbs by sequential injection analysis-anodic stripping voltammetry using screen-printed carbon nanotubes electrodes, *Anal. Chim. Acta.* 668 (2010) 54–60.
 - [22] H. Wei, J.J. Sun, Y. Xie, C.G. Lin, Y.M. Wang, W.H. Yin, G.N. Chen, Enhanced electrochemical performance at screen-printed carbon electrodes by a new pretreating procedure, *Anal. Chim. Acta.* 588 (2007) 297–303.
 - [23] K.C. Honeychurch, J.P. Hart, D.C. Cowell, *Voltammetric Behavior and Trace Determination of Lead at a Mercury-free Screen-printed Carbon Electrode* *Electroanalysis*, vol. 12, 2000, pp. 171–177.
 - [24] D. Li, R.B. Kaner, Graphene-based materials, *Science* 320 (2008) 1170–1171.
 - [25] S.J. Guo, S.J. Dong, Graphene and its derivative-based sensing materials for analytical devices, *J. Mater. Chem.* 21 (2011) 18503–18516.
 - [26] M. Armand, F. Endres, D.R. MacFarlane, H. Ohno, B. Scrosati, Ionic-liquid materials for the electrochemical challenges of the future, *Nat. Mat.* 8 (2009) 621–629.
 - [27] X.H. Niu, H.L. Zhao, M.B. Lan, Disposable screen-printed antimony film electrode modified with carbon nanotubes/ionic liquid for electrochemical stripping measurement, *Electrochim. Acta.* 56 (2011) 9921–9925.
 - [28] Z. Wang, H. Wang, Z. Zhang, G. Liu, Electrochemical determination of lead and cadmium in rice by a disposable bismuth/electrochemically reduced graphene/ionic liquid composite modified screen-printed electrode, *Sens. Actuators B Chem.* 199 (2014) 7–14.
 - [29] H. Bagheri, A. Afkhami, H. Khoshshafar, M. Rezaei, S.J. Sabounchei, M. Sarlakifar, Simultaneous electrochemical sensing of thallium, lead and mercury using a novel ionic liquid/graphene modified electrode, *Anal. Chim. Acta.* 870 (2015) 56–66.
 - [30] N. Amini, M.B. Gholivand, M. Shamsipur, Electrocatalytic determination of traces of insulin using a novel silica nanoparticles-Nafion modified glassy carbon electrode, *J. Electroanal. Chem.* 714 (2014) 70–75.
 - [31] K. Keawkim, S. Chuanuwatanakul, O. Chailapakul, S. Motomizu, Determination of lead and cadmium in rice samples by sequential injection/anodic stripping voltammetry using a bismuth film/crown ether/Nafion modified screen-printed carbon electrode, *Food Control.* 31 (2013) 14–21.
 - [32] K. Kalcher, I. Svancara, R. Metelka, K. Vytras, A. Walcarius, Heterogeneous carbon electrochemical sensors, *Encycl. Sensors* 4 (2006) 283–430.
 - [33] I. Svancara, K. Kalcher, A. Walcarius, K. Vytras, *Electroanalysis with Carbon Paste Electrodes*, CRC Press, Francis & Taylor, 2012.
 - [34] F. Xu, F. Wang, D. Yang, Y. Gao, H. Li, Electrochemical sensing platform for L-CySH based on nearly uniform Au nanoparticles decorated graphene nanosheets, *Mater. Sci. Eng. C* 38 (2014) 292–298.
 - [35] I. Palchetti, S. Laschi, M. Mascini, Miniaturised stripping-based carbon modified sensor for in field analysis of heavy metals, *Anal. Chim. Acta.* 530 (2005) 1–7.
 - [36] S. Chuanuwatanakul, W. Dungchai, O. Chailapakul, S. Motomizu, Determination of trace heavy metals by sequential injection-anodic stripping voltammetry using bismuth film screen-printed printed carbon electrode, *Anal. Sci.* 24 (2008) 589–594.
 - [37] L. Fu, X. Li, J. Yu, J. Ye, Facile and simultaneous stripping determination of zinc, cadmium and lead on disposable multiwalled carbon nanotubes modified screen-printed electrode, *Electroanalysis* 25 (2013) 567–572.
 - [38] N. Ruecha, N. Rodthongkum, D.M. Cate, J. Volckens, O. Chailapakul, C.S. Henry, Sensitive electrochemical sensor using a graphene-polyaniline nanocomposite for simultaneous detection of Zn(II), Cd(II), and Pb(II), *Anal. Chim. Acta.* 874 (2015) 40–48.
 - [39] Y. Li, X. Liu, X. Zeng, Y. Liu, X. Liu, W. Wei, S. Luo, Simultaneous determination of ultra-trace lead and cadmium at a hydroxyapatite-modified carbon ionic liquid electrode by square-wave stripping voltammetry, *Sens. Actuators B Chem.* 139 (2009) 604–610.
 - [40] Z. Es'laghi, T. Heidari, E. Mazloomi, In situ pre-concentration and voltammetric determination of trace lead and cadmium by a novel ionic liquid mediated hollow fiber-graphite electrode and design of experiments via Taguchi method, *Electrochim. Acta.* 147 (2014) 279–287.
 - [41] E. Nagles, V. Arancibia, R. Rios, C. Rojas, Simultaneous determination of lead and cadmium in the presence of Morin by adsorptive stripping voltammetry with a Nafion-ionic liquid-coated mercury film electrode, *Int. J. Electrochem. Sci.* 7 (2012) 5521–5533.
 - [42] P. Zhang, S. Dong, G. Gu, T. Huang, Simultaneous determination of Cd²⁺, Pb²⁺, Cu²⁺ and Hg²⁺ at a carbon paste electrode modified with ionic liquid-functionalized ordered mesoporous silica, *Bull. Korean Chem. Soc.* 30 (2010) 2949–2954.
 - [43] N. Promphet, P. Rattanasat, R. Rangkupan, O. Chailapakul, N. Rodthongkum, An electrochemical sensor based on graphene/polyaniline/polystyrene nanoporous fibers modified electrode for simultaneous determination of lead and cadmium, *Sens. Actuators B Chem.* 207 (2015) 526–534.
 - [44] S. Bose, T. Kuila, A.K. Mishra, R. Rajasekar, N.H. Kim, J.H. Lee, Carbon-based nanostructured materials and their composites as supercapacitor electrodes, *J. Mater. Chem.* 22 (2012) 767–784.
 - [45] S.H. Aboutalebi, A.T. Chidembo, M. Salari, K. Konstantinov, D. Wexler, H.K. Lou, S.X. Dou, Comparison of GO, GO/MWCNTs composite and MWCNTs as potential electrode materials for supercapacitors, *Energy Environ. Sci.* 4 (2011) 1855–1865.
 - [46] C. Biwas, Y.H. Lee, Graphene versus carbon nanotubes in electronic devices, *Adv. Funct. Mater.* 21 (2011) 3806–3826.
 - [47] C. Liu, S. Alwarappan, Z.F. Chen, X.X. Kong, C.Z. Li, Membraneless enzymatic biofuel cells based on graphene nanosheets, *Biosens. Bioelectron.* 25 (2010) 1829–1833.
 - [48] J. Nriagu, *Zinc Toxicity in Humans*, Elsevier Publication, 2007, pp. 1–7. Available: http://www.extranet.elsevier.com/homepage_about/mrwd/nvrn/Zinc%20Toxicity%20in%20Humans.pdf.
 - [49] M.A. Bhat, C.K. Dutta, G.M. Rather, Exploring physicochemical aspects of N-alkylimidazolium based ionic liquids, *J. Mol. Liquid* 181 (2013) 142–151.
 - [50] J. Wang, Stripping analysis at bismuth electrodes: a review, *Electroanalysis* 17 (2005) 1341–1346.



Hydrophilic graphene surface prepared by electrochemically reduced micellar graphene oxide as a platform for electrochemical sensor

Nontapol Akkarachainon^a, Pranee Rattanawaleedirojn^b, Orawon Chailapakul^{a,c,*},
Nadnudda Rodthongkum^{b,*,**}

^a *Electrochemistry and Optical Spectroscopy Research Unit, Department of Chemistry, Faculty of Science, Chulalongkorn University, Phayathai Road, Pathumwan, Bangkok 10330, Thailand*

^b *Metallurgy and Materials Science Research Institute, Chulalongkorn University, Soi Chula 12, Phayathai Road, Pathumwan, Bangkok 10330, Thailand*

^c *National Center of Excellence for Petroleum, Petrochemicals, and Advanced Materials, Chulalongkorn University, Phayathai Road, Pathumwan, Bangkok 10330, Thailand*

ARTICLE INFO

Keywords:

Graphene oxide
Electrochemically reduced micellar graphene oxide
Electrochemical detection
Carbofuran
Carbendazim

ABSTRACT

Graphene is one of the promising hydrophobic carbon-based nanomaterials used for electrode modification in electrochemical sensor. However, hydrophobicity of graphene makes it incompatible with aqueous electrolyte solution, leading to significant impediment to the electron transfer process. Here, we aim to alter graphene property to be hydrophilicity by using an electrochemically reduced micellar graphene oxide for electrode surface modification. Then, this system was applied for the simultaneous determination of toxic pesticides (e.g. carbofuran and carbendazim). Interestingly, the modified electrode offers an improved electrochemical sensitivity, verified by a drastic increase in current signal of carbofuran (4 times) and carbendazim (12 times) compared to an unmodified electrode. Under the optimal conditions, low detection limits of carbofuran and carbendazim were found to be $10 \mu\text{g L}^{-1}$ and $5 \mu\text{g L}^{-1}$, respectively. Ultimately, this system was successfully applied for the sensitive and simultaneous determination of carbofuran and carbendazim residues in various agricultural products.

1. Introduction

With the advent of nanotechnology, various nanomaterials, such as metallic nanoparticles [1,2] and carbon based nanomaterials (*i.e.* fullerenes [3], carbon nanofibers [4], carbon nanotubes [5], carbon nanodots [6], graphene) have been used to modify the electrode surfaces. Among carbon based nanomaterials, graphene (G) [7–12] has become a promising material for electrode modification due to its outstanding properties, such as large surface area, fast electron transfer kinetics and high electrical conductivity. However, the use of pristine G always suffers from a high tendency of self-agglomeration and re-stacking via Van der Waals interaction, leading to loss of effective surface area and conductivity; thus, it is necessary to prevent the self-agglomeration of G. Alternatively, graphene oxide (GO), containing oxygen groups on the plane of carbon atom, has become an attractive material. An important property of GO is well dispersibility in water due to the high polarity of oxygen; nonetheless, GO is often classified as an electrical insulator because of the disruption from the oxygen groups. Therefore, GO is used as a precursor and reduced into pristine

G by removal of oxygen-groups, described as a reduction reaction. GO which is reduced into G is called reduced graphene oxide (RGO). There are several methods for producing of RGO [13–16] including chemical reduction, thermal reduction and electrochemical reduction. From the previous reports [17], although RGO prepared by chemical reduction is a large scale method; however, it was contaminated by the reducing agents resulting in poor-quality yields. Likewise, for thermal reduction at high temperature, it usually produces the very high surface area of RGO, but the heating process can damage the structure of RGO sheets [18]. Nevertheless, GO which is reduced by electrochemical method, denoted as an electrochemically reduced graphene oxide (ERGO) [19,20], can be created as the best quality compared to others. Unfortunately, because of the entire carbon structure of G, it is classified as a hydrophobic material [21]. Thus, the surface of graphene refuses to closely contact with an aqueous solution. In this work, we aim to alter a property of graphene surface to be hydrophilic by simply using a common surfactant for improving of the interfacial property.

Surfactants are the surface-active compounds consisting of hydrophilic heads on one side and long chain hydrophobic tails on another

* Corresponding author.

** Corresponding author.

E-mail addresses: corawon@chula.ac.th (O. Chailapakul), Nadnudda.R@chula.ac.th (N. Rodthongkum).

side. Normally, the surfactant molecules possess an important property of reducing the interfacial tension. Previously, surfactants were used to prevent the self-agglomeration of G by intercalation between G sheets [22–24]. Furthermore, it has been previously reported that surfactant can improve the interface property between electrode and electrolyte solution [25]. Also, it was well known that micelles are formed spontaneously in aqueous solution at a sufficiently high concentration of surfactant. There are several applications that use micelles for electrode modification to improve the electrode surface properties [26,27]. Accordingly, surfactant becomes a material of interest for the development of a new electrode for an electrochemical sensor. Here, cetyltrimethylammonium bromide (CTAB), a positively charged surfactant with quaternary ammonium group, is used along with GO for the electrode surface modification.

One of the current environmental problems which our world is confronting is a contamination of natural resource by toxic chemical substances, especially for the pesticide residues. Carbofuran (CBF) and carbendazim (CBZ), generally used as an insecticide and a fungicide, are considered as one of the most hazardous pesticides. Both of them have potential to wreak widespread destruction of natural environment and potentially contaminate in various agricultural products. With inadvertent use of them, there will be inevitable contamination in air, food and water and adversely impact through the food chain [28]. Consequently, they not only devastate wildlife, but also severely harm to the human health. Previously, it was reported that CBF and CBZ are the carcinogenic substances causing chronic and acute diseases [29–31]. Thus, the development of sensitive sensor for detection of these compounds is essential to control the contamination in environment.

Traditional analytical methods are commonly used for CBF and CBZ determination, such as ultraviolet spectroscopy [32], spectrophotometry [33], gas chromatography [34], high-performance liquid chromatography [35,36] and capillary electrophoresis [37]. Unfortunately, these techniques still have some drawbacks, for example, high cost, non-portability, long analysis time and complicated sample pretreatment. Thus, electrochemical technique has become an interesting option due to its inexpensiveness, fast analysis and portability; however, the performance of conventional electrodes has not sufficed to accomplish the sensitive analyses. To unravel this problem, modification of working electrode surface to improve both analytical performance and sensitivity of electrochemical sensor is very crucial.

Herein, the modified electrodes were fabricated by using an electrochemically reduced micellar graphene oxide (ERMGO) and CTAB, and then this system was applied for the simultaneous detection of CBF and CBZ in the agricultural products. The electrode preparation was thoroughly optimized, and the analytical performances of ERMGO modified electrode were compared with ERGO modified electrode and unmodified electrode. Overall, this system offers several advantages, such as fast and easy fabrication, excellent electrochemical sensitivity, high analytical performance and extremely low cost. Indeed, this novel platform might be an alternative approach for further development of high performance electrochemical sensor in various applications.

2. Experimental

2.1. Materials

Graphene oxide (GO) was purchased from XF Nano, Inc. (Nanjing, China). Cetyltrimethylammonium bromide (CTAB), potassium dihydrogen phosphate (KH_2PO_4) and disodium hydrogen phosphate (Na_2HPO_4) were obtained from Sigma-Aldrich (St. Louis, MO, USA). All aqueous solutions were prepared in Milli-Q water (18.2 M Ω cm). Carbon graphene ink and silver/silver chloride ink were purchased from Gwent group (Torfaen, United Kingdom) for screen-printed carbon electrode preparation.

2.2. Apparatus

The electrochemical measurements using square-wave voltammetry (SWV) and cyclic voltammetry (CV) were performed on a 910 PSTAT mini (Metrohm Siam Company Ltd). SWV measurements of CBF and CBZ were carried out using an applied potential ranging from 0 to 1.0 V with the optimal parameters including step potential of 10 mV, amplitude of 20 mV and frequency of 10 Hz. Furthermore, electrochemical impedance spectroscopy (EIS) was performed on μ AUTOLAB type III potentiostat (Metrohm Siam Company Ltd.) using a solution of 0.5 M KCl containing 1 mM $[\text{Fe}(\text{CN})_6]^{3-/4-}$ with a frequency range from 0.1 to 10^5 Hz and an amplitude of 0.01 V.A. JSM-6400 field emission scanning electron microscope (Japan Electron Optics Laboratory Co., Ltd., Japan) was used for electrode surface morphology characterization. Contact angle measurement was performed by using a 200-k1 goniometer (Rame-hart Instrument Co).

2.3. Preparation of screen-printed carbon electrode (SPCE)

A three-electrode configuration of screen-printed carbon electrode pattern was designed by Adobe Illustrator. The electrodes were prepared by using an in-house screen-printing procedure. Firstly, silver/silver chloride was screened on PVC substrate as reference electrode (RE) and conducting pad, and then heated up at 55 °C until the ink was dried out. Afterwards, carbon graphene ink was screened over as working electrode (WE) and counter electrode (CE), and heated up at 55 °C till the ink was dried out [38].

2.4. Preparation of GO solution for electrode modification

To prepare GO solution, 1.6 mg of GO was dispersed in 1 mL of water with an ultrasonication for 2 h. After that, the dispersed GO solution was mixed with 0.1 M phosphate buffer solution pH 7 at the ratio of 1:1, denoted as GO solution. Likewise, micellar graphene oxide solution was prepared. Firstly, 0.02 g of CTAB was dissolved in 10 mL of water. Secondly, 1.6 mg of GO was sonicated in 1 mL of water for 2 h. Afterwards, the mixture of dispersed GO solution, 0.1 M phosphate buffer solution pH 7 and CTAB solution was mixed at a ratio of 10:9:1, denoted as MGO solution.

2.5. Fabrication of electrochemically reduced graphene oxide modified electrode

To fabricate electrochemically reduced graphene oxide modified electrode, 100 μ L of GO solution was dropped onto a SPCE, covering over 3 electrodes. Cyclic voltammetry was performed from -0.5 to -1.7 v (vs Ag/AgCl) at a scan rate of 100 mV s $^{-1}$ for 10 cycles. Eventually, reduced graphene oxide was deposited on the working electrode surface. This modified electrode is called ERGO modified electrode. Similarly, to fabricate electrochemically reduced micellar graphene oxide modified electrode, 100 μ L of MGO solution was dropped onto a SPCE. Then, the reducing process was carried out by cyclic voltammetry in a potential range of -0.5 to -1.5 V (vs Ag/AgCl) at a scan rate of 100 mV s $^{-1}$ for 10 cycles. Finally, reduced micellar graphene oxide would be deposited onto the working electrode surface. This modified electrode model is denoted as ERMGO modified electrode.

2.6. Real sample preparation

Three agricultural products were selected as real samples including soybeans, rice and tomatoes. They were purchased as raw products from local markets. To prepare the real samples, agricultural product specimens were infused in 50 mL of chloroform and leaved them for a day. Next, 30 mL of chloroform was collected, and removed by rotary evaporator. Then, 10 mL of ethanol was added instead and collected

5 mL of supernatants to avoid dregs and oil part. Then, CBF and CBZ standard solutions were spiked into the solution. Next, 2 mL of 0.01 M NaOH was mixed together with 5 mL of the pesticide solution. The solution was heated up at 85 °C in a closed system for 20 min [39], and then cooled down at a room temperature. After that, 2 mL of 0.01 M HClO₄ was added to neutralize NaOH. Finally, the pesticide solution was diluted with 41 mL of 0.01 M PB solution pH of 7 for a final volume of 50 mL, which has the final concentration of 200, 1000 and 4000 µg L⁻¹ for CBF and 50, 500 and 2000 µg L⁻¹ for CBZ prior to analyses.

3. Results and discussion

3.1. Electrode characterization

3.1.1. Visual characterization

Initially, when CTAB was added into GO solution and the concentration of CTAB reached its critical micelle concentration (CMC), the formation of micellar graphene oxide (MGO) was observed. Suddenly, the micelles were spontaneously formed with CTAB surrounding GO, called micellization. Hydrophilic heads form outer assemblies to contact with aqueous solution, and hydrophobic tail sequesters within the interior. As shown in Fig. 1, it exhibits the alterant features of 0.8 mg mL⁻¹ of GO solution with different CTAB concentrations. Firstly, Fig. 1A shows an appearance of GO solution in the absence of CTAB. An original feature of GO solution was observed as a turbid and dark-brown solution. Secondly, GO solution in the presence of 0.0025% CTAB is shown in Fig. 1B with an unchanged appearance, indicating that CTAB micelles are not formed at this concentration which is below its CMC. Thirdly (Fig. 1C), GO solution was prepared with 0.010% CTAB, and the appearance shows dark-brown micellar sediment of GO suspending in the solution, and micellization takes place by an aggregation of CTAB and GO [40], verifying that the CTAB concentration is above its CMC. Lastly, the appearance of GO solution with 0.020% CTAB was observed with an increased amount of suspended sediment of GO (Fig. 1D); therefore, the micellar CTAB-GO are further aggregated with an increasing amount of CTAB in the solution.

3.1.2. Electrochemical reduction of GO and MGO

To generate ERGO, an electrochemical reducing process was carried out by applying highly negative potential to force the reduction of oxygen groups on the surface of GO sheets. Initially, 0.8 mg mL⁻¹ of GO solution was prepared in the absence and presence of 0.010% CTAB. Afterwards, the reducing process was operated by using cyclic voltammetry scanning in a potential range from -0.5 to -1.7 V (vs Ag/AgCl) for 10 cycles at a scan rate of 100 mV s⁻¹ as shown in Fig. 2. In this work, the cyclic voltammograms present 10 cycles of reduction reactions of GO and MGO. The first cycle of cathodic peaks always provides the highest current signal, explained that the reduction process of GO takes place almost entirely. Next, for the subsequent

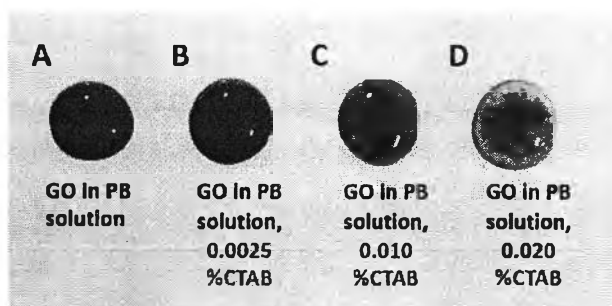


Fig. 1. Appearances of GO solution in an absence (A) and presence of different CTAB concentrations (B–D).

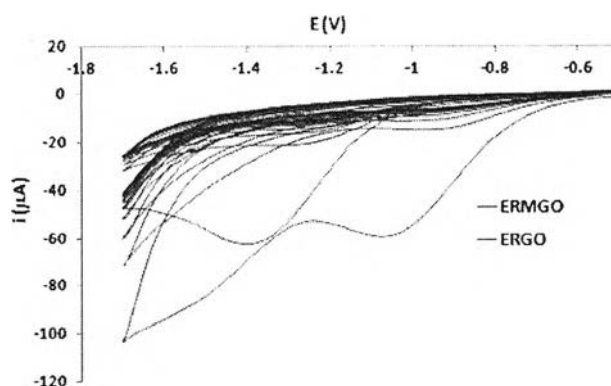


Fig. 2. Cyclic voltammograms of electrodeposition of GO (blue line) and MGO (red line) modified electrode. (For interpretation of the references to color in this figure legend, the reader is referred to the web version of this article.)

cycles, the cathodic peaks become lower and vanish successively because GO exhausts almost completely. Eventually, reduced GO is cumulatively deposited on the electrode surface. Fig. 2 shows the comparisons of cyclic voltammograms of reduction reaction between ERGO (blue line) and ERMGO (red line) modified electrode. The cyclic voltammograms of ERGO display that the reduction of GO begins at a potential of -1.0 V, and reaches the maximum current at -1.4 V. On the other hand, cyclic voltammograms of ERMGO show that the onset potential of reducing process of MGO is at -0.6 V, and the cathodic peak appears at -1.0 V. Considering the first cycles, ERMGO provides positively shifted compared with ERGO, indicating that a rate of electron transfer is promoted in the process of reducing MGO. This phenomenon is possibly explained that the positively charged outer shells of MGO consist of hydrophilic heads of quaternary ammonium group. Then, the negative potential was applied to the electrode surface, so the negatively charged surface attracts the positively charged micelles by an electrostatic interaction resulting in an accelerated migration of MGO.

3.1.3. Scanning electron microscopy

To prove the successful electrodeposition of RGO on the electrode surfaces, the morphologies of unmodified electrode, ERGO and ERMGO modified electrode were characterized by scanning electron microscopy (SEM) as shown in Fig. 3A–C. According to Fig. 3A, a SEM image shows an appearance of unmodified electrode surface, exhibiting the sheet-like architecture with plenty of graphite flakes on the surface. Fig. 3B shows a SEM image of ERGO modified electrode that demonstrates ERGO film covering over the sheet-like morphology and concealing all graphite flakes of unmodified electrode. Fig. 3C, thin ERMGO film also covers the entire sheet-like morphology. In addition, ERMGO is a translucent film because it can be seen through the opposite site with clear visibility. Thereby, it can be concluded that the ERMGO film is more transparent than ERGO film, implying that ERMGO film is much thinner than ERGO film. Furthermore, in order to confirm the elemental composition of the working electrode surfaces, unmodified electrode, ERGO modified electrode and ERMGO modified electrode were characterized by using an energy-dispersive x-ray spectroscopy (SEM-EDX), and the obtain spectra were shown in Fig. S1 in the Supporting information.

3.1.4. Contact angle (CA) measurement

Contact angle measurement is one of the techniques used for investigation of the hydrophobic/hydrophilic property or wettability of the solid surface. In this work, CA values of an unmodified electrode, ERGO and ERMGO modified electrode surface were measured using a static sessile drop method as presented in Table 1, and the water drop behaviors on the electrode surface are shown in the Fig. 4A–C. As seen in Fig. 4A, it shows the water drop behavior on the unmodified

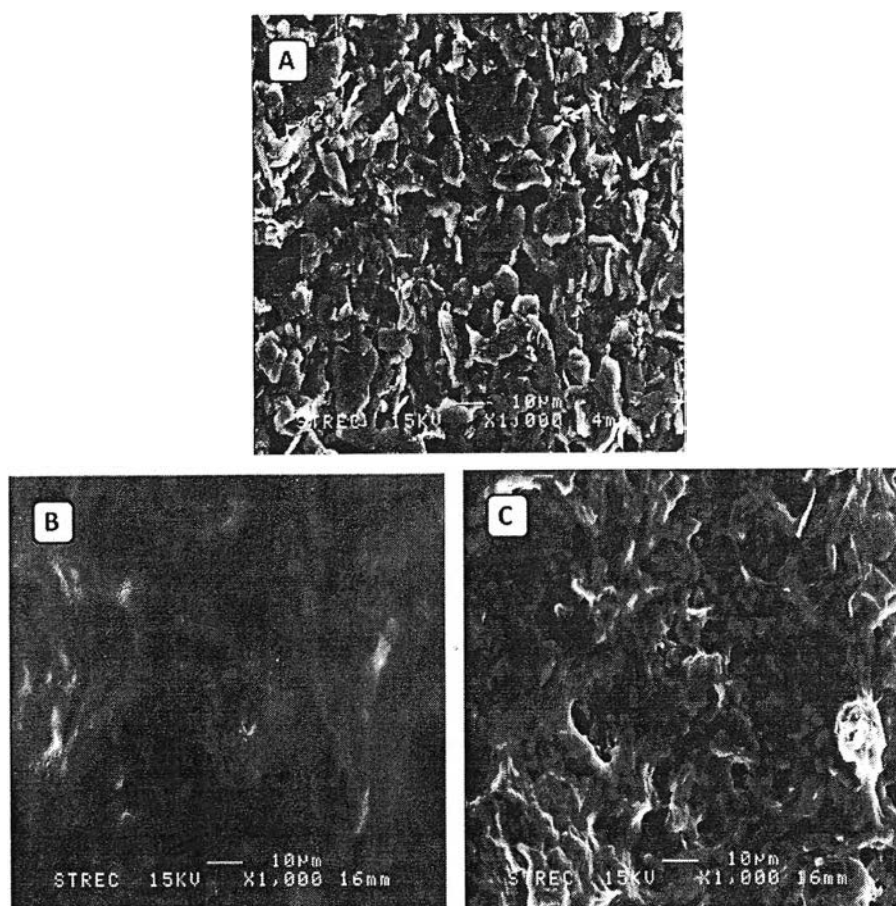


Fig. 3. SEM images of unmodified electrode surface (A), ERGO modified electrode surface (B) and ERMGO modified electrode surface (C) with 1000× magnification.

Table 1
Comparison of contact angle values on the surface of different electrodes.

Electrode	Average contact angle values ($^{\circ} \pm SD$)
Unmodified	133.18 \pm 2.02
ERGO	127.52 \pm 3.51
ERMGO	68.86 \pm 3.90

electrode surface. The water drop is almost spherical, and a CA value is found to be 133.18°. Obviously, a CA value obtained from unmodified electrode is larger than 90°, considered as hydrophobic surface or low wettability. This phenomenon can be described that screened carbon ink composition consists of carbon ink, graphite, graphene flakes, organic solvent and additives etc. All the components are hydrophobic, so the unmodified electrode surface repels the water droplet. Likewise, Fig. 4B presents the water drop behavior on ERGO modified electrode surface. The shape of water drop is also spherical similar to the drop on the unmodified electrode, and a CA value is 127.52°. ERGO modified electrode surface is also classified as hydrophobic surface or low wettability. As that result, ERGO was produced from the removal of oxygen functionalities on the GO sheets by reduction reaction. Consequently, ERGO remains merely entire carbon structure, so it is hydrophobic as well. On the contrary, Fig. 4C shows the water drop behavior on ERMGO modified electrode surface. The water drop pervasively spread over the surface, and a CA value is 68.86°, which is smaller than 90°, suggesting that the wetting on the surface is favorable. Thus, ERMGO modified electrode surface is classified to be hydrophilic surface or high wettability. This phenomenon can be described that CTAB has a property of reducing surface tension

between interfacial phases. In other words, CTAB has ability for the improvement of miscibility between polar and non-polar phases. Thus, the adjustment of ERGO surface with micelle of CTAB takes an advantage of improving compatibility of ERMGO and water.

3.1.5. Electrochemical impedance spectroscopy

Also, the interfacial properties of electrode surface were investigated by using an electrochemical impedance spectroscopy (EIS). The charge-transfer resistance (R_{ct}) depends on dielectric and insulating features at the electrode-electrolyte interface. The R_{ct} value derived from a diameter of semicircle portion of Nyquist plots is related to the charge transfer resistance and electronic resistance of the electrodes. The semicircular portion of Nyquist plots can indicate the efficiency of electron transfer from electrode surface to an aqueous electrolyte solution. As shown in Fig. 5, the Nyquist plots represent the comparison among unmodified electrode (blue line), ERGO modified electrode (green line) and ERMGO modified electrode (red line) in the presence of 1.0 mM of $Fe(CN)_6^{3-/4-}$ in 0.1 M KCl. The Nyquist curve of unmodified electrode shows the largest semicircular portion of all with an R_{ct} value of 16329.4 Ω , indicating that an unmodified electrode has high charge-transfer resistance, leading to poor electron transfer through the surface. For the curve of ERGO modified electrode, the semicircular portion is smaller than on an unmodified electrode, and an R_{ct} value substantially decreases to 4984.2 Ω . The small diameter on the curve can indicate that G has an ability to accelerate the electron transfer between electrode surface and electrolyte solution. After modifying electrode with ERMGO, a semicircular domain does not exist, and the relation is almost straight line; thus, R_{ct} value is not available. This result suggests that the rate of electron transfer on ERMGO modified electrode is very fast. Theoretically, CTAB is

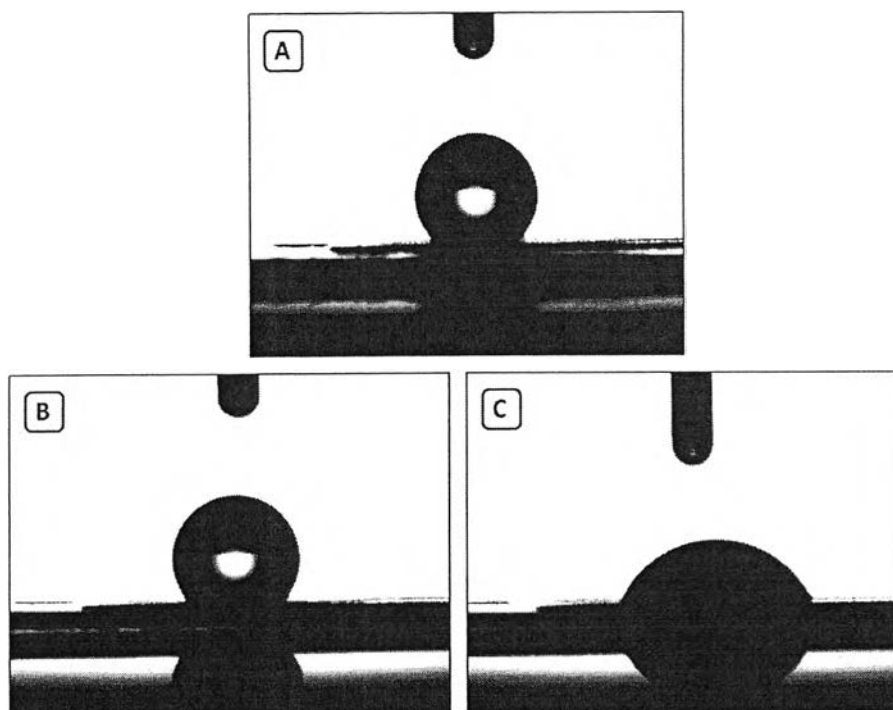


Fig. 4. Images of water droplet on unmodified electrode surface (A), ERGO modified electrode surface (B) and ERMGO modified electrode surface (C) obtained from CA measurements.

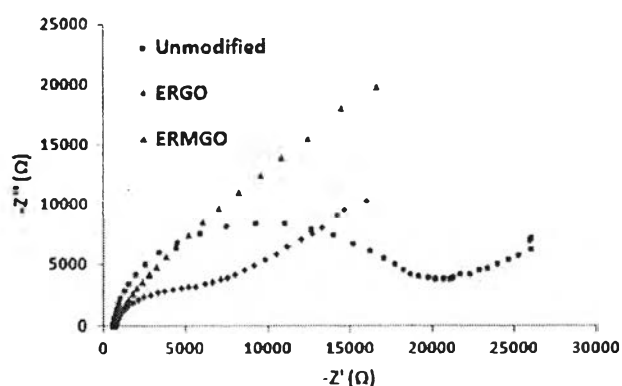


Fig. 5. EIS of an unmodified electrode (blue), ERGO modified electrode (green) and ERMGO modified electrode (red) in the presence of 1.0 mM of $\text{Fe}(\text{CN})_6^{3-/4-}$ in 0.5 M KCl. (For interpretation of the references to color in this figure legend, the reader is referred to the web version of this article.)

surfactant which has no property of direct improvement of the electrical conductivity. For this reason, adding the CTAB might have impeded the electron transfer and obstructed the access of analytes from bulk solution. Thus, the Nyquist curve on ERMGO modified electrode should have possessed the largest semicircular portion. However, ERMGO provides the lowest charge-transfer resistance, implying that CTAB orientation on ERMGO surface facilitates the electron transfer process between ERMGO surface and aqueous electrolyte solution.

According to the characterization, although G possesses several exceptional properties, it is still not suitable for directly modification of an electrode surface which is used to detect analytes in an aqueous solution due to the water refusal of hydrophobic G. To bring out the maximum efficiency of G, ERMGO modified electrode was developed in this study. The G surface was adjusted by the orientation of micellar CTAB which improves hydrophilicity of the surfaces. Then, ERMGO modified electrode can improve the compatibility between the analytes and G surface, leading to enhanced electron transfer as a result of high electrode performance.

3.2. Electrochemical determination of CBF and CBZ

In this work, voltammetry is a technique which is used for CBF and CBZ detection. Square-wave voltammetry (SWV) is selected for the simultaneous determination of CBF and CBZ. Fig. 6A shows the square-wave voltammograms of 20 mg L^{-1} of CBF and 5 mg L^{-1} of CBZ measured on unmodified electrode (red line), ERGO modified electrode (green line) and ERMGO modified electrode (blue line). The SWV was operated under a step potential of 10 mV, an amplitude of 20 mV and a frequency of 10 Hz. From the voltammograms, the results show the well-separated cathodic peaks of two compounds at the potential of 0.18 and 0.53 V belonging to CBF and CBZ, respectively. The peak currents were measured by current integration from each peak as shown in Fig. 6B. For the voltammogram measured on an unmodified electrode, it exhibits two cathodic peaks which are low current response signal and broad peak shape. For the current response measured on ERGO modified electrode, the peak currents of both CBF and CBZ are higher than measuring on an unmodified electrode, approximately 1.5-fold for CBF and 4-fold for CBZ. The significant increase of current signal can be described by the excellent properties of G, such as a high electrical conductivity, a high surface area and a high electrocatalytic activity. ERMGO modified electrodes were used for the simultaneous determination of CBF and CBZ. The obtained voltammogram presents the well-defined peak shape and have the highest current response compared to an unmodified electrode and an ERGO modified electrode. The peak current measured on ERMGO modified electrode is 4-fold higher than an unmodified electrode for CBF and 12-fold higher for CBZ. Due to a drastic enhancement of current signal, it substantiates that ERMGO modified electrode has an excellent efficiency for the simultaneous determination of CBF and CBZ.

According to the characterization results, the important roles of CTAB orientation on graphene surfaces, influencing on the electrochemical behaviors, could be explained as follows:

- Due to hydrogen bonding among oxygen functional groups on GO sheets, GO tends to re-agglomeration. The addition of CTAB, which

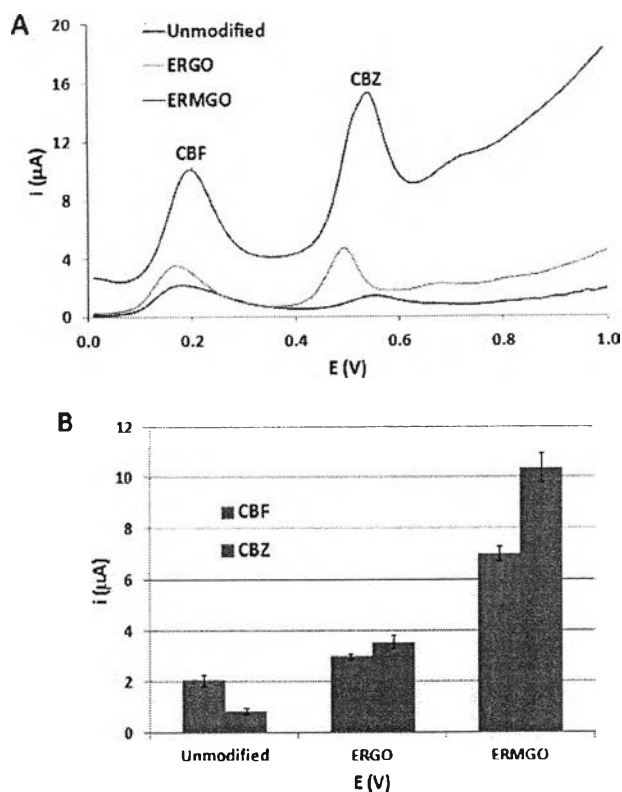


Fig. 6. Square-wave voltammograms (SWV) of 20 mg L⁻¹ CBF and 5 mg L⁻¹ CBZ measured on unmodified electrode (blue), ERGO modified electrode (green) and ERMGO modified electrode (red) (A) and a histogram showing peak currents obtained from SWV using unmodified electrode, ERGO modified electrode and ERMGO modified electrode (B). (For interpretation of the references to color in this figure legend, the reader is referred to the web version of this article.)

reduces surface tension of water and intercalates between GO sheets, can inhibit the agglomeration, so it has ability to stabilize GO dispersibility [41]. Thus, the obtained reduced GO layers dispersed with CTAB are significantly thinner than reduced GO

alone, resulting in better electrical conductivity (Scheme 1A).

- ERMGO was deposited on the electrode surface. CTAB on the G sheet will form by arranging the hydrophobic tails towards G, and expose the hydrophilic outwards to the aqueous solution as a result of reduction of surface tension of water. In the previous works [42–44], they reported that the surface tension is related to diffusion coefficient by an inverse variation. Consequently, with the decreasing surface tension, a diffusion coefficient will increase. According to the Randles-Sevcik equation (Eq. (1)) [45,46], the equation shows the relation of current (i_p) and diffusion coefficient (D). The current is directly proportional to the diffusion coefficient.

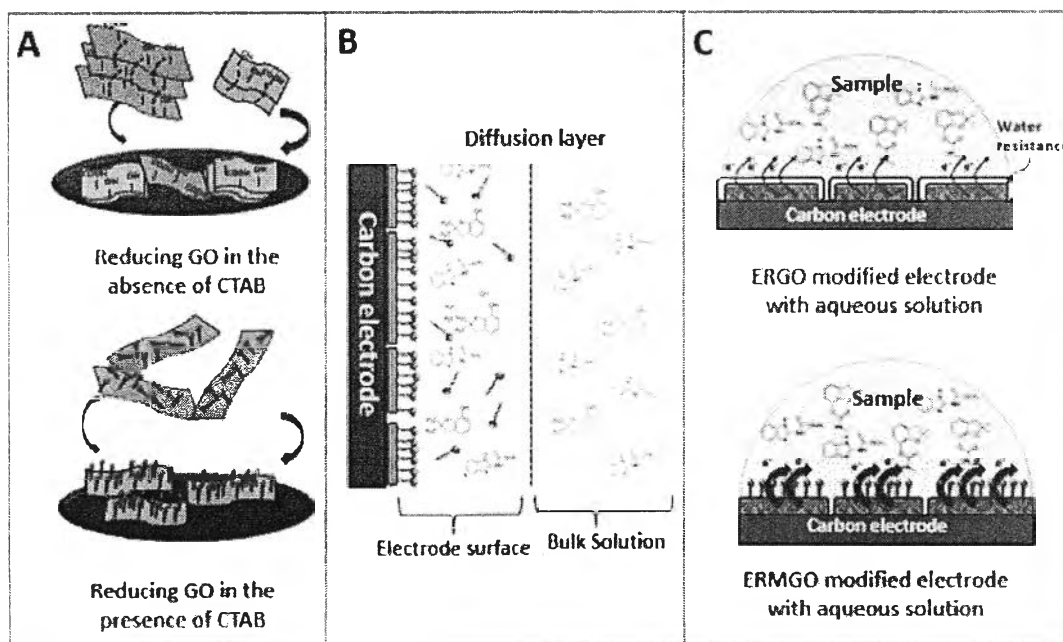
$$i_p = (2.69 \times 10^5) n^{3/2} A C D^{1/2} \nu^{1/2} \quad (1)$$

where n=number of electron transfer, A=electrode surface area (cm²), C=concentration of the electroactive species (mol cm⁻³), D=diffusion coefficient (cm² s⁻¹) and ν =scan rate (v s⁻¹).

From the following equation, it is inferred that decreasing surface tension causes the increase of current. Thus, using ERMGO for CBF and CBZ detection can amplify the current signal, leading to an enhanced electrochemical sensitivity (Scheme 1B).

- From EIS along with CA measurement, since G consists of entire carbon atom, the property of ERGO is hydrophobic. Therefore, using ERGO modified electrode with aqueous solution will produce the water resistance between ERGO sheet and water which impedes the electron transfer across the phases. On the contrary, on ERMGO modified electrode, CTAB orientation will adjust hydrophobic surface to be hydrophilic surface. Accordingly, the contact of water on ERMGO surface is even more compatible, so the analytes can easily access to the electrode surface. Thereby, it helps to facilitate the electron transfer from ERMGO surface to electrolyte solution (Scheme 1C).

According to Randles-Sevcik equation (Eq. (1)), it is obvious that the electrode surface area is directly proportional to the peak current responses. For the increasing of sensitivity, using the high surface area materials (i.e. nanoparticles [1,2,47]) and the suitable electrode modification process (i.e. electrospraying [48,49] or electrospinning [50,51]) are the important factors. For this system, the use of ERMGO



Scheme 1. The roles of CTAB on the modified electrode surfaces.

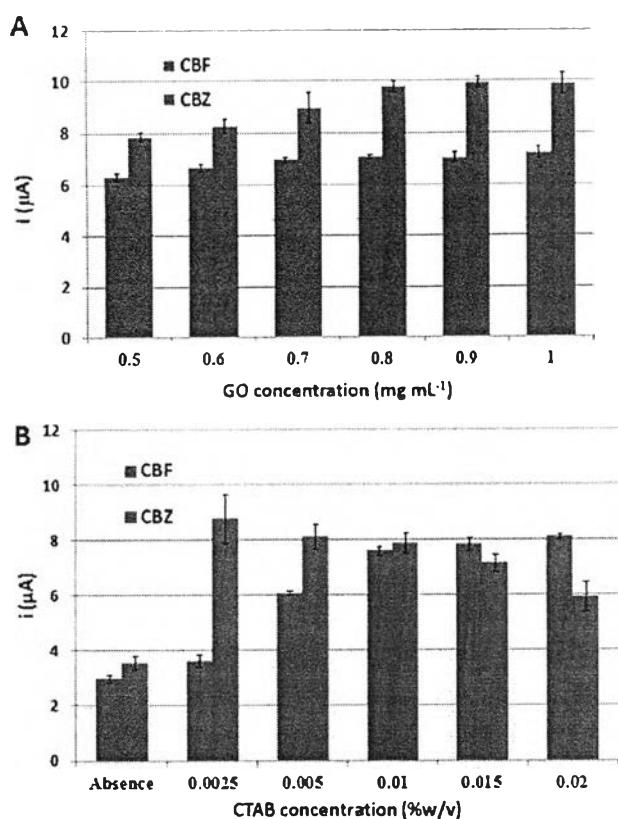


Fig. 7. Optimization of GO concentration (mg mL⁻¹) using ERMGO modified electrode (A) of CTAB concentration (%w/v) using ERMGO modified electrode (B).

also significantly improved the electrode surface area and thus the electrochemical sensitivity.

3.3. Optimization of ERMGO modified electrode fabrication

For the fabrication of ERMGO modified electrode, the important parameters concerning in MGO solution including CTAB concentration, GO concentration, scan rate of reducing process and number of scan were optimized. The selected conditions were obtained from that particular condition that provides both highest peak current and well-defined peak shape. First of all, GO concentration in MGO solution was optimized. The GO concentration was varied within the concentration range of 0.5, 0.6, 0.7, 0.8, 0.9 and 1.0 mg mL⁻¹ as shown in Fig. 7A. The current responses continuously increase until the concentration reaches to 0.8 mg mL⁻¹, and then it plateaus; thus, 0.8 mg mL⁻¹ of GO was selected as an optimum concentration. CTAB concentration in MGO solution was investigated within a concentration range of 0.0025%, 0.005%, 0.010%, 0.015% and 0.020%w/v compared with the absence of CTAB as shown in Fig. 7B. As the result, at the condition without CTAB, peak currents of CBF and CBZ show the lowest signal. After adding CTAB, the current responses of both analytes significantly increase. At the concentration of 0.0025% CTAB, the current of CBF slightly increase as the current of CBZ substantially increases. After varying the concentration of CTAB from 0.005% to 0.020%, the current responses of CBF rapidly increase as the current responses of CBZ slightly decrease. Obviously, CBF response to CTAB is higher than CBZ response. According to these results, the compromising selection of this parameter is 0.010% for the preparation of MGO solution. Lastly, in the process of reducing MGO, the parameters of scan rate and number of scan were optimized (Figs. S2 and S3). The selected condition would be considered from the condition which is obtained from the suitability of compromise between the current response and operation time.

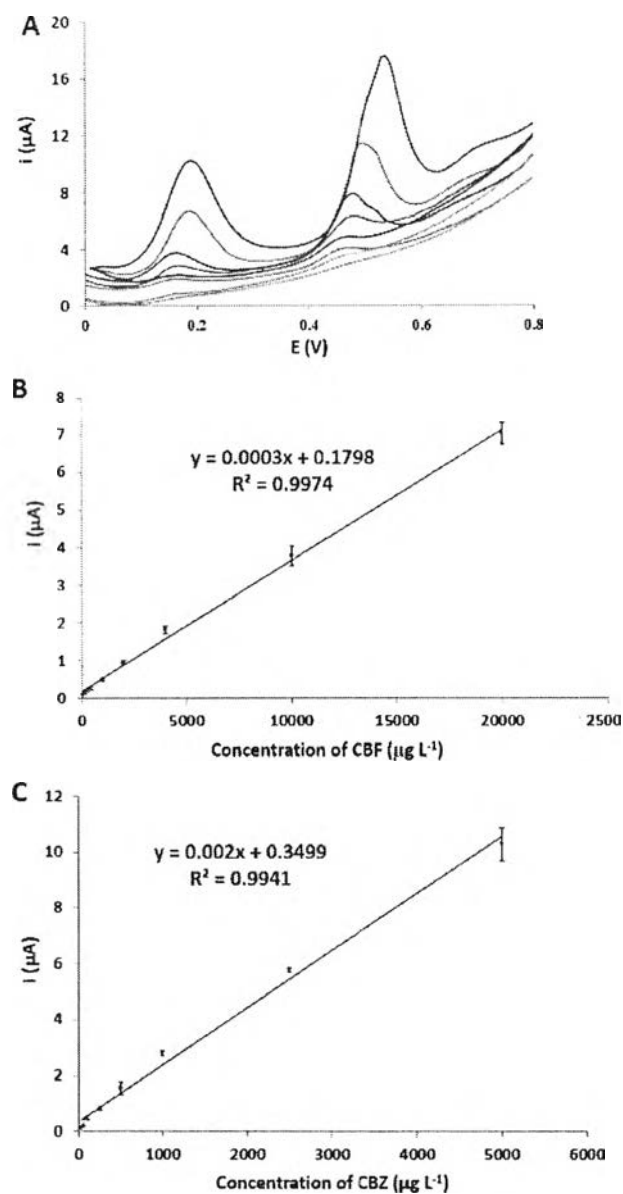


Fig. 8. Square-wave voltammograms of CBF and CBZ in a concentration range of 40–10,000 μg L⁻¹ and 25–5000 μg L⁻¹, respectively, in PB solution at pH 7 (A), a calibration plot of CBF concentrations versus current signal (B) and a calibration plot of CBZ concentrations versus current signal (C).

Ultimately, the optimal conditions of 100 mV s⁻¹ and 10 cycles were chosen for further experiments.

3.4. Analytical performances of ERMGO modified electrode

The analytical performances of ERMGO modified electrode in the simultaneous determination of CBF and CBZ were evaluated. To investigate the detection capability, different concentrations of analytes were determined for five replicates (n=5) at a concentration range of 40, 100, 200, 400, 1000, 2000, 4000, 10,000 and 20,000 μg L⁻¹ for CBF and 25, 50, 100, 250, 500, 1000, 2500 and 5000 μg L⁻¹ for CBZ (Fig. 8A). The calibration curves of CBF and CBZ concentrations were plotted versus the current response signals, and the current responses increase linearly with the increase of analyte concentrations. As for CBF detection, a calibration plot (Fig. 8B) is linear over a range of 40–20,000 μg L⁻¹ with a correlation coefficient (R²) of 0.997. On the other hand, a calibration curve of CBZ (Fig. 8C) was obtained over a range of

Table 2.1
Comparison of the purposed electrode to other modified electrodes in the determination of CBF.

Modified electrode	Method	Supporting electrolyte	Linear range ($\mu\text{g L}^{-1}$)	Detection limit ($\mu\text{g L}^{-1}$)	Other analytes	References
Co-RGO/GCE	DPV	0.1 M B-R (pH4): acetonitrile	95.5–13,370	3.82	Carbaryl (simultaneous)	[54]
MIP-RGO@Au/GCE	DPV	0.1 M KCl	9.55–3820	3.82	–	[55]
Heated – SPCE	DPV	Borate buffer (pH 10)	76.4–76,400	9.55	–	[39]
Micellar CTAB-RGO/SPCE	SWV	PB solution (pH7)	40–20,000	10	Carbendazim (simultaneous)	This work

Table 2.2
Comparison of the purposed electrode to other modified electrodes in the determination of CBZ.

Modified electrode	Method	Supporting electrolyte	Linear range ($\mu\text{g L}^{-1}$)	Detection limit ($\mu\text{g L}^{-1}$)	Other analytes	References
SiO ₂ MWNTs/GCE	SWV	0.1 M PB Solution (pH 8)	38.2–764	11	–	[56]
MWNTs-PMRE/GCE	LSV	0.6 M H ₂ SO ₄	38.2–1910	1.7	–	[57]
GO-MWNTs/GCE	DPV	B-R solution (pH 1.8)	1.91–764	1.0	–	[58]
Diamond electrode	SWV	0.1 M Na ₂ HPO ₄ (pH 2)	95.5–2865	22	–	[59]
TCP/SPCE	Stripping-DPV	B-R solution (pH 4.0)	95.5–1910	57.3	–	[60]
G/SPCE	Stripping-SWV	1.0 M HClO ₄	500–10,000	110	Isoproturon (simultaneous)	[61]
Micellar CTAB-RGO/SPCE	SWV	PB Solution (pH 7)	25–5,000	5	Carbofuran (simultaneous)	This work

25–5000 $\mu\text{g L}^{-1}$ with a correlation coefficient (R^2) of 0.994. The experimental limit of detection (LOD) was evaluated based on signal-to-noise ratio of three ($S/N=3$) and LODs of CBF and CBZ were found to be 10 and 5 $\mu\text{g L}^{-1}$ for CBF and CBZ, respectively. According to maximum acceptable amounts of CBF and CBZ from Maximum Residue Limits (MRLs) [52,53], there are 50–2000 $\mu\text{g L}^{-1}$ for CBF and 50–15,000 $\mu\text{g L}^{-1}$ for CBZ. Apparently, LODs obtained from ERMGO modified electrode are low and wide. Hence, this system is sufficiently sensitive enough for the simultaneous determination of CBF and CBZ in real agricultural products.

The comparison of the analytical performances of our system with the previous reports are shown in Tables 2.1 and 2.2. Considering the previous works, our system provides the comparable analytical performances for the simultaneous determination of CBF and CBZ. Interestingly, by comparing with the similar platforms ERMGO modified electrodes provide lower LOD and wider linear range. Moreover, the most important purpose of modifying screen-printed carbon electrode is using as disposable sensors. Therefore, it will be wasted if the electrodes were modified with the noble metal nanoparticles (gold nanoparticles, cobalt phthalocyanine etc.) or expensive materials (diamond electrode etc.) or complicated preparation (molecular imprinting etc.) or double/triple modification steps. As seen, the materials used for the electrode modification in our proposed system are much simpler and cheaper than others. Moreover, the preparation procedure is a one-step operation of electrodeposition, so several advantages of our system are easy, simple and fast preparation.

3.5. Interference study

Sample preparation is a crucial step to eliminate the interferences, especially for real sample analyses. In this study, the crop samples were initially infused in chloroform for extraction. This step was carried out to eliminate ions and polar compounds (e.g. ascorbic acid) which can potentially interfere the analyte detection. After the extraction by chloroform, the infusions were re-solvated by ethanol, and then collected a clear part from ethanol solution for elimination of dregs and other non-polar compounds (e.g. pigment oils). It can presume that prepared samples do not have any interference, proved by assuring that the current signal of CBF and CBZ in standard solution and real

samples, which had been already prepared, are perfectly matched at every level of concentration (Fig. S4). Thus, the real sample analysis can be determined by using an external standard method.

3.6. Real sample analyses

To validate method applicability, ERMGO modified electrodes were used for simultaneous detection of CBF and CBZ in the real samples. Three types of agricultural products which have possibility of being used of both pesticides were selected as the real samples, namely soy beans, rice and tomatoes. For our analytical method, three levels of pesticide concentration were spiked into the real samples. For CBF, the concentrations of 200, 1000 and 4000 $\mu\text{g L}^{-1}$ were added. Likewise, 50, 500 and 2000 $\mu\text{g L}^{-1}$ of CBZ were spiked into the real samples. Afterwards, the amounts of these pesticides in the real samples were determined by external standard method. Each sample was detected thrice ($n=3$), and the average values are shown in Tables 3.1 and 3.2. The percent recoveries were found in the ranges of 95–102% and 97–103% for CBF and CBZ, respectively. The percent RSD is significantly acceptable in every single range of concentration according to a standard AOAC guideline [62], indicating that this developed system can be applied for the simultaneous determination of CBF and CBZ in the actual agricultural samples with high accuracy and precision.

Table 3.1
Determination of CBF in three agricultural crop samples using ERMGO modified electrode ($n=3$).

Samples	Concentration ($\mu\text{g L}^{-1}$)		Recovery (%)	RSD (%)
	Added	Found		
Soy bean	4000	4023.50 \pm 227.98	100.6	5.7
	1000	997.67 \pm 46.67	99.8	4.7
	200	191.42 \pm 7.68	95.7	4.0
Rice	4000	4033.20 \pm 239.36	100.8	5.9
	1000	994.33 \pm 65.66	99.4	6.6
	200	207.88 \pm 12.14	102.8	5.8
Tomato	4000	3917.70 \pm 63.86	97.7	1.6
	1000	974.33 \pm 58.41	97.4	6.0
	200	199.75 \pm 15.61	99.9	7.8

Table 3.2
Determination of CBZ in three agricultural crop samples using ERMGO modified electrode (n=3).

Samples	Concentration ($\mu\text{g L}^{-1}$)		Recovery (%)	RSD (%)
	Added	Found		
Soy bean	2000	2072.30 \pm 41.66	103.6	2.0
	500	527.63 \pm 10.95	105.5	2.1
	50	97.00 \pm 6.61	97.0	6.8
Rice	2000	2065.10 \pm 104.18	103.3	5.0
	500	517.42 \pm 15.44	103.5	3.0
	50	101.17 \pm 4.02	97.8	3.9
Tomato	2000	2046.80 \pm 74.10	102.3	3.6
	500	502.00 \pm 15.44	100.4	1.0
	50	99.08 \pm 9.36	99.1	9.5

4. Conclusions

ERMGO modified SPCE was developed as a novel platform of high performance electrochemical sensor for the sensitive determination of CBF and CBZ. The use of G along with CTAB improved the electrode surface area, leading to substantially increased electrochemical sensitivity of the system. By using ERMGO modified electrode along with SWV, linear ranges of 40–20,000 $\mu\text{g L}^{-1}$ and 25–5000 $\mu\text{g L}^{-1}$ were obtained for CBF and CBZ, respectively. The detection limits (LODs) were found to be 10 $\mu\text{g L}^{-1}$ for CBF and 5 $\mu\text{g L}^{-1}$ for CBZ. Ultimately, this system was successfully applied for the simultaneous determination of pesticide residues in real agricultural crops with high accuracy and precision. Besides, this system can be created with fast and simple fabrication process with low cost. Thus, it might be an interesting prototype for the electrode modification using ERMGO for other application fields.

Acknowledgements

Nontapol Akkarachainon gratefully appreciates The Center of Excellence on Petrochemical and Materials Technology (PETROMAT) through High Performance and Smart Materials (HPSM) research program. This research was funded by the Ratchadapisek Sompoch Endowment Fund (2015), Chulalongkorn University (CU-58-029-AM). Orawon Chailapakul also would like to thank to the Thailand Research Fund through Research Team Promotion Grant (RTA5780005).

Appendix A. Supporting information

Supporting information associated with this article can be found in the online version at doi:10.1016/j.talanta.2016.12.092.

References

- [1] E. Bernalte, C. Marin Sánchez, E. Pimilla Gil, Gold nanoparticles-modified screen-printed carbon electrodes for anodic stripping voltammetric determination of mercury in ambient water samples. *Sens. Actuators B: Chem.* 161 (2012) 669–674.
- [2] M. Pal, V. Ganesan, Electrochemical determination of nitrite using silver nanoparticles modified electrode. *Analyst* 135 (2010) 2711–2716.
- [3] R.N. Goyal, V.K. Gupta, N. Bachheti, Fullerene-C60-modified electrode as a sensitive voltammetric sensor for detection of nandrolone—an anabolic steroid used in doping. *Anal. Chim. Acta* 597 (2007) 82–89.
- [4] Y. Yue, G. Hu, M. Zheng, Y. Guo, J. Cao, S. Shao, A mesoporous carbon nanofiber-modified pyrolytic graphite electrode used for the simultaneous determination of dopamine, uric acid, and ascorbic acid. *Carbon* 50 (2012) 107–114.
- [5] B. Habibi, M. Abazari, M.H. Pournaghi-Azar, A carbon nanotube modified electrode for determination of caffeine by differential pulse voltammetry. *Chin. J. Catal.* 33 (2012) 1783–1790.
- [6] S. Zhao, C. Li, H. Huang, Y. Liu, Z. Kang, Carbon nanodots modified cobalt phosphate as efficient electrocatalyst for water oxidation. *J. Mater.* 1 (2015) 236–244.
- [7] A.A. Balandin, S. Ghosh, W. Bao, I. Calizo, D. Teweldebrhan, F. Miao, C.N. Lau, Superior thermal conductivity of single-layer graphene. *Nano Lett.* 8 (2008) 902–907.
- [8] A.K. Geim, K.S. Novoselov, The rise of graphene. *Nat. Mater.* 6 (2007) 183–191.
- [9] N. Huang, M. Liu, H. Li, Y. Zhang, S. Yao, Synergetic signal amplification based on electrochemical reduced graphene oxide-ferrocene derivative hybrid and gold nanoparticles as an ultra-sensitive detection platform for bisphenol A. *Anal. Chim. Acta* 853 (2015) 249–257.
- [10] M. Liu, L. Wang, J. Deng, Q. Chen, Y. Li, Y. Zhang, H. Li, S. Yao, Highly sensitive and selective dopamine biosensor based on a phenylethynyl ferrocene/graphene nanocomposite modified electrode. *Analyst* 137 (2012) 4577–4583.
- [11] M. Liu, J. Deng, Q. Chen, Y. Huang, L. Wang, Y. Zhao, Y. Zhang, H. Li, S. Yao, Sensitive detection of rutin with novel ferrocene benzene derivative modified electrodes. *Biosens. Bioelectron.* 41 (2013) 275–281.
- [12] M. Liu, Q. Chen, C. Lai, Y. Zhang, J. Deng, H. Li, S. Yao, A double signal amplification platform for ultrasensitive and simultaneous detection of ascorbic acid, dopamine, uric acid and acetaminophen based on a nanocomposite of ferrocene thiolate stabilized Fe₃O₄@Au nanoparticles with graphene sheet. *Biosens. Bioelectron.* 48 (2013) 75–81.
- [13] S. Pei, H.-M. Cheng, The reduction of graphene oxide. *Carbon* 50 (2012) 3210–3228.
- [14] S. Stankovich, R.D. Piner, X. Chen, N. Wa, S.T. Nguyen, R.S. Ruoff, Stable aqueous dispersions of graphitic nanoplatelets via the reduction of exfoliated graphite oxide in the presence of poly(sodium 4-styrenesulfonate). *J. Mater. Chem.* 16 (2006) 155–158.
- [15] H.C. Schniepp, J.-L. Li, M.J. McAllister, H. Sai, M. Herrera-Alonso, D.H. Adamson, R.K. Prud'homme, R. Car, D.A. Saville, I.A. Aksay, Functionalized single graphene sheets derived from splitting graphite oxide. *J. Phys. Chem. B* 110 (2006) 8535–8539.
- [16] S.J. An, Y. Zhu, S.H. Lee, M.D. Stoller, T. Enslin, S. Park, A. Velamakanni, J. An, R.S. Ruoff, Thin film fabrication and simultaneous anodic reduction of deposited graphene oxide platelets by electrophoretic deposition. *J. Phys. Chem. Lett.* 1 (2010) 1259–1263.
- [17] J.D.L. Fuente, Reduced graphene oxide - what is it? How is it created? (<http://www.graphenea.com/pages/reduced-graphene-oxide.s.VrBMBtJ971U>) (accessed 20.12.15).
- [18] K.N. Kudin, B. Ozbas, H.C. Schniepp, R.K. Prud'homme, I.A. Aksay, R. Car, Raman spectra of graphite oxide and functionalized graphene sheets. *Nano Lett.* 8 (2008) 36–41.
- [19] M.A. Raj, S.A. John, Fabrication of electrochemically reduced graphene oxide films on glassy carbon electrode by self-assembly method and their electrocatalytic application. *J. Phys. Chem. C* 117 (2013) 4326–4335.
- [20] L. Chen, Y. Tang, K. Wang, C. Liu, S. Luo, Direct electrodeposition of reduced graphene oxide on glassy carbon electrode and its electrochemical application. *Electrochim. Commun.* 13 (2011) 133–137.
- [21] D.J. Preston, D.L. Mafra, N. Miljkovic, J. Kong, E.N. Wang, Scalable graphene coatings for enhanced condensation heat transfer. *Nano Lett.* 15 (2015) 2902–2909.
- [22] Y. Fan, Y. Liu, Q. Cai, Y. Liu, J. Zhang, Synthesis of CTAB-intercalated graphene/poly pyrrole nanocomposites via in situ oxidative polymerization. *Synth. Met.* 162 (2012) 1815–1821.
- [23] X. Ma, M. Chao, Z. Wang, Electrochemical determination of Sudan I in food samples at graphene modified glassy carbon electrode based on the enhancement effect of sodium dodecyl sulphate. *Food Chem.* 138 (2013) 739–744.
- [24] Y. Mao, Q. Fan, J. Li, L. Yu, L.-B. Qu, A novel and green CTAB-functionalized graphene nanosheets electrochemical sensor for Sudan I determination. *Sens. Actuators B: Chem.* 203 (2014) 759–765.
- [25] C. Hu, S. Hu, Electrochemical characterization of cetyltrimethyl ammonium bromide modified carbon paste electrode and the application in the immobilization of DNA. *Electrochim. Acta* 49 (2004) 405–412.
- [26] X.-L. Wen, Y.-H. Jia, Z.-L. Liu, Micellar effects on the electrochemistry of dopamine and its selective detection in the presence of ascorbic acid. *Talanta* 50 (1999) 1027–1033.
- [27] P. Manisankar, G. Selvanathan, C. Vedhi, Determination of pesticides using heteropolyacid montmorillonite clay-modified electrode with surfactant. *Talanta* 68 (2006) 686–692.
- [28] F.C. Moraes, L.H. Mascaro, S.A.S. Machado, C.M.A. Brett, Direct electrochemical determination of carbaryl using a multi-walled carbon nanotube/cobalt phthalocyanine modified electrode. *Talanta* 79 (2009) 1406–1411.
- [29] H. Marshall, Carbendazim 57 (2002).
- [30] Q.X. Li, B.D. Hammock, J.N. Seiber, Development of an enzyme-linked immunosorbent assay for the herbicide bentazone. *J. Agric. Food Chem.* 39 (1991) 1537–1544.
- [31] B.V.C. Toxicity, Section. murray state university. hopkinsville. kentucky carbofuran toxicity. *J. Toxicol. Environ. Health* (1994) 383–418.
- [32] A. Moral, M.D. Sicilia, S. Rubio, D. Pérez-Bendito, Multifunctional sorbents for the extraction of pesticide multiresidues from natural waters. *Anal. Chim. Acta* 605 (2008) 61–72.
- [33] G.N. Fu, Y.Z. He, C.Z. Yu, Y. Gao, W.E. Gan, Preconcentration and determination of carbamate pesticide residues in vegetable samples by electrokinetic flow analysis with on-line hollow fiber liquid-liquid microextraction and spectrophotometry. *Spectrosc. Lett.* 42 (2009) 305–311.
- [34] X.M. Xu, S. Yu, R. Li, J. Fan, S.H. Chen, H.T. Shen, J.L. Han, B.F. Huang, Y.P. Ren, Distribution and migration study of pesticides between peel and pulp in grape by online gel permeation chromatography-gas chromatography/mass spectrometry. *Food Chem.* 135 (2012) 161–169.
- [35] M. Godejohann, J.D. Berser, D. Muffl, Non-targeted analysis of wastewater treatment plant effluents by high performance liquid chromatography-time slice-solid phase extraction-nuclear magnetic resonance/time-of-flight-mass spectro-

- metry. *J. Chromatogr. A* 1218 (2011) 9202–9209.
- [36] Y. Wen, J. Li, F. Yang, W. Zhang, W. Li, C. Liao, L. Chen, Salting-out assisted liquid–liquid extraction with the aid of experimental design for determination of benzimidazole fungicides in high salinity samples by high-performance liquid chromatography, *Talanta* 106 (2013) 119–126.
- [37] J. Domínguez-Álvarez, M. Mateos-Vivas, D. García-Gómez, E. Rodríguez-Gonzalo, R. Carabias-Martínez, Capillary electrophoresis coupled to mass spectrometry for the determination of anthelmintic benzimidazoles in eggs using a QuEChERS with preconcentration as sample treatment, *J. Chromatogr. A* 1278 (2013) 166–174.
- [38] C. Saengsookwaow, R. Rangkupan, O. Chailapakul, N. Rodthongkum, Nitrogen-doped graphene–polyvinylpyrrolidone/gold nanoparticles modified electrode as a novel hydrazine sensor, *Sens. Actuators B: Chem.* 227 (2016) 524–532.
- [39] H. Wei, J.J. Sun, Y.M. Wang, X. Li, G.N. Chen, Rapid hydrolysis and electrochemical detection of trace carbofuran at a disposable heated screen-printed carbon electrode, *Analyst* 133 (2008) 1619–1624.
- [40] W. Meng, E. Gall, F. Ke, Z. Zeng, B. Kopchick, R. Timsina, X. Qiu, Structure and interaction of graphene oxide–cetyltrimethylammonium bromide complexation, *J. Phys. Chem. C* 119 (2015) 21135–21140.
- [41] K. Zhang, L. Mao, L.L. Zhang, H.S. On Chan, X.S. Zhao, J. Wu, Surfactant-intercalated, chemically reduced graphene oxide for high performance supercapacitor electrodes, *J. Mater. Chem.* 21 (2011) 7302.
- [42] P. Joos, E. Killaerts, Theory on the determination of the dynamic surface tension with the drop volume and maximum bubble pressure methods, *J. Colloid Interface Sci.* 79 (1981) 96–100.
- [43] E.R. Washburn, H.N. Dunning, The determination of diffusion coefficients by measurements of surface tension, *J. Am. Chem. Soc.* 73 (1951) 1311–1313.
- [44] J. Soós, K. Koczó, Measurement of dynamic surface tension of surfactant solution with the drop volume method using an automatic drop detector, *Period. Polytech. Chem. Eng.* 33 (1989) 269–274.
- [45] D. Salinas-Torres, F. Huerta, F. Montilla, E. Morallón, Study on electroactive and electrocatalytic surfaces of single walled carbon nanotube-modified electrodes, *Electrochim. Acta* 56 (2011) 2464–2470.
- [46] C. Wang, J. Du, H. Wang, C.E. Zou, F. Jiang, P. Yang, Y. Du, A facile electrochemical sensor based on reduced graphene oxide and Au nanoplates modified glassy carbon electrode for simultaneous detection of ascorbic acid, dopamine and uric acid, *Sens. Actuators B: Chem.* 204 (2014) 302–309.
- [47] E. Punrat, C. Maksud, S. Chuanwatanakul, W. Wonsawat, O. Chailapakul, Polyaniline/graphene quantum dot-modified screen-printed carbon electrode for the rapid determination of Cr(VI) using stopped-flow analysis coupled with voltammetric technique, *Talanta* 150 (2016) 198–205.
- [48] N. Ruecha, R. Rangkupan, N. Rodthongkum, O. Chailapakul, Novel paper-based cholesterol biosensor using graphene/polyvinylpyrrolidone/polyaniline nanocomposite, *Biosens. Bioelectron.* 52 (2014) 13–19.
- [49] N. Thammasoontaree, P. Rattanarat, N. Ruecha, W. Siangproh, N. Rodthongkum, O. Chailapakul, Ultra-performance liquid chromatography coupled with graphene/polyaniline nanocomposite modified electrode for the determination of sulfonamide residues, *Talanta* 123 (2014) 115–121.
- [50] N. Rodthongkum, N. Ruecha, R. Rangkupan, R.W. Vachet, O. Chailapakul, Graphene-loaded nanofiber-modified electrodes for the ultrasensitive determination of dopamine, *Anal. Chim. Acta* 804 (2013) 84–91.
- [51] N. Promphet, P. Rattanarat, R. Rangkupan, O. Chailapakul, N. Rodthongkum, An electrochemical sensor based on graphene/polyaniline/polystyrene nanoporous fibers modified electrode for simultaneous determination of lead and cadmium, *Sens. Actuators B: Chem.* 207 (Part A) (2015) 526–534.
- [52] T.C.A. Commission Maximum residue limits for carbofuran. (<http://www.codexalimentarius.net/>) (accessed 13.12.15).
- [53] T.C.A. Commission Maximum residue limits for carbendazim. (<http://www.codexalimentarius.net/>).
- [54] M. Wang, J. Huang, M. Wang, D. Zhang, J. Chen, Electrochemical nonenzymatic sensor based on CoO decorated reduced graphene oxide for the simultaneous determination of carbofuran and carbaryl in fruits and vegetables, *Food Chem.* 151 (2014) 191–197.
- [55] X. Tan, Q. Hu, J. Wu, X. Li, P. Li, H. Yu, X. Li, F. Lei, Electrochemical sensor based on molecularly imprinted polymer reduced graphene oxide and gold nanoparticles modified electrode for detection of carbofuran, *Sens. Actuators B: Chem.* 220 (2015) 216–221.
- [56] C.A. Razzio, L.F. Sgobbi, T.C. Canevari, J. Cancino, S.A.S. Machado, Sensitive determination of carbendazim in orange juice by electrode modified with hybrid material, *Food Chem.* 170 (2015) 360–365.
- [57] J. Li, Y. Chi, Determination of carbendazim with multiwalled carbon nanotubes–polynetric methyl red film modified electrode, *Pestic. Biochem. Phys.* 93 (2009) 101–104.
- [58] S. Luo, Y. Wu, H. Gou, A voltammetric sensor based on GO–MWNTs hybrid nanomaterial-modified electrode for determination of carbendazim in soil and water samples, *Ionics* 19 (2013) 673–680.
- [59] R.F. França, H.P.M. de Oliveira, V.A. Pedrosa, L. Codognato, Electroanalytical determination of carbendazim and fenamiphos in natural waters using a diamond electrode, *Diam. Relat. Mater.* 27–28 (2012) 54–59.
- [60] A.M.D. Ashrafi, J. Guzvavy, V. Svancara, I. Petrovic, T.T. Purenovic, M. Vytras, K. Trace, determination of carbendazim fungicide using adsorptive stripping voltammetry with a carbon paste electrode containing tricresyl phosphate, *Int. J. Electrochem. Sci.* 7 (2012) 9717–9731.
- [61] P. Noyrod, O. Chailapakul, W. Wonsawat, S. Chuanwatanakul, The simultaneous determination of isoproturon and carbendazim pesticides by single drop analysis using a graphene-based electrochemical sensor, *J. Electroanal. Chem.* 719 (2014) 54–59.
- [62] Aoac manual for peer verified methods program. (www.pfigueiredo.org/Bromono2b.pdf) (accessed 20.12.15).



Voltammetric detection of carbofuran determination using screen-printed carbon electrodes modified with gold nanoparticles and graphene oxide

Apaond Jirasirichote^a, Eakkasit Punrat^b, Akkapol Suea-Ngam^a, Orawon Chailapakul^a,
Suchada Chuanuwatanakul^{a,*}

^a *Electrochemistry and Optical Spectroscopy Center of Excellent (EOSCE), Department of Chemistry, Faculty of Science, Chulalongkorn University, Phayathai Road, Pathumwan, Bangkok 10330, Thailand*

^b *Department of Chemistry, Faculty of Science, Ramkhamhaeng University, Bangkok, Bangkok 10240, Thailand*

ARTICLE INFO

Keywords:

Graphene oxide
Gold nanoparticles
Central composite design
Carbofuran
Screen-printed carbon electrode

ABSTRACT

Carbofuran is a highly toxic pesticide that is heavily used in agriculture due to its high effectiveness and low cost. Improved methods that are simpler and lower cost are needed for carbofuran detection in food and agricultural samples. Herein, we describe the development of a unique electrochemical method for carbofuran-phenol, which is the main hydrolysis product of carbofuran. We have successfully developed a highly accurate and precise method in a portable size using a screen-printed carbon electrode (SPCE) that is modified with graphene oxide (GO) and gold nanoparticles (AuNPs). Consequently, the developed electrode is highly sensitive to and selective for carbofuran. Using the central composite design (CCD) approach, we optimized the method for analysis parameters including the electrode surface loadings of GO and AuNPs as well as the working solution pH. The method exhibited a wide linear range of 1–250 μM for analyte detection using differential pulse voltammetry (DPV) on AuNPs/GO-SPCE under the optimized conditions. The limits of detection and quantitation were 0.22 and 0.72 μM , respectively. In addition, we also report the application of the method for carbofuran determination in real cucumber and rice samples. This sensitive and selective carbofuran detection method is very promising for simple and low cost analysis in real agricultural fields.

1. Introduction

Carbofuran, a carbamate pesticide, has been classified as a hazardous substance for humans that acts by inhibiting acetylcholinesterase activity in the central nervous system [1]. Although carbofuran has been banned in Canada and the European Union, it is still used in many areas, particularly in developing countries. Due to its low cost and high effectiveness, carbofuran is widely applied to field crops such as potatoes, corn, and soybeans. Therefore, the detection of carbofuran is crucial with regards to issues of consumer health and environmental quality [2].

Several analytical approaches to carbofuran detection have been developed, including methods based on gas chromatography (GC) [3], high-performance liquid chromatography (HPLC) [4], capillary electrophoresis (CE) [5], and mass spectrometry (MS) [6]. However, these methods are time-consuming, complicated, require bulky instruments, and leave relatively large carbon foot-prints due their consumption of large quantities of solvents. Electrochemical methods are analytical techniques that provide a high sensitivity, short analysis time, in-

expensive instrumentation and very low quantitation limit [7,8]. Moreover, the electroanalytical process has been widely used for the determination of trace organic analytes in biological and environmental samples [9–11]. Thus, the development of electrochemical sensors for carbofuran detection has been an active area of research in recent years due to their simplicity, portability, low cost, and consumption of relatively small amounts of materials.

Electrochemical sensors for carbofuran detection have been developed to improve the sensitivity and selectivity by coupling with enzymatic materials such as acetylcholinesterase immobilized on an iron oxide-chitosan nanocomposite [12] and an Eupenicillium shearii FREI-39 esterase and multiwalled carbon nanotube-modified electrode [13]. However, enzymatic assays are costly and require a skillful scientist to handle the system. In order to avoid the disadvantages of enzyme-based sensors, non-enzymatic electrochemical sensors such as a cobalt oxide-reduced graphene oxide/glassy carbon electrode [14] and a Hemin-graphene oxide/glassy carbon electrode [15] have been reported. Recently, non-enzymatic methods have required the hydrolysis of carbofuran to carbofuran-phenol to increase the electrochemi-

* Corresponding author.

E-mail address: suchada.e@chula.ac.th (S. Chuanuwatanakul).

cal response [16]. However, phenol derivatives cause electrode fouling upon oxidation due to the rapid polymerization of electrogenerated phenoxy radicals. The electrochemically generated passive film adheres strongly to the electrode surface, making a time-consuming clean-up step necessary [14]. A screen-printed carbon electrode (SPCE) is an attractive alternative choice due to that it is versatile, disposable, inexpensive, easy to fabricate, and can be operated over a wide potential range [17]. A single-use SPCE can be easily and rapidly replaced after each measurement [18].

To date, electrochemical measurements using electrodes that are chemically modified with nanomaterials have been reported [19–21]. Nanomaterials with unique properties have become interesting as electrode-modifying substances due to their high surface area and great enhancement of sensitivity, as described using the Cottrell equation [22,23]. One of the nanomaterials widely used for electrode modification is gold nanoparticles (AuNPs) [24], which have several benefits such as a large effective surface area, good biocompatibility, and good electro-catalytic as well as electronic properties [25,26]. Graphene oxide (GO), a well-known two-dimensional (2D) carbon material that has hydroxyl and carbonyl functional groups on its surface [27], is also used for electrode modification because it could increase the electrode's sensitivity due to its high adsorption capacity and large surface area [28]. In the project described herein, we prepared electrodes that are modified with a mixture of these two aforementioned substances.

The overall aim of this study was to develop an electrochemical sensor for the determination of carbofuran-phenol that is based on a SPCE modified with GO and AuNPs (AuNPs/GO-SPCE). To optimize the analytical conditions, we used central composite design (CCD) for several variables with a minimum number of experiments [29]. This method allows not only a linear relationship but also a quadratic relationship to be considered with increasing or decreasing one of the variables. These responses could be mapped as a response surface to determine the optimum point of the system [30]. Three analytical conditions including the amount of GO, the concentration of AuNPs, and pH were optimized using the CCD method. Finally, the optimized method was successfully applied for the determination of carbofuran concentrations in agricultural products.

2. Materials and methods

2.1. Reagents and solutions

All reagents used were of analytical reagent grade and were used without further purification. Standard carbofuran, standard carbofuran-phenol, graphite powder (particle size < 20 μM), chloroauric acid (1000 ppm gold solution), sodium citrate, NaH_2PO_4 , and Na_2HPO_4 were obtained from Sigma-Aldrich (Bangkok, Thailand). Screen-printing ink including carbon and silver/silver chloride (Ag/AgCl) pastes were obtained from the Gwent Group, Singapore. The screen-printed templates were designed by our laboratory, and then made by the Chaiyaboon Co. Ltd., Thailand. All aqueous solutions were prepared in ultra-purified water ($R \geq 18.2 \text{ M}\Omega \text{ cm}$) obtained from a water purification system of Merck Millipore (USA).

A standard 1.0 mM carbofuran solution was prepared by dissolving 0.022 g of carbofuran in 100 mL of 0.1 M NaOH. Prior to analysis, the standard solution was heated at 70 $^\circ\text{C}$ for 40 min to ensure the complete hydrolysis of carbofuran to carbofuran-phenol (Fig. S1) [15]. Potentially interfering pesticides (chlorpyrifos, metalaxyl, carben-dazim, carbaryl, propoxur, isoprocarb, methiocarb and methomyl) were purchased from Sigma-Aldrich (Thailand). These interfering solutions were prepared and hydrolyzed by the same methods as standard carbofuran.

Electrochemical measurements were conducted on a potentiostat (PGSTAT30 model, Metrohm-Autolab, The Netherlands). A disposable screen-printed carbon electrode (SPCE) was fabricated in-house by the

screen-printing technique. Scanning electron microscopy (SEM) (JEOL, Japan) and energy-dispersive X-ray spectroscopy (EDX) (JEOL, Japan) were used to investigate the surface morphology of the electrode. The synthesized GO and AuNPs were characterized using attenuated total reflectance Fourier transform infrared spectroscopy (ATR FT-IR) (Thermo Fisher Scientific, USA) and UV-visible spectroscopy (UV-vis) (Agilent Technologies, USA).

2.2. Fabrication and modification of the electrodes

GO and AuNPs were synthesized by the methods of Hummers and Turkevich, respectively [31,32]. Graphene oxide modified screen-printed carbon electrodes (GO-SPCEs) were fabricated by a screen-printing technique on a polyvinylchloride (PVC) substrate. Briefly, Ag/AgCl paste was screen-printed onto a PVC sheet to form a reference electrode and then dried in an oven at 55 $^\circ\text{C}$ for 1 h. A mixture of carbon paste and a suitable amount of GO were screen-printed onto the dried PVC sheet to form working and counter electrodes, and then, they were heated again in an oven at 55 $^\circ\text{C}$ for 1 h. Finally, the working electrode was modified with AuNPs by drop casting, and then, the electrode was allowed to dry at room temperature ($\sim 25 \text{ }^\circ\text{C}$).

2.3. Electrochemical detection

Cyclic voltammetry (CV) and differential pulse voltammetry (DPV) were carried out using a PG101 model potentiostat from Metrohm Autolab (Thailand). All electrochemical experiments were derived from three repeats and performed at room temperature without purging a working solution with nitrogen gas. DPV was carried out under the following conditions: step potential, 0.01 V; interval time, 1 s; modulation time, 0.3 s; modulation amplitude, 0.15 V; accumulation potential, + 0.0 V; and accumulation time, 60 s.

2.4. Central composite design (CCD) for the optimization of the conditions

We optimized the method with respect to three variables including the amount of GO, concentration of AuNPs, and pH of the working solution, while the dependent variable or the electrochemical response of this method is the peak current. The variables to be optimized were assigned to five levels to design 20 experiments; the actual and code values of all variables are available in Table S1 (Supplementary material). In order to avoid the bias in data analysis, the regression model with the variables and parameters in individual, interaction and quadratic terms were employed using code values [33]. The predicted responses (i.e., currents) were calculated using the obtained regression model to fit the surface response. The suitable conditions that provided the highest predicted responses were determined.

2.5. High performance liquid chromatography (HPLC)

The HPLC setup with which carbofuran was detected included a C18-column (150 mm \times 4.6 mm) and UV detector. HPLC measurements were performed in triplicate using a Prostar 330 model HPLC under the following conditions: isocratic elution with an acetonitrile: water (65:35 v/v) mobile phase, 1.0 mL min^{-1} flow rate, 20 μL injection volume, and absorbance detection at 280 nm [15].

3. Results and discussion

3.1. Material and electrode characterization

The synthesized GO was characterized and compared to a graphite reference material by attenuated total reflectance Fourier transform infrared spectroscopy (ATR FT-IR). A number of characteristic peaks were observed including the following: O-H stretching at

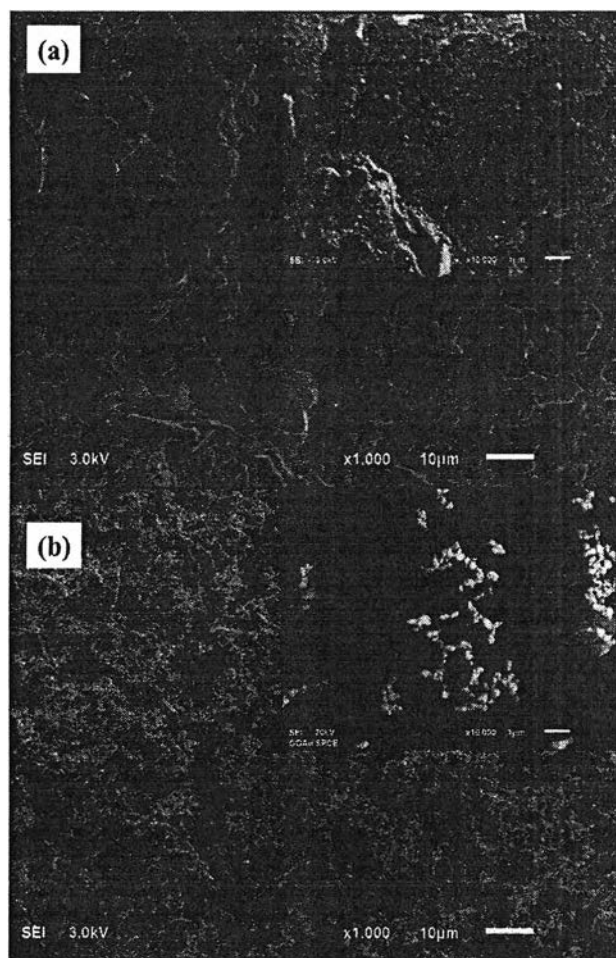


Fig. 1. SEM images of a SPCE (a) and a AuNPs/GO-SPCE (b).

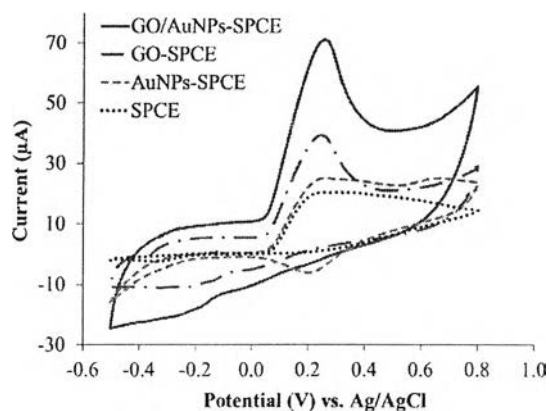


Fig. 2. Typical cyclic voltammograms of 2.0 mM carbofuran-phenol in 0.1 M phosphate buffer (pH = 7.4) on a SPCE (dotted line), a AuNPs-SPCE (dashed line), a GO-SPCE (dash-dotted line), and a AuNPs/GO-SPCE (solid line).

3120.71 cm^{-1} , C=O stretching at 1715.92 cm^{-1} and residual sp^2 stretching at 1574.43 cm^{-1} (Fig. S2a). AuNPs were characterized by UV–visible spectroscopy, and the resulting spectrum (Fig. S2b) shows a single band at $\approx 520\text{ nm}$, which is the characteristic peak of the surface plasmon absorption of AuNPs [34].

The electrodes were also characterized by scanning electron microscopy (SEM) and energy-dispersive X-ray spectroscopy (EDX). The surface morphologies of a bare SPCE and a AuNPs/GO-SPCE are seen in the SEM images in Fig. 1. These SEM images confirm that the

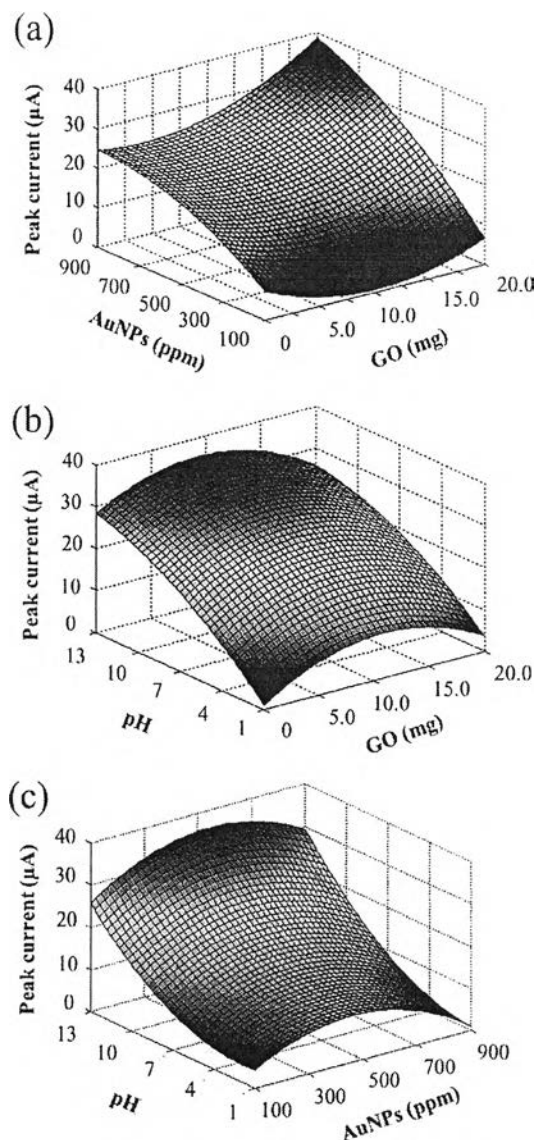


Fig. 3. Response surface plots showing the effects of the concentration of AuNPs and amount of GO (a), pH of the working solution and amount of GO (b), and pH of the working solution and concentration of AuNPs (c) on the peak current of carbofuran-phenol.

electrodes were successfully modified with GO and AuNPs. When the percent of Au on a AuNPs/GO-SPCE was determined by EDX (Fig. S2c), the modified electrode surface was found to have a Au coverage of 7.15%.

Thereafter, we compared the following four different electrodes: i) a bare SPCE, ii) a AuNPs-SPCE, iii) a GO-SPCE and iv) a AuNPs/GO-SPCE. The four electrode types were analyzed by cyclic voltammetry in solutions containing 2.0 mM carbofuran-phenol in 0.1 M phosphate buffer (pH = 7.4). The observed cyclic voltammograms are shown in Fig. 2. All of the modified SPCEs provided higher anodic peak currents than the bare SPCE. In particular, the peak current for the AuNPs/GO-SPCE was approximately 3-fold higher than that of the bare SPCE. This observation suggests that GO and AuNPs are promising materials that can improve the electrochemical sensitivity of electrodes for carbofuran detection.

3.2. Optimization of the analytical conditions

During the optimization, the amount of GO and the concentration

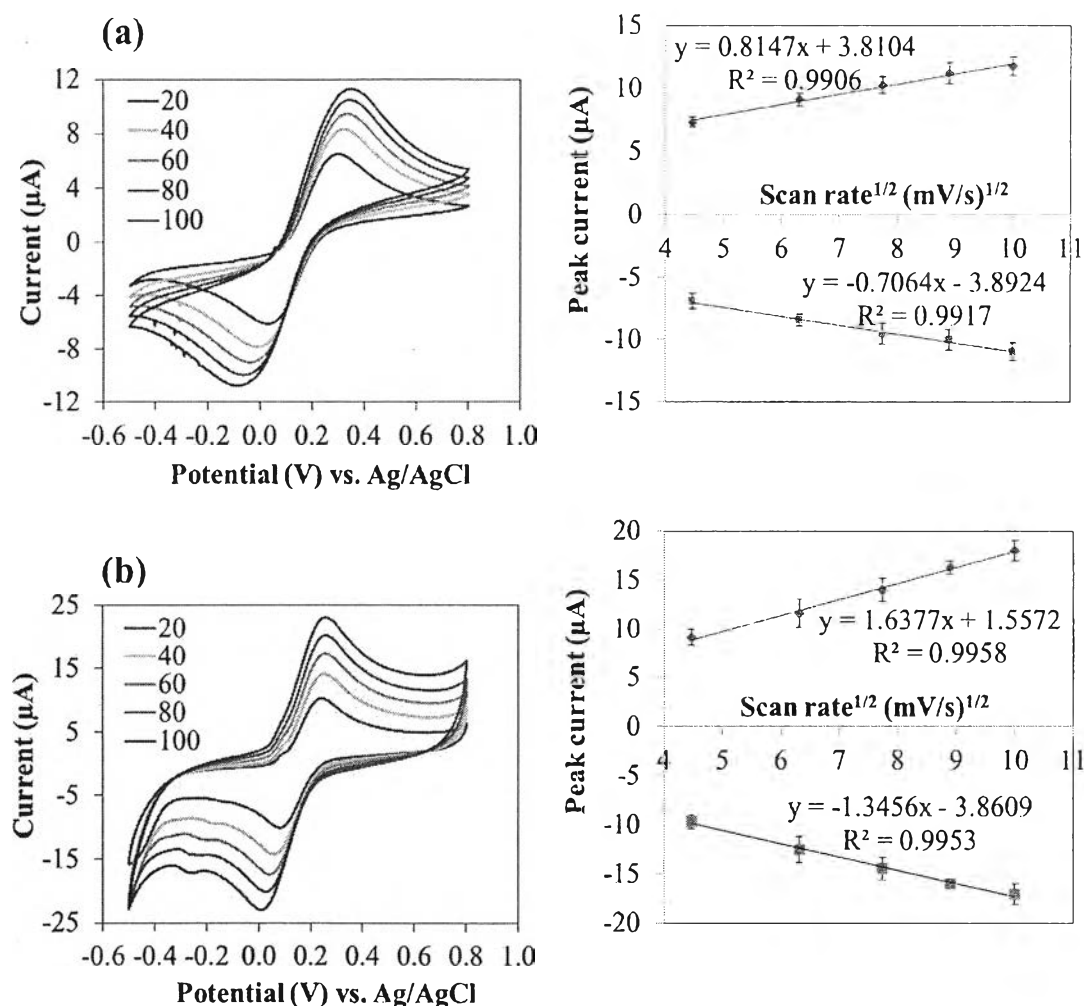


Fig. 4. Typical cyclic voltammograms (left) and I_p - $v^{1/2}$ plots of $1.0 \text{ mM Fe(CN)}_6^{4-/3-}$ on a bare SPCE (a) and a AuNPs/GO-SPCE (b) at various scan rates from 20 to 100 mV s^{-1} .

of AuNPs in the solution used to modify the electrodes were varied from 1.6 to 18.4 mg and 164–836 ppm, respectively. Furthermore, the pH of the working solution was varied over the range of 2–12 because pH is the factor that disrupts the negative charge on citrate resulting in the aggregation of the nanoparticles and hence decreases the stability of the AuNPs. Using the coded values so as to prevent systematic bias in the CCD method (see the details in Table S1), the results were calculated by multiple linear regression to predict a model or statistical equation as follows:

$$I_p = 27.21 + 6.21(\text{GO}) + 1.72(\text{AuNPs}) + 0.04(\text{pH}) - 1.02(\text{GO})^2 + 1.55(\text{AuNPs})^2 - 2.08(\text{pH})^2 + 0.94(\text{GO} \times \text{AuNPs}) - 0.31(\text{GO} \times \text{pH}) + 0.44(\text{AuNPs} \times \text{pH})$$

where GO and AuNPs are the coded values of the amount of GO and concentration of AuNPs, respectively, modified on a SPCE, pH is the coded value of the pH of the working solution, and I_p is the dependent variable of the resulting peak current.

According to the equation, the major variables affecting the resulting peak current are the amount of GO and the concentration of AuNPs, which is shown in the interaction term of (GO \times AuNPs) and the quadratic terms of (GO)² and (AuNPs)². The high values of the coefficients of the GO and AuNPs indicate that when the amount of GO or the concentration of AuNPs increase, the resulting peak current increases. The graph of the response surface in Fig. 3a also shows that the highest peak current was obtained from the CCD experiment using 18.4 mg of GO and 836 ppm of AuNPs. Meanwhile,

the pH of the working solution did not significantly affect the peak current due to the low value of the coefficient of the pH, and the counter plots of GO-pH and AuNPs-pH, which are shown in Fig. 3b and c, also indicate that pH was an independent variable of this proposed method. The pH value of 7.4 was chosen because it will be able to be applied in future applications such as in enzymatic assays or immuno-assays.

Nevertheless, 18.4 mg of GO and 836 ppm of AuNPs that provided the highest response were the upper limits of the examined values. To improve the resolution of the optimization, the amount of GO was re-optimized from 10 to 80 mg, and the experiment using 40 mg of GO provided the highest response (Fig. S3a). When the concentration of AuNPs was re-investigated, it was found that the AuNPs were limited at 836 ppm. Consequently, 40 mg of GO, 836 ppm of AuNPs, and a pH of 7.4 were determined to be the optimal conditions for carbofuran-phenol determination by this method.

3.3. Microscopic electrode area

The CV of a solution containing $1.0 \text{ mM Fe(CN)}_6^{4-/3-}$ in 0.1 M KCl was performed with different potential scan rates to study the microscopic electrode areas of a bare SPCE and a AuNPs/GO-SPCE. The electroactive surface areas (A) were calculated according to the Randles-Sevcik equation [35]:

$$I_p = 20.69 \times 10^5 \text{ A C n}^{3/2} \text{ D}^{1/2} \nu^{1/2}$$

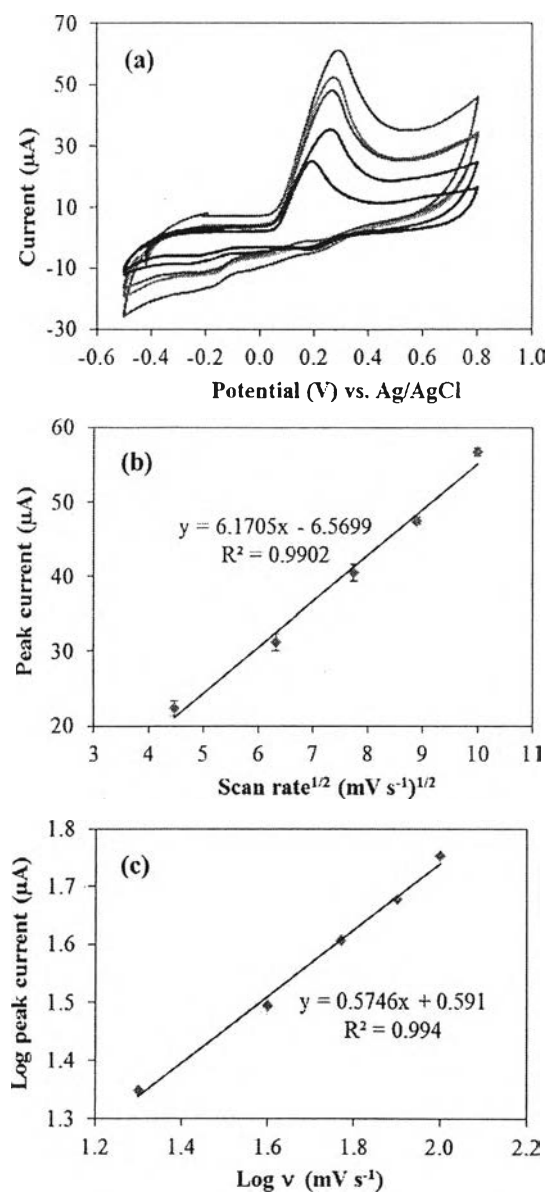


Fig. 5. Typical cyclic voltammograms (a), I_p - $v^{1/2}$ plot (b), and $\log I_p$ - $\log v$ plot (c) of 2.0 mM carbofuran-phenol in 0.1 M phosphate buffer (pH = 7.4) at various scan rates.

where I_p is the obtained peak current, C is the concentration of $\text{Fe}(\text{CN})_6^{4-/3-}$ (1.0 mM), n is the number of involved electrons (1 electron), D is the diffusion coefficient of $\text{Fe}(\text{CN})_6^{4-/3-}$ ($7.6 \times 10^{-6} \text{ cm}^2 \text{ s}^{-1}$), and v is the potential scan rate.

Plotting I_p versus $v^{1/2}$ (Fig. 4), the electroactive surface areas were calculated to be 0.110 and 0.221 cm^2 for a bare SPCE and a AuNPs/GO-SPCE, respectively.

3.4. Study of the electrochemical process

The electrochemical process of carbofuran-phenol on a AuNPs/GO-SPCE was studied by CV with various potential scan rates from 20 to 100 mV s^{-1} ; the resulting voltammograms are shown in Fig. 5a. The peak potential shifted to a more positive potential when a higher potential scan rate was used. The relationship between the peak current (I_p) and the square-root of the potential scan rate ($v^{1/2}$) was linear with a R^2 of 0.9902, as shown in Fig. 5b; this is a characteristic of a diffusion-controlled electrochemical process. Moreover, the results were also confirmed by another plot between $\log I_p$ and $\log v$

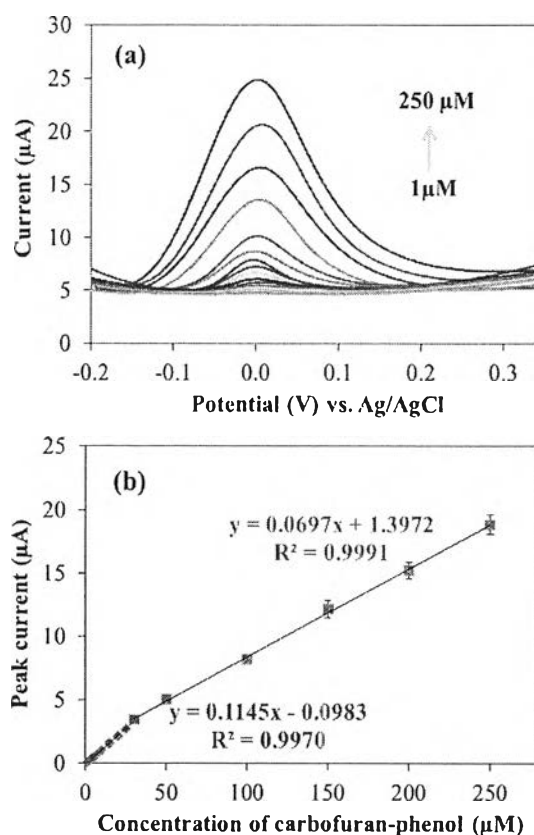


Fig. 6. Typical voltammograms (a) and a standard calibration graph (b) of carbofuran-phenol in 0.1 M phosphate buffer (pH = 7.4) determined by DPV using a AuNPs/GO-SPCE.

(Fig. 5c). The slope of the plot was 0.57, which was close to the theoretically expected value of 0.5 for a purely diffusion-controlled current [36].

3.5. Differential pulse voltammetry

DPV was used to improve the electrochemical sensitivity of carbofuran detection. Using the optimized conditions, four types of buffer solutions including acetate, borate, phosphate, and Britton-Robinson buffer solution were varied with a fixed concentration of 0.1 M and a pH of 7.4. The highest peak current was achieved from the experiment using 0.1 M phosphate buffer (Fig. S4a).

The accumulation time was also investigated in the range of 0–120 s. The obtained peak current increased when the accumulation time increased from 0 to 60 s, and then, it did not significantly change at longer accumulation times of 90 and 120 s (Fig. S4b). Furthermore, the accumulation potential was varied between -0.2 and $+0.2$ V. It was found that the accumulation potential did not affect the anodic peak current of carbofuran-phenol (Fig. S4c). Therefore, an accumulation time of 60 s and an accumulation potential of $+0.0$ V were used in subsequent analyses.

3.6. Analytical performance

Using the optimized conditions, DPV was carried out to determine the carbofuran-phenol in the concentration range of 1–250 μM ; the resulting voltammograms are shown in Fig. 6. The relationship between the carbofuran-phenol concentration and the obtained peak current was linear in the 2 concentration ranges of 1–30 and 30–250 μM with R^2 values of 0.9970 and 0.9991, respectively. The limit of detection (LOD) and the limit of quantification (LOQ) were 0.22 μM

Table 1

Determination of the carbofuran concentration in spiked samples by the developed method using a AuNPs/GO-SPCE. The results were compared with the results from the conventional HPLC [15].

Sample	Spiked (mg/kg)	DPV on AuNPs/GO-SPCE		HPLC-UV	
		Found (mg/kg)	Recovery (%)	Found (mg/kg)	Recovery (%)
Cucumber	–	Not detected	–	Not detected	–
	1.11	1.19 ± 0.21	107.2	1.17 ± 0.14	105.4
	6.64	6.16 ± 0.65	92.8	6.20 ± 0.18	93.4
Rice	–	Not detected	–	Not detected	–
	1.11	1.15 ± 0.47	103.6	1.16 ± 0.31	104.5
	6.64	6.95 ± 0.82	104.7	7.12 ± 0.46	107.2

Data are shown as the mean ± SD (N = 3) and derived from three repeats.

and 0.72 μM, respectively, which were obtained from the former calibration curve.

3.7. Interference study

Eight other pesticides, namely chlorpyrifos, metalaxyl, carbendazim, carbaryl, propoxur, isoprocarb, methiocarb and methomyl, were studied for their effects on the determination of carbofuran by DPV using a AuNPs/GO-SPCE. In the presence of each of the other pesticides, these pesticides were analyzed by the proposed method with 5 μM standard carbofuran-phenol in 0.1 M phosphate buffer (pH = 7.4).

It was found that the peaks of the foreign pesticides at high concentrations overlapped the peak of carbofuran. Due to no resulting DPV peaks of chlorpyrifos and metalaxyl, they did not affect the carbofuran detection. The other DPV signals are shown in Fig. S5. Carbendazim, a fungicide, did not interfere with carbofuran detection either because the oxidation peaks of carbendazim and carbofuran-phenol did not overlap and the interference tolerance limit was 40-fold. Some aryl carbamates, which are carbaryl and propoxur, showed peaks at adjacent potentials to the peak of carbofuran-phenol. However, isoprocarb, methiocarb and methomyl, which are carbamate pesticides, exhibited oxidation peaks with different potentials than carbofuran-phenol; the interference tolerance limits were 1-fold, 1-fold and 36-fold carbofuran-phenol's concentration for isoprocarb, methiocarb and methomyl, respectively. Meanwhile, the peak of carbofuran-phenol was higher than the peaks of isoprocarb, methiocarb and methomyl. This result demonstrates that the AuNPs/GO-SPCE was a highly selective sensor for carbofuran detection.

3.8. Real sample analysis

The developed method for the determination of carbofuran by DPV using a AuNPs/GO-SPCE was applied in real cucumber and rice samples. The samples spiked with carbofuran standard were analyzed by the standard addition method, and the results are shown in Table 1. Recovery results were 92.8–107.2%, and the concentrations of carbofuran found by the developed method and by the conventional HPLC method were not significantly different, indicating that the method has good accuracy.

4. Conclusions

A screen-printed carbon electrode (SPCE), which is inexpensive and easy to fabricate, was modified by graphene oxide (GO) and gold nanoparticles (AuNPs) to be a new highly sensitive electrochemical sensor for carbofuran detection. The AuNPs/GO-SPCE was characterized by ATR FT-IR, SEM and EDX. Under the optimized conditions, the modified SPCE was successfully applied to determine the carbofuran concentration in real samples. The proposed method is promising as an alternative and highly sensitive electrochemical method.

Acknowledgements

We gratefully acknowledge financial support from the Thailand Research Fund through Research Team Promotion Grant (RTA5780005), Electrochemistry and Optical Spectroscopy Center of Excellent, Department of Chemistry, Faculty of Science, Chulalongkorn University and the 90th Anniversary of Chulalongkorn University Fund (Ratchadaphiseksomphot Endowment Fund). We are grateful to Dr. David Kreller for his help in English editing and improving the manuscript.

Appendix A. Supplementary material

Supplementary data associated with this article can be found in the online version at doi:10.1016/j.talanta.2017.07.050.

References

- [1] R.C. Gupta, Carbofuran toxicity, *J. Toxicol. Environ. Health* 33 (4) (1994) 383–418.
- [2] P.O. Otieno, J.O. Lalah, M. Virani, J.O. Jondiko, K.W. Schraum, Carbofuran and its toxic metabolites provide forensic evidence for furadan exposure in vultures (*Gyps africanus*) in Kenya, *Bull. Environ. Contam. Toxicol.* 84 (5) (2010) 536–544.
- [3] A.M. Filho, F.N. dos Santos, P.A.P. Pereira, Development, validation and application of a method based on DI-SPME and GC-MS for determination of pesticides of different chemical groups in surface and groundwater samples, *Microchem. J.* 96 (1) (2010) 139–145.
- [4] L.E. Vera-Avila, B.P. Marquez-Lira, M. Villanueva, R. Covarrubias, G. Zelada, V. Thibert, Determination of carbofuran in surface water and biological tissue by sol-gel immunoaffinity extraction and on-line preconcentration/HPLC/UV analysis, *Talanta* 88 (2012) 553–560.
- [5] H.Y. Xie, Y.Z. He, W.E. Gan, G.N. Fu, L. Li, F. Han, Y. Gao, On-column liquid-liquid microextraction coupled with base stacking as a dual preconcentration method for capillary zone electrophoresis, *J. Chromatogr. A* 1216 (15) (2009) 3353–3359.
- [6] L. Latrous El Atrache, R. Ben Sghaier, B. Bejaoui Kefi, V. Haldys, M. Dachraoui, J. Tortajada, Factorial design optimization of experimental variables in preconcentration of carbamate pesticides in water samples using solid phase extraction and liquid chromatography-electrospray-mass spectrometry determination, *Talanta* 117 (2013) 392–398.
- [7] S. Tajik, M.A. Taher, H. Beitollahi, Mangiferin DNA biosensor using double-stranded DNA modified pencil graphite electrode based on guanine and adenine signals, *J. Electroanal. Chem.* 720–721 (2014) 134–138.
- [8] S. Mohammadi, H. Beitollahi, A. Mohadesi, Electrochemical behaviour of a modified carbon nanotube paste electrode and its application for simultaneous determination of epinephrine, uric acid and folic acid, *Sens. Lett.* 11 (2) (2013) 388–394.
- [9] H. Beitollahi, M. Mostafavi, Nanostructured base electrochemical sensor for simultaneous quantification and voltammetric studies of Levodopa and Carbidopa in pharmaceutical products and biological samples, *Electroanalysis* 26 (5) (2014) 1090–1098.
- [10] H. Beitollahi, S. Mohammadi, Selective voltammetric determination of norepinephrine in the presence of acetaminophen and tryptophan on the surface of a modified carbon nanotube paste electrode, *Mater. Sci. Eng.: C. Mater. Biol. Appl.* 33 (6) (2013) 3214–3219.
- [11] A. Mohadesi, H. Beitollahi, Electrochemical and catalytic investigations of levodopa and folic acid by modified carbon nanotube paste electrode, *Anal. Methods* 3 (11) (2011) 2562.
- [12] T. Jeyapragasam, R. Saraswathi, Electrochemical biosensing of carbofuran based on acetylcholinesterase immobilized onto iron oxide-chitosan nanocomposite, *Sens. Actuators B: Chem.* 191 (2014) 681–687.

- [13] G.F. Grawe, T.R. de Oliveira, E. de Andrade Narciso, S.K. Mocellini, A.J. Terezo, M.A. Soares, M. Castilho, Electrochemical biosensor for carbofuran pesticide based on esterases from *Fusarium solani* FRES-39 endophytic fungus. *Biosens. Bioelectron.* 63 (2015) 407–413.
- [14] M. Wang, J. Huang, M. Wang, D. Zhang, J. Chen, Electrochemical nonenzymatic sensor based on CoO decorated reduced graphene oxide for the simultaneous determination of carbofuran and carbaryl in fruits and vegetables. *Food Chem.* 151 (2014) 191–197.
- [15] A. Wong, F.M. Materon, M.D.P.T. Sotomayor, Development of a biomimetic sensor modified with hemin and graphene oxide for monitoring of carbofuran in food. *Electrochim. Acta* 146 (2014) 830–837.
- [16] H. Wei, J.J. Sun, Y.M. Wang, X. Li, G.N. Chen, Rapid hydrolysis and electrochemical detection of trace carbofuran at a disposable heated screen-printed carbon electrode. *Analyst* 133 (11) (2008) 1619–1624.
- [17] V.K. Rao, M.K. Sharma, P. Pandey, K. Sekhar, Comparison of different carbon ink based screen-printed electrodes towards amperometric immunosensing. *World J. Microbiol. Biotechnol.* 22 (11) (2006) 1135–1143.
- [18] M.K. Sharma, A.K. Goel, L. Singh, V.K. Rao, Immunological biosensor for detection of vibrio cholerae O1 in environmental water samples. *World J. Microbiol. Biotechnol.* 22 (11) (2006) 1155–1159.
- [19] S. Chaiyo, E. Mehmeti, K. Zagar, W. Siangproh, O. Chailapakul, K. Kalcher, Electrochemical sensors for the simultaneous determination of zinc, cadmium and lead using a Nafion/ionic liquid/graphene composite modified screen-printed carbon electrode. *Anal. Chim. Acta* 918 (2016) 26–34.
- [20] H. Beitollahi, H. Karimi-Maleh, H. Khabazzadeh, Nanomolar and selective determination of epinephrine in the presence of norepinephrine using carbon paste electrode modified with carbon nanotubes and novel 2-(4-Oxo-3-phenyl-3,4-dihydro-quinazolinyl)-N'-phenyl-hydrazinecarbothioamide. *Anal. Chem.* 80 (24) (2008) 9848–9851.
- [21] S. Tajik, M.A. Taher, H. Beitollahi, First report for simultaneous determination of methyldopa and hydrochlorothiazide using a nanostructured based electrochemical sensor. *J. Electroanal. Chem.* 704 (2013) 137–144.
- [22] K. Charoenkitamorn, O. Chailapakul, W. Siangproh, Development of gold nanoparticles modified screen-printed carbon electrode for the analysis of thiram, disulfiram and their derivative in food using ultra-high performance liquid chromatography. *Talanta* 132 (2015) 416–423.
- [23] C. Saengsookwaow, R. Rangkapan, O. Chailapakul, N. Rodthongkum, Nitrogen-doped graphene-polyvinylpyrrolidone/gold nanoparticles modified electrode as a novel hydrazine sensor. *Sens. Actuators B: Chem.* 227 (2016) 524–532.
- [24] B. Rafiee, A.R. Fakhari, M. Ghaffarzadeh, Impedimetric and stripping voltammetric determination of methamphetamine at gold nanoparticles-multiswelled carbon nanotubes modified screen printed electrode. *Sens. Actuators B: Chem.* 218 (2015) 271–279.
- [25] M. Das, K.H. Shim, S.S.A. An, D.K. Yi, Review on gold nanoparticles and their applications. *Toxicol. Environ. Health Sci.* 3 (4) (2012) 193–205.
- [26] E.R. Santana, C.A. de Lima, J.V. Piovesan, A. Spirelli, An original ferrocene oxide and gold nanoparticles-modified glassy carbon electrode for the determination of bisphenol A. *Sens. Actuators B: Chem.* 240 (2017) 487–496.
- [27] J. Chen, Y. Li, L. Huang, C. Li, G. Shi, High-yield preparation of graphene oxide from small graphite flakes via an improved Hummers method with a simple purification process. *Carbon* 81 (2015) 826–834.
- [28] X. Gong, Y. Bi, Y. Zhao, G. Liu, W.Y. Teoh, Graphene oxide-based electrochemical sensor: a platform for ultrasensitive detection of heavy metal ions. *RSC Adv.* 4 (47) (2014) 24653.
- [29] A. Suea-Ngam, P. Rattanarat, K. Wongravee, O. Chailapakul, M. Srisa-Art, Droplet-based glucosamine sensor using gold nanoparticles and polyaniline-modified electrode. *Talanta* 158 (2016) 134–141.
- [30] S. Mohajeri, H.A. Aziz, M.H. Isa, M.A. Zahed, M.N. Adlan, Statistical optimization of process parameters for landfill leachate treatment using electro-Fenton technique. *J. Hazard Mater.* 176 (1–3) (2010) 749–758.
- [31] W.S. Hummers, R.E. Offeman, Preparation of graphitic oxide. *J. Am. Chem. Soc.* 80 (1958) (1339–1339).
- [32] J. Kimling, M. Maier, B. Okenve, V. Kotaidis, H. Ballot, A. Plech, Turkevich method for gold nanoparticle synthesis revisited. *J. Phys. Chem. B* 110 (32) (2006) 15700–15707.
- [33] R. Zare-Dorabeh, S.M. Ferdowsi, A. Barzin, A. Tadjarodi, Highly efficient simultaneous ultrasonic-assisted adsorption of Pb(II), Cd(II), Ni(II) and Cu(II) ions from aqueous solutions by graphene oxide modified with 2,2'-dipyridylamine: central composite design optimization. *Ultrason. Sonochem.* 32 (2016) 265–276.
- [34] X. Huang, M.A. El-Sayed, Gold nanoparticles: optical properties and implementations in cancer diagnosis and photothermal therapy. *J. Adv. Res.* 1 (1) (2010) 13–28.
- [35] A. Suea-Ngam, P. Rattanarat, O. Chailapakul, M. Srisa Art, Electrochemical droplet-based microfluidics using chip-based carbon paste electrodes for high-throughput analysis in pharmaceutical applications. *Anal. Chim. Acta* 883 (2015) 45–54.
- [36] S. Jampasa, W. Siangproh, K. Duangmal, O. Chailapakul, Electrochemically reduced graphene oxide-modified screen-printed carbon electrodes for a simple and highly sensitive electrochemical detection of synthetic colorants in beverages. *Talanta* 160 (2016) 113–124.



Label-free immunosensor based on graphene/polyaniline nanocomposite for neutrophil gelatinase-associated lipocalin detection



Jutiporn Yukird^a, Tossapon Wongtangprasert^b, Ratthapol Rangkupan^c,
Orawon Chailapakul^b, Trairak Pisitkun^d, Nadnudda Rodthongkum^{c,*}

^a Petrochemical and Polymer Science, Faculty of Science, Chulalongkorn University, Phayathai Road, Patumwan, Bangkok, 10330 Thailand

^b Electrochemistry and Optical Spectroscopy Research Unit, Department of Chemistry, Faculty of Science, Chulalongkorn University, Phayathai Road, Patumwan, Bangkok, 10330 Thailand

^c Metallurgy and Materials Science Research Institute, Chulalongkorn University, Soi Chula 12, Phayathai Road, Patumwan, Bangkok, 10330 Thailand

^d Chulalongkorn University Systems Biology Center, Faculty of Medicine, Chulalongkorn University, Phayathai Road, Patumwan, Bangkok, 10330 Thailand

ARTICLE INFO

Article history:

Received 14 June 2016

Received in revised form

16 August 2016

Accepted 18 August 2016

Available online 20 August 2016

Keywords:

Graphene

Polyaniline

Electrospraying

Electropolymerization

Immunosensor

Neutrophil gelatinase-associated lipocalin (NGAL)

Acute kidney injury (AKI)

ABSTRACT

A novel label-free electrochemical immunosensor for neutrophil gelatinase-associated lipocalin (NGAL) detection has been developed. The immunosensor has been constructed by immobilization of NGAL capture antibodies to electropolymerized aniline deposited on top of an electrosprayed graphene/polyaniline (G/PANI) modified screen printed carbon electrode. Electrospraying of G/PANI increases the electrode surface area while electropolymerization of aniline increases the number of amino groups (-NH₂) for antibody immobilization. The factors affecting the sensor sensitivity (i.e. aniline concentration, scan number and scan rate of electropolymerization) have been optimized. In a prior report, Kannan et al. reported a broad oxidation peak in cyclic voltammetry upon the binding between NGAL with its antibody. In this study, a dramatic increase (58-fold) in the oxidation current upon the binding between NGAL and its antibody is obtained when compared to an unmodified electrode, verifying a substantial improvement in the electrochemical sensitivity of this system. Under optimal conditions, this system exhibits high sensitivity with a limit of detection (LOD) of 21.1 ng mL⁻¹, wide linearity (50–500 ng mL⁻¹) and high specificity toward NGAL detection from small samples (10 μL). As an example application, the sensor is tested for the detection of NGAL in human urine, and the results correspond well with the values obtained from a standard ELISA. Compared to the ELISA method, our system requires less analysis time (≤ 30 min/sample), less sample and less operating cost.

© 2016 Elsevier B.V. All rights reserved.

1. Introduction

Acute kidney injury (AKI) has been reported in 5 to 7% of hospitalized patients worldwide (Cruz et al., 2007; Himmelfarb and Izkizler, 2007; Mandelbaum et al., 2011). AKI results in loss of kidney function within hours, days or weeks. Importantly, AKI increases the risk of end-stage renal disease in the elderly and death after cardiac surgery (Ishani et al., 2009; Rosner, 2012). Thus, the diagnostic approach for AKI has been continually developed to improve the accuracy and sensitivity for an earlier diagnosis of patients. The standard diagnostic method for AKI is relied on the determination of serum creatinine (SCr) (Bagshaw et al., 2009; Weisbord et al., 2006; Zappitelli et al., 2009a, 2009b). Unfortunately, the use of SCr has a practical limitation i.e. the

concentration of SCr will not significantly changed unless the kidney has lost at least 50% of its function (Wagener et al., 2006). Recently, several biomolecules have been used as better, alternative biomarkers for early diagnosis of AKI including urinary interleukin-18 (IL-18), kidney injury molecule-1 (KIM-1), cystatin C and neutrophil gelatinase-associated lipocalin (NGAL) (Devarajan, 2007; Hall et al., 2010; Nguyen and Devarajan 2008). Among all, NGAL is one of the most promising biomarkers for AKI diagnosis (Devarajan, 2010a, 2010b). NGAL is identified as a 25 kDa protein, found in association with gelatinase from neutrophils. This protein is expressed at very low concentrations in human tissues such as kidney, lung, stomach, and colon (Dent et al., 2007; Gabbard et al., 2010; Mishra et al., 2005). In AKI, urinary NGAL concentration is highly associated with SCr concentration (Wagener et al., 2006). After surgery, it usually takes 1–3 days before a diagnosis of AKI can be made using an SCr level, but this diagnosis can be reached within 2–6 h using an increase in urine NGAL level. Given the importance of NGAL as a biomarker, we have explored a new approach for detecting this protein as an early indicator of AKI.

* Corresponding author.

E-mail addresses: trairak@gmail.com (T. Pisitkun), Nadnudda.r@chula.ac.th (N. Rodthongkum).

Various analytical techniques have been used for the determination of NGAL, including immunoblotting (Wagener et al., 2006) and enzyme-linked immunosorbent assays (ELISA) (Dent et al., 2007; Hirsch et al., 2007); however, these techniques require expensive laboratory equipment and are time-consuming. To solve these problems, electrochemical techniques have been considered as alternative tools for NGAL detection due to its high robustness, ease of use, low cost and rapid analysis (Kannan et al., 2012). Moreover, it can be used for both qualitative and quantitative analyses. Electrochemistry has been used for sensitive protein detection (Cai et al., 2013; Cheng et al., 2012), for biomarkers such as cytochrome C, a heme-containing protein that transfer electron in human cells (Furbee et al., 1993). It was reported that the electrochemical detection of NGAL relies on the increasing of oxidation peak current upon antibody-NGAL binding (Kannan et al., 2012); however, the mechanism was not reported (Iannetti et al., 2008; Schmidt-Ott et al., 2007). One possible reason for the enhanced signal is that NGAL binds iron and thus electron transfer could be facilitated upon antibody-NGAL binding.

In an electrochemical biosensor, a working electrode is usually miniaturized to make the biosensor portable and compatible with small biological samples (i.e. urine). Nonetheless, a small working electrode inevitably limits the surface area and therefore the sensitivity of the developed sensor. Further modification of the working electrode is required to improve the electrochemical sensitivity of a sensor. In recent years, carbon-based nanomaterials, such as carbon nanotubes (Zhang et al., 2013), carbon nanofibers (Promphet et al., 2015; Rodthongkum et al., 2013), carbon nanodots (Dai et al., 2012) and graphene have been used to modify working electrodes to improve their electrochemical performance. Graphene (G) has attracted considerable attention due to its large specific surface area, high electrochemical conductivity, high stability, and relatively low cost. G possesses a single layer of carbon atoms in a closely-packed honeycomb two-dimensional lattice (Zhang et al., 2013). To prevent the agglomeration of G, conducting polymers are used along with G for electrode surface modification. A nanocomposite between G and a conducting polymer makes this hybrid nanomaterial more suitable for electrode fabrication and biofunctionalization than a pure G. It has been reported that the use of G/conducting polymer nanocomposite-modified electrodes significantly enhance the electrochemical sensitivity of sensors (Ruecha et al., 2015; Tirawattanakoson et al., 2016). Different conducting polymers have been used for electrode surface modification, such as polyaniline (PANI) (Fan et al., 2011; Radhapyari et al., 2013), polypyrrole (PPy) (Bora and Dolui, 2012; Xing et al., 2012) and poly(3,4-ethylenedioxythiophene) (PEDOT) (Wisitsoraat et al., 2013; Zhang et al., 2012). Among these, PANI is the most appealing material due to its low cost, easy synthesis, good environmental stability, reversible redox properties and high biocompatibility (Bo et al., 2011; Fan et al., 2011).

G/PANI nanocomposite-modified electrodes are fabricated by electrospaying since this technique can create well-defined nanodroplets on the electrode surface. G/PANI nanodroplet-modified electrodes show higher specific surface area than unmodified and thin-film modified electrodes, leading to enhanced electrochemical sensitivity (Thammasoontaree et al., 2014). Unfortunately, G/PANI nanodroplets produced by electrospaying are randomly distributed on the electrode surface, resulting in sub-optimal exposure of amino groups ($-NH_2$). Thus, developing a method that helps organize and increase the number of amino groups on the electrode surface for biomolecule immobilization is required. In this study, electropolymerization of aniline on the top of G/PANI nanodroplets is carried out to increase the number of amino groups on the electrode surface. Then, NGAL capture antibodies were conjugated to the active amino groups via peptide bonds using EDC/NHS coupling chemistry. The resulting

immunosensor was tested for NGAL detection and applied for the analysis of NGAL in complex biological fluids (i.e. normal human urine VS pooled patient urine).

2. Materials and methods

2.1. Chemicals and materials

Graphene nanopowder was purchased from SkySpring Nanomaterials Inc. (Houston, TX, USA). Recombinant NGAL and NGAL-selective antibody were obtained from R&D Systems, Inc. (Minneapolis, MN, USA) and used as manufacturer instruction. Polyaniline emeraldine base ($M_w=65,000$), (+)-camphor-10-sulfonic acid (CSA), polystyrene ($M_w=180,000$), potassium ferricyanide ($K_3[Fe(CN)_6]$), potassium ferrocyanide ($K_2[Fe(CN)_6]$), 1-ethyl-3-(3-dimethylaminopropyl) carbodiimide (EDC), N-hydroxysuccinimide (NHS) were purchased from Sigma-Aldrich (St. Louis, MO, USA). Potassium dihydrogen phosphate (KH_2PO_4), chloroform, dichloromethane, *N,N*-dimethylformamide (DMF) were obtained from Carlo Erba Reagents (Milano, Italy). Disodium hydrogen phosphates (Na_2HPO_4) and potassium chloride (KCl) were purchased from Merck (Darmstadt, Germany). Carbon ink and silver/silver chloride ink were obtained from Gwent group (Torfaen, UK). Filter paper grade no.1 (size, $46 \times 57 \text{ cm}^2$) was purchased from Whatman International, Ltd (Maidstone, UK). All solutions were prepared in Milli-Q water (Millipore, USA, $R \geq 18.2 \text{ M}\Omega \text{ cm}^{-1}$). A phosphate-buffered solution was prepared by dissolving 0.144% (w/v) Na_2HPO_3 , 0.024% (w/v) KH_2PO_4 in Milli-Q water.

2.2. Apparatus

All electrochemical measurements, including cyclic voltammetry and amperometry, were performed on a μ AUTOLAB type III potentiostat (Metrohm Siam Company Ltd, Bangkok, Thailand) controlled by General Purpose Electrochemical System (GPES) software. A three-electrode system was used. The working electrode (WE) was fabricated by modification of a screen-printed carbon electrode surface (4 mm in diameter) with G/PANI nanodroplets via electrospaying and electropolymerized aniline via cyclic voltammetry. A JSM-6400 field emission scanning electron microscope (Japan Electron Optics Laboratory Co., Ltd, Tokyo, Japan) with an accelerating voltage of 15 kV, a JEM-2100 transmission electron microscope (Japan Electron Optics Laboratory Co., Ltd, Tokyo Japan) and atomic force microscope (Bruker, Karlsruhe, Germany) were used for electrode surface characterization.

2.3. Electrospaying of G/PANI nanocomposites on screen-printed carbon electrodes

A three-electrode system (working, counter, and reference) was fabricated on a polyvinyl chloride (PVC) substrate using a screen-printing technique. The patterned electrode was designed by Adobe Illustrator and an ink-blocking stencil was fabricated by Chaiyaboon Co. (Bangkok, Thailand). First, silver/silver chloride ink was printed on the PVC substrate for all electrodes. The reference electrode and conductive pads were used without further modification. Next, carbon ink was printed on top of one silver/silver chloride layer to generate the working and counter electrodes, respectively. Finally, the screen-printed electrode was dried at 50°C for 1 h to remove the residual solvent.

For electrode modification, G/PANI nanodroplets were created on the working electrode using electrospaying. The composite solution of G/PANI was prepared as follows. G nanopowder and PVP (2:2 mg) were dispersed in 1 mL DMF using an ultrasonicator for 24 h at a room temperature. PANI (0.4 g) was doped with CSA

(0.516 g) and dissolved in 15 mL chloroform. After that, the PANI solution was stirred at 1000 rpm for 12 h at a room temperature and filtered through filter paper (Whatman No. 1) to remove any particulate matter. G/PVP and PANI solutions were mixed together, and 0.1% (v/v) PS was added into the mixture. The electro spray setup consists of a syringe pump, high-voltage power supply, ground collector, syringe, and stainless-steel needle. The nano-composite solution of G/PVP/PANI was added into a syringe, and a voltage of 7.5 kV was applied to the solution. The flow rate of the solution was controlled at 1.0 mL h^{-1} , and the distance between needle and collector was fixed at 5 cm. The optimal electro spraying time was 5 min as investigated in the previous study (Ruecha et al., 2014).

2.4. Electrochemical experiments

For the cyclic voltammetry experiments, the potential was scanned from -0.5 V to $+1.0 \text{ V}$ for electropolymerization of aniline monomer, -0.5 V to $+1.0 \text{ V}$ for a standard ferri/ferrocyanide detection and -0.2 V to $+0.6 \text{ V}$ for NGAL detection. The detection potential for NGAL determination was optimized by using hydrodynamic voltammetry at a potential range of $0.1\text{--}0.6 \text{ V}$. For NGAL detection, NGAL solution was directly dropped on the electrode surface, and amperometry was performed at an optimum potential. After that, the anodic current was recorded at a steady state current of 75 s.

2.5. Functionalization of the modified electrode

After electropolymerization of aniline was carried out, the available $-\text{NH}_2$ groups of polyaniline were further attached to $-\text{COOH}$ group of anti-NGAL antibody using EDC/NHS coupling chemistry by covalent bonding as explained in details in the previous report (Bagshaw et al., 2009; Lee et al., 2011). A $10 \mu\text{L}$ solution of EDC/NHS ($0.2/0.2 \text{ M}$) and the NGAL antibody ($360 \mu\text{g mL}^{-1}$) was pipetted on the working electrode and incubated in the dark for 3 h at a room temperature. Then, the fully functionalized electrode was washed with a phosphate-buffered solution ($\text{pH } 7.0$) and Milli-Q water to remove any free antibodies.

2.6. Preparation of modified electrode for electrochemical detection of NGAL

For NGAL detection, a solution of recombinant NGAL was pipetted on the electrode surface and incubated for 30 min at room temperature ($25 \pm 2 \text{ }^\circ\text{C}$). Then the modified electrode was washed with a phosphate-buffered solution ($\text{pH } 7.0$) and Milli-Q water to remove any unbound NGAL. Finally, the modified electrode was used for the electrochemical detection of NGAL.

2.7. Preparation of urine sample

Urine samples were collected from healthy human volunteers. After collection, the samples were centrifuged at 1600 rpm with an ultracentrifuge (Cole-Parmer, USA) for 20 min, and the supernatants were kept for further analyses. A standard addition method was used for the detection of NGAL in the urine samples. Standard solutions of NGAL were added in a 1:1 ratio to undiluted human urine, and the percentages of recovery were determined. All samples were analyzed on the electropolymerized aniline on G/PANI nanodroplet modified SPCEs using amperometry.

The pooled patient urine samples were collected after surgery. Then, they were centrifuged at 1600 rpm for 20 min, and the supernatants were kept for ELISA analysis and electrochemical detection. The quantitative measurement of NGAL by ELISA was performed using Human Lipocalin-2/NGAL Quantikine ELISA Kit

(Cat# DLCN20, R&D Systems, MN) following the manufacturer's instructions.

3. Results and discussion

3.1. Electrode optimization and electrochemical characterization

Before using our novel immunosensor for detecting NGAL, the steps required to functionalize the electrode were optimized. To increase the surface area of working electrode, electro spraying of G/PANI was used. The important electro spraying parameters that affect the surface morphology and electrochemical sensitivity of modified electrodes were identified in our previous report (Ruecha et al., 2014). In this study, the effect of aniline electropolymerization (i.e. aniline concentration, scan number, scan rate of electropolymerization, etc.) on the sensor performance was investigated. Among all the parameters, the aniline concentration was found to be an important factor controlling the electrochemical sensitivity of the system. $100 \mu\text{L}$ of different aniline concentrations, ranging from 0.01 to 0.10 M were dropped on each electrode and aniline monomer was electropolymerized by using cyclic voltammetry. For electropolymerization, cyclic voltammetry was employed using a potential range of -0.5 to $+1.0 \text{ V}$ at a scan rate of 100 mV s^{-1} . After electropolymerization, the electrochemical sensitivity of modified electrode was determined by measuring the current response of $1.0 \text{ mM } [\text{Fe}(\text{CN})_6]^{3-/4-}$, which is a standard redox couple used for investigating the electrocatalytic property of newly developed electrodes prior to use for target analyte determination (Emami et al., 2014; Promphet et al., 2015; Saengsookwaow et al., 2016), as shown in Fig. 1. Higher aniline concentrations increased the anodic peak current of a $1.0 \text{ mM } [\text{Fe}(\text{CN})_6]^{3-/4-}$ and thus increased the sensitivity of the system. From Fig. 1, it is clear that 0.10 M aniline provides the highest anodic peak current while still maintaining a well-defined cyclic voltammogram for $[\text{Fe}(\text{CN})_6]^{3-/4-}$ (see an inset of Fig. 1). As shown in Fig. S1, Supporting information, at higher aniline concentration (0.15 M , 0.20 M), cyclic voltammogram peak shape are distorted, which is undesirable for the system since another reaction mechanism (e.g. adsorption) will take place on the electrode surface instead of the desirable diffusion current. Therefore, 0.10 M aniline was selected for subsequent electrode functionalization.

Electropolymerization scan number and rate were also studied (Fig. S2 and S3, Supporting information). The scan number was varied from 2 to 10 cycles and a well-defined, symmetric cyclic

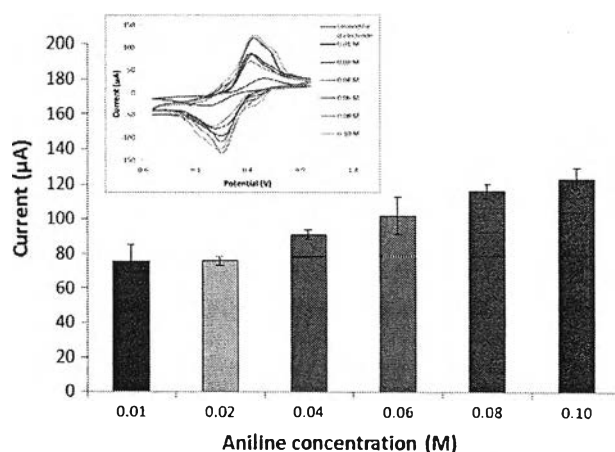


Fig. 1. The anodic peak currents of standard $1.0 \text{ mM } [\text{Fe}(\text{CN})_6]^{3-/4-}$ obtained from cyclic voltammograms (inset) measured on different modified electrodes functionalized via electropolymerization with different aniline concentrations.

voltammogram of 1.0 mM standard $[\text{Fe}(\text{CN})_6]^{3-/4-}$ was obtained with the highest anodic current response at a scan number of 4 cycles. Moreover, SEM images (Fig S4, Supporting information) shows the thicker layer of electropolymerized aniline on electrode surface at a higher scan number of 10 (S4, b) compared with a lower scan number of 4 (S4, a). The thicker polyaniline layer was easily scratched out and peeled off from the electrode surface leading to low electrode reproducibility. Thus, a scan number of 4 was selected for electropolymerization. The scan rate appears to play a less important role on the sensor performance since the current signals do not significantly change with the scan rate. In this study, the scan rate was varied from 60 to 110 mV s^{-1} , and a constant scan rate of 100 mV s^{-1} was selected for further experiments. Since the electrochemical activity of each compound is different, we also performed the similar experiments with NGAL and these results confirmed that 0.10 M aniline, 4 cycles of scan number and 100 mV s^{-1} of scan rate are the optimal conditions for NGAL detection. Thus, these parameters were used for all subsequent experiments.

The electrochemical characteristics of the modified electrode were investigated by cyclic voltammetry using 1.0 mM $[\text{Fe}(\text{CN})_6]^{3-/4-}$ as a well-known standard redox couple used for electrochemical characterization of newly developed electrodes (Rodthongkum et al., 2013; Saengsookwaow et al., 2016). As shown in Fig. 2, cyclic voltammetric measurements were performed on three different electrodes, including an unmodified carbon electrode, a G/PANI nanodroplet-modified carbon electrode, and aniline functionalized G/PANI nanodroplet-modified carbon electrode. Both anodic and cathodic currents of 1.0 mM $[\text{Fe}(\text{CN})_6]^{3-/4-}$ show well-defined peaks for all three electrodes. The current response for the aniline functionalized electrode (red line) is approximately 4 times higher than the unmodified carbon electrode (green line) and 2 times higher than the G/PANI nanodroplet-modified carbon electrode (blue line), indicating that the aniline functionalized electrode substantially increases the electrochemical sensitivity of the system. Furthermore, the peak potential difference (ΔE_p) of the aniline functionalized electrode ($\Delta E_p=0.45$; red line) decreases compared to the unmodified carbon electrode ($\Delta E_p=0.66$; green line), verifying that the electropolymerized aniline on the G/PANI-modified electrode accelerates electron transfer at the electrode.

3.2. Physical characterization

The surface morphology of the electrosprayed G/PANI

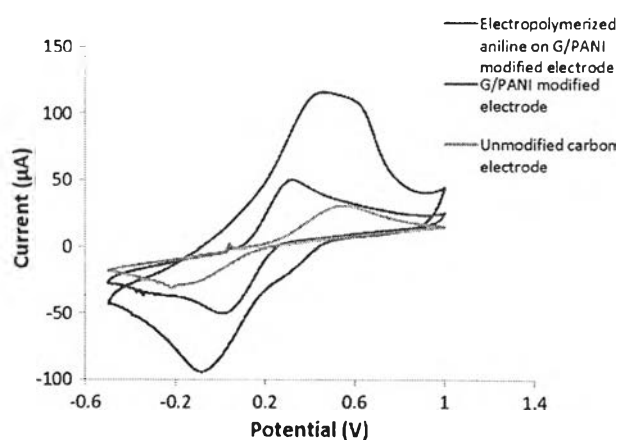


Fig. 2. Cyclic voltammogram of 1.0 mM $[\text{Fe}(\text{CN})_6]^{3-/4-}$ measured on an unmodified screen-printed carbon electrode (green line), G/PANI nanodroplet-modified carbon electrode (blue line) and an aniline functionalized G/PANI nanodroplet-modified electrode (red line). (For interpretation of the references to color in this figure legend, the reader is referred to the web version of this article.)

nanodroplet modified electrode was reported in our previous study. The average size of G/PANI droplets prepared in this study were approximately 180 ± 1.0 nm (Ruecha et al., 2014). The dispersion of G within the nanodroplets was characterized by transmission electron microscopy (TEM). TEM (Fig. 3a) confirms that G sheets are well dispersed inside the nanocomposites without severe agglomeration and re-stacking. Electron diffraction (an inset of Fig. 3a) further confirms that pure G is dispersed in the composites, which corresponds well with our previous work (Rao et al., 2014). The surface morphology of the aniline-modified G/PANI electrodes was characterized by scanning electron microscopy (SEM) as shown in Fig. 3b. SEM shows a 3D-sponge-like porous network with high uniformity of PANI on the modified electrode surface, confirming that aniline can be polymerized and attached onto the nanodroplet-modified electrode. Moreover, the surface area and surface roughness of the modified electrodes were investigated by atomic force microscopy (AFM) as shown in Fig. 3c. AFM image demonstrates that the modified electrodes have a higher surface area with surface roughness of 0.16 ± 0.02 μm , which is higher than observed for unmodified carbon electrodes that have a surface roughness of 0.02 ± 0.03 μm . The large surface area and high surface roughness of the modified electrode improves the sensitivity of the electrochemical sensor.

3.3. Determination of NGAL

3.3.1. Cyclic voltammetry

For NGAL detection, the experiments were performed on NGAL in phosphate buffer (pH 7.0) without ferri/ferrocyanide by using cyclic voltammetry (CV). To make this electrode system specific for NGAL, antibodies were immobilized onto the aniline functionalized electrodes using EDC/NHS coupling. According to a previous report, electrochemical detection of NGAL relies on an increase in the broad oxidation peak current on the modified electrodes upon NGAL binding to its antibody over a potential range of 0–0.6 V (Kannan et al., 2012). In this study, as shown in Fig. 4a, 90 ng mL^{-1} solution of NGAL causes a dramatic increase in the anodic current as compared to a buffered solution over a potential range of –0.2 to 0.8 V.

The performances of different electrodes for the detection of NGAL were studied. Three electrodes including unmodified carbon electrode, G/PANI nanocomposite modified carbon electrode and electropolymerized aniline on G/PANI nanocomposite modified carbon electrode were used for the determination of 90 ng mL^{-1} of NGAL as shown in Fig. 4b. An approximately 58-fold increase in anodic peak current is observed (green line) compared to an unmodified electrode (blue line) and 9-fold compared to G/PANI modified electrode (red line), which indicates the value of antibody-functionalized modified electrode. The determination of NGAL using EDC/NHS coupling for anti-NGAL immobilization on an unmodified electrode was unsuccessful (no peak observed) as shown in Fig. 4b (blue line) since there is no $-\text{NH}_2$ group on the unmodified electrode surface to attach with $-\text{COOH}$ of anti-NGAL antibodies. Also, the low oxidation current signal was observed on G/PANI modified electrode shown in Fig. 4b (red line) since there are not enough $-\text{NH}_2$ group on the electrode surface to attach with anti-NGAL antibodies. As for electropolymerized aniline on G/PANI nanocomposite modified electrode, increasing amount of $-\text{NH}_2$ group on the electrode surface by electropolymerization of aniline promotes the binding between NGAL and its antibodies leading to substantially enhance the current response signal (green line). An explanation for this substantial increasing anodic current signal on electropolymerized aniline on G/PANI nanocomposite modified carbon electrode (green line) is that NGAL facilitates the electron transfer upon the binding with its antibody since NGAL plays an important role for iron transport (i.e. iron) in cells and thus may be

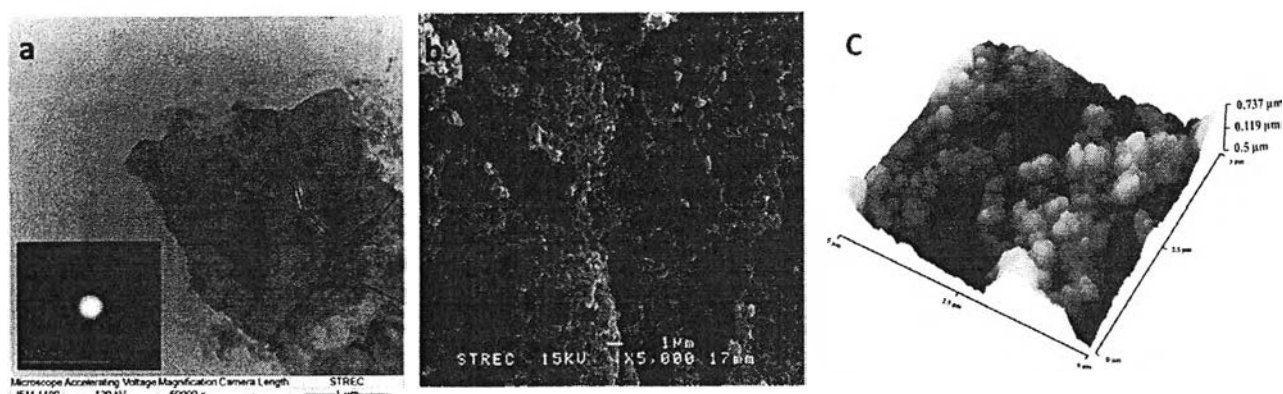


Fig. 3. TEM image of G dispersion within G/PANI nanodroplets with an electron diffraction pattern of graphene as an inset. (a), SEM image of electropolymerized aniline on G/PANI nanodroplet-modified electrode with a magnification of 5000x. (b), and AFM image of electropolymerized aniline on G/PANI nanodroplet modified electrode (c).

electrochemically active when bound to the surface of the modified electrode (Schmidt-Ott et al., 2007). While this is the proposed mechanism, determining the exact mechanism was outside of the scope of the proposed effort.

3.3.2. Chronoamperometry

After testing the performance of modified electrode for NGAL detection, the immunosensor was further tested using chronoamperometry to improve the electrochemical sensitivity of the system. Chronoamperometry was used to identify an optimum detection potential for NGAL in a range of 0.1–0.6 V. As shown in Fig. 5a, the anodic current signal of NGAL significantly decreases as the detection potential increases from 0.1 to 0.4 V. At higher voltages, 0.4–0.6 V, the anodic current signal slightly increases; however, the background current also increases. Consequently, the signal-to-background ratio (S/B) ratio is found to be the highest at a detection potential of 0.3 V. Thus, this potential was selected for further experiments.

After the detection potential of NGAL was optimized, the other parameters (e.g. incubation time for antibody immobilization, concentration of antibody and incubation time of NGAL prior to electrochemical detection) were also investigated using chronoamperometry to obtain the highest immunosensor performance. As shown in Figs. S5–S7 in the supporting information, 3h incubation for anti-NGAL antibody immobilization, 360 $\mu\text{g}/\text{mL}$ of anti-NGAL antibody and 30 mins incubation of NGAL prior to amperometric detection were the optimum conditions offering the highest immunosensor sensitivity with shortest analysis time;

thus these parameters were used for subsequent experiments.

3.4. Calibration curve

The analytical figures of merit for the immunosensor were also evaluated. Using NGAL concentrations between 50 and 500 ng mL^{-1} , amperometric measurements were made at 75 s to create a calibration curve (Fig. 6). The anodic current response was found to be linearly proportional to NGAL concentration over the studied range. From these measurements, we determined the limit of detection (LOD) and limit of quantitation (LOQ) for NGAL to be 21.1 ng mL^{-1} and 70.4 ng mL^{-1} , respectively. The LOD was calculated by $\text{LOD} = 3S_b/m$ and LOQ was calculated by $\text{LOQ} = 10 S_b/m$, where S_b is a standard deviation of the blank (estimated by five replicates of blank signal) and m is the slope of the calibration curve. The level of NGAL in normal human urine is lower than 20 ng mL^{-1} (Kannan et al., 2012), whereas the level of NGAL in patient urine after surgery is in the range of 50–1000 ng mL^{-1} (Bennett et al., 2008), indicating that our electrode system is sensitive enough to detect NGAL in patient urine thereby making it a useful tool for early diagnosis of AKI.

3.5. Reproducibility and stability

The reproducibility and stability of the electrode system were investigated by amperometric detection of 200 ng mL^{-1} samples of NGAL in a phosphate buffer (pH 7.0). The %RSD of NGAL concentrations were found to be between 1.49% and 9.20% for

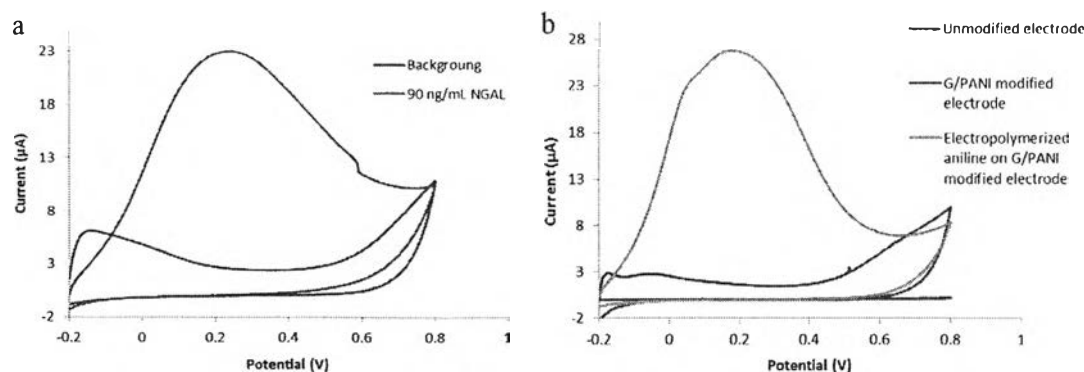


Fig. 4. Cyclic voltammograms of 90 ng mL^{-1} of NGAL in phosphate buffer solution (pH 7.0) measured on the antibody-functionalized modified electrode (blue line), and a cyclic voltammogram of a phosphate buffer solution (pH 7.0) measured on the antibody-functionalized electrode without NGAL (red line) at a scan rate of 50 mV s^{-1} (a). Cyclic voltammograms of 90 ng mL^{-1} of NGAL measured on unmodified electrode (blue line), G/PANI modified electrode (red line) and electropolymerized aniline on G/PANI modified electrode (green line) at a scan rate of 50 mV s^{-1} (b). (For interpretation of the references to color in this figure legend, the reader is referred to the web version of this article.)

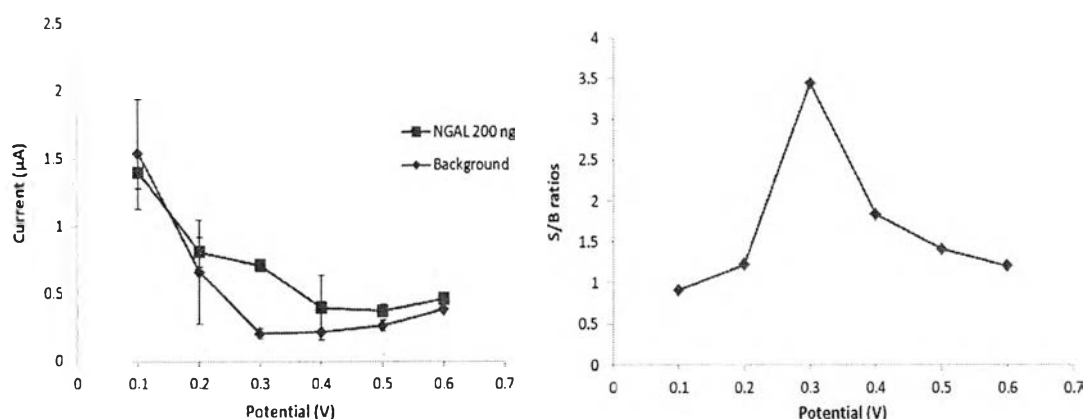


Fig. 5. Hydrodynamic voltammograms of 200 ng mL⁻¹ of NGAL (red line) and background (blue line) in 0.1 M phosphate buffer solution at pH 7.0 for 75 s, measured on the antibody-modified electrode (a) and the signal-to-background ratios (S/B) obtained from hydrodynamic voltammograms (b). (For interpretation of the references to color in this figure legend, the reader is referred to the web version of this article.)

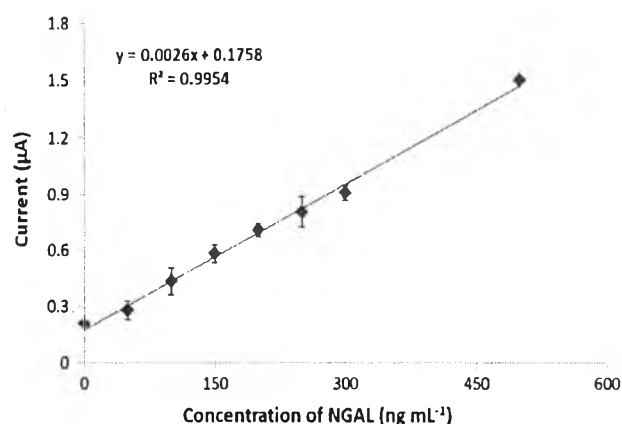


Fig. 6. A calibration plot obtained from amperometric detection of NGAL in 0.1 M phosphate buffer solution at pH 7.0 using the antibody-modified electrode. The standard deviations are obtained from 4 measurements ($n=4$).

5 measurements on different electrodes. The stability of the electrode system was also evaluated by storing the modified electrodes in a phosphate buffer solution (pH 7.0) at a room temperature for 3 days before using it to measure NGAL. The current responses were found to decrease only 2–9% after storage, indicating that this system is relatively stable.

3.6. Specificity

The specificity of commercial anti-NGAL antibody was verified by the information brochure of human Lipocalin-2/NGAL (DY1757). It was reported that anti-NGAL antibody exhibits no cross-reactivity with recombinant human Lipocalin-1, recombinant human MMP-9, recombinant mouse and rat Lipocalin-2 at a concentration of 50 ng/mL. For the experiments, there is no significant difference of current response signal between 0.1 M PB solution and normal urine sample as shown in Fig. S8 in Supporting information implying that other proteins and substances presenting in human urine do not interfere the detection of NGAL. Moreover, the specificity of this NGAL sensor was investigated toward bovine serum albumin (BSA). BSA derived from cow is commonly used as a represented standard protein instead of human serum albumin (HSA), which is the highest abundant human protein to test specificity of antigen-antibody binding of the developed sensor. For the assessment of BSA interference, 0.1 M PB solution (background), different concentrations of BSA, a mixture of BSA and NGAL and a pure NGAL solution were incubated and

the amperometric current responses were measured on the modified electrode as shown in Fig. S9 in the Supporting information. As seen in the results, the oxidation current of various BSA concentrations are not different from background. Obviously, the oxidation current increases in the presence of NGAL due to specific binding between anti-NGAL antibody and NGAL on electrode surface. Moreover, the current response of NGAL in the presence of BSA (dark blue bar) and absence of BSA (red bar) are not significant different, indicating that our developed sensor is highly specific to NGAL in the presence of BSA.

3.7. Sample analyses

To evaluate the applicability of the immunosensor, the modified electrodes were used to determine NGAL in human urine. The human urine samples were freshly collected and centrifuged at 1600 rpm for 20 min. Then, the supernatants were measured by amperometry. The solutions of the NGAL at different concentrations were added at a 1:1 ratio to undiluted human urine samples, and the percent recovery was determined (Table 1). The percent recoveries were found to be in a range of 97.5–104.4% and %RSD values were less than 5.0%, suggesting that this electrode system is suitable for the determination of NGAL in human urine.

The accuracy of this electrode system was investigated via comparison with a standard ELISA method. The modified electrode was used for amperometric detection of NGAL in AKI patient urine samples. The percent recoveries were found to be in the range of 93.5–99.8%, confirming that this system is very accurate. Moreover, the results obtained from our system correspond well with the results obtained from a conventional ELISA method as shown in Table 2. Compared with ELISA, since our developed system requires less analysis time (30 min VS hours for ELISA), less sample volume (10 µL VS 100 µL for ELISA) and lower operating cost while offers higher precision for quantitative analysis, it might be a promising tool for early AKI diagnosis.

Table 1
Determination of different concentrations of NGAL spiked into normal human urine.

Added (ng mL ⁻¹)	Found (ng mL ⁻¹)	Recovery (%)
0	ND	–
100	97.5 ± 1.0	97.5
200	208.7 ± 1.4	104.4
400	413.4 ± 2.1	103.3

Table 2

Determination of NGAL in patient urine samples by this approach compared with conventional ELISA method.

AKI patient urine samples	ELISA (ng mL ⁻¹)	Found (ng mL ⁻¹)	Recovery (%)
1	200	199.5 ± 13.5	99.8
2	1645	1642.0 ± 14.7	93.5

4. Conclusions

In summary, attaching an NGAL-specific antibody to a G/PANI nanodroplet-modified electrode enables the selective, sensitive, and robust determination of NGAL. The electrochemical signal of NGAL from this functionalized electrode is 58 times higher than from an unmodified electrode. The electrode system was found to have a LOD and LOQ of 21.1 ng mL⁻¹ and 70.4 ng mL⁻¹, respectively, and preliminary validation indicates that NGAL can be measured in human urine with excellent recoveries (i.e. 97.5–104.4%) and precision (i.e. %RSD < 5.0%). Importantly, NGAL levels in AKI patient urine samples measured by this system correspond well with the results obtained from a standard ELISA method, while our system offers easier process of fabrication, faster analysis (≤ 30 mins/sample), lower sample volume requirement (10 μL), and especially less operating cost. Thus, our system might be an alternative tool for early diagnosis of AKI in medical applications.

Acknowledgments

The authors gratefully acknowledge the financial support from Ratchadapisek Sompoch Endowment Fund, Chulalongkorn University under Outstanding Research Performance Program (2016) and Ratchadapiseksompotch Fund, Faculty of Medicine, Chulalongkorn University, CU – 57 – 091 – IC and RA57/063. Prof. Dr. Orawon Chailapakul would like to thank to the Thailand Research Fund through Research Team Promotion Grant (RTA5780005). Also, Dr. Tossapon Wongtangprasert would like to thank to Ratchadapisek Sompote Fund Chulalongkorn University for post-doctoral fellowship.

Appendix A. Supplementary material

Supplementary data associated with this article can be found in the online version at <http://dx.doi.org/10.1016/j.bios.2016.08.062>.

References

- Bagshaw, S.M., Uchino, S., Cruz, D., Bellomo, R., Morimatsu, H., Morgera, S., Schetz, M., Tan, I., Bouman, C., Macedo, E., Gibney, N., Tolwani, A., Oudemans-van Straalen, H.M., Ronco, C., Kellum, J.A., 2009. *Nephrol. Dial. Transpl.* 24 (9), 2739–2744.
- Bennett, M., Dent, C.L., Ma, Q., Dastrala, S., Grenier, F., Workman, R., Syed, H., Ali, S., Barasch, J., Devarajan, P., 2008. *Clin. J. Am. Soc. Nephrol.* 3 (3), 665–673.
- Bo, Y., Yang, H., Hu, Y., Yao, T., Huang, S., 2011. *Electrochim. Acta* 56 (6), 2676–2681.
- Bora, C., Dolui, S.K., 2012. *Polymer* 53 (4), 923–932.

- Cai, Z., Song, Y., Wu, Y., Zhu, Z., James Yang, C., Chen, X., 2013. *Biosens. Bioelectron.* 41, 783–788.
- Cheng, W., Ding, S., Li, Q., Yu, T., Yin, Y., Ju, H., Ren, G., 2012. *Biosens. Bioelectron.* 36 (1), 12–17.
- Cruz, D.N., Boigan, L., Perazella, M.A., Bonello, M., de Cal, M., Corradi, V., Polanco, N., Ocampo, C., Nalesso, F., Piccini, P., Ronco, C., 2007. *Clin. J. Am. Soc. Nephrol.* 2 (3), 418–425.
- Da, H., Xu, G., Gong, L., Yang, C., Lin, Y., Tong, Y., Chen, J., Chen, G., 2012. *Electrochim. Acta* 80 (0), 362–367.
- Dent, C.L., Ma, Q., Dastrala, S., Bennett, M., Mitsnefes, M.M., Barasch, J., Devarajan, P., 2007. *Crit. Care Med.* 11 (6), R127–R127.
- Devarajan, P., 2007. *Contrib. Nephrol.* 156, 203–212.
- Devarajan, P., 2010a. *Nephrology (Carlton)* 15 (4), 419–428.
- Devarajan, P., 2010b. *Biomark. Med.* 4 (2), 265–280.
- Emami, M., Shamsipur, M., Saber, R., Iradjirad, R., 2014. *Analyst* 139 (11), 2858–2866.
- Fan, Y., Liu, J.-H., Yang, C.-P., Yu, M., Liu, P., 2011. *Sens. Actuators B-Chem.* 157 (2), 669–674.
- Furbee, J.W., Thomas, C.R., Kelly, R.S., Malachowski, M.R., 1993. *Anal. Chem.* 65 (13), 1654–1657.
- Gabbar, W., Milbrandt, E.B., Kellum, J.A., 2010. *Crit. Care Med.* 14 (4), 318–318.
- Hall, I.E., Yarlalagadda, S.G., Coca, S.G., Wang, Z., Doshi, M., Devarajan, P., Han, W.K., Marcus, R.J., Parikh, C.R., 2010. *J. Am. Soc. Nephrol.* 21 (1), 189–197.
- Himmelfarb, J., Ikizler, T.A., 2007. *Kidney Int.* 71 (10), 971–976.
- Hirsch, R., Dent, C., Priem, H., Allen, J., Beekman 3rd, R.H., Ma, Q., Dastrala, S., Bennett, M., Mitsnefes, M., Devarajan, P., 2007. *Pediatr. Nephrol.* 22 (12), 2089–2095.
- Iannetti, A., Pacifico, F., Acquaviva, R., Lavorgna, A., Crescenzi, E., Vascotto, C., Tell, G., Salzano, A.M., Scaloni, A., Vuttariello, E., Chiappetta, G., Formisano, S., Leonardi, A., 2008. *Proc. Natl. Acad. Sci. USA* 105 (37), 14058–14063.
- Ishani, A., Xue, J.L., Himmelfarb, J., Eggers, P.W., Kimmel, P.L., Molitoris, B.A., Collins, A.J., 2009. *J. Am. Soc. Nephrol.* 20 (1), 223–228.
- Kannan, P., Tiong, H.Y., Kim, D.-H., 2012. *Biosens. Bioelectron.* 31 (1), 32–36.
- Lee, L., Luo, X., Cui, X.T., Yun, M., 2011. *Biosens. Bioelectron.* 26 (7), 3297–3302.
- Mandelbaum, T., Scott, D.J., Lee, J., Mark, R.G., Malhotra, A., Waikar, S.S., Howell, M. D., Talmor, D., 2011. *Crit. Care Med.* 39 (12), 2659–2664.
- Mishra, J., Dent, C., Tarabishi, R., Mitsnefes, M.M., Ma, Q., Kelly, C., Ruff, S.M., Zahedi, K., Shao, M., Bean, J., Mori, K., Barasch, J., Devarajan, P., 2005. *Lancet* 365 (9466), 1231–1238.
- Nguyen, M., Devarajan, P., 2008. *Pediatr. Nephrol.* 23 (12), 2151–2157.
- Promphet, N., Rattanasat, P., Rangkupan, R., Chailapakul, O., Rodthongkum, N., 2015. *Sens. Actuators B-Chem.* 207, 526–534.
- Radhapari, K., Kotoly, P., Das, M.R., Khan, R., 2013. *Talanta* 111 (0), 47–53.
- Rao, K.S., Senthilnathan, J., Liu, Y.-F., Yoshimura, M., 2014. *Sci. Rep.* 4.
- Rodthongkum, N., Ruecha, N., Rangkupan, R., Vachet, R.W., Chailapakul, O., 2013. *Anal. Chim. Acta* 804 (0), 84–91.
- Rosner, M., 2012. Acute kidney injury associated with cardiac surgery. In: Machiraju, V.R., Schaff, H.V., Svensson, L.G. (Eds.), *Redo Cardiac Surgery in Adults*. Springer, New York, pp. 37–52.
- Ruecha, N., Rangkupan, R., Rodthongkum, N., Chailapakul, O., 2014. *Biosens. Bioelectron.* 52 (0), 13–19.
- Ruecha, N., Rodthongkum, N., Cate, D.M., Volckens, J., Chailapakul, O., Henry, C.S., 2015. *Anal. Chim. Acta* 874, 40–48.
- Saengsookwaow, C., Rangkupan, R., Chailapakul, O., Rodthongkum, N., 2016. *Sens. Actuators B-Chem.* 227, 524–532.
- Schmidt-Ott, K.M., Mori, K., Li, J.Y., Kalandadze, A., Cohen, D.J., Devarajan, P., Barasch, J., 2007. *J. Am. Soc. Nephrol.* 18 (2), 407–413.
- Thammasontaree, N., Rattanasat, P., Ruecha, N., Siangproh, W., Rodthongkum, N., Chailapakul, O., 2014. *Talanta* 123, 115–121.
- Tirawattanakoson, R., Rattanasat, P., Ngamrojavanich, N., Rodthongkum, N., Chailapakul, O., 2016. *J. Electroanal. Chem.* 767, 68–75.
- Wagener, G., Jan, M., Kim, M., Mori, K., Barasch, J.M., Sladen, R.N., Lee, H.T., 2006. *Anesthesiology* 105 (3), 485–491.
- Weisbord, S.D., Chen, H., Stone, R.A., Kip, K.E., Fine, M.J., Saul, M.I., Palevsky, P.M., 2006. *J. Am. Soc. Nephrol.* 17 (10), 2871–2877.
- Wisitsoraat, A., Pakapongpan, S., Sriprachuabwong, C., Phokharatkul, D., Sritongkham, P., Lomas, T., Tuantranont, A., 2013. *J. Electroanal. Chem.* 704 (0), 208–213.
- Xing, X., Liu, S., Yu, J., Lian, W., Huang, J., 2012. *Biosens. Bioelectron.* 31 (1), 277–283.
- Zappitelli, M., Bernier, P.L., Saczkowski, R.S., Tchervenkov, C.I., Gottesman, R., Dancea, A., Hyder, A., Alkandari, O., 2009a. *Kidney Int.* 76 (8), 885–892.
- Zappitelli, M., Bernier, P.-L., Saczkowski, R.S., Tchervenkov, C.I., Gottesman, R., Dancea, A., Hyder, A., Alkandari, O., 2009b. *Kidney Int.* 76 (8), 885–892.
- Zhang, B.-T., Zheng, X., Li, H.-F., Lin, J.-M., 2013. *Anal. Chim. Acta* 784 (0), 1–17.
- Zhang, Y., Wang, Y., Jia, J., Wang, J., 2012. *Sens. Actuators B-Chem.* 171–172, 580–587.



Highly sensitive colorimetric detection of lead using maleic acid functionalized gold nanoparticles

Nalin Ratnarathorn^a, Orawon Chailapakul^b, Wijitar Dungchai^{a,*}

^a Department of Chemistry, Faculty of Science, King Mongkut's University of Technology Thonburi, Prachautid Road, Thungkru, Bangkok 10140, Thailand

^b Center of Excellence for Petroleum, Petrochemicals, and Advanced Materials, Chulalongkorn University, Patumwan, Bangkok 10330, Thailand

ARTICLE INFO

Article history:

Received 5 August 2014

Received in revised form

6 October 2014

Accepted 10 October 2014

Available online 23 October 2014

Keywords:

Colorimetric sensing

Gold nanoparticles

Lead

ABSTRACT

Highly sensitive colorimetric detection for Pb^{2+} has been developed using maleic acid (MA) functionalized GNP. The $-\text{COOH}$ on MA was used to modify GNP surface whereas the other $-\text{COOH}$ functional group have strong affinity to coordination behavior of Pb^{2+} allowing the selective formation more than other ions. MA-GNPs solution changed from red to blue color after the addition of Pb^{2+} due to nanoparticle aggregation. The different optical absorption and discriminate of particle size between the MA-GNPs solution with and without Pb^{2+} were characterized by UV-visible spectroscopy and transmission electron microscopy (TEM), respectively. The color intensity as a function of Pb^{2+} concentration gave a linear response in the range of $0.0\text{--}10.0 \mu\text{g L}^{-1}$ ($R^2=0.990$). The detection limit was found at $0.5 \mu\text{g L}^{-1}$ by naked eye and can be completed the analysis within 15 min. The MA-GNPs aggregated with Pb^{2+} showed high selectivity when was compared to other metal ions (As^{3+} , Ca^{2+} , Cd^{2+} , Co^{2+} , Cu^{2+} , Fe^{3+} , Hg^{2+} , Mg^{2+} , Mn^{2+} , Ni^{2+} , Pb^{2+} and Zn^{2+}) and anions (Cl^- , NO_3^- and SO_4^{2-}). Our proposed method was also applied for the determination of Pb^{2+} in real drinking water samples from 5 sources. The result of real water samples were not statistically significant different from the standard methods at the 95% confidence level (pair t-test method). Moreover, we evaluated our proposed method for the determination of trace Pb^{2+} concentration in real breast milk samples. The recoveries were acceptable and ranged from 101 to 104% for spiked Pb^{2+} in real breast milk samples. Thus, MA-GNP colorimetric sensing provides a simple, rapid, sensitive, easy-to-use, inexpensive and low detection limit for the monitoring of Pb^{2+} .

© 2014 Elsevier B.V. All rights reserved.

1. Introduction

The present food and drinking water are often contaminated with harmful substances for humans, either as part of the production process, natural or caused by the additives added to it. Lead (Pb^{2+}) is a major environmental pollutant and ranks second in the list of toxic substances that cause renal malfunction and damage to the brain and kidneys [1]. It has also been classified as carcinogenic agents by the World Health Organization (WHO) and International Agency for Research on cancer. Moreover, the long-term exposure to low concentrations of these metals causes adverse health effects. Therefore, WHO controlled level of lead in drinking water is not over $10 \mu\text{g L}^{-1}$ [2]. Several methods have been used for the detection of lead such as atomic absorption spectrometry (AAS) [3–5], inductively coupled plasma mass spectrometry (ICP/MS) [6], inductively coupled plasma atomic emission spectroscopy (ICP/AES)

[7], electrochemical method [8] and X-ray fluorescence spectrometry [9]. Although, these methods can detect lead sensitively and accurately, but there are limits in their complicated sample preparation processes, expensive, and required any specialized as well as sophisticated instrumentation [10].

Colorimetric sensors for Pb^{2+} determination attract much attention for their conveniences of visual observation and simple operations. They allow the direct analysis by the naked eyes without costly instruments compared with other methods. In recent year, gold nanoparticles (GNPs) have been widely used for colorimetric assays because their extinction coefficients are high relative to common organic compound [11–13]. GNPs have been extensively employed as colorimetric sensors for the detection of small concentrations of toxic metals such as arsenic, cadmium, cobalt, nickel and lead [14–16]. Kim et al. used GNPs capped with 11-mercaptoundecanoic acid to be capable of detecting Pb^{2+} through the coordination between the carboxylic groups and Pb^{2+} [17]. Moreover, Lu and co-workers reported a colorimetric sensor for Pb^{2+} detection using DNA-functionalized GNPs [18]. In 2010, GNPs capped with gallic acid (GA-GNPs) for the detection of Pb^{2+} has been reported. Huang and

* Corresponding author. Tel.: +66 2 470 9553; fax: +66 2 470 8840.

E-mail address: wijitar.dun@kmutt.ac.th (W. Dungchai).

co-workers have also demonstrated the aggregation of GA-GNPs in aqueous solutions and its minimum detectable concentration for Pb^{2+} in drinking water is 10 nM or $2.1 \mu\text{g L}^{-1}$ [12]. The detection limits of GA-GNPs are lower than the maximum allowable contamination level of Pb^{2+} in drinking water (WHO). However, the European Food Safety Authority (EFSA) reported that even using a low concentration of Pb^{2+} in drinking water ($2.1 \mu\text{g L}^{-1}$), adverse effect children's intelligence development can be observed [19,20]. In the absence of a safe exposure limit of children to Pb^{2+} and because of its ability to accumulate in the body for a long time, a great interest in the evaluation of the adverse effects of Pb^{2+} in low concentrations has emerged. Moreover, Human Health State of the Science in Canada has studied the trace Pb^{2+} concentration in breast milk because it is good biomarkers of maternal and infant exposure to Pb^{2+} . The Pb^{2+} level in human milk was found in the range from 0.025 to $15.8 \mu\text{g L}^{-1}$ in 210 mothers cross Canada [21,22]. Therefore, a highly sensitive, selective, simple and rapid method for the detection and quantification of trace Pb^{2+} is still required not only for the acceptance criteria of food safety but also toxicology.

Maleic acid, which has two carboxylic groups ($\text{HO}_2\text{CCH}=\text{CHCO}_2\text{H}$), should be suitable for the modification of nanoparticles surface. In the previous reports, GNPs was modified by thiol compounds such as glutathiol [10], cysteine [23], alkyl phosphate [24] and 11-mercaptoundecanoic acid [25] for the determination of Pb^{2+} in micromole level but maleic acid functionalized GNPs has been not investigated for the colorimetric detection of Pb^{2+} . Thus, the aim of this work was to develop the highly sensitive, selective, simple and rapid colorimetric sensor for trace Pb^{2+} determination using maleic acid modified GNPs. Maleic acid is easy to modify on GNPs surface within 1 h. MA-GNPs solution changed from red to blue color after the addition of Pb^{2+} and can be observed by the naked eye. The pH effect and the reaction time were studied in this work. The low limits of detection for Pb^{2+} at sub $\mu\text{g L}^{-1}$ level with a short analysis time of 15 min were obtained by our proposed assay. Finally, our developed method was successfully applied for determination of trace levels of Pb^{2+} in drinking water samples and the human breast milk samples.

2. Experimental

2.1. Chemicals and materials

All chemicals used in experiment were analytical reagent (AR) grade and solutions were prepared using high pure water with a resistance of $18 \text{ M}\Omega \text{ cm}^{-1}$. Dithiothreitol (DTT), glutathione (Glu), homocysteine (Hcy), L-cysteine (L-cys), maleic acid (MA), metal ions (As^{3+} , Cd^{2+} , Co^{2+} , Cu^{2+} , Fe^{3+} , Hg^{2+} , Mg^{2+} , Mn^{2+} , Ni^{2+} , Pb^{2+} , Zn^{2+} using atomic absorption grade), KCl, KNO_3 and K_2SO_4 were bought from Sigma-Aldrich (St. Louis, Missouri). Whatman No. 1 filter paper was bought from Cole-Parmer (Vernon Hills, IL). All glassware was thoroughly cleaned with freshly prepared 1:1 HCl/ HNO_3 and rinsed with high pure water prior to use. All metal ions stock solutions were prepared in 50 mM phosphate buffer pH 5.8.

2.2. Instrumentation

UV-visible absorption spectra were recorded in a quartz cuvette (1-cm pathlength) using a UV-visible spectrometer (Lambda 35, Perkin Elmer Instruments, USA). Size distribution of particles was recorded by Transmission Electron Microscope (TEM, TECNAI T20 G², FEI, Netherland). Photographic results were recorded using a digital camera (PowerShot S95, 10.1 Megapixels, Canon). An atomic absorption spectrometer (AAS) with a hollow cathode lamp and standard air/acetylene flame (Analyst 300, Perkin Elmer Instruments, USA)

was used for atomic absorbance measurements. A hollow cathode lamp was used under the following operations conditions: wavelength: 283.3 nm; slit-width: 0.7 H nm; lamp current: 10 mA.

2.3. Synthesis of GNPs

100 mL of HAuCl_4 (0.01%) was added into a 250 mL Erlenmeyer flask and then boiled. After that, 3.5 mL of trisodium citrate (1%) was added and further rapidly stirred for 15 min. We continually stirred for 30 min without heating. The solution was cooled to room temperature which was stored in the refrigerator 4 °C before further use [15].

The MA-GNPs solution was prepared using self-assembly of the organic compound on the GNP surface. A red of GNP solution (~20 nm in diameter) was first prepared from GNPs stock solution. Then, 0.20 mL of 0.01 M MA was added into 0.40 mL of GNP solution to generate MA-GNPs. Organic compound was self-assembled on to the surface of GNPs by incubating the GNPs with the MA solutions for 1 h at room temperature. After this step, the GNP aggregation was characterized using UV-visible Spectrometry.

2.4. Detection of lead

0.60 mL of MA-GNP solution in the eppendorf was mixed with 0.40 mL of metal ion solutions (As^{3+} , Ca^{2+} , Cd^{2+} , Co^{2+} , Cu^{2+} , Fe^{3+} , Hg^{2+} , Mg^{2+} , Mn^{2+} , Ni^{2+} , Pb^{2+} and Zn^{2+}) and anions solutions (KCl, KNO_3 and K_2SO_4) in 50 mM phosphate buffer at pH 5.8. For background (Bg), 0.40 mL of buffer was mixed 0.60 mL of MA-GNP solution (Bg-MA-GNPs). Then, the mixture was incubated for 15 min at the room temperature and analysis by the spectrometer and TEM.

2.5. Sample preparation for transmission electron microscopy (TEM)

Transmission electron microscope (TEM) measurements were performed on TECNAI T20 G² instrument which operated at an accelerating voltage of 120 kV and the 25000× magnification. The sample solutions for TEM studies were prepared by placing a drop of GNPs, MA-GNPs, Bg-MA-GNPs and Pb^{2+} -MA-GNPs on a formvar coated copper grid. The films on the TEM grids were allowed to dry for 1 h. The size of nanoparticle studies was performed in aqueous solution by Center of Nanoimaging, Mahidol University.

2.6. Applications

To evaluate the utility of our proposed method, the Pb^{2+} in the drinking water samples from five different sources was quantified. Our method was validated against AAS. Prior to analysis by AAS, pre-concentration was carried out on all samples. 1.5 L of sample was mixed with 1 mL of 0.1 M HCl and then heated to evaporate excess water until 5.0 mL of samples remained. For AAS, samples were adjusted to a final volume of 10 mL with deionized water. For our proposed method, 0.60 mL of MA-GNP solution in the eppendorf was mixed with 0.40 mL of the water sample without any pretreatment. Then, the mixture was incubated for 15 min at the room temperature and analysis by spectrometer. For testing of trace levels of Pb^{2+} in the human breast milk, the sample was divided two parts. The first was analyzed by our method without spiking Pb^{2+} and the second was spiked with the standard Pb^{2+} solution at 10.0, 25.0 and $50.0 \mu\text{g L}^{-1}$ to obtain the final concentration at 1.0, 2.5 and $5.0 \mu\text{g L}^{-1}$, respectively. Prior to analysis, spiked samples were precipitated the protein by adding 0.75 mL of sample with 0.15 mL of 10% w/v TCA (Tri chloroacetic acid). After that, samples were stored at 4 °C for 15 min and then subjected to centrifugation at 14,500 rpm for 10 min. The precipitate was removed from the supernatant and kept only supernatant for analysis.

3. Results and discussion

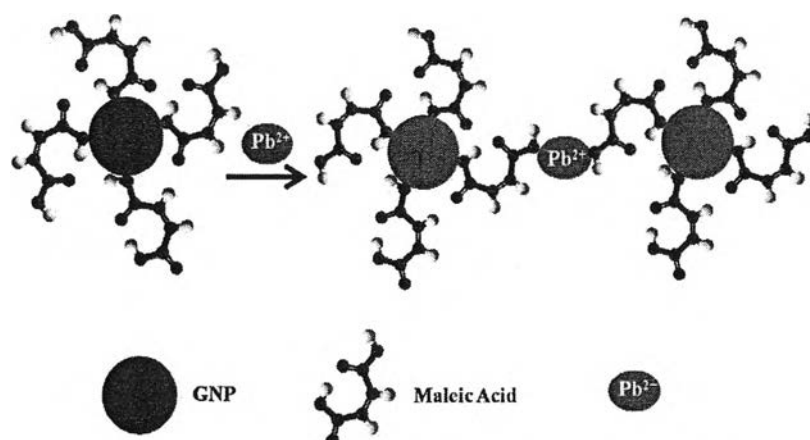
3.1. Characterization of GNP aggregation

Maleic acid has two carboxylic groups ($\text{HO}_2\text{CCH}=\text{CHCO}_2\text{H}$) so one carboxylic group should be suitable for the modification of nanoparticles surface and the other carboxylic group can capture Pb^{2+} in aqueous solution as shown in Scheme 1. In this experiment, the color of solution change from dark pink to blue after adding $1.0 \mu\text{g L}^{-1}$ of Pb^{2+} in the MA-GNPs solution (Fig. 1). MA-GNPs in the presence and absence of Pb^{2+} were characterized by UV-vis Spectroscopy and Transmission Electron Microscope (TEM). A characteristic band of MA-GNPs was observed at approximate 520 nm. After the addition of Pb^{2+} , the wavelength at 520 nm decreased and a new red-shifted change at 600 nm (Fig. 1), so Pb^{2+} can induce aggregation of MA-GNPs. To confirm the mechanism of the interaction between MA-GNPs and Pb^{2+} , the solution of GNPs, MA-GNPs, Bg-MA-GNPs and Pb^{2+} -MA-GNPs were analyzed by TEM as shown in Fig. S1. The prepared GNPs were dispersed an average particle size under ~ 20 nm in diameter, whereas the nanoparticles remain

isolated and randomly distributed in the absence of Pb^{2+} ions (Fig. S1a–c). Upon addition of Pb^{2+} into MA-GNPs, the solution turned blue color. TEM studies clearly indicate that Pb^{2+} induces aggregation of nanoparticles (Fig. S1d). Possible mechanism is the obstructive aggregation of MA-GNPs in the absence of Pb^{2+} due to the electrostatic repulsion against van der Waals attraction of carboxylic of MA on the GNPs surface [13]. After the addition Pb^{2+} , the other $-\text{COOH}$ group of MA can binds with Pb^{2+} and it is specificity than other metals (Fig. 1) because of the coordination number of Pb^{2+} more over the other metal cations. Other metal cations interact only with lesser numbers of ligands, leaving the nanoparticles isolated; hence, no spectral change and no color of solution change were observed under the experimental conditions [26].

3.2. Selectivity study

We investigated the change in values of absorption ratio ($A_{600/520}$) for MA-GNPs that measured after 15 min upon the addition of the metal ions. The concentration of other metal ions was studied for 15 min at higher than 100 times of Pb^{2+} concentration ($1.0 \mu\text{g L}^{-1}$ of



Scheme 1. Schematic of aggregating process of MA-GNPs induced by adding Pb^{2+} .

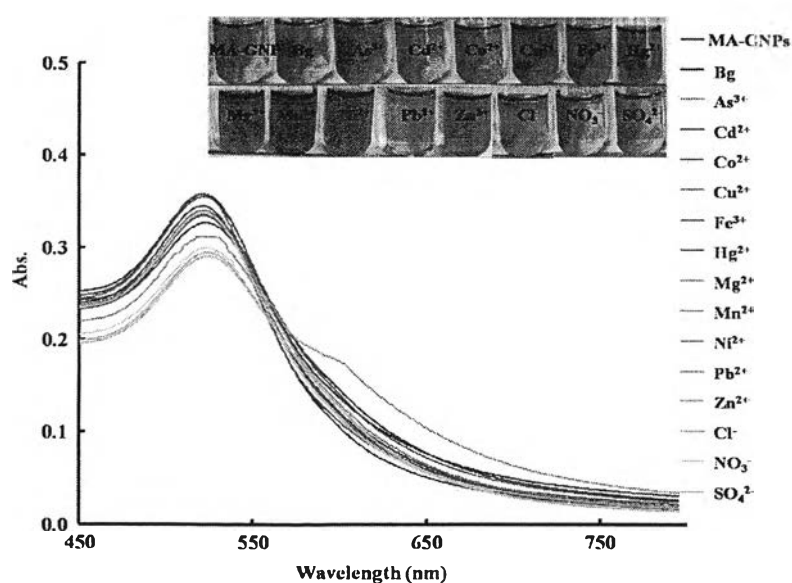


Fig. 1. UV-visible spectra of MA-GNPs solutions with cations ($1.0 \mu\text{g L}^{-1}$ of Pb^{2+} and 0.1 mg L^{-1} of other cations) and anions ($250.0 \text{ mg L}^{-1} \text{ Cl}^-$, $45.0 \text{ mg L}^{-1} \text{ NO}_3^-$ and $200.0 \text{ mg L}^{-1} \text{ SO}_4^{2-}$ following Guidelines for drinking-water quality by [2]). (For interpretation of the references to color in this figure legend, the reader is referred to the web version of this article.)

Pb^{2+} and 0.1 mg L^{-1} of As^{3+} , Cd^{2+} , Co^{2+} , Cu^{2+} , Fe^{3+} , Hg^{2+} , Mg^{2+} , Mn^{2+} , Ni^{2+} and Zn^{2+}). Most interference levels in this study were higher than the permissible limit in the drinking water by WHO (For example; 0.003 , 0.05 and 0.02 mg L^{-1} for Cd^{2+} , Co^{2+} and Ni^{2+} , respectively). Moreover, interference effect of anions at the levels containing in drinking-water ($250.0 \text{ mg L}^{-1} Cl^{-}$, $45.0 \text{ mg L}^{-1} NO_3^{-}$ and $200.0 \text{ mg L}^{-1} SO_4^{2-}$ by [2]) was studied. The result showed that the color of solution didn't change to blue color after the addition of anions and other metal ions as shown in Fig. 1. The absorbance ratio ($A_{600/520}$) of MA-GNPs with different metal ions and anions is shown in Fig. 2. Only Pb^{2+} can be observed a significant $A_{600/520}$ value. Possible mechanism is the unique coordination behavior of Pb^{2+} as $[Xe]4f^{14}5d^{10}6s^2$ electronic configuration. It appears as a borderline acid, able to bind to wide families of ligands within very flexible bond length and geometry so it allows the formation of a stable supra-molecular complex. Other metal cations interact only with lesser numbers of ligands, leaving the nanoparticles isolated because of the rigid coordination geometry or may result from other factors e.g., the

change in particle geometry. Hence, no spectral and color change were observed under the experimental conditions [26,27]. On the aforementioned results, MA-GNPs can be utilized to detect Pb^{2+} with high selectivity.

GNPs surface can be typically modified by carboxylic, amino, and thiols group to achieve selective cross-linking (and thus aggregation) therefore we also investigated the effect of cross-linking group in this part. DTT, Hcy, ι -Cys and Glu were studied due to the active group in their molecules. All modified GNPs synthesized by our method showed an absorbance at 520 nm wavelength and observed a red solution. After adding $1.00 \mu\text{g L}^{-1}$ various metals including Pb^{2+} , As^{3+} , Cd^{2+} , Co^{2+} , Cu^{2+} , Fe^{3+} , Hg^{2+} , Mg^{2+} , Mn^{2+} , Ni^{2+} and Zn^{2+} in the solution of DTT-GNPs, Hcy-GNPs and ι -Cys-GNPs at $\text{pH } 5.8$, the color of the solution for all metals changes from red to violet and spectra shifts from 520 nm to 600 nm (Fig. S2a–c). Whereas, Glu-GNPs (Fig. S2d) showed no change occurs, the absorption spectrum is still intact. Therefore, Glu-GNPs, DTT-GNPs, Hcy-GNPs and ι -Cys-GNPs gave no specificity to Pb^{2+} under this condition.

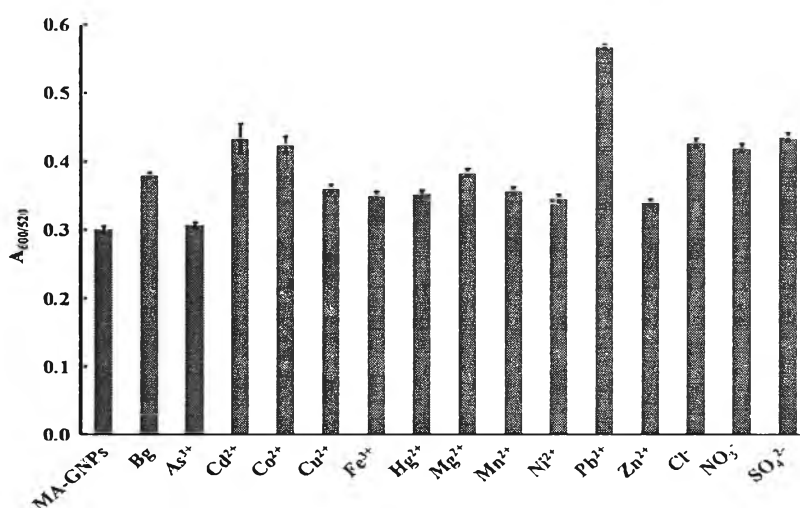


Fig. 2. The values ($A_{600/520}$) of MA-GNPs upon the addition of $1.0 \mu\text{g L}^{-1} Pb^{2+}$ and 0.1 mg L^{-1} of other cations and $250.0 \text{ mg L}^{-1} Cl^{-}$, $45.0 \text{ mg L}^{-1} NO_3^{-}$ and $200.0 \text{ mg L}^{-1} SO_4^{2-}$. The error bars represent standard deviations based on three independent measurements.

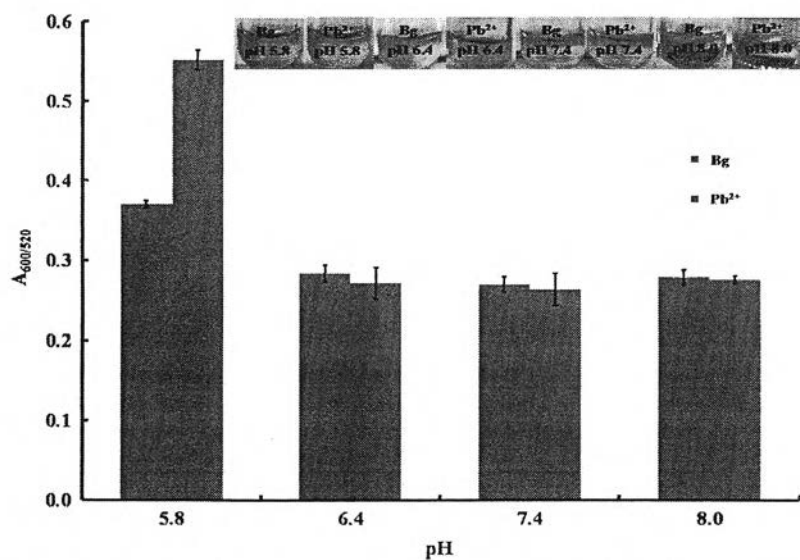


Fig. 3. Effect of pH $0.6 \mu\text{L}$ of MA-GNPs mixed $0.4 \mu\text{L}$ of Pb^{2+} ($1.0 \mu\text{g L}^{-1}$) in phosphate buffer pH 5.8, 6.4, 7.4 and 8.0 for 15 min error bar at $n=3$.

3.3. Effect of pH and reaction time

We investigated the colorimetric response of MA-GNPs with Pb^{2+} at different pH (5.8, 6.4, 7.4 and 8.0). Only MA-GNPs with Pb^{2+} at pH 5.8 showed the color change and higher absorbance ratio ($A_{600/520}$) than buffer (Bg). While at pH 6.4, 7.4 and 8.0 show no significant difference of the absorbance ratio ($A_{600/520}$) and color solution between presence and absence of Pb^{2+} (Fig. 3). Additionally, Bg-MA-GNPs slightly change color at low pH (< 6.58) and the absorbance ratio was larger than at high pH (Fig. 3). MA-GNPs ionizable of structure would be affected by the pH value, which was high enough for ionization, taking the pK_{a1} (1.93) and pK_{a2} (6.58) value of MA into consideration. The electrostatic repulsion between the MA-GNPs would increase and disintegrated to all ions at pH more than pK_{a2} , while the electrostatic repulsion between the MA-GNPs would decrease and occur van der Waals attraction between $-COOH$ group of MA with GNPs at pH less than pK_{a2} . The mechanism can be attributed to the function of Pb^{2+} with MA-GNP in a chelating reaction. The aggregation of MA-GNPs was induced by the coordination between Pb^{2+} and carboxylate of MA at pH 5.8. The various metal cations including As^{3+} , Cd^{2+} , Co^{2+} , Cu^{2+} , Fe^{3+} , Hg^{2+} , Mg^{2+} , Mn^{2+} , Ni^{2+} , Pb^{2+} and Zn^{2+} no changed of color occurs after adding into the MA-GNPs at pH 6.4,

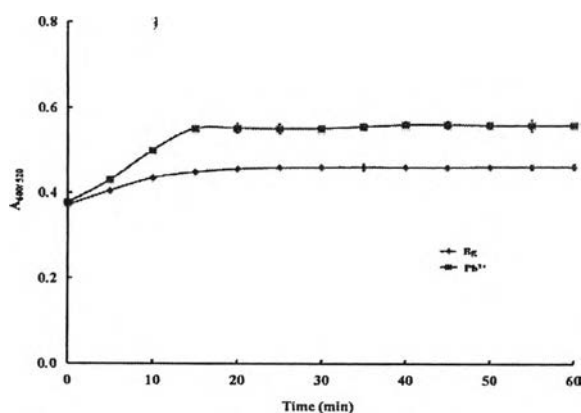


Fig. 4. Effect of reaction time between 0 and 60 min (0.6 μ L of MA-GNPs mixed 0.4 μ L of Pb^{2+} (1.0μ g L^{-1}) in phosphate buffer pH 5.8) Error bar at $n=3$.

7.4 and 8.0 (Fig. S3). Therefore, we selected the optimum pH at pH 5.8 for Pb^{2+} detection by the naked eye.

The effect of reaction time between MA-GNPs and Pb^{2+} was investigated. The ratio between the absorbance at a wavelength of 520 nm to 600 nm was used to evaluate as shown in Fig. 4. We found that for low concentration of Pb^{2+} (1.0μ g L^{-1}) absorbance ratio reached equilibrium within 15 min. This result represents the fast performance of this assay for Pb^{2+} .

3.4. Calibration

The different concentrations of Pb^{2+} were added to MA-GNPs. The degree of aggregation of MA-GNPs depended on concentration of Pb^{2+} . Fig. 5 shows that the absorbance changed with the addition of different concentrations of Pb^{2+} . The maximal absorption at 520 nm decreased and a new peak at 600 nm increased with increasing Pb^{2+} concentration, which indicated the aggregating between MA-GNPs and Pb^{2+} has a relationship with the concentration. Thus, the MA-GNPs for the detection of different concentrations of Pb^{2+} was processed directly using the UV-vis absorbance ratio ($A_{600/520}$). A linear correlation existed between the absorbance ratio ($A_{600/520}$) and the concentration of Pb^{2+} ranging from 0.0 to 10.0μ g L^{-1} ($R^2=0.990$) as shown in Fig. 5. The detection limit was found at 0.5μ g L^{-1} . In the presence of high concentration of Pb^{2+} more than 10.0μ g L^{-1} , the UV-Vis absorption spectra of Pb^{2+} -MA-GNPs became broader and shifted to much longer wavelength (> 600 nm). The value is not in a linear range. Consequently, the concentration of Pb^{2+} ranging from 0.0 to 10.0μ g L^{-1} made this assay suitable for the determination of Pb^{2+} in aqueous solution. Compared with the other colorimetric methods based on nanoparticles (Table 1), our method has the higher sensitivity and more rapid.

3.5. Analytical applications

To validate our assay for the determination of Pb^{2+} in real samples, drinking water samples from 5 sources were analyzed by our assay and the traditional method (Atomic Absorption Spectroscopy, AAS) as shown in Table 2. The data were then compared by a paired t-test. Our results were not statistically significant different from the standard methods at the 95% confidence level

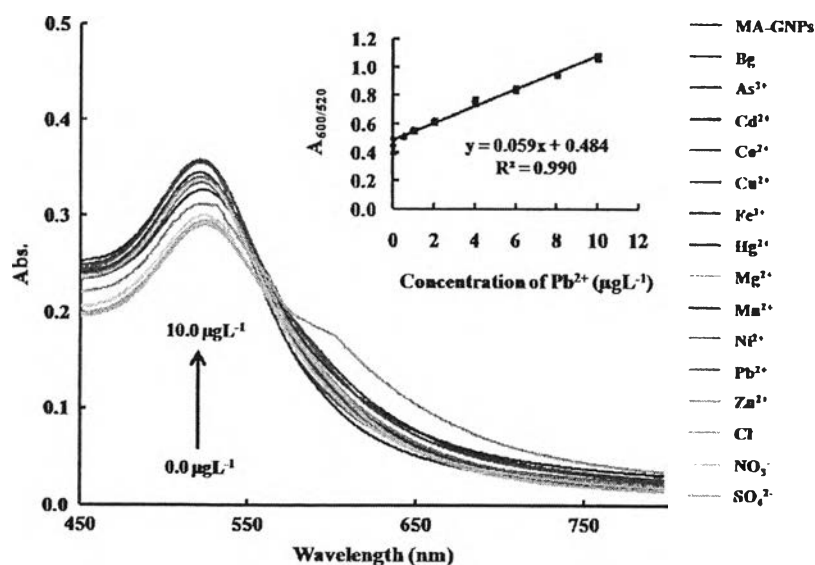


Fig. 5. UV-visible spectra of MA-GNP solutions with various concentrations of Pb^{2+} in the range from 0.0 to 10.0μ g L^{-1} at 15 min.

Table 1
Nanoparticles optical assays for the detection of Pb²⁺.

Probe unit	LOD	Linear range	Real sample	Time (min)	Refs.
DNAzyme and GNPs	103.6 µg L ⁻¹	N/A ^a	N/A ^a	20	[28]
Gallic acid-GNPs	2.1 µg L ⁻¹	2.1–207.2 µg L ⁻¹	N/A ^a	30	[12]
Gallic acid-GNPs or Gallic acid-AgNPs	N/A ^a	6.2–62.2 mg L ⁻¹	N/A ^a	N/A ^a	[26]
Gallic acid-GNPs	5.2 µg L ⁻¹	10.4–207.2 µg L ⁻¹	Drinking water	N/A ^a	[29]
Papain-GNPs	41.4 µg L ⁻¹	N/A ^a	N/A ^a	N/A ^a	[30]
Cysteine-alanine-leucine-asparagine-asparagine-GNPs	20.7 µg L ⁻¹	20.7 µg L ⁻¹ –6.2 mg L ⁻¹	N/A ^a	N/A ^a	[16]
Alkyl Phosphate-GNPs	621.6 µg L ⁻¹	0.0–2.1 mg L ⁻¹	N/A ^a	15	[24]
Maleic acid-GNPs	0.5 µg L ⁻¹	0.0–10.0 µg L ⁻¹	Drinking water and milk	15	Our method

^a Not available.

Table 2
Levels of Pb²⁺ in drinking water samples were measured using our method and AAS.

Water samples	Concentration of Pb ²⁺ (µg L ⁻¹)	
	AAS	Our method
Sample 1	6.74±0.02	6.42±0.51
Sample 2	7.71±0.03	7.95±1.38
Sample 3	7.90±0.01	9.21±0.77
Sample 4	7.74±0.03	8.68±0.79
Sample 5	10.20±0.06	11.42±0.04

The standard deviation of water samples at n=5.

(t-test value=0.67, t critical value=2.31). Moreover, we also evaluated the utility of our method by analysis low level of Pb²⁺ in human breast milk samples. We found that Pb²⁺ in the human breast milk samples were not detectable under our detection limit (0.5 µg L⁻¹). Thus, known amounts of Pb²⁺ were spiked into milk samples to get the final concentration at 1.0, 2.5 and 5.0 µg L⁻¹. It was found the level of Pb²⁺ at 1.09±0.20, 2.93±0.62, and 5.06±0.29 µg L⁻¹, respectively (n=7) and the percentage recovery in the range 101–105%. Therefore, the MA-GNPs can be used to measure the low amount of Pb²⁺ in real samples. It is an easy to measure without the need for analyze complex or expensive, used of less levels and does not require expert analysis.

4. Conclusions

In summary, a simple, rapid, highly sensitive, easy-to-use, inexpensive, and portable alternative point-of-measurement monitoring for Pb²⁺ using MA-GNPs colorimetric assay has been developed. The Pb²⁺-induced MA-GNPs aggregation results in a marked red shift in the UV-vis absorption spectra and a visible color change from red to blue. The detection limit of this method by the detection of naked eye is 0.5 µg L⁻¹ which lower than other GNPs colorimetric probs. Furthermore, Pb²⁺ was clearly distinguishable color change from the other heavy metal ions under the optimum conditions at the critical level of Pb²⁺ in drinking water prescribed by WHO. Finally, our method was successfully applied to analysis of Pb²⁺ in water samples and the human breast milk samples. Therefore, this method should be applicable to detect low level of Pb²⁺ in drinking water and some biological samples.

Acknowledgements

Orawon Chailapakul and Wijitar Dungchai gratefully acknowledge the financial support from Thailand Research Fund through TRF Senior Research Scholar (RTA5780005).

Appendix A. Supporting information

Supplementary data associated with this article can be found in the online version at <http://dx.doi.org/10.1016/j.talanta.2014.10.024>.

References

- [1] L. Fewtrell, R. Kaufmann, A.P. Ustun, Lead, W.H.O. (Environmental Burden of Disease Series) Geneva, 2003, pp. 5–21.
- [2] Guidelines for Drinking-Water Quality, third ed., W.H.O. Geneva, 2004, pp. 8–35.
- [3] A.A. Jigam, B.E.N. Dauda, T. Jimoh, H.N. Yusuf, Z.T. Umar, Afr. J. Food Sci. 5 (2011) 156–160.
- [4] M.H. Shagal, H.M. Maina, R.B. Donatus, K. Tadzabia, Glob. Adv. Res. J. Environ. Sci. Toxicol 1 (2012) 18–22.
- [5] K. Bakkali, N.R. Martos, B. Souhail, E. Ballesteros, Food Chem. 2 (2009) 590–594.
- [6] H.W. Liu, S.J. Jiang, S.H. Liu, Spectrochim. Acta, Part B 54 (1999) 1367–1375.
- [7] E. Pehlivan, G. Arslan, F. Gode, T. Altun, M.M. Ozcan, Grasas Aceites 59 (2008) 239–244.
- [8] Z. Zou, A. Jang, E. MacKnight, P.M.i. Wu, J. Do, P.L. Bishop, C.H. Ahn, Sens. Actuators, B 134 (2008) 18–24.
- [9] D.H.S. Richardson, M. Shoreb, R. Hartreeb, R.M. Richardson, Sci. Total. Environ. 176 (1995) 97–105.
- [10] F. Chai, C. Wang, T. Wang, L. Li, Z. Su, Appl. Mater. Interfaces 2 (2010) 1466–1470.
- [11] R. Elghamian, J.J. Storhoff, R.C. Mucic, R.L. Letsinger, C.A. Mirkin, Science 277 (1997) 1997 (1080).
- [12] K.W. Huang, C.J. Yu, W.L. Tseng, Biosens. Bioelectron. 25 (2010) 984–989.
- [13] Z. Chen, Z. Wang, J. Chen, S. Wang, X. Huang, Analyst 137 (2012) 3132–3137.
- [14] J.R. Kalluri, T. Arbnesi, S.A. Khan, A. Neely, P. Candice, B. Varisli, M. Washington, S. McAfee, B. Robinson, S. Banerjee, A.K. Singh, D. Senapati, P.C. Ray, Angew. Chem. Int. Ed. 48 (2009) 1–5.
- [15] M. Zhang, Y.Q. Liux, B.C. Ye, Analyst 137 (2012) 601–607.
- [16] X.K. Li, Z.X. WANG, Chem. Res. Chin. Univ. 2 (2010) 194–197.
- [17] Y. Kim, R.C. Johnson, J.T. Hupp, Nano Lett. 1 (2001) 165–167.
- [18] J. Liu, Y. Lu, J. Am. Chem. Soc. 127 (2005) 12677–12683.
- [19] Lead Standard in Drinking Water, The SCHER, 2011.
- [20] EFSA Panel on Contaminants in the Food Chain (CONTAM), EFSA Journal 8 1147. Available online: (<http://www.efsa.europa.eu/en/efsajournal/pub/1570.htm>).
- [21] The Minister of Health, Final Human Health State of the Science Report on Lead. (2013). Available online: (<http://www.hc-sc.gc.ca/ewh-scmt/pubs/contaminants/dhhssrl-rpccsceph/index-eng.php>).
- [22] G.A.K. Koyashiki, M.M.B. Paoliello, P.B. Tchounwou, Rev. Environ. Health 25 (2010) 243–253.
- [23] Y.P. Zhanga, J. Chena, L.Y. Baib, X.M. Zhou, L.M. Wang, J. Chin. Chem. Soc. 57 (2010) 972–975.
- [24] S.K. Kim, S. Kim, E.J. Hong, M.S. Han, Korean Chem. Soc. 31 (2010) 3806–3808.
- [25] C. Fan, S. He, G. Liu, L. Wang, S. Song, Sensors 12 (2012) 9467–9475.
- [26] K. Yoosaf, B.I. Ipe, C.H. Suresh, K.G. Thomas, J. Phys. Chem. C 111 (2007) 12839–12847.
- [27] L.S. Livny, J.P. Glusker, C.W. Bock, Inorg. Chem. 37 (1998) 1853–1867.
- [28] H. Wei, B. Li, J. Li, S. Dong, E. Wang, Nanotechnology 19 (2008) 1–5.
- [29] N. Ding, Q. Cao, H. Zhao, Y. Yang, L. Zeng, Y. He, K. Xiang, G. Wang, Sensors 10 (2010) 11144–11155.
- [30] Y. Guo, Z. Wang, W. Qu, H. Shao, X. Jiang, Biosens. Bioelectron. 26 (2011) 4064–4069.



Simple and fast colorimetric detection of inorganic arsenic selectively adsorbed onto ferrihydrite-coated silica gel using silver nanoplates



Weena Siangproh^a, Orawan Chailapakul^b, Kriangsak Songsrirote^{a,*}

^a Department of Chemistry, Faculty of Science, Srinakharinwirot University, Sukhumvit 23, Wattana, Bangkok 10110, Thailand

^b Electrochemistry and Optical Spectroscopy Research Unit, Department of Chemistry, Faculty of Science, Chulalongkorn University, 254 Phayathai Road, Pathumwan, Bangkok 10330, Thailand

ARTICLE INFO

Article history:

Received 13 December 2015

Received in revised form

4 March 2016

Accepted 6 March 2016

Available online 7 March 2016

Keywords:

Arsenic

Silver nanoplates

Colorimetry

Ferrihydrite-coated silica gel

Optical detection

ABSTRACT

The optical detection for inorganic arsenic (As) semi-quantitative determination is presented by using silver nanoplates (AgNPs). The color of AgNPs is immediately changed in the presence of As(III) and As(V) with the same sensitivity. To improve the selectivity of AgNPs for As detection, ferrihydrite-coated silica gel (SiO₂-Fh) was specifically exploited as adsorbent for arsenic prior to As detection by AgNPs. The developed method provides the detection limit of 0.5 ppm with the detection range between 0.5 ppm and 30.0 ppm for As determination observed with naked eye, and allows to determine total inorganic arsenic. This is the first report of As detection approach combining As removal technology together with nanotechnology. This combined technique provides a rapid, sensitive and selective method for monitoring As levels in aqueous samples, and can be employed as a testing field kit to screen arsenic contamination outside of a laboratory.

© 2016 Elsevier B.V. All rights reserved.

1. Introduction

Arsenic is a serious environmental contaminant because of its toxicity and also carcinogenicity. This toxic element occurs as a major constituent in more than 200 minerals. Arsenic is unevenly distributed in the earth's crust and is found in soil, rocks, and minerals around the world. Furthermore, arsenic contamination of water resources both surface and subsurface has been reported in many parts of the world, as arsenic can be released into water systems once mineral deposits or rocks containing arsenic are dissolved. In addition, some anthropogenic activities also accelerate arsenic exposure to the environment e.g. mining, agricultural and industrial activities, and waste and fossil-fuel burning. Arsenic exists in four oxidation states: As(-III), As(0), As(III) and As(V) with numerous forms, both organic and inorganic, resulting in complexity of its chemistry and mobility in the environment. The major arsenic species found in environmental and biological samples are arsenite As(III), arsenate As(V), arsenious acids, arsenic acids, monomethylarsonate (MMA), dimethylarsinate (DMA), arsenobetaine (AB), arsenocholine (AC), and arsenosugars. Different species of arsenic have different toxic levels of which organic species are considered to be substantially less harmful in comparison to inorganic forms. Among the existing arsenic species in

the environment, arsenite and arsenate, inorganic species, are the most concerned species because of their high toxicity in which arsenite is 10 and 70 times more toxic than arsenate and the methylated species, respectively [1,2].

Due to its toxicity, arsenic contaminations in a wide range of samples such as water, food, soils, and plants etc. were monitored [3–8]. To determine the accurate quantity of arsenic in samples, expensive and sophisticated instruments and facilities together with skilled staff are required. Several analytical techniques have been applied for arsenic determination such as atomic absorption spectroscopy (AAS) [3,9], atomic emission spectroscopy (AES) [10–12], electrochemical methods [13–16], atomic fluorescence spectrometry [17,18], neutron activation analysis (NAA) [19,20], capillary electrophoresis (CE) [21,22], and chromatographic methods (hyphenated techniques) [3,9,23,24]. To date, field test kits for determining arsenic semi-quantitatively have been developed and extensively used for arsenic in water samples. Most of the test kits commercially available are based on the classical Gutzeit method, developed over 100 years ago [25] used for hydride generation to generate a toxic arsine gas, AsH₃. However, the user must be very careful, as the test kit protocols involve the use of a strong reducing agent and acid, and toxic gas production.

Nowadays, nanoparticle optical detection based on colorimetry have been gaining great attention from researchers especially for biological and environmental sample analysis because of their simplicity, low cost, less time consuming, and ease of data interpretation. Nanotechnology is rapidly growing in the field of optical

* Corresponding author.

E-mail address: kriangsaks@g.swu.ac.th (K. Songsrirote).

detections, as nanoparticles (NPs) have unique physical, chemical, and biological properties compared to their macro-scaled counterparts. Different types of NPs provide different optical, fluorescent and magnetic properties. Therefore, NPs with distinctive optical property related to the size and shape of the NPs especially gold- and silver-NPs show potential to be exploited in a wide range of applications. Gold nanoparticles (AuNPs) have been intensively studied for numerous applications as optical detections for heavy metals [26–29] including As(III) [30] and As(V) [31], aromatic compounds [32,33], organophosphate [34], and stimulant [35] etc. Colorimetric detections of mercury(II) ion using AgNPs were reported for environmental [36,37] and biological sample [38] analyses. The selective detection of Co^{2+} using glutathione-modified AgNPs was also presented [39].

In this study, silver nanoplates (AgNPs) were elucidated for As(III) and As(V) detections. However, due to the matrix effect which possibly interferes the detection, iron oxide-coated silica gel was exploited to selectively adsorb arsenic prior to the detection with AgNPs. Since several technologies have been used for arsenic removal from water to improve the water quality such as oxidation [40], co-precipitation [41], ion exchange [42,43], and membrane [44] etc. Adsorption onto sorptive media [45–51] is one of the most common technologies utilized to remove arsenic. Iron(III) oxide is widely used as arsenic adsorbent [45–48]. The synthesis and properties of ferrihydrite-coated silica gel ($\text{SiO}_2\text{-Fh}$) for As removal were studied and explained clearly by Arifin [45]. $\text{SiO}_2\text{-Fh}$ showed good efficiency on both As(III) and As(V) removals with easy synthesis procedure. Therefore, the iron oxide-coated silica gel was applied for arsenic detection herein. Thus, the developed approach of using the As removal technology combined with silver nanotechnology was first demonstrated for the detection of inorganic arsenic in contaminated water for the first time.

2. Experimental section

2.1. Chemicals and materials

Silver nanoplates (AgNPs) with dark blue color were obtained from the Sensor Research Unit at the Department of Chemistry, Chulalongkorn University. Synthesis of AgNPs employed a facial method that used starch as the stabilizer without capping agents. Analytical grade reagents and 18 M Ω cm resistance deionized water (obtained from a Millipore Milli-Q purification system) were used throughout. Arsenic trioxide, arsenic pentoxide, iron(III) nitrate nonahydrate, mercury chloride, silver nitrate, trisodium phosphate were purchased from Sigma-Aldrich. Sodium chloride, zinc chloride, magnesium chloride, lead nitrate, sodium sulfate, sodium carbonate, calcium chloride, ammonium chloride, and magnesium sulfate were purchased from Analytical univar reagent Ajax Finechem.

2.2. Preparation of the ferrihydrite-coated silica gel

Ferrihydrite-coated silica gel ($\text{SiO}_2\text{-Fh}$) was modified from the protocol developed by Eric Arifin et al. [45]. Briefly, 20 g of silica gel 60 (70–230 mesh ASTM) and 2.8 g of $\text{Fe}(\text{NO}_3)_3 \cdot 9\text{H}_2\text{O}$ and 50 mL deionized water were loaded into 250 mL flask. The pH of the mixture was adjusted to neutral (pH 7) by using NH_4OH solution. The mixture was stirred for 2 h at room temperature. The modified silica bead was then filtered using vacuum filtration and washed with deionized water to remove free ferrihydrite from the beads. Finally, the $\text{SiO}_2\text{-Fh}$ was oven dried at 60 °C for 2 h, and then stored in a glass vial for further use.

2.3. Arsenic adsorption on the ferrihydrite-coated silica gel

Approximate 0.3 g of $\text{SiO}_2\text{-Fh}$ was added to the 100 mL of sample solution and then stirred with slow speed for 45 min. The solid was then filtrated using vacuum filtration and washed with large volume of deionized water. The solid was oven dried at 50 °C for 1 h, and then stored in a glass vial until the determination.

2.4. Colorimetric measurements of inorganic As and AgNPs

The absorption spectra of the AgNPs with and without inorganic arsenic added were obtained by using a UV–vis absorption spectrometer (Shimadzu, 2401 PC). In addition, AgNPs were characterized and reported in our previous work [36].

2.5. Analysis of real samples

To test the practical application capability of the develop approach, water samples from different sources were collected and filtered through a 0.45 μm membrane. Standard addition method was applied to prepare a series of samples by spiking standard solutions of As(III) to tap water, groundwater, and canal water. Prior to arsenic determination using AgNPs, the pretreated water samples were applied to $\text{SiO}_2\text{-Fh}$ following the procedure described in Section 2.3. In addition, inductively coupled plasma-optical emission spectrometry (Thermo Scientific iCAP 7000 Series ICP-OES) was exploited as validation method for the proposed approach.

3. Results and discussion

3.1. Conditions of AgNPs for inorganic As determination

The dark blue colored AgNPs were obtained with an initial concentration of 400 ppm. The AgNPs showed maximum absorption at 575 nm. The dark blue color of AgNPs was changed to purple, pink, orange, and yellow, respectively, depending on the concentrations of As added to the solution. Fig. 1 is UV–vis spectra of 50 ppm AgNPs and also of the 50 ppm AgNPs with 50 ppm As(III) at the ratio 1:1. The spectra of AgNPs containing As(III) were

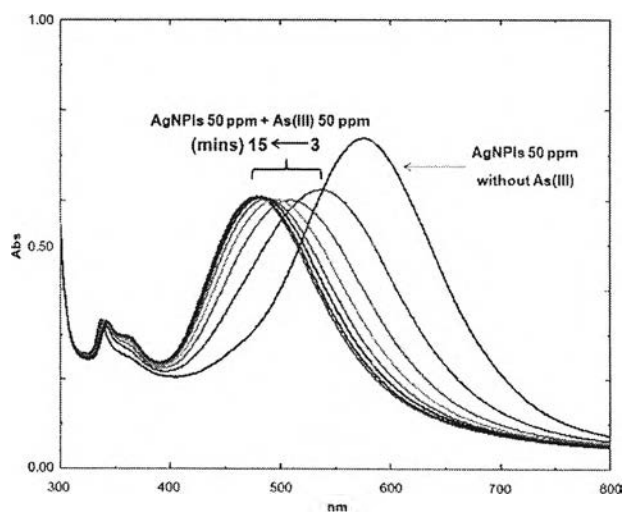


Fig. 1. The UV–vis spectra of AgNPs at 50 ppm without As(III) added (Blue line) and with 50 ppm As(III) addition, which were recorded every 2 min for 15 min started from the third minute after adding As(III) to AgNPs. (For interpretation of the references to color in this figure legend, the reader is referred to the web version of this article.)

recorded for 15 min to monitor the optical changes of AgNPLs. After As(III) addition to AgNPLs, the color of AgNPLs gradually changed from dark blue to yellow (maximum absorption occurred at approximately 470 nm) within 7 min. Subsequent to this no further change in color was observed.

The concentrations of AgNPLs also effected for As detection. To achieve the optimum concentration of AgNPLs for As detection, the series of 25, 50, 100, 150, and 200 ppm of AgNPLs were treated with different concentrations of As(III). 50 ppm of AgNPLs provided the best sensitivity for As detection with LOD of 0.5 ppm. With 25 ppm AgNPLs, LOD was found to be 5 ppm, while higher concentrations of AgNPLs than 50 ppm also presented less sensitivity for As detection. In the case of too high concentrations of AgNPLs, dark blue color can interfere the visual resulting in difficulty to differentiate the slightly-changed color. However, too low concentrations cause poor sensitivity for As detection. Therefore, 50 ppm of AgNPLs was chosen as the optimal concentration for the further studies.

In aqueous systems, arsenic normally exists in the form of oxyanion either arsenite or arsenate depending on the conditions of the water. Thus, behaviors of both As(III) and As(V) on changing color of AgNPLs were studied. Interestingly, both As(III) and As(V) resulted in the similar color changes of AgNPLs (Fig. 2). Therefore, the AgNPLs at the concentration of 50 ppm provided detection range for inorganic arsenic between 0.5–30 ppm. The color of AgNPLs was changed from dark blue to purple, pink, orange, and yellow according to the concentrations of As presented from low to high levels in the tested solutions. The solutions which contain As more than 30 ppm turned the color of AgNPLs to undifferentiated yellow color. Since inorganic arsenic resulted in a blue shift effect, namely maximum absorption of AgNPLs was decreased in the presence of As(III) and As(V), this indicated that the sizes of AgNPLs become smaller upon the increased concentrations of As. Therefore, the changes of AgNPL colors are not caused by aggregation mechanism. In addition, as both As(III) and As(V) demonstrated the same behavior on the AgNPL-color changes, thus, oxidation of Ag(0) to Ag(I) by As(III) is not a promising mechanism. The reduction potential of Ag(I) is also higher than those of As(III) and As(V). To confirm the origin of the observed color changes of the AgNPLs, transmission electron microscope (TEM) was exploited. Predictably, the TEM images (Fig. 3) show that arsenic ions caused a decrease in the size AgNPLs by dispersion resulting in the blue-shift effect observed in UV-vis spectra.

3.2. Selectivity of AgNPLs for As detection using ferrihydrite-coated silica gel

The selectivity of AgNPLs for inorganic As was studied by treating AgNPLs with several potential interferences including CaCl₂, HgCl₂, NaCl, Na₂CO₃, Na₃PO₄, NH₄Cl, MgCl₂, MgSO₄, Pb(NO₃)₂, and ZnCl₂. All of the studied salts were prepared at the concentration of 2,000 ppm, and added individually to 50 ppm AgNPLs with the ratio of 1:1. Chloride salts were found to interfere As detection, as they were able to change the color of dark blue AgNPLs, while metal ions with other counter anions; CO₃²⁻, PO₄³⁻, SO₄²⁻, and NO₃⁻, had no effect on changing the color of the original AgNPLs. As the color of AgNPLs was not selectively changed only by arsenite and arsenate, different observed chloride salts showed different effects on the color changes with different mechanisms [36]. The tolerant levels of AgNPL-color changes on the presence of these chloride salts were as follows: 40 ppm for NaCl and ZnCl₂, 30 ppm for CaCl₂, 20 ppm for NH₄Cl, 15 ppm for MgCl₂, and 5 ppm for HgCl₂.

To overcome the interference effect from other metal ions and their counter anions, iron oxide (ferrihydrite)-coated silica gel was exploited to adsorb only As(III) and As(V) to the surface of the

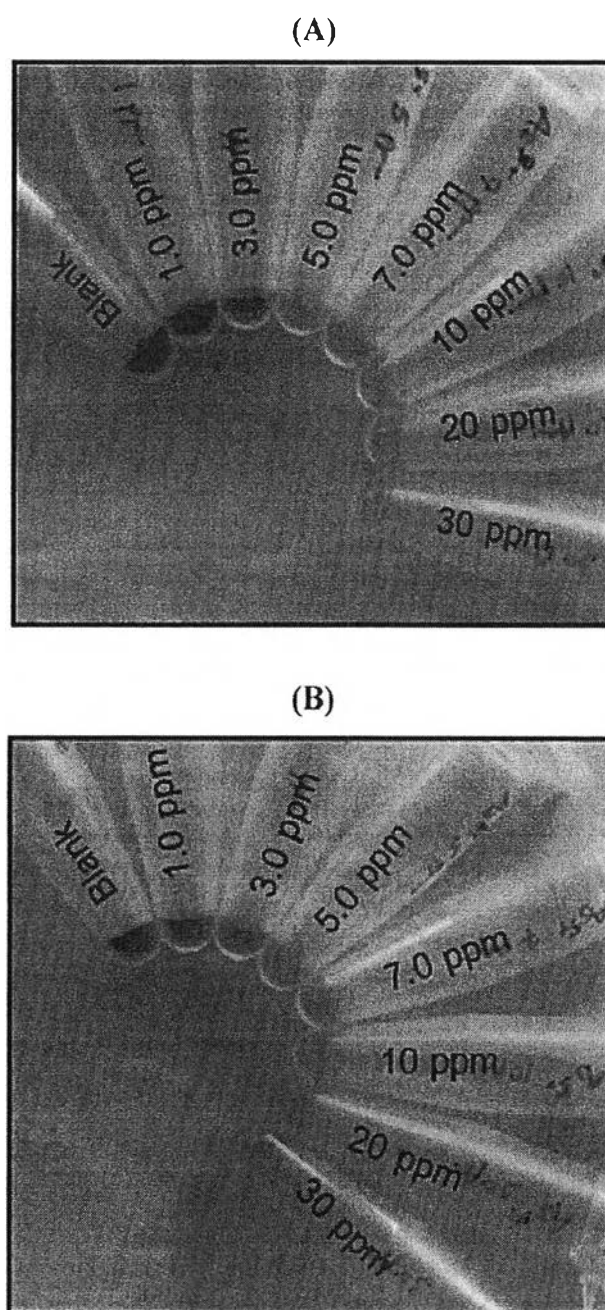


Fig. 2. Color changes of 50 ppm AgNPLs after the addition of (A) As(III) and (B) As(V) at different final concentrations.

adsorbent prior to As detection. Arsenic in water is normally presented as arsenic oxyanion; arsenite (AsO₃³⁻) and arsenate (AsO₄³⁻). Iron-oxide is well known and has been used as As adsorbent material to remove As from water due to the great affinity towards arsenic. Several kinds of iron-oxide have been developed for As removal [44–47]. In this work, ferrihydrite-coated silica gel (SiO₂-Fh) was applied for As detection, since its selectivity to As adsorption and allowing the adsorbed As to be detected by AgNPLs.

The 0.3 g of SiO₂-Fh was stirred for 45 min in the As(III) solutions 100 mL containing 6 chlorides salts including HgCl₂, MgCl₂, CaCl₂, NH₄Cl, ZnCl₂, and NaCl of which the concentration of each salt is 2000 ppm. The solid was then filtrated and washed with 200 mL deionized water, and oven dried. The dried solid was divided approximately 0.03 g for As test. After the 50 μL of AgNPLs

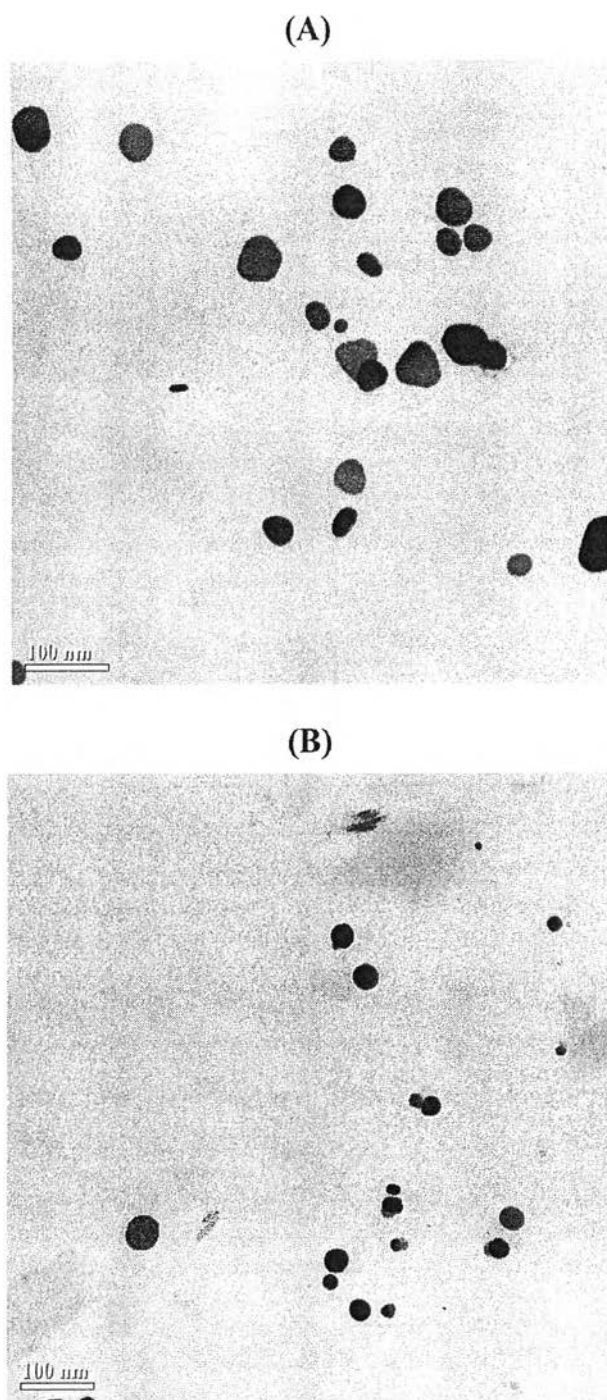


Fig. 3. TEM images of 50 ppm AgNPs without (A) and with (B) 20 ppm As(III) addition.

was applied to the As-adsorbed $\text{SiO}_2\text{-Fh}$, the blue color of AgNPs was changed immediately according to the concentrations of As adsorbed onto the $\text{SiO}_2\text{-Fh}$ without interference effect from chloride salts in the solution. Fig. 4 demonstrates the color changes of AgNPs covered on the $\text{SiO}_2\text{-Fh}$ applied to the solutions containing 1.0 and 5.0 ppm As(III) (Fig. 4B.2 and B.4, respectively) in the presence of chloride salts. There was no difference between the colors of AgNPs applied to standard As(III) solutions with no chloride salts (Fig. 4B.1 and B.3) and applied to $\text{SiO}_2\text{-Fh}$ after As adsorption in the presence of chloride salts.

However, the amounts of $\text{SiO}_2\text{-Fh}$ and also the volumes of

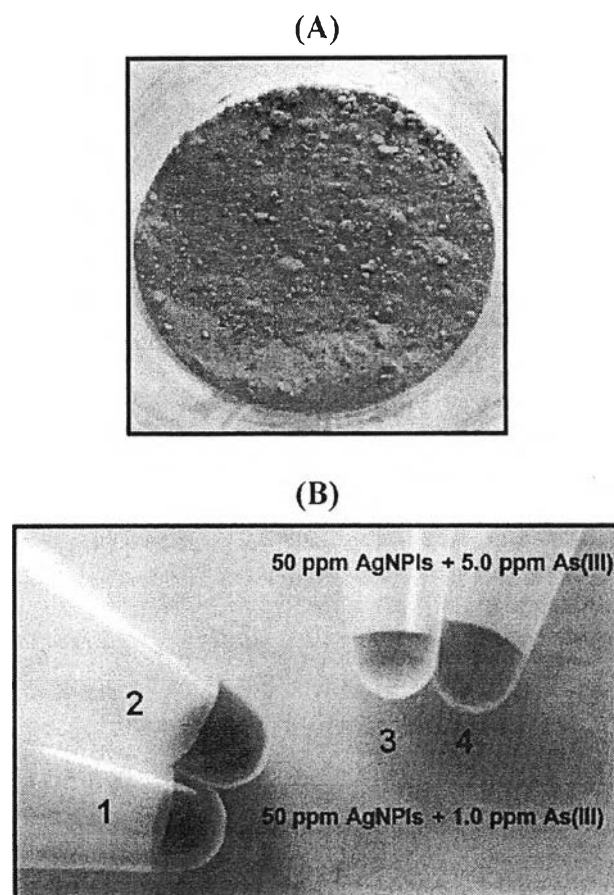


Fig. 4. (A) Physical appearance of ferrihydrate-coated silica gel. (B) Comparing the colors of AgNPs between the application to standard As(III) solutions, 1.0 and 5.0 ppm, with no chloride salts (B.1 and B.3, respectively) and application to $\text{SiO}_2\text{-Fh}$ after As adsorption in the presence of chloride salts (B.2 and B.4).

testing solution used in As adsorption protocol influence sensitivity of As detection. With higher amounts of $\text{SiO}_2\text{-Fh}$ or lower volumes of solution, the sensitivity is reduced, while lower amounts of $\text{SiO}_2\text{-Fh}$ or higher volumes of solution can improve sensitivity for As detection. The 1.0 g of $\text{SiO}_2\text{-Fh}$ was preliminary employed for As adsorption. The color changes of AgNPs were not observed from the $\text{SiO}_2\text{-Fh}$ treated to As solutions with concentrations less than 30 ppm (data not shown). Therefore, the sensitivity of As detection using this approach can be improved by reducing the amount of $\text{SiO}_2\text{-Fh}$ and increasing the volume of testing solution.

To elucidate the detection of both As(III) and As(V) using the combination of $\text{SiO}_2\text{-Fh}$ and AgNPs, adsorption of As(V) onto $\text{SiO}_2\text{-Fh}$ prior to the detection with AgNPs was also carried out. Since the sensitivities of As(III) and As(V) detection using AgNPs without adsorption onto $\text{SiO}_2\text{-Fh}$ were not significantly different, the results of using $\text{SiO}_2\text{-Fh}$ to adsorb As(III) and As(V) prior to the detection also provided the similar color changes of AgNPs. Fig. 5 shows the appearance of color changes of AgNPs after As adsorption protocol. The tested solutions also contained chloride salts at the concentration of 2000 ppm. At the same concentration of As(III) and As(V) in the solutions, the same color of AgNPs was observed. In addition, the total inorganic arsenic was also determined by using the developed method, as the color changes of AgNPs applied to the mixture solution of As(III) and As(V) represented total amount of both As species in the solution.

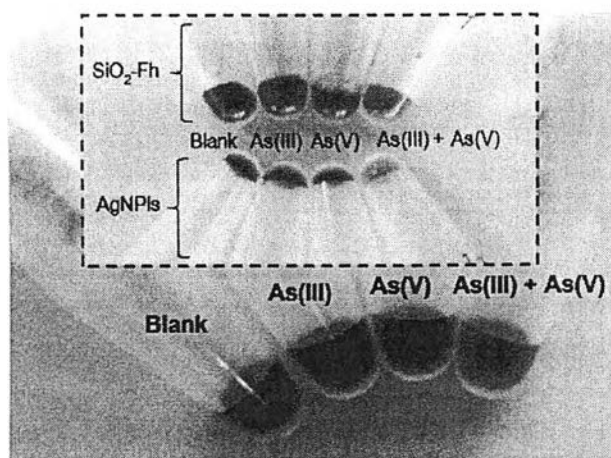


Fig. 5. The color changes of AgNPIs applied to As-adsorbed $\text{SiO}_2\text{-Fh}$ with different As concentrations; no arsenic (blank), 2.5 ppm As(III), 2.5 ppm As(V), and 2.5 ppm As(III)+2.5 ppm As(V). An inset presents the appearance of the AgNPI solutions separated from their $\text{SiO}_2\text{-Fh}$ solid.

3.3. Analysis of real sample

After the proposed approach was successfully applied to standard As solutions, samples of natural water including tap water, groundwater, and canal water were tested. A series of samples with different As concentrations were determined using the proposed approach. As shown in Fig. 6, there was no color change of AgNPIs applied to groundwater with no standard As added. However, the pretreated groundwater samples with 1.0, 10.0, and 20.0 ppm standard As resulted in color changes of AgNPIs from blue to purple, orange, and yellow, respectively, which corresponded to the results of standard As detection. In addition, a series of samples of tap water and canal water showed the similar results to the groundwater, which means that As contaminations in the selected natural water samples are less than 0.5 ppm.

ICP-OES was also performed to determine concentration and recovery of As in the real samples. The results are shown in

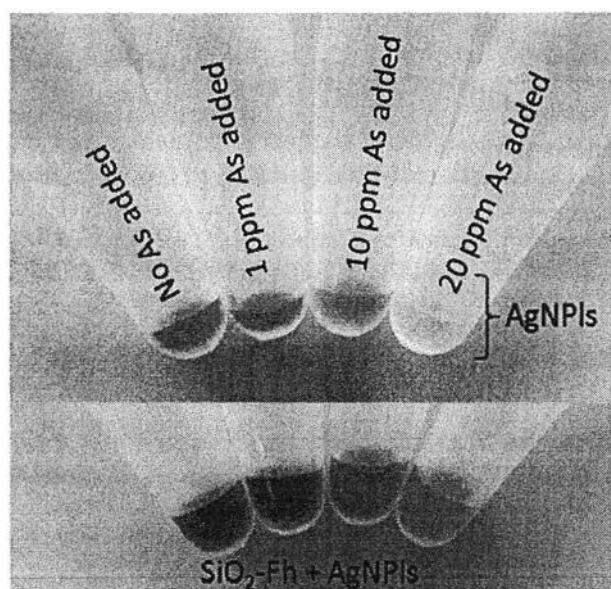


Fig. 6. The color changes of AgNPIs applied to As-adsorbed $\text{SiO}_2\text{-Fh}$ from the pretreated canal water samples; no arsenic added, 1.0 ppm As(III), 10.0 ppm As(III), and 20.0 ppm As(III) (lower). The upper presents the appearance of the AgNPI solutions separated from their $\text{SiO}_2\text{-Fh}$ solid.

Table 1
The results of As(III) determination in real sample ($n=3$) using ICP-OES and the proposed method.

Samples	ICP-OES				Proposed method Conc. of As (ppm) compared to the colors of standard As
	Added (ppm)	Found (ppm)	Recovery (%)	RSD (%)	
Tap water	0.0	ND	–	–	< 0.5
	1.0	1.05	105.0	1.27	1–2
	10.0	8.48	84.8	0.63	5–10
	20.0	17.04	85.2	0.33	15–20
Ground water	0.0	ND	–	–	< 0.5
	1.0	0.92	92.0	0.18	1–2
	10.0	8.30	83.0	0.35	5–10
	20.0	16.82	84.1	0.38	15–20
Canal water	0.0	ND	–	–	< 0.5
	1.0	1.01	101.0	0.44	1–2
	10.0	8.37	83.7	0.54	5–10
	20.0	17.58	87.9	0.62	15–20

ND is not detectable.

Table 1, the recovery of As(III) was between 84.8–105.0% for tap water, 83.0–93.0% for groundwater, and 83.7–101.0% for canal water. Moreover, arsenic in all of real samples cannot be detected which agreed with the results obtained from the developed approach, indicating that the approach was practically applicable for the detection of inorganic arsenic in real samples.

4. Conclusions

The inorganic arsenic screening method has been developed based on colorimetric detection using AgNPIs which are able to change the color in the presence of As in the tested solution. The visible color changes were observed with the blue shift of absorption spectra of AgNPIs suggesting that the average particle size of the AgNPIs decreased as the As concentration increased resulting from AgNPI dispersion in the presence of As in the solution. In addition, the $\text{SiO}_2\text{-Fh}$ was exploited to overcome interference from other ions potentially existing in the tested solution. With the naked eye, LOD of As was 0.5 ppm with the detection range between 0.5–30 ppm. Total inorganic As determination can be achieved using this developed method, as both arsenite and arsenate can be adsorbed onto the $\text{SiO}_2\text{-Fh}$ and they also exhibited the same sensitivity on AgNPI optical detection. Therefore, this method can be applicable for screening As levels in water samples or monitoring quality of wastewater after a treatment.

Acknowledgments

The authors acknowledge scholarship support from Srinakharinwirot University, Thailand (Grant no. 044/2557), and partial support from the Thailand Research Fund through Research Team Promotion Grant (RTA5780005).

Appendix A. Supplementary material

Supplementary data associated with this article can be found in the online version at <http://dx.doi.org/10.1016/j.talanta.2016.03.028>.

References

- [1] K.S. Squibb, B.A. Fowler, Biochemical mechanisms of arsenical toxicity, in: F. A. Fowler (Ed.), *Biological and Environmental Effects of Arsenic*, Elsevier, Amsterdam, 1983, pp. 233–270.
- [2] N.E. Korte, Q. Fernando, *Crit. Rev. Environ. Ctrl.* 21 (1991) 1–39.
- [3] F.H. Ko, S.L. Chen, M.H. Yang, *J. Anal. Atom. Spectrom.* 12 (1997) 589–595.
- [4] J.R. Behari, R. Prakash, *Chemosphere* 63 (2006) 17–21.
- [5] A.N. Anthemidis, G.A. Zachariadis, J.A. Stratis, *Anal. Chim. Acta* 547 (2005) 237–242.
- [6] R. Schaeffer, C. Soeroes, I. Ipolyi, P. Fodor, N.S. Thomaidis, *Anal. Chim. Acta* 547 (2005) 109–118.
- [7] J. Mattusch, R. Wennrich, A.C. Schmidt, W. Reisser, *Fresenius J. Anal. Chem.* 366 (2000) 200–203.
- [8] M.K. Paik, M.J. Kim, W.I. Kim, J.H. Yoo, B.J. Park, G.J. Im, J.E. Park, M.K. Hong, *J. Korean Soc. Appl. Biol. Chem.* 53 (2010) 634–638.
- [9] X.C. Le, W.R. Cullen, K.J. Reimer, *Talanta* 41 (1994) 495–502.
- [10] E. Bulska, P. Tschopel, J.A.C. Broekaert, G. Tolg, *Anal. Chim. Acta* 271 (1993) 171–181.
- [11] B.A. Fernandez, C.V.H. Temporano, dI.C. Fernandez, D.L. Campa, A. Sanz-Medel, P. Neil, *Talanta* 39 (1992) 1517–1523.
- [12] E. Bulska, J.A.C. Broekaert, P. Tschopel, G. Tolg, *Anal. Chim. Acta* 276 (1993) 377–384.
- [13] I. Eguiarte, R.M. Alonso, R.M. Jimenez, *Analyst* 121 (1996) 1835–1838.
- [14] G. Henze, W. Wagner, S. Sander, *Fresenius J. Anal. Chem.* 358 (1997) 741–744.
- [15] T. Ferri, R. Morabito, B.M. Petronio, E. Pitti, *Talanta* 36 (1989) 1259–1263.
- [16] H. Li, R.B. Smart, *Anal. Chim. Acta* 325 (1996) 25–32.
- [17] Z. Mester, P. Fodor, *Spectrochim. Acta B* 52 (1997) 1763–1771.
- [18] J. Moreda-Pineiro, M.L. Cervera, M. de la Guardia, *J. Anal. At. Spectrom.* 12 (1997) 1377–1380.
- [19] W.M. Mok, C.M. Wai, *Talanta* 35 (1988) 183–186.
- [20] K.W. Sims, E.S. Gladney, *Anal. Chim. Acta* 251 (1991) 297–303.
- [21] P.D. Zhang, G.W. Xu, J.H. Xiong, Y.F. Zheng, Q. Yang, F.S. Wei, *J. Sep. Sci.* 25 (2002) 155–159.
- [22] E.J. Prest, S.J. Baldock, P.R. Fielden, N.J. Goddard, B.J. Treves Brown, *J. Chromatogr. A* 990 (2003) 325–334.
- [23] S. Saverwyns, X. Zhang, F. Vanhaecke, R. Cornelis, L. Moens, R. Dams, *J. Anal. At. Spectrom.* 12 (1997) 1047–1052.
- [24] C. Demesmay, M. Olle, M. Porthault, *Fresenius J. Anal. Chem.* 348 (1994) 205–210.
- [25] W. Holak, *Anal. Chem.* 41 (1969) 1712–1713.
- [26] C.K. Darbha, A.K. Singh, U.S. Rai, E. Yu, H. Yu, P.C. Ray, *J. Am. Chem. Soc.* 130 (2008) 8038–8043.
- [27] D. Li, A. Wieckowska, I. Willner, *Angew. Chem. Int. Ed. Engl.* 47 (2008) 3927–3931.
- [28] T. Li, S. Dong, E. Wang, *Anal. Chem.* 81 (2009) 2144–2149.
- [29] X. Xue, F. Wang, X. Liu, *J. Am. Chem. Soc.* 130 (2008) 3244–3245.
- [30] J.R. Kalluri, T. Arbneshi, S.A. Khan, A. Neely, P. Candice, B. Varisli, M. Washington, S. McAfee, B. Robinson, S. Banerjee, A.K. Singh, D. Senapati, P. C. Ray, *Angew. Chem. Int. Ed.* 48 (2009) 9668–9671.
- [31] M. Lakatos, S. Matys, J. Raff, W. Pompe, *Talanta* 144 (2015) 241–246.
- [32] W.L. Daniai, M.S. Han, J.S. Lee, C.A. Mirkkin, *J. Am. Chem. Soc.* 131 (2009) 6362–6363.
- [33] N. Xiao, C. Yu, *Anal. Chem.* 82 (2010) 3659–3663.
- [34] J.D.S. Newman, J.M. Robert, G.J. Blanchard, *Anal. Chem.* 79 (2007) 3443–3454.
- [35] X. Zhang, H. Zhao, Y. Xue, Z. Wu, Y. Zhang, Y. He, X. Li, Z. Yuan, *Biosens. Bioelectron.* 34 (2012) 112–117.
- [36] A. Apilux, W. Siangproh, N. Praphairaksit, O. Chailapakul, *Talanta* 97 (2012) 388–394.
- [37] S. Stanly, John Xavier, M.S. Selvakumar, D. Prem Anand, A. Pius, *SAX* 4 (2013) 103–110.
- [38] Y. Wang, F. Yang, X. Yang, *ACS Appl. Mater. Interfaces* 2 (2010) 339–342.
- [39] H.K. Sung, S.Y. Oh, C. Park, Y. Kim, *Langmuir* 29 (2013) 8978–8982.
- [40] M.L. Pierce, C.B. Moore, *Water Res.* 16 (1982) 1247–1253.
- [41] J.G. Hering, P.Y. Chen, J.A. Wilkie, M. Elimelech, S. Liang, *J. Am. Water Works Ass.* 88 (1996) 155–167.
- [42] J. Kim, M.M. Benjamin, *Water Res.* 38 (2004) 2053–2062.
- [43] F.P. Garciaa, F.P. Morenob, Y.M. Santillana, *IJAST* 2 (2012) 14–16.
- [44] J.I. Oh, K.K. Yamamoto, H. Kitawaki, S. Nakao, T. Sagawara, M.M. Rahaman, M. H. Rahaman, *Desalination* 132 (2000) 307–314.
- [45] E. Arifin, J. Cha, J.K. Lee, *Bull. Korean Chem. Soc.* 34 (2013) 2358–2366.
- [46] L. Zeng, *Water Res.* 37 (2003) 4351–4358.
- [47] S. Zhang, H. Niu, Y. Cai, X. Chao, Y. Shi, *Chem. Eng. J.* 158 (2010) 599–607.
- [48] G.S. Zhang, J.H. Qu, H.J. Liu, R.P. Liu, G.T. Li, *Environ. Sci. Technol.* 41 (2007) 4613–4619.
- [49] X. Guo, F. Chen, *Environ. Sci. Technol.* 39 (2005) 6808–6818.
- [50] W. Chen, R. Parette, J. Zou, F.S. Cannon, B.A. Dempsey, *Water Res.* 41 (2007) 1851–1858.
- [51] A. Gupta, N. Sankararamkrishnan, *Bioresour. Technol.* 101 (2010) 2173–2179.



ELSEVIER

Contents lists available at ScienceDirect

Talanta

journal homepage: www.elsevier.com/locate/talanta

Novel colorimetric assay for paraquat detection on-silica bead using negatively charged silver nanoparticles

Weena Siangproh^a, Thachkorn Somboonsuk^a, Orawan Chailapakul^b, Kriangsak Songsrirote^{a,*}

^a Department of Chemistry, Faculty of Science, Srinakharinwirot University, Sukhumvit 23, Wattana, Bangkok 10110, Thailand

^b Electrochemistry and Optical Spectroscopy Research Unit, Department of Chemistry, Faculty of Science, Chulalongkorn University, 254 Phayathai Road, Pathumwan, Bangkok 10330, Thailand

ARTICLE INFO

Keywords:

Paraquat
Silver nanoparticles
Colorimetry
On-silica bead
Optical detection

ABSTRACT

A simple, rapid, sensitive, and economical method based on colorimetry for the determination of paraquat, a widely used herbicide, was developed. Citrate-coated silver nanoparticles (AgNPs) were synthesized as the colorimetric probe. The mechanism of the assay is related to the aggregation of negatively charged AgNPs as induced by positively-charged paraquat resulting from coulombic attraction which causes the color to change from a deep greenish yellow to pale yellow in accordance with the concentrations of paraquat. Silica gel was exploited as the paraquat adsorbent for purification and pre-concentration prior to the direct determination with negatively charged AgNPs without the requirement of the elution step. The validity of the proposed approach was evaluated by spiking standard paraquat in water and plant samples. Recoveries of paraquat in water samples were 93.6% and 95.4% for groundwater and canal water, respectively, while those in plant samples were 89.5% and 86.6% for Chinese cabbage and green apple, respectively, after using the optimized extraction procedure. The absorbance of AgNPs at 400 nm was linearly related to the concentration of paraquat over the range of 0.05–50 mg L⁻¹, with detection limits of 0.05 mg L⁻¹ for water samples, and 0.10 mg L⁻¹ for plant samples by naked eye determination.

1. Introduction

Paraquat (1,1-dimethyl-4,4-bipyridium dichloride) is a fast-acting non-selective contact herbicide. It has been widely used as an active component in several commercial herbicides to control broad-leaved weeds in both agricultural and non-agricultural areas in over 130 countries since 1962. Although residual paraquat can be degraded by microbiological and photochemical processes, the slowness of the degradation process, as well as the overuse of paraquat, increases the contamination risk for the environment, consequently causing a potential danger for human and animal health. Therefore, it has been banned in some countries [1]. However, due to its relatively low cost and high efficiency, paraquat is unlikely to be superseded in the near future, resulting in illicit usage, and it is still legally used in several countries. Hence, large-scale usage of paraquat will be a long-lasting problem of serious concern.

As it is one of the most commonly used herbicides worldwide, agricultural workers are easily exposed to it from either accidental or direct contact, resulting in a problem for human health. In addition, with a property of high solubility in water, an intensive use of paraquat

also damages the aquatic environment affecting algae, fish, insects, and other aquatic organisms [2]. Thus, contamination of paraquat in water is a great concern. Moreover, exposure to paraquat and other pesticides can potentially occur through residues on food crops, as the human diet consists largely of vegetables and fruit. Therefore, plants are effective carriers of paraquat to the consumer, as paraquat is absorbed into plant cells easily and simple washing may not adequately remove it completely. The maximum content of paraquat residue allowed in most foodstuffs is 0.05 mg/kg [1], and the acceptable daily intake is 0.004 mg/kg (body weight) [1,3].

There is a wide variety of analytical techniques which have been reported for paraquat determination such as gas and liquid chromatography [4,5], mass spectrometry [6], electrophoretic methods [7,8], electrochemistry [9–11], flow injection analysis [12], and spectrophotometry [13–15]. Although these techniques can be effectively used for paraquat determination with high selectivity and sensitivity, they are however time-consuming, sample-treatment requiring techniques, complicated in operation with high cost, and off-site detection. Therefore, it will be very useful to have a simple tool which everyone can use for quickly screening paraquat levels on-site to obtain real-time

* Corresponding author.

E-mail address: kriangsaks@g.swu.ac.th (K. Songsrirote).

determination.

Visualizing the color changes is one of the simplest ways to interpret a signal for everyone, with no scientific skill needed. The reduction of paraquat solution in an alkaline medium to develop a blue color is a well-known reaction, as intensity of the developed color simply represents paraquat levels. Several reactions based on conversion of color after treatment with reducing agents such as sodium borohydride, sodium dithionite, and natural reducing agents e.g. ascorbic acid and glucose have been reported for paraquat determination using simple colorimetry. Each of these provides different advantages and disadvantages in different applications [12–14,16–19].

With distinctively optical properties, nanotechnology is rapidly growing in the field of optical detections, as nanoparticles (NPs) have unique physical, chemical, and biological properties compared to their macro-scaled counterparts. Different types of NPs provide different optical, fluorescent and magnetic properties. Therefore, optical properties related to the size and shape of NPs, especially gold- and silver-NPs, show potential for exploitation in a wide range of applications. Gold nanoparticles (AuNPs) have been intensively studied for numerous applications as optical sensors for heavy metals [20–22], aromatic compounds [23], stimulants [24], etc. The optical detection of organophosphate and organophosphonate species, used as nerve agents and pesticides, using silica microparticles in conjunction with AuNPs, has been demonstrated [25]. Colorimetric detections of heavy metals using AgNPs were also reported for environmental [26] and biological sample [27] analyses. In addition, paraquat determination using cyclen dithiocarbamate-functionalized AgNPs for colorimetric sensing has previously been presented [28].

In this work, the determination of paraquat using a simple synthesized negatively charged AgNPs as a colorimetric probe is proposed. Due to size and shape dependences, the negatively charged AgNPs were aggregated by the coulombic attraction with paraquat, positively charged species, causing the color changes. Moreover, silica gel was employed for paraquat purification and concentration to improve the detection performance prior to the determination using negatively charged AgNPs. The applications of silica gel as an adsorbent for quaternary ammonium herbicides were well documented by Pico, et al. [29]. From our best knowledge, this is the first report on the use of silica gel and AgNPs for pre-concentration and detection of paraquat. The proposed approach was also applied for determining paraquat in contaminated water and plant samples.

2. Experimental section

2.1. Chemicals and materials

Analytical grade reagents and 18 M Ω cm deionized (DI) water (obtained from a Millipore Milli-Q purification system) were used throughout. Paraquat, diquat, difenzoquat, and silver nitrate (AgNO₃) were purchased from Sigma-Aldrich. Sodium borohydride (NaBH₄), sodium hydroxide (NaOH), hydrochloric acid (HCl), sulfuric acid (H₂SO₄), trisodium citrate (TSC), and methanol (MeOH) were purchased from Merck. The salts for interference study were purchased from Analytica univar reagent Ajax Finechem. Silica gel with particle size of 0.05–0.20 nm was purchased from Carlo Erba Reagenti. Plant samples were purchased from a local supermarket.

2.2. Preparation of negatively charged silver nanoparticles

The protocol for synthesizing AgNPs was adapted from S. Agnohotri, et al. [30]. Briefly, 40 mL of the mixture of 5×10^{-4} mol L⁻¹ NaBH₄ and 3.5×10^{-3} mol L⁻¹ TSC was heated at 60 °C for 30 min in the dark with vigorous stirring. Then, 10 mL of 2.0×10^{-3} mol L⁻¹ AgNO₃ was added drop-wise to the mixture while the temperature was increased to 90 °C. Then, the pH of the solution was adjusted to 10.5 using 0.1 mol L⁻¹ NaOH while the heating was

continued for 20 min until the color of the reaction changed to a deep greenish-yellow solution. The synthesized AgNPs were then allowed to cool at room temperature and stored at 4 °C until use.

2.3. Sample preparation for the determination of paraquat in water and plant samples with silica gel adsorbent

2.3.1. Determination of paraquat in water

Natural groundwater and canal water were collected in PTFE bottles. Approximate 0.2 g of silica gel was added to the 50 mL of filtered sample solutions and then stirred at a speed of around 300–500 rpm for 30 min. The beads were then collected using vacuum filtration and washed with a large volume of DI water. The beads were then oven-dried at 50 °C for 1 h, and stored in a plastic vial until the determination.

2.3.2. Determination of paraquat in plants

In this study, chinese cabbage and green apples were selected as a model for determining paraquat in plants. Several extraction procedures previously reported were adapted and carried out to compare the extraction efficiency for paraquat detection [1,13,28–32]. To evaluate extraction efficiency, 10 g of plant samples was weighed and homogenized. Then, 500 μ L of the paraquat standard (1000 mg L⁻¹) was added and the slurry was allowed to stand for 10 min prior to the addition of 20 mL of each extraction solvent including (I) 6 mol L⁻¹ H₂SO₄, (II) 6 mol L⁻¹ HCl, (III) 50:50 MeOH/0.1 mol L⁻¹ HCl, and (IV) DI water. The extractions using the above extraction solvent were performed in two different conditions of either a water bath at 80 °C or sonication at 50 °C for 30 min. Then, the extract was centrifuged at 5000 rpm for 10 min. An aliquot was filtered through a syringe filter (0.45 μ m), and transferred to a plastic bottle and made up to a final volume of 50 mL with DI water. In addition, the acidic extraction solutions were neutralized with 1 mol L⁻¹ NaOH before the pre-concentration step. Approximately 0.2 g of silica gel was added to the diluted extract solutions and then stirred at a speed of around 300–500 rpm for 30 min. The beads were then collected using vacuum filtration and washed with a large volume of DI water. The beads were oven-dried at 50 °C for 1 h, and then stored in a plastic vial until the determination. Because it was found that paraquat had strong absorption to glassware [1,32], plasticware was used throughout the experiment.

2.4. Colorimetric measurement of paraquat using AgNPs probe

The absorption spectra of the AgNPs either added directly to in-solution paraquat or to on-silica bead paraquat were obtained using a UV–Vis absorption spectrometer (Shimadzu, 2401 PC) with an ultramicroquartz cuvette for micro-scale analysis. In the case of direct reaction between AgNPs and sample solution, 50 μ L of AgNPs was added to 50 μ L of the sample solution. For determining paraquat adsorbed onto silical gels, 100 μ L of AgNPs was added to 0.05 g of silica gels. In both cases, the mixtures were well mixed, and allowed to stand for 5 min prior to the colorimetric measurement.

2.5. Method validation experiments

Both external standard (using DI water or extraction solution as a dilution solvent) and standard addition calibrations over a working range of 0.01–50.0 mg L⁻¹ were constructed to monitor the matrix effect in the samples. Approximately 0.2 g of silica gel was added to the standard solutions and extraction solutions of spiked samples following the protocol of sample preparation.

The results obtained from the proposed approach were compared with the conventional colorimetric method of paraquat reduction by using NaBH₄ in an alkaline medium. Briefly, 0.05 g of paraquat-adsorbed silica gels was transferred to a plastic vial, and then 50 μ L

of saturated ammonium chloride was added to elute the paraquat. 100 μL of 1% NaBH_4 (aq) and 300 μL of 2 mol L^{-1} NaOH were then added [13]. The absorbance of the blue solution of paraquat radical cation was measured at 605 nm using a UV-Vis absorption spectrometer (Shimadzu, 2401 PC).

3. Results and discussions

3.1. Synthesis and characterization of negatively charged silver nanoparticles

The AgNPs were synthesized using NaBH_4 as the primary reductant and TSC as the secondary reductant as well as stabilizing agent. After finishing the preparation protocol, a deep greenish yellow solution was obtained with a particle size of approximately 40 nm according to transmission electron microscope (TEM) measurement. The solution of suspended AgNPs was characterized using UV-Vis spectrophotometry, and maximum absorption (λ_{max}) at 400 nm was observed. The mechanism of negatively charged AgNPs formation is well described by Agnohotri et al. [30].

3.2. The color changes of AgNPs upon paraquat concentrations

In a preliminary observation, the concentration of AgNPs was optimized for paraquat determination, as at high concentrations the dark color of AgNPs causes difficulty for monitoring the color changes, while too low concentrations result in poor sensitivity of detection. Therefore, 50 μL of 70 mg L^{-1} of negatively charged AgNPs was added to 50 mL of paraquat solutions for paraquat detection by using AgNPs as the colorimetric probe. The color of AgNPs changed from yellow to metallic black with increasing concentrations of paraquat (Fig. 1) resulting from the aggregation of negatively charged AgNPs induced by positively charged paraquat. At high concentrations of paraquat, the aggregation of AgNPs suspended in the solution began to develop a dark metallic color which was clearly observed by the naked eye, and the aggregated AgNPs accumulated and eventually settled to the bottom of the vial.

3.3. Interference for paraquat determination

The selectivity of the synthesized AgNPs was assessed by investigating the effect of other quaternary ammonium pesticides and some salts in the analysis of paraquat (Fig. 2). The tolerance limit levels of different foreign species on the color change of AgNPs are presented in Table 1.

Diquat caused a color change in AgNPs similar to paraquat with a little less sensitivity, possibly due to related structures between the two compounds, while the AgNPs showed a very high tolerance to difenzoquat. In addition, different salts affected the color change of the AgNPs at different tolerance values, in which Cu^{2+} had the lowest

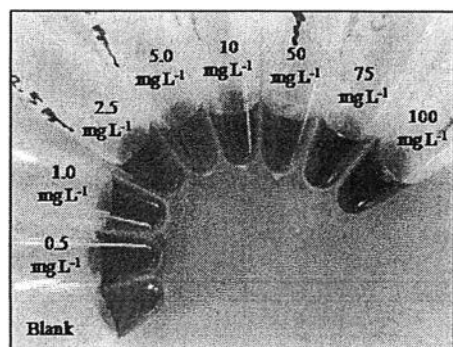


Fig. 1. The colors of 70 mg L^{-1} AgNPs added with different paraquat solutions from 0 to 100 mg L^{-1} .

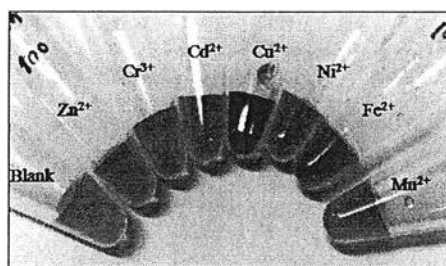


Fig. 2. The effect of heavy metal salts (100 mg L^{-1} of Zn^{2+} , Cr^{3+} , Cd^{2+} , Cu^{2+} , Ni^{2+} , Fe^{2+} , and Mn^{2+}) on the color change of AgNPs.

Table 1

Effect of foreign species on the color change of AgNPs (50 μL , 70 mg L^{-1}).

Foreign species	Tolerance limit (mg L^{-1})	Foreign species	Tolerance limit (mg L^{-1})
Paraquat	10	Ni^{2+} , Fe^{2+}	500
Diquat	20	Zn^{2+} , Cd^{2+}	120
Difenzoquat	2000	Mn^{2+}	100
Cr^{3+}	1000	Cu^{2+}	30

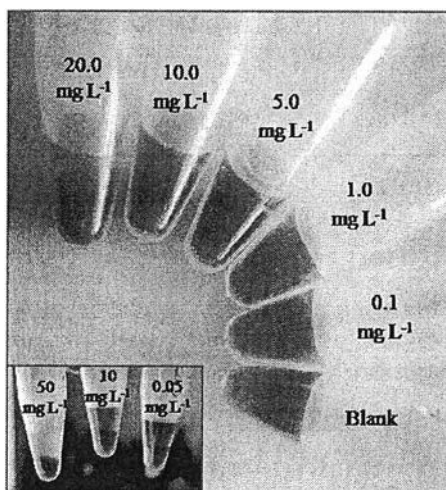


Fig. 3. The appearance of 70 mg L^{-1} AgNPs added to different concentrations of paraquat adsorbed on silica gel.

tolerance limit, while the system could easily tolerate the contamination of Cr^{3+} . The selectivity of the AgNPs on paraquat detection could be mainly from the size of paraquat, which possibly fits well with the size of the AgNPs. In addition, paraquat is relatively large when compared to the size of heavy metal salts. This could lead to a more aggregation-induced effect of the AgNPs. Consequently, the color change of the AgNPs solution is more clearly visualized. Moreover, there are two charged sites on the structure of paraquat dissolved in an aqueous solution. This could increase an interaction opportunity between paraquat and the AgNPs. The detection of difenzoquat showed poor sensitivity possibly because of its relatively low solubility in water compared to paraquat, and there is only one charged site on the structure.

3.4. Application of silica gel as paraquat adsorbent prior to the detection with AgNPs

As shown in Fig. 1, using the naked eye, the color of less than 10 mg L^{-1} paraquat-added AgNPs solutions cannot be differentiated from the color of blank AgNPs. Owing to such a poor limit of the direct in-solution detection, pre-concentration protocol was required to

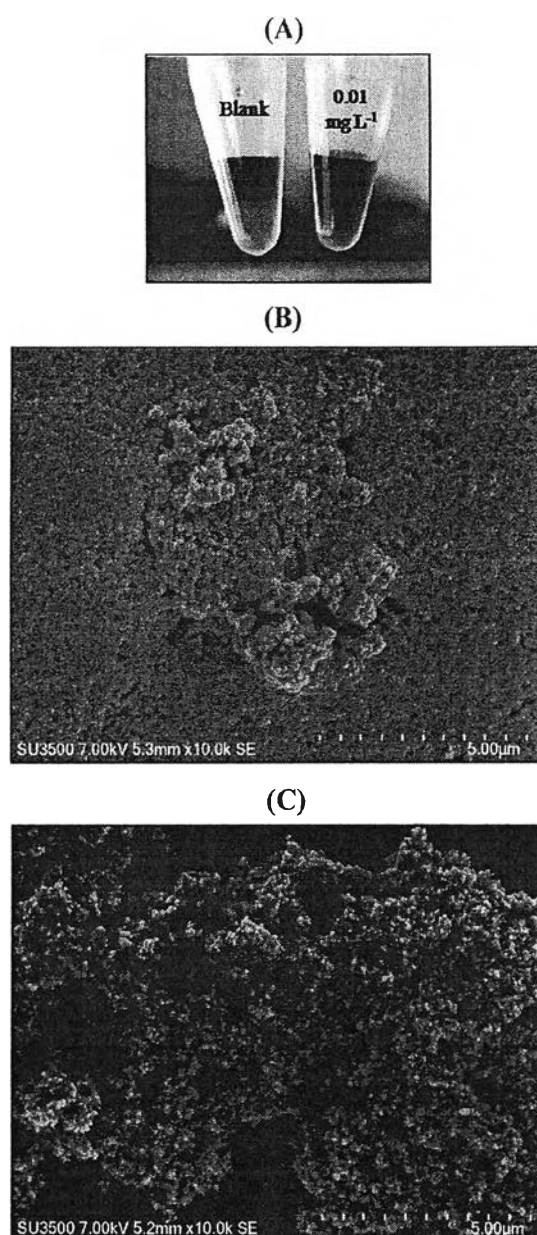


Fig. 4. The appearance of AgNPs solutions added to blank and 0.01 mg L⁻¹ paraquat-adsorbed silica gels (A), and scanning electron microscope images of silica gel without and with paraquat adsorption (B and C, respectively).

improve the sensitivity of the detection. Unmodified silica gels were conventionally used as an adsorbent for quaternary ammonium species [5,13,14,19,34–36]. Generally, in all colorimetric-based approaches previously reported, the elution step was needed to leach the paraquat out of the silica gel prior to the color forming reaction procedure. However, paraquat adsorbed on the surface of silica gel can be determined directly, with no elution step required in this work.

Similar results to in-solution detection were observed in which the color of AgNPs was changed according to the concentration levels of paraquat adsorbed onto the silica gel. However, the color of AgNPs applied to an on-silica bead system and the trend of color change were different from those using an in-solution system. In the case of the on-silica bead system, the color of AgNPs changed from a dark-greenish yellow solution to lighter yellow or pale yellow according to the concentrations of paraquat (Fig. 3), because there was no dilution of the initial AgNPs solution by sample or standard solutions. In addition,

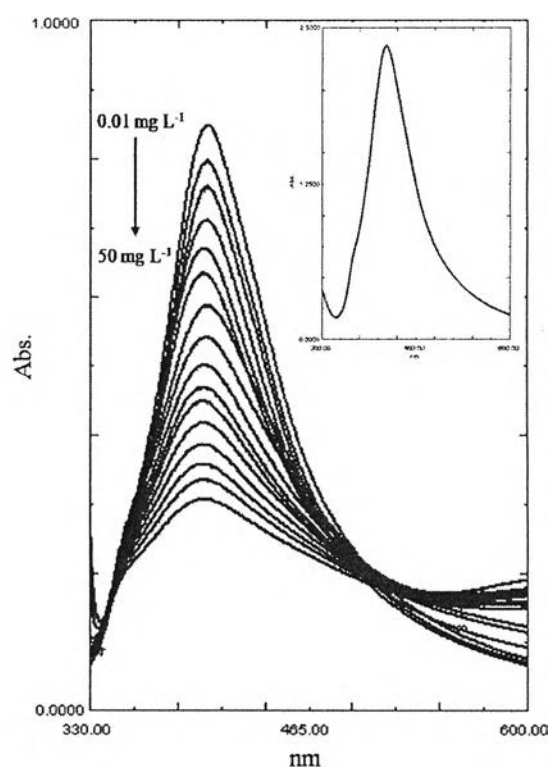


Fig. 5. Absorption spectra of AgNPs after addition of different concentrations of standard paraquat adsorbed on silica gel. The inset shows spectrum of the AgNPs (200 mg L⁻¹) without paraquat added.

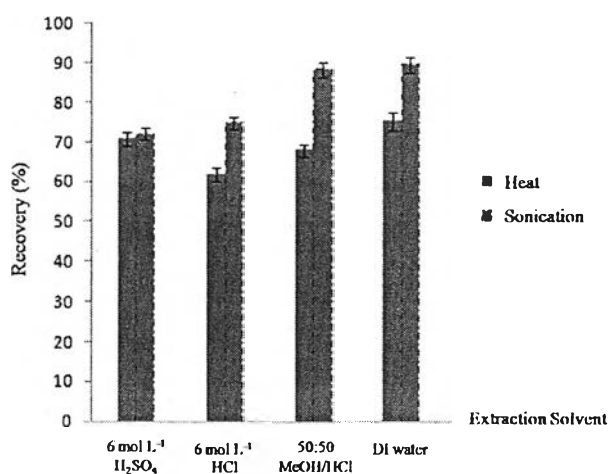


Fig. 6. Comparing efficiency of different methods for paraquat extraction from homogenized Chinese cabbage spiked with standard paraquat solutions, 500 µL of 1000 mg L⁻¹, (n=3).

high concentrations of paraquat adsorbed on silica gel, such as 50 mg L⁻¹ as shown in Fig. 3, resulted in the color bleaching of AgNPs, while the in-solution system caused the color to change from yellow to a dark metallic color.

Interestingly, at a low concentration of paraquat, 0.01–0.05 mg L⁻¹, the color change of AgNPs solutions could not easily be observed with the naked eye, but there was clear differentiation in color between the silica gels with and without paraquat adsorbed on their surfaces (Fig. 4). The color of silica gel with adsorbed paraquat turned black, resulting from AgNPs aggregation induced by coulombic attraction with paraquat, and the aggregated AgNPs were consequently adsorbed on the surface of the silica gel. This phenomenon explains the reason for AgNPs color bleaching in the on-silica bead system, as

Table 2

The results of paraquat determination in real samples ($n=3$) using the proposed on-silica bead with AgNPs method and the conventional colorimetric method.

Samples	Standard Added (mg L ⁻¹)	Proposed method Found (mg L ⁻¹) ^a	Conventional method Found (mg L ⁻¹) ^a	Limit of detection Naked eye (mg L ⁻¹)
Ground water	0.05	0.03 ± 0.02	0.04 ± 0.02	0.05
	1.00	0.87 ± 0.04	1.20 ± 0.07	
	25.00	23.37 ± 1.16	26.10 ± 1.02	
Canal water	0.05	0.03 ± 0.01	0.04 ± 0.01	0.05
	1.00	0.74 ± 0.07	0.80 ± 0.08	
	25.00	23.80 ± 0.98	22.70 ± 1.22	
Chinese cabbage	0.05	ND	ND	0.10
	1.00	0.78 ± 0.15	1.00 ± 0.11	
	25.00	26.60 ± 0.92	26.5 ± 1.14	
Green apple	0.05	ND	ND	0.10
	1.00	0.86 ± 0.09	0.90 ± 0.08	
	25.00	26.13 ± 1.29	22.80 ± 1.25	

ND = Not detectable.

^a UV-Vis spectrometric measurement.

the negatively charged AgNPs were attracted to accumulate on the silica gel surface coated by positively charged paraquat. Therefore, instead of dispersing throughout the solution to make a dark metallic color, the AgNPs were attracted to the silica gel surface, causing the removal of AgNPs from the solution.

3.5. Application of on-silica bead system for paraquat detection in real samples

3.5.1. Water sample determination

The absorption spectra of AgNPs were proportionally decreased according to the increase of paraquat concentrations added (Fig. 5). To investigate the matrix effect from natural water samples, groundwater and canal water, a standard solution of paraquat was added to the water sample. The results showed that matrices in natural water samples had no obviously adverse effect on the determination. By using the on-silica bead protocol, the recoveries of paraquat from groundwater and canal water were 93.6% and 95.4%, respectively, calculated by comparison with external standard calibration.

3.5.2. Plant sample determination

Extraction efficiency was studied to achieve satisfactory recovery of paraquat from plant matrices. Although literature reported the successful extraction of paraquat from plant samples with good recovery by using a strong acid [13,36], in this experiment the results showed relatively poor recovery. Furthermore, extractions with sonication provided greater recovery than with heating. Among the studied extraction procedures for Chinese cabbage, using DI water with sonication showed the best recovery at 89.5%, while using 50:50 MeOH/HCl with sonication provided slightly less recovery at 88.5%

(Fig. 6), as calculated using the external standard calibration, while green apple matrices resulted in slightly less recovery, 86.6% using DI water with sonication (data not shown). Therefore, DI water was chosen for further experiments. It was also compatible with AgNPs detection, since AgNPs are very sensitive to acidic conditions. Several extraction procedures were also performed and reported by T. Zou, et al. for the determination of paraquat in vegetables, and the maximum recovery was at 73.5% using water as an extraction solvent in the sonication system. The reason for incomplete extraction is possibly because paraquat can penetrate plant cells rapidly and resides tightly inside the cells. When a very low concentration of paraquat is spiked into a plant sample, very low recovery is obtained [1].

3.5.3. Method validation

As DI water with sonication was chosen as the extraction method for plant samples, the measurement of paraquat in the real samples using the proposed approach was compared to a conventional colorimetric method for paraquat determination by using a reducing agent under alkaline conditions. Standard addition calibrations over the range of 0.01–50 mg L⁻¹ for each sample were constructed, and the spiked samples with final concentrations of 0.05, 1.00 and 25.00 mg L⁻¹ were additionally prepared. After extraction and pre-concentration steps, AgNPs were added to the silica gel coated with paraquat followed by UV-Vis spectrometric measurement. The results are shown in Table 2.

By using the proposed method to determine paraquat in the spiked sample, paraquat contents were calculated by comparing to the standard addition calibration. Satisfactory results were achieved. The working range of the method was 0.05–50 mg L⁻¹ with the detection limit of 0.015 mg L⁻¹ by using UV-Vis spectrometric determination, in the case of water sample analysis. However, since the proposed approach was aimed to be applied as an optical assay for simple semi-quantitation analysis as on-site detection, therefore the limit of detection was also determined with the naked eye. Owing to incomplete extraction from plant solid matrices, the detection limit of paraquat in plant samples (LOD of 0.1 mg L⁻¹) was higher than that of paraquat in water samples (LOD of 0.05 mg L⁻¹) determined by visualizing the color of AgNPs solution.

With the application of negatively charged AgNPs for colorimetric detection of paraquat, the present method shows a good alternative approach in terms of simplicity, sensitivity, and economy. The method is compared to other published colorimetric and chromatographic methods as shown in Table 3.

4. Conclusion

This work presents a novel, simple, rapid, economic, and sensitive on-silica bead approach for paraquat detection, because it is one of the most widely used toxic chemicals as a herbicide. Negatively charged AgNPs were used as a colorimetric probe of which the levels of contaminated paraquat can be determined with the naked eye.

Table 3

Comparison of the proposed approach with other colorimetric and chromatographic methods for paraquat determination (modified from Rai et al. [13]).

Methods	Detection range/limit (mg L ⁻¹)	Remarks
Forming complex with tetra-iodomercurate [16]	3	Reaction time is relatively long, and reagent is toxic and expensive.
Reduction with ascorbic acid [14]	1.2–9.6	Less sensitive than the proposed method.
Reduction with sodium borohydride [13]	0.05–0.50	Elution of analyst from SPE prior to reduction is needed.
Host-guest chemistry using cyclen dithiocarbamate-functionalized silver nanoparticles [28]	1.85	Less sensitive and more expensive reagent than the proposed method.
HPLC with silica column and UV detection [5]	0.01–0.50	Method is more sensitive, but relatively more complicated.
HPLC coupled to ESI-MS [6]	2.0 × 10 ⁻⁴	Method is very sensitive, but the instrument is complicated and expensive.
On-silica bead detection with negatively charged AgNPs as colorimetric probe (present method)	0.05 [*]	Method is simple, selective, and sensitive. LOD can be as low as 0.01 ppm for water determination by visualizing color of silica gel coated with paraquat. [*] By visualizing the color of AgNPs solution with naked eye for water sample.

Moreover, the elution step can be ignored after pre-concentration protocol, as AgNPs can be applied directly to the paraquat adsorbed onto silica gel for monitoring paraquat concentrations. The approach was successfully applied for paraquat determination in water and plant samples with a relatively low limit of detection as compared to the previous reports of colorimetric methods for paraquat detection. Therefore, this approach can be applied as a quick scanning assay for paraquat contamination in food and environmental samples.

Acknowledgement

The authors acknowledge scholarship support from the Thailand Research Fund through Research Team Promotion Grant (RTA5780005).

Appendix A. Supporting information

Supplementary data associated with this article can be found in the online version at doi:10.1016/j.talanta.2017.06.045.

References

- [1] T. Zou, P. He, J. Cao, Z. Li, Determination of paraquat in vegetables using HPLC-MS-MS, *J. Chromatogr. Sci.* 53 (2015) 204–209.
- [2] V.Y. Taguchi, S.W.D. Jenkins, P.W. Crozier, D.T. Wand, Wand, Determination of diquat and paraquat in water by liquid chromatography-(electrospray ionization) mass spectrometry, *J. Am. Soc. Mass Spectrom.* 9 (1998) 830–839.
- [3] S. Jafarnejad, Recent advances in determination of herbicide paraquat in environmental waters and its removal from aqueous solution: a review, *Int. Res. J. Appl. Basic. Sci.* 9 (2015) 1758–1774.
- [4] S.M. Pond, Manifestations and management of paraquat poisoning, *Med. J. Aust.* 152 (1990) 256–259.
- [5] T.M. Chichila, Liquid chromatographic determination of paraquat and diquat in crops using a silica column with aqueous ionic mobile phase, *J. Assoc. Off. Anal. Chem.* 74 (1991) 961–967.
- [6] V.Y. Taguchi, S.W.D. Jenkins, P.W. Crozier, D.T. Wang, Determination of diquat and paraquat in water by liquid chromatography-(electrospray ionization) mass spectrometry, *J. Am. Soc. Mass Spectrom.* 9 (1998) 830–839.
- [7] O. Nunez, E. Moyano, M.T. Galceran, Solid-phase extraction and sample stacking-capillary electrophoresis for the determination of quaternary ammonium herbicides in drinking water, *J. Chromatogr. A* 946 (2002) 275–282.
- [8] O. Nunez, E. Moyano, M.T. Galceran, Capillary electrophoresis-mass spectrometry for the analysis of quaternary ammonium herbicides, *J. Chromatogr. A* 974 (2002) 243–255.
- [9] H.El Harmoudi, M. Achak, A. Farahi, S. Lahrich, L.El Gani, M. Abdennoiri, A. Bouzidi, M. Bakasse, M.A. El Mhammedi, Sensitive determination of paraquat by square wave anodic stripping voltammetry with chitin modified carbon paste electrode, *Talanta* 115 (2013) 172–177.
- [10] A. Walcarius, L. Lamberts, Square wave voltammetric determination of paraquat and diquat in aqueous solution, *J. Electroanal. Chem.* 406 (1996) 59–68.
- [11] X. Ye, Y. Gu, C. Wang, Fabrication of the Cu₂O/polyvinyl pyrrolidone-graphene modified glassy carbon-rotating disk electrode and its application for sensitive detection of herbicide paraquat, *Sens. Actuat. B-Chem.* 173 (2012) 530–539.
- [12] A. Jain, K.K. Verma, A. Townshend, Determination of paraquat by flow-injection spectrophotometry, *Anal. Chim. Acta* 284 (1993) 275–279.
- [13] M.K. Rai, J.V. Das, V.K. Gupta, A sensitive determination of paraquat by spectrophotometry, *Talanta* 45 (1997) 343–348.
- [14] P. Shivhare, V.K. Gupta, Spectrophotometric method for the determination of paraquat in water, grain and plant materials, *Analyst* 116 (1991) 391–393.
- [15] Official Methods of Analysis, 15th ed AOAC, Arlington, VA, Sec. 969.09 (accessed 22 December 2016), 1990.
- [16] S.H. Yuen, J.E. Bagness, D. Myles, Spectrophotometric determination of diquat and paraquat in aqueous herbicide formulations, *Analyst* 92 (1967) 375–381.
- [17] M. Agudo, M. Rios, M. Valcárcel, Automatic continuous-flow determination of paraquat at the subnanogram per millilitre level, *Anal. Chim. Acta* 281 (1993) 103–109.
- [18] E.C. Guijarro, P. Yáñez-Sedeño, L.M. Polo Díez, Determination of paraquat by flow-injection spectrophotometry, *Anal. Chim. Acta* 199 (1987) 203–208.
- [19] R. Kesari, M. Rai, V.K. Gupta, Spectrophotometric method for determination of paraquat in food and biological samples, *J. AOAC Int.* 80 (1997) 388–391.
- [20] G.K. Darbha, A.K. Singh, U.S. Rai, E. Yu, H. Yu, P.C. Ray, Selective detection of mercury (II) ion using nonlinear optical properties of gold nanoparticles, *J. Am. Chem. Soc.* 130 (2008) 8038–8043.
- [21] D. Li, A. Wiecekowska, I. Willner, Optical analysis of Hg²⁺ ions by oligonucleotide gold nanoparticle hybrids and DNA based machines, *Angew. Chem. Int. Ed. Engl.* 47 (2008) 3927–3931.
- [22] T. Li, S. Dong, F. Wang, Label-free colorimetric detection of aqueous mercury ion (Hg²⁺) using Hg²⁺-modulated G-Quadruplex-based DNAzymes, *Anal. Chem.* 81 (2009) 2144–2149.
- [23] H. Gu, K. Hu, D. Li, Y. Long, SERS detection of polycyclic aromatic hydrocarbons using a bare gold nanoparticles coupled film system, *Analyst* 141 (2016) 4359–4365.
- [24] X. Zhang, H. Zhao, Y. Xue, Z. Wu, Y. Zhang, Y. He, X. Li, Z. Yuan, Colorimetric sensing of clenbuterol using gold nanoparticles in the presence of melamine, *Biosens. Bioelectron.* 34 (2012) 112–117.
- [25] J.D.S. Newman, J.M. Robert, G.J. Blanchard, Optical organophosphate sensor based upon gold nanoparticle functionalized fused silica gel, *Anal. Chem.* 79 (2007) 3448–3454.
- [26] A. Apilux, W. Siangproh, N. Praphairaksit, C. Chailapakul, Simple and rapid colorimetric detection of Hg(II) by a paper-based device using silver nanoplates, *Talanta* 97 (2012) 388–394.
- [27] S. Mohammadi, G. Khayatian, Highly selective and sensitive photometric creatinine assay using silver nanoparticles, *Microchim. Acta* 182 (2015) 1379–1386.
- [28] J.V. Rohit, S.K. Kailasa, Cyclen dithiocarbamate-functionalized silver nanoparticles as a probe for colorimetric sensing of thiram and paraquat pesticides, *J. Nanopart. Res.* 16 (2014) 2585–2601.
- [29] Y. Pico, G. Font, J.C. Molto, J. Manes, Solid-phase extraction of quaternary ammonium herbicides, *J. Chromatogr. A* 885 (2000) 251–271.
- [30] S. Agnohotri, S. Mukherji, S. Mukherji, Size-controlled silver nanoparticles synthesized over the range 5–100 nm using the same protocol and their antibacterial efficacy, *RSC Adv.* 4 (2014) 3974–3983.
- [31] M.S. Young, J.C. Shia, K.V. Tran, UPLC-MS/MS determination of paraquat and diquat in potato and wheat using the CORTECS UPLC HILIC column, Application note, Waters Corporation. (<http://www.waters.com/webassets/cms/library/docs/720004851en.pdf>)(accessed 12 January 2017).
- [32] D.I.S. Kolberg, D. Mack, M. Anastassiades, M.T. Hetmanski, R.J. Fussell, T. Meijer, H.G.J., Development and independent laboratory validation of a simple method for the determination of paraquat and diquat in potato, cereals and pulses, *Mol. Anal. Bioanal. Chem.* 404 (2012) 2465–2474.
- [33] M. Ibañez, Y. Pico, J. Manes, On-Line liquid chromatographic trace enrichment and high performance liquid chromatographic determination of paraquat and difenzoquat in water, *J. Chromatogr. A* 728 (1996) 325–331.
- [34] T.M.P. Chichila, D.M. Gilydis, Determination of paraquat and diquat in low-moisture food crops using silica column cleanup and liquid chromatography with UV detection, *J. AOAC Int.* 76 (1993) 1323–1328.
- [35] J.L. Tadeo, C. Sanchez-Brunete, R.A. Perez, M.D. Fernandez, Analysis of herbicide residues in cereals, fruits and vegetables, *J. Chromatogr. A* 882 (2000) 175–191.

Review

Biomedical Probes Based on Inorganic Nanoparticles for Electrochemical and Optical Spectroscopy Applications

Abdulhadee Yakoh ¹, Chanika Pinyorosphathum ¹, Weena Siangproh ^{2,*} and Orawon Chailapakul ^{1,*}

¹ Electrochemistry and Optical Spectroscopy Research Unit (EOSRU), Department of Chemistry, Faculty of Science, Chulalongkorn University, 254 Phayathai Road, Patumwan, Bangkok 10330, Thailand; E-Mails: i_style@windowslive.com (A.Y.); n8h7@hotmail.com (C.P.)

² Department of Chemistry, Faculty of Science, Srinakharinwirot University, Sukhumvit 23, Wattana, Bangkok 10110, Thailand

* Authors to whom correspondence should be addressed: E-Mails: weena@g.swu.ac.th or weenasi@hotmail.com (W.S.); corawon@chula.ac.th (O.C.); Tel.: +66-2-640-5000 (ext. 18208) (W.S.); +66-2-218-7615 (O.C.); Fax: +66-2-259-2098 (W.S.); +66-2-218-7615 (O.C.).

Academic Editor: Shinya Maenosono

Received: 30 June 2015 / Accepted: 10 August 2015 / Published: 28 August 2015

Abstract: Inorganic nanoparticles usually provide novel and unique physical properties as their size approaches nanometer scale dimensions. The unique physical and optical properties of nanoparticles may lead to applications in a variety of areas, including biomedical detection. Therefore, current research is now increasingly focused on the use of the high surface-to-volume ratios of nanoparticles to fabricate superb chemical- or biosensors for various detection applications. This article highlights various kinds of inorganic nanoparticles, including metal nanoparticles, magnetic nanoparticles, nanocomposites, and semiconductor nanoparticles that can be perceived as useful materials for biomedical probes and points to the outstanding results arising from their use in such probes. The progress in the use of inorganic nanoparticle-based electrochemical, colorimetric and spectrophotometric detection in recent applications, especially bioanalysis, and the main functions of inorganic nanoparticles in detection are reviewed. The article begins with a conceptual discussion of nanoparticles according to types, followed by numerous applications to analytes including biomolecules, disease markers, and pharmaceutical substances. Most of the references cited herein, dating from 2010 to 2015, generally mention one or more of the following characteristics: a low detection limit, good signal amplification and simultaneous detection capabilities.

Keywords: biomedical probes; inorganic nanoparticles; electrochemical detection; colorimetry; spectrophotometric detection; biosensors; bioanalysis

1. Introduction

Among the various nanomaterials, inorganic nanoparticles are extremely important in the development of sensors. Not only can they be easily synthesized, but also cheaply mass produced. For this reason, they can also be more readily integrated into a variety of applications. Recently, inorganic nanoparticles of different kinds and dimensions have become widely exploited as versatile and sensitive sensors or probes. The main objective of designer inorganic nanoparticles, enhanced sensitivity in bio-sensing applications, greatly benefits from their small size, where their properties are strongly influenced by increasing their surface area. Thus, the combination of inorganic nanoparticles and sensors is one of the most exciting areas in modern analytical detection development because they offer excellent prospects for designing highly sensitive and selective sensors. Electrochemical sensing and spectrophotometric detection based on the modification or use of a particular variety of inorganic nanoparticles constitute a fascinating research area in biomedical applications. The remarkable features resulting from the use of inorganic nanoparticles are now widely employed in various detection systems. Presently, inorganic nanoparticle electrochemical sensors and optical spectrophotometric sensors used for bioanalysis purposes are collected. In this review the electrochemical and optical spectrophotometric characteristics of biomedical probes based on inorganic nanoparticles and the sensing applications possible with these materials are discussed, and their advantages and weaknesses are also explored. We also summarize the promising future anticipated for the use of these inorganic nanoparticles in both electrochemical and spectrophotometric detection as shown in the following sections.

2. Types of Nanoparticles

2.1. Gold Nanoparticles

Gold nanoparticles (AuNPs), one of the most commonly used metal nanoparticles, have been applied in various fields. The range of applications for AuNPs is growing rapidly and includes: electronics, photodynamics, therapeutic agent delivery, sensors, probes, diagnostics and catalysis. AuNPs possess several advantages: (1) AuNPs can be synthesized in a straightforward manner and can be made highly stable; (2) AuNPs possess unique optoelectronic properties; (3) AuNPs provide high surface-to-volume ratio with excellent biocompatibility; (4) these properties of AuNPs can be readily tuned by varying their size, shape, and the surrounding chemical environment and (5) AuNPs offer a suitable platform for multifunctionalization with a wide range of organic or biological ligands for the selective binding and detection of small molecules and biological targets [1]. Due to the abovementioned advantages, AuNPs have been utilized in various sensing strategies.

2.2. Magnetic Nanoparticles

Magnetic nanoparticles are nanoparticles composed of magnetic elements, particularly iron oxide. A large surface-to-volume ratio owing to their small size provides them with a high immobilization density and high surface reactivity [2–4]. Prior to their use in any detection procedure, most magnetic nanoparticles have to be functionalized with enzymes, metals, or metal oxides in order to improve their physiochemical properties and stability [5,6]. This refinement has to be employed since bare magnetic nanoparticles tend to form large aggregates and have few active groups. Moreover, they are easily oxidized and dissolved in acid media, leading to poor stability [5]. Their plethora of applications benefit from their low toxicity, biocompatibility, and easy separation utilizing external magnetic fields [7–10]. A facile separation of magnetic nanoparticles is not only able to reduce the background interference but also enhance target immobilization [11]. Consequently, magnetic nanoparticles have been extensively applied in biomedicine, immunology, biocatalysis, bioanalysis, and especially the separation and purification of target molecules [9,11].

2.3. Nanocomposites

Nanocomposites are one of the new composite materials formed by nanometer-sized materials dispersed in a 3-D substrate. Nanocomposites offer an exciting and practical approach for designing and fabricating new technological products and materials with superior mechanical, electrical, optical, antimicrobial, catalytic, and reactive properties [12]. Nanocomposites provide better performance over conventional composite materials and are suitable candidates to overcome the limitations of many materials owing to the high surface to volume ratio of the reinforcing phase and its high aspect ratio. Nanocomposite materials can be classified, according to their matrix materials, into three different categories including ceramic matrix nanocomposites (CMNC), metal matrix nanocomposites (MMNC) and polymer matrix nanocomposites (PMNC) [13]. Herein, to the best of our knowledge, all the various applications of nanocomposites in the biomedical field are presented.

2.4. Semiconductor Nanostructures

Semiconductor nanostructures have recently attracted considerable attention due to their unique physical properties that give rise to many potential applications. Semiconductor particles of nanometer size can refer to nanoparticles, nanoclusters, nanocrystals, quantum dots, *etc.* Semiconductor nanostructures are generally categorized into three types: two-dimensional (2D) nanostructures (e.g., quantum wells (QWs)), one-dimensional (1D) nanostructures (quantum wires (QWRs) and nanowires (NWs)), and zero-dimensional (0D) nanostructures (quantum dots (QDs)) [14]. Colloidally synthesized semiconductor nanoparticles often possess a strong band-gap luminescence tunable by size as a result of the quantum confinement effect, which makes them interesting for different applications [15]. Because QDs are zero-dimensional, they have a sharper state density than higher-dimensional structures and as a result, they have superior transport and optical properties and are being researched for use in laser diodes, solar cells, and several biological sensors [14].

2.5. Silver Nanoparticles

Silver nanoparticles have received tremendous attention due to their unique properties that are absent from their bulk forms. Their unusual features, including physiochemical and electronic properties, lead to enormous sensing applications in biosensors, electronics, catalysis, pharmaceutical, and therapeutics [16,17]. Enhancement of the local electric field supports the use of silver nanoparticles as substrates for surface-enhanced Raman scattering (SERS) extending the various uses of silver nanoparticles as detection probes [18]. Silver nanoparticles, moreover, are applied as a sensor modification in order to increase the electrochemical sensitivity, selectivity, and reproducibility [19]. In addition, the aggregation of silver nanoparticles induced by various conditions causes shifting and broadening of the plasma band [16]. This simplicity has allowed the development of abundant naked eye and optical detection uses. Furthermore, the utilization of silver nanoparticles offers benefits of minimal material consumption and no need for sophisticated instruments [16].

2.6. Other Nanoparticles

Other metals such as nickel, copper, palladium, and platinum have been used to synthesize metallic nanoparticles. A variety of applications are proposed elsewhere due to their special properties at the nanoscale. Many metal nanoparticles are candidates for electrochemical applications thanks to their conductivity enhancement and signal amplification properties. In addition to an increment in sensitivity, these nanoparticles are often employed due to their cost-effectiveness and environmental friendliness. Most of these applications focusing on electrochemical techniques are described in this review.

3. Biomedical Applications

3.1. Amino Acids

Amino acids are biological organic compounds that play critical functions in animals. Thiol-containing amino acids, including cysteine and tryptophan, has been frequently reported as disease biomarkers [20], due to the fact that their deficiency leads to numerous disorders, such as Alzheimer's disease, slowed growth, lethargy, liver damage, skin lesions, *etc.* [21,22]. A rapid quantification of amino acids, especially sulfur-containing compounds, is consequently an important objective for health diagnosis.

3.1.1. Electrochemical Detection

Gold nanoparticles with carbon nanotubes pre-cast on a glassy carbon electrode (AuNP-CNT/GCE) had been fabricated for the detection of tryptophan in pharmaceutical samples with a low detection limit. The hybrid nanomaterial substantially decreased the overpotential of tryptophan because of a remarkable synergistic effect of the modified electrode on the electrocatalytic activity toward the oxidation of the analyte [23].

Fe₃O₄-based nanoparticles with graphene oxide have been cast on glassy carbon electrodes. They show high catalytic effects in the oxidation of amino acids. The composite provided the advantages of

excellent catalytic activity, high sensitivity, and good stability. The techniques were able to detect cysteine and N-acetylcysteine at low μM levels [24].

A glassy carbon electrode (GCE) was fabricated with silver nanoparticles/graphene oxide (AgNPs/GO) and glucose as a reducing and stabilizing agent. The modified electrode possessed specific features typical of both silver nanoparticles and graphene oxide. The properties of high specific area and fast electron transfer rate improved the electrocatalytic performance and enhanced the activity for oxidation of tryptophan by ten-fold compared with graphene oxide films. The AgNPs/GO/GCE was also free of interferences from tyrosine and coexisting species [25].

Cobalt and nickel nanoparticle-modified electrodes have also been used for the detection of amino acids [21,22,26]. Essential compounds in living cells of animals could be simultaneously detected by a carbon paste electrode (CPE) modified with a (9,10-dihydro-9,10-ethananoanthracene-11,12-dicarboximido)-4-ethylbenzene-1,2-diol (DEDE) and a NiO/CNT nanocomposite. The modified electrode had a potent and persistent electron-mediating behavior and well-separated oxidation peaks of cysteine, nicotinamide adenine dinucleotide (NADH), and folic acid were observed [26]. Another work reported nickel oxide nanoparticles modified on a glassy carbon electrode with DNA as a new platform for entrapment of an osmium (III) complex as an excellent electron transfer mediator. The GC/DNA/NiO_xNPs/O_s(III)-complex modified electrode exhibited excellent selectivity, electrocatalytic activity, stability, remarkable antifouling properties, and allowed the simultaneous detection of cysteine and homocysteine without interferences from low molecular mass biothiol derivatives and electroactive biological species [21]. Cysteine was electrochemically detected by an electrode modified with cobalt hexacyanoferrate nanoparticles with a core shell structure. In the presence of cysteine, the anodic peak current of the Fe(II)/Fe(III) transition was increased while the corresponding cathodic peak current was decreased. In contrast, the peak current of Co(II)/Co(III) remained almost unchanged. The results indicated that the nanoparticles oxidized cysteine via a surface mediated electrocatalytic mechanism. The detection limits of cysteine in batch and flow mode with this modified electrode were as low as 40 and 20 nM, respectively.

3.1.2. Colorimetric and Spectrophotometric Detection

Carboxymethyl cellulose-functionalized gold nanoparticles were synthesized with sodium carboxymethyl-cellulose (CMC-AuNPs) for cysteine detection based on a colorimetric method. The novel nanoparticles would protect particles against salt-induced aggregation. In the presence of cysteine, colloid solutions in sodium chloride were aggregated and displayed color changes, as well as UV-Vis absorption spectra changes. The method was applied to real urine samples [27]. Biothiols including Cys, GSH, and Hcys were detected by a colorimetric assay. *S*-adenosyl-L-methionine (SAM) that interacted electrostatically with unmodified gold nanoparticles (AuNPs) induced selective aggregation. In the presence of bioethics, AuNPs prefer to react with thiols rather than SAM due to the formation of AuS bonds, thus the aggregation of AuNPs changes to the disperse state. The color change was detected by UV-Vis spectrometry and by the naked eye. This assay exhibited rapid operation, high selectivity and sensitivity, and allowed the simultaneous detection of three biothiols compound [28].

Magnetic particles were functionalized with amine and Ni²⁺ for the detection of histidine. A highly specific interaction between the histidine and Ni²⁺ formed a complex, which in the presence of formic

acid would liberate gaseous nickel tetracarbonyl which separated from the sample matrix. The gas was determined by atomic absorption/fluorescence spectrometry. Ten to hundred fold improvements over conventional methods was seen with the method. The approach promises high sensitivity, simple design, and convenient operation [29].

Fluorescence responses of Hcy, L-cys, and GSH of CdTe QDs using L-cysteine as capping reagent were investigated. The probe offered good sensitivity, and selectivity for detecting Hcy, L-cys, and GSH in the presence of 20 amino acids, metal ions, and other molecules in biological fluids. It was applied in four serum samples, cell extract sample from two cancer cell lines (Hela and HepG2) with a detection limit of 46 nM, 43 nM, and 63 nM for Hcy, L-cys, and GSH, respectively [30]. Mono-6-SH- β -cyclodextrin capped Mn-doped ZnS quantum dots (β -CD-MnZnS QDs) had dual photoluminescence (PL) at 430 and 598 nm upon excitation at 315 nm to detect tryptophan enantiomers differently. The D-isomer showed little effect whereas L-tryptophan displayed a large time-dependent enhancement in the PL intensity of QDs. This selectivity is due to different inclusion constants for tryptophan enantiomers of the coating on the surface of Mn-ZnS QDs. L-Tryptophan can be detected in the presence of its stereoisomer with a 5.4 nM detection limit [31].

Silver nanoparticles has been primarily reported for detection of amino acids due to the strong interaction of thiol groups towards nanoparticles [32]. Silver nanoparticles induced an aggregation or an anti-aggregation mechanism in the presence of cations and surface modified material. This basis was used for sensing various amino acids. For example, in the presence of cysteine, the color of the silver nanoparticles changed from yellow to pink. The color change was detected visually and could be estimated metrically by measuring the surface plasmon resonance absorption. The method could be applied for the detection of cysteine at ultralow levels [32]. Moreover, nonionic fluorosurfactant-capped silver nanoparticles were aggregated as a result of the presence of cysteine. The modified nanoparticles exhibited selectivity towards cysteine in the determination of this amino acid in human urine and plasma samples [16]. Calcium ion was used as a cross-linking agent for a rapid detection of cysteine. By monitoring the color change from yellow to red, cysteine could be quantified in biological fluids, such as serum and artificial cerebrospinal fluid [33]. Another demonstration stated that cysteine was selectively detected in the presence of Ca^{2+} and NaCl. The result showed other amino acids had no effect on the color change due to the absence of thiol groups [34]. Chromium ion had a similar interaction. In a solution composed of silver nanoparticles and Cr^{3+} , cysteine was able to induce aggregation and displayed accolor change from yellow to purple. The techniques also exhibited the selectivity towards cysteine in the presence of other amino acids [35]. Amino acids without thiol functional groups such as tryptophan could be quantified using surface plasmon absorption. The modification of 4,4-bipyridine-functionalized onto silver nanoparticles changed the color of the solutions from yellow to red. The absorption could be detected at 390 nm and 556 nm, respectively. This approach demonstrated the selectivity of the functionalized nanoparticles over other neutral amino acids with low detection limits [36].

3.2. Antigen-Antibody

Antigens are many substances that stimulate the immune system to produce antibodies. There is a specific antibody for each antigen, thus, each one can be used to detect the presence of the other. The

detection of particular antigens/antibodies is a widespread method used in medical diagnostics of many diseases. Several different methods may be employed, including the following:

3.2.1. Electrochemical Detection

In recent years, gold nanoparticles (AuNPs) have found wide use and have gained much attention in the electrochemical sensor field due to their great properties as described above. Interestingly, an electrochemical immunosensing platform has been developed for the detection of the human lung cancer-associated antigen ENO1, by first fabricating a polyethylene glycol (PEG) layer on a screen printed electrode and subsequently using anti-ENO1-tagged AuNPs congregate bioprobes as signal amplifiers to improve the sensitivity of the assay. The electrochemical signal from the bound AuNPs congregates was obtained after oxidizing, followed by the reduction of AuCl_4^- in square wave voltammetry (SWV) mode as shown in Figure 1A. This AuNPs congregate-based assay provides an amplification approach for detecting ENO1 at trace levels, leading to a detection limit as low as 11.9 fg (equivalent to 5 μL of a 2.38 pg/mL solution) [37]. A number of groups have also proposed a signal amplification strategy for ultrasensitive immunosensors. For example, using human and mouse IgG as model analytes, a multiplexed immunoassay has been developed by combining alkaline phosphatase (ALP)-labeled antibody functionalized AuNPs (ALP-Ab/AuNPs) and enzyme-AuNPs catalyzed deposition of silver nanoparticles (AgNPs) on an immunosensor array (Figure 1B). After sandwich-type immunoreactions, the ALP-Ab/AuNPs were captured on an immunosensor surface to catalyze the hydrolysis of 3-indoxyl phosphate, which produced an indoxyl intermediate to reduce Ag^+ . The silver deposition process was catalyzed by both ALP and AuNPs, which amplified the detection signal. The deposited silver was then measured by anodic stripping analysis in KCl solution [38]. Based on a similar concept, a triple signal amplification strategy was also designed as illustrated in Figure 1C. An enhancement in signal resulted from the use of a graphene modified immunosensor surface which accelerated electron transfer, PSA (poly(styrene-co-acrylic acid) microbeads that carried AuNPs as tracing tags to label signal antibody (Ab_2) and AuNPs induced silver deposition in KCl solution for anodic stripping analysis [39].

3.2.2. Colorimetric and Spectrophotometric Detection

Nanomaterials have found widespread use for the detection of different antigen/antibody combinations. Various optical immunoassay detection methods are of interest in early diagnostic and screening detection, such as a surface-enhanced Raman scattering (SERS)-based gradient optofluidic sensor developed by Chon *et al.*, for testing a specific target marker (rabbit immunoglobulin (IgG)) [40]. The sensor is composed of three components consisting of the gradient channel, the injection and mixing area of antibody-conjugated hollow gold nanospheres and magnetic beads, and a sandwich immunoassay trapping area. This system, using antibody-conjugated HGNS and magnetic beads, provides advantages over the SERS immunoassay performed in microwells owing to the automatically control of the microfluidic system, so the tedious manual dilution process and time consuming assay was eliminated.

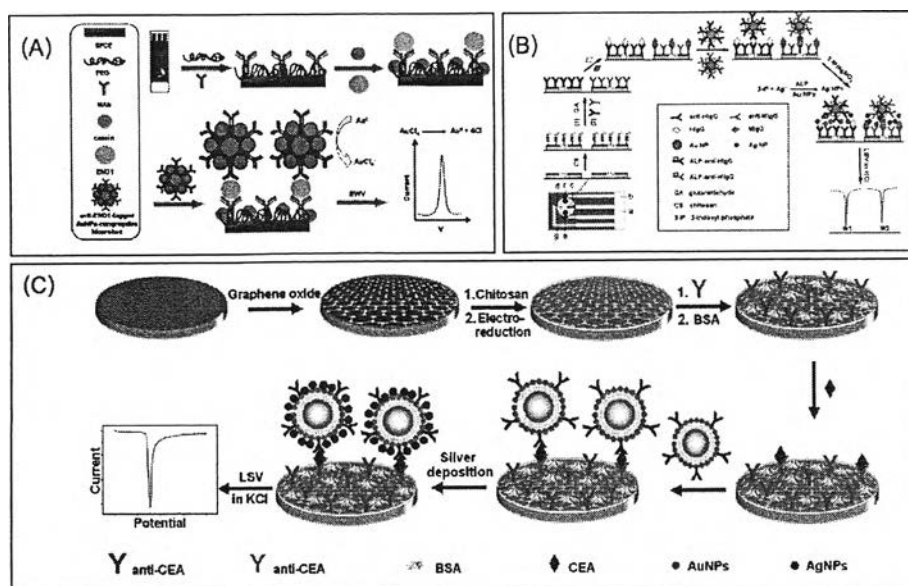


Figure 1. Schematic representation of (A) the operation of the electrochemical immunosensor for the detection of ENO1 [37]. Reprinted with permission from (Ho, J.A.A.; Chang, H.C.; Shih, N.Y.; Wu, L.C.; Chang, Y.F.; Chen, C.C.; Chou, C. Diagnostic detection of human lung cancer-associated antigen using a gold nanoparticle-based electrochemical immunosensor. *Anal. Chem.* **2010**, *82*, 5944–5950.). Copyright (2010) American Chemical Society.; (B) preparation of immunosensor array and detection strategy by sandwich-type immunoassay and linear sweep voltammetric stripping analysis of enzymatically deposited AgNPs [38]. Reprinted (adapted) with permission from (Lai, G.; Yan, F.; Wu, J.; Leng, C.; Ju, H. Ultrasensitive multiplexed immunoassay with electrochemical stripping analysis of silver nanoparticles catalytically deposited by gold nanoparticles and enzymatic reaction. *Anal. Chem.* **2011**, *83*, 2726–2732.). Copyright (2011) American Chemical Society; and (C) the immunosensor fabrication and sandwich-type immunoassay procedure [39]. Reprinted (adapted) with permission from (Lin, D.; Wu, J.; Wang, M.; Yan, F.; Ju, H., Triple signal amplification of graphene film, polybead carried gold nanoparticles as tracing tag and silver deposition for ultrasensitive electrochemical immunosensing. *Anal. Chem.* **2012**, *84*, 3662–3668.). Copyright (2012) American Chemical Society.

Based on magnetic core/shell $\text{Fe}_3\text{O}_4/\text{SiO}_2$ and $\text{Fe}_3\text{O}_4/\text{Ag}/\text{SiO}_2$ nanoparticles, a surface plasmon resonance (SPR) biosensor for the detection of goat anti-rabbit IgG was developed. The modified magnetic nanoparticles (MNPs)-based biosensor has two main advantages over traditional biosensors. First, the MNPs can easily be immobilized on the Au film, which greatly simplifies the operation; Second, in contrast to the traditional biosensor that contained only one layer of receptor molecules on the surface of the gold film, the modified MNPs have larger surface areas, better compatibilities and more numbers of receptor molecules, which are more beneficial for the immobilization of antibodies [5].

Nanocomposites have also been used for carcinoembryonic antigen (CEA) detection. A sandwich type electrochemiluminescence (ECL) immunosensor based on a Ag/graphene nanocomposite was designed using nanoporous Pd as a catalytically promoted nanolabel. The main advantages of the developed immunosensor can be attributed to two aspects: first, the obtained Ag/graphene

nanocomposite could be an ideal substrate for antibody immobilization with good stability and bioactivity. Second, the novel ECL label of nanoporous Pd exhibited excellent ECL activity [41]. A versatile immunosensor using a CdTe quantum dot (QDs) coated silica nanosphere (Si/QDs) as a label was also developed for the detection of a biomarker (rabbit IgG). In this approach, goat anti-rabbit IgG antibody was covalently bound to CdTe QDs on the surface of silica nanospheres (Si/QD/Ab₂) attached onto the gold electrode surface through a subsequent sandwich immunoreaction. The resulting immunosensor exhibited a signal amplification in both the ECL and square-wave voltammetry techniques which could be attributed to the high loading of CdTe QDs [42]. An electrochemiluminescence (ECL) immunosensor based on the amplifying ECL of luminol by hemin-reduced graphene oxide (hemin-rGO) and silver nanoparticles (AgNPs) decorated reduced graphene oxide (Ag-rGO) was constructed for the detection of carcinoembryonic antigen (CEA).

In brief, AuNPs electrodeposited (DpAu) onto hemin-rGO constituted the base for the immunosensor, which amplified the ECL signal of luminol and served as carrier to immobilize primary antibody (Ab₁). Moreover, AgNPs-rGO were used to load secondary antibody (Ab₂) and GOD. In the presence of oxygen, the loaded GOD immediately catalyzed the oxidation of glucose in the detection of *in situ* generated H₂O₂, which could promote the oxidation of luminol with an amplified ECL signal. Additionally, hemin and AgNPs could further enhance the ECL signal of luminol owing to the decomposable catalysis of H₂O₂ to produce increased amounts of reactive oxygen species [43].

3.3. Antioxidants

Antioxidants are a broad group of organic compounds that are widespread in food [44]. Their properties are understood to involve the inhibition of free radical chain reactions. The reactions initiated by free radicals cause damage to proteins, lipids, and nucleic acids [45]. Glutathione (GSH) as an example of antioxidants prevents aging, cancer, and other diseases [46]. In addition, it functions in protein synthesis, enzyme activity, and cell protection [47]. Another example is ascorbic acid (AA) or vitamin C, which acts as a supplement and is frequently consumed in tablets. Mostly, it is used for treating colds, scurvy, and promoting health development [48]. The benefits of other antioxidants are abundantly reported, therefore, their quantification is of importance.

3.3.1. Electrochemical Detection

Modified nanocomposites are responsible for the improvement of electrochemical signals, as a consequence of the good properties of the various materials and nanoparticles fabricated into an electrode. A *N*-(4-hydroxyphenyl)-3,5-dinitrobenenamide-FePt/CNTs carbon paste electrode was used for the detection of GSH in the presence of piroxican. The modified nanocomposite exhibited a good electron-mediating behavior. As a result, the oxidation peaks were well separated. Moreover, the approach could detect GSH and piroxican at low nM concentrations [46]. The synergistic effect of a Fe₂O₃/graphene nanocomposite modified electrode was improved for ascorbic acid and uric acid detection [48]. The nanocomposite modified onto the electrode was able to resolve the overlapping anodic peaks of these two analytes. It had advantages of simplicity, high sensitivity, and good selectivity.

Silver nanoparticles/carboxylated multiwalled carbon nanotubes/polyaniline film (AgNPs/c-MWCNT/PANI) have been synthesized on gold electrodes and further covalently immobilized with

glutathione oxidase for the detection of glutathione in hemolysated erythrocytes. The modified electrode held a great promise of stability, lower response time and could perform without interferences [47].

Electrodeposition of nickel oxide nanoparticles onto a glassy carbon electrode offered low oxidation potential toward GSH, while other organic compounds like ascorbic acid, uric acid, dopamine, and glucose had no interaction in the method. Additionally, nickel oxide nanoparticles modified with ethylferrocene (EF) and multiwalled carbon nanotubes (MWCNT) on carbon paste electrode (CPE) showed excellent individual peak separation characteristics for the electrooxidation of glutathione and acetaminophen [49]. Other nanoparticles such as platinum nanoparticles had been employed as a nanocomposite for Pt-nanoparticles/polyelectrolyte-functionalized ionic liquid (PFIL)/graphene sheet (GS) modified electrodes. Independent oxidation peaks of ascorbic acid and dopamine were observed in urine samples [50].

3.3.2. Colorimetric and Spectrophotometric Detection

Glutathione was detected based on an anti-aggregation mechanism. The solution of gold nanoparticles changed from a dispersion to an aggregated state in the presence of glutathione, which resulted in a color change from red to blue. This anti-aggregation activity was preferable to have higher selectivity. This approach had selectivity towards glutathione relative to natural amino acids, homocysteine, and glutathione disulfide [51]. Gold nanoclusters coated with Hg^{2+} and Au^+ were able to quench the emission of NIR fluorescence, and the mechanism was used for the detection of glutathione. In the addition of the analyte, the signal was enhanced as a result of the affinity between glutathione and Hg^{2+} . The method had been employed for the detection of glutathione in living cells and human blood samples. It possessed advantages of high sensitivity and low spectral interferences [52].

CdS nanotube (NT) films and $\text{K}_2\text{S}_2\text{O}_8$ as coreactant were modified on an indium tin oxide substrate. Nanosemiconductors coated on this substrate exhibited strong electrochemiluminescent emission. The quench was differently affected by hydroxyl moieties in the benzene ring. This quenching property was used for the simultaneous determination of phenolic compounds, namely catechol, phenol, hydroquinone, and resorcinol with good reproducibility [53]. CdS-2-mercapto-propionic acid or CdS-2-MPA was used for the luminescent detection of rutin. The signal resulted from the inner filter effect and a statistic luminescence quenching component. Rutin was quantified in this technique without interferences from the flavonoids hesperidin and herperetin [54].

Due to the color change of silver nanoparticles from colorless to yellow caused by ascorbic acid, the method could be used for quantification of this antioxidant by LSPR with low detection limit [55]. Another approach presented the immobilization of silver nanoparticles on the surface of magnetic particles for the detection of glutathione by surface plasmon resonance. In the presence of crystal violet, the glutathione competed for the adsorption on the particles. As a result, the Raman signal was decreased and inversely proportional with the increase of glutathione concentration. This method was applied to blood samples with high sensitivity, selectivity, and stability [56].

3.4. Cancer

According to the National Cancer Institute (NCI), a biomarker is a biological molecule found in blood, other body fluids, or tissues that is a sign of a normal or abnormal process, or of a condition or disease. A biomarker may be used to see how well the body responds to a treatment for a disease or condition such as cancer. Cancer biomarkers can include a broad range of biochemical entities, such as nucleic acids, proteins, and small metabolites as well as whole tumor cells that indicate the presence of cancer in the body. Cancer biomarkers can be used to screen for cancer diagnosis. Moreover, recent technological advancements have enabled the examination of many potential biomarkers, providing great opportunities for improving the management of cancer patients.

3.4.1. Electrochemical Detection

Electrochemical detection combined with several nanomaterials offers great potential for the detection of clinically significant cancer biomarkers, and recently, various electrochemical biosensors for the detection of cancer biomarkers have been established. For example, an inkjet-printed gold nanoparticles (AuNPs) array immunosensor was fabricated for the multiple detection of the cancer biomarker interleukin-6 (IL-6) in serum. The AuNPs ink was printed on a flexible, heat resistant polyimide Kapton substrate. Captured antibodies for IL-6 were linked onto the eight electrode array, and used in sandwich immunoassays. In addition, a biotinylated secondary antibody with 16–18 horseradish peroxidase labels was used, and detection was achieved by hydroquinone mediated amperometry. These promising sensors are easily fabricated at relatively low cost, and could be mass-produced with commercial inkjet printers [57]. Furthermore, an electrochemical single nucleotide polymorphism (SNP) genotyping sensor for the analysis of a cancer-related gene sequence has also been reported. Combination of the gold nanoparticles (AuNPs)-base enrichment effect with the surface hybridization-based dragging strategy can improve detection sensitivity and signal amplification. With a large number of ferrocene (Fc) probes enriched with AuNPs and then dragged into close proximity to the electrode surface through DNA hybridization, a detection limit at the femtomolar level was achieved [58].

An aptamer-based competition assay for the electrochemical detection of acute leukemia cells was developed with high sensitivity. It utilized the competitive binding of cell-specific aptamers to acute leukemia cells and subsequent voltammetric quantification of the metal signature. Enhanced sensitivity was achieved with dual signal amplification using Fe_3O_4 magnetic nanoparticles (MNPs) as carrier to load a large amount of AuNPs and AuNPs-catalyzed silver deposition [59].

With aptamer-DNA concatamer-quantum dots (QDs) as recognizing probes, model cancer cells (CCRF-CEM cells) were detected using a MWCNTs@PDA@AuNPs modified electrode. The as-prepared electrode was applied to bind concanavalin A (Con A) for cell capture as shown in Figure 2. The developed supersandwich cytosensor showed high sensitivity with a detection limit of $50 \text{ cells}\cdot\text{mL}^{-1}$. More importantly, it could distinguish cancer cells from normal cells, which indicated the promising applications of the method in the clinical diagnosis and treatment of cancers [60]. Other sensors have recently been demonstrated for the electrochemical detection of specific DNA sequences of bladder cancer cells based on CdTe quantum dots (QDs) modified glassy carbon electrode (GCE).

Methylene blue (MB) was intercalated into the hybridized double stranded DNA (dsDNA) and used as electrochemical indicator for the detection of target DNA in a differential pulse voltammetry (DPV) mode. The CdTe QDs provided advantages of excellent electrochemical signal amplification due to their larger surface area, which can immobilize more single stranded DNA (ssDNA) probes on the electrode surface [61].

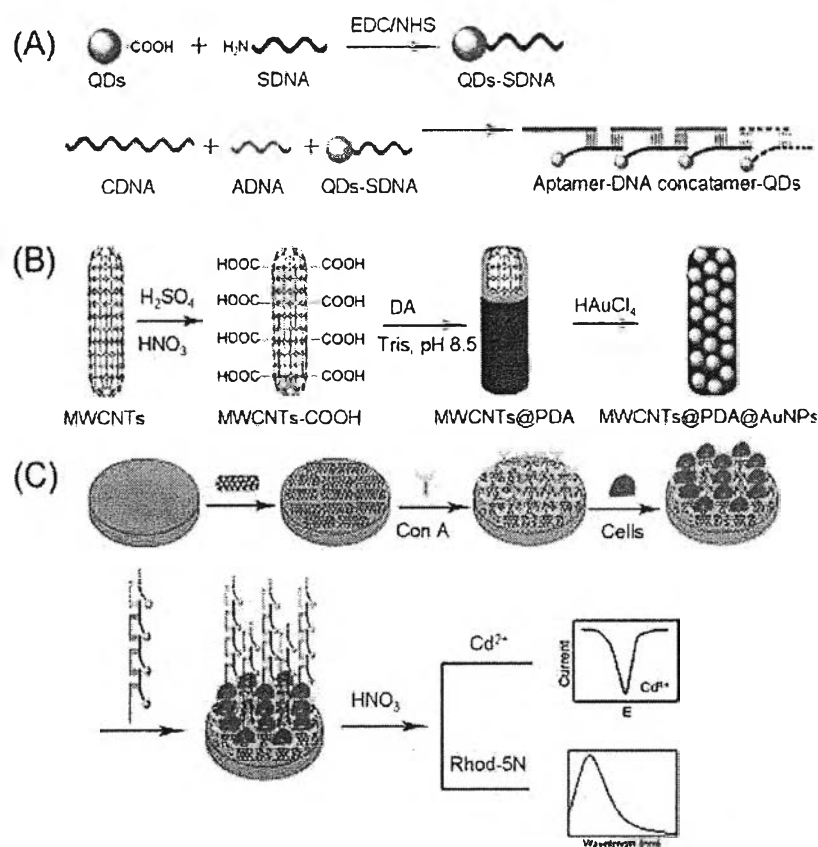


Figure 2. Procedures for the Fabrication of Aptamer-DNA Concatamer-QDs (A) MWCNTs@PDA@AuNPs Composites; (B) and Supersandwich Cytosensor; (C) [60]. Reprinted with permission from (Liu, H.; Xu, S.; He, Z.; Deng, A.; Zhu, J.J. Supersandwich cytosensor for selective and ultrasensitive detection of cancer cells using aptamer-DNA concatamer-quantum dots probes. *Anal. Chem.* **2013**, *85*, 3385–3392.). Copyright (2013) American Chemical Society.

3.4.2. Colorimetric and Spectrophotometric Detection

Many methods have been used to detect cancer biomarkers, such as a simple colorimetric assay reported by Wang *et al.* [62] for testing human telomerase activity. Telomerase is over-expressed in over 85% of all known human tumors. The working principle is based on the elongated primers conjugated to the gold nanoparticles (AuNPs) surface, which can fold into a G-quadruplex to protect the AuNPs from aggregation. Their assay has also been used for initial screening of telomerase inhibitors as anticancer drug agents. Recently, based on a localized surface plasmon resonance (LSPR) and the coupling plasmon mode of AuNPs, a strategy for the one-step dual detection of tumor-specific mutations (E542K and E545K) and methylation of circulating tumor DNA (ctDNA) of PIK3CA gene

has been reported. Peptide nucleic acid (PNA) is used as probe to capture and enrich the 69-bp PIK3CA ctDNA. Immunogold colloids are exploited as methylation detectors and plasmon coupling based enhancement for secondary response. Their results demonstrated that the sensor can simultaneously detect hot-spot mutations and epigenetic changes on ctDNA with this platform [63].

Magnetic nanoparticles (MNPs) have found widespread use for the detection of various cancer biomarkers. For example, the simultaneous detection of two biomarker of T helper cancer cells has been established. One biomarker conjugates with immunofunctionalized MNPs, enabling the separation of the T helper cells from a mixed population of cells. The other biomarker is used for the detection during ELISA analysis. The specific T helper cells can be quantified according to their ELISA absorbance values following magnetic separation [64]. In a similar assay, functionalized MNPs were also utilized for signal enhancement in conjunction with surface plasmon resonance (SPR) on gold nanoslits to detect mRNA heterogeneous nuclear ribonucleoproteins (hnRNP B1) in two cancer cell lines (CL1-0 and CL1-5). In this approach, MNPs were applied for a dual purpose: to isolate the target molecule from the sample matrix to prevent non-specific binding and to enhance the SPR response. The approach for the detection includes double hybridization at two different specific locations in two steps. First, the biomarker target molecules are captured with MNPs, and second, MNPs carrying the target molecules are introduced to the SPR chip to hybridize with probe immobilized on the gold nanoslits [65]. Another work has been reported by Fang *et al.* [66]. In their study, aptamer-conjugated upconversion nanoparticles (UCNPs) was used as nanoprobe to recognize circulating tumor cells (CTC), which were then enriched by attaching magnetic nanoparticles (MNPs) and placing them in the presence of a magnetic field. Owing to the autofluorescence-free nature of upconversion luminescence imaging, as well as the use of magnetic separation to further reduce background signals this method shows promise for CTC detection in medical diagnostics. Up to date, ELISA have most widely been applied in immunoassays. However, several unavoidable limitations of natural enzymes have hindered their widespread applications. Interestingly, an efficient colorimetric detection of target cells utilizing the superior catalytic activity of graphene oxide-magnetic-platinum nanohybrids has been presented. The nanohybrids consisted of Fe₃O₄ magnetic nanoparticles (MNPs) and platinum nanoparticles (PtNPs), simultaneously immobilized on the surface of graphene oxide (GO). Due to the highly catalytically active PtNPs and MNPs on GO whose frameworks possess high substrate affinity, the nanohybrid is able to achieve up to 30-fold higher maximal reaction velocity (V-max) compared to that of free GO for the colorimetric reaction of the peroxidase substrate, and enable rapid detection of target cancer cells. Specifically, using this assay system, breast cancer cells can be detected in 5 min with high specificity and sensitivity [67].

Detection of cancer biomarkers using semiconductor quantum dots (QDs) is another promising area of the research. Highly enhanced electrochemiluminescence (ECL) from a novel hybrid gold/silica/CdSE-CdS quantum dots nanostructures has been established for the first time, and successfully applied to develop an ultrasensitive ECL immunosensor for the detection of a protein tumor marker [68]. Liu *et al.* [69] also reported the use of multiplexed QDs and wavelength-resolved imaging to detect and characterize a class of low-abundant tumor cells in Hodgkin's lymphoma. To overcome the cellular heterogeneity and rarity problem, they have developed multicolor QD antibody conjugates to simultaneously detect a panel of four protein biomarkers (CD15, CD30, CD45, and Pax5) directly in human tissue biopsies. Furthermore, a versatile electrochemiluminescence (ECL)

assay for cancer cells based on dendrimer/CdSE-ZnS-quantum dot nanoclusters (NCs) as ECL probe has been reported. Capture DNA was designed as a high affinity aptamer to the target cell; a novel ECL biosensor for cancer cells was directly accomplished using the biobarcode technique to avoid cross-reaction. Moreover, magnetic beads (MBs) for aptamer immobilization were combined with a dendrimer/QD NCs probe for signal production in an ECL assay of cancer cells, which simplified the separation procedures. In particular, a cycle-amplifying technique using a DNA device on MBs was further employed in the ECL assay of cancer cells, which greatly improved sensitivity [70].

3.5. Chemical Substances

A large number of both organic and inorganic compounds are related to good physical condition and disease biomarkers. A group of chemical substances including drugs and ions are described in company with nanoparticles that enhance the sensitivity of the analysis in the following section.

3.5.1. Electrochemical Detection

The side effects of chemical substances, namely drugs used for treating acute pain, cancer, heart conditions, bacterial infections, neurological disorders, and respiratory disorders, are concentration dependent, and for this reason, their accurate quantification is critical. In this section, electrochemical detection using nanoparticles as modifiers are reviewed according to the sequential chemical substances listed above.

Nimesulide, zolmitriphan, acetaminophen or paracetamol (*N*-acetylaminophenol) are drugs used as analgesics. Nimesulide in medical tablets was detected by magnetic nanoparticles modified on a glassy carbon electrode. The results had a remarkable catalytic and enhancement effect on the reduction of the analyte and the reduction peak shifted positively compared with a bare electrode [10]. Silver nanoparticles/multiwalled carbon nanotube-modified glassy carbon electrodes showed an enhancement of oxidation peaks and were applied for the detection of zolmitriphan without interferences. The method was simple, sensitive, and reproducible [71]. The electrochemical detection of acetaminophen was reported in numerous references [72–74]. For example, electrochemically reduced graphene (ERG)-loaded nickel oxide (Ni₂O₃-NiO) nanoparticles coated onto a glassy carbon electrode displayed high electrocatalytic activity ascribed to the synergistic effect of the special composite structure and the physical properties of nickel oxide nanoparticles and graphene [73]. Acetaminophen had also been simultaneously detected in the presence of ascorbic acid, dopamine, and uric acid. Its detection limit as low as 0.05 μM benefited from coupling phenylethynyl ferrocene thiolate (Fc-SCA)-modified Fe₃O₄@Au NPs with a graphene sheet/chitosan modified glassy carbon electrode. The modified electrode exhibited synergistic catalytic and amplification effects towards the analytes [75].

Adriamycin is a trade name of doxorubicin, a drug known for cancer treatment. Its presence in calf thymus DNA was quantified with a glassy carbon electrode modified with silver nanoparticles and multiwalled carbon nanotubes with carboxy groups. The results showed excellent stability and low limit of detection [76].

Amiodarone, atenolol, and digoxin are employed in patients with heart disorder conditions, *i.e.*, cardiovascular disease and cardiac dysrhythmias. Magnetic nanoparticles were combined with a modified electrode to determine the amount of drugs. For amiodarone and atenolol, the nanoparticles

were loaded in crystalline material-41 grafted with 3-amiropropyl groups and modified on a carbon paste electrode. The anodic peak currents increased owing to the adsorption of amiodarone and atenolol [77]. Magnetic nanoparticles was coated on core-shell gold nanoparticles ($\text{Fe}_3\text{O}_4\text{-Au-NPs}$), labeled with antigen, and later modified on a screen-printed carbon electrode for the analysis of digoxin with a low detection limit. The modified electrode offered simplicity, low cost, high sensitivity, stability, and reliability [78].

Anti-bacterial drugs are ubiquitous since encounters with bacteria are inevitable. Oxacillin and rifampicin are examples of anti-bacterial drugs that can be detected by electrochemistry. With the fabrication of an indium tin oxide electrode including cobalt nanoparticles, the resulting sensor had an excellent selectivity and amplification of the electrochemical response signal for oxacillin detection in human blood serum samples [79]. Nickel hydroxide nanoparticles-reduced graphene oxide nanosheets ($\text{Ni(OH)}_2\text{-RGO}$) were prepared layer-by-layer on a graphene oxide (GO) film pre-cast on a glassy carbon electrode surface. The modified electrode exhibited a distinctly higher activity for the electro-oxidation of rifampicin. The peak currents was enhanced as a result of the fast electron transfer kinetics that arose from the excellent properties of RGO nanosheets and the exclusive properties of nanoparticles [80].

Chlorpromazine, clonazepam, and thioridazine are drugs used in the management of psychotic conditions. Cobalt nanoparticles modified on a carbon paste electrode showed high sensitivity for the detection of chlorpromazine in biological samples [81]. A glassy carbon electrode composed of silver nanoparticles and multiwalled carbon nanotubes was fabricated and had high electrocatalytic activity toward the reduction of clonazepam. Nanodiamond graphite, in addition, was decorated with silver nanoparticles for thioridazine detection. The enhancement in microscopic area and strong absorption of thioridazine increased the peak currents and offered high sensitivity. Moreover, the modification of nanoparticles displayed high stability, uniformity, and reproducibility [17].

Silver nanoparticles functionalized on various electrodes were used as sensitive tools for respiratory disorder drugs, for example, difficult breathing and tuberculosis. Amperometric detection of isoniazid exploiting a screen-printed carbon electrode modified with silver hexacyanoferrate in simulated human urine samples exhibited a detection limit as low as $2.6 \mu\text{M}$ [82]. Melamine functionalized silver nanoparticles were immobilized on the surface of an electrode and used for the determination of clenbuterol in biological fluids and illegal usage in livestock feeding. The approach had advantages of simplicity, rapid detection, highly sensitivity, and selectivity [83].

3.5.2. Colorimetric and Spectrophotometric Detection

Chemical substances including drugs and ions can be detected by optical methods and provide high sensitivity and selectivity similar to electrochemical detection. Sample analytes in this part are divided into anti-bacterial and antiviral drug, drugs for relieving heart failure, pain, skeleton muscle performance, and ions.

Entecavir and 5-fluorocytosine are used as antiviral and antimitotic drugs, respectively. The detection concept of both analytes was based on the aggregation of modified silver nanoparticles. The change from a dispersion to an aggregation resulted in a color change from yellow to wine red in the presence of entecavir. The aggregation was due to neutralization of the electrostatic repulsion. This

method was applied to real samples of human urine [84]. Along with *p*-aminobenzenesulfonic acid and silver nanoparticles, 5-fluorocytosine caused a color change from yellow to green and a SPR shift. The aggregation gave a green color to the solution due to an electron donor/acceptor reaction. The result was detectable by the naked eye at concentrations as low as 0.08 ppm [85].

Plasmon absorbance decreased with increasing amounts of captopril, a drug for hypertension and some types of heart failure. Modified silver nanoparticles composed of ascorbic acid as a reducer and sodium dodecyl sulfate as stabilizer were used as probe. The results exhibited a low detection limit in pharmaceutical formulation samples [86].

The tripan family drugs are used for migraines and cluster headache treatment. Silver nanoparticles were capped by citrate and utilized for detection. The results were observed as a color change from yellow, to orange, and to brown. The simple, sensitive, and rapid technique was employed in pharmaceutical tablets and nasal sprays [87]. Semiconductor CdTe quantum dots were fabricated as S- β -CD-MSA-CdTe. In the presences of acetylsalicylic acid (ASA), the fluorescence was enhanced. The method could be employed for detection of aspirin [88].

An inhibition of the chemiluminescent signal was observed after the addition of baclofen into L-cysteine-capped CdS quantum dots, KMnO_4 , and $\text{Na}_2\text{S}_2\text{O}_3$. The technique was applied for the detection of spasticity drugs showing higher sensitivity than CD-IMS [89].

Many ions act as a good representatives for disease and abnormal health status detection. For example, calcium ion as illustrative of bone condition and iodated salt as a health indicator are described [90,91]. Amino-functionalized carbon dots mixed with glutamic acid and hyaluronic acid were found to bind at bone cracks. Thus, the process was able to locate micro-cracks and map calcium deposition by fluorescence imaging [90]. Conjugated polyelectrolyte-stabilized silver nanoparticles were synthesized as light absorbers and 4-oxo-4(pyren-1-ylmethoxy) butanoic acid was used as an ideal fluorescence probe. Light absorbers quenched the ideal fluorophore and could be recovered after the addition of hydrogen peroxide and iodine ion based on the inner filter effect (IFE). The technique was used for determination of an iodate salt in urine samples [91].

3.6. Hormones

A hormone is a chemical messenger produced by the endocrine system that regulates body physiology and behavior such as growth and development, metabolism, sexual function, reproduction and mood. Endocrine glands secrete hormones directly into the blood, which transports the hormones through the body. Cells in a target tissue have receptor sites for specific hormones. However, too much or too little of a certain hormone can be serious. It takes only a tiny amount to cause big changes in cells or even the whole body. Thus, various laboratory tests for measuring hormone levels in biological fluids have been reported.

3.6.1. Electrochemical Detection

A simple, cost effective, selective and sensitive detection method is required for routine monitoring of the endocrine-disrupting compounds in real samples. Thus, an electrochemical aptasensor for endocrine disrupting 17β -estradiol based on a poly(3,4-ethylenedioxythiophene) (PEDOT) doped with gold nanoparticles (AuNPs) platform has been reported. The prepared electrode was employed for the

immobilization of biotinylated aptamer for the detection of the target. The electrochemical signal generated from the aptamer-target molecule interaction was monitored electrochemically using square wave voltammetry in the presence of $[\text{Fe}(\text{CN})_6]^{-3/-4}$ as a redox probe [92]. Moreover, an aptamer-based label free electrochemical biosensor was also used for 17β -estradiol detection. In that work, an aptamer was immobilized on a layered tungsten disulfide nanosheets/gold nanoparticle-modified glassy carbon electrode through Au-S interaction. The layered tungsten disulfide nanosheet/AuNPs film acted as an efficient platform for the assembly of bio-probes. After blocking with bovine serum albumin, the aptamer probe was then bound with the addition of 17β -estradiol to form an estradiol/aptamer complex on the electrode surface, which led to a significant decrease in peak current. The aptamer sensor holds great promise of sensitivity, reproducibility and could be extended to other analytes [93].

In addition, determination of insulin was also established by using a nickel oxide nanoparticles modified Nafion-multiwalled carbon nanotubes screen printed electrode (NiONPs/Nafion-MWCNTs/SPE). Cyclic voltammetric studies showed that the NiONPs/Nafion-MWCNTs film modified SPE lowered the overpotentials and improved the electrochemical behavior during insulin oxidation, as compared with the bare SPE. Moreover, amperometry was used to evaluate the analytical performance of the modified electrode in the quantitation of insulin. Excellent analytical performance was achieved under optimized conditions [94].

3.6.2. Colorimetric and Spectrophotometric Detection

Using multifunctional gold nanoparticles (AuNPs), a surface plasmon resonance (SPR) biosensor was developed for insulin detection in human serum. Bifunctional hydroxyl/thiol-functionalized fourth-generation polyamidoamine dendrimer (G4-PAMAM)-encapsulated AuNPs were synthesized and immobilized on a gold surface. Part of the dendrimer thiol groups were converted to hydrazide functionalities providing an activated surface available to subsequently immobilize the receptor. Herein, the resulting AuNPs dendrimer-modified surface provided an assay with high stability, significantly enhanced sensitivity, and a detection limit for analyzing insulin of 0.5 pM. The SPR detection of insulin was amplified due to the changes in the dielectric properties of the matrixes, occurring upon the biorecognition processes on the sensor surface, through the coupling of the localized plasmon of the NPs with the surface plasmon wave [95].

Europium (Eu(III)) chelate-bonded silica nanoparticles have been developed as a fluorescent label for a time-resolved immunofluorometric assay (TrIFA) for human thyroid stimulating hormone (hTSH). The fluorescent nanoparticle label allowed directly reading of the fluorescent signal, omitting the signal development step required for the commercial dissociation-enhanced lanthanide fluorescence immunoassay (DELFI) system. In combination of high sensitivity, short period of assay time, this developed method can be potentially used in hospitals for daily clinical practice in hTSH screening [96].

3.7. Lipids

Most of the fat found in food is in the form of triglycerides, cholesterol, and phospholipids. High cholesterol is one of the major controllable risk factors for coronary heart disease, heart attacks and strokes. Many people do not know their cholesterol is too high because there are usually no symptoms.

Therefore, the monitoring of cholesterol level is very important for clinical diagnosis. Many analytical methods have been developed for cholesterol determination using either enzymatic or non-enzymatic based methods.

3.7.1. Electrochemical Detection

To the present, electrochemical methods have been widely used to measure cholesterol levels. A gold nanoparticles (AuNPs)-modified cholesterol oxidase-based bioelectrode has been fabricated for the amperometric detection of cholesterol in human serum samples. The fabrication procedure was based on the deposition of AuNPs on a 1,6-hexanedithiol-modified gold electrode, functionalization of the surface of the deposited AuNPs with carboxyl groups using 11-mercaptopundecanoic acid and then covalent immobilization of cholesterol oxidase on the surface of the AuNPs film using *N*-ethyl-*N'*-(3-dimethylaminopropyl carbodimide) and *N*-hydroxysuccinimide ligand chemistry. The AuNPs provided an environment for enhanced electrocatalytic activities and thus resulted in an enhanced analytical response [97].

Besides, a porous tubular silver nanoparticles (AgNPs)-modified glassy carbon electrode (GCE) was also constructed as a working electrode for non-enzymatic cholesterol detection. The modified electrode showed markedly improved electrocatalytic activity toward cholesterol oxidation compared with solid Ag nanorods [98]. Likewise, a AgNPs-modified glassy carbon electrode (AgNPs/GCE) fabricated by an electrochemical deposition technique has also been reported for the determination of cholesterol in bovine serum based on coupling of enzymatic assay and electrochemical detection. The AgNPs catalyst possesses catalytic activity in hydrogen peroxide reduction, with no observed interference from easily oxidizable species such as ascorbic acid and uric acid. In addition, the main advantages for the use of AgNPs/GCE are in term of high sensitivity, high accuracy, and simple fabrication [99].

3.7.2. Colorimetric and Spectrophotometric Detection

Several examples of electrochemiluminescence (ECL)-based nanoparticles for cholesterol detection have been demonstrated. For example, an ECL biosensor based on an anodic ECL of luminol at low potential has been demonstrated. Firstly, C-60 was functionalized with L-cysteine (L-cys) giving an L-cys-C-60 composite, which was modified onto the surface of glassy carbon electrodes for adsorbing gold colloidal nanoparticles (AuNPs). Subsequently, cholesterol oxidase (ChO_x) was dropped onto the surface of the modified electrode to fabricate a cholesterol biosensor. This approach promises good reproducibility, stability and anti-interference ability [100].

In a second example, an ECL biosensor for cholesterol detection based on multifunctional core-shell structured microspheres (Fe₃O₄@SiO₂-Au@mpSiO₂) has been reported. These microspheres consist of a core of silica-coated magnetite nanoparticles, an active transition layer of gold nanoparticles (AuNPs) and a mesoporous silica shell. The microspheres possess a large surface area that can increase enzyme loading and an active transition layer AuNPs can also enhance the ECL signal, providing a better analytical performance [101].

3.8. Microorganism

Over millions of years, microbes and humans have formed a unique relationship. The huge majority of the microbes in the body are rendered harmless by the protective effects of the immune system. Microbes are even useful for various applications such as a source of antibiotics and vaccines to treat and prevent infectious diseases, but there are many ways that bacteria and other microbes can negatively affect human life.

3.8.1. Electrochemical Detection

A regenerating electrochemical impedance immunosensor has been constructed for the detection of type 5 adenovirus. The multi-layered immunosensor fabrication involved modification steps on gold electrodes: (1) modification with a self-assembled monolayer (SAM) of 1,6-hexanedithiol to which gold nanoparticles (AuNPs) were attached via the distal thiol groups; (2) formation of SAM of 11-mercaptoundecanoic acid onto the AuNPs; (3) covalent immobilization of monoclonal anti-adenovirus 5 antibody, with EDC/NHS coupling reaction on the nanoparticles. The immunosensor displayed a very good detection limit of 30 virus particles/mL and a wide linear dynamic range. An electrochemical reductive desorption technique was employed to completely desorb the components of the immunosensor surface, then re-assemble the sensing layer and reuse the sensor [102].

3.8.2. Colorimetric and Spectrophotometric Detection

Recently, a platform based on conjugating long spacer arms (LSA) of carboxymethylated glucan (CMG) onto magnetic nanoparticles (MNPs) was developed to enhance the chemiluminescence (CL) detection of infectious pathogens (hepatitis B virus (HBV)). CMG-MNPs are designed to have low steric hindrance and high suspension properties, which allow for facile modification and hybridization reactions that enhance the CL sensitivity and detection. The biotinylated amplicon of HBV was hybridized to DNA probes functionalized on CMG-MNPs. The magnetic complexes were then incubated with streptavidin-alkaline phosphatase (SA-AP) to form linkages. Finally, the magnetic complexes were mixed with AMPPD to generate a CL signal that is proportional to the concentration of HBV target. When optimized, the platform showed high specificity and a detection limit of 0.5 pM, which exhibited great promise for the early clinical diagnosis of infectious diseases [103]. In addition, a method for the detection of RNA virus (hepatitis C virus (HCV)) based on enzyme free MNPs extraction of nucleic acid and chemiluminescence has been reported. The specific lysis buffer conditions helped the nucleic acid adsorb on the surface of MNPs. The CL detection of HCV was achieved by incubating the biotin labeled RT-PCR products with probe-labeled MNPs and streptavidin-alkaline phosphatase (SA-AP) [104].

Simultaneous determination of human enterovirus 71 (EV71) and coxsackievirus B3 (CVB3) was also possible using dual-color quantum dots (QDs), as shown in Figure 3. The QDs are streptavidin-conjugated quantum dots (SA-QDs), and the antibodies are biotinylated antibodies. Biotinylated EV71 antibody (Ab_1) was associated with 525 nm green colored SA-QDs via biotin-streptavidin interaction forming QDs- Ab_1 , whereas biotinylated CVB3 antibody (Ab_2) was associated with 605 nm red colored SA-QDs via biotin-streptavidin interaction forming QDs- Ab_2 .

Graphene oxide (GO) was a quencher to the fluorescent of both QDs-Ab₁ and QDs-Ab₂. The target of EV1 and CVB3 can break up the complex of QDs-AB and GO, recovering the fluorescence of QDs-Ab₁ and QDs-Ab₂, respectively. Using these dual-color QDs, the two enterovirus can be simultaneously quantitatively determined with a single excitation light [105].

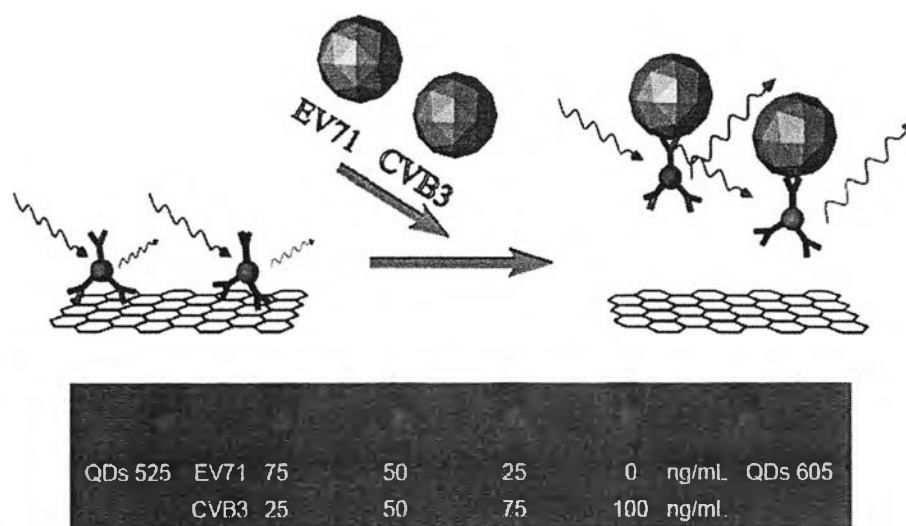


Figure 3. Schematic Presentation of the Multicolored QDs-Ab and GO Based EV71 and CVB3 Determination Biosensor and photovisualization of semiquantitative simultaneous determination of EV71 and CVB3 [105]. Reprinted with permission from (Chen, L.; Zhang, X.; Zhou, G.; Xiang, X.; Ji, X.; Zheng, Z.; He, Z.; Wang, H. Simultaneous determination of human enterovirus 71 and coxsackievirus b3 by dual-color quantum dots and homogeneous immunoassay. *Anal. Chem.* **2012**, *84*, 3200–3207.). Copyright (2012) American Chemical Society.

3.9. Neurotransmitters

Neurotransmitters have received considerable attention due to their important role in the human brain and body [106]. Dopamine has been recently an interesting target analyte of many research groups. Its deficiency causes cognitive malfunctions, such as Parkinson's disease [107]. Other neurotransmitters, *i.e.*, L-dopa, choline, and serotonin, also have essential role in animals.

3.9.1. Electrochemical Detection

Gold nanoparticle-modified electrodes have been individually and simultaneously used for detection of dopamine and L-dopa. For example, a gold nanoparticles functionalized carbon nanotubes (AuNP-CNT)-modified pyrolytic graphite electrode (AuNP-CNT/PGE) decreased the oxidation potential whereas oxidation currents were increased by five-fold compared with PGE in the determination of L-dopa [107]. Dopamine was detected simultaneously in urine serum with a modified glassy carbon electrode. The biosensor was fabricated by electrodeposition of Au-nanoclusters on a poly(3-amino-5-mercapto-1,2,4-triazole) (p-TA) film-modified glassy carbon electrode (GCE). The combination of materials produced a large surface area electrode and provided biological compatibility as well as good conductivity, stability, high sensitivity, and selectivity [108].

Ascorbic acid was a serious interference in the analysis of dopamine, thus a negatively charged electrode surface using PEGylated arginine functionalized magnetic nanoparticles was fabricated to resolve the problem. Dopamine interacted with the charged electrode and exhibited high sensitivity and selectivity for detection at a low concentration [109]. The fabrication of glassy carbon electrode modified-NiF₂O₄ magnetic nanoparticles decorated with multiwalled carbon nanotubes showed a synergistic effect toward the oxidation of dopamine without interference from other organic compounds, especially ascorbic acid, uric acid, cysteine, and urea. The results indicated a low detection limit and wide linear dynamic range for dopamine quantification in pharmaceutical, urine, and human blood serum samples [110].

A nanocomposite film of choline oxidase, multiwalled carbon nanotubes, gold nanoparticles, and poly(diallyldimethylammonium chloride) (PDDA) was used for choline detection. Gold nanoparticles was coated on the multiwalled carbon nanotubes by the interaction of gold and thiols. PDDA was utilized as dispersant and binder material. The film had good reproducibility and long term stability with anti-interference ability [111]. Other nanocomposites of cuprous oxide nanoparticles [112], gold nanoparticles [113,114], palladium nanoparticles [106], and zinc oxide nanosheets [115] present corresponding advantages resulting from their nanoparticles, including excellent sensitivity, selectivity, coupled with good stability.

Dopamine in commercial available human serum samples was analyzed without interferences using chitosan-stabilized silver nanoparticles and *p*-toluenesulfonic acid-doped ultrathin polypyrrole film. The results indicated a low detection limit of 0.58 nM [116]. Dopamine was detected simultaneously in the presence of uric acid and ascorbic acid [117,118]. For example, a silver nanoparticles-decorated reduced graphene oxide composite (AgNPs/rGO) was responsible for excellent electrocatalytic activity and well separated oxidation peaks. The method had good stability, sensitivity, and selectivity. It was applied for detection of these three compounds in commercial pharmaceutical samples, such as vitamin C tablets and dopamine injections [117]. Other neurotransmitters, namely serotonin, were detectable in plasma serum samples with a detection limit as low as 0.15 μM by utilizing a platinum electrode modified with multiwalled carbon nanotubes, polypyrrole, and colloidal silver nanoparticles [19].

Other metal nanoparticles were coated onto electrodes for the determination of dopamine, epinephrine, and L-dopa. To illustrate this, palladium nanoparticles with multiwalled carbon nanotubes and ionic liquids were decorated onto a carbon paste electrode for the simultaneous detection of dopamine, ascorbic acid, and uric acid. The results displayed three sharp and well separated peaks. The detection limit was in the nM range [119]. Epinephrine was detected in the presence of dopamine by square wave voltammetry. A glassy carbon electrode modified with nickel oxide nanoparticles and carbon nanotubes within a dihexadecylphosphate film was used for analysis of these compounds in human body fluids consisting of cerebrospinal fluid, human serum, and lung fluid [120]. Cobalt hydroxide nanoparticles and multiwalled carbon nanotubes was constructed on a carbon ionic liquid electrode for the detection of L-dopa and melatonin in pharmaceutical and human urine samples. The electrode provided high sensitivity as well as convenient preparation and high stability [121].

3.9.2. Colorimetric and Spectrophotometric Detection

Recent applications show that modified gold nanoparticles can be used for the visual detection of dopamine. For example, the use of BSA-stabilized Au nanoclusters (BSA-AuNCs) showed dramatically decreased the fluorescence intensity that could be inhibited upon the addition of dopamine. The signal decrease was due to the dopamine electrostatically attached to the BSA-AuNCs [122]. Moreover, melamine-induced aggregation of gold nanoparticles was inhibited in the presence of dopamine. The color changed from red to blue and could be detected by the naked eye. The aggregation was a consequence of strong hydrogen bonding between melamine and dopamine [123]. Dopamine was capped on the surface of gold nanoparticles and subsequently caused the aggregation. The reaction was catalyzed by thioglycolic acid that was modified through hydrolysis promoting Au-S bond formation. The addition of dopamine changed the solution color from red to purple, or red to yellow. The method provided a detection limit lower than the level of existence of dopamine in urine [124].

Many magnetic nanoparticles are reported to have peroxidase mimetic activity. As an illustration, $\text{Co}_x\text{Fe}_{3-x}\text{O}_4$ magnetic particles were synthesized and could effectively catalyze the reaction between 3,3',5,5'-tetramethylbenzidine or TMB and H_2O_2 . Dopamine, which possesses a hydroxyl group, was able to react as a reducing agent and consume the H_2O_2 . The blue color due to the interaction between TMB and H_2O_2 is eventually faded. The technique could quantify dopamine in human serum samples at low μM levels [125].

Silver nanoparticles have the ability to enhance the co-luminescent effects of rare earth ions such as Tb^{3+} and Y^{3+} . Dopamine could increase the luminescent intensity of the ions. The analyte in hydrochloride injection was determined at concentrations as low as nM level using this metal-enhanced fluorescence concept [126].

3.10. Nucleic Acids

Nucleic acids are nucleotide biopolymers. Nucleotides are composed of 5-carbon sugars, phosphate groups, and nitrogenous bases. RNA and DNA are types of nucleic acid. The two have different sugars, thus RNA is composed of ribose, whereas DNA is composed of deoxyribose. The nitrogenous bases are derivatives of pyrimidine (*i.e.*, cytosine, thymine, and uracil) and purine bases (*i.e.*, adenine and guanine). DNA and RNA are associated with gene expression. NADH is two nucleotides joined together at a phosphate group or so-called dinucleotide. It is a coenzyme that carries electrons from one reaction to another. Due to the prevalence of these substances in living cells, the detection of nucleic acids and their composition is important.

3.10.1. Electrochemical Detection

Gold nanoparticles were modified onto a mercapto-diazoaminobenzene monolayer-modified electrode (AuNPs-ATP-diazo-ATP) based on self-assembly for the detection of complementary single-stranded DNA. The DNA was determined with a detection limit of 9.10×10^{-11} M by differential pulse voltammetry with the use of $\text{Co}(\text{phen})_3^{3+}$ as an electrochemical indicator. The gold nanoparticles were assumed to be responsible for the efficient electron transfer ability. The modified electrode had in consequence good selectivity and was easily regenerated [127].

Magnetic nanoparticles were immobilized with linker DNA and CdS NPs for the hybridization of the target DNA. Utilizing the nicking endonuclease for cutting the specific strand of linker DNA, the target DNA was liberated and able to re-hybridize with other modified nanoparticles. When the linker DNA was transected, the CdS NPs was released. Hence, the amount of released nanoparticles was enhanced. The amplification signal was detected by SWV with a detection limit of 0.08 fM. The method possessed high sensitivity, satisfactory reproducibility, and excellent stability [128]. Fe₃O₄ magnetic nanoparticles were loaded onto the surface of a MWC-NTs-modified GC electrode for the detection of NADH by amperometric detection. The modified electrode presented the advantages of both MNPs and MWC-NTs. Fe₃O₄ has similar redox properties to mediators that favor the electron transfer between NADH and the electrode. As a result, the modified electrode catalyzed the oxidation of NADH at low potential and the overpotential was decreased. NADH could be detected with this technique with a detection limit of 0.3 μM. In addition, the method was used for detection of lactate by coupled dehydrogenase enzymes with a modified electrode. The detection limit for lactate using DPV was 0.5 μM. The method promised to offer an efficient transducer for the design of biosensors [129].

A TiO₂-graphene nanocomposite was modified on a glassy carbon electrode for the determination of purine bases, namely adenine and guanine. The detection limits of adenine and guanine were 0.10 and 0.15 μM, respectively. The electrocatalytic activity was improved because the modified electrode had a high adsorptivity and conductivity [130]. AuNPs/rGO was formed on GCE with redox mediators and enzymes for NADH detection. The modified electrode produced an excellent direct electrocatalytic oxidation of NADH due to a large active surface area and a favorable environment for electron transfer between NADH and the electrode. The electrocatalytic current density was 2–3 times higher compared with AuNPs alone. The detection limit was 1.13 nM (S/N = 3). The interferences, *i.e.*, glutathione, glucose, ascorbic acid, guanine, were negligible. The method was applied in human urine samples [131]. CdSe QDs-GO was immobilized on a paraffin wax-impregnated graphite electrode (PIGE) for adenine and guanine detection. The modified electrode showed excellent electrocatalytic activity for the oxidative determination of adenine and guanine with a good peak separation of 0.31 V. The detection limits of adenine and guanine were 0.028 and 0.055 μM, respectively. The method was employed for herring sperm DNA as an example of a real sample [132].

Poly(styrene-co-acrylic acid) microbeads were functionalized with CdTe quantum dots for the detection of DNA. The engagement of quantum dots made the polybeads an effective platform for labelling DNA and protein. The CdTe-tagged polybeads with a DNA probe specific to breast cancer was used for determination of DNA using SWV to measure Cd²⁺ after dissolution of CdTe tags with HNO₃. The detection limit of this technique was 0.52 fM [133].

Graphene was easily coated with polydopamine and funtionalized with AgNPs in order to assemble an electrode for the detection of the nucleic acid derivatives. The confirmation of electrode doping was illustrated by comparing pre-coating images obtained by SEM, TEM, and XRD with post-coating images. HS-SSDNA was immobilized and methylene blue was utilized as an electrochemical indicator for the determination of DNA. The results showed the detection limit of 3.2×10^{-15} M (S/N = 3) and high selectivity of differentiation of one-base mismatched DNA [134]. A similar technique for the determination of adenine and guanine was reported having a detection limit of 2.0 and 4.0 nM, respectively. The modified electrode showed more favorable electron transfer kinetics than both Gr-modified GCEs and AgNPs-modified GCEs [135].

Nickel and nickel oxide nanoparticles were modified on a GCE for the detection of DNA and NADH. NADH was detected with a NiO_xNPs/GC electrode by chronoamperometry without using any electron mediator. The detection limit was 106 nM (S/N = 3). The modified electrode possessed excellent electrocatalytic activity toward oxidation of NADH at a reduced voltage [136]. Likewise, a GCE was modified with NiNPs dispersed on PDAN for the detection of NADH. The modified electrode provided a positively synergistic effect in the electrochemical oxidation of NADH with excellent selectivity. Three types of voltammetry were employed including CV, SWV, and DPV. Each had a different detection limit of 0.378, 0.122, and 0.02 μM, respectively [137]. In another reference the immobilization of a DNA probe and a [Ru(NH₃)₅Cl]PF₆ complex onto a NiO_x(NP) modified GCE was reported. NiO_x(NP) provided strong affinity for phosphate groups, thus oligonucleotide probes with a terminal phosphate group can be attached to the surface of the modified electrode for the detection of DNA. The detection limit was 6.8×10^{-11} M. The Ru-complex only responded to the complementary sequence of DNA. The technique has the advantages of good selectivity, good sensitivity, excellent reproducibility, stability, and simplicity [138].

3.10.2. Colorimetric and Spectrophotometric Detection

The Stx-2 gene that causes disease in human was used as an example of colorimetric detection by gold nanoparticles (GNPs). GNPs were functionalized with thiolated ssDNA complementary to a target specific based-pair of stx-2 genes [139]. A detection and capture probe were reported in another reference for miRNA determination. The detection probe consisted of thiol-DNA and gold nanoparticles, while the capture probe had biotin-single strand DNA as a combination. Avidin immobilized on a flow strip could capture the avidin-biotin-Au-sample complex so that miRNA was detected at levels as low as 1 fM without silver enhancement [140].

Magnetic nanoparticles were functionalized for the detection of DNA. There were two probes for trapping and sensing, respectively. Complementary DNA was covalently immobilized on the target for the fabrication of the trapping probe, which had the responsibility of concentrating the target DNA from complex. The detection probe, on the other hand, was made from Fe₃O₄@Al₂O₃ magnetic nanoparticles and riboflavin-5-monophosphate (RFMP) through Al-phosphate chelation. RFMP is a fluorescent dye used in a reaction in which the displacement of DNA on the probe would release RFMP into the solution and enhanced fluorescent intensity. Ultimately, the DNA remaining on the probe was detected by MALDI-MS [141]. Target mutant DNA with a hairpin loop portion consisted of biotin at 3' and isothiocyanate (FITC) at 5' forming a nicking site for nicking endonuclease (NEase). NEase would cleave the hairpin and DNA, releasing parts with fluorescence for signal detection and DNA that was able to initiate the recycling process. Hence, the amount of fluorescence was increased and could be quantified. The method was applied for the detection of p53 gene and had high selectivity toward mismatched DNA [142].

HIV-1 and HIV-2 at a single molecule level could be detected by functionalized quantum dots (QDs). The QDs had two functions. One was to act as a concentrator, and another as fluorescence pair. The technique was simple, showing high sensitivity and low sample consumption with short analysis times [61].

The determined of adenine with magnetic nanoparticles decorated with silver nanoparticles via photochemical reduction was proposed. The modified particles had a seven-fold signal enhancement and could be used for the detection of adenine at a few hundred nanomolar concentration [143].

A sandwich-type DNA sensor was fabricated. Magnetic nanoparticles were functionalized at the amino group of DNA, whereas the other DNA had a carboxyl functionalized by gold nanoparticles. Cobalt nanoparticles were modified onto DNA-functionalized gold nanoparticles to amplify the detection signals. Later, the mixture of functionalized magnetic and modified gold nanoparticles would liberate cobalt ions in the presence of acid, and the chemiluminescence of the cobalt ions could be detected in the presence of luminol and H_2O_2 with a low detection limit [144].

3.11. Proteins

Proteins are large biomolecules composed of amino acids that polymerizes to polypeptides. Proteins are essential compounds to many living beings, especially animals. They influence health through dietary consumption, and protein deficiency affects growth, therefore, the quantification of proteins is important. There are many forms of protein that play critical roles in the living systems, but most publications refer to thrombin due to its crucial property as a part of the blood coagulation system. Other protein and protein derivative analytes are also described in the following subsections.

3.11.1. Electrochemical Detection

Gold nanoparticles with antithrombin-aptamer as molecular recognition element improved the sensitivity for thrombin detection. The combination was self-assembled on the surface of a bare electrode using 1,6-hexanedithiol. The redox couple was monitored for the electron transfer resistance of the aptasensor. The detection limit was 0.013 nM. The aptasensor showed good selectivity toward thrombin against other proteins [145]. Another approach presented an aptamer-gold nanoparticles-horseradish peroxidase (HRP) sensor for the detection of thrombin. A capture probe of aptamer 1 immobilized onto the core/shell Fe_3O_4/Au magnetic nanoparticles and a detection probe of aptamer 2 labeled with AuNPs and HRP was fabricated. Thrombin linked the captured and detection probe together causing an amplification of the signal. The method was simple, rapid, and selective. It showed great performance in the determination of thrombin in disease diagnosis [146].

An electrochemical platform based on $Fe_3O_4@polyaniline$ nanoparticles ($Fe_3O_4@PANI$ NPs) has been developed for the detection of creatinine in human plasma and urine. The creatinine target molecule was self-assembled on the surface of nanoparticles through N-H hydrogen bonding. Molecular imprinted polymers (MIPs) were established on a magnetic glassy carbon electrode. The sensors exhibited high sensitivity and selectivity for creatinine with a low detection limit [147]. The electrochemical signals modified by micro- and nanoparticles for detection of *Plasmodium falciparum* histidine-rich protein (HRP2) that is related to malaria were compared. The particles were immobilized with HRP2-antibody and horseradish peroxidase (HRP), and then captured by graphite-epoxy composite (m-GEC) which was used as the transducer for the detection. The results showed that magnetic nanoparticles had better analytical performance for a rapid, simple, cost-effective, and on-site detection of HRP2 in blood [148]. The schematic of the detection method is illustrated in Figure 4.

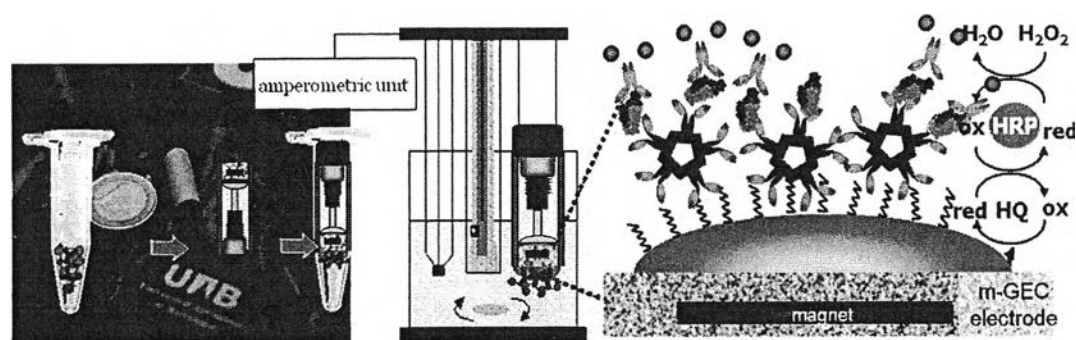


Figure 4. Schematic representation of the experimental details of the *P. falciparum* antigen (HRP2) related to malaria disease in human serum for the electrochemical magneto immunosensor [148]. Adapted with permission from (de Souza Castilho, M.; Laube, T.; Yamanaka, H.; Alegret, S.; Pividori, M.I. Magneto immunoassays for plasmodium falciparum histidine-rich protein 2 related to malaria based on magnetic nanoparticles. *Anal. Chem.* **2011**, *83*, 5570–5577.). Copyright (2011) American Chemical Society.

Graphene/3,4,9,10-perylenetetracarboxylic acid (GPD) with a three-dimensional porous structure had been fabricated as a redox probe. The novel probe has a high electrochemically active area and conductivity. In thrombin detection, the probe showed higher sensitivity compared with other redox probes [149]. ST6Gal-I is a protein marker of tumors and cancer. It was detected using a modification of nanocomposites and gold nanoparticles. The nanocomposites were Prussian Blue-based (PB). The technique had excellent sensitivity and selectivity and could be used for quantification of the protein in human serum samples with a detection limit as low as $3 \text{ pg} \cdot \text{mL}^{-1}$ [150].

Silver nanoparticles decorated with ZnO nanotubes were used as tools for the detection of D-dimer. D-dimer is present in humans under thrombosis (DVT) disorder conditions. Firstly, ZnO nanorods were etched into nanotubes that later would be covered with silver nanoparticles. The biosensor exhibited a low detection limit with acceptable selectivity and reproducibility. The method promised specific detection of D-dimer in clinical and real samples [151].

3.11.2. Colorimetric and Spectrophotometric Detection

Thrombin is detected by various colorimetric techniques. For example, gold nanoparticles with the addition of thrombin in an excess of fibrinogen induced the formation of insoluble fibrin-AuNPs as a result of the polymerization of the unconjugated and conjugated fibrinogen. The absorbance of the supernatants decreased as the amount of thrombin increased. This probe exhibited high sensitivity and selectivity over other proteins. The limit of detection is lower than those obtained using other nanomaterial- and aptamer-based detection methods. The technique has potential for the detection of thrombin in disease diagnosis [152]. Another reference [153] reported a technique similar to the previous one for quantification of thrombin without interferences from proteins such as bovine serum albumin, pepsin, trypsin, *etc.* The catalytic activity of gold nanoparticles in the luminol H_2O_2 chemiluminescent method (CL) was used for the detection of thrombin. The effective binding of the target protein and aptamer could induce the aggregation of gold nanoparticles, and subsequently

enhance the CL reaction. This biosensor provided a simple, cheap, rapid, and sensitive method for detection of thrombin [154].

The parallel concept of aptamer-induced aggregation was applied in magnetic nanoparticles for thrombin detection. Gold-coated iron oxide nanoparticles were synthesized. The synthesized nanoparticles had a flowerlike or nanorose shape. The nanorose changed from well dispersed to an aggregated state in the presence of human- α thrombin, which resulted in an alteration of the UV-Vis absorption spectra. The dual detection of qualification and quantification was advantageous as it provided more reliable results. The technique was used for detection of thrombin at low detection limits [155]. Likewise, magnetic nanoparticles with antithrombin aptamer conjugated on SPR gold film was used for detection of thrombin by SPR spectroscopy with a low detection limit. The selectivity of the technique was tested using three kinds of protein including BSA, human IgM, and human IgE. The results showed that the nanoparticles were an excellent amplification reagent in SPR detection of thrombin and had great performance [11]. Other approaches were employed for the quantification of thrombin, the signal enhancement being due to core-shell gold capped magnetic nanoparticles (GMPs) was an example. In a solution comprised of thrombin aptamer 1 and GMP5-Apt2 conjugates a remarkably increase in SPR angle was displayed due to the larger mass and higher refractive index of GMP5-Apt2 compared with gold nanoparticles. Thus, a low level detection limit could be achieved. The method presented a novel option for protein detection and disease diagnosis [156]. Besides thrombin, various analytes such as C-reactive protein (CRP), bovine serum albumin (BSA), and cardiac troponin I (cTnI) have utilized magnetic nanoparticles as a significant features for colorimetric detection [4,7,157].

Quantum dot coupling with thrombin aptamer was used for the quantification of thrombin. QDs-apt:B was constructed by assembling the quantum dots with a single-stranded aptamer, then staining the duplex regions of the aptamer with a DNA intercalating dye (BOBO-3). The dye was released as thrombin induced the folding of the aptamer. The QD fluorescence resonance energy transfer (FRET)-mediated BOBO-3 emission decreased, therefore, the technique could be applied to evaluate the thrombin level [158]. Moreover, quantum dots functionalized with aptamer as well as magnetic nanoparticles functionalized by aptamer showed ability for the determination of thrombin with low detection limits. The system was assembled on a chip using fluorescence as a detection technique. The results revealed that the on-chip platform had advantages of speed and efficiency [159].

A protein derivative such as an amino acid can be detected using nanoparticles too. For example, short peptide chains were hydrolyzed into the negative peptide apart and positively charged dipeptides, in the presence of trypsin. The dipeptides were able to cap on the surface of silver nanoparticles and induce aggregation under salt conditions. The interaction caused a change in the color of the solution, which could be detected by UV-Vis spectrophotometry and the naked eye. This technique provided a novel strategy for trypsin determination in clinical applications [160]. An aptamer was functionalized on silver nanoparticles (apt-AgNPs) for the determination of platelet derived growth factor-BB (PDGF-BB) protein. First, the aptamer and ssDNA were loaded on the nanoparticle surface to form a probe. Second, the probe could cause metal deposition by catalyzing the reduction of metallic ions in a color agent. The corresponding results could be captured by the naked eye. There were two coloring agents, namely silver enhance solution, and color agent 1 which was a solution of HAuCl_4 and hydroquinone. The results demonstrated that color agent 1 had benefits over the other option,

especially at low detection limits due to its superior sensitivity. The development showed good potential in complex biological samples [29].

3.12. Sugars

Diabetes is a metabolic disease, which can cause serious health effect such as heart disease and kidney failure. Thus, monitoring of glucose levels is required for the diagnosis and control of diabetes. For this purpose, various analytical methods based on the use of the nanomaterials have been established for glucose monitoring.

3.12.1. Electrochemical Detection

According to the sugar determination, this approach can be classified into two main groups: enzymatic and non-enzymatic methods. Enzymatic methods are highly selective, fast and sensitive, but several parameters can affect enzyme activity. To overcome these disadvantages, many glucose sensors that have been made are based on non-enzymatic methods such as those of Ismail *et al.* [161] who reported a non-enzymatic electrochemical glucose sensor based on a graphene oxide nanoribbon (GONRs)-gold nanoparticle (AuNPs) hybrid. They found that AuNPs supported by GONRs were greatly superior to the unsupported conventional bare gold electrode, with a greatly enhanced current density (approximately by 200%). This is attributed not only to the high total surface area of the AuNPs compared to that of a Au sheet, but also to the three-dimensional specific interaction between the functional groups on the GONRs and the Au active sites with the reactant and the intermediates that promote the reaction kinetics. Another non-enzymatic glucose sensor was also developed based on the electrocatalytic oxidation activity of nanoporous gold (NPG) toward glucose. The NPG electrode was prepared by a rapid one-step square-wave oxidation reduction cycle (SWORC). The prepared NPG electrode had high roughness, and excellent electrocatalytic activity toward glucose electrooxidation. In addition, Nafion was selected as a protective film to enhance the specificity of the developed glucose sensor with no interference from ascorbic acid and uric acid [162].

To increase the sensitivity of enzymatic glucose biosensors, several articles have been published based on the use of magnetic nanoparticles (MNPs) as an immobilization platform for glucose oxidase (GOD). A conductive-catalyst system that consisted of Fe_3O_4 MNPs and oxidative enzymes co-entrapped in the pores of mesoporous carbon, forming a magnetic mesoporous carbon (MMC) has been fabricated. GOD is subsequently immobilized in the remaining pores of the MMC using glutaraldehyde cross-linking to prevent enzyme leaching. H_2O_2 is generated by the catalytic action of GOD in proportion to the amount of the glucose and is subsequently reduced in H_2O by the peroxidase mimetic activity of MNPs generating a cathodic current, which can be detected through the conductive carbon matrix [163]. Furthermore, a practical glucose biosensor with immobilization of glucose oxidase (GOD) enzyme on the surface of citric acid (CA)-assisted cobalt ferrite (CF) magnetic nanoparticles (GOD/CA-CF/GCE) has been reported. This approach worked on the principle of detection of H_2O_2 which is produced by the enzymatic oxidation of glucose to gluconic acid. This sensor has tremendous potential for application in glucose biosensing due to its higher sensitivity and a substantial increment of the anodic peak current [164]. In order to improve the sensitivity, an amperometric glucose sensor based on an enhanced catalytic reduction of oxygen using GOD adsorbed

onto core-shell $\text{Fe}_3\text{O}_4@\text{silica}@\text{Au}$ MNPs has been reported. The authors found that the immobilized GOD retained its bioactivity with protein load and exhibited a fast heterogeneous electron transfer rate [165]. Another work demonstrated magnetic single-enzyme nanoparticles (MSEs) encapsulated within a composite $\text{Fe}_3\text{O}_4/\text{poly}(\text{pyrrole-N-propylsulfonic acid})$ network. The MSEs were then modified onto a magnetic glassy carbon electrode (MGCE) through magnetic immobilization. The modified electrode exhibited high selectivity, stability and rapid operation for the detection of glucose [9].

Nanocomposites have also found widespread use for monitoring glucose. This is due to their greatly enhanced electrocatalytic activity toward glucose in the electrochemical detection step. In these systems, chronoamperometry or amperometry are often performed, which are very suitable for the determination of glucose. Using a PtPd/MCV nanocomposite (PtPd bimetallic alloy nanoparticles on onion-like mesoporous carbon vesicle (MCV))-modified glassy carbon electrode, a nonenzymatic glucose sensor has been reported. Compared with Pt/MCV nanocomposite, the PtPd/MCV nanocomposite displays an enhanced current response toward glucose. The particular lamellar structure of the MCV also resulted in favorable transport passage for glucose [166]. Glucose was also measured based on integration of glucose oxidase (GOD) with a Pt nanoparticles/ordered mesoporous carbon (OMC) nanocomposite-modified electrode. In this approach, GOD was immobilized by entrapment in an electropolymerized pyrrole film for the construction of a glucose biosensor, providing great sensitivity [167]. Moreover, a non-enzymatic glucose sensor based on a glassy carbon electrode has been recently modified with copper oxide (CuO) nanocubes-graphene nanocomposite [168], nickel hydroxide/graphene nanocomposite [169]. GOD immobilized on poly(methylene blue) doped silica nanocomposites ($\text{PMB}@\text{SiO}_2$) was also constructed on a glassy carbon electrode. Compared with poly(methylene blue) film, $\text{PMB}@\text{SiO}_2$ had more advantages in facilitating electron transfer between GOD and the electrode surface [170]. Recently, a high performance non-enzymatic glucose sensor based on polyvinylpyrrolidone (PVP)-stabilized graphene nanosheets (GNs)-chitosan (CS) nanocomposite was demonstrated. Benefitting from the synergistic effect of GNs (large surface area and high conductivity), NiNPs (high electrocatalytic activity in glucose oxidation) and CS (good film-forming and antifouling ability), this enzyme-free sensor was established with outstanding detection limits and attractive selectivity [171]. An *in-situ* polypyrrole cross-linked chitosan/glucose oxidase/gold bionanocomposite film was fabricated to construct a simple glucose sensor. The resulting bionanocomposite provided a suitable environment for the enzyme to retain its bioactivity under quite extreme conditions, and the decorated AuNPs in the bionanocomposite offer good enzyme affinity [172]. Glucose was also measured by an enzyme-free sensor based on chemical oxidative polymerization of pyrrole monomers on the surface of CuFe_2O_4 nanoparticles (core-shell- $\text{CuFe}_2\text{O}_4/\text{PPY}$ nanocomposite). It was shown that the presence of pyrrole increased the electronic interaction between NPs and the polypyrrole matrices [173]. To improve the sensitivity and prevent GOD from leaching away, a sensitive glucose sensor based on the immobilization of GOD on hollow Pt nanospheres assembled on graphene oxide (GO)-Prussian Blue (PB)-3,4,9,10-perylenetetracarboxylic dianhydride derivative (PTC- NH_2) nanocomposite film has been reported [174]. Interestingly, to pursue high performance for non-enzymatic glucose sensors, the modified electrode coupling with concentrated hydroxide electrolyte based on a fast conversion of the redox couple ($\text{Ni}(\text{OH})_2 \leftrightarrow \text{NiOOH}$: $\text{Ni}^{\text{II}}/\text{Ni}^{\text{III}}$) on $\text{Ni}(\text{OH})_2$ nanoparticles-modified carbon ($\text{Ni}(\text{OH})_2/\text{C}$) nanocomposites has been established. The excellent performance for glucose detection is attributed to

the fast conversion of $\text{Ni}^{\text{II}}/\text{Ni}^{\text{III}}$ which is accelerated by an adequate hydroxide electrolyte concentration, fast electron transfer in the carbon skeleton, and high activity of $\text{Ni}(\text{OH})_2/\text{C}$ nanocomposite [175].

Silver nanoparticles (AgNPs) are of interest for the electrochemical detection of glucose. Several papers have been published based on the use of AgNPs for the modification of the electrode. For example, an enzymatic glucose sensor based on immobilizing glucose oxidase (GOD) on a AgNPs-decorated multiwalled carbon nanotube (AgNP-MWNT) modified glass carbon electrode (GCE) has been reported. The AgNP-MWNT composite membrane showed improved biocompatibility for GOD immobilization and an enhanced electrocatalytic activity toward reduction of oxygen due to the decoration of AgNPs on MWNT surfaces. The AgNPs also accelerated the direct electron transfer between the redox-active site of GOD and the GCE surface because of their excellent conductivity and large capacity for protein loading, leading to direct electrochemistry of GOD [176]. In a second example, an amperometric glucose sensor based on silver nanowires (AgNWs) and chitosan (CS)-glucose oxidase (GOD) film was demonstrated. The results indicated that AgNWs play an important role in the enhanced electron transfer between the immobilized GOD and the surface of electrode, which are attributed to large surface-to-volume ratio and high conductivity of AgNWs [177]. Recently, a simple method for the decoration of graphene oxide (GO) with AgNPs as the catalyst material was used for the glucose sensor applications. The total response of the sensor was improved significantly, mainly because of the synergistic interaction between the AgNPs and GO [178].

Owing to the unique properties of the mentioned metal nanoparticles, other metal nanoparticles have also been used in non-enzymatic sensors to enhance the sensitivity. Cobalt nanoparticles (CoNPs) are alternative metal nanoparticles that have good potential for glucose sensing due to a prominent electrocatalytic activity toward glucose. For instance, a non-enzymatic amperometric sensor based on a cobalt oxide nanoparticle-modified glassy carbon (CONM/GC) electrode was reported. The modified electrode exhibited excellent performance for glucose determination, sensitivity and fast response times [179]. Moreover, a selective sensor based on cobalt oxide nanoparticles electrodeposited on reduced graphene oxide was also used, which displayed a remarkably selectivity toward glucose [180]. Another sensor has been reported using a new type of cobalt nanoparticle modified indium tin oxide electrode made by an ion implantation technique [181].

Nickel nanoparticles (NiNPs) are another type of metal nanoparticles that exhibit excellent electrocatalytic ability toward glucose broadly used in glucose sensors. Nie *et al.* [182] reported a non-enzymatic glucose sensor based on using well-distributed NiNPs on straight multi-walled carbon nanotubes (SMWNTs) nanohybrids, which were synthesized through an *in situ* precipitation procedure. The observed remarkable enhancement in electrocatalytic activity can be attributed to the synergistic effect of SMWNTs and $\text{Ni}^{2+}/\text{Ni}^{3+}$ redox couple. Nickel hexacyanoferrate nanoparticles (NiHCF)-modified TiO_2 nanotube arrays (TNTs) were also applied for the non-enzymatic detection of glucose. NiNPs were deposited on TNTs by a pulse electrodeposition method and then converted to NiHCF by cyclic voltammetry in a solution containing $[\text{Fe}(\text{CN})_6]^{3-}$ [183]. Furthermore, NiNPs electrodeposited on reduced graphene oxide film have also been reported [184]. In order to achieve a higher sensitivity, a single layer of nickel hydroxide nanoparticles ($\text{Ni}(\text{OH})_2\text{NPs}$) covered on a porous Ni foam electrode was successfully applied for the quantification of glucose by an amperometric method [185].

Palladium nanoparticles (PdNPs) are also of interest as a great potential catalyst for improving the performance of glucose sensors. For example, PdNPs modified on functional carbon nanotubes (FCNTs) have been reported. Based on the electrochemical results, PdNPs efficiently catalyzed the oxidation of glucose and showed excellent resistance towards poisoning from interfering species such as ascorbic acid and uric acid [186]. Similarly, PdNPs were also electrodeposited on an epoxy-silver electrode, where the PdNPs act as catalyst for the direct oxidation of glucose [187]. Well-dispersed PdNPs were also prepared on graphene oxide (PdNPs/GO) using a simple ultrasonic method. The results showed that GO acted as a good supportive substrate for controlling the size and activity of PdNPs [6]. PdNPs deposited on surfactant-functionalized multi-walled carbon nanotubes (MWCNTs) were also synthesized by a facile spontaneous redox method. The as-prepared Pd catalyst showed excellent catalytic activity toward oxidation of ethanol and glucose which indicated a great potential for improving the performance of direct ethanol fuel cells and glucose sensors [188]. Furthermore, PdNPs supported on multi-walled carbon nanotubes (MWCNTs) were also synthesized by a simple *in situ* ultrasonication process at room temperature. The PdNPs could help increase the current signal due to their high surface area and the physical adsorption of the glucose molecules onto the large surface area of the electrode. More importantly, the electrode is highly resistant against poisoning by the interference from the oxidation of common interfering agents [189].

3.12.2. Colorimetric and Spectrophotometric Detection

Colloidal gold is extensively used for molecular sensing because of the flexibilities it offers in terms of modification of the gold nanoparticles (AuNPs) surface with a variety of functional groups. To enable glucose detection, the naked eye detection of glucose in urine has been reported. Thiol-capped AuNPs were functionalized with glucose oxidase (GOD) using carbodiimide chemistry. A visible color change of the GOD-functionalized AuNPs from red to blue was observed [190], as shown in Figure 5. Another colorimetric assay for the detection of sugars was also demonstrated. The synthesis of Au-NPs in presence of glucose as reducing agent in different conditions has been achieved, allowing the formation of pink or blue color NPs, and this has been employed in the design of two colorimetric assays. Both assays rely on the analyte-induced intensity increase (without any shift) of the NPs plasmon band absorption. The pink assay is based on the sugar-assisted chemical synthesis of NPs while the other is based on the AuNPs synthesis catalyzed by the glucose oxidase enzyme. This colorimetric assay did not suffer from bleaching of the final color because the stability of the AuNPs [191].

A fluorometric method for the determination of glucose and hydrogen peroxide using BiFeO₃ magnetic nanoparticles (BFO MNPs) has been reported. The authors found that BFO MNPs can catalyze the decomposition of H₂O₂ to produce OH radicals, which in turn oxidize the weakly fluorescent benzoic acid to a strongly fluorescent hydroxylated product with a maximum emission at 405 nm [192]. Moreover, a renewable glucose biosensor based on GOD immobilized on MNPs was constructed. The GOD was covalently cross-linked to the surface of synthesized Fe₃O₄ nanoparticles, then adhered to a solid parafin carbon paste electrode by magnetic force to fabricate a working electrode. H₂O₂ was produced by the enzymatic reaction of GOD and electrochemiluminescence (ECL) could be obtained by the reaction between luminol and H₂O₂ [193]. Furthermore, a colorimetric detection of glucose based MFe₂O₄ (M = Mg, Ni, Cu) MNPs has been proposed. This nanomaterial

exhibited catalytic activities similar to those of biological enzymes that could catalyze H_2O_2 to produce hydroxyl radicals, which oxidized peroxidase substrate to produce a color [194].

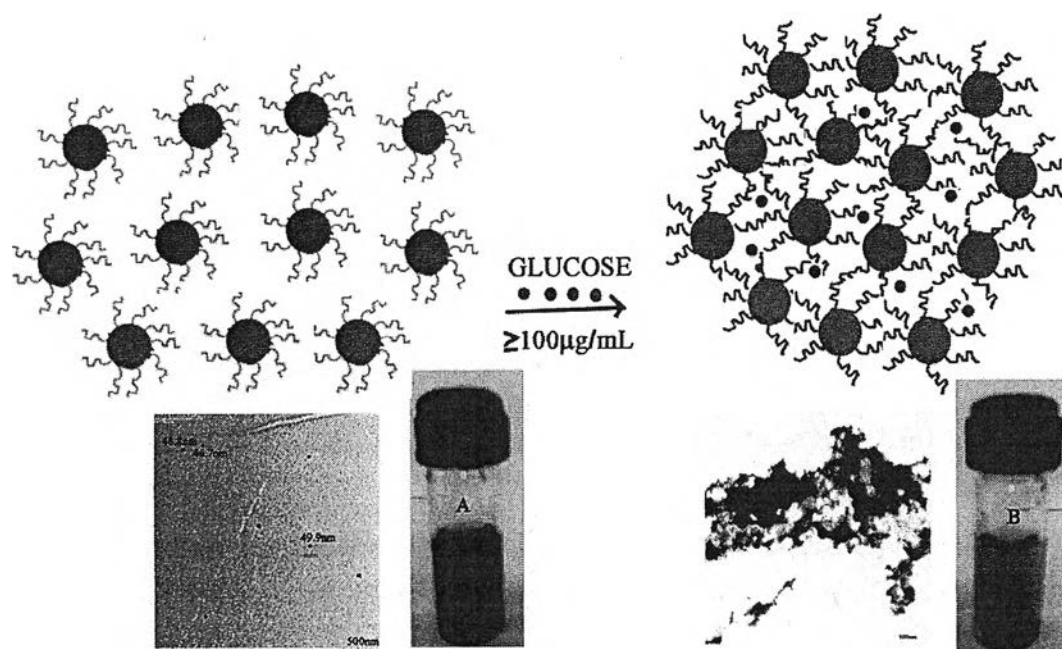


Figure 5. Color of (A) GNPs and (B) GOD-GNP on reacting with $\geq 100 \mu\text{g/mL}$ glucose, with mechanism [190]. Reprinted with permission from (Radhakumary, C.; Sreenivasan, K. Naked eye detection of glucose in urine using glucose oxidase immobilized gold nanoparticles. *Anal. Chem.* **2011**, *83*, 2829–2833.). Copyright (2011) American Chemical Society.

Colorimetric detection based on assemblies of 5-amino-2-fluorophenylboronic acid-modified silver nanoparticles (FPBA-AgNPs) has been demonstrated. The glucose-modulated assembly of the FPBA-AgNPs occurred by the regulable formation of interparticle linkages via the bridge binding of 1,2-*cis*-diols and 5,6-*cis*-diols (for the furanose form) or 4,6-*cis*-diols (for the pyranose form), respectively, of a glucose molecule to two FPBA-AgNPs. Furthermore, the glucose level variations associated with a model biological reaction process can be monitored by using FPBA-AgNPs, whilst the reaction mechanism remains nearly unchanged [195]. A new assembled glucose sensor based on the AgNPs-enhanced fluorescence of CdSe quantum dots was also demonstrated. Compared to that of bare CdSe QDs, a fluorescence signal enhancement and a clear blue shift of the emission peak for AgNP-CdSe QD complexes were observed, which is attributed to the surface plasmon resonance of AgNPs. In addition, the as-formed complexes are gradually disassembled in the presence of glucose molecules because they can replace the AgNPs by competitive binding with boronic acid groups, resulting in the weakening of the fluorescence enhancement [196].

4. Analytical Performance

Analytical performance of selected samples are listed in tables that categorized according to their detection methods including electrochemical (Table 1), and colorimetric and spectrophotometric techniques (Table 2), respectively.

Table 1. Selected examples of recent reports on biomedical targets using various nanoparticles by electrochemical techniques.

Group of Analytes	Detection *	Materials	Analytes	Detection Limit	Linear Dynamic Range	Ref.
Amino acids	Amperometry	AuNP-CNT/GCE	Trypsin	10 nM	30 nM–2.5 μ M	[23]
	CV	Fe ₃ O ₄ -GO/GCE	Cysteine	56 μ M	0.5–13.5 mM	[24]
			Acetaminophen	25 μ M	0.12–13.3 mM	
	DPV	AgNPs/GO/GCE	Trypsin	2.0 nM	0.01–50 μ M	[25]
CA	GC/DNA/NiOxNPs/Os(III)-complex electrode	Cysteine	0.07 μ M	50.0–800.0 μ M		
Antigens-antibodies	SV	AuNPs	CEA	0.12 pg·mL ⁻¹	0.5 pg·mL ⁻¹ –0.5ng·mL ⁻¹	[39]
Antioxidants	SWV	NiO/MWCNT nanocomposite	Glutathione	0.006 μ M	0.01–200 μ M	[49]
			Acetaminophen	0.5 μ M	0.8–600 μ M	
	CV	Fe ₂ O ₃ /RG nanocomposite	Ascorbic acid	0.543 μ M	0.57–3.97 μ M	[48]
	Amperometry	AgNPs/CMWCNT/PANI/Au electrode	Glutathione	0.3 μ M	0.3–3500 μ M	[47]
Cancer biomarkers	-	AuNP	Cancer-related gene sequence	4 fM	10 fM–1 nM	[58]
	Voltammetry	Fe ₃ O ₄ MNPs	Leukemia cells	10 cells	-	[59]
	DPV	CdTe QDs/CGE	DNA sequences of bladder cancer cells	6.435 $\times 10^{-13}$ M	1 $\times 10^{-12}$ –1 $\times 10^{-8}$ M	[61]
Chemical substances	CV	Fe ₃ O ₄ -Au-NPs	Digoxin	0.05 ng·mL ⁻¹	0.5–5 ng·mL ⁻¹	[78]
	CV/DPV/LSV	Fe ₃ O ₄ /GCE	Nimesulide	1.3 $\times 10^{-7}$ M	2.6 $\times 10^{-6}$ –1.0 $\times 10^{-4}$ M	[10]
	DPV	AgNP/MWCNTs-COOH/GCE	Adriamycin	1.7 $\times 10^{-9}$ M	8.2 $\times 10^{-9}$ –19.0 $\times 10^{-9}$ M	[76]
Hormones	-	WS2/AuNPs/GCE	17 β -estradiol	2 pM	0.1 pM–5 nM	[93]
	Amperometry	NiOPs/Nafion-MWCNTs/SPE	Insulin	6.1 nM	20–60 nM	[94]
Lipids	Amperometry	AuE/dithiol/AuNPs/MUA/ ChOx	Cholesterol	34.6 μ M	0.04–0.22 mM	[97]
	CA	AgNPs/GCE	Cholesterol	0.99 mg·dL ⁻¹	3.9–773.4 mg·dL ⁻¹	[99]
Microorganisms	EIS	EDC/NHS activated Au/1,6-HDT/AuNP/MUA	Type 5 adenovirus	30 virus particle·mL ⁻¹	10–10 ⁸ virus particle·mL ⁻¹	[102]
Nurotransmitters	DPV	AuNP-CNTs/PGE	L-Dopa	50 nM	0.1–150 μ M	[107]

Table 1. Cont.

Group of Analytes	Detection *	Materials	Analytes	Detection Limit	Linear Dynamic Range	Ref.
Neurotransmitters	DPV	NiFe ₂ O ₄ -MWCNT modified GCE	Dopamine	0.02 μM	0.05–6.0 μM 6.0–100 μM	[110]
	CV/LSV	RGO-Pd-NPs composite modified GCEs	Dopamine	0.233 μM	1–150 μM	[106]
	CV/DPA	PPyox-PTSA/Ag NP/Pt electrode	Dopamine	0.58 nM	1 × 10 ⁻⁹ –1.2 × 10 ⁻⁷ M	[116]
Nucleic acids	DPV	AuNPs-ATP-diazo-ATP/Au electrode	ssDNA	9.10 × 10 ⁻¹¹ M	3.01 × 10 ⁻¹⁰ –1.32 × 10 ⁻⁸ M	[127]
	Amperometry /CA/ CV/DPV	Fe ₃ O ₄ /MWCNT/LDH/NAD ⁺ modified GC electrode	NADH	0.3 μM	Up to 300 μM	[129]
	Amperometry /CV	Au nanoparticle/rGO GCE	NADH	1.13 nM	50 nM–500 μM	[131]
	CV	CdSe QDs-GO	Adenine Guanine	0.028 μM	0.083–291 μM	[132]
				0.055 μM	0.167–245 μM	
Nucleic acids	DPV	AgNPs-Pdop@Gr /GCE	DNA	3.2 × 10 ⁻¹⁵ M	1 × 10 ⁻¹³ –1 × 10 ⁻⁸ M	[134]
	CA	NiOxNPs/GC	NADH	106 nM	Up to 1 mM	[136]
Proteins	DPV	AuMNPs-Apt1/thrombin/ Apt2-AuNPs-HRP modified Au electrode	Thrombin	30 fM	0.1–60 pM	[146]
	DPV	MNPs/CS-MWCNTs	Bovine serum albumin	2.8 × 10 ⁻¹¹ g·mL ⁻¹	1.0 × 10 ⁻⁴ –1.0 × 10 ⁻¹⁰ g·mL ⁻¹	[7]
Sugars	CA	AuNPs/GONRs/CS	Glucose	0.5 μM	2 μM–1.375 mM 1.375–15 mM	[162]
	Amperometry	MSENs/MGCE	Glucose	0.2 μM	0.5 μM–3.5 mM	[9]
	Amperometry	PVP-GNs-NiNPs-CS	Glucose	30 nM	0.1 μM–0.5 mM	[171]
	Amperometry	GOD-CS/AgNWs/ GCE	Glucose	2.83 μM	10 μM–0.8 mM	[177]
	Amperometry	CONM/GC	Glucose	0.15 μM	0.7–60 μM	[179]
	Amperometry	RGO-NiNPs/GCE	Glucose	0.1 μM	2 μM–2.1 mM	[184]
	Amperometry	Pd-MWCNTs	Glucose	0.2 μM	1–22 mM	[189]

* Detection methods were; (CA) Chronoamperometry, (CV) Cyclic Voltammetry, (DPV) Differential Pulse Voltammetry, (EIS) Electrochemical Impedance Spectroscopy (LSV) Linear Sweep Voltammetry, (SWV) Square Wave Voltammetry.

Table 2. Selected examples of recent reports on biomedical targets using various nanoparticles by colorimetric and spectrophotometric techniques.

Group of Analytes	Detections *	Materials	Analytes	Detection Limit	Linear Dynamic Range	Ref.
Amino acids	UV-Vis	CMC-AuNPs	Cysteine	ND	10.0–100.0 μM	[27]
	UV-Vis	Non-fluorosurfactant capped AgNPs	Cysteine	0.05 μM	1.5–6.0 μM	[16]
	SERS	AuNPs	Rabbit IgG	1–10 $\text{ng}\cdot\text{mL}^{-1}$	0–100 $\text{ng}\cdot\text{mL}^{-1}$	[40]
Antigens-antibodies	SPR	$\text{Fe}_3\text{O}_4/\text{SiO}_2$ and $\text{Fe}_3\text{O}_4/\text{Ag}/\text{SiO}_2$ MNPs	Rabbit IgG	ND	1.25–20 $\mu\text{g}\cdot\text{mL}^{-1}$ (for $\text{Fe}_3\text{O}_4/\text{SiO}_2$) 0.3–20 $\mu\text{g}\cdot\text{mL}^{-1}$ (for $\text{Fe}_3\text{O}_4/\text{Ag}/\text{SiO}_2$)	[5]
	ECL	Ag/graphene	CEA	0.6 $\text{pg}\cdot\text{mL}^{-1}$	1 $\text{pg}\cdot\text{mL}^{-1}$ –500 $\text{ng}\cdot\text{mL}^{-1}$	[41]
	ECL	Si/CdTe/Ab ₂	Rabbit IgG	1.3 $\text{pg}\cdot\text{mL}^{-1}$	5 $\text{pg}\cdot\text{mL}^{-1}$ –10 $\text{ng}\cdot\text{mL}^{-1}$	[42]
	ECL	AgNPs-rGO-Ab ₂ -GOD	CEA	0.03 $\text{pg}\cdot\text{mL}^{-1}$	0.1 $\text{pg}\cdot\text{mL}^{-1}$ –160 $\text{ng}\cdot\text{mL}^{-1}$	[43]
	Fluorescence	CdS-2MPA	Rutin	1.2 $\times 10^{-6}$ M	up to 4 $\times 10^{-5}$ M	[54]
Antioxidants	Spectrophotometry	BSA-AgNCs	Ascorbic acid	0.16 μM (38)	2.0–50.0 μM	[55]
	Colorimetric	Primer conjugated AuNPs	Human telomerase activity	1 HeLa cell $\cdot\mu\text{L}^{-1}$	ND	[62]
Cancer biomarkers	Colorimetric	Fe_3O_4 MNPs and PtNPs nanohybrids	Target cancer cells (breast cancer)	ND	ND	[67]
	Wavelength-resolved imaging	Multiplexed QDs	Tumor cells in Hodgkin's lymphoma	ND	ND	[69]
Chemical substances	CL	L-cysteine capped CdS QDs	Baclofen	0.0035 $\text{mg}\cdot\text{L}^{-1}$	0.012–24.0 $\text{mg}\cdot\text{L}^{-1}$	[89]
Hormones	SPR	AuNPs-G4-OH SAM	Insulin	0.5 pM	2–43 pM	[95]
	Fluorescence	Eu(III) chelated-bonded SiNPs	Human thyroid stimulating hormone	0.0007 $\text{mL}\cdot\text{UL}^{-1}$	0.005–100 $\text{mL}\cdot\text{UL}^{-1}$	[96]
Lipids	ECL	AuNPs	Cholesterol	5.7 nM	0.17 nM–0.3 mM	[100]
	ECL	$\text{Fe}_3\text{O}_4@\text{SiO}_2\text{-Au}@mp\text{SiO}_2$	Cholesterol	0.28 μM	0.83–2.62 mM	[101]
Microorganisms	CL	CMG-MNPs	HBV	0.5 pM	ND	[103]
	Fluorescence	Dual color QDs	Human enterovirus 71	0.42 $\text{ng}\cdot\text{mL}^{-1}$ (for EV71) 0.39 $\text{ng}\cdot\text{mL}^{-1}$ (for CVB3)	1–14 $\text{ng}\cdot\text{mL}^{-1}$ (For EV 71) 1–19 $\text{ng}\cdot\text{mL}^{-1}$ (for CVB3)	[105]

Table 2. Cont.

Group of Analytes	Detections *	Materials	Analytes	Detection Limit	Linear Dynamic Range	Ref.
Neurotransmitters	Fluorescence	AgNPs	6-thioguanine	9.7 nM	1.5×10^{-8} – 7.5×10^{-7} M	[105]
	Spectrophotometry	AuNPs	Dopamine	33 nM	33 nM–3.33 mM	[123]
	UV-Vis	Co _x Fe _{3-x} O ₄ MNPs	Dopamine	0.13 μM	0.6–8.0 μM	[125]
Nucleic acids	Colorimetric in flow strip	Oligonucleotides-modified AuNPs	miRNA	1 fM (without silver enhancement)	ND	[140]
	Fluorescence	NEase-amplified MNPs	p53 gene	198 fM	ND	[142]
	CL	Oppy-PdNPs/Au	Sequence-specific DNA	6.0×10^{-17} M	1.0×10^{-16} – 1.0×10^{-15} M	[196]
Proteins	Colorimetric	Fib-AuNPs	Thrombin	ND	0.1–10 pM	[152]
	UV-Vis	Fe ₃ O ₄ @AuNPs	Thrombin	1.0 nM	1.6–30.4 nM	[155]
Proteins	Fluorescence	QD-apt nanoconjugates	Thrombin	1 nM	nM–μM	[158]
	Naked eyes	Apt-AgNPs	PDGF-BB	1.56 ng·mL ⁻¹	1.56 ng·mL ⁻¹ –100 ng·mL ⁻¹	[29]
Sugars	Colorimetric	AuNPs	Glucose	10 μM (for pink assay) 5 μM (for blue assay)	Extended to 1.5 mM (for pink assay) Extended to 1.0 mM (for blue assay)	[191]
	Fluorescence	BiFeO ₃ MNPs	Glucose	4.5 nM	0.2 nM–0.2 μM	[193]
	Colorimetric	FPBA-AgNPs	Glucose	89 μM	ND	[195]

* Detections were; (CL) Chemiluminescence, (ECL) Electrochemiluminescence, (SERS) Surface Enhanced Raman Scattering, (SPR) Surface Plasmon Resonance, (UV-Vis) UV-visible spectrophotometry.

5. Conclusions

Due to the good properties of inorganic nanoparticles, they have been prevalently used as powerful sensors and probes. Each type of nanoparticle exhibits its own fascinating properties. However, they shared a similarity of enhancing probe sensitivity owing to their high surface area-to-volume ratios. Metal particles mostly synthesized from their bulk material display remarkably properties and exceptional features due to their miniature size, while the excellent behavior of semiconductor and nanocomposites results from their combinations of various materials. They have been utilized in a variety of applications for numerous analytes as described in this review for both electrochemical and optical spectrophotometric detection. The use of nanoparticles is an excellent approach for biomedical detection. Various groups of examples as discussed clarify the efficiency of nanoparticles by an increment of signal. In addition to modification, nanoparticles are capable of providing selectivity against interferences and complicated matrix effects. Many benefits of nanoparticles have been revealed, although more feasible practices still need to be developed to overcome difficulties such as the tendency to agglomeration and precision in size-control. Moreover, differences in the synthesized products from day to day led to uncertain properties which stimulate the search for solutions. Applications of nanoparticles in biomedical detection are abundant as well. Among essential substances, small clusters such as single molecules or cells as early stage disease markers are recently of interest. Therefore, improved comprehension of the advantages resulting from the use of nanoparticles and curiosity is challenging many research groups and should lead to novel discoveries in the future.

Acknowledgments

The authors also greatly thank for financial support from the Thailand Research Fund through Research Team Promotion Grant (RTA5780005), Chulalongkorn University (Ratchadaphiseksomphot Endowment Fund) and Srinakharinwirot University.

Conflicts of Interest

The authors declare no conflict of interest.

References

1. Saha, K.; Agasti, S.S.; Kim, C.; Li, X.; Rotello, V.M. Gold nanoparticles in chemical and biological sensing. *Chem. Rev.* **2012**, *112*, 2739–2779.
2. Wang, M.; Lei, C.; Nie, Z.; Guo, M.; Huang, Y.; Yao, S. Label-free fluorescent detection of thrombin activity based on a recombinant enhanced green fluorescence protein and nickel ions immobilized nitrotriactic acid-coated magnetic nanoparticles. *Talanta* **2013**, *116*, 468–473.
3. Wang, G.; Chen, L.; He, X.; Zhu, Y.; Zhang, X. Detection of polynucleotide kinase activity by using a gold electrode modified with magnetic microspheres coated with titanium dioxide nanoparticles and a DNA dendrimer. *Analyst* **2014**, *139*, 3895–3900.

4. Tang, L.; Casas, J.; Venkataramasubramani, M. Magnetic nanoparticle mediated enhancement of localized surface plasmon resonance for ultrasensitive bioanalytical assay in human blood plasma. *Anal. Chem.* **2013**, *85*, 1431–1439.
5. Wang, L.; Sun, Y.; Wang, J.; Wang, J.; Yu, A.; Zhang, H.; Song, D. Preparation of surface plasmon resonance biosensor based on magnetic core/shell Fe₃O₄/SiO₂ and Fe₃O₄/Ag/SiO₂ nanoparticles. *Coll. Surf. B Biointerfaces* **2011**, *84*, 484–490.
6. Wang, Q.; Cui, X.; Chen, J.; Zheng, X.; Liu, C.; Xue, T.; Wang, H.; Jin, Z.; Qiao, L.; Zheng, W. Well-dispersed palladium nanoparticles on graphene oxide as a non-enzymatic glucose sensor. *RSC Adv.* **2012**, *2*, 6245–6249.
7. Chen, H.J.; Zhang, Z.H.; Luo, L.J.; Yao, S.Z. Surface-imprinted chitosan-coated magnetic nanoparticles modified multi-walled carbon nanotubes biosensor for detection of bovine serum albumin. *Sens. Actuators B Chem.* **2012**, *163*, 76–83.
8. Rezaei, B.; Ensafi, A.A.; Haghghatnia, F.; Aalaye, S.E., Application of beta-cyclodextrin/MnFe₂O₄ magnetic nanoparticles as a catalyst for fast chemiluminescence determination of glutathione in human blood using luminol-diperiodatoargentate(III) system. *J. Braz. Chem. Soc.* **2012**, *23*, 2248–2257.
9. Yang, Z.; Zhang, C.; Zhang, J.; Huang, L. Development of magnetic single-enzyme nanoparticles as electrochemical sensor for glucose determination. *Electrochim. Acta* **2013**, *111*, 25–30.
10. Zhang, J.L.; Tan, X.C.; Zhao, D.D.; Tan, S.W.; Liu, L.; Wang, L.; Huang, Z.W. Fe₃O₄ magnetic nanoparticles modified electrode as a sensor for determination of nimesulide. *Chem. Res. Chin. Univ.* **2011**, *27*, 566–569.
11. Wang, J.; Zhu, Z.; Munir, A.; Zhou, H.S. Fe₃O₄ nanoparticles-enhanced SPR sensing for ultrasensitive sandwich bio-assay. *Talanta* **2011**, *84*, 783–788.
12. Abu-Thabit, N.Y.; Makhlof, A.S.H. Chapter 24—Recent Advances in Nanocomposite Coatings for Corrosion Protection Applications. In *Handbook of Nanoceramic and Nanocomposite Coatings and Materials*; Makhlof, A.S.H., Scharnweber, D., Eds.; Elsevier: MA, USA, 2015; pp. 515–549.
13. Camargo, P.H.C.; Satyanarayana, K.G.; Wypych, F. Nanocomposites: Synthesis, structure, properties and new application opportunities. *Mater. Res.* **2009**, *12*, 1–39.
14. Tomioka, K.; Fukui, T. 18—Growth of Semiconductor Nanocrystals. In *Handbook of Crystal Growth (Second Edition)*; Nishinaga, T., Ed.; Elsevier: Boston, MA, USA, 2015; pp. 749–793.
15. Rogach, A.L.; Talapin, D.V.; Weller, H. Semiconductor Nanoparticles. In *Colloids and Colloid Assemblies*; Wiley-VCH Verlag GmbH & Co. KGaA: Weinheim, Germany, 2004; pp. 52–95.
16. Chen, S.; Gao, H.; Shen, W.; Lu, C.; Yuan, Q. Colorimetric detection of cysteine using noncrosslinking aggregation of fluorosurfactant-capped silver nanoparticles. *Sens. Actuators B Chem.* **2014**, *190*, 673–678.
17. Shahrokhian, S.; Nassab, N.H. Nanodiamond decorated with silver nanoparticles as a sensitive film modifier in a jeweled electrochemical sensor: Application to voltammetric determination of thioridazine. *Electroanalysis* **2013**, *25*, 417–425.
18. Ghosh, D.; Chattopadhyay, N. Gold and silver nanoparticles based superquenching of fluorescence: A review. *J. Lumin.* **2015**, *160*, 223–232.

19. Cesarino, I.; Galesco, H.V.; Machado, S.A.S. Determination of serotonin on platinum electrode modified with carbon nanotubes/polypyrrole/silver nanoparticles nanohybrid. *Mater. Sci. Eng. C Mater. Biol. Appl.* **2014**, *40*, 49–54.
20. Parsons, B.J.; Spickett, C.M. Special issue on “Analytical methods for the detection of oxidized biomolecules and antioxidants”. *Free Rad. Res.* **2015**, *49*, 473–476.
21. Sharifi, E.; Salimi, A.; Shams, E. DNA/nickel oxide nanoparticles/osmium(III)-complex modified electrode toward selective oxidation of L-cysteine and simultaneous detection of L-cysteine and homocysteine. *Bioelectrochemistry* **2012**, *86*, 9–21.
22. Sattarahmady, N.; Heli, H. An electrocatalytic transducer for L-cysteine detection based on cobalt hexacyanoferrate nanoparticles with a core-shell structure. *Anal. Biochem.* **2011**, *409*, 74–80.
23. Guo, Y.; Guo, S.; Fang, Y.; Dong, S. Gold nanoparticle/carbon nanotube hybrids as an enhanced material for sensitive amperometric determination of tryptophan. *Electrochim. Acta* **2010**, *55*, 3927–3931.
24. Song, Y.; He, Z.; Hou, H.; Wang, X.; Wang, L. Architecture of Fe₃O₄-graphene oxide nanocomposite and its application as a platform for amino acid biosensing. *Electrochim. Acta* **2012**, *71*, 58–65.
25. Li, J.; Kuang, D.; Feng, Y.; Zhang, F.; Xu, Z.; Liu, M.; Wang, D. Green synthesis of silver nanoparticles-graphene oxide nanocomposite and its application in electrochemical sensing of tryptophan. *Biosens. Bioelectron.* **2013**, *42*, 198–206.
26. Karimi-Maleh, H.; Biparva, P.; Hatami, M. A novel modified carbon paste electrode based on NiO/CNTs nanocomposite and (9, 10-dihydro-9, 10-ethanoanthracene-11, 12-dicarboximido)-4-ethylbenzene-1, 2-diol as a mediator for simultaneous determination of cysteamine, nicotinamide adenine dinucleotide and folic acid. *Biosens. Bioelectron.* **2013**, *48*, 270–275.
27. Wei, X.; Qi, L.; Tan, J.; Liu, R.; Wang, F. A colorimetric sensor for determination of cysteine by carboxymethyl cellulose-functionalized gold nanoparticles. *Anal. Chim. Acta* **2010**, *671*, 80–84.
28. Li, X.; Li, G.; Yang, M.; Chen, L.C.; Xiong, X.L. Gold nanoparticle based signal enhancement liquid crystal biosensors for tyrosine assays. *Sens. Actuators B Chem.* **2015**, *215*, 152–158.
29. Hu, H.; Li, H.; Zhao, Y.; Dong, S.; Li, W.; Qiang, W.; Xu, D. Aptamer-functionalized silver nanoparticles for scanometric detection of platelet-derived growth factor-BB. *Anal. Chim. Acta* **2014**, *812*, 152–160.
30. Cui, X.; Lv, Y.; Liu, Y.; Wu, B. Aqueous synthesis of near-infrared CdTe quantum dots for biothiols detection in biological fluids. *Acta Chim. Sin.* **2014**, *72*, 75–82.
31. Wei, Y.; Li, H.; Hao, H.; Chen, Y.; Dong, C.; Wang, G. beta-Cyclodextrin functionalized Mn-doped ZnS quantum dots for the chiral sensing of tryptophan enantiomers. *Polym. Chem.* **2015**, *6*, 591–598.
32. Borase, H.P.; Patil, C.D.; Salunkhe, R.B.; Suryawanshi, R.K.; Kim, B.S.; Bapat, V.A.; Patil, S.V. Bio-functionalized silver nanoparticles: A novel colorimetric probe for cysteine detection. *Appl. Biochem. Biotechnol.* **2015**, *175*, 3479–3493.
33. Han, C.; Xu, K.; Liu, Q.; Liu, X.; Li, J. Colorimetric sensing of cysteine using label-free silver nanoparticles. *Sens. Actuators B Chem.* **2014**, *202*, 574–582.

34. Hajizadeh, S.; Farhadi, K.; Forough, M.; Molaei, R. Silver nanoparticles in the presence of Ca^{2+} as a selective and sensitive probe for the colorimetric detection of cysteine. *Anal. Methods* **2012**, *4*, 1747–1752.
35. Ravindran, A.; Mani, V.; Chandrasekaran, N.; Mukherjee, A. Selective colorimetric sensing of cysteine in aqueous solutions using silver nanoparticles in the presence of Cr^{3+} . *Talanta* **2011**, *85*, 533–540.
36. Li, H.; Li, F.; Han, C.; Cui, Z.; Xie, G.; Zhang, A. Highly sensitive and selective tryptophan colorimetric sensor based on 4,4-bipyridine-functionalized silver nanoparticles. *Sens. Actuators B Chem.* **2010**, *145*, 194–199.
37. Ho, J.A.A.; Chang, H.C.; Shih, N.Y.; Wu, L.C.; Chang, Y.F.; Chen, C.C.; Chou, C. Diagnostic detection of human lung cancer-associated antigen using a gold nanoparticle-based electrochemical immunosensor. *Anal. Chem.* **2010**, *82*, 5944–5950.
38. Lai, G.; Yan, F.; Wu, J.; Leng, C.; Ju, H. Ultrasensitive multiplexed immunoassay with electrochemical stripping analysis of silver nanoparticles catalytically deposited by gold nanoparticles and enzymatic reaction. *Anal. Chem.* **2011**, *83*, 2726–2732.
39. Lin, D.; Wu, J.; Wang, M.; Yan, F.; Ju, H. Triple signal amplification of graphene film, polybead carried gold nanoparticles as tracing tag and silver deposition for ultrasensitive electrochemical immunosensing. *Anal. Chem.* **2012**, *84*, 3662–3668.
40. Chon, H.; Lim, C.; Ha, S.M.; Ahn, Y.; Lee, E.K.; Chang, S.I.; Seong, G.H.; Choo, J. On-chip immunoassay using surface-enhanced raman scattering of hollow gold nanospheres. *Anal. Chem.* **2010**, *82*, 5290–5295.
41. Li, S.; Liu, F.; Ge, S.; Yu, J.; Yan, M. Application of nanoporous Pd as catalytically promoted nanolabels for ultrasensitive electrochemiluminescence immunosensor based on Ag/graphene nanocomposite. *Sens. Actuators B Chem.* **2015**, *210*, 460–467.
42. Qian, J.; Zhang, C.; Cao, X.; Liu, S. Versatile immunosensor using a quantum dot coated silica nanosphere as a label for signal amplification. *Anal. Chem.* **2010**, *82*, 6422–6429.
43. Jiang, X.; Chai, Y.; Wang, H.; Yuan, R. Electrochemiluminescence of luminol enhanced by the synergetic catalysis of hemin and silver nanoparticles for sensitive protein detection. *Biosens. Bioelectron.* **2014**, *54*, 20–26.
44. Fernandez-Lucas, J. Multienzymatic synthesis of nucleic acid derivatives: A general perspective. *Appl. Microbiol. Biotechnol.* **2015**, *99*, 4615–4627.
45. Matemadombo, F.; Apetrei, C.; Nyokong, T.; Rodriguez-Mendez, M.L.; de Saja, J.A. Comparison of carbon screen-printed and disk electrodes in the detection of antioxidants using CoPc derivatives. *Sens. Actuators B Chem.* **2012**, *166*, 457–466.
46. Karimi-Maleh, H.; Tahernejad-Javazmi, F.; Ensafi, A.A.; Moradi, R.; Mallakpour, S.; Beitollahi, H. A high sensitive biosensor based on FePt/CNTs nanocomposite/*N*-(4-hydroxyphenyl)-3,5-dinitrobenzamide modified carbon paste electrode for simultaneous determination of glutathione and piroxicam. *Biosens. Bioelectron.* **2014**, *60*, 1–7.
47. Narang, J.; Chauhan, N.; Jain, P.; Pundir, C.S. Silver nanoparticles/multiwalled carbon nanotube/polyaniline film for amperometric glutathione biosensor. *Int. J. Biol. Macromol.* **2012**, *50*, 672–678.

48. Yu, Z.; Li, H.; Lu, J.; Zhang, X.; Liu, N.; Zhang, X. Hydrothermal synthesis of Fe₂O₃/graphene nanocomposite for selective determination of ascorbic acid in the presence of uric acid. *Electrochim. Acta* **2015**, *158*, 264–270.
49. Shahmiri, M.R.; Bahari, A.; Karimi-Maleh, H.; Hosseinzadeh, R.; Mirnia, N. Ethynylferrocene-NiO/MWCNT nanocomposite modified carbon paste electrode as a novel voltammetric sensor for simultaneous determination of glutathione and acetaminophen. *Sens. Actuators B Chem.* **2013**, *177*, 70–77.
50. Li, F.; Chai, J.; Yang, H.; Han, D.; Niu, L. Synthesis of Pt/ionic liquid/graphene nanocomposite and its simultaneous determination of ascorbic acid and dopamine. *Talanta* **2010**, *81*, 1063–1068.
51. Li, Y.; Wu, P.; Xu, H.; Zhang, H.; Zhong, X. Anti-aggregation of gold nanoparticle-based colorimetric sensor for glutathione with excellent selectivity and sensitivity. *Analyst* **2011**, *136*, 196–200.
52. Tian, D.; Qian, Z.; Xia, Y.; Zhu, C. Gold nanocluster-based fluorescent probes for near-infrared and turn-on sensing of glutathione in living cells. *Langmuir* **2012**, *28*, 3945–3951.
53. Wen, Y.; Luo, F.; Yang, Y.; Lin, L.; Du, J.; Guo, Y.; Xiao, D.; Choi, M.M.F. CdS nanotubes thin film for electrochemiluminescence analysis of phenolic compounds. *Anal. Methods* **2012**, *4*, 1053–1059.
54. Carvalho, J.M.; Leandro, K.C.; da Silva, A.R.; Aucelio, R.Q. Selective determination of rutin by fluorescence attenuation of the cds-2-mercaptopropionic acid nanocrystal probe. *Anal. Lett.* **2013**, *46*, 207–224.
55. Yang, X.H.; Ling, J.; Peng, J.; Cao, Q.E.; Wang, L.; Ding, Z.T.; Xiong, J. Catalytic formation of silver nanoparticles by bovine serum albumin protected-silver nanoclusters and its application for colorimetric detection of ascorbic acid. *Spectrochim. Acta Part. Mol. Biomol. Spectrosc.* **2013**, *106*, 224–230.
56. Ouyang, L.; Zhu, L.; Jiang, J.; Tang, H. A surface-enhanced Raman scattering method for detection of trace glutathione on the basis of immobilized silver nanoparticles and crystal violet probe. *Anal. Chim. Acta* **2014**, *816*, 41–49.
57. Jensen, G.C.; Krause, C.E.; Sotzing, G.A.; Rusling, J.F. Inkjet-printed gold nanoparticle electrochemical arrays on plastic. Application to immunodetection of a cancer biomarker protein. *Phys. Chem. Chem. Phys.* **2011**, *13*, 4888–4894.
58. Qiu, L.; Qiu, L.; Zhou, H.; Wu, Z.; Shen, G.; Yu, R. Sensitive and selective electrochemical DNA sensor for the analysis of cancer-related single nucleotide polymorphism. *New J. Chem.* **2014**, *38*, 4711–4715.
59. Zhang, K.; Tan, T.; Fu, J.J.; Zheng, T.; Zhu, J.J. A novel aptamer-based competition strategy for ultrasensitive electrochemical detection of leukemia cells. *Analyst* **2013**, *138*, 6323–6330.
60. Liu, H.; Xu, S.; He, Z.; Deng, A.; Zhu, J.J. Supersandwich cytosensor for selective and ultrasensitive detection of cancer cells using aptamer-DNA concatamer-quantum dots probes. *Anal. Chem.* **2013**, *85*, 3385–3392.
61. Zhang, C.Y.; Hu, J. Single quantum dot-based nanosensor for multiple DNA detection. *Anal. Chem.* **2010**, *82*, 1921–1927.
62. Wang, J.; Wu, L.; Ren, J.; Qu, X. Visualizing human telomerase activity with primer-modified Au nanoparticles. *Small* **2012**, *8*, 259–264.

63. Nguyen, A.H.; Sim, S.J. Nanoplasmonic biosensor: Detection and amplification of dual bio-signatures of circulating tumor DNA. *Biosens. Bioelectron.* **2015**, *67*, 443–449.
64. Cheng, H.Y.; Lai, L.J.; Ko, F.H. Rapid and sensitive detection of rare cancer cells by the coupling of immunomagnetic nanoparticle separation with ELISA analysis. *Int. J. Nanomed.* **2012**, *7*, 2967–2973.
65. Mousavi, M.Z.; Chen, H.Y.; Wu, S.H.; Peng, S.W.; Lee, K.L.; Wei, P.K.; Cheng, J.Y. Magnetic nanoparticle-enhanced SPR on gold nanoslits for ultra-sensitive, label-free detection of nucleic acid biomarkers. *Analyst* **2013**, *138*, 2740–2748.
66. Fang, S.; Wang, C.; Xiang, J.; Cheng, L.; Song, X.; Xu, L.; Peng, R.; Liu, Z. Aptamer-conjugated upconversion nanoprobe assisted by magnetic separation for effective isolation and sensitive detection of circulating tumor cells. *Nano Res.* **2014**, *7*, 1327–1336.
67. Kim, M.I.; Kim, M.S.; Woo, M.A.; Ye, Y.; Kang, K.S.; Lee, J.; Park, H.G. Highly efficient colorimetric detection of target cancer cells utilizing superior catalytic activity of graphene oxide-magnetic-platinum nanohybrids. *Nanoscale* **2014**, *6*, 1529–1536.
68. Jie, G.F.; Liu, P.; Zhang, S.S. Highly enhanced electrochemiluminescence of novel gold/silica/CdSe-CdS nanostructures for ultrasensitive immunoassay of protein tumor marker. *Chem. Commun.* **2010**, *46*, 1323–1325.
69. Liu, J.; Lau, S.K.; Varma, V.A.; Kairdolf, B.A.; Nie, S. Multiplexed detection and characterization of rare tumor cells in hodgkin's lymphoma with multicolor quantum dots. *Anal. Chem.* **2010**, *82*, 6237–6243.
70. Jie, G.; Wang, L.; Yuan, J.; Zhang, S. Versatile electrochemiluminescence assays for cancer cells based on dendrimer/cdse-zns-quantum dot nanoclusters. *Anal. Chem.* **2011**, *83*, 3873–3880.
71. Karadas, N.; Bozal-Palabiyik, B.; Uslu, B.; Ozkan, S.A. Functionalized carbon nanotubes-with silver nanoparticles to fabricate a sensor for the determination of zolmitriptan in its dosage forms and biological samples. *Sens. Actuators B Chem.* **2013**, *186*, 486–494.
72. Kumary, V.A.; Divya, J.; Nancy, T.E.M.; Sreevalsan, K. Voltammetric detection of paracetamol at cobalt ferrite nanoparticles modified glassy carbon electrode. *Int. J. Electrochem. Sci.* **2013**, *8*, 6610–6619.
73. Liu, G.T.; Chen, H.F.; Lin, G.M.; Ye, P.P.; Wang, X.P.; Jiao, Y.Z.; Guo, X.Y.; Wen, Y.; Yang, H.F. One-step electrodeposition of graphene loaded nickel oxides nanoparticles for acetaminophen detection. *Biosens. Bioelectron.* **2014**, *56*, 26–32.
74. Razmi, H.; Habibi, E. Amperometric detection of acetaminophen by an electrochemical sensor based on cobalt oxide nanoparticles in a flow injection system. *Electrochim. Acta* **2010**, *55*, 8731–8737.
75. Liu, M.; Chen, Q.; Lai, C.; Zhang, Y.; Deng, J.; Li, H.; Yao, S. A double signal amplification platform for ultrasensitive and simultaneous detection of ascorbic acid, dopamine, uric acid and acetaminophen based on a nanocomposite of ferrocene thiolate stabilized Fe₃O₄@Au nanoparticles with graphene sheet. *Biosens. Bioelectron.* **2013**, *48*, 75–81.
76. Zhang, K.; Zhang, Y. Electrochemical behavior of adriamycin at an electrode modified with silver nanoparticles and multi-walled carbon nanotubes, and its application. *Microchim. Acta* **2010**, *169*, 161–165.

77. Hasanzadeh, M.; Pournaghi-Azar, M.H.; Shadjou, N.; Jouyban, A. Magnetic nanoparticles incorporated on functionalized mesoporous silica: An advanced electrochemical sensor for simultaneous determination of amiodarone and atenolol. *RSC Adv.* **2014**, *4*, 4710–4717.
78. Ahmadi, A.; Shirazi, H.; Pourbagher, N.; Akbarzadeh, A.; Omidfar, K. An electrochemical immunosensor for digoxin using core-shell gold coated magnetic nanoparticles as labels. *Mol. Biol. Rep.* **2014**, *41*, 1659–1668.
79. Hu, Y.; Zhang, Z.; Zhang, H.; Luo, L.; Yao, S. A sensitive and selective sensor-coated molecularly imprinted sol-gel film incorporating beta-cyclodextrin-multi-walled carbon nanotubes and cobalt nanoparticles-chitosan for oxacillin determination. *Surf. Interface Anal.* **2012**, *44*, 334–341.
80. Rastgar, S.; Shahrokhian, S. Nickel hydroxide nanoparticles-reduced graphene oxide nanosheets film: Layer-by-layer electrochemical preparation, characterization and rifampicin sensory application. *Talanta* **2014**, *119*, 156–163.
81. Parvin, M.H.; Golivand, M.B.; Najafi, M.; Shariaty, S.M. Carbon paste electrode modified with cobalt nanoparticles and its application to the electrocatalytic determination of chlorpromazine. *J. Electroanal. Chem.* **2012**, *683*, 31–36.
82. De Oliveira, P.R.; Oliveira, M.M.; Zarbin, A.J.G.; Marcolino-Junior, L.H.; Bergamini, M.F. Flow injection amperometric determination of isoniazid using a screen-printed carbon electrode modified with silver hexacyanoferrates nanoparticles. *Sens. Actuators B Chem.* **2012**, *171*, 795–802.
83. Miao, P.; Han, K.; Sun, H.; Yin, J.; Zhao, J.; Wang, B.; Tang, Y. Melamine functionalized silver nanoparticles as the probe for electrochemical sensing of clenbuterol. *ACS Appl. Mater. Interfaces* **2014**, *6*, 8667–8672.
84. Gao, M.; Lin, R.; Li, L.; Jiang, L.; Ye, B.; He, H.; Qiu, L. Label-free silver nanoparticles for the naked eye detection of entecavir. *Spectrochim. Acta Part Mol. Biomol. Spectrosc.* **2014**, *126*, 178–183.
85. Gong, W.J.; Dong, C.X.; Chen, J.; Zhang, T.Y.; Zhang, Y.P.; Bai, L.Y. Preparation of a chemical sensor based on modified silver nanoparticles for quick recognition of 5-fluorocytosine. *Asian J. Chem.* **2012**, *24*, 3695–3698.
86. Rastegarzadeh, S.; Hashemi, F. A surface plasmon resonance sensing method for determining captopril based on *in situ* formation of silver nanoparticles using ascorbic acid. *Spectrochim. Acta Part Mol. Biomol. Spectrosc.* **2014**, *122*, 536–541.
87. Laliwala, S.K.; Mehta, V.N.; Rohit, J.V.; Kailasa, S.K. Citrate-modified silver nanoparticles as a colorimetric probe for simultaneous detection of four triptan-family drugs. *Sens. Actuators B Chem.* **2014**, *197*, 254–263.
88. Algarra, M.; Campos, B.B.; Aguiar, F.R.; Rodriguez-Borges, J.E.; Esteves da Silva, J.C.G. Novel beta-cyclodextrin modified CdTe quantum dots as fluorescence nanosensor for acetylsalicylic acid and metabolites. *Mater. Sci. Eng. C Mater. Biol. Appl.* **2012**, *32*, 799–803.
89. Khataee, A.; Hasanzadeh, A.; Iranifam, M.; Joo, S.W. A novel flow-injection chemiluminescence method for determination of baclofen using L-cysteine capped CdS quantum dots. *Sens. Actuators B Chem.* **2015**, *215*, 272–282.
90. Krishna, A.S.; Radhakumary, C.; Sreenivasan, K. *In vitro* detection of calcium in bone by modified carbon dots. *Analyst* **2013**, *138*, 7107–7111.

91. Xiao, Y.; Zhang, Y.; Huang, H.; Zhang, Y.; Du, B.; Chen, F.; Zheng, Q.; He, X.; Wang, K. Conjugated polyelectrolyte-stabilized silver nanoparticles coupled with pyrene derivative for ultrasensitive fluorescent detection of iodide. *Talanta* **2015**, *131*, 678–683.
92. Olowu, R.A.; Arotiba, O.; Mailu, S.N.; Waryo, T.T.; Baker, P.; Iwuoha, E. Electrochemical aptasensor for endocrine disrupting 17 beta-estradiol based on a poly(3,4-ethylenedioxythiophene)-Gold nanocomposite platform. *Sensors* **2010**, *10*, 9872–9890.
93. Huang, K.J.; Liu, Y.J.; Zhang, J.Z.; Liu, Y.M. A novel aptamer sensor based on layered tungsten disulfide nanosheets and Au nanoparticles amplification for 17 beta-estradiol detection. *Anal. Methods* **2014**, *6*, 8011–8017.
94. Rafiee, B.; Fakhari, A.R. Electrocatalytic oxidation and determination of insulin at nickel oxide nanoparticles-multiwalled carbon nanotube modified screen printed electrode. *Biosens. Bioelectron.* **2013**, *46*, 130–135.
95. Frasconi, M.; Tortolini, C.; Botre, F.; Mazzei, F. Multifunctional Au nanoparticle dendrimer-based surface plasmon resonance biosensor and its application for improved insulin detection. *Anal. Chem.* **2010**, *82*, 7335–7342.
96. Zhou, Y.; Xia, X.; Xu, Y.; Ke, W.; Yang, W.; Li, Q. Application of europium(III) chelates-bonded silica nanoparticle in time-resolved immunofluorometric detection assay for human thyroid stimulating hormone. *Anal. Chim. Acta* **2012**, *722*, 95–99.
97. Saxena, U.; Chakraborty, M.; Goswami, P. Covalent immobilization of cholesterol oxidase on self-assembled gold nanoparticles for highly sensitive amperometric detection of cholesterol in real samples. *Biosens. Bioelectron.* **2011**, *26*, 3037–3043.
98. Li, Y.; Bai, H.; Liu, Q.; Bao, J.; Han, M.; Dai, Z. A nonenzymatic cholesterol sensor constructed by using porous tubular silver nanoparticles. *Biosens. Bioelectron.* **2010**, *25*, 2356–2360.
99. Nantaphol, S.; Chailapakul, O.; Siangproh, W. Sensitive and selective electrochemical sensor using silver nanoparticles modified glassy carbon electrode for determination of cholesterol in bovine serum. *Sens. Actuators B Chem.* **2015**, *207*, 193–198.
100. Ou, X.; Tan, X.; Wei, S.; Chen, S.; Zhang, J.; Liu, X. Electrochemiluminescence biosensor for cholesterol detection based on AuNPs/L-cys-C-60 nanocomposites. *Anal. Methods* **2014**, *6*, 3804–3810.
101. Zhang, J.; Chen, S.; Tan, X.; Zhong, X.; Yuan, D.; Cheng, Y. Highly sensitive electrochemiluminescence biosensors for cholesterol detection based on mesoporous magnetic core-shell microspheres. *Biotechnol. Lett.* **2014**, *36*, 1835–1841.
102. Lin, D.; Tang, T.; Harrison, D.J.; Lee, W.E.; Jemere, A.B. A regenerating ultrasensitive electrochemical impedance immunosensor for the detection of adenovirus. *Biosens. Bioelectron.* **2015**, *68*, 129–134.
103. Yang, H.; Liang, W.; Si, J.; Li, Z.; He, N. Long spacer arm-functionalized magnetic nanoparticle platform for enhanced chemiluminescent detection of hepatitis B virus. *J. Biomed. Nanotechnol.* **2014**, *10*, 3610–3619.
104. Ali, Z.; Liang, W.; Jin, L.; Tang, Y.; Mou, X.; Shah, M.A.A.; Yang, H.; Deng, Y.; He, N.; Li, Z. Development of magnetic nanoparticles based nucleic acid extraction method and application in hepatitis c virus chemiluminescent detection. *Sci. Adv. Mater.* **2015**, *7*, 1233–1240.

105. Chen, L.; Zhang, X.; Zhou, G.; Xiang, X.; Ji, X.; Zheng, Z.; He, Z.; Wang, H. Simultaneous determination of human enterovirus 71 and coxsackievirus b3 by dual-color quantum dots and homogeneous immunoassay. *Anal. Chem.* **2012**, *84*, 3200–3207.
106. Palanisamy, S.; Ku, S.; Chen, S.M. Dopamine sensor based on a glassy carbon electrode modified with a reduced graphene oxide and palladium nanoparticles composite. *Microchim. Acta* **2013**, *180*, 1037–1042.
107. Hu, G.; Chen, L.; Guo, Y.; Wang, X.; Shao, S. Selective determination of L-dopa in the presence of uric acid and ascorbic acid at a gold nanoparticle self-assembled carbon nanotube-modified pyrolytic graphite electrode. *Electrochim. Acta* **2010**, *55*, 4711–4716.
108. Wang, C.; Yuan, R.; Chai, Y.; Zhang, Y.; Hu, F.; Zhang, M. Au-nanoclusters incorporated 3-amino-5-mercapto-1,2,4-triazole film modified electrode for the simultaneous determination of ascorbic acid, dopamine, uric acid and nitrite. *Biosens. Bioelectron.* **2011**, *30*, 315–319.
109. Chandra, S.; Arora, K.; Bahadur, D. Impedimetric biosensor based on magnetic nanoparticles for electrochemical detection of dopamine. *Mater. Sci. Eng. B-Adv. Funct. Solid-State Mater.* **2012**, *177*, 1531–1537.
110. Ensafi, A.A.; Arashpour, B.; Rezaei, B.; Allafchian, A.R. Voltammetric behavior of dopamine at a glassy carbon electrode modified with NiFe₂O₄ magnetic nanoparticles decorated with multiwall carbon nanotubes. *Mater. Sci. Eng. C Mater. Biol. Appl.* **2014**, *39*, 78–85.
111. Qin, X.; Wang, H.; Wang, X.; Miao, Z.; Chen, L.; Zhao, W.; Shan, M.; Chen, Q. Amperometric biosensors based on gold nanoparticles-decorated multiwalled carbon nanotubes-poly(diallyldimethylammonium chloride) biocomposite for the determination of choline. *Sens. Actuators B Chem.* **2010**, *147*, 593–598.
112. Zhang, F.; Li, Y.; Gu, Y.E.; Wang, Z.; Wang, C. One-pot solvothermal synthesis of a Cu₂O/Graphene nanocomposite and its application in an electrochemical sensor for dopamine. *Microchim. Acta* **2011**, *173*, 103–109.
113. Li, J.; Yang, J.; Yang, Z.; Li, Y.; Yu, S.; Xu, Q.; Hu, X. Graphene-Au nanoparticles nanocomposite film for selective electrochemical determination of dopamine. *Anal. Methods* **2012**, *4*, 1725–1728.
114. Zhao, Z.; Zhang, M.; Li, Y.; Cheng, S.; Chen, X.; Wang, J. Evaluation of electrochemically reduced gold nanoparticle-graphene nanocomposites for the determination of dopamine. *Anal. Lett.* **2015**, *48*, 1437–1453.
115. Wang, W.; Wang, W.; Davis, J.J.; Luo, X. Ultrasensitive and selective voltammetric aptasensor for dopamine based on a conducting polymer nanocomposite doped with graphene oxide. *Microchim. Acta* **2015**, *182*, 1123–1129.
116. Saha, S.; Sarkar, P.; Turner, A.P.F. Interference-free electrochemical detection of nanomolar dopamine using doped polypyrrole and silver nanoparticles. *Electroanalysis* **2014**, *26*, 2197–2206.
117. Kaur, B.; Pandiyan, T.; Satpati, B.; Srivastava, R. Simultaneous and sensitive determination of ascorbic acid, dopamine, uric acid, and tryptophan with silver nanoparticles-decorated reduced graphene oxide modified electrode. *Coll. Surfaces B Biointerfaces* **2013**, *111*, 97–106.

118. Noroozifar, M.; Khorasani-Motlagh, M.; Taheri, A. Preparation of silver hexacyanoferrate nanoparticles and its application for the simultaneous determination of ascorbic acid, dopamine and uric acid. *Talanta* **2010**, *80*, 1657–1664.
119. Rafati, A.A.; Afraz, A.; Hajian, A.; Assari, P. Simultaneous determination of ascorbic acid, dopamine, and uric acid using a carbon paste electrode modified with multiwalled carbon nanotubes, ionic liquid, and palladium nanoparticles. *Microchim. Acta* **2014**, *181*, 1999–2008.
120. Figueiredo-Filho, L.C.S.; Silva, T.A.; Vicentini, F.C.; Fatibello-Filho, O. Simultaneous voltammetric determination of dopamine and epinephrine in human body fluid samples using a glassy carbon electrode modified with nickel oxide nanoparticles and carbon nanotubes within a dihexadecylphosphate film. *Analyst* **2014**, *139*, 2842–2849.
121. Babaei, A.; Taheri, A.R.; Farahani, I.K. Nanomolar simultaneous determination of levodopa and melatonin at a new cobalt hydroxide nanoparticles and multi-walled carbon nanotubes composite modified carbon ionic liquid electrode. *Sens. Actuators B Chem.* **2013**, *183*, 265–272.
122. Tao, Y.; Lin, Y.; Ren, J.; Qu, X. A dual fluorometric and colorimetric sensor for dopamine based on BSA-stabilized Au nanoclusters. *Biosens. Bioelectron.* **2013**, *42*, 41–46.
123. Chen, Z.; Zhang, C.; Zhou, T.; Ma, H. Gold nanoparticle based colorimetric probe for dopamine detection based on the interaction between dopamine and melamine. *Microchim. Acta* **2015**, *182*, 1003–1008.
124. Leng, Y.; Xie, K.; Ye, L.; Li, G.; Lu, Z.; He, J. Gold-nanoparticle-based colorimetric array for detection of dopamine in urine and serum. *Talanta* **2015**, *139*, 89–95.
125. Niu, X.; Xu, Y.; Dong, Y.; Qi, L.; Qi, S.; Chen, H.; Chen, X. Visual and quantitative determination of dopamine based on $\text{CoFe}_3\text{-xO}_4$ magnetic nanoparticles as peroxidase mimetics. *J. Alloys Compd.* **2014**, *587*, 74–81.
126. Li, H.; Wu, X. Silver nanoparticles-enhanced rare earth co-luminescence effect of Tb (III)-Y(III)-dopamine system. *Talanta* **2015**, *138*, 203–208.
127. Li, F.; Feng, Y.; Dong, P.; Tang, B. Gold nanoparticles modified electrode via a mercapto-diazoaminobenzene monolayer and its development in DNA electrochemical biosensor. *Biosens. Bioelectron.* **2010**, *25*, 2084–2088.
128. Dong, X.; Zhao, W.; Xu, J.; Chen, H. Magnetic particles and cadmium sulfide nanoparticles tagging for signal-amplifying detection of nucleic acids. *Sci. China Chem.* **2011**, *54*, 1304–1310.
129. Teymourian, H.; Salimi, A.; Hallaj, R., Low potential detection of NADH based on Fe_3O_4 nanoparticles/multiwalled carbon nanotubes composite: Fabrication of integrated dehydrogenase-based lactate biosensor. *Biosens. Bioelectron.* **2012**, *33*, 60–68.
130. Fan, Y.; Huang, K.J.; Niu, D.J.; Yang, C.P.; Jing, Q.S. TiO_2 -graphene nanocomposite for electrochemical sensing of adenine and guanine. *Electrochim. Acta* **2011**, *56*, 4685–4690.
131. Govindhan, M.; Amiri, M.; Chen, A. Au nanoparticle/graphene nanocomposite as a platform for the sensitive detection of NADH in human urine. *Biosens. Bioelectron.* **2015**, *66*, 474–480.
132. Kalaivani, A.; Narayanan, S.S. Simultaneous determination of adenine and guanine using cadmium selenide quantum dots-graphene oxide nanocomposite modified electrode. *J. Nanosci. Nanotechnol.* **2015**, *15*, 4697–4705.

133. Dong, H.; Yan, F.; Ji, H.; Wong, D.K.Y.; Ju, H. Quantum-dot-functionalized poly(styrene-co-acrylic acid) microbeads: step-wise self-assembly, characterization, and applications for sub-femtomolar electrochemical detection of DNA hybridization. *Adv. Funct. Mater.* **2010**, *20*, 1173–1179.
134. Huang, K.J.; Liu, Y.J.; Wang, H.B.; Wang, Y.Y. A sensitive electrochemical DNA biosensor based on silver nanoparticles-polydopamine@graphene composite. *Electrochim. Acta* **2014**, *118*, 130–137.
135. Huang, K.J.; Wang, L.; Wang, H.B.; Gan, T.; Wu, Y.Y.; Li, J.; Liu, Y.M. Electrochemical biosensor based on silver nanoparticles-polydopamine-graphene nanocomposite for sensitive determination of adenine and guanine. *Talanta* **2013**, *114*, 43–48.
136. Sharifi, E.; Salimi, A.; Shams, E. Electrocatalytic activity of nickel oxide nanoparticles as mediatorless system for NADH and ethanol sensing at physiological pH solution. *Biosens. Bioelectron.* **2013**, *45*, 260–266.
137. Hassan, K.M.; Hathoot, A.A.; Ashour, W.F.D.; Abdel-Azzem, M. Electrochemical and analytical applications for NADH detection at glassy carbon electrode modified with nickel nanoparticles dispersed on poly 1,5-diaminonaphthalene. *J. Solid State Electrochem.* **2015**, *19*, 1063–1072.
138. Noorbakhsh, A.; Salimi, A. Development of DNA electrochemical biosensor based on immobilization of ssDNA on the surface of nickel oxide nanoparticles modified glassy carbon electrode. *Biosens. Bioelectron.* **2011**, *30*, 188–196.
139. Jyoti, A.; Pandey, P.; Singh, S.P.; Jain, S.K.; Shanker, R. Colorimetric detection of nucleic acid signature of shiga toxin producing escherichia coli using gold nanoparticles. *J. Nanosci. Nanotechnol.* **2010**, *10*, 4154–4158.
140. Hou, S.Y.; Hsiao, Y.L.; Lin, M.S.; Yen, C.C.; Chang, C.S. MicroRNA detection using lateral flow nucleic acid strips with gold nanoparticles. *Talanta* **2012**, *99*, 375–379.
141. Lin, J.Y.; Chen, Y.C. Functional magnetic nanoparticle-based trapping and sensing approaches for label-free fluorescence detection of DNA. *Talanta* **2011**, *86*, 200–207.
142. Li, N.; Gao, Z.F.; Kang, B.H.; Li, N.B.; Luo, H.Q. Sensitive mutant DNA biomarker detection based on magnetic nanoparticles and nicking endonuclease assisted fluorescence signal amplification. *RSC. Adv.* **2015**, *5*, 20020–20024.
143. Alula, M.T.; Yang, J. Photochemical decoration of silver nanoparticles on magnetic microspheres as substrates for the detection of adenine by surface-enhanced Raman scattering. *Anal. Chim. Acta* **2014**, *812*, 114–120.
144. Chen, L.; Zhang, L.; Qiu, T.; Cao, W. Chemiluminescent detection of DNA hybridization based on signal DNA probe modified with gold and cobalt nanoparticles. *Int. J. Electrochem. Sci.* **2011**, *6*, 5325–5336.
145. Li, L.D.; Zhao, H.T.; Chen, Z.B.; Mu, X.J.; Guo, L. Aptamer biosensor for label-free impedance spectroscopy detection of thrombin based on gold nanoparticles. *Sens. Actuators B Chem.* **2011**, *157*, 189–194.
146. Zhao, J.; Zhang, Y.; Li, H.; Wen, Y.; Fan, X.; Lin, F.; Tan, L.; Yao, S. Ultrasensitive electrochemical aptasensor for thrombin based on the amplification of aptamer-AuNPs-HRP conjugates. *Biosens. Bioelectron.* **2011**, *26*, 2297–2303.

147. Wen, T.; Zhu, W.; Xue, C.; Wu, J.; Han, Q.; Wang, X.; Zhou, X.; Jiang, H. Novel electrochemical sensing platform based on magnetic field-induced self-assembly of Fe₃O₄@Polyaniline nanoparticles for clinical detection of creatinine. *Biosens. Bioelectron.* **2014**, *56*, 180–185.
148. de Souza Castilho, M.; Laube, T.; Yamanaka, H.; Alegret, S.; Pividori, M.I. Magneto immunoassays for plasmodium falciparum histidine-rich protein 2 related to malaria based on magnetic nanoparticles. *Anal. Chem.* **2011**, *83*, 5570–5577.
149. Yuan, Y.; Gou, X.; Yuan, R.; Chai, Y.; Zhuo, Y.; Ye, X.; Gan, X. Graphene-promoted 3,4,9,10-perylenetetracarboxylic acid nanocomposite as redox probe in label-free electrochemical aptasensor. *Biosens. Bioelectron.* **2011**, *30*, 123–127.
150. Zhang, J.; He, J.; Xu, W.; Gao, L.; Guo, Y.; Li, W.; Yu, C. A novel immunosensor for detection of beta-galactoside alpha-2, 6-sialyltransferase in serum based on gold nanoparticles loaded on Prussian blue-based hybrid nanocomposite film. *Electrochim. Acta* **2015**, *156*, 45–52.
151. Ibupoto, Z.H.; Jamal, N.; Khun, K.; Liu, X.; Willander, M. A potentiometric immunosensor based on silver nanoparticles decorated ZnO nanotubes, for the selective detection of D-dimer. *Sens. Actuators B Chem.* **2013**, *182*, 104–111.
152. Chen, C.K.; Huang, C.C.; Chang, H.T. Label-free colorimetric detection of picomolar thrombin in blood plasma using a gold nanoparticle-based assay. *Biosens. Bioelectron.* **2010**, *25*, 1922–1927.
153. Niu, Y.; Wang, P.; Zhao, Y.; Fan, A. Turn-on colorimetric sensor for ultrasensitive detection of thrombin using fibrinogen-gold nanoparticle conjugate. *Analyst* **2013**, *138*, 1475–1482.
154. Qi, Y.; Li, B. A sensitive, label-free, aptamer-based biosensor using a gold nanoparticle-initiated chemiluminescence system. *Chem. Eur. J.* **2011**, *17*, 1642–1648.
155. Liang, G.; Cai, S.; Zhang, P.; Peng, Y.; Chen, H.; Zhang, S.; Kong, J. Magnetic relaxation switch and colorimetric detection of thrombin using aptamer-functionalized gold-coated iron oxide nanoparticles. *Anal. Chim. Acta* **2011**, *689*, 243–249.
156. Chen, H.; Qi, F.; Zhou, H.; Jia, S.; Gao, Y.; Koh, K.; Yin, Y. Fe₃O₄@Au nanoparticles as a means of signal enhancement in surface plasmon resonance spectroscopy for thrombin detection. *Sens. Actuators B Chem.* **2015**, *212*, 505–511.
157. Yang, J.Y.; Lin, Y.J.; Su, M.Y.; Li, W.J.; Liu, M.Y. Use of magnetic nanoparticles and a microplate reader with fluorescence detection to detect C-reactive protein. *J. Chin. Chem. Soc.* **2014**, *61*, 221–226.
158. Chi, C.W.; Lao, Y.H.; Li, Y.S.; Chen, L.C. A quantum dot-aptamer beacon using a DNA intercalating dye as the FRET reporter: Application to label-free thrombin detection. *Biosens. Bioelectron.* **2011**, *26*, 3346–3352.
159. Tennico, Y.H.; Hutanu, D.; Koesdjojo, M.T.; Bartel, C.M.; Remcho, V.T. On-chip aptamer-based sandwich assay for thrombin detection employing magnetic beads and quantum dots. *Anal. Chem.* **2010**, *82*, 5591–5597.
160. Miao, P.; Liu, T.; Li, X.; Ning, L.; Yin, J.; Han, K. Highly sensitive, label-free colorimetric assay of trypsin using silver nanoparticles. *Biosens. Bioelectron.* **2013**, *49*, 20–24.

161. Ismail, N.S.; Le, Q.H.; Yoshikawa, H.; Saito, M.; Tamiya, E., Development of non-enzymatic electrochemical glucose sensor based on graphene oxide nanoribbon—Gold nanoparticle hybrid. *Electrochim. Acta* **2014**, *146*, 98–105.
162. Zhong, G.X.; Zhang, W.X.; Sun, Y.M.; Wei, Y.Q.; Lei, Y.; Peng, H.P.; Liu, A.L.; Chen, Y.Z.; Lin, X.H. A nonenzymatic amperometric glucose sensor based on three dimensional nanostructure gold electrode. *Sens. Actuators B Chem.* **2015**, *212*, 72–77.
163. Kim, M.I.; Ye, Y.; Won, B.Y.; Shin, S.; Lee, J.; Park, H.G. A highly efficient electrochemical biosensing platform by employing conductive nanocomposite entrapping magnetic nanoparticles and oxidase in mesoporous carbon foam. *Adv. Funct. Mater.* **2011**, *21*, 2868–2875.
164. Krishna, R.; Titus, E.; Chandra, S.; Bardhan, N.K.; Krishna, R.; Bahadur, D.; Gracio, J. Fabrication of a glucose biosensor based on citric acid assisted cobalt ferrite magnetic nanoparticles. *J. Nanosci. Nanotechnol.* **2012**, *12*, 6631–6638.
165. Wang, A.J.; Li, Y.F.; Li, Z.H.; Feng, J.J.; Sun, Y.L.; Chen, J.R. Amperometric glucose sensor based on enhanced catalytic reduction of oxygen using glucose oxidase adsorbed onto core-shell Fe₃O₄@silica@Au magnetic nanoparticles. *Mater. Sci. Eng. C Mater. Biol. Appl.* **2012**, *32*, 1640–1647.
166. Bo, X.; Bai, J.; Yang, L.; Guo, L. The nanocomposite of PtPd nanoparticles/onion-like mesoporous carbon vesicle for nonenzymatic amperometric sensing of glucose. *Sens. Actuators B Chem.* **2011**, *157*, 662–668.
167. Jiang, X.; Wu, Y.; Mao, X.; Cui, X.; Zhu, L. Amperometric glucose biosensor based on integration of glucose oxidase with platinum nanoparticles/ordered mesoporous carbon nanocomposite. *Sens. Actuators B Chem.* **2011**, *153*, 158–163.
168. Luo, L.; Zhu, L.; Wang, Z. Nonenzymatic amperometric determination of glucose by CuO nanocubes-graphene nanocomposite modified electrode. *Bioelectrochemistry* **2012**, *88*, 156–163.
169. Qiao, N.; Zheng, J. Nonenzymatic glucose sensor based on glassy carbon electrode modified with a nanocomposite composed of nickel hydroxide and graphene. *Microchim. Acta* **2012**, *177*, 103–109.
170. Xiao, X.; Zhou, B.; Zhu, L.; Xu, L.; Tan, L.; Tang, H.; Zhang, Y.; Xie, Q.; Yao, S. An reagentless glucose biosensor based on direct electrochemistry of glucose oxidase immobilized on poly(methylene blue) doped silica nanocomposites. *Sens. Actuators B Chem.* **2012**, *165*, 126–132.
171. Liu, Z.; Guo, Y.; Dong, C. A high performance nonenzymatic electrochemical glucose sensor based on polyvinylpyrrolidone-graphene nanosheets-nickel nanoparticles-chitosan nanocomposite. *Talanta* **2015**, *137*, 87–93.
172. Senel, M. Simple method for preparing glucose biosensor based on *in-situ* polypyrrole cross-linked chitosan/glucose oxidase/gold bionanocomposite film. *Mater. Sci. Eng. C Mater. Biol. Appl.* **2015**, *48*, 287–293.
173. Shahnavaz, Z.; Lorestani, F.; Meng, W.P.; Alias, Y. Core-shell-CuFe₂O₄/PPy nanocomposite enzyme-free sensor for detection of glucose. *J. Solid State Electrochem.* **2015**, *19*, 1223–1233.

174. Xu, W.; He, J.; Gao, L.; Zhang, J.; Hui, J.; Guo, Y.; Li, W.; Yu, C. A sensitive glucose biosensor based on the abundant immobilization of glucose oxidase on hollow Pt nanospheres assembled on graphene oxide-Prussian Blue-PTC-NH₂ nanocomposite film. *J. Electroanal. Chem.* **2015**, *741*, 8–13.
175. Wang, L.; Tang, Y.; Wang, L.; Zhu, H.; Meng, X.; Chen, Y.; Sun, Y.; Yang, X.J.; Wan, P. Fast conversion of redox couple on Ni(OH)₂/C nanocomposite electrode for high-performance nonenzymatic glucose sensor. *J. Solid State Electrochem.* **2015**, *19*, 851–860.
176. Chen, L.; Xie, H.; Li, J. Electrochemical glucose biosensor based on silver nanoparticles/multiwalled carbon nanotubes modified electrode. *J. Solid State Electrochem.* **2012**, *16*, 3323–3329.
177. Wang, L.; Gao, X.; Jin, L.; Wu, Q.; Chen, Z.; Lin, X. Amperometric glucose biosensor based on silver nanowires and glucose oxidase. *Sens. Actuators B Chem.* **2013**, *176*, 9–14.
178. Joshi, A.C.; Markad, G.B.; Haram, S.K. Rudimentary simple method for the decoration of graphene oxide with silver nanoparticles: Their application for the amperometric detection of glucose in the human blood samples. *Electrochim. Acta* **2015**, *161*, 108–114.
179. Sattarahmady, N.; Heli, H. A non-enzymatic amperometric sensor for glucose based on cobalt oxide nanoparticles. *J. Exp. Nanosci.* **2012**, *7*, 529–546.
180. Li, S.J.; Du, J.M.; Chen, J.; Mao, N.N.; Zhang, M.J.; Pang, H. Electrodeposition of cobalt oxide nanoparticles on reduced graphene oxide: A two-dimensional hybrid for enzyme-free glucose sensing. *J. Solid State Electrochem.* **2014**, *18*, 1049–1056.
181. Wang, T.; Yu, Y.; Tian, H.; Hu, J. A Novel non-enzymatic glucose sensor based on cobalt nanoparticles implantation-modified indium tin oxide electrode. *Electroanalysis* **2014**, *26*, 2693–2700.
182. Nie, H.; Yao, Z.; Zhou, X.; Yang, Z.; Huang, S. Nonenzymatic electrochemical detection of glucose using well-distributed nickel nanoparticles on straight multi-walled carbon nanotubes. *Biosens. Bioelectron.* **2011**, *30*, 28–34.
183. Yu, S.J.; Zhang, Y.H.; Xiao, P.; Li, X.L.; Meng, X.Q.; Yang, Y.N. An amperometric non-enzymatic glucose sensor by nickel hexacyanoferrate nanoparticles modified TiO₂ nanotube arrays. *Chin. J. Anal. Chem.* **2012**, *40*, 313–316.
184. Zhang, Y.; Xiao, X.; Sun, Y.; Shi, Y.; Dai, H.; Ni, P.; Hu, J.; Li, Z.; Song, Y.; Wang, L. Electrochemical deposition of nickel nanoparticles on reduced graphene oxide film for nonenzymatic glucose sensing. *Electroanalysis* **2013**, *25*, 959–966.
185. Kung, C.W.; Cheng, Y.H.; Ho, K.C. Single layer of nickel hydroxide nanoparticles covered on a porous Ni foam and its application for highly sensitive non-enzymatic glucose sensor. *Sens. Actuators B Chem.* **2014**, *204*, 159–166.
186. Chen, X.M.; Lin, Z.J.; Chen, D.J.; Jia, T.T.; Cai, Z.M.; Wang, X.R.; Chen, X.; Chen, G.N.; Oyama, M. Nonenzymatic amperometric sensing of glucose by using palladium nanoparticles supported on functional carbon nanotubes. *Biosens. Bioelectron.* **2010**, *25*, 1803–1808.
187. Gutes, A.; Carraro, C.; Maboudian, R. Nonenzymatic glucose sensing based on deposited palladium nanoparticles on epoxy-silver electrodes. *Electrochim. Acta* **2011**, *56*, 5855–5859.

188. Cai, Z.X.; Liu, C.C.; Wu, G.H.; Chen, X.M.; Chen, X. Palladium nanoparticles deposit on multi-walled carbon nanotubes and their catalytic applications for electrooxidation of ethanol and glucose. *Electrochim. Acta* **2013**, *112*, 756–762.
189. Singh, B.; Bhardwaj, N.; Jain, V.K.; Bhatia, V. Palladium nanoparticles decorated electrostatically functionalized MWCNTs as a non enzymatic glucose sensor. *Sens. Actuators A Phys.* **2014**, *220*, 126–133.
190. Radhakumary, C.; Sreenivasan, K. Naked eye detection of glucose in urine using glucose oxidase immobilized gold nanoparticles. *Anal. Chem.* **2011**, *83*, 2829–2833.
191. Palazzo, G.; Facchini, L.; Mallardi, A. Colorimetric detection of sugars based on gold nanoparticle formation. *Sens. Actuators B Chem.* **2012**, *161*, 366–371.
192. Luo, W.; Li, Y.S.; Yuan, J.; Zhu, L.; Liu, Z.; Tang, H.; Liu, S. Ultrasensitive fluorometric determination of hydrogen peroxide and glucose by using multiferroic BiFeO₃ nanoparticles as a catalyst. *Talanta* **2010**, *81*, 901–907.
193. Xiong, Z.G.; Li, J.P.; Tang, L.; Cheng, Z.Q. A novel electrochemiluminescence biosensor based on glucose oxidase immobilized on magnetic nanoparticles. *Chin. J. Anal. Chem.* **2010**, *38*, 800–804.
194. Su, L.; Qin, W.; Zhang, H.; Rahman, Z.U.; Ren, C.; Ma, S.; Chen, X. The peroxidase/catalase-like activities of MFe₂O₄ (M = Mg, Ni, Cu) MNPs and their application in colorimetric biosensing of glucose. *Biosens. Bioelectron.* **2015**, *63*, 384–391.
195. Cao, K.; Jiang, X.; Yan, S.; Zhang, L.; Wu, W. Phenylboronic acid modified silver nanoparticles for colorimetric dynamic analysis of glucose. *Biosens. Bioelectron.* **2014**, *52*, 188–195.
196. Tang, Y.; Yang, Q.; Wu, T.; Liu, L.; Ding, Y.; Yu, B. Fluorescence enhancement of cadmium selenide quantum dots assembled on silver nanoparticles and its application to glucose detection. *Langmuir* **2014**, *30*, 6324–6330.

Chapter III

The development of paper-based analytical sensors

In this chapter, we presented the new alternative analytical devices using paper. Paper-based analytical devices were recognized as a promising and powerful platform that have shown great potential in the development for the next generation of analytical devices. A paper-based microfluidic device combines many advantages of paper strip tests with the utility of microfluidics. They have the potential to be good alternatives for various applications over the traditional methods because they are capable of simultaneous multiplex analyte detection. In addition, they are portable, easy to use, require only a small volume of sample and provide rapid analysis. There are 8 publications obtained from the proposed idea under the objective of this project. The publications can be classified into 3 groups according to their detection modes:

1. Colorimetric detection

1.1 K. Talalak, J. Noiphung, T. Songjaroen, O. Chailapakul, W. Laiwattanapaisal, A facile low-cost enzymatic paper-based assay for the determination of urine creatinine, *Talanta*, 144 (2015) 915-921.

1.2 S. Chaiyo, A. Apiluk, W. Siangproh, O. Chailapakul, High sensitivity and specificity simultaneous determination of lead, cadmium and copper using μ PAD with dual electrochemical and colorimetric detection, *Sensors and Actuators B-Chemical*, 233 (2016) 540-549.

1.3 P. Teengam, W. Siangproh, A. Tuantranont, T. Vilaivan, O. Chailapakul, C. S. Henry, Multiplex Paper-Based Colorimetric DNA Sensor Using PyrrolidinyI Peptide Nucleic Acid-Induced AgNPs Aggregation for Detecting MERS-CoV, MTB, and HPV Oligonucleotides, *Analytical Chemistry*, 89 (2017) 5428-5435.

2. Electrochemical detection

2.1 Y. Boonyasit, O. Chailapakul, W. Laiwattanapaisal, A multiplexed three-dimensional paper-based electrochemical impedance device for simultaneous label-free affinity sensing of total and glycosylated haemoglobin: The potential of using a specific single-frequency value for analysis, *Analytica Chimica Acta*, 936 (2016) 1-11.

2.2 F.N. Maluin, M. Sharifah, P. Rattanarat, W. Siangproh, O. Chailapakul, A.M. Issam, N.S.A. Manan, Synthesis of PANI/hematite/PB hybrid nanocomposites and fabrication as screen printed paper based sensors for cholesterol detection, *Analytical Methods*, 8 (2016) 8049-8058.

2.3 P. Ruengpirasiri, E. Punrat, O. Chailapakul, S. Chuanuwatanakul*, Graphene Oxide-Modified Electrode Coated with in-situ Antimony Film for the Simultaneous Determination of Heavy Metals by Sequential Injection-Anodic Stripping Voltammetry, *Electroanalysis*, 28 (2016) 462-468.

2.4 S. Nantaphol, R. B. Channon, T. Kondo, W. Siangproh, O. Chailapakul, C. S. Henry, Boron Doped Diamond Paste Electrodes for Microfluidic Paper-Based Analytical Devices, *Analytical Chemistry*, 89 (2017) 4100-4107.

3. Dual detection by combining colorimetric and electrochemical detection

3.1 S. Chaiyo, A. Apiluk, W. Siangproh, O. Chailapakul, High sensitivity and specificity simultaneous determination of lead, cadmium and copper using mu PAD with dual electrochemical and colorimetric detection, *Sensors and Actuators B-Chemical*, 233 (2016) 540-549.

Detail of each work is presented in the subsequent part.



A facile low-cost enzymatic paper-based assay for the determination of urine creatinine

Kwanrutai Talalak^a, Julaluk Noiphung^a, Temsiri Songjaroen^b, Orawon Chailapakul^{c,d},
Wanida Laiwattanapaisal^{e,*}

^a Clinical Biochemistry and Molecular Medicine, Faculty of Allied Health Sciences, Chulalongkorn University, Patumwan, Bangkok 10330, Thailand

^b Department of Clinical Chemistry, Faculty of Allied Health Sciences, Chulalongkorn University, Patumwan, Bangkok 10330, Thailand

^c Electrochemistry and Optical Spectroscopy Research Unit (EOSRU), Department of Chemistry, Faculty of Science, Chulalongkorn University, Patumwan, Bangkok 10330, Thailand

^d Center of Excellence on Petrochemical and Materials Technology (PETROMAT), Chulalongkorn University, Patumwan, Bangkok 10330, Thailand

^e Department of Clinical Chemistry, Faculty of Allied Health Sciences, Chulalongkorn University, Patumwan, Bangkok 10330, Thailand

ARTICLE INFO

Article history:

Received 26 February 2015

Received in revised form

6 July 2015

Accepted 13 July 2015

Available online 14 July 2015

Keywords:

Lab-on-paper

Paper-based analytical devices

Dead-volume reagent

Enzymatic assay

Urinary creatinine

Low-cost diagnostic

ABSTRACT

Creatinine is one of many markers used to investigate kidney function. This paper describes a low-cost enzymatic paper-based analytical device (enz-PAD) for determining urine creatinine. The disposable dead volumes of creatinine enzyme reagents from an automatic analyser cassette were utilised. Whatman No. 3 paper was cut into long rectangular shapes ($4 \times 40 \text{ mm}^2$) on which the enzyme reagents, R1 and R2, were adsorbed in two consecutive regions. The assay was performed by immersing test strips into urine samples contained in microwells to allow creatinine in the sample to react with immobilised active ingredients and, then, traverse via capillary action to the detection area where chromogen products accumulated. The method is based on hydrogen peroxide (H_2O_2) formation via creatinine conversion using creatininase, creatinase, and sarcosine oxidase. The liberated H_2O_2 reacts with 4-aminophenazone and 2,4,6-triiodo-3-hydroxybenzoic acid to form quinoneimine with a pink-red colour at the detection zone. The linear range of the creatinine assay was $2.5\text{--}25 \text{ mg dL}^{-1}$ ($r^2=0.983$), and the detection limit was 2.0 mg dL^{-1} . The colorimetric enz-PAD for the creatinine assay was highly correlated with a conventional alkaline picrate method when real urine samples were evaluated ($r^2=0.977$; $n=40$). This simple and nearly zero-cost paper-based device provides a novel alternative method for screening urinary creatinine and will be highly beneficial for developing countries.

© 2015 Elsevier B.V. All rights reserved.

1. Introduction

Creatinine is the end product of creatine metabolism, which normally exists in serum and is eradicated from the blood circulation via glomerular filtration at a constant excretion rate [1,2]. Abnormal levels of creatinine in serum or urine indicate impaired kidney function, and creatinine has been accepted as a marker for monitoring the impact of treatment in haemodialysis patients [2]. Moreover, urinary creatinine concentration is widely used as an index for urine dilution [3] and as an internal standard for normalising the ratios of other urinary biomarkers, such as microalbumin [4], protein [5], cystatin-c [6], α -dicarbonyl compounds [7], and bisphenol A (BPA) [8].

Creatinine assays are routine in most clinical laboratories. The original method, the alkaline picrate Jaffé reaction, was replaced

by the Jaffe kinetic assay, which is still widely used for determining creatinine in many laboratories [9,10]. However, the method is characterised by poor specificity. Specifically, many substances, such as glucose [11], albumin [12], cycloketones [13], pseudochromogen [14] and carbonyl compounds [15], may interfere with the assay. Therefore, the Jaffe assay has been widely replaced by enzymatic methods [16]. In addition to enzymatic methods, numerous creatinine assays have been developed, such as high performance liquid chromatography (HPLC) [17], capillary electrophoresis [18], isotope-dilution mass spectrometry (IDMS) [19], tandem mass spectrometry [20], flow injection analysis [21], sequential injection analysis systems [22], microfluidic systems [23], zone fluidic multichannel kinetic spectrophotometry [24], surface-enhanced Raman spectroscopy [25] and antibody-based sensors [26]. However, these methods are not commonly used in general laboratories because they require expensive instruments and are cumbersome for routine use [17,19]. In addition, these methods require well-trained personnel to operate the machinery and to interpret the results [27,28].

* Corresponding author. Fax: +66 02 218 1082.

E-mail address: Wanida.L@chula.ac.th (W. Laiwattanapaisal).

In contrast, enzymatic-based methods are now widely accepted due to their high specificity. In addition, enzymatic reagents can be analysed using general spectrophotometers that are available in most laboratories. Alternatively, enzymatic methods can be assayed in parallel with other analytes using automatic analysers.

Moreover, the results of enzymatic methods have been reported to closely mirror the gold standard method, isotope-dilution-mass spectrometry (IDMS) [16]. However, the main disadvantage of enzymatic methods is the high cost because, many enzyme types (e.g., 4–6 enzymes) are utilised for a given reaction. Batch enzymatic assays consume a relatively large reagent volume and require a large space for instrumentation. Therefore, such methods are not suitable for bedside patient use or for use in remote, low-income areas in developing countries.

Even though many automatic analysers have been developed to reduce the dead volume of reagents in cassettes, approximately 1–3 mL of reagent remains in a reagent cassette because the reagent probe of automated machines does not extend into the enzyme reagent deeper than its sensor level. Generally, the remaining reagents that are left in the cassettes are neglected in clinical laboratories. They are discarded daily, even though the reagents still contain active ingredients, i.e., enzymes and substrates. These small reagent volumes can be utilised in miniaturised systems that consume low reagent volumes, such as microfluidic devices or paper-based analytical devices (PADs). The latter approach is promising for being developed as a point-of-care-testing (POCT) for use in developing countries [29] because of its simplicity and an extremely low-cost of paper substrates.

Many researchers have proposed microfluidic paper-based analytical devices (μ PADs) for many types of clinical analyses, such as for assessing glucose [30–32], protein [30,31], pathogens [33], blood type [34] and liver function [35]. Due to a small scale of paper-based devices, these devices require small reagent and sample volumes. Additionally, paper exhibits a special solution wicking via capillary action characteristic. Thus, a liquid can flow through paper without the use of external forces [30]. Because of this property, paper is extensively used in both the conventional lateral-flow immunochromatography [36] and bidirectional approaches [37]. Several researchers have developed fabrication methods for paper-based devices using photolithography [30], paper cutting [38], wax-printing [39] and wax-dipping [31,40].

In this study, an extremely low-cost diagnostic paper device is proposed for use in urinary creatinine assays based on an enzymatic method. The disposable dead volumes of creatinine reagents from cassettes of an automatic analyser were pooled for use in this application. Because enzymatic reactions occur in a specific order and depend on reagents in cassettes, R1 and R2, the reagents were adsorbed on two consecutive regions on the paper. Endogenous creatine needs to be eliminated in the first step by enzymes present in R1. A continuous capillary force from the sample solution drives the enzyme reagents into the reaction zone and facilitates generation of the quinoneimine products that accumulate at the end of the PADs. The colour change intensity is analysed using a scanner or a digital camera for quantitative assays. This facile, simple and low-cost paper-based device provides a new alternative method for determining urinary creatinine. This approach can be extended to other similar enzymatic reactions and will be highly beneficial for use in developing countries.

2. Materials and methods

2.1. Materials and chemicals

Creatinine ($C_4H_7N_3O$), potassium phosphate monobasic (KH_2PO_4) and potassium phosphate dibasic (K_2HPO_4) were

obtained from Merck (Darmstadt, Germany). Creatinine reagents (CREP2-Creatinine plus ver.2, Roche Diagnostics, Basel, Switzerland; ref. 03263991, lot no. 687743) were collected from the disposable dead volume of automatic analyser cassettes used at a local hospital in Bangkok, Thailand. The remaining reagents were pooled from ten cassettes that were collected on different days within two months after opening. The creatinine assay kits (CREATININE liquicolor) based on the Jaffe kinetic reaction were purchased from HUMAN diagnostic (Wiesbaden, Germany). L-ascorbic acid, D-(+)-glucose, uric acid and human serum albumin were obtained from Sigma-Aldrich (St. Louis, United States). Bilirubin was obtained from Fluka (Seelze, Germany). Whatman filter papers (Nos. 1, 3 and 42) were purchased from Whatman International Ltd. (Maidstone, England). White pellets of beeswax were purchased from a local shop in Bangkok, Thailand. A hot plate (model C-MAG HS7) and thermometer (model ETS-DS) from IKA (Wilmington, USA) were used to melt the beeswax.

2.2. Sample preparation

Forty urine samples from healthy volunteers were collected from the first morning urination without additives. The urine samples were centrifuged at 3000 rpm for 5 min and diluted 10- to 20-fold with a 100 mM potassium phosphate buffer at pH 7.5 before assaying with enz-PADs. The experiments were approved by The Ethics Review Committee for Research Involving Human Research Subjects, Health Science Group, Chulalongkorn University, Bangkok, Thailand (COA No. 159/2557).

2.3. Design and fabrication of enz-PADs

The discarded reagents from cassettes were pooled and analysed for total protein content before utilising to avoid lot-to-lot variation of the enzyme reagents. In this study, the pooled enzyme reagents, R1 and R2, contained protein concentrations of 4.76 ± 0.46 mg mL⁻¹ and 0.73 ± 0.05 mg mL⁻¹, respectively. According to the manufacturer's description, the R1 reagent contained creatinase, sarcosine oxidase, ascorbate oxidase, catalase, 2,4,6-triiodo-3-hydroxybenzoic acid (HTIB) and N-tris-(hydroxymethyl) methyl-3-aminopropanesulfonic acid (TAPS). The R2 reagent consisted of creatininase, peroxidase, 4-aminophenazone, potassium hexacyanoferrate [II] and N-tris-(hydroxymethyl) methyl-3-aminopropanesulfonic acid (TAPS). The assay is based on hydrogen peroxide (H_2O_2) production following the creatinine conversion with creatininase, creatinase, and sarcosine oxidase. The generated H_2O_2 reacts with 4-aminophenazone and HTIB to yield pink-red quinoneimine dye. The colour intensity of the formed quinone imine chromogen is directly proportional to the creatinine concentration in the sample.

Unless otherwise stated, Whatman No. 3 filter paper was used to fabricate the enz-PADs because the paper has appropriate pore sizes and thickness suitable for our approach. The Whatman No. 3 filter paper was designed to consist of five zones, which included two reagent adsorption zones (R1: 4×10 mm² and R2: 4×7 mm²), a sample dipping zone (4×5 mm²), a detection zone (4×3 mm²) and a hydrophobic holder zone (4×15 mm²). It is necessary to adsorb the R1 and R2 enzyme reagents on separated zones for the following reasons. The existing endogenous creatine in the sample needs to be eliminated in the first step during the contact with R1 before a reaction with creatininase is started in R2. Additionally, the generated H_2O_2 from the creatinase and sarcosine oxidase reaction needs to be destroyed using the catalase in the R1 zone. The, the catalase is inhibited with sodium azide when it flows to R2, so the actual H_2O_2 that is generated from the creatinine reaction does not interfere. The patterned papers were printed using an HP LaserJet P1102 printer and then, were cut into

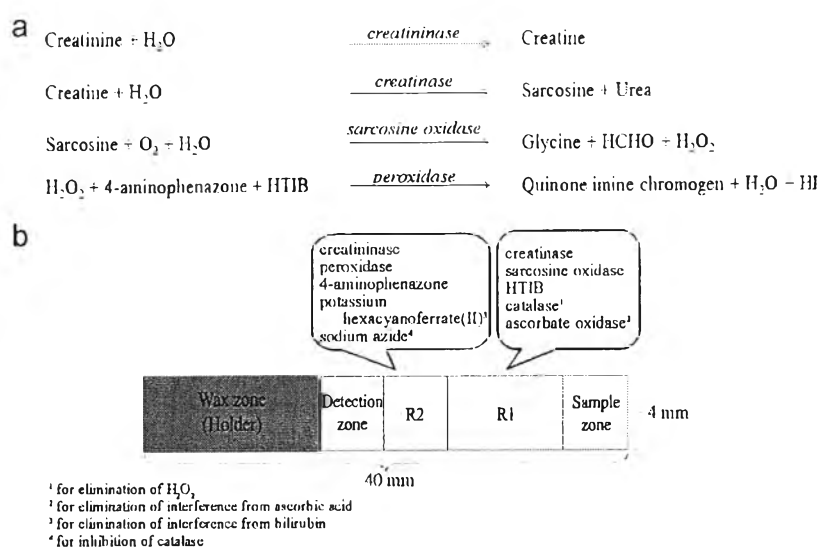


Fig. 1. Schematic diagram of the enzymatic colorimetric assay of enz-PADs. (a) The operating principle of the enzymatic assay for urinary creatinine. (b) The enz-PAD design used in this study.

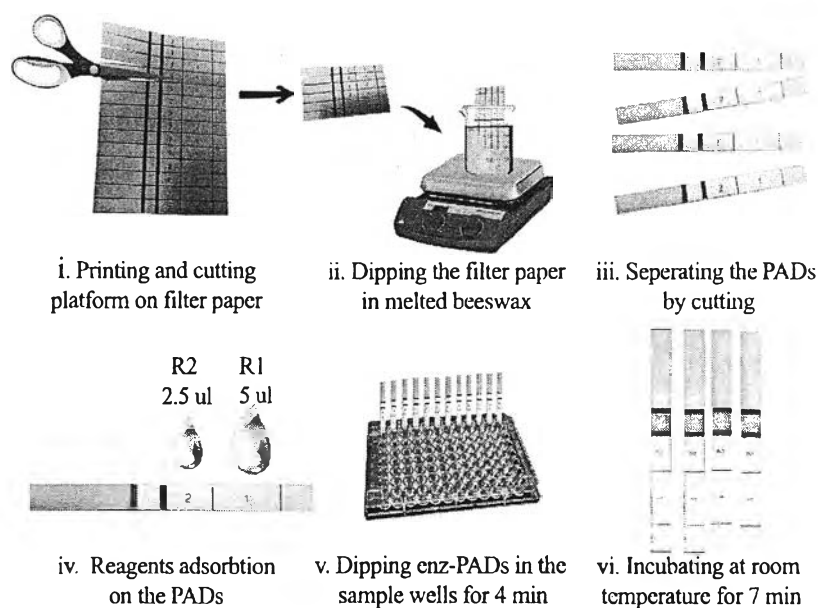


Fig. 2. The enz-PADs fabrication steps and the creatinine assay procedure.

small rectangular shapes ($4 \times 40 \text{ mm}^2$). Furthermore, a hydrophobic holder zone was created by dipping one end of the paper into a melted wax chamber at $108 \pm 3 \text{ }^\circ\text{C}$ for 3 s. In addition, the wax holder zone acted as a barrier for the accumulating quinone imine products. The enz-PAD design is shown in Fig. 1.

Following the manufacturer instructions, a 2:1 ratio of R1–R2 is recommended for a reaction mixture of the enzymatic creatinine assay. Therefore, the same proportion of both reagents was utilised in this study. The PADs were placed on a cleaned lab bench, in which the printed pattern was side up. Then, the reagents were applied to the desired areas using a pipetting technique, in which $5 \mu\text{L}$ of R1 and $2.5 \mu\text{L}$ of R2 were adsorbed on the desired regions separately (Fig. 1b). To carry the enz-PAD, it was touched only at the hydrophobic holder zone. Next, the enz-PADs were allowed to air dry at room temperature, and a vacuum sealer (SINBO™) was used to seal the enz-PADs in a plastic bag for storage at $4 \text{ }^\circ\text{C}$ until future use. Based on the 1–3 mL dead volume of the obtained reagents, 200–600 enz-PADs were fabricated. This, demonstrated a

very low or near zero-cost for this paper device.

2.4. Creatinine detection using enz-PADs

The creatinine assay principle consisted of four continuous enzyme reactions, including (1) a conversion of creatinine into creatine by creatininase, (2) a further conversion of creatine into sarcosine by creatinase, followed by (3) an oxidation of sarcosine by sarcosine oxidase that produces H₂O₂ and (4) a liberated H₂O₂ reaction with 4-aminophenazone and HTIB to form a pink-red quinoneimine chromogen via the peroxidase function, as depicted in Fig. 1a and b. However, the complete assay reaction is initiated by creatininase after the adsorbed reagents on R1 move to R2 zone via capillary force. Although catalase, present in R1 to remove H₂O₂ generated from the endogenous creatine elimination reaction, moves to R2, catalase does not interfere with the peroxidase reaction in R2 because it is inhibited by the sodium azide contained in R2.

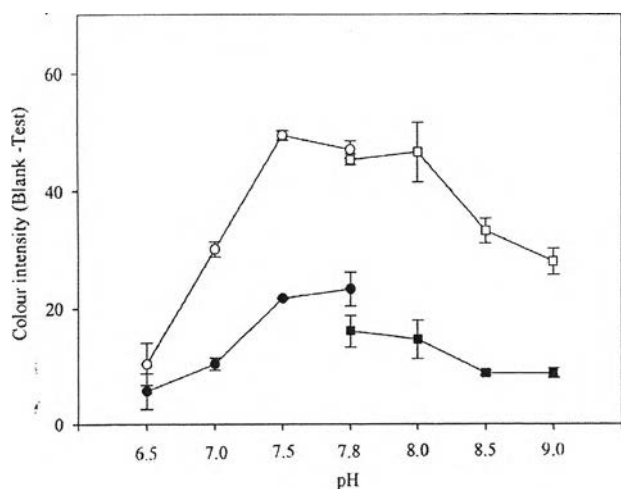


Fig. 3. Effect of the sample pH on colour intensity development in the enz-PADs. The error bars represent standard deviation based on triplicate assays. (●) 5 mg dL⁻¹ of creatinine with 100 mM potassium phosphate buffer; (○) 20 mg dL⁻¹ of creatinine with 100 mM potassium phosphate buffer. (■) 5 mg dL⁻¹ of creatinine with 100 mM Tris-HCl buffer; (□) 20 mg dL⁻¹ of creatinine with 100 mM Tris-HCl buffer.

To initiate the assay, 50 μ L of standard solutions and urine samples was pipetted into microwells. Each sample underwent triplicate assays and was tested in parallel with creatinine standard solutions. The sample zone of each enz-PAD was dipped into wells of the standard or urine solutions to allow creatinine in the sample to react with the pre-impregnated R1 and R2 reagents via the natural capillary force for 4 min. Meanwhile, the water front usually reached and covered the detection zone. Then, the enz-PAD devices were removed from the sample wells, and the colour was allowed to completely develop using air-drying in the detection zone for another 7 min (Fig. 2). Finally, the enz-PAD was imaged using a scanner (HP Deskjet F370 All-in-One scanner) at 600 dpi resolution in jpeg format. The detection zone, a fixed size corresponding to 70 \times 90 pixels in rectangular area on the enz-PAD, was selected for measuring the colour intensity. An average intensity value of the rectangular area was obtained from the histogram panel of RGB channel in the Adobe Photoshop CS2 programme.

To compare this method, the creatinine content in the samples was quantified using a commercial kit (Creatinine liquicolor, HUMAN) and was measured using a spectrophotometer (Evolution 600, Thermo Scientific). Briefly, a urine sample was diluted 50-fold with distilled water and then, it reacted with 1000 μ L of the alkaline picrate working solution. After 30 s, the absorbance A1 was read, and after 2 min, the absorbance A2 was read at 500 nm.

3. Results and discussions

3.1. Type of paper

In this study, the pore-size and colour development intensity of Whatman papers Nos. 1, 3 and 42 were investigated using 20 mg dL⁻¹ creatinine testing. The formed colour in the Whatman No. 3 detection zone was smoother than that of Whatman No. 1 upon a naked eyes observation (data not show). This is a result of, the pore size in Whatman No. 3 (6 μ m) being smaller than the pore size in Whatman No. 1 (11 μ m). The pore size differences lead to different wicking rates. Thus, the wicking flow rate in Whatman No. 3 is 90 s per 100 mL, whereas the flow rate in Whatman No. 1 is 40 s per 100 mL. The developed colour in Whatman No. 1 in

the detection zone exhibited a rocket-like shape. Specifically, the colour at the edge of the hydrophilic zone was more intense than in the middle of the paper. This caused imprecision of the captured colour intensity from this area. These findings suggest that a homogeneous colour in the detection zone is better obtained from papers with slow wicking rates. Nevertheless, when using Whatman No. 42 (2.5 μ m pore-size and, a 240 s per 100 mL wicking rate), a consistent colour development in the detection zone was not significantly improved compared with Whatman No. 3. Whatman No. 3 is two times cheaper than No. 42. Thus, Whatman No. 3 was selected for further experiments. The detection zone was designed to be a small rectangular shape (4 \times 3 mm²) for it be readily observable and to allow colour intensity measurement. Using the chosen detection zone size, a smooth and evenly developed colour intensity was observed, and the rocket shaped colour pattern development was not observed. Intensity of the developed colour at the detection zone was randomly analysed for 10 replicates on the same enz-PAD using a fixed size of 70 \times 90 pixels, and the average colour intensity of the entire square was recorded. As shown in Fig. S.1 (Supplementary data), variation coefficients (% CV) were obtained with values of 0.26, 0.30 and 0.46% when assayed with standard creatinine solution at 2.5, 10 and 25 mg dL⁻¹, respectively. In addition, the colour intensities of small areas (17.5 \times 22.5 pixels) were analysed for 16 consecutive areas until the entire detection zone of an enz-PAD was covered. The results are displayed in Table S.1 (Supplementary data). Specifically, % CVs were obtained with values of 2.94, 4.38, and 6.45% when assayed with 2.5 mg dL⁻¹, 10 mg dL⁻¹ and 25 mg dL⁻¹, respectively. These findings confirmed that the developed colour in the detection zone of the proposed enz-PAD was sufficiently smooth and evenly developed.

3.2. Effect of sample pH

In this study, determination of creatinine is based on an enzymatic method. Therefore, the pH of an assay reaction influences enzymatic activity and the colour intensity development. In our enz-PAD platform, urine samples represent a relatively large volume compared with the reagent that was impregnated on the paper. Therefore, each urine sample should be adjusted to the same optimised pH before the assay is performed. The average pH of healthy urine samples ranges from 6.5 to 8.0. In the experiment, a variety of buffers with pH ranging from 6.5 to 9.0 was used to dilute the samples and to determine the optimal pH. The results demonstrated in Fig. 3 show that the colour intensity increased when pH of the sample increased. However, a pH of samples higher than 7.5 did not influence the enzyme activity, such as for the use of potassium phosphate buffer, and therefore, a colour intensity plateau was observed. Clearly, if the pH of the sample was higher than 7.8, the colour intensity was dramatically decreased. Therefore, in this study, a 100 mM potassium phosphate buffer with a pH of 7.5 was selected to dilute samples before the enz-PAD analysis.

3.3. Effect of reaction time

To determine the optimal reaction time for enzymatic reaction before capturing the image intensity, 2.5 and 20 mg dL⁻¹ creatinine sample solution were tested with the proposed enz-PADs. When the sample solution reached and covered the detection zone, the devices were removed from the sample wells, and the reaction time was immediately recorded. The colour intensity in the detection zone was captured using a scanner for another 15 min at 1-min intervals. As shown in Fig. 4, the colour intensity was developed proportional to time within the first 3–7 min. As the reaction extended longer than 7 min, the colour intensity was

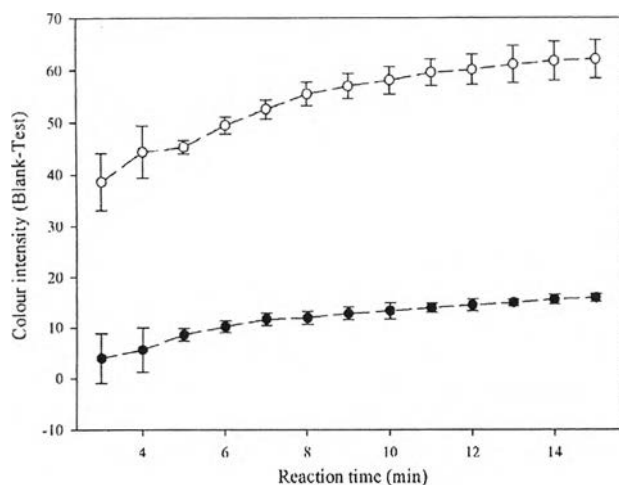


Fig. 4. The colour intensities obtained for the optimisation study of the reaction time for determining creatinine using enz-PADs. (●) 2.5 mg dL⁻¹ of creatinine; (○) 20 mg dL⁻¹ of creatinine. Each point indicates the mean value from triplicate assays; error bars represents standard deviation.

slowly developed. As a compromise between the sensitivity of the assay and the assay time, a reaction time of 7 min was selected for the creatinine measurements using enz-PADs in the subsequent experiments.

3.4. Analytical range and limit of detection

For the proper conditions described in Section 2.4, creatinine concentrations up to 40 mg dL⁻¹ were analysed using enz-PADs, and triplicate assays were performed for each concentration. The results demonstrated a linear range from 2.5 to 25 mg dL⁻¹ of creatinine ($r^2=0.983$), as shown in Fig. 5.

The limit of detection (LOD) was calculated based on three standard deviations of a blank sample ($n=10$) divided by the slope of the analytical curve in the linear range. In our study, the obtained detection limit for creatinine was 2.0 mg dL⁻¹. Compared with previously published studies, our paper device offers the same sensitivity level. For example, electrochemical sensors based on the Jaffé reaction exhibit a linear range of 4.19–40.72 mg dL⁻¹ and a limit of detection of 0.97 mg dL⁻¹ [41]. However, our method is 10–20 times less sensitive than the previously

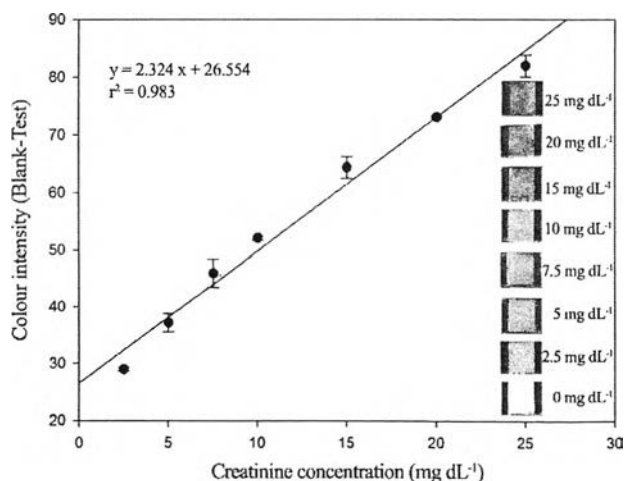


Fig. 5. Analytical curve of enz-PADs for determining urinary creatinine. The analytical linear range obtained from 2.5 to 25 mg dL⁻¹ of creatinine by measuring colour intensity (RGB mode) in the detection zone ($r^2=0.983$, assays for each sample were performed in triplicate).

published methods. Zone fluidic multichannel kinetic spectrophotometry, which relies on the Jaffé reaction, exhibits a LOD of 0.076 mg dL⁻¹ [24], whereas the LOD of a previously reported portable microfluidic system was 0.33 mg dL⁻¹ [23]. However, such methods require sophisticated equipment and well-trained personal to operate the machinery. Compared with portable POCT assays, such as Clinitek[®] (Siemens), that detect both microalbumin and creatinine, Clinitek[®] provides semi-quantitative results and reports urine creatinine content ranging from 10 to 300 mg dL⁻¹, allowing the undiluted urine sample to be assayed directly. A major drawback is that the strip is expensive (approximately \$3.2–6 per test strip), and haemoglobin or myoglobin (≥ 5 mg dL⁻¹) may cause falsely elevated results in both the albumin and creatinine tests. Although our proposed enz-PAD does not provide a very low LOD, its sensitivity is satisfactory and is sufficient for clinical diagnoses, and its linear range covers both the normal and pathological concentrations.

3.5. Precision of enz-PADs

To evaluate the reproducibility of enz-PADs for the creatinine assay, 20 pieces of enz-PADs fabricated on the same day were used to perform assays with 5 mg dL⁻¹ and 20 mg dL⁻¹ of creatinine. The results showed that within-day precisions with coefficients of variation (CVs) of 8.82% and 6.86% were obtained for assays of 5 mg dL⁻¹ ($n=10$) and 20 mg dL⁻¹ ($n=10$) of creatinine, respectively. Between day precisions at 11.57% and 9.39% coefficients of variation (CVs) were obtained when evaluated with 5 mg dL⁻¹ and 20 mg dL⁻¹ of creatinine standard on three consecutive days ($n=30$), respectively.

In addition, the enz-PADs were also analysed with 3 levels of creatinine, 11.6 mg dL⁻¹ ($n=20$), 172.0 mg dL⁻¹ ($n=20$) and 328.2 mg dL⁻¹ ($n=20$), from real urine samples. The results of the within-day precision with CVs of 14.2%, 6.9% and 5.9% were obtained when evaluated with the abovementioned three urine samples, respectively. The between-day precision with CVs of 16.6%, 6.4% and 6.1% was obtained when evaluated for the abovementioned real urine samples with different levels of creatinine assayed on ten consecutive days, respectively.

3.6. Interference study

Currently, determination of creatinine based on enzyme reactions is accepted and is used in most clinical laboratories, because this method exhibits several advantages over the Jaffé-based assays, especially regarding the specificity. To study the effect of interfering substances on creatinine determination, several common interfering substances were spiked into the creatinine standard to correspond to a final creatinine concentration of 10 mg dL⁻¹. The results revealed that the presence of 300 mg dL⁻¹ glucose, 150 mg dL⁻¹ human serum albumin, 100 mg dL⁻¹ haemoglobin, 50 mg dL⁻¹ ascorbic acid, 35 mg dL⁻¹ bilirubin, 20 mg dL⁻¹ uric acid and 1 mg dL⁻¹ creatine did not significantly interfere with enz-PADs. We obtained recoveries of 96.0–101.8% from the undiluted triplicates samples (Table 1). Nevertheless, for the proposed method, the urine samples must be diluted 10- to 20-fold with 100 mM phosphate buffer, pH 7.5, before analysis. For this reason, it is assumed that the proposed enz-PADs will not significantly interfere with contaminant concentrations 10- to 20-fold lower than the concentrations that were tested.

To confirm efficiency of the designed enz-PADs for a complete elimination of endogenous creatine in the R1 zone, creatine was spiked into the standard or urine sample, and the assay recoveries were studied. As shown in Table S.2 (Supplementary data), the results show that 1 mg dL⁻¹ creatine did not significantly interfere with the proposed enz-PADs. This implies that enzymes in R1 of enz-

Table 1
Effects of the tested substances on the creatinine assay using the proposed enz-PADs.

Tested substances	% Recovery
None	100.0 ± 5.7
300 mg dL ⁻¹ of glucose	96.0 ± 8.5
150 mg dL ⁻¹ of human serum albumin	101.5 ± 3.4
100 mg dL ⁻¹ of haemoglobin	97.2 ± 8.8
50 mg dL ⁻¹ of ascorbic acid	99.7 ± 3.5
35 mg dL ⁻¹ of bilirubin	101.5 ± 10.1
20 mg dL ⁻¹ of uric acid	96.3 ± 9.2
1 mg dL ⁻¹ of creatine	101.8 ± 2.3

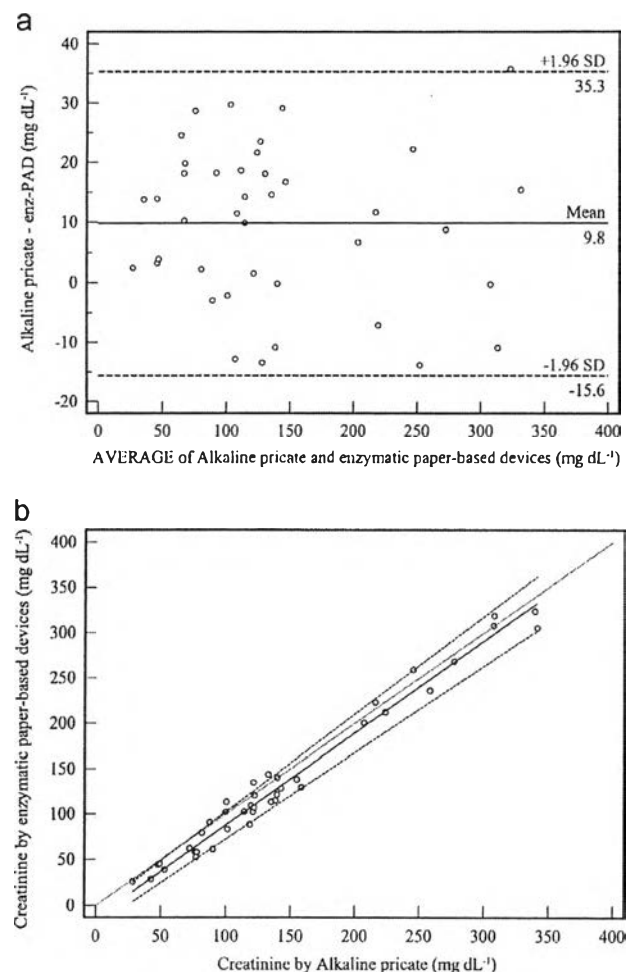


Fig. 6. Comparison of results obtained using the enz-PAD method and the alkaline picrate method for determining urinary creatinine. The results are shown as (a) a Bland–Altman bias plot and (b) a Passing–Bablok regression analysis.

PADs can completely eliminate the endogenous creatine up to 10 mg dL⁻¹ from undiluted urine samples. In general, urine creatine can be found in the range of 0–40 mg/day and 0–80 mg/day in males and in females, respectively [42]. If the average excreted urine volume is 1.5 L/day, the creatine concentration should be 0–2.7 mg dL⁻¹ and 0–5.3 mg dL⁻¹ in males and in females, respectively. Therefore, the urine creatine levels do not interfere with the enzymatic reactions utilised in the proposed enz-PADs for creatinine determination.

3.7. Analysis of real urine samples

To evaluate the accuracy of enz-PADs for analysing real samples,

forty urine samples were quantified, and the results were compared with a conventional alkaline picrate method. Urine samples ($n=40$) were diluted 10- to 20-fold with 100 mM potassium phosphate buffer, pH 7.5. A scatter-plot of the results obtained using both methods is shown with a correlation coefficient of 0.977 ($n=40$), as shown in Fig S.2. The enz-PADs had no bias for detecting urinary creatinine because the differences between the two methods fell within the mean \pm 1.96 SD, as shown in the Bland–Altman plot (Fig. 6a). The Passing–Bablok regression was employed to assess the correlation of the methods, for which the equation $y=1.0159x-13.8390$ was obtained, and no significant deviation from linearity ($P>0.10$) was observed, as shown in Fig. 6b. Therefore, the proposed enz-PADs can be used for quantitative creatinine assays of real samples and exhibit good agreement with the alkaline picrate method without bias. Moreover, using the 96-well microplates, the enz-PADs can be used to analyse multiple samples simultaneously. Because the enz-PAD requires 11 min per test, approximately 480 samples can be assayed per hour, and more samples can be analysed with intervals of 4 min. The throughput of enz-PADs is similar to automatic analysers, which assay 600 samples per hour. The high-throughput of the proposed method is important for clinical diagnoses, particularly for in the field analyses. The sample analysis frequency was better than for the electrochemical sensors and flow injection analyses [23,41,43,44].

4. Conclusion

A sensitive and specific paper-based diagnostic analytical device for determining urinary creatinine based on an enzymatic assay was successfully developed. The assay format is simple, rapid and highly promising for performing high-throughput assays of several samples within a short period of time. The major advantage of an enz-PAD is that it exploits the small remaining creatinine assay reagent volume in cassettes of automatic analysers, which allows the detection cost to be extremely low or negligible. To analyse urine creatinine using our PADs, no expensive instruments are required. The PAD is a novel device that exhibits good reproducibility and allows fully portable analyses. The proposed PAD provide an alternative and inexpensive platform for screening urinary creatinine and will be highly beneficial for the low-income or developing countries.

Acknowledgements

This research was financially supported by the 90th Anniversary of Chulalongkorn University Fund (Ratchadaphiseksomphot Endowment Fund) from Chulalongkorn University (Grant no. GCUGR11255725106M), and the Thailand Research Fund through Research Team Promotion Grant (RTA5780005). K.T. acknowledges the Overseas Academic Presentation Scholarship for Graduate Students, Chulalongkorn University.

Appendix A. Supplementary information

Supplementary data associated with this article can be found in the online version at <http://dx.doi.org/10.1016/j.talanta.2015.07.040>.

References

- [1] E. Mohabbati-Kalejahi, V. Azimirad, M. Bahrami, A. Ganbari, Talanta 97 (2012) 1–8.
- [2] E.P. Randviir, C.E. Banks, Sens. Actuators B Chem. 183 (2013) 239–252.

- [3] S. Gamagedara, H. Shi, Y. Ma, *Anal. Bioanal. Chem.* 402 (2012) 763–770.
- [4] W. Siangproh, N. Teshima, T. Sakai, S. Katoh, O. Chailapakul, *Talanta* 79 (2009) 1111–1117.
- [5] G. Xin, M. Wang, L.-l Jiao, G.-b Xu, H.-y Wang, *Clin. Chim. Acta* 350 (2004) 35–39.
- [6] K. Uchida, A. Goroh, *Clin. Chim. Acta* 323 (2002) 121–128.
- [7] M. del Carmen Hurtado-Sánchez, A. Espinosa-Mansilla, M.I. Rodríguez-Cáceres, E. Martín-Tornero, I. Durán-Merás, *J. Sep. Sci.* 35 (2012) 2575–2584.
- [8] L.A. McGuinn, A.A. Ghazarian, L. Joseph, Su, G.L. Ellison, *Environ. Res.* 136 (2015) 381–386.
- [9] H. Husdan, A. Rapoport, *Clin. Chem.* 14 (1968) 222–238.
- [10] M.L. Bishop, E.P. Fody, L.E. Schoeff, *Clinical Chemistry: Principles, Techniques, and Correlations*, Lippincott Williams & Wilkins, Philadelphia, 2013.
- [11] S. Viraraghavan, K.G. Blass, *J. Clin. Chem. Clin. Biochem.* 28 (1990) 95–105.
- [12] H.L. Pardue, B.L. Bacon, M.G. Nevius, J.W. Skoug, *Clin. Chem.* 33 (1987) 278–285.
- [13] M.H. Kroll, N.A. Roach, B. Poe, R.J. Elin, *Clin. Chem.* 33 (1987) 1129–1132.
- [14] J.R. Delanghe, M.M. Speeckaert, *NDT Plus* 4 (2011) 83–86.
- [15] J.A. Weber, A.P. van Zanten, *Clin. Chem.* 37 (1991) 695–700.
- [16] M. Panteghini, *Clin. Chem. Lab. Med.* 46 (2008) 567–572.
- [17] D. Tsikas, A. Wolf, J.C. Frölich, *Clin. Chem.* 50 (2004) 201–203.
- [18] V. Pavlicek, P. Tuma, J. Matejkova, E. Samcova, *Electrophoresis* 35 (2014) 956–961.
- [19] M.J. Welch, A. Cohen, H.S. Hertz, K.J. Ng, R. Schaffer, P. Van der Lijn, Et White, *Anal. Chem.* 58 (1986) 1681–1685.
- [20] R. Hušková, P. Chrástina, T. Adam, P. Schneiderka, *Clin. Chim. Acta* 350 (2004) 99–106.
- [21] A. Radomska, E. Bodenszac, B.S. Gla, R. Koncki, *Talanta* 64 (2004) 603–608.
- [22] [20] R.I. Stefan-van Staden, R.G. Bokretson, J.F. van Staden, H.Y. Aboul-Enem, *Prep. Biochem. Biotechnol.* 36 (2006) 287–296.
- [23] T. Songjaroen, T. Matusos, A. Sappat, A. Tuantrianont, W. Laiwattanapaisal, *Anal. Chim. Acta* 647 (2009) 78–83.
- [24] S.I. Ohira, A.B. Kirk, P.K. Dasgupta, *Anal. Biochem.* 384 (2009) 238–244.
- [25] M. Tadele Alula, J. Yang, *Talanta* 130 (2014) 55–62.
- [26] A. Benkert, F. Scheller, W. Schossler, C. Hentschel, B. Mischeel, O. Behrsing, G. Scharte, W. Stocklein, A. Warsinke, *Anal. Chem.* 72 (2000) 916–921.
- [27] F. Mitchell, *Pure Appl. Chem.* 57 (1985) 571–573.
- [28] C.F. Banks, E.P. Randviir, *Bioanalysis* 6 (2014) 109–111.
- [29] D. Mabey, R.W. Peeling, A. Ustianowski, M.D. Perkins, *Nat. Rev. Microbiol.* 2 (2004) 231–240.
- [30] A.W. Martinez, S.T. Phillips, M.J. Butte, G.M. Whitesides, *Angew. Chem. Int. Ed. Engl.* 46 (2007) 1318–1320.
- [31] T. Songjaroen, W. Dungchai, O. Chailapakul, W. Laiwattanapaisal, *Talanta* 85 (2011) 2587–2593.
- [32] J. Noiphung, T. Songjaroen, W. Dungchai, C.S. Henry, O. Chailapakul, W. Laiwattanapaisal, *Anal. Chim. Acta* 788 (2013) 39–45.
- [33] J.C. Jakerst, J.A. Adkins, B. Bisha, M.M. Mentele, L.D. Goodridge, C.S. Henry, *Anal. Chem.* 84 (2012) 2900–2907.
- [34] M. Li, J. Tian, M. Al-Tamimi, W. Shen, *Angew. Chem. Int. Ed. Engl.* 51 (2012) 5497–5501.
- [35] S.J. Vella, P. Beattie, R. Cademartiri, A. Laromaine, A.W. Martinez, S.T. Phillips, K.A. Mirica, G.M. Whitesides, *Anal. Chem.* 84 (2012) 2883–2891.
- [36] T. Teerinen, T. Lappalainen, T. Erho, *Anal. Bioanal. Chem.* 406 (2014) 5955–5965.
- [37] S.M.Z. Hossain, R.E. Luckham, M.J. McFadden, J.D. Brennan, *Anal. Chem.* 81 (2009) 9055–9064.
- [38] E.M. Fenton, M.R. Mascarenas, G.P. López, S.S. Sibbett, *ACS Appl. Mater. Interfaces* 1 (2008) 124–129.
- [39] Y. Lu, W. Shi, J. Qin, B. Lin, *Anal. Chem.* 82 (2009) 329–335.
- [40] T. Songjaroen, W. Dungchai, O. Chailapakul, C.S. Henry, W. Laiwattanapaisal, *Lab Chip* 12 (2012) 3392–3398.
- [41] J.C. Chen, A.S. Kumar, H.H. Chung, S.H. Chien, M.C. Kuo, J.M. Zen, *Sens. Actuators B Chem.* 115 (2006) 473–480.
- [42] E.R.A. Carl A. Burtis (Ed.), *Tietz Fundamentals of Clinical Chemistry*, 5th ed., Saunders/Elsevier, St. Louis, 2001.
- [43] C.-H. Chen, M.S. Lin, *Biosens. Bioelectron.* 31 (2012) 90–94.
- [44] K. Ponghong, N. Teshima, K. Grudpan, J. Vichapong, S. Moromizu, T. Sakai, *Talanta* 133 (2015) 71–76.



Contents lists available at ScienceDirect

Analytica Chimica Acta

journal homepage: www.elsevier.com/locate/aca

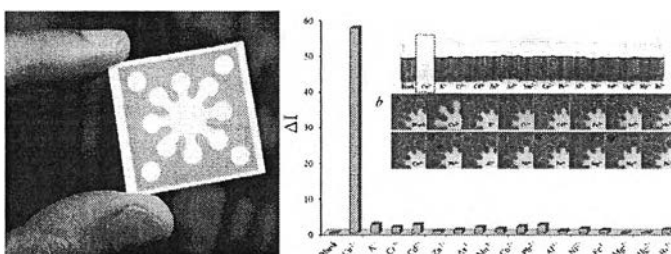
Highly selective and sensitive paper-based colorimetric sensor using thiosulfate catalytic etching of silver nanoplates for trace determination of copper ions

Sudkate Chaiyo^a, Weena Siangproh^b, Amara Apilux^{c,*}, Orawon Chailapakul^{a,d,*}^a *Electrochemistry and Optical Spectroscopy Research Unit, Department of Chemistry, Faculty of Science, Chulalongkorn University, 254 Phayathai Road, Pathumwan, Bangkok 10330, Thailand*^b *Department of Chemistry, Faculty of Science, Srinakharinwirot University, Sukhumvit 23, Wattana, Bangkok 10110, Thailand*^c *Center for Innovation Development and Technology Transfer, Faculty of Medical Technology, Mahidol University, 999 Phuttamonthon 4 Road, Salaya, Nakhon Pathom 73170, Thailand*^d *Center for Petroleum, Petrochemicals and Advanced Materials, Chulalongkorn University, 254 Phayathai Road, Pathumwan, Bangkok 10330, Thailand*

HIGHLIGHTS

- Novel, highly selective and sensitive μ PAD for determination of Cu^{2+} was achieved.
- The limit of detection was found to be very low at 1.0 ng mL^{-1} by visual detection.
- This method was successfully applied for determination of Cu^{2+} in real samples.

GRAPHICAL ABSTRACT



ARTICLE INFO

Article history:

Received 24 October 2014

Received in revised form 19 January 2015

Accepted 28 January 2015

Available online 30 January 2015

Keywords:

Copper ions

Colorimetric detection

Paper-based sensor

Silver nanoplates

Thiosulfate

ABSTRACT

A novel, highly selective and sensitive paper-based colorimetric sensor for trace determination of copper (Cu^{2+}) ions was developed. The measurement is based on the catalytic etching of silver nanoplates (AgNPLs) by thiosulfate ($\text{S}_2\text{O}_3^{2-}$). Upon the addition of Cu^{2+} to the ammonium buffer at pH 11, the absorption peak intensity of AuNPLs/ $\text{S}_2\text{O}_3^{2-}$ at 522 nm decreased and the pinkish violet AuNPLs became clear in color as visible to the naked eye. This assay provides highly sensitive and selective detection of Cu^{2+} over other metal ions (K^+ , Cr^{3+} , Cd^{2+} , Zn^{2+} , As^{3+} , Mn^{2+} , Co^{2+} , Pb^{2+} , Al^{3+} , Ni^{2+} , Fe^{3+} , Mg^{2+} , Hg^{2+} and Bi^{3+}). A paper-based colorimetric sensor was then developed for the simple and rapid determination of Cu^{2+} using the catalytic etching of AgNPLs. Under optimized conditions, the modified AgNPLs coated at the test zone of the devices immediately changes in color in the presence of Cu^{2+} . The limit of detection (LOD) was found to be 1.0 ng mL^{-1} by visual detection. For semi-quantitative measurement with image processing, the method detected Cu^{2+} in the range of $0.5\text{--}200 \text{ ng mL}^{-1}$ ($R^2 = 0.9974$) with an LOD of 0.3 ng mL^{-1} . The proposed method was successfully applied to detect Cu^{2+} in the wide range of real samples including water, food, and blood. The results were in good agreement according to a paired *t*-test with results from inductively coupled plasma-optical emission spectrometry (ICP-OES).

© 2015 Elsevier B.V. All rights reserved.

* Corresponding author at: Electrochemistry and Optical Spectroscopy Research Unit, Department of Chemistry, Faculty of Science, Chulalongkorn University, 254 Phayathai Road, Pathumwan, Bangkok 10330, Thailand. Tel.: +66 2 218 7615; fax: +66 2 218 7615.

** Corresponding author. Tel.: +66 2 441 4371; fax: +66 2 441 4380.

E-mail addresses: amara.apl@mahidol.ac.th (A. Apilux), corawon@chula.ac.th (O. Chailapakul).

1. Introduction

Copper ions (Cu^{2+}) are an essential trace element for life. Cupric ions play an important role in many body functions as an enzyme co-factor and are involved in the formation of red blood cells [1]. However, an excessive uptake of Cu^{2+} can cause serious health problems, including ischemic heart disease, kidney disease, neurodegenerative disease, anemia and bone disorders [2]. Because of their toxicity, the maximum contamination value of Cu^{2+} in the environment and in food was set by several organizations throughout the world to protect human health. For example, the United States Environmental Protection Agency (USEPA) issued the maximum contamination level of Cu^{2+} in drinking water at 1.30 mg L^{-1} [3]. In Thailand, the pollutant control organization permitted a Cu^{2+} concentration of 2.00 mg L^{-1} in surface water [4]. In addition, the concentration limit of Cu^{2+} for exposure from foods is in the range of 1.2–4.2 mg copper/day as set by The European Food Safety Authority (EFSA) [5]. Therefore, the monitoring of Cu^{2+} contaminants in water, food and the environment is necessary.

Conventional methods for the measurement of Cu^{2+} include atomic absorption spectrometry (AAS) [6], inductively coupled plasma atomic emission spectrometry (ICP-AES) [7], inductively coupled plasma mass spectrometry (ICP-MS) [8], voltammetry [9] and fluorescence spectrometry [10]. Although these methods provide high sensitivity and selectivity, they require expensive instrumentation, laboratory setup, and high operating cost, which makes these methods unsuitable for field monitoring. Therefore, there is an increasing interest in the development of simple and low-cost sensors for the highly sensitive and selective detection of Cu^{2+} that can allow reliable on-site real time detection.

Recently, colorimetric sensors based on noble metal nanoparticles such as gold nanoparticles (AuNPs) [11] or silver nanoparticles (AgNPs) [12] for the visual determination of Cu^{2+} have gained increased attention. AgNPs is particularly of interest because it has a higher extinction coefficient compared to AuNPs of the same size and a lower cost compared to AuNPs [13]. Zhou et al. reported on the colorimetric detection of Cu^{2+} by using 4-mercaptobenzoic acid (4-MBA) modified AgNPs. The measurement was based on the aggregation of 4-MBA-AgNPs in the presence of Cu^{2+} via ion-templated chelation [12]. Miao et al. proposed a colorimetric detection method of Cu^{2+} with high sensitivity and selectivity by utilizing the redox reaction between starch-stabilized AgNPs and Cu^{2+} [14]. Ratnarathorn et al. presented the colorimetric measurement on μPAD by using the homocysteine (Hcy) and dithiothreitol (DTT) modified AgNP surface that is able to induce the aggregation of AgNPs in the presence of Cu^{2+} [15]. In addition, a sensitive and selective colorimetric method was developed based on catalytic thiosulfate leaching of nanoparticles including silver coated gold nanoparticles (Ag/Au NPs) [16] or AuNPs [17] by Cu^{2+} . Cu^{2+} can accelerate the leaching rate of NPs and leads to a dramatic decrease in its surface plasmon resonance (SPR) absorption because the nanoparticles size is decreased. Although these assays provided high sensitivity, they are time-consuming (25–60 min) and large volumes of solution are required.

A paper-based sensor or microfluidic paper-based analytical devices (μPADs) are a new alternative methodology of a micro total analytical system (μTAS) applied to food analysis, environmental monitoring, and clinical diagnosis. They provide several advantages such as ease of use, high throughput, disposability, low sample and reagents consumption, low expense, and portability [18–20]. The μPADs were first introduced by Martinez et al., where the hydrophilic microchannels on devices were fabricated by creating a hydrophobic wall using photolithography [21]. To date, several methods were proposed to fabricate these devices, including inkjet-printing [22], plotting [23], wax-printing [24], plasma treatment [25], and screen printing [26]. Herein, the wax

printing method, which is easy and is a quick fabrication process, was applied to create paper-based devices. This paper-based colorimetric sensor is based on the catalytic etching of silver nanoplates (AgNPLs) with thiosulfate ($\text{S}_2\text{O}_3^{2-}$) and is developed for the highly selective and sensitive detection of trace Cu^{2+} .

2. Experimental

2.1. Chemicals and materials

Copper sulfate (CuSO_4) and ammonium hydroxide (NH_4OH) were purchased from BDH (England). Sodium thiosulfate, hexadecyltrimethylammonium bromide (CTAB), magnesium sulfate (MgSO_4), manganese chloride (MnCl_2) and ammonium dichromate ($(\text{NH}_4)_2\text{Cr}_2\text{O}_7$) were obtained from Sigma-Aldrich (Missouri). Ammonium chloride (NH_4Cl) was obtained from Ajax (NSW, Australia). Standard solutions of $1000 \mu\text{g mL}^{-1}$ Hg^{2+} , Bi^{3+} , As^{3+} , Pb^{2+} , Co^{2+} , Cd^{2+} and Zn^{2+} were purchased from Spectrosol (Poole, UK), and standard solutions of $1000 \mu\text{g mL}^{-1}$ Ni^{2+} and Al^{3+} were purchased from Merck (Darmstadt, Germany). The following chemicals were used as received: iron chloride hexahydrate ($\text{FeCl}_3 \cdot 6\text{H}_2\text{O}$) (Merck, Darmstadt, Germany) and potassium chloride (KCl) (Univar, Redmond, WA). All chemicals were analytical-grade. All reagents were prepared with $18 \text{ M}\Omega \text{ cm}^{-1}$ resistance in deionized water (obtained from a Millipore Milli-Q purification system).

2.2. Instrumentation

The absorbance measurement was carried out by a UV-visible spectrophotometer (HP HEWLETT PACKARD 8453, UK) using a 1.0 cm path length quartz cell. The modified surface morphology of the paper-based device was characterized by scanning electron microscopy (SEM) (JEOL, Ltd., Japan). Transmission electron microscopy (TEM) was recorded by a H-7650 transmission electron microscope (Hitachi Model, Japan). The levels of Cu^{2+} in real samples were analyzed by inductively coupled plasma optical emission spectrometry (ICP-OES) (CAP 6000 series ICP-OES, Thermo Scientific, USA).

2.3. Synthesis of the modified AgNPLs

AgNPLs [27] were obtained from the Sensor Research Unit at the Department of Chemistry, Faculty of Science, Chulalongkorn University. Briefly, the AgNPLs were synthesized by reduction of AgNO_3 using NaBH_4 and the shape transformation using a 30% H_2O_2 solution [27]. First, the NaBH_4 was added into the AgNO_3 under vigorously magnetic stirring. The solution turned light yellow, indicating the formation of NPs. The shape transformation reaction was done by an injection of the 30% H_2O_2 solution at the rate of $13.45 \text{ mL min}^{-1}$ into AgNs. After the complete addition of the H_2O_2 solution, the colloid was further stirred for 10 min to complete the shape conversation process. The solution turned color from light yellow to the blue of AgNPLs. For the modification of AgNPLs hexadecyltrimethylammonium bromide (CTAB) capped AgNPLs were prepared by the dilution of AgNPLs to $200 \mu\text{g mL}^{-1}$ in a total final volume of $1000 \mu\text{L}$ with a 0.1 M ammonia buffer at pH 11. Then, $10 \mu\text{L}$ of 0.1 M CTAB was added to produce the CTAB-capped AgNPLs. Sequentially, $5 \mu\text{L}$ of 1.0 M $\text{Na}_2\text{S}_2\text{O}_3$ was added to the CTAB-capped AgNPLs followed by incubation of the mixture for 5 min at room temperature.

2.4. Device design and fabrication

In order to obtain highly reproducible measurements, the dendritic hydrophilic channel terminated in the eight detection

zone to enable repeating eight measurements at the same time, and in the four circular area of the control zone that was designed on the paper-based sensor using Adobe illustrator CS4. The wax printing method was used to pattern the resulting design. The fabrication process includes two steps: (1) printing of the wax pattern on the surface of the filter paper (Whatman no. 1) by using the wax printer (Xerox Color Qube 8570, Japan) and (2) melting the wax-printed paper on a hot plate at 175 °C for 40 s. The wax covered area was hydrophobic, while the area without wax was hydrophilic. These processes can be finished within 2 min.

2.5. Colorimetric assay of Cu^{2+} on paper based devices

The modified AgNPLs at 0.8 μL were dropped onto the detection zone and control zone, and allowed to dry. For Cu^{2+} measurement, 20 μL of the standard/sample solutions was added to the sample application zone and then the solution flowed into the detection zone. The color change at the test zone can be observed within 2 min. For quantitative analysis, the photograph of the results on the paper-based sensor was recorded by a digital camera (Cannon EOS 1000 D1, Japan) in a light control box. Then, color intensity of the testing area on the device was measured using ImageJ 1.45s (National Institutes of Health, USA). Finally, the color intensity values were used to obtain a calibration curve.

2.6. Analysis of Cu^{2+} in real world samples

2.6.1. Mineral water and groundwater

The mineral water samples were purchased from a local supermarket. The groundwater samples were obtained from the paddy field of the Suphanburi province, Thailand. All of the water samples were filtered using 0.45 μm member filters before testing.

2.6.2. Tomato juices

The tomato juices were purchased from a local supermarket. A 1.5 mL aliquot of the juices was centrifuged for 40 min at 6000 rpm [28]. The centrifuged juice samples were then filtered using cotton and a 0.45 μm membrane filter.

2.6.3. Rice

The rice sample was obtained from a Surin Provincial source, Thailand. The samples were digested by an acid digestion method [29]. A 0.5 g of rice sample was added in the mixing between concentrated nitric acid and concentrated perchloric acid in the ratio 1:1 (v/v) and heated to 150 °C and stirred for 4 h. The solution was evaporated to less than 2 mL of volume. Sequentially, the concentrated hydrogen peroxide was added dropwise under heating until the solution was colorless after the solution was evaporated. Finally, the sample solution was filtered through a 0.45 μm membrane filter.

2.6.4. Blood

The leftover blood samples were obtained from the local hospital. The whole blood samples (1 mL) were added to 4 mL of the mixture solution of concentrated nitric acid and concentrated perchloric acid (3:1 v/v) [30] and heated to near dryness. The sample solution was then filtered using a 0.45 μm member filter.

For all cases, the filtered solution was diluted with 0.1 M ammonia buffer at pH 11 before measurement. Fortunately, after preparation of the real samples, the solution obtained was colorless. Therefore, there was no interference effect from color of sample.

3. Results and discussion

3.1. UV–visible absorption spectra and Mechanism of AgNPLs the presence of Cu^{2+}

To understand the mechanism of the catalytic etching of AgNPLs by $\text{S}_2\text{O}_3^{2-}$ for the measurement of Cu^{2+} , the SPR absorption was investigated as shown in Fig. 1. The CTAB/AgNPLs in 0.1 M ammonia buffer at pH 11 exhibited an absorption maximum (λ_{max}) of 563 nm (curve a). After the addition of 1 M $\text{Na}_2\text{S}_2\text{O}_3$ at 1.5 μL in 3 mL of CTAB/AgNPLs the λ_{max} of the CTAB/AgNPLs was decreased (curve b) and blue shifted to 522 nm. This is due to the decreased AuNPLs size through oxidation of AgNPLs with oxygen (O_2). By the addition of Cu^{2+} , the color of the solutions changed from violet-red to colorless within 5 min. The absorbance peak at 522 nm decreased with an increase in concentration of Cu^{2+} from 50 to 200 ng mL^{-1} (curves c–e). The insets of Fig. 1 show the color change of CTAB/AgNPLs caused by the catalytic etching of CTAB/AgNPLs by $\text{S}_2\text{O}_3^{2-}$ in the presence of Cu^{2+} .

Upon the addition of $\text{S}_2\text{O}_3^{2-}$ ions to CTAB/AgNPLs the AgNPLs can be oxidized by dissolved O_2 leading to reduction of the particle size of AgNPLs (Scheme S1). However, it was found that this reaction is very slow because the $\text{Ag}(\text{S}_2\text{O}_3)_2^{3-}$ complexes immediately generated a passive layer on the surface AgNPLs. By adding Cu^{2+} , the Cu^{2+} in the 0.1 M ammonia buffer at pH 11 forms the $\text{Cu}(\text{NH}_3)_4^{2+}$ complex and the standard potential of $\text{Cu}(\text{NH}_3)_4^{2+}/\text{Cu}^{2+}$ in the presence of $\text{S}_2\text{O}_3^{2-}$ was increased (Eq. (2)). The Cu^{2+} could accelerate the etching rate of the AgNPLs by forming $\text{Cu}(\text{S}_2\text{O}_3)_3^{5-}$ and the complexes could also be oxidized to Cu^{2+} by dissolved oxygen (Eq. (3)). The etching of $\text{S}_2\text{O}_3^{2-}/\text{CTAB/AgNPLs}$ increased with increasing concentration of Cu^{2+} . As a result, the color solution changes from violet-red to colorless. Therefore, the colorimetric detection based on the catalytic etching of modified AgNPLs provides a simple and sensitive method for the measurement of trace Cu^{2+} .

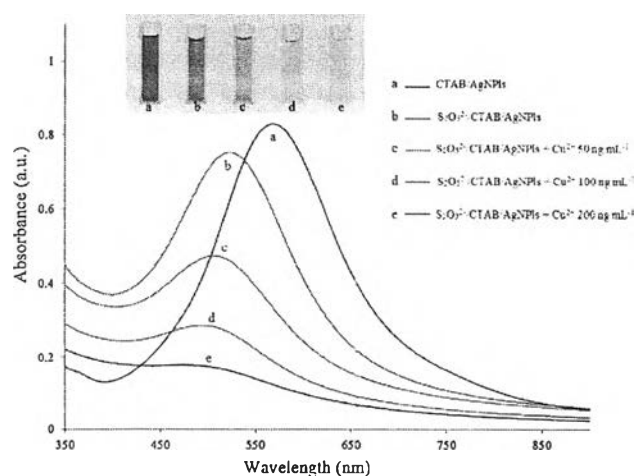
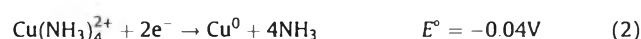
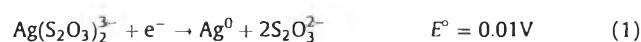
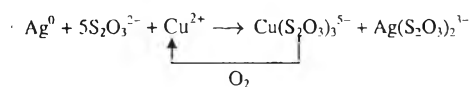
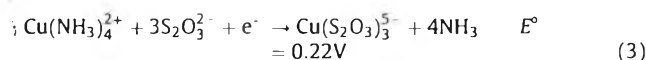


Fig. 1. The absorption spectra of AgNPLs (a) CTAB/AgNPLs ($\lambda_{\text{max}} = 563 \text{ nm}$, $A = 0.827$); (b) $\text{S}_2\text{O}_3^{2-}/\text{CTAB/AgNPLs}$ ($\lambda_{\text{max}} = 522 \text{ nm}$, $A = 0.749$); (c) $\text{S}_2\text{O}_3^{2-}/\text{CTAB/AgNPLs} + 50 \text{ ng mL}^{-1}$ of Cu^{2+} ($A = 0.473$); (d) $\text{S}_2\text{O}_3^{2-}/\text{CTAB/AgNPLs} + 100 \text{ ng mL}^{-1}$ of Cu^{2+} ($A = 0.284$); (e) $\text{S}_2\text{O}_3^{2-}/\text{CTAB/AgNPLs} + 200 \text{ ng mL}^{-1}$ of Cu^{2+} ($A = 0.174$). The experiment was carried out at room temperature in 0.1 M ammonia buffer pH 11. The UV–vis spectra was investigated after 5 min. (Inset: the color product of the catalytic etching of modified CTAB/AgNPLs with $\text{S}_2\text{O}_3^{2-}$ for measurement of Cu^{2+}).



3.2. Paper-based sensor for tract determination of Cu^{2+}

To improve the colorimetric determination of Cu^{2+} for rapid on-site screening applications, the developed approach using a paper-based sensor was applied. The $\text{S}_2\text{O}_3^{2-}$ /CTAB/AgNPLs was pre-prepared with the test zone and control zone on the paper-based sensor as fabricated by wax printing method (Fig. 2a). For Cu^{2+} measurement, the sample solution at $20 \mu\text{L}$ was applied at the sample zone and then the solution flowed outward via capillary forces to the eight detection zones. In the absence of Cu^{2+}

, the color results at the detection zone were not changed (Fig. 2b). However, in the presence of Cu^{2+} , the color at the detection zones changed from violet-red to colorless with increasing Cu^{2+} concentration, which can be monitored by the naked eye after 120 s (Fig. 2c and d). The SEM image of the paper based-sensor at the detection zone is shown in Fig. 2 both (e) without and (f) with AgNPLs and (g) AgNPLs in the presence of Cu^{2+} . The results indicated that the modified AgNPLs were etched by Cu^{2+} . Additionally, the TEM image (Fig. 2h) clearly shows that the $\text{S}_2\text{O}_3^{2-}$ /CTAB/AgNPLs was well dispersed in the aqueous solution. The average size of $\text{S}_2\text{O}_3^{2-}$ /CTAB/AgNPLs was approximately 30 nm. After the addition of Cu^{2+} (Fig. 2i), the $\text{S}_2\text{O}_3^{2-}$ /CTAB/AgNPLs would be catalytically oxidized and etched into the solution. The average size of $\text{S}_2\text{O}_3^{2-}$ /CTAB/AgNPLs were decreased after incubation for 5 min at room temperature.

3.3. Optimization of the detection conditions

The sensitivity of the paper-based colorimetric sensors containing the modified AgNPLs for Cu^{2+} detection is related to various factors including, pH of buffer solutions, concentrations of AgNPLs

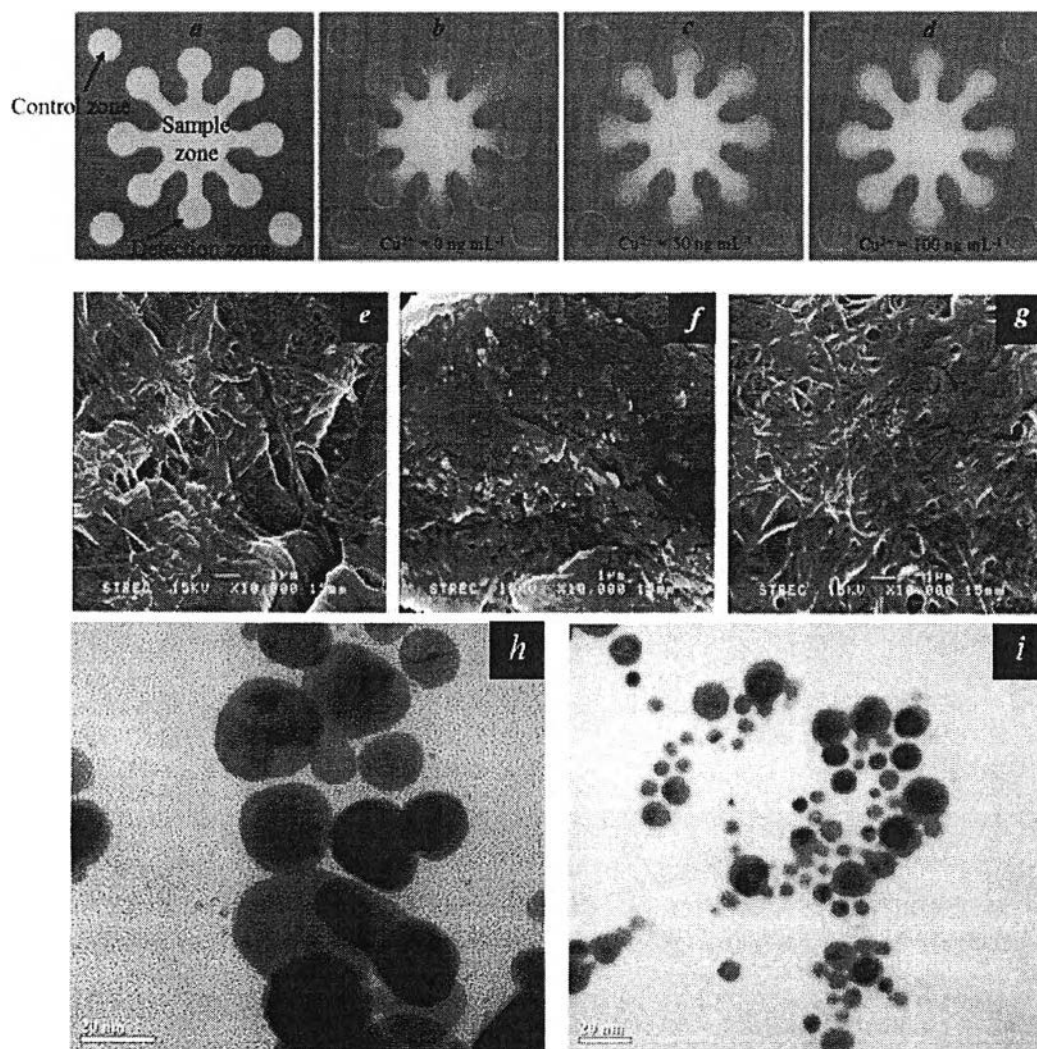


Fig. 2. Paper-based colorimetric sensor based on the catalytic etching mechanism of the CTAB/AgNPLs with $\text{S}_2\text{O}_3^{2-}$ for measurement of Cu^{2+} at (a) image of paper-based devices; image of paper-based devices after measurement of Cu^{2+} (b) 0 ng mL^{-1} , (c) 50 ng mL^{-1} and (d) 100 ng mL^{-1} of Cu^{2+} ; the SEM images of paper-based sensor at the detection zone (e) without CTAB/AgNPLs (f) with CTAB/AgNPLs (g) CTAB/AgNPLs in the presence of 100 ng mL^{-1} Cu^{2+} ; the TEM images of $\text{S}_2\text{O}_3^{2-}$ /CTAB/AgNPLs without Cu^{2+} (h) and with 100 ng mL^{-1} of Cu^{2+} (i).

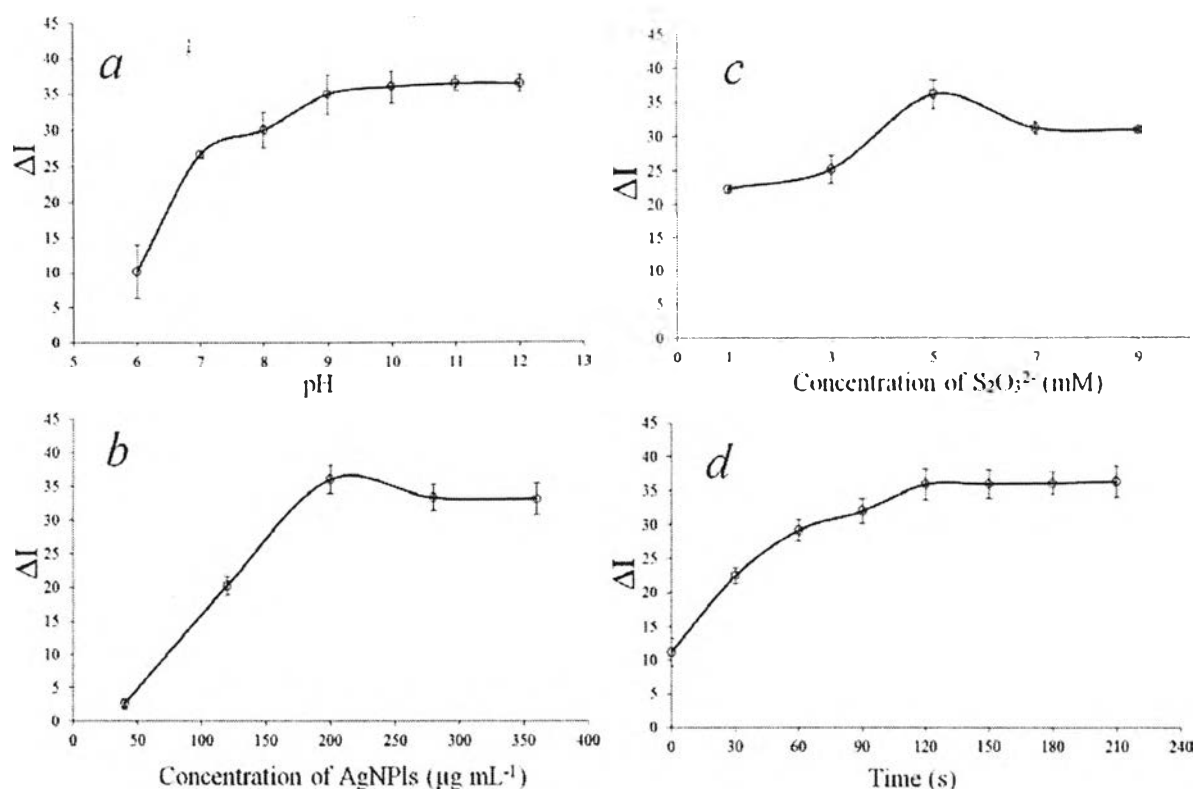


Fig. 3. Effect of experimental conditions for Cu^{2+} measurement on paper-based sensor; (a) pH of ammonia buffer, (b) concentration of AgNPLs (c) concentration of $\text{S}_2\text{O}_3^{2-}$ and (d) incubation time.

and $\text{S}_2\text{O}_3^{2-}$ and incubation time. Therefore, these parameters were optimized by using 100 ng mL^{-1} of Cu^{2+} . The difference in the color intensity values of the AgNPLs before and after the addition of Cu^{2+} ($\Delta I = I_{\text{sample}} - I_{\text{blank}}$) was determined.

3.3.1. Effect of the pH of the ammonia buffer

The influence of the pH on this system was investigated in pH range of 6.0–11.0 (Fig. 3a). At pH lower than 8, the ΔI decreased

because the $\text{S}_2\text{O}_3^{2-}$ was not stable and broke down into sulfate, sulfide, sulfite tetrathionate, trithionate, polythionates and polysulfides [31]. However, in the pH range of 9–12, the complex $\text{Cu}(\text{NH}_3)_4^{2+}$ concentration increased with increasing NH_3 concentration, enabling the oxidation of AgNPLs by $\text{Cu}(\text{NH}_3)_4^{2+}$. The intensity color of modified AgNPLs was almost constant above pH 11 in the presence Cu^{2+} . Therefore, pH 11 was selected as the optimal value for all experiment.

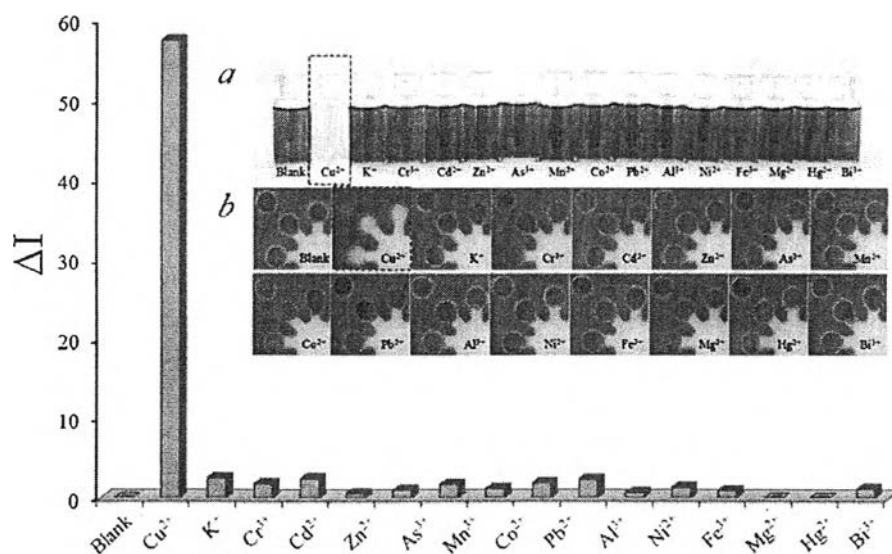


Fig. 4. The mean color intensity values of the modified AgNPLs on paper-based sensor after addition of different metal ions at concentration of 100 ng mL^{-1} Cu^{2+} and $10 \mu\text{g mL}^{-1}$ others metals. Inset: the photographic images results of colorimetric determination of metal ions (a) in solution (b) on paper-based devices.

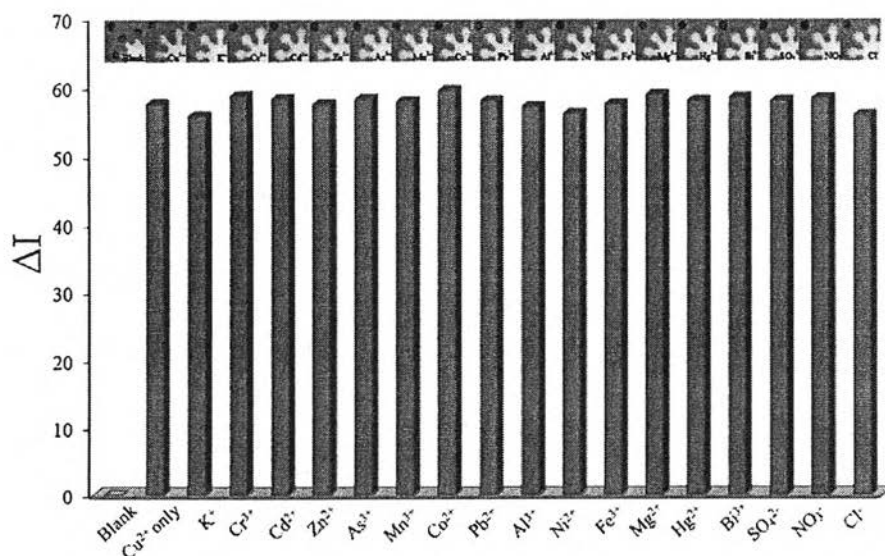


Fig. 5. Effect of other common ions ($10 \mu\text{g mL}^{-1}$) on the determination of $100 \text{ ng mL}^{-1} \text{ Cu}^{2+}$. Inset: corresponding photographs of the paper-based sensor at the detection zone after addition of Cu^{2+} and Cu^{2+} with various other common ions.

3.3.2. Effect of the concentration of AgNPLs

The effect of AgNPLs concentration was investigated in the range of $40\text{--}360 \mu\text{g mL}^{-1}$. As the results show in Fig. 3b, ΔI increased with increasing AgNPLs concentration and tends to be stable above $200 \mu\text{g mL}^{-1}$. Therefore, $0.8 \mu\text{L}$ of $200 \mu\text{g mL}^{-1}$ AgNPLs was used to prepare the detection and control zone on the paper-based sensor in future experiments.

3.3.3. Effect of the concentration of $\text{S}_2\text{O}_3^{2-}$ and the incubation time

The concentration of $\text{S}_2\text{O}_3^{2-}$ and the incubation time have influences on the detection of Cu^{2+} . The effect of the $\text{S}_2\text{O}_3^{2-}$ concentration was examined in range of $1.0\text{--}9.0 \text{ mM}$ (Fig. 3c). The

ΔI value increased with increasing $\text{S}_2\text{O}_3^{2-}$ concentration and slightly decreased above 5.0 mM . Therefore, the concentration of 5.0 mM $\text{S}_2\text{O}_3^{2-}$ was selected as the optimized concentration. Furthermore, the effect of incubation time on the Cu^{2+} detection was studied. The ΔI increased with increasing incubation time and remains constant above 120 s (Fig. 3d). This indicated that the developed method provides a rapid measurement of Cu^{2+} .

3.4. Selectivity of the modified AgNPLs for the determination of Cu^{2+}

In order to evaluate the selectivity of the colorimetric assay for the determination of Cu^{2+} , the other environmentally relevant

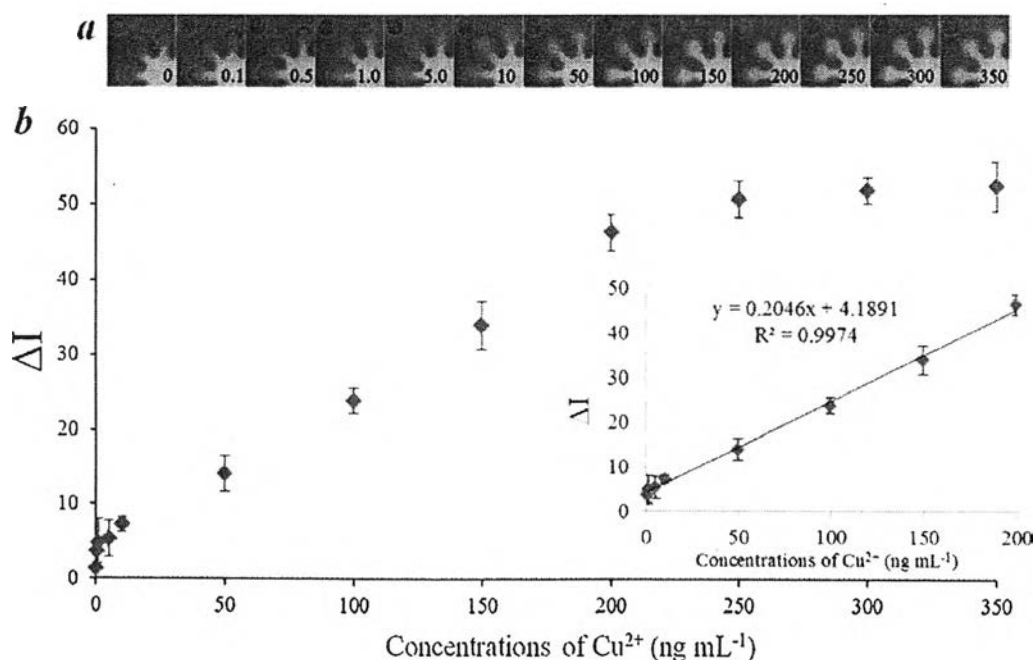


Fig. 6. (a) Corresponding photographs of the paper-based sensor at detection zone for detection of Cu^{2+} at various concentrations. (b) The plot of the mean intensity of the AgNPLs color determined by photograph analysis using NIH ImageJ vs. Cu^{2+} concentration ($0\text{--}350 \text{ ng mL}^{-1}$). Inset: linear regression analysis and best fit line in the concentration range of $0.5\text{--}200 \text{ ng mL}^{-1} \text{ Cu}^{2+}$.

Table 1
Comparison of the performance of different nanoparticles for the detection of Cu²⁺.

Nanoparticles	Method	LOD (ng mL ⁻¹)	Linearity range (ng mL ⁻¹)	Incubation time (min)	Ref.
Starch-stabilized silver nanoparticles	Colorimetric assay	31.75	6.35–63.5	10	[32]
o-Penicillamine/gold nanoparticles	Colorimetric assay	1.9	3.17–117.47	12	[33]
CTAB/thiosulfate/gold nanoparticles	Colorimetric assay	0.32	0.63–5.08	25	[17]
4-Mercaptobenzoic acid/silver nanoparticles	Colorimetric assay	1.58	6.35 to 6350	30	[12]
Gold nanorods	Colorimetric assay	13.97	5.08–304.8	25	[35]
NaSCN/H ₂ O ₂ /gold nanorods	Colorimetric assay	0.65	0.65–19.05	17	[36]
ZnO@ZnS core-shell nanoparticles	Colorimetric paper assay	952.5	952.5–95,250	20	[34]
Homocysteine/dithiothreitol/silver nanoparticles	Colorimetric paper assay	0.5	0.5–3.98	5	[15]
CTAB/thiosulfate/silver nanoplates	Colorimetric paper assay	0.3	0.5–200	2	In this work

Table 2
Recovery tests of the proposed method and standard method for the determination of Cu²⁺ in real samples (n = 3).

Sample	Proposed method				Standard method ^a			
	Cu(II) (ng mL ⁻¹)		%Recovery	%RSD	Cu(II) (ng mL ⁻¹)		%Recovery	%RSD
	Added	Found			Added	Found		
Drinking water	10.00	9.89 ± 1.77	98.95	7.91	10.00	9.98 ± 0.43	99.80	4.31
	50.00	49.95 ± 3.26	99.89	6.52	50.00	50.64 ± 1.03	101.28	2.03
	100.0	98.06 ± 0.96	98.06	0.9	100.0	100.23 ± 0.84	100.23	0.84
Groundwater	10.00	10.20 ± 0.69	101.99	6.78	10.00	10.11 ± 0.20	101.10	1.98
	50.00	53.27 ± 1.25	106.57	2.35	50.00	50.71 ± 1.19	101.42	2.35
	100.0	95.23 ± 0.83	95.23	0.87	100.0	98.92 ± 0.39	98.92	0.39
Tomato	10.00	11.90 ± 0.41	119.01	3.41	10.00	10.78 ± 0.12	107.80	1.11
	50.00	48.88 ± 0.97	97.76	1.99	50.00	50.21 ± 0.43	100.42	0.86
	100.0	102.36 ± 0.93	102.36	0.91	100.0	99.21 ± 0.53	99.21	0.53
Rice	10.00	9.90 ± 0.76	99.01	7.71	10.00	10.12 ± 0.22	101.20	2.17
	50.00	46.30 ± 3.44	92.60	7.44	50.00	46.30 ± 1.24	92.60	2.68
	100.0	99.04 ± 2.15	99.04	2.17	100.0	98.21 ± 1.50	98.21	1.53
Blood	10.00	10.40 ± 0.95	103.98	9.16	10.00	11.02 ± 0.53	110.20	4.81
	50.00	52.90 ± 3.23	105.80	6.11	50.00	50.01 ± 1.66	100.02	3.32
	100.0	98.06 ± 1.83	98.06	1.87	100.0	100.61 ± 0.98	100.61	0.97

^a Inductively coupled plasma optical emission spectrometry (ICP-OES).

metallic ions including K⁺, Cr³⁺, Cd²⁺, Zn²⁺, As³⁺, Mn²⁺, Co²⁺, Pb²⁺, Al³⁺, Ni²⁺, Fe³⁺, Mg²⁺, Hg²⁺ and Bi³⁺ were investigated under optimized conditions. The metal ions were prepared in 0.1 M ammonia buffer at pH 11 at concentration of 100 times higher than Cu²⁺. The plots of the mean color intensity as determined by NIH ImageJ analysis of the results image versus the concentration of metal ions are shown in Fig. 4. As a result, only Cu²⁺ can oxidize modified AgNPLs causing the color change of the modified AgNPLs from violet-red to colorless, and this change can be monitored by the naked eye.

In order to study the influence of other ions on the catalytic etching of AgNPLs induced by Cu²⁺, competitive experiments were carried out in the presence of 100 ng mL⁻¹ Cu²⁺ and 10 μg mL⁻¹ of other metal ions including K⁺, Cr³⁺, Cd²⁺, Zn²⁺, As³⁺, Mn²⁺, Co²⁺, Pb²⁺, Al³⁺, Ni²⁺, Fe³⁺, Mg²⁺, Hg²⁺, Bi³⁺, SO₄²⁻, NO₃⁻ and Cl⁻. The results obtained by measurement of the mixture solution of Cu²⁺ and a

common ion were not different from Cu²⁺ alone (Fig. 5). This indicates that the proposed method offers a high selectivity for the determination of Cu²⁺.

3.5. Analytical performance

The performance of the developed method was evaluated for the quantitative detection of Cu²⁺. Under the optimized conditions, the color intensity values of modified AuNPLs at the detection zone on paper-based devices were examined at room temperature in the presence of Cu²⁺ in the range of 0–350 ng mL⁻¹. The pinkish of the violet colors at the test zone changed to colorless after adding Cu²⁺ to over 0.1 ng mL⁻¹, and these results can easily be distinguished by the naked eye as shown in Fig. 6a. The plots of the mean intensity and concentration of Cu²⁺ show a reasonable linearity in the range of 0.5–200 ng mL⁻¹ (R² = 0.9974), with a LOD and LOQ of 0.35 and

Table 3
Determination of Cu²⁺ in real samples using paper-based colorimetric sensor based on thiosulfate catalytic etching of AgNPLs at room temperature.

Sample	Proposed method (n = 8) (ng mL ⁻¹)	Standard method ^a (n = 3) (ng mL ⁻¹)
Drinking water	14.26 ± 0.92	13.75 ± 0.39
Groundwater	30.93 ± 1.56	29.48 ± 0.18
Blood	34.27 ± 1.72	27.10 ± 0.08
Tomato	2.10 ± 0.47	2.18 ± 0.14
Rice	4.37 ± 1.08	4.13 ± 0.09

^a Inductively coupled plasma optical emission spectrometry (ICP-OES).

1.16 ng mL⁻¹, respectively (Fig. 6b), which is lower than that obtained from the other nanoparticles. (Table 1). The obtained LOQ values are lower than the maximum allowable levels of 1.30 μg mL⁻¹ in the United States for drinking water [3], and ~2.00 μg mL⁻¹ in Thailand for surface water [4].

3.6. Semi-quantitative determination of Cu²⁺ in real samples

To demonstrate the utility of our approach, the developed devices were evaluated for detecting Cu²⁺ in real samples, including mineral water, groundwater, tomato, rice and blood samples. Cu²⁺ was spiked into the samples at concentration levels of 10, 50 and 100 ng mL⁻¹ and was measured using the developed devices. The recovery results are shown in Table 2, the recoveries and %RSDs of Cu²⁺ were found in the range of 92.60–119.01% and 0.87–9.16%, respectively, which suggests that this method is reliable. In addition, the unknown samples were then determined by both the developed method and the standard method, i.e., inductively coupled plasma optical emission spectrometry (ICP-OES) (Table 3). The results from the developed method were in good agreement with those from the ICP-OES method (paired *t*-test at the 95% confidence level gave *t*_{calculated} (1.346) below *t*_{critical} at *t* = 2.776 with 4 degrees of freedom). These results indicate that the developed paper-based colorimetric sensor that is based on the thiosulfate catalytic etching of AgNPs is applicable for Cu²⁺ detection in real samples.

4. Conclusion

A paper-based device with a highly sensitive and selective colorimetric assay that is based on the catalytic etching of modified AgNPs by thiosulfate was developed for the rapid detection of Cu²⁺. The developed sensor was easily fabricated by a wax screen printing method. In the presence of Cu²⁺, the color of modified AgNPs changed from pinkish-violet to colorless at the detection zone and the change can be easily detected by the naked eye. The approach demonstrated good selectivity for Cu²⁺ against other metal ions. For semi-quantitative analysis, the color intensity values of the paper-based sensor photograph were digitized by NIH ImageJ software to obtain the calibration curve. The color intensity values are linear with the concentration of Cu²⁺ ranging from 0.5 to 200 ng mL⁻¹ with a coefficient of 0.9974, and shows good sensitivity with a LOD = 0.35 ng mL⁻¹. Furthermore, this method was successfully used for the determination of Cu²⁺ in real samples (mineral water, groundwater, tomato, rice and blood). The developed paper-based colorimetric sensor that is based on the thiosulfate etching of silver nanoplates has great potential for the low-cost, rapid, simple, portable, highly sensitive and selective determination of Cu²⁺ levels.

Acknowledgments

SC gratefully acknowledges the partially financial supports from Thailand Research Fund (TRF) through the Royal Golden Jubilee Ph.D. program (Grant number PHD/0127/2556). OC, AA and WS greatly thank the Thailand Research Fund through Research Team Promotion Grant (RTA5780005), the Thai Government Stimulus Package 2 (TKK2555), under the Project for Establishment of Comprehensive Center for Innovative Food, Health Products and Agriculture, Chulalongkorn University.

Appendix A. Supplementary data

Supplementary data associated with this article can be found, in the online version, at <http://dx.doi.org/10.1016/j.aca.2015.01.042>.

References

- M.B. Gholivand, A. Sohrabi, S. Abbasi, Determination of copper by adsorptive stripping voltammetry in the presence of calcein blue. *Electroanalysis* 19 (2007) 1609–1615.
- S.A. Reddy, K.J. Reddy, S.L. Narayan, A.V. Reddy, Analytical applications of 2,6-diacetylpyridine bis-4-phenyl-3-thiosemicarbazone and determination of Cu(II) in food samples. *Food Chem.* 109 (2008) 654–659.
- U.S. Environmental Protection Agency Report EPA/625/R-04/108 (2004).
- Thailand State of Pollution Report, Ministry of Science, Technology and Environment, Bangkok, Thailand, 2006.
- F. Aguilar, U.R. Charrondiere, B. Dusemund, P. Galtier, J. Gilbert, D.M. Gott, S. Grilli, R. Guertler, G.E.N. Kass, J. Koenig, C. Lambré, J.-C. Larsen, J.-C. Leblanc, A. Mortensen, D. Parent-Massin, I. Pratt, I.M.C.M. Rietjens, I. Stankovic, P. Tobback, T. Verguieva, R.A. Woutersen, Copper(II) oxide as a source of copper added for nutritional purposes to food supplements, scientific opinion of the panel on food additives and nutrient sources added to food, EFSA J. 1089 (2009) 1–15.
- N. Pourreza, R. Hoveizavi, Simultaneous preconcentration of Cu, Fe and Pb as methylthymol blue complexes on naphthalene adsorbent and flame atomic absorption determination. *Anal. Chim. Acta* 549 (2005) 124–128.
- D. Atanassova, V. Stefanova, E. Russeva, Co-precipitative pre-concentration with sodium diethyldithiocarbamate and ICP-AES determination of Se, Cu, Pb, Zn, Fe, Co, Ni, Mn, Cr and Cd in water. *Talanta* 47 (1998) 1237–1243.
- Y.B. Zhu, K. Inagaki, K. Chiba, Determination of Fe, Cu, Ni, and Zn in seawater by ID-ICP-MS after preconcentration using a syringe-driven chelating column. *J. Anal. At. Spectrom.* 24 (2009) 1179–1183.
- S. Chaiyo, O. Chailapakul, T. Sakai, N. Teshima, W. Siangproh, Highly sensitive determination of trace copper in food by adsorptive stripping voltammetry in the presence of 1,10-phenanthroline. *Talanta* 108 (2013) 1–6.
- S. Zhang, T. Yu, M. Sun, H. Yu, Z. Zhang, S. Wang, H. Jiang, Highly sensitive and selective fluorescence detection of copper(II) ion based on multi-ligand metal chelation. *Talanta* 126 (2014) 185–190.
- Z. Weng, H. Wang, J. Vongsivut, R. Li, A.M. Glushenkov, J. He, Y. Chen, C.J. Barrow, W. Yang, Self-assembly of core-satellite gold nanoparticles for colorimetric detection of copper ions. *Anal. Chim. Acta* 803 (2013) 128–134.
- Y. Zhou, H. Zhao, Y. He, N. Ding, Q. Cao, Colorimetric detection of Cu²⁺ using 4-mercaptobenzoic acid modified silver nanoparticles. *Colloids Surf. A* 391 (2011) 179–183.
- X.C. Jiang, A.B. Yu, Silver nanoplates: a highly sensitive material toward inorganic anions. *Langmuir* 24 (2008) 4300–4309.
- L.J. Miao, J.W. Xin, Z.Y. Shen, Y.J. Zhang, H.Y. Wang, A.G. Wu, Exploring a new rapid colorimetric detection method of Cu²⁺ with high sensitivity and selectivity. *Sens. Actuators B Chem.* 176 (2013) 906–912.
- N. Ratnarathorn, O. Chailapakul, C.S. Henry, W. Dungchai, Simple silver nanoparticle colorimetric sensing for copper by paper-based devices. *Talanta* 99 (2012) 552–557.
- T. Lou, L. Chen, Z. Chen, Y. Wang, L. Chen, J. Li, Colorimetric detection of trace copper ions based on catalytic leaching of silver-coated gold nanoparticles. *ACS Appl. Mater. Interfaces* 3 (2011) 4215–4220.
- R. Liu, Z. Chen, S. Wang, C. Qu, L. Chen, Z. Wang, Colorimetric sensing of copper (II) based on catalytic etching of gold nanoparticles. *Talanta* 112 (2013) 37–42.
- W.A. Zhao, A. van den Berg, Lab on paper. *Lab Chip* 8 (2008) 1988–1991.
- N. Dungchai, O. Chailapakul, C.S. Henry, Electrochemical detection for paper-based microfluidics. *Anal. Chem.* 81 (2009) 5821–5826.
- A. Apilux, W. Dungchai, W. Siangproh, N. Praphairaksit, C.S. Henry, O. Chailapakul, Lab-on-paper with dual electrochemical/colorimetric detection for simultaneous determination of gold and iron. *Anal. Chem.* 82 (2010) 1727–1732.
- A.W. Martinez, S.T. Phillips, M.J. Butte, G.M. Whitesides, Patterned paper as a platform for inexpensive low-volume, portable bioassays. *Angew. Chem. Int. Ed.* 46 (2007) 1318–1320.
- K. Abe, K. Suzuki, D. Citterio, Inkjet-printed microfluidic multianalyte chemical sensing paper. *Anal. Chem.* 80 (2008) 6928–6934.
- D.A. Bruzewicz, M. Reches, G.M. Whitesides, Low-cost printing of poly (dimethylsiloxane) barriers to define microchannels in paper. *Anal. Chem.* 80 (2008) 3387–3392.
- E. Carrilho, A.W. Martinez, G.M. Whitesides, Understanding wax printing: a simple micropatterning process for paper-based microfluidics. *Anal. Chem.* 81 (2009) 7091–7095.
- X. Li, J. Tian, T. Nguyen, W. Shen, Paper-based microfluidic devices by plasma treatment. *Anal. Chem.* 80 (2008) 9131–9134.
- W. Dungchai, O. Chailapakul, C.S. Henry, A low-cost, simple, and rapid fabrication method for paper-based microfluidics using wax screen-printing. *Analyst* 136 (2011) 77–82.
- T. Parnklang, C. Lertvachirapaiboon, P. Pienpinijtham, K. Wongravee, C. Thammachareon, S. Ekgasit, H₂O₂-triggered shape transformation of silver nanospheres to nanoprisms with controllable longitudinal LSPR wavelengths. *RSC Adv.* 3 (2013) 12886–12894.
- S. Abbasi, H. Khani, R. Tabaraki, Determination of ultra-trace levels of copper in food samples by a highly sensitive adsorptive stripping voltammetric method. *Food Chem.* 123 (2010) 507–512.
- Q.Y. Ye, Y. Li, Y. Jiang, X.P. Yan, determination of trace cadmium in rice by flow injection on-line filterless precipitation-dissolution-preconcentration coupled

- with flame atomic absorption spectrometry, *J. Agric. Food Chem.* 51 (2003) 2111–2114.
- [30] T. Attar, Y. Harek, L. Larabi, determination of ultra trace levels of copper in whole blood by adsorptive stripping voltammetry, *J. Korean Chem. Soc.* 57 (2013) 568–573.
- [31] A.C. Grosse, G.W. Dicoski, C.W. Shaw, P.R. Haddad, Leaching and recovery of gold using ammoniacal thiosulfate leach liquors (a review), *Hydrometallurgy* 69 (2003) 1–21.
- [32] L.J. Miao, J.W. Xin, Z.Y. Shen, Y.J. Zhang, H.Y. Wang, A.G. Wu, Exploring a new rapid colorimetric detection method of Cu^{2+} with high sensitivity and selectivity, *Sens. Actuators B Chem.* 176 (2013) 906–912.
- [33] M.R.H. Nezhad, S.A. Moayed, A sensitive and selective colorimetric method for detection of copper ions based on anti-aggregation of unmodified gold nanoparticles, *Talanta* 129 (2014) 227–232.
- [34] A. Sadollahkhani, A. Hatamie, O. Nur, M. Willander, B. Zargar, I. Kazeminezhad, Colorimetric disposable paper coated with ZnO@ZnS core-shell nanoparticles for detection of copper ions in aqueous solutions, *ACS Appl. Mater. Interfaces* 6 (2014) 17694–17701.
- [35] J.M. Liu, L. Jiao, L.P. Lin, M.L. Cui, X.X. Wang, L.H. Zhang, Z.Y. Zheng, S.L. Jiang, Non-aggregation based label free colorimetric sensor for the detection of Cu^{2+} based on catalyzing etching of gold nanorods by dissolve oxygen, *Talanta* 117 (2013) 425–430.
- [36] S. Wang, Z. Chen, L. Chen, R. Liu, L. Chen, Label-free colorimetric sensing of copper(II) ions based on accelerating decomposition of H_2O_2 using gold nanorods as an indicator, *Analyst* 137 (2013) 2080–2084.

Multiplex Paper-Based Colorimetric DNA Sensor Using Pyrrolidinyl Peptide Nucleic Acid-Induced AgNPs Aggregation for Detecting MERS-CoV, MTB, and HPV Oligonucleotides

Prinjaporn Teengam,[†] Weena Siangproh,[‡] Adisorn Tuantranont,[§] Tirayut Vilaivan,^{||} Orawon Chailapakul,^{*,1,#} and Charles S. Henry^{*,○}

[†]Program in Petrochemistry, Faculty of Science, ^{||}Organic Synthesis Research Unit, Department of Chemistry, Faculty of Science, [‡]Electrochemistry and Optical Spectroscopy Research Unit, Department of Chemistry, and [#]National Center of Excellence for Petroleum, Petrochemicals, and Advanced Materials, Chulalongkorn University, Pathumwan, Bangkok, 10330, Thailand

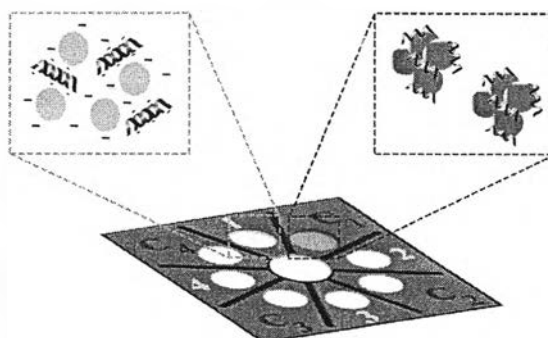
[‡]Department of Chemistry, Faculty of Science, Srinakharinwirot University, Bangkok, 10110, Thailand

[§]Nanoelectronics and MEMS Laboratory, National Electronics and Computer Technology Center, Pathumthani 12120, Thailand

[○]Departments of Chemistry and Chemical and Biological Engineering, Colorado State University, Fort Collins, Colorado 80523, United States

Supporting Information

ABSTRACT: The development of simple fluorescent and colorimetric assays that enable point-of-care DNA and RNA detection has been a topic of significant research because of the utility of such assays in resource limited settings. The most common motifs utilize hybridization to a complementary detection strand coupled with a sensitive reporter molecule. Here, a paper-based colorimetric assay for DNA detection based on pyrrolidinyl peptide nucleic acid (acpcPNA)-induced nanoparticle aggregation is reported as an alternative to traditional colorimetric approaches. PNA probes are an attractive alternative to DNA and RNA probes because they are chemically and biologically stable, easily synthesized, and hybridize efficiently with the complementary DNA strands. The acpcPNA probe contains a single positive charge from the lysine at C-terminus and causes aggregation of citrate anion-stabilized silver nanoparticles (AgNPs) in the absence of complementary DNA. In the presence of target DNA, formation of the anionic DNA-acpcPNA duplex results in dispersion of the AgNPs as a result of electrostatic repulsion, giving rise to a detectable color change. Factors affecting the sensitivity and selectivity of this assay were investigated, including ionic strength, AgNP concentration, PNA concentration, and DNA strand mismatches. The method was used for screening of synthetic Middle East respiratory syndrome coronavirus (MERS-CoV), *Mycobacterium tuberculosis* (MTB), and human papillomavirus (HPV) DNA based on a colorimetric paper-based analytical device developed using the aforementioned principle. The oligonucleotide targets were detected by measuring the color change of AgNPs, giving detection limits of 1.53 (MERS-CoV), 1.27 (MTB), and 1.03 nM (HPV). The acpcPNA probe exhibited high selectivity for the complementary oligonucleotides over single-base-mismatch, two-base-mismatch, and noncomplementary DNA targets. The proposed paper-based colorimetric DNA sensor has potential to be an alternative approach for simple, rapid, sensitive, and selective DNA detection.



Infectious diseases represent a major threat to human health in developed and developing countries alike. DNA alterations contribute to different types of diseases; therefore, the detection of specific DNA sequences plays a crucial role in the development method for early stage treatment and monitoring of genetic-related diseases. DNA diagnostics can provide sequence-specific detection, especially for single-nucleotide polymorphisms (SNPs),¹ which critical for a range of applications including the diagnosis of human diseases and bacterial/viral infections.

Middle East respiratory syndrome (MERS), tuberculosis (TB), and cervical cancers related to human papilloma virus

(HPV) are examples of infectious diseases caused by bacterial and viral infections that benefit greatly from DNA detection. TB is an infectious disease caused by mycobacteria, usually *M. tuberculosis* (MTB) in humans.² HPV has been shown to be a major cause of cervical cancer.³ Middle East Respiratory Syndrome coronavirus (MERS-CoV) has recently emerged as an infectious disease with a high fatality rate in humans.⁴

Received: January 20, 2017

Accepted: April 10, 2017

Published: April 10, 2017

Diagnostic methods developed for these infectious diseases include reverse transcription polymerase chain reaction (RT-PCR) for MERS-CoV,⁵ sputum smear microscopy, culture of bacilli, and molecular species diagnostics for MTB^{6–11} and Digene Hybrid Capture assay (HC2) and Pap smear test for HPV.^{12,13} While these techniques have been used for successful detection, they are difficult to implement in point-of-care clinical diagnostics particularly in developing countries lacking specialized medical facilities and skilled personnel. Therefore, simple, rapid, low-cost, and highly accurate on-site diagnostic platforms amenable to nucleic acid detection remain a challenge for early detection of infectious diseases for better patient management and infection control. Although DNA amplification is still needed with the current method to provide high sensitivity, we seek to further improve selectivity and assay

simplicity to give immediate and quantitative responses in resource limited settings.

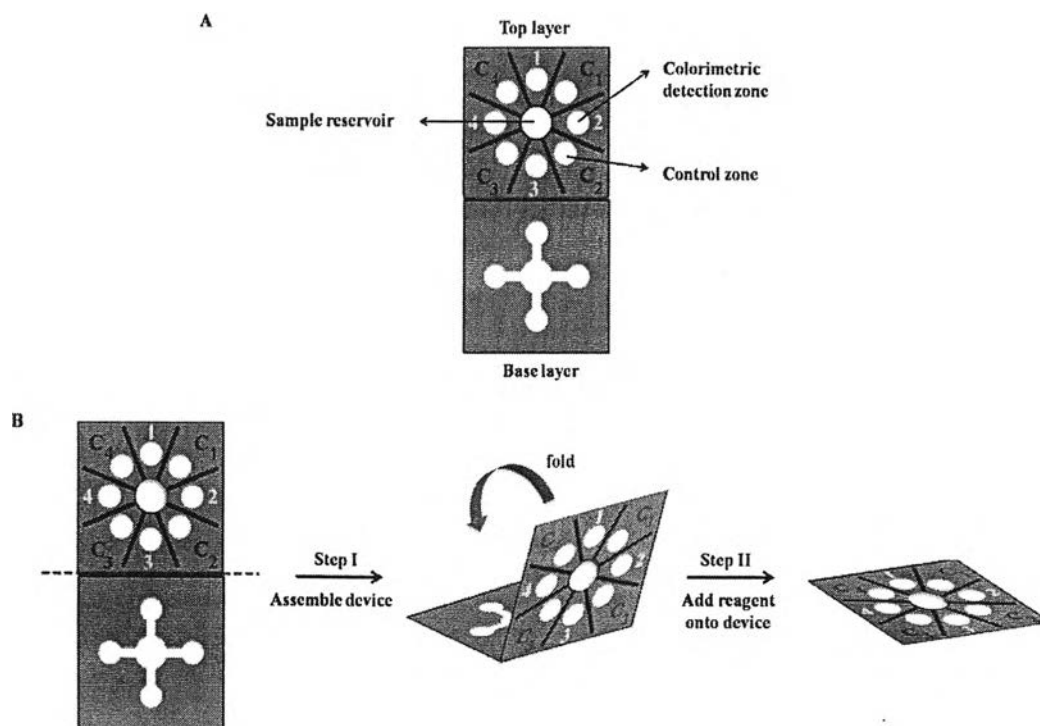
Paper-based analytical devices (PADs) are a point-of-use technology that recently received renewed interest because they are simple, inexpensive, portable, and disposable.^{14–16} To date, PADs have been extensively used for applications ranging from environmental analysis to clinical diagnostic assays.^{15,17,18} Colorimetric assays are particularly attractive when coupled with PADs due to their ease-of-use, lack of complicated external equipment and ability to provide semiquantitative results.^{19–21} Moreover, quantitative analysis of colorimetric assays can be accomplished using simple optical technologies such as digital cameras^{22–24} and office scanners^{20,25} combined with image processing software to carry out color, hue, and intensity measurements. In the field of clinical diagnostics, the advantages of simplicity, sensitivity, and low-cost are key reasons that make PADs coupled with colorimetric detection an effective diagnostic tool relative to traditional methods.

Colorimetric assays based on the aggregation of silver (AgNPs) and gold nanoparticles (AuNPs) have attracted increasing attention in biomedical applications. The optical properties of these nanomaterials depend on their size and shape.^{26–31} AgNPs are known to have a higher extinction coefficient compared to AuNPs,^{32–34} leading to improved optical sensitivity. Chemical reduction of silver salts is frequently used to synthesize AgNPs; while specific control of shape and size distribution is achieved by varying the reducing agents and stabilizers.^{35–37} Among stabilizing agents, negatively charged citrate has been widely used.^{38,39} Recently, colorimetric assays based on AgNPs aggregation for DNA detection has been reported.³⁴ Colorimetric DNA detection using AgNPs usually involves modifying the particles with a DNA probe and mixing them with the DNA target containing the complementary

Table 1. List of Oligonucleotide Used in This Study

oligonucleotide	sequence (5'-3')
MERS-CoV	
complementary DNA	5'-CGATTATGTGAAGAG-3'
two-base-mismatch	5'-CGATTATCTGAGGAG-3'
noncomplementary DNA	5'-TTCGCACAGTGGTCA-3'
MTB	
complementary DNA	5'-ATAACGTGTTTCTTG-3'
single-base-mismatch	5'-ATAACGTCTTCTTG-3'
noncomplementary DNA 1	5'-TGGCTAGCCGCTCCT-3'
noncomplementary DNA 2	5'-CACTTGCCACACCA-3'
HPV	
complementary DNA (HPV type 16)	5'-GCTGGAGGTGTATG-3'
noncomplementary DNA 1 (HPV type 18)	5'-GGATGCTGCACCG-3'
noncomplementary DNA 2 (HPV type 31)	5'-CCAAAAGCCCAAGG-3'
noncomplementary DNA 3 (HPV type 33)	5'-CACATCCACCCGCA-3'

Scheme 1. (A) Design and (B) Operation of Multiplex Paper-Based Colorimetric Device



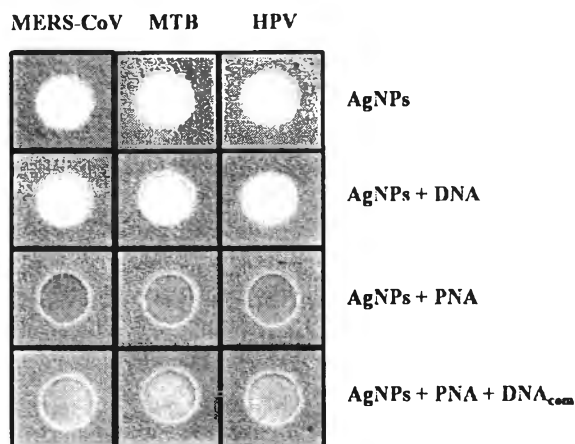
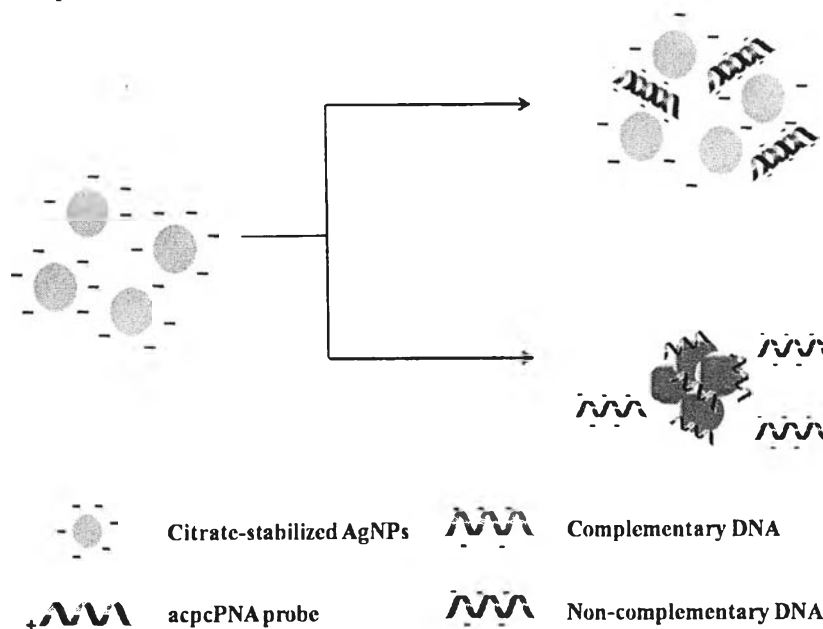
Scheme 2. Process of acpcPNA-Induced AgNP Aggregation in the Presence of DNA_{com} and DNA_{nc}

Figure 1. Photograph of visual color changes obtained from detection of MERS-CoV, MTB, and HPV in the presence of DNA_{com}.

sequence. When the hybridization of probe and target DNA occurs, the AgNPs aggregate and change color.^{33,34} The assay principal has been further adopted using charge-neutral peptide nucleic acids (PNA)^{40,41} as the hybridization agent. PNA causes aggregation of metal nanoparticles in solution without immobilization, thus, simplifying the assay.^{42,43} Finally, PNA-based nanoparticle aggregation assays also provide a high hybridization efficiency of PNA-DNA duplexes leading to a rapid color change.⁴³

Recently, Vilaivan's group proposed a new conformationally constrained pyrrolidinyl PNA system which possesses an α,β -peptide backbone derived from D-proline/2-aminocyclopentanecarboxylic acid (known as acpcPNA).^{44,45} Compared to Nielsen's PNA,⁴⁰ acpcPNA exhibits a stronger affinity and higher sequence specificity binding to DNA. acpcPNA exhibits the characteristic selectivity of antiparallel binding to the target DNA and low tendency to self-hybridize. Moreover, the

nucleobases and backbone of acpcPNA can be modified to increase molecular functionality. These combined properties make acpcPNA an attractive candidate as a probe for biological applications.^{46–48}

Here, the multiplex colorimetric PAD for DNA detection based on the aggregation of AgNPs induced by acpcPNA is reported. acpcPNA bearing a positively charged lysine modification at C-terminus was designed as the probe. The cationic PNA probe can interact with the negatively charged AgNPs leading to nanoparticle aggregation and a significant color change. This proposed sensor was used for simultaneous detection of MERS-CoV, MTB, and HPV. The developed paper-based DNA sensor has potential as an alternative diagnostic device for simple, rapid, sensitive, and selective DNA/RNA detection.

EXPERIMENTAL SECTION

Chemicals and Materials. Analytical grade reagents, including AgNO₃, NaBH₄, and sodium citrate from Sigma-Aldrich, KH₂PO₄ and KCl from Fisher Scientific, Na₂HPO₄ from Mallinckrodt, and NaCl from Macron, were used without further purification. A total of 18 M $\Omega\text{-cm}^{-1}$ resistance water was obtained from a Millipore Milli-Q water system. Synthetic DNA oligonucleotides were obtained from Biosearch Technologies. The sequences of DNA oligonucleotides are shown in Table 1.

Synthesis of AgNPs. The AgNPs were synthesized using the citrate-stabilization method.⁴⁹ Briefly, 4 mL of 12.6 mM sodium citrate and 50 mL of 0.3 mM AgNO₃ were mixed together. Then, 1 mL of 37 mM NaBH₄ was added to the mixture under vigorous stirring and the solution turned yellow. The formation of AgNPs and their size distribution were verified by dynamic light scattering measurement, and the average size of AgNPs was found to be 19 nm (Figure S1).

Synthesis of acpcPNA Probes. The acpcPNA probes were designed to detect the synthetic oligonucleotide targets

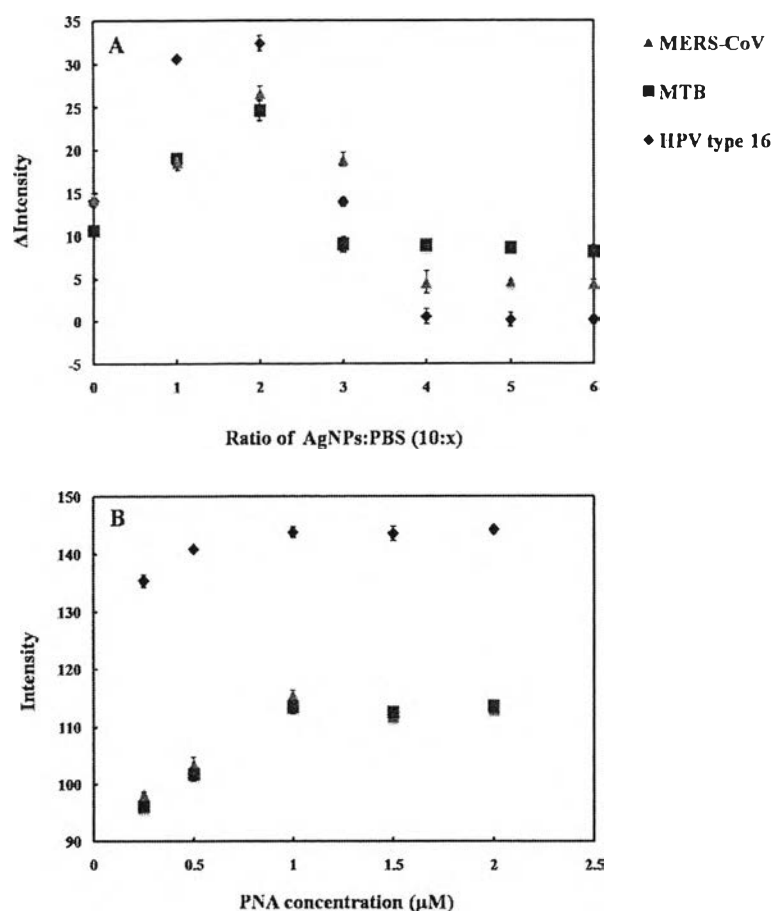


Figure 2. Influence of (A) AgNPs/PBS ratio and (B) acpPNA probe concentration on color intensity for MERS-CoV, MTB, and HPV detection. The error bars represent one standard deviation (SD) obtained from three independent measurements ($n = 3$).

with sequences corresponding to MERS-CoV, MTB, and HPV type 16. The sequences of acpPNA probes are as follows:

MERS-CoV: CTCTTCACATAATCG-LysNH₂

MTB: CAAGAAACACGTTAT-LysNH₂

HPV type 16: CATACACCTCCAGC-LysNH₂

*(written in the N → C direction)

The acpPNA probe was synthesized by solid-phase peptide synthesis using Fmoc chemistry, as previously described.⁴⁴ At the C-terminus, lysinamide was included as a positively charged group that could induce nanoparticle aggregation. All PNA were purified by reverse-phase HPLC (C18 column, 0.1% (v/v) trifluoroacetic acid (TFA) in H₂O–MeOH gradient). The identity of the acpPNA was verified by MALDI-TOF MS analysis (Figure S2), and the purity was confirmed to be >90% by reverse-phase HPLC.

Design and Operation of Paper-Based Multiplex DNA Sensor. A wax-printing technique was used to create PADs.⁵⁰ The sensor was designed using Adobe Illustrator. The wax colors were selected to be complementary to the colorimetric reactions to enhance visualization. For paper-based device fabrication, the wax design was printed onto Whatman grade 1 filter paper (VWR) using a wax printer (Xerox Phaser 8860). The wax pattern was subsequently melted at 175 °C for 50 s to generate the hydrophobic barriers and hydrophilic channels. The sensor was based on Origami concept consisting of two layers.^{51,52} As shown in Scheme 1A, the base layer contains four

wax-defined channels extending outward from the sample reservoir (6 mm i.d.) and the top layer contains four detection and control zones (4 mm i.d.). Scheme 1B illustrates operation of the multiplex sensor. First, the sample reservoir of the top layer was punched to provide a solution connection directly from the top to the bottom layer, and then the device was assembled by folding the top layer over the base layer to create the three-dimension origami paper-based device. A polydimethylsiloxane (PDMS) lid was used for holding the two layers together. The lid consisting of one 6 mm diameter hole over the colorimetric detection and control zones was aligned over the device to provide consistent pressure across the surface of the device. Next, the acpPNA probe and AgNPs solution were added onto the detection and control zones. Finally, the sample solution was added onto the sample reservoir and flow through the channels to wet the colorimetric detection zones.

Colorimetric Detection of MERS-CoV, MTB, and HPV DNA Target. According to the concept of PNA-induced AgNPs aggregation,^{42,43} acpPNA was designed as a specific probe for quantitative detection of synthetic MERS-CoV, MTB, and HPV DNA targets. For colorimetric detection, the detection zone was prepared by adding 10 μL of AgNPs in 0.1 M phosphate buffer saline (PBS) pH 7.4 in a ratio of 5:1 (AgNPs: PBS), followed by 1 μL of specific acpPNA probe. Control zones were prepared using the same conditions as the colorimetric

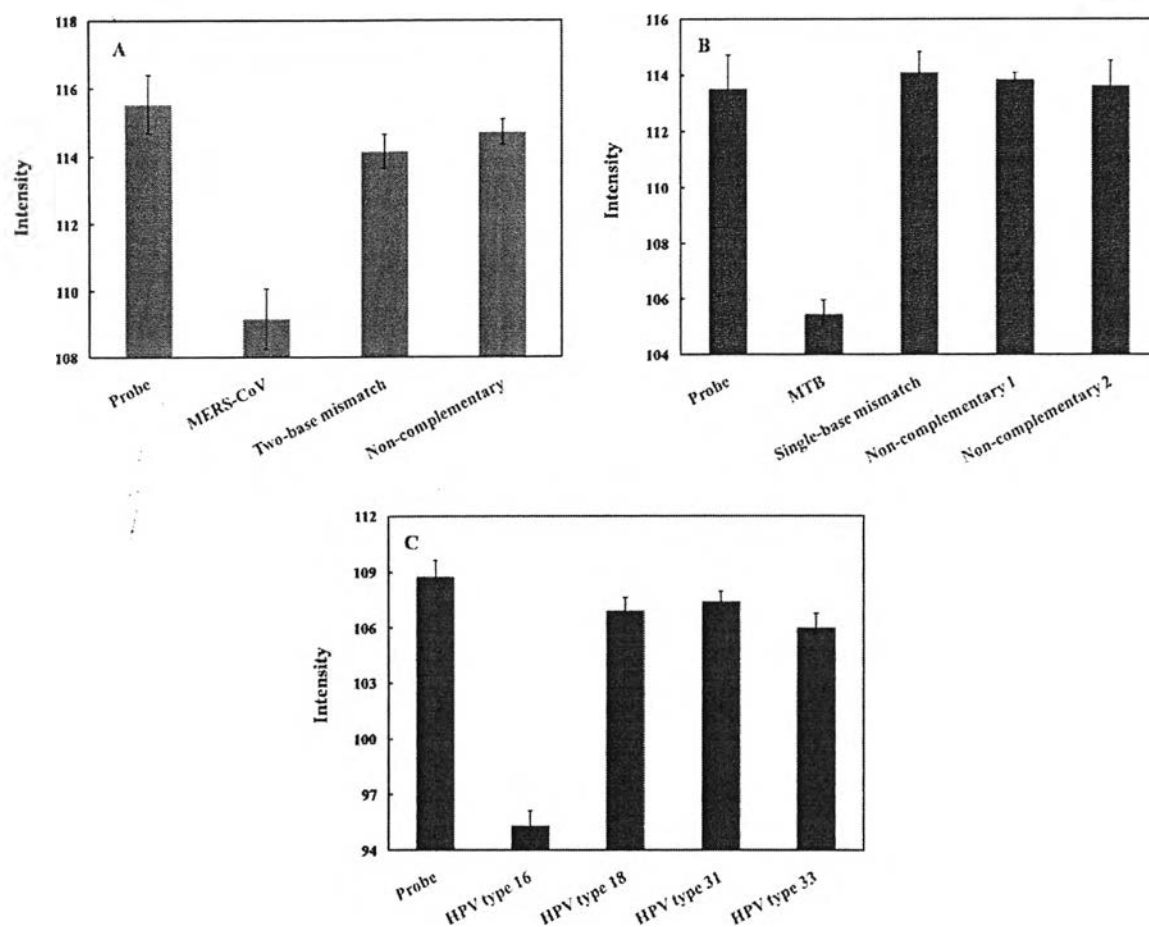


Figure 3. Color intensity of (A) MERS-CoV, (B) MTB, and (C) HPV detection after hybridization of DNA_{m1}, DNA_{m2}, and DNA_{nc}. The error bars represent one standard deviation (SD) obtained from three independent measurements ($n = 3$).

detection zones. Next, 25 μL of DNA target was added to the open sample reservoir. Upon sample addition, solution moved outward through the channels to wet the colorimetric detection zone of the top layer. Finally, the AgNPs aggregation occurred and the color intensity was measured.

Image Processing. The detection images were recorded using a scanner (XEROX DocuMate 3220) and saved in JPEG format at 600 dpi. ImageJ software (National Institutes of Health) was used to analyze the mean intensity of the color for each colorimetric reaction zone by applying a color threshold window for removing the blue background. Images were then inverted, and the mean intensity was measured.^{20,53}

RESULTS AND DISCUSSION

acpcPNA-Induced AgNPs Aggregation. The process of acpcPNA-induced AgNPs aggregation is shown in Scheme 2. The anionic AgNPs are initially well dispersed due to electrostatic repulsion. On addition of the cationic acpcPNA, the electrostatic repulsion is shielded, resulting in nanoparticle aggregation. When complementary DNA (DNA_{com}) is present, the specific PNA–DNA interaction outcompetes the less specific PNA–AgNPs interaction, resulting in a negatively charged PNA–DNA_{com} duplex and deaggregation of the anionic nanoparticles. Upon addition of noncomplementary DNA (DNA_{nc}), the acpcPNA should remain bound to the AgNPs and no color

change occurs. To prove the concept, we designed and synthesized acpcPNA probes to detect synthetic oligonucleotide targets with sequences corresponding to MERS-CoV, MTB, and HPV type 16. The photographs of the results are shown in Figure 1. The yellow AgNPs turned red when the acpcPNA was added. When the solution contained of the acpcPNA and DNA_{nc}, the color also changed to red due to aggregation of the AgNPs. On the other hand, the color changed from red (aggregated) to yellow (nonaggregated) in the presence of DNA_{com} with the intensity dependent on the DNA concentration. Next, the sequence of adding the PNA probe and DNA target was investigated. As shown in Figure S3, when equimolar DNA_{com} was added either before or after the addition of acpcPNA probe into the AgNPs, the same color intensities were obtained indicating that the sequence of adding acpcPNA and DNA_{com} did not impact the final signal.

Critical Coagulation Concentration (CCC). The influence of electrolyte solution on the aggregation behavior of citrate-stabilized AgNPs was investigated based on the CCC.⁵⁴ The CCC represents the electrolyte concentration required to cause aggregation of the nanoparticles in the absence of acpcPNA. In Figure S4, the color intensity of citrate-stabilized AgNPs in the absence of acpcPNA probe is shown as a function of NaCl concentration. The intensity and, therefore, the degree of aggregation, increased with the concentration of NaCl,

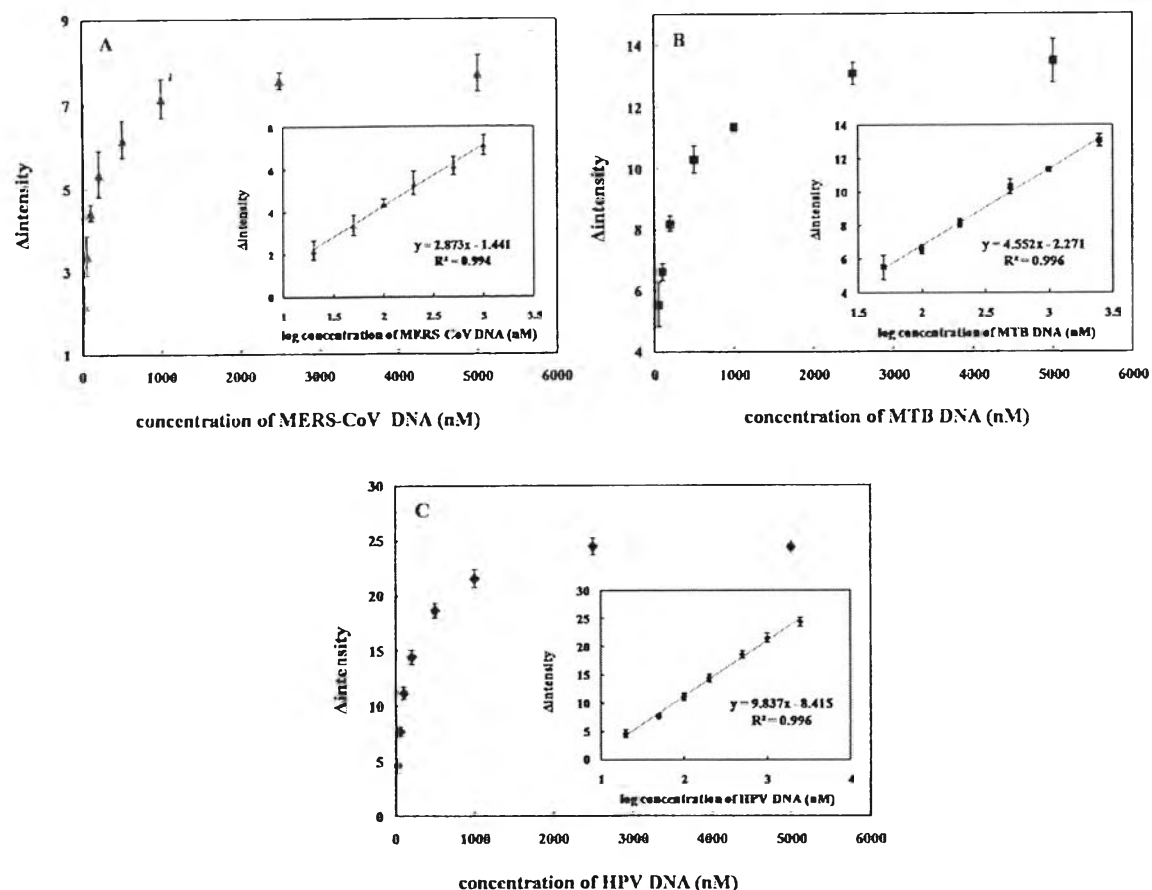


Figure 4. Change of probe color intensity vs DNA target concentration (ΔI) and calibration graph between ΔI and log DNA target concentration (inset) for (A) MERS-CoV, (B) MTB, and (C) HPV detection. The error bars represent standard deviation (SD) obtained from three independent measurement ($n = 3$).

Table 2. Summarized Analytical Performance of the Multiplexed 3DPAD for Colorimetric DNA Assay

DNA target	linearity (nM)	LOD (nM)	%RSD ($n = 3$)
MERS-CoV	20–1000	1.53	0.17–0.50
MTB	50–2500	1.27	0.12–0.67
HPV	20–2500	1.03	0.43–0.93

indicating that increasing ionic strength led to enhanced aggregation.⁵⁵ We believe that the ionic strength can decrease the electrostatic repulsion of citrate-stabilized AgNPs as a result of shielding, accelerating the AgNPs aggregation. The CCC was obtained when the degree of aggregation reached a maximum and became independent of NaCl concentration. In this experiment, the CCC of citrate-stabilized AgNPs was found to be 30 mM. Above this concentration, PNA-induced aggregation was not observed.

Optimization of Assay Parameters. For a colorimetric assay based on acpcPNA-induced AgNPs aggregation, assay parameters including 0.1 M PBS (pH 7.4) ratio and acpcPNA concentration were optimized using a simple paper-based design. The degree of AgNPs aggregation was determined by measuring the color intensity of the resulting solution in the presence of acpcPNA without target DNA. First, the impact of the PBS concentration on AgNPs aggregation was measured. The differential color intensity (Δ intensity, ΔI) obtained before and

after addition of acpcPNA as a function of AgNPs to PBS ratio is shown in Figure 2A. ΔI increased until the ratio of AgNPs/PBS reached 5:1 and then decreased until it plateaued at 5:2. Thus, the ratio of 5:1 AgNPs/PBS was selected as the optimal condition because it gave the largest ΔI . Another important aspect for the DNA assay is probe concentration. The influence of acpcPNA probe concentration on absolute intensity was studied. As shown in Figure 2B, the acpcPNA concentration was varied within a range of 0–2.5 μ M, and the highest aggregation was obtained at the concentration of 1.0 μ M. At this concentration, the aggregation became independent of acpcPNA concentration, which was desirable for simplifying the assay. Higher concentrations of AgNPs were not tested in order to minimize reagent consumption. As a result, the optimal conditions consisting of AgNPs/PBS ratio of 5:1 and acpcPNA concentration of 1.0 μ M were selected for further experiments.

Selectivity of MERS-CoV, MTB, and HPV Detection. To investigate the selectivity of this system, the color intensity obtained from the DNA_{com} of MERS-CoV, MTB, and HPV was compared to that of single-base mismatch (DNA_{m1}), two-base mismatch (DNA_{m2}), and DNA_{nc} sequences. The color intensity decreased significantly in the presence of DNA_{com}, whereas, the intensity did not change for the mismatched and noncomplementary targets (Figure 3). We believe the affinity of PNA–DNA hybridization was reduced due to the contribution of one- and two-base mismatches, leaving free PNA to aggregate

the nanoparticles. PNA–DNA_{com} complex can retard the ability of PNA to induce AgNPs aggregation as discussed above and result in different color intensities. These results suggest that the fully complementary DNA selectively hybridized the acpcPNA probe and yielded measurable signals. In addition, bovine serum albumin (BSA), which is commonly used in cell culture protocols, was used to investigate the protein interference of the proposed system. The DNA target was prepared in the presence of 3% BSA solution. It was observed that the color intensities of the DNA targets for MERS-CoV, MTB, and HPV in 3% BSA solution were statistically identical to the ones without BSA (Figure S5). Hence, common proteins should not negatively affect the analysis of this system.

Analytical Performance. To assess the sensitivity of the proposed method for DNA quantification, the intensity as a function of the target DNA concentration was determined. The color intensity decreases with the target DNA concentration. The calibration curves for each species are shown in Figure 4A, B, and C for MERS-CoV, MTB, and HPV, respectively. The linear range for each DNA target using a logarithmic DNA concentration and color intensity (Figure 4, inset) was also obtained. The analytical performances for all three DNA targets are summarized in Table 2. It can be seen that a sufficiently low detection limit could be obtained for MERS-CoV, MTB, and HPV detection without the need for multiple PCR cycles. Moreover, this multiplex system can provide sensitive and selective detection for simultaneous analysis of multiple DNA targets in a single device, which simplifies the analysis compared to traditional diagnostics.^{9,56–59}

Device Design. Next, a multiplex device (Scheme 1) was designed for simultaneous detection of MERS-CoV, MTB, and HPV. The top layer contained four detection zones and four control zones. Each zone contained AgNPs with a single acpcPNA probe to provide selectivity for DNA. The base layer contained four wax-defined channels extending outward from a sample inlet. After the device was folded and stacked together,

the channels of the base layer were connected to four detection zones of the top layer. Upon sample addition, the solution moved outward through the channels of the base layer to wet the colorimetric detection zones of the top layer and lead to color change. Figure 5 illustrates the ability of the proposed sensor for detection of 100 nM MERS-CoV, MTB, and HPV. Only the colorimetric detection zones that contained the selective probes changed color compared to their control zones. This result indicated that the multiplex paper-based colorimetric sensor is promising for simultaneous determination of MERS-CoV, MTB, and HPV.

CONCLUSIONS

A multiplex colorimetric PAD was developed for simultaneous detection of DNA associated with viral and bacterial infectious diseases, including Middle East respiratory syndrome coronavirus (MERS-CoV), *Mycobacterium tuberculosis* (MTB), and human papillomavirus (HPV). AgNPs were used as a colorimetric reagent for DNA detection based on acpcPNA-induced nanoparticle aggregation. This colorimetric DNA sensor exhibited high selectivity against single-base mismatch, two-base mismatch and noncomplementary target DNA. Under the optimized condition, the limit of detection for MERS-CoV, MTB, and HPV were found to be 1.53, 1.27, and 1.03 nM, respectively. As a result, this developed multiplex colorimetric PAD could be a low-cost and disposable alternative tool for rapid screening and detecting in infectious diagnostics.

ASSOCIATED CONTENT

Supporting Information

The Supporting Information is available free of charge on the ACS Publications website at DOI: 10.1021/acs.analchem.7b00255.

Supporting Figures S1–S5 (PDF).

AUTHOR INFORMATION

Corresponding Authors

*E-mail: chuck.henry@colostate.edu.

*E-mail: corawon@chula.ac.th.

ORCID

Charles S. Henry: 0000-0002-8671-7728

Notes

The authors declare no competing financial interest.

ACKNOWLEDGMENTS

P.T. gratefully appreciates the financial supports from Thailand Graduate Institute of Science and Technology (TGIST 01-55-014) and The Thailand Research Fund (RTA5780005). C.S.H. acknowledges financial support from Colorado State University and the United States Department of Agriculture through the National Wildlife Research Center (1574000859CA). T.V. acknowledges technical assistance of Ms. Chotima Vilaivan (Organic Synthesis Research Unit, Chulalongkorn University) and the financial support from Thailand Research Fund (DPG5780002, to T.V.) for the PNA synthesis. The authors thank Dr. Yuanyuan Yang for assistance with manuscript editing. The authors also acknowledge important discussions with Dr. Christopher Ackerson surrounding the critical coagulation concentration.

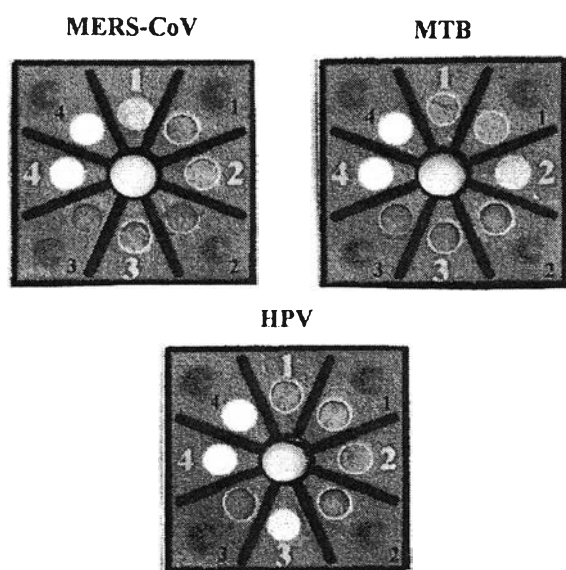


Figure 5. Selectivity of 100 nM MERS-CoV, MTB, and HPV detection using multiplex colorimetric PAD (1, C₁ = AgNPs + MERS-CoV acpcPNA probe; 2, C₂ = AgNPs + MTB acpcPNA probe; 3, C₃ = AgNPs + HPV acpcPNA probe).

■ REFERENCES

- (1) Wei, F.; Lillehoj, P. B.; Ho, C.-M. *Pediatr. Res.* **2010**, *67*, 458–468.
- (2) Smith, I. *Clin. Microbiol. Rev.* **2003**, *16*, 463–496.
- (3) Burd, E. M. *Clin. Microbiol. Rev.* **2003**, *16*, 1–17.
- (4) de Wit, E.; Rasmussen, A. L.; Falzarano, D.; Bushmaker, T.; Feldmann, F.; Brining, D. L.; Fischer, E. R.; Martellaro, C.; Okumura, A.; Chang, J.; Scott, D.; Benecke, A. G.; Katze, M. G.; Feldmann, H.; Munster, V. J. *Proc. Natl. Acad. Sci. U. S. A.* **2013**, *110*, 16598–16603.
- (5) Bhadra, S.; Jiang, Y. S.; Kumar, M. R.; Johnson, R. F.; Hensley, L. E.; Ellington, A. D. *PLoS One* **2015**, *10*, e0123126.
- (6) Davies, P. D. O.; Pai, M. *International Journal of Tuberculosis and Lung Disease* **2008**, *12*, 1226–1234.
- (7) Steingart, K. R.; Ng, V.; Henry, M.; Hopewell, P. C.; Ramsay, A.; Cunningham, J.; Urbanczik, R.; Perkins, M. D.; Aziz, M. A.; Pai, M. *Lancet Infect. Dis.* **2006**, *6*, 664–674.
- (8) Lee, J. J.; Suo, J.; Lin, C. B.; Wang, J. D.; Lin, T. Y.; Tsai, Y. C. *International Journal of Tuberculosis and Lung Disease* **2003**, *7*, 569–574.
- (9) Al-Zamel, F. A. *Expert Rev. Anti-Infect. Ther.* **2009**, *7*, 1099–1108.
- (10) Noordhoek, G. T.; Kolk, A. H.; Bjune, G.; Catty, D.; Dale, J. W.; Fine, P. E.; Godfrey Faussett, P.; Cho, S. N.; Shinnick, T.; Svenson, S. B. *Journal of Clinical Microbiology* **1994**, *32*, 277–284.
- (11) Yang, Y.-C.; Lu, P.-L.; Huang, S. C.; Jenh, Y.-S.; Jou, R.; Chang, T. C. *Journal of Clinical Microbiology* **2011**, *49*, 797–801.
- (12) Lörcincz, A.; Anthony, J. *Papillomavirus Report* **2001**, *12*, 145–154.
- (13) Gravitt, P. E.; Jamshidi, R. *Infectious Disease Clinics of North America* **2005**, *19*, 439–458.
- (14) Martinez, A. W.; Phillips, S. T.; Butte, M. J.; Whitesides, G. M. *Angew. Chem., Int. Ed.* **2007**, *46*, 1318–1320.
- (15) Cate, D. M.; Adkins, J. A.; Mettakoonpitak, J.; Henry, C. S. *Anal. Chem.* **2015**, *87*, 19–41.
- (16) Yetisen, A. K.; Akram, M. S.; Lowe, C. R. *Lab Chip* **2013**, *13*, 2210–2251.
- (17) Adkins, J.; Boehle, K.; Henry, C. *Electrophoresis* **2015**, *36*, 1811–1824.
- (18) Mettakoonpitak, J.; Boehle, K.; Nantaphol, S.; Teengam, P.; Adkins, J. A.; Srisa-Art, M.; Henry, C. S. *Electroanalysis* **2016**, *28*, 1420–1436.
- (19) Nery, E. W.; Kubota, L. T. *Anal. Bioanal. Chem.* **2013**, *405*, 7573–7595.
- (20) Rattanarat, P.; Dungchai, W.; Cate, D.; Volckens, J.; Chailapakul, O.; Henry, C. S. *Anal. Chem.* **2014**, *86*, 3555–3562.
- (21) Liana, D. D.; Raguse, B.; Gooding, J. J.; Chow, E. *Sensors* **2012**, *12*, 11505.
- (22) Apilux, A.; Siangproh, W.; Praphairaksit, N.; Chailapakul, O. *Talanta* **2012**, *97*, 388–394.
- (23) Apilux, A.; Dungchai, W.; Siangproh, W.; Praphairaksit, N.; Henry, C. S.; Chailapakul, O. *Anal. Chem.* **2010**, *82*, 1727–1732.
- (24) Chaiyo, S.; Siangproh, W.; Apilux, A.; Chailapakul, O. *Anal. Chim. Acta* **2015**, *866*, 75–83.
- (25) Cate, D. M.; Nanthasurasak, P.; Riwkulkajorn, P.; L'Orange, C.; Henry, C. S.; Volckens, J. *Ann. Occup. Hyg.* **2014**, *58*, 413–423.
- (26) Shim, S.-Y.; Lim, D.-K.; Nam, J.-M. *Nanomedicine* **2008**, *3*, 215–232.
- (27) Baptista, P.; Pereira, E.; Eaton, P.; Doria, G.; Miranda, A.; Gomes, I.; Quaresma, P.; Franco, R. *Anal. Bioanal. Chem.* **2008**, *391*, 943–950.
- (28) Zhao, W.; Brook, M. A.; Li, Y. *ChemBioChem* **2008**, *9*, 2363–2371.
- (29) Thaxton, C. S.; Georganopoulou, D. G.; Mirkin, C. A. *Clin. Chim. Acta* **2006**, *363*, 120–126.
- (30) Li, H.; Cui, Z.; Han, C. *Sens. Actuators, B* **2009**, *143*, 87–92.
- (31) Vilela, D.; González, M. C.; Escarpa, A. *Anal. Chim. Acta* **2012**, *751*, 24–43.
- (32) Wei, H.; Chen, C.; Han, B.; Wang, E. *Anal. Chem.* **2008**, *80*, 7051–7055.
- (33) Lee, J.-S.; Lytton-Jean, A. K. R.; Hurst, S. J.; Mirkin, C. A. *Nano Lett.* **2007**, *7*, 2112–2115.
- (34) Thompson, D. G.; Enright, A.; Faulds, K.; Smith, W. E.; Graham, D. *Anal. Chem.* **2008**, *80*, 2805–2810.
- (35) Yeo, S. Y.; Lee, H. J.; Jeong, S. H. *J. Mater. Sci.* **2003**, *38*, 2143–2147.
- (36) Chimentao, R. J.; Kirm, I.; Medina, F.; Rodriguez, X.; Cesteros, Y.; Salagre, P.; Sueiras, J. E. *Chem. Commun.* **2004**, 846–847.
- (37) He, B.; Tan, J. J.; Liew, K. Y.; Liu, H. *J. Mol. Catal. A: Chem.* **2004**, *221*, 121–126.
- (38) Abou El-Nour, K. M. M.; Eftaiha, A. a.; Al-Warthan, A.; Ammar, R. A. *Arabian J. Chem.* **2010**, *3*, 135–140.
- (39) Irvani, S.; Korbekandi, H.; Mirmohammadi, S. V.; Zolfaghari, B. *Research in Pharmaceutical Sciences* **2014**, *9*, 385–406.
- (40) Nielsen, P.; Egholm, M.; Berg, R.; Buchardt, O. *Science (Washington, DC, U. S.)* **1991**, *254*, 1497–1500.
- (41) Egholm, M.; Buchardt, O.; Christensen, L.; Behrens, C.; Freier, S. M.; Driver, D. A.; Berg, R. H.; Kim, S. K.; Norden, B.; Nielsen, P. E. *Nature* **1993**, *365*, 566–568.
- (42) Su, X.; Kanjanawarut, R. *ACS Nano* **2009**, *3*, 2751–2759.
- (43) Kanjanawarut, R.; Su, X. *Anal. Chem.* **2009**, *81*, 6122–6129.
- (44) Vilaivan, T.; Srisuwannaket, C. *Org. Lett.* **2006**, *8*, 1897–1900.
- (45) Vilaivan, T. *Acc. Chem. Res.* **2015**, *48*, 1645–1656.
- (46) Jampasa, S.; Wonsawat, W.; Rodthongkum, N.; Siangproh, W.; Yanatatsaneejit, P.; Vilaivan, T.; Chailapakul, O. *Biosens. Bioelectron.* **2014**, *54*, 428–434.
- (47) Kongpeth, J.; Jampasa, S.; Chaumpluk, P.; Chailapakul, O.; Vilaivan, T. *Talanta* **2016**, *146*, 318–325.
- (48) Jirakittiwut, N.; Panyain, N.; Nuanyai, T.; Vilaivan, T.; Praneenarat, T. *RSC Adv.* **2015**, *5*, 24110–24114.
- (49) Laliwala, S. K.; Mehta, V. N.; Rohit, J. V.; Kailasa, S. K. *Sens. Actuators, B* **2014**, *197*, 254–263.
- (50) Carrilho, E.; Martinez, A. W.; Whitesides, G. M. *Anal. Chem.* **2009**, *81*, 7091–7095.
- (51) Liu, H.; Crooks, R. M. *J. Am. Chem. Soc.* **2011**, *133*, 17564–17566.
- (52) Liu, H.; Xiang, Y.; Lu, Y.; Crooks, R. M. *Angew. Chem.* **2012**, *124*, 7031–7034.
- (53) Mentele, M. M.; Cunningham, J.; Koehler, K.; Volckens, J.; Henry, C. S. *Anal. Chem.* **2012**, *84*, 4474–4480.
- (54) Huynh, K. A.; Chen, K. L. *Environ. Sci. Technol.* **2011**, *45*, 5564–5571.
- (55) Li, X.; Lenhart, J. J.; Walker, H. W. *Langmuir* **2010**, *26*, 16690–16698.
- (56) Shirato, K.; Yano, T.; Senba, S.; Akachi, S.; Kobayashi, T.; Nishinaka, T.; Notomi, T.; Matsuyama, S. *Viral. J.* **2014**, *11*, 139–139.
- (57) Azhar, E. I.; Hashem, A. M.; El-Kafrawy, S. A.; Sohrab, S. S.; Aburizaiza, A. S.; Farraj, S. A.; Hassan, A. M.; Al-Saeed, M. S.; Jamjoom, G. A.; Madani, T. A. *mBio* **2014**, *5*, e01450.
- (58) Abreu, A. L. P.; Souza, R. P.; Gimenes, F.; Consolaro, M. E. L. *Viral. J.* **2012**, *9*, 262–262.
- (59) Villa, L. L.; Denny, L. *Int. J. Gynecol. Obstet.* **2006**, *94*, S71–S80.



ELSEVIER

Contents lists available at ScienceDirect

Analytica Chimica Acta

journal homepage: www.elsevier.com/locate/aca

A multiplexed three-dimensional paper-based electrochemical impedance device for simultaneous label-free affinity sensing of total and glycated haemoglobin: The potential of using a specific single-frequency value for analysis

Yuwadee Boonyasit^a, Orawon Chailapakul^b, Wanida Laiwattanapaisal^{c,*}

^a Graduate Program in Clinical Biochemistry and Molecular Medicine, Faculty of Allied Health Sciences, Chulalongkorn University, Bangkok, 10330, Thailand

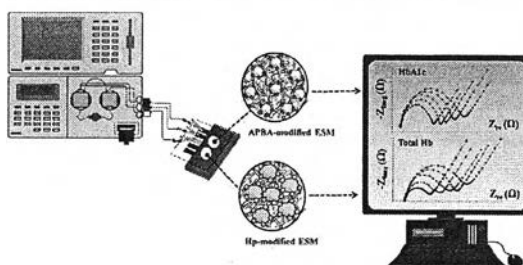
^b Electrochemistry and Optical Spectroscopy Research Unit (EOSRU), Department of Chemistry, Faculty of Science, Chulalongkorn University, Bangkok, 10330, Thailand

^c Department of Clinical Chemistry, Faculty of Allied Health Sciences, Chulalongkorn University, Bangkok, 10330, Thailand

HIGHLIGHTS

- A cost-effective 3D-PEID was developed for label-free impedimetric affinity sensing of total and glycated haemoglobin.
- Determination of the optimal binding frequency facilitates fast impedance measurements using a single frequency.
- Hp and APBA are recognition elements for selective binding of total and glycated haemoglobin, respectively.
- The proposed system meets the clinical requirements for glycaemic assessment in diabetic patients.

GRAPHICAL ABSTRACT



ARTICLE INFO

Article history:

Received 23 March 2016

Received in revised form

30 May 2016

Accepted 31 May 2016

Available online 3 June 2016

Keywords:

Glycated haemoglobin

Three-dimensional paper-based

electrochemical impedance device

3-Aminophenylboronic acid

Haptoglobin

Eggshell membrane

Label-free electrochemical detection

ABSTRACT

A novel three-dimensional paper-based electrochemical impedance device (3D-PEID) is first introduced for measuring multiple diabetes markers. Herein, a simple 3D-PEID composed of a dual screen-printed electrode on wax-patterned paper coupled with a multilayer of magnetic paper was fabricated for label-free electrochemical detection. The results clearly demonstrated in a step-wise manner that the haptoglobin (Hp)-modified and 3-aminophenylboronic acid (APBA)-modified eggshell membranes (ESMs) were highly responsive to a clinically relevant range of total (0.5–20 g dL⁻¹; $r^2 = 0.989$) and glycated haemoglobin (HbA1c) (2.3%–14%; $r^2 = 0.997$) levels with detection limits (S/N = 3) of 0.08 g dL⁻¹ and 0.21%, respectively. The optimal binding frequencies of total haemoglobin and HbA1c to their specific recognition elements were 5.18 Hz and 9.99 Hz, respectively. The within-run coefficients of variation (CV) were 1.84%, 2.18%, 1.72%, and 2.01%, whereas the run-to-run CVs were 2.11%, 2.41%, 2.08%, and 2.21%, when assaying two levels of haemoglobin and HbA1c, respectively. The CVs for the haemoglobin and HbA1c levels measured on ten independently fabricated paper-based sheets were 1.96% and 2.10%, respectively. These results demonstrated that our proposed system achieved excellent precision for the simultaneous detection of total haemoglobin and HbA1c, with an acceptable reproducibility of fabrication. The long-term stability of the Hp-modified eggshell membrane (ESM) was 98.84% over a shelf-life of 4 weeks, enabling the possibility of storage or long-distance transport to remote regions.

* Corresponding author.

E-mail address: Wanida.L@chula.ac.th (W. Laiwattanapaisal).

particularly in resource-limited settings; however, for the APBA-modified ESM, the stability was 92.35% over a one-week period. Compared with the commercial automated method, the results demonstrated excellent agreement between the techniques (p -value < 0.05), thus permitting the potential application of 3D-PEID for the monitoring of the glycaemic status in diabetic patients.

© 2016 Elsevier B.V. All rights reserved.

1. Introduction

The implementation of microfluidic paper-based analytical devices (μ PADs) in clinical off-site diagnoses has recently emerged as a distinctive field of simple telemedicine in remote areas [1]. The multiplexed measurement of a panel of biomarkers has recently attracted considerable interest due to its great potential for monitoring patient compliance, evaluating the effectiveness of therapy, and early screening for diseases. During recent years, μ PADs coupled with optical imaging for colourimetric detection have provided an affordable point-of-care platform for the multiplexed analysis of biomarkers, such as the transaminase assays for liver function assessment [2,3], detection of metabolic biomarkers for glycaemic control [4,5], urinalysis assays [1,6], and simultaneous detection of glucose, uric acid and lactate [7]. Alternatively, other detection methods for assaying multiple biomarkers on a single 3D- μ PAD have been demonstrated, including electrochemical [8–13], chemiluminescence [14], and electrochemiluminescence [15] techniques, most of which relied heavily on ultrasensitive immunodevices for multiplexed quantification of cancer biomarkers. To date, considering the existing paper-based electrochemical devices for measuring metabolic biomarkers, considerable efforts have been focused only on establishing a proof-of-concept work on the determination of glucose, uric acid, and lactate [16,17]. However, there has been minimal validation of μ PADs using actual clinical specimens. Thus far the label-free impedimetric sensing of diabetes markers for the long-term assessment of glycaemic control on a single 3D- μ PAD has yet to be investigated. As an alternative to the single-analyte assays, the multiplexed 3D- μ PAD allows simultaneous measurement of multiple analytes on a single device, which provides an accurate basis for clinical diagnoses and decreases the assay time. To our knowledge, there have been no attempts to use a single three-dimensional paper-based electrochemical impedance device (3D-PEID) for measuring multiple diabetes markers.

Currently, electrochemical impedance spectroscopy (EIS)-based point-of-care diagnostic platforms for determining a panel of biomarkers have attracted great interest in the clinical assessment of early disease detection. Known as an informative and nondestructive technique for biosensing applications, EIS has an enormous potential for the label-free and ultrasensitive biomarker detection with the capability to measure multiple markers simultaneously as it can be used to study the interfacial events or diffusion effects occurring at the surface of the electrodes. Because acquisition of impedance spectra is relatively time consuming, many attempts have been made to use a single frequency value for analysis [18–22]. More recently, multiplexed sensor array designs, most of which depend on antibody-based molecular recognition, have been implemented for the determination of various inflammatory markers using a unique frequency upon binding of the target molecule to the sensor [23,24]. The biological reaction between each target and its molecular recognition element results in a unique binding frequency that is specific to each reaction. Thus, the differences in frequency signals from each reaction can be detected on a single platform due to the effective discrimination of the target binding frequencies from the others. Using this

underlying principle, by immobilising recognition elements for different biomarkers on the sensor interface, each target molecule can be measured simultaneously by monitoring their optimal binding frequency, thereby making this platform suitable for multiplexed assays of makers in a single device. The specific optimal binding frequency depends on several factors such as the sensor material, molecular recognition element, and the linkers used for immobilisation [25]. For instance, EIS in combination with technology for the management of patients with diabetes mellitus (DM) was implemented using a specific frequency for glucose-glucose oxidase binding interaction [26]. A few years later, the feasibility of EIS in detecting 1,5-anhydroglucitol levels at its optimal binding frequency was also demonstrated using the enzyme pyranose oxidase [27]. However, there are no relevant data as of yet on the label-free affinity biosensing for measuring multiple diabetes markers on a single device. Hence, a multiplexed single-sensor diabetes marker assay needs to be further developed to meet the clinical requirements for a point-of-care testing (POCT) system.

Typically, in clinical practice, the quantitative measurement of glycated haemoglobin (HbA1c) is an indispensable index for the long-term monitoring of glycaemic control in both the diagnosis and routine management of diabetes. The intensive monitoring of glycaemic status is needed to avoid diabetic complications. In general, the HbA1c level is measured as the percentage of glycated haemoglobin in the total haemoglobin (i.e., mmol mol^{-1} or %). According to the consensus statement of the International Federation of Clinical Chemistry and Laboratory Medicine (IFCC) and the National Glycohemoglobin Standardization Program (NGSP) on the standard interpretation norms of HbA1c values, HbA1c results are reported worldwide together with the haemoglobin value as mmol of HbA1c or a percentage of HbA1c in the total haemoglobin, respectively [28]. HbA1c analysis has been accomplished using a wide range of techniques, including mass spectrometry [29–31], electrophoresis [32], chromatography [33,34], immunoassays [35–39], electrochemistry [40–49], enzyme assays [50–53], piezoelectric sensing [54–56], and optical spectroscopy [57–59]. However, most of the aforementioned approaches require the use of highly sophisticated instruments at high operating costs by experienced personnel. Moreover, they fail to satisfy the analytical requirements of sensitivity, specificity, reproducibility, storage stability, simplicity, and portability. For these reasons, further improvements of cost-effective diagnostic POCT devices are still required for the clinical assessment of glycaemic status in diabetes patients. Thus far, there have been no reports in the literature regarding simultaneous detection of both total haemoglobin and HbA1c based on a single affinity-based sensing device. In our preceding work, the label-free boronate-modified eggshell membrane (ESM)-based affinity sensor for long-term glycaemic monitoring was first demonstrated via the cis-diol interaction between HbA1c and the boronate recognition element [60]. Using the boronate-modified sensing surface, our device could distinguish between HbA1c and non-glycated haemoglobin (HbAo). However, acquisition of impedance spectra typically required a scanning time of 15 min for the entire frequency range. Therefore, in the present work, we have further developed the affinity membrane-based

analytical device for detecting HbA1c in parallel with total haemoglobin contents using a specific single-frequency value for analysis to circumvent the time-intensive procedure of acquiring entire impedance spectra.

Herein, to combine a multiplexed biomarker assay with a selective low-cost platform, we demonstrated a simple 3D-PEID for simultaneous quantitative detection of total haemoglobin and HbA1c using an ESM-based affinity sensor. The impedance response as a function of analyte concentration was also investigated in a single- or limited-frequency range by attaching the molecular recognition elements, i.e., haptoglobin (Hp) or 3-aminophenylboronic acid (APBA), to the sensor surface. Due to the distinctive features of Hp and APBA, which are promising recognition elements for total haemoglobin and HbA1c, selective binding was obtained via non-covalent protein-protein interactions and cis-diol interactions, respectively. Therefore, each target analyte could be detected by monitoring the optimal binding frequency specific to that reaction using a single 3D-PEID platform. This affinity device was also validated to suit the clinical requirements and applied to the determination of the total haemoglobin and HbA1c levels in real clinical blood samples. To our knowledge, no previous attempts have been made to assess the clinical applicability of a label-free 3D-PEID for assaying both total haemoglobin and HbA1c in actual patient-derived specimens. This reliable and inexpensive device for assaying total haemoglobin in parallel with HbA1c is an ideal sensing platform for point-of-care diagnostics. Our proposed system demonstrates the considerable future potential for long-term independent bedside monitoring of the glycaemic status of diabetes patients, particularly in resource-limited settings.

2. Materials and methods

2.1. Reagents and chemicals

All reagents and chemicals were of analytical grade or the highest purity available and used as received without further purification. APBA, human haptoglobin phenotype 1-1 (Hp), human haemoglobin, 4-ethylmorpholine, sodium chloride (NaCl), potassium chloride (KCl), potassium hexacyanoferrate II, potassium hexacyanoferrate III, a glutaraldehyde solution (25% w/w), ethanolamine, sodium acetate trihydrate, potassium cyanide, sodium phosphate monobasic, sodium phosphate dibasic, potassium phosphate monobasic, potassium phosphate dibasic, sodium hydroxide, urea, and haemoglobin-Ao were acquired from Sigma (St. Louis, MO, USA). Hydrochloric acid, ethanol, and absolute acetic acid were purchased from Merck (Darmstadt, Germany). A Lyphochek[®] HbA1c linearity set and Lyphochek[®] diabetes controls were obtained from BioRad Laboratories (Hercules, CA, USA). Ultrapure water obtained from a Millipore water purification system (18 M Ω cm, Milli-Q, Millipore) was used throughout the study. The instruments used for measuring the haematocrit (Hct) values, including micro-haematocrit tubes, a micro-capillary reader, and a micro-haematocrit centrifuge, were manufactured by Vitrex Medical A/S (Herlev, Denmark), International Equipment Company (Needham Heights, MA, USA), and Hawksley and Sons Ltd. (Sussex, England), respectively. For the preparation of the screen-printed electrodes, the carbon ink (C2030519P4) and silver chloride ink (C2090225P7) were supplied by Gwent group (Torfaen, United Kingdom). An A4 sheet of 180 g per square metre (gsm) office paper was available from a local stationery store. The custom-ordered blocking stencils and a rubber squeegee were readily available from the local service provider. For the ESM preparation, the chicken eggs were purchased from a local supermarket and stored at 4 °C before use. An *in vitro* test for the quantitative measurement of HbA1c in whole blood using a Tina-quant[®] HbA1c Gen.2 clinical chemistry analyser (Roche Diagnostics,

Switzerland) was employed to validate the method based on a turbidimetric inhibition immunoassay.

2.2. Design and fabrication of the 3D-PEID

The simple 3D-PEID was composed of a dual screen-printed electrode on a wax-patterned paper coupled with a multilayer of magnetic paper. For the preparation of the wax-based pattern on the 180 gsm office paper, the designed patterns of hydrophobic barriers as a dark blue-colour on a white background were fabricated using a slightly modified wax-printing procedure described previously [61]. Briefly, the wax-patterned paper containing a dual circular and rectangular zone was designed using Adobe Illustrator CS6 software (Adobe Systems Inc., San Jose, CA) and then printed onto the A4 sheet of 180 gsm office paper with a Xerox ColorQube 8570 solid ink printer. The wax-printed paper was transferred to a 150 °C hot plate with the wax side up for 180 s, and the printed wax was allowed to melt and penetrate through the paper to form the blue-coloured hydrophobic and insulating barriers. After cooling at room temperature, the wax-printed paper sheet was then ready for the printing of the three-electrode areas and conductive pads on its hydrophilic zones. Following our in-house screen printing technique, dual working and counter electrodes comprising the conductive pads were screen-printed on the defined hydrophilic areas on the wax-printed paper sheet using carbon ink. After that, to cure the carbon ink, the screen-printed paper was baked in an oven at 65 °C for 30 min before starting the next round of the screen-printing process. A reference electrode with its conductive pad was then screen-printed in the defined hydrophilic zone on the same paper sheet using silver/silver chloride ink before baking again at 65 °C for 30 min. Finally, after allowing the screen-printed paper to cool to room temperature, a dual screen-printed electrode on a wax-patterned paper layer was then adhered onto a customised magnetic paper sheet before assembling the whole system. To complete the proposed 3D-PEID, a dual screen-printed electrode layer adhered to a bottom magnetic paper layer and a top magnetic-paper lid containing two circular wells were all aligned and assembled with a permanent magnet underneath, as illustrated in Fig. 1A. The designed wax-patterned paper electrochemical cell was composed of two paper working zones (4 mm in diameter) surrounded by shared reference (geometric area approximately 3 mm²) and counter electrodes (geometric area approximately 17 mm²). The wax patterns around the three electrodes constituted an insulator for the electrochemical cell and served as a reservoir with a volume of approximately 60 μ L after alignment with the top magnetic-paper layer containing two circular holes. To characterise the surface structure of the screen-printed paper, scanning electron microscope (SEM) images of the proposed device were recorded on a field emission scanning electron microscope (JSM-7610F, JEOL, Tokyo, Japan).

2.3. ESM preparation

A circular double-layered ESM was prepared according to the procedure described previously [62]. Briefly, after soaking the chicken eggs in absolute acetic acid at 4 °C for 18 h, the membrane was subsequently peeled off and cleansed with a copious amount of ultrapure water before being cut into circular pieces (7 mm in diameter). The circular ESMs were then stored in a working buffer for assaying total haemoglobin and HbA1c until further use. To observe the microstructure of the ESM with and without the immobilised haemolysate samples containing the total haemoglobin, a dried circular ESM was adhered onto a piece of glass using carbon double-sided adhesive tape before placing on a specimen stub and coating with a thin layer of gold for the SEM analysis.

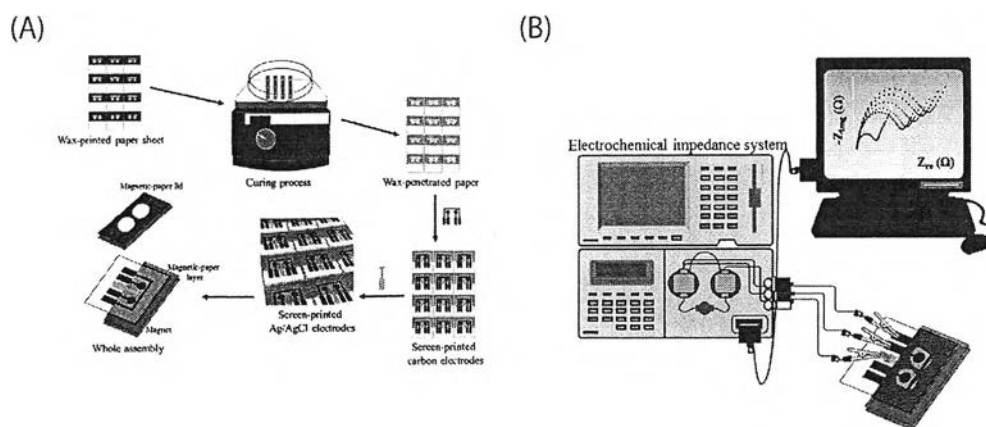


Fig. 1. Schematic representation of the proposed 3D-PEID illustrating (A) the fabrication process for the paper-based electrodes and (B) the configuration of the label-free electrochemical impedance system set-up. Two pieces of the affinity-based ESMs were placed on the two defined areas acting as the paper-based working electrodes for the selective sensing of total haemoglobin and HbA1c.

2.4. Surface modification with Hp and APBA

An affinity ESM-based impedance sensor was prepared by immobilising Hp or APBA on the surface of the ESM via glutaraldehyde cross-linking. Unless otherwise stated, the membrane was activated with the 25% glutaraldehyde solution for 1 min and washed with 100 mM phosphate buffer solution at pH 7 (PBS), then $10 \mu\text{g mL}^{-1}$ Hp was applied to the membrane surface and reacted at room temperature for 10 min. The sensing interface was subsequently rinsed with 10 mM ethanolamine, followed by an additional wash before allowing it to react with the various concentrations of total haemoglobin for 5 min. The EIS measurement was carried out in a step-wise manner with the electroactive redox probe. The Hp-modified ESMs could be used repeatedly after washing with a regeneration buffer, i.e., 5 M urea containing 0.15 M sodium chloride at pH 11. For the fabrication of the APBA-modified ESM, the selective binding of HbA1c was performed using a procedure described in our previous work [60], with slight modifications. Briefly, after activating the ESM with the 25% glutaraldehyde solution for 1 min, a 10 mM 4-ethylmorpholine buffer solution containing 0.25 M KCl and 0.1 M NaCl at a pH of 8.5 was used as a working buffer for rinsing the excess aldehyde functional groups. Next, 0.25 mg mL^{-1} of APBA was immobilised on the ESM for 5 min and washed with working buffer. The remaining aldehyde groups were then blocked with 10 mM ethanolamine buffer and washed with working buffer again. Finally, different concentrations of HbA1c were added to the selective sensor and allowed to incubate for 5 min at room temperature, followed by washing with working buffer according to the procedure described above. The APBA-modified ESMs could be regenerated using a 10 mM sodium acetate buffer at pH 5 due to the unstable cis-diol interactions under acidic conditions.

2.5. Apparatus set-up for the electrochemical impedance measurement

After assembling a multi-layered 3D-PEID, the impedance detection system, i.e., a potentiostat/galvanostat instrument (Autolab PGSTAT30, Eco Chemie, The Netherlands) equipped with the Frequency Response Analyser software, was then connected to the 3D-PEID using alligator clips. The configuration of the proposed system is illustrated in Fig. 1B. The whole assembly, including the dual screen-printed electrode layer adhered to the magnetic paper and the top magnetic-paper layer, was held together by a magnetic

force. Two pieces of the circular thin-layered ESMs (7 mm in diameter) were carefully placed on the screen-printed electrodes covering the working, counter, and reference electrodes. Each membrane was used as an immobilising platform for the specific recognition elements, i.e., Hp and APBA, used in the selective sensing of total haemoglobin and HbA1c, respectively. The redox ions, i.e., a 5 mM $\text{Fe}(\text{CN})_6^{3-/4-}$ solution prepared in a working buffer, was used as an electroactive probe throughout the experiment. The EIS measurement was conducted over a wide frequency range from 100 kHz to 10 mHz with an alternating-current amplitude of 10 mV. After recording the EIS data over the entire range of frequencies, the impedance spectra were fitted to an equivalent-circuit model using the NOVA 1.9 software and investigated for the optimal binding frequency of the interaction between the analyte of interest and its molecular recognition element.

2.6. Ethical conduct of research and sample preparation

Healthy and diabetic volunteers were enrolled in our study of their own volition. All subjects voluntarily gave written informed consent before the start of the study on the development of membrane-based biosensors for diabetes makers, which was approved by the Ethics Review Committee for Research Involving Human Research Subjects, Health Sciences Group, Chulalongkorn University (ECCU) under approval number COA No. 057/2557. Whole blood samples were drawn into vacuum blood collection tubes with tripotassium ethylenediaminetetraacetic acid (K_3EDTA) as an anticoagulant, and the Hct levels were measured using microcapillary tubes. The plasma was separated from the whole blood and discarded to eliminate other glycosylated proteins and sugars present in the blood plasma. To remove the plasma completely, the remaining red blood cells were carefully washed thrice with a 0.9% sodium chloride solution. A haemolysing buffer solution prepared according to the previous study [40] was used to lyse the red blood cells prior to the EIS measurement.

2.7. Real sample analysis

Unless otherwise stated, after preparing the Hp-modified and APBA-modified ESMs, approximately $40 \mu\text{L}$ of the haemolysate sample was allowed to incubate for 5 min, then washed with the working buffers for the total and glycosylated haemoglobin assays before recording the impedance spectra using the electroactive redox probes. The impedance signals on each paper-based sensing

electrode were sequentially measured via a one-channel potentiostat instrument. In this study, our proposed multi-layered 3D-PEID performed an independent EIS measurement for each specific analyte by using each modified-ESM location on the surface of each paper-based electrode. By sharing the counter and reference electrodes, each adjacent paper based working electrode could be operated independently to sense the two glycaemic markers.

3. Results and discussion

3.1. Surface characterisation of the 3D-PEID

After the curing process, the wax-patterned A4 sheet was prepared for the screen-printing of the three-electrode configuration onto the hydrophilic zones. Fig. 2 shows scanning electron micrographs (Panels A–C) of the porous structures and microfibrils of the pure office paper, the boundary of the wax-patterned paper, and the wax-penetrated paper. The melted wax penetrates the pores of the pure office paper and decreases its hydrophilicity remarkably. The functional hydrophobic areas prevent the aqueous solution from wicking and penetrating unwanted zones and act as an insulating region to confine all the reagents and solutions within the defined working electrode areas. The unprinted-paper zone remained highly hydrophilic and flexible and thus did not affect the screen-printing of the electrodes. The surface morphology of the screen-printed working electrodes is essential for assessing the sensing performance of the electrochemical devices; therefore, we investigated the surface structure of the screen-printed paper-based working electrode. As shown in Fig. 2D, a homogeneous structure was observed on the bare electrode surface, which was particularly helpful in producing paper-based electrodes with a reproducible response. For the preparation of the affinity membrane-based device, an entire sheet of ESM was used as a platform for the selective sensing of either total haemoglobin or HbA1c. Fig. 2E presents the inner surface of the ESM, showing a network-like structure that contains highly cross-linked protein fibres and cavities. The interlacing fibres of the inner layer were uniform and smooth, which was beneficial for protein immobilisation. The surface of the interlacing ESM fibres with immobilised Hp was saturated by haemoglobin after exposure to a red blood cell

lysate, as depicted in Fig. 2F. These results indicated that haemoglobin from the red blood cell lysate was successfully immobilised on the surface of the ESM.

3.2. EIS characterisation of the sensing interface

The inner surface of the ESM was subjected to step-wise modifications with the screen-printed working paper electrodes underneath. To investigate the specific binding of the total haemoglobin and HbA1c to the ESM interfaces, EIS measurements were carried out following each step of the surface modification. Nyquist plots acquired in the presence of 5 mM $\text{Fe}(\text{CN})_6^{3-/4-}$ at different stages of the modification process are shown in Figs. S1A and B (Supplementary material). A semicircular region could be observed at the higher frequencies, corresponding to the charge transfer resistance (R_{ct}) and double layer capacitance, as well as a straight line at the lower frequencies, representing the diffusion-limited process. The spectra obtained with the bare paper-based electrodes showed a semicircle with a relatively small diameter, which indicated a low R_{ct} of the redox couple. Comparatively, 2-fold increase in the R_{ct} values was observed when the ESMs were placed on the paper-based electrodes, which resulted from the blocking of the diffusion of the redox species to the electrode surface by the interlacing networks of the fibrous ESM. After modification of the ESM with the glutaraldehyde solution, a substantial increase in R_{ct} was observed. The glutaraldehyde-activated ESM was further modified with Hp and APBA before exposure to the various concentrations of total haemoglobin and HbA1c. The results showed that the impedance spectra acquired on electrodes having the Hp-modified and APBA-modified ESM had significantly lower R_{ct} compared to those only having the glutaraldehyde-treated ESM. In the case of APBA modification, the decrease in R_{ct} could be at least partly explained by electrostatic attraction of the negatively charged redox probe due to the presence of amino groups of APBA molecules that were actually bound to the glycoproteins of the ESM [60]. On the other hand, the decrease in R_{ct} after immobilisation of Hp cannot be fully explained since the protein acquires negative charge at pH 7 (pI of Hp ≤ 6), which rather causes repulsion of the redox probe. To investigate whether the ESM surfaces had successfully immobilised Hp and APBA, control experiments were also

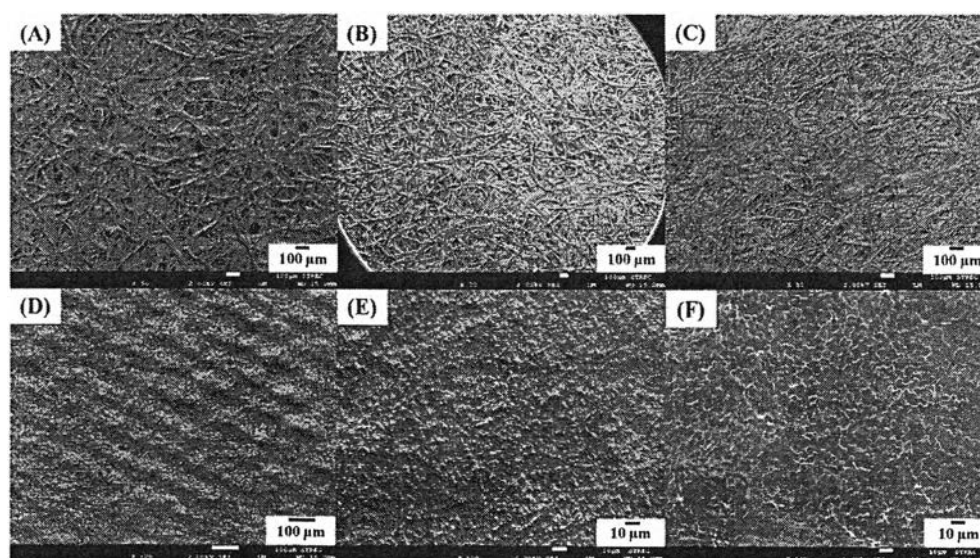


Fig. 2. SEM images of (A) pure office paper; (B) the boundary of the wax pattern, with the wax-printed office paper on the left side and the pure office paper on the right; (C) front face of wax-penetrated office paper; (D) screen-printed working electrode; (E) inner surface of the ESM; (F) after exposure to total haemoglobin.

performed using an ESM without immobilised Hp and APBA prepared in the same manner. The impedance response to various concentrations of total haemoglobin and HbA1c remained unchanged compared to the baseline signals of the ESMs, as shown in Figs. S2A and B (Supplementary material), respectively. These results confirmed the successful immobilisation of Hp and APBA on the ESM surfaces, implying that the changes in impedance were due to the specific binding of the total haemoglobin and HbA1c to the modified ESMs via non-covalent protein-protein and cis-diol interactions, respectively.

3.3. Analytical performance

Under optimal conditions, a remarkable increase in impedance was observed with increasing concentrations of total haemoglobin, as depicted in the Nyquist plot of Fig. 3A. The binding interaction between the Hp-modified ESM and the total haemoglobin contents hindered the diffusion of redox species to the surface of paper-based electrode, thus making the redox process more difficult and causing the impedance to increase. Due to the specific binding between the Hp-modified ESM and haemoglobin via non-covalent protein-protein interactions, the Hp-modified ESM was responsive to the various concentrations of total haemoglobin. The substantial increases in impedance signal were directly proportional to haemoglobin levels over the concentration range of 0.5 g dL^{-1} to 20 g dL^{-1} . Moreover, dramatic changes in impedance were noticed at the lower frequency range, as shown in Fig. 3B, thereby demonstrating the sensitive response of the Hp-modified ESM towards haemoglobin. The phase shift increased steadily upon the immobilisation of haemoglobin and subsequent addition of higher haemoglobin concentrations, as shown in Fig. 3C. The experimental

impedance data are approximated using the modified Randles' equivalent circuit model shown in Fig. 3D (inset), which includes a series of two constant-phase elements (CPEs) in parallel with two charge-transfer resistances (R_{ct1} , R_{ct2}) and the Warburg impedance (W), along with the ohmic resistance of the electrolyte solution (R_s). The R_{ct1} and R_{ct2} correspond to the membrane resistance and charge-transfer kinetics at the paper-based electrode, respectively. This equivalent circuit appears to be the optimal model that matches the experimental impedance spectra with good fitting results, as shown in Fig. S3A in the Supplementary material. The bulk properties and diffusion features of the redox probe solution, W and R_s , respectively, were not modified by the stepwise modification process, whereas the CPE and R_{ct} , the dielectric and insulating features at electrode/electrolyte interface, are controlled by the changes occurring at the electrode surface. The capacitance changes are not as sensitive as the charge transfer resistance. According to the impedance values obtained from the fit to this equivalent circuit, an increase in the membrane resistance was observed in the presence of increasing haemoglobin concentrations. The normalised resistances derived from the fitted resistance values were plotted versus the various concentrations of haemoglobin. As illustrated in Fig. 3D, the results showed that the normalised response was linear up to 20 g dL^{-1} of haemoglobin, with a regression equation of $y = 0.0642x + 0.2281$ ($r^2 = 0.989$) and a detection limit ($S/N = 3$) of 0.08 g dL^{-1} . For the HbA1c detection, a substantial increase in impedance with increasing concentrations of HbA1c was observed, as shown in Fig. 4A. The changes in impedance were observed at the lower frequencies; conversely, at higher frequencies, the impedance responses did not depend on the presence of HbA1c and were thus not useful for HbA1c detection, as shown in Fig. 4B. A significant phase shift with increasing

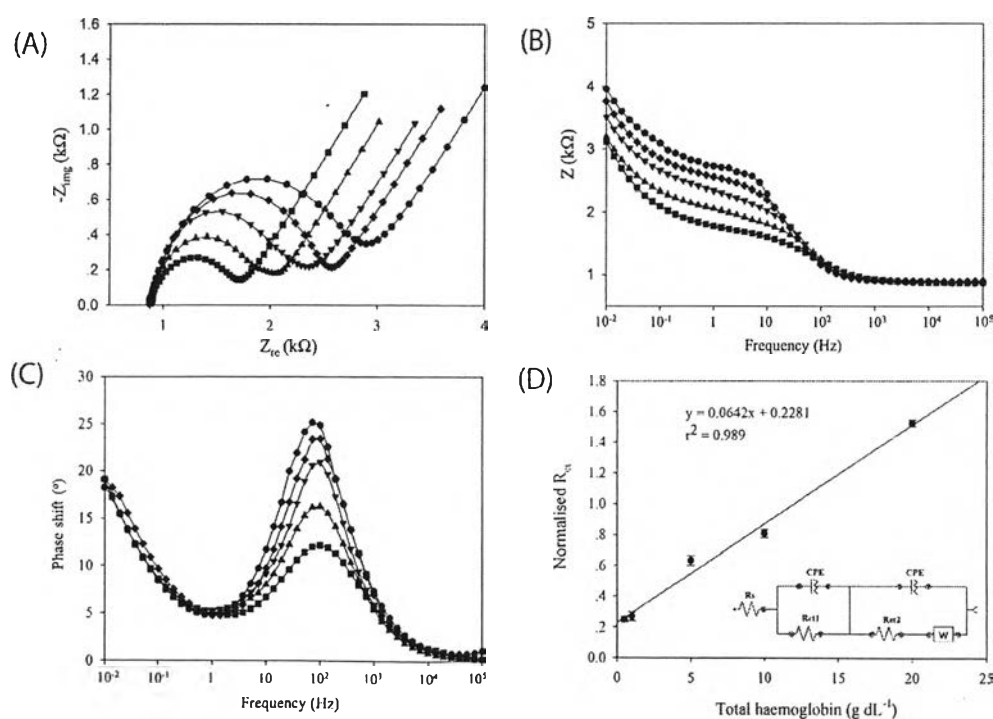


Fig. 3. Impedance data obtained from (A) the Nyquist plot; (B) the Bode-modulus plot of the Hp-modified ESM after it was exposed to various concentrations of total haemoglobin: (■) 0.5 g dL^{-1} , (▲) 1 g dL^{-1} , (▼) 5 g dL^{-1} , (◆) 10 g dL^{-1} , and (●) 20 g dL^{-1} ; and (C) the Bode-phase plot and (D) variation of the normalised R_{ct} with respect to the concentration of total haemoglobin. Inset right: an equivalent circuit for analysing the impedance data; R_s , R_{ct} , CPE, and W represent the solution resistance, charge-transfer resistance, constant-phase element, and Warburg impedance, respectively. The EIS spectra were obtained in $5 \text{ mM Fe(CN)}_6^{3-/4-}$ solution prepared in a working buffer at an open circuit voltage from 100 kHz to 10 mHz (ac amplitude, 10 mV).

concentrations of HbA1c is clearly demonstrated in Fig. 4C. Good fits to normal and diabetic HbA1c concentrations were also obtained over the entire measurement frequency range as shown in Fig. S3B in the Supplementary material. The APBA-modified ESM was responsive to HbA1c concentrations covering the clinically required range. The good relationship between the normalised Rct and the concentration of HbA1c was observed up to 14% of HbA1c, with a regression equation of $y = 0.0846x + 0.9118$ ($r^2 = 0.997$), as depicted in Fig. 4D. The resulting limit of detection was 0.21% ($S/N = 3$).

The correlation between the haemoglobin concentration and each frequency was investigated to determine the optimal binding frequency at a specific binding constant. The relationship between the impedance derived from the Hp-modified ESM and haemoglobin concentration was compared at each frequency point in the range from 100 kHz to 10 mHz and further analysed by reaching a compromise between the R-squared value and the correlation's slope, at which the maximised values were selected as the optimum binding target. The R-squared value and the slope from a duplicate measurement on a single paper-based electrode were plotted versus the frequency range, as shown in Fig. 5A. The R-squared value increased from the baseline and reached a maximum value close to 1 before returning to a lower level, whereas the slope gradually decreased until reaching a value close to 0 as the frequency increased. Hence, the optimal frequency of the binding interaction between the Hp-modified ESM and haemoglobin was determined to be 5.18 Hz. The correlation, as shown in Fig. 5B, represents an average impedance value of two different paper-based electrodes at a frequency of 5.18 Hz over a wide concentration range from 0.5 g dL⁻¹ to 20 g dL⁻¹, with a regression equation of $y = 0.0500x + 1.8250$ ($r^2 = 0.987$). We further investigated whether the standard curve obtained from an impedance

measurement at a specific single-frequency could be used in lieu of that from an impedance measurement recording the entire frequency range. Within the 95% confidence interval, a paired statistical analysis showed no significant differences between the two methods (p -value = 0.001), indicating the potential benefit of using a single frequency value for analysis. The optimal binding frequency for the APBA-modified ESM and HbA1c interaction was also evaluated using two parallel measurements on a single paper-based electrode, as demonstrated in Fig. 5C, and determined to be 9.99 Hz based on the full EIS sweep, at which the R-squared value was close to 1 and the constant slope was approximately zero. Fig. 5D shows a good correlation between the average impedance response at a specific frequency and its associated HbA1c concentration over a clinically relevant range, with a regression equation of $y = 0.0869x + 1.6527$ ($r^2 = 0.991$). Compared with the results obtained from the impedance measurements recording the whole frequency range of the EIS spectrum, the single-frequency measurements showed no significant differences, at the 95% confidence interval (p -value = 0.001). These findings support the use of a single-frequency as an optimal binding frequency for constructing a calibration curve.

As demonstrated here, our proposed 3D-PEID for measuring multiple diabetes markers not only improves the assay time by using a single specific-frequency measurement, but also offers a great sensitivity to total haemoglobin and HbA1c values within the clinically required ranges, where 13.5–17.5 g dL⁻¹ (male), 12.0–16.0 g dL⁻¹ (female) of haemoglobin, and 3.8–6.4% of HbA1c are considered the normal reference ranges [63]. Our paper-based device is the first report on the simultaneous detection of total haemoglobin and HbA1c based on a single affinity sensing device covering a broad clinical range [40,47–49]. Table S1 in the Supplementary material provides a brief summary of the current

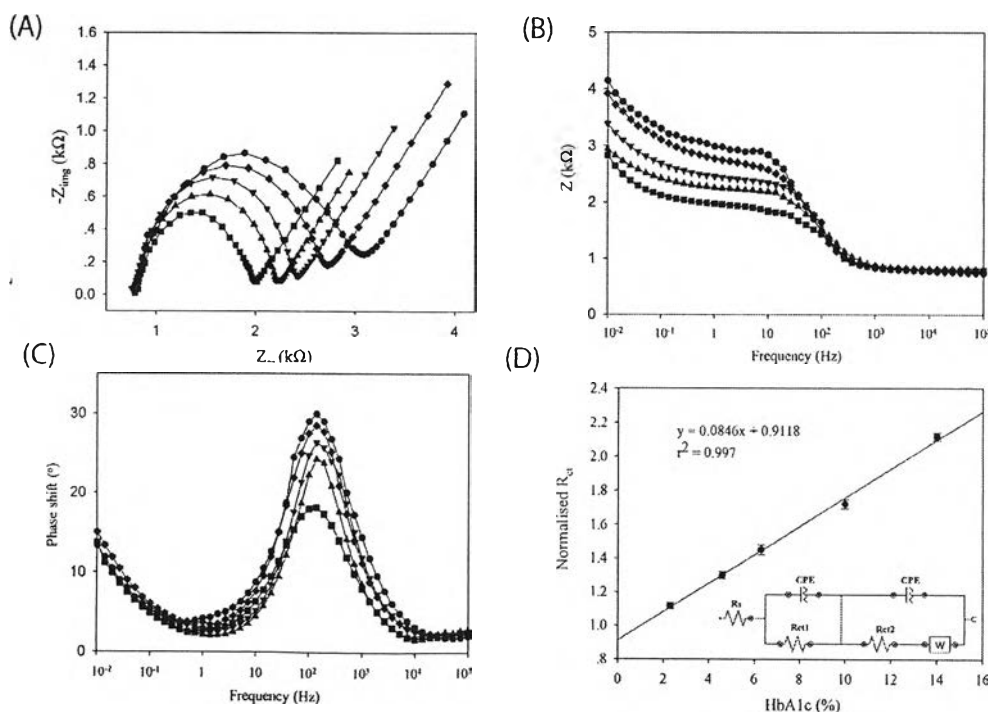


Fig. 4. Impedance data obtained from (A) the Nyquist plot; (B) the Bode-modulus plot of the APBA-modified ESM after it was exposed to various concentrations of HbA1c: (■) 2.3%, (▲) 4.6%, (▼) 6.3%, (◆) 10%, and (●) 14% HbA1c; and (C) the Bode-phase plot and (D) variation of the normalised Rct with respect to the concentration of HbA1c (%). Inset right: an equivalent circuit for analysing the impedance data. The EIS spectra were obtained in 5 mM Fe(CN)₆^{3-/4-} solution prepared in a working buffer at an open circuit voltage from 100 kHz to 10 mHz (ac amplitude, 10 mV).

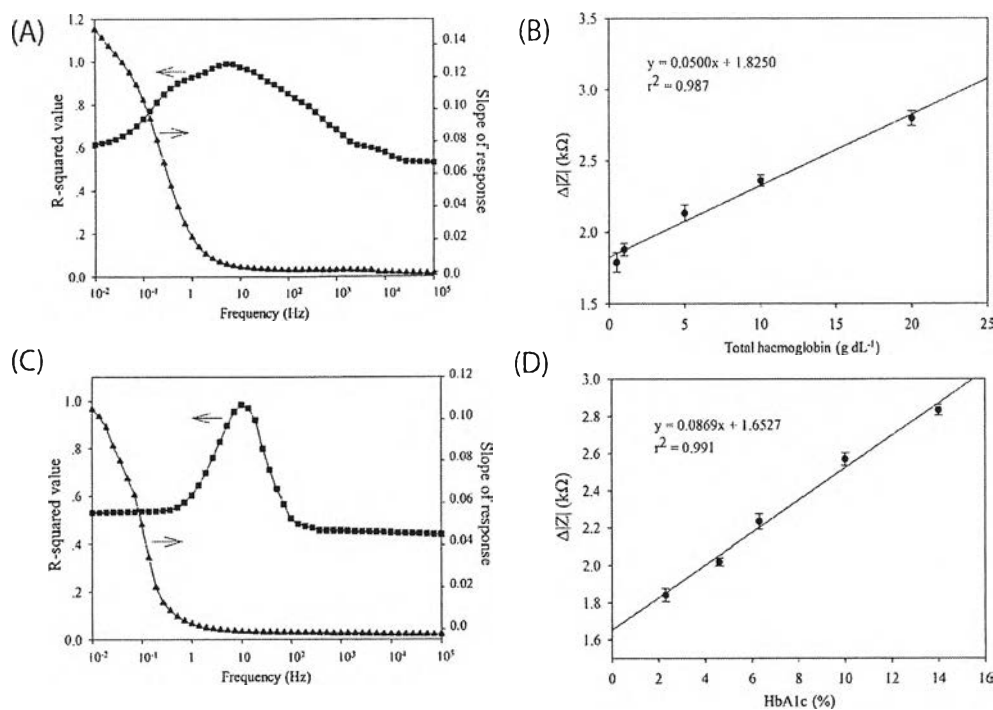


Fig. 5. Optimal binding frequency for (A) the Hp-modified ESM and total haemoglobin interaction and (C) the APBA-modified ESM and HbA1c interaction: (■) R-squared value of response versus frequency, (▲) slope of response versus frequency; and (B&D) correlation between the average impedance response at a specific frequency and its associated total haemoglobin and HbA1c concentration, respectively.

boronate-based electrochemical devices for assaying HbA1c. Thus, our proposed paper-based system provides a sensitive and cost-effective approach for glycaemic monitoring in individuals with diabetes, particularly for developing countries.

3.4. Regeneration and reproducibility

The reversibility of the interaction between haemoglobin and HbA1c and their specific recognition elements was also investigated to assess the method's potential for low-cost applications. To evaluate the performance of the regeneration procedure, the regeneration efficiency (RE) was calculated according to the following equation [64]: $RE = [1 - (RT - B)/T] \times 100\%$, where the RT represents the impedance response obtained after the regeneration cycle, B is the impedance response for the blank, and T is the impedance response before applying any regeneration step. Fig. S4A in the Supplementary material presents Nyquist plots for the reversible binding interaction of haemoglobin with its interface. The impedance of the Hp-modified ESM in the absence of haemoglobin (curve a) was smaller than that of the Hp-modified ESM in the presence of 1 g dL⁻¹ haemoglobin (curve b). After applying the regeneration buffer (5 M urea containing 0.15 M sodium chloride at a pH of 11), the impedance decreased due to the release of the bound haemoglobin from the Hp-modified ESM (curve c). The impedance increased again after exposure to 10 g dL⁻¹ of haemoglobin, indicating the rebinding of haemoglobin onto the Hp-modified ESM (curve d). After the second round of regeneration, the regeneration efficiency was 99.14% (curve e). The increase in impedance was then observed after re-incubating with 1 g dL⁻¹ of haemoglobin (curve f). The reversible binding of HbA1c onto the APBA interface was also observed, as shown in Fig. S4B in the Supplementary material. Compared with the baseline signal of the APBA-modified ESM (curve a), a significant increase in resistance was observed after exposure to 4.6% HbA1c (curve b). After the first

round of regeneration using 10 mM sodium acetate buffer at a pH of 5, the impedance decreased after the first rinse (curve c) but remained greater than the initial curve (curve a). The APBA-modified ESM was then re-incubated with 10% HbA1c, resulting in a dramatic increase in resistance (curve d). After applying the subsequent round of regeneration, the impedance significantly decreased (curve e), with a regeneration efficiency of 99.07%. The increase in impedance was observed again after re-incubating with 4.6% HbA1c (curve f). After repeating the same procedure for 10 cycles, the regeneration efficiencies of the Hp-modified ESM and APBA-modified ESM were found to be 90.11% and 89.97%, respectively. These results showed that the proposed 3D-PEID could be used as a reusable sensing platform due to the reversible binding of haemoglobin and HbA1c to their recognition interfaces.

The reproducibility of the proposed device was examined using two levels of haemoglobin and HbA1c, i.e., 10 g dL⁻¹ and 20 g dL⁻¹ of haemoglobin; 4.6% and 10% HbA1c, with measurements performed on the same day and on three consecutive days using the same ESM device. The within-run reproducibility for each concentration (n = 10), expressed as coefficient of variation (CV), was 1.84%, 2.18%, 1.72%, and 2.01% for 10 g dL⁻¹ and 20 g dL⁻¹ of haemoglobin and 4.6% and 10% HbA1c, respectively. The run-to-run reproducibility for each concentration (n = 30) was 2.11%, 2.41%, 2.08%, and 2.21%, assessed on three consecutive days, for 10 g dL⁻¹ and 20 g dL⁻¹ of haemoglobin and 4.6% and 10% HbA1c, respectively. The CV representing the variation between ten independently fabricated paper-based sheets was 1.96% and 2.10%, for 10 g dL⁻¹ of haemoglobin and 4.6% HbA1c, respectively. These results indicate that our proposed system provides a great precision for the simultaneous detection of total haemoglobin and HbA1c with an acceptable reproducibility of fabrication.

The storage stability of the Hp-modified ESM and APBA-modified ESM was evaluated over a period of 4 weeks by storing the membrane in 100 mM phosphate buffer solution (pH 7) at 4 °C.

To evaluate the performance of the Hp-modified ESM and APBA-modified ESM, the impedance response was measured after incubation with the same concentration of haemoglobin (10 g dL^{-1}) and HbA1c standard solution (4.6%), respectively. The results showed the long-term stability of the Hp-modified ESM to be 98.84% over a shelf-life of at least 4 weeks, as shown in Fig. S5A in the Supplementary material, indicating that the Hp-modified ESM would be suitable for long-distance transport to remote regions, particularly in resource-limited settings. The remarkable stability of the Hp-modified ESM was largely due to the biocompatible microenvironment of the ESM comprising the net-veined structure and the gas-permeable hydrophilicity, which may stabilise the activity of the protein during the long-term storage. For the stability of APBA-modified ESM, as shown in Fig. S5B in the Supplementary material, the activity of the APBA sensing interface was 92.35% over a one-week period; however, the signal response gradually decreased until reaching an activity of 53.75% after a four-week storage period. The decrease in signal was probably caused by the loss of APBA activity during the prolonged storage period.

3.5. Selectivity study

The evaluation of endogenous and exogenous interfering substances present in clinical specimens is essential before the diagnostic system can be implemented clinically. Whole blood specimens contain not only haemoglobin, but also glucose, glycated albumin, and other glycosylated proteins and sugars found in serum. The boronate recognition group is able to bind to the diol group of any glycosylated protein or sugar present in the blood matrix. Accordingly, the sample pre-treatment process is crucial to remove the interfering species in the whole blood before being subjected to the impedance measurement. As stated earlier, in our study, the interfering agents present in plasma were negligible due to the well-prepared treatment of blood samples. Thus, to assess the

analytical performance of the proposed system for measuring multiple diabetes markers, human serum albumin and non-glycosylated haemoglobin (HbAo) were tested as potential interferences in the sensing interfaces. Figs. S6A and B in the Supplementary material show the Nyquist plots for examining the selectivity of the Hp-modified ESM and APBA-modified ESM for varying levels of human serum albumin and HbAo, respectively. Compared with the signal baseline obtained from the Hp-modified ESM and APBA-modified ESM, the impedance responses remain virtually unchanged by human serum albumin and HbAo over the concentration range of $3\text{--}6 \text{ g dL}^{-1}$ and $10\text{--}20 \text{ g dL}^{-1}$, respectively. These results indicate that the proposed system was highly selective in determining the haemoglobin and HbA1c values in actual specimens, enabling the possibility of using the present method to assess the glycaemic levels in clinical practice. Most importantly, compared with other available methods for HbA1c determination, the boronate affinity assay was less affected by the presence of genetic variants and chemical derivatives of haemoglobin [65, 66]. For the interpretation of the HbA1c results, additional relevant factors, such as severe iron-deficiency anaemia, haemolytic anaemia or any condition that directly affects the erythrocyte lifespan, e.g., renal failure, should be taken into account in practical considerations.

3.6. Real sample analysis and assay comparison

A demonstration of the ability of the diagnostic system to detect the percentage of HbA1c in real human blood samples is essential before it can be implemented clinically. Thus, to further investigate its potential in practical applications, the effectiveness of the proposed 3D-PEID for measuring the total haemoglobin and HbA1c values was assessed using the real blood samples of healthy and diabetic volunteers, for which the haematocrit values were within the range of 37–48%. Each red blood cell lysate sample was

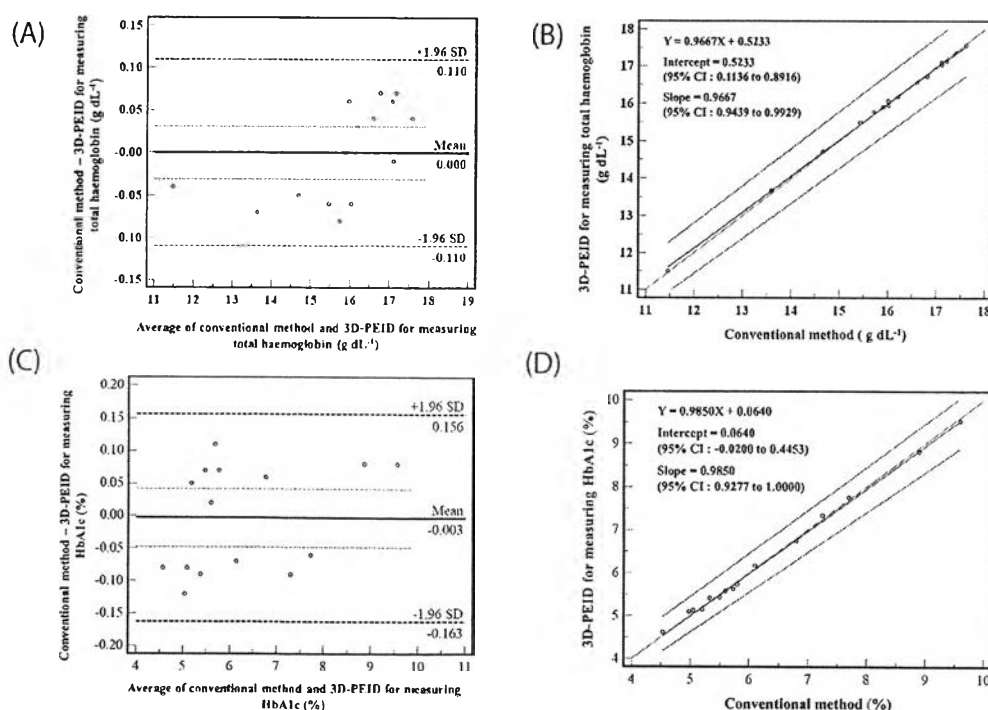


Fig. 6. Comparison of the proposed 3D-PEID and the current large-scale method for total haemoglobin and HbA1c measurements using (A&C) a Bland-Altman bias plot and (B&D) Passing-Bablok regression analysis, respectively.

measured individually using our system and with the automated clinical chemistry analyser. The results obtained from the proposed 3D-PEID were compared with those determined with the turbidimetric inhibition immunoassay on an automated large-scale analyser. The agreement and correlation between the two approaches were evaluated by Bland-Altman bias plot and Passing-Bablok regression analysis, respectively. As demonstrated in Fig. 6A and C, the data showed acceptable agreement between the results provided by our proposed device and the commercially available kit within an agreement interval of ± 1.96 SD. These results also showed zero bias and a reliable relationship, which indicates that these two approaches could be used interchangeably. Moreover, as shown in Fig. 6B and D, the regression equations according to the Passing-Bablok analysis of the total haemoglobin and HbA1c were $y = 0.9667x + 0.5233$ and $y = 0.9850x + 0.0640$, respectively. These results indicated a good correlation between the two methods throughout the entire measurement range. Within a 95% confidence interval, the values of the y-intercept (0.5233 g dL^{-1}) and the slope (0.9667) were significantly reliable and covered a range of 0.1136 – 0.8916 g dL^{-1} and 0.9439 to 0.9929 , respectively. Additionally, for the determination of HbA1c, the values of the y-intercept (0.0640%) and the slope (0.9850) were trustworthy and covered a range of -0.0200 – 0.4453% and 0.9277 to 1.0000 , respectively. The data presented in this proof-of-concept work demonstrates the validity of the proposed device for the simultaneous detection of total haemoglobin and HbA1c in clinical diagnostics using actual clinical specimens. Our paper-based device offers the great benefit for onsite clinical monitoring of the glycaemic status in individuals with diabetes.

4. Conclusions

We have demonstrated a selective 3D-PEID for multiplexed determination of diabetes markers using a single EIS platform. By monitoring at a single frequency value, the proposed device has a considerable advantage over the conventional EIS measurements in terms of assay time, allowing a decrease in data acquisition time by a factor of 15. However, further improvement on the EIS processing software would be needed to run EIS at the desired frequency value. As demonstrated here, our proposed 3D-PEID not only provides a precise measurement with a wide linear concentration range but also offers a great sensitivity for the total haemoglobin and HbA1c values within the clinically relevant ranges. Such capabilities make this cost-effective device useful for monitoring the glycaemic status in individuals with diabetes. In addition to being a proof-of-concept work, our system performed well compared with the commercial automated method using actual clinical samples, even in specimens obtained from diabetic patients. Conceivably, the successful development of this multiplexed 3D-PEID would be suitable for near-patient monitoring in remote areas. However, POCT systems require not only the production of affordable and portable devices but also the development of the detection instruments to measure the signal using a portable multi-channel device.

Acknowledgements

This research was financially supported by the Thailand Research Fund through Research Team Promotion Grant (RTA5780005) and the Ratchadapisek Sompot Endowment Fund of Chulalongkorn University (WCU-58-002-HR). Y.B. acknowledges the Thailand Research Fund through the Royal Golden Jubilee Ph.D. Program (under grant No. PHD/0164/2553) and the Graduate School, Chulalongkorn University for the Tuition Fee Scholarship. Dr. Poomrat Rattanarat is acknowledged for providing excellent technical assistance with the screen-printed fabrication process.

Appendix A. Supplementary data

Supplementary data related to this article can be found at <http://dx.doi.org/10.1016/j.aca.2016.05.047>.

References

- [1] A.W. Martinez, S.T. Phillips, E. Carrilho, S.W. Thomas III, H. Sindi, G.M. Whitesides, Simple telemedicine for developing regions: camera phones and paper-based microfluidic devices for real-time, off-site diagnosis, *Anal. Chem.* 80 (2008) 3699–3707.
- [2] S.J. Vella, P. Beattie, R. Cademartiri, A. Laromaine, A.W. Martinez, S.T. Phillips, K.A. Mirica, G.M. Whitesides, Measuring markers of liver function using a micropatterned paper device designed for blood from a fingerstick, *Anal. Chem.* 84 (2012) 2883–2891.
- [3] N.R. Pollock, J.P. Rolland, S. Kumar, P.D. Beattie, S. Jain, F. Noubary, V.I. Wong, R.A. Pohlmann, U.S. Ryan, G.M. Whitesides, A paper-based multiplexed transaminase test for low-cost, point-of-care liver function testing, *Sci. Transl. Med.* 4 (2012) 1–10.
- [4] Y. Boonyasit, W. Laitwanapaisal, A microfluidic paper-based analytical device for the assay of albumin-corrected fructosamine values from whole blood samples, *Bioanalysis* 7 (2015) 79–90.
- [5] M. Yamaguchi, S. Kambe, T. Eto, M. Yamakoshi, T. Kouzuma, N. Suzuki, Point of care testing system via enzymatic method for the rapid, efficient assay of glycated albumin, *Biosens. Bioelectron.* 21 (2005) 426–432.
- [6] A.W. Martinez, S.T. Phillips, M.J. Butte, G.M. Whitesides, Patterned paper as a platform for inexpensive, low-volume, portable bioassays, *Angew. Chem. Int. Ed.* 46 (2007) 1318–1320.
- [7] W. Dungchai, O. Chailapakul, C.S. Henry, Use of multiple colorimetric indicators for paper-based microfluidic devices, *Anal. Chim. Acta* 674 (2010) 227–233.
- [8] Y. Wu, P. Xue, Y. Kang, K.M. Hui, Paper-based microfluidic electrochemical immunodevice integrated with nanobioprobes onto graphene film for ultrasensitive multiplexed detection of cancer biomarkers, *Anal. Chem.* 85 (2013) 8661–8668.
- [9] P. Wang, L. Ge, M. Yan, X. Song, S. Ge, J. Yu, Paper-based three-dimensional electrochemical immunodevice based on multi-walled carbon nanotubes functionalized paper for sensitive point-of-care testing, *Biosens. Bioelectron.* 32 (2012) 238–243.
- [10] D. Zang, L. Ge, M. Yan, X. Song, J. Yu, Electrochemical immunoassay on a 3D microfluidic paper-based device, *Chem. Commun.* 48 (2012) 4683–4685.
- [11] S. Ge, L. Ge, M. Yan, X. Song, J. Yu, J. Huang, A disposable paper-based electrochemical sensor with an addressable electrode array for cancer screening, *Chem. Commun.* 48 (2012) 9397–9399.
- [12] L. Li, W. Li, H. Yang, C. Ma, J. Yu, M. Yan, X. Song, Sensitive origami dual-analyte electrochemical immunodevice based on polyaniline/Au-paper electrode and multi-labeled 3D graphene sheets, *Electrochim. Acta* 120 (2014) 102–109.
- [13] W. Li, L. Li, M. Li, J. Yu, S. Ge, M. Yan, X. Song, Development of a 3D origami multiplex electrochemical immunodevice using a nanoporous silver-paper electrode and metal ion functionalized nanoporous gold–chitosan, *Chem. Commun.* 49 (2013) 9540–9542.
- [14] L. Ge, S. Wang, X. Song, S. Ge, J. Yu, 3D origami-based multifunction-integrated immunodevice: low-cost and multiplexed sandwich chemiluminescence immunoassay on microfluidic paper-based analytical device, *Lab. Chip* 12 (2012) 3150–3158.
- [15] L. Ge, J. Yan, X. Song, M. Yan, S. Ge, J. Yu, Three-dimensional paper-based electrochemiluminescence immunodevice for multiplexed measurement of biomarkers and point-of-care testing, *Biomaterials* 33 (2012) 1024–1031.
- [16] W. Dungchai, O. Chailapakul, C.S. Henry, Electrochemical detection for paper-based microfluidics, *Anal. Chem.* 81 (2009) 5821–5826.
- [17] C. Zhao, M.M. Thuo, X. Liu, A microfluidic paper-based electrochemical biosensor array for multiplexed detection of metabolic biomarkers, *Sci. Technol. Adv. Mater.* 14 (2013) 054402.
- [18] J. Wang, J.A. Profit, M.J. Puglia, I.I. Suni, Au nanoparticle conjugation for impedance and capacitance signal amplification in biosensors, *Anal. Chem.* 78 (2006) 1769–1773.
- [19] R.K. Shervedani, S.A. Mozaffari, Impedimetric sensing of uranyl ion based on phosphate functionalized cysteamine self-assembled monolayers, *Anal. Chim. Acta* 562 (2006) 223–228.
- [20] R.K. Shervedani, A. Hatefi-Mehrjardi, Electrochemical characterization of directly immobilized glucose oxidase on gold mercaptosuccinic anhydride self-assembled monolayer, *Sens. Actuator E-Chem.* 126 (2007) 415–423.
- [21] R.K. Shervedani, M. Bagherzadeh, H. Sabzyan, R. Safari, One-impedance for one-concentration impedimetry as an electrochemical method for determination of the trace zirconium ion, *J. Electroanal. Chem.* 633 (2009) 259–263.
- [22] E. Katz, L. Alfonsa, I. Willner, Chronopotentiometry and Faradaic impedance spectroscopy as methods for signal transduction in immunosensors, *Sens. Actuator B-Chem.* 76 (2001) 134–141.
- [23] J.T. La Belle, U.K. Demirok, D.R. Patel, C.B. Cook, Development of a novel single sensor multiplexed marker assay, *Analyst* 136 (2011) 1496–1501.
- [24] A.B. Fairchild, K. McAferty, U.K. Demirok, J.T. La Belle, A label-free, rapid multimarker protein impedance-based immunosensor, in: *Complex Medical Engineering*, CME/ICME International Conference on, IEEE, 2009, pp. 1–5.

- [25] U. Demirok, A. Verma, J.T. La Belle, The development of a label-free electrochemical impedance based point-of-care technology for multimarker detection, *J. Biosens. Bioelectron.* 12 (2013).
- [26] T.L. Adamson, F.A. Eusebio, C.B. Cook, J.T. LaBelle, The promise of electrochemical impedance spectroscopy as novel technology for the management of patients with diabetes mellitus, *Analyst* 137 (2012) 4179–4187.
- [27] T.L. Adamson, C.B. Cook, J.T. LaBelle, Detection of 1, 5-Anhydroglucitol by electrochemical impedance spectroscopy, *J. Diabetes Sci. Technol.* 8 (2014) 350–355.
- [28] Consensus Committee, Consensus statement on the worldwide standardisation of the HbA1c measurement, *Diabetologia* 50 (2007) 2042–2043.
- [29] E. del Castillo, M. Montes-Bayón, E. Anón, A. Sanz-Medel, Quantitative targeted biomarker assay for glycosylated haemoglobin by multidimensional LC using mass spectrometric detection, *J. Proteomics* 74 (2011) 35–43.
- [30] N.B. Roberts, A.B. Amara, M. Morris, B.N. Green, Long-term evaluation of electrospray ionization mass spectrometric analysis of glycosylated hemoglobin, *Clin. Chem.* 47 (2001) 316–321.
- [31] J.O. Jeppsson, U. Kobold, J. Barr, A. Finke, W. Hoelzel, T. Hoshino, K. Miedema, A. Mosca, P. Mauri, R. Paroni, Approved IFCC reference method for the measurement of HbA1c in human blood, *Clin. Chem. Lab. Med.* 40 (2002) 78–89.
- [32] R. Mullins, G. Austin, Sensitivity of isoelectric focusing, ion exchange, and affinity chromatography to labile glycosylated hemoglobin, *Clin. Chem.* 32 (1986) 1460–1463.
- [33] F. Frantzen, K. Grimrud, D.-E. Heggli, E. Sundrehagen, Protein-boronic acid conjugates and their binding to low-molecular-mass cis-diols and glycosylated hemoglobin, *J. Chromatogr. B Biomed. Sci. Appl.* 670 (1995) 37–45.
- [34] S. Eckerborn, Y. Bergqvist, J.O. Jeppsson, Improved method for analysis of glycosylated haemoglobin by ion exchange chromatography, *Ann. Clin. Biochem.* 31 (1994) 355–360.
- [35] H.H. Chen, C.-H. Wu, M.-L. Tsai, Y.J. Huang, S.H. Chen, Detection of total and A1c-glycosylated hemoglobin in human whole blood using sandwich immunoassays on polydimethylsiloxane-based antibody microarrays, *Anal. Chem.* 84 (2012) 8635–8641.
- [36] D. Stöllner, W. Stocklein, F. Scheller, A. Warsinke, Membrane-immobilized haptoglobin as affinity matrix for a hemoglobin-A1c immunosensor, *Anal. Chim. Acta* 470 (2002) 111–119.
- [37] G. Liu, S.M. Khor, S.G. Iyengar, J.J. Gooding, Development of an electrochemical immunosensor for the detection of HbA1c in serum, *Analyst* 137 (2012) 829–832.
- [38] C. RamanaSuri, Zeta potential based colorimetric immunoassay for the direct detection of diabetic marker HbA1c using gold nanopores. *Chem. Commun.* 46 (2010) 5755–5757.
- [39] J. Szymezak, N. Leroy, E. Lavalard, P. Gillery, Evaluation of the DCA vantage analyzer for HbA1c assay, *Clin. Chem. Lab. Med.* 46 (2008) 1195–1198.
- [40] D.M. Kim, Y.B. Shim, Disposable amperometric glycosylated hemoglobin sensor for the finger prick blood test, *Anal. Chem.* 85 (2013) 6536–6543.
- [41] T. Tanaka, S. Tsukube, K. Izawa, M. Okochi, T.-K. Lim, S. Watanabe, M. Harada, T. Matsunaga, Electrochemical detection of HbA1c, a marker for diabetes, using a flow immunoassay system, *Biosens. Bioelectron.* 22 (2007) 2051–2056.
- [42] S. Liu, U. Wollenberger, M. Katterle, F.W. Scheller, Ferroceneboronic acid-based amperometric biosensor for glycosylated hemoglobin, *Sens. Actuator B-Chem.* 113 (2006) 623–629.
- [43] Y. Zhou, H. Dong, L. Liu, Y. Hao, Z. Chang, M. Xu, Fabrication of electrochemical interface based on boronic acid-modified pyrroloquinoline quinine/reduced graphene oxide composites for voltammetric determination of glycosylated hemoglobin, *Biosens. Bioelectron.* 64 (2015) 442–448.
- [44] S.Y. Song, H.C. Yoon, Boronic acid-modified thin film interface for specific binding of glycosylated hemoglobin (HbA1c) and electrochemical biosensing, *Sens. Actuator B-Chem.* 140 (2009) 233–239.
- [45] S.Y. Song, Y.D. Han, Y.M. Park, C.Y. Jeong, Y.J. Yang, M.S. Kim, Y. Ku, H.C. Yoon, Bioelectrocatalytic detection of glycosylated hemoglobin (HbA1c) based on the competitive binding of target and signaling glycoproteins to a boronate-modified surface, *Biosens. Bioelectron.* 35 (2012) 355–362.
- [46] H. Liu, R.M. Crooks, Determination of percent hemoglobin A1c using a potentiometric method, *Anal. Chem.* 85 (2012) 1834–1839.
- [47] K.M. Hsieh, K.C. Lan, W.L. Hu, M.K. Chen, L.S. Jang, M.H. Wang, Glycosylated hemoglobin (HbA1c) affinity biosensors with ring-shaped interdigital electrodes on impedance measurement, *Biosens. Bioelectron.* 49 (2013) 450–456.
- [48] J.Y. Park, B.Y. Chang, H. Nam, S.M. Park, Selective electrochemical sensing of glycosylated hemoglobin (HbA1c) on thiophene-3-boronic acid self-assembled monolayer covered gold electrodes, *Anal. Chem.* 80 (2008) 8035–8044.
- [49] Y.C. Chuang, K.C. Lan, K.M. Hsieh, L.S. Jang, M.K. Chen, Detection of glycosylated hemoglobin (HbA1c) based on impedance measurement with parallel electrodes integrated into a microfluidic device, *Sens. Actuator B-Chem.* 171 (2012) 1222–1230.
- [50] L. Fang, W. Li, Y. Zhou, C.C. Liu, A single-use, disposable indium-modified electrochemical biosensor for fructosyl valine for the glycosylated hemoglobin detection, *Sens. Actuator B-Chem.* 137 (2009) 235–238.
- [51] K. Ogawa, D. Stöllner, F. Scheller, A. Warsinke, F. Ishimura, W. Tsugawa, S. Ferri, K. Sode, Development of a flow-injection analysis (FIA) enzyme sensor for fructosyl amine monitoring, *Anal. Bioanal. Chem.* 373 (2002) 211–214.
- [52] A. Sakaguchi, W. Tsugawa, S. Ferri, K. Sode, Development of highly-sensitive fructosyl-valine enzyme sensor employing recombinant fructosyl amine oxidase, *Electrochemistry* 71 (2003) 442–445.
- [53] W. Tsugawa, F. Ishimura, K. Ogawa, K. Sode, Development of an enzyme sensor utilizing a novel fructosyl amine oxidase from a marine yeast, *Electrochemistry* 68 (2000) 869–871.
- [54] J. Haláček, U. Wollenberger, W. Stocklein, F. Scheller, Development of a biosensor for glycosylated hemoglobin, *Electrochim. Acta* 53 (2007) 1127–1133.
- [55] J. Příbyl, P. Skládal, Quartz crystal biosensor for detection of sugars and glycosylated hemoglobin, *Anal. Chim. Acta* 530 (2005) 75–84.
- [56] J. Příbyl, P. Skládal, Development of a combined setup for simultaneous detection of total and glycosylated hemoglobin content in blood samples, *Biosens. Bioelectron.* 21 (2006) 1952–1959.
- [57] J.T. Liu, L.Y. Chen, M.C. Shih, Y. Chang, W.Y. Chen, The investigation of recognition interaction between phenylboronate monolayer and glycosylated hemoglobin using surface plasmon resonance, *Anal. Biochem.* 375 (2008) 90–96.
- [58] M. Adamczyk, Y.Y. Chen, D.D. Johnson, P.G. Mattingly, J.A. Moore, Y. Pan, R.E. Reddy, Chemiluminescent acridinium-9-carboxamide boronic acid probes: application to a homogeneous glycosylated hemoglobin assay, *Bioorg. Med. Chem. Lett.* 16 (2006) 1324–1328.
- [59] M. Syamala Kiran, T. Itoh, K. Yoshida, N. Kawashima, V. Biju, M. Ishikawa, Selective detection of HbA1c using surface enhanced resonance Raman spectroscopy, *Anal. Chem.* 82 (2010) 1342–1348.
- [60] Y. Boonyasit, A. Heiskanen, O. Chailapakul, W. Laiwattanapaisal, Selective label-free electrochemical impedance measurement of glycosylated haemoglobin on 3-aminophenylboronic acid-modified eggshell membranes, *Anal. Bioanal. Chem.* (2015) 1–11.
- [61] E. Carrilho, A.W. Martinez, G.M. Whitesides, Understanding wax printing: a simple micropatterning process for paper-based microfluidics, *Anal. Chem.* 81 (2009) 7091–7095.
- [62] F. Yeni, D. Odaci, S. Timur, Use of eggshell membrane as an immobilization platform in microbial sensing, *Anal. Lett.* 41 (2008) 2743–2758.
- [63] A. Kratz, M. Ferraro, P.M. Sluss, K.B. Lewandrowski, Laboratory reference values, *N. Engl. J. Med.* 351 (2004) 1548–1564.
- [64] J. Yakovleva, R. Davidsson, A. Lobanova, M. Bengtsson, S. Eremin, T. Laurell, J. Ernéus, Microfluidic enzyme immunoassay using silicon microchip with immobilized antibodies and chemiluminescence detection, *Anal. Chem.* 74 (2002) 2994–3004.
- [65] S. Jaisson, N. Leroy, C. Desroches, M. Tonye-Libyh, E. Guillard, P. Gillery, Interference of the most frequent haemoglobin variants on quantification of HbA_{1c}: comparison between the LC–MS (IFCC reference method) and three routinely used methods, *Diabetes Metab.* 39 (2013) 363–369.
- [66] I. Byt, P.C. Chen, D.B. Sacks, Effects of hemoglobin variants and chemically modified derivatives on assays for glycohemoglobin, *Clin. Chem.* 47 (2001) 153–163.

CrossMark
click for updatesCite this: *Anal. Methods*, 2016, 8, 8049

Synthesis of PANI/hematite/PB hybrid nanocomposites and fabrication as screen printed paper based sensors for cholesterol detection

Farhatun N. Maluin,^{ab} Sharifah M.,^{ab} Poomrat Rattanarat,^c Weena Siangproh,^d Orawon Chailapakul,^{ce} Issam A. M.^a and Ninie S. A. Manan^{*ab}

In this work, the composites of polyaniline/nano-hematite (α -Fe₂O₃)/Prussian Blue (PB) were successfully synthesized *via* a sonochemical method. This nanocomposite (PB/CPANI) has been used for the modification of paper-based sensors for cholesterol detection. The electrochemical studies of this nanocomposite showed a well-defined cyclic voltammogram for hydrogen peroxide (H₂O₂) with a remarkable electrochemical sensitivity. This nanocomposite modified paper-based electrode also showed excellent electrocatalytic activity towards H₂O₂ in the interference-free cathodic region. In addition, cholesterol oxidase was immobilized on the PB/CPANI-modified paper-based electrode for selective detection of cholesterol. Under optimum conditions, a linear range of 0.6–6.0 mM with a very low detection limit of 0.52 mM for cholesterol and a good sensitivity of 411.7 μ A mM⁻¹ cm⁻² were obtained which indicated that the method presented is outstandingly appropriate to determine cholesterol in bovine serum albumin. This work might be an alternative, interference-free, and cost-effective approach for biomonitoring of cholesterol both in methodological studies and in clinical laboratories

Received 3rd September 2016

Accepted 13th October 2016

DOI: 10.1039/c6ay02478e

www.rsc.org/methods

Introduction

Awareness on the importance of monitoring cholesterol levels in blood has increased the interest in the development of cholesterol biosensors.^{1,2} Cholesterol is one of the most important biomarkers for cardiovascular disease, high blood pressure, coronary artery disease, and anemia.³ The National Cholesterol Education Program reports that the total cholesterol in blood should be lower than 0.011 M to be considered as normal, while 0.011–0.013 M is borderline-high and above 0.013 M is considered as high cholesterol levels.⁴ Thus, monitoring the cholesterol level in blood is very important for prevention and therapy. However, low-cost medical diagnoses and treatments are still necessary especially in developing countries. In order to develop a low cost device, printing of

functional materials on a paper substrate has drawn great attention recently.⁵ Paper-based biosensors offer several advantages such as low cost, requirement of small volumes of reagents and samples, biocompatibility and disposability.⁶ Among the detection techniques, methods based on electrochemical sensors have attracted much attention due to their small size, portability, low cost, high sensitivity, and high selectivity by an appropriate choice of detection potential and/or electrode materials.⁷ However, the limitation of paper-based electrochemical biosensors is their limited sensitivity for detection of trace biomarkers.⁶ Therefore, modification of paper based biosensors with nanomaterials, such as metallic nanoparticles, nano-carbon based materials, metal oxide nanostructures and conducting polymers, is still greatly required to improve the sensor sensitivity. Nanomaterials have been widely applied in biosensing systems which benefit from the unique chemical, physical and size properties of the nanomaterials.⁸

Metal oxide NPs emerge as remarkable materials for sensing purposes with several advantages such as wide band gaps, low cost synthesis, high resistance to corrosion, facile fabrication, controllable sizes, ease of surface modification and ability to promote the electron-transfer kinetics.^{9,10} Hematite (α -Fe₂O₃) NPs have also been used for the detection of glucose,¹¹ dopamine,¹² hydrazine,¹³ *etc.* On the other hand, electroactive conducting polymers (CPs) such as polyaniline (PANI), polypyrrole (PPy) and polythiophene are promising host materials for

^aDepartment of Chemistry, Faculty of Science, University of Malaya, 50603 Kuala Lumpur, Malaysia. E-mail: ninie.manana@um.edu.my; Fax: +60-3-79677188; Tel: +60-3-79677022

^bUniversity of Malaya Center for Ionic Liquid (UMCIL), University of Malaya, 50603 Kuala Lumpur, Malaysia

^cElectrochemistry and Optical Spectroscopy Unit (EOSRU), Department of Chemistry, Faculty of Science, Chulalongkorn University, Phayathai Road, Patumwan, Bangkok, 10330, Thailand

^dDepartment of Chemistry, Faculty of Science, Srinakharinwirot University, Sukhumvit 23, Wattana, Bangkok 10110, Thailand

^eNational Center of Excellence for Petroleum, Petrochemicals, and Advanced Materials, Chulalongkorn University, Phayathai Road, Patumwan, Bangkok, 10330, Thailand

inorganic semiconductors owing to the high mobility of charge carriers, good conductivity and electrochemical stability.^{14,15} Among the conducting polymers, polyaniline (PANI) is a promising material due to its excellent electrochemical properties, high environmental stability and low toxicity.

Nowadays, the development of polymer/inorganic hybrid nanocomposites has been receiving significant attention due to their wide range of nanotechnology applications in various fields.^{16–25} Combining the properties of the organic polyaniline and inorganic nano- α - Fe_2O_3 will improve the properties of the nanocomposite and this can overcome the drawbacks due to the individual counterparts as well as improve the physical and chemical properties of the materials. Bandgar *et al.*²⁶ proved that PANI- Fe_2O_3 hybrid nanocomposites showed higher oxidation and doping degree than pure PANI.

Cholesterol oxidase (ChOx) is a commonly used enzyme for sensor fabrication and has been immobilized on various modified electrodes.²⁷ ChOx contains the flavin adenine dinucleotide (FAD) cofactor which can undergo an enzymatic reaction by oxidizing the cholesterol to cholest-5-en-3-one. The reduced flavin cofactor then undergoes a further enzymatic reaction to form hydrogen peroxide (H_2O_2).^{6,28} Therefore, H_2O_2 is usually used for indirect quantification of cholesterol.^{29,30} The main problem in direct detection of H_2O_2 is the presence of other compounds (*e.g.* ascorbic acid, glucose, uric acid, *etc.*) in real samples which might be oxidized at the electrode surface together with H_2O_2 .³¹ Thus, in order to minimize or avoid this electrochemical interference, the electrocatalytic reduction of H_2O_2 by Prussian blue (PB) has been widely and thoroughly investigated.³²

Hybrid structures have proven their superior characteristics in several applications such as solar cells, sensors and energy storage devices.¹⁰ In this contribution, a new nanocomposite with the combination of α - Fe_2O_3 , PANI and PB (PB-CPANI) was synthesized to possess the properties of the individual components with a synergistic effect. This new nanocomposite has been used to modify the working electrode of a paper-based biosensor. The performance of this sensing system was optimized. The developed method was validated according to the International Council on Harmonisation (ICH) guidelines and was found to be linear, sensitive, specific, precise and accurate.^{33,34} The developed method was applied for determination of cholesterol in real samples. To the best of our knowledge, the proposed hybrid nanostructure has not been investigated before for cholesterol detection by electrochemistry or other techniques.

Experimental

Reagent and materials

Potassium ferrocyanide ($\text{K}_3[\text{Fe}(\text{CN})_6]$) and iron(III) chloride (FeCl_3) were purchased from R&M Chemicals (Essex, United Kingdom). Aniline, hydrochloric acid (HCl) (37%), and uric acid ($\text{C}_5\text{H}_4\text{N}_4\text{O}_3$) were purchased from Fisher Scientific (Selangor, Malaysia), Friendemann and Schmidt (Parkwood, Australia), and Wako (Shanghai, China), respectively. Cholesterol, 100 U mL^{-1} cholesterol oxidase (ChOx) from *Streptomyces* sp.,

polyoxyethylene octyl phenyl ether (Triton X-100), and acetaminophen (paracetamol) were obtained from Sigma-Aldrich (St. Louis, Missouri, USA). Potassium dihydrogen phosphate (KH_2PO_4) and D -glucose anhydrous were purchased from Carlo Erba Reagenti-SDS (Valde Reuil, France). 1-Butyl-3-methylimidazolium bis(trifluoromethylsulfonyl)imide ($[\text{C}_4\text{mim}][\text{NTf}_2]$), *N*-methyl pyrrolidone (NMP), ascorbic acid, disodium hydrogen phosphate (Na_2HPO_4), potassium chloride (KCl), and sodium chloride (NaCl) were purchased from Merck (Darmstadt, Germany). Carbon and silver/silver chloride inks were obtained from Gwent group (Torfaen, United Kingdom). Filter paper grade no. 1 (size; $46 \times 57 \text{ cm}^2$) was purchased from Whatman (Sigma-Aldrich, St. Louis, Missouri, USA). All chemicals were used without further purification, and all solutions were prepared using high-purity water ($18.2 \text{ M}\Omega \text{ cm}$) from a MilliQ Water System (Millipore, Billerica, Massachusetts, USA). For the real sample analysis, blank bovine serum albumin (BSA) was obtained from Nacalai Tesque Inc. (Kyoto, Japan). Phosphate buffer saline (pH 7.4) was prepared by dissolving 0.8% (w/v) NaCl, 0.02% (w/v) KCl, 0.144% (w/v) Na_2HPO_3 , and 0.024% (w/v) KH_2PO_4 in MilliQ water. Cholesterol solutions were prepared by slowly heating 5% w/v of Triton X-100 in a 60°C water bath and were diluted in MilliQ water. They were stored at 4°C prior to use.

Instrumentation

FTIR spectra were obtained using a Perkin-Elmer RX1 FT-IR spectrometer in the range of $4000\text{--}400 \text{ cm}^{-1}$ while powder XRD was carried out using a Siemens D5000, with Cu $K\alpha$ radiation ($\lambda = 0.15418 \text{ nm}$) in the range of $2\theta = 10\text{--}80^\circ$ with a step of 0.07° per second. The morphological and elemental components were analyzed using a FESEM JEOL JAMP-9500F (Peabody, Massachusetts, USA) and a HR-TEM JEOL JEM-2100F (Tokyo, Japan). The electrochemical measurements (cyclic voltammetry and amperometry) were performed using an Autolab Potentiostat & Galvanostat Metrohm with NOVA software (Riverview, Florida, USA). A three-electrode system was used and PB/CPANI was dropcast directly on the working carbon electrode surface.

Synthesis of the Prussian blue/polyaniline nanocomposite (PB/CPANI)

In a separate 50 mL beaker, 20% w/v aniline was dissolved in an ionic liquid ($[\text{C}_4\text{mim}][\text{NTf}_2]$) and 1.2 g of iron(III) chloride, $\text{FeCl}_3 \cdot 6\text{H}_2\text{O}$, was dissolved in a 1 : 1 (w/v) ratio mixture of 37% HCl and MilliQ water respectively. The two solutions were combined and a green layer was formed within the interface after several minutes and allowed to rest overnight. The ionic liquid ($[\text{C}_4\text{mim}][\text{NTf}_2]$) was used as a stabilizer for the formation of nano-hematite in the polyaniline matrix. The crude product of CPANI was collected *via* filtration and washed with ethanol and water to remove any unreacted chemicals and aniline oligomers. CPANI was dried under vacuum and further dried in an oven overnight at $50\text{--}60^\circ \text{C}$.³⁵ Next, 0.2% w/v of CPANI was dissolved in 37% HCl. This solution was subjected to mild sonication for 30 min. To the solution, 25 mL of 0.005 M

potassium ferrocyanide was added. The mixture was stirred for 3 hours and then left overnight. The aqueous phase was removed by using a rotatory evaporator and the product was washed with MilliQ water in order to remove any unreacted chemicals.

Fabrication of the screen printed paper-based electrode (SPE)

Paper-based electrodes were fabricated by designing the desired pattern using Adobe Illustrator. The pattern was printed on a filter paper (Whatman no. 1) using a wax printer (Xerox Color Qube 8570, Tokyo, Japan) to create a hydrophobic area (covered with wax). Three electrodes were screen-printed on the wax-patterned paper. Both working (WE) and auxiliary electrodes (AE) were printed using carbon ink, while silver/silver chloride (Ag/AgCl) ink was used to form the reference electrode and act as a conductive pad.

Fabrication of the PB/CPANI nanocomposite paper-based biosensor

The PB/CPANI nanocomposite was dispersed in *N*-methyl pyrrolidone (NMP) with 30 min mild ultrasonication to achieve a homogenous suspension. Then, 2 μL of the nanocomposite suspension was directly cast on the surface area of the working carbon electrode (diameter of 4 mm) of the prepared screen printed paper based electrode (SPE). After that, the coated electrode was heated at 50 $^{\circ}\text{C}$ in an oven for 30 minutes. For layer optimization, 2 μL of the nanocomposite suspension was cast for each layer. The study was done from 0 up to 5 layers of PB/CPANI.

Preparation of bovine serum albumin (BSA)

The stock solution of 20 mg of bovine serum albumin (BSA) was diluted in 10 mL of MilliQ water prior to analysis. 40 mL BSA was further diluted in PBS with the addition of 10 mL of cholesterol at different concentrations (0.5, 1.0, 2.0, 4.0, and 6.0 mM).

Electrochemical measurements

For cyclic voltammetry measurements, the potential value was scanned from -0.8 V to $+0.8$ V at 10 mV s^{-1} for the first analytical performance study of 1 mM H_2O_2 and for the layer

optimization study. For the scan rate studies, the potential was scanned from -1.0 V to $+1.0$ V (between 100 mV s^{-1} and 900 mV s^{-1}). The optimum potential for the reduction of H_2O_2 by cyclic voltammetry was in the range of 0.0 V to -0.8 V. Furthermore, amperometric measurements at the optimum detection potential were employed for cholesterol detection. The amperometric steady-state current at 90 s was recorded and used for the cholesterol measurement.

Results and discussion

Synthesis and physicochemical characterization of PB/CPANI

In this research, a composite of PANI/hematite, CPANI, was synthesized *via* interfacial polymerization. The synthesized CPANI was reacted with 37% HCl and was subjected to sonication for 30 minutes. During this time, hematite ($\alpha\text{-Fe}_2\text{O}_3$) from CPANI leached out Fe^{3+} ions which then reacted with $[\text{Fe}(\text{CN})_6]^{4-}$ from potassium ferrocyanide, resulting in a greenish-blue solution indicating the complete formation of the composite nano-hybrid of PB/CPANI. Fig. 1 displays the summarized pathway of PB/CPANI nanocomposite synthesis.

Structural characterization. The FTIR spectra of the CPANI and PB/CPANI are shown in Fig. 2(a). In Fig. 2(a), the FTIR spectra of PB/CPANI (ii) show strong peaks at 2070 cm^{-1} and 530 cm^{-1} which were attributed to the CN stretching in the $[\text{Fe}^{\text{II}}\text{-CN-Fe}^{\text{III}}]$ units.³⁶ These peaks can be obviously seen in the spectra of Fig. 2(a)(i), which proved the existence of PB in the composite. The absorption bands at 1447 cm^{-1} and 1556 cm^{-1} corresponding to the C=C stretching of quinoid rings and the C=C stretching of benzenoid rings, respectively, were observed, matching the peaks in the CPANI composite (Fig. 2(a)(iii)). The bands at 500 cm^{-1} were attributed to the characteristic of Fe-O which is related to hematite, $\alpha\text{-Fe}_2\text{O}_3$.³⁷

The polycrystalline structure of PB/CPANI was also confirmed by the X-ray scattering pattern. As shown in Fig. 2(b)(i), strong and sharp peaks were found at 2θ values of 17.72° ($2\ 0\ 0$), 28.72° ($2\ 2\ 2$), 40.84° ($4\ 2\ 0$), 50.04° ($4\ 4\ 0$), and 58.83° ($6\ 2\ 2$), which are related to the characteristics of the face-centered-cubic phase of $\text{Fe}_4[\text{Fe}(\text{CN})_6]_3$ crystal particles. These patterns are almost identical to the standard patterns of the PB crystal (Fig. 2(b)(ii)) and have been confirmed through the XRD library; JCPDS file no. 73-0689. The peaks at 2θ values of 24.26° ($0\ 1\ 2$), 35.61° ($1\ 1\ 0$), 39.36° ($0\ 0\ 6$), 54.09° ($1\ 1\ 6$), and 57.59°

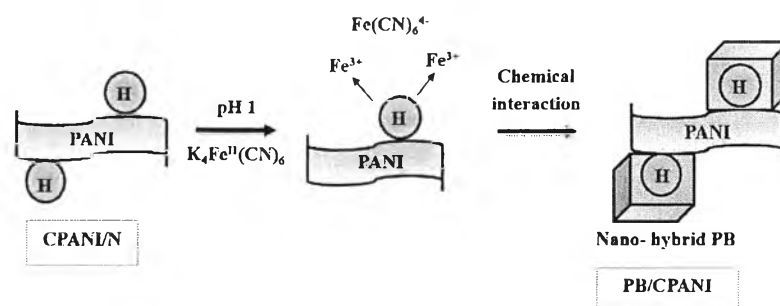


Fig. 1 A schematic diagram of the synthesis of PB/CPANI nanocomposites.

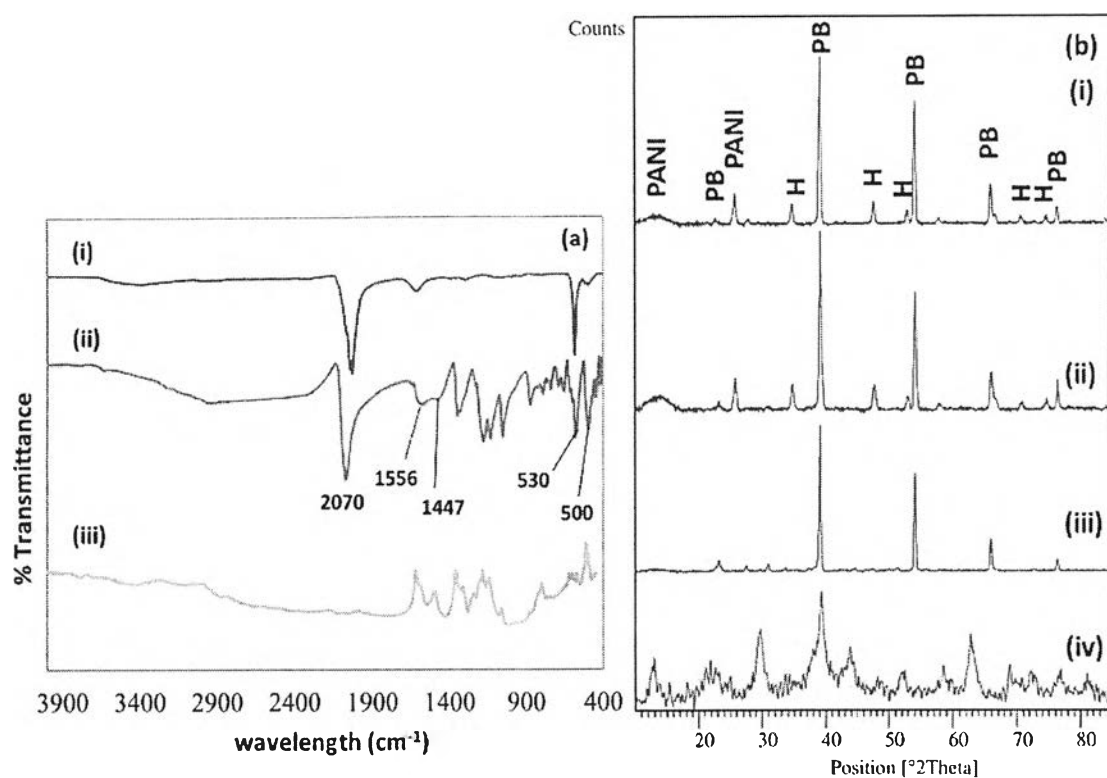


Fig. 2 (a) FTIR of (i) PB, (ii) PB/CPANI, and (iii) CPANI; (b) XRD spectra of (i) PB/CPANI, (ii) PB, (iii) CPANI and (iv) PANI.

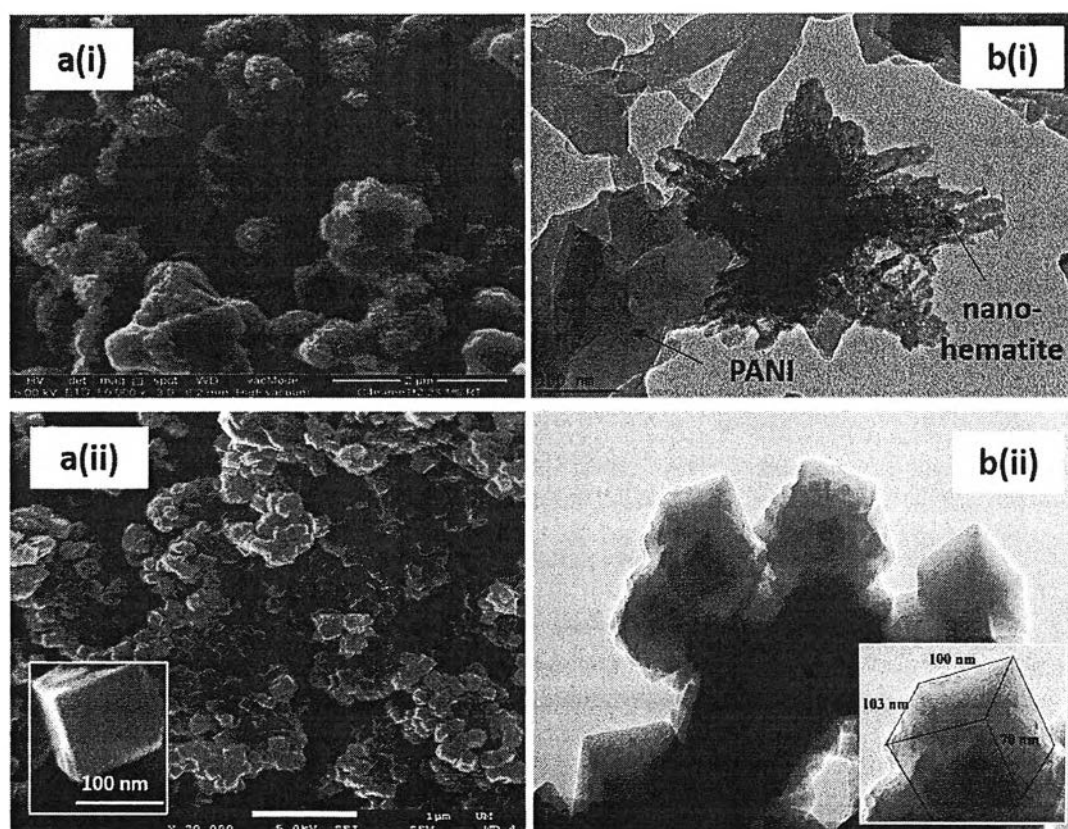


Fig. 3 FESEM (a) images of (i) CPANI, (ii) PB/CPANI; (b) HR-TEM images of (i) CPANI, (ii) PB/CPANI.

(0 1 8) belong to hematite peaks (Fig. 2(b)(iii)) and are related to the rhombohedral shape of hematite which utterly match the ref. code 00-033-0664 (ICDD Database). Therefore, the XRD results revealed that the crystalline PB phase was embedded with hematite and amorphous forms of PANI.

Morphological analysis. The presence of PB in PB/CPANI was further investigated using FESEM and TEM as shown in Fig. 3(a) and (b) respectively. Fig. 3(a)(i) and (b)(i) show the PANI being well-coated with fibrils of nano-hematite. This hematite then leached out Fe^{3+} ions and they reacted with $[\text{Fe}(\text{CN})_6]^{4-}$ to form PB/CPANI. Fig. 3(a)(ii) and (b)(ii) show that both images of PB/CPANI are in the nano-cubic structure which is in good agreement with the PB crystal structure reported in the Open Chemistry Database (compound summary code; ID 27242510).

Analytical application

Electrochemical study of the PB/CPANI/SPE. The study of electrochemical performance of the PB/CPANI/SPE was done by cyclic voltammetry. In Fig. 4(a)(i), no electrochemical response of H_2O_2 was observed at the bare SPE. The PB/SPE (Fig. 4(a)(ii)) shows a quasi-reversible redox couple at around 0.22 V and -0.13 V vs. Ag/AgCl, corresponding to the oxidation and reduction of H_2O_2 , respectively.³⁸ It is well known that Prussian blue has certain intrinsic peroxidase-like activity due to its close

similarity to peroxidase, and thus it can be used to catalyze the reduction of hydrogen peroxide.^{39–41} The CPANI/SPE produces the same response towards H_2O_2 with better current signals, which is due to the ability of PANI to enhance the electroactive area (Fig. 4(a)(iii)). A remarkably high current signal can be seen for the PB/CPANI/SPE (Fig. 4(a)(iv)). Both anodic and cathodic peak currents of H_2O_2 enhanced approximately seven-fold compared to the PB/SPE (Fig. 4(a)(ii)). These results confirmed that the presence of PANI considerably promotes the electron transfer rate and further enhances the electrocatalytic behavior of redox PB towards H_2O_2 .

Further layer optimization studies were done for PB/CPANI ranging from zero to five layers using cyclic voltammetry as shown in Fig. 4(b). The measurements of anodic (i_{pa}) and cathodic currents (i_{pc}) against the number of deposited layers were plotted as shown in Fig. 4(c) in which four layers of PB/CPANI had shown the highest current signal and was chosen for further study. The measurement of peak current was performed by using NOVA software and based on “baseline” from which to define the magnitude of a peak.

The electrochemical behavior of H_2O_2 using optimized layer deposition of the PB/CPANI/SPE was further investigated. Cyclic voltammograms of different scan rates were obtained ranging from 100 mV s^{-1} to 900 mV s^{-1} (Fig. 5(a)). The plots of peak

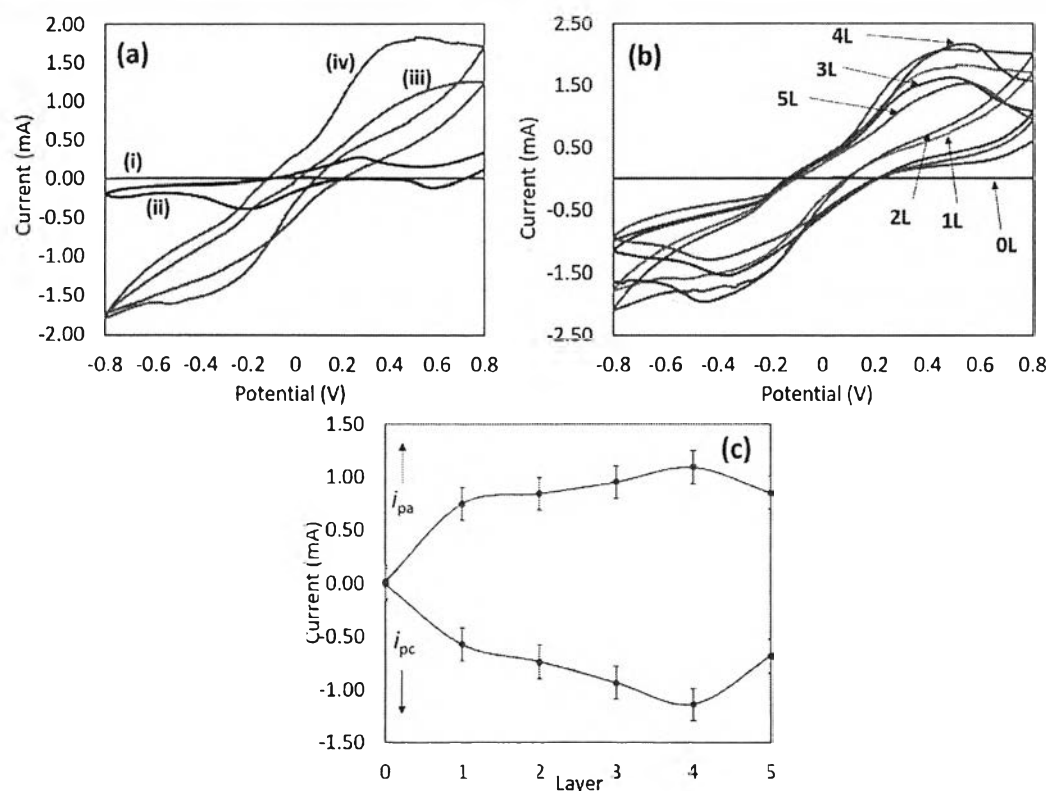


Fig. 4 (a) Cyclic voltammetric behaviors of (i) the bare SPE, (ii) PB/SPE, (iii) CPANI/SPE, and (iv) PB/CPANI/SPE in the presence of $1 \text{ mM H}_2\text{O}_2$ in phosphate buffer saline at pH 7.4 and a scan rate of 100 mV s^{-1} ; (b) cyclic voltammogram of different layers (0 layer to 5 layers) of deposited PB/CPANI on the SPE in the presence of $1 \text{ mM H}_2\text{O}_2$ in phosphate buffer saline at pH 7.4 and a scan rate of 100 mV s^{-1} ; (c) plot current vs. layer optimization of PB/CPANI ranging from 0 to 5 layers in the presence of $1 \text{ mM H}_2\text{O}_2$ in phosphate buffer saline at pH 7.4 and a scan rate of 100 mV s^{-1} .

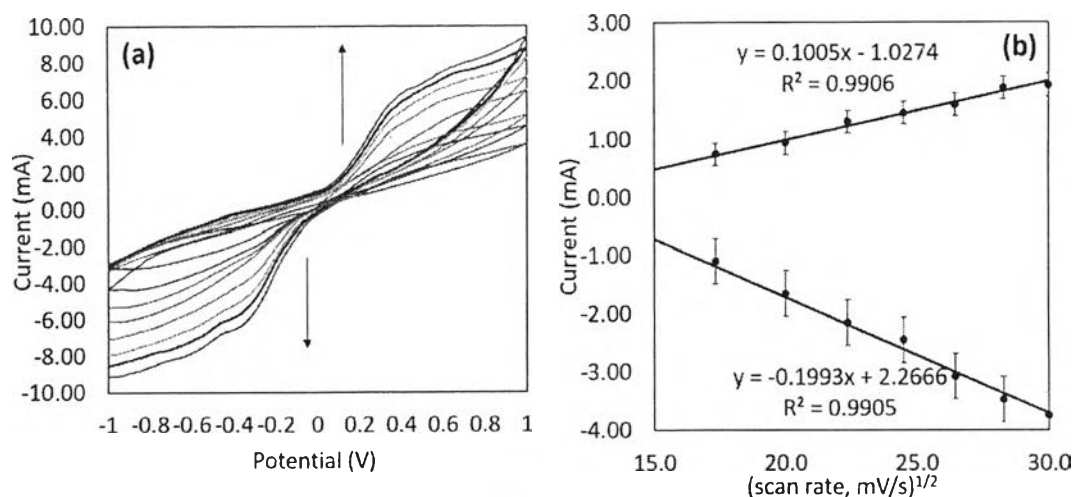


Fig. 5 (a) Cyclic voltammogram of 1 mM H_2O_2 in phosphate buffer saline at pH 7.4 and at different scan rates ranging from 100 to 900 mV s^{-1} ; (b) the relationship between the square root of the scan rate ($v^{1/2}$) and peak current.

current vs. square root of the scan rate produced linear plots for both oxidative and reductive processes as shown in Fig. 5(b), showing the diffusion-controlled process.

Amperometry is another great technique with several advantages including high sensitivity, wide applicability, easy interpretation, and reproducibility.⁴² This technique was chosen to study the cathodic signal current, corresponding to the H_2O_2 reduction. The cathodic region can be regarded as an interference-free region as mentioned in the Introduction part. The optimization study of the potential has been conducted to find the best potential for H_2O_2 reduction and cholesterol detection. The voltammogram of H_2O_2 showed the increase of current for both the electrolyte background (PBS, pH 7.4) and analyte signal (1 mM of H_2O_2) as shown in Fig. 6(a). The signal-to-background (S/B) current ratio was plotted against the potential (Fig. 6(b)). From the graph plotted, the S/B current

ratio at -0.2 V vs. Ag/AgCl showed the highest signal current and sensitivity towards H_2O_2 . Therefore, this potential was chosen for further amperometric detection of cholesterol.

Cholesterol detection. For cholesterol detection, cholesterol oxidase (ChOx) was directly dropped on the surface of the PB/CPANI/SPE. This enzyme immobilization method involves van der Waals forces, ionic bonding or hydrophobic forces.⁴³ The enzymatic reaction between cholesterol and the ChOx PB/CPANI/SPE is explained in Fig. 7. The flavin factor of ChOx catalyzes the oxidation and isomerization of cholesterol, yielding H_2O_2 .^{43,44} The H_2O_2 then underwent further electrocatalytic reduction at the PB/CPANI surface matrix to OH^- .

The immobilization of enzymes plays an important role in the success of the biosensor as it depends on how well the enzymes bind to the surface matrix.⁴⁵ Thus, the optimization of the ChOx volume was done to get the optimum volume of ChOx

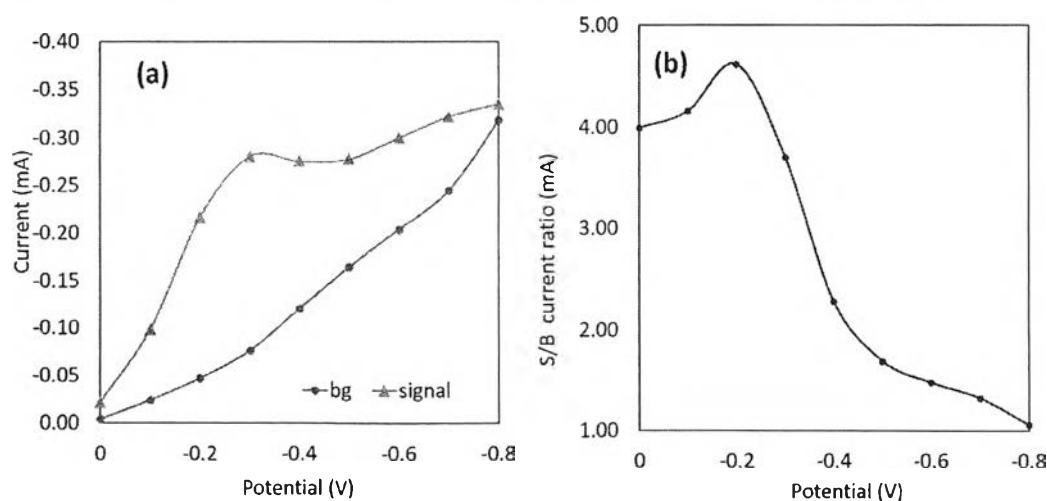


Fig. 6 (a) Hydrodynamic voltammogram of 1 mM H_2O_2 (signal) and background (bg) in 0.1 M phosphate buffer saline at pH 7.4 at a 90 s sampling time; (b) hydrodynamic voltammogram of signal-to-background current ratios (S/B).

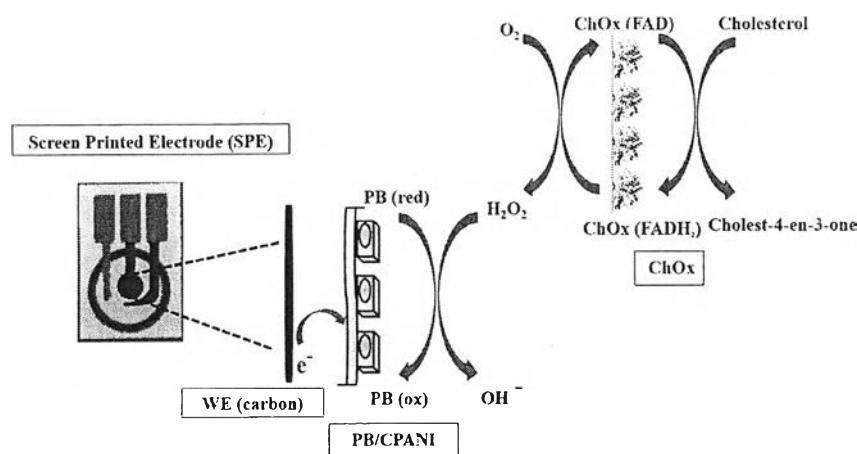


Fig. 7 The enzymatic reaction pathway between the cholesterol/enzyme/electrode paper-based biosensor and cholesterol.

on the PB/CPANI/SPE. Different volumes of ChOx were directly dropped on the PB/CPANI/SPE (Fig. 8). By using the optimum potential, the optimum volume obtained was 1.2 μL .

Further quantification of cholesterol was studied by applying the optimum volume of ChOx (1.2 μL) and the optimum electrocatalytic reduction potential ($-0.2\text{ V vs. Ag/AgCl}$) using the amperometric method. The steady-state current response at 90 s was recorded and used for the calibration curve plotting (Fig. 9). The calibration curve plotted shows a linearity between electrocatalytic current and concentration ranging from 0.6 mM to 6.0 mM with a correlation coefficient of 0.9983.

$$\text{Current (mA)} = 0.0583 (\text{cholesterol conc. (mM)}) + 0.0299 \quad (1)$$

From the calibration curve obtained, the limit of detection (LOD) and limit of quantification (LOQ) as well as the sensitivity of our proposed electrode can be calculated based on the equations given below:

$$\text{LOD} = (\text{SD} \times 3)/\text{slope} \quad (2)$$

$$\text{LOQ} = (\text{SD} \times 10)/\text{slope} \quad (3)$$

$$\text{Sensitivity} = \text{slope}/\text{area} \quad (4)$$

where SD is the standard deviation of the blank sample (PBS). The sensitivity calculated by using a projection area of the SPE was $411.7\ \mu\text{A cm}^{-2}\ \text{mM}^{-1}$. The LOD and LOQ calculated were 0.52 mM and 0.53 mM, respectively.

The comparisons of electrochemical performance between our PB/CPANI/SPE and previous selected work for cholesterol detection based on ChOx are listed in Table 1. As listed, our PB/CPANI/SPE showed competitive performance with high sensitivity in electrocatalytic cathodic current (interference free region) with a low potential value. The LOD value of this developed method revealed the suitability of this method as an efficient cholesterol detector since the normal cholesterol level in blood should be lower than $0.011 \times 10^3\ \text{mM}$.

Interference study. The co-electrooxidation of common interfering molecules in the detection of cholesterol may cause overestimation of the current signal. Therefore, the amperometric detection of cholesterol in the presence of glucose, ascorbic acid, uric acid, and paracetamol using the PB/CPANI/SPE was investigated. The current signal was recorded in the presence of interferents at normal levels in human serum (5 mM glucose (Glu), 1 mM ascorbic acid (AA), 1 mM uric acid (UA) and 0.1 mM paracetamol (Para)) during the detection of cholesterol at a working potential of $-0.2\text{ V vs. Ag/AgCl}$ (Fig. 10). The amperometric current signal showed an almost negligible effect for all interfering agents. Therefore, these results indicated that the proposed cholesterol biosensor showed an excellent performance where the influence of interfering agents can be greatly minimized. It could be said that the developed method is highly selective.

Reproducibility study. The reproducibility for five PB/CPANI/SPEs was evaluated by comparing the cathodic

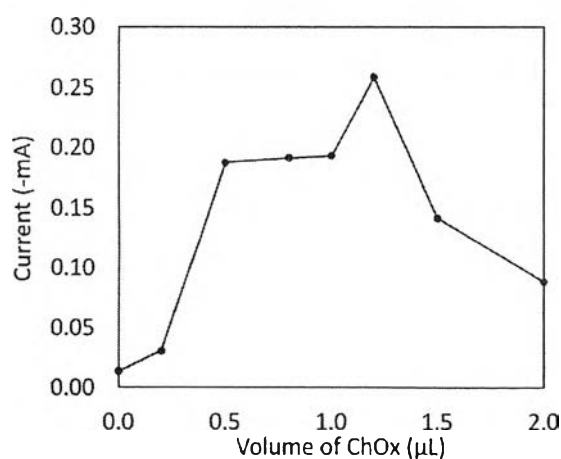


Fig. 8 The effect of the ChOx enzyme volume ($100\ \text{U mL}^{-1}$).

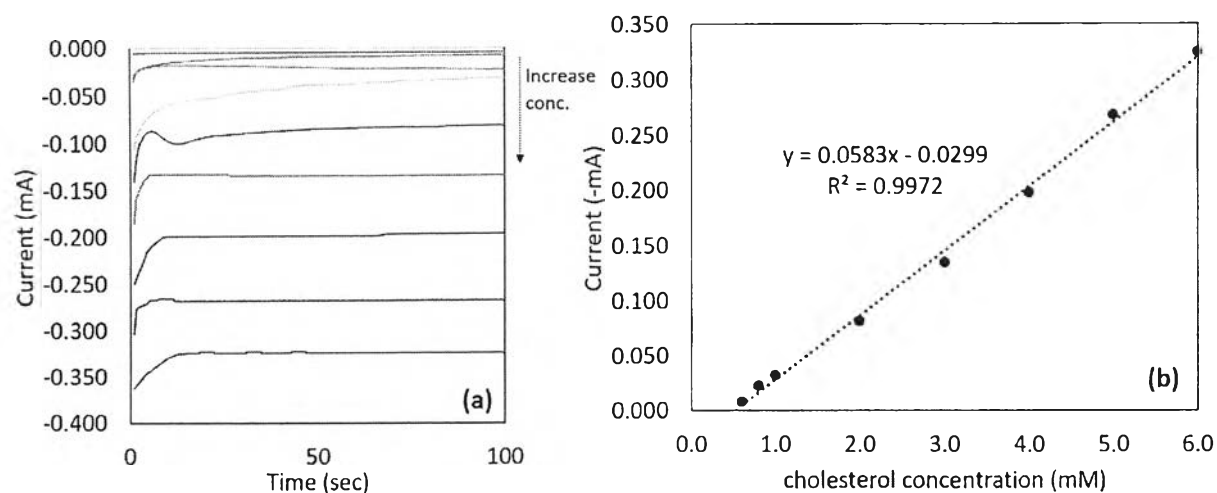


Fig. 9 (a) Chronoamperometry detection using the PB/CPANI/SPE at different cholesterol concentrations ranging from 0.6 mM to 6.0 mM; (b) calibration graph of the PB/CPANI/SPE in the detection of cholesterol at different cholesterol concentrations at a 90 s sampling time.

Table 1 The comparison of the performance of various cholesterol biosensors based on cholesterol oxidase^a

Electrode	Modification procedure	Applied potential (V vs. Ag/AgCl)	Sensitivity ($\mu\text{A mM}^{-1} \text{cm}^{-2}$)	LOD (mM)	Linear range (mM)	Reference
PB(NPs)/CPANI (90–100 nm)	Drop casting on the SPE	-0.2	411.7	0.52	0.6–6.0	This work
AuPt/chitosan/ILs	Electrodeposition	-1.0	90.7	0.01	0.05–6.2, 6.2–11.12	Safavi <i>et al.</i> (2011) ⁴⁶
PANI/MWCNT	Indium tin oxide (ITO)-coated glass plate	0.3	6.8	—	1.26–1.29	Dhand <i>et al.</i> (2008) ⁴⁷
CNT/chitosan	Deposited on Pt	0.4	44.0	0.005	—	Tsai <i>et al.</i> (2008) ⁴⁸
Graphene/PVP/PANI	Electro-spraying on the SPE	0.6	34.8	0.001	0.05–10.0	Ruecha <i>et al.</i> (2013) ⁶

^a Abbreviations: SPE, screen printed electrode; GCE, glassy carbon electrode; PVP, polyvinylpyrrolidone; CNT, carbon nanotube; MWCNT, multiwall carbon nanotube; and Pt, platinum electrode.

current of cholesterol. It was investigated by using the amperometric detection of cholesterol under optimal conditions. At 1, 3, and 6 mM of cholesterol, the relative standard deviation (RSD) was found to be 3.91%, 4.78%, and 5.47% ($n = 5$), respectively. Consequently, these results demonstrate good reproducibility of this paper-based device.

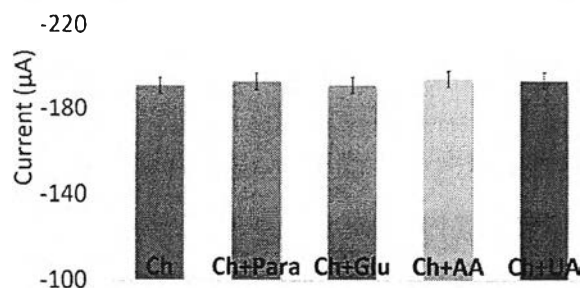


Fig. 10 Study of common interfering molecules in the detection of cholesterol.

Demonstration of cholesterol detection. To investigate the applicability to analytical samples, the PB/CPANI/SPE was further tested in bovine serum albumin (BSA) solution. Blank BSA was spiked with different concentrations of cholesterol (0.5, 1.0, 2.0, 4.0, and 6.0 mM). As seen in Table 2, the cholesterol concentration found for all concentrations showed good

Table 2 Determination of cholesterol in bovine serum albumin ($n = 3$)

Cholesterol concentration					
Added amount (mM)	Found amount (mM)	Accuracy ^a %	Recovery%	RSD%	
0.5	0.50 ± 0.015	0	100.3 ± 8.6	3.0	
1.0	1.04 ± 0.032	4	103.8 ± 9.9	3.0	
2.0	2.01 ± 0.047	0.5	101.0 ± 4.1	2.3	
4.0	4.01 ± 0.120	0.25	100.3 ± 4.2	3.0	
6.0	6.27 ± 0.200	4.5	104.4 ± 4.3	3.2	

^a Bias%: $\frac{(\text{found} - \text{added})}{\text{added}} \times 100\%$.

accuracy, recovery and acceptable precision results.³³ Thus, these results indicate that our fabricated PB/CPANI/SPE has demonstrated great potential for application in determining cholesterol levels.

Conclusion

The PB/CPANI/SPE exhibited excellent electrocatalytic activity towards the oxidation and reduction of H₂O₂. Furthermore, cholesterol oxidase (ChOx) was immobilized on the PB/CPANI/SPE to develop a highly sensitive amperometric cholesterol biosensor. The electrocatalytically reduced H₂O₂ generated during the enzymatic reaction of ChOx and cholesterol showed a linear curve with good sensitivity and a low detection limit. The proposed electrode was stable, and interference-free with good sensitivity and a low detection limit which make it a promising candidate to be applied for a wide range of applications of biosensors related to the detection of hydrogen peroxide as the product of the enzymatic reaction.

Acknowledgements

F. N. gratefully acknowledges the fellowship from the University of Malaya and Mymaster from the Ministry of Higher Education Malaysia for the financial support. Thanks to the ASEAN Scholarships program from Chulalongkorn University, Thailand for the financial support during the stay in Chulalongkorn University, Thailand. This research was financially supported by the University of Malaya Grant, UMRG-Program RP020B-16SUS and FP045-2014A. This research was also supported by the Thailand Research Fund through the Research Team Promotion Grant (RTA578005). P. R. would like to thank the financial support from the Graduate School of Chulalongkorn University for the Postdoctoral Fellowship (Ratchadaphiseksomphot Endowment Fund).

References

- S. Cao, L. Zhang, Y. Chai and R. Yuan, *Talanta*, 2013, **109**, 167–172.
- R. Manjunatha, G. S. Suresh, J. S. Melo, S. F. D'Souza and T. V. Venkatesha, *Talanta*, 2012, **99**, 302–309.
- X. Tan, M. Li, P. Cai, L. Luo and X. Zou, *Anal. Biochem.*, 2005, **337**, 111–120.
- D. S. Goodman, S. B. Hulley, L. T. Clark, C. Davis, V. Fuster, J. C. LaRosa, A. Oberman, E. J. Schaefer, D. Steinberg and W. V. Brown, *Arch. Intern. Med.*, 1988, **148**, 36–69.
- W. Kit-Anan, A. Olarnwanich, C. Sriprachubwong, C. Karuwan, A. Tuantranont, A. Wisitsoraat, W. Srituravanich and A. Pimpin, *J. Electroanal. Chem.*, 2012, **685**, 72–78.
- N. Ruecha, R. Rangkupan, N. Rodthongkum and O. Chailapakul, *Biosens. Bioelectron.*, 2014, **52**, 13–19.
- W. Dungchai, O. Chailapakul and C. S. Henry, *Anal. Chem.*, 2009, **81**, 5821–5826.
- X. Ge, A. M. Asiri, D. Du, W. Wen, S. Wang and Y. Lin, *TrAC, Trends Anal. Chem.*, 2014, **58**, 31–39.
- K. Singh, A. Kaur, A. Umar, G. Chaudhary, S. Singh and S. Mehta, *J. Appl. Electrochem.*, 2015, **45**, 253–261.
- F. A. Harraz, A. A. Ismail, S. Al-Sayari, A. Al-Hajry and M. Al-Assiri, *Sens. Actuators, B*, 2016, **234**, 573–582.
- X. Cao and N. Wang, *Analyst*, 2011, **136**, 4241–4246.
- A. S. Adekunle, B. O. Agboola, J. Pillay and K. I. Ozoemena, *Sens. Actuators, B*, 2010, **148**, 93–102.
- S. Mehta, K. Singh, A. Umar, G. Chaudhary and S. Singh, *Sci. Adv. Mater.*, 2011, **3**, 962–967.
- M. Ates, T. Karazehir and A. Sezai Sarac, *Curr. Phys. Chem.*, 2012, **2**, 224–240.
- Y.-Z. Long, M.-M. Li, C. Gu, M. Wan, J.-L. Duvail, Z. Liu and Z. Fan, *Prog. Polym. Sci.*, 2011, **36**, 1415–1442.
- P. H. C. Camargo, K. G. Satyanarayana and F. Wypych, *Mater. Res.*, 2009, **12**, 1–39.
- M. L. Yola and N. Atar, *Electrochim. Acta*, 2014, **119**, 24–31.
- M. L. Yola, T. Eren and N. Atar, *Electrochim. Acta*, 2014, **125**, 38–47.
- M. L. Yola, T. Eren and N. Atar, *Biosens. Bioelectron.*, 2014, **60**, 277–285.
- M. L. Yola, N. Atar, T. Eren, H. Karimi-Maleh and S. Wang, *RSC Adv.*, 2015, **5**, 65953–65962.
- O. Akyıldırım, G. Kotan, M. L. Yola, T. Eren and N. Atar, *Ionics*, 2016, **22**, 593–600.
- M. L. Yola, T. Eren, N. Atar, H. Saral and İ. Ermiş, *Electroanalysis*, 2016, **28**, 570–579.
- G. Kotan, F. Kardaş, Ö. A. Yokuş, O. Akyıldırım, H. Saral, T. Eren, M. L. Yola and N. Atar, *Anal. Methods*, 2016, **8**, 401–408.
- N. Atar, M. L. Yola and T. Eren, *Appl. Surf. Sci.*, 2016, **362**, 315–322.
- W. Lian, S. Liu, J. Yu, J. Li, M. Cui, W. Xu and J. Huang, *Biosens. Bioelectron.*, 2013, **44**, 70–76.
- D. Bandgar, S. Navale, S. Vanalkar, J. Kim, N. Harale, P. Patil and V. Patil, *Synth. Met.*, 2014, **195**, 350–358.
- X. Liu, Z. Nan, Y. Qiu, L. Zheng and X. Lu, *Electrochim. Acta*, 2013, **90**, 203–209.
- J. Katrlík, M. Valach and L. Jantošová, *Acta Fac. Pharm. Univ. Comenianae*, 2005, 116–124.
- T. Mizoguchi, T. Edano and T. Koshi, *J. Lipid Res.*, 2003, **45**, 396–401.
- J. P. Li and H. N. Gu, *J. Chin. Chem. Soc.*, 2006, **53**, 575–582.
- F. Scheller, D. Pfeiffer, F. Schubert, R. Reneberg and D. Kirstein, *Biosensors: Fundamental and Applications*, 1987.
- A. A. Karyakin, E. E. Karyakina and L. Gorton, *J. Electroanal. Chem.*, 1998, **456**, 97–104.
- M. L. Yola and N. Özaltın, *Rev. Anal. Chem.*, 2011, **30**, 29–36.
- M. L. Yola and N. Ozaltın, *Rev. Chim.*, 2011, **62**, 420–426.
- H. Gao, T. Jiang, B. Han, Y. Wang, J. Du, Z. Liu and J. Zhang, *Polymer*, 2004, **45**, 3017–3019.
- I. O. Ali, T. M. Salama, M. S. Thabet, K. S. El-Nasser and A. M. Hassan, *Mater. Chem. Phys.*, 2013, **140**, 81–88.
- G. Xie, P. Xi, H. Liu, F. Chen, L. Huang, Y. Shi, F. Hou, Z. Zeng, C. Shao and J. Wang, *J. Mater. Chem.*, 2012, **22**, 1033–1039.
- X. Yang, X. Chen, X. Zhang, W. Yang and D. G. Evans, *Sens. Actuators, B*, 2008, **134**, 182–188.

- 39 R. Vittal, K.-J. Kim, H. Gomathi and V. Yegnaraman, *J. Phys. Chem. B*, 2008, **112**, 1149–1156.
- 40 H. Ju, Z. Xueji and J. Wang, *NanoBiosensing: Principles, Development and Application*, Springer Science & Business Media, 2011.
- 41 L. Gao, J. Zhuang, L. Nie, J. Zhang, Y. Zhang, N. Gu, T. Wang, J. Feng, D. Yang and S. Perrett, *Nat. Nanotechnol.*, 2007, **2**, 577–583.
- 42 A. A. Karyakin, O. V. Gitelmacher and E. E. Karyakina, *Anal. Chem.*, 1995, **67**, 2419–2423.
- 43 G. Li, J. Liao, G. Hu, N. Ma and P. Wu, *Biosens. Bioelectron.*, 2005, **20**, 2140–2144.
- 44 S. K. Arya, M. Datta and B. D. Malhotra, *Biosens. Bioelectron.*, 2008, **23**, 1083–1100.
- 45 W. H. Scouten, J. H. Luong and R. S. Brown, *Trends Biotechnol.*, 1995, **13**, 178–185.
- 46 A. Safavi and F. Farjami, *Biosens. Bioelectron.*, 2011, **26**, 2547–2552.
- 47 C. Dhand, S. K. Arya, M. Datta and B. Malhotra, *Anal. Biochem.*, 2008, **383**, 194–199.
- 48 Y.-C. Tsai, S.-Y. Chen and C.-A. Lee, *Sens. Actuators, B*, 2008, **135**, 96–101.

DOI: 10.1002/elan.201500406

Development of Electrochemical Paper-based Glucose Sensor Using Cellulose-4-aminophenylboronic Acid-modified Screen-printed Carbon Electrode

Tipawan Rungsawang,^[a, b] Eakkasit Punrat,^[b] Jaclyn Adkins,^[c] Charles Henry,^{*, [c]} and Orawon Chailapakul^{*, [b, d]}

Abstract: The present work describes the fabrication of paper-based analytical devices (μ PADs) by immobilization of glucose oxidase onto the screen printed carbon electrodes (SPCEs) for the electrochemical glucose detection. The sensitivity towards glucose was improved by using a SPCE prepared from homemade carbon ink mixed with cellulose acetate. In addition, 4-aminophenyl-

boronic acid (4-APBA) was used as a redox mediator giving a lower detection potential for improvement selectivity. Under optimized condition, the detection limit was 0.86 mM. The proposed device was applied in real samples. This μ PAD has many advantages including low sample consumption, rapid analysis method, and low device cost.

Keywords: Paper-based analytical device · 4-aminophenylboronic acid (4-APBA) · Glucose · Biosensor

1 Introduction

Determination of glucose is very important, especially in the fields of healthcare, clinical, food and beverage industries [1–2]. In food and beverage industries, the determination of glucose is required for quality control and fermentation processes. [3]. In the clinical field, glucose determination is important because high glucose levels can indicate diabetes mellitus, insulin deficiency and hyperglycemia [4–5]. Normal concentrations of glucose are 3.5–5.5 mM in whole blood, 2.5–5.3 mM in serum, and 0.1–5.3 mM in urine [6]. Although conventional method of high performance liquid chromatography (HPLC) coupled with enzyme assays have been reported for the glucose determination, they require many steps while consuming of time, reagents and samples. Therefore, a simple, fast and low cost method is still needed to develop for the determination of glucose.

Here, several paper-based analytical devices were developed and used as a diagnostic devices. Since 2007 when Whitesides and co-workers demonstrated microfluidic devices made from photoresist-patterned paper or μ PADs, extensive efforts have been placed on developing low-cost sensors with using naked eyes colorimetric detection [7–9]. Moreover, other detection techniques such as absorption spectroscopy [10], chemiluminescence [11–12], and electrochemistry [13–18] have been proposed to provide better sensitivity and selectivity. Electrochemical detection is of particular interest when combined with a μ PAD due to its low cost, portability, high accuracy at low analyte concentrations, low sample consumption, and the ability for miniaturization.

Screen-printed carbon electrodes (SPCEs) have many advantages for μ PADs due to their low cost, ease of preparation, flexible design, and ease of modification by vari-

ous chemicals for sensing applications [19–22]. On the other hand, a bare SPCE lacks its sensitivity in trace analysis when it is compared with a modified electrode. Electrode modification can also reduce the effect of interferences at high over-potentials [23–24]. Hence, the type of modifying chemicals is important to investigate for each analysis. In this work, cellulose was chosen as a modifying chemical mixed with carbon ink, which was used for fabrication of SPCEs. Due to a network structure and a large number of porous, cellulose has a large surface area that is suitable for improvement of sensitivity of electrochemical detection.


Redox mediators are interesting for electrode modification in glucose biosensors because they can enhance the

[a] T. Rungsawang
Program in Biotechnology, Faculty of Science,
Chulalongkorn University, Phayathai Road, Pathumwan,
Bangkok 10330 Thailand

[b] T. Rungsawang, E. Punrat, O. Chailapakul
Electrochemistry and Optical Spectroscopy Research Unit,
Department of Chemistry, Faculty of Science, Chulalongkorn
University, Phayathai Road, Pathumwan, Bangkok 10330
Thailand
Tel.: +66-2-218-7615; Fax: +66-2-254-1309;
*e-mail: orawon.c@chula.ac.th

[c] J. Adkins, C. Henry
Department of Chemistry, Colorado State University, Fort
Collins, Colorado 80523-1872 USA
Tel.: +1-970-491-2852; Fax: +1-970-491-1801;
*e-mail: chuck.henry@colostate.edu

[d] O. Chailapakul
Center of Excellence for Petroleum, Petrochemicals, and
Advanced Materials, Chulalongkorn University, Patumwan,
Bangkok 10330, Thailand

 Supporting information for this article is available on the
WWW under <http://dx.doi.org/10.1002/elan.201500406>.

efficiency of electron transfer between glucose and the electrode surface as part of the enzymatic detection of glucose [25]. An oxidized redox mediator can be reduced instead of oxygen during the enzymatic assay, and then re-oxidized at the electrode surface while amperometric signal is obtained. Thus, mediators can improve the sensitivity and selectivity of the glucose determination at low levels in samples such as whole blood, blood serum, and urine [26]. Recently, there are several publications targeted at improving sensor performance using redox mediators [27–29]. In several examples, aminophenol and its derivatives are used as the redox mediator because they can react with several enzymes, and are also non-toxic and inexpensive [23,30].

Hence, a novel SPCE fabricated from cellulose-mixed carbon ink and modified by 4-aminophenylboronic acid (4-APBA) [31] was first developed on a μ PAD for electrochemical determination of glucose. Moreover, this glucose sensor was cheap (<0.07 USD per device), low consumption of reagents (2.5 μ L) and sample (25 μ L), and easy to fabricate. The μ PADs were modified with glucose oxidase to provide glucose selectivity. Under the optimized conditions, the detection limit of the developed μ PADs was found to be 0.86 mM and the μ PADs were used to analyze artificial blood serum, soft drink, sweet tea and apple juice with good accuracy that were acceptable with the traditional clinical diagnostic assays (using student t-test; $p < 0.05$). This proposed μ PADs would be an alternative biomarker for diagnostic of diabetes mellitus and for quality control in food and beverage industries.

2 Experimental

2.1 Chemicals and Reagents

D-(+)-glucose oxidase (from *Aspergillus niger*), trehalose, potassium ferricyanide, and potassium ferrocyanide were obtained from Sigma-Aldrich (St. Louis, MO, USA). Sodium chloride and monobasic/dibasic sodium phosphate were obtained from Fisher Scientific (Pittsburgh, PA, USA). The chemicals were in analytical grade and were used without further purification. All working standard solutions and sample solutions were prepared daily by dissolving in 0.1 M phosphate buffer solution (PBS) at pH 7.

2.2 Preparation of the Paper-based Analytical Devices

2.2.1 Wax-printing Technique

Filter paper (Whatman No 1, Cole-Parmer, IL, USA) was used for the preparation of the paper-based analytical devices. The filter paper was cut into A4 size (210 mm \times 297 mm), and then it was brought into a wax-printer (model of ColorQube 8870 DN, Xerox) at which a pattern of wax wells were simply printed via common computer software; the pattern was designed by Adobe® Illustrator® CS6 with radius of each well to be 3 mm (Figure 1a).

After that, the wax-printed paper was heated on a hot plate at 150 °C for 2 min. The wax melted and flowed along the thickness of the paper by capillary force. Next, the paper was allowed to cool down at room temperature ($22 \pm 2^\circ$). The wax provides a hydrophobic barrier to control the spreading out of sample and reagent flow while the inner circle of wax pattern is hydrophilic (Figure 1b). Next, a three-electrode system of electrochemical detection was prepared on the paper by screen-printing technique (see in Section 2.2.3)

2.2.2 Cellulose-mixed Carbon Ink

A cellulose-mixed carbon ink was in-lab prepared for fabrication of SPCE by the following steps. First, a cellulose acetate (Sigma-Aldrich, MO, USA) solution was prepared at a concentration of 7.5% w/w in ink solvent of 1:1 v/v cyclohexanone and acetone (Mallinckrodt Chemicals, NJ, USA). The mixture was mixed under magnetic stirrer for 2 h until cellulose acetate was dissolved. Next, 0.5 g of graphite powder (<20 nm) (Sigma-Aldrich, MO, USA) was added to 1.25 g of the mixture, and then mixed for 3 min to yield a homogeneous cellulose-mixed carbon ink.

2.2.3 Screen-printed Carbon Electrodes

Electrochemical detection was performed with a three-electrode system consisting of a working electrode (WE), a reference electrode (RE) and a counter electrode (CE). The three electrodes were prepared by screen printing with the cellulose-mixed carbon ink (Figure 1c). The screen template was designed via CorelDraw computer software and fabricated on a transparent sheet using a laser cutter (Zing 24 Laser, Epilog Laser, CO, USA). To reduce effects of uncompensated resistance, the WE (with geometric area of 3.14 mm²) was placed within 0.5 mm of the RE. The μ PADs were heated in an oven at 65 °C for 20 min to dry and remove the organic solvent in the ink. After that, a tape ring was placed on the μ PAD to definite the electrochemical detection area.

2.3 Modification of the μ PAD with the Redox Mediator and Glucose Oxidase Enzyme

Three microliters of 20 mM 4-APBA (Sigma-Aldrich, MO, USA) in 0.1 M PBS (pH 7) were dropped onto the wax well of the μ PAD and then allowed to dry at room temperature for 30 min. Next, the μ PAD was modified with 2.5 μ L of a solution containing 800 U mL⁻¹ glucose oxidase in 0.1 M PBS (pH 7) and 0.3 M trehalose. The μ PAD was dried again at room temperature for at least 20 min before use.

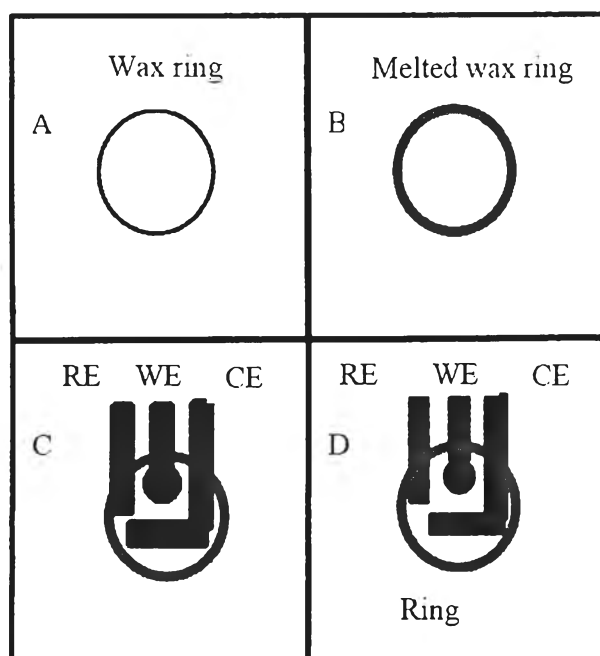


Fig. 1. The μ PAD in each preparation step of wax printing (a), wax melting (b), electrode screen-printing (c), and ring tape putting (d). WE is a working electrode; RE is a reference electrode; and CE is a counter electrode.

2.4 Electrochemical Method for the Determination of Glucose

The potentiostat used in this work was a CHI 1207A (CH Instruments, TX, USA). Cyclic voltammetry with a solution containing 1 mM each of ferricyanide and ferrocyanide in 0.1 M KCl was used to characterize bare and modified SPCEs. For the determination of glucose, 25 μ L of glucose standard solution or sample solution was introduced onto the μ PAD and then incubated for 3 min to dissolve the reagents, incubate and equilibrate the enzyme reaction. After that, chronoamperometry was used. Optimal parameters were investigated resulting in the use of an applied potential of 0.2 V. All experiments were performed at room temperature ($22 \pm 2^\circ$). Under optimal conditions, the developed μ PAD was applied to real samples including control samples of blood serum, soft drink, tea, juice, and energy drinks. Control samples of human serum (levels I and II, from Pointe Scientific, MI, USA) were mixed with 5.0 mL deionized water before analysis, according to supplier instructions.

3 Results and Discussion

Microfluidic devices made ordinary filter paper as the substrate material have been developed for various applications due to the low cost, ease of design and modification, and suitability for many detection techniques including spectroscopy, colorimetry, and electrochemistry [32–36]. Although such techniques have linearity ranges which are suitable for clinical test, detection limits are

still insufficient and the analysis times are more than 5 min. To improve limits of detection and reduce analysis time, this work reports the use of μ PAD with electrochemical detection using 4-APBA-cellulose-modified SPCE. The final cost of the μ PAD was very cheap about 0.1 USD per each as shown in Table S1.

3.1 Electrochemical Characterization of Cellulose-modified SPCE on μ PAD

To investigate the electrochemical performance of a cellulose-modified SPCE on μ PAD, ferri/ferrocyanate solution was used as a representative of electrochemically active specie because is a well-known reversible reaction with one electron transfer and widely used as a model analyte for characterization the modified electrode. Therefore, cellulose-modified SPCE was investigated electrochemical response compared with a bare SPCE by cyclic voltammetry in a solution containing 1 mM ferri/ferrocyanate in 0.1 M KCl. Typical cyclic voltammograms are shown in Figure 2. As seen, the cellulose-modified SPCE gave a higher oxidation current ($45.88 \pm 0.22 \mu\text{A}$) at peak potential of 0.3 V compared to a SPCE without cellulose acetate ($34.04 \pm 0.33 \mu\text{A}$). Based on the network structure and large number of porous of cellulose acetate, thus, the use of mixture between carbon ink and cellulose acetate provided the large surface area compared to those carbon ink leading to the improvement in the electrochemical sensitivity.

3.2 Effect of 4-APBA

4-APBA, a redox mediator, was chosen to modify the SPCE to improve the sensitivity and selectivity for the glucose determination. Various concentrations in the range of 20 to 35 mM of 4-APBA in PBS pH 7.0 were added in 2.5 μ L increments to the working electrode of each μ PAD. After drying at room temperature, the μ PADs were modified with 2.5 μ L of 200 U mL^{-1} glucose oxidase in 0.1 M PBS (pH 7) and 0.3 M trehalose. The effect of 4-APBA concentration on the determination of glucose was investigated at concentrations between 0 and 30 mM (Figure 3).

For all glucose concentrations, increasing 4-APBA concentrations increased the detection signal. At higher 4-APBA concentrations (30 and 35 mM), however, the linear range was narrow between 7 and 20 mM glucose concentration. Hence the optimal concentration of 4-APBA that provided the best combination of sensitivity and linear range was found to be 20 mM.

3.3 Effect of the Concentration of Glucose Oxidase

Enzymes are widely used to improve selectivity and sensitivity in sensors as well as providing lower limit of detection, thus, the investigation of enzyme concentration is next studied. For glucose oxidase, glucose reacts with oxygen to generate hydrogen peroxide and gluconic acid.

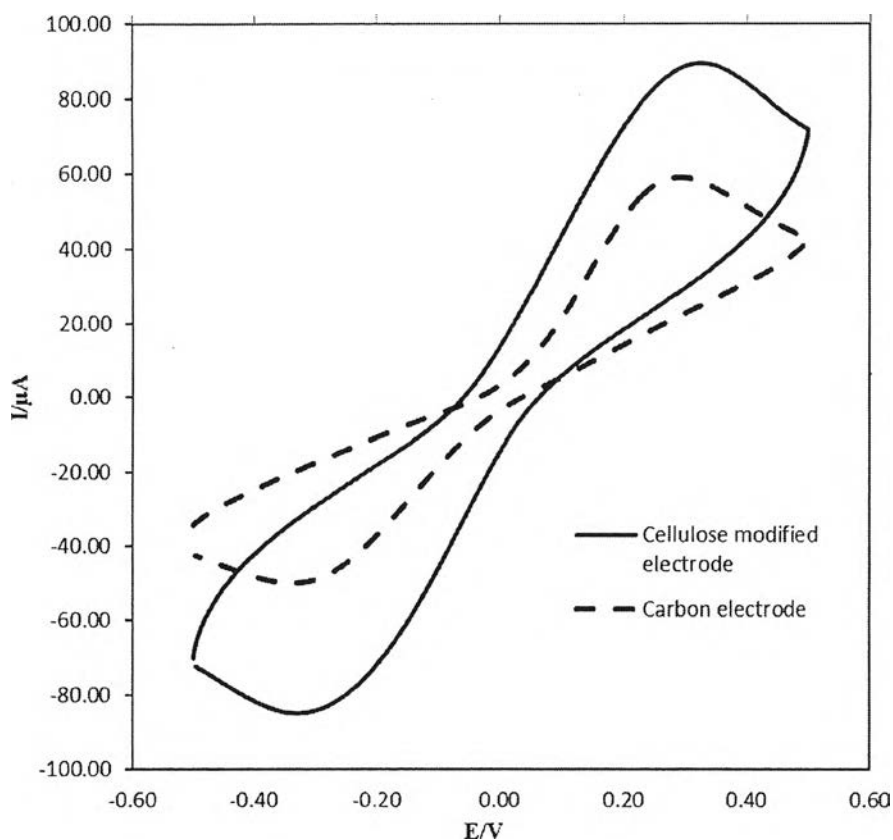


Fig. 2. Typical cyclic voltammograms with a potential scan rate of 0.5 V s^{-1} in a solution containing 1 mM ferri/ferrocyanate in 0.1 M KCl on a cellulose-modified SPCE (solid line) and a bare SPCE (dash line).

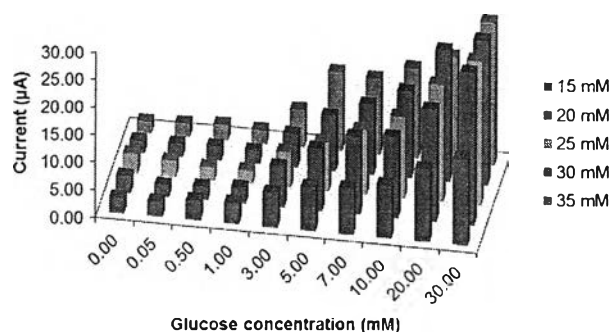


Fig. 3. Effect of the concentration of 4-APBA on anodic current of standard glucose solutions at various concentrations between 0 and 30 mM by chronoamperometry using μPADs with following conditions: sampling time of 25 s , applied potential of 0.2 V , concentration of glucose oxidase of 200 U mL^{-1} , reaction time of 3 min , and buffer solution of 0.1 mM PBS, $\text{pH } 7$.

Here, hydrogen peroxide is released as a product of this reaction and *p*-aminophenylboronic acid was reduced [37]. The reaction generates 4-aminophenol (4-AP) and tetrahydroxyborate ions with the 4-AP detected at the working electrode. Figure 4 shows linear electrochemical response as a function of the amount of glucose oxidase deposited on the electrode. In this example, glucose concentrations ranging from 0 and 100 mM were tested using

the various concentrations of glucose oxidase (200 – 1200 U mL^{-1}). The anodic current response was directly proportional to the glucose oxidase concentration up to 1200 U mL^{-1} . The response current obtained from 1200 U mL^{-1} glucose oxidase was higher than that obtained from 800 U mL^{-1} glucose oxidase. However, the concentration of 800 U mL^{-1} glucose oxidase was selected to use for the subsequent work because this concentration provided a wider linear range. In addition, to compromise between signal and cost of enzyme, an enzyme concentration of 800 U mL^{-1} was chosen as optimal.

3.4 Effect of the Reaction Time

In this work, the response signal was obtained within 25 sec . However, the enzymatic process was required the waiting time or reaction time to dissolve, incubate, and equilibrate the enzyme reaction before the signal was detected by chronoamperometry. Using the reaction times in the range of 0 and 30 min , it can be observed that the current response increases up to 15 min and then remains constant (data not shown). Given the ultimate goal of fast response times, 15 min was selected to compare with 3 min to determine the effect of time on linear range. Figure 5 shows the linear range was not improved as the time increased because of a limitation of substrate (glu-

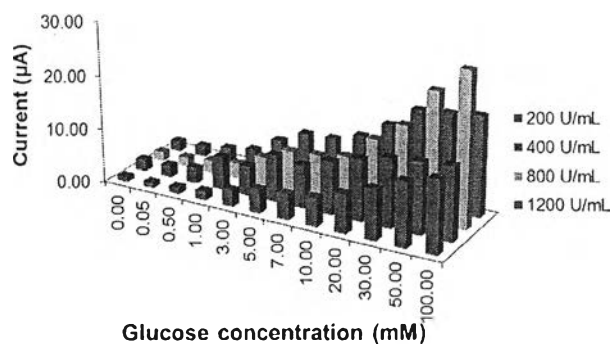


Fig. 4. Effect of the concentration of glucose oxidase on anodic current of standard glucose solutions at various concentrations between 0 and 100 mM by chronoamperometry using μ PADs with following conditions: sampling time of 25 s, applied potential of 0.2 V, concentration of 4-APBA of 20 mM, reaction time of 3 min, and buffer solution of 0.1 mM PBS, pH 7.

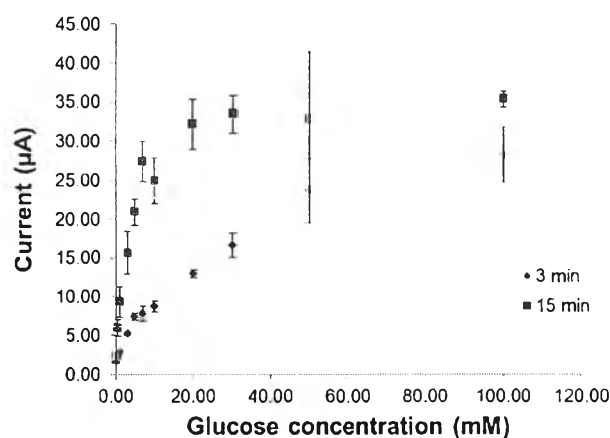


Fig. 5. Relationship between glucose concentration and anodic current obtained from chronoamperometry using μ PADs with different reaction times of 3 min and 15 min. Other experimental conditions are applied potential of 0.2 V, concentration of 4-APBA of 20 mM, concentration of glucose oxidase of 800 U mL^{-1} , and buffer solution of 0.1 mM PBS, pH 7.

cose). As a result, the reaction time of 3 min was selected to use in the chronoamperometric experiments.

3.5 Effect of Potential

Due to the pseudo-reference electrode, the electrode cannot maintain an accurately constant potential, however this reference electrode can be used for a specific condition. To obtain the correct potential for 4-AP, the investigation of the reasonable potential for the detection using the proposed SPCE was studied by hydrodynamic voltammetry and found that the use of applied potential of 200 mV is reasonable for detection 4-AP as shown in Figure 6. Chronoamperometry was used to determine the optimal detection potential in the range of 50 to 350 mV vs cellulose-modified pseudo-reference electrode. While increasing the detection potential increased the analyte

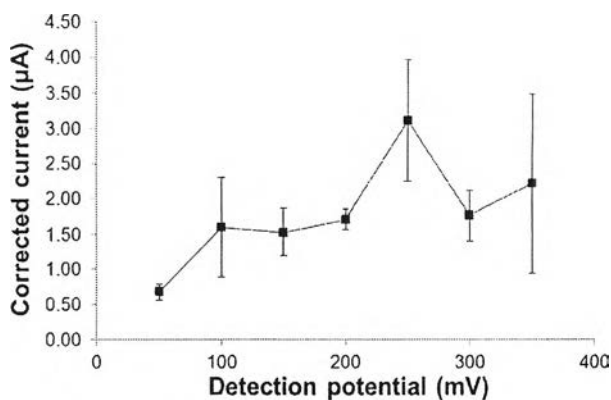


Fig. 6. Effect of applied potentials between 50 and 350 mV on corrected currents (subtracted sample signal with a blank signal) of 1.0 M glucose by chronoamperometry using μ PADs with following conditions: concentration of 4-APBA of 20 mM, concentration of glucose oxidase of 800 U mL^{-1} , reaction time of 3 min and buffer solution of 0.1 mM PBS, pH 7.

current, the background current also increased significantly. Figure 6 shows a comparison of signal to noise ratio as a function of detection potential. The signal to noise ratio reached a maximum at 250 mV versus the carbon reference electrode. However, the standard deviation of this point was higher than 200 mV and the higher potential can generate more matrix interference. As a result, a detection potential of 200 mV vs cellulose-modified pseudo-reference electrode was selected for the further studies.

3.6 Repeatability

The paper-based analytical devices with modified electrode were shown a good repeatability of the determination of glucose. The relative standard deviation (RSD) for 10 times of 5.0 mM and 30.0 mM were not over 6.52 %.

3.7 Analytical Performance

At 25 sec, the anodic current was recorded while obtained the steady state under the optimal condition to generate a calibration curve and linearity (Figure 7). To establish the suitable concentration range for glucose determination, the analyte concentration and response current was demonstrated in a wide range (0.05–100 mM). Linear calibration of the anodic current against the glucose concentrations within a range of 0 and 100 mM, and the coefficient of determination (R^2) was 0.992. LOD of 0.86 mM and LOQ of 2.85 mM for glucose were calculated from the 3 and 10 times of signal that produced from the standard deviation of blank ($n = 10$).

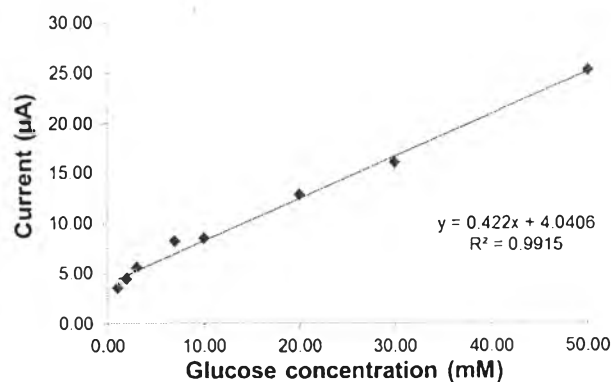


Fig. 7. Relationship between glucose concentration and anodic peak currents obtained from chronoamperometry using μ PADs with following conditions: applied potential of 0.2 V, concentration of 4-APBA of 20 mM, concentration of glucose oxidase of 800 U mL^{-1} , reaction time of 3 min and buffer solution of 0.1 mM PBS, pH 7.

3.8 Analytical Application

In order to evaluate the electrochemical paper-based analytical devices with the artificial blood serum samples were prepared with glucose in two levels, 5.0 and 30.0 mM. The samples were analyzed without any pre-treatment and the results obtained using the proposed method was to be satisfied. The recovery values were obtained in the range of 92.58–102.64%. Furthermore, soft drink (diet), apple juice, and sweet tea were successfully analyzed using this proposed μ PAD with acceptable results compared with the labelled values by student's t-test at 95% confident level. This proposed glucose sensor was used at low over-potential, which common interferences such as uric acid, ascorbic acid and acetaminophen did not affect the glucose determination. This results obtained are agreed with the previous research. [31]. The important mention of this work that the analysis time is short. The paper-based analytical devices can be analyzed in less than 4 min, including enzymatic reaction and the steps of electrochemical detection.

4 Conclusions

The work presented here has clearly demonstrated that glucose sensor using screen-printed carbon electrodes (modified with cellulose acetate) with 4-APBA as a mediator using with paper-based analytical devices to improve the performance for the glucose determination.

Enzymatic reaction and electrochemical detection can be performed within 3 min in the detection zone that was the hydrophilic circular area created on paper. The enzyme and redox mediator was added into the detection zone without any step of modification electrode. Also, the proposed devices have a long linearity, high sensitivity and good stability.

Thus, the new biosensor has been successfully applied to the glucose determination in human blood serum, soft

drink (diet), apple juice, and sweet tea. We believe this low-cost devices can be extended to use in plant materials, and food products.

Acknowledgements

TR gratefully acknowledges financial support from the office of the Higher Education Commission, Thailand under the program strategic scholarships for frontier research network for the joint PhD program Thai Doctoral Degree (Grant No. 73/2551), OC thanks the Thailand Research Fund through Research Team Promotion Grant (RTA5780005), EP is grateful for financial support from Ratchadaphiseksomphot Endowment Fund for Postdoctoral Fellowship, Chulalongkorn University.

References

- [1] A. L. Galant, R. C. Kaufman, J. D. Wilson, *Food Chemistry* **2015**, *188*, 149–160.
- [2] I. Delfino, C. Camerlingo, M. Portaccio, B. D. Ventura, L. Mita, D. G. Mita, M. Lepore, *Food Chemistry* **2011**, *127*, 735–742.
- [3] N. G. Patel, S. Meier, K. Cammann, G. C. Chemnitz, *Sensors and Actuators B* **2001**, *75*, 101–110.
- [4] D. Kuppinger, W. H. Hartl, *Nutrition* **2013**, *29*, 708–712.
- [5] C. J. Shih, E. A. Smith, *Analytica Chimica Acta* **2009**, *653*, 200–206.
- [6] P. B. Luppá, C. Müller, A. Schichtiger, H. Schlebusch, *Trends in Analytical Chemistry* **2011**, *30*, 887–898.
- [7] A. W. P. Martinez, S. T.; Butte, G. M. Whitesides, *Angew. Chem. Int. Ed.* **2007**, *46*, 1318–1320.
- [8] A. W. Martinez, S. T. Philips, E. Carrilho, S. W. Thomas, H. Sindi, G. M. Whitesides, *Analytical Chemistry* **2008**, *80*, 3699–3707.
- [9] A. W. Martinez, S. T. Philips, G. M. Whitesides, E. Carrilho, *Analyst* **2010**, *82*, 3–10.
- [10] N. Ratnarathorn, O. Chailapakul, C. S. Henry, W. Duangchai, *Talanta* **2012**, *99*, 552–557.
- [11] J. L. Delaney, C. F. Hogan, J. F. Tian, W. Shen, *Analytical Chemistry* **2011**, *83*, 1300–1306.
- [12] J. H. Yu, L. Ge, J. D. Huang, S. M. Wang, S. G. Ge, *Lab on a Chip* **2011**, *11*, 1286–1291.
- [13] M. Florescu, C. M. A. Brett, *Talanta* **2005**, *65*, 306–312.
- [14] K. Abe, K. Suzuki, D. Citterio, *Analytical Chemistry* **2008**, *80*, 6928–6934.
- [15] W. Dungchai, O. Chailapakul, C. S. Henry, *Analytical Chemistry* **2009**, *81*, 5821–5826.
- [16] Z. H. Nie, F. Deiss, X. Y. Liu, O. Akbulut, G. M. Whitesides, *Lab on a Chip* **2010**, *10*, 3163–3169.
- [17] Z. H. Nie, C. A. Nijhuis, J. Gong, X. Chen, A. Kumachev, A. W. Martinez, M. Narovlyansky, G. M. Whitesides, *Lab on a Chip* **2010**, *10*, 477–483.
- [18] L. Y. Shiroma, M. Santhiago, A. L. Gobbi, L. T. Kubota, *Analytica Chimica Acta* **2012**, *725*, 44–50.
- [19] A. W. Stephen, P. H. John, *Analytica Chimica Acta* **1990**, *231*, 203–212.
- [20] M. Johirul, A. Shiddiky, R. E. Kim, Y. B. Shim, *Electrophoresis* **2005**, *26*, 3043–3054.
- [21] N. German, A. Ramanaviciene, J. Voronovic, A. Ramanavicius, *Microchimica Acta* **2010**, *168*, 221–229.
- [22] L. Berisha, K. Kalcher, A. Hajrizi, T. Arbneshi, *American Journal of Analytical Chemistry* **2013**, *4*, 27–35.

- [23] M. L. Fultz, R. A. Durst, *Analytica Chimica Acta* **1982**, *140*, 1–18.
- [24] J. Liu, J. Wang, *Food Technology and Biotechnology* **2001**, *39*, 55–58.
- [25] A. K. Amine, J. M.; Patriarche, *Talanta* **1991**, *38*, 107–110.
- [26] E. H. Yoo, S. Y. Lee, *Sensors* **2010**, *10*, 4558–4576.
- [27] F. Ricci, A. Amine, C. S. Tuta, A. A. Ciucu, F. Lucarelli, G. Palleschi, D. Moscone, *Analytica Chimica Acta* **2003**, *485*, 111–120.
- [28] J. Razumiene, V. Gereviciene, A. Vilkanauskyte, L. Marcinkeviciene, I. Bachmotova, R. Meskys, V. Laurinavicius, *Sensors and Actuators B* **2003** *95*, 378–383.
- [29] M. E. Ghica, C. M. A. Brett, *Analytica Chimica Acta* **2005**, *532*, 145–151.
- [30] M. Senel, C. Nergiz, M. Dervisevic, E. Cevik, *Electroanalysis* **2013**, *5*, 1194–1200.
- [31] M. Santhiago, L. T. Kubota, *Sensors and Actuators B* **2013**, *177*, 224–230.
- [32] J. Noiphung, T. Songjaroen, W. Dungchai, C. S. Henry, O. Chailapakul, W. Laiwattanapaisal, *Analytica Chimica Acta* **2013**, *788*, 39–45.
- [33] P. Rattanarat, W. Dungchai, D. M. Cate, W. Siangproh, J. Volckens, O. Chailapakul, C. S. Henry, *Analytica Chimica Acta* **2013**, *800*, 50–55.
- [34] M. Santhiago, C. S. Henry, L. T. Kubota, *Electrochimica Acta* **2014**, *130*, 771–777.
- [35] C. R. Ispas, G. Crivat, S. Andreescu, *Analytical Letters* **2012**, *45*, 168–186.
- [36] B. Liu, D. Du, X. Hua, X.-Y. Yu, Y. Lin, *Electroanalysis* **2014**, *26*, 1214–1223.
- [37] D. Das, D. M. Kim, D. S. Park, Y. B. Shim, *Electroanalysis* **2011**, *23*, 2036–2041.

Received: June 16, 2015

Accepted: July 15, 2015

Published online: August 14, 2015

Boron Doped Diamond Paste Electrodes for Microfluidic Paper-Based Analytical Devices

Siriwan Nantaphol,[†] Robert B. Channon,[‡] Takeshi Kondo,[§] Weena Siangproh,^{||} Orawon Chailapakul,^{*,†} and Charles S. Henry^{*,‡}

[†]Department of Chemistry, Faculty of Science, Chulalongkorn University, Patumwan, Bangkok 10330, Thailand

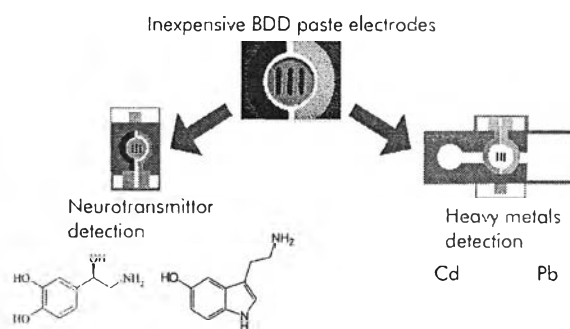
[‡]Department of Chemistry, Colorado State University, Fort Collins, Colorado 80523, United States

[§]Department of Pure and Applied Chemistry, Faculty of Science and Technology, Tokyo University of Science, 2641 Yamazaki, Noda, Chiba 278-8510, Japan

^{||}Department of Chemistry, Faculty of Science, Srinakharinwirot University, Sukhumvit 23, Wattana, Bangkok 10110, Thailand

Supporting Information

ABSTRACT: Boron doped diamond (BDD) electrodes have exemplary electrochemical properties; however, widespread use of high-quality BDD has previously been limited by material cost and availability. In the present article, we report the use of a BDD paste electrode (BDDPE) coupled with microfluidic paper-based analytical devices (μ PADs) to create a low-cost, high-performance electrochemical sensor. The BDDPEs are easy to prepare from a mixture of BDD powder and mineral oil and can be easily stencil-printed into a variety of electrode geometries. We demonstrate the utility and applicability of BDDPEs through measurements of biological species (norepinephrine and serotonin) and heavy metals (Pb and Cd) using μ PADs. Compared to traditional carbon paste electrodes (CPE), BDDPEs exhibit a wider potential window, lower capacitive current, and are able to circumvent the fouling of serotonin. These results demonstrate the capability of BDDPEs as point-of-care sensors when coupled with μ PADs.



Since microfluidic paper-based analytical devices (μ PADs) were first reported in 2007 for multiplexed diagnostic detection,¹ they have emerged as a promising technology to address the growing need for simple, quantitative, and point-of-need assay platforms. μ PADs provide the advantages of low cost, low sample consumption, ease of use, portability, and ease of disposability, making them ideal sensors for resource-limited settings.² Moreover, flow can be generated via capillary forces, precluding the need for mechanical or electrical pumps.³ The hydrophobic barriers which constrain the flow can be easily manufactured by a variety of methods, such as wax printing,⁴ photolithography,⁵ or printing of hydrophobic polymers.^{6,7} Furthermore, μ PADs are compatible with many classical detection motifs such as colorimetry,^{4,8} electrochemistry,^{5,9} electrochemiluminescence,^{10,11} chemiluminescence,^{12,13} and fluorescence.^{14,15}

Electrochemical detection is a particularly attractive partner for μ PADs, due to its instrumental simplicity, fast analysis times, high sensitivity, high accuracy, simple instrumentation, and low power requirements. Electrochemical paper-based analytical devices (ePADs), first reported in 2009 by Dungchai et al.,⁵ have used various electrode materials (e.g., carbon, metals, microwires, and nanoparticles) and fabrication techniques (e.g., screen/stencil-printing, pencil/pen drawing,

inkjet-printing, and wire placement).^{16–23} Carbon electrodes, especially screen-printed carbon paste electrodes (CPE), have been extensively employed in ePADs due to their easy fabrication, low cost, and potential for large-scale production.^{24,25} Despite these advantages, CPEs are prone to surface fouling, which negatively impacts on analyte adsorption, electron-transfer kinetics, and electrocatalysis, resulting in poor limits of detection and a reduced device lifetime.^{26–28} The electrochemical response of the CPEs is also heavily dependent on the manufacturing process, where key small technical details are difficult to include in publications or reports. Furthermore, commercial CPE are often more expensive than their homemade counterparts, and are limited by the available geometries and functionalities of the electrodes. Finally, though other electrode materials have been employed as disposable electrodes, such as sputtered Au or Pt, these are often more difficult in terms of time and cost to make, and are significantly more prone to surface fouling than CPEs, limiting their applicability.

Received: December 20, 2016

Accepted: March 6, 2017

Published: March 6, 2017

Boron doped diamond (BDD) is a carbon-based p-type semiconductor, which exhibits quasi-metallic conductivity at boron doping concentrations of around 1 boron atom per 1700 carbon atoms.²⁹ The attractive features of BDD electrodes include remarkably low background currents, high mechanical robustness, stability in strong alkaline and acidic media, very wide potential window, and a high resistance to fouling.^{30–32} As with the vast majority of carbon-based electrode materials, the particular properties of the BDD depend on the synthesis and processing. For example, freestanding BDD electrodes exhibit very low background currents and a particularly wide potential window, due to the minimal sp² carbon content, but are often difficult and costly to manufacture and process, requiring highly specialized machinery and techniques for polishing and sealing.³³ In contrast, thin-film BDD electrodes are easier to manufacture; they are typically grown by chemical vapor deposition on a silicon wafer substrate.^{34,35} However, the electrochemical cell is typically clamped to the thin-film electrode,³⁶ which limits the available electrode and cell geometries and applications. Freestanding and thin-film BDD electrodes have been previously coupled with microfluidic devices to combine the electrochemical advantages of BDD with the higher sensitivities and lower detection limits afforded through convective flow,^{37,38} and this remains an active research area in the field.^{39,40} However, currently available commercial and academic BDD electrodes are incompatible with point-of-care sensors, in terms of limited geometry, manufacturing time, and cost.

Conductive BDD powder was first demonstrated by Fischer and Swain in 2005.⁴¹ The BDD powder is easily prepared from an insulating diamond powder substrate (8–12 μm diameter) through microwave plasma-assisted chemical vapor deposition (MPCVD). Combination of the BDD powder with a conducting ink, followed by screen printing, yields a BDD paste electrode (BDDPE), which can potentially overcome the aforementioned limitations of conventional BDD electrodes.^{42–44} Specifically, these BDDPE are an attractive alternative to conventional BDD electrodes in terms of lower cost, simpler and faster electrode fabrication, and are ideal as a disposable and portable platform. Additionally, previous investigations with a simple BDDPE have demonstrated reduced electrode fouling for dopamine electrooxidation compared to CPEs, suggesting that the BDDPE will outperform conventional CPEs.⁴³

In this work, we demonstrate the use of BDD powder for the fabrication of disposable BDDPEs in a μPAD platform. Electrode performance is contrasted with conventional CPEs and traditional BDD electrodes. To demonstrate the scope of this device, the BDDPE ePADs are employed for two applications; the quantitative detection of norepinephrine (NE) and serotonin (5-hydroxytryptamine, 5-HT) and the anodic stripping voltammetry of heavy metals. The simultaneous determination of NE and 5-HT is of great importance, as low levels of NE and 5-HT have been related to several disorders, including depression, migraine, and anxiety.⁴⁵ However, previous investigations with CPEs have found significant electrode fouling with 5-HT.^{46,47} BDD is expected to alleviate this problem due to the chemical inertness of the surface, as has been previously shown on conventional freestanding and thin-film electrodes.^{48,49} Additionally, NE and 5-HT have similar electrooxidation potentials on carbon electrodes, making codetection challenging.⁵⁰ Therefore, an electrochemically reduced grapheme oxide (ERGO)-modified

BDDPE is used herein for simultaneous NE and 5-HT detection due to its high electroactive surface area, rapid electron transfer, and small charge-transfer resistance. In addition, we further demonstrate the application of BDDPEs in a flow-through μPAD , for the simultaneous determination of two heavy metals, Cd(II) and Pb(II). The presence of these toxic elements in the environment is of particular concern due to their adverse effects on ecosystems and human health.^{51,52} Using a flow-through design, coupled with square-wave anodic stripping voltammetry (SWASV), preaccumulation can be carried out online, enhancing the efficiency for the metal deposition and, consequently, improving the detection sensitivity. Aside from their individual importance as analytical targets, NE, 5-HT, Cd(II), and Pb(II) are important analytes as they allow direct comparison to other studies which have previously investigated these species using CPEs, freestanding BDD electrodes, and thin-film BDD electrodes, in order to demonstrate the significant potential of BDDPE as point-of-care sensors.

■ EXPERIMENTAL SECTION

Materials, Equipment, and Chemicals. BDD powder was prepared through a previously reported procedure.⁴³ In short, natural diamond powder (Micron+SND, Element Six, particle diameter <500 nm) was washed in aqua regia and 30% hydrogen peroxide at 60 °C for 30 min to remove possible metallic contaminants, followed by rinsing with Milli-Q water and drying. To grow BDD on the substrate powder surface, the pretreated diamond powder was spread on a molybdenum susceptor and subjected to MPCVD for 8 h, using previously described conditions.⁴³ Finally, the BDD powder was ground using a mortar and pestle and oxidized in air using a muffle furnace at 425 °C for 5 h to remove graphitic impurities, resulting in an oxygen-terminated surface.⁵³

Graphene oxide (GO) was acquired from XF Nano, Inc. (Nanjing, China). 5-HT was acquired from Alfa Aesar (Ward Hill, MA). NE, potassium phosphate monobasic, sodium phosphate dibasic, and standard solutions of all metals Cd(II), Pb(II), and Bi(III) were acquired from Sigma-Aldrich (St. Louis, MO). Acetic acid, sodium acetate, and light mineral oil were acquired from Fischer Scientific (New Jersey). Potassium ferrocyanide ($\text{Fe}(\text{CN})_6^{4-}$) was acquired from Mallinckrodt (St. Louis, MO). All chemicals were analytical grade and used as received, and all solutions were prepared by using purified water (18.2 M Ω cm) from a Milli-Q Millipore water purification system.

Whatman 1 chromatography paper was acquired from Fisher Scientific (Pittsburgh, PA). A XEROX Phaser 8860 printer was used to print wax patterns on μPAD s following established protocols. An Isotemp hot plate from Fischer Scientific, set at 150 °C, was used to melt the wax on the paper. Ag/AgCl ink from Gwent Group (Torfaen, U.K.) was used to construct the conducting pads and reference electrode (RE). Carbon ink from Ercon Incorporated (Wareham, MA) was used for the construction of the counter electrode (CE).

Device Fabrication. Wax printing and Whatman 1 chromatography paper were selected for the construction of the devices following previously reported methods.⁵⁴ The CE, RE, and conducting pads on wax-printed paper were stencil-printed in-house. For fabrication of the BDD paste working electrode (WE), stencil-printed Ag/AgCl on a transparency sheet substrate was prepared as a conducting pad. To minimize BDD paste consumption, a second stencil containing three

smaller openings (0.1 mm × 2 mm rectangles) was fabricated using a laser engraving system (Epilog, Golden, CO). The BDD paste WE was prepared by mixing BDD powder and mineral oil (70:30, w/w) and stencil-printed onto the mask. A photograph of the BDDPEs is shown in Figure 1a. Double-sided tape was

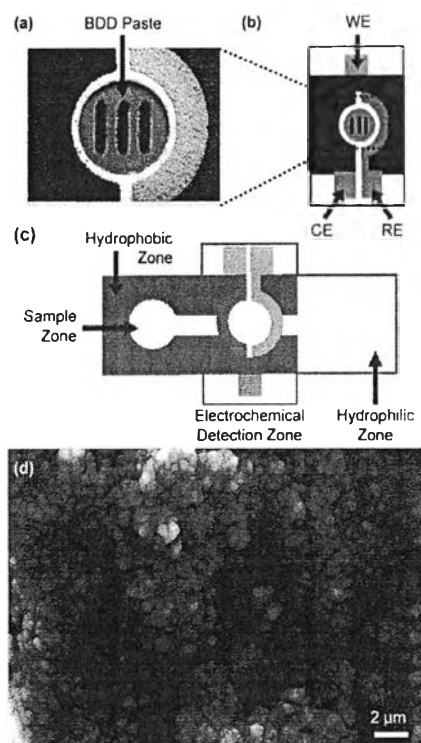


Figure 1. Device design for BDDPE: (a) photograph of the BDDPE, (b) ePAD design for NE and 5-HT analysis, (c) μ PAD design for the measurement of Pb and Cd, and (d) SEM image of the BDDPE.

used to attach the CE (stencil-printed carbon) and RE (stencil-printed Ag/AgCl) section to the WE section. Figure 1b shows the device design for NE and 5-HT detection, which was carried out by pipetting a 50 μ L aliquot atop the BDDPE. For heavy metal analysis, a flow-through pattern μ PAD was designed, consisting of a sample zone (where a 50 μ L sample

aliquot was added), an electrochemical detection zone, and a hydrophilic area at the outlet of the paper channel, as shown in Figure 1c. Further details of the fabrication procedures are provided in the Supporting Information, Figure S1.

Electrochemical Detection. All electrochemical experiments were performed with a model 660B potentiostat (CH Instruments, Austin, TX) at room temperature (22 ± 1 °C). For NE and 5-HT detection, an ERGO-modified BDDPE was used as the WE. Details of the ERGO-modified electrode preparation is described in Supporting Information, section 2. Standard solutions of NE and 5-HT were prepared in 0.1 M phosphate buffer (PBS) pH 8.0, and a 50 μ L aliquot was used for the experiments. For differential pulse voltammetry (DPV), an amplitude of 60 mV, potential increment of 4 Hz, and a pulse width of 0.05 s were used.

For Pb and Cd detection, SWASV was employed with the flow-through device for the simultaneous determination of Cd(II) and Pb(II). All standard metals were prepared in 0.1 M acetate buffer pH 4.5. Bismuth-modified BDDPE were used as WE, prepared by chronoamperometry in a 4 ppm Bi(III) solution at -1.2 V for 20 min. A 50 μ L aliquot was added to the sample zone, and SWASV was performed after the solution flowed to electrochemical detection zone (ca. 1 min). SWASV used a frequency of 25 Hz, potential increment of 15 mV, and an amplitude of 50 mV, with an electrochemical deposition step at -1.2 V for 5 min, an equilibration period of 5 s, and a square-wave voltammetric stripping range of -1.1 to -0.5 V.

RESULTS AND DISCUSSION

Characterization of BDD Paste Electrodes. The BDDPE morphology was characterized by scanning electron microscopy (SEM) as shown in Figure 1d. The BDDPE has a homogeneous distribution of ~ 1 μ m sized particles, with a surface roughness of tens of micrometers, which is in agreement with previous studies on BDDPEs.⁴³ Furthermore, the boron concentration can be estimated from the carrier concentration of the thin-film growth material, through a Hall effect measurement,⁵⁵ yielding a boron concentration of $\sim 10^{20}$ – 10^{21} boron atoms/cm³, suggesting the BDDPEs should have metallic conductivity.⁵⁶ The BDDPE quality was then characterized and contrasted with a CPE via double layer capacitance (C_{dl}) and solvent window measurements, as shown in Figure 2, parts a and b, respectively. Cyclic voltammograms (CVs) were run between -0.1 and 0.1 at 0.2 V s⁻¹ in 0.1 M

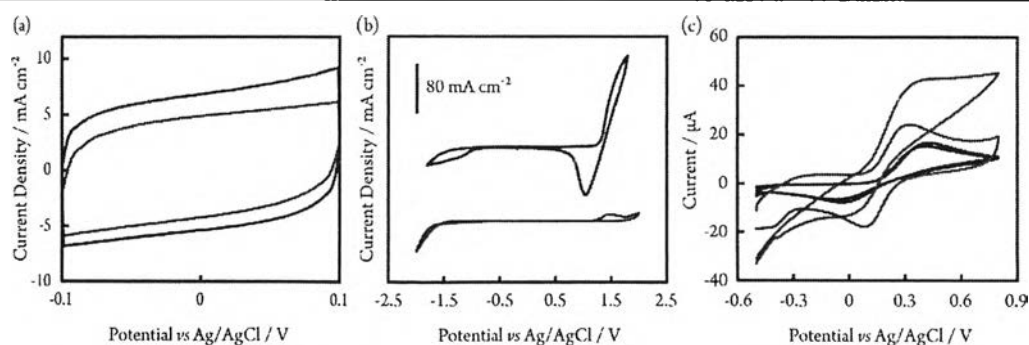


Figure 2. (a) CVs in aerated 0.1 M KNO₃, recorded at 0.2 V s⁻¹ over the potential range of -0.1 to 0.1 V, for the BDDPE (red line) and CPE (blue line). (b) CVs in 0.1 M KNO₃, recorded at 0.2 V s⁻¹ over the potential range of -2 to 2 V, for the BDDPE (red line) and -1.8 to 1.8 V for the CPE (blue line). (c) CVs performed with a BDDPE (blue line), CPE (black line), ERGO-modified BDDPE (red line), and ERGO-modified CPE (green line), at 0.05 V s⁻¹, using 4 mM Fe(CN)₆⁴⁻ in 0.1 M KCl.

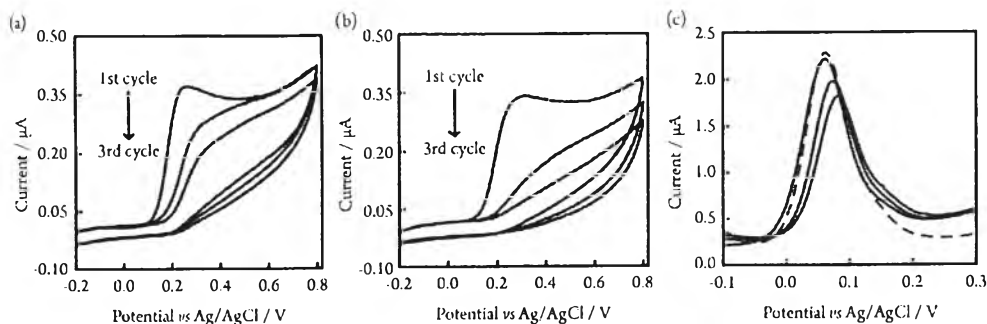


Figure 3. Three successive CVs of 10 μM 5-HT with a (a) BDDPEs and (b) CPEs in 0.1 M PBS (pH 8.0) at 0.05 V s^{-1} . (c) Three consecutive DPVs of 10 μM 5-HT in 0.1 M PBS (pH 8.0) at a BDDPE before (solid lines) and after (red dashed line) anodic polarization.

KNO_3 , and C_{dl} of each electrode was determined at 0 V versus screen-printed Ag/AgCl using³³

$$C_{\text{dl}} = \frac{i_{\text{average}}}{\nu A_{\text{geometric}}} \quad (1)$$

where i_{average} is the current average from the forward and reverse sweep in amperes, ν is the scan rate in volts per second, and $A_{\text{geometric}}$ is the geometric electrode area in square centimeters. The capacitive currents at CPEs and BDDPEs were 61.74 ± 0.36 and $42.29 \pm 0.24 \mu\text{F cm}^{-2}$, respectively ($n = 3$ electrodes, Figure 2a). The BDDPE capacitance compares favorably with conventional BDD electrodes reported in the literature,³³ considering the simple electrode fabrication and application. For example, thin-film BDD electrodes are typically $3.9\text{--}381 \mu\text{F cm}^{-2}$ and freestanding BDD electrodes are typically $2.9\text{--}11 \mu\text{F cm}^{-2}$.³³

The potential window was recorded for each electrode material using CV in 0.1 M KNO_3 at 0.1 V s^{-1} (Figure 2b). Using the definition of BDD solvent window as the anodic and cathodic potential limits to generate a current of $\pm 0.4 \text{ mA cm}^{-2}$ from water electrolysis,³³ the solvent window of the BDDPE was found to be 2.25 V. For the CPE, the potential window is much narrower as shown in Figure 2b. The solvent window of our BDD electrodes compare well with thin-film BDD electrodes (2.30–1.38 V) and freestanding BDD electrodes (4.11–3.53 V).³³ In addition, a peak was observed at $\sim +1.5$ V in the BDDPE CV, characteristic of non-diamond carbon species (sp^2 carbon) or impurities situated in the grain boundaries of the diamond surface, as is expected for paste or thin-film electrodes.³³ The capacitance and solvent window data confirm that BDDPEs have smaller background currents and wider potential windows than the CPEs typically employed with ePADs, which should translate to improved limits of detection (LOD).

The electrochemical characteristics of the electrodes were investigated through measurement of the peak currents and peak-to-peak separation (ΔE_p) of the inner-sphere redox couple, $\text{Fe}(\text{CN})_6^{4-}$, via CV. As shown in Figure 2c, symmetrical voltammograms are observed for $\text{Fe}(\text{CN})_6^{4-}$ electrooxidation with BDDPEs and CPEs ($\Delta E_p = 410 \pm 10$ and 400 ± 20 mV, respectively, $n = 3$ electrodes). After modification with ERGO, the ERGO-BDDPEs exhibited symmetrical cathodic and anodic peaks and greater electrochemical reversibility than the ERGO-CPEs, as illustrated through smaller ΔE_p (200 ± 30 and 280 ± 30 mV, respectively). The large ΔE_p for the BDDPEs are indicative of ohmic resistive effects, likely originating from the nonohmic contact between the BDD

powder and the mineral oil or Ag/AgCl screen-printed contact pad. This hypothesis is supported by ΔE_p of 75 and 89 mV for the outer-sphere couples FcTMA^+ and $\text{Ru}(\text{NH}_3)_6^{3+}$ (1 mM in 0.1 M KNO_3 , not shown).

Serotonin and Norepinephrine Detection. The two-electron irreversible electrooxidation of serotonin (5-HT) is known to produce hydroxylated products, dimers, and other species that can irreversibly adsorb to the electrode, fouling the surface.⁴⁷ Electrode fouling decreases sensitivity, making 5-HT determination on carbon electrodes challenging. Previous studies have shown BDD is not as prone to 5-HT fouling due to the relative surface inertness.⁵⁷ Parts a and b of Figure 3 show CVs for 10 μM 5-HT at a BDDPE and CPE, respectively. Well-defined oxidation peaks were observed for both electrodes for the initial CV. The decrease of oxidation peak current and peak potential shift after the first cycle are indicative of electrode fouling, although the fouling is less severe for BDDPEs compared to CPEs. We attribute this phenomena to the lower adsorption of the organic species on BDDPEs when compared with CPEs.⁴³

In order to improve resistance to electrode fouling, electrode pretreatment was tested to reactivate the electrode surface. Several methods have been described for the pretreatment of BDD thin-film electrodes. Duran et al. investigated the effect of anodic, cathodic, or a combined anodic and cathodic galvanostatic polarization on the response of a diamond microelectrode for two inner-sphere redox couples, $\text{Fe}(\text{CN})_6^{4-}$ and 5-HT. Cathodic pretreatment and combined pretreatment performed by the anodic step followed by the cathodic step were found to be effective for activating a fouled microelectrode.²⁷ Similarly, Sarada et al. showed the CV of 5-HT at a BDD electrode before and after pretreating the electrode by oxidizing the surface in PBS. Relative to a fresh diamond electrode, the 5-HT oxidation peak potential and current for a diamond electrode after anodic pretreatment remained unchanged.⁴⁸ Therefore, the effect of anodic pretreatment on the electrochemical response of BDDPEs was investigated for 5-HT as shown in Figure 3. Figure 3c shows the effect of anodic cleaning on the response of fouled BDDPEs by comparing the DPV of 10 μM 5-HT on BDDPE before and after treatment. Three DPVs were performed on the same electrode without a cleaning step, resulting in an oxidation current decrease and positive peak potential shift, likely due to the adsorption of a quinone as the oxidation product of 5-HT.⁴⁷ Subsequently, anodic pretreatment was carried out by oxidizing the fouled electrode with at +1.2 V for 5 min in PBS solution, leading to a peak current and peak potential similar to those of the fresh

BDDPEs (red dashed line). These results indicate that the BDDPE was returned to its native activity state after anodic treatment, and subsequently anodic treatment was used for all S-HT and NE measurements.

Next, the electrochemical behavior of NE and S-HT on BDDPEs was investigated by CV (Figure 4a). Due to their

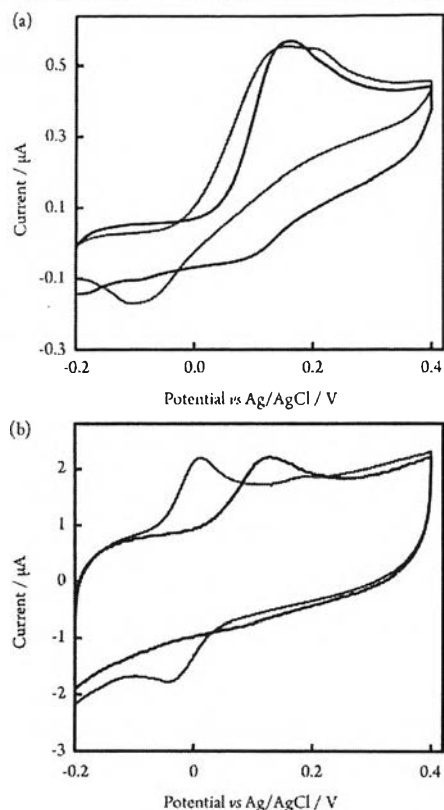


Figure 4. CVs performed with bare BDDPEs (a) and ERGO-BDDPEs (b) for the oxidation of 25 μM NE (red line) and 10 μM S-HT (black line) in 0.1 M PBS (pH 8.0).

similar oxidation potentials, NE and S-HT could not be discriminated using bare BDDPEs. Therefore, ERGO was chosen to modify the BDDPEs in an attempt to enable simultaneous detection of both analytes. CVs of BDDPEs and ERGO-BDDPEs at varying scan rates from 0.01 to 0.1 V s^{-1} using $\text{Fe}(\text{CN})_6^{4-}$ are shown in Figure S2, parts a and b, respectively. ΔE_p at the unmodified BDDPEs increases from 190 ± 4 mV at 0.01 V s^{-1} to 387 ± 7 mV at 0.1 V s^{-1} , whereas ΔE_p at the ERGO-BDDPEs increases from 120 ± 5 mV at 0.01 V s^{-1} to 280 ± 7 mV at 0.1 V s^{-1} . The lower ΔE_p for the ERGO-BDDPEs implies faster electron-transfer kinetics from the ERGO modification.⁵⁸ Figure S2c shows a linear dependence of the peak current versus square root of the ν for both unmodified and modified electrodes, indicating that the electrochemical processes at both electrodes are diffusion-controlled.⁵⁹

The surface area of the electrodes was determined by using Randles–Sevcik equation⁶⁰

$$i_{pa} = (2.69 \times 10^5)n^{2/3}AD_0^{1/2}\nu^{1/2}C_0^* \quad (2)$$

where i_{pa} is the peak current in amperes, A is the area of the electrode in square centimeters, C_0^* is the concentration of electroactive species in millimoles per liter, and D is the diffusion coefficient in square centimeters per second. Given $D = 7.26 \times 10^{-6} \text{ cm}^2 \text{ s}^{-1}$ for $\text{Fe}(\text{CN})_6^{4-}$,⁵¹ A for each electrode can be calculated from the slope of the i_p versus $\nu^{1/2}$ plot. The surface areas (A) of the electrodes were found to be 8.66×10^{-2} and $16.7 \times 10^{-2} \text{ cm}^2$ for the BDDPEs and ERGO-BDDPEs, respectively. The results demonstrated the ERGO layer is effective at increasing the electroactive surface area.

CVs of NE and S-HT at the ERGO-BDDPE are shown in Figure 4b. Following modification, the E_{pa} of NE decreased from 0.13 ± 0.0047 V to -0.006 ± 0.0052 V, while the E_{pa} of S-HT decreased from 0.14 ± 0.0061 to 0.12 ± 0.0035 V, showing a clear separation in NE and S-HT oxidation peaks. To evaluate the mass transfer of the analytes toward the electrode, CV was performed at different scan rates. As seen in Figure S3, parts a and b, the anodic peak currents of NE and S-HT oxidation increase with increasing ν as predicted. Moreover, the peak currents of both compounds are linearly proportional to the square root of ν in the range of 0.01–0.1 V s^{-1} , suggesting that the electrochemical processes are diffusion-controlled.

Analytical Performance. Next, DPV was employed for the simultaneous determination of NE and S-HT. The linear range of NE and S-HT was studied at ERGO-BDDPEs, with a fixed concentration of the other species. As shown in Figure S4, parts a and b, the peak currents of NE or S-HT increased linearly with the concentration. For NE detection, a linear calibration plot was found over a range of 2.5–100 μM with a sensitivity of $0.030 \mu\text{A } \mu\text{M}^{-1}$ and correlation coefficient (R^2) of 0.9991. For S-HT, a linear calibration plot was obtained over a range of 0.5–7.5 μM with a sensitivity of $0.069 \mu\text{A } \mu\text{M}^{-1}$ and R^2 of 0.9938. The experimental LODs were 2.5 and 0.5 μM for NE and S-HT, respectively. Although this device exhibits higher LOD values than other BDD electrode materials,^{48,57} it has other advantages in terms of ease of use, low cost, and disposability.

Next, the device repeatability was evaluated through repeated measurements of 10 μM NE and 5 μM S-HT ($n = 10$, not shown). The relative standard deviations (RSDs) were 6.93% and 8.43%, for NE and S-HT, respectively. The intradevice reproducibility was evaluated using DPV detection of 10 μM NE and 5 μM S-HT. The RSDs of six different devices under the same conditions were found to be 6.02% and 7.68%, for NE and S-HT, respectively. All of these values are in line with other ePAD systems.

Detection of Heavy Metals. The contamination of the environment by heavy metals [e.g., Cd(II) and Pb(II)] remains a serious problem because of their environmental persistence and high toxicity.⁶² In order to show the scope of the developed sensor, BDDPEs were employed for heavy metal determination. SWASV is a particularly attractive electrochemical technique for trace heavy metal determination, as it greatly reduces the background noise arising from capacitive charging currents during the potential scan.⁶³ Conventional ASV measurements consist of two steps: first, in the preconcentration step, metal ions are electrochemically deposited onto the electrode surface, typically under controlled stirring conditions. Then, the stirring is ceased and the deposited metal is oxidized or stripped from the electrode, back into the solution. The resulting anodic diffusion current is then used to determine the concentration of the metal. However, this approach is not ideal for in-field

measurements due to the practicality and difficulty of synchronizing stirring and ASV procedures.

To overcome this limitation, BDDPEs on static and flow-through PADs were applied for the simultaneous determination of Cd(II) and Pb(II), using SWASV. For simplicity, the preconcentration step was performed without stirring, which will affect the device sensitivity as preaccumulation of analytes in stripping is limited by diffusion. Therefore, to increase electrode sensitivity, Bi was used to modify BDDPEs, forming a metal–bismuth alloy on the electrode surface, which facilitates the nucleation process during metal ion deposition.⁶⁴ The PADs were designed as a flow-through pattern by adding a hydrophilic area in the outlet of a paper channel (Figure 1c). This design allows the continuous wicking of solution across the electrodes in the preconcentration step, facilitating the accumulation of metals onto the electrode surface.⁶⁵ During the preconcentration step, -1.2 V was applied for 5 min, providing enough time to stop the flow before the stripping step.

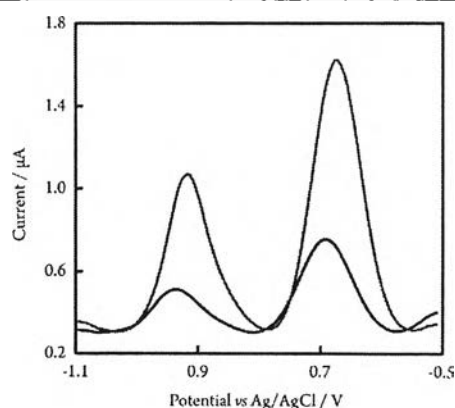


Figure 5. SWASV for a 50 ppb solution of Cd(II) and Pb(II) in 0.1 M acetate buffer (pH 4.5), at a Bi-modified BDDPE, using the static ePAD system (black line) and the flow through μ PAD system (red line).

Figure 5 shows the SWASV for static and flow-through devices for the simultaneous detection of 50 ppb Cd(II) and Pb(II). The voltammogram obtained from the flow-through PADs, in which the sample solution continuously flowed in the paper microchannel, showed well-defined separated peaks for Cd(II) and Pb(II), at -0.93 and -0.67 V versus the Ag/AgCl reference electrode, respectively. In contrast, the voltammogram obtained from the static PAD, in which the sample solution was directly dropped onto the electrodes, showed a much lower current signal. These results demonstrate that the flow-through PADs exhibit a much higher sensitivity than the static system [4.3 and 3.1 times higher for Cd(II) and Pb(II), respectively]. This is likely due to the increased mass transport as a result of convection through PAD, enhancing the efficiency of the metal accumulation.

The analytical performance of the flow-through PADs for Cd(II) and Pb(II) determination was evaluated using SWASV under the optimized experimental conditions. SWASV of different concentrations of Pb(II) and Cd(II) are shown in Figure 6a. The resulting calibration plots were linear over the concentration range from 1 to 200 ppb for Pb(II) and 25–200 ppb for Cd(II) (Figure 6b) with sensitivities of 0.305 and 0.218 $\mu\text{A } \mu\text{M}^{-1}$, respectively. The experimental LODs were 1 and 25

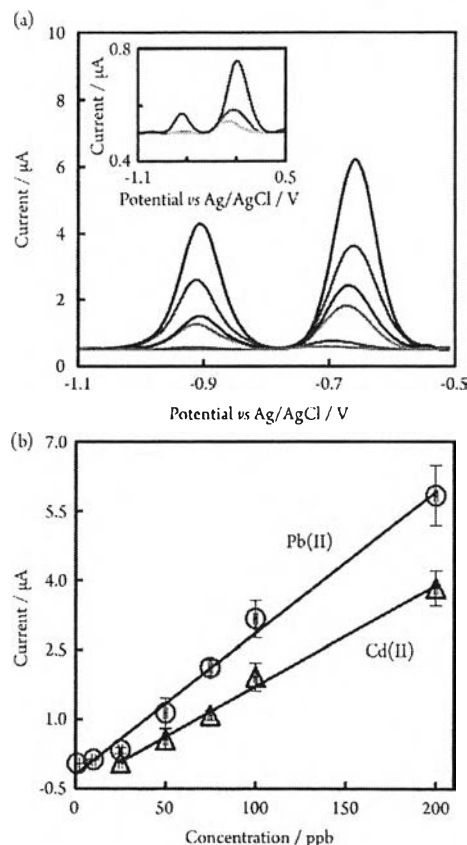


Figure 6. (a) SWASV of Cd(II) and Pb(II) from 1 to 200 ppb in 0.1 M acetate buffer (pH 4.5), at a Bi-modified BDDPE, using the flow through μ PAD, with low concentrations in the inset. (b) Corresponding calibration curves for increasing concentrations of Pb(II) (1 to 200 ppb, sensitivity = 0.0305 $\mu\text{A/ppb}$, $R^2 = 0.9910$) and Cd(II) (25 to 200 ppb, sensitivity = 0.0218 $\mu\text{A/ppb}$, $R^2 = 0.9938$).

ppb for Pb(II) and Cd(II), respectively. These results indicate that the devices are not only simple and inexpensive, but also provide the good linearity and LODs compared to alternate methods which are often more expensive and require complicated fabrication procedures.^{66–68} While these detection limits are higher than other optimized materials using Bi codeposition, the LOD value of Pb is below the EPA action limit of contaminants in drinking water⁶⁹ and also demonstrate applicability of the system to inorganic as well as organic analytes.

The effects of some possible interferences [Mn(II), Cr(III), Fe(III), Zn(II), Cu(II), Ca(II), Na(I), and K(I)] were investigated by adding them into a solution containing 50 ppb of Cd(II) and Pb(II) in 0.1 M acetate buffer pH 4.5. The tolerance ratio is defined as the mass ratio of interfering species relative to the target metal that makes a change in peak current of $\pm 5\%$. By limiting the scanning potential in the system from -1.1 to -0.5 V, the maximum tolerable concentrations of foreign species are shown in Table S1. These findings indicate that the aforementioned common metal ions do not interfere with the determination of Cd(II) and Pb(II).

To demonstrate the method applicability, flow-through μ PAD devices were used to detect Cd(II) and Pb(II) in spiked drinking water samples. The drinking water samples were bought from a local supermarket (Bangkok, Thailand). For

analysis, the drinking water was diluted (1:5) with acetate buffer (pH 4.5) and recovery studies were carried out by spiking Cd(II) and Pb(II) to the drinking water samples at three different concentrations (5, 25, and 59 ppb). The percentages of recoveries were found in a range from 93.01% to 103.10% and the acceptable %RSD ($n = 3$) was below 4.77% (Table S2). In addition, the unknown samples were determined by both the proposed method and a standard method (inductively coupled plasma optical emission spectroscopy, ICP-OES) (Table S3). The results from the developed method were in good agreement with those from the ICP-OES method. These results clearly indicate the ability to measure Cd(II) and Pb(II) levels in drinking water samples.

CONCLUSIONS

In this work, we report for the first time the fabrication and electrochemical characterization of BDDPE for μ PADs. The BDDPE exhibits very useful electrochemical properties such as wide solvent window, low background currents, and resistance to surface fouling, which play an important role in the analytical performance of electrochemical sensors. The BDDPEs demonstrated here can be easily fabricated and integrated with ePADs. In addition, the BDDPEs are cheaper and more amenable to disposable and portable platforms compared with conventional BDD electrodes (the prices are \sim \\$0.1/each and \\$310/each for BDDPEs and polycrystalline BDD electrodes, respectively). To demonstrate the scope of the BDDPEs, the material is applied in ePAD and μ PAD formats for the quantitative detection of biological species and heavy metals. In case of biological species, the ePAD device was capable of simultaneously detecting NE and 5-HT in wide concentration ranges and with low limit of detections. In addition, electrode fouling from 5-HT electrooxidation is easily overcome through anodic electrode treatment, opening this sensor for use with multiple measurements (e.g., testing of 20 different samples in situ with one electrode). For heavy metal quantitation, a flow-through μ PAD design with SWASV enhances the efficiency of metal deposition, thereby improving the detection sensitivity compared to a static ePAD system. The developed sensor is applicable to a range of analytes and, through overcoming analytical challenges such as electrode fouling and peak shielding, should open up ePADs and μ PAD to wide adoption across a range of fields.

ASSOCIATED CONTENT

Supporting Information

The Supporting Information is available free of charge on the ACS Publications website at DOI: 10.1021/acs.analchem.6b05042.

Details of the BDDPE fabrication, preparation of the ERGO-modified BDDPE, a scan rate study of Fe(CN)₆⁴⁻, NE, and 5-HT, calibration curves for NE and 5-HT oxidation on the ePAD, an interference study for heavy metals analysis, and analysis of spiked real drinking water samples for heavy metal analysis (PDF)

AUTHOR INFORMATION

Corresponding Authors

*E-mail: chuck.henry@colostate.edu.

*E-mail: Orawon.C@chula.ac.th.

ORCID

Robert B. Channon: 0000-0001-5416-7736

Charles S. Henry: 0000-0002-8671-7728

Notes

The authors declare no competing financial interest.

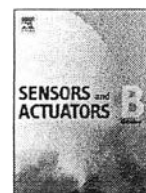
ACKNOWLEDGMENTS

We gratefully acknowledge funding for this project from the Thailand Research Fund (TRF) via the Research Team Promotion Grant (RTA5780005). Partial support was provided through the National Institute of Occupational Safety and Health (R01OH010662) for C.S.H. and R.B.C. S.N. thanks the Royal Golden Jubilee Ph.D. Program (Grant No. PHD/0123/2554).

REFERENCES

- (1) Martinez, A. W.; Phillips, S. T.; Butte, M. J.; Whitesides, G. M. *Angew. Chem., Int. Ed.* 2007, 46, 1318–1320.
- (2) Martinez, A. W.; Phillips, S. T.; Whitesides, G. M.; Carrilho, E. *Anal. Chem.* 2010, 82, 3–10.
- (3) Cate, D. M.; Noblitt, S. D.; Volckens, J.; Henry, C. S. *Lab Chip* 2015, 15, 2808–2818.
- (4) Jokerst, J. C.; Adkins, J. A.; Bisha, B.; Mentele, M. M.; Goodridge, L. D.; Henry, C. S. *Anal. Chem.* 2012, 84, 2900–2907.
- (5) Dungchai, W.; Chailapakul, O.; Henry, C. S. *Anal. Chem.* 2009, 81, 5821–5826.
- (6) Sameenoi, Y.; Nongkai, P. N.; Nouanthavong, S.; Henry, C. S.; Nacapricha, D. *Analyst* 2014, 139, 6580–6588.
- (7) Cate, D. M.; Adkins, J. A.; Mettakoonpitak, J.; Henry, C. S. *Anal. Chem.* 2015, 87, 19–41.
- (8) Chaiyo, S.; Siangproh, W.; Apilux, A.; Chailapakul, O. *Anal. Chim. Acta* 2015, 866, 75–83.
- (9) Santhiago, M.; Wydallis, J. B.; Kubota, L. T.; Henry, C. S. *Anal. Chem.* 2013, 85, 5233–5239.
- (10) Gao, C.; Su, M.; Wang, Y.; Ge, S.; Yu, J. *RSC Adv.* 2015, 5, 28324–28331.
- (11) Wu, L.; Ma, C.; Ge, L.; Kong, Q.; Yan, M.; Ge, S.; Yu, J. *Biosens. Bioelectron.* 2015, 63, 450–457.
- (12) Wang, S.; Ge, L.; Song, X.; Yu, J.; Ge, S.; Huang, J.; Zeng, F. *Biosens. Bioelectron.* 2012, 31, 212–218.
- (13) Liu, W.; Guo, Y.; Li, H.; Zhao, M.; Lai, Z.; Li, B. *Spectrochim. Acta, Part A* 2015, 137, 1298–1303.
- (14) He, M.; Liu, Z. *Anal. Chem.* 2013, 85, 11691–11694.
- (15) Thom, N. K.; Lewis, G. G.; Yeung, K.; Phillips, S. T. *RSC Adv.* 2014, 4, 1334–1340.
- (16) Nurak, T.; Praphairaksit, N.; Chailapakul, O. *Talanta* 2013, 114, 291–296.
- (17) Ruecha, N.; Rangkupan, R.; Rodthongkum, N.; Chailapakul, O. *Biosens. Bioelectron.* 2014, 52, 13–19.
- (18) Santhiago, M.; Kubota, L. T. *Sens. Actuators, B* 2013, 177, 224–230.
- (19) Dossi, N.; Toniolo, R.; Terzi, F.; Impellizzeri, F.; Bontempelli, G. *Electrochim. Acta* 2014, 146, 518–524.
- (20) Adkins, J. A.; Henry, C. S. *Anal. Chim. Acta* 2015, 891, 247–254.
- (21) Fosdick, S. E.; Anderson, M. J.; Renault, C.; DeGregory, P. R.; Loussaert, J. A.; Crooks, R. M. *Anal. Chem.* 2014, 86, 3659–3666.
- (22) Määtänen, A.; Ihalainen, P.; Pulkkinen, P.; Wang, S.; Tenhu, H.; Peltonen, J. *ACS Appl. Mater. Interfaces* 2012, 4, 955–964.
- (23) Kit-Anan, W.; Olarnwanich, A.; Sriprachubwong, C.; Karuwan, C.; Tuantranont, A.; Wisitsoraat, A.; Srituavanich, W.; Pimpin, A. J. *Electroanal. Chem.* 2012, 685, 72–78.
- (24) Pereira, S. V.; Bertolino, F. A.; Fernandez-Baldo, M. A.; Messina, G. A.; Salinas, E.; Sanz, M. I.; Raba, J. *Analyst* 2011, 136, 4745–4751.
- (25) Mettakoonpitak, J.; Boehle, K.; Nantaphol, S.; Teengam, P.; Adkins, J. A.; Srisa-Art, M.; Henry, C. S. *Electroanalysis* 2016, 28, 1420–1436.
- (26) Swamy, B. E. K.; Venton, B. J. *Analyst* 2007, 132, 876–884.

- (27) Duran, B.; Brocenschi, R. F.; France, M.; Galligan, J. J.; Swain, G. M. *Analyst* 2014, 139, 3160–3166.
- (28) Chandra, S.; Miller, A. D.; Bendavid, A.; Martin, P. J.; Wong, D. K. Y. *Anal. Chem.* 2014, 86, 2443–2450.
- (29) Hutton, L.; Newton, M. E.; Unwin, P. R.; Macpherson, J. V. *Anal. Chem.* 2009, 81, 1023–1032.
- (30) Luong, J. H. T.; Male, K. B.; Glennon, J. D. *Analyst* 2009, 134, 1965–1979.
- (31) Balmer, R. S.; Brandon, J. R.; Clewes, S. L.; Dhillon, H. K.; Dodson, J. M.; Friel, I.; Inglis, P. N.; Madgwick, T. D.; Markham, M. L.; Mollart, T. P.; Perkins, N.; Scarsbrook, G. A.; Twitchen, D. J.; Whitehead, A. J.; Wilman, J. J.; Woollard, S. M. *J. Phys.: Condens. Matter* 2009, 21, 364221.
- (32) Compton, R. G.; Foord, J. S.; Marken, F. *Electroanalysis* 2003, 15, 1349–1363.
- (33) Hutton, L. A.; Iacobini, J. G.; Bitziou, E.; Channon, R. B.; Newton, M. E.; Macpherson, J. V. *Anal. Chem.* 2013, 85, 7230–7240.
- (34) Kondo, T.; Tamura, Y.; Hoshino, M.; Watanabe, T.; Aikawa, T.; Yuasa, M.; Einaga, Y. *Anal. Chem.* 2014, 86, 8066–8072.
- (35) Watanabe, T.; Ivandini, T. A.; Makide, Y.; Fujishima, A.; Einaga, Y. *Anal. Chem.* 2006, 78, 7857–7860.
- (36) Granger, M. C.; Witek, M.; Xu, J.; Wang, J.; Hupert, M.; Hanks, A.; Koppang, M. D.; Butler, J. E.; Lucazeau, G.; Mermoux, M.; Strojek, J. W.; Swain, G. M. *Anal. Chem.* 2000, 72, 3793–3804.
- (37) Granger, M. C.; Xu, J.; Strojek, J. W.; Swain, G. M. *Anal. Chim. Acta* 1999, 397, 145–161.
- (38) Jolley, S.; Koppang, M.; Jackson, T.; Swain, G. M. *Anal. Chem.* 1997, 69, 4099–4107.
- (39) van den Brink, F. T. G.; Zhang, T.; Ma, L.; Bomer, J.; Odijk, M.; Olthuis, W.; Permentier, H. P.; Bischoff, R.; van den Berg, A. *Anal. Chem.* 2016, 88, 9190–9198.
- (40) Stanković, D. M.; Kalcher, K. *Sens. Actuators, B* 2016, 233, 144–147.
- (41) Fischer, A. E.; Swain, G. M. *J. Electrochem. Soc.* 2005, 152, B369–B375.
- (42) Kondo, T.; Udagawa, I.; Aikawa, T.; Sakamoto, H.; Shitanda, I.; Hoshi, Y.; Itagaki, M.; Yuasa, M. *Anal. Chem.* 2016, 88, 1753–1759.
- (43) Kondo, T.; Sakamoto, H.; Kato, T.; Horitani, M.; Shitanda, I.; Itagaki, M.; Yuasa, M. *Electrochem. Commun.* 2011, 13, 1546–1549.
- (44) Kondo, T.; Horitani, M.; Sakamoto, H.; Shitanda, I.; Hoshi, Y.; Itagaki, M.; Yuasa, M. *Chem. Lett.* 2013, 42, 352–354.
- (45) Graeff, F. G.; Guimaraes, F. S.; De Andrade, T. G. C. S.; Deakin, J. F. W. *Pharmacol., Biochem. Behav.* 1996, 54, 129–141.
- (46) Wang, Y.; Wang, S.; Tao, L.; Min, Q.; Xiang, J.; Wang, Q.; Xie, J.; Yue, Y.; Wu, S.; Li, X.; Ding, H. *Biosens. Bioelectron.* 2015, 65, 31–38.
- (47) Patel, A. N.; Unwin, P. R.; Macpherson, J. V. *Phys. Chem. Chem. Phys.* 2013, 15, 18085–18092.
- (48) Sarada, B. V.; Rao, T. N.; Tryk, D. A.; Fujishima, A. *Anal. Chem.* 2000, 72, 1632–1638.
- (49) Wang, J.; Chen, G.; Chatrathi, M. P.; Fujishima, A.; Tryk, D. A.; Shin, D. *Anal. Chem.* 2003, 75, 935–939.
- (50) Ponchon, J. L.; Cespuglio, R.; Gonon, F.; Jouvet, M.; Pujol, J. F. *Anal. Chem.* 1979, 51, 1483–1486.
- (51) Kemper, T.; Sommer, S. *Environ. Sci. Technol.* 2002, 36, 2742–2747.
- (52) Chaiyo, S.; Mehmeti, E.; Žagar, K.; Siangproh, W.; Chailapakul, O.; Kalcher, K. *Anal. Chim. Acta* 2016, 918, 26–34.
- (53) Osswald, S.; Yushin, G.; Mochalin, V.; Kucheyev, S. O.; Gogotsi, Y. J. *Am. Chem. Soc.* 2006, 128, 11635–11642.
- (54) Nantaphol, S.; Chailapakul, O.; Siangproh, W. *Anal. Chim. Acta* 2015, 891, 136–143.
- (55) Huang, J. T.; Guo, W. H.; Hwang, J.; Chang, H. *Appl. Phys. Lett.* 1996, 68, 3784–3786.
- (56) Lagrange, J. P.; Deneville, A.; Gheeraert, E. *Diamond Relat. Mater.* 1998, 7, 1390–1393.
- (57) Guell, A. G.; Meadows, K. E.; Unwin, P. R.; Macpherson, J. V. *Phys. Chem. Chem. Phys.* 2010, 12, 10108–10114.
- (58) Vidya, H.; Swamy, B. E. K. *J. Mol. Liq.* 2015, 211, 705–711.
- (59) Nantaphol, S.; Chailapakul, O.; Siangproh, W. *Electroanalysis* 2014, 26, 1024–1030.
- (60) Bai, L.; Yuan, R.; Chai, Y.; Yuan, Y.; Wang, Y.; Xie, S. *Chem. Commun.* 2012, 48, 10972–10974.
- (61) Konopka, S. J.; McDuffie, B. *Anal. Chem.* 1970, 42, 1741–1746.
- (62) Chaiyo, S.; Apiluk, A.; Siangproh, W.; Chailapakul, O. *Sens. Actuators, B* 2016, 233, 540–549.
- (63) Ramaley, L.; Krause, M. S. *Anal. Chem.* 1969, 41, 1362–1365.
- (64) Wang, J.; Lu, J.; Hocevar, S. B.; Farias, P. A. M.; Ogorevc, B. *Anal. Chem.* 2000, 72, 3218–3222.
- (65) Nie, Z.; Nijhuis, C. A.; Gong, J.; Chen, X.; Kumachev, A.; Martinez, A. W.; Narovlyansky, M.; Whitesides, G. M. *Lab Chip* 2010, 10, 477–483.
- (66) Xiao, L.; Xu, H.; Zhou, S.; Song, T.; Wang, H.; Li, S.; Gan, W.; Yuan, Q. *Electrochim. Acta* 2014, 143, 143–151.
- (67) Zhao, D.; Guo, X.; Wang, T.; Alvarez, N.; Shanov, V. N.; Heineman, W. R. *Electroanalysis* 2014, 26, 488–496.
- (68) Wu, Y.; Li, N. B.; Luo, H. Q. *Sens. Actuators, B* 2008, 133, 677–681.
- (69) U. S. Environmental Protection Agency. Table of Regulated Drinking Water Contaminants. 2003.



High sensitivity and specificity simultaneous determination of lead, cadmium and copper using μ PAD with dual electrochemical and colorimetric detection

Sudkate Chaiyo^a, Amara Apiluk^b, Weena Siangproh^{c,*,**}, Orawon Chailapakul^{a,d,*}

^a *Electrochemistry and Optical Spectroscopy Research Unit (EOSRU), Department of Chemistry, Faculty of Science, Chulalongkorn University, 254 Phayathai Road, Patumwan, Bangkok 10330, Thailand*

^b *Center for Innovation Development and Technology Transfer, Faculty of Medical Technology, Mahidol University, 999 Phuttamonthon 4 Road, Salaya, Nakhon Pathom 73170, Thailand*

^c *Department of Chemistry, Faculty of Science, Srinakharinwirot University, Sukhumvit 23, Wattana, Bangkok 10110, Thailand*

^d *National Center of Excellence for Petroleum, Petrochemicals and Advanced Materials, Chulalongkorn University, Patumwan, Bangkok 10330, Thailand*

ARTICLE INFO

Article history:

Received 1 March 2016

Received in revised form 11 April 2016

Accepted 19 April 2016

Available online 22 April 2016

Keyword:

Lead

Cadmium

Copper

Microfluidic paper-based analytical device

Dual detection

ABSTRACT

A bismuth-modified electrode can increase the sensitivity of lead and cadmium detection. However, use of a bismuth-modified electrode in the detection of copper remains limited because the bismuth signal overlaps with the signal for copper. In this study, we developed a new microfluidic paper-based analytical device (μ PAD) coupled with dual electrochemical and colorimetric detection to obtain high sensitivity and specificity for the simultaneous determination of lead, cadmium and copper. The μ PAD is divided into two parts. The first part is electrochemical detection for the determination of lead and cadmium using a bismuth-modified, boron-doped diamond electrode (Bi-BDDE). The limit of detection was 0.1 ng mL^{-1} (for both metals). The second part is colorimetric detection for the determination of copper based on the catalytic etching of silver nanoplates (AgNPLs) by thiosulfate ($\text{S}_2\text{O}_3^{2-}$). The color of AgNPLs on μ PAD changed from pinkish violet to colorless after the addition of copper; this change can be monitored by naked eyes and its detection limit was 5.0 ng mL^{-1} by the Image J analysis. The proposed method was applied for the simultaneous determination of these three metals in real samples and no significant differences in accuracy and precision were observed compared to the standard method.

© 2016 Elsevier B.V. All rights reserved.

1. Introduction

Heavy metal ions are hazardous pollutants to living organisms that can accumulate in the human body via the food chain and cause adverse effects on the immune, central nervous and reproductive systems [1]. Metal ions such as lead (Pb(II)), cadmium (Cd(II)), copper (Cu(II)), mercury (Hg(II)), and zinc (Zn(II)) are serious hazards that cannot be degraded in the environment. Therefore, a rapid, sensitive, and simple method for the determination of these trace heavy metal ions is critically important.

Several techniques for the determination of trace heavy metal ions, including atomic absorption spectroscopy (AAS) [2], inductively coupled plasma-mass spectrometry (ICP-MS) [3] and inductively coupled plasma optical emission spectrometry (ICP-OES) [4], are available. However, these techniques have some drawbacks; they are time-consuming, costly and require complex and expensive instrumentation. Therefore, they are unsuitable for field analysis. Currently, electrochemical detection has attracted extensive attention due to their intrinsic advantages of simplicity, portability, low cost, high sensitivity, and excellent selectivity [5]. Early electroanalytical methods were frequently conducted with hanging mercury drop electrodes [6] and mercury-film working electrodes [7]. However, the toxicity of mercury and mercury salt for humans and the environment has significantly hindered the use of this electrode. Currently, the bismuth-modified electrode has attracted considerable interest because its behavior is similar to the behavior of a mercury-film electrode and presents significantly low toxicity [8]. Bismuth film electrodes, formed by electrochemi-

* Corresponding author.

** Corresponding author at: Department of Chemistry, Faculty of Science, Srinakharinwirot University, Sukhumvit 23, Wattana, Bangkok 10110, Thailand.

E-mail addresses: weena@gswu.ac.th, weenasi@hotmail.com (W. Siangproh), corawon@chula.ac.th (O. Chailapakul).

cal deposition on substrates, including glassy carbon electrodes [9], screen-printed carbon electrodes (SPCEs) [10], carbon paste electrode (CPEs) [11] and boron doped diamond electrodes (BDDEs) [12]. Among these electrode substrates, the BDDEs offers the most favorable electroanalytical properties. These beneficial properties include a wide potential window, a low background current, chemical inertness, and the readily renewable surface of the BDDEs [13]. Therefore, the BDDEs is a potentially ideal substrate electrode for the application of a bismuth-modified electrode.

Cu(II) is commonly detected in environmental samples, which poses a problem for the environmental analysis of a trace heavy metal. The use of a bismuth-modified electrode for the detection of Cu(II) remains limited because the signal of stripping bismuth overlaps with the signal of Cu(II) [14,15]. Therefore, the simultaneous determination of Cu(II) in samples with other trace heavy metals is important and challenging. Based on this problem, the development of a simple colorimetric detection to the simultaneous determination of Cu(II) with trace heavy metals (Pb(II) and the detection of Cd(II)) using a bismuth-modified boron doped diamond electrode (Bi-BDDE) is our primary objective.

In 2007, the concept of a microfluidic paper-based analytical device (μ PAD) was developed by the Whitesides group [16]. The μ PAD is a new alternative device that can be applied to food analysis, environmental monitoring, and clinical diagnosis due to their advantages of simplicity, high throughput, disposability, low sample and reagent consumption, low cost, and portability [17–20]. Several detectors of μ PADs are proposed: for example, colorimetry [17], electrochemical [18], chemiluminescence [19], electrochemiluminescence [20] and electrical [21] methods. These techniques have advantages and disadvantages in terms of sensitivity, simplicity and cost-effectiveness. Recently, an interesting sensing approach for μ PADs involved the realization of a dual-detection device. The first hybrid paper-based device, which consisted of colorimetric and electrochemical detection, was proposed for the simultaneous detection of Au(III) and Fe(III) in industrial waste solutions [22]. Although hybrid detection instruments are a feasible alternative to single-type sensing assays, they require multiple readout mechanisms.

The objective of this study is to develop μ PADs combined with dual electrochemical and colorimetric detection for high sensitivity, specificity, rapidity, simplicity, portability, and the simultaneous determination of Pb(II), Cd(II) and Cu(II). Electrochemical detection with bismuth-modified boron doped diamond electrodes (Bi-BDDEs) was employed to measure Pb(II) and Cd(II), whereas colorimetric detection for the determination of Cu(II) based on the catalytic etching of silver nanoplates (AgNPLs) by thiosulfate ($S_2O_3^{2-}$) [23] was proposed. In the presence of Cu(II), the catalytic etching system induced a distinct decrease in the size of the AgNPLs and concomitantly produced a red-shift with a pinkish violet to colorless change. The proposed devices were successfully applied to the simultaneous determination of Pb(II), Cd(II) and Cu(II) in real samples.

2. Experimental

2.1. Reagents and apparatus

Standard solutions of $1000 \mu\text{g mL}^{-1}$ Pb(II), Cd(II), Hg(II), Bi(III), As(III), Co(II) and Zn(II) were purchased from Spectrosol (Poole, UK), and standard solutions of $1000 \mu\text{g mL}^{-1}$ Ni(II) and Al(III) were purchased from Merck (Darmstadt, Germany). Copper sulfate (CuSO_4 , BDH, UK), ammonium hydroxide (NH_4OH , BDH, England), sodium thiosulfate ($\text{Na}_2\text{S}_2\text{O}_3$, Sigma-Aldrich, Missouri), hexadecyltrimethylammonium bromide (CTAB, Sigma-Aldrich, Missouri), magnesium sulfate (MgSO_4 , Sigma-Aldrich, Missouri), manganese

chloride (MnCl_2 , Sigma-Aldrich, Missouri), ammonium dichromate ($(\text{NH}_4)_2\text{Cr}_2\text{O}_7$, Sigma-Aldrich, Missouri), ammonium chloride (NH_4Cl , Ajax, Australia), iron chloride hexahydrate ($\text{FeCl}_3 \cdot 6\text{H}_2\text{O}$, Merck, Germany), sodium chloride (NaCl , Univar, Redmond, WA) and potassium chloride (KCl , Univar, Redmond, WA) were used as received. All chemicals were analytical-grade chemicals. Ultrapure water (resistivity $\geq 18.2 \text{ M}\Omega \cdot \text{cm}$ at 25°C) was used to prepare all aqueous solutions (obtained from a Millipore Milli-Q purification system).

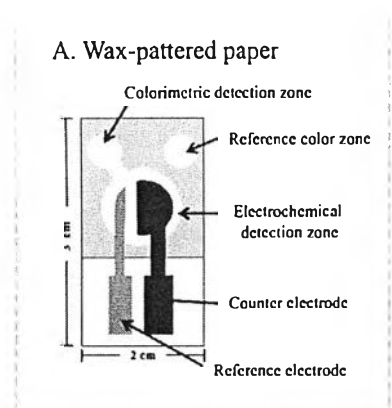
Electrochemical measurements were performed using a model—the PGSTAT 101 Autolab Electrochemical System—controlled with the NOVA software package (Kanaalweg 29-G 3526 KM Utrecht, The Netherlands). A three-electrode system, in which a silver/silver chloride paste 70/30 (Gwent Electronic Materials Ltd., UK) served as the reference electrode, a carbon ink (Acheson, California, USA) served as the auxiliary electrode and BDDE served as working electrode, was employed. The screen-printed block was fabricated by Chaiyaboon Co. Ltd. (Bangkok, Thailand). The absorbance measurement was conducted by a UV-visible spectrophotometer (HP HEWLETT PACKARD 8453, UK) using a 1.0 cm path length quartz cell. Transmission electron microscopy (TEM) was recorded by an H-7650 transmission electron microscope (Hitachi Model, Japan).

2.2. Design and fabrication of the μ PAD

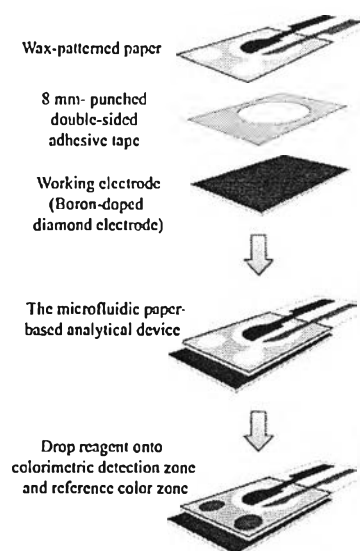
The design of the wax-patterned paper, including the electrochemical detection zone (cycle, diameter = 1 cm), the colorimetric detection zone (cycle, diameter = 3 mm), the channel connection among the electrochemical detection zone, the colorimetric detection zone (channel, 1 #XPS#9617; \times #XPS#9617; 1 mm) and the reference color zone (cycle, diameter = 3 mm), as defined in Fig. 1A, was created using Adobe Illustrator software (Adobe Systems, Inc.). The wax-pattern was printed onto Whatman grade 1 filter paper using a solid-wax printer (Xerox Color Qube 8570, Japan). After printing the wax pattern, the printed paper is placed on a hot plate and the wax on the filter paper is melted and spread throughout the thickness of the filter paper. The wax-covered area was hydrophobic, whereas the area without wax was hydrophilic. For the electrochemical detection zone, the two electrodes were fabricated on wax-patterned paper using the screen-printing method, carbon ink served as the counter electrode and silver/silver chloride ink served as the reference electrode (Fig. 1A). After each printing step, the wax-patterned paper was cured in the oven at 65°C for 30 min. The finished product is shown in Fig. 1A. To complete the device, a BDD electrode was attached to the wax-patterned paper using 8 mm-punched double-sided adhesive tape, and the modified AgNPLs at $0.8 \mu\text{L}$ were dropped onto the colorimetric detection zone and the reference color zone. All fabrication procedures of the μ PAD are shown in Fig. 1B.

2.3. Electrochemical detection of Pb(II) and Cd(II)

Anodic stripping voltammetry (ASV) was chosen for the determination of trace heavy metals due to its high sensitivity, simplicity, speed, low cost and low detection limits [24]. ASV measurements were performed with *in situ* bismuth film preparation. For the analytical procedures, $50 \mu\text{L}$ of the mixture between $2 \mu\text{g mL}^{-1}$ Bi(III) and appropriate amounts of Pb(II) and Cd(II) in 0.2 M NaCl solutions (pH 6.0) was added to the electrochemical detection zone of μ PAD, which caused the solution flows through the channels to the colorimetric detection zones, whereas the solution covered the three electrodes. A preconcentration was performed at -1.2 V for 120 s, where Bi(III) and the target metals were simultaneously deposited on the surface of the electrode. After the accumulation time, the



B. Fabrication procedure for the PAD



C. Analytical procedure for metal assays

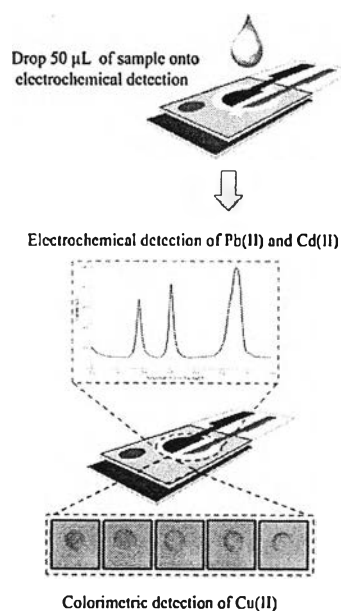


Fig. 1. Drawings of μ PAD coupled the dual electrochemical/colorimetric detection (A). Schematics of the fabrication procedure for a μ PAD (B). Analytical procedures for the simultaneous determination of Pb(II), Cd(II) and Cu(II) (C).

voltammogram was recorded between -1.2 V and 0.2 V (Fig. 1C). All experiments were conducted at room temperature (25°C).

2.4. Colorimetric detection of Cu(II)

AgNPs were synthesized by the reported procedure using the chemical reduction process [25]. Sodium borohydride and methyl cellulose solution served as the reducing agent and the stabilizer, respectively, and the shape transformation was achieved using a 30% H_2O_2 solution. AgNPs solutions were obtained from the Sensor Research Unit at the Department of Chemistry, Faculty of Science, Chulalongkorn University. For the modification of AgNPs, $200\ \mu\text{g mL}^{-1}$ AgNPs solution was prepared from the dilution of $1000\ \mu\text{g mL}^{-1}$ AgNPs stock solution with 0.1 M ammonia buffer at pH 11. Subsequently, $10\ \mu\text{L}$ of 0.1 M CTAB was added to 1 mL of $200\ \mu\text{g mL}^{-1}$ AgNPs. Sequentially, $5\ \mu\text{L}$ of 1.0 M $\text{Na}_2\text{S}_2\text{O}_3$ were added to the CTAB-capped AgNPs followed by incubation of the mixture for 5 min at room temperature. To complete the measurement, $0.8\ \mu\text{L}$ of modified AgNPs solution was added to the colorimetric detection zone, and $50\ \mu\text{L}$ of standard/sample solution were added to the electrochemical detection zone of μ PAD; the solution flowed into the colorimetric detection zone by capillary force. The color change in the test zone was observed within 120 s. A digital camera (Cannon EOS 1000 D1, Japan) was used to record a μ PAD image of the colorimetric measurements. All experiments of colorimetric detection were performed in a light control box. For the quantitative analysis, the color intensity of the colorimetric detection area on a μ PAD was measured using ImageJ 1.45s (National Institutes of Health, USA).

2.5. Simultaneous determination of Pb(II), Cd(II) and Cu(II) in real samples

2.5.1. Stream water and groundwater

Stream water (collected in Saen Saep stream, Bangkok, Thailand) and groundwater (collected in Suphanburi, Thailand) were filtered through a $0.45\ \mu\text{m}$ membrane filter to remove suspended particles. Subsequently, 2 mL of each sample solution was transferred to a volumetric flask and diluted to 10 mL with 0.2 M NaCl. The pH of the sample solutions was adjusted to pH 6.0 by the addition of NaOH solution prior to analysis using the proposed devices.

2.5.2. Rice and fish

The commercial rice and fish samples were purchased from a local market. The treatment process was performed according to published literature with slight modifications [26]. The sample (rice or fish) was ground by a blender machine into a fine powder for the rice sample or small pieces for the fish sample. Subsequently, 0.2 g of the sample (rice or fish) was digested with 3 mL of the mixture of HNO_3 and HClO_4 (1:1). The samples were heated at 100°C for 4 h to digest the samples and evaporate the solvent. Then, 10 mL of 0.2 M NaCl was added and heated until a clear solution was formed (~ 1 h). The residue was adjusted to 10 mL with 0.2 M NaCl (pH 6.0), and the resulting mixture was filtered through a membrane with a pore size of $0.45\ \mu\text{m}$. Prior to measurement, the pH of the digest solutions was adjusted to pH = 6.0 by adding an appropriate amount of NaOH solution.

3. Results and discussion

3.1. Comparison of the electrochemical response between bi-BDEs and Bi-SPCEs

In our first study, we discussed the attractive stripping behavior of bismuth-coated electrodes for trace measurements of Pb(II) and Cd(II). Fig. 2 shows the ASV analytical characteristics from

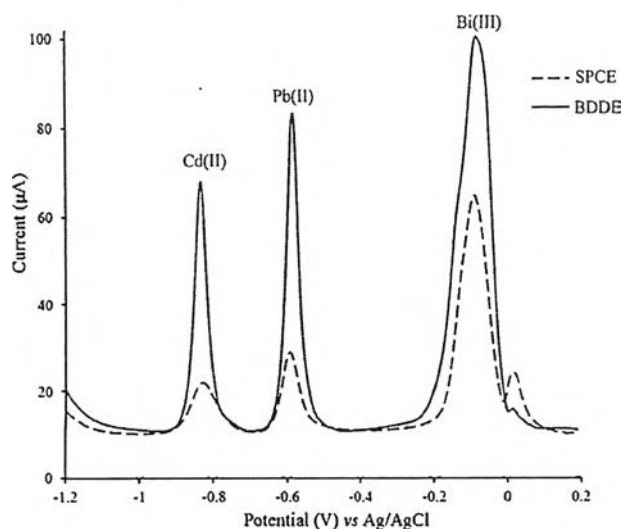


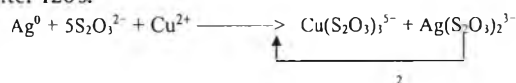
Fig. 2. Anodic stripping voltammograms of 50 ng mL^{-1} for both Pb(II) and Cd(II) in 0.2 M NaCl ($\text{pH} = 6.0$) on Bi-SPCE (dotted line) and Bi-BDDE (solid line). The accumulation potential was -1.2 V , and the accumulation time was 120 s .

use of a screen printing carbon electrode (SPCE) and a BDDE by *in situ* plating bismuth film on paper devices. The stripping voltammograms were recorded using 0.2 M NaCl ($\text{pH} = 6.0$), which contained 50 ng mL^{-1} Pb(II) and Cd(II) and $2 \text{ } \mu\text{g mL}^{-1}$ Bi(III). The stripping peaks were observed at -0.85 V and -0.58 V for Cd(II) and Pb(II), respectively, at both bismuth-modified SPCE and BDDE. The bismuth-modified electrodes exhibited superior voltammetric performance, and yielded well-defined, sharp and separated stripping peaks for both Pb(II) and Cd(II). The improved stripping responses at the bismuth-modified electrodes can be attributed to the fact that bismuth can form “fused” alloys with Pb(II) and Cd(II), which renders them ready to be reduced [27,28]. However, the stripping peaks at the Bi-BDDE (solid line) were significantly higher than the stripping peak current that was observed on the Bi-SPCE (dotted line) by four-fold and five-fold for Pb(II) and Cd(II), respectively. This suggests that the use of a BDD electrode can enhance the sensitivity for the determination of Pb(II) and Cd(II) with the proposed μPAD .

3.2. Colorimetric detection of Cu(II)

For the determination of Cu(II) in parallel to the electrochemical measurement, we developed a highly selective and sensitive colorimetric sensor based on the catalytic etching of silver nanoplates (AgNPLs) with thiosulfate ($\text{S}_2\text{O}_3^{2-}$). As shown in Fig. 3A, the addition of Cu(II) and $\text{S}_2\text{O}_3^{2-}$ to AgNPLs caused a reduction in the sizes of the AgNPLs and a distinct change of color from pinkish violet to colorless after the addition of Cu(II). These results explain that $\text{S}_2\text{O}_3^{2-}$ can be strongly adsorbed to the surfaces of the AgNPLs to form the $\text{Ag}(\text{S}_2\text{O}_3)_2^{3-}$ complexes in the presence of dissolved oxygen and the complexes immediately generated a passive layer on the surface of AgNPLs. For this reason, the etching reaction slowly occurred because the surfaces of the AgNPLs was blocked by the passive layer. In the presence of Cu(II), the etching rate of this reaction can be accelerated by forming $\text{Cu}(\text{S}_2\text{O}_3)_3^{5-}$, and the complexes can also be oxidized to Cu(II) by dissolved oxygen Eq. (1). To understand the role of Cu(II) in the catalytic etching of AgNPLs, the absorption spectra of AgNPLs was monitored for the conditions of varying Cu(II) concentrations, as shown in Fig. 3B. The CTAB-stabilized AuNPLs (CTAB/AuNPLs) in ammonia buffer exhibited the absorption spectra located at 563 nm (curve a). For the addition of $\text{S}_2\text{O}_3^{2-}$ solution, the absorption spectra of CTAB/AuNPLs are blue-shifted ($\lambda = 522 \text{ nm}$)

and absorbance-decreased (curve b); therefore, the color of the CTAB/AuNPLs solutions changed from blue to pinkish violet. In the presence of Cu(II), the absorbance at 522 nm decreased when the concentration of Cu(II) increased (curves c and d). The color of the solutions gradually changed from pinkish violet to colorless. For the detection of Cu(II) on μPAD , $0.8 \text{ } \mu\text{L}$ of the modified AgNPLs was added to the colorimetric detection zone. The sample solution at $50 \text{ } \mu\text{L}$ was subsequently dropped on the electrochemical detection zone and the solution flowed outward via capillary forces to the colorimetric detection zones. The color at the colorimetric detection zones changed from pinkish violet to colorless as the concentration of Cu(II) increased, which could be monitored by the naked eye after 120 s .



As shown in the TEM images, the size of the initial AgNPLs was $\sim 30 \text{ nm}$ (Fig. 3C). The size of the AgNPLs reduced to $\sim 15 \text{ nm}$ with the addition of Cu(II) after incubation for 5 min at room temperature (Fig. 3D), which indicates that Cu(II) can accelerate the etching rate of the AgNPLs. The morphology and size changes of AgNPLs effectively proved the sensing mechanism.

To investigate the selectivity of the modified AgNPLs toward Cu(II), different common metal ions, including $10 \text{ } \mu\text{g mL}^{-1}$ of K(I), Cr(III), Cd(II), Zn(II), As(III), Mn(II), Co(II), Pb(II), Al(III), Ni(II), Fe(III), Mg(II), Hg(II) and Bi(III), were tested by this method (the concentration at $10 \text{ } \mu\text{g mL}^{-1}$ are excess amount of metal found in the environment). As shown in Fig. 4, only Cu(II) (100 ng mL^{-1}) can etch the modified AgNPLs and cause the color change of modified AgNPLs from pinkish violet to colorless, which suggests that this detection system exhibited a high selectivity for Cu(II) [33,34].

3.3. Optimization of operation conditions

3.3.1. Optimization of the parameters for the electrochemical detection of Pb(II) and Cd(II) levels

The operating conditions and parameters of electrochemical detection, including supporting electrolyte, accumulation potential, accumulation time and concentration of Bi(III), were subsequently investigated. The supporting electrolyte can affect both the electrochemical sensor and the colorimetric sensor. The preliminary experiments were conducted with aqueous solution, including HCl, NaCl and ammonia buffer that served as the supporting electrolyte. From the results, 0.1 M HCl ($\text{pH} = 2.0$) provided a high sensitivity for Pb(II) and Cd(II) detection because the acidic chloride ions are a better ligand for metal ions compared with other ions [8] (as shown in Fig. S1). Conversely, the intensity of detecting Cu(II) by colorimetry was attributed to its low sensitivity because the $\text{S}_2\text{O}_3^{2-}$ was not stable and broke down to form sulfate, sulfide, sulfite, tetrathionate, trithionate, polythionates and polysulfides [29]. For the results of ammonia buffer ($\text{pH} = 9.0$), the detection of Cu(II) using a colorimetric sensor provided a high-intensity color change. However, the sensitivity of Pb(II) and Cd(II) detection decreased because the OH^- may be complexed with Pb(II) or Cd(II) by forming $\text{Pb}(\text{OH})_2$ or $\text{Cd}(\text{OH})_2$ [30]. Thus, 0.2 M NaCl ($\text{pH} = 6.0$) was used throughout this study to optimize simultaneous electrochemical and colorimetric detection using the same solution because this supporting electrolyte provided not only high sensitivity of Pb(II) and Cd(II) using electrochemistry but also a high intensity of Cu(II) by colorimetry.

The effect of accumulation potential on the stripping peaks current for Pb(II) and Cd(II) was individually examined over the potential range of -0.6 to -1.4 V vs Ag/AgCl. The accumulation potential of -1.2 V vs Ag/AgCl was optimal because it yielded the

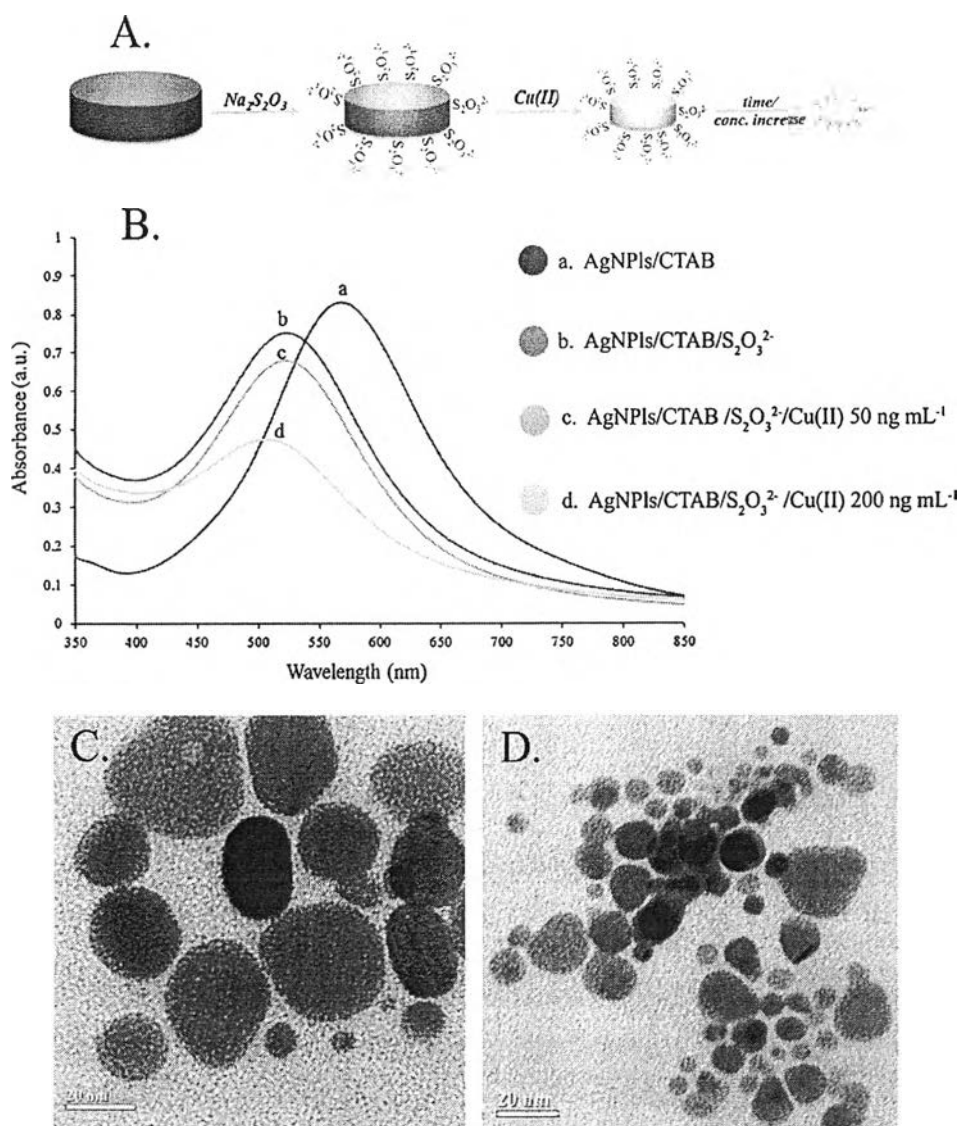


Fig. 3. Schematic mechanism of sensing Cu(II) based on catalytic etching of silver nanoplates (AgNPs) with thiosulfate ($S_2O_3^{2-}$) (A). The absorption spectra of AgNPs/CTAB/AgNPs (a), $S_2O_3^{2-}$ /CTAB/AgNPs (b), $S_2O_3^{2-}$ /CTAB/AgNPs + 50 ng mL⁻¹ of Cu²⁺ (c) and $S_2O_3^{2-}$ /CTAB/AgNPs + 200 ng mL⁻¹ of Cu²⁺ (d) (B). The experiment was performed at room temperature, and the UV-vis spectra was investigated after 5 min. The TEM images of $S_2O_3^{2-}$ /CTAB/AgNPs without Cu(II) (C) and with 100 ng mL⁻¹ of Cu(II) (D).

Table 1
Operating conditions and parameters for the simultaneous determination of Pb(II), Cd(II) and Cu(II).

Optimization parameter	Range of study	Selected
Supporting electrolyte	HCl, NaCl, Ammonia buffer pH 9	NaCl
Deposition potential	-0.6 to -1.4 V	-1.2 V
Deposition time or incubation time	0 to 180 s	120 s
Concentration of Bi(III)	0.5 to 3 μg mL ⁻¹	2 μg mL ⁻¹
Concentration of AgNPs	100 to 900 μg mL ⁻¹	500 μg mL ⁻¹
Concentration of Na ₂ S ₂ O ₃	1 to 10 mM	5 mM

highest stripping peak currents (Fig. S2A). The effect of the accumulation potential on both electrochemical detection and colorimetric detection was examined in the range of 0–180 s. Fig. S2B indicated that the stripping peak currents of Pb(II) and Cd(II) increased with an increase in the accumulation time. Therefore, an accumulation time of 120 s was used throughout this study. In addition, this accumulation time provides not only high sensitivity but also a short analysis time.

Next, the effect of the bismuth film was optimized by varying the concentration of the Bi(III) plating solution in the range of 0.5–3 μg mL⁻¹. As shown in Fig. S2C, the stripping peak currents of the Pb(II) and Cd(II) increased with an increase in concentration of Bi(III) from 0 to 2 μg mL⁻¹ and subsequently decreased at 2.5–3 μg mL⁻¹ Bi(III) concentrations, which is probably due to the fact that the thick bismuth film might hinder the mass transfer of both metal ions during the stripping step [31]. Therefore, the

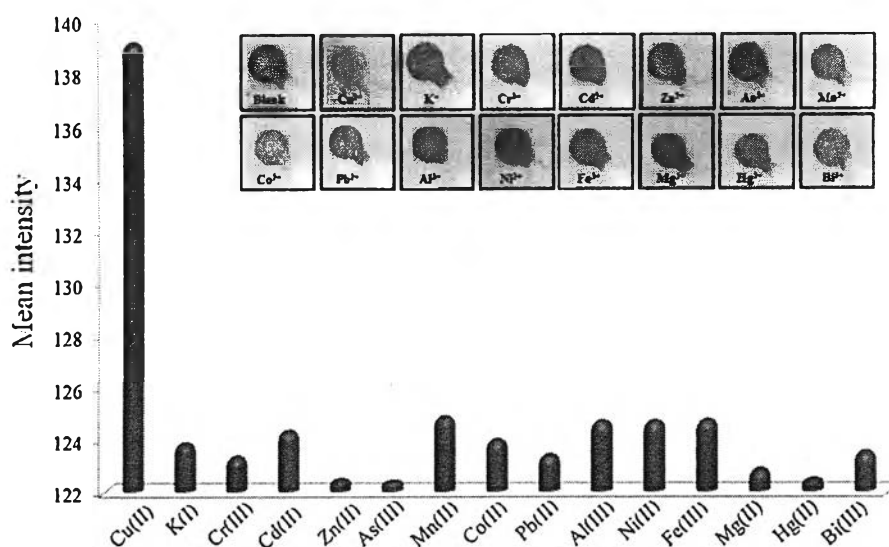


Fig. 4. Mean color intensity values of the modified AgNPIs on μ PAD after the addition of different common metal ions at the concentration of 100 ng mL^{-1} Cu(II) and $10 \text{ }\mu\text{g mL}^{-1}$ common metals. Inset: photographic images of the colorimetric determination of metal ions on paper-based devices.

Bi(III) plating solution concentration of $2 \text{ }\mu\text{g mL}^{-1}$ was chosen for the determinations of Pb(II) and Cd(II).

3.3.2. Optimization of the parameters for the colorimetric detection of Cu(II) levels

For the system that contains 100 ng mL^{-1} of Cu(II), a number of parameters, including the concentrations of the AgNPIs, concentration of $\text{S}_2\text{O}_3^{2-}$ and incubation time were investigated. The difference in the color intensity values before and after the addition of Cu(II) ($\Delta I = I_{\text{sample}} - I_{\text{blank}}$) was considered for determining the optimal conditions. For the effect of AgNPI concentration, different concentrations of AgNPIs in the range of $100\text{--}900 \text{ }\mu\text{g mL}^{-1}$ was investigated. The best ΔI was determined at $500 \text{ }\mu\text{g mL}^{-1}$ (Fig. S3A). Thus, $500 \text{ }\mu\text{g mL}^{-1}$ was used in the subsequent experiments. Then, the influence of $\text{S}_2\text{O}_3^{2-}$ concentration on ΔI is examined and illustrated in Fig. S3B. The ΔI increased with an increase in the concentration of $\text{S}_2\text{O}_3^{2-}$ and slightly decreased above 5.0 mM . Therefore, the concentration at 5.0 mM $\text{S}_2\text{O}_3^{2-}$ was selected as the optimized concentration. The effect of incubation time was investigated in the range of $0\text{--}210 \text{ s}$ as shown in Fig. S3C. The ΔI increased linearly with an increase in incubation time. Then, 120 s was selected as the optimum reaction time to obtain a distinct color difference in our paper devices. Table 1 summarized all optimum experimental conditions for the simultaneous determination of Pb(II), Cd(II) and Cu(II) using the proposed μ PAD.

3.4. Interferences

For electrochemical detection, the interference study was performed by adding common metal ions into a standard solution that contains 50 ng L^{-1} Pb(II) and Cd(II). Using $\pm 5.0\%$ tolerance ratios (Fig. 5A), the results indicated that the 1000-fold (green-column) K(I), Mg(II), Mn(II), Al(III), 500-fold (light green-column) As(III), Fe(III), Cr(III), 400-fold (yellow-column) Zn(II), Hg(II), Co(II), Ni(II) and 200-fold (red-column) Cu(II) had no significant effect on the signals of Pb(II) and Cd(II). For colorimetric detection, the concentration of common metal ions was investigated at more than 100 times the Cu(II) concentration (100 ng L^{-1} of Cu(II) and $10 \text{ }\mu\text{g mL}^{-1}$ of K(I), Cr(III), Cd(II), Zn(II), As(III), Mn(II), Co(II), Pb(II), Al(III), Ni(II), Fe(III), Mg(II), Hg(II) and Bi(III)). The results indicated that the color of solution did not change to colorless after the addition of these common metal ions, as shown in Fig. 5B. This finding indicates that

these common metal ions did not interfere in the determination of Cu(II) based on the catalytic etching of AgNPIs with $\text{S}_2\text{O}_3^{2-}$ using μ PAD.

3.5. Analytical performance of μ PAD coupled dual electrochemical and colorimetric detection

Calibration curves for the simultaneous determination of Pb(II), Cd(II) and Cu(II) were achieved by μ PAD with dual electrochemical and colorimetric detection in optimal conditions. For electrochemical detection, the anodic stripping voltammetry (ASV) of the different concentrations of Pb(II) and Cd(II) are shown in Fig. 6. The resulting calibration plots are linear over the concentration range from 0.5 to 70 ng mL^{-1} for both Pb(II) and Cd(II). The detection limit of Pb(II) and Cd(II), which was calculated based on three times the signal of the background noise ($3S/N$), were 0.1 ng L^{-1} (Pb(II) = 0.48 nM and Cd(II) = 0.89 nM) for both target metals. The relative standard deviation (RSD) for the electrochemical detection was 4.13% and 4.22% for Pb(II) and Cd(II), respectively. For colorimetric detection, the increasing concentrations of Cu(II) in the range of $0\text{--}450 \text{ ng mL}^{-1}$, the color of the modified AuNPIs on μ PADs gradually changed from pinkish violet to colorless (Fig. 7). A linear correlation between ΔI and the concentration of Cu(II) was observed in the range from 10 to 350 ng mL^{-1} (as shown in inset). We can probably discriminate the concentration of Cu(II) using the naked eye compared with the reference color zone. The detection limit of the colorimetric detection was calculated based on $3sd/\text{slope}$, where sd is the standard deviation of the blank samples and the slope was obtained from the standard correlation curve between the intensity of the signals and the concentration of Cu(II). The statistical analysis revealed that the detection limit of Cu(II) was 4.12 ng mL^{-1} or 64.8 nM , which is significantly lower than the maximum allowable levels of $\sim 20 \text{ }\mu\text{M}$ in the United States, $\sim 30 \text{ }\mu\text{M}$ in the European Union, and $\sim 31 \text{ }\mu\text{M}$ in Thailand [32].

3.6. Analytical application

A μ PAD was successfully applied for the simultaneous determination of Pb(II), Cd(II) and Cu(II) in several samples, such as groundwater, stream water, fish and rice samples. The results are summarized in Table 2; the % recovery of the spiked Pb(II), Cd(II) and Cu(II) were $82.2\text{--}102.6\%$, $81.6\text{--}102.9\%$ and $71.7\text{--}96.9\%$, respec-

Table 2
Simultaneous determination of Pb(II), Cd(II) and Cu(II) in real sampl.

Samples	Electrochemical detection						Colorimetric detection					
	Cadmium			Lead			Copper					
	Concentration of Cd (II) (ng mL ⁻¹)		Mean%Recovery (X̄ ± SD)	RSD (%)	Concentration of Pb (II) (ng mL ⁻¹)		Mean%Recovery (X̄ ± SD)	RSD (%)	Concentration of Cu (II) (ng mL ⁻¹)		Mean%Recovery (X̄ ± SD)	RSD (%)
	Amount of added	Amount of found		Amount of added	Amount of found			Amount of added	Amount of found			
Groundwater	0	ND	–	–	0	ND	–	–	0	30.93	–	–
	5	4.24	84.82 ± 2.84	3.34	5	4.74	94.70 ± 4.37	4.62	10	38.23	73.01 ± 4.59	6.29
	30	26.37	87.91 ± 1.94	2.21	30	24.66	82.20 ± 5.21	6.34	50	75.98	90.12 ± 4.23	4.69
	60	55.68	92.79 ± 1.52	1.64	60	61.59	102.64 ± 3.69	3.60	100	123.43	92.53 ± 3.21	3.47
Stream water	0	ND	–	–	0	ND	–	–	0	43.22	–	–
	5	4.08	81.68 ±	3.09	5	4.62	92.34 ± 5.06	5.48	10	50.39	71.71 ± 3.93	5.48
	30	28.23	94.12 ± 4.60	4.89	30	25.81	86.04 ± 4.38	5.09	50	89.05	91.66 ± 4.23	4.61
	60	58.82	98.04 ± 1.89	1.93	60	59.06	98.43 ± 2.10	2.13	100	139.64	96.42 ± 3.12	3.24
Rice	0	ND	–	–	0	ND	–	–	0	47.74	–	–
	5	4.27	85.35 ± 4.26	4.99	5	4.28	85.50 ± 0.96	1.12	10	55.83	80.94 ± 3.84	4.74
	30	28.52	95.07 ± 8.77	9.22	30	26.09	86.96 ± 5.73	6.59	50	92.45	89.42 ± 2.12	2.37
	60	58.39	97.32 ± 6.59	6.77	60	58.28	97.14 ± 3.61	3.71	100	143.22	95.48 ± 1.34	1.40
Fish	0	ND	–	–	0	ND	–	–	0	18.86	–	–
	5	4.77	95.31 ± 1.39	1.46	5	4.72	94.31 ± 3.01	3.19	10	26.23	73.72 ± 3.63	4.92
	30	30.22	100.72 ± 1.54	1.53	30	28.95	96.50 ± 3.65	3.78	50	67.32	96.92 ± 3.42	3.53
	60	61.77	102.94 ± 1.82	1.76	60	59.22	98.70 ± 3.95	4.00	100	111.96	93.13 ± 1.99	2.14

ND = Not detection.

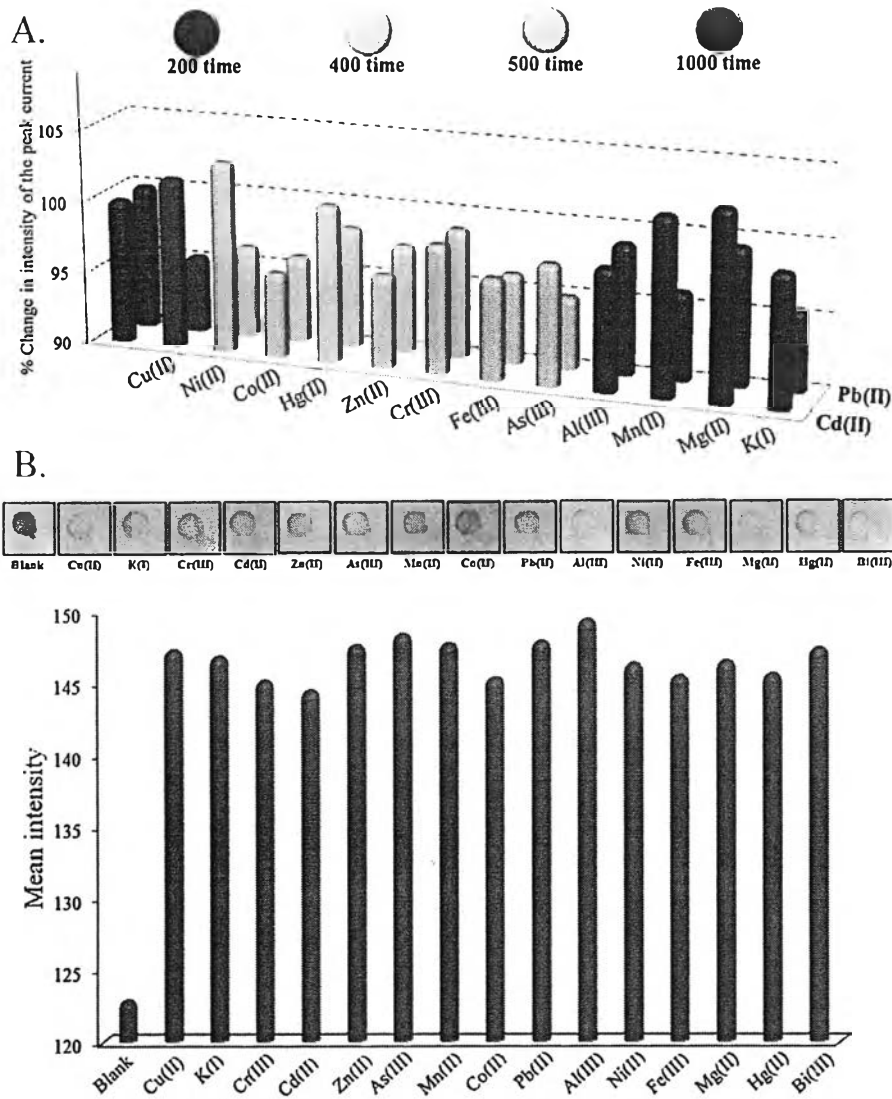


Fig. 5. Tolerance ratio of interfering ions in the electrochemical determination of 50 ng mL^{-1} of Pb(II) and Cd(II) (A). Effect of common metal ions ($10 \mu\text{g mL}^{-1}$) in the colorimetric determination of 100 ng mL^{-1} of Cu(II) (B). Inset (B): corresponding photographs of the paper-based sensor at the colorimetric detection zone after the addition of Cu(II) with various common metal ions.

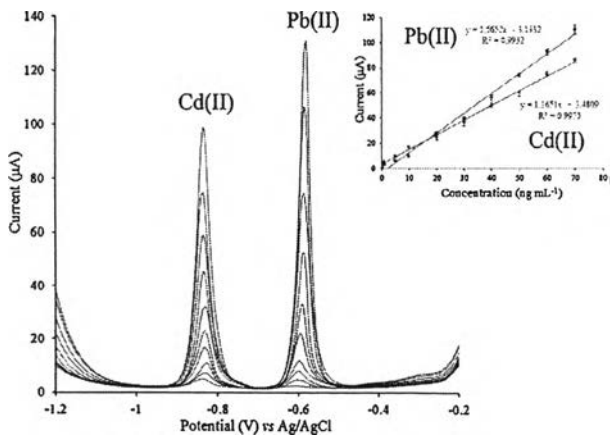


Fig. 6. Anodic stripping voltammograms and respective calibration curves or increasing concentration of Pb(II) and Cd(II) ($0.5\text{--}70 \text{ ng mL}^{-1}$) in 0.2 M NaCl solution at Bi-BDDE.

tively. The excellent average recoveries suggest that the proposed method offers benefits for various samples that contain Pb(II), Cd(II) and Cu(II). To validate the accuracy of this method, the results from μPAD were compared with the results obtained by inductively coupled plasma optical emission spectrometry (ICP – OES). A paired t-test at the 95% confidence level was performed; the statistics revealed that the $t_{\text{calculated}}$ of Pb(II) and Cd(II) were below t_{critical} (4.30), which suggests no significant difference between the two methods and indicates the applicability and reliability of the proposed method.

4. Conclusions

A new microfluidic paper-based analytical device that combines electrochemical and colorimetric detection was developed for the simultaneous determination of Pb(II), Cd(II) and Cu(II). The bismuth-modified boron doped diamond electrode was employed as a working electrode for the highly sensitive determination of Pb(II) and Cd(II). The specific determination of Cu(II) is based on colorimetric detection using the catalytic etching of silver nanoplates

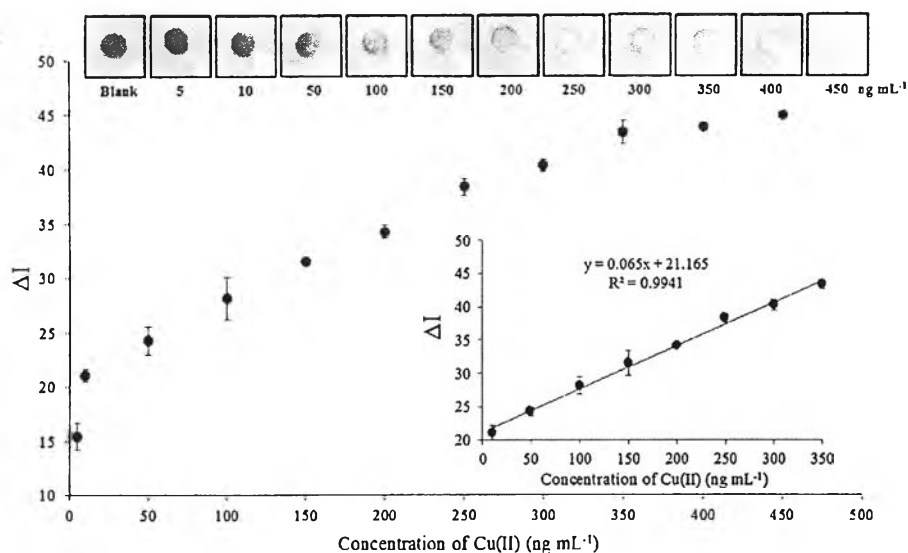


Fig. 7. Photographs of the paper-based sensor at the colorimetric detection zone for the detection of Cu(II) at various concentrations (A). The plot of the mean intensity of the color of the AgNPs determined by photograph analysis using NIH ImageJ vs. Cu(II) concentration (0–450 ng mL⁻¹) (B). Inset: linear regression analysis and best-fit line in the concentration range of 10–350 ng mL⁻¹.

by thiosulfate. In optimal conditions, the minimum detection limits of 0.1 ng L⁻¹ for both Pb(II) and Cd(II) were achieved by electrochemical detection, and the minimum detection limits of 4.12 ng mL⁻¹ of Cu(II) were achieved by colorimetric detection. We have demonstrated the ability of the microfluidic paper-based analytical device for the simultaneous determination of Pb(II), Cd(II) and Cu(II) in several samples; they were validated using the ICP-OES method, which confirmed the accuracy and reliability of the approach. Therefore, we propose that these devices are cost-effective and simple for the simultaneous determination of Pb(II), Cd(II) and Cu(II) without the need for complicated instrumentation, which could be very useful for food and environmental analysis.

Acknowledgments

This study was financially supported by the Thailand Research Fund (TRF) via the Royal Golden Jubilee Ph.D. program (Grant Number PHD/0127/2556), the Thailand Research Fund via the Research Team Promotion Grant (RTA5780005) and the 90th Anniversary of Chulalongkorn University Fund (GCUGR1125582008D). WS would to thank partially financial supported by Srinakharinwirot University.

Appendix A. Supplementary data

Supplementary data associated with this article can be found, in the online version, at <http://dx.doi.org/10.1016/j.snb.2016.04.109>.

References

- [1] T. Kemper, S. Sommer, Estimate of heavy metal contamination in soils after a mining accident using reflectance spectroscopy, *Environ. Sci. Technol.* 36 (2002) 2742–2747.
- [2] M.E. Mahmoud, I.M.M. Kenawy, M.M.A.H. Hafez, R.R. Lashein, Removal, preconcentration and determination of trace heavy metal ions in water samples by AAS via chemically modified silica gel N-(1-carboxy-6-hydroxy) benzylidene propylamine ion exchanger, *Desalination* 250 (2010) 62–70.
- [3] B. Dai, M. Cao, G. Fang, B. Liu, X. Dong, M. Pan, S. Wang, Schiff base-chitosan grafted multiwalled carbon nanotubes as a novel solid-phase extraction adsorbent for determination of heavy metal by ICP-MS, *J. Hazard. Mater.* 219–220 (2012) 103–110.
- [4] I. Jarić, Ž. Višnjić-Jeftić, G. Cvijanović, Z. Gačić, L. Jovanović, S. Skorić, M. Lenhardt, Determination of differential heavy metal and trace element accumulation in liver, gills, intestine and muscle of sterlet (*Acipenser ruthenus*) from the Danube River in Serbia by ICP-OES, *Microchem. J.* 98 (2011) 77–81.
- [5] H. Huang, T. Chen, X. Liu, H. Ma, Ultrasensitive and simultaneous detection of heavy metal ions based on three-dimensional graphene-carbon nanotubes hybrid electrode materials, *Anal. Chim. Acta* 852 (2014) 45–54.
- [6] J.A. Rodrigues, C.M. Rodrigues, P.J. Almeida, L.M. Valente, L.M. Gonçalves, R.G. Compton, A.A. Barros, Increased sensitivity of anodic stripping voltammetry at the hanging mercury drop electrode by ultracathodic deposition, *Anal. Chim. Acta* 701 (2011) 152–156.
- [7] C.M.A. Brett, D.A. Fungaro, Poly(ester sulphonic acid) coated mercury thin film electrodes: characterization and application in batch injection analysis stripping voltammetry of heavy metal ions, *Talanta* 50 (2000) 1223–1231.
- [8] S. Chuanwatanakul, W. Dungchai, O. Chalapakul, S. Motomizu, Determination of trace heavy metals by sequential injection-anodic stripping voltammetry using bismuth film screen-printed carbon electrode, *Anal. Sci.* 24 (2008) 589–594.
- [9] L. Zhu, L. Xu, B. Huang, N. Jia, L. Tan, S. Yao, Simultaneous determination of Cd(II) and Pb(II) using square wave anodic stripping voltammetry at a gold nanoparticle-graphene-cysteine composite modified bismuth film electrode, *Electrochim. Acta* 115 (2014) 471–477.
- [10] U. Injang, P. Noyrod, W. Siangproh, W. Dungchai, S. Motomizu, O. Chalapakul, Determination of trace heavy metals in herbs by sequential injection analysis-anodic stripping voltammetry using screen-printed carbon nanotubes electrodes, *Anal. Chim. Acta* 668 (2010) 54–60.
- [11] L. Cao, J. Jia, Z. Wang, Sensitive determination of Cd and Pb by differential pulse stripping voltammetry with in situ bismuth-modified zeolite doped carbon paste electrodes, *Electrochim. Acta* 53 (2008) 2177–2182.
- [12] K.E. Toghiani, G.G. Wildgoose, A. Moshar, C. Mulcahy, R.G. Compton, The fabrication and characterization of a bismuth nanoparticle modified boron doped diamond electrode and its application to the simultaneous determination of cadmium(II) and lead(II), *Electroanalysis* 20 (2008) 1731–1737.
- [13] K. Pecková, J. Musilová, J. Barek, Boron-doped diamond film electrodes—new tool for voltammetric determination of organic substances, *Crit. Rev. Anal. Chem.* 39 (2009) 148–172.
- [14] D. Yang, L. Wang, Z. Chen, M. Megharaj, R. Naidu, Investigation of copper(II) interference on the anodic stripping voltammetry of lead(II) and cadmium(II) at bismuth film electrode, *Electroanalysis* 25 (2013) 2637–2644.
- [15] J. Wang, J. Lu, A. Kirgiz, S.B. Hocevar, B. Ogorevc, Insights into the anodic stripping voltammetric behavior of bismuth film electrodes, *Anal. Chim. Acta* 434 (2001) 29–34.
- [16] A.W. Martinez, S.T. Phillips, M.J. Butte, G.M. Whitesides, Patterned paper as a platform for inexpensive low-volume, portable bioassays, *Angew. Chem. Int. Ed.* 46 (2007) 1318–1320.
- [17] S.M. Hossain, J.D. Brennan, β-galactosidase-based colorimetric paper sensor for determination of heavy metals, *Anal. Chem.* 83 (2011) 8772–8778.
- [18] W. Dungchai, O. Chalapakul, C.S. Henry, Electrochemical detection for paper-based microfluidics, *Anal. Chem.* 81 (2009) 5821–5826.
- [19] J. Yu, L. Ge, J. Huang, S. Wang, S. Ge, Microfluidic paper-based chemiluminescence biosensor for simultaneous determination of glucose and uric acid, *Lab Chip* 11 (2011) 1286–1291.

- [20] J.L. Delaney, C.F. Hogan, J. Tian, W. Shen, Electrogenated chemiluminescence detection in paper-based microfluidic sensors, *Anal. Chem.* 83 (2011) 1300–1306.
- [21] A.C. Siegel, S.T. Phillips, B.J. Wiley, G.M. Whitesides, Thin, lightweight, foldable thermochromic displays on paper, *Lab Chip* 9 (2009) 2775–2781.
- [22] A. Apilux, W. Dungchai, W. Siangproh, N. Praphairaksit, C.S. Henry, O. Chailapakul, Lab-on-paper with dual electrochemical/colorimetric detection for simultaneous determination of gold and iron, *Anal. Chem.* 82 (2010) 1727–1732.
- [23] S. Chaiyo, W. Siangproh, A. Apilux, O. Chailapakul, Highly selective and sensitive paper-based colorimetric sensor using thiosulfate catalytic etching of silver nanoparticles for trace determination of copper ions, *Anal. Chim. Acta* 866 (2015) 75–83.
- [24] Kh. Z. Brainina, N.Y. Stozhko, G.M. Belysheva, O.V. Inzhevatoeva, L.I. Kolyadina, C. Cremisini, M. Galletti, Determination of heavy metals in wines by anodic stripping voltammetry with thick-film modified electrode, *Anal. Chim. Acta* 514 (2004) 227–234.
- [25] T. Parnklang, C. Lertvachirapaiboon, P. Pienpinijtham, K. Wongravee, C. Thammacharoen, S. Ekgasit, H₂O₂-triggered shape transformation of silver nanospheres to nanoprisms with controllable longitudinal LSPR wavelengths, *RSC Adv.* 3 (2013) 12886–12894.
- [26] K. Keawkim, S. Chuaniwatanakul, O. Chailapakul, S. Motomizu, Determination of lead and cadmium in rice samples by sequential injection/anodic stripping voltammetry using a bismuth film/crown ether/Nafion modified screen-printed carbon electrode, *Food Control* 31 (2013) 14–21.
- [27] S.B. Hocevar, B. Ogorevc, J. Wang, B. Pihlar, A study on operational parameters for advanced use of bismuth film electrode in anodic stripping voltammetry, *Electroanalysis* 14 (2002) 1707–1712.
- [28] J.H. Luo, X.X. Jiao, N.B. Li, H.Q. Luo, Sensitive determination of Cd(II) by square wave anodic stripping voltammetry with in situ bismuth-modified multiwalled carbon nanotubes doped carbon paste electrodes, *J. Electroanal. Chem.* 689 (2013) 130–134.
- [29] A.C. Grosse, G.W. Dicoski, G.W. Shaw, P.R. Haddad, Leaching and recovery of gold using ammoniacal thiosulfate leach liquors (a review), *Hydrometallurgy* 69 (2003) 1–21.
- [30] G. Y. Li, Y. Sun, C. Zhang, N. Ge, Y. Wang Bao, A glassy carbon electrode modified with bismuth nanotubes in a silsesquioxane framework for sensing of trace lead and cadmium by stripping voltammetry, *Microchim. Acta* 181 (2014) 751–757.
- [31] G.G. Giles, Q.G. Carina, S.S. Paulo, S. Almir, In situ bismuth-film electrode for square-wave cathodic voltammetric detection of pendimethalin at nanomolar level, *Electrochim. Acta* 168 (2015) 379–385.
- [32] X. Wang, L. Chen, L. Chen, Colorimetric determination of copper ions based on the catalytic leaching of silver from the shell of silver-coated gold nanorods, *Microchim. Acta* 181 (2014) 105–110.
- [33] T. Lou, L. Chen, Z. Chen, Y. Wang, L. Chen, J. Li, Colorimetric detection of trace copper ions based on catalytic leaching of silver-coated gold nanoparticles, *ACS Appl. Mater. Interfaces* 3 (2011) 4215–4220.
- [34] R. Liu, Z. Chen, S. Wang, C. Qu, L. Chen, Z. Wang, Colorimetric sensing of copper(II) based on catalytic etching of gold nanoparticles, *Talanta* 112 (2013) 37–42.

Biographies

Sudkate Chaiyo is candidate Ph.D. at Department of Chemistry, Chulalongkorn University, Thailand. Her research field is development of electrochemical method for inorganic and organic compounds.

Amara Apiluk is Lecturer of Center for Innovation Development and Technology Transfer at Mahidol University. Her current research areas are biosensor, paper-based sensor and electrochemistry.

Weena Siangproh is Associate Professor of Department of Chemistry at Srinakharinwirot University. Her current research areas are electroanalytical applications, diamond electrode, flow-based system and lab-on-chip devices for quantitative drug and biological diagnostics, immunoassay, modified sensors.

Orawon Chailapakul is Professor of Department of Chemistry at Chulalongkorn University. Her research fields are electroanalytical detection, flow-based system and lab-on-chip, devices for various applications, immunoassay, and battery.

Chapter IV

The development of microfluidic and/or flow-based systems

Microfluidic systems have been utilized for analysis in a variety of applications, including chemical, biological, medical, environmental and pharmaceutical fields. Taking advantages from micron-scale systems, microfluidic devices offer a number of advantages, including small amount of samples and reagents required, fast analysis time, high analytical performances, portability and possibility for high-throughput analysis. Nowadays, microfluidics for medical analysis has attracted considerable attraction because of its high potential to be developed as point-of-care (POC) medical diagnostic systems. One of the most challenging tasks for developing microfluidic systems for POC analysis is that a system should be rapid, simple to use (less equipment and training), cost-effective, reliable and easily interpretable. Herein, a simple microfluidic system is developed for medical applications and further applied to be a microfluidic-based POC system and would be eventually attained to be a home-care device. There are 4 publications obtained from this project as shown below:

1. P. Rattanarat, P. Teengam, W. Siangproh, R. Ishimatsu, K. Nakano, O. Chailapakul, T. Imato, An Electrochemical Compact Disk-type Microfluidics Platform for Use as an Enzymatic Biosensor, *Electroanalysis*, 27 (2015) 703-712.
2. P. Rattanarat, A. Suea-Ngam, N. Ruecha, W. Siangproh, C.S. Henry, S.A. Monpichar, O. Chailapakul, Graphene-polyaniline modified electrochemical droplet-based microfluidic

sensor for high-throughput determination of 4-aminophenol, *Analytica Chimica Acta*, 925 (2016) 51-60.

3. A. Suea-Ngam, P. Rattanarat, O. Chailapakul, M. Srisa-Art, Electrochemical droplet-based microfluidics using chip-based carbon paste electrodes for high-throughput analysis in pharmaceutical applications, *Analytica Chimica Acta*, 883 (2015) 45-54. (IF 2015 = 4.712)

4. A. Suea-Ngam, P. Rattanarat, K. Wongravee, O. Chailapakul, M. Srisa-Art*, Droplet-based glucosamine sensor using gold nanoparticles and polyaniline-modified electrode, *Talanta*, 158 (2016) 134-141. (IF 2015 =4.035)

To overcome the limitation of batch system in term of time-consuming and require large volume of reagent. Flow-based analysis systems for various applications have been reported by several research groups to increase the speed and reproducibility of analytical methods. The present project describes the use of an automated sequential injection analysis (SIA) system and highly sensitive electrochemical detection for the determination of many kinds of target analytes in real samples. There are two reasons prompted us to develop the automatic system for analysis. Firstly, the introduction of selection valve analysers has made the measurements of analyte concentrations more generally available, and they are often made when they are requested. Furthermore, there are few publications that support the use of the automatic system for detection. This accurate and precise proposed system should be useful to routine analysis. There are 4 publications obtained from this project as shown below:

1. S. Chaiyo, O. Chailapakul, W. Siangproh, Highly sensitive determination of mercury using copper enhancer by diamond electrode coupled with sequential injection–anodic stripping voltammetry, *Analytica Chimica Acta*, 852 (2014) 55-62.
2. E. Punrat, C. Maksuk, S. Chuanuwatanakul, W. Wonsawat, O. Chailapakul, Polyaniline/graphene quantum dot-modified screen-printed carbon electrode for the rapid determination of Cr(VI) using stopped-flow analysis coupled with voltammetric technique, *Talanta*, 150 (2016) 198-205.
3. P. Ruengpirasiri, E. Punrat, O. Chailapakul, S. Chuanuwatanakul, Graphene Oxide-Modified Electrode Coated with in-situ Antimony Film for the Simultaneous Determination of Heavy Metals by Sequential Injection-Anodic Stripping Voltammetry, *Electroanalysis*, 29 (2017) 1022-1030.
4. E. Punrat, P. Tutiyaarn, S. Chuanuwatanakul, W. Wonsawat, O. Chailapakul* Determination of nickel(II) by ion-transfer to hydroxide medium using sequential injection-electrochemical analysis (SIECA), *Talanta*, 168 (2017) 286-290.

The detail of each work is shown in the following part.

DOI: 10.1002/elan.201400590

An Electrochemical Compact Disk-type Microfluidics Platform for Use as an Enzymatic Biosensor

Poomrat Rattanarat,^[a] Prinjaporn Teengam,^[b] Weena Siangproh,^[c] Ryoichi Ishimatsu,^[d] Koji Nakano,^[d] Orawon Chailapakul,^{*,[a,e]} and Toshihiko Imato^{*,[d]}

Abstract: A novel centrifuge-based microfluidic device coupled with an electrochemical detector for the determination of glucose in control human serum is described. The electrochemical compact disk (eCD) platform was based on a poly(dimethylsiloxane) (PDMS) material containing reservoir, a mixing chamber, a spiral channel, a carbon-paste electrode (CPE) detector, and a waste reservoir. For electrode fabrication, a mixture consisting of cobalt phthalocyanine (CoPC), graphite powder, PDMS, and mineral oil was printed and formulated into a PDMS-based electrode pattern. To enhance electrochemical sensitivity, a graphene-polyaniline (G-PANI) nanocomposite solution was cast onto the working electrode surface. During the rotation of the eCD platform at a rotation speed of ~1000 rpm, a glucose solution and a glucose oxidase solution in separated reservoirs were

mixed in a spiral channel to produce hydrogen peroxide by an enzymatic reaction. The produced hydrogen peroxide was determined using the electrode detector set at an applied potential of +0.4 V vs. CPE (pseudo reference electrode). Under optimal conditions, a linear calibration ranging from 1 to 10 mM with a limit of detection (LOD) of 0.29 mM ($S/N=3$) and a limit of quantitation (LOQ) of 0.97 mM ($S/N=10$) was obtained. Various common interference compounds including ascorbic acid, uric acid, paracetamol, and L-cysteine were tested. Finally, glucose in control serum samples containing certified concentrations were amperometrically determined and validated. Glucose levels measured using the eCD system matched actual values for the certified reference serum samples with satisfactory accuracy.

Keywords: Compact disk-type microfluidics • Electrochemical detection • Glucose oxidase • Human serum

1 Introduction

Miniaturized systems including test strips and microfluidic devices continuously used in numerous applications such as point of care testing, agricultural quality control, food analysis, and environmental monitoring [1–4]. With its capability, which including portability, prompt response time, and low cost of manufacturing, miniaturized testing devices have proven to be beneficial for handling on-site analysis in remote areas. In terms of clinical diagnosis, the devices can act as a preliminary screening tool which would be able to reduce potential risks associated with aggressive diseases and improve the quality of life for many people. Microfluidics is an innovative technology platform which is geometrically designed in sub-millimeter scale. This device is frequently fabricated on glass [5] or a polymer [6] containing a micropattern platform. In general, the flow of liquids through their channels can be controlled using liquid mechanical pumping or a high voltage power supply for normal flow injection and electrokinetic systems [7–8], respectively. For detection, various common analytical measurements comprising of optical imaging [9], absorbance [10] and fluorescence spectroscopy [11], and mass spectrometry [12] have been used. The main disadvantages of complicated propulsion and detection systems are their high cost and difficulty to couple with miniaturized systems for fieldwork applica-

tions. Therefore, all of these developments present novel analytical challenges which need to be addressed.

Compact disk (CD)-based microfluidics is a new class of miniaturized high-throughput screening systems incor-

- [a] P. Rattanarat, O. Chailapakul
Electrochemistry and Optical Spectroscopy Research Unit,
Department of Chemistry, Faculty of Science, Chulalongkorn
University
Patumwan, Bangkok 10330, Thailand
*e-mail: corawon@chula.ac.th
- [b] P. Teengam
Program in Petrochemistry, Faculty of Science,
Chulalongkorn University
Patumwan, Bangkok 10330, Thailand
- [c] W. Siangproh
Department of Chemistry, Faculty of Science,
Srinakharinwirot University
Sukhumvit 23, Wattanna, Bangkok, 10110, Thailand
- [d] R. Ishimatsu, K. Nakano, T. Imato
Department of Applied Chemistry, Graduate School of
Engineering, Kyushu University
Fukuoka, 819-0395, Japan
*e-mail: imato@cstf.kyush-u.ac.jp
- [e] O. Chailapakul
National Center of Excellence for Petroleum,
Petrochemicals, and Advanced Materials, Chulalongkorn
University
Bangkok 10330, Thailand

porate various laboratory functionalities such as sampling, mixing, reaction, and detection [13–14]. The testing and reagent solutions are allowed to flow by centrifugal force. Furthermore, the flow rate can be varied by adjustment of the speed of rotation of the disk via the use of a portable rotary motor system. The solution from the reservoir located at the center of the disk is pumped through the channels and then flows towards to outer perimeter of disk. The advantageous centrifugal pumping is that it is relatively insensitive to physicochemical properties such as pH, ionic strength or chemical composition (in contrast to electroosmotic pumping). The utility of CD technology has progressed and is not used in applications in biomedical diagnosis, food safety, and environmental monitoring. Some reports [13, 15–18] have concentrated on measuring several analyte of interest using CD microfluidics. For example, various applications have been reported including enzyme-linked immunosorbent assay (ELISA) for rat immunoglobulin G (IgG) [18] and immunoglobulin A (IgA) [15], cultivation and behavioral observation of *Caenorhabditis elegans* [17], a label-free haptoglobin assay [13], and simultaneous determination of cationic and anionic nutrients (nitrite, nitrate and nitrite, ammonium, orthophosphate, and silicate) in water samples [16]. All of these analyses used spectrophotometric detection. To the best of our knowledge, only a few publications concerning electrochemical detection in centrifugal CD-based microfluidics have appeared.

Electrochemical detection offers great promise with excellent features including remarkable sensitivity, inherent miniaturization of both the detector and control instrumentation [3, 19–21]. Moreover, this technique is independence of sample turbidity or optical path length, is low cost, and power demands are minimal. Among the electrochemical enzymatic sensors, glucose sensors have been broadly developed because their effectiveness in the point-of-care testing of diabetic human subjects. Over the past five decades, the classical glucose biosensor was based on the consumption of oxygen due to an enzymatic reaction between glucose and glucose oxidase (GOx) and measurement of hydrogen peroxide (H_2O_2), the product of the reaction [22]. Unfortunately, a high applied potential value of H_2O_2 electro-oxidation for amperometric detection is required [23].

As a result, the objective of this research was to develop a novel CD-based microfluidics instrument coupled with a screen-printed electrode for the determination of glucose. To accomplish this, a screen-printed carbon paste electrode was first incorporated onto a CD-based microfluidics platform for in-microchannel detection within the CD-flow pattern. Outstanding electrode modifiers consisting of graphene-polyaniline (G-PANI) nanocomposite and cobalt phthalocyanine (CoPc) electrocatalyst were selected to reduce the applied potential to 0.4 V. vs. CPE for monitoring the H_2O_2 product produced in the enzymatic reaction. This modified electrode also enhanced the electrochemical response of produced H_2O_2 [24–25]. Due to the centrifugal force, a test sample solution and a glu-

cose oxidase (GOx) (an enzyme) solution were physically mixed at the mixing chamber of the CD microfluidics platform. Significant parameters including rotating speed, applied potential, GOx concentration were then optimized. Common interfering substances at the highest levels that are present in human serum (except paracetamol) have a negligible effect towards glucose detection. Finally, our proposed method was applied to the quantitation of glucose in human serum and the results were found to be acceptable.

2 Experimental

2.1 Chemicals and Reagents

The SU-8 negative photoresist and developer were purchased from MicroChem Corp. (Newton, MA). All chemicals were analytical grade. The following materials and chemicals were used as received: mineral oil (Perkin Elmer, Thailand), graphite powder ($\leq 20 \mu\text{m}$, Sigma-Aldrich, Singapore), and poly(dimethylsiloxane) (PDMS) Sylgard 184 elastomer kit (Dow Corning, USA). Sodium chloride (NaCl), disodium hydrogen phosphate (Na_2HPO_4), potassium dihydrogen phosphate (KH_2PO_4), potassium chloride (KCl) and albumin were purchased from Wako Pure Chemicals Industry (Japan) for preparation of phosphate buffer saline (PBS) 0.1 M pH 7.4. Glucose oxidase (GOx) and potassium ferricyanide ($K_3[Fe(CN)_6]$) were obtained from Sigma-Aldrich (Singapore). Glucose (Glu), dopamine hydrochloride (DA), ascorbic acid (AA), uric acid (UA), paracetamol (PA), cysteine (Cys), citric acid, fructose, glycine, urea, and albumin were purchased from Wako Pure Chemicals Industry (Japan). Polyaniline and camphor-10-sulfonic acid ($C_{10}H_{16}O_4S$) were purchased from Merck (Darmstadt, Germany). Graphene (G) was purchased from A. C.S (Medford, USA). Control human serum samples consisting of level I and II were obtained from Aalto Scientific, Ltd. (San Marcos, CA, USA). Millipore filtered water on a Milli-Q system (Nihon Millipore, Tokyo, Japan) was used throughout this experiment.

2.2 Fabrication of Electrochemical Compact-Disk (eCD system)

2.2.1 Compact-Disk Microfluidic Platform

Figure 1a shows the conceptual design of the compact-disk microfluidics set up, comprised of 2 layers of PDMS-based microchannel and electrode. The configuration of eCD platform was described as follows; for upper PDMS layer, microchannel width was $500 \mu\text{m}$ while the thickness was $100 \mu\text{m}$. The reservoir diameter on the CD platform was 5 mm. The radius between each reservoir and the center of the compact disk was 35 mm and 27 mm for testing solution and washing solution, respectively. Microchannel was constructed of PDMS using a soft lithography method as follows [26]. Briefly, the SU-8 negative photoresist was coated onto a silicon wafer substrate

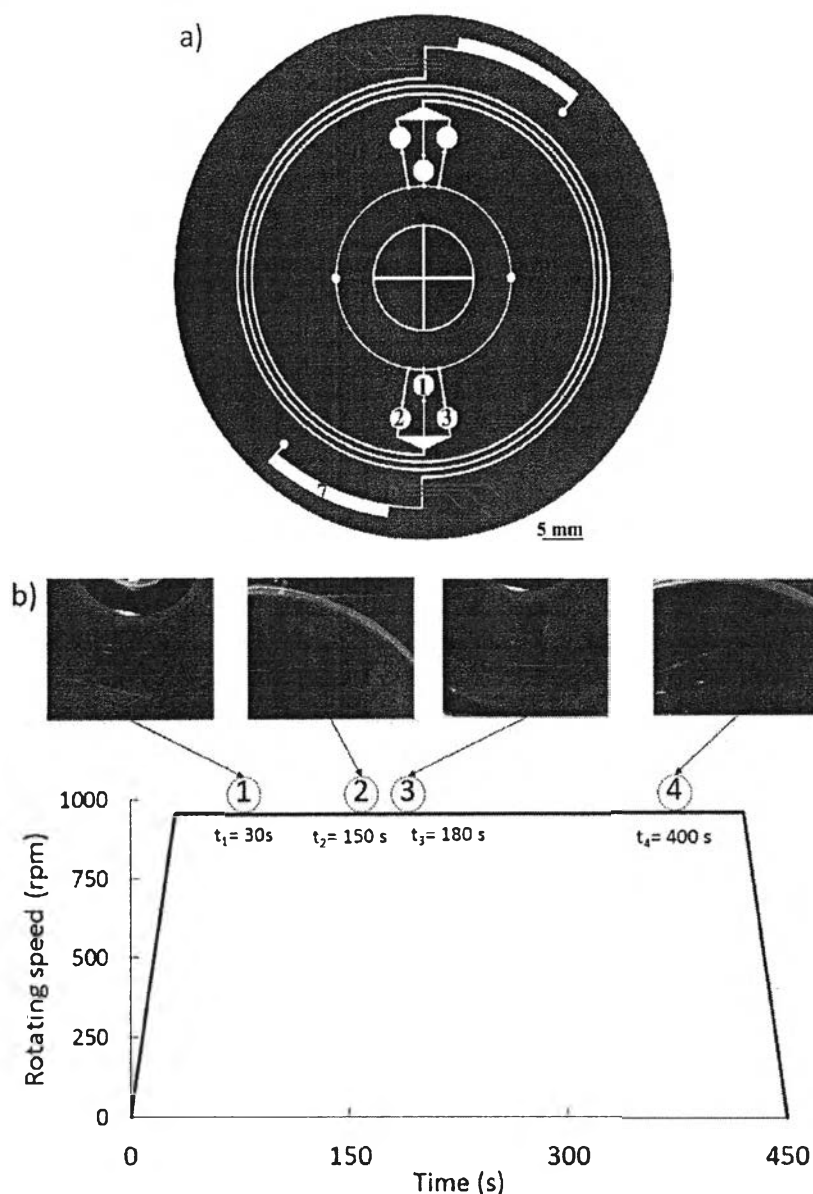


Fig. 1. a) Concept design of eCD microchip consisting of 1: washing solution reservoir, 2: enzyme reservoir, 3: sample reservoir, 4: spiral mixing channel, 5: G-PANI/CoPc-CPE, 6: detection zone, and 7: waste reservoir. b) Rotating speed set up to the centrifugal force for controlling the delivery of the solution system inside CD microchip within 450 s (Inset) captured frames obtained from high speed camera.

using a spin coater (K-359S1, Kyowariken, Tokyo, Japan) at 500 rpm for 20 s and 2000 rpm for 30 s, respectively. The silicon substrate was baked at 65°C for 5 min and 95°C for 45 min. The transparent films containing the microchannel and electrode design (Figure 1 a) were aligned onto the baked silicon wafer. The baked silicon wafer was then exposed to ultra-violet (UV) light using UV exposure device (BOX-W98, Sunhayato, Tokyo, Japan). The SU-8 master template of CD microfluidic was obtained after treating by SU-8 developer and isopropanol, respectively. Next, the mixture between PDMS and a curing agent in a 10:1 ratio was prepared and degassed under vacuum conditions to remove air bubbles in the PDMS

mixture. The clear PDMS mixture was poured over both SU-8 masters and baked in an oven at 65°C for at least 2 h. The cross-linked PDMS was peeled off the mold and punched by using a circular punch to create the reservoirs.

2.2.2 Graphene-Polyaniline Nanocomposite Modified Cobalt Phthalocyanide-Carbon Paste Electrode (G-PANI/CoPc-CPE)

We followed the previous procedures reported by Samee-noi et al. [27] to fabricate the screen-printed carbon-paste electrode for in-channel detection within the CD micro-

fluidics platform. First, CoPC and a graphite composite (10% w/w) was prepared by adding CoPc to graphite powder and mixing with diethylether to provide a well homogenized CoPc-graphite mixture. The diethylether was completely evaporated to produce a dehydrated powder of 10% (w/w) CoPc-graphite composite. Next, a paste comprised of CoPc-graphite powder, PDMS, and mineral oil in a ratio of 2:1:1 was extensively mixed and then spread onto the PDMS electrode channel. Excess carbon paste was removed using Scotch Magic Tape until a clear carbon paste electrode was obtained.

For the electrode modifier, graphene-polyaniline (G-PANI) nanocomposite was prepared using a liquid/liquid interfacial polymerization method [28]. Briefly, graphene powder was dispersed in a hydrochloric acid solution containing FeCl_3 , which was used as the water phase. The oil phase was prepared by dissolving aniline monomer in chloroform. Both solutions consisting of an oil and a water phase were transferred to a beaker and the polymerization of polyaniline was allowed to proceed for 2 days. Finally, the product was collected by filtration and rinsed with distilled water, following drying step in a vacuum oven at 60°C for 1 day. A JEM-2100 transmission electron microscope (Japan Electron Optics Laboratory Co., Ltd, Japan) was used for the electrode characterization.

In the next step, the G-PANI nanocomposite was redispersed in an NMP solution and carefully cast onto surface area of the carbon-paste working electrode. The cast CPE was baked in an oven at 65°C . For both electrochemical sensing in batch and eCD systems, a second PDMS layer (consisting of 8 mm diameter hole or CD microchannel) was plasma-sealed to PDMS layer containing G-PANI/CoPc-CPE. The actual working electrode area for the batch system was 4 mm^2 while the eCD system was 0.25 mm^2 . Finally, copper wires were connected to the end of the CPE using silver paint (SPI supplies, West Chester, PA) and epoxy glue, respectively.

2.3 Centrifugal Rotating Procedure

The eCD microchip was set on a turn table fabricated by Kyusgu Keisoku Co., Ltd., Japan. Prior to the analysis, $10\ \mu\text{L}$ of 0.1 M PBS was added to reservoir No. 1 used as the washing solution while $10\ \mu\text{L}$ aliquots of 100 U/mL GOx and the test solution were dropped into reservoirs No. 2 and 3, respectively. Scotch Magic Tape was also used to cover all reservoirs and the waste area to prevent the leakage of solution during rotation of the CD microchip. The LabView software was used to control the rotating speed of the CD microchip by adjusting the applied voltage. In order to observe flow characteristic in the CD microchannel, a high speed camera (VW-Z1, Keyence, Co., Japan) was used to indicate the required rotating speed to provide the optimal centrifugal force to initiate solution flow. Figure 1b shows a captured photograph using a pink Rose Bengal solution for visible observation within the CD microchannel. The speed of rotation was

increased to 957 rpm within 30 s and maintained at the same speed for 390 s to generate a solution flow via centrifugal force. The mixing solution from reservoir No. 2, 3 and the flow of the washing solution were generated, respectively. All solutions had completely flowed to the waste reservoir within 400 s.

2.4 Electrochemical Detection of Glucose

For cyclic voltammetry and amperometry, a commercially available potentiostat (ALS/chi Electrochemical Analyzer Model 715AN, CH instruments, Austin, TX, USA) was used. The working electrode was either a G-PANI/CoPc-CPE or a CPE. The auxiliary and reference electrodes were CPE. All experiments were conducted at room temperature. For the batch system, cyclic voltammetry was used to characterize the electrochemical performance of the bare CPE and the G-PANI/CoPc-CPE. A cyclic voltammogram of hydrogen peroxide (H_2O_2) was recorded in the range of -0.2 to 1.0 V vs. CPE at scan rate of 100 mV/s .

An amperometric method was used for the detection of produced H_2O_2 in the eCD microchip system. To optimize the amperometric applied potential, hydrodynamic voltammetry in a range of 0.2 – 0.8 V vs. CPE was examined. The hydrodynamic voltammogram was plotted between the peak current and applied potential. The amperometric measurements were performed at the potential of 0.4 V vs. CPE which obtained from the maximum signal-to-background (S/B) ratio in the hydrodynamic voltammograms. A calibration graph between the anodic current and glucose concentration was created using the linear least square regression method. The limit of detection (LOD) and the limit of quantitation (LOQ) were calculated from $3SD_{bl}/S$ to $10SD_{bl}/S$, respectively, where SD_{bl} is the standard deviation of the blank measurement ($n=7$) and S is the slope of the linearity or sensitivity of the method. In addition, the selectivity in this work was examined by observing whether any electroactive interference, present as a main component in normal human serum was an issue. For glucose determination in control human serum, all samples were directly tested using the eCD microchip system without any pretreatment procedure.

3 Results and Discussion

3.1 eCD Design

To investigate the flow characteristic of a solution within a channel, the fluidic manipulation of Rose Bengal solutions inside the microfluidic platform was recorded using a high-speed CCD camera. Images of the solutions in the reservoir at each rotation speed are shown in Figure 1b. When the rotation speed was increased (at 0–30 s), the solutions were forced by centrifugal force to flow toward the bottom side of reservoir No. 2 and 3. At 30 s, the solution in reservoir No. 2 and 3 flowed out and mixed at

a critical rotation speed of 957 rpm. At 150 s, the solution was moved to the electrochemical detection zone while the washing solution was started to flow at 180 s with the same critical rotation speed. Finally, all of the solutions had completely flowed out and moved to the waste reservoir at 400 s. The mixing between solutions in reservoirs No. 2 and 3 occurred simultaneously due to the similar distance between the channel inlet and the center of the CD. Moreover, the washing solution in reservoir No. 1 which was located at a shorter distance from the center of the CD, was subjected to a higher centrifugal force. Thus, the solution in reservoirs No. 2 and 3 began to flow before the solution in reservoir No. 1 with a calculated flow rate of $0.17 \mu\text{L/s}$. In addition, the solution in reservoir No. 2 and 3 can be completely mixed in 120 s within a spiral channel which is beneficial for the reaction time of glucose and glucose oxidase which require a mixing time of at least 2 min. As a result, our system is particularly suitable for use in an enzymatic assay in the microchip channel with a simple manual operation and substantially reduced reagent consumption.

3.2 H_2O_2 Detection of G-PANI/CoPc-CPE

An electrochemical enzymatic biosensor based on glucose oxidase (GOx) has played an important role in simple easy-to-use blood glucose testing. H_2O_2 , the product of the reaction between glucose and GOx was electrochemically measured at the electrode. Therefore, the amount of H_2O_2 produced in the GOx reaction can be used to indirectly determine glucose levels. In this work, a G-PANI/CoPc-CPE was used for the sensitive detection of H_2O_2 and glucose using cyclic voltammetry and amperometry. An electrode modifier comprised of a CoPc electrocatalyst and a G-PANI nanocomposite was used. The role of the CoPc is to provide electrocatalytic activity by reducing the working potential of the carbon-paste electrode as follows [29]. First, Co(III) is chemically reduced by H_2O_2 to Co(II). Then, Co(II) is electrochemically oxidized to Co(III). Moreover, a G-PANI nanocomposite can be used to enhance the electrochemical sensitivity of the electrode due to the large surface area of its nanostructure [24–25]. Comparison of electrochemical performance between G-PANI/CoPc-CPE and bare CPE are illustrated in Figure 2a.

Compared to a bare CPE (dashed line), a well-defined irreversible anodic peak with a significant increase in anodic current of H_2O_2 by using G-PANI/CoPc-CPE was observed, indicating that G-PANI nanocomposite and CoPc electrocatalyst might be a promising electrode modifier for sensitive detection of glucose due to its excellent electrocatalytic activity.

Figure 2b shows the amperometric response of 1 mM H_2O_2 in 0.1 M PBS pH 7.4, obtained from the eCD system based on a G-PANI/CoPc-CPE. According to the period of time required for the H_2O_2 solution to flow to the electrode surface (between 150 to 300 s), the anodic current decreased with time which is related to the Cot-

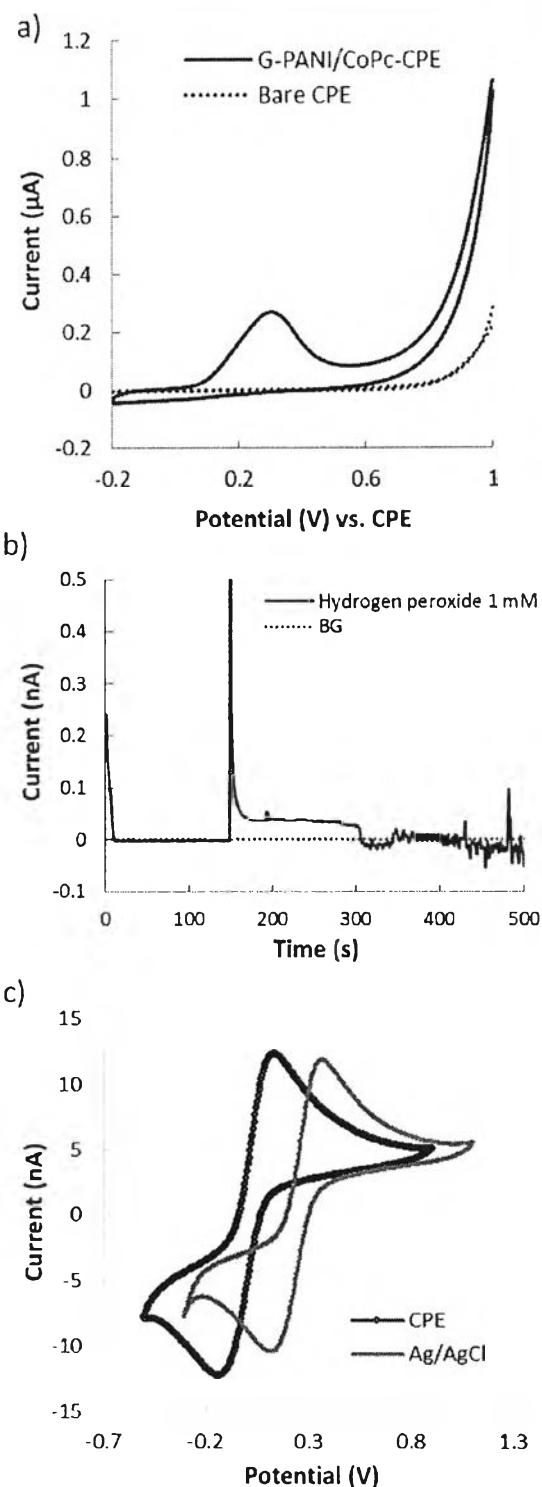


Fig. 2. a) Cyclic voltammograms of 1 mM H_2O_2 in 0.1 M PBS pH 7.4 measured in electrochemical batch cell based on a G-PANI/CoPc-CPE (solid line) and bare CPE (dashed line) at a scan rate of 100 mV/s. b) Amperogram of 1 mM H_2O_2 in 0.1 M PBS pH 7.4 measured by eCD system based on a G-PANI/CoPc-CPE. c) Comparison of reference potential between the CPE and standard Ag/AgCl electrode.

rel equation [30]. The anodic current then decreased because the washing solution passed through the electrode surface. For the further determination of glucose using the eCD system, the amperometric currents were recorded at a steady state current of 300 s (before the signal dropped) [31].

To investigate reference potential of CPE compared to the standard Ag/AgCl electrode, a cyclic voltammogram of the 1 mM ferrocyanide solution was obtained as shown in Figure 2c. The reference potential of CPE was found to be lower than that of the standard Ag/AgCl reference electrode by 0.22 V. The cathodic potential shift might be due to the fact that the working and reference electrodes were fabricated from the same carbon-based material and immersed in the same testing solution [32]. Moreover, stability and reproducibility of the potential of CPE as the reference electrode were tested. The %RSD obtained from cyclic voltammetric measurements of the 1 mM ferrocyanide solution for both 30 experimental runs ($n=30$) and 10 different carbon-paste electrode were found to be less than 5%. Therefore, this CPE can be also used as a reference electrode with acceptable stability.

3.3 Optimization of Conditions

Various optimization conditions were examined, including applied potential, rotating speed, and GOx concentration.

3.3.1 Applied Potential

To obtain the optimal potential for amperometric detection in the eCD system, the hydrodynamic voltammetry of 1 mM H_2O_2 was studied, as shown in Figure 3a. A hydrodynamic voltammetric i - E curve obtained at the G-PANI/CoPc-CPE electrode for 1 mM H_2O_2 (solid line) vs. 0.1 M PBS pH 7.4 (dashed line).

The anodic current of H_2O_2 obviously increased as a function of the detection potential; however, the background current increased as well. The S/B ratios were calculated from the data in Figure 3a at each potential. The resulting curve for the S/B ratios vs. potential is shown in Figure 3b.

The result shows that the maximum S/B ratio was found to be 0.4 V vs. CPE. Higher potentials over 0.8 V vs. CPE were not investigated in order to reduce the tendency for interfering compounds (e.g. ascorbic acid (AA), uric acid (UA), and paracetamol (PA)) to be oxidized [23]. Therefore, this optimal applied potential of 0.4 V vs. CPE was selected for quantitative amperometric detection in the eCD experiments.

3.3.2 Rotating Speed

The speed of rotation of eCD is related to the flow rate of the solution. When the rotating speed is increased, the flow rate of a solution within the microfluidic platform also increases. Figure 4a displays amperograms for

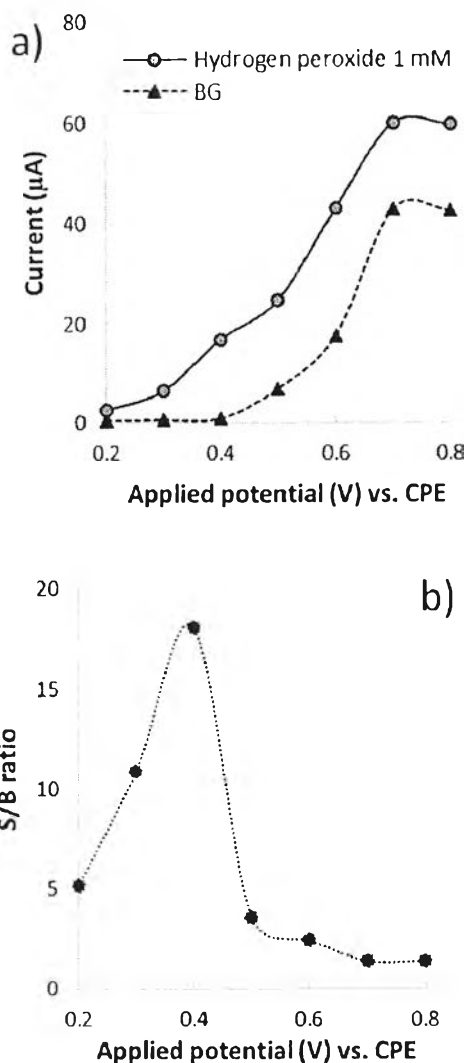


Fig. 3. a) A hydrodynamic voltammetric i - E curve obtained at the G-PANI/CoPc-CPE electrode for 1 mM H_2O_2 (solid line) versus 0.1 M PBS pH 7.4 (dashed line). b) A signal-to-background (S/B) ratios extracted from Figure 3a.

a 1 mM H_2O_2 solution obtained using different rotating speeds in the range of 957–1598 rpm.

The results show that the peak width decreased with increasing flow rate, as increasing the rotation speed. Lower flow rates below 957 rpm were not studied because the flow of all solutions through the electrochemical detection zone was incomplete. The anodic current for H_2O_2 increased with rotating speed in the range of 957–1085 rpm. This result can be explained by the fact that the diffusion layer on the working electrode becomes thinner due to increase in the rotation speed. However, the anodic current decreased at higher rotating speed than 1085 rpm. The limited electrode response at fast rotating speeds higher than 1085 rpm may be attributed to the shorter residence time for the charge transfer reaction of the oxidation of hydrogen peroxide occurring at the electrode surface. Indeed similar results have been re-

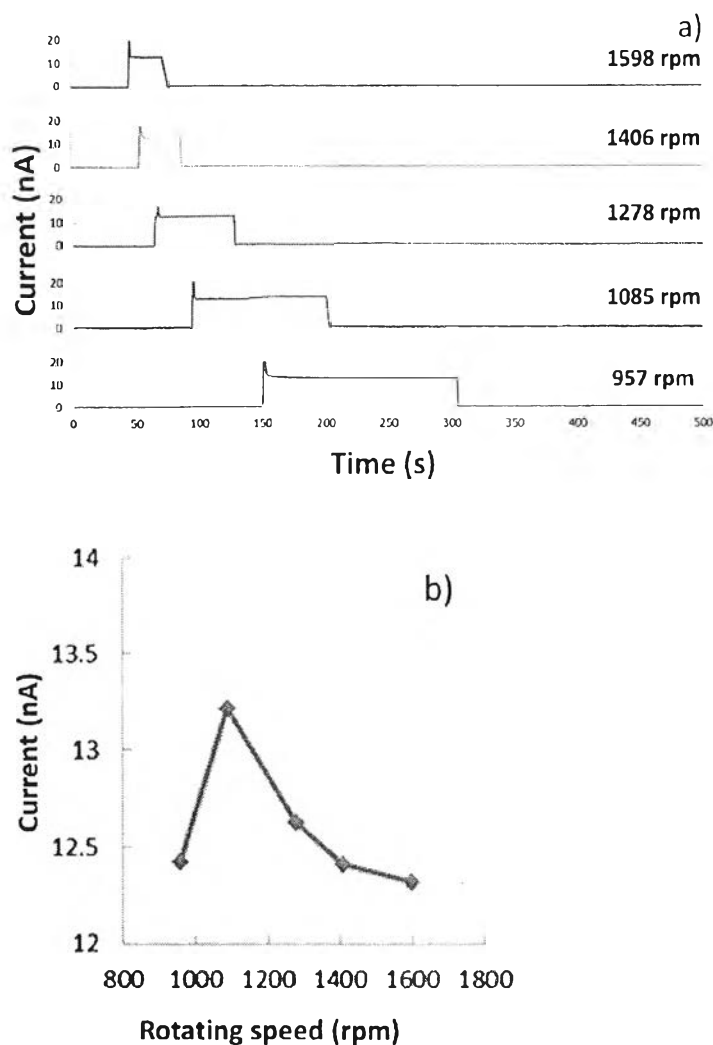


Fig. 4. a) Amperogram and b) anodic current vs. rotating speed plot displaying the influence of rotating speed on the amperometric detection of 1 mM H_2O_2 in 0.1 M PBS pH 7.4 using eCD system based on a G-PANI/CoPc-CPE at applied potential of +0.4 V vs. CPE.

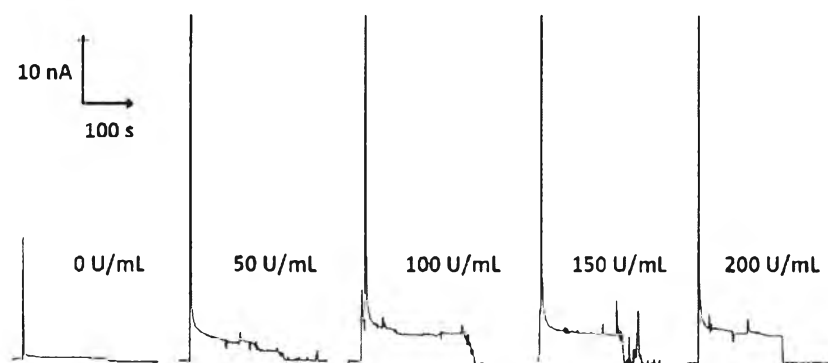


Fig. 5. Amperogram of 2 mM glucose with different concentration of GOx (0–200 U/mL) in 0.1 M PBS pH 7.4 measured by eCD system based on a G-PANI/CoPc-CPE at applied potential of +0.4 V vs. CPE.

ported [33–34]. Although a rotating speed at 1085 rpm provided the highest oxidation current of H_2O_2 , the mixing time is shorter than a rotating speed of 957 rpm.

As a result, the optimal rotating speed in this eCD system was found to be 957 rpm.

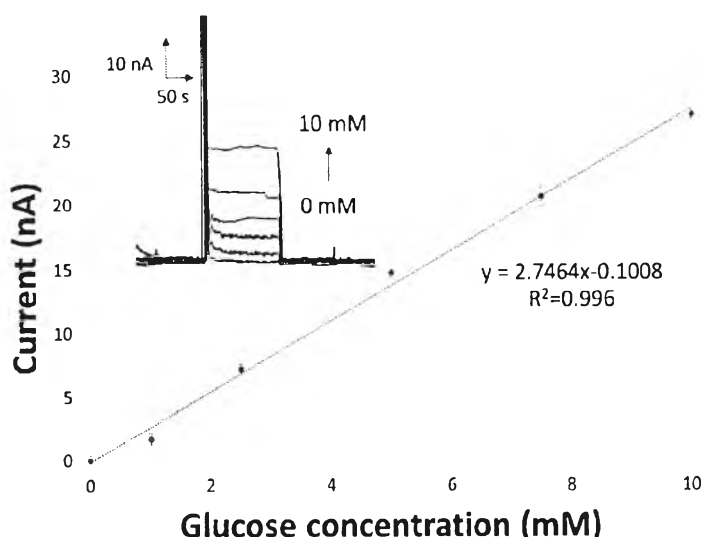


Fig. 6. Calibration curve and amperogram (Inset) for glucose assay using eCD system based on a G-PANI/CoPc-CPE at applied potential of +0.4 V vs. CPE.

3.3.3 GOx Concentration

The influence of GOx concentration in reservoir No. 2 on the response to the 2 mM glucose substrate was investigated. The current increased rapidly when the GOx concentration was increased from 0 U/mL to 100 U/mL, and then reached a plateau from 100 U/mL to 200 U/mL. We believe that this plateau phenomena is due to the complete consumption of glucose by an excess GOx concentration. Therefore, the optimal concentration was found to be 100 U/mL.

3.4 Analytical Performance

The optimized conditions for glucose detection using the eCD system consisting of 100 U/mL GOx, an applied potential of +0.4 V vs. CPE, and a rotating speed of 957 rpm were used to construct the calibration curve, which is shown in Figure 6. Using the optimal conditions, the linear calibration was in the range of 1 to 10 mM with a correlation coefficient of 0.996 and relative standard deviation (%RSD) of 4.26%.

The limit of detection (LOD , $S/N=3$) and limit of quantitation (LOQ , $S/N=10$) were found to be 0.29 mM and of 0.97 mM, respectively. These results indicate that our eCD system provided a low detection limit and a wide linear range for the determination of glucose. Usually, the normal glucose levels in whole blood and serum are in the range of 3.5–5.3 mM and 2.5–5.3 mM, respectively [35]. Our eCD can be effectively used for measurements in this range; therefore, this proposed system can be applied to the determination of glucose in both whole blood and serum within our linear calibration range.

Although the LOD and LOQ values reported here are higher than those reported in previous studies [29,36–39], our eCD system requires an extremely low sample volume (only 10 μ L) for each glucose assay. In addition,

this proposed method included all of these steps, i.e., sample-enzyme mixing, electrochemical measurement, and washing steps; therefore, it provides more advantages than conventional electrochemical batch systems in that the for an analysis and reagent/sample consumption are reduced substantially. Moreover, our eCD system can be designed to perform the simultaneous determination of various biomarkers within a single CD system. The simultaneous detection using various oxidase enzyme reactions (e.g. cholesterol oxidase, lactase, uricase) can be also conducted within a single eCD device. Thus, measurements using this eCD approach can be an ideal platform for an on-site and universal screening for medical diagnosis.

3.5 Interference Study

In order to evaluate the selectivity of this eCD system, the effect of various foreign compounds on the determination of 2 mM glucose by the proposed method was investigated.

Generally, for the electrochemical detection of glucose in biological fluids, some coexisting electroactive species including ascorbic acid (AA), uric acid (UA), paracetamol (PA), and L-cysteine (Cys) have been considered because these compounds can also be oxidized at an anodic potential similar to that for H_2O_2 [23,29]. The results are summarized in Figure 7 and Table 1.

The tolerance limit was defined as the concentration of an interfering compound required to generate a change in the electrochemical response of more than or equal to 5% when compared to the response obtained from the standard concentration. The result shows that 5% tolerance concentration from adding interfering compounds was observed over their highest normal level found in human serum. This serves to confirm that there were no significant interferences in blood or plasma. Unfortunately,

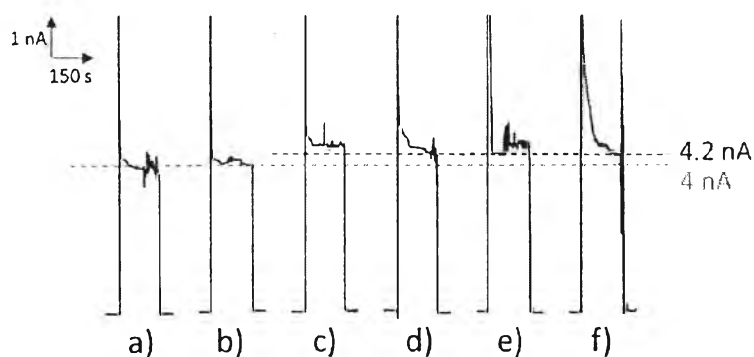


Fig. 7. Amperograms of 2 mM glucose and 100 U/mL GOx with/without interfering compounds at the highest concentration found in normal human serum and 5% tolerance concentration (mM). Conditions: a) glucose without interfering compound, b) glucose with 0.08 mM AA, 0.4 mM UA, 0.05 mM PA, and 0.2 mM Cys, c) glucose with 0.16 mM AA, d) glucose with 0.8 mM UA, e) glucose with 0.1 mM PA, and f) glucose with 0.2 mM Cys.

Table 1. Influence of electroactive interfering species on glucose assay using eCD system.

Interference	Highest normal level in serum (mM)	5% Tolerance concentration (mM)
Ascorbic acid	0.08	0.16
Uric acid	0.4	0.8
Paracetamol	0.1	0.1
L-Cysteine	0.05	0.2

Table 2. Determination of glucose in control serum samples.

Sample	Glucose concentration (mM \pm SD [a])	
	Certified level	Proposed method
Human serum level I	4.77 \pm 0.39	4.62 \pm 0.09
Human serum level II	15.54 \pm 1.28	16.00 \pm 0.28

[a] SD = standard deviation ($n=7$)

ly, only PA appeared to have an impact on the selectivity of the proposed eCD system; therefore, PA needed to be diluted or removed to a level where it no longer influenced the analytical results.

3.6 Determination of Glucose in Human Serum

To evaluate the eCD microfluidic system with actual samples, seven replicate determinations ($n=7$) of glucose in clinical control samples was performed. The control samples are common systems for evaluating the accuracy of diagnostic tests in a biologically relevant matrix without worry of blood borne pathogens. The results are shown in Table 2. The paired *t*-test was used to validate our method versus both control levels for glucose. No significant difference was found at the 95% confidence level. Thus, the analyzed values of glucose in human serum are acceptable. Therefore, it can be successfully applied to the determination of glucose in control samples.

4 Conclusions

We demonstrated the potential of using a CD microfluidic biosensor in the quantitative measurement of critical diabetes markers in serum for the first time. Using a G-PANI nanocomposite, significant electrochemical enhancement was achieved, along with an improvement in selectivity due to a shift in oxidation potential by using CoPc electrocatalyst. This spiral channel platform has been suitably designed for achieving optimal mixing between glucose and oxidase enzyme within a 2 min period. Eventually, this eCD system was used in the selective determination of glucose in human serum samples and the results were in reasonable agreement with actual glucose levels in the serum. Therefore, this practical eCD system has considerable potential for use in a variety of electrochemical detections where a mixing step is needed, such as in an enzymatic reaction. Additionally, this eCD model can be further extended to several other applications such as point-of-care testing, quality control of foods and/or beverages, and environmental monitoring.

Acknowledgements

This research was supported by the Ratchadaphiseksomphot Endowment Fund 2013 of Chulalongkorn University (CU-56-904-AM) the Thailand Research Fund (RTA5780005). Also, P. R. wishes to acknowledge financial support from Chulalongkorn University and the Thailand Research Fund, through the Royal Golden Jubilee Ph.D. Program (Grant No. PHD/0251/2552). This research was supported by National Electronics and Computer Technology Center (NECTEC) and Technology for Development Agency and Thailand Graduate Institute of Science and Technology (TGIST). This research was also supported in part by the Japan Society for the Promotion of Science (JSPS) KAKENHI Grant No. 252880651.

References

- [1] M. H. Ghanim, M. Z. Abdullah, *Talanta* **2011**, *85*, 28–34.
- [2] M. Pumera, *Talanta* **2005**, *66*, 1048–1062.
- [3] W. Siangproh, W. Dungchai, P. Rattanasat, O. Chailapakul, *Anal. Chim. Acta* **2011**, *690*, 10–25.
- [4] S. A. Sundberg, A. Chow, T. Nikiforov, H. G. Wada, *Drug Discov. Today* **2000**, *5*, 92–103.
- [5] O. Chailapakul, S. Korsrisakul, W. Siangproh, K. Grudpan, *Talanta* **2008**, *74*, 683–689.
- [6] N. Ruecha, W. Siangproh, O. Chailapakul, *Talanta* **2011**, *84*, 1323–1328.
- [7] R. Liu, R. Ishimatsu, M. Yahiro, C. Adachi, K. Nakano, T. Imato, *Talanta* **2015**, *132*, 96–105.
- [8] W. Siangproh, O. Chailapakul, R. Laocharoensuk, J. Wang, *Talanta* **2005**, *67*, 903–907.
- [9] O. Hugon, I. A. Paun, C. Ricard, B. van der Sanden, E. Lacot, O. Jacquin, A. Witomski, *Ultramicroscopy* **2008**, *108*, 523–528.
- [10] Q. Lu, C. L. Copper, G. E. Collins, *Anal. Chim. Acta* **2006**, *572*, 205–211.
- [11] C. Liu, D. Cui, X. Chen, *J. Chromatogr. A* **2007**, *1170*, 101–106.
- [12] X. He, Q. Chen, Y. Zhang, J.-M. Lin, *TrAC – Trends Anal. Chem.* **2014**, *53*, 84–97.
- [13] D. D. Nolte, *Rev. Sci. Instrum.* **2009**, *80*, 3236681.
- [14] M. Vázquez, D. Brabazon, F. Shang, J. O. Omamogho, J. D. Glennon, B. Paull, *TrAC – Trends Anal. Chem.* **2011**, *30*, 1575–1586.
- [15] A. Hemmi, T. Usui, A. Moto, T. Tobita, N. Soh, K. Nakano, H. Zeng, K. Uchiyama, T. Imato, H. Nakajima, *J. Separation Sci.* **2011**, *34*, 2913–2919.
- [16] H. Hwang, Y. Kim, J. Cho, J.-y. Lee, M.-S. Choi, Y.-K. Cho, *Anal. Chem.* **2013**, *85*, 2954–2960.
- [17] N. Kim, C. M. Dempsey, J. V. Zoval, J.-Y. Sze, M. J. Madou, *Sens. Actuators B, Chem.* **2007**, *122*, 511–518.
- [18] S. Lai, S. Wang, J. Luo, L. J. Lee, S. T. Yang, M. J. Madou, *Anal. Chem.* **2004**, *76*, 1832–1837.
- [19] M. Trojanowicz, *Anal. Chim. Acta* **2009**, *653*, 36–58.
- [20] E. Bakker, Y. Qin, *Anal. Chem.* **2006**, *78*, 3965–3984.
- [21] D. W. Kimmel, G. LeBlanc, M. E. Meschievitz, D. E. Cliffel, *Anal. Chem.* **2011**, *84*, 685–707.
- [22] A. Heller, B. Feldman, *Chem. Rev.* **2008**, *108*, 2482–2505.
- [23] W.-Z. Jia, K. Wang, X.-H. Xia, *TrAC – Trends Anal. Chem.* **2010**, *29*, 306–318.
- [24] N. Ruecha, R. Rangkupan, N. Rodthongkum, O. Chailapakul, *Biosens. Bioelectron.* **2014**, *52*, 13–19.
- [25] N. Rodthongkum, N. Ruecha, R. Rangkupan, R. W. Vachet, O. Chailapakul, *Anal. Chim. Acta* **2013**, *804*, 84–91.
- [26] J. A. Rogers, R. G. Nuzzo, *Mater. Today* **2005**, *8*, 50–56.
- [27] Y. Sameenoi, M. M. Mensack, K. Boonsong, R. Ewing, W. Dungchai, O. Chailapakul, D. M. Cropek, C. S. Henry, *Analyst* **2011**, *136*, 3177–3184.
- [28] Q. Hao, H. Wang, X. Yang, L. Lu, X. Wang, *Nano Res.* **2011**, *4*, 323–333.
- [29] K. Wang, J.-J. Xu, H.-Y. Chen, *Biosens. Bioelectron.* **2005**, *20*, 13881396.
- [30] J. G. M. Castro Júnior, G. M. M. Ferreira, F. G. de Oliveira, F. S. Damos, R. d. C. S. Luz, *J. Electroanal. Chem.* **2014**, *732*, 93–100.
- [31] H. Liu, R. M. Crooks, *Lab Chip* **2013**, *13*, 1364–1370.
- [32] M. Santhiago, C. S. Henry, L. T. Kubota, *Electrochim. Acta* **2014**, *130*, 771–777.
- [33] P. A. Raymundo-Pereira, C. S. Martin, M. F. Bergamini, N. Bocchi, M. F. S. Teixeira, *Electrochim. Acta* **2011**, *56*, 2552–2558.
- [34] S. Prabhu, J. L. Anderson, *Anal. Chem.* **1987**, *59*, 157–163.
- [35] W. Dungchai, O. Chailapakul, C. S. Henry, *Anal. Chem.* **2009**, *81*, 5821–5826.
- [36] K. Tian, M. Prestgard, A. Tiwari, *Mater. Sci. Eng. C* **2014**, *41*, 100–118.
- [37] K.-C. Lin, Y.-C. Lin, S.-M. Chen, *Electrochim. Acta* **2013**, *96*, 164–172.
- [38] C.-L. Sun, W.-L. Cheng, T.-K. Hsu, C.-W. Chang, J.-L. Chang, J.-M. Zen, *Electrochem. Commun.* **2013**, *30*, 91–94.
- [39] S. Park, H. Boo, T. D. Chung, *Anal. Chim. Acta* **2006**, *556*, 46–57.

Received: October 15, 2014

Accepted: November 25, 2014

Published online: February 12, 2015



Graphene-polyaniline modified electrochemical droplet-based microfluidic sensor for high-throughput determination of 4-aminophenol

Poomrat Rattanarat^a, Akkapol Suea-Ngam^{a, b}, Nipapan Ruecha^c, Weena Siangproh^d, Charles S. Henry^{e, f}, Monpichar Srisa-Art^{a, b}, Orawon Chailapakul^{a, g, *}

^a Electrochemistry and Optical Spectroscopy Research Unit (EOSRU), Department of Chemistry, Faculty of Science, Chulalongkorn University, Patumwan, Bangkok 10330, Thailand

^b Chromatography and Separation Research Unit (ChSRU), Department of Chemistry, Faculty of Science, Chulalongkorn University, Patumwan, Bangkok 10330, Thailand

^c Program in Macromolecular Science, Faculty of Science, Chulalongkorn University, Patumwan, Bangkok 10330, Thailand

^d Department of Chemistry, Faculty of Science, Srinakharinwirot University, Sukhumvit 23, Wattana, Bangkok 10110, Thailand

^e Department of Chemistry, Colorado State University, Fort Collins, CO 80523, United States

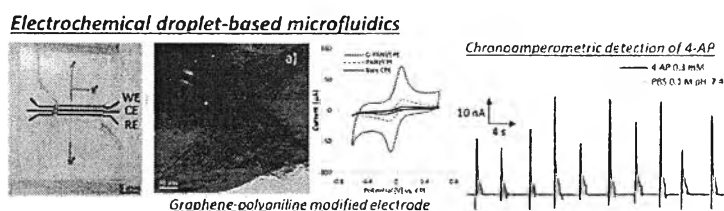
^f School of Biomedical Engineering, Colorado State University, Fort Collins, CO 80523, United States

^g National Center of Excellent of Petroleum, Petrochemicals and Advanced Materials, Chulalongkorn University, Patumwan, Bangkok 10330, Thailand

HIGHLIGHTS

- A novel combination of G-PANI/CPE and droplet-based microfluidic device for determination of 4-AP was achieved.
- G-PANI nanocomposite increases the surface area and improved electrochemical sensitivity of the electrode.
- This novel droplet-based system was successfully applied for 4-AP monitoring in commercial PA samples.

GRAPHICAL ABSTRACT



ARTICLE INFO

Article history:

Received 23 September 2015

Received in revised form

29 December 2015

Accepted 7 March 2016

Available online 8 April 2016

Keywords:

Droplet-based microfluidics

Electrochemical detection

Graphene

Polyaniline

ABSTRACT

We report herein the first development of graphene-polyaniline modified carbon paste electrode (G-PANI/CPE) coupled with droplet-based microfluidic sensor for high-throughput detection of 4-aminophenol (4-AP) in pharmaceutical paracetamol (PA) formulations. A simple T-junction microfluidic platform using an oil flow rate of 1.8 $\mu\text{L}/\text{min}$ and an aqueous flow rate of 0.8 $\mu\text{L}/\text{min}$ was used to produce aqueous testing microdroplets continuously. The microchannel was designed to extend the aqueous droplet to cover all 3 electrodes, allowing for electrochemical measurements in a single droplet. Parameters including flow rate, water fraction, and applied detection potential (E_{det}) were investigated to obtain optimal conditions. Using G-PANI/CPE significantly increased the current response for both cyclic voltammetric detections of ferri/ferrocyanide [$\text{Fe}(\text{CN})_6^{3-/4-}$] (10 times) and 4-AP (2 times), compared to an unmodified electrode. Using the optimized conditions in the droplet system, 4-AP in the presence of PA was selectively determined. The linear range of 4-AP was 50–500 μM ($R^2 = 0.99$), limit of detection (LOD, $S/N = 3$) was 15.68 μM , and limit of quantification (LOQ, $S/N = 10$) was 52.28 μM . Finally, the

Selected paper from Flow Analysis XIII Conference, 5–10 July 2015 in Prague, Czech Republic.

* Corresponding author. Electrochemistry and Optical Spectroscopy Research Unit (EOSRU), Department of Chemistry, Faculty of Science, Chulalongkorn University, Patumwan, Bangkok 10330, Thailand.

E-mail address: corawon@chula.ac.th (O. Chailapakul).

<http://dx.doi.org/10.1016/j.aca.2016.03.010>

0003-2670/© 2016 Elsevier B.V. All rights reserved.

4-Aminophenol
Paracetamol

system was used to determine 4-AP spiked in commercial PA liquid samples and the amounts of 4-AP were found in good agreement with those obtained from the conventional capillary zone electrophoresis/UV–Visible spectrophotometry (CZE/UV–Vis). The proposed microfluidic device could be employed for a high-throughput screening (at least 60 samples h^{-1}) of pharmaceutical purity requiring low sample and reagent consumption.

© 2016 Elsevier B.V. All rights reserved.

1. Introduction

Since the mid-1940s, paracetamol (PA, acetaminophen or *N*-acetyl-*p*-aminophenol) has been commonly used as an antipyretic and analgesic drug around the world [1,2]. Many PA formulations, such as tablets, syrups, injections, and suppositories, have been available and highly effective for a variety of patients including children, pregnant women, and the elderly. Unfortunately, 4-aminophenol (4-AP) residue might be present as an impurity in PA formulations obtained from its synthesis or as a result of degradation [3]. Consuming 4-AP unintentionally can cause numerous pathologies (e.g. nephrotoxicity and hepatotoxicity) [3–5]. The European, United States, British, German, and Chinese Pharmacopoeias have set the maximum allowable limit of 4-AP in the PA drug formulations at 50 ppm (0.005% w/w) [5]. Several analytical approaches to determine 4-AP in PA formulations have been developed including high performance liquid chromatography (HPLC) coupled with UV–Visible [6,7] or fluorescence [8] detection, electrochemical detection [9], capillary electrophoresis [10,11], and flow-based analytical techniques [4,12]. Although these techniques offer highly selective, and sensitive quantification of 4-AP in PA formulations, these techniques are time consuming, have high operation costs, and are available only in sophisticated laboratories.

Recently, droplet microfluidic systems have held great promise for analytical measurements due to their portability, fast analysis time, low manufacturing cost, low reagent/sample consumption, and high-throughput screening [13]. Droplet microfluidic systems are capable of generating and manipulating small droplets encapsulated by an immiscible phase. Among other microfluidic platforms, droplet microfluidics has gained attention because of superior mixing efficiency and low dispersion/adsorption of sample within the microchannel [14]. The utility of droplet-based technology has been demonstrated for many applications, such as biomedical diagnosis [15,16], food safety [17,18], and environmental monitoring [19]. Other demonstrated applications include protein crystallization [20] and enzymatic kinetic assays [21], emulsion-based polymerase chain reaction [22], chemical synthesis [23,24], and single cell-based analysis [25]. For detection in droplet microfluidics, various detection methods have been used including laser-induced fluorescence [26], mass spectrometry [27], Raman spectroscopy [28], absorption spectroscopy [29], and bright-field microscopy [30]. Although these techniques offer highly selective, sensitive and accurate quantification, the main disadvantages are high equipment cost and challenge of coupling them with miniaturized systems for on-site applications.

Electrochemical detection is an attractive and alternative detection method for microfluidics because it is high speed, high sensitivity, cost-effectiveness, and independence of sample turbidity or optical path length [31]. Currently, there have been a few reports on electrochemical detection for droplet microfluidic systems. For example, Liu et al. used chronoamperometry for the detection of droplet contents and characterization of droplet

generation (e.g. frequency, size and velocity) [32]. Han et al. developed an amperometric droplet microfluidic device to investigate the kinetics of enzymatic decomposition of H_2O_2 using catalase [33]. Gu et al. used a Pt-black modified electrochemical droplet-based microfluidic sensor for enzymatic glucose assays in biological fluids [34]. Itoh et al. demonstrated a novel droplet-based microdevice with an electrochemical ATP-sensing function for fish freshness determination [35].

The use of nanomaterials to improve electrode performance in microfluidic devices has drawn increasing attention in recent years. Numerous nanomaterials (e.g. gold nanoparticles, silver nanoparticles, single-wall carbon nanotubes, and multi-wall carbon nanotubes) are currently available and can increase active surface area of the working electrode, leading to enhance electrochemical sensitivity and conductivity [34,36–38]. Graphene (G) has received substantial attention for chemical modification of electrodes [39], owing to its large surface area, extraordinary electrical conductivity, high mechanical strength and potentially low manufacturing cost. In addition, G has been also used to modify electrode surface in order to improve the electrochemical properties of the electrodes. One problem associated with G-based electrode modification is the potential for self-agglomeration of pure G on the electrode surface. One solution is use of a nanocomposite consisting of conducting polymer and G to increase the distribution of graphene [40]. Among conducting polymers, polyaniline (PANI) has been widely used for electrode modification because of its inherent electrochemical properties, biocompatibility and stability [41,42]. Previous reports have used G-PANI hybrid modified electrochemical sensors for electrochemiluminescent detection of luminol [43], voltammetric determination of dopamine [41] and dobutamine [44], and electrochemical immunoassays for estradiol [45] and salbutamol [46]. To the best of our knowledge, there are no previous reports combining a novel G-PANI modified electrodes and droplet microfluidics for electrochemical determination of 4-AP.

Herein, the aim of this work is to develop a high-throughput and sensitive method using G-PANI modified electrochemical droplet-based microfluidic sensor for determination of 4-AP in pharmaceutical PA products. An improved selectivity for 4-AP was achieved using G-PANI modified carbon-paste electrodes (G-PANI/CPE) operating at the optimized detection potential for highly selective detection of 4-AP in the presence of PA. This system offers an alternative method to measure 4-AP level in acceptable concentration range. Finally, this approach was successfully applied for the determination of 4-AP in commercial PA liquid samples, giving high correlation with a CZE/UV–Vis method. Accordingly, measurements using this approach can provide a fast and high-throughput route and could be an ideal platform for screening of purity in pharmaceutical products with small sample consumption. Furthermore, the development of this microfluidic model can be further extended to various applications such as medical testing, environmental monitoring and quality control of foods or beverages.

2. Experimental

2.1. Materials and chemicals

The following materials were used as received: poly(dimethylsiloxane) (PDMS) Sylgard 184 elastomer kit (Dow Corning, USA), mineral oil (Perkin Elmer, Thailand), silver paint (SPI supplies, USA), graphite powder ($\leq 20 \mu\text{m}$, Sigma–Aldrich, Singapore), and graphene (A.C.S Medford, USA). All chemicals were analytical grade: sodium chloride (NaCl: Merck, Thailand), disodium hydrogen phosphate (Na_2HPO_4 : Merck, Thailand), potassium dihydrogen phosphate (KH_2PO_4 : Carlo ERBA, Thailand), potassium chloride (KCl: Ajax Finechem, Thailand), and ethanol (Merck, Thailand). Potassium ferricyanide ($\text{K}_3[\text{Fe}(\text{CN})_6]$) and potassium ferrocyanide ($\text{K}_4[\text{Fe}(\text{CN})_6]$) were obtained from Sigma–Aldrich (Singapore). Polyaniline and camphor-10-sulfonic acid ($\text{C}_{10}\text{H}_{16}\text{O}_4\text{S}$) were purchased from Merck (Darmstadt, Germany). N-Methyl-2-pyrrolidone (NMP), 4-aminophenol (4-AP) and paracetamol (PA) were purchased from Sigma–Aldrich (Singapore). Commercial PA drugs consisting of Infants' TYLENOL[®] (Janssen-Cilag, Ltd., Thailand), TEMPRA[®] (Taisho Pharmaceutical Co., Ltd., Thailand), SARA[®] (Thai Nakorn Patana Co., LTD, Thailand) were purchased from a local pharmacy in Thailand. For droplet generation, a 10:2 (v/v) mixture of perfluorodecalin (mixture of *cis* and *trans*, 95%, Sigma–Aldrich, Germany) and 1H, 1H, 2H, 2H-perfluoro-1-octanol (97%, Sigma–Aldrich, Germany) was used as an oil solution. All aqueous solutions were prepared using deionized water (18.0 MU cm. Milli-Q Gradient System, Millipore, Thailand). Phosphate buffer saline (PBS) pH 7.4 at a concentration of 0.1 M was used as a supporting electrolyte. To prepare 0.1 M PBS, the mixture comprising of 2.0 g NaCl, 0.05 g KCl, 0.36 g Na_2HPO_4 and 0.06 g KH_2PO_4 was dissolved in a 250 mL volumetric flask using deionized water. All aqueous stock standards of 4-AP and PA were prepared in 0.1 M PBS.

2.2. Fabrication of patterned PDMS

In this work, solutions were pumped through the device using syringe pumps (Harvard Apparatus PHD 2000, Harvard Apparatus, Holliston, MA). Both aqueous and oil phases were prepared and stored in 1 mL plastic syringes (Nipro, Thailand). Polyethylene tubing (0.38 mm I.D., 1.09 mm O.D., PORTEX, Belgium) connecting the inlets of microfluidic device with syringe pumps was secured using commercial epoxy. For microfluidic experiments, a T-junction microchannel and electrode layout originally published by Liu et al. was used [47]. Briefly, the SU-8 negative photoresist was coated onto a silicon wafer using a spin coater and then baked at 95 °C for 45 min. Next, the transparency film containing the microchannel and electrode pattern was placed over the coated wafer, and exposed to ultra-violet (UV) light for pattern. The final SU-8 template was obtained by washing with the SU-8 developer and isopropanol, respectively. Microchannel platforms were fabricated using the traditional soft lithography using a 10:1 ratio of the PDMS precursor to curing agent (Sylgard 184, Dow Corning) [48,49]. The mixture was degassed under vacuum to remove dissolved air. The PDMS mixture was poured onto the SU-8 master and baked in the oven at 65 °C for 3 h. The cross-linked PDMS was peeled off the mold, and inlets were created using a circular biopsy puncher. Two PDMS replicas containing the microchannel layer and the electrode layer were obtained. The depth of all microchannels was 100 μm . For upper PDMS layer, the main channel of 500 μm width (having two inlets and one outlet) was narrowed to be a confined channel (50 μm width and 1 cm length). For lower electrode layer, three parallel electrode channels (100 μm depth and 500 μm width) with a spacing between each electrode of 500 μm were used according to

previous reports [48,50].

2.3. Fabrication and modification of electrode

Electrode fabrication was accomplished in two steps, screen-printing of the carbon-paste electrode and electrode modification using G-PANI nanocomposite. PDMS cross-linked carbon paste electrodes (CPEs) were created using the previously published method from Sameenoi et al. [48,50]. Briefly, a carbon paste containing graphite powder, mineral oil, and PDMS mixture in a ratio of 2:1:1 was spread over the electrode channels in the PDMS. Excess paste was removed using Scotch Magic Tape[™] until well-defined carbon paste electrodes were obtained.

For electrode modification, G-PANI nanocomposite was prepared using a simple physical mixing procedure [40]. G in NMP solution (2 mg mL^{-1}) was prepared and dispersed using an ultrasonic bath for 12 h at room temperature. The conductive form of PANI was prepared by doping with camphor-10-sulfonic acid and dissolved in chloroform. Then, the G and PANI solutions were mixed and sonicated for 12 h to obtain a well-dispersed G-PANI nanocomposite solution. Next, 1 μL -aliquot of G-PANI nanocomposite was casted onto the surface area of a carbon-paste working electrode. The modified CPE was baked in the oven at 65 °C in order to evaporate NMP solution. The morphology of G-PANI nanocomposite was observed using a JSM-6400 field emission scanning electron microscope and a JEM-2100 transmission electron microscope (Japan Electron Optics Laboratory Co., Ltd, Japan). For electrochemical detection in batch and droplet-based systems, a second PDMS layer (containing 10 mm diameter hole or T-junction microchannel) was sealed over PDMS layer containing G-PANI/CPE using reversible ethanol bonding method. Ethanol was dropped onto both PDMS surfaces, the surfaces were then carefully aligned before being baked at 65 °C for 1 h in order to evaporate the NMP within the casted modifier layer. Electrical connections were made using wires glued to the electrodes using silver paste (SPI supplies, West Chester, PA) and epoxy. The actual working electrode area for the batch system was 5 mm² while droplet system was 0.025 mm² (due to the confined channel). Examples of microfluidic and batch devices are shown in the Fig. 1b.

2.4. Electrochemical detection using G-PANI modified CPE

Electrochemical measurements including cyclic voltammetry, square-wave voltammetry, and chronoamperometry were performed using a commercially available potentiostat (eDAQ, ED410, 410-088, Australia) using standard three-electrode configuration. The working electrode was either a bare CPE or G-PANI/CPE. Both pseudo-reference and auxiliary electrodes were CPEs. Cyclic voltammetry was used to compare electrochemical performance of each working electrode type using the working potential ranges of -0.60 to $+0.60$ V and -0.50 to $+1.20$ V vs. CPE for ferri/ferrocyanide and 4-AP, respectively.

To study mass transfer of 4-AP on G-PANI/CPE, the dependence of scan rates was performed in the range of 0.01 – 0.20 V s⁻¹. To measure 4-AP and PA simultaneously, square-wave voltammetry with a potential range of -0.20 to $+0.80$ V vs. CPE was used. Voltammograms were recorded in the positive sweep direction to observe the anodic responses of both 4-AP and PA. All electrochemical experiments were carried out at room temperature.

2.5. Chronoamperometric determination of 4-AP

For microfluidic system, droplets were generated using an oil carrier phase (perfluorodecalin and 1H, 1H, 2H, 2H-perfluoro-1-octanol at a ratio of 10:2 (v/v)) and an aqueous testing solution.

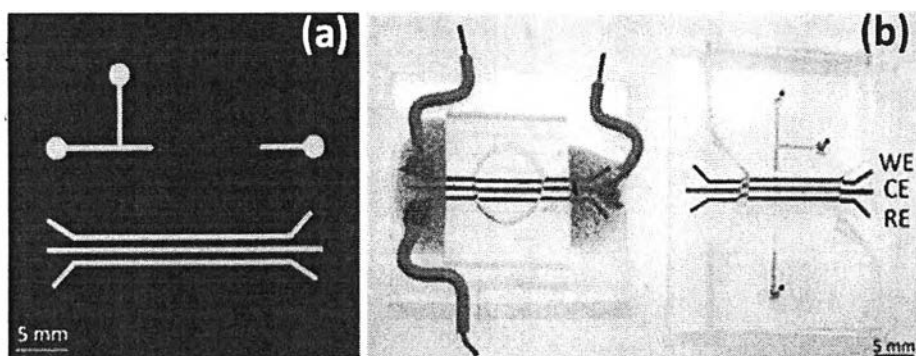


Fig. 1. (a) Schematic of microchannels (top) and electrode patterns (bottom). (b) An electrochemical batch cell (left) and a microfluidic device comprising of main channel and confined channel coupled with microband electrodes (WE-working electrode, CE-counter electrode, and RE-reference electrode).

Chronoamperometric detection was performed for the detection of 4-AP in the droplets. The oil phase flow rate was $1.8 \mu\text{L min}^{-1}$ while the aqueous phase flow rate was $0.8 \mu\text{L min}^{-1}$. The water fraction (W_f) was calculated from following equation [51].

$$W_f = F_w / (F_w + F_o) \quad (1)$$

where W_f is the water fraction, F_w is aqueous-phase flow rate, and F_o is the aqueous- and oil-phase flow rates, respectively.

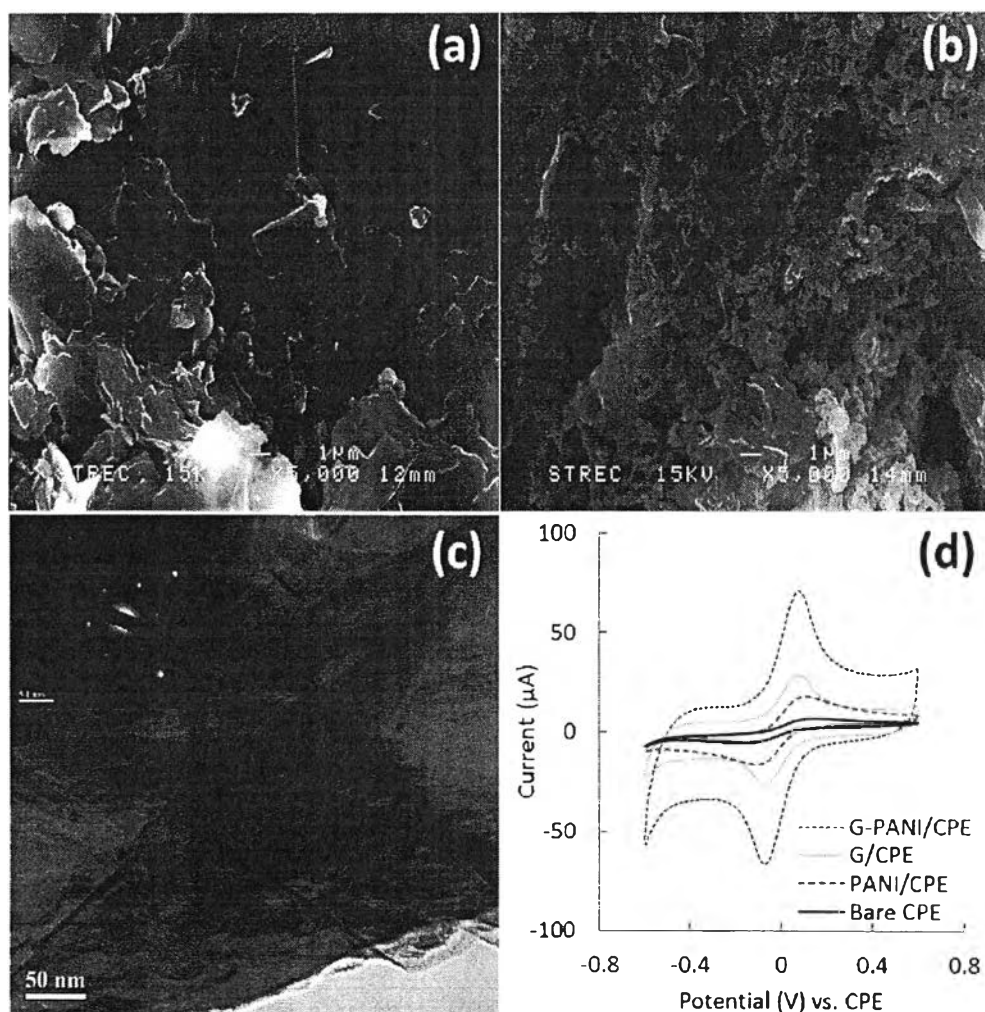


Fig. 2. SEM images of (a) bare SPCE, (b) G-PANI/SPCE, (c) A TEM image of G-PANI nanocomposite with an electron diffraction pattern of G (the inset of c) and (d) cyclic voltammograms of 1 mM ferri/ferrocyanide in 0.1 M KCl at bare CPE (black line), PANI/CPE (green line), G/CPE (yellow line) and G-PANI/CPE (red line). (For interpretation of the references to color in this figure legend, the reader is referred to the web version of this article.)

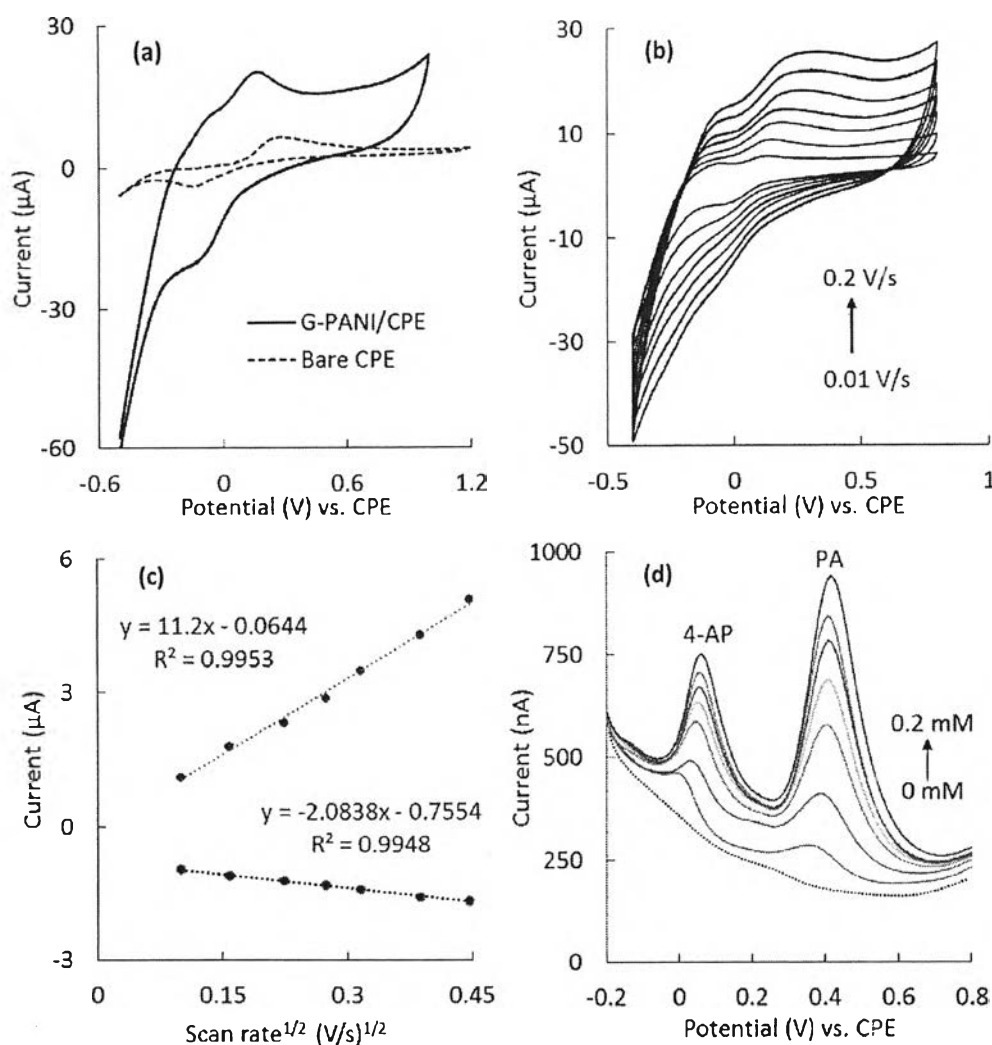


Fig. 3. (a) Comparison of cyclic voltammograms of 1 mM 4-AP obtained from the G-PANI/CPE and bare CPE at a scan rate of 0.1 V/s, (b) cyclic voltammograms of 1 mM 4-AP at the G-PANI/CPE with various scan rates in the range of 0.01–0.2 V/s, (c) peak currents of 4-AP as a function of the square root scan rate ($v^{1/2}$), and (d) square-wave voltammograms of 4-AP and PA (0–0.2 mM) at the G-PANI/CPE with the scanning potential range of –0.2–0.8 V vs. CPE.

Here, the total flow rate was $2.6 \mu\text{L min}^{-1}$, corresponding to a linear flow velocity of 0.86 mm s^{-1} and a water fraction of 0.31. Chronoamperometric responses from droplet contents were measured while droplets passing through the three-electrode system. Data was collected for 1 min and averaged currents were plotted versus detection potential (E_{det}) to generate hydrodynamic voltammograms (HDVs) in the range of 0.00–0.40 V vs. CPE for optimizing the detection potential as defined by the highest signal-to-noise ratio (S/N). The limits of detection (LOD) and quantitation (LOQ) were obtained from $\text{LOD} = 3(\text{SD}_{\text{bl}}/S)$ and $\text{LOQ} = 10(\text{SD}_{\text{bl}}/S)$, respectively, where SD_{bl} is the standard deviation of the blank measurement ($n = 10$) and S is the slope of the linear calibration. Finally, our method was applied for 4-AP determination in PA liquid samples. Prior to analysis, the PA liquid samples was diluted using 0.1 M PBS pH 7.4. The 4-AP concentration levels in all samples were determined and compared with those obtained for the standard CZE/UV–Vis method [52].

CZE separation was performed using a MDQ automated CE system coupled with a diode array detector (Beckman), fluid-cooled column cartridge and automatic injector [11]. A fused-silica capillary column of 57 cm (50 cm length to

detector) $\times 75 \mu\text{m i.d.}$ and $375 \mu\text{m o.d.}$ was used. For each CE run, the capillary column was first rinsed with 0.1 M sodium hydroxide for 1 min at high pressure (20 psi), followed by rinsing with the running buffer (50 mM borate buffer pH 9.2) for 1 min. Samples were hydrodynamically injected for 10 s and a voltage of +20 kV was applied for separation. UV absorption was monitored at 250 nm.

3. Results and discussion

3.1. Morphology and electrochemical characterization and of G-PANI/CPE

Various reports have used G-PANI nanocomposites to improve the electrochemical sensitivity of carbon electrodes with the resulting performance improvement being attributed to the increase in electrode surface area [3,5,37,39–46]. To observe the changes of electrode morphology, scanning electron microscope (SEM) and transmission electron microscopy (TEM) were used to characterize G-PANI nanocomposite as shown in Fig. 2a, 2b, and 2c. Both SEM and TEM images clearly show a well dispersion of G with

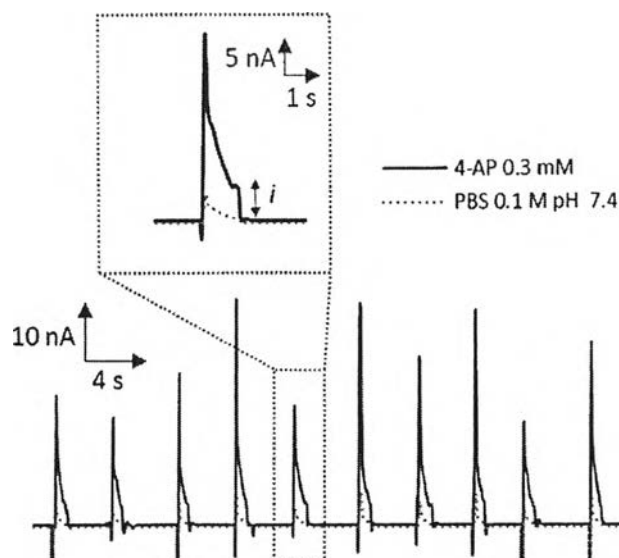


Fig. 4. A chronoamperogram of droplets containing 0.3 mM 4-AP in 0.1 M PBS pH 7.4. The optimal conditions: a detection potential (E_{det}) of +0.2 V vs. CPE, a total flow rate of $2.6 \mu\text{L min}^{-1}$ (0.016 mm s^{-1}) and $W_f = 0.31$.

slight agglomeration on the electrode surface; moreover, the electron diffraction pattern of G sheet (the inset of Fig. 2c) is matched with the previous published report [42].

Next, cyclic voltammetry of standard ferri/ferrocyanide redox species was used to characterize the electrochemical properties of the bare CPE, PANI/CPE, G/CPE, and G-PANI/CPE electrodes (Fig. 2d). Compared to the PANI/CPE and bare CPE, G-PANI/CPE exhibited well-defined anodic and cathodic ferri/ferrocyanide current responses which were 10-fold higher than those obtained from the bare CPE and 3-fold greater than those of PANI/CPE and G/CPE. Moreover, peak potential separation between anodic and cathodic peaks was noticeably reduced when using G-PANI/CPE compared to those measured from the PANI/CPE and bare CPE, indicating that the G-PANI nanocomposite can be also used as an electrode

modifier to improve the electron transfer kinetics.

3.2. Electrochemical detection of 4-AP and PA using G-PANI/CPE

Next, the electrochemical behavior of 4-AP and PA using the G-PANI/CPE in the batch cell was investigated using cyclic voltammetry with the comparison between the G-PANI/CPE and bare CPE, which is shown in Fig. 3a. Cyclic voltammograms of the G-PANI/CPE exhibited quasi-reversible redox peaks with significantly increased redox current (2-fold) and reduced redox potentials ($\sim 100 \text{ mV}$) when compared to bare CPE. These results can be ascribed to good electrocatalytic activity of G-PANI nanocomposite towards 4-AP, demonstrating that the nanomodifier offers improved sensitivity for 4-AP, compared to the unmodified CPE. Therefore, the G-PANI nanocomposite can be used as an excellent electrode modifier in the electrochemical system.

To study the mass transfer process of 4-AP on the G-PANI/CPE surface, a current dependence on scan rate was performed (Fig. 3b and c). A slight shift of both anodic and cathodic peak potentials was observed owing to the adsorption of 4-AP on the electrode surface. Both anodic ($i_{p,a}$) and cathodic ($i_{p,c}$) peak currents increased linearly with the square root of scan rate ($v^{1/2}$) with correlation coefficients (R^2) over 0.99. These results verify that the redox process was controlled by diffusion of 4-AP corresponding to the Randles–Sevcik equation (Equation (2)).

$$i_p = 2.686 \times 10^5 n^{3/2} A C D^{1/2} v^{1/2} \quad (2)$$

where i_p is the peak current of 4-AP in A, n is the number of electrons involved (to reduce/oxidize one molecule of 4-AP), A is the electrode area in cm^2 , D is the diffusion coefficient of 4-AP in $\text{cm}^2 \text{ s}^{-1}$, C is the concentration of 4-AP in mol cm^{-3} , and $v^{1/2}$ is the scan rate in V s^{-1} .

Subsequently, square-wave voltammetry was used to determine detection limits and linearity. Fig. 3d displays representative square-wave voltammograms of 4-AP and PA at concentrations between 50 and 200 μM . For the response from both 4-AP and PA, anodic peak currents are linearly proportional to their concentrations with an LOD ($S/N = 3$) of 4.33 μM and 2.12 μM for 4-AP and PA, respectively. The peak potential separation between 4-AP and PA is

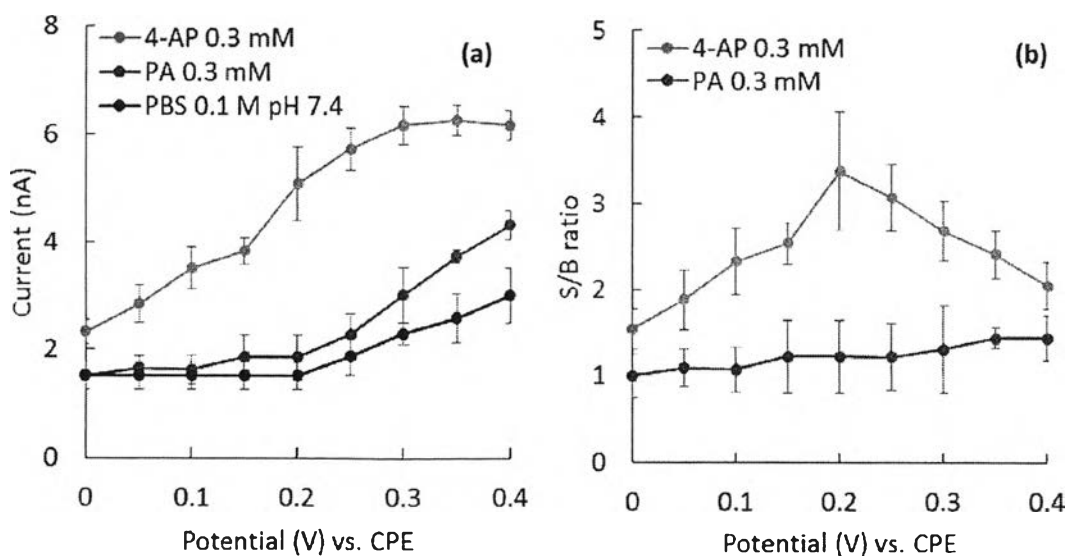


Fig. 5. (a) Hydrodynamic voltammogram and (b) signal to background ratio of 0.3 mM 4-AP and 0.3 mM PA. The measurements were carried out using a total flow rate of $2.6 \mu\text{L min}^{-1}$ (0.016 mm s^{-1}) and $W_f = 0.31$.

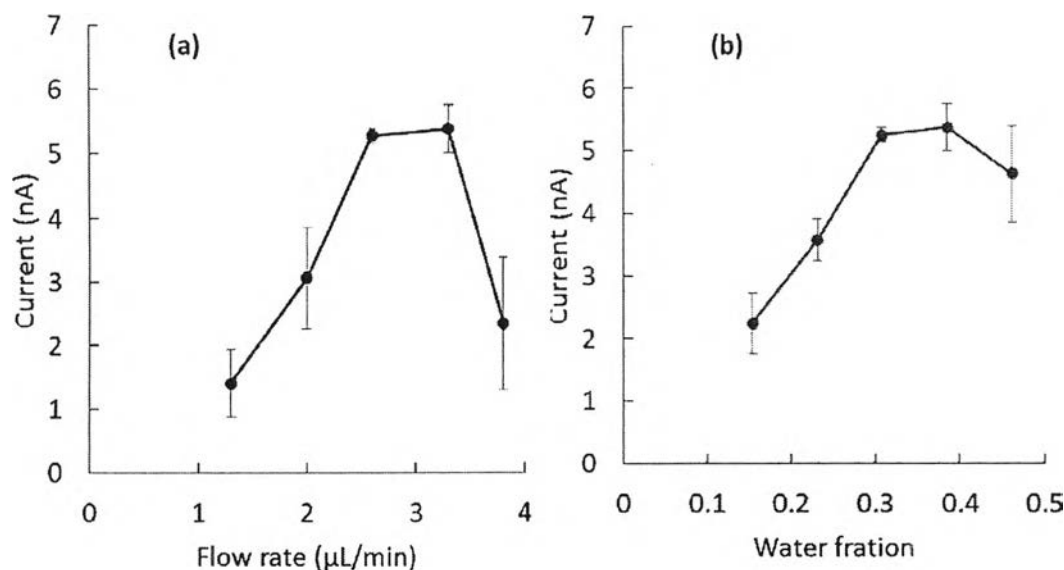


Fig. 6. Effects of (a) total flow rate and (b) water fraction on chronoamperometric detection of 0.3 mM 4-AP. Conditions: an detection potential (E_{det}) of +0.2 V vs. CPE, total flow rate of $2.6 \mu\text{L min}^{-1}$ (0.016 mm s^{-1}) and $W_f = 0.31$.

clearly observed with an anodic potential difference ($E_{PA} - E_{4-AP}$) of 380 mV. As a result, the selection of potential to use in further chronoamperometric experiments would be particularly useful for selective electrochemical detection of 4-AP in the presence of PA.

3.3. Chronoamperometric detection in droplets

Chronoamperometric detection has been broadly used in the various flow-based systems due to its ease of operation and low background current. Fig. 4 shows a representative chronoamperogram of 300 μM 4-AP in droplets in which each discrete peak corresponds to an individual droplet. When the droplet front began to pass through the electrode array, the current increased sharply. With the electrooxidation reaction of 4-AP proceeded, its concentration region at the nearby electrode surface exponentially decreased, resulting that the current slowly decayed with time corresponding to Cottrell equation [50]. Subsequently, the current approaches a steady state level of $5.14 \pm 0.11 \text{ nA}$ ($n = 10$) which can be assigned to the diffusion-limited current of 4-AP. For quantification, the current was measured during this regime.

3.3.1. Selection of the optimal detection potential (E_{det})

Selective detection of 4-AP in the presence of PA in the flow-based system was assessed. According to Fig. 3d, the selection of E_{det} lower than +0.3 V vs. CPE should achieve selective detection of 4-AP in the presence of PA. To select an optimal E_{det} for chronoamperometric detection of 4-AP and PA in the droplet-based flow system, hydrodynamic voltammetry (Fig. 5a) experiments were conducted. The anodic peak current of 4-AP increased with E_{det} . There is no signal response from PA and background (BG) solution (0.1 M PBS pH 7.4) in the range of 0.0–0.2 V vs. CPE while both anodic current signals of 300 μM PA and BG solution also increased with E_{det} over +0.2 V vs. CPE.

Thus, the E_{det} for chronoamperometric detection in the range between 0.0 and 0.2 V vs. CPE can be used for selective detection of 4-AP without an interfering response from PA. To optimize the E_{det} for chronoamperometric detection of droplet contents, the signal-to-background (S/B) ratio of 4-AP and PA was plotted as a function of E_{det} . As seen from Fig. 5b, an E_{det} of +0.2 V vs. CPE showed the highest S/B ratio for 4-AP detection; accordingly, +0.2 V vs. CPE was chosen as the optimal chronoamperometric E_{det} for quantitative measurements of 4-AP for further experiment.

3.3.2. Effect of water fraction and total flow rate

The influence of water fraction (W_f) and total flow rate on

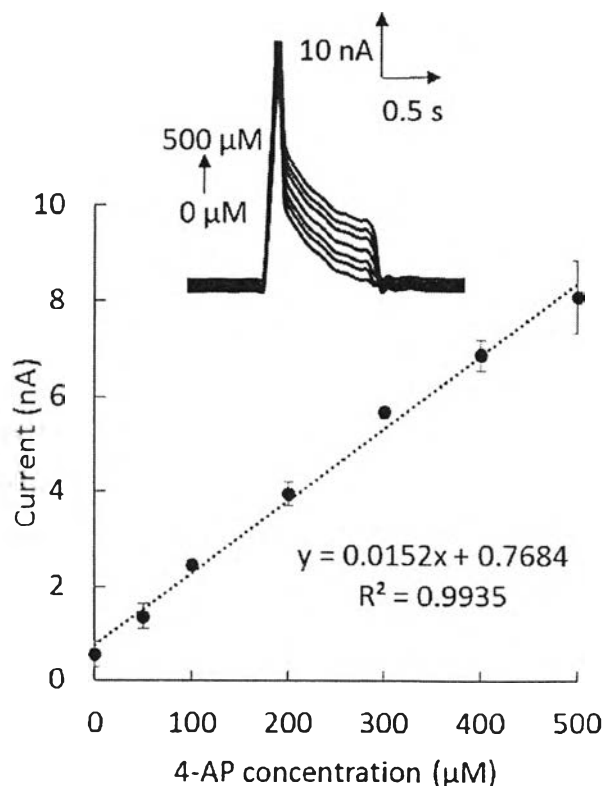


Fig. 7. A linear calibration plot of 4-AP in the concentration range of 0–500 μM . The optimal conditions: an detection potential (E_{det}) of +0.2 V vs. CPE, total flow rate of $2.6 \mu\text{L min}^{-1}$ (0.016 mm s^{-1}) and $W_f = 0.31$. (Inset) A chronoamperogram of 4-AP current vs. time.

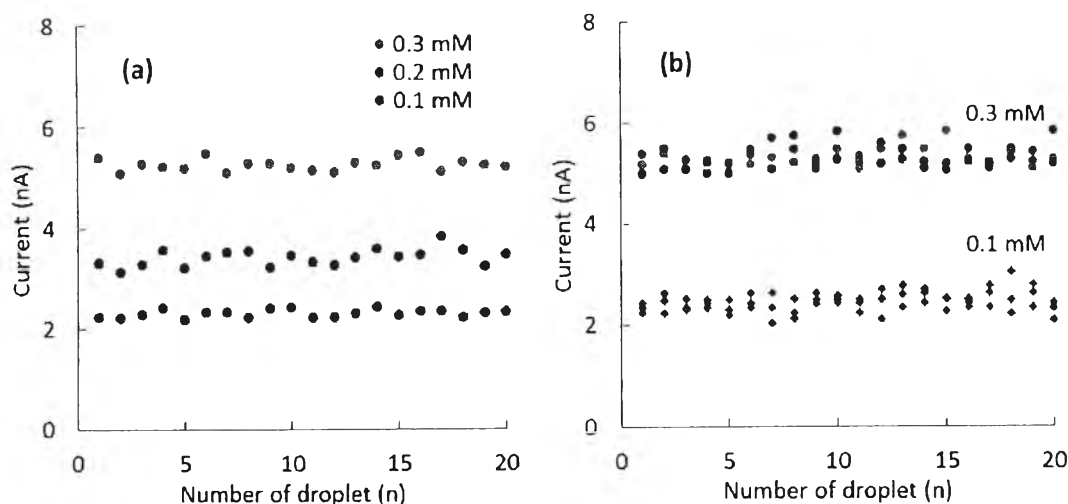


Fig. 8. Intra-day measurements of (a) 4-AP at concentrations of 0.1, 0.2 and 0.3 mM and (b) inter-day measurements of 0.1 and 0.3 mM 4-AP for three days ($n = 3$).

Table 1
Effect of foreign ions on the determination of 0.3 mM 4-AP.

Foreign species	5% Tolerable molar ratio
Na ⁺ , K ⁺ , Mg ²⁺ , Ca ²⁺ , NO ₃ ⁻ , SO ₄ ²⁻ , PO ₄ ³⁻ , Cl ⁻ , Glucose, Sucrose	>10000
Cu ²⁺ , Fe ²⁺ , Fe ³⁺	300
Acetylsalicylic acid, Glutathione	1000
Uric acid, Dopamine	500
Ascorbic acid, Cysteine	200
Paracetamol	100

chronoamperometric measurements were then studied. W_f is a well-known factor strongly affecting droplet size with droplet size increasing with W_f . In this work, the droplet sizes at W_f values in the range of 0.15–0.46 were generated by adjusting the flow rate ratio between oil and aqueous solutions while the total flow rate was kept constant at $2.6 \mu\text{L min}^{-1}$. As shown in Fig. 6a, when the water fraction was lower than 0.31, unstable droplets with small sizes were produced, resulting in low anodic current. For W_f values over 0.38, droplet length was too long, resulting that the anodic steady-state current decreased due to amperometrically exponential decay. The highest current was obtained at a water fraction of 0.31. Accordingly, the water fraction of 0.31 was found to be the optimal W_f to produce stable droplets, and all subsequent

experiments were performed using this conditions.

Another important factor influencing on chronoamperometric response is total flow rate. The effect of total flow rate was investigated as shown in Fig. 6b. While the water fraction was kept at a constant of 0.31, total flow rate was varied between 1.30 and $3.90 \mu\text{L min}^{-1}$, corresponding to a linear flow velocity in the range of 0.43 – 1.29 mm s^{-1} . Results show that for flow rates $< 2.6 \mu\text{L min}^{-1}$ (linear velocity $< 0.43 \text{ mm/s}$), a low steady-state current was obtained due to the long residence time of a single droplet passing over the electrode surface. When the total flow rate was $> 3.25 \mu\text{L min}^{-1}$ (linear velocity $> 1.08 \text{ mm/s}$), the current also reduced significantly. We believe that this high total flow rates provided short residence time which was not sufficient for the

Table 2
The % recovery of the our proposed method ($n = 20$) for determination of 4-AP in PA samples vs. conventional CZE/UV–Vis method ($n = 3$).

Sample	Spiked 4-AP concentration (μM)	This proposed method ($n = 20$)		CZE/UV–Vis method ($n = 3$)	
		%Recovery ($\pm\text{SD}$)	%RSD	%Recovery ($\pm\text{SD}$)	%RSD
Infants' TYLENOL®	100	91.21 \pm 2.51	2.75	99.74 \pm 1.01	1.01
	200	91.29 \pm 3.29	3.60	102.95 \pm 3.29	3.20
	300	101.12 \pm 4.12	4.07	98.89 \pm 2.11	2.13
	400	97.34 \pm 3.93	4.04	99.19 \pm 1.71	1.72
	500	101.25 \pm 4.19	4.14	101.91 \pm 2.41	2.36
TEMPRA®	100	99.97 \pm 3.21	3.21	99.24 \pm 1.31	1.32
	200	98.08 \pm 2.94	3.00	98.93 \pm 1.92	1.94
	300	95.25 \pm 3.17	3.33	102.25 \pm 1.27	1.24
	400	105.34 \pm 2.94	2.78	103.04 \pm 2.14	2.08
	500	91.93 \pm 2.74	2.98	99.91 \pm 0.24	0.24
SARA®	100	97.51 \pm 3.19	3.27	102.01 \pm 2.45	2.40
	200	101.12 \pm 1.92	1.90	99.92 \pm 1.29	1.29
	300	102.12 \pm 2.25	2.20	101.01 \pm 2.01	1.99
	400	103.34 \pm 1.89	1.83	103.34 \pm 1.71	1.65
	500	101.25 \pm 2.97	2.93	103.15 \pm 1.31	1.27

electrochemical process to occur. The highest steady-state current values were obtained from the total flow rates at 2.6 and 3.25 $\mu\text{L min}^{-1}$. In addition, use of high flow rates to produce droplets increases reagent/sample consumption. Therefore, an optimal total flow rate of 2.6 $\mu\text{L min}^{-1}$ (linear velocity = 0.86 mm s^{-1}) was selected to use in further experiments.

3.4. Analytical performance

The analytical performance of the droplet microfluidics coupled with G-PANI/CPE was investigated. Chronoamperometric detection of 4-AP at E_{det} of +0.2 V vs. CPE was performed using the optimal conditions as mentioned above. Calibration curve of 4-AP was plotted between anodic current as a function of the standard 4-AP concentration as shown in Fig. 7. A linear range was found to be 50–500 μM with correlation coefficient (R^2) of 0.99. The limit of detection (LOD, $S/N = 3$) was found to be 15.68 μM while limit of quantitation (LOQ, $S/N = 10$) was found to be 52.28 μM . The European, United States, British, German, and Chinese Pharmacopoeias report the maximum allowable limit of 4-AP in PA products is 50 ppm (0.005% w/w); therefore, our system can determine 4-AP at the relevant concentration in commercial PA samples.

In this work, a chronoamperometric measurement within droplet volume of 0.625 nL was performed. This volume of testing solution was lower than those required from conventional electrochemical batch cells (normally require sample volumes at least 0.5 mL), corresponding to a high limit of detection of our proposed system. Although the LOD and LOQ values reported here are higher than those obtained from the previous publications [2,3,5,7,10], our approach offers simplicity and inexpensive operation. In addition, small aliquot (<1 mL) of testing sample/reagent was required to operate the droplet generation within the microfluidic system, leading to a fast and high-throughput analysis of 4-AP.

In addition to assess the stability of this system, chronoamperometric detection of standard 4-AP at different concentrations by 20 successive measurements was performed for intra-day and inter-day precisions as shown in the Fig. 8. For intra-day and inter-day results, relative standard deviations (RSDs) were found to be less than 5% ($n = 20$). Therefore, these results verify that our proposed system had the good stability. Moreover, the reproducibility of the microfluidic sensor was evaluated using chronoamperometric detection of 0.3 mM 4-AP. The %RSD of seven different devices was found to be 3.5%, indicating that the fabricated microfluidic sensor had a good precision.

3.5. Interference study and determination of 4-AP in commercial PA samples

The effect of various foreign species on the detection of 0.3 mM 4-AP was studied. The 5% tolerable ratio of foreign species is shown in Table 1. The tolerable ratio was defined as the level of foreign species, generating a change in intensity of the peak current of $\pm 5\%$. From the results, these species were tolerated at a high level, demonstrating the good selectivity of the proposed method.

Additionally, since 4-AP is produced from the degradation of pharmaceutical PA samples, the selectivity of this method towards the determination of 4-AP in the presence of PA in commercial samples was evaluated. The tolerance concentration is defined as the concentration of 4-AP, generating a change in signal response of $\pm 5\%$. Results show that 30 mM PA gave a 5% change in the detection of 0.3 mM 4-AP; therefore, the PA sample was diluted to a lower concentration. Next, the application of our method was tested by measuring the spiked 4-AP concentrations (100, 200, 300, 400, and 500 μM) in each diluted PA sample.

As shown in the Table 2, the % recovery of this system was found

in the range of 91.21%–105.34% ($n = 20$). Moreover, to validate our method, the results obtained from the proposed system was compared to those obtained from the conventional capillary zone electrophoresis/UV–Visible spectrophotometric technique (CZE/UV–Vis) [11] using a paired t-test at 95% confidential interval. The experimental t-values ($t_{\text{calculated}}$) obtained by this proposed method was found to be -2.20 which were significantly lower than the critical t-values of 1.76. Results show that there is no significant difference between the results obtained from our method and CZE/UV–Vis method. As a result, our electrochemical droplet system is an alternative and high-throughput method (at least 60 samples h^{-1}) for determining the 4-AP contamination in commercial PA formulations.

4. Conclusions

In this work, we report a novel electrochemical droplet microfluidic device for determination of 4-AP in commercial PA formulations. The G-PANI/CPE was first coupled with the droplet system to perform chronoamperometric detection of 4-AP. The improvement in electrochemical sensitivity was attributed to an enhancement of the active surface area of electrode and increased electrochemical conductivity. Our proposed method can perform a high-throughput and rapid measurement of 4-AP in commercial PA products with required small consumption of reagent/sample. Eventually, this system was successfully applied for the determination of 4-AP in PA liquid samples with high precision and good recovery; therefore, this system might be an alternative analytical device for routine analysis of 4-AP residue in pharmaceutical products.

Acknowledgments

P. R. wishes to thank the financial support from Chulalongkorn University and the Thailand Research Fund, through the Royal Golden Jubilee Ph.D. Program (Grant No. PHD/0251/2552). Moreover, this research has been supported by the Thailand Research Fund through Research Team Promotion Grant (RTA5780005) and National Research University project, Office of Higher Education Commission (WCU-032-AM-57).

References

- [1] K. Vijayakaran, K. Kannan, M. Kesavan, S. Suresh, P. Sankar, S.K. Tandan, S.N. Sarkar, *Environ. Toxicol. Pharmacol.* 37 (2014) 438.
- [2] I.Y. Shiroma, M. Santhiago, A.L. Gobbi, L.T. Kubota, *Anal. Chim. Acta* 725 (2012) 44.
- [3] H. Yin, Q. Ma, Y. Zhou, S. Ai, L. Zhu, *Electrochim. Acta* 55 (2010) 7102.
- [4] M.S. Bloomfield, *Talanta* 58 (2002) 1301.
- [5] Y. Fan, J.-H. Liu, C.-P. Yang, M. Yu, P. Liu, *Sensors Actuators B Chem.* 157 (2011) 669.
- [6] A. Brega, P. Prandini, C. Amaglio, E. Pafumi, *J. Chromatogr. A* 535 (1990) 311.
- [7] C.-M. Zou, H. Yu, M.-Y. Wang, *Chin. Chem. Lett.* 25 (2014) 201.
- [8] B. Schultz, *J. Chromatogr. A* 299 (1984) 484.
- [9] B.C. Lourenção, R.A. Medeiros, R.C. Rocha-Filho, L.H. Mazo, O. Fatibello-Filho, *Talanta* 78 (2009) 748.
- [10] Q. Chu, L. Jiang, X. Tian, J. Ye, *Anal. Chim. Acta* 606 (2008) 246.
- [11] T. Pérez-Ruiz, C. Martínez-Lozano, V. Tomás, R. Galera, *J. Pharm. Biomed. Anal.* 38 (2005) 87.
- [12] A.B. Vishnikin, M.I.E.A. Al-Shwaiyat, G.A. Petrushina, L.P. Tsigarik, V. Andrush, Y.R. Bazel, H. Sklenářová, P. Solich, *Talanta* 96 (2012) 230.
- [13] Y. Zhu, Q. Fang, *Anal. Chim. Acta* 787 (2013) 24.
- [14] C.-G. Yang, Z.-R. Xu, J.-H. Wang, *TrAC Trends Anal. Chem.* 29 (2010) 141.
- [15] S. Park, Y. Zhang, S. Lin, T.-H. Wang, S. Yang, *Biotechnol. Adv.* 29 (2011) 830.
- [16] B. Ramaswamy, Y.-T.T. Yeh, S.-Y. Zheng, *Sensors Actuators B Chem.* 180 (2013) 21.
- [17] Y.T. Atalay, S. Vermeir, D. Witters, N. Vergauwe, B. Verbruggen, P. Verboven, B.M. Nicolai, J. Lammertyn, *Trends Food Sci. Technol.* 22 (2011) 386.
- [18] M. Safavi, S. Nahar, M. Zourob, M.U. Ahmed, in: A.K. Bhunia, M.S. Kim, C.R. Taitt (Eds.), *High Throughput Screening for Food Safety Assessment*, Woodhead Publishing, 2015, p. 327.

- [19] Z.-X. Guo, Q. Zeng, M. Zhang, L.-Y. Hong, Y.-F. Zhao, W. Liu, S.-S. Guo, X.-Z. Zhao, *Sensors Actuators A Phys.* 172 (2011) 546.
- [20] S. Teychené, B. Biscans, *Chem. Eng. Sci.* 77 (2012) 242.
- [21] M.-P.N. Bui, C.A. Li, K.N. Han, J. Choo, E.K. Lee, G.H. Seong, *Anal. Chem.* 83 (2011) 1603.
- [22] H. Tsuchiya, M. Okochi, N. Nagao, M. Shikida, H. Honda, *Sensors Actuators B Chem.* 130 (2008) 583.
- [23] J. Ji, Y. Zhao, L. Guo, B. Liu, C. Ji, P. Yang, *Lab Chip* 12 (2012) 1373.
- [24] I. Lignos, L. Protesescu, S. Stavrakis, L. Piveteau, M.J. Speirs, M.A. Loi, M.V. Kovalenko, A.J. deMello, *Chem. Mater.* 26 (2014) 2975.
- [25] T. Konry, M. Dominguez-Villar, C. Baecher-Allan, D.A. Haller, M.L. Yarmush, *Biosens. Bioelectron.* 26 (2011) 2707.
- [26] S.-W. Lin, C.-H. Chang, C.-H. Lin, *Genomic Med. Biomarkers Health Sci.* 3 (2011) 27.
- [27] J. Lee, H.K. Musyimi, S.A. Soper, K.K. Murray, *J. Am. Soc. Mass Spectrom.* 19 (2008) 964.
- [28] M.P. Cecchini, J. Hong, C. Lim, J. Choo, T. Albrecht, A.J. deMello, J.B. Edel, *Anal. Chem.* 83 (2011) 3076.
- [29] G. Aubry, S. Méance, L. Couraud, A.M. Haghiri-Gosnet, Q. Kou, *Microelectron. Eng.* 86 (2009) 1368.
- [30] J. Clausell-Tormos, D. Lieber, J.-C. Baret, A. El-Harrak, O.J. Miller, L. Frenz, J. Blouwolf, K.J. Humphry, S. Köster, H. Duan, C. Holtze, D.A. Weitz, A.D. Griffiths, C.A. Meriten, *Chem. Biol.* 15 (2008) 427.
- [31] J. Wang, *Talanta* 56 (2002) 223.
- [32] S. Liu, Y. Gu, R.B. Le Roux, S.M. Matthews, D. Bratton, K. Yunus, A.C. Fisher, W.T.S. Huck, *Lab Chip* 8 (2008) 1937.
- [33] Z. Han, W. Li, Y. Huang, B. Zheng, *Anal. Chem.* 81 (2009) 5840.
- [34] S. Gu, Y. Lu, Y. Ding, L. Li, H. Song, J. Wang, Q. Wu, *Biosens. Bioelectron.* 55 (2014) 106.
- [35] D. Itoh, F. Sassa, T. Nishi, Y. Kani, M. Murata, H. Suzuki, *Sensors Actuators B Chem.* 171–172 (2012) 619.
- [36] W. Siangproh, W. Dungchai, P. Rattanarat, O. Chailapakul, *Anal. Chim. Acta* 690 (2011) 10.
- [37] M. Arvand, T.M. Gholizadeh, *Colloids Surfaces B Bionterfaces* 103 (2013) 84.
- [38] H. Ghadimi, R.M.A. Tehrani, A.S.M. Ali, N. Mohamed, S. Ab Ghani, *Anal. Chim. Acta* 765 (2013) 70.
- [39] S. Wu, Q. He, C. Tan, Y. Wang, H. Zhang, *Small* 9 (2013) 1160.
- [40] N. Thammasoontaree, P. Rattanarat, N. Ruecha, W. Siangproh, N. Rodthongkum, O. Chailapakul, *Talanta* 123 (2014) 115.
- [41] N. Rodthongkum, N. Ruecha, R. Rangkipan, R.W. Vachet, O. Chailapakul, *Anal. Chim. Acta* 804 (2013) 84.
- [42] N. Ruecha, R. Rangkipan, N. Rodthongkum, O. Chailapakul, *Biosens. Bioelectron.* 52 (2014) 13.
- [43] Y.-P. Dong, J. Zhang, Y. Ding, X.-F. Chu, J. Chen, *Electrochim. Acta* 91 (2013) 240.
- [44] E. Asadian, S. Shahrokhian, A.I. zad, E. Jokaer, *Sensors Actuators B Chem.* 196 (2014) 582.
- [45] J. Li, S. Liu, J. Yu, W. Lian, M. Cui, W. Xu, J. Huang, *Sensors Actuators B Chem.* 188 (2013) 99.
- [46] J. Huang, Q. Lin, X. Zhang, X. He, X. Xing, W. Lian, M. Zuo, Q. Zhang, *Food Res. Int.* 44 (2011) 92.
- [47] H. Liu, R.M. Crooks, *Lab a Chip* 13 (2013) 1364.
- [48] Y. Sameenoi, M.M. Mensack, K. Boonsong, R. Ewing, W. Dungchai, O. Chailapakul, D.M. Crokek, C.S. Henry, *Analyst* 136 (2011) 3177.
- [49] N. Ruecha, W. Siangproh, O. Chailapakul, *Talanta* 84 (2011) 1323.
- [50] A. Suea-Ngam, P. Rattanarat, O. Chailapakul, M. Srisa-Art, *Anal. Chim. Acta* 883 (2015) 45.
- [51] J.D. Tice, A.D. Lyon, R.F. Ismagilov, *Anal. Chim. Acta* 507 (2004) 73.
- [52] T. Németh, P. Jankovics, J. Németh-Palotás, H. Kőszegi-Szalai, *J. Pharm. Biomed. Anal.* 47 (2008) 746.



Electrochemical droplet-based microfluidics using chip-based carbon paste electrodes for high-throughput analysis in pharmaceutical applications



Akkapol Suea-Ngam^{a,b}, Poomrat Rattanarat^b, Orawon Chailapakul^{b,c},
Monpichar Srisa-Art^{a,b,*}

^a Chromatography and Separation Research Unit (ChSRU), Department of Chemistry, Faculty of Science, Chulalongkorn University, Patumwan, Bangkok 10330, Thailand

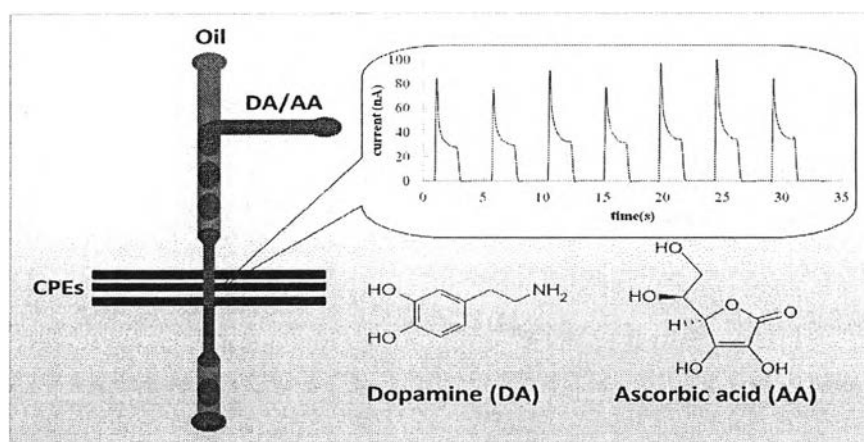
^b Electrochemistry and Optical Spectroscopy Research Unit (EOSRU), Department of Chemistry, Faculty of Science, Chulalongkorn University, Patumwan, Bangkok 10330, Thailand

^c Center of Excellence on Petrochemical and Materials Technology, Chulalongkorn University, Patumwan, Bangkok 10330, Thailand

HIGHLIGHTS

- Droplet microfluidics with CPEs was developed for pharmaceutical applications.
- This system was used to quantitative analysis of DA and AA in intravenous drugs.
- Highly accurate and precise analysis of DA and AA using this system was achieved.

GRAPHICAL ABSTRACT



ARTICLE INFO

Article history:

Received 1 May 2014

Received in revised form 10 February 2015

Accepted 4 March 2015

Available online 9 March 2015

Keywords:

Droplet-based microfluidics

Carbon paste electrode

Dopamine

Ascorbic acid

ABSTRACT

This paper presents the first example of a pharmaceutical application of droplet-based microfluidics coupled with chronoamperometric detection using chip-based carbon paste electrodes (CPEs) for determination of dopamine (DA) and ascorbic acid (AA). Droplets were generated using an oil flow rate of $1.80 \mu\text{L min}^{-1}$, whereas a flow rate of $0.80 \mu\text{L min}^{-1}$ was applied to the aqueous phase, which resulted in a water fraction of 0.31. The optimum applied potential for chronoamperometric measurements in droplets was found to be 150 mV. Highly reproducible analysis of DA and AA was achieved with relative standard deviations of less than 5% for both intra-day and inter-day measurements. The limit of detection (LOD) and limit of quantitation (LOQ) were found to be 20 and $70 \mu\text{M}$ for DA and 41 and $137 \mu\text{M}$ for AA, respectively. Linearity of this method was in the ranges of 0.02–3.0 mM for DA and 0.04–3.0 mM for AA. This system was successfully applied to determine the amounts of DA and AA in intravenous drugs.

* Corresponding author at: Chromatography and Separation Research Unit (ChSRU), Department of Chemistry, Faculty of Science, Chulalongkorn University, Patumwan, Bangkok 10330, Thailand. Tel.: +66 221 87610; fax: +66 221 87598.

E-mail address: monpichar.s@chula.ac.th (M. Srisa-Art).

Calibration curves of DA and AA for quantitative analysis were obtained with good linearity with R^2 values of 0.9984 and 0.9988, respectively. Compared with the labeled amounts, the measured concentrations of DA and AA obtained from this system were insignificantly different, with error percentages of less than $\pm 3.0\%$, indicating a high accuracy of the developed method.

© 2015 Elsevier B.V. All rights reserved.

1. Introduction

Droplet-based microfluidic systems were introduced into scientific research a decade ago in order to overcome the classical problems of slow mixing and sample zone dispersion associated with laminar flow microfluidic platforms [1]. Since then the droplet technology has grown rapidly and been widely exploited in a diverse range of applications [2–5], such as chemical synthesis [6], biological and cell studies [7–10], medical applications and pharmaceutical sciences [11,12]. This is due to the fact that droplet-based microfluidic systems have successfully exploited the outstanding advantages of miniaturization, including small sample consumption, high analytical performance, low cost, portability, the potential for parallel analysis and short analysis times. In addition, droplet systems possess uniquely superb performance. For example, precisely defined volume droplets can be controllably produced at high generation frequencies up to 1 kHz or above. This renders droplet microfluidics a promising platform for high-throughput analysis, in which each isolated droplet can serve as a micro/nano reactor. Significantly, the compartmentalization of droplets not only prevents diffusion of sample zone, surface adsorption and cross-contamination [1,13], but also enhances rapid mixing [3,14]. These allow reactions occurring within droplets to be accurately and precisely controlled and monitored.

Apart from droplet generation and manipulation, the online detection and characterization of an individual droplet is also a challenge. There have been various detection methods, such as fluorescence spectroscopy [1,8,15], mass spectrometry [16,17], electrochemical detection [18–22], Raman spectroscopy [23–25], that have been used to characterize droplet contents. Among these detection techniques, fluorescence has been the most attractive detection system due to its high sensitivity and fast response. However, this detection method encounters the problems of complexity, high cost and large instrumentation which is not ideally compatible with microfluidic systems. Unlike other detection systems, electrochemical detection offers an alternative relatively simple, cheap, sensitive, selective and label-free method for droplet detection. Importantly, the size of the electrochemical detection setup is perfectly suitable to be incorporated with microfluidic systems. Accordingly, electrochemical detection holds a great promise to be a detection method for droplet-based microfluidics. To date, there have been limited published reports on electrochemical detection for droplet-based microfluidic systems. For example, Liu et al. [26] successfully demonstrated a chronoamperometric method using gold microband electrodes, to determine droplet contents and characterize droplet generation frequency, size and velocity. In addition, Han et al. [27] developed a droplet-based microfluidic system coupled with amperometric detection using Pt wire electrodes to monitor the kinetics of the decomposition of H_2O_2 by catalase occurring within droplets. Using this system, the complete Michaelis–Menten kinetics of catalase was successfully measured. Furthermore, Filla et al. [28] presented a corona discharge electrode to create a hydrophilic/hydrophobic interface in order to desegment the flow into separate oil and aqueous streams. The desegmented droplets' contents were subsequently analyzed using electrochemistry or microchip electrophoresis with electrochemical detection. Additionally, potentiometric [29] and coulometric [30] detection systems have

also successfully been used for the analysis of droplet contents. Recently, highly reproducible chronoamperometric analysis of microdroplets containing 0.1 mM $Ru(NH_3)_6^{3+}$ was presented by Liu et al. [22]. A narrow section of the microchannel, which was placed across gold microband electrodes, was used to elongate droplets to attain reproducible current measurements.

In all situations, electrochemical detection methods have shown their abilities for analyzing droplet contents. However, all published reports have focused on metal electrodes. The main problems of using metal electrodes are fouling and narrow working potentials. Therefore, in this work, it was successfully demonstrated for the first time that chip-based carbon paste electrodes (CPEs) fabricated as three microbands within the microfluidic device can be used to monitor electrochemical activities within droplets. The chip-based CPEs were originally developed by Henry's research group [31]. Unlike metal electrodes, the CPEs have attracted considerable attention because of their unique property to withstand fouling and flow-based systems and they possess a larger potential range [31,32]. A confined channel design previously presented by Liu et al. [22] was also exploited to obtain reproducible chronoamperometric measurements within droplets. Using this approach, chronoamperometric measurements of dopamine and ascorbic acid in real samples of intravenous drugs were successfully achieved.

2. Experimental

2.1. Materials and chemicals

All chemicals were analytical grade. The following materials and chemicals were used as received: sodium chloride (NaCl: Merck, Thailand), disodium hydrogen phosphate (Na_2HPO_4 : Merck, Thailand), potassium dihydrogen phosphate (KH_2PO_4 : Carlo ERBA, Thailand), potassium chloride (KCl: Ajax Finechem, Thailand), Noujol mineral oil (PerkinElmer, Thailand), silver paint (SPI supplies, USA), graphite powder ($\leq 20 \mu m$, Sigma–Aldrich, Singapore), ethanol (Merck, Thailand) and poly(dimethylsiloxane) (PDMS) Sylgard 184 elastomer kit (Dow Corning, USA). Potassium ferricyanide ($K_3[Fe(CN)_6]$) and potassium ferrocyanide ($K_4[Fe(CN)_6]$) were obtained from Sigma–Aldrich (Singapore). Dopamine hydrochloride (DA) and ascorbic acid (AA) were purchased from Sigma–Aldrich (Singapore) and BDH (AnalaR, England), respectively.

Intravenous drugs containing either DA or AA were purchased from the King Chulalongkorn Memorial Hospital (Thailand) and a local pharmacy. Three samples of DA which are Upamine (Umeda Co., Ltd., Thailand), Domine-250 (Modern Menu Co., Ltd., Thailand) and Dopamex (Biolab Co., Ltd., Thailand) were determined. The labeled amounts of DA contained in Upamine, Domine-250 and Dopamex are 250 mg/10 mL, 250 mg/10 mL and 200 mg/10 mL, respectively. A sample of ascorbic acid is a product of Atlantic Laboratories Corporation Ltd. (Thailand) and contains AA at a concentration of 500 mg/2 mL.

The oil solution for droplet generation was a 10:2 (v/v) mixture of perfluorodecalin (mixture of *cis* and *trans*, 95%, Sigma–Aldrich, Germany) and 1H, 1H, 2H, 2H-perfluoro-1-octanol (97%, Sigma–Aldrich, Germany). All aqueous solutions were prepared with deionized water ($18.0 M\Omega cm$, Milli-Q Gradient System, Millipore, Thailand).

2.2. Instrumentation

All electrochemical measurements were conducted using a commercially available potentiostat (eDAQ, ED410, 410-088, Australia). In this work, both aqueous and carrier phases stored in 1 mL plastic syringes (Nipro, Thailand) were connected to the inlets of a microfluidic device using polyethylene tubing (0.38 mm I.D., 1.09 mm O.D., PORTEX, Belgium). The solutions were driven through the device using syringe pumps (Harvard Apparatus 11 Plus).

2.3. Procedures

2.3.1. Preparation of solutions

Phosphate buffer saline (PBS) pH 7.4 at a concentration of 0.1 M was used as a supporting electrolyte for all experiments. To prepare: 0.1 M PBS, 2.0 g NaCl, 0.05 g KCl, 0.36 g Na_2HPO_4 and 0.06 g KH_2PO_4 were dissolved using deionized water in a 250 mL

volumetric flask. All aqueous solutions were prepared in 0.1 M PBS. Stock solutions of DA and AA at a concentration of 80 mM were prepared separately by dissolving 15.17 mg of DA and 14.09 mg of AA in 1.0 mL of 0.1 M PBS in safe-lock tubes (Eppendorf, Thailand). Desired concentrations of DA and AA were diluted from the stock solutions. Real samples of DA and AA from intravenous drugs were prepared in 0.1 M PBS at concentrations of 1.0 and 1.5 mM, respectively.

2.3.2. Microfluidic device design and fabrication

The design of a microfluidic device used for electrochemical detection in this experiment followed the layout originally presented by Liu et al. [22]. A T-junction PDMS microfluidic device was fabricated using traditional soft lithography [33]. Two types of SU-8 masters, electrode-patterned and channel-patterned PDMS molding, were produced. Two PDMS replicas (channel-patterned and electrode-patterned) were cast from the SU-8 masters. The PDMS replicas are shown in Fig. 1(a) and (b).

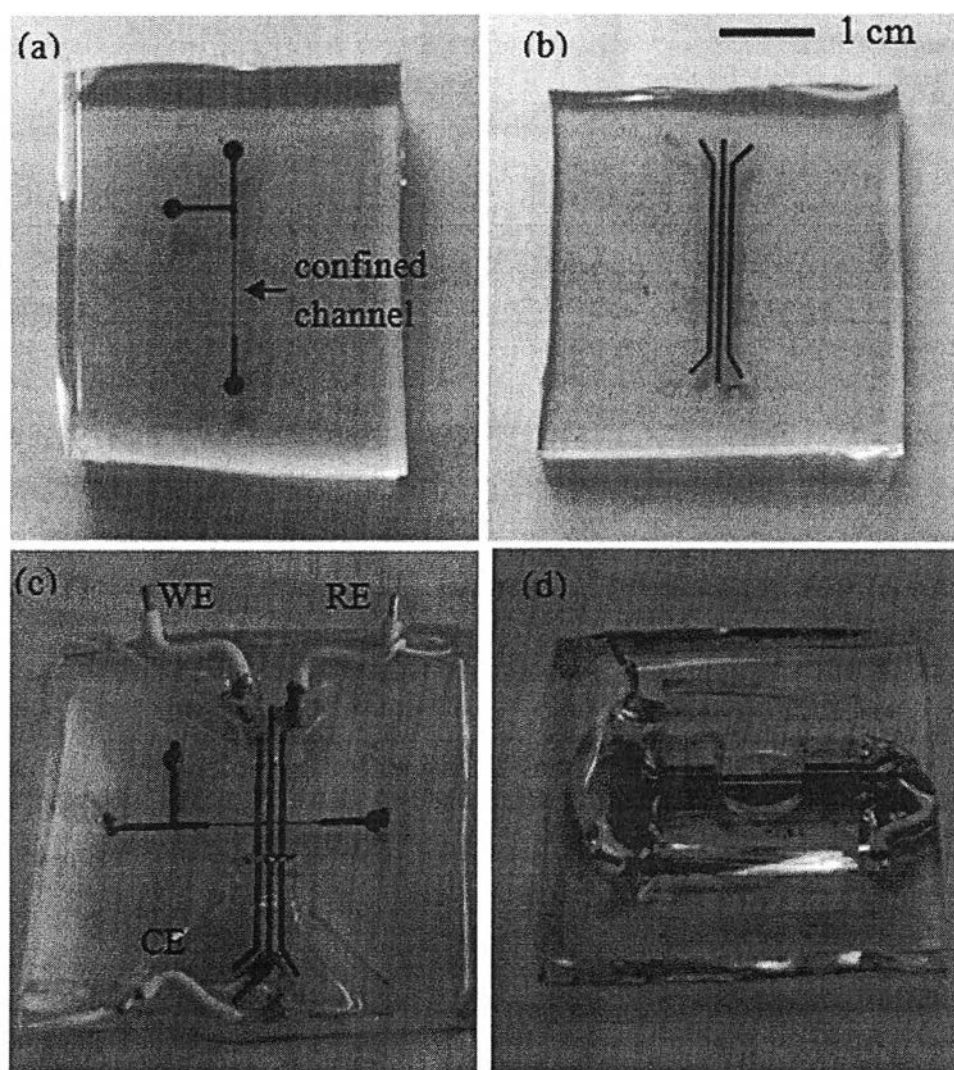


Fig. 1. A microfluidic device with electrochemical sensors for chronoamperometric measurements in droplets. (a) A channel patterned PDMS replica filled with a dye for visualization. (b) An electrode patterned PDMS replica screen-printed with carbon paste. (c) A complete microfluidic device consisting of a main channel (100 μm deep and 500 μm wide) and a confined channel (100 μm deep, 50 μm wide and 1 cm long) at the detection area where microband electrodes (100 μm deep and 500 μm wide) were placed across the confined channel with a distance of 500 μm between electrodes; WE – working electrode, CE – counter electrode, RE – reference electrode. (d) A batch microfluidic device consisting of a well with a diameter of 1 cm.

2.3.3. Fabrication of electrodes

Electrodes used in this work were PDMS-modified carbon paste, embedded within an electrode-patterned PDMS replica consisting of three parallel channels (100 μm deep and 500 μm wide with a spacing of 500 μm) designed for chip-based electrodes. Carbon paste electrodes (CPEs) were fabricated using a previously published procedure [31]. Briefly, carbon paste (a mixture of PDMS elastomer, curing agent, Noujol oil and graphite powder at a weight ratio of 0.91, 0.09, 1.0 and 2.0 g, respectively) was spread on the electrode-patterned PDMS replica by means of screen printing. Before spreading the paste, Scotch Magic Tape™ was applied around the electrode channels to act as borders of CPEs and for easy cleaning. Excess paste was removed using a scraper to wipe over the electrode channels. Finally, the tape was removed from the PDMS, leaving a CPEs-patterned PDMS plate, as shown in Fig. 1(b).

2.3.4. Microfluidic device assembly

For device assembly, the channel-patterned PDMS plate was bonded with the electrode-patterned PDMS plate using either oxygen plasma treatment (irreversible bonding) or reversible bonding using ethanol. For plasma bonding, both PDMS plates were placed into a plasma oven (Harrick plasma, USA) and exposed to the plasma at a high level for 1 min. One PDMS plate was then placed on top of the other for bonding. For ethanol bonding, both PDMS plates were cleaned using nitrogen gas. Ethanol was then dropped onto the to-be-bonded surfaces of both PDMS plates. Subsequently, one PDMS plate was placed carefully onto the other plate for bonding. Finally, the bonded PDMS plate was placed in a 65 °C oven for 1 h to ensure bonding.

For electrical connection, electric wires were attached to each electrode of the microfluidic device. Before attaching the wires, the parts of electrodes that were not covered by the PDMS plate and not used for connection were removed in order to prevent electrical short-circuiting. Silver paste was then glued as a connector between each electrode and its wire. Finally, epoxy glue was applied to the connection area for protecting electrodes and reducing background noise. A complete microfluidic device for electrochemical detection is shown in Fig. 1(c). This device consists of a T-junction with two inlets and one outlet. The main channel of 500 μm width was confined into a narrow section of 50 μm width and 1 cm length for the electrochemical detection of droplets. The depth of all channels was 100 μm . The patterned CPEs (500 μm wide and 100 μm deep) were in a cross position with the confined channel. This results in an electrode working area of 0.025 mm².

2.3.5. Electrode characterization

The CPEs were electrochemically characterized by cyclic voltammetry (CV) using a standard solution of ferri/ferrocyanide ($[\text{Fe}(\text{CN})_6]^{3-/4-}$). A microfluidic device specially designed to have a circle reservoir (1 cm diameter) covering the CPEs was used to perform CV. This device was called a batch microfluidic device and is shown in Fig. 1d. A potential range from -1.0 to $+1.0$ V was scanned using scan rates from 0.20 to 1.0 V s⁻¹. Prior to chronoamperometric measurements of DA and AA in droplets, the electrochemical performance of the CPEs was also determined by CV using 1 mM DA and 1 mM AA. The CV for DA was carried out using scan rates in the range of 0.025–0.175 V s⁻¹ over an applied potential range from -0.3 to $+1.2$ V.

2.3.6. Chronoamperometry in droplets

Hydrodynamic voltammograms were generated to find an optimum applied potential providing the highest signal-to-noise ratio (S/N) of current. To perform hydrodynamic measurements, droplets were generated using an oil carrier phase, consisting of perfluorodecalin and 1H, 1H, 2H, 2H-perfluoro-1-octanol as a

surfactant at a ratio of 10:2 (v/v), and an aqueous phase, which was either 0.1 M DA or 0.1 M AA. Flow rates of the oil and aqueous phases were set to be 0.8 and 1.8 $\mu\text{L min}^{-1}$, respectively. This resulted in a total flow rate of 2.6 $\mu\text{L min}^{-1}$, corresponding to a linear flow velocity of 0.86 mm s⁻¹ and a water fraction of 0.31. In this work, the water fraction (W_f) is simply defined as $W_f = F_w / (F_w + F_o)$ [14], where F_w and F_o are the total aqueous- and oil-phase flow rates, respectively. Applied potentials were 0, 50, 100, 150, 200, 250, 300, 350, 400, 450 and 500 mV (vs. CPE). Chronoamperometric currents arising from droplet contents were monitored while the droplets were squeezing through the confined channel and passing the microband CPEs. Data were collected for 1 min and averaged currents from 10 droplets ($n = 10$) were subsequently plotted versus applied potential to generate hydrodynamic voltammograms.

3. Results and discussion

3.1. Electrode characterization

Traditionally, CV was used as an effective tool to monitor the electron transfer process of electrodes and electrode characteristics. It was found that plasma bonding significantly affected the sensitivity of the CPEs. Accordingly, two batch microfluidic devices, one bonded with oxygen plasma (irreversible bonding) and the other bonded using ethanol (reversible bonding), were used to generate cyclic voltammograms and compare the electrochemical efficiency of the CPEs. Comparison of electrode performance when using oxygen plasma and ethanol bonding for the detection of

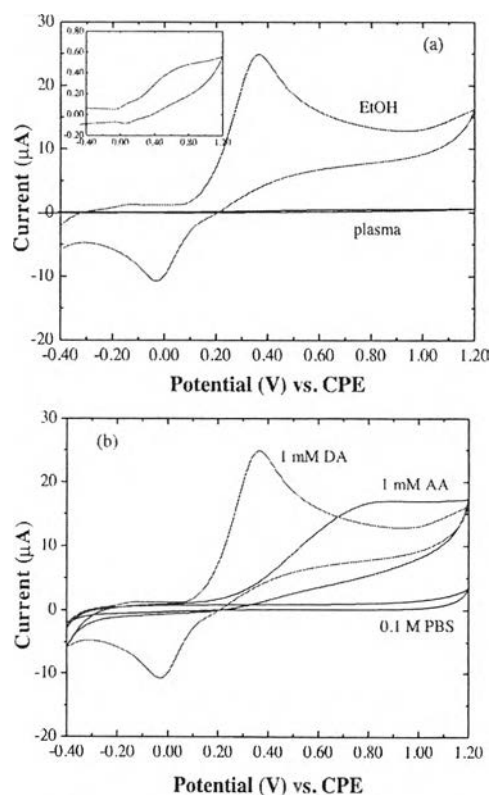


Fig. 2. (a) Cyclic voltammograms of 1 mM DA in 0.1 M PBS (pH 7.4) using irreversible oxygen plasma bonding and reversible ethanol bonding. The inset defines a close-up of the cyclic voltammogram obtained from the plasma bonding. (b) Comparison of cyclic voltammograms of 1 mM DA, 1 mM AA and 0.1 M PBS (background) obtained using the ethanol (EtOH) device.

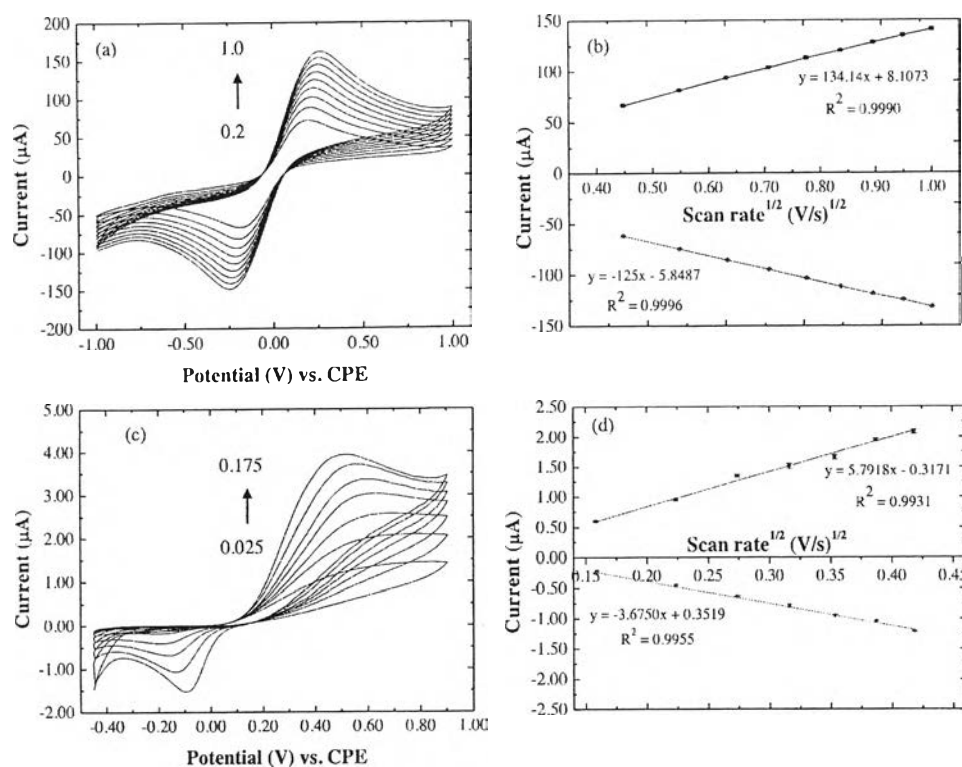


Fig. 3. Cyclic voltammograms of (a) 1.0 mM $[\text{Fe}(\text{CN})_6]^{3-/4-}$ in 0.1 M KCl at scan rates in the range of 0.2–1.0 V s^{-1} and (c) 1.0 mM DA at scan rates in the range of 0.025–0.175 V s^{-1} . Plots of the anodic (top) and cathodic (bottom) peak currents as a function of square root of scan rate; (b) 1.0 mM $[\text{Fe}(\text{CN})_6]^{3-/4-}$ in 0.1 M KCl and (d) 1 mM DA.

0.1 M DA in 0.1 M PBS (pH 7.4) is shown in Fig. 2a. Significant enhancement, approximately 50 times of the highest current response, obtained from the CPEs without plasma treatment was observed. This could be because oxygen plasma caused the decomposition of the Nujol mineral oil which was used as a binder of the CPEs. Normally, oxygen plasma is well known as a cleaning method for removing organic matter. Accordingly, the efficiency of the CPEs treated with oxygen plasma could be significantly decreased when compared to that of the CPEs without plasma treatment. Recently, Sameenoi et al. [31] has reported that exposure of PDMS-CPEs to oxygen plasma increased the peak current density; the longer the plasma exposure time, the higher the sensitivity of the chip-based CPEs. However, a comparison of the electrode sensitivity between with and without oxygen plasma treatment has not been studied yet. It should be noted that plasma treatment is normally unavoidable for chip-based electrodes because it is widely known as a bonding method for microfluidic device assembly. Accordingly, the reversible bonding using ethanol was applied for all device assemblies in this work to attain high sensitivity of the chip-based CPEs. In addition, it is interesting to note that the cyclic voltammogram of 1 mM DA obtained when using the ethanol-bonded device was quasi-reversible (Fig. 2a), whereas an irreversible voltammogram was observed from the plasma-bonded device. Normally, the redox reaction of dopamine is known as an irreversible reaction [34]. Accordingly, the CPEs without plasma treatment exhibited a wider working potential range, including the cathodic region. This could be beneficial because determination of DA using this system can be performed using cathodic potentials, which have less interference. A cyclic voltammogram of 1 mM AA was generated using the same procedure as that of 1 mM DA. Compared with DA, the cyclic voltammogram of AA was irreversible with no appearance of a cathodic peak current (Fig. 2b).

To electrochemically characterize the CPEs, a standard solution of 1.0 mM $[\text{Fe}(\text{CN})_6]^{3-/4-}$ was used to observe the electron transfer process of the CPEs. Cyclic voltammograms of 1.0 mM $[\text{Fe}(\text{CN})_6]^{3-/4-}$ at different scan rates (0.2, 0.3, 0.4, 0.5, 0.6, 0.7, 0.8, 0.9 and 1.0 V s^{-1}) obtained from the ethanol-bonded device are presented in Fig. 3a. As expected, both anodic and cathodic peak currents increased with the scan rate. As predicted by the Randles–Sevcik equation [34], plots of peak currents as a function of the square root of the scan rate (Fig. 3b) exhibited a linear relationship, with R^2 values of 0.9990 and 0.9996 for anodic and cathodic peak currents, respectively, indicating a diffusion limited reversible reaction. The Randles–Sevcik equation is shown below:

$$I = 2.69 \times 10^5 A C n^{3/2} D^{1/2} \nu^{1/2}$$

where I is anodic or cathodic current of electroactive species (e.g. $[\text{Fe}(\text{CN})_6]^{3-/4-}$ and DA), A is the electrode surface area (cm^2), n is the number of transferred electrons, D is the diffusion coefficient of electroactive species ($\text{cm}^2 \text{s}^{-1}$), ν is the scan rate (mV s^{-1}), and C is the concentration of analyte (mol cm^{-3}). Prior to analysis of DA, the CPEs were also characterized using CV and cyclic voltammograms of 1.0 mM DA are shown in Fig. 3c. Linear relationship with R^2 values of 0.9931 and 0.9955 were obtained from plots of peak currents (anodic and cathodic, respectively) as a function of square root of the scan rate, as shown in Fig. 3d. However, the anodic potential is slightly shifted less than 100 mV, which could be due to adsorption of DA and its oxidation product at the electrode surface [35,36].

3.2. Chronoamperometry in droplets

3.2.1. Selection of the optimal applied potential

To determine an optimal potential for chronoamperometric analysis of DA and AA in the droplet system, hydrodynamic

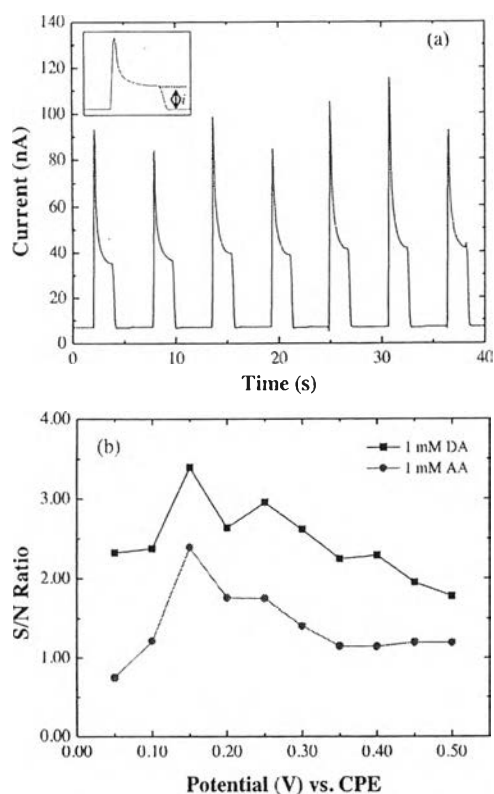


Fig. 4. (a) Chronoamperometric readout of a 40-s window for droplets containing 2 mM DA in 0.1 M PBS pH 7.4. The inset shows the zone of the droplet peak used to measure the current (i). The measurements were carried out using a total flow rate of $2.6 \mu\text{L min}^{-1}$ (0.016 mm s^{-1}) and $W_f=0.31$ and the applied potential was 150 mV. (b) Hydrodynamic voltammograms of 1 mM DA and 1 mM AA.

measurements were performed using standard solutions of DA and AA at a concentration of 1 mM. Fig. 4a shows representative data over a period of 40 s obtained from chronoamperometric measurements of 2 mM DA droplets. Each peak in Fig. 4a corresponds to an individual droplet. As seen from Fig. 4a, for each droplet, the initial current is high and then exponentially decays with time, which corresponds to the results from previous work [22]. This follows the Cottrell equation describing the exponential decay of chronoamperometric current with respect to time [37]. Accordingly, lower currents are obtained if they are measured at a later time. Therefore, measured currents not only depend on analyte concentration, but also rely on the measurement time. Normally, the chronoamperometric current can be measured at any time; however, in this work, currents were simply measured at the end of droplet peaks. As seen in Fig. 4a, averaged peak currents of 2 mM DA were found to be approximately 22.3 ± 0.5 nA.

To generate hydrodynamic voltammograms, the signal-to-noise ratio (S/N) of chronoamperometric current obtained from the analytes (DA and AA) to that obtained from the background (0.1 M PBS, pH 7.0) was plotted as a function of applied potential in a range of 50–500 mV. As seen from Fig. 4b, an applied potential of 150 mV showed the highest S/N ratios for both DA and AA. Therefore, 150 mV was chosen as the optimum applied potential for quantitative measurements of DA and AA in the droplet system.

3.2.2. Effect of droplet size on chronoamperometric measurements

Droplet size affects the analysis time for chronoamperometric measurements. Droplet length should be sufficient to cover the three-microband CPEs to complete the electrochemical process.

Accordingly, the length of elongated droplets should not be shorter than 2.5 mm after being elongated by the confined channel. This length was calculated from the width of $500 \mu\text{m}$ of each microband CPE combined with its spacing of $500 \mu\text{m}$. However, if the droplet length is too long, it would affect chronoamperometric measurements due to the exponential decay of the chronoamperometric current. Consequently, longer droplet lengths would result in lower currents. A widely known factor strongly affecting droplet size is water fraction (W_f), with a higher W_f leading to a larger droplet size [14]. To study the effect of droplet size on chronoamperometric measurements, droplets were generated using 1 mM DA at different water fractions in the range of 0.15–0.46. These were performed by changing the flow rates of the aqueous solution in the range of 0.40 – $1.20 \mu\text{L min}^{-1}$ and the oil inlet in the range of 2.20 – $1.40 \mu\text{L min}^{-1}$, resulting in a constant total flow rate of $2.60 \mu\text{L min}^{-1}$. The applied potential was held at 150 mV for chronoamperometric measurements. Results are shown in Fig. 5a. As expected, at high W_f values (0.38 and 0.46), low currents were achieved because the currents were measured from long droplets. The highest current was obtained from a water fraction of 0.31. Slightly lower currents were observed when using W_f lower than 0.31. This could be due to unstable droplet formation (as seen from the error bars) caused by the low flow rates applied to the aqueous inlet. Accordingly, the water fraction of 0.31 (corresponding to droplet lengths of 1.25 and 12.5 mm before and after elongation, respectively) was found to be suitable for this experiment because it provides the highest current of 10.1 ± 0.4 nA for 1 mM DA.

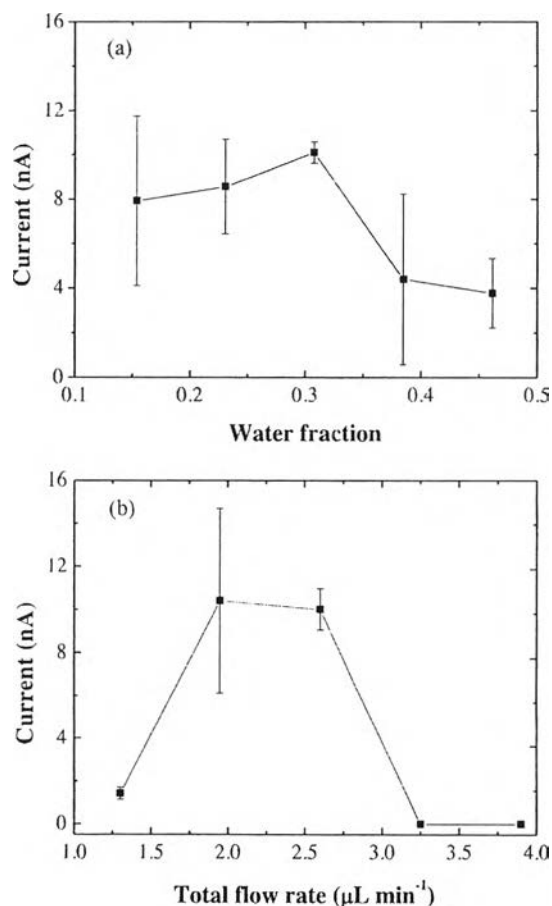


Fig. 5. Effects of (a) water fraction (W_f) and (b) total flow rate on chronoamperometric measurements of 1 mM DA in droplets. Other conditions are shown in Fig. 4.

3.2.3. Effect of total flow rate on chronoamperometric measurements

In flow-based systems coupled with electrochemical detection, residence time is crucial because it affects the sensitivity of the measurements [38]. Accordingly, the effect of total flow rate on chronoamperometric measurements in the droplet system was investigated. To perform this investigation, droplets were generated from 1 mM DA by maintaining a water fraction at 0.31 to obtain droplets with the same size of approximately 1.25 mm and the total flow rate was varied from 1.30 to 3.90 $\mu\text{L min}^{-1}$. This was performed by changing the flow rates of the aqueous solution in the range of 0.40–1.20 $\mu\text{L min}^{-1}$ and the oil inlet from 0.90 to 2.70 $\mu\text{L min}^{-1}$. Fig. 5b presents results obtained when using different total flow rates in the range of 1.30–3.90 $\mu\text{L min}^{-1}$, corresponding to a linear flow velocity in the range of 0.43–1.29 mm s^{-1} . Two maximum current values of 10.4 and 10.0 nA were obtained when using the total flow rates of 1.95 and 2.60 $\mu\text{L min}^{-1}$, respectively. When the total flow rate was changed to be higher than 2.60 $\mu\text{L min}^{-1}$, the current was found to decrease drastically and was unable to be measured if the flow rates were higher than 3.25 $\mu\text{L min}^{-1}$ (1.08 mm s^{-1}). This could be because the droplets traveled too fast, resulting in relatively short residence time for the electrochemical process to occur. In addition, it was found that when using the flow rate of 1.30 $\mu\text{L min}^{-1}$ (0.43 mm s^{-1}), the measured current was relatively low, which could be due to excessively long residence time caused by relatively slow droplet movement when passing the CPEs. This could make the chronoamperometric currents exponentially decrease with time

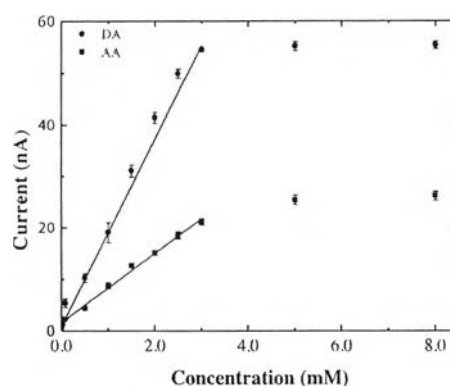


Fig. 6. Linear dynamic ranges obtained from the chronoamperometric measurements of DA and AA using the proposed system. Droplets were generated using flow rates of 1.80 $\mu\text{L min}^{-1}$ for the oil phase and 0.80 $\mu\text{L min}^{-1}$ for the aqueous solution, resulting in a total flow rate of 2.60 $\mu\text{L min}^{-1}$ (0.86 mm s^{-1}) and a water fraction of 0.31. The applied potential was 150 mV.

and almost reach the background level. Although the total flow rate of 1.95 $\mu\text{L min}^{-1}$ gave the highest current value, lower flow rates were applied to each inlet when compared to the total flow rate of 2.60 $\mu\text{L min}^{-1}$. Using low flow rates to generate droplets encounters a high possibility to obtain unstable droplet formation. Therefore, the total flow rate of 2.60 $\mu\text{L min}^{-1}$ (corresponding to a linear flow velocity of 0.86 mm s^{-1}) was chosen for

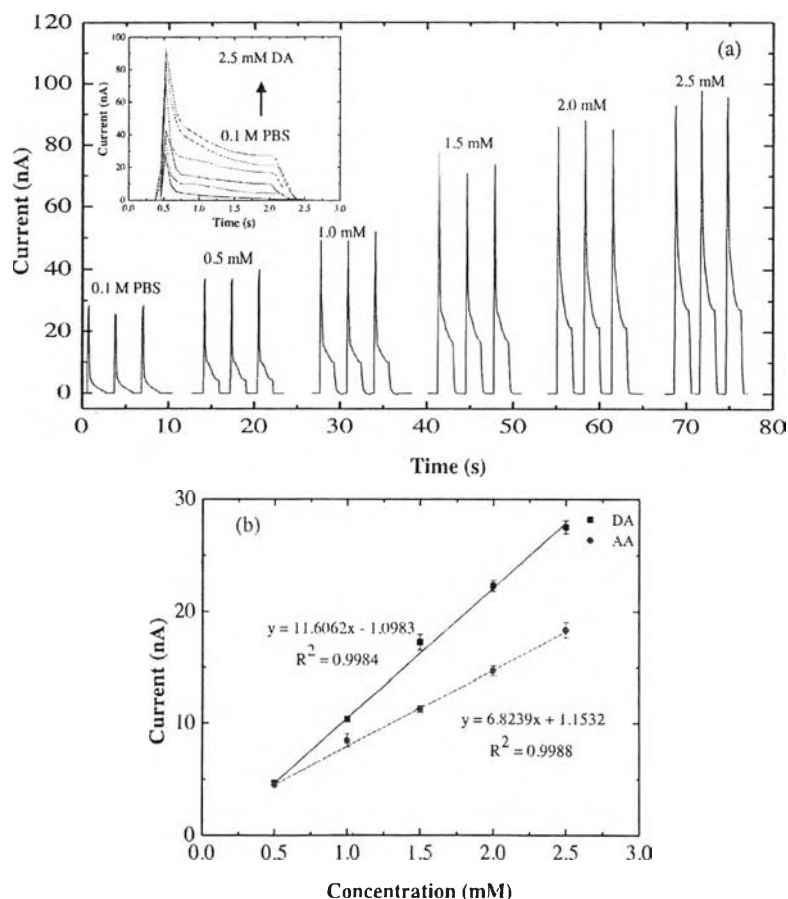


Fig. 7. (a) Examples of typical readout of current signals obtained from droplets containing DA at different concentrations. The background signal was measured from 0.1 M PBS. The inset defines overlay signals measured from an individual droplet containing different DA concentrations. (b) Calibration curves of DA and AA. All experiments were carried out using the conditions shown in Fig. 6.

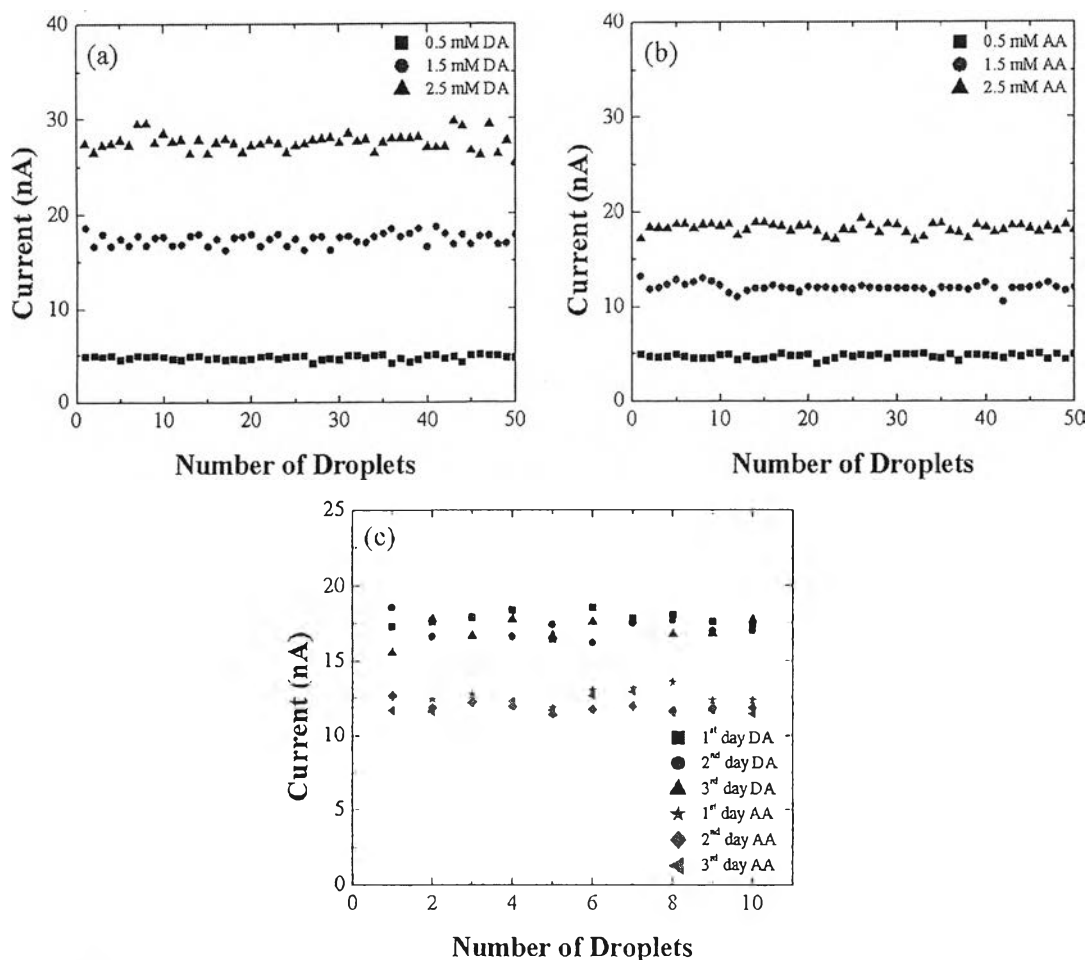


Fig. 8. Intra-day measurements of (a) DA and (b) AA at concentrations of 0.5, 1.5 and 2.5 mM. The currents were measured from 50 droplets ($n=50$). (c) Inter-day measurements of 1.5 mM DA and AA, which were performed for three days ($n=3$). All experiments were carried out using the conditions shown in Fig. 6.

chronoamperometric measurements in this system and at this flow rate a current value of 10.0 ± 0.9 nA was achieved from 1 mM DA.

3.3. Validation of the method

3.3.1. Linearity, limit of detection and limit of quantitation

Before utilizing this system for the quantitative analysis of DA and AA, the performance of the droplet platform coupled with the electrochemical detection system was investigated under the optimized conditions. Droplets were generated using flow rates of $1.80 \mu\text{L min}^{-1}$ for the oil phase and $0.80 \mu\text{L min}^{-1}$ for the aqueous solution, resulting in a total flow rate of $2.60 \mu\text{L min}^{-1}$ (0.86 mm s^{-1}) and a water fraction of 0.31. As seen from Fig. 6, it was found that linearity was in the ranges of 0.02–3.0 mM and 0.04–3.0 mM

with R^2 values of 0.9921 and 0.9970 for DA and AA, respectively. The limit of detection (LOD) and limit of quantitation (LOQ) evaluated using signal-to-noise ratios (S/N) of three ($S/N=3$) and ten ($S/N=10$) were found to be 20 and $70 \mu\text{M}$, respectively for DA and 40 and $137 \mu\text{M}$, respectively for AA.

3.3.2. Calibration curves

Calibration curves for quantitative determination of DA and AA were constructed by plotting measured current as a function of the analyte concentration. Standard DA and AA solutions for the calibration curves were prepared in the range of 0.5–2.5 mM. Fig. 7a presents examples of typical readouts of current signals obtained from droplets containing five different DA concentrations and the background (0.1 M PBS). The inset shows overlay current signals obtained from five single droplets with different DA

Table 1
Comparison of modified CPEs for determination of dopamine.

Modifier	Working area (mm^2)	Linear range (μM)	Detection limit (μM)	System	Ref.
CNT-TNCPE	19.63	0.1–80	0.03	Batch	[40]
CNFs	1.13	0.04–5.6	0.04	Batch	[41]
Pd/CNFs	1.13	0.5–160	0.2	Batch	[42]
SDS	3.10	8–134	3.7	Batch	[43]
MWCNT/Gly	3.14	0.5–40	0.012	Batch	[44]
PBD/MWCNT	9.62	30–800	1.0	Batch	[45]
PDMS/Nujol oil	0.25	20–3000	20	Microfluidics	This work

Abbreviations: CNFs, carbon nanofibers; CNT, carbon nanotube; Gly, glycerol; MWCNT, multi-walled carbon nanotube; PDB, 2,2'-((1E)-(1,2-phenylenebis(azananylylidene))bis(methanylylidene))bis(benzene-1,4-diol); PDMS, poly(dimethylsiloxane); SDS, sodium dodecyl sulphate; TNCPE, thionine-nafion supported carbon paste electrode.

concentrations and the background. Calibration plots of DA and AA are presented in Fig. 7b. The relationship between current and concentration was found to be linear with high correlation coefficients of R^2 , equal to 0.9984 and 0.9988 for DA and AA, respectively.

3.3.3. Precision

Precision of the system was investigated within the same day (intra-day precision) and among 3 days (inter-day precision). The intra-day precision was performed using three concentrations of DA and AA (0.5, 1.5 and 2.5 mM). For each concentration, the chronoamperometric measurements were recorded for 1 min and the measured currents were then averaged from 50 droplets. The inter-day precision was carried out using 1.5 mM DA and AA. The measurements were performed for three days and currents were averaged from 10 droplets. For intra-day and inter-day measurements, relative standard deviation (RSD) was found to be less than 5%. Results obtained from intra-day and inter-day measurements are shown in Fig. 8. Using a one-way ANOVA statistical analysis, results obtained from inter-day measurements of DA and AA among three days (inter-day precision, $n = 3$) were found to be not statistically different (at a 95% confidence level) with p values of 0.146 and 0.323 for DA and AA, respectively. These results indicate high intraday and inter-day precisions of the method.

A result comparison between the proposed method and previous work for the determination of DA is shown in Table 1. The current system has shown a wide linear range of 20–3000 μM when compared to the batch methods. It should be noted that, in this work, the CPEs integrated within a microfluidic channel, namely chip-based CPEs, were microband electrodes possessing a

Table 2

Quantitative determination of DA and AA in real samples of intravenous drugs.

Content	Sample	Labeled amount	Determined amount	% RSD	%Error
DA	Upamine	250 (mg/10 mL)	252.3 \pm 7.1 (mg/10 mL)	2.80	+0.90
	Domine-250	250 (mg/10 mL)	254.2 \pm 7.9 (mg/10 mL)	3.09	+1.69
	Dopamex	200 (mg/10 mL)	197.1 \pm 5.0 (mg/10 mL)	2.52	-1.46
AA	Ascorbic acid	500 (mg/2 mL)	514.0 \pm 23.0 (mg/2 mL)	4.61	+2.86

small working area and the measurements were carried out in a flow-based system. These could lead to a high limit of detection of the system when compared to other methods. However, the outstanding benefit of using a microfluidic system is that small amount of samples is required. In this work, a chronoamperometric measurement was performed within a droplet having a volume of 0.625 nL. This volume was significantly lower than the sample volumes needed for classical electrochemical measurements or batch methods, which normally require sample volumes of at least 0.5 mL. Accordingly, microfluidic analysis would be an excellent alternative when samples are limited or expensive, especially biological/medical samples. In addition, high-throughput analysis is simply applicable with microfluidic systems.

3.4. Application to real samples

The proposed system was applied for the quantitative determination of DA and AA contained in intravenous drugs, which have the main component either DA or AA. The final concentrations of DA and AA in the samples were prepared to be 1.0 and 1.5 mM, respectively. For each sample, measured currents were averaged currents from 10 droplets and their concentrations were calculated using the calibration plots in Fig. 7b. Chronoamperograms obtained from the measurements of real DA and AA samples are presented in Fig. 9. It can be seen that the pattern of exponential decay of the chronoamperometric current and the peak shape obtained from the real samples are similar to those of the standard solutions. These confirm that no electrode fouling was observed when the real samples were measured. Table 2 shows the amounts of DA and AA found in the samples. The determined amounts of DA and AA were insignificantly different from the labels with %RSD below 5% and percentage error less than $\pm 3\%$. In addition, statistical analysis using t -test (at 95% confidence level) showed no significant difference between the determined and labeled amounts, indicating a high accuracy of the proposed system.

4. Conclusions

We have successfully demonstrated the first application of a droplet microfluidic system coupled with chronoamperometric detection using chip-based CPEs for highly reproducible and accurate measurements of dopamine and ascorbic acid in real samples of medical injections. The chip-based CPEs have shown high electrochemical performance and allow for ease of electrode patterning and microfluidic device fabrication at a low cost. Although detection limits of the proposed system for analysis of dopamine and ascorbic acid are not as low as those reported in previous work [39], this system offers an alternative route to determine the amount of DA and AA in real samples containing high DA and AA concentration levels (e.g. medical substances). In addition, measurements using this approach can be performed in a high-throughput manner with small sample consumption, which

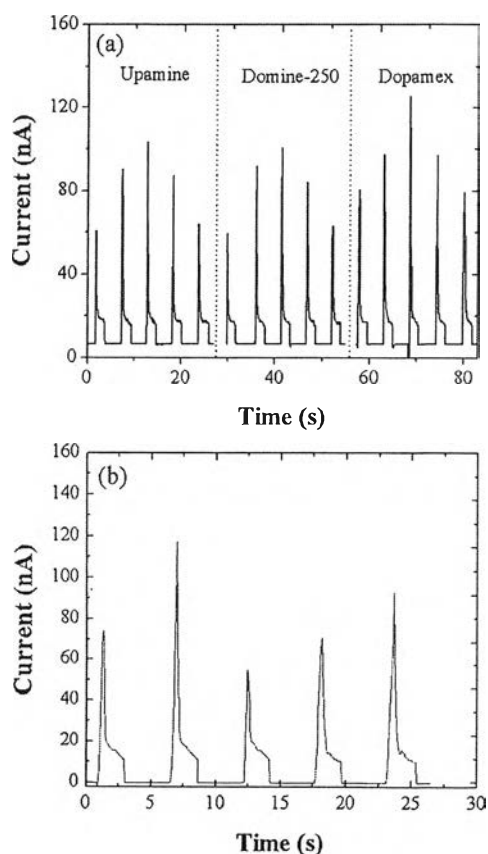


Fig. 9. Examples of chronoamperograms obtained from the measurements of intravenous drugs containing (a) DA (Upamine, Domine and Dopamex) and (b) AA. All experiments were carried out using the conditions shown in Fig. 6.

could be an ideal platform for on-site measurements for medical diagnosis. From this work, the droplet system would pave the way for other applications of a new generation of droplet microfluidic systems integrated with electrochemical detection for applications in medical diagnosis and online monitoring of environmental pollution (e.g. heavy metals). We are currently extending our approach for drug analysis, which would result in the basis of a future publication.

Acknowledgements

This work was supported by National Research University Project, Office of Higher Education Commission (WCU-032-AM-57) and the Thailand Research Fund (RTA5780005). Special thanks to Professor Charles S. Henry at Colorado State University for providing facilities for SU-8 master fabrication. P.R. would like to thank a Postdoctoral Fellowship (Ratchadaphiseksomphot Endowment Fund).

References

- [1] H. Song, J.D. Tice, R.F. Ismagilov, A microfluidic system for controlling reaction networks in time, *Angew. Chem. Int. Ed.* 42 (2003) 768.
- [2] S.Y. Teh, R. Lin, L.H. Hung, A.P. Lee, Droplet microfluidics, *Lab Chip* 8 (2008) 198.
- [3] H. Song, D.L. Chen, R.F. Ismagilov, Reactions in droplets in microfluidic channels, *Angew. Chem. Int. Ed.* 45 (2006) 7336.
- [4] X.C.I. Solvas, A. deMello, High-throughput age synchronisation of *Caenorhabditis elegans*, *Chem. Commun.* 47 (2011) 9801.
- [5] M.T. Guo, A. Rotem, J.A. Heyman, D.A. Weitz, Droplet microfluidics for high-throughput biological assays, *Lab Chip* 12 (2012) 2146.
- [6] I. Shestopalov, J.D. Tice, R.F. Ismagilov, Multi-step synthesis of nanoparticles performed on millisecond time scale in a microfluidic droplet-based system, *Lab Chip* 4 (2004) 316.
- [7] K. Ohno, K. Tachikawa, A. Manz, Microfluidics: applications for analytical purposes in chemistry and biochemistry, *Electrophoresis* 29 (2008) 4443.
- [8] M. Srisa-Art, A.J. deMello, J.B. Edel, High-throughput DNA droplet assays using picoliter reactor volumes, *Anal. Chem.* 79 (2007) 6682.
- [9] J.J. Agresti, E. Antipov, A.R. Abate, K. Ahn, A.C. Rowat, J.-C. Baret, M. Marquez, A.M. Klibanov, A.D. Griffiths, D.A. Weitz, Ultrahigh-throughput screening in drop-based microfluidics for directed evolution, *PNAS* 107 (2010) 4004.
- [10] M.T. Guo, A. Rotem, J.A. Heyman, D.A. Weitz, Droplet microfluidics for high-throughput biological assays, *Lab Chip* 12 (2012) 2146.
- [11] J. Pihl, M. Karlsson, D.T. Chiu, Microfluidic technologies in drug discovery, *Drug Discov. Today* 10 (2005) 1377.
- [12] L.F. Kang, B.G. Chung, R. Langer, A. Khandemhosseini, Microfluidics for drug discovery and development: from target selection to product lifecycle management, *Drug Discov. Today* 13 (2008) 1.
- [13] J. Clauseil-Tormos, D. Lieber, J.C. Baret, A. El-Harrak, O.J. Miller, L. Frenz, J. Blouwolf, K.J. Humphry, S. Koster, H. Duan, C. Holtze, D.A. Weitz, A.D. Griffiths, C.A. Merten, Droplet-based microfluidic platforms for the encapsulation and screening of mammalian cells and multicellular organisms, *Chem. Biol.* 15 (2008) 875.
- [14] J.D. Tice, H. Song, A.D. Lyon, R.F. Ismagilov, Formation of droplets and mixing in multiphase microfluidics at low values of the Reynolds and the capillary numbers, *Langmuir* 19 (2003) 9127.
- [15] M. Srisa-Art, A.J. deMello, J.B. Edel, High-efficiency single-molecule detection within trapped aqueous microdroplets, *J. Phys. Chem. B* 114 (2010) 15766.
- [16] T. Hatakeyama, D.L.L. Chen, R.F. Ismagilov, Microgram-scale testing of reaction conditions in solution using nanoliter plugs in microfluidics with detection by MALDI-MS, *J. Am. Chem. Soc.* 128 (2006) 2518.
- [17] L.M. Fidalgo, G. Whyte, B.T. Ruotolo, J.L.P. Benesch, F. Stengel, C. Abell, C.V. Robinson, W.T.S. Huck, Coupling microdroplet microreactors with mass spectrometry: reading the contents of single droplets online, *Angew. Chem. Int. Ed.* 48 (2009) 3665.
- [18] R. Silva, E. Almeida, A. Rabelo, A. Silva, L. Ferreira, E. Richter, Three electrode electrochemical microfluidic cell: construction and characterization, *J. Braz. Chem. Soc.* 20 (2009) 1235.
- [19] C. Lou, X. Yang, Q. Fu, M. Sun, Q. Ouyang, Y. Chen, H. Ji, Picoliter-volume aqueous droplets in oil: electrochemical detection and yeast cell electroporation, *Electrophoresis* 27 (2006) 1977.
- [20] S. Liu, Y. Gu, R.B.L. Roux, S.M. Matthews, D. Bratton, K. Yunus, A.C. Fisher, W.T.S. Huck, The electrochemical detection of droplets in microfluidic devices, *Lab Chip* 8 (2008) 1937.
- [21] Z. Han, W. Li, Y. Huang, B. Zheng, Measuring rapid enzymatic kinetics by electrochemical method in droplet-based microfluidic devices with pneumatic valves, *Anal. Chem.* 81 (2009) 5840.
- [22] H. Liu, R.M. Crooks, Highly reproducible chronoamperometric analysis in microdroplets, *Lab Chip* 13 (2013) 1364.
- [23] K.R. Strehle, D. Gialla, P. Posch, T. Henkel, M. Kohler, J. Popp, A reproducible surface-enhanced Raman spectroscopy approach. Online SERS measurements in a segmented microfluidic system, *Anal. Chem.* 79 (2007) 1542.
- [24] G. Cristobal, I. Arbouet, F. Sarrazin, D. Talaga, J.L. Bruneel, M. Joanicot, L. Servant, On-line laser Raman spectroscopic probing of droplets engineered in microfluidic devices, *Lab Chip* 6 (2006) 1140.
- [25] S.E. Barnes, Z.T. Cygan, J.K. Yates, K.L. Beers, E.J. Amis, Raman spectroscopic monitoring of droplet polymerization in a microfluidic device, *Analyst* 131 (2006) 1027.
- [26] S. Liu, Y. Gu, R.B. Le Roux, S.M. Matthews, D. Bratton, K. Yunus, A.C. Fisher, W.T.S. Huck, The electrochemical detection of droplets in microfluidic devices, *Lab Chip* 8 (2008) 1937.
- [27] Z. Han, W. Li, Y. Huang, B. Zheng, Measuring rapid enzymatic kinetics by electrochemical method in droplet-based microfluidic devices with pneumatic valves, *Anal. Chem.* 81 (2009) 5840.
- [28] L.A. Filla, D.C. Kirkpatrick, R.S. Martin, Use of a corona discharge to selectively pattern a hydrophilic/hydrophobic interface for integrating segmented flow with microchip electrophoresis and electrochemical detection, *Anal. Chem.* 83 (2011) 5996.
- [29] Z. Han, Y.Y. Chang, S.W. Ngor, B. Zheng, Measuring rapid kinetics by a potentiometric method in droplet-based microfluidic devices, *Chem. Commun.* 48 (2012) 1601.
- [30] F. Sassa, H. Laghzaoui, J. Fukuda, H. Suzuki, Coulometric detection of components in liquid plugs by microfabricated flow channel and electrode structures, *Anal. Chem.* 82 (2010) 8725.
- [31] Y. Sameenoi, M.M. Mensack, K. Boonsong, R. Ewing, W. Dungchai, O. Chailapakul, D.M. Crokek, C.S. Henry, Poly(dimethylsiloxane) cross-linked carbon paste electrodes for microfluidic electrochemical sensing, *Analyst* 136 (2011) 3177.
- [32] C.F. Gonzalez, D.M. Crokek, C.S. Henry, Photopatternable carbon electrodes for chip-based electrochemical detection, *Electroanalysis* 21 (2009) 2171.
- [33] J.C. McDonald, G.M. Whitesides, Poly(dimethylsiloxane) as a material for fabricating microfluidic devices, *Acc. Chem. Res.* 35 (2002) 491.
- [34] N. Rodthongkum, N. Ruecha, R. Rangakupun, R.W. Vacher, O. Chailapakul, Graphene-loaded nanofiber-modified electrodes for the ultrasensitive determination of dopamine, *Anal. Chim. Acta* 804 (2013) 84.
- [35] A. Salimi, H. Mamkhezri, R. Hallaj, Simultaneous determination of ascorbic acid, uric acid and neurotransmitters with a carbon ceramic electrode prepared by sol-gel technique, *Talanta* 70 (2006) 823.
- [36] N.F. Atta, A. Galal, R.A. Ahmed, Poly(3,4-ethylene-dioxythiophene) electrode for the selective determination of dopamine in presence of sodium dodecyl sulfate, *Bioelectrochemistry* 80 (2011) 132.
- [37] Y. Wang, Q. Liu, Q. Qi, J. Ding, X. Gao, Y. Zhang, Y. Sun, Electrocatalytic oxidation and detection of *N*-acetylcysteine based on magnetite/reduced graphene oxide composite-modified glassy carbon electrode, *Electrochim. Acta* 111 (2013) 31.
- [38] D. Mackoul, D.C. Johnson, Effect of variation in flow rate on amperometric detection in flow injection analysis, *Anal. Chem.* 56 (1984) 436.
- [39] M.J. Song, S.K. Lee, J.H. Kim, D.S. Lim, Dopamine sensor based on a boron-doped diamond electrode modified with a polyaniline/Au nanocomposites in the presence of ascorbic acid, *Anal. Sci.* 28 (2012) 583.
- [40] S. Shahrokhanian, H.R.Z. Mehrjardi, Application of thionine-nation supported on multi-walled carbon nanotube for preparation of a modified electrode in simultaneous voltammetric detection of dopamine and ascorbic acid, *Electrochim. Acta* 52 (2007) 6310.
- [41] Y. Liu, J.S. Huang, H.Q. Hou, T.Y. You, Simultaneous determination of dopamine, ascorbic acid and uric acid with electrospun carbon nanofibers modified electrode, *Electrochem. Commun.* 10 (2008) 1431.
- [42] J.S. Huang, Y. Liu, H.Q. Hou, T.Y. You, Simultaneous electrochemical determination of dopamine, uric acid and ascorbic acid using palladium nanoparticle-loaded carbon nanofibers modified electrode, *Biosens. Bioelectron.* 24 (2008) 632.
- [43] E. Colín-Orozco, M.T. Ramírez-Silva, S. Corona-Avenidaño, M. Romero-Romo, M. Palomar-Pardavé, Electrochemical quantification of dopamine in the presence of ascorbic acid and uric acid using a simple carbon paste electrode modified with SDS micelles at pH 7, *Electrochim. Acta* 85 (2012) 307.
- [44] T. Thomas, R.J. Mascarenhas, B.E.K. Swamy, P. Martis, Z. Mekhalif, B.S. Sherigara, Multi-walled carbon nanotube/poly(glycine) modified carbon paste electrode for the determination of dopamine in biological fluids and pharmaceuticals, *Colloids Surf. B: Biointerfaces* 110 (2013) 458.
- [45] M. Mazloum-Ardakani, M. Abolhasani, B.-F. Mirjalili, M.A. Sheikh-Mohseni, A. Dehghani-Firouzabadi, A. Khoshroo, Electrocatalysis of dopamine in the presence of uric acid and folic acid on modified carbon nanotube paste electrode, *Chin. J. Catal.* 35 (2014) 201.



Droplet-based glucosamine sensor using gold nanoparticles and polyaniline-modified electrode

Akkapol Suea-Ngam^{a,b}, Poomrat Rattanarat^b, Kanet Wongravee^c, Orawon Chailapakul^{b,d},
Monpichar Srisa-Art^{a,b,*}

^a Chromatography and Separation Research Unit (ChSRU), Department of Chemistry, Faculty of Science, Chulalongkorn University, Bangkok 10330, Thailand

^b Electrochemistry and Optical Spectroscopy Research Unit (EOSRU), Department of Chemistry, Faculty of Science, Chulalongkorn University, Bangkok 10330, Thailand

^c Nanotec-CU Center of Excellence on Food and Agriculture, Faculty of Science, Department of Chemistry, Chulalongkorn University, Bangkok, 10330, Thailand

^d National Center of Excellence on Petrochemical and Materials Technology, Chulalongkorn University, Bangkok 10330, Thailand

ARTICLE INFO

Article history:

Received 14 February 2016

Received in revised form

16 May 2016

Accepted 16 May 2016

Available online 16 May 2016

Keywords:

Droplet-based microfluidics

Glucosamine

Carbon paste electrode

Central composition design,

chronoamperometry

ABSTRACT

A droplet-based electrochemical sensor for direct measurement of D-glucosamine was developed using carbon paste electrodes (CPEs) modified with gold nanoparticles (AuNPs) and polyaniline (PANI). Central composition design (CCD) was employed as a powerful method for optimization of parameters for electrode fabrication. The optimized amounts of AuNPs and PANI obtained from the response surface were determined as 300 and 3000 mg L⁻¹, respectively. Coupled with a droplet microfluidic system, the analysis of glucosamine was performed in a high-throughput manner with a sample throughput of at least 60 samples h⁻¹. In addition, the adsorption of the analyte on the electrode surface was prevented due to compartmentalization in droplets. Linearity of the proposed system was found to be in the range of 0.5–5 mM with a sensitivity of 7.42 × 10⁻³ A mol⁻¹ L cm⁻² and limits of detection and quantitation of 0.45 and 1.45 mM, respectively. High intraday and interday (evaluated among 3 days) precisions for the detection of 50 droplets containing glucosamine were obtained with relative standard deviation less than 3%. The system was successfully used to determine the amounts of glucosamine in supplementary products with error percentage and relative standard deviation less than 3%. In addition, the amounts of glucosamine measured using the developed sensor were in good agreement with those obtained from a CE method. These indicate high accuracy and precision of the proposed system.

© 2016 Elsevier B.V. All rights reserved.

1. Introduction

Osteoarthritis (OA) or a degenerative joint disease is a group of mechanical abnormalities of joints, which especially occurs in the elderly and overweight people as well as athletes [1]. D-Glucosamine (GlcN), an amino monosaccharide found in connective tissues and gastrointestinal mucosal membranes [2], is widely used to alleviate the symptoms of OA because it has been believed that GlcN prevents the deterioration of the cartilage and surrounding fluid in the joints [3]. Therefore, GlcN is manufactured as supplementary products and marketed to people suffering from OA [4]. Nowadays, the use of GlcN supplements for treatment of OA is growing rapidly, leading to a variety of commercial brands of GlcN supplements distributed into the markets. Therefore, a simple and rapid method for quantitative analysis of GlcN is required to

control the quality of GlcN products during manufacturing processes and the products distributed into the markets.

Previously, the analysis of GlcN was achieved using several methods, including fluorescent sensors [5], capillary electrophoresis with fluorescence detection [6] and high-performance liquid chromatography with a variety of detection systems, such as electrochemical detection [7,8], mass spectrometry [9–11], refractive index [11,12], fluorescence [2,6,13] and UV detection [3]. Since GlcN is a monosaccharide derivative of glucose, quantitative determination using fluorescence detection was required a derivatization step using a fluorescent dye. Therefore, electrochemical detection was favorably performed by taking advantages of sugar compounds exhibiting electrochemical properties. Accordingly, the analysis of GlcN using electrochemical detection was easily achieved with its native structure. Therefore, we present herein a facile and reliable method using an electrochemical sensor as an alternative for quantitative determination of GlcN supplements. Since less matrix effect is generally found in supplementary products when compared to biological fluids, an electrochemical sensor was developed for a direct measurement of GlcN without a separation step. In addition, a GlcN sensor was coupled

*Corresponding author at: Chromatography and Separation Research Unit (ChSRU), Department of Chemistry, Faculty of Science, Chulalongkorn University, Bangkok 10330, Thailand.

E-mail address: monpichar.s@chula.ac.th (M. Srisa-Art).

with a droplet microfluidic system in order to perform the analysis in a high-throughput manner with small sample consumption. Moreover, compartmentalization in droplets prevented the adsorption of analytes on the electrode surface. Accordingly, no washing and drying steps between consecutive runs were required, resulting in minimization of analysis time compared with batch-wise electrochemical sensing methods. Therefore, advantages of a droplet system, including rapid mixing, no sample dispersion and adsorption, low sample consumption, portability and high throughput analysis, enhance the analytical performance of the chip-based GlcN sensor.

In this work, carbon paste electrodes (CPEs) were selected to fabricate a chip-based GlcN sensor. CPEs are easily to fabricate into a chip-based format and possess a wide working potential and withstand electrode fouling [14]. Gold nanoparticles (AuNPs) were used to modify chip-based CPEs because it was previously reported that gold electrodes were able to catalyze the oxidation of carbohydrates [7] and AuNPs modified carbon electrodes were used to monitor GlcN during the synthesis of glucosaminic acid [15]. The advantages of AuNPs are that they are inexpensive and possess more surface area when compared to gold-pad electrodes. In addition, polyaniline (PANI), a well-known conducting polymer, was also employed for electrode modification to enhance electrochemical signal due to its excellent electrochemical properties, good environmental stability and non-toxicity [16]. Central composition design (CCD) was used in this work to optimize pH of the working medium and the amounts of PANI and AuNPs for electrode modification. The box-like design of experiments was carried out and a responsive surface was then plotted to formulate an equation to find the optimized conditions of each parameter (pH, the amounts of PANI and AuNPs) [17,18]. Under the optimized conditions, the analytical performance of the developed system for determination of GlcN was evaluated. Finally, the proposed system was employed for quantitative analysis of GlcN in supplementary products. This approach offers a fast, low cost, simple and reliable platform for determination of glucosamine products. In addition, the proposed system could be an ideal route for screening product quality in both markets and manufacturing processes by further developing the whole system to be fully automated. This could make manufacturing quality control far more efficient.

2. Experimental

2.1. Materials and instrumentation

All chemicals are analytical grade. Gold nanoparticles were synthesized from HAuCl_4 (Sigma-Aldrich, Singapore) and 1% sodium citrate (Sigma-Aldrich, Singapore) using a conventional chemical reduction method [19]. Polyaniline was grounded with (+)-camphor-10-sulfonic acid and dissolved in 2-methyl-N-pyrrolidone (NMP) (Sigma-Aldrich, Singapore). Materials and chemicals were used as received: D-(+)-glucosamine hydrochloride (Fluka Chemica CH-9471, Switzerland), sodium chloride (NaCl: Merck, Thailand), disodium hydrogen phosphate (Na_2HPO_4 : Merck, Thailand), potassium dihydrogen phosphate (KH_2PO_4 : Carlo ERBA, Thailand), potassium chloride (KCl: Ajax Finechem, Thailand), nujol mineral oil (Perkin Elmer, Thailand), silver paint (SPI supplies, USA), graphite powder ($\leq 20 \mu\text{m}$, Sigma-Aldrich, Singapore), ethanol (Merck, Thailand) and Sylgard 184 elastomeric kit (Dow Corning, USA). Electrochemical measurements were conducted using a commercially available potentiostat (eDAQ, ED410, 410–088, Australia). For microfluidic experiments, all solutions were contained in 1 mL plastic syringes (Nipro, Thailand) connected to the inlets of a microfluidic device using polyethylene tubing (0.38 mm I. D., 1.09 mm O.D., PORTEX, Belgium). The solutions were driven through the device using syringe pumps (PHD 2000, Harvard Apparatus, USA).

2.2. Preparation of solutions

All aqueous solutions were prepared using Milli-Q water (18.0 M Ω cm, Milli-Q Gradient System, Millipore, Thailand). Phosphate buffer saline (PBS) pH 7.4 at a concentration of 0.1 M was prepared by dissolving 2.0 g NaCl, 0.05 g KCl, 0.36 g Na_2HPO_4 and 0.06 g KH_2PO_4 using Milli-Q water in a 250 mL volumetric flask. To adjust pH of the PBS buffer, 0.1 M phosphoric acid and 0.1 M NaOH were used to obtain a desired pH. A stock solution of D-glucosamine at a concentration of 100 mM was prepared by dissolving 21.56 mg of D-glucosamine in 1.0 mL of 0.1 M PBS in a safe-lock tube (Eppendorf, Thailand). A mixture of AuNPs and PANI was prepared by dissolving AuNPs and PANI in NMP in a safe-lock tube. The mixture was vortexed before use. For droplet-based microfluidic experiments, an oil solution for droplet generation was a 10:2 (v/v) mixture of perfluorodecalin (mixture of *cis* and *trans*, 95%, Sigma-Aldrich, Germany) and 1*H*, 1*H*, 2*H*, 2*H*-perfluoro-1-octanol (97%, Sigma-Aldrich, Germany). D-Glucosamine supplementary products were purchased from a local drugstore (Thailand). All samples were prepared in 0.1 M PBS to have a final concentration of 3.0 mM.

2.3. Design and fabrication of microfluidic devices

There were two designs of PDMS microfluidic devices; one was a device consisting of a circular reservoir with a diameter of 0.8 cm (a well-like device) for measurements using cyclic voltammetry and the other was a device with microchannels for electrochemical measurements in droplets. The design of microchannels followed the microfluidic layout presented in previous work [14]. PDMS devices were fabricated using traditional soft lithography [20]. Each device was composed of two PDMS layers. The top layer was a microchannel- or reservoir-patterned plate and the bottom layer was an electrode-patterned plate. The microchannels consisted of a major channel (500 μm wide) and a confined channel (50 μm wide) and all channel depth was 100 μm . The electrode-patterned PDMS plate consisted of three microchannels with 500 μm width and 100 μm depth for fabrication of three microelectrode bands.

Chip-based CPEs were fabricated by means of screen printing [14]. Graphite powder, nujol oil and PDMS were mixed and then filled into the microchannels of the electrode-patterned PDMS plate. A rubber scraper was used to spread the carbon paste onto the electrode area to smooth out the surface of the electrodes. The excessive paste was cleaned up using Scotch Magic Tape™. Subsequently, for electrode modification, 1 μL of the mixed solution of AuNPs and PANI microfibers was applied onto the middle electrode using the drop-casting technique and the electrodes were then left in a 65 °C oven for 1 h.

To make a well-like device with a circular reservoir, a square piece of PDMS was punched using a 0.8 cm diameter puncher. For device assembly using plasma treatment, only the punched PDMS or microchannel PDMS was exposed to plasma, not the electrode-patterned PDMS. This was because the nujol oil component from the electrodes could be decomposed upon plasma treatment [21], resulting in low efficiency of the CPEs. Electric wires were then attached at the end of each electrode using silver paint. In order to reduce the noise, epoxy glue was applied over the silver paint area and left to be cured for 1 h. Thereafter, the devices were ready to use. The complete devices are shown in Fig. 1(a) and (b).

2.4. Central composition design (CCD) for electrode modification

The amounts of AuNPs and PANI used for electrode modification were optimized to achieve maximum current signal. Stock solutions of 1000 mg L⁻¹ AuNPs and 10,000 mg L⁻¹ PANI were prepared in NMP and the desired amounts were used for electrode modification. Effect of pH of the working buffer was studied because both AuNPs and PANI are pH dependent. CCD was used for optimization

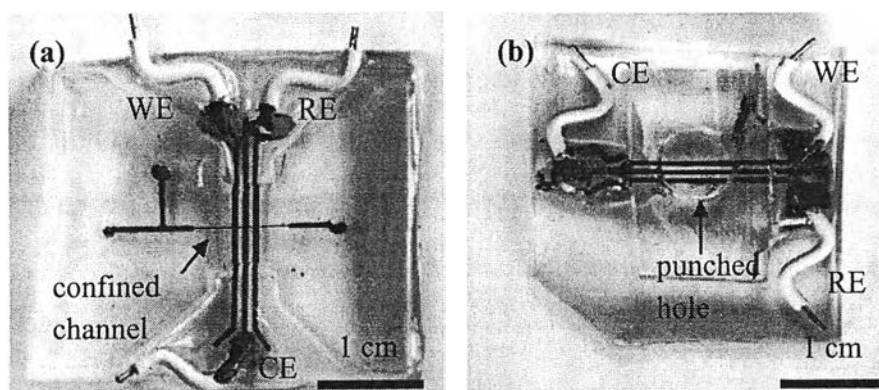


Fig. 1. (a) A microfluidic device consisting of two PDMS layers. The top PDMS plate contains a main channel (500 μm wide and 100 μm deep) and a confined channel (50 μm wide, 100 μm deep and 1 cm long) as a detection window. The bottom PDMS plate has three parallel channels (500 μm wide and 100 μm deep) screen printed with carbon paste to be used as working, counter and reference electrodes (WE, CE and RE, respectively). The working electrode was modified with PANI and AuNPs. The distance between each electrode is 500 μm . (b) A well-like device with a 0.8 mm punched hole to serve as a reservoir.

of these parameters (the amounts of AuNPs and PANI and pH). Actual and coded values for the factors investigated in the study are given in Table S1 (ESI); a total of 20 experiments were performed. A regression model with the parameters with individual, interaction and quadratic terms were constructed using code values in order to avoid data bias [4,22]. The predicted responses (current in this case) were calculated using the obtained regression model to extrapolate the optimized conditions from the surface responses.

2.5. Electrode characterization

After electrode modification using each condition shown in Table S1 (ESI), the modified CPEs were electrochemically characterized using cyclic voltammetry (CV) to find the optimized condition which was considered from the maximum current obtained from cyclic voltammograms. CV measurements were performed in a well-like device using 40 or 100 mM GlcN in 0.1 M PBS and background current was obtained from 0.1 M PBS. Scan rates were used in the range of 50–500 mV s^{-1} with a potential window from -1.00 to 1.30 V. Moreover, the morphology of mixed modifiers (AuNPs and PANI) was observed using scanning electron microscope (SEM, Japan Electron Optics Laboratory Co., Ltd., Japan).

2.6. Electrochemical detection in droplets

To generate droplets in a microfluidic device, a mixture of perfluorodecalin and perfluorooctanol at a volume ratio of 10:2 v/v was used as an oil phase and an aqueous phase was either GlcN or 0.1 M PBS. Applied potentials in the range of 50–500 mV were studied to achieve a maximum ratio of the current signal to background. The current signals were measured from droplets containing 5 mM GlcN, while 0.1 M PBS pH 4 was used to produce droplets for the background current. Chronoamperometric measurements of the droplet content were performed while droplets were passing through the confined channel in which the modified microband CPEs were located. Current data was monitored for 1 min and averaged currents from ten droplets were used to construct a hydrodynamic voltammogram, a plot of the ratio of current signal to background (S/B) as a function of applied potential. An applied potential providing the highest S/B ratio was selected for further chronoamperometric measurements in droplets.

To optimize droplet size and velocity for electrochemical measurements, water fraction (W_f), the ratio between the flow rate of aqueous phase and the total flow rate ($W_f = F_{aq}/(F_{aq} + F_{oil})$), in which F_{aq} and F_{oil} are the flow rates of aqueous and oil phases, respectively [14]. Both water fraction and total flow rate were concomitantly

studied using W_f equal to 0.3, 0.4 and 0.5 and total flow rate in the range of 1.0–3.0 $\mu\text{L min}^{-1}$. For example, to study the velocity of droplet on the chronoamperometric measurement, W_f was fixed at 0.3 and the total flow rate was varied from 1.0 to 3.0 $\mu\text{L min}^{-1}$. After that the experiments were repeated using the same flow rates but changing W_f to 0.4 and 0.5, respectively.

3. Results and discussion

3.1. CCD experiments for electrode modification

A regression model including linear, interactive and quadratic parameters correlating to the current efficiency was calculated using the multiple linear regression (MLR). From the regression function, it was found that all experimental parameters (pH and the amounts of AuNPs and PANI) affected the current signal and they were strongly correlated. Thus, in the case, a "one factor at a time" approach was not satisfied to determine the optimized conditions. Therefore, it was necessary to generate the response surface to discover the condition which gave the highest current. First, we attempted to visualize all interactions in one surface plot by setting the x- and y-axis to be the amounts of AuNPs (X_2) and PANI (X_3), respectively, together with the surface layers corresponding to the different pH values. Each response surface layers were superimposed in order to include all interactions. Fig. 2a shows the estimation of current at different pH values. It suggests that pH has a strong effect on the current. When increasing pH values, current signal tends to be decreased. This is in good agreement with the coefficient in the regression functions where a negative sign for pH (X_1) was observed. Lower current signal obtained when increasing pH could be due to the conducting PANI converted to a non-conducting form in neutral or alkaline pH [23]. To better visualize the optimized conditions, current contour plots at pH ~ 5 were constructed by simultaneously varying the two factors (the amounts of AuNP and PANI), as shown in Fig. 2b. It was observed from the surface plots that the highest current should be obtained when using the amounts of AuNPs and PANI in the ranges of 100–300 mg L^{-1} and 1000–3000 mg L^{-1} , respectively (as shown in the filled area in Fig. 2b). Results obtained from CV experiments confirmed that 300 mg L^{-1} AuNPs and 3000 mg L^{-1} PANI showed the highest current (Table S1, ESI). It was found that low current signal was obtained when using higher amounts of PANI ($> 3000 \text{ mg L}^{-1}$) and AuNPs ($> 300 \text{ mg L}^{-1}$). This could be because thick PANI film accounts for high background current due to high charging current, while AuNPs at high concentrations could aggregate, resulting in less surface area.

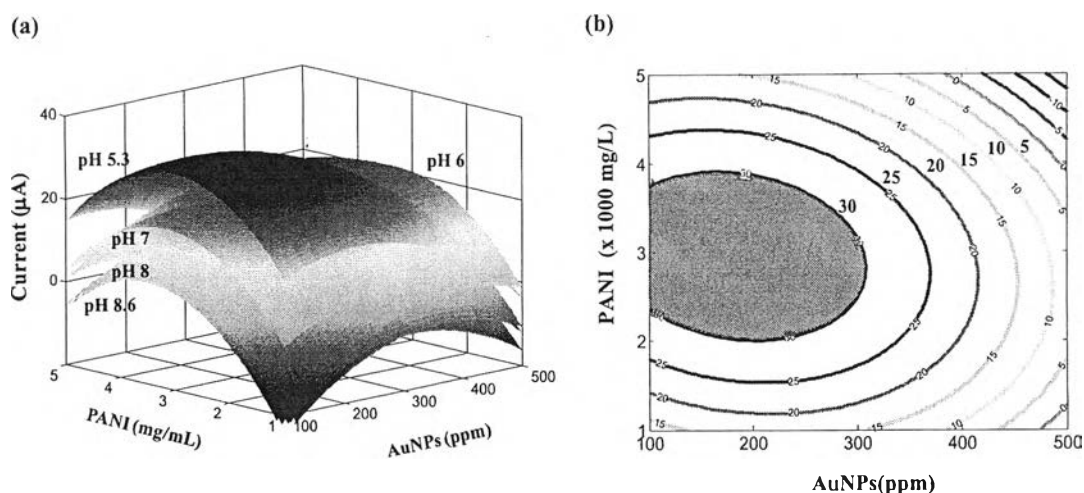


Fig. 2. Responsive surfaces of central composition calculated using the regression model: $y_{\text{current}} = 13.58 - 1.76X_1 + 1.12X_2 - 1.42X_3 + 4.91X_1^2 - 4.56X_2^2 - 2.69X_3^2 + 1.64X_1X_2 + 2.89X_1X_3 - 1.08X_2X_3$ where, X_1 , X_2 and X_3 are linear terms corresponding to pH, the amounts of AuNPs and PANI, respectively. X_1^2 , X_2^2 , X_3^2 and X_1X_2 , X_1X_3 , X_2X_3 are quadratic terms and interaction terms of the parameters. (a) Estimation of response surface of the current by plotting the amounts of AuNPs and PANI with superimposition of surface layers which represent different pH values. (b) Response surface contours of the current by plotting the amounts of AuNPs and PANI at pH \sim 5. The range of the optimized conditions to obtain the highest current is chosen from the overlapped area labeled in brown. (For interpretation of the references to color in this figure legend, the reader is referred to the web version of this article.)

From the surface plots (Fig. 2a), it was also noticed that when the pH was increased to pH 8, current signal was slightly increased. This could be due to AuNPs, which is known that gold is a good electrocatalyst for electrochemical processes in alkaline media [15], playing a dominant role in the reaction. Accordingly, pH values outside of the CCD range (pH 5.3–8.7) were studied with the optimized amounts of AuNPs (300 mg L^{-1}) and PANI (3000 mg L^{-1}) for electrode modification. CV measurements of 100 mM GlcN were carried out using the modified electrodes. It was found that two maximum current values of $70 \text{ } \mu\text{A}$ and $35 \text{ } \mu\text{A}$ were obtained when using the working electrolytes (0.1 M PBS) at pH 4 and pH 12, respectively. A quasi-reversible cyclic voltammogram was obtained when using pH 4, while an irreversible cyclic voltammogram was observed at pH 12 (Fig. 3). The quasi-reversible process would occur due to the effect of PANI which provided better electron transfer at low pH [23]. Therefore, pH 4 was selected for further experiments.

3.2. Electrode characterization

To study the mass transfer behavior of GlcN using the AuNPs and PANI modified CPE (AuNPs-PANI/CPE) with the optimized amounts of 300 mg L^{-1} AuNPs and 3000 mg L^{-1} PANI, CV measurements of both 40 and 100 mM GlcN were performed using a potential window from -1.00 to $+1.30 \text{ V}$ with scan rates ranging from 50 to 500 mV s^{-1} and cyclic voltammograms are shown in Fig. 4a and c. Peak currents obtained from the cyclic voltammograms were plotted as a function of scan rate and square root of scan rate to determine whether the reaction is an adsorption- or diffusion-controlled process. Generally, a diffusion controlled-process is described using the Randles-Sevcik equation ($i_p = 2.69 \times 10^5 F A C n^{3/2} D^{1/2} \nu^{1/2}$), where i_p is peak current (A), A is the electrode surface area (cm^2), n is the number of transferred electrons, C is the concentration of analyte (mol cm^{-3}), D is the diffusion coefficient of electroactive species ($\text{cm}^2 \text{ s}^{-1}$), F is Faraday's constant ($96,485 \text{ C mol}^{-1}$) and ν is scan rate (mV s^{-1}) [14]. According to the Randles-Sevcik equation, if a plot between peak current and square root of scan rate is linear, the reaction is characterized as a diffusion-controlled process. As seen from Fig. 4b, when using 40 mM GlcN, plots of peak current as a function of square root of scan rate exhibited linear relationships. However, linear plots of peak current as a function of scan rate were obtained when using 100 mM GlcN

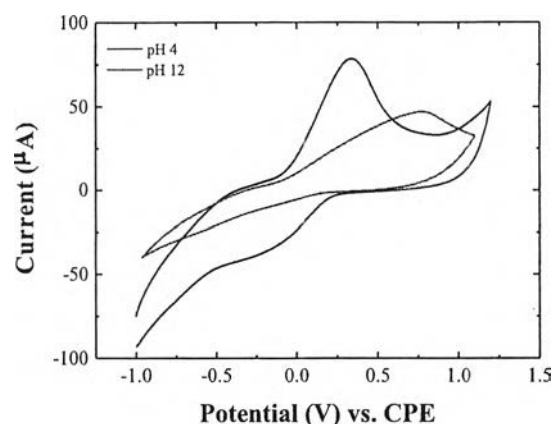


Fig. 3. Cyclic voltammograms (CVs) of 100 mM GlcN in 0.1 M PBS buffer. A quasi-reversible CV was obtained at pH 4, while an irreversible CV was observed at pH 12. The measurements were carried out using a scan rate of 100 mV s^{-1} with a potential window from -1.00 to 1.30 V vs. CPE.

(Fig. 4d). These implied that at low concentrations of GlcN, the reaction was controlled by diffusion, whereas an adsorption-controlled process played an important role at high concentrations of GlcN. In addition, a small change in peak shift was observed for the diffusion-controlled process, which could be due to adsorption of GlcN and glucosaminic acid (a product) at the electrode surface.

Moreover, the morphology of the mixed modifiers (AuNPs and PANI) was characterized using SEM. SEM images in Fig. 5 illustrate that AuNPs self-assembled on the surface of PANI microfibers. Previously, it was reported that PANI microfibers were used as a reducer for the synthesis of AuNPs from chloroauric acid (HAuCl_4) without a stabilizer [24]. The nitrogens along the polymer chains act as physical supporters for AuNPs. Therefore, AuNPs can be simply synthesized on the surface of PANI microfibers using only physical mixing or an applied potential. A proposed model of AuNPs grown on a PANI modified CPE is shown in Fig. S1a (ESI). With the presence of GlcN, the amino group of GlcN interacted with AuNPs, resulting in a sandwich-like configuration (Fig. S1b, ESI). This configuration would enhance the electrochemical signal because of high electron density on the AuNPs surface from the amino group of GlcN.

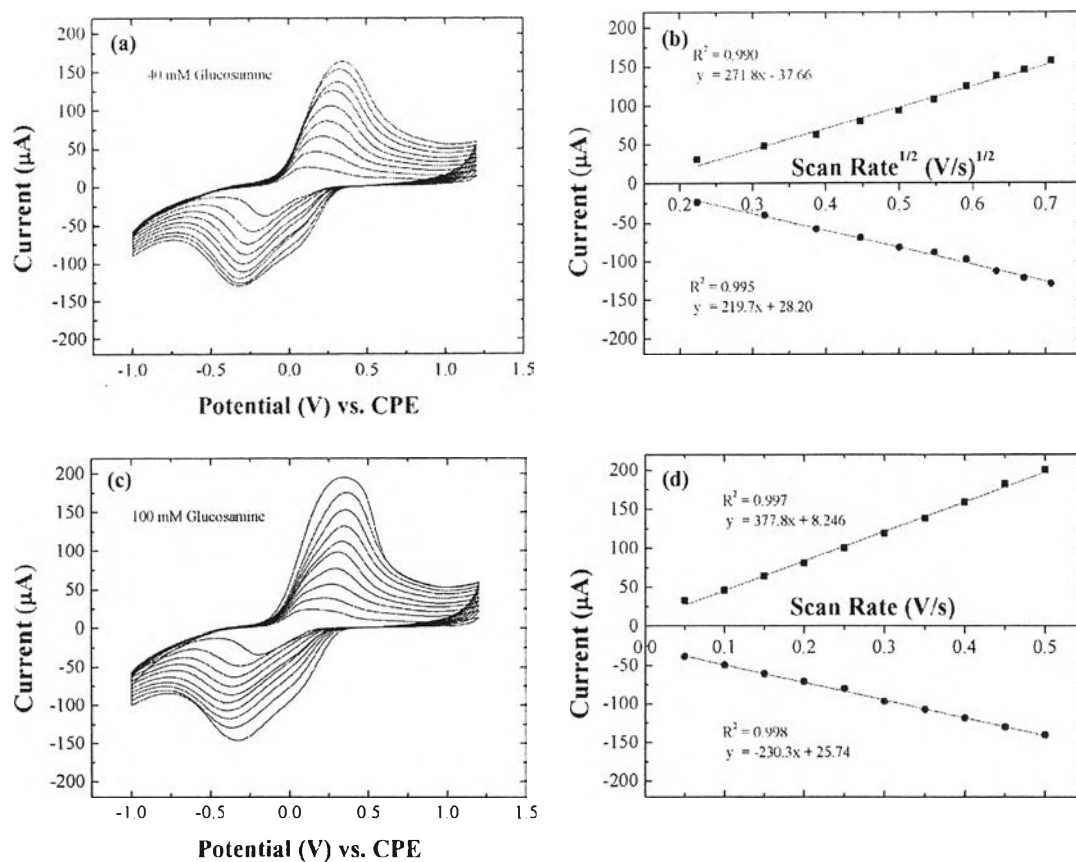


Fig. 4. Cyclic voltammograms (CVs) of (a) 40 mM and (c) 100 mM GlcV in 0.1 M PBS pH 4 at scan rates in the range of 50–500 mV s^{-1} . Plots of the anodic (top) and cathodic (bottom) peak currents obtained from the CVs as a function of square root of scan rate (b) and as a function of scan rate (d).

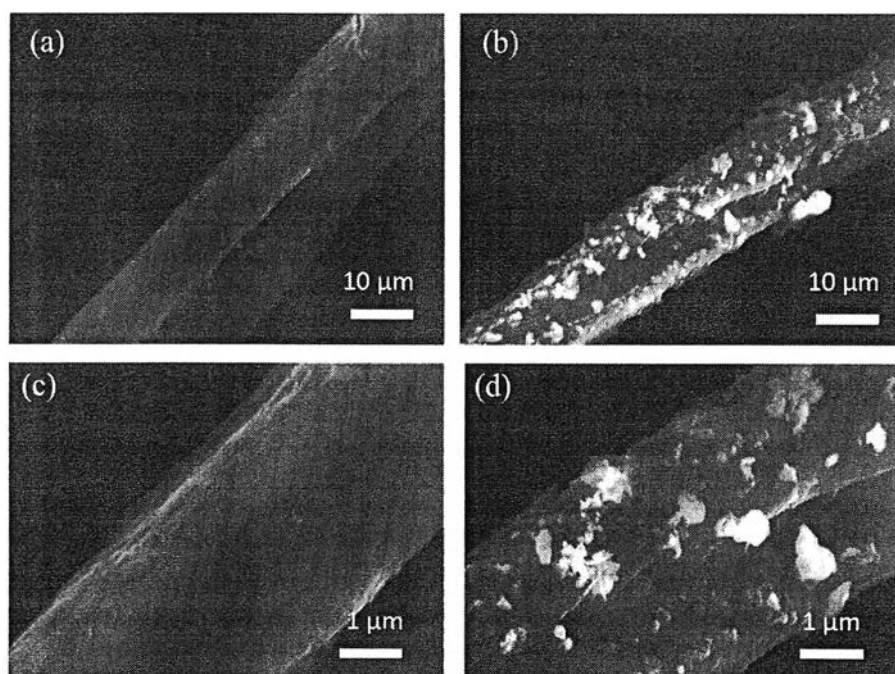


Fig. 5. SEM images of PANI microfibers (a and c) and PANI microfibers with AuNPs (b and d).

3.3. Chronoamperometric measurements in droplets

3.3.1. Optimization of an applied potential

Droplet-based microfluidics was employed in this work not

only for high-throughput experiments, but also for preventing adsorption of analytes on electrodes [25]. Chronoamperometric measurements were performed at the detection window, in which droplets were elongated to cover the modified CPEs. When

droplets passing through the modified CPEs, electrochemical signal exhibited the highest current at the beginning of the droplet signal and then decreased exponentially to the steady-state, which followed the Cottrell equation [26]. Generally, chronoamperometric current signal is measured at the steady-state. However, for high accuracy and reproducibility, chronoamperometric currents were measured at the end of droplet peaks where the current reached a semi-steady-state value [27]. Chronoamperometric readout of droplets containing a concentration series of GlcN was presented in Fig. 6a. Each peak corresponds to chronoamperometric signal from an individual droplet.

To optimize an applied potential for chronoamperometric measurements in droplets, hydrodynamic experiments were performed by generating droplets containing 2.5 mM GlcN. Subsequently, the droplet contents were measured for currents using different applied potentials ranging from 50 to 500 mV. The S/B ratio was then plotted as a function of applied potential to construct a hydrodynamic voltammogram, as shown in Fig. 6b. It can be seen that when using an applied potential of 100 mV, the highest S/B ratio was obtained. Therefore, an applied potential of 100 mV was selected for further chronoamperometric measurements using the droplet system.

3.3.2. Effects of droplet size and velocity on chronoamperometric measurements

Since chronoamperometric current measurements were taken at the end of droplet signals, effects of droplet size and velocity on the currents were investigated to maximize the current signals. To optimize the velocity of droplets, droplet size was fixed by maintaining W_f at 0.3, 0.4 and 0.5 for droplet generation whilst total flow rate was varied in the range of 1.0–3.0 $\mu\text{L min}^{-1}$ for each W_f . Fig. 7a illustrates effect of droplet velocity on current signal for each W_f .

It was found that at the same velocity the lower the water fraction, the higher the electrochemical signal. This is due to the exponential decay of chronoamperometric current with time, resulting in lower current signal for longer droplets (higher W_f). Therefore, W_f equal to 0.3 was selected for droplet generation. In addition, the velocity of droplets was found to affect the current signal. When increasing the total flow rate, current signal was increased (Fig. 7a) due to short residence time caused by fast droplet movement when passing the CPEs. It should be noted that chronoamperometric currents were measured at semi-steady state of the exponential decay; therefore, shorter residence (higher droplet velocity) time would result in higher current signal. However, it was found that unstable current signals were observed at high flow velocities (2.5 and 3.0 $\mu\text{L min}^{-1}$). This could be due to the fact that at high flow velocities, the residence time was too short, resulting in uncertainty of the measured current signals. Accordingly, chronoamperometric measurements of the droplet content were performed using the flow rates of 1.4 $\mu\text{L min}^{-1}$ and 0.6 $\mu\text{L min}^{-1}$ for oil and aqueous solutions, respectively, resulting in a total flow rate of 2.0 $\mu\text{L min}^{-1}$ (corresponding to a linear velocity of 0.66 mm s^{-1}).

3.4. Analytical performance

3.4.1. Linearity and limits of detection and quantitation (LOD and LOQ)

To investigate linearity of the droplet system for determination of GlcN, droplets were produced using GlcN at different concentrations. Flow rates of GlcN and the oil phase were set to be 0.6 and 1.4 $\mu\text{L min}^{-1}$, respectively. Currents measured from the droplet system were then plotted as a function of GlcN concentration to observe a linear range. Fig. 7b shows linearity of this system, which was found to be in the range of 0.45–5 mM with a sensitivity of $7.42 \times 10^{-3} \text{ A mol}^{-1} \text{ L cm}^{-2}$. In addition, LOD and LOQ of the droplet system for determination of GlcN, calculated using 3 and 10 times of signal-to-background ratios, were found to be 0.45 and

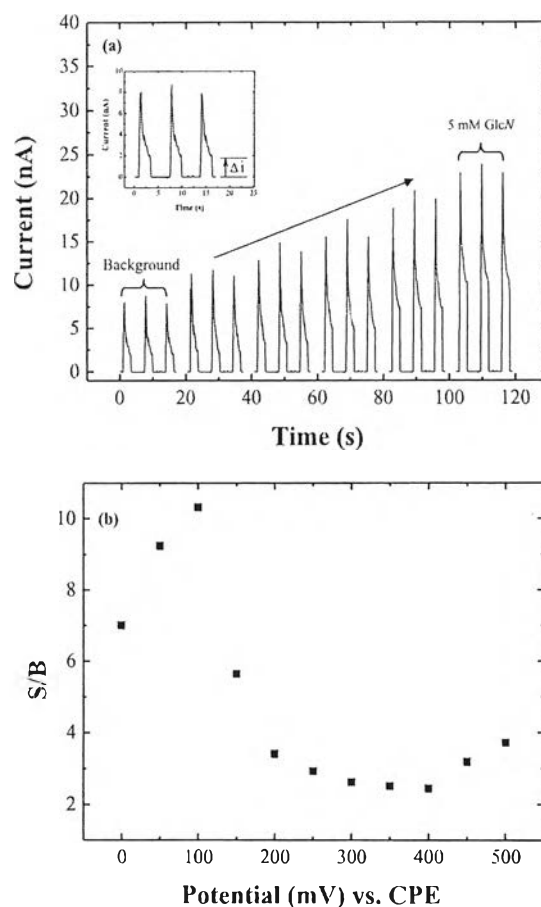


Fig. 6. (a) Chronoamperometric readout of a concentration series of GlcN from 0 to 5 mM. The inset shows an example of current measurement of a droplet peak. The measurements were carried out using a total flow rate of 2.0 $\mu\text{L min}^{-1}$ and $W_f=0.3$ to generate droplets containing GlcN. The applied potential was 100 mV vs. CPE. (b) A hydrodynamic voltammogram of 2.5 mM GlcN.

1.45 mM, respectively. It should be noted that the chip-based CPEs used in this work were microband electrodes possessing a small working area of $2.5 \times 10^{-4} \text{ cm}^2$ and the measurements were carried out in a flow-based system to allow for high-throughput analysis. Accordingly, the linear range and LOD of the proposed system are not as good as those reported from the previous work [28]. However, the advantages of using a droplet system are that small amount of samples (typically in nanoliters) is required for the measurements when compared to batch methods which are normally required sample volumes of at least 0.5 mL and the proposed approach not only allows for high-throughput analysis (at least 60 samples h^{-1}), but also prevents the adsorption of analytes on the electrode surface due to the compartmentalization of droplets. These minimize the analysis time to be approximately 1 min for a sample because no washing and drying steps are required between consecutive runs, compared to batch methods which normally take at least 5 min for a sample. In addition, the proposed platform could be further developed to be fully automated for high throughput sample monitoring for quality control of products in manufacturing processes.

3.4.2. Precision

Intra-day and inter-day precisions of the droplet system for chronoamperometric measurements of GlcN were evaluated. Three concentration levels (1.5, 2.5 and 3.5 mM) of GlcN were used to generate droplets for assessment of both precisions. Intra-day precision was observed from current measurements of 50 droplets

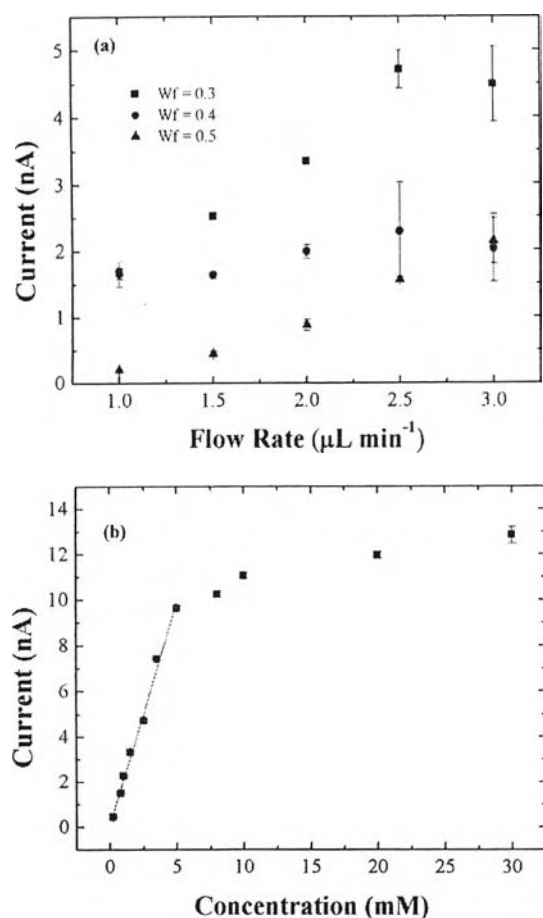


Fig. 7. (a) Effects of water fraction and total flow rate on chronoamperometric measurements of GlcN in droplets. (b) A dynamic range (0.45–5.0 mM) of the droplet system for determination of GlcN. Droplets were generated using a total flow rate of $2.0 \mu\text{L min}^{-1}$ and $W_f=0.3$. The applied potential was 100 mV.

($n=50$) for each concentration within the same day, while inter-day precision was investigated from current measurements of droplet contents among 3 days ($n=3$). Results showed that current signals obtained from the intra-day measurements (Fig. S2a, ESI) were highly reproduced with the percentage of relative standard deviation (% RSD) of less than 3%. For inter-day precision (Fig. S2b, ESI), % RSD of the currents measured from 3 days ($n=3$) were found to be less than 5%. Using the t -test, the currents obtained among three days for inter-day experiments were not statistically different at a 95% confidence level ($t_{\text{cal}}=0.21 < t_{\text{crit}}=4.30$). These indicate high repeatability of the droplet system for intra-day and inter-day measurements of GlcN.

3.5. Study of interference

Generally, GlcN can be synthesized from hydrolysis of chitosan with *N*-acetylglucosamine (GlcNAc) as a by-product. Both GlcN and GlcNAc have similar chemical structures with a hydrogen of the amine group of GlcN being replaced by an acetyl group to form GlcNAc (Fig S3, ESI). Therefore, study of interference caused by GlcNAc for determination of GlcN using the droplet system was performed. To study effect of GlcNAc on determination of GlcN, the concentration of GlcN was maintained at 5 mM (the control) and mixed solutions between GlcN and GlcNAc were prepared at different concentration ratios of 1:10, 2:10, 3:10, 4:10 and 5:10 (GlcNAc: GlcN), resulting in 10%, 20%, 30%, 40% and 50% GlcNAc in GlcN solutions. Subsequently, all solutions were chronoamperometrically measured for currents using the

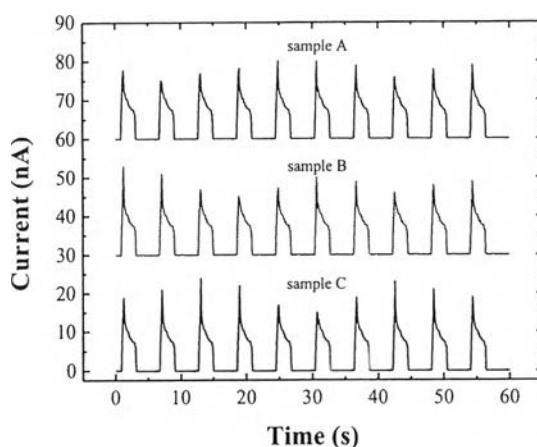


Fig. 8. Examples of chronoamperograms obtained from the measurements of GlcN in supplementary products. All experiments were carried out using the conditions shown in Fig. 7b.

droplet system. From the results (Fig. S4, ESI), it was determined that at concentration ratios of 1:10, 2:10, 3:10, 4:10, currents were found to be insignificantly different (only 0.4%, 0.6%, 1.6% and 3.0% increase, respectively) when compared to the current obtained from 5 mM GlcN. At the ratio of 5:10 (50% GlcNAc), 14% of current enhancement was found. However, the relative percent composition of GlcNAc in supplementary products is not expected to reach 50%. Therefore, GlcNAc does not interfere GlcN measurements using this method.

3.6. Application to real samples

The proposed method was applied for determination of GlcN in dietary supplements (A, B and C). Three marketed GlcN products were prepared in 0.1 M PBS pH 4. Consequently, droplets of real samples were generated and measured for chronoamperometric currents. An example of droplet signal containing GlcN supplements is shown in Fig. 8. Averaged currents from 10 droplets for each sample were then used to calculate the amount of GlcN using a linear equation of $y = 1.854x + 0.489$ with $R^2 = 0.997$ obtained from a calibration curve plotted between current (nA) and concentration in the range of 1–5 mM. The amounts of GlcN determined using the droplet system are shown in Table 1. Error percentages of the difference between the determined amounts of GlcN in real samples and the labeled amounts were found to be less than 0.1%. In addition, results from t -test at a 95% confidence level showed that the calculated t values ($t_{\text{cal}}=0.15, 0.49$ and 0.21 for samples A, B and C, respectively) did not exceed the critical t value ($t_{\text{crit}}=2.26, n=10$), confirming that there was no significant difference between the determined and labeled amounts of GlcN in real samples. Moreover, to further validate the proposed system, results obtained from real sample measurements were compared to those from the measurements using the traditional capillary electrophoresis (CE) with UV detection [29]. Statistical analysis using t -test (at a 95% confidence interval) showed that t_{cal} equal to 0.45 was significantly lower than t_{crit} of 2.91, indicating no significant difference between the results determined using the proposed approach and the CE method. This confirmed a high accuracy of the proposed system for quantitative analysis of GlcN supplements.

4. Conclusions

A chip-based electrochemical sensor using the AuNPs-PANI/CPES for monitoring of GlcN in supplementary products was successfully developed for the first time. Using CCD experiments, optimization

Table 1.
Measurements of GlcN in supplementary products.

Real sample	Labeled amount (mg)	This method			CE method		
		Measured amount (mg)	%RSD	%Error	Measured amount (mg)	%RSD	%Error
A	1500	1516	2.08	1.07	1516	2.85	1.07
B	1500	1499	0.71	0.06	1513	2.07	0.87
C	1500	1510	1.68	0.67	1505	2.75	0.33

of pH of the working medium and the amounts of AuNPs and PANI for electrode fabrication was easily and accurately achieved. The proposed system has shown its ability for measurements of GlcN with good sensitivity and high accuracy and precision. Integration with a droplet system expedited the analysis into a high-throughput manner and prevented adsorption of samples on the electrode surface. Although the detection limit of the proposed system for analysis of GlcN is not as low as that reported in previous work [3], this platform offers a direct, facile and convenient route to determine the amount of GlcN, which could be employed for quality control of GlcN products during manufacturing processes and for monitoring the quality of GlcN supplements distributed into the markets. In addition, dietary supplements always contain GlcN at high concentrations; therefore, an analytical method with a low detection limit is not necessary. From this work, droplet microfluidics integrated with an electrochemical sensor has put a strong emphasis on feasible applications for controlling and monitoring the quality of products during manufacturing processes and in the growing dietary supplement market.

Acknowledgements

This work was supported by the 90th Anniversary of Chulalongkorn University, Rachadapisek Sompote Fund, the Rachadapiseksomphot Endowment Fund 2013 of Chulalongkorn University (CU-56-498-AM) and the Thailand Research Fund through Research Team Promotion Grant (RTA5780005). Special thanks to K. Chindaphan for CE analysis. K. Wongravee would like to thank the Nanotechnology center (NANOTEC) for the good encouragements and opportunities.

Appendix A. Supplementary material

Supplementary data associated with this article can be found in the online version at <http://dx.doi.org/10.1016/j.talanta.2016.05.052>.

References

- [1] D.J. Hunter, F. Eckstein, Exercise and osteoarthritis, *J. Anat.* 214 (2009) 197–207.
- [2] L.-J. Zhang, T.-M. Huang, X.-I. Fang, X.-N. Li, Q.-S. Wang, Z.-W. Zhang, X.-Y. Sha, Determination of glucosamine sulfate in human plasma by precolumn derivatization using high performance liquid chromatography with fluorescence detection: its application to a bioequivalence study, *J. Chromatogr. B* 842 (2006) 8–12.
- [3] Y. Shao, R. Alluri, M. Mummeri, U. Koetter, S. Lech, A stability-indicating HPLC method for the determination of glucosamine in pharmaceutical formulations, *J. Pharm. Biomed. Anal.* 35 (2004) 625–631.
- [4] M.F. Adams, Hype about glucosamine, *Lancet* 354 (1999) 353–354.
- [5] R. Cheng, Y. Liu, S. Ou, Y. Pan, S. Zhang, H. Chen, L. Dai, J. Ou, Optical turn-on sensor based on graphene oxide for selective detection of D-glucosamine, *Anal. Chem.* 84 (2012) 5641–5644.
- [6] A. Aghazadeh-Habashi, S. Sattari, F. Pasutto, F. Jamali, High performance liquid chromatographic determination of glucosamine in rat plasma, *J. Pharm. Pharm. Sci.* 5 (2002) 176–180.
- [7] T.R.I. Cataldi, C. Campa, G.E. De Benedetto, Carbohydrate analysis by high-performance anion-exchange chromatography with pulsed amperometric detection: the potential is still growing, *Fresenius J. Anal. Chem.* 368 (2000) 739–758.
- [8] E. Pashkova, A. Pirogov, A. Bendryshev, E. Ivanaynen, O. Shpigun, Determination of underivatized glucosamine in human plasma by high-performance liquid chromatography with electrochemical detection: Application to pharmacokinetic study, *J. Pharm. Biomed. Anal.* 50 (2009) 671–674.
- [9] S. Zhong, D. Zhong, X. Chen, Improved and simplified liquid chromatography/electrospray ionization mass spectrometry method for the analysis of underivatized glucosamine in human plasma, *J. Chromatogr. B* 854 (2007) 291–298.
- [10] Y. Liu, Z. Li, G. Liu, J. Jia, S. Li, C. Yu, Liquid chromatography–tandem mass spectrometry method for determination of N-acetylglucosamine concentration in human plasma, *J. Chromatogr. B* 862 (2008) 150–154.
- [11] M.O.P. Crespo, M.V. Martínez, J.L. Hernández, M.A. Lage Yusty, High-performance liquid chromatographic determination of chitin in the snow crab, *Chionoecetes opilio*, *J. Chromatogr. A* 1116 (2006) 189–192.
- [12] W.K. Way, K.G. Gibson, A.G. Breite, Determination of glucosamine in nutritional supplements by reversed-phase ion-pairing HPLC, *J. Liq. Chromatogr. Relat. Technol.* 23 (2000) 2861–2871.
- [13] K. Račaitytė, S. Kiessig, F. Kálmán, Application of capillary zone electrophoresis and reversed-phase high-performance liquid chromatography in the biopharmaceutical industry for the quantitative analysis of the monosaccharides released from a highly glycosylated therapeutic protein, *J. Chromatogr. A* 1079 (2005) 354–365.
- [14] A. Suea-Ngam, P. Rattanasart, O. Chailapakul, M. Srisa-Art, Electrochemical droplet-based microfluidics using chip-based carbon paste electrodes for high-throughput analysis in pharmaceutical applications, *Anal. Chim. Acta* 883 (2015) 45–54.
- [15] M. Tomimaga, M. Nagashima, I. Taniguchi, Controlled-potential electro-synthesis of glucosaminic acid from glucosamine at a gold electrode, *Electrochim. Commun.* 9 (2007) 911–914.
- [16] C. Dhand, M. Das, M. Datta, B.D. Malhotra, Recent advances in polyaniline based biosensors, *Biosens. Bioelectron.* 26 (2011) 2811–2821.
- [17] E. Fernandez, I. Vidal, J. Iniesta, J.P. Metters, C.E. Banks, A. Canals, Screen-printed electrode-based electrochemical detector coupled with in-situ ionic-liquid-assisted dispersive liquid-liquid microextraction for determination of 2,4,6-trinitrotoluene, *Anal. Bioanal. Chem.* 406 (2014) 2197–2204.
- [18] S.M. Ghoreishi, M. Behpour, A. Khoobi, Central composite rotatable design in the development of a new method for optimization, voltammetric determination and electrochemical behavior of betaxolol in the presence of acetaminophen based on a gold nanoparticle modified electrode, *Anal. Methods* 4 (2012) 2475–2485.
- [19] A.D. McFarland, C.L. Haynes, C.A. Mirkin, R.P. Van Duyne, H.A. Godwin, *Color My nanoworld*, *J. Chem. Educ.* 81 (2004) 544A.
- [20] J.C. McDonald, G.M. Whitesides, Poly(dimethylsiloxane) as a material for fabricating microfluidic devices, *Acc. Chem. Res.* 35 (2002) 491–499.
- [21] H.D. Ward, J. Alroy, B.I. Lev, G.T. Keusch, M.E. Pereira, Biology of *Giardia lamblia*. Detection of N-acetyl-D-glucosamine as the only surface saccharide moiety and identification of two distinct subsets of trophozoites by lectin binding, *J. Exp. Med.* 167 (1988) 73–88.
- [22] R.G. Brereton, *Chemometrics: Data Analysis for the Laboratory and Chemical Plant*, John Wiley & Sons Ltd., Chichester, UK, 2003.
- [23] J. Anthony Smith, M. Josowicz, J. Janata, Gold-polyaniline composite Part I. Moving electrochemical interface, *Phys. Chem. Chem. Phys.* 7 (2005) 3614–3618.
- [24] C.O. Baker, B. Shedd, R.J. Tseng, A.A. Martinez-Morales, C.S. Ozkan, M. Ozkan, Y. Yang, R.B. Kaner, Size control of gold nanoparticles grown on polyaniline nanofibers for bistable memory devices, *ACS Nano* 5 (2011) 3469–3474.
- [25] X. Hu, X. Lin, Q. He, H. Chen, Electrochemical detection of droplet contents in polystyrene microfluidic chip with integrated micro film electrodes, *J. Electroanal. Chem.* 726 (2014) 7–14.
- [26] Y. Wang, Q. Liu, Q. Qi, J. Ding, X. Gao, Y. Zhang, Y. Sun, Electrocatalytic oxidation and detection of N-acetylcysteine based on magnetite/reduced graphene oxide composite-modified glassy carbon electrode, *Electrochim. Acta* 111 (2013) 31–40.
- [27] H. Liu, R.M. Crooks, Highly reproducible chronoamperometric analysis in microdroplets, *Lab Chip* 13 (2013) 1364–1370.
- [28] N.A. Al-arfa'i, M.F. El-Tohamy, Carbon paste and modified carbon nanotubes paste sensors for determination of reducing-osteoarthritis drug glucosamine sulphate in bulk powder and in its pharmaceutical formulations, *Int. J. Electrochem. Sci.* 7 (2012) 11023–11034.
- [29] S. Hoffstetter-Kuhn, A. Paulus, E. Gassmann, H.M. Widmer, Influence of borate complexation on the electrophoretic behavior of carbohydrates in capillary electrophoresis, *Anal. Chem.* 63 (1991) 1541–1547.



Highly sensitive determination of mercury using copper enhancer by diamond electrode coupled with sequential injection–anodic stripping voltammetry

Sudkate Chaiyo^a, Orawon Chailapakul^{b,c}, Weena Siangproh^{a,*}

^a Department of Chemistry, Faculty of Science, Srinakharinwirot University, Thailand

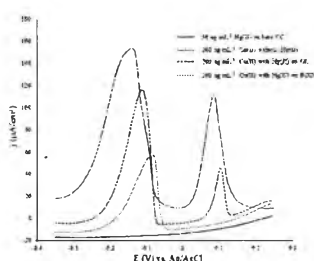
^b Department of Chemistry, Faculty of Science, Chulalongkorn University, Thailand

^c Center for Petroleum, Petrochemicals, and Advanced Materials, Chulalongkorn University, Thailand

HIGHLIGHTS

- Highly sensitive determination of Hg(II) using SI–ASV–BDD was achieved.
- Electrochemical detection of Hg(II) using Cu(II) enhancer was accomplished.
- LOD and LOQ were found to be very low at 40.0 ppt and 135.0 ppt.
- This method was successfully applied for determination of Hg(II) in real samples.

GRAPHICAL ABSTRACT



ARTICLE INFO

Article history:

Received 25 June 2014

Received in revised form 5 September 2014

Accepted 9 September 2014

Available online 16 September 2014

Keyword:

Mercury

Copper enhancer

Sequential injection–anodic stripping voltammetry (SI–ASV)

Boron-doped diamond thin film electrode (BDD)

ABSTRACT

A highly sensitive determination of mercury in the presence of Cu(II) using a boron-doped diamond (BDD) thin film electrode coupled with sequential injection–anodic stripping voltammetry (SI–ASV) was proposed. The Cu(II) was simultaneously deposited with Hg(II) in a 0.5 M HCl supporting electrolyte by electrodeposition. In presence of an excess of Cu(II), the sensitivity for the determination of Hg(II) was remarkably enhanced. Cu(II) and Hg(II) were on-line deposited onto the BDD electrode surface at -1.0 V (vs. Ag/AgCl, 3 M KCl) for 150 s with a flow rate of $14 \mu\text{L s}^{-1}$. An anodic stripping voltammogram was recorded from -0.4 V to 0.25 V using a frequency of 60 Hz, an amplitude of 50 mV, and a step potential of 10 mV at a stopped flow. Under the optimal conditions, well-defined peaks of Cu(II) and Hg(II) were found at -0.25 V and $+0.05$ V (vs. Ag/AgCl, 3 M KCl), respectively. The detection of Hg(II) showed two linear dynamic ranges (0.1 – 30.0 ng mL^{-1} and 5.0 – 60.0 ng mL^{-1}). The limit of detection ($S/N = 3$) obtained from the experiment was found to be 0.04 ng mL^{-1} . The precision values for 10 replicate determinations were 1.1, 2.1 and 2.9% RSD for 0.5, 10 and 20 ng mL^{-1} , respectively. The proposed method has been successfully applied for the determination of Hg(II) in seawater, salmon, squid, cockle and seaweed samples. A comparison between the proposed method and an inductively coupled plasma optical emission spectrometry (ICP–OES) standard method was performed on the samples, and the concentrations obtained via both methods were in agreement with the certified values of Hg(II), according to the paired t-test at a 95% confidence level.

© 2014 Elsevier B.V. All rights reserved.

* Corresponding author. Tel.: +66 649 5000ext.18208; fax: +66 259 2054.

E-mail addresses: weena@swu.ac.th, weenasi@hotmail.com, weenasi@yahoo.com (W. Siangproh).

1. Introduction

Mercury is a well-recognized global pollutant and one of the most toxic elements [1]. Its toxicity, bioavailability and bioaccumulation in living organisms are dependent on its chemical form [2]. Due to its solubility in water, which provides a pathway for contamination in large amounts of water, Hg(II) is one of the most common and stable forms of mercury pollution. By this means, Hg(II) can accumulate in vital organs throughout the food chain and cause severe damage to the brain, nervous system, kidneys, heart and endocrine system [3]. Therefore, it is very important to routinely monitor the Hg(II) in the environment. Due to its high toxicity, the United States Environmental Protection Agency (USEPA) limits the mercury level in drinking water to 0.002 mg L^{-1} [4], and the pollutant control department in Thailand allows the mercury level in industrial effluent to be 0.005 mg L^{-1} [5]. For the determination of such very low levels of Hg(II) in environmental samples, the development of a highly sensitive detection method is really important.

Several techniques can be used for mercury quantification, such as cold-vapor atomic fluorescence spectrometry (CV-AFS) [6], cold-vapor atomic absorption spectrometry (CV-AAS) [7], inductively coupled plasma-mass spectrometry (ICP-MS) [3] and inductively coupled plasma atomic emission spectrometry (ICP-AES) [8]. Even though, these methods are sensitive for the detection of low concentrations, to meet the sensitivity requirement, they need extensive sample preparation and long analysis times. Consequently, these techniques are not suitable for on-line monitoring. On the other hand, electrochemical techniques are an alternative choice for the detection of trace metals because of their simplicity and high sensitivity. Anodic stripping voltammetry especially offers a highly sensitive method for the detection of metal ions because it contains a pre-concentration step before analysis. Thus, this method has significant advantages as an automatic on-line monitoring method.

Anodic stripping voltammetry (ASV) [9] is a popular technique used for the determination of various heavy metals. Recently, ASV has been widely used for the trace and ultra-trace analysis of metal ions due to its wide linear dynamic range, high sensitivity and low detection limit. The additional advantages of ASV over AAS, ICP-AES and ICP-MS are the low instrument cost and small equipment. To overcome the traditional batch analysis, ASV can be combined with sequential injection analysis (SIA). This combination has significant advantages over the batch system, including the speed of analysis and low reagent consumption as well as improved accuracy and precision [10,11]. Moreover, sequential injection-anodic stripping voltammetry (SI-ASV) can be performed as a fully automated system. The detection of mercury in solutions using anodic stripping voltammetry (ASV) has been reported using several different electrodes, including graphite [12], carbon paste [13], glassy carbon [14], modified glassy carbon [15],

screen-printed carbon [16] and gold [17]. In some of these cases, electrode preparation techniques such as polishing, chemical modification or electrode pre-treatment are essential for the detection of low levels of mercury or to increase the reproducibility of the detection.

Boron-doped diamond (BDD) thin film electrodes have been increasingly used in electrochemical applications due to the characteristics of diamond, such as its durability, electrical conductivity, and corrosion resistance [18,19]. The excellent chemical inertness combined with the low background current and the large potential range between the onset of oxygen and hydrogen evolution makes the use of diamond popular for the detection of variety of electroactive species [20–22]. Boron-doped diamond thin film electrodes have attracted considerable attention for use in the electroanalytical detection of a variety of analytes including mercury [23,24].

From literature reviews related to the electrochemical detection of mercury, we found that copper is the major interfering ion in the determination. In the presence of copper ions, the peak current of mercury increased with increasing concentrations of copper ions [25,26]. Based on this idea Borgo et al. recently reported the determination of Hg(II) by stripping voltammetry using an antimony film electrode in the presence of Cu(II) [27]. However, this method is a batch analysis method. Furthermore, Ashrafi and Vytrás revealed a method introducing additional Cd(II) into the Hg(II) using an antimony film modified carbon paste electrode. However, this method is highly toxic due to the Cd(II) [28]. Therefore, the aim of the present work was to develop a highly sensitive and automated method for the determination of Hg(II) ions in the presence of Cu(II) to obtain a high sensitivity. The BDD thin film electrode was selected because this electrode provided the sensitivity to detect Hg(II). However, there is no report of the use of a BDD thin film electrode as a sensor in an automated system. The developed method was successfully applied for determination of trace levels of Hg(II) in seawater, salmon, cockles, squid and seaweed samples.

2. Experimental

2.1. Reagents

A standard solution of Hg(II) was prepared daily by an appropriate dilution of the stock standard solutions of $\text{Hg}(\text{NO}_3)_2$ (1000 mg L^{-1} atomic absorption analysis hydrochloric acid solution obtained from Ajax, Australia). The stock standard solutions of 0.5 M Cu(II) solution were prepared by dissolving CuSO_4 (BDH, England) in a 0.5 M hydrochloric acid solution. The 0.5 M hydrochloric acid solution, which served as a supporting electrolyte, was prepared by the dilution of concentrated hydrochloric acid (analytical reagent grade, 37% , 1.19 g mL^{-1} ; Merck, Germany) with milli-Q water. The 1.0 M nitric acid solution

Table 1
Step sequence for the determination of Hg(II) by SI-ASV.

Step	Description	Position of selection valve	Volume (μL)	Flow rate ($\mu\text{L s}^{-1}$)	Time (s)	Electrode potential (V)
1	Aspirate sample solution into holding coil	1	1400	100	14	–
2	Aspirate Cu(II) solution into holding coil	2	700	100	7	–
3	Dispense Cu(II) solution and sample solution into flow cell for <i>in situ</i> plating of Cu(II) and metal ion	3	2100	14	150	–1.0
4	Equilibration	3	0	0	5	–1.0
5	Stripping and recording of voltammogram	3	0	0	10	–0.4 to 0.25
6	Aspirate 0.5 M HCl into holding coil	4	200	100	2	–
7	Dispense 0.5 M HCl into flow cell for electrode cleaning	3	200	20	10	+1.0
8	Aspirate 1.0 M HNO_3 into holding coil	5	1200	100	12	–
9	Dispense 1.0 M HNO_3 into flow cell for electrode cleaning	3	1200	20	60	+1.0

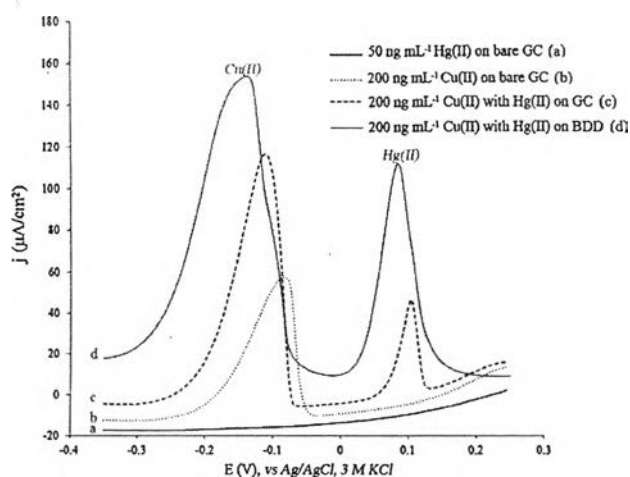


Fig. 1. Sequential injection-anodic stripping voltammograms (SI-ASV) of 50 ng mL⁻¹ Hg(II) on bare GC (a), 200 ng mL⁻¹ Cu(II) without Hg(II) (b), 200 ng mL⁻¹ Cu(II) with 50 ng mL⁻¹ Hg(II) on GC (c) and 200 ng mL⁻¹ Cu(II) with 50 ng mL⁻¹ Hg(II) on BDD (d). The deposition potential was -1.0 V; the deposition time, 150 s; flow rate was set at 14 $\mu\text{L s}^{-1}$. Electrode areas: GC is 0.1413 cm² and BDD is 0.3406 cm².

was prepared by the dilution of concentrated nitric acid (analytical reagent grade, 65%, 1.39 g mL⁻¹; Merck, Germany) with milli-Q water.

2.2. Apparatus

A sequential injection system for the determination of Hg(II) by ASV consisted of a syringe pump (Hamilton, USA) and an 8-port selection valve (Hamilton, USA). PTFE tubing was used for the flow lines (1.5 mm i.d.) and a holding coil (1.5 mm i.d., 2.5 m). The system was computer controlled by a program written with visual basic software. Electrochemical measurements were carried out in a thin-layer flow cell (Bioanalytical Systems, USA) using the potentiostat (Autolab, The Netherlands). The thin-layer flow cell consisted of a gasket as a spacer, a BDD electrode as a working electrode, an Ag/AgCl electrode (3 M KCl) as a reference electrode, and a stainless-steel tube as a counter electrode as well as a solution outlet of the flow cell.

2.3. SI-ASV procedure

The step sequences for the determination of Hg(II) are shown in Table 1. The sample and the Cu(II) enhancer solution were sequentially aspirated into the holding coil and dispensed into a thin-layer flow cell while an electrode potential of -1.0 V was applied for 150 s in which Cu(II) and Hg(II) were deposited onto the electrode (steps 1–3). After a 5 s equilibration time with a stopped flow (step 4), a square wave voltammogram using a frequency of 60 Hz, a step potential of 10 mV, and a pulse amplitude of 50 mV was recorded from -0.4 V to +0.25 V (step 5). Finally, the electrode was cleaned at +1.0 V to remove any remaining analyte metals on the electrode surface, and 0.5 M hydrochloric acid was flowed for

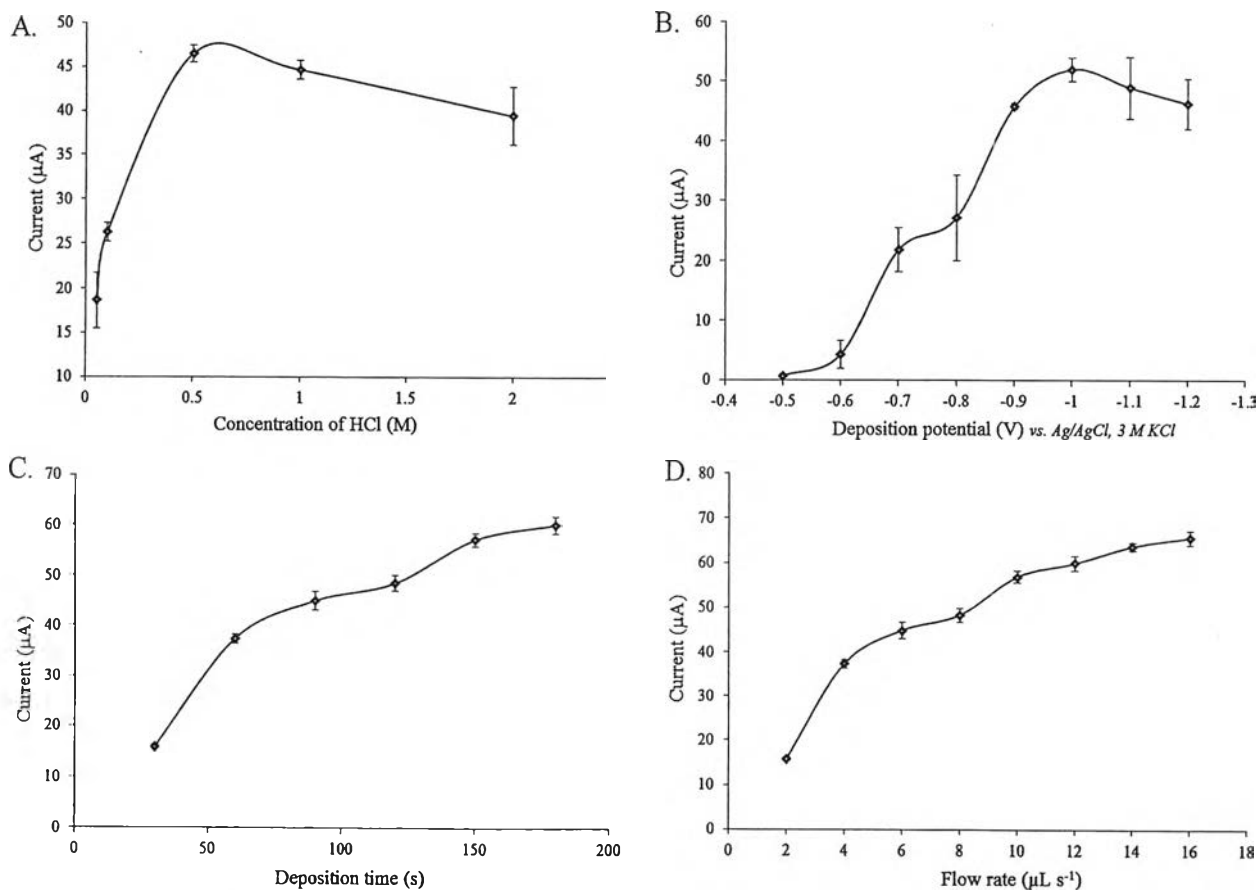


Fig. 2. Effect of optimized experimental conditions for the determination of Hg(II) such as concentration of HCl (A), deposition potential (B), deposition time (C) and flow rate (D). All other conditions were the same as those in Fig. 1.

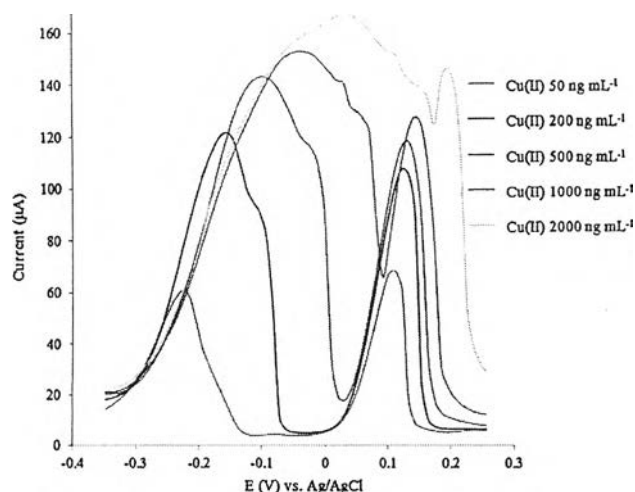


Fig. 3. SI-ASV of 50 ng mL^{-1} Hg(II) in various concentration of Cu(II). All other conditions were the same as those in Fig. 1.

10 s and 1.0 M nitric acid was flowed for 60 s (steps 6–9). All of the experiments were performed at room temperature.

2.4. Sample preparation

2.4.1. Preparation of seawater

The seawater sample was filtered through membranes ($0.45 \mu\text{m}$) to remove the suspended particles. Five milliliters of this filtrate volume was diluted to 25 mL with 0.5 M HCl. This solution was stored at 4°C in a refrigerator.

2.4.2. Preparation of salmon, cockle, squid and seaweed

Two grams of sample were accurately weighed into a 100 mL borosil beaker, and a mixture of 2 mL HNO_3 and 1 mL HClO_4 was added [29]. The mixture was then heated at a temperature of 100°C until the solution was clear. The solution was then cooled to room temperature, filtered through a $0.45 \mu\text{m}$ membrane filter and then the filtrate was diluted to a total volume of 10 mL with 0.5 M HCl.

3. Results and discussion

3.1. Behavior of mercury on bare GC and BDD electrodes

The major objective of the present work is to determine the mercury content using a BDD electrode. However, a comparison was also performed using a bare glassy carbon (GC) electrode to emphasize the unique properties of the BDD electrode. From Fig. 1, it can be observed that there is no voltammetric response of 50 ng mL^{-1} Hg(II) in 0.1 M HCl at a GC electrode (curve a). Curve b shows the oxidation peak obtained from 200 ng mL^{-1} Cu(II) in 0.1 M HCl at a GC electrode, and this peak was found at a potential of -0.10 V . As shown in curve c, 200 ng mL^{-1} Cu(II) was added to 50 ng mL^{-1} Hg(II), and they were then simultaneously on-line

Table 3

Tolerance ratio of interfering ions in the determination of 50 ng mL^{-1} of Hg(II).

Ions	Tolerance ratio ($W_{\text{ion}}/W_{\text{Hg(II)}}$)
Na^+ , Ba^{2+} , Co^{2+} , NO_3^- , CO_3^{2-} , HPO_4^{2-} , OH^- , Br^-	2000
Fe^{2+} , SO_4^{2-}	1500
Li^+ , Ni^{2+} , Cl^- , Mn^{2+} , NO_2^-	1000
CH_3COO^-	800
Mg^{2+}	400
Zn^{2+}	200
Cd^{2+} , Ag^+ , K^+	100
As^{3+} , Ca^{2+}	20
CN^- , I^- , Pb^{2+}	10

deposited on a GC. A Cu(II) peak was found at a potential of -0.15 V , and a new peak of Hg(II) was generated at a potential of $+0.10 \text{ V}$. Using the same conditions as curve c except for the GC electrode being replaced by a BDD electrode, a peak of 50 ng mL^{-1} Hg(II) at the BDD electrode greatly increased (curve d). This suggests that a BDD electrode can improve the sensitivity of the determination of mercury in this automated system.

3.2. Optimization of the parameters

The operating conditions and parameters, such as the supporting electrolyte, concentration of the supporting electrolyte, deposition potential, deposition time, concentration of Cu(II), and flow rate, were subsequently investigated.

3.2.1. Effect of the supporting electrolyte

Preliminary experiments were carried out with four acids (HCl, HNO_3 , HClO_4 and H_2SO_4) used as the supporting electrolyte, with each being used at the same concentration of 0.5 M. These experiments revealed that the highest peak currents and well-defined peak shapes were obtained using a 0.5 M HCl solution. Therefore, HCl was chosen as the optimal supporting electrolyte for this work. Next, the effect of varying the HCl concentration on the obtained current signal of Hg(II) was evaluated with 0.01, 0.1, 0.5, 1.0 and 5.0 M HCl. The highest stripping peak currents of Hg(II) were obtained by SI-ASV using 0.5 M HCl (Fig. 2A). It could be a concern that at this electrolyte concentration, the migration current was completely suppressed. However, a decrease in the stripping signal of Hg(II) occurred at higher concentrations because of the greater effect of hydrogen evolution. Therefore, 0.5 M HCl was selected as the optimum supporting electrolyte for the proposed method.

3.2.2. Effect of the deposition potential and deposition time

The dependence of the stripping peak current on the deposition potential was examined over the range -0.5 to -1.2 V . The solution consisted of 50 ng mL^{-1} Hg(II) and 200 ng mL^{-1} Cu(II), and a fixed flow rate of $14 \mu\text{L s}^{-1}$ was used. The results are presented in Fig. 2B. The stripping peak increases rapidly as the deposition potential becomes more negative. However, the peak current leveled off as the deposition potential approached -1.0 V and dropped when the potential was more negative than -1.0 V . Thus, an optimal deposition potential of -1.0 V was selected.

Table 2

Operating conditions and parameters for the determination Hg(II) by SI-ASV.

Optimization parameter	Range study	Selected
Deposition potential	$+0.5$ to -1.2 V	-1.0 V
Deposition time	30–210 s	150 s
Supporting electrolyte	HCl, HClO_4 , HNO_3 , H_2SO_4	HCl
Concentration supporting electrolyte	0.1–2 M	0.5 M
Concentration of Cu(II)	5–2000 ng mL^{-1}	50–200 ng mL^{-1}
Flow rate	2–16 $\mu\text{L s}^{-1}$	14 $\mu\text{L s}^{-1}$

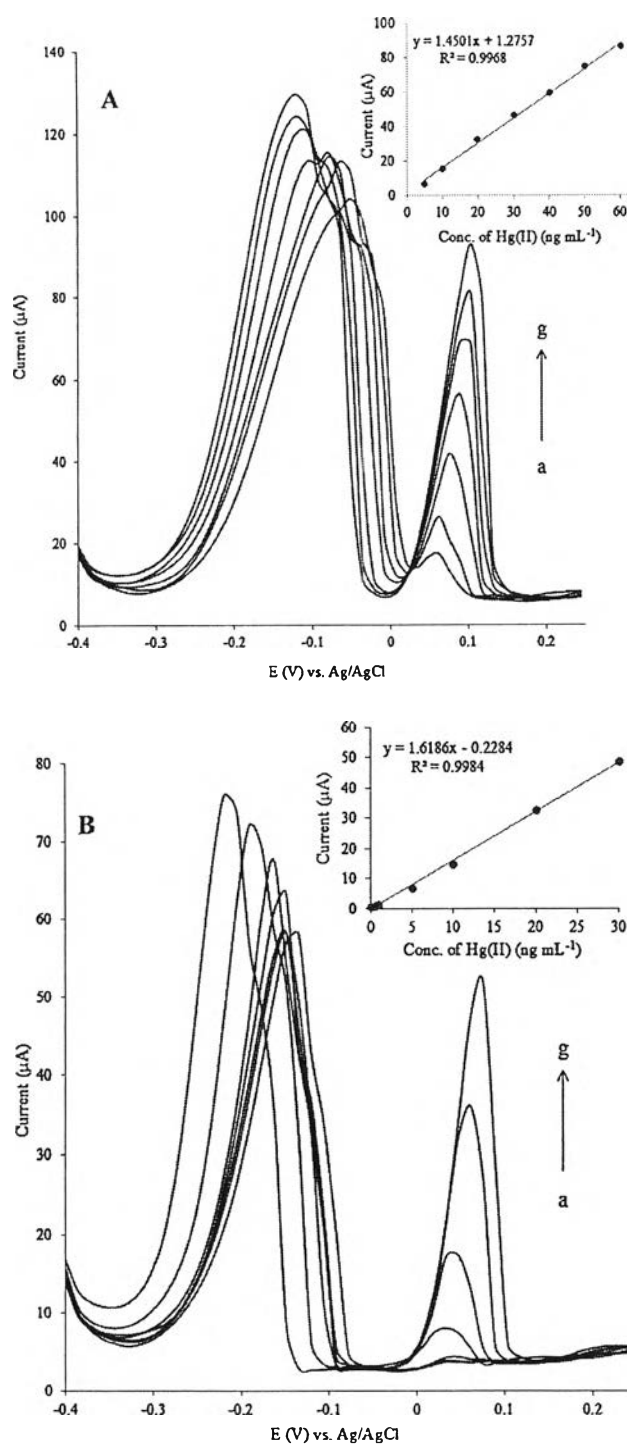


Fig. 4. (A) SI-ASV of the Hg(II) + 50 ng mL⁻¹ Cu(II) with different concentration of Hg(II), (a–g) 0.1, 0.5, 1.0, 5.0, 10.0, 20.0, and 30.0 ng mL⁻¹. Calibration plots (insert) for increasing concentrations of Hg(II) under optimum conditions. (B) SI-ASV of the Hg(II) + 200 ng mL⁻¹ Cu(II) with different concentration of Hg(II), (a–g) 5, 10, 20, 30, 40, 50, and 60 ng mL⁻¹. Calibration plots (insert) for increasing concentrations of Hg(II) under optimum conditions.

For the deposition time, the dependence of the Hg(II) peak heights was examined over the range of 30–200 s at a fixed flow rate of 14 $\mu\text{L s}^{-1}$ in the presence of 50 ng mL⁻¹ Hg(II) and 200 ng mL⁻¹ Cu(II). As illustrated in Fig. 2C, the peak currents increased almost linearly with the deposition time. The current signals increased with an increasing deposition time up to the maximum studied deposition time of 200 s. To balance the

sensitivity and analysis time, a deposition time of 150 s was selected here for all of the analyses.

3.2.3. Effect of the square-wave parameters

The square wave parameters investigated were the amplitude, the frequency and the step potential. These parameters together have an effect on the peak shape and peak current of the Hg(II)

Table 4
Determination of mercury by electrochemical analysis.

Electrode	Electrochemistry	LOD (ng mL ⁻¹)	System	Deposition time (s)	Ref.
Copper/antimony/glassy carbon electrode	ASV ^a	0.39	Batch	120	[27]
Thiophenol/single-walled carbon nanotubes/gold electrode	ASV	0.6	Batch	120	[30]
Palladium oxide/graphite composite electrode	DPASV ^b	3.87	Batch	180	[31]
Gold atomic cluster based nanocomposites/cetyl trimethyl ammonium bromide(CTAB)/biopolymer/chitosan/gold electrode	DPASV	1.6 × 10 ⁻⁶	Batch	15	[32]
Platinum microelectrode	FI-LAV ^c	112	Automatic	-	[33]
Solid gold and gold film electrode	FI-ASV ^d	0.05	Automatic	540	[34]
Gold film/screen-printed carbon electrode	SI-ASV ^e	0.22	Automatic	200	[16]
Copper/BDD	SI-ASV	0.04	Automatic	150	This work

^a ASV: anodic stripping voltammetry.

^b DPASV: differential pulse anodic stripping voltammetry.

^c FI-LSV: flow injection-linear scan voltammetry.

^d FI-ASV: flow injection-anodic stripping voltammetry.

^e SI-ASV: sequential injection-anodic stripping voltammetry.

response. The peak currents of Hg(II) increased as the square-wave frequency and step potential increased, but at high frequencies and step potentials, an increase in the background current was also found. This increase in the background current resulted in a lower signal to noise ratio, which may be due to that at a high frequency and step potential. The capacitive charging current does not significantly decay and contributes to the measured response. The peak current of Hg(II) increases with an increase in the square-wave amplitude up to 50 mV. Further increasing the amplitude decreases and broadens the Hg(II) stripping peak. Thus, the optimum amplitude, frequency and step potential selected for the square-wave stripping voltammetry were 50 mV, 60 Hz and 10 mV, respectively, and these parameters were used for all of the subsequent measurements.

3.2.4. Effect of the flow rate

The flow rate is an important parameter that affects the sensitivity and analysis time of mercury ion detection by SI-ASV. Hence, the influence of the flow rate on the stripping peak currents was investigated throughout the range of 2–16 $\mu\text{L s}^{-1}$. The

deposition time was fixed at 150 s, and a ratio between the mercury ion solution and Cu(II) solution of 2:1 was used. The result was that the peak current of Hg(II) increased with an increasing flow rate up to a maximum flow rate of 16 $\mu\text{L s}^{-1}$ as shown in Fig. 2D. Hence, a flow rate of 14 $\mu\text{L s}^{-1}$ was used throughout this work because this flow rate not only offers a high sensitivity but also provided a lower consumption of the sample and reagents.

3.2.5. Effect of the Cu(II) enhancer

Previous research reported that Cu(II) ions can interfere in the electrochemical detection of mercury. In addition, we found that Cu(II) can enhance the Hg(II) signal by a colorimetric method [26]. Therefore, we are interested in the use of Cu(II) as an enhancer. From the results, it can be observed that the Cu(II) enhancer could increase the signal of Hg(II). Therefore, the stripping peak currents are affected by the concentration of Cu(II). The effect of varying the Cu(II) concentration was investigated over the range of 50–2000 ng mL⁻¹. The stripping peak currents of Hg(II) and Cu(II) increased with increasing Cu(II) concentrations, but the signal of Cu(II) overlapped with the stripping peak currents of Hg(II) at

Table 5
The intra- and inter-day precisions and recoveries of the proposed method.

Samples	Concentration of Hg(II) (ng mL ⁻¹)	Intra-day		Inter-day	
		Mean %recovery (±SD)	RSD (%)	Mean %recovery (±SD)	RSD (%)
Seawater	1.0	82.25 ± 3.02	3.67	90.12 ± 14.18	15.73
	5.0	95.19 ± 6.69	7.03	94.68 ± 5.31	5.61
	10.0	101.80 ± 2.81	2.76	102.22 ± 4.00	3.91
	30.0	100.11 ± 0.23	0.23	99.91 ± 0.41	0.41
Salmon	1.0	77.08 ± 11.62	15.08	79.86 ± 5.07	6.35
	5.0	96.09 ± 10.94	11.38	97.45 ± 10.37	10.64
	10.0	100.80 ± 4.51	4.47	99.00 ± 6.06	10.47
	30.0	100.04 ± 0.31	0.31	100.20 ± 0.39	0.40
Squid	1.0	74.73 ± 2.61	3.50	81.76 ± 16.64	20.34
	5.0	108.18 ± 7.58	7.01	100.57 ± 19.60	19.49
	10.0	94.97 ± 4.45	4.69	96.71 ± 6.03	6.23
	30.0	100.58 ± 0.26	0.26	100.37 ± 0.24	0.24
Cockle	1.0	80.37 ± 9.34	11.62	86.33 ± 4.45	5.15
	5.0	97.60 ± 5.91	6.05	96.23 ± 5.96	6.20
	10.0	99.79 ± 6.22	6.23	97.74 ± 2.59	2.65
	30.0	100.10 ± 0.60	0.60	100.63 ± 0.57	0.57
Seaweed	1.0	80.27 ± 16.26	20.36	83.30 ± 12.72	15.27
	5.0	92.84 ± 13.78	4.07	88.88 ± 10.54	11.86
	10.0	101.21 ± 1.13	1.12	102.83 ± 2.53	2.46
	30.0	99.27 ± 1.68	1.69	100.02 ± 0.41	0.41

Table 6
Determination of mercury in real samples.

Samples	Added concentrations (ng mL ⁻¹)	Founded concentrations	
		Proposed method (ng mL ⁻¹)	Standard method ^a (ng mL ⁻¹)
Seawater	0.0	ND	ND
	1.0	0.83 ± 0.10	1.09 ± 0.10
	5.0	4.74 ± 0.06	4.36 ± 0.14
	10.0	10.65 ± 0.38	9.19 ± 0.11
	30.0	29.83 ± 0.12	30.37 ± 0.05
Salmon	0.0	ND	ND
	1.0	0.86 ± 0.10	1.09 ± 0.12
	5.0	4.27 ± 0.03	5.17 ± 0.33
	10.0	10.60 ± 0.42	9.76 ± 0.55
	30.0	29.93 ± 0.13	30.05 ± 0.20
Squid	0.0	ND	ND
	1.0	1.01 ± 0.21	0.87 ± 0.08
	5.0	3.90 ± 0.31	3.96 ± 0.20
	10.0	10.34 ± 0.80	10.72 ± 0.23
	30.0	30.07 ± 0.23	29.94 ± 0.08
Cockle	0.0	ND	ND
	1.0	0.90 ± 0.17	1.10 ± 0.15
	5.0	4.67 ± 0.92	5.47 ± 0.28
	10.0	9.81 ± 0.69	10.21 ± 0.54
	30.0	30.13 ± 0.08	29.85 ± 0.15
Seaweed	0.0	ND	ND
	1.0	0.66 ± 0.10	1.03 ± 0.08
	5.0	5.01 ± 0.19	4.72 ± 0.33
	10.0	9.99 ± 0.53	9.48 ± 0.36
	30.0	30.01 ± 0.17	30.22 ± 0.08

^a Inductively couple plasma-optical emission spectrometer (ICP-OES).

high concentrations of Cu(II) (500–2000 ng mL⁻¹) as shown in Fig. 3. Hence, the optimum concentration of the Cu(II) enhancer for the determination of Hg(II) by SI-ASV is between 50 and 500 ng mL⁻¹.

3.2.6. Effect of the interference from other ions

Various ions were examined regarding their interference in the determination of Hg(II). Possible interference with the stripping peak currents of Hg(II) by other ions was investigated by the addition of the possible interfering ion to a solution containing 50 ng mL⁻¹ of Hg(II) under the optimized conditions (summarized in Table 2). The tolerance limit was defined as the concentration that gave an error of ±5.0% in the determination of 50 ng mL⁻¹ Hg(II). The results of this study are summarized in Table 3. According to the results, no interference was caused by the investigated cations and anions; hence, the proposed method offers a very high selectivity.

3.2.7. Analytical characteristics

Under the experimental conditions (Table 2), the stripping peak currents of Hg(II) provided a linear relationship with the Hg(II) concentration. The dynamic ranges were examined using different concentrations of Cu(II). The calibration curves of the proposed method showed two different linear ranges. The first calibration was for high concentrations of Hg(II) obtained throughout the range of 5.0–60 ng mL⁻¹ ($R^2 = 0.9968$) in the presence of a Cu(II) concentration of 200 ng mL⁻¹ (Fig. 4A). The second calibration was for low concentrations of Hg(II) obtained throughout the range of 0.1–30 ng mL⁻¹ ($R^2 = 0.9968$) in the presence of a Cu(II) concentration of 50 ng mL⁻¹ (Fig. 4B). The benefit of different linear ranges is that the method can directly determine the Hg(II) at high concentrations without dilution or at low concentrations without pre-concentration before analysis. The detection limit and quantification limit, which were calculated based on three times (3 S/N) and ten times (10 S/N) the signal of the blank, were

40.0 pg mL⁻¹ and 135.0 pg mL⁻¹, respectively, whereas repetitive measurements yielded a relative standard deviation (%RSD) of 2.1% (20 ng mL⁻¹, $n = 10$). We have compared this method with some other methods, and the results are listed in Table 4. As observed from Table 4, the proposed method has the highest sensitivity among all of the other methods. Moreover, we proposed a method that can be automated and work in a closed system, thus reducing the risk of mercury toxicity.

3.2.8. The precision and accuracy

The precision and accuracy were evaluated under the optimal conditions to verify the use of SI-ASV for quantifying the Hg(II) in real samples (seawater, salmon, cockle, squid and seaweed). The intra-day ($n = 3$) and inter-day (3 days) experiments were performed and evaluated using samples spiked with four levels (1.0, 5.0, 10.0 and 30.0 ng mL⁻¹) of Hg(II). As shown in Table 5, the intra-day/inter-day accuracy for seawater, salmon, cockle, squid and seaweed samples were in the ranges of 82.25–101.80%/90.12–102.22%, 77.08–100.80%/79.86–100.20%, 74.73–108.18%/81.76–100.57%, 80.37–100.10%/86.33–86.33% and 80.27–101.21%/83.30–102.83%, respectively ($n = 3$). The precisions (%RSD) for the seawater, salmon, cockle, squid and seaweed samples were in the ranges of 0.23–7.03%/0.41–15.73%, 0.31–15.08%/0.40–10.67%, 0.26–7.01%/0.24–20.34%, 0.60–11.62%/0.57–5.15% and 1.12–20.36%/0.41–15.27%, respectively. This outstanding performance makes the developed method attractive for use as an automated analytical system for the analysis of Hg(II) in real samples.

3.2.9. Analysis of real samples

Under the optimal conditions, the proposed method was applied to determine the Hg(II) contamination in seawater, salmon, cockle, squid and seaweed samples. The utility of this method was evaluated by recovery studies at spiked concentration levels of 1, 5, 10 and 30 ng mL⁻¹. Each concentration was based on

three replicate runs. Results are shown in Table 6. No Hg(II) was found in the real samples. The relative recoveries and %RSD values were in the ranges of 74.73–108.18% and 0.26–17.38%, respectively. To validate the proposed method, the results obtained by this method were compared to those obtained from the ICP-OES method. The comparison of the results obtained from the two techniques is shown in Table 6. These results showed good agreement with the results obtained by the standard method, which means that the proposed alternative method can be accepted.

4. Conclusions

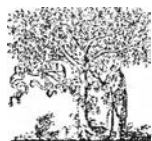
A highly sensitive, selective, rapid, automatic and low-cost electroanalytical method was successfully developed for the determination of ultra-trace levels of mercury ions in food and environmental samples. This method did not require any separation or pre-concentration steps and was directly applied for the determination of ultra-trace levels of mercury ions in food and environmental samples. The method exhibits an excellent linear dynamic range, which is divided into 2 ranges that offer the opportunity for application for both high ($5.0\text{--}60.0\text{ ng mL}^{-1}$) and low ($0.1\text{--}30.0\text{ ng mL}^{-1}$) concentrations of the analyte. A very low detection limit with an accumulation time of 150 s was obtained compared to those obtained in previous works. The results showed that the method is sensitive and accurate for real samples, and the results for the samples were in good agreement with the values obtained using inductively couple plasma-optical emission spectroscopy. Overall, the present method is promising for the electroanalysis of trace Hg(II) using an environmentally friendly procedure. Therefore, the proposed method is recommended as an alternative option for the analysis of various products contaminated with mercury.

Acknowledgments

The authors gratefully acknowledge partially financial support from Srinakharinwirot University under the Government Budget 2556 (Grant No. 117/2556) and the Thailand Research Fund (RTA5780005). The Thai Government Stimulus Package 2 (TKK2555), under the Project for Establishment of Comprehensive Center for Innovative Food Health Products and Agriculture (PERFECTA).

References

- [1] G.A. Drasch, Mercury, in: H.G. Seiler, A. Sigel (Eds.), *Handbook on Metals in Clinical and Analytical Chemistry*, Marcel Dekker Inc., New York, 1994.
- [2] P. Krystek, R. Ritsema, Determination of methylmercury and inorganic mercury in shark fillets, *Appl. Organomet. Chem.* 18 (2004) 640–645.
- [3] Z. Gu, M. Zhao, Y. Sheng, A. Bentolila, Y. Tang, Detection of mercury ion by infrared fluorescent protein and its hydrogel-based paper assay, *Anal. Chem.* 83 (2011) 2324–2329.
- [4] <http://water.epa.gov/drink/contaminants/basicinformation/mercury.cfm>.
- [5] http://www.pcd.go.th/info_serv/en_reg_std_water04.html
- [6] K. Leopold, L. Harwardt, M. Schuster, G. Schlemmer, A new fully automated on-line digestion system for ultra-trace analysis of mercury in natural waters by means of FI-CV-AFS, *Talanta* 76 (2008) 382–388.
- [7] D.P. Torres, V.L.A. Frescura, A.J. Curtius, Simple mercury fractionation in biological samples by CV AAS following microwave-assisted acid digestion or TMAH pre-treatment, *Microchem. J.* 93 (2009) 206–210.
- [8] Y. Wu, Y. Lee, L. Wu, X. Hou, Simple mercury speciation analysis by CVG-ICP-MS following TMAH pre-treatment and microwave-assisted digestion, *Microchem. J.* 103 (2012) 105–109.
- [9] X. Chai, X. Chang, Z. Hu, Q. He, Z. Tu, Z. Li, Solid phase extraction of trace Hg(II) on silica gel modified with 2-(2-oxoethyl)hydrazine carbothioamide and determination by ICP-AES, *Talanta* 82 (2010) 1791–1796.
- [10] H.J. Kim, D.W. Son, J.M. Park, D.Y. Hwang, C.Y. Mo, S.W. Park, C. Kim, J.B. Eun, Application of an in situ bismuth-coated glassy carbon electrode for electroanalytical determination of Cd(II) and Pb(II) in Korean polished rices, *Food Sci. Biotechnol.* 19 (2010) 1211–1217.
- [11] G.D. Christian, Sequential injection analysis for electrochemical measurements and process analysis, *Analyst* 119 (1994) 2309–2314.
- [12] E.A. Viltchinskaja, L.L. Zeigmann, S.G. Morton, Application of stripping voltammetry for the determination of mercury, *Electroanalysis* 7 (1995) 264–269.
- [13] Z. Navratilova, P. Kula, Modified carbon paste electrodes for the study of metal-humic substances complexation, *Anal. Chim. Acta* 273 (1993) 305–311.
- [14] S. Meyer, F. Scholz, R. Trittl, Determination of inorganic ionic mercury down to $5 \times 10^{-14}\text{ mol L}^{-1}$ by differential-pulse anodic stripping voltammetry, *Fresenius J. Anal. Chem.* 356 (1996) 247–252.
- [15] I. Svančara, M. Matoušek, E. Sikora, K. Schachl, K. Kalcher, K. Vytras, Carbon paste electrodes plated with a gold film for the voltammetric determination of mercury(II), *Electroanalysis* 9 (1997) 827–833.
- [16] E. Punrat, S. Chuanuwatanakul, T. Kaneta, S. Motomizu, O. Chailapakul, Method development for the determination of mercury(II) by sequential injection/ anodic stripping voltammetry using an in situ gold-film screen-printed carbon electrode, *J. Electroanal. Chem.* 727 (2014) 78–83.
- [17] M. Korolczuk, Sensitive and selective determination of mercury by differential pulse stripping voltammetry after accumulation of mercury vapour on a gold plated graphite electrode, *Fresenius J. Anal. Chem.* 357 (1997) 389–391.
- [18] K.E. Spear, J.P. Dismukes (Eds.), *Synthetic Diamond: Emerging CVD Science and Technology*, John Wiley & Sons, Inc., New York, 1994.
- [19] D. Pletcher, F.C. Walsh, *Industrial Electrochemistry*, 2nd ed., Chapman and Hall, London, 1990.
- [20] H.B. Martin, A. Argoitia, U. Landau, A.B. Anderson, J.C. Angus, Hydrogen and oxygen evolution on boron-doped diamond electrodes, *J. Electrochem. Soc.* 143 (1996) 133–136.
- [21] G.M. Swain, The susceptibility to surface corrosion in acidic fluoride media: a comparison of diamond, HOPG, and glassy carbon electrodes, *J. Electrochem. Soc.* 141 (1994) 3382–3393.
- [22] J. Wu, J. Zhu, L. Shan, N. Cheng, Voltammetric and amperometric study of electrochemical activity of boron-doped polycrystalline diamond thin film electrodes, *Anal. Chim. Acta* 333 (1996) 125–130.
- [23] A. Manivannan, M.S. Seehra, A. Fujishim, Detection of mercury at the ppb level in solution using boron-doped diamond electrodes, *Fuel Process. Technol.* 85 (2004) 513–519.
- [24] A. Manivannan, L. Ramakrishnan, M.S. Seehra, E. Granite, J.E. Butler, D.A. Tryk, A. Fujishima, Trace analysis of mercury at boron-doped diamond electrodes, *J. Electroanal. Chem.* 577 (2005) 287–293.
- [25] O. Fusun, F.N. Ertaş, İ.İ. Gökcel, H. Tural, Anodic stripping voltammetric behavior of mercury in chloride medium and its determination at a gold film electrode, *Turk. J. Chem.* 29 (2005) 355–366.
- [26] A. Apilux, W. Siangproh, N. Praphairaksit, A. O. Chailapakul, Simple and rapid colorimetric detection of Hg(II) by a paper-based device using silver nanoplates, *Talanta* 97 (2012) 388–394.
- [27] S.D. Borgo, V. Jovanovski, S.B. Hocevar, Antimony film electrode for stripping voltammetric measurement of Hg(II) in the presence of Cu(II), *Electrochim. Acta* 88 (2013) 713–717.
- [28] A.M. Ashrafi, K. Vytřas, Stripping voltammetric determination of mercury(II) at antimony-coated carbon paste electrode, *Talanta* 85 (2011) 2700–2702.
- [29] L. Tayebi, S. Sobhanardakani, A. Farmany, M. Cheraghi, Mercury content in edible part of otoliths ruber marketed in Hamedan, Iran, *WASET* 5 (2011) 11–20.
- [30] J. Wei, D. Yang, H. Chen, Y. Gao, H. Li, Stripping voltammetric determination of mercury(II) based on SWCNT-PhSH modified gold electrode, *Sens. Actuators B Chem.* 190 (2014) 968–974.
- [31] F.E. Aroui, S. Lahrach, A. Farahi, M. Achak, L.E. Gaini, B. Manoun, M. Bakasse, A. Bouzidi, M.A.E. Mhammedi, Electrochemical determination of mercury(II) in ambient water at palladium oxide/graphite composite electrodes, *J. Taiwan Inst. Chem. E.* (2014) (In press).
- [32] P.K. Aneesh, S.R. Nambiar, T.P. Rao, A. Ajayaghosh, Electrochemical synthesis of a gold atomic cluster–chitosan nanocomposite film modified gold electrode for ultra-trace determination of mercury, *Phys. Chem. Chem. Phys.* 16 (2014) 8529–8535.
- [33] R. Lai, E.L. Huang, F. Zhou, D.Q. Wipf, Selective determination of methylmercury by flow-injection fast-scan voltammetry, *Electroanalysis* 10 (1998) 926–930.
- [34] P. Richter, M.I. Toral, B. Abbott, Anodic stripping voltammetric determination of mercury in water by using a new electrochemical flow through cell, *Electroanalysis* 14 (2014) 1288–1293.



ELSEVIER

Contents lists available at ScienceDirect

Talanta

journal homepage: www.elsevier.com/locate/talanta

Polyaniline/graphene quantum dot-modified screen-printed carbon electrode for the rapid determination of Cr(VI) using stopped-flow analysis coupled with voltammetric technique

Eakkasit Punrat^a, Chakkarin Maksuk^{a,b}, Suchada Chuanuwatanakul^a,
Wanida Wonsawat^{c,*}, Orawon Chailapakul^{a,**}

^a *Electrochemistry and Optical Spectroscopy Research Unit, Department of Chemistry, Faculty of Science, Chulalongkorn University, Phayathai Road, Pathumwan, Bangkok 10330, Thailand*

^b *Program in Biotechnology, Faculty of Science, Chulalongkorn University, Phayathai Road, Pathumwan, Bangkok 10330, Thailand*

^c *Department of Chemistry, Faculty of Science and Technology, Suan Sunandha Rajabhat University, U-Thong Nok Road, Dusit, Bangkok 10300, Thailand*

ARTICLE INFO

Article history:

Received 17 September 2015

Received in revised form

10 December 2015

Accepted 10 December 2015

Available online 11 December 2015

Keywords:

Chromium(VI)

Polyaniline

Graphene quantum dot

Stopped-flow analysis

Voltammetry

ABSTRACT

Polyaniline/graphene quantum dots (PANI/GQDs) were used to modify a screen-printed carbon electrode (SPCE) in a flow-based system. A method for rapidly determining the Cr(VI) concentrations by using stopped-flow analysis has been developed using an Auto-Pret system coupled with linear-sweep voltammetry using the PANI/GQD-modified SPCE. The GQDs, synthesized in a bottom-up manner from citric acid, were mixed with aniline monomer in an optimized ratio. The mixture was injected into an electrochemical flow cell in which electro-polymerization of the aniline monomer occurred. Under conditions optimized for determining Cr(VI), wide linearity was obtained in the range of 0.1–10 mg L⁻¹, with a detection limit of 0.097 mg L⁻¹. For a sample volume of 0.5 mL, the modified SPCE can be used continuously with a sample-throughput of more than 90 samples per hour. In addition, this proposed method was successfully applied to mineral water samples with acceptable accuracy, and the quantitative agreement was accomplished in deteriorated Cr-plating solutions with a standard traditional method for Cr(VI) detection.

© 2015 Elsevier B.V. All rights reserved.

1. Introduction

Since graphene was isolated from highly oriented pyrolytic graphite using the mechanical exfoliation method known as the “Scotch-tape method”, which was reported by Geim and Novoselov in 2004 [1], research into graphene’s characteristic and potential application has grown exponentially due to its excellent mechanical, thermal, optical and electrical properties [2]. Recently, graphene-based nanomaterials such as graphene oxide (GO) [3], graphene nanoribbons (GNRs) [4] and graphene quantum dots (GQDs) [5] have gained interest in various fields of research. GQD especially displays unique optical and electrical properties due to the quantum confinement effect [6]. GQD is a chemically inert, low

toxicity and low cost nanomaterial compared to other nanomaterials. Moreover, it is a water-soluble nanocarbon [7]. Therefore, GQDs are attractive for use in analytical chemistry applications, particularly in spectroscopy [8–11] and electrochemistry [12].

Polyaniline (PANI) is a conducting polymer that is ideal for improving the sensitivity of electrochemical detection because it is easy to prepare, stable and provides good electrical conductivity [13,14]. The conductivity of polyaniline has made its composite useful for application in solar cells [15,16], super-capacitors [17], and analytical sensors [18–20].

Chromium is extensively used and exists abundantly in two oxidation states of Cr(III) and Cr(VI) which are both toxic, but Cr(VI) is the primary subject of concern for various international environmental agencies because it has more mutagenic properties than Cr(III) [21,22]. The maximum permissible concentration of Cr(VI) in drinking water according to the US Environmental Protection Agency is 0.1 mg L⁻¹ [23], which is one reason why the accurate determination of Cr(VI) levels is very important in water analysis.

Screen-printing technology has emerged as an exciting tool for

* Corresponding author at: Department of Chemistry, Faculty of Science and Technology, Suan Sunandha Rajabhat University, U-Thong Nok Road, Dusit, Bangkok 10300, Thailand. Fax: +66 2 160 1146.

** Corresponding author at: Fax: +66 2 254 1309.

E-mail addresses: Wanida.Wo@ssru.ac.th (W. Wonsawat), corawan@chula.ac.th (O. Chailapakul).

preparing electrodes for electrochemical detection and has provided a new opportunity to perform electrochemical techniques for environmental applications outside of a laboratory. Screen-printing also lends itself to the mass production of highly reproducible electrodes with consistent chemical makeup. The preferred material for this purpose is carbon due to its low price and ease of production. Although many kinds of screen-printed carbon electrodes (SPCEs) are commercially available, SPCEs can be easily fabricated at the laboratory scale and the SPCE surface can be modified with ease to fit the aim of an analysis related to a specific analyte. Over the past several years, SPCEs have been successfully applied to improve analysis by incorporating various modifiers into the surface, including enzymes, immuno-reagents, noble metals and inorganic nanocomposites [24–30].

As mentioned above, PANI and GQDs were used to modify a SPCE in this research for increasing the electrochemical response, and the modified SPCE exhibits direct electron transfer [5]. A flow-based technique using an Auto-Pret system was developed to promote the automation of electrode modification. The Auto-Pret system is well known as a sequential injection system that provides high precision and compatibility with several detection modes [31–33]. Using the Auto-Pret system, the synthesized GQDs were used to modify SPCEs by electro-polymerization of polyaniline composites.

This is the first report on the on-line determination of Cr(VI) using on-line electro-polymerization of aniline monomer and GQDs mixture on SPCE with very short analysis time. The aim of this study was to develop a rapid method for quantifying Cr(VI) concentrations with good accuracy and precision by using the Auto-Pret system coupled with electrochemical detection using a novel PANI/GQD-modified SPCE. The proposed method was applied to the determination of the Cr(VI) concentration in mineral drinking water and in deteriorated Cr-plating samples.

2. Experimental

2.1. Chemicals and materials

Cr(VI) standard solutions were prepared from potassium dichromate ($K_2Cr_2O_7$) purchased from BDH Laboratory Supplies, England. Potassium chloride (KCl), sodium hydroxide (NaOH) and sulfuric acid (fuming 95–97% H_2SO_4) were acquired from Merck, Germany. Citric acid (99.8%) was obtained from Farmitalia Carlo Erba, Italy. Aniline monomers were purchased from Sigma, St. Louis, MO. In addition, in the interference study, several cation solutions were prepared from chloride and sulfate salts including NaCl, KCl, $MgCl_2$, $CaSO_4 \cdot 2H_2O$, $CuSO_4$, and $FeCl_3$ (Sigma-Aldrich, USA), while others were prepared by diluting standard solutions (atomic absorption standard solution, 1000 mg L^{-1} , BDH Chemicals, England) of $Zn(NO_3)_2$, $Pb(NO_3)_2$, $Cd(NO_3)_2$. Anion solutions were prepared from the following sodium and potassium salts: NaCl, Na_2SO_4 , K_2CO_3 , NaH_2PO_4 , and $NaNO_3$ (Sigma-Aldrich, USA). Ultra purified water ($R \geq 18.2 \text{ M}\Omega \text{ cm}^{-1}$, Milli-Q water from Merck Millipore, Singapore) was used throughout the experiments.

Screen-printed carbon electrodes (SPCEs) used in this research were prepared in-house by screen-printing carbon ink (Electrodag PF-407C, Acheson, USA) onto a PVC substrate. The SPCEs, as shown in Fig. 1, were dried in an oven at $55 \text{ }^\circ\text{C}$ for 1 h. Next, the screen-printing and drying steps were repeated again to obtain the SPCE that was subsequently modified with polyaniline/graphene quantum dots (PANI/GQDs) by electro-polymerization using the Auto-Pret system. Next, the PANI/GQD-modified SPCE was used as a working electrode for Cr(VI) detection.

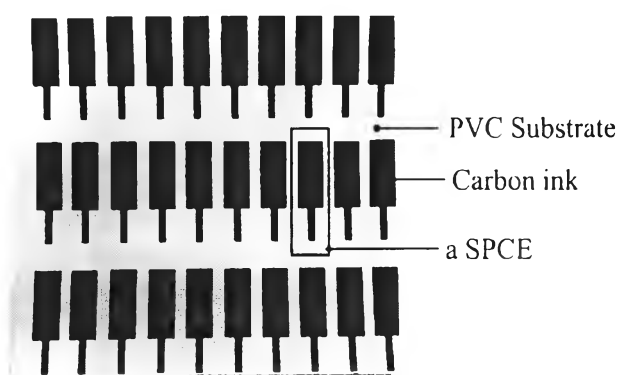


Fig. 1. Screen-printed carbon electrodes (SPCEs).

2.2. Apparatus

The Auto-Pret system with the MGC Auto-Pret MP-014S model (MGC Japan), which consists of a 2.5 mL syringe pump with a 3-way syringe valve, an 8-port selection valve, a 6-port switching valve (not used in this research), a 3.0 mL PTFE holding coil (0.8 mm i.d.), and PTFE tubing (0.8 mm i.d.) with PEEK connectors, was used for the on-line modification of the electrodes and the determination of Cr(VI). The Auto-Pret system was computer-controlled by SIA MPV ver 5.0 software (MGC Japan). All electrochemical measurements were carried out in a complete flowcell (cross-flow MF-1093, Bioanalytical System Inc., USA) using a portable 910 PSTAT Mini potentiostat (Metrohm Autolab, Switzerland). The complete flowcell consisted of a 0.5 mm thick silicone gasket as a spacer, and a three-electrode configuration of a PANI/GQD-modified SPCE, an Ag/AgCl electrode (3 M NaCl) and stainless steel outlet tube as a working electrode, a reference electrode and a counter electrode, respectively.

A schematic diagram of the Auto-Pret system coupled with the electrochemical detection method for the modification of PANI/GQDs on a SPCE and the determination of the Cr(VI) concentration is shown in Fig. 2. The experiments were performed under air-conditioned room temperature ($\sim 25 \text{ }^\circ\text{C}$).

2.3. Preparation of graphene quantum dots (GQDs)

The GQDs were prepared by an easy bottom-up method using the pyrolysis of citric acid [6]. Briefly, 2 g of citric acid was heated and melted by a heating mantle at $200 \text{ }^\circ\text{C}$. After 30 min of heating, the melted citric acid became orange due to the formation of the GQDs. The liquid was instilled into 100 mL of 10 mg mL^{-1} NaOH solution drop by drop while vigorous stirring. Next, the solution was adjusted to pH 4 with a 1.0 M H_2SO_4 solution and diluted to 250.00 mL in a volumetric flask with ultra-purified water. The obtained GQDs solution was kept refrigerated at $4 \text{ }^\circ\text{C}$.

2.4. On-line modification of PANI/GQDs on a SPCE

The electrode-modifying solution was a mixture of aniline monomer and GQD solution that was prepared as follows. A $90 \text{ }\mu\text{L}$ aliquot of aniline monomer was pipetted into a 10.00 mL volumetric flask and $360 \text{ }\mu\text{L}$ of GQD solution was added. The mixture was then sonicated for 5 min before adding 2.50 mL of 4 M H_2SO_4 and diluting the solution to the final volume of 10.00 mL with Milli-Q water. The result was an electrode-modifying solution containing 1:4 v/v aniline monomer and GQD solution in 1 M H_2SO_4 .

The step sequence for on-line modification of PANI/GQDs on a SPCE using the Auto-Pret system coupled with the potentiostat is

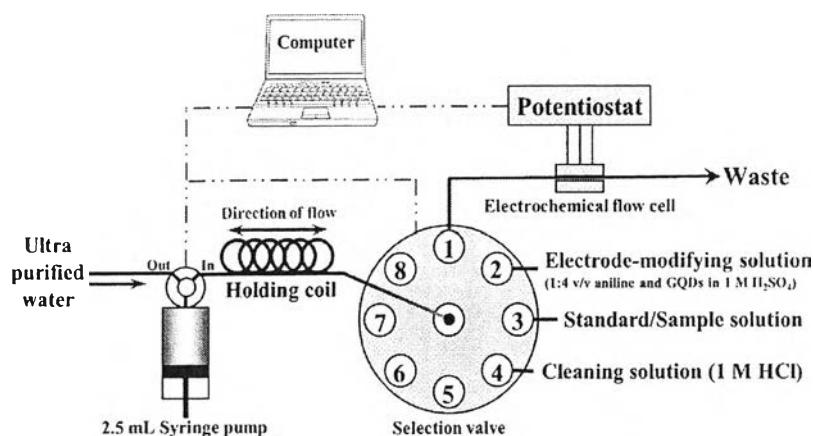


Fig. 2. Schematic diagram of the Auto-Pret system coupled with electrochemical detection for on-line modification of the SPCE with PANI/GQD and the determination of Cr(VI) concentrations.

Table 1

Step sequence for on-line modification of PANI/GQD on a SPCE by electro-polymerization using the Auto-Pret system coupled with a potentiostat.

Step	Operating description	Auto-Pret system				Potentiostat	Time (s)
		Selection valve position	Syringe pump status	Volume (μL)	Flow rate ($\mu\text{L s}^{-1}$)		
1	Aspirate an electrode-modifying solution into the holding coil	Port 2: Aniline/GQD	Aspirate	500	100	Standby	5
2	Dispense the electrode-modifying solution into the flow cell	Port 1: Flow cell	Dispense	500	50	Standby	10
3	Apply cyclic voltammetry for modification of PANI/GQD on the SPCE by electro-polymerization (Scan rate of 50 mV s^{-1} , 10 cycles)	–	Stop	–	–	Potential applied in the range of -1.3 V and $+0.8 \text{ V}$	840
4	Aspirate cleaning solution into the holding coil	Port 4: 1 M HCl	Aspirate	500	100	Standby	5
5	Rinse the PANI/GQD-modified SPCE with the cleaning solution	Port 1: Flow cell	Dispense	500	50	Standby	10

Table 2

Step sequence for the determination of Cr(VI) concentration by stopped-flow analysis with the Auto-Pret system coupled with linear sweep voltammetry using PANI/GQD-modified SPCE.

Step	Operating description	Auto-Pret system				Potentiostat	Time (s)
		Selection valve position	Syringe pump status	Volume (μL)	Flow rate ($\mu\text{L s}^{-1}$)		
1	Aspirate a sample solution into the holding coil	Port 3: Sample	Aspirate	500	100	Standby	5
2	Dispense the sample solution into the flow cell	Port 1: Flow cell	Dispense	500	50	Standby	10
3	Apply the accumulation potential to the electrochemical flow cell	–	Stop	–	–	Potential applied at $+0.5 \text{ V}$	5
4	Record the linear sweep voltammogram (scan rate of 50 mV s^{-1})	–	Stop	–	–	Potential applied from $+0.7 \text{ V}$ to -0.2 V	18

shown in Table 1. A volume of $500 \mu\text{L}$ of the electrode-modifying solution was aspirated into the holding coil and subsequently injected through the flowcell, resulting in the entire SPCE surface being covered with the solution. Next, the flow was stopped, the PANI/GQD composite was prepared, and the composited was accumulated on the SPCE by one-step electro-polymerization using cyclic voltammetry. Cyclic voltammetry was carried out for 10 cycles with a scan rate of 50 mV s^{-1} by scanning the potential between -1.3 and $+0.8 \text{ V}$ vs Ag/AgCl, and the aniline monomer was polymerized at anodic potentials [34]. Finally, the PANI/GQD-modified SPCE was rinsed with $500 \mu\text{L}$ of 1 M HCl . The PANI/GQD-modified SPCE was then capable for being used to quantify Cr(VI) levels several times over without renewal or re-modification of the electrode.

2.5. Determination of Cr(VI) by stopped-flow analysis

To determine concentrations of Cr(VI), a $500 \mu\text{L}$ aliquot of the Cr(VI)-containing sample or standard solution was aspirated into the holding coil, and subsequently injected into the flowcell. After the flow stopped, an accumulation potential of $+0.5 \text{ V}$ vs Ag/AgCl was applied for 5 s, and then a linear sweep voltammetry was executed using potentials scanned in the cathodic direction from $+0.7 \text{ V}$ to -0.2 V vs Ag/AgCl with a scan rate of 50 mV s^{-1} . The step sequence is shown in Table 2. Due to the excess volume of sample/standard solution (which can be ascribed to a $200 \mu\text{L}$ -void injection volume), this procedure can be performed continuously for Cr(VI) determination in other samples without employing an electrode cleaning process. The highest sample throughput was

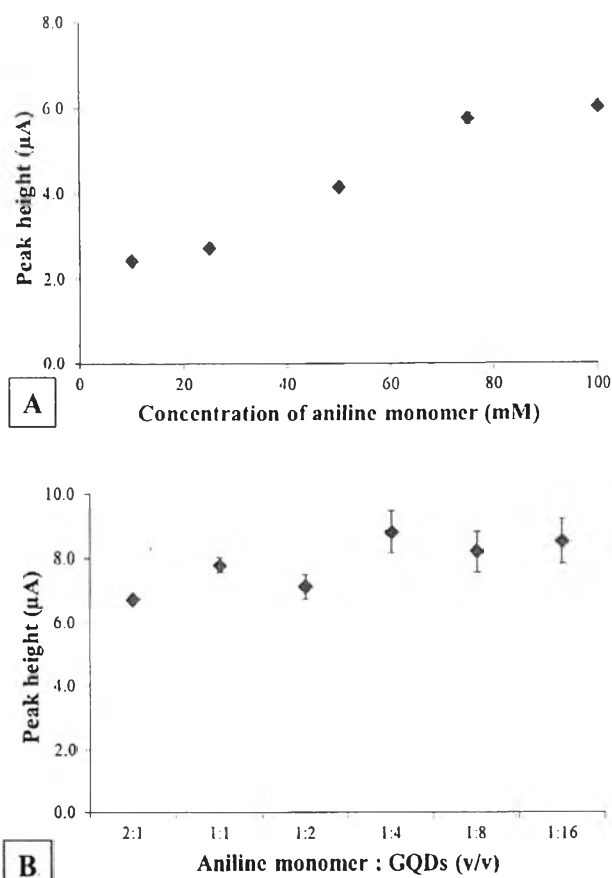


Fig. 3. Effects of the aniline monomer concentration (A) and the aniline monomer solution: GQD solution volume ratio (B) used to modify the SPCE on the Cr(VI) cathodic peak height measured for a solution containing 5 mg L^{-1} Cr(VI) in 1 M HCl.

greater than 90 samples per hour.

3. Results and discussion

3.1. Electrochemical detection of Cr(VI)

Characterization of the electrochemical process of Cr(VI) on the SPCE was carried out by cyclic voltammetry of 5 mg L^{-1} Cr(VI) in 1 M HCl at a scanned potential between -0.5 and $+0.8 \text{ V}$ and with various potential scan rates of 5, 10, 50, 100, and 500 mV s^{-1} . The obtained voltammograms exhibited a cathodic peak corresponding to Cr(VI) at approximately $+0.3 \text{ V}$, while no anodic peak of Cr(VI) was found. Therefore, the electrochemical process of Cr(VI) was irreversible at the scanned potentials. The electrochemical process was found to be limited by diffusion process due to the linear relationship ($R^2 = 0.9979$) between the cathodic peak current and the square root of the potential scan rate [35]. This result proved that other processes, like adsorption that can cause electrode fouling, did not occur. The most well defined cathodic peak of Cr(VI) was obtained by using a potential scan rate of 50 mV s^{-1} , which was chosen for conducting further experiments.

3.2. Optimization of the conditions for PANI/GQD modification on SPCE

Because of the irreversible electrochemical reaction, linear sweep voltammetry was selected instead of CV to quantify Cr(VI).

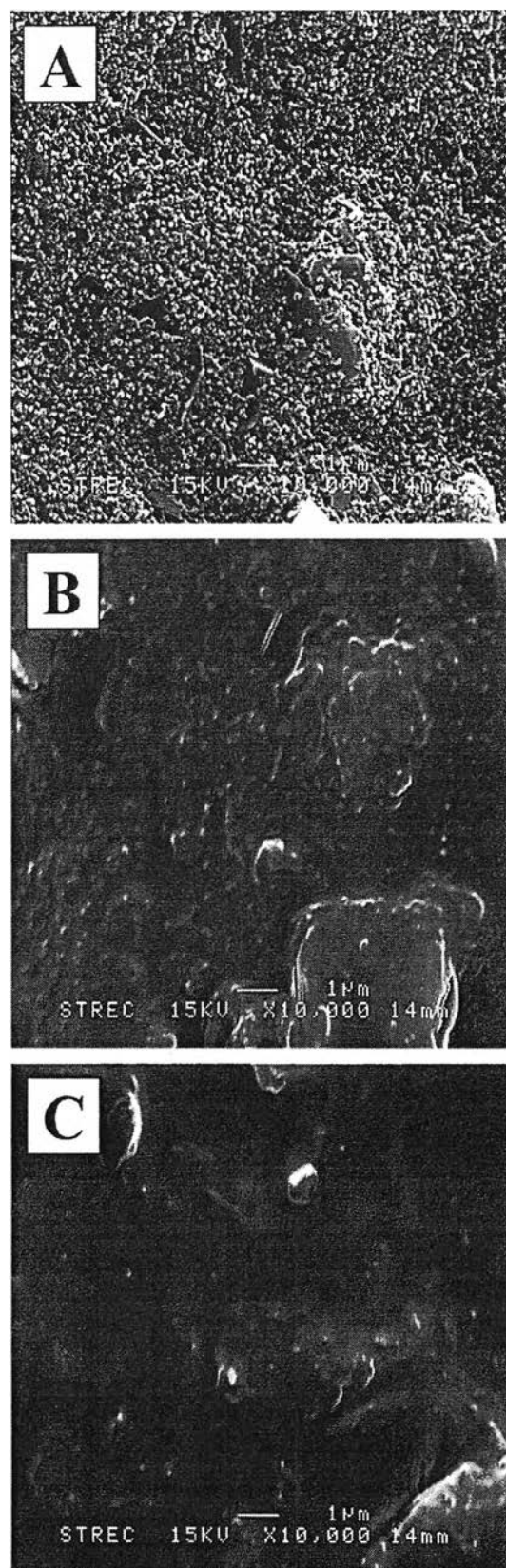


Fig. 4. SEM images of a bare SPCE (A), a PANI-modified SPCE (B), and a PANI/GQD-modified SPCE (C).

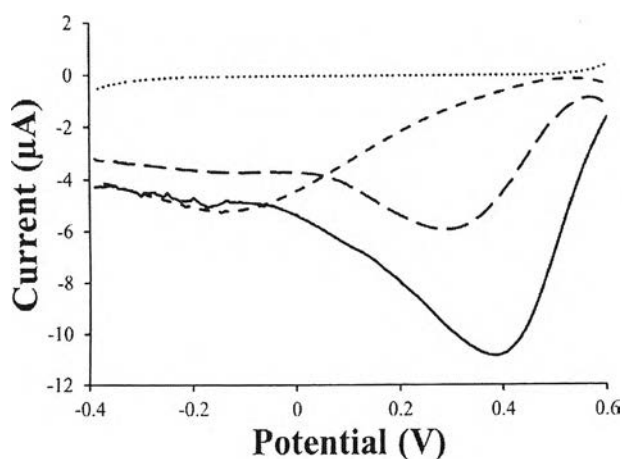


Fig. 5. Typical linear-sweep voltammograms of an 1 M HCl solution (dot line) and a solution containing 5 mg L^{-1} Cr(VI) in 1 M HCl on various electrodes: a bare SPCE (short-dashed line), a PANI-modified SPCE (long-dashed line), and a PANI/GQD-modified SPCE (solid line).

First, the concentration of aniline monomer used for the modification of the SPCE was studied across a range of 10–100 mM. The results are shown in Fig. 3A. It was found that the cathodic peak height of Cr(VI) increased when higher concentrations of aniline monomer were used, because polyaniline (PANI) is a conducting polymer. However, aniline monomer was difficult to dissolve at concentrations higher than 100 mM. The optimum concentration of aniline monomer was therefore 100 mM. Next, the effect of the concentration of GQDs was investigated. Mixtures, in which the final concentration of aniline monomer was held at 100 mM, were varied with aniline monomer and synthesized GQDs ratios of 2:1, 1:1, 1:2, 1:4, 1:8, and 1:16 v/v for SPCE modification. The

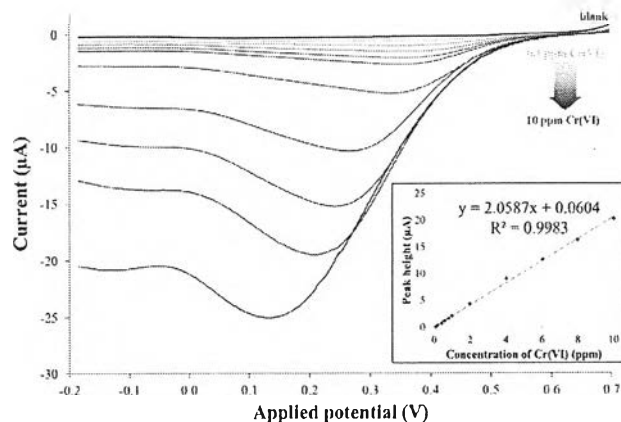


Fig. 7. Representative linear-sweep voltammograms and calibration graph (inset) of Cr(VI) standard solutions at concentrations between 0.1 and 10 mg L^{-1} in 1 M HCl by stopped-flow analysis using a PANI/GQDs-modified SPCE.

voltammograms of 5 mg L^{-1} Cr(VI) were recorded using the modified SPCEs. The resultant Cr(VI) cathodic peak heights are shown in Fig. 3B. The obtained peak height increased when the volume of GQDs increased up to 1:4 v/v of aniline monomer:GQD due to the increment of electrode's surface area by GQDs. However, when using higher volume ratio of GQDs, GQD can partially coagulate increasing the surface area. The solution containing 1:4 v/v aniline monomer and GQDs was chosen as the suitable electrode-modifying solution.

3.3. Characterization of PANI/GQD-modified SPCE

The electrode surface of a PANI/GQD-modified SPCE was characterized using scanning electron microscopy (SEM), as were a

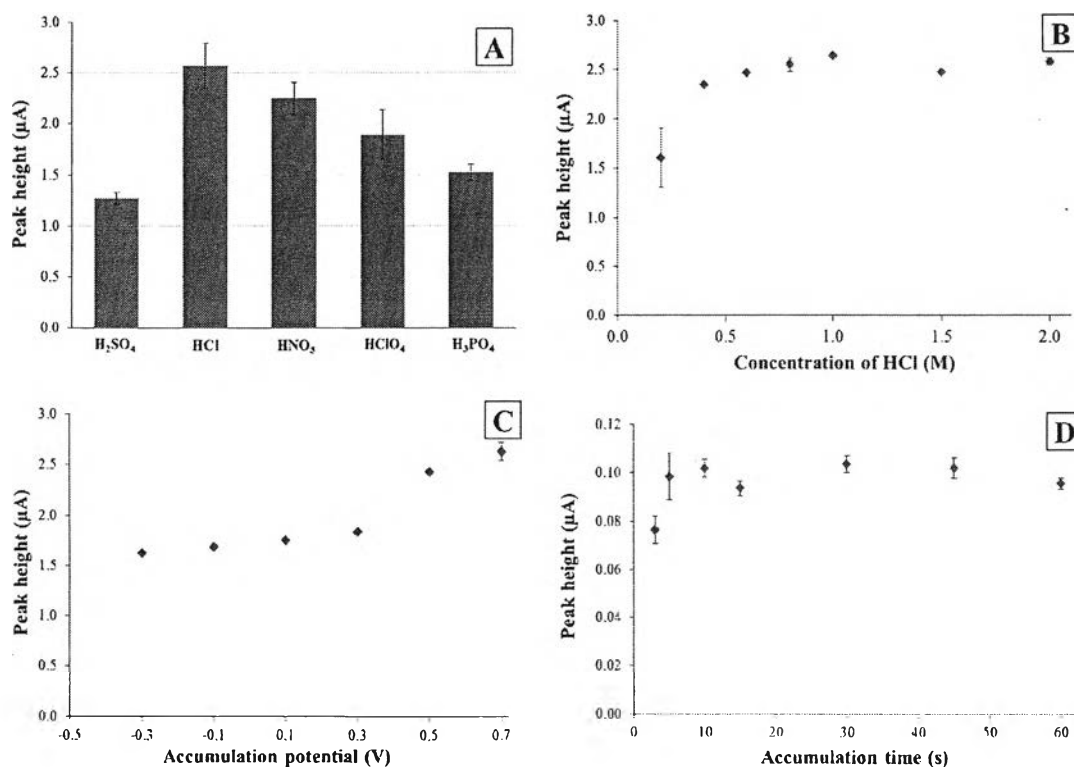


Fig. 6. Effects of type of electrolyte solution (A), concentration of HCl electrolyte solution (B), accumulation potential (C), and accumulation time (D) on the cathodic peak height of Cr(VI) of a solution containing 1 mg L^{-1} of Cr(VI) in 1 M of each electrolyte on a PANI/GQDs-modified SPCE. (Accumulation time (D) was studied in 0.1 mg L^{-1} of Cr(VI) solution.).

Table 3
Comparison of analytical performances between screen-printed electrodes for Cr(VI) detection developed by different authors.

Working electrode	Electrochemical technique	Quantitative range (mg L ⁻¹)	Detection limit (mg L ⁻¹)	Approximate time of analysis	Ref.
PANI/GQD-modified SPCE	Linear sweep cathodic voltammetry	0.1–10	0.097	< 1 min	This work
Quercetin/multi walled carbon nanotubes-modified SPCE	Differential pulse cathodic voltammetry	0.05–10	0.016	15 min	[40]
Glucose oxidase-modified SPCE	Chronoamperometry	0.005–0.04	0.005	10 min	[41]
Thick-film SPCE	Amperometry	0.2–300	0.05	5 min	[42]
Screen-printed gold electrode	Differential pulse cathodic voltammetry	0.1–10	0.05	No report	[43]
Gold nanoparticle-modified SPCE	Square wave voltammetry	0.01–5	0.005	2 min	[44]

Table 4
Tolerance ratios of various interfering ions for the determination of Cr(VI) by using stopped-flow analysis coupled with linear-sweep voltammetry.

Cations	Tolerance ratios	Anions	Tolerance ratios
K ⁺	> 100	Cl ⁻	> 1000
Na ⁺	> 100	SO ₄ ²⁻	> 1000
Mg ²⁺	> 100	CO ₃ ²⁻	> 1000
Ca ²⁺	> 100	PO ₄ ³⁻	> 1000
Zn ²⁺	> 100	NO ₃ ⁻	> 1000
Cd ²⁺	> 100		
Cr ³⁺	> 100		
Pb ²⁺	> 10		
Cu ²⁺	> 10		
Fe ³⁺	> 1		

Table 5
Determination of Cr(VI) in mineral drinking water by stopped-flow analysis coupled with linear-sweep voltammetry.

Samples	Cr(VI) concentration (mg L ⁻¹)		Recovery (%)	RSD (%)
	Spiked	Found		
Mineral water 1	0.00	Not detect	–	–
	0.50	0.43 ± 0.03	85.1	7.0
	2.00	1.61 ± 0.04	80.3	2.5
	4.00	3.90 ± 0.09	97.5	2.3
Mineral water 2	0.00	Not detect	–	–
	0.50	0.41 ± 0.03	81.7	7.3
	2.00	1.64 ± 0.08	82.0	4.9
	4.00	4.25 ± 0.07	106	1.6
Mineral water 3	0.00	Not detect	–	–
	2.00	1.96 ± 0.02	98.1	1.0
	5.00	4.51 ± 0.01	90.2	0.2
	8.00	7.22 ± 0.06	90.3	0.8

bare SPCE and a PANI-modified SPCE for comparison. As shown in Fig. 4, the aniline monomer was electro-polymerized as a PANI film on a SPCE that presented a smooth surface and the surface of PANI/GQD-modified SPCE. Although the PANI-modified and PANI/GQD-modified SPCEs did not appear different from the microscopic images, the reduction of Cr(VI) onto the modified SPCEs was easier than onto bare SPCE, as shown by the fact that the cathodic peak of Cr(VI) on the modified SPCEs appeared at a more positive potential as shown in Fig. 5. In addition, the electrochemical

Table 6
Comparison of the Cr(VI) concentration in deteriorated Cr-plating solution determined by stopped-flow analysis coupled with linear-sweep voltammetry and the DPC standard method.

Samples	Found Cr(VI) concentration (mg L ⁻¹)		<i>t</i> -value of the two method (<i>t</i> _{critical, two-tails, α=0.05} = 3.182)
	This method	DPC standard method	
Cr-plating solution 1	11.9 ± 0.7	15.6 ± 4.9	2.33
Cr-plating solution 2	10.3 ± 1.2	11.2 ± 8.5	0.15

response of the PANI/GQD-modified SPCE was clearly higher than that obtained from a PANI-modified SPCE because GQD has a high surface area that can additionally improve the sensitivity as shown in the supplementary Fig. S1.

3.4. Optimization of conditions for the Cr(VI) determination

The electrolyte solution, a crucial factor in Cr(VI) quantitation, was optimized by studying several types of acid solutions that were chosen because PANI is electrically conductive in acidic media [36]. Five acid, H₂SO₄, HCl, HNO₃, HClO₄ and H₃PO₄, were examined. Linear-sweep voltammograms of 1 mg L⁻¹ Cr(VI) using a PANI/GQD-modified SPCE were recorded in triplicate, and the typical voltammograms are shown in the supplementary Fig. S2. The Cr(VI) peak heights were measured as shown in Fig. 6A. The highest peak was obtained with HCl as an electrolyte, because chloride ion from HCl could improve the signal-to-noise characteristic of Cr(VI) detection [37], in agreement with the work of Compton et al. [38]. The effects of the concentration of the HCl solution were investigated by analyzing 1 mg L⁻¹ Cr(VI) in various HCl concentrations ranging from 0.2 to 2.0 M. The results in Fig. 6B shows that the most suitable electrolyte solution for determining Cr(VI) was 1 M HCl.

To improve sensitivity, an accumulation potential was applied before the accumulated analyte on the electrode surface was reduced in the measuring step. The accumulation time was varied from 5 s to 60 s, and the accumulation potential was tuned to various values between -0.3 and +0.7 V vs Ag/AgCl. As described in Fig. 6C and D, optimal accumulation was achieved by applying a potential of +0.7 V for 5 s providing good sensitivity with little impact on time of analysis.

3.5. Analytical performance of the developed method

A calibration curve was established by plotting Cr(VI) concentrations and cathodic peak heights, as obtained by stopped-flow analysis with linear sweep voltammetry using a PANI/GQD-modified SPCE under the optimal conditions. The relationship was linear across a wide range from 0.1 to 10 mg L⁻¹ Cr(VI) with a slope of 2.059 ± 0.110 μA L mg⁻¹ and an R² of 0.9983 (Fig. 7). The relative standard deviation (RSD) of 10 replicates for Cr(VI) concentrations of 0.1, 4.0 and 10.0 mg L⁻¹ were 6.6, 0.81 and 0.40%,

respectively. The repeatability of this proposed method, therefore, was acceptable according to the AOAC Guideline (%RSD < 8) [39]. To investigate the operation stability, a PANI/GQD-modified SPCE was used to measure a standard solution containing 2 mg L^{-1} Cr(VI) 100 times. The RSD for the 100 replicates was found to be only 4.9%. It shows that the PANI/GQD-modified SPCE can be used at least 100 times with no significant effect on the sensitivity.

The limit of detection (LOD; the concentration corresponding to 3 times the standard deviation (SD) of the obtained blank signal, $n=10$) and the limit of quantification (LOQ; the concentration corresponding to 10 times the SD of the obtained blank signal, $n=10$) were 0.097 and 0.32 mg L^{-1} , respectively. The LOD was in the $\mu\text{g/L}$ range which was similar to the results obtained from previous researches [40–44], however, our method was performed with very short analysis time compared with others as shown in Table 3.

3.6. Interference study

The presence of other cations and anions in a sample could potentially interfere with the developed method, therefore the tolerance ratio tests of several potential interfering cations and anions were performed by recording stopped-flow linear-sweep voltammograms of a solution containing 1 mg L^{-1} Cr(VI) in 1 M HCl in the presence of each interfering ion. A concentration of such ions that changed cathodic peak height by more than 5% was considered to be interfering. The results of this study are listed in Table 4.

When the interfering cations were introduced in 100-fold excess, the results varied significantly: the presence of Pb(II) decreased analyte peak height but Cu(II) and Fe(III) both increased the peak height, while the other cations including Cr(III) had no significant effect. The Fe(III) reduction peak overlapped the Cr(VI) peak, even when the concentration ratio was as low as 1:1. Future work, therefore, will need to address Fe(III) removal from the analysis solution by using additional procedures such as electro-coagulation [45–47], adsorption [48,49] and solvent extraction [50]. The interference of anions, meanwhile, was studied at a high concentration of 1000-fold excess because this is likely the concentration of such anions in environmental samples. It was found that even at this concentration ratio there are no appreciable interferences observed from these anionic species.

3.7. Real sample analysis

To demonstrate the applicability of this method, stopped-flow analysis coupled with linear-sweep voltammetry using the PANI/GQD-modified SPCE was used to evaluate Cr(VI) levels in mineral drinking water samples. The water samples were spiked with Cr(VI) at various concentrations, and were diluted with 4 M HCl (3:1 v/v), so that the working solutions were in 1 M HCl electrolyte. Each solution was analyzed in triplicate using the standard addition method, and the analytical results are summarized in Table 5. The recoveries of the spiked samples ranged from 80.3–106%, with RSDs ($n=3$) below 8%, indicating that the accuracy and precision of this method were acceptable [39].

Complicated samples of deteriorated Cr-plating solutions were also analyzed by using the proposed method. The samples were diluted by a factor of 10 to be within the appropriate concentration range, and were then analyzed using the standard addition method. The results of this method were compared with those obtained by the traditional method for the detection of Cr(VI); that is, by spectroscopy using 1,5-diphenylcarbazide (DPC) as a reagent [51,52]. The samples were diluted 1000-fold before being measured by the DPC method. The results were corrected by multiplication with the dilution factors. To evaluate the two different

methods, the student's *t*-test was used. As shown in Table 6, the calculated *t*-values were smaller than the t_{critical} -value, therefore, it can be concluded that there is no significant difference at a confidence level of 95% between the traditional method and the method proposed here.

4. Conclusion

A rapid method for the determination of Cr(VI) by stopped-flow analysis coupled with linear-sweep voltammetry using a PANI/GQD-modified SPCE has been successfully developed. The method was fully computer-controlled with accurate synchronization between the Auto-Pret system and the potentiostat. The PANI/GQD-modified SPCE was prepared using a simple two-step method and a low-cost screen-printing technique to fabricate the SPCE and on-line modification of the SPCE with PANI/GQD. The modified SPCE could be used several times without any renewal processes. Under optimized conditions, the proposed method provided acceptable accuracy and precision for the rapid determination of Cr(VI) concentrations in aqueous samples with throughput of more than 90 samples per hour. The proposed method has been successfully applied to mineral drinking water and deteriorated Cr-plating solutions, and the results of the latter were statistically equivalent to those obtained by the traditional spectroscopic method. This method, moreover, provided high sensitivity with a detection limit as low as 0.097 mg L^{-1} .

Acknowledgments

The authors are grateful for financial support from the Thailand Research Fund through Research Team Promotion Grant (RTA5780005) and The Thai Government Stimulus Package 2 (TKK2555), under the Project for Establishment of Comprehensive Center for Innovative Food, Health Products and Agriculture (PERFECTA). E.Punrat thanks the Ratchadaphiseksomphot Endowment Fund, Chulalongkorn University for the Postdoctoral Fellowship. We greatly appreciate Prof. Dr. Shoji Motomizu and Asst. Prof. Dr. Lukman Hakim of the Okayama University, Japan for their kind supports regarding the Auto-Pret system.

Appendix A. Supplementary material

Supplementary data associated with this article can be found in the online version at <http://dx.doi.org/10.1016/j.talanta.2015.12.016>.

References

- [1] K.S. Novoselov, A.K. Geim, S.V. Morozov, D. Jiang, Y. Zhang, S.V. Dubonos, I. V. Grigorieva, A.A. Firsov, Electric Field Effect in Atomically Thin Carbon Films, *Science* 306 (2004) 666–669.
- [2] A.K. Geim, Graphene: Status and Prospects, *Science* 324 (2009) 1530–1534.
- [3] K. Toda, R. Furue, S. Hayami, Recent progress in applications of graphene oxide for gas sensing: a review, *Anal. Chim. Acta* 878 (2015) 43–53.
- [4] X. Li, X. Wang, L. Zhang, S. Lee, H. Dai, Chemically Derived, Ultrasmooth Graphene Nanoribbon Semiconductors, *Science* 319 (2008) 1229–1232.
- [5] S. Benítez-Martínez, M. Valcárcel, Graphene quantum dots in analytical science, *Trends Anal. Chem.* 72 (2015) 93–113.
- [6] Y. Dong, J. Shao, C. Chen, H. Li, R. Wang, Y. Chi, X. Lin, G. Chen, Blue luminescent graphene quantum dots and graphene oxide prepared by tuning the carbonization degree of citric acid, *Carbon* 50 (2012) 4738–4743.
- [7] Q. Li, B.W. Noffke, Y. Liu, L.-S. Li, Understanding fundamental processes in carbon materials with well-defined colloidal graphene quantum dots, *Current Opinion in Colloid & Interface Science*, DOI (<http://dx.doi.org/10.1016/j.cocis.2015.10.008>).

- [8] Y. Dong, G. Li, N. Zhou, R. Wang, Y. Chi, G. Chen, Graphene Quantum Dot as a Green and Facile Sensor for Free Chlorine in Drinking Water, *Anal. Chem.* 84 (2012) 8378–8382.
- [9] J. Ju, W. Chen, Synthesis of highly fluorescent nitrogen-doped graphene quantum dots for sensitive, label-free detection of Fe (III) in aqueous media, *Biosens. Bioelectron.* 58 (2014) 219–225.
- [10] L. Lin, M. Rong, F. Luo, D. Chen, Y. Wang, X. Chen, Luminescent graphene quantum dots as new fluorescent materials for environmental and biological applications, *Trac. Trends Anal. Chem.* 54 (2014) 83–102.
- [11] V. Stengl, S. Bakardjeva, J. Henych, K. Lang, M. Kormunda, Blue and green luminescence of reduced graphene oxide quantum dots, *Carbon* 63 (2013) 537–546.
- [12] C.S. Lim, K. Hala, A. Ambrosi, R. Zboril, M. Pumera, Graphene and carbon quantum dots electrochemistry, *Electrochem. Commun.* 52 (2015) 75–79.
- [13] G. Čirić-Marjanović, Recent advances in polyaniline research: Polymerization mechanisms, structural aspects, properties and applications, *Synth. Met.* 177 (2013) 1–47.
- [14] U. Rana, N.D. Paul, S. Mondal, C. Chakraborty, S. Malik, Water soluble polyaniline coated electrode: a simple and nimble electrochemical approach for ascorbic acid detection, *Synth. Met.* 192 (2014) 43–49.
- [15] S. Ghani, R. Sharif, S. Bashir, A. Ashraf, S. Shahzadi, A.A. Zaidi, S. Rafique, N. Zafar, A.H. Kamboh, Dye-sensitized solar cells with high-performance electrodeposited gold/polyaniline composite counter electrodes, *Mater. Sci. Semicond. Process.* 31 (2015) 588–592.
- [16] K. Saranya, M. Rameez, A. Subramania, Developments in conducting polymer based counter electrodes for dye-sensitized solar cells – An overview, *Eur. Polym. J.* 66 (2015) 207–227.
- [17] V.R. Gedela, V.V.S.S. Srikanth, Electrochemically active polyaniline nanofibers (PANi NFs) coated graphene nanosheets/PANi NFs composite coated on different flexible substrates, *Synth. Met.* 193 (2014) 71–76.
- [18] N. Ruecha, N. Rodthongkum, D.M. Cate, J. Volckens, O. Chailapakul, C.S. Henry, Sensitive electrochemical sensor using a graphene–polyaniline nanocomposite for simultaneous detection of Zn(II), Cd(II), and Pb(II), *Anal. Chim. Acta* 874 (2015) 40–48.
- [19] I. Fratoddi, I. Venditti, C. Cametti, M.V. Russo, Chemiresistive polyaniline-based gas sensors: a mini review, *Sensors Actuators B: Chem.* 220 (2015) 534–548.
- [20] P.-Z. Liu, X.-W. Hu, C.-J. Mao, H.-L. Niu, J.-M. Song, B.-K. Jin, S.-Y. Zhang, Electrochemiluminescence immunosensor based on graphene oxide nanosheets/polyaniline nanowires/CdSe quantum dots nanocomposites for ultrasensitive determination of human interleukin-6, *Electrochim. Acta* 113 (2013) 176–180.
- [21] S. Langard, M. Costa, *Handbook on the Toxicology of Metals*, in: G.F.N.A. F. Nordberg (Ed.), *Handbook on the Toxicology of Metals*, Fourth Edition, Academic Press, San Diego, 2015, pp. 717–742, Chapter 33–Chromium.
- [22] B. Markiewicz, J. Komorowicz, A. Sajnóg, M. Belter, D. Baralkiewicz, Chromium and its speciation in water samples by HPLC/ICP-MS – technique establishing metrological traceability: a review since 2000, *Talanta* 132 (2015) 814–828.
- [23] United States Environmental Protection Agency (EPA), Chromium in drinking water (<http://water.epa.gov/drink/info/chromium/>), 2012.
- [24] M.F. Bergamini, D.P. Santos, M.V.B. Zanoni, Determination of isoniazid in human urine using screen-printed carbon electrode modified with poly-L-histidine, *Bioelectrochemistry* 77 (2010) 133–138.
- [25] F.R. Caetano, A. Gevaerd, E.G. Castro, M.F. Bergamini, A.J.G. Zarbin, L. H. Marcolino-Junior, Electroanalytical application of a screen-printed electrode modified by dodecanethiol-stabilized platinum nanoparticles for dopamine determination, *Electrochimica Acta* 66 (2012) 265–270.
- [26] À. Dago, J. Navarro, C. Ariño, J.M. Díaz-Cruz, M. Esteban, Carbon nanotubes and graphene modified screen-printed carbon electrodes as sensitive sensors for the determination of phytochelatin in plants using liquid chromatography with amperometric detection, *J. Chromatogr. A* 1409 (2015) 210–217.
- [27] S. Palanisamy, B. Thirumalraj, S.-M. Chen, M.A. Ali, F.M.A. Al-Hemaid, Palladium nanoparticles decorated on activated fullerene modified screen printed carbon electrode for enhanced electrochemical sensing of dopamine, *J. Colloid Interface Sci.* 448 (2015) 251–256.
- [28] K. Keawkim, S. Chuanuwatanakul, O. Chailapakul, S. Motomizu, Determination of lead and cadmium in rice samples by sequential injection/anodic stripping voltammetry using a bismuth film/crown ether/Nafion modified screen-printed carbon electrode, *Food Control.* 31 (2013) 14–21.
- [29] P. Noyrod, O. Chailapakul, W. Wonsawat, S. Chuanuwatanakul, The simultaneous determination of isoproturon and carbendazim pesticides by single drop analysis using a graphene-based electrochemical sensor, *J. Electroanal. Chem.* 719 (2014) 54–59.
- [30] E. Punrat, S. Chuanuwatanakul, T. Kaneta, S. Motomizu, O. Chailapakul, Method development for the determination of arsenic by sequential injection/anodic stripping voltammetry using long-lasting gold-modified screen-printed carbon electrode, *Talanta* 116 (2013) 1018–1025.
- [31] R.K. Katarina, M. Oshima, S. Motomizu, On-line collection/concentration and determination of transition and rare-earth metals in water samples using Multi-Auto-Pret system coupled with inductively coupled plasma-atomic emission spectrometry, *Talanta* 78 (2009) 1043–1050.
- [32] R.B.R. Mesquita, A.O.S.S. Rangel, A review on sequential injection methods for water analysis, *Anal. Chim. Acta* 648 (2009) 7–22.
- [33] C.L.C. Silvestre, P.C.A.G. Pinto, M.A. Segundo, M.L.M.F.S. Saraiva, J.L.F.C. Lima, Enzyme based assays in a sequential injection format: A review, *Anal. Chim. Acta* 689 (2011) 160–177.
- [34] E. Asadian, S. Shahrokhan, A.I. zad, E. Jokar, In-situ electro-polymerization of graphene nanoribbon/polyaniline composite film: Application to sensitive electrochemical detection of dobutamine, *Sensors Actuators B: Chem.* 196 (2014) 582–588.
- [35] A.J. Bard, L.R. Faulkner, *Electrochemical methods: fundamentals and applications*, 2nd ed., John Wiley & Sons, Inc., New York, 2000.
- [36] G. Boara, M. Sparpaglione, Synthesis of polyanilines with high electrical conductivity, *Synth. Met.* 72 (1995) 135–140.
- [37] I. Švancara, M. Galik, K. Vytras, Stripping voltammetric determination of platinum metals at a carbon paste electrode modified with cationic surfactants, *Talanta* 72 (2007) 512–518.
- [38] C.M. Welch, O. Nekrassova, R.G. Compton, Reduction of hexavalent chromium at solid electrodes in acidic media: reaction mechanism and analytical applications, *Talanta* 65 (2005) 74–80.
- [39] AOAC International, *Append. K.: Guid. Diet. Suppl. Bot.* (2012) (http://www.eoma.aoc.org/app_k.pdf).
- [40] S. Sadeghi, A. Garmroodi, A highly sensitive and selective electrochemical sensor for determination of Cr(VI) in the presence of Cr(III) using modified multi-walled carbon nanotubes/quecetin screen-printed electrode, *Mater. Sci. Eng.: C* 33 (2013) 4972–4977.
- [41] A. Calvo-Pérez, O. Domínguez-Renedo, M. Alonso-Lomillo, M. Arcos-Martínez, Speciation of chromium using chronoamperometric biosensors based on screen-printed electrodes, *Anal. Chim. Acta* 833 (2014) 15–21.
- [42] S.A. Miscoria, C. Jacq, T. Maeder, R. Martin Negri, Screen-printed electrodes for electroanalytical sensing, of chromium VI in strong acid media, *Sensors Actuators B: Chem.* 195 (2014) 294–302.
- [43] D. Li, J. Li, X. Jia, Y. Xia, X. Zhang, E. Wang, A novel Au–Ag–Pt three-electrode microchip sensing platform for chromium(VI) determination, *Anal. Chim. Acta* 804 (2013) 98–103.
- [44] G. Liu, Y. Y. Lin, H. Wu, Y. Lin, Voltammetric Detection of Cr(VI) with Disposable Screen-Printed Electrode Modified with Gold Nanoparticles, *Environ. Sci. Technol.* 41 (2007) 8129–8134.
- [45] D. Ghosh, H. Solanki, M.K. Purkait, Removal of Fe(II) from tap water by electrocoagulation technique, *J. Hazard. Mater.* 155 (2008) 135–143.
- [46] J.A.G. Gomes, P. Daida, M. Kesmez, M. Weir, H. Moreno, J.R. Parga, G. Irwin, H. McWhinney, T. Grady, E. Peterson, D.L. Cocke, Arsenic removal by electrocoagulation using combined Al–Fe electrode system and characterization of products, *J. Hazard. Mater.* 139 (2007) 220–231.
- [47] M. Kobyá, U. Gebologlu, F. Ulu, S. Oncel, E. Demirbas, Removal of arsenic from drinking water by the electrocoagulation using Fe and Al electrodes, *Electrochimica Acta* 56 (2011) 5060–5070.
- [48] P. Mondal, C.B. Majumder, B. Mohanty, Effects of adsorbent dose, its particle size and initial arsenic concentration on the removal of arsenic, iron and manganese from simulated ground water by Fe³⁺ impregnated activated carbon, *J. Hazard. Mater.* 150 (2008) 695–702.
- [49] A.T. Paulino, L.B. Santos, J. Nozaki, Removal of Pb²⁺, Cu²⁺, and Fe³⁺ from battery manufacture wastewater by chitosan produced from silkworm chrysalides as a low-cost adsorbent, *React. Funct. Polym.* 68 (2008) 634–642.
- [50] J.H. Luo, J. Li, X.X. Duan, Study on removal of Fe³⁺ from sodium dihydrogen phosphate by emulsification solvent extraction, *J. Ind. Eng. Chem.* 19 (2013) 727–731.
- [51] Standard method for the examination of water and wastewater, 19th ed., American Public Health Association, Washington DC, 1995.
- [52] Environmental Protection Agency (EPA), Method 7196A.

DOI: 10.1002/elan.201600568

Graphene Oxide-Modified Electrode Coated with *in-situ* Antimony Film for the Simultaneous Determination of Heavy Metals by Sequential Injection-Anodic Stripping Voltammetry

Prasongporn Ruengpirasiri,^[a] Eakkasit Punrat,^[a] Orawon Chailapakul,^[a] and Suchada Chuanuwatanakul^{*[a]}

Abstract: The proposed chemically modified electrode was graphene oxide that was synthesized via Hummer's method followed by reduction of antimony film by *in-situ* electrodeposition. The experimental process could be concluded in three main steps: preparation of antimony film, reduction of analyte ions on the electrode surface and stripping step under the conditions of square wave anodic stripping voltammetry (SWASV). A simple and rapid approach was developed for the determination of heavy metals simultaneously based on a sequential injection (SI), an automated flow-based system, coupled with voltammetric method using antimony-graphene

oxide modified screen-printed carbon electrode (SbF-GO-SPCE). The effects of main parameters involved with graphene oxide, antimony and measurement parameters were also investigated. Using SI-SWASV under the optimal conditions, the proposed electrode platform has exhibited linear range from 0.1 to 1.5 M. Calculated limits of detection were 0.054, 0.026, 0.060, and 0.066 μM for Cd (II), Pb(II), Cu(II) and Hg(II), respectively. In addition, the optimized method has been successfully applied to determine heavy metals in real water samples with acceptable accuracy of 94.29 – 113.42 % recovery.

Keywords: Graphene oxide · Antimony film · Heavy metal · Screen-printed electrode · Sequential injection analysis

1 Introduction

The use of the chemically modified electrode extremely improves the sensitivity of the quantitative electrochemical measurements. Recently, the discovery of nanotechnology reveal that these outstanding nanomaterial were interesting to use as a modifier of electrode. The nanomaterials have attached much interest for the modification of electrodes due to their great chemical and electronic properties in comparison with conventional materials. Especially, graphene is a relatively new material discovered in 2004. The incredible electrical natures of graphene have been widely studied and used in electrical devices, composites, and sensors [1]. Graphene oxide, which is one of derivatives of graphene [2], has functional groups such as hydroxyl and carbonyl, which are advantageous for adsorbing heavy metal ions. The decorated oxygen groups allowed GO to produce stable dispersion in various non polar and polar solvents such as water which is commonly used as solvents for supporting electrolyte. Moreover, it is stable under both acidic and basic conditions [2b]. Interestingly, very few reports on the graphene oxide decorated with metal film or metal oxides nanoparticles could be found in electrochemical detecting of heavy metal ions. Huang and coworkers [3] reported that the SnO₂/reduced graphene oxide nanocomposite modified glassy carbon could be used for the simultaneous and sensitive electrochemical detection of Cd(II), Pb(II), Cu(II), and Hg(II) in drinking water. This

modified electrode showed a very great sensitivity and selectivity upon heavy metal ions using square wave anodic stripping voltammetry (SWASV). However, the synthesis of nanoparticles was complicated, time consuming and under extreme conditions.

On the other hand, the traditional material that is very popularly used for determination of heavy metal ions is mercury because of superior electroanalytical performance. Unfortunately, mercury is very toxic, therefore it is hard to handling, storage, and disposal. Alternative materials which have the same capability to mercury are bismuth and antimony due to intermetallic compounds of analytes and these materials. Because the bismuth film modified electrode was not suitable for determination of copper(II) and mercury(II) ions [4], antimony film modified electrode [5] became an attractive material for simultaneous detection of cadmium(II), lead(II), copper (II), and mercury(II). Hocevar and coworkers [6] reported the *in-situ* antimony film carbon paste electrode (SbF-CPE) as an electrochemical sensor. The comparison of

[a] P. Ruengpirasiri, E. Punrat, O. Chailapakul, S. Chuanuwatanakul
Electrochemistry and Optical Spectroscopy Research Unit, Department of Chemistry, Faculty of Science, Chulalongkorn University, Phayathai Road, Pathumwan, Bangkok, 10330 Thailand
E-mail: suchada.c@chula.ac.th

different modified electrodes showed that the antimony film modified electrode has a lower baseline and the better peak shape. This modified electrode revealed a great stripping current responses of Cd(II) and Pb(II) ions using SWASV. Antimony film was proved to be potential for detection of heavy metal ions in the same way as mercury did with lower toxicity [7]. The synergistic influence of GO which can increase electrode surface area and higher heavy metal ion adsorption and antimony which help formation of intermetallic compounds of analytes would be a good combination for improvement of sensitivity because only antimony is not enough to increasing detectable signal [8].

To make the determination more automatic, a sequential injection (SI) system is used as an automated approach to sample handling that allows automating *in-situ* antimony film modification of electrode and SWASV procedures in a rapid, precise, and efficient manner. Small solution zones are manipulated under controlled dispersion conditions in narrow bore tubing. This system will reduce human's error, glassware and risk of health problems of the operator on direct contact with toxic metal ions. Guzványi, Imato and coworkers [9] reported the alternative applying of antimony-film modified glassy carbon electrode in SI system for determination of Pb(II) and Cd(II) by ASV. The antimony film was electrodeposited from an antimony(III) solution onto the electrode surface after that analyte metals were deposited from a sample solution automatically under SI system. This modified electrode performed a great reproducibility. The developed SI-ASV process was practically used in a tap water sample. In order to achieve more convenient usage, screen-printed electrodes (SPEs) were a promising candidate as a platform to modify and combine with SIA system because of their reproducibility, mass production, disposable, and miniaturized size which provide a chance to be a part of portable instrumentation [10].

The aim of this work was to improve the sensitivity of simultaneous quantification of heavy metal ions by the use of antimony film in combination with graphene oxide to increase the electron transfer rate in the system and enhance the adsorption of heavy metal ions at the electrode surface.

2 Experimental

2.1 Chemicals and Reagents

All reagents used in this study were analytical reagent grade and were used without further purification. Ultrapure water from Milli-Q water purification system (Millipore, Bedford, USA) of 18 M Ω cm resistivity was used to prepare reagents and solutions. Antimony, cadmium, lead, copper and mercury standard stock solutions (1000 mg L⁻¹, atomic absorption standard solution) were obtained from BDH (BDH, UK). Hydrochloric acid (HCl) were purchased from Merck (Merck, Germany). Graphite powder (particle size < 20 μ m) was from Sigma-Aldrich.

For the interferences study, five cations stock solutions were prepared by dilution from each standard stock solution (1000 mg L⁻¹) which are NaCl, KCl, MgCl₂, CaCl₂, and AlCl₃ (analytical grade, Wako Pure Chemical Industries, Japan). And seven anions stock solutions of each anion were prepared by dissolving the following sodium salts (analytical grade, Wako Pure Chemical Industries, Japan) which are NaF, NaBr, NaNO₃, NaHCO₃, Na₂CO₃, and Na₂SO₄.

2.2 Instrumentations

A sequential injection (SI) system (MGC Auto-Pret MP-014S, MGC, Japan) comprising of a 8-port selection valve, a 6-port switching valve (not be used in this work), a 2.5 mL syringe pump and 5.74 mL holding coil was used. This system was controlled via SIA MPV Lite ver. 2.50 software (MGC, Japan). The electrochemical measurements were carried out at room temperature in a transparent in-house developed flow cell with the antimony film-graphene oxide modified screen-printed carbon electrode (SbF-GO-SPCE) as the working electrode, a stainless steel tube counter electrode and a Ag/AgCl (3 mol L⁻¹ NaCl) reference electrode (RE-3 V model, Bioanalytical System Inc., USA). All measurements were performed using a potentiostat, PGSTAT 101 instrument (Autolab Eco Chemie, The Netherlands) attached to a personal computer with data acquisition software (NOVA version 1.11.2, Eco Chemie). The surface morphology characterization was carried out by a scanning electron microscope JSM-5410LV (JEOL, Japan).

2.3 Preparation of the Modified Electrode

Graphene oxide was first synthesized by Hummers' method [11]. Then, the graphene oxide modified screen-printed carbon electrodes (GO-SPCEs) were fabricated in house using carbon ink (Electrodag PF-407C, Acheson, USA) mixed with graphene oxide at appropriate amount on PVC substrate. After that, electrodes were baked to dry in an oven at 55 °C for 1 hour. The SbF-GO-SPCE was prepared by on-line *in-situ* electrodepositing the antimony film from a solution consisting of Sb(III) and HCl, at optimum conditions.

2.4 Analytical Procedure

The *in-situ* antimony film modification of the GO-SPCE and SWASV measuring steps are shown in Table 1. The sample solution and the Sb(III) solution were sequentially aspirated into the holding coil. Next, the deposition potential was set at -1.4 V vs Ag/AgCl while solutions were flowed directly to the flow cell as electrodeposition of antimony film and the preconcentration of analytes. Then, the flow was stop for 10 s as equilibration. Square wave voltammogram with a frequency of 50 Hz, a step potential of 6 mV, and an amplitude of 40 mV was recorded from -1.4 V to +0.4 V vs Ag/AgCl. Lastly, the

Table 1. Step sequence for the Sb film modification of the GO-SPCE and the determination of heavy metal ions by SI-SWASV.

Step	Description	Valve position	Flow rate ($\mu\text{L s}^{-1}$)	Duration (s)	Electrode Potential (V)
1	Aspirate sample solution into holding coil	5	200	5	+ 0.4
2	Aspirate Sb(III) solution into holding coil	6	200	2.5	+ 0.4
3	Dispense Sb(III) solution and sample solution into flow cell	8	10	150	-1.4
4	Equilibration	8	0	10	-1.4
5	Stripping and recording of voltammogram	8	0	5	-1.0 to + 0.4
6	Aspirate 0.5 M HCl into holding coil	4	200	2.5	-
7	Dispense 0.5 M HCl into flow cell for electrode cleaning	8	30	17	-

electrode was cleaned to remove any remaining analyte metals and antimony film in flowing supporting electrolyte at flow rate of $30 \mu\text{L s}^{-1}$ for 17 seconds without any applied potential. One measurement cycle for 4 analytes including Cd(II), Pb(II), Cu(II), and Hg(II) is about 3 min. A 0.5 M HCl solution was used as a supporting electrolyte for all steps. Every experiment was performed without removing oxygen from the solutions.

2.5 Sample Preparation

For real sample analysis, water samples were prepared by mixing 0.05 mL of sample solution and specific volume of metal standard solutions. Then, the prepared solutions were diluted with the supporting electrolyte which is 0.5 M HCl to the final volume of 10 mL. After that, the concentration from standard addition method and the percent recovery from spiked sample solutions were calculated by analytical curve.

3 Results and Discussion

3.1 Characterization of Synthesized Graphene Oxide

Graphene oxide was obtained 6.27 grams from 4.0 grams of graphite powder. The Attenuated Total Reflectance Fourier Transform infrared (ATR-FTIR) spectra of graphite and graphene oxide are shown in Figure S1. It can be seen that a characteristic peaks of graphene oxide are O–H stretching vibration at 3208 cm^{-1} , C=O stretching vibration at 1717 cm^{-1} and the remaining sp^2 stretching vibration at 1617 cm^{-1} [2a, 12].

UV-visible spectroscopy was also used to characterize graphene oxide (Figure S2). The spectrum of graphene oxide has an absorption peak at 232 nm. This peak is attributed to $\pi \rightarrow \pi^*$ transition of aromatic C–C bond, and a shoulder at about 300 nm can be assigned to the $\pi \rightarrow \pi^*$ transition of C=O bonds. Also, this result, which is consistent with the result by ATR-FTIR, confirms the existence of oxygen-containing functional groups in graphene oxide [13].

3.2 Comparison of Working Electrodes

The SWASV response towards metals detection using various modified electrodes was compared including bare electrodes (SPCE), GO-SPCEs, SbF-SPCEs, and SbF-GO-SPCEs as shown in Figure 1. The result showed that, when using SbF-GO-SPCE, the anodic current was raised by 5 to 7 times higher than SPCE. We believed that the increase of electrochemical response is due to the synergistic influence of GO and SbF. These electrode modifiers were an interesting combination because GO can increase active electrode surface of working electrode and SbF can improve SWASV performance due to the intermetallic formation between antimony and these metals of interest during accumulation step of SWASV. Therefore, the proposed SbF-GO-SPCE was chosen as an electrochemical detector in sequential injection system for the further experiment.

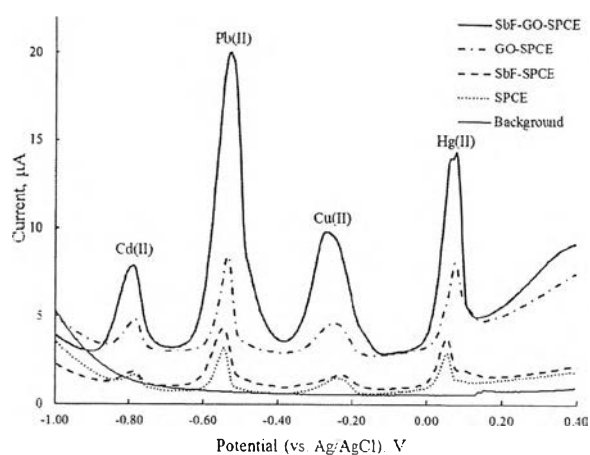


Fig. 1. Comparison of SPCE (dot line), SbF-SPCE (dash line), GO-SPCE (dash dot line) and SbF-GO-SPCE (solid line) upon the stripping voltammetric response at $100 \mu\text{g L}^{-1}$ of Pb(II), Cd(II), Cu(II), and Hg(II). Other conditions: supporting electrolyte of 0.5 M HCl, deposition potential of $-1.4 \text{ V vs. Ag/AgCl}$, frequency of 50 Hz, amplitude of 40 mV. Electrode conditions: 1% (w/w) of GO, $500 \mu\text{g L}^{-1}$ of Sb(III) solution.

To investigate the morphology of electrode, scanning electron microscopy (SEM) was performed. The SEM

images illustrated that the electrodeposited antimony film was successfully covered the area of the electrode (Figure S3b) compared to GO-SPCE (Figure S3a). Moreover, the SEM images of antimony film present the different shape from GO-SPCE. The results indicate that the SbF and GO can be an alternative electrode modifier which can enhance the electrochemical performance of the detector in in sequential injection system.

To understand more about the factor that improve proposed method, the evaluation of effective areas of SbF-GO-SPCEs, GO-SPCEs and SPCEs were calculated by using Randles-Sevcik equation [14]. The slope of the relationship between I_{pa} versus $v^{1/2}$ for each electrode were obtained. For a reversible process,

$$I_{pa} = (2.69 \times 10^5) n^{2/3} A_{eff} D^{1/2} v^{1/2} C_0$$

For 5 mM $K_3[Fe(CN)_6]$, $n=1$, D (diffusion coefficient) = $7.6 \times 10^{-6} \text{ cm}^2 \text{ s}^{-1}$, the effective surface areas were shown in Table 2.

Table 2. The calculated effective electrode surface area.

Electrodes	Slope ($\text{A s}^{1/2} \text{V}^{-1/2}$)	A_{eff} (cm^2)
SPCEs	1.05×10^{-5}	7.08×10^{-11}
GO-SPCEs	1.37×10^{-5}	9.24×10^{-11}
SbF-GO-SPCEs	2.06×10^{-5}	13.9×10^{-11}

From the results showed that after modified SPCEs with GO, the effective surface area increased which consistent to the SEM image that illustrate roughly surface. Moreover, when coated GO-SPCEs with antimony film, the surface area also increased. This result suggested that the synergistic influence of GO and SbF was achieved by increasing both surface area and co-electrodeposition into antimony film.

3.3 Optimization of Parameters and Conditions

3.3.1 Amount of Graphene Oxide in Carbon Ink

GO-SPCEs were fabricated from mixtures of graphene oxide and carbon ink. GO was chosen as an electrode modifier because of their high electrical conductivity and high surface area which provide greater potential for heavy metal analysis. However, they generate a higher background current than bare SPCEs. In order to achieve the highest signal-to-noise ratio for heavy metal detection, the percentages of GO to carbon ink with 0%, 1%, 2%, 3%, and 4% (w/w) were investigated by SI-SWASV. Square wave anodic stripping voltammograms of $100 \mu\text{g L}^{-1}$ Cd(II), Pb(II), Cu(II), and Hg(II) on SbF-GO-SPCEs at various percentages of GO are illustrated in Figure 2a. It can be seen that peak current of both heavy metals decreased with increasing percentage of GO. Owing to increase the electrode surface area of GO could be the

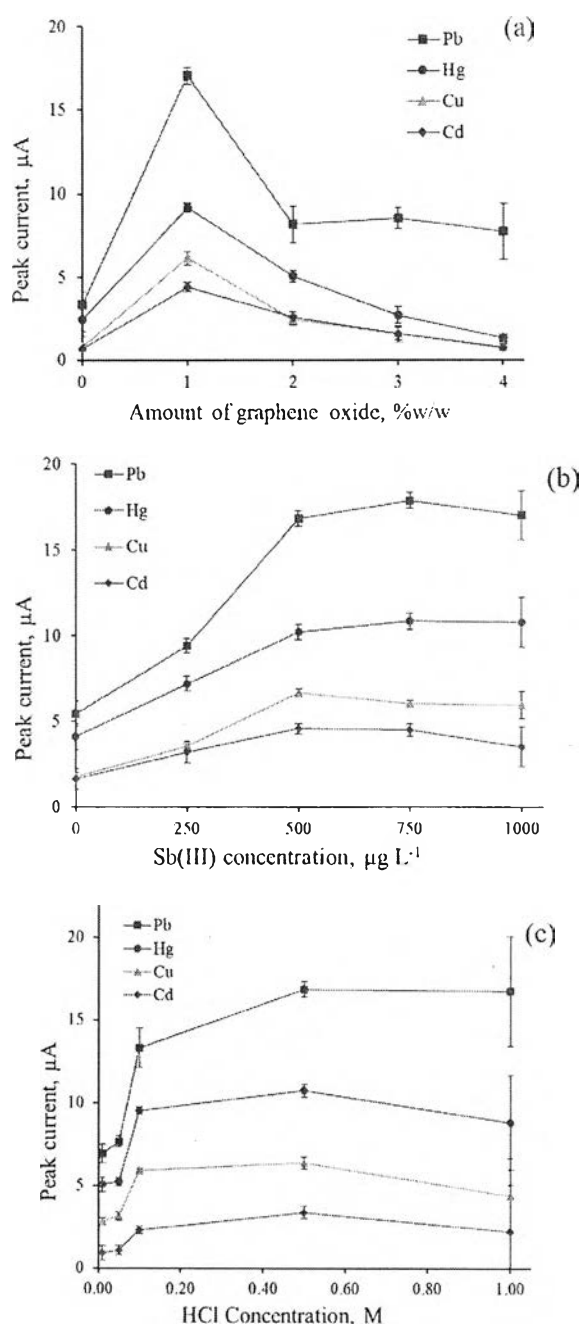


Fig. 2. Effect of the amount of GO (a), concentration of Sb(III) (b), and concentration of HCl (supporting electrolyte) (c) in SbF-GO-SPCE upon the stripping voltammetric response at $100 \mu\text{g L}^{-1}$ of Pb(II), Cd(II), Cu(II), and Hg(II).

result of the larger background current [1a, 15]. Therefore, 1% (w/w) was selected as optimum amount of GO.

3.3.2 Concentration of Antimony(III)

Antimony film was selected to modify on GO-SPCE by on-line in situ electrodeposition between each analysis. Sb (III) solution was introduced into the flow system

followed by aspiration of sample solution into the holding coil. Then, all solutions were dispensed to detection zone in the flow cell in order that the antimony was electro-deposited first, followed by the heavy metals in the sample solution. After finished each detection, the Sb film was cleaned by flowing supporting electrolyte without applied any potential for 17 s. The concentration of Sb(III) was optimized by varying concentration from 0 to 1000 $\mu\text{g L}^{-1}$ while the volume of Sb(III) solution remained constant. The peak current increased when increased Sb(III) concentration and then reached the highest value at 500 $\mu\text{g L}^{-1}$ of Sb(III) solution with small standard deviation for all heavy metal ions. After that, the signals remained rather constant for Pb(II), Hg(II), and Cu(II) and slightly decreased for Cd(II), as shown in Figure 2b. Therefore, 500 $\mu\text{g L}^{-1}$ of Sb(III) solution was selected as optimum concentration to minimize the amount of Sb(III).

3.3.3 Concentration of Supporting Electrolyte

There has been widely reported that HCl is a good supporting electrolyte for heavy metal analysis [9,16]. The optimization of concentration of HCl as supporting electrolyte was carried out at different concentration from 0.01 to 1.00 M. The results showed that signal of all analytes increased with increasing HCl concentration and slightly decreased after 0.50 M of HCl due to hydrogen evolution at highly negative potential (Figure 2c). The standard deviations for all heavy metal ions at 0.50 M HCl were small. Moreover, at this concentration, it is enough amount of HCl to be a supporting electrolyte and the electrode can be cleaned, therefore 0.50 M of HCl was selected as optimum concentration of supporting electrolyte solution.

3.3.4 Electrochemical Parameters

In order to obtain the best detection and good reproducibility, parameters of SWASV were studied including deposition potential, square wave frequency, square wave amplitude and increment potential. Thus, all conditions were investigated under previous optimized SbF-GO-SPCE and 0.50 M HCl as supporting electrolyte. To begin with, the effect of deposition potential was evaluated from -1.6 to -1.0 V with frequency of 50 Hz, amplitude of 40 mV and increment potential of 6 mV (Figure S4a). For all of heavy metal ions determination, the maximum anodic peak current was achieved with a deposition potential of -1.4 V vs. Ag/AgCl. For other deposition potential, the peaks current were lower and poorer reproducibility (bigger standard deviation). Thus, -1.4 V vs. Ag/AgCl was selected as optimum deposition potential.

The frequency affected to the scan rate of determination system and was evaluated from 10 to 90 Hz at -1.4 V vs. Ag/AgCl as deposition potential, amplitude of 20 mV and increment potential of 4 mV (Figure S4b). The results showed that at 50 Hz high peak current with small standard deviation, well-separated peak shape for all

heavy metal ions and fast determination were achieved. Therefore, optimum frequency of 50 Hz was selected.

Next, square wave amplitude was studied from 20 to 100 mV, with -1.4 V vs. Ag/AgCl as deposition potential, frequency of 50 Hz and increment potential of 4 mV (Figure S4c). The signals of all heavy metals were steadily increased and after 80 mV, signal were started to decrease. Increasing of amplitude also increased all signals for both background and analytes therefore the shape of peaks should be considered. For this reason, amplitude of 40 mV was selected.

Finally, the influence of increment potential was investigated from 2 to 10 mV, with deposition potential of -1.4 V vs. Ag/AgCl, frequency of 50 Hz and amplitude of 4 mV (Figure S4d). The increasing of increment potential would lower the number of points of measurement graph (lower precision of determined peak current position). However, at high increment potential, the signal obtained was high thus the peak current and number of data point must be considered. As a result, increment potential of 6 mV shown enough point for forming the graph and small standard deviation of peak for all heavy metal ions was selected.

3.3.5 Parameters of Flow-Based Operation

The other factors that influence the sensitivity and analysis time of each SWASV detection in flow-based analysis are sample volume and flow rate of the solution in the electrodeposition step. These parameters are related to deposition time, changing the sample volume and/or the flow rate will affect to the deposition time. Hence, the sample volume was set at 1.0 mL. The effect of flow rate was studied in the range of 5 to 40 $\mu\text{L s}^{-1}$ and at different deposition times (Figure 3a). It can be seen that the peak current decreased when the flow rate was increased. The highest signal was obtained at 5 $\mu\text{L s}^{-1}$ however at that speed the analysis was time-consuming and had poor reproducibility. Thus, the flow rate of 10 $\mu\text{L s}^{-1}$ performed high current, smaller standard deviation for all heavy metal ions and shorter analysis time was selected.

After finish each analysis, the antimony film and all deposited metal was cleaned by flowing 0.5 M HCl which was the supporting electrolyte. To reduce waste, cleaning solution volume was investigated. The results showed that at 300 μL of 0.5 M HCl a small peak at around $+0.05$ V was still observed, whereas 500 μL of 0.5 M HCl can clean the electrode surface for all heavy metal ions (Figure 3b). Therefore, 500 μL of 0.5 M HCl was selected as optimum volume of cleaning solution.

3.4 Analytical Performance

Under the optimized conditions, the calibration data for the simultaneous detection of the heavy metal ions was studied in the concentration range of 0.1 to 1.5 μM (Figure 4). The peak currents were found to be directly

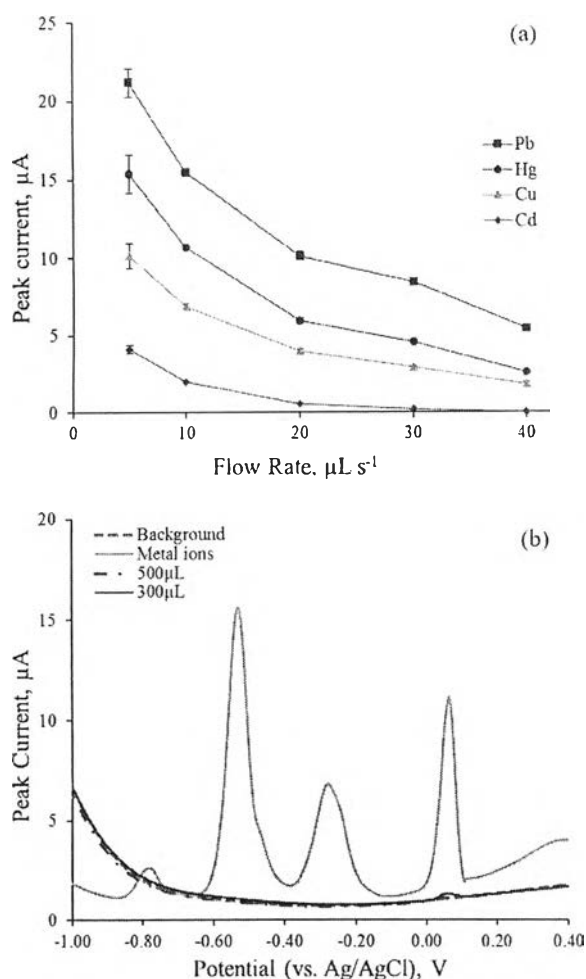


Fig. 3. Effect of the flow rate during deposition (a) and 0.5 M HCl at 500 µL (dash dot line) and 300 µL (solid line) of cleaning solution (b) in SbF/GO/SPCE upon the stripping voltammetric response at 100 µg L⁻¹ of Pb(II), Cd(II), Cu(II), and Hg(II).

proportional to the concentration of all analytes, with good linear regression correlation coefficients (R^2) of 0.996. The limit of detection (LOD) and limit of quantitation (LOQ) were achieved from $3\sigma/S$ and $10\sigma/S$, where σ is the standard deviation of the blank measurement ($n=10$) and S is the slope of curve. Summary of analytical data are presented in Table 3.

Table 3. The analytical performance of simultaneous determination of heavy metal ions by SI-SWASV using SbF-GO-SPCE under optimized conditions.

Metal ion	Linear range (µM)	R^2	LOD (µM)	LOQ (µM)
Cd(II)	0.3-1.5	0.9974	0.054	0.178
Pb(II)	0.1-1.3	0.9971	0.026	0.087
Cu(II)	0.3-1.5	0.9969	0.060	0.202
Hg(II)	0.1-1.3	0.9983	0.066	0.222

Moreover, under the same optimal conditions, each of heavy metal was analyzed separately. The relationship of anodic peak currents and the concentration was obtained (Figure S5). Analytical characteristics for individual determination of heavy metal ions are summarized in Table S1. Under the same condition, it can be seen that LOD of Cd(II), Pb(II) and Cu(II) for individual detection were better when compared to simultaneous detection, however, the LOD of Hg(II) under simultaneous detection was better than that of individual detection. This phenomenon could be explaining by the intermetallic compounds [17] formed among the four target heavy metal ions and the competition for the limited area of active site on the modified electrode, although, the exactly reason for how these ions influence on each other is remain vague at present. Moreover, the activity of each metal is different from each other, thus single determination of Hg(II) was poorer performance because mercury can [17a] form intermetallic compound with the other heavy metal ions and commonly used to improve the sensitivity in heavy metal ions detection. Absent of other metal ions caused the lower sensitivity of Hg(II) as well. Nevertheless, the separation between the anodic stripping peaks is big enough, hence the simultaneous or selective detection using SbF-GO-SPCE is practicable.

The comparison of electrodes reported by several publications for the determination of the analytes are shown in Table 4. Even though the sensitivity of this modified electrode was not the best when compared with some work reported before, SbF-GO-SPCE can be easily fabricated and provided simultaneous analysis of four analytes. Besides, SbF-GO-SPCE could use repeatedly with renewable of electrode surface between successive detection and can also be used for a long total experimental time.

3.5 Interference Study

To analyze these target heavy metal ions in real water sample, various ions in such that water can be found. Hence, the interference of many cations (Na^+ , K^+ , Mg^{2+} , Ca^{2+} and Al^{3+}) and some of anions (F^- , Br^- , NO_3^- , HCO_3^- , CO_3^{2-} and SO_4^{2-}) that might be found in sewage or sea water were investigated. The concentration of all interference was 100-fold higher than analyte concentration. The recovery of all target metal ions was in the range of 95.0 – 105.0% which was acceptable according to Guidelines for Dietary Supplements and Botanicals. The results showed that none of the selected ions were considered interfered with the voltammograms of the solution of all heavy metal ions.

3.6 Real Sample Applications

To evaluate the proposed method, this system was applied under optimized conditions for the simultaneous quantification of all target ions in sewage, fertilizer waste and sea water. All sample solutions were prepared by mixed 50 µL

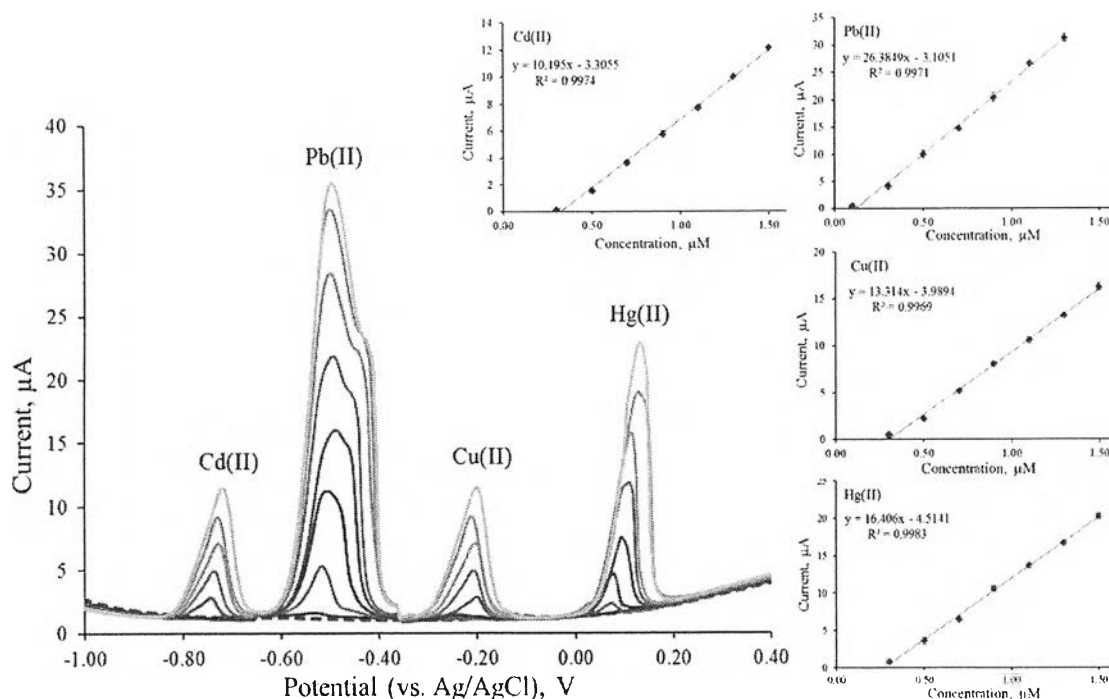


Fig. 4. SI-SWASV signals of the SbF/GO/SPCE at different concentration of Cd(II), Pb(II), Cu(II) and Hg(II) on 0.5 M HCl, simultaneously. Inset is the calibration plot of signal and the heavy metal concentration.

Table 4. The comparison of analytical performances from several electrodes for the determination of the metal ions.

Electrodes	Method	Linear range (µM)	LOD (nM)	Ref.
G/CeO ₂ /GCE	DPASV	Cd(II), 0.2–2.5	0.1	[18]
		Pb(II), 0.2–2.5	0.2	
		Cu(II), 0.2–2.5	0.2	
		Hg(II), 0.2–2.5	0.3	
NG/GCE	DPSV	Cd(II), 0.05–1008	50	[19]
		Pb(II), 0.01–9	5	
		Cu(II), 0.01–5	5	
MWCNT's/ poly(PCV)/ Bi/GCE	DPASV	Cd(II), 0.009–2.7	2	[20]
		Pb(II), 0.005–1	2	
SnO ₂ /RGO/ GCE	SWASV	Cd(II), 0.3–1.2	0.1	[3]
		Pb(II), 0.3–1.2	0.2	
		Cu(II), 0.3–1.2	0.2	
		Hg(II), 0.3–1.2	0.3	
Bi/GR/IL-SPCE	SWASV	Cd(II), 0.009–0.7	0.7	[21]
		Pb(II), 0.005–0.4	0.5	
<i>in-situ</i> Sb/SPCE	DPASV	Cd(II), 0.1–0.6	30	[7a]
		Pb(II), 0.08–0.3	20	
		Cu(II), 0.08–1.6	20	
N/SbF/GCE	AdSV	Cd(II), 0.009–0.1	4	[5]
		Pb(II), 0.005–0.06	2	
		Cu(II), 0.1–1.5	60	
SbF/GO/ SPCE	SWASV	Cd(II), 0.1–1.5	54	This work
		Pb(II), 0.1–1.5	26	
		Cu(II), 0.1–1.5	60	
		Hg(II), 0.1–1.5	66	

of each filtered water sample with 0.5 M HCl which was a supporting electrolyte to final volume of 10 mL. Prepared samples were introduced to determination system without any further pretreatment.

For sewage and fertilizer waste from a metal-plating factory in Thailand, preliminary testing found that only Cu(II) was detected. Thus, standard addition method was used to quantify concentration of copper solely. The average concentration of Cu(II) in sewage and fertilizer were found to be 38.02 µM and 68.70 µM, respectively (Figure S6). In addition, the calculated standard deviations were relatively small, which suggested an acceptable level of reproducibility. To validate the proposed method, the results were compared with standard method obtained by AAS. A paired *t*-test with degrees of freedom of 4 was achieved on the data obtained. The calculated *t*-values between the two pairs of methods were 0.8369 for sewage and 0.2466 for fertilizer waste. Statistical analysis shown that the *t*-value for 4 degree of freedom at 95% confidence interval (2.7764) was greatly larger than the above-mentioned experimental *t*-values. The results indicated that there was no significant difference between two methodologies for the heavy metals determination. It can be concluded that the proposed method is successful and suggesting that these results are reliable and acceptable.

For sea water, the concentration of target ions was studied by calibration method without pretreatment. No anodic peak current of heavy metal ions was obtained in the unspiked sea water sample. The average concentrations of analytes in spiked samples were detected to be

Table 5. Determination of the heavy metal ion concentrations in spiked sea water samples by SI-SWASV using SbF-GO-SPCE under optimized conditions.

Spiked concentration (μM)	Found concentration (μM)			
	Cd(II)	Pb(II)	Cu(II)	Hg(II)
0.00	Not detected	Not detected	Not detected	Not detected
0.30	0.32 ± 0.03	0.32 ± 0.08	0.33 ± 0.03	0.34 ± 0.14
0.50	0.54 ± 0.06	0.52 ± 0.17	0.47 ± 0.05	0.50 ± 0.14
1.00	1.05 ± 0.12	1.01 ± 0.28	1.00 ± 0.17	1.08 ± 0.16

slightly higher than expected amount, with a 94.29 – 113.42% recovery when spiked at 0.30, 0.50, 1.00 μM (Figure S7). However, the reproducibility represented by standard deviations was reliable, which suggested by relatively low standard deviation (Table 5).

3.6 Conclusions

In this study, we successfully developed a new electrochemical platform using *in-situ* antimony film and graphene oxide modified screen-printed electrode coupled with automated SI-SWASV. The purposed system provides relatively low-cost, rapid, selective, and sensitive quantification method for Cd(II), Pb(II), Cu(II) and Hg(II) individually and simultaneously. This method can analyze 18 samples per hour with high precision and small sample consumption over batch analysis system. Finally, it could be shown that applications of real water samples monitoring for heavy metal ion detection was achieved.

4 Acknowledgements

The authors would like to acknowledge the financial support from Thailand Research Fund through Research Team Promotion Grant (RTA5780005), the 90th Anniversary of Chulalongkorn University Fund (Ratchadaphiseksomphot Endowment Fund) and the Electrochemistry and Optical Spectroscopy Research Unit, Department of Chemistry, Faculty of Science, Chulalongkorn University. Eakkasit Punrat is also grateful for financial support from Ratchadaphiseksomphot Endowment Fund for Postdoctoral Fellowship, Chulalongkorn University.

References

- [1] a) A. K. Geim, K. S. Novoselov, *Nat Mater* **2007**, *6*, 183–191; b) V. K. Gupta, M. L. Yola, N. Atar, Z. Ustundag, A. O. Solak, *Electrochim. Acta* **2013**, *112*, 541–548; c) W. K. Chee, H. N. Lim, I. Harrison, K. F. Chong, Z. Zainal, C. H. Ng, N. M. Huang, *Electrochim. Acta* **2015**, *157*, 88–94; d) H. Chang, L. Tang, Y. Wang, J. Jiang, J. Li, *Anal. Chem.* **2010**, *82*, 2341–2346.
- [2] a) M. R. Pourjavid, A. A. Sehat, M. Arabieh, S. R. Yousefi, M. H. Hosseini, M. Rezaee, *Mater Sci Eng C Mater Biol Appl* **2014**, *35*, 370–378; b) A. U. Chaudhry, V. Mittal, B. Mishra, *Mater. Chem. Phys.* **2015**, *163*, 130–137.
- [3] Y. Wei, C. Gao, F. L. Meng, H. H. Li, L. Wang, J. H. Liu, X. J. Huang, *Journal of Physical Chemistry C* **2012**, *116*, 1034–1041.
- [4] a) G. H. Hwang, W. K. Han, J. S. Park, S. G. Kang, *Talanta* **2008**, *76*, 301–308; b) R. O. Kadara, I. E. Tothill, *Anal. Chim. Acta* **2008**, *623*, 76–81.
- [5] V. Arancibia, E. Nagles, C. Rojas, M. Gomez, *Sensors and Actuators B-Chemical* **2013**, *182*, 368–373.
- [6] E. Tesarova, L. Baldrianova, S. B. Hocevar, I. Svancara, K. Vytras, B. Ogorevc, *Electrochim. Acta* **2009**, *54*, 1506–1510.
- [7] a) V. Sosa, C. Barcelo, N. Serrano, C. Arino, J. M. Diaz-Cruz, M. Esteban, *Anal. Chim. Acta* **2015**, *855*, 34–40; b) E. Svobodova-Tesarova, L. Baldrianova, M. Stoces, I. Svancara, K. Vytras, S. B. Hocevar, B. Ogorevc, *Electrochim. Acta* **2011**, *56*, 6673–6677; c) A. M. Ashrafi, S. Cerovac, S. Mudric, V. Guzsvany, L. Husakova, I. Urbanova, K. Vytras, *Sensors and Actuators B-Chemical* **2014**, *191*, 320–325.
- [8] C. W. Foster, A. P. de Souza, J. P. Metters, M. Bertotti, C. E. Banks, *Analyst* **2015**, *140*, 7598–7612.
- [9] V. Guzsvany, H. Nakajima, N. Soh, K. Nakano, T. Imato, *Anal. Chim. Acta* **2010**, *658*, 12–17.
- [10] a) F. Arduini, L. Micheli, D. Moscone, G. Palleschi, S. Piermarini, F. Ricci, G. Volpe, *TrAC, Trends Anal. Chem.* **2016**, *79*, 114–126; b) C. Rojas-Romo, N. Serrano, C. Ariño, V. Arancibia, J. M. Díaz-Cruz, M. Esteban, *Talanta* **2016**, *155*, 21–27; c) C. Barcelo, N. Serrano, C. Ariño, J. M. Díaz-Cruz, M. Esteban, *Electroanalysis* **2016**, *28*, 640–644.
- [11] W. S. Hummers, R. E. Offeman, *J. Am. Chem. Soc.* **1958**, *80*, 1339–1339.
- [12] a) K. Hamsawahini, P. Sathishkumar, R. Ahamad, A. R. Yusoff, *Talanta* **2015**, *144*, 969–976; b) K. Z. Setshedi, M. Bhaumik, M. S. Onyango, A. Maity, *Chem. Eng. J.* **2015**, *262*, 921–931; c) S. Su, B. Chen, M. He, B. Hu, *Talanta* **2014**, *123*, 1–9.
- [13] a) Rattana, S. Chaiyakun, N. Witit-anun, N. Nuntawong, P. Chindaudom, S. Oaew, C. Kedkeaw, P. Limsuwan, *Procedia Engineering* **2012**, *32*, 759–764; b) F. T. Thema, M. J. Moloto, E. D. Dikio, N. N. Nyangiwe, L. Kotsedi, M. Maaza, M. Khenfouch, *Journal of Chemistry* **2013**, *2013*, 6.
- [14] a) J.-S. Ye, Y. Wen, W. De Zhang, H. F. Cui, G. Q. Xu, F.-S. Sheu, *Electroanalysis* **2005**, *17*, 89–96; b) M. P. Siswana, K. I. Ozoemena, T. Nyokong, *Electrochim. Acta* **2006**, *52*, 114–122.
- [15] a) S. Park, R. S. Ruoff, *Nat Nanotechnol* **2009**, *4*, 217–224; b) A. A. Balandin, S. Ghosh, W. Bao, I. Calizo, D. Teweldebrhan, F. Miao, C. N. Lau, *Nano Lett.* **2008**, *8*, 902–907; c) R. F. Service, *Science* **2009**, *324*, 875–877.
- [16] a) W. Wonsawat, S. Chuanwatanakul, W. Dungchai, E. Punrat, S. Motomizu, O. Chailapakul, *Talanta* **2012**, *100*, 282–289; b) E. Punrat, S. Chuanwatanakul, T. Kaneta, S. Motomizu, O. Chailapakul, *Talanta* **2013**, *116*, 1018–1025.
- [17] a) J. Pei, M. L. Tercier-Waeber, J. Buffle, *Anal. Chem.* **2000**, *72*, 161–171; b) A. H. I. Ben-Bassat, A. Azrad, *Electrochim. Acta* **1978**, *23*, 63–69; c) R. J. Grim, *The Journal of Physical*

- Chemistry* **1942**, *46*, 464–469; d) J. Schiewe, K. B. Oldham, J. C. Myland, A. M. Bond, V. A. VicenteBeckett, S. Fletcher, *Anal. Chem.* **1997**, *69*, 2673–2681.
- [18] Y.-L. Xie, S.-Q. Zhao, H.-L. Ye, J. Yuan, P. Song, S.-Q. Hu, *J. Electroanal. Chem.* **2015**, *757*, 235–242.
- [19] H. Xing, J. Xu, X. Zhu, X. Duan, L. Lu, W. Wang, Y. Zhang, T. Yang, *J. Electroanal. Chem.* **2016**, *760*, 52–58.
- [20] M. A. Chamjangali, H. Kouhestani, F. Masdarolomoor, H. Daneshinejad, *Sensors and Actuators B: Chemical* **2015**, *216*, 384–393.
- [21] Z. Wang, H. Wang, Z. Zhang, G. Liu, *Sensors and Actuators B: Chemical* **2014**, *199*, 7–14.

Received: September 6, 2016

Accepted: December 5, 2016

Published online on December 28, 2016



Determination of nickel(II) by ion-transfer to hydroxide medium using sequential injection-electrochemical analysis (SIECA)



Eakkasit Punrat, Panunporn Tutiyaarn, Suchada Chuanuwatanakul, Orawon Chailapakul^a

Electrochemistry and Optical Spectroscopy Research Unit (EOSRU), Department of Chemistry, Faculty of Science, Chulalongkorn University, Phayathai Road, Pathumwan, Bangkok 10330, Thailand

ARTICLE INFO

Keywords:

Nickel detection
Sequential injection analysis
Square-wave voltammetry
Screen-printed carbon electrode
Stripping voltammetry

ABSTRACT

A method for the determination of Ni(II) using ion-transfer to a hydroxide medium has been developed by the sequential injection-electrochemical analysis (SIECA), a combination between an automated flow-based analysis and electrochemical techniques with a homemade screen-printed carbon electrode (SPCE). A sample/standard solution was introduced into an electrochemical flow cell where the Ni(II) in the solution was electrochemically reduced and accumulated on the SPCE. The accumulated Ni was then oxidized to Ni(II) in a hydroxide medium, which led to the formation of nickel hydroxide (Ni(OH)₂) and nickel oxyhydroxide (NiOOH) on the SPCE. The electrochemical response associated with Ni(OH)₂ and NiOOH was subsequently determined by square-wave voltammetry to account for Ni(II). Under optimal conditions, the proposed method provides a low detection limit of 0.02 mg mL⁻¹. This method was further applied to determine the Ni(II) content of standard-spiked mineral water samples with satisfactory results.

1. Introduction

Nickel (Ni) is a silvery-white metallic element found in the Earth's crust. This element is one of the metals that humans have exploited for daily life since its discovery in 1751 [1]. Because of its properties, which include good corrosion resistance and strength, nickel is commonly used to make coins, stainless steels, magnets, jewelry, electronic devices, and even catalyst [2]. Consequently, these industries are common sources of nickel pollution, which can be released into the environment at ppm-level concentration [3]. A large amount of nickel in any environmental compartment must be considered life threatening if it exposes living organisms to the metal. To be more precise, prolonged contact with nickel can cause dermatitis and nasopharyngeal carcinoma [4]. On the basis of the hazards of nickel, the World Health Organization (WHO) has set the Ni concentration limit in drinking water to not exceed 0.07 mg L⁻¹ [5]. Hence, a rapid, sensitive, selective, inexpensive and simple method for determining of Ni needs to be developed to monitor and control the amount of Ni in the environment.

Atomic absorption spectroscopy (AAS) and inductively coupled plasma (ICP) techniques are well-known standard methods for the determination of Ni in water sample [6,7]. Other methods, including UV–visible absorption spectroscopy [8] and capillary electrophoresis [9,10], have also been extensively used for Ni detection. However, these techniques are time-consuming, expensive in terms of instrumenta-

tions and maintenance costs, and non-portable, which makes them inconvenient for fieldwork monitoring. An electrochemical method is a viable alternative for fieldwork monitoring and on-line analysis because it can be miniaturized using relatively low-cost devices; it also features high sensitivity, good selectivity, simplicity, and a short analysis time.

Stripping voltammetry is one of the most powerful electrochemical method for the determination of trace metal ions, including Ni(II), in environmental and biological samples because of its excellent limits of detection, high selectivity and suitability for automated analysis [11,12]. However, the conventional stripping voltammetry provides a low electrochemical signal for Ni because the electrochemical reaction of the Ni(s)/Ni(II) redox couple is an irreversible reduction at a highly negative potential of more than -1.1 V vs SCE [13]. The adsorptive mode of stripping voltammetry overcomes these problems by incorporating dimethylglyoxime (DMG), a chelating agent, into the solution to improve the sensitivity, as reported in several publications [14–16]. However, the chelating agent and its Ni complex are toxic. To avoid any chelating agents, this work therefore proposes an alternative stripping voltammetric method using ion-transfer to a hydroxide medium. Instead of the measuring the Ni(s)/Ni(II) redox couple, Ni(s) is oxidized in a hydroxide solution at a highly positive potential to form nickel oxyhydroxide (NiOOH) and then the electrochemical response of the Ni(II)/Ni(III) redox couple is subsequently recorded by voltammetry. To achieve a convenient and low-cost method, a disposable

^a Correspondence to: Department of Chemistry, Faculty of Science, Chulalongkorn University, Pathumwan, Bangkok 10330, Thailand.
E-mail address: corawan@chula.ac.th (O. Chailapakul).

electrode specifically, a screen-printed carbon electrode (SPCE) was selected because it is easily mass produced at the laboratory scale and because its surface can be easily modified to fit the aim of the analysis related to a specific analyte.

To automatically replace a sample solution with hydroxide solution in the stripping step, sequential injection analysis (SIA) is used as an automated approach because of its high-throughput, precision and accuracy compared to batch analysis. This system requires a small volume of sample and reagents, and the solution zones can be manipulated in narrow-bore tubing. Moreover, SIA can reduce human and glassware errors and mitigate health risks associated with direct contact with toxic chemicals.

Hence, the aim of this work is to develop a chelating-agent-free method for the automated determination of Ni(II) ion content through the electrochemical response of a Ni(II)/Ni(III) redox couple by ion-transfer to a hydroxide medium using sequential injection-electrochemical analysis (SIECA).

2. Experimental

2.1. Chemicals

All chemicals were of analytical grade and used without further purification. Ni(II) standard solution (999 mg L^{-1} , standard solution for AAS) was obtained from Fluka Analytical, New York, USA. Sodium hydroxide (NaOH) and hydrochloric acid (fuming 37% HCl) were purchased from Merck, Germany. Sodium chloride (NaCl) was acquired from Carlo Erba, France. All aqueous solutions were prepared with ultrapure water (resistivity of $18 \text{ M}\Omega \text{ cm}$) from a Milli-Q® water purification system (Merck-Millipore, Singapore). For the interference study, several solutions of heavy-metal ions Pb(II), Cd(II), Zn(II), Cu(II) and Au(III) were prepared from their respective standard solution (1000 mg L^{-1} , analytical grade for AAS, VWR International, Belgium).

2.2. Electrodes and electrochemical flow cell

In-house SPCEs used as a working electrode were fabricated by screen-printing carbon sensor paste (C2030519P4, Gwent Group, Singapore) onto a PVC substrate (0.3 mm thick). The printed PVC plate were baked in an oven for 1 h at $55 \text{ }^\circ\text{C}$ to dry the carbon paste. The carbon paste was printed onto the PVC plate and baked under the same conditions again to obtain SPCEs. The SPCEs were stored in a desiccator at room temperature.

A cross-flow cell, model MF-1093, was purchased from Bioanalytical Systems Inc. (USA). The flow cell consisted of a 1.0-mm-thick silicone gasket as a spacer and a three-electrode system in which a SPCE was used as the working electrode instead of a commercial glassy carbon electrode. An Ag/AgCl electrode (RE-3V, ALS, Japan) and a stainless steel outlet tube of the flow cell were used as the reference electrode and the auxiliary electrode, respectively.

2.3. Instrumentations

A schematic of SIECA for the determination of Ni(II) ion by ion-transfer to a hydroxide medium is shown in Fig. 1. All electrochemical techniques were carried out using a portable potentiostat, PalmSens3 (PalmSens BV, The Netherlands) that was controlled via a laptop with PSTrace 4.4 software. The sequential injection system used in this work was an MGC Auto-Pret MP-014S (MGC Japan) which consisted of a 5.0 mL syringe pump with a syringe valve (PSD/4, Hamilton, USA), a 5.3 mL PTFE holding coil (0.8 mm i.d.), an 8-port selection valve (HVXM 8-5, Hamilton, USA), and a 0.5 mm i.d. PTFE tubing with PEEK connectors. This system was controlled via SIA MPV Ver. 5.0 software (MGC Japan) which included a special command to start the PSTrace 4.4 software. Therefore, the sequential injection system and

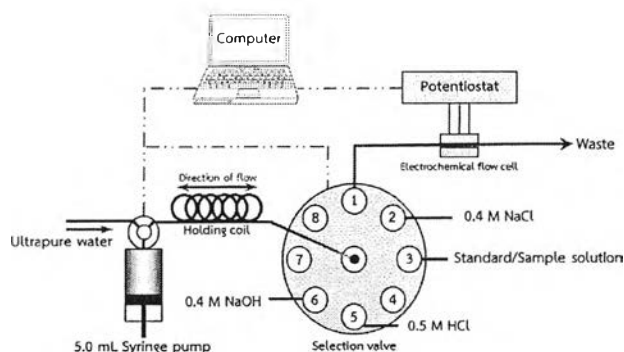
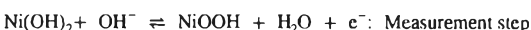
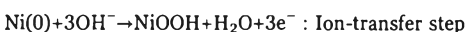
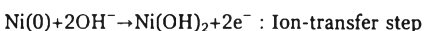
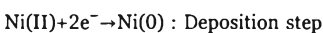


Fig. 1. Schematic of the sequential injection-electrochemical analysis (SIECA) for the determination of Ni(II) concentration by ion-transfer to hydroxide medium.

the potentiostat were completely synchronized for the flow analysis using electrochemical techniques.

2.4. Analytical procedure

To determine Ni(II) concentration by ion-transfer to hydroxide medium using SIECA, the step sequence including important parameters shown in Table 1 was followed. The method can be divided into 5 steps: the initial, deposition, oxidation, measurement, and cleaning steps. Five hundred microliters of a 0.6 M NaOH solution and $1800 \mu\text{L}$ of sample solution were sequentially aspirated into the holding coil in the initial step. In the deposition step, the aspirated solutions were injected in the reverse direction into the flow cell in which the deposition potential (E_{dep}) was applied at $-2.0 \text{ V vs Ag/AgCl}$. The Ni(II) in the sample solution was reduced to Ni(0), which accumulated on the electrode surface. Then, the NaOH solution was injected to push the remaining sample solution out of the flow cell. In the oxidation step, $900 \mu\text{L}$ of a NaOH solution was injected into the flow cell while the oxidation potential (E_{ox}) of $+1.0 \text{ V vs Ag/AgCl}$ was simultaneously applied to oxidize the accumulated Ni in the hydroxide medium to form nickel oxyhydroxide (NiOOH) and nickel hydroxide ($\text{Ni}(\text{OH})_2$) which was oxidized again to NiOOH because of the highly positive potential; this step is called the ion-transfer step. Next, square-wave voltammetry (SWV) was carried out to record the electrochemical response of the Ni(II)/Ni(III) redox couple by scanning the potential from $+0.0$ to $+0.8 \text{ V vs Ag/AgCl}$ with square wave parameters of 50 Hz frequency, 50 mV amplitude and 6 mV potential step. Finally, the electrode was cleaned with 0.5 M HCl solution that flowed through the flow cell at a high flow rate of $50 \mu\text{L s}^{-1}$ while the cleaning potential was applied at $+1.0 \text{ V vs Ag/AgCl}$. The end of the flow stream was a blank solution of 0.4 M NaCl for conditioning the flow cell for the next measurement. All experiments were performed at room temperature ($\sim 25 \text{ }^\circ\text{C}$). The overall mechanisms are as follows:



3. Results and discussion

3.1. Electrochemical behavior of Ni(II)/Ni(III) redox couple in hydroxide medium

According to the step sequence in Table 1, a solution containing 1.00 mg L^{-1} Ni(II) in 0.4 M NaCl was determined by ion-transfer to a hydroxide medium (0.4 M NaOH); hydroxyl compounds of Ni(II) and

Table 1
Step sequence for the determination of Ni(II) concentration by ion-transfer to hydroxide medium using SIECA.

Step	Operating description	Selection valve position ^a	Syringe pump status	Volume (μL)	Flow rate ($\mu\text{L s}^{-1}$)	Electrochemical potential (V)
Initial step						
1	Aspirate a NaOH solution into the holding coil	Port 6	Aspirate	500	100	Standby
2	Aspirate a sample solution into the holding coil	Port 3	Aspirate	1800	100	
Deposition step						
3	Inject the sample solution into the flow cell for electrochemical reduction of Ni(II) ion.	Port 1	Dispense	1800	10	-2.0
4	Push the remaining sample solution out of the flow cell.	Port 1	Dispense	500	50	
Ion-transfer/oxidation step						
5	Aspirate a NaOH solution into the holding coil	Port 6	Aspirate	900	100	+1.0
6	Inject the NaOH solution into the flow cell	Port 1	Dispense	900	30	
Measurement step						
7	Record a square wave voltammogram ^b	-	Stop	-	-	+0.0 to +0.8
Cleaning step						
8	Aspirate a NaCl solution into the holding coil	Port 2	Aspirate	500	100	+1.0 V
9	Aspirate 0.5 M HCl solution into the holding coil	Port 5	Aspirate	3000	200	
10	Clean the electrode and the flow cell	Port 1	Dispense	3500	50	

^a See the description of each port of the selection valve in Fig. 1.

^b Potential step=6 mV; frequency=50 Hz; amplitude=50 mV.

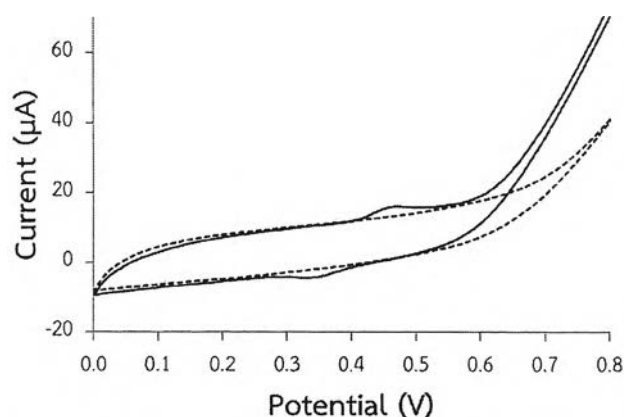


Fig. 2. Typical cyclic voltammograms of the Ni(II)/Ni(III) redox couple in a solution containing 1.00 mg L^{-1} Ni(II) and 0.4 M NaCl , the analysis was achieved by ion-transfer to hydroxide medium (0.4 M NaOH) using SIECA (solid line). The voltammogram of a blank solution, 0.4 M NaCl (dashed line) on a screen-printed carbon electrode is included for comparison.

Ni(III) were formed as Ni(OH)_2 and NiOOH , respectively. The electrochemical behavior of the Ni(II)/Ni(III) redox couple was investigated by cyclic voltammetry in the measurement step. Using a potential scan rate of 0.1 V s^{-1} , we collected cyclic voltammograms of the blank solution (0.4 M NaCl) and the standard solution; the results are shown in Fig. 2. The electrochemical process of the Ni(II)/Ni(III) redox couple in the hydroxide medium represented a quasi-reversible transformation; two well-defined peaks, a cathodic peak and an anodic peak at $+0.34$ and $+0.46 \text{ V}$, respectively, were observed.

3.2. Conditions of deposition step

According to the literatures, sodium chloride (NaCl) has been widely used in several applications as an electrolyte solution for Ni(II) detection by stripping voltammetry due to its good electrical conductivity, ease of uses and preparation, and green chemical properties [17–19]. Therefore, a NaCl solution was used as the electrolyte solution in the present work. The deposition potential and the concentration of NaCl for the detection of Ni(II) using SIECA were optimized by traditional square-wave anodic stripping voltammetry (SWASV) without an ion-transfer technique.

The constant deposition potential was investigated in the range from -1.4 to $-2.0 \text{ V vs Ag/AgCl}$. A standard solution of 1.00 mg L^{-1}

Ni(II) in 0.6 M NaCl was injected through the flow cell with 200 s deposition time to reduce Ni(II) to Ni(0). Next, the electrochemical response of the Ni(0) oxidation was recorded by SWASV with a potential step of 5 mV , a square-wave amplitude of 10 mV and a square-wave frequency of 25 Hz . The effect of the deposition potentials are shown in Fig. 3a. No peak was observed at the deposition potential of -1.4 V , indicating that the potential was not sufficient for reducing Ni(II). The highest peak with the lowest standard deviation was

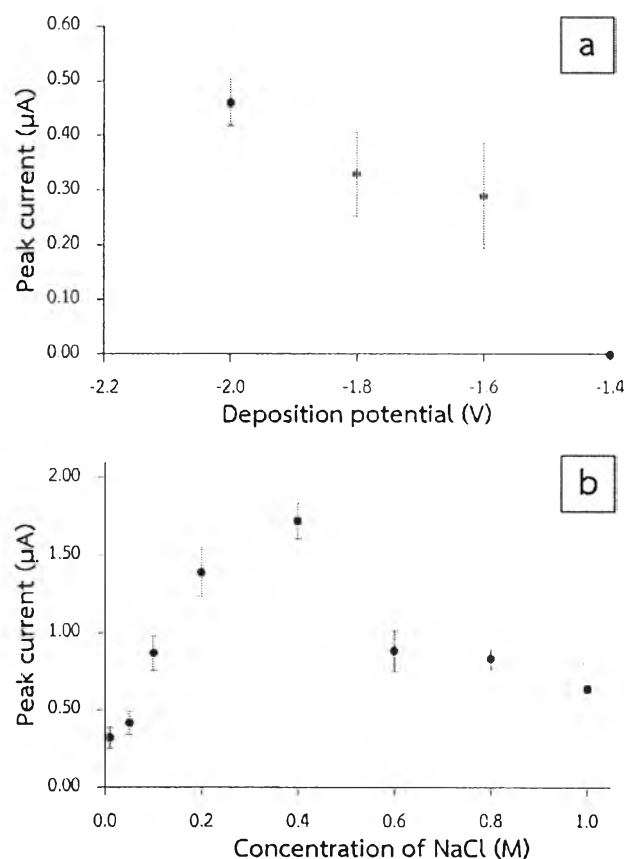


Fig. 3. Effect of the deposition potential (a) and NaCl concentration (b) on the obtained peak current of a standard solution containing 1.00 mg L^{-1} Ni(II) in a NaCl electrolyte solution using the traditional SWASV on a SPCE via SIECA.

obtained using a highly negative potential; therefore, a deposition potential of -2.0 V was chosen.

In addition, the concentration of the NaCl electrolyte solution was also varied in the range from 0.01 to 1.0 M; the results are shown in Fig. 3b. The obtained peak current increased when the concentration of NaCl was increased to 0.4 M because of the increase in the electrical conductivity of the solution; however, the peak current decreased when the concentration of NaCl was increased further because the viscosity of the resulting solution limited the ion mobility. Hence, a NaCl concentration of 0.4 M was used in subsequent experiments.

3.3. Parameters of square-wave voltammetric detection

In this part, the step sequence shown in Table 1 was carried out to determine Ni(II) concentration in a standard solution containing 1.00 mg L⁻¹ Ni(II) and 0.4 M NaCl by ion-transfer to a hydroxide medium using SIECA. Square-wave voltammetry was performed in the measurement step to record the electrochemical response of the Ni(II)/Ni(III) redox couple in the hydroxide medium with varying frequency, amplitude and step potential parameters.

First, the frequency was evaluated in the range from 25 to 100 Hz with an amplitude of 100 mV and a step potential of 10 mV. The highest peak current with a well-defined peak shape and a small standard deviation was achieved at a frequency of 50 Hz (Fig. S1a). Therefore, this frequency was chosen to optimize the next parameter, the square-wave amplitude, which was varied between 10 and 100 mV. The obtained peak currents increased when a higher amplitude was used; however, the standard deviations were larger (Fig. S1b). The suitable amplitude that provided a high response with good precision was 50 mV. Lastly, the step potential was also investigated from 2 to 10 mV. Using a higher step potential theoretically provided a higher peak current (Fig. S1c) but the lowered a number of data points in the voltammogram. Because the number of data point must be considered, the optimal step potential for this proposed method with the highest peak current was 6 mV.

3.4. Conditions of ion-transfer to hydroxide medium

In the oxidation step, 0.4 M NaOH was injected into the flow cell while an oxidation potential of $+1.0$ V vs Ag/AgCl was applied. The flow-based operation of the NaOH injection was considered; hence, flow parameters, including the flow rate and the volume of the NaOH solution, were investigated. Because these parameters were also related to the oxidation time, the oxidation time was studied by varying the volume of the NaOH solution in the range from 500 to 2500 μ L with a fixed flow rate of 50 μ L s⁻¹ such that the oxidation times were between 15 and 55 s (including 5 s aspiration time). The results in Fig. 4a show that the obtained peak currents moderately rose when the volume of the NaOH solution was increased to 1500 μ L (oxidation time of 35 s) and then remained constant when a larger volume was used. Therefore, the NaOH volume of 1500 μ L and the oxidation time of 35 s were determined to be suitable for the analysis.

Furthermore, to reduce reagent consumption, the flow rate of NaOH injection was lowered from 50 to 10 μ L s⁻¹ whereas the oxidation time was fixed at 35 s; therefore, the volume of the NaOH solution varied between 300 and 1500 μ L. The effect of the flow rate is shown in Fig. 4b. The optimal NaOH solution flow rate that provided the highest peak current was 30 μ L s⁻¹.

3.5. Analytical performance

Under the optimized condition for the determination of Ni(II) concentration by ion-transfer to hydroxide medium with SIECA using the step sequence in Table 1, the relationship between the obtained peak current and the Ni(II) concentration was studied over a wide concentration range. A linear calibration curve with $R^2=0.9930$ was

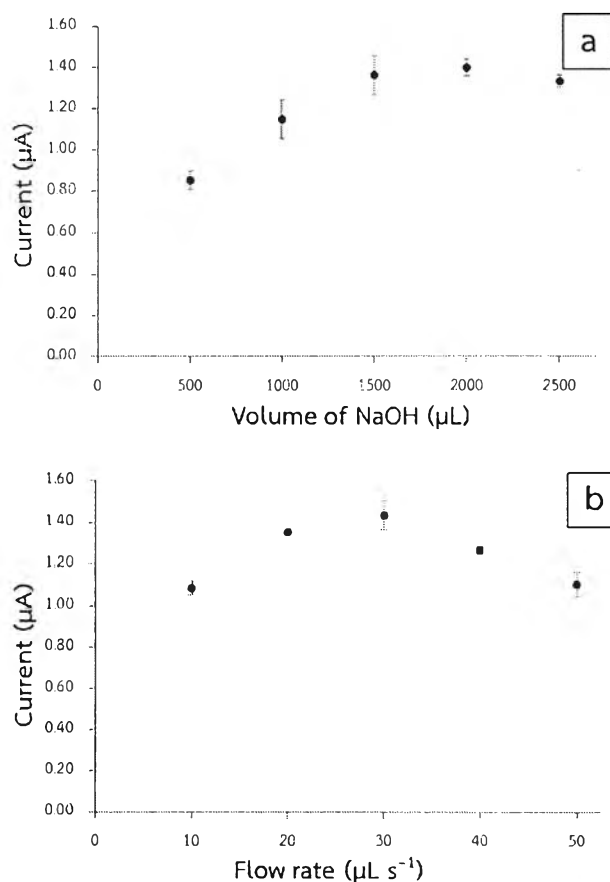


Fig. 4. Effect of the volume of 0.4 M NaOH (a) and the flow rate of NaOH injection (b) on the obtained peak current of a standard solution containing 1.00 mg L⁻¹ Ni(II) in 0.4 M NaCl electrolyte solution by ion-transfer to hydroxide medium using SIECA.

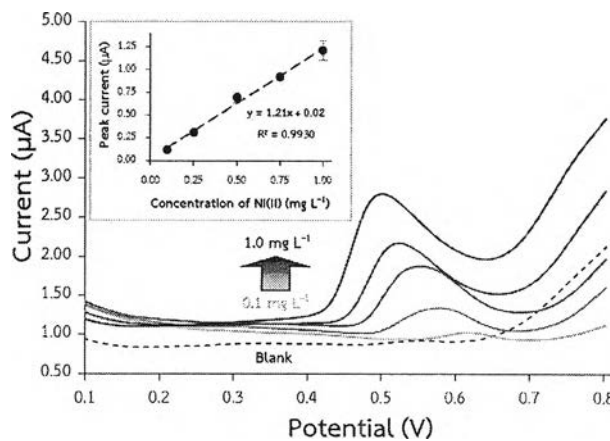


Fig. 5. Typical square-wave voltammograms of standard solutions containing different concentration of Ni(II) in 0.4 M NaCl by ion-transfer to hydroxide medium using SIECA. The inset shows the linear relationship between the Ni(II) concentration and the obtained peak current from the determination of Ni(II)

established in the range from 0.10 to 1.00 mg L⁻¹ Ni(II), as shown in Fig. 5. Good sensitivity was achieved at a slope of 1.21 μ A L mg⁻¹. We investigated the repeatability by analyzing a standard solutions. Three standard solutions with Ni(II) levels of 0.10 , 0.50 and 1.00 mg L⁻¹ were determined using the proposed method (ion-transfer to hydroxide medium using SIECA) in replicates of 10 times; the relative standard deviations (RSDs) were 13% , 7.4% and 3.9% , respectively, which are acceptable according to the Association of Analytical Communities

Table 2
Determination of Ni(II) concentration in mineral water samples by ion-transfer to hydroxide medium using SIECA.

Sample	Concentration of Ni (II) (mg L ⁻¹)		%Recovery
	Spiked	Found	
Mineral water I	0.00	Not detected	–
	0.10	0.094 ± 0.019	94
	0.50	0.496 ± 0.050	99
Mineral water II	0.00	Not detected	–
	0.20	0.194 ± 0.003	97
	0.40	0.378 ± 0.008	94

(AOAC)'s guidelines for dietary supplements and botanicals [20]. The reproducibility of the proposed method using different SPCEs was also investigated in terms of the sensitivity RSD obtained from the slope of the linear calibration curve. The average slope from three calibration curves was $1.08 \pm 0.12 \mu\text{A L mg}^{-1}$ with an acceptable RSD of 11%.

The limit of detection (LOD), the concentration corresponding to $3\sigma/S$, was 0.02 mg L^{-1} ; where σ is the standard deviation ($n=10$) of the signal from a standard solution containing the lowest concentration in the linear range, 0.10 mg L^{-1} Ni(II), and S is the slope of the calibration curve for the same SPCE.

In addition, the interference effect of some metal ions, including Pb(II), Cd(II), Zn(II), Cu(II) and Au(III), was studied. The results indicated that the signals for Ni(II) did not significantly change at 95% confidence intervals when the standard solutions were contaminated until the concentrations of the foreign ions were more than 100 times the Ni(II) concentration.

3.6. Real water sample analysis

The proposed method for the determination of Ni(II) by ion-transfer to a hydroxide medium using SIECA was evaluated under the optimized conditions by determining the Ni(II) concentration in mineral water samples. The samples were filtered without further purification and were then spiked with various concentrations of Ni(II). The spiked samples were diluted with 2 M NaCl (4:1 w/v) to obtain working solutions with 0.4 M NaCl electrolyte. The samples were then analyzed by a standard addition method in triplicates. Table 2 summarizes the results, which indicate that the accuracy of the proposed method was very good, with recovery in the range from 94% to 99%.

4. Conclusions

An alternative method for the determination of Ni(II) ion concentration through the electrochemical response of the Ni(II)/Ni(III) redox couple has been achieved by ion-transfer to a hydroxide medium using SIECA, which is a perfect combination of an automated flow-based system and a highly sensitive electrochemical techniques. An inexpensive sensor, i.e., a homemade SPCE, was also successfully used in this proposed method. Under the optimized conditions, the method provided good linearity over the concentration range from 0.10 to 1.00 mg L^{-1} and a low detection limit of 0.02 mg L^{-1} . In addition, the proposed methods was successfully applied to the determination of Ni(II) concentrations in standard-spiked water samples, with good accuracy.

Acknowledgments

The authors thank the Thailand Research Fund through Research Team Promotion Grant (RTA5780005). E. Punrat is grateful to the Ratchadaphiseksomphot Endowment Fund, Chulalongkorn University,

for a Postdoctoral Fellowship. We also greatly appreciate Professor Dr. Shoji Motomizu and Assistant Professor Dr. Lukman Hakim from Okayama University, Okayama, Japan, for their supports with the sequential injection system. In addition, we thank the National Nanotechnology Center (NANOTEC), NSTDA, Ministry of Science and Technology, Thailand, through its Center of Excellence Network program.

Appendix A. Supplementary material

Supplementary data associated with this article can be found in the online version at doi:10.1016/j.talanta.2017.03.062.

References

- [1] Markin Metal Powders (UK) Ltd., Infographic: History of Metals Timeline, 2016. (<http://www.markin-metals.com/about/history-of-metals-infographic/>), (Accessed 10 August 2016).
- [2] C. Barcelo, N. Serrano, C. Arino, J.M. Diaz-Cruz, M. Esteban, Ex-situ antimony screen-printed carbon electrode for voltammetric determination of Ni(II)-ions in wastewater, *Electroanalysis* 28 (3) (2016) 640–644.
- [3] M.I. Ansari, A. Malik, Seasonal variation of different microorganisms with nickel and cadmium in the industrial wastewater and agricultural soils, *Environ. Monit. Assess.* 167 (1) (2010) 151–163.
- [4] Nickel Institute, *Safe Use of Nickel in the Workplace*, 3rd ed., 2008.
- [5] World Health Organization, *Guidelines for Drinking-water Quality*, Geneva, 2008.
- [6] A. Ferancová, M.K. Hattunieni, A.M. Sesay, J.P. Räsý, V.T. Virtanen, Rapid and direct electrochemical determination of Ni(II) in industrial discharge water, *J. Hazard. Mater.* 306 (2016) 50–57.
- [7] R. Soomro, S.Q. Memon, M.J. Ahmed, N. Memon, A. Mallah, Bis(salicylaldehyde) orthophenylenediamine as complexing reagent in simultaneous determination of gold, chromium, iron, uranyl, and nickel using capillary zone electrophoresis, *Acta Chromatogr.* 24 (4) (2012) 543–558.
- [8] H.R. Rajabi, S. Razmpour, Synthesis, characterization and application of ion imprinted polymeric nanobeads for highly selective preconcentration and spectrophotometric determination of Ni(2+)(+) ion in water samples, *Spectrochim. Acta A Mol. Biomol. Spectrosc.* 153 (2016) 45–52.
- [9] K.L. Sze, W.S. Yeung, Y.S. Fung, Separation and determination of metal cations in milk and dairy products by CE, *Electrophoresis* 28 (22) (2007) 4156–4163.
- [10] L.L. Zhao, S.X. Zhong, K.M. Fang, Z.S. Qian, J.R. Chen, Determination of cadmium(II), cobalt(II), nickel(II), lead(II), zinc(II), and copper(II) in water samples using dual-cloud point extraction and inductively coupled plasma emission spectrometry, *J. Hazard. Mater.* 239 (2012) 206–212.
- [11] S. Intarakamhang, W. Seuhmann, A. Schulte, Robotic heavy metal anodic stripping voltammetry: ease and efficacy for trace lead and cadmium electroanalysis, *J. Solid State Electrochem.* 17 (6) (2013) 1535–1542.
- [12] A. Economou, Recent developments in on-line electrochemical stripping analysis – an overview of the last 12 years, *Anal. Chim. Acta* 683 (1) (2010) 38–51.
- [13] R.P. Baldwin, J.K. Christensen, L. Kryger, Voltammetric determination of traces of nickel(II) at a chemically modified electrode based on dimethylglyoxime-containing carbon paste, *Anal. Chem.* 58 (8) (1986) 1790–1798.
- [14] A. Economou, P.R. Fielden, Selective determination of Ni(II) and Co(II) by flow injection analysis and adsorptive cathodic stripping voltammetry on a wall jet mercury film electrode, *Talanta* 46 (5) (1998) 1137–1146.
- [15] M. Morfobos, A. Economou, A. Voulgaropoulos, Simultaneous determination of nickel(II) and cobalt(II) by square wave adsorptive stripping voltammetry on a rotating disc bismuth-film electrode, *Anal. Chim. Acta* 519 (1) (2004) 57–64.
- [16] A. Bobrowski, A. Króllicka, M. Maczuga, J. Zarębski, A novel screen-printed electrode modified with lead film for adsorptive stripping voltammetric determination of cobalt and nickel, *Sens. Actuators B: Chem.* 191 (2014) 291–297.
- [17] T. Nurak, N. Praphairaksit, O. Chailapakul, Fabrication of paper-based devices by jacquer spraying method for the determination of nickel (II) ion in waste water, *Talanta* 114 (2013) 291–296.
- [18] S. Neodo, M. Nie, J.A. Wharton, K.R. Stokes, Nickel-ion detection on a boron-doped diamond electrode in acidic media, *Electrochim. Acta* 88 (2013) 718–724.
- [19] J. Davis, D.H. Vaughan, D. Stirling, L. Nei, R.G. Compton, Cathodic stripping voltammetry of nickel: sonoelectrochemical exploitation of the Ni(III)/Ni(II) couple, *Talanta* 57 (6) (2002) 1045–1051.
- [20] AOAC, *Appendix K: Guidelines for Dietary Supplements and Botanicals*, AOAC International, 2013.

Chapter V

Conclusions

We are successful in the development of novelty in analytical chemistry for innovation of detection as following our objectives set for this project. First, we obtained novel nanomaterial-based chemical sensors for electrochemical and/or colorimetric detection. The methods were successfully applied for analysis of many important analytes in real samples. Second, the paper-based analytical sensors were successfully designed and applied for detection target analytes in real samples. These devices could be a low-cost and disposable alternative tool for rapid screening and detecting in various applications. Third, the automatic and sensitive microfluidic and sequential injection system coupled with electrochemical detection for the determination of metals and organic compound were developed. They were successfully applied for the determination of target analytes in real samples, with results comparable to those obtained by the comparison procedures. Moreover, the proposed methodologies are less laborious, inexpensive, reliable, and more rapid when compared to the conventional methods.

With mentioned satisfying results, all developed systems obtained from this project could be a choice for routine assessment of clinical, food and environmental detection as an alternative way to the conventional procedures. These lead to analytical systems that are more portable than comparable systems, which make these systems especially suitable for on field analysis. Its future use in portable and/or automatic tool for screening and

determination of various predictors of health status or disease risk or environmental safety in humans can be visualized.

Chulalinet



3 0021 01376481 6



